LABORATORY DIRECTED RESEARCH AND DEVELOPMENT 2004

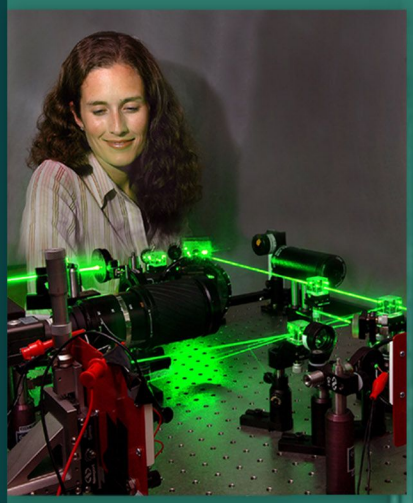

Science, Technology, and Engineering

Mission Technologies

Grand Challenges

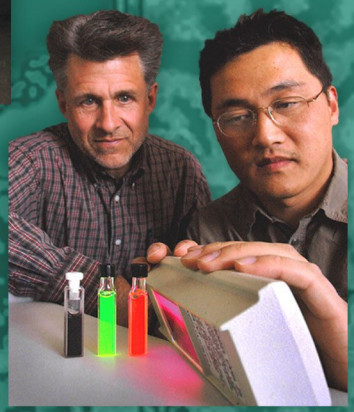

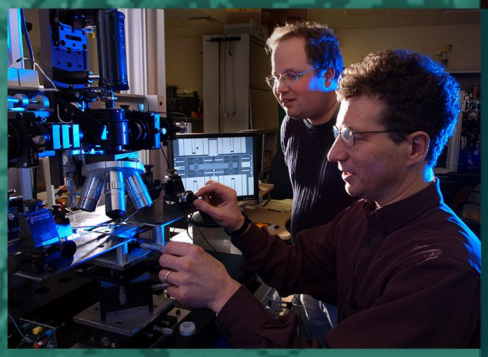

Sandia National Laboratories

A Department of Energy National Laboratory

NNSA National Nuclear Security Administration

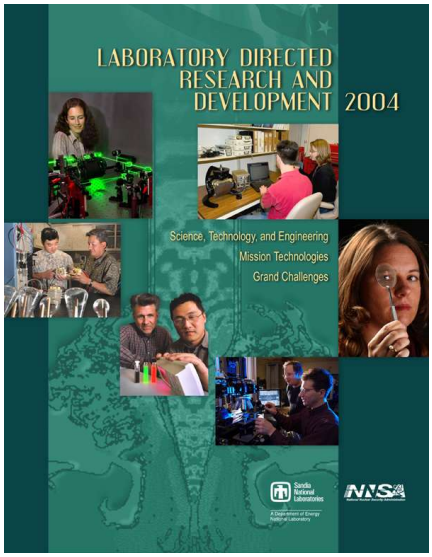

Cover photos (top right going clockwise):
(1) developing novel control/image-formation algorithms to support next-generation synthetic-aperture radar (SAR), (2) looking through a substrate that was made for the new cantilever epitaxy growth process, (3) investigating friction at the microscale using a recently developed nanotractor actuator fabricated using the Sandia Ultraplanar MicroMachine Technology (SUMMiT V^{TM}) process, (4) observing satisfactory fluorescence by their well-trained nanocrystals in water solution. The dark green vial holds gold nanocrystals, the orange and green are semiconductor nanocrystals, (5) holding a test micro fuel cell with the Sandia membrane, (6) looking at very fine motion previously unobservable by the human eye, now revealed by laser beam interaction with unusual diffraction grating.

Issued by Sandia National Laboratories, operated for the United States Department of Energy by Sandia Corporation.

NOTICE: This report was prepared as an account of work sponsored by an agency of the United States Government. Neither the United States Government, nor any agency thereof, nor any of their employees, nor any of their contractors, subcontractors, or their employees, make any warranty, express or implied, or assume any legal liability or responsibility for the accuracy, completeness, or usefulness of any information, apparatus, product, or process disclosed, or represent that its use would not infringe privately owned rights. Reference herein to any specific commercial product, process, or service by trade name, trademark, manufacturer, or otherwise, does not necessarily constitute or imply its endorsement, recommendation, or favoring by the United States Government, any agency thereof, or any of their contractors or subcontractors. The views and opinions expressed herein do not necessarily state or reflect those of the United States Government, any agency thereof, or any of their contractors.

Printed in the United States of America. This report has been reproduced directly from the best available copy.

Available to DOE and DOE contractors from
U.S. Department of Energy
Office of Scientific and Technical Information
P.O. Box 62
Oak Ridge, TN 37831

Telephone: (865)576-8401
Facsimile: (865)576-5728
E-Mail: reports@adonis.osti.gov
Online ordering: https://www.osti.gov/doebridge/

Available to the public from
U.S. Department of Commerce
National Technical Information Service
5285 Port Royal Rd
Springfield, VA 22161

Telephone: (800)553-6847
Facsimile: (703)605-6900
E-Mail: orders@ntis.fedworld.gov
Online order: http://www.ntis.gov/help/ordermethods.asp?loc=7-4-0#online

Abstract

This report summarizes progress from the Laboratory Directed Research and Development (LDRD) program during fiscal year 2004. In addition to a programmatic and financial overview, the report includes progress reports from 352 individual R&D projects in 15 categories.

Sandia is a multiprogram laboratory operated by Sandia Corporation, a Lockheed Martin Company, for the United States Department of Energy's National Nuclear Security Administration under Contract DE-AC04-94-AL85000.

SAND 2005-1988
March 2005

LDRD Annual Report Staff:

Sandia National Laboratories

Hank Westrich
Cynthia H. McDonald
Donna Chavez
Keith Ortiz
Danielle Montoya

TECHnically WRITE

Rhonda Reinert
Carol Whiddon
Donna Drayer
Douglas Prout

Table of Contents

16 "...exceptional service in the national interest."

17 An Overview of Sandia's FY 2004 Laboratory Directed Research and Development (LDRD) Program

24 Stewardship of Sandia National Laboratories' FY 2004 Laboratory Directed Research and Development (LDRD) Program

Advanced Concepts

28 Agent-Based Modeling of Middle East Terrorist Recruitment

30 Automatic Generation of Terrorist Operation Plan Hypotheses

33 Radiation-/Geometry-Driven Jets: Proof-of-Principle Tests

36 Systems Assessment of Water-Savings Impact of Controlled-Environment Agriculture Utilizing Wirelessly Networked SDACs

38 Climate Change Effects on International Stability

Advanced Manufacturing

41 Microfabrication with Femtosecond Laser Processing

44 Mesoscale Controlled Motion for a Microfluidic Drop Ejector

46 Atomic Layer Deposition of Highly Conformal Tribological Coatings

50 Assembly of Microsystems Using Exothermic Multilayer Thin Films

52 Intelligent Interaction Control as Applied to Metrology and Assembly of Microscale Components

55 Rapid-Prototyping High-Density Circuitry (RpHdc)

57 Elucidating the Mysteries of Wetting

60 Next-Generation Spindles for Micromilling

63 Miniature High-Power RF Components Enabled by Mesoscale Manufacturing

66 Rapid Prototyping to the Nanometer Scale

67 Robust Manufacturing of Gel-Based Components for Nuclear Weapons

69 Meso-/Microoptical System Interface Coupling Solutions

71 Injection Molding of Net-Shape Active Ceramic Components

73 Macro-/Meso-/Microsystems Integration in LTCC

Biotechnology

77 Physical and Electronic Changes Caused by Membrane Signaling as a Transduction Pathway in Affinity-Based Biosensors

80 Cellular Observatory: Simultaneous Time- and Frequency-Resolved Microscopy

82 Modeling Biomembranes

84 Reverse-Engineering Biological Networks: Applications in Immune Responses to Bioterrorism Threats

Table of Contents

88 High-Throughput Identification of Molecular Machines Involved in Membrane Signaling and Toxin Pathways

91 Studies of Signaling Domains in Model and Biological Membranes Through Advanced Imaging Techniques

93 Imaging Self-Organization of Proteins in Membranes by Photocatalytic Nanotagging

96 Protein Microarrays for Biowarfare-Agent Detection and Characterization

99 Interaction of Proteins with Lipid Films

103 New Technologies for Understanding Membrane-Protein Recognition and Signaling

Chemical and Earth Sciences

107 Sequestration of Pathogens on Nanoengineered Surfaces

111 A Combined Preconcentrator and Sensor for Live Waterborne Pathogens

113 Geophysical Subsurface Imaging and Interface Identification

Computational and Information Sciences

116 Graduated Embodiment for Sophisticated-Agent Evolution and Optimization

119 Scalable Fault-Tolerant Algorithms for Linear-Scaling Coupled-Cluster Electronic Structure Methods

121 Micromagnetic Suspension

123 Sensitivities for Large-Scale Simulation Codes

126 IP Storage: A Performance and Security Study

129 A Parallel Circuit Simulator for Cell Biology

131 Developing a Computationally Efficient Dynamic Multilevel Hybrid Optimization Scheme Using Multifidelity Model Interactions

134 Robust Large-Scale Parallel Nonlinear Solvers for Simulations

137 Development of Computational Algorithms and Inversion Capabilities for Transport/Reaction Simulations of Chemical/Biological/ Radiological Terrorist Attack Scenarios in Support of Homeland Security

140 Massively Parallel Linear Programming

143 A Method of Evaluating Research Using New Innovation, Risk, and Impact Indicators

145 Massively Parallel, Scalable Atmosphere Model

147 High-Performance Processing Architecture

149 Substructured Multibody Molecular Dynamics

151 Enhancing Simulation Performance on Clusters with Configurable Auxiliary Devices

154 A Hybrid Level-Set/Particle Method for Modeling Surface Evolution During Feature-Scale Etching and Deposition Processes

157 Penetrator Reliability Investigation and Design Exploration (PRIDE)

160 Topology Optimization for Improving Sensor Performance

Differentiating Technologies

164 Microengine for Advanced Power Generation

Table of Contents

Electronics and Photonics

168 Engineered Superconductivity in Electron-Hole Bilayers

171 Silicon-Based RF MEMS Components

173 Nanoelectromechanical Oscillators (NEMOs) for RF Filtering

176 Continuous-Wave Intersubband Terahertz Sources

178 Microsystems for Chemical Signature and Reagent Delivery

180 Microfluidic Cellular-Sample Pretreatment

183 Active Photonic-Crystal Devices for Integrated Photonics and Silicon Photonics

185 Co-Processing of Chalcogenide-Based Radiation-Hard Nonvolatile Memories by Sandia's MDL and BAE Systems

187 Functionalized Nanoparticles for Sensor Applications

190 Novel *In Situ* Mechanical Testers to Enable Integrated Metal Surface Micromachines

193 Compliant Thermomechanical MEMS Actuators

196 An Integrated, Stacked System-on-a-Chip

199 Micromass Spectrometer-on-a-Chip

201 Quantum Coherence in Semiconductor Nanostructures for Improved Lasers and Detectors

203 MOSFET–MEMS Integration

205 Microoptical Gyroscope Via Monolithic Active/Passive Optical Integration

207 Materials Physics and Device Development for Improved Efficiency of GaN HEMT High-Power Amplifiers

209 Leaky-Mode VCSELs for Photonic Logic Circuits

211 Advanced Polychromator Systems for Remote Chemical Sensing

213 Characterization and Application of Dielectrics with Controlled Leakage

216 Nano-G Accelerometers Using Nanophotonic Motion-Detection System

218 Bragg Fiber Development

220 Microwave-to-Millimeter-Wave Electrodynamic Response and RF Applications of Semiconductor Quantum Nanostructures

222 Development of GaN 20–100 Watt Ku-Band Power Amplifiers for Micro-SAR

225 Evanescent-Wave Planar Photonic Biosensor

227 Passive Electronically Steerable Array (PESA) for Miniature Synthetic-Aperture Radar (Mini-SAR), Precision Guidance, and Intelligence/Surveillance/Reconnaissance (ISR)

Emerging Threats

231 Automated Visual Direction of Mobile Manipulation

233 Miniature Fourier-Transform Ion-Mobility Spectrometer for Real-Time Detection and Identification of Explosives and Chemical Agents

235 EM Interactions with Systems to Enhance Security

Table of Contents

236 Use of Seismic and Acoustic Responses to Assess Bomb Damage to Underground Facilities

238 Free-Space Electrooptic Sampling and Remote Mapping of Electromagnetic Fields from Emitting Structures Using Femtosecond Terahertz Transceivers

241 Identification of Chemical Plumes: Range-Resolved IR Lidar Enabled by New Photonic Technologies

243 Critical Technology Development for Hard-Target-Defeat High-G-Tolerant Fuze and High Explosives

245 Immunological Basis for High-Reliability Systems Control

247 Moving-Target Identification Using Ultrahigh-Range-Resolution Data

249 Advanced Mobile Networking, Sensing, and Controls Using Graph Theory

252 Compact Terahertz Sources for Emerging-Threats Applications

255 Understanding Communication in Counterterrorism Crisis Management

258 Hypervelocity Impact-Generated Flash

260 Improving Human/System Interactions in Systems-of-Systems

262 Distributed Detection and ID Algorithm Architecture for Unattended Ground Sensors

264 Secure Chaotic Communications

266 System-of-Systems Modeling and Analysis

268 Eye-Safe Short-Range Standoff Aerosol-Cloud Finder

270 Microflame-Based Detector Suite for Universal Gas Sensing

273 Nonlethal Technologies for the War on Terrorism

275 Advancements in Sensing and Perception Using Structured Lighting Techniques and an Innovative Design Tool

278 Biophysics of BW-Warhead Defeat with a Kinetic Interceptor

281 Dispersal in Urban Canyons, Source Identification, and Collateral Damage/ Mitigation Assessment

283 Weaponization of Thermobaric Explosives

286 Development of an Enterprise-Scale Agent-Based Autonomic Logistics Simulation Model

289 Mobile-Node Authentication in a Wireless *Ad Hoc* Environment

292 Novel Processing, Affordable Motion Compensation, and Mode Multiplexing for Miniaturized Synthetic-Aperture Radar

295 Coilgun Technology Demonstration Test-Bed

298 Enhanced Perception for Remote 3-D Mapping of Unknown Indoor and Outdoor Environments

300 A Modular Micromagnetic Accelerometer in Support of the mTalon Vision

302 MICROFUZE Integration

304 Analysis of Technology Impacts on Operations in Complex Environments

306 CBW Cloud Knockdown and Neutralization

308 Assessment of Biokillers in EDS for Biological-Agent Destruction

Table of Contents

310 Adaptive-Force-Feedback Surface Control

312 High-Capacity Earth-Penetrator Instrumentation

314 Systems Analysis of Networked Sensors

317 Deployable Object Tracker for NMD Flights

319 Continuous-Flow Detector for Rapid Pathogen Identification

321 Simulating Human Behavior for National Security

323 Compact Ultrabright Multikilovolt X-Ray Sources for Advanced Material Studies, 3-D Nanoimaging, and Attosecond X-Ray Technology

326 Magnetophoretic Bead Trapping in a High-Flowrate Biological Detection System

329 TPV Energy Scavenging for Hypervelocity Vehicles

Energy and Critical Infrastructures

332 Natural-Gas Production Problems: Solutions, Methodologies, and Modeling

335 Time-Domain Reflectometry for Remote, Real-Time Water-Quantity/-Quality Monitoring of Perennial and Ephemeral Streams

338 Functionalized Nanoelectrode Arrays for *In Situ* Identification and Quantification of Regulated Chemicals in Water

341 Water Desalination

344 Revolutionary Systems for Catalytic Combustion and Diesel Catalytic Particulate Traps

348 Potential Application of Microsensor Technology in Radioactive-Waste Management—With Emphasis on Headspace Gas Detection

351 Beyond Nanoparticles—Attack on a Chemical "Holy Grail"

354 Advanced Proton-Exchange Materials for Energy-Efficient Fuel Cells

357 Alanate-Hydride Fuel-Cell Demonstration Project

360 Real-Time Discriminatory Sensors for Water-Contamination Events

362 Advanced High-Efficiency Direct-Cycle Gas Power-Conversion Systems for Small Special-Purpose Nuclear-Power Reactors

365 Securing Mobile Code

368 Novel Catalysts for Hydrogen Fuel-Cell Applications

372 Linking Optimization and Simulation in Critical-Infrastructure Systems

375 Hydrogen Futures Dynamic Simulation Model

377 Agent-Based Control of Distributed Infrastructure Resources

380 Biological-Security Decontamination Technology—Reducing the Threat of Infectious-Agent Spread

383 Consequence Management, Recovery, and Restoration after an Intentional Contamination Event

386 Fully Integrated System-Dynamics Toolbox for Water Resources Planning

Table of Contents

390 Predicting System Performance of Proton-Exchange-Membrane Fuel Cells: Computational Modeling with Experimental Discovery and Validation

393 Optimal Allocation of Terrorist Countermeasures Using Risk-Based Systems Pathways Analysis

396 Silicon Field-Emission Electric Propulsion Arrays (FEEP) Powered by Orbital Nuclear Reactors

398 Advanced Fuel-Cell Reactor for the Direct Cogeneration of Electricity During Selective Partial Oxidation of Hydrocarbons

401 New Hydrogen-Storage Material: Metal-N-H System

403 Intrusion Detection for Wireless Networks

405 Membranes for H_2 Generation from Nuclear-Powered Thermochemical Cycles

408 Microfabricated BTU Monitoring Device for System-Wide Natural-Gas Monitoring

411 "Tunable" Ion Conductors for Low-Temperature Oxide-Based Fuel Cells

414 Nuclear Nanobatteries: On-Board Power for Independent MEMS Devices

417 Integrated Tunable Light Sources for Miniature Sensors

419 Design and Fabrication of Advanced Device Structures for Ultrahigh-Efficiency Solid-State Lighting

421 Develop a System-Dynamics Modeling Framework for Assessing Factors that Influence Water Resource Consumption

423 Develop a Cooperative Water-Management Process, Creating a System-Dynamics Model of Water Resources in the Lower Rio Grande Basin

425 Energy-Systems Analysis Framework and Modeling

427 A Mathematical Method for Quantifying the Effectiveness of Management Strategies

429 Inactivation of Avian Influenza (Bird Flu) with Sandia-Developed Decontamination Formulations

431 GeSi–Strained Nanostructure Self-Assembly for Nano- and Optoelectronics

Engineering Sciences

434 A Robust, Coupled Approach for Atomistic-Continuum Simulation

438 Microscale Rarefied-Gas Dynamics and Surface Interactions for EUVL and MEMS Applications

441 High-Fidelity Frictional Models for MEMS

444 Soot Formation, Transport, and Radiation in Unsteady Diffusion Flames

447 Coupled Solid-Fluid-Mechanical-Computational Modeling of Fracture and Fragmentation in Geomaterials, such as Hard and Deeply Buried Targets (HDBTs)

450 Novel Diagnostics for Rarefied Flows in MEMS Applications

452 Ray Model of High-Frequency Cavity Scarring

455 New Smart Material to Address Issues of Structural Health Monitoring

458 Noncontact Surface Thermometry for Microsystems

Table of Contents

461 High-Speed Interferometric Deformation Measurements

463 Fundamentals of Nanofluidics

465 Simulating Self-Assembly and Growth of Biological Nanostructured Materials

468 A Low-Power, Ultrafast-Current Transient Measuring Device

470 A Capillary Valve for Microfluidic Systems

Grand Challenges

473 Biomicrofuel Cell (BMFC)

476 Augmented Cognition: Next-Generation Intelligent Systems

480 TALON

483 Near-Real-Time Characterization for Assured HDBT Defeat

486 Prompt Global Response

488 Winning the War: A Systems Approach to Defending Our Borders

Materials Science and Technology

493 The Basics of Aqueous Nanofluidics: “Interphase” Structure and Surface Forces

497 Design, Synthesis, and Characterization of Soft-Matter Nanolayer Superlattices

499 Photocontrol of Nanointeractions in Microsystems

501 Electrochemically Deposited Alloys with Tailored Nanostructures for LIGA Micromachines

503 Nanostructured Materials for Directed Transport of Excitation Energy

505 Modeling Local Chemistry in the Presence of Collective Phenomena

507 Solution-Based Nanoengineering of Materials

510 Assembly and Actuation of Nanomaterials Using Active Biomolecules

514 Decomposition of Contaminants Using Photochemically Active Nanoparticles

516 Thermally Cleavable Surfactants

518 Transition-Metal Catalyzation of Complex-Hydride Absorption/Desorption Reactions

520 Quantification of Environments and Surfaces Within Micropackages

523 Assembly of Ordered Electrooptical and Bioactive Materials and Composites

525 Advanced Packaging/Joining Technology for Microsystems

528 Magnetostrictive Elastomers for Actuators and Sensors

530 Experimental and Computational Study of Liquid-Solid Transition in Tin

532 Active Photonic Nanostructures

534 Electrochemically Switchable Materials for (Bio)Microfluidics

537 Modeling of Friction-Induced Deformation and Microstructure

540 Reversible Antibody Trapping for Selective Sensor Devices

Table of Contents

542 Correlated and Comprehensive Analytical Techniques for Homeland Defense

545 Development of High-Energy-Density Dielectric Materials for Integrated Microsystems

549 Nanolithography-Directed Materials Growth and Self-Assembly

552 Development of a Novel Technique to Assess the Vulnerability of Micromechanical System Components to Environmentally Assisted Cracking

554 3-D Optical Sectioning with a New Hyperspectral Deconvolution Fluorescence Imaging System

558 The Science of Solutes: Transition Metals in LIGA Nickel

560 Novel Gel-Based Technology for Sensors and Weapons

562 Coupled Nanomechanical Oscillator Arrays for the Study of Internal Dissipation in Nanoscale Structures and Collective Behavior in Large Systems

565 Precisely Controlled Picoliter Vessels with Rapid Sample Preparation for Trace Biotoxin Detection

568 Developing the Foundation for Polyoxoniobate Chemistry: Highly Tunable and Exploitable Materials

Nonproliferation and Materials Control

572 Agile, Microsystems-Enabled Receiver

576 Development of a High-Throughput Microfluidic Integrated Microarray for the Detection of Chimeric Bioweapons

578 Zero-Power Radio Receiver

581 Completely Passive Microwave Tag

584 Security Coatings for Multichip Modules

586 Detailed Modeling and Simulation of Contaminant Transport in Architectural Spaces

588 Content-Based Video and Image Indexing System

591 Bioaerosol Collection and Concentration for Microseparations-Based Detectors

594 Detecting the Toolmarks of Genetic Engineering in Bioweapons Strains

596 Joint Authentication/Encryption

598 Ultrahigh-Temperature Ceramics for Hypersonic Vehicle Applications

601 Leveraging Robotic Planning for Physical-Security Analysis

604 Ultralightweight Telescope with MEMS Adaptive Optic for Distortion Correction

606 Modeling Signals from Earth-Penetrating Nuclear Weapons for Remote Kill Assessment

607 Novel Micropreconcentrators for CW, Explosives, and Water Surety

610 Ion-Mobility Spectrometer/Mass Spectrometer

612 Cryptographic Assurance of Execution Correctness and Confidentiality

615 Characterization, Performance, and Optimization of PVDF as a Piezoelectric Film for Advanced Space Mirror Concepts

618 Adaptive Optics and Phase-Diversity Imaging for Responsive Space Applications

Table of Contents

621 Infrastructural Development for Flexible Network of Devices

622 Monolithic Reconfigurable Radio-Frequency Microelectromechanical Systems (RF MEMS) Antennas

625 Next-Generation 3-D Inspection System for Facility Monitoring

627 Risk-Assessment Metatool

629 Featureless Spread-Spectrum Waveform Design and Processing

631 Tracking Slow-Moving Objects in a GPS–Denied Environment

632 Optical Communications

633 A Unique Vibration-Based Miniature Power Generator for National Security Applications

636 Image Georectification Using Digital Elevation Model Shadows

639 Vulnerability Assessment of State-of-the-Art Microelectronics

640 Nonlinear Optical Detection of Biological and Chemical Aerosol Agents Using Femtosecond Lasers

643 Polymer Electronic Devices and Materials

647 Small Circuits for Cryptography

649 Analysis of Multichannel Internet Communication

650 Receiver for Ultralow-Power Wake-Up and Command

652 Extraordinary Optical Transmission Through Patterned Subwavelength Apertures

654 Reconstruction Algorithm Development and Assessment for a Computed Tomography–Based Spectral Imager

657 Power-Combining Techniques for Solid-State Power Amplifiers

659 Dispersive Diffractive Optical Elements for the Infrared

661 Atmospheric Propagation of Terahertz Radiation

663 High-Confidence Estimation of Relative Event Locations from Space-Based Sensors

665 Critical-Infrastructure System-of-Systems Assessment Methodology

667 Dynamic Vulnerability Assessment

669 Inflatable Antenna with Adaptive Actuators

671 Data-Driven Dynamic Models of Conflict

673 Microoptical Radar (MOR) Facial-Recognition Project

676 Automatic-Target-Recognition Algorithms for Uncooled Thermal Imagery

678 Vulnerability Analysis for SCADA

679 Randomness Complexity and Cryptography

681 System Study: Adaptive Optics for Weapon, Reconnaissance, and Military Space Applications

Pulsed Power and High Energy Density Sciences

684 Simulations of Intense Petawatt Laser Pulses with Dense Z-Pinch Plasmas

Table of Contents

686 Development of an Efficient Large-Aperture High-Damage-Threshold Sol-Gel Diffraction Grating

689 Laser Triggering of Water Switches in Terawatt-Class Pulse-Power Accelerators

691 Electrical Conductivity of Metal Alloys

694 Efficient Implicit Multigroup Radiation Calculations

696 Model for Channel Resistance in Water Breakdown

698 Embeddable Shock Physics Sensors

Corporate Objectives

701 Nanoscale Energetic Materials by Inverse Micellar Synthesis

704 Modeling of Rock Penetration

707 Direct Simulation of Solid-Fluid Systems

710 Support–Active Site Interactions in Heterogeneous Catalysts

712 An Analysis of the Automotive Industry as a Source for Weapon Components and Manufacturing Processes

713 High-Speed Micro-EDM

715 Microexternal-Combustion Engine: The P3 Engine Prototype

717 Lipid Membranes on Nanostructured Silicon

720 Resin Infusion Between Double Flexible Tooling

723 Studies on the Disbonding Initiation of Interfacial Cracks

725 Compliant Membranes for MEMS Microphones

727 Multiscale Experimental/Numerical Study

730 Predictive Accelerated Aging of Microsystems: The Science of Dormancy

733 Surety and Accountability Enhancements for Storage Containers

735 Nuclear-Safety Weaklinks for Thermal and Mechanical Environments

738 Advanced Packaging Technology for Optical Firesets

740 Miniature Transmitter Filter for JTA Using LIGA Technology

743 Novel and Robust Environmental Sensing Devices (ESDs)

745 Advanced Neutron Monitors for JTA and Stockpile Monitoring

747 Design and Control of the Magnetic Properties of Nanoparticles

749 Flow Control and Mixing in Microfluidic Devices

752 Atomic-Scale Scanning-Tunneling Microscopy Measurements of Nucleation and Growth of Ge/Si Alloy Structures

754 Micro-/Nanoscale Thermomechanical Manufacturing

756 Evolution of Near-Surface Scalar Concentrations Through a Compact Cylinder Array Embedded in the Atmospheric Surface Layer

757 Design of Biospecific Surfaces to Control Specific Cellular Responses

Table of Contents

760 Nanomagnetic Films

762 A Multiscale Approach to Modeling Carbon Nanotube–Reinforced Composites

765 Integrated Superhard and Metallic Coatings for MEMS

769 Microscale Separations of Biological Compounds Using Novel Polymeric Separations Materials

772 Friction in Micromachine Interfaces

774 Lipid Microarray Biosensor for Biotoxin Detection

777 Advanced Manufacturing Techniques Using Rapid Prototyping

779 Robust Hermetic Packaging Techniques for MEMS Integrated Microsystems

781 3-D Large-Eddy Simulation of Turbulent Flow Based on One-Dimensional Turbulence Modeling

784 Photonic Encryption Using All-Optical Logic

786 Nanoporous-Carbon Adsorbers for Chemical Microsensors

789 Direct Single-Ion Machining of Nanopores

792 Investigation of the Effects of Intense Pulsed Particle Beams on the Durability of Metal-to-Plastic Interfaces

794 Advanced Techniques for Multiobjective Discrete Optimization

796 Nonradioactive Safety and Performance Issues with Supercritical Water Reactor (SCWR) Safety Technologies

798 Radiation Performance Issues with Advanced Coolants for Next-Generation Reactor

800 MEMS/Fuze Diagnostic Extraction in High-G Environments

802 Smart Detectors of Enrichment of Bioaerosols

805 Computational Studies of JP-8 Diffusion Flames with Detailed Chemistry and Particulate Formation

808 Molecular Simulation of Beta-Amyloid (A-beta) Peptide Interaction with Phospholipid Membranes

809 Nanoscale Testing of Deformation and Fracture in Engineering Materials

812 Nanocrystal-Polymer Composites for High-Luminous-Efficiency LEDs

817 Outstanding Challenges for AlGaInN MOCVD

820 Nanoporous Polymeric Materials for Chemically and Spatially Multiplexed Sensing of Bioagents

823 Evolutionary Complexity for Protection of Critical Assets

825 Nanomechanical Stochastic Resonators

826 Augmented Musculature Device

828 Biomolecular Decision-Making Processes for Self-Assembly

830 Light-Powered Nanovehicle Propulsion

832 System-Dynamics Modeling to Assist Regional Water Planning: Modeling the Nonmarket Value of Water

834 Interactive Water-Quality Modeling to Assist Regional Water Planning

Table of Contents

837 Microbe-Exuded Polymers and the Enhanced Corrosion of Carbonate Materials

840 Nerve-Cell Function and the Development of Cognitive Networks

843 Ultrahigh-Gain Fusion Concept

844 Nanofluidic Devices for Rapid Detection of Virus Particles

846 Solution Behavior of PEO: The Ultimate Biocompatible Polymer

848 New Self-Assembled Nanocrystal Micelles for Biolabels

851 Rapid Detection of Biothreat Agents Based on Cellular Machinery

853 Patterning Quantum-Dot Arrays Using DNA Replication Principles

856 Adaptive Algorithms for Use in the Rejection of Periodic Disturbances of Unknown Frequency

858 Property-Based Testing for Cybersecurity Assurance

860 Self-Assembled Ordered Carbon-Nanotube Arrays and Membranes

863 Chemical Cross-Linking and Mass-Spectrometry Studies of the Structure and Dynamics of Membrane Proteins and Receptors

866 Toxin Studies Using an Integrated Biophysical and Structural Biology Approach

869 Top-Down Structural Studies

871 Molecular Dynamics of Membrane Proteins

874 Model-Building Codes for Membrane Proteins

878 Poroelastic-Wave Propagation on the Earth Simulator

882 Development of Microreformers for Fuel Cells

884 Superhydrophobic Surface Coatings for Microfluidics and MEMS

886 Determining Explosive Ignition Criteria for Miniaturized Devices

888 Quantum Squeezed Light for Probing Mitochondrial Membranes and Study of Neuroprotectants

890 Characterization of a New Class of Surface-Micromachined Pumps

893 Risk of Biological Terrorism to Water-Distribution Systems

895 Explicit and Implicit Measures in Human Aversive Classical Conditioning

898 Assessment of Advanced Pulsed-Power Fusion Concepts

901 Developing Algorithms for Predicting Protein-Protein Interactions from Experimental Constraints

904 Instrumentation Development for Real-Time Brain-Wave Monitoring

906 Maximally Autonomous Autodirective Antenna Array Technology

907 Miniaturized Electronic Steerable-Array Synthetic-Aperture Radar

910 Full-Earth-Monitoring Sensor MESAWorks

913 Deciphering the Genetic Regulatory Code Using an Inverse Error Control Coding Framework

Table of Contents

916 Generalized Continuum Models for Inelasticity in Solids: Formulation of Theories and Variational Methods for Computation

918 Molten Salt-Based Growth of Bulk GaN and InN

921 Appendix A: Project Number/Title Index

935 Appendix B: Awards/Recognition List

937 Appendix C: Project Performance Measures

958 Appendix D: DOE Critical Technologies

976 Appendix E: Major National Programs

996 Appendix F: Dual Benefit Areas and Single-Use Categories

1020 Author and Title Index

“...exceptional service in the national interest.”

Science and technology are the heart of the United States industrial competitiveness, national security, energy resources, environmental quality, and leadership in fundamental and applied science.

At Sandia, the Laboratory Directed Research and Development Program provides the knowledge that drives our future. We initiate research and development that spawn the knowledge that revolutionizes technology. Areas of emphasis center on our core technical competencies and the major strategic thrusts of Sandia’s Institutional Plan. Leading-edge experiments that validate our work are constructed and operated on schedule, within budget, and in a safe and environmentally responsible manner.

Our work continues to produce many scientific and technological breakthroughs that lead to new technologies, markets, and businesses for the nation.

To all those who have contributed so generously of their time and talent, thanks and congratulations for a job well done.

An Overview of Sandia's FY 2004 Laboratory Directed Research and Development (LDRD) Program

K. Ortiz and D. Montoya

Breakthrough Innovation

Innovation is a dance between two questions: "What is possible?" and "What is needed?"[1] Sometimes innovation begins with new science or technology, and the innovator seeks possible applications—"What is possible?" At other times, the innovator seeks solutions to a problem, and innovation begins with "What is needed?" Thomas Edison's laboratory is a famous example of the "What is needed?" approach. Sandia's µChemLab™ (pronounced Micro-ChemLab) is an example of the "What is possible?" approach.

In 1997, three coordinated Laboratory Directed Research and Development (LDRD) Grand Challenges projects,[2] collectively known as µChemLab™, began with the premise that technological advances in surface micromachining could re-create the instruments found in typical chemistry laboratories on a vastly smaller scale. For example, a 1 m-high gas-chromatography column could be placed as a hairwidth spiral on a 1 cm^2 piece of silicon. Combined with advanced sensors and other technology, a "chemistry-lab-on-a-chip" could be created.

The original goal of µChemLab™ was to create a swarm of autonomous, mobile robots that could detect explosives to locate landmines and unexploded ordnance. The need for such a capability was evident to the researchers from the war in Bosnia-Herzegovina, from Princess Diana's campaign against landmines, and from the cleanup efforts on military bases.

However, as the project continued, it became apparent that a more critical need existed for detecting chemical warfare (CW) agents, such as sarin, and that the detector units could be hand-held. As "What is needed?" became clearer, the direction of technology development followed. For example, sensor capabilities were tailored to CW agents.

The need to detect CW agents was unexpectedly validated after the Grand Challenges projects ended. Sandia was asked to deploy emergency prototype units of µChemLab™ in high-risk

[1] Mark Stefik and Barbara Stefik, *Breakthrough: Stories and Strategies of Radical Innovation* (MIT Press, 2004).

[2] 3522020000, "Autonomous Micro-Chem Laboratory (µChemLab™)"; 3522010000, "Science on the Microdomain"; 3522030000, "Cooperative, Distributed Sensing and Action Using Microminiature, Intelligent Agents."

public places in the wake of the September 2001 anthrax attacks in Washington, D.C. Since then, other units have been deployed in a variety of national security applications.

Today, µChemLab™ refers to a technology platform that can perform two kinds of chemical analysis—gas chromatography and liquid separation—in small, compact units.[3] µChemLab™ units are small, relatively inexpensive, highly sensitive, and extremely reliable. Multiple sponsors, including the Department of Homeland Security, the Department of Defense, and the Department of Energy, provide current funding. Commercialization of the technology is beginning. In December 2004, a Cooperative Research and Development Agreement (CRADA) was signed between Sandia and two industrial partners, Tenix and CH2M Hill, to develop µChemLab™ for an unattended water-safety system.[4]

In addition to sponsored work, Sandia continues to fund high-risk, high-value LDRD projects that increase µChemLab™ capabilities, for example, in the science of microfluidics. Notably, research to develop better valves for the liquid-phase system resulted in an *R&D Magazine* R&D 100 Award in 2003.[5]

The LDRD Program provides the stable, predictable funding base necessary to conduct high-risk, long-term R&D like µChemLab™. This is possible because LDRD is funded through an assessment (tax) on all work conducted by the Laboratories, and the assessment is pooled into an indirect (overhead) account. As a result, the projects are decoupled from the original funding sources, allowing the researchers to work toward broad mission goals and to adjust the goals as the R&D progresses, as seen in the case of µChemLab™. LDRD also allows the projects to pursue paths that benefit multiple missions of the Laboratories, again as exemplified by µChemLab™.

The LDRD Program is of great importance to the Laboratories. It allows the Laboratories to create their future through innovation. The LDRD Program can anticipate and respond to future national security needs far faster than programmatically directed R&D can. The benefit to national security is evident from the list of the Laboratories' current users, who are reaping the benefits of innovations funded by

[3] See the µChemLab™ Web site at http://www.ca.sandia.gov/chembio/tech_projects/detection/micro-chem-lab.html.

[4] See the news release at http://www.sandia.gov/news-center/news-releases/2004/tech-trans/tenix.html.

[5] The award presented to "Isolated Cast-in-Place Microvalves" resulted from project 11130, "Molecular Integrated Microsystems (MIMS)."

their predecessors and, in turn, are paying for innovations that will pay off in the future.

Therefore, the Laboratories must get maximum value from the LDRD Program. Let us address the performance of the LDRD Program in fiscal year (FY) 2004.

Performance Against DOE Objectives

The present form of LDRD was authorized by Congress in 1991 to be the sole source of discretionary research funds. It is implemented under DOE Order 413.2A, "Laboratory Directed Research and Development," which identifies the following five objectives for the program:

- Maintain scientific and technical vitality of the Laboratories,
- Enhance the Laboratories' ability to address future Department of Energy (DOE) missions,
- Foster creativity and stimulate exploration of forefront science and technology,
- Serve as a proving ground for new research, and
- Support high-risk, potentially high-value R&D.

One measure of the FY 2004 program is with respect to these objectives.

Scientific and Technical Vitality. LDRD is essential to attracting and retaining young staff. In the last 4 years, almost a quarter of Sandia's staff supported LDRD projects. Over 46% of the full-time employee (FTE) hours spent on FY 2004 LDRD projects are from staff with fewer than 5 years of experience. In addition, LDRD projects support more postdocs (49%) than any other program at Sandia.

Future DOE Missions. LDRD is essential to creating the capabilities that bring customers to Sandia, both new and returning. For example, the LDRD Program anticipated the need for research into technologies to counter chemical or biological warfare agents and other problems in homeland security several years before the 9/11 attacks.

Forefront Science and Technology. LDRD research is at the forefront of Sandia's R&D. The two R&D 100 awards won by Sandia in FY 2004 were both based on LDRD projects. In FY 2002 and 2003, nearly 20% of the Laboratories' scientific and engineering publications were generated by LDRD research.

New Research. The importance of biotechnology to national security is now recognized, for instance, in defense against biowarfare and bioterrorism. In fewer than 10 years, LDRD has placed Sandia's biotechnology initiative on the map.

The two R&D 100 awards won by Sandia in FY 2004 were both based on LDRD projects. In FY 2002 and 2003, nearly 20% of the Laboratories' scientific and engineering publications were generated by LDRD research.

Sandia's biotech publications have grown from virtually nothing to rivaling the impact of the other national laboratories.

High-Risk, High-Value R&D. LDRD projects conduct high-risk research that would not be funded by programmatic sources, i.e., neither the DOE nor Other Federal Agencies (OFAs). Often, after an LDRD project reduces the initial risk, another sponsor will step in to fund follow-on work. The µChemLab™ is a perfect example.

In calendar year 2003..., LDRD contributed to 413 refereed publications. In the period from 1999 through 2003..., Sandia LDRD produced 529 papers, of which 70% were cited one or more times.

Performance Against OMB Measures

Another way to measure the LDRD Program is to compare it against the three criteria stipulated by the Office of Management and Budget and the President's Office of Science in 2002[6]: Relevance, Quality, and Performance.

Relevance. Sandia's LDRD Program is designed to fund mission-relevant R&D. Investment areas (IAs) issue calls for new R&D ideas; there is a strong programmatic component to the proposal reviews, and the IAs often jointly fund projects of mutual interest.

Quality. The quality of the program is represented by external recognition, publications, and intellectual property.

As previously mentioned, both of Sandia's FY 2004 R&D 100 awards (honoring demonstrable technological significance relative to competing products and technologies) were based on LDRD research. The award-winning "Cantilever Epitaxy" was made possible by a 3-year, $6.6 million LDRD Grand Challenge: project 27328, "A Revolution in Lighting: Building the Science and Technology Base for Ultraefficient Solid-State Lighting." "TRILINOS," part of a broad effort to achieve a high-fidelity computational modeling and simulation approach to science and engineering, was enabled by LDRD project 26517, "Parallel Repartitioning for Optimal Solver Performance," also funded through FY 2003. In addition, 10 other LDRD projects received awards or recognition for outstanding research in FY 2004. (Please refer to Appendix B, Awards/Recognition List.)

In calendar year 2003 (the last complete year for which data are available), LDRD contributed to 413 refereed publications. In the period from 1999 through 2003 (the most recent 5 years for which data are available), Sandia LDRD produced 529 papers, of which 70% were cited one or more times. The Institute for Scientific Information's impact metric measures the impact on the scientific community by tallying the number of times published research is cited by other researchers.

[6] Marburger and Daniels, "FY 2004 Interagency Research and Development Priorities" (30 May 2002).

Sandia's LDRD–related optics and acoustics publications from 1999 through 2003 were cited eight times the world average, placing us first among the 140 institutions measured. In materials science and engineering, LDRD papers were cited nearly three times the world average, placing LDRD seventh among these institutions publishing more than 25 papers in 5 years. In physics, LDRD papers were cited over two times the world average, placing LDRD ninth among these same 140 institutions. Two of the five most highly cited Sandia papers in 2003 were from LDRD projects.

In terms of intellectual property, the LDRD Program is responsible for over 40% of Sandia's total number of technical advances, close to 40% of issued patents, and 30% of Sandia's total income for patent licenses. Since 1992, the number of patents granted and copyrights issued has increased substantially. In FY 1992, Sandia submitted 15 patent applications, 49 technical disclosures, and 6 copyrights. The FY 2004 LDRD Program yielded the submission of 70 patent applications, 159 technical disclosures, and 16 copyrights.

Performance. The FY 2004 program is funded at approximately $106M, which is 5.7% of the total operating budget. [7] Approximately 87% of the projects are defense-related; 70% are identified as potentially dual-use (i.e., applying to both defense and nondefense). The program closed FY 2004 within 1% of its projected cost.

A measure of project performance is progress against identified research goals and milestones. Project milestones are determined for approximately every $300K of funding and identify specific accomplishments in research progress. Goals refer to certain capabilities that are desired within the overall framework of a project's research activities. In scientific inquiry, meeting all of the intended milestones and goals indicates that the research challenges have been set too low. So project teams are encouraged to create a deliberate mismatch between the group's research aspirations and its present knowledge and resources. In FY 2004, almost 95% of LDRD projects met at least two-thirds of their milestones, and over 80% substantially met or achieved their goals. This indicates that while researchers work hard to meet projected goals and

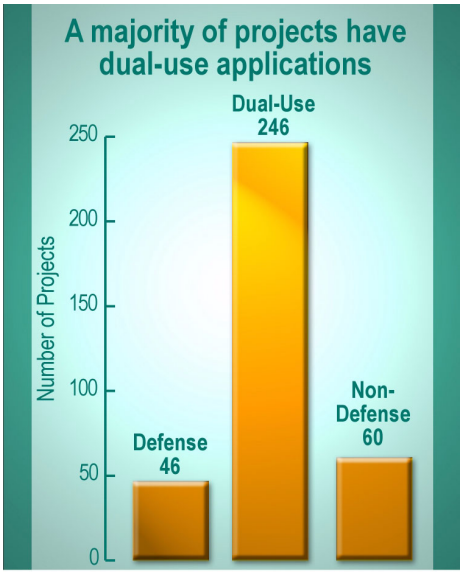

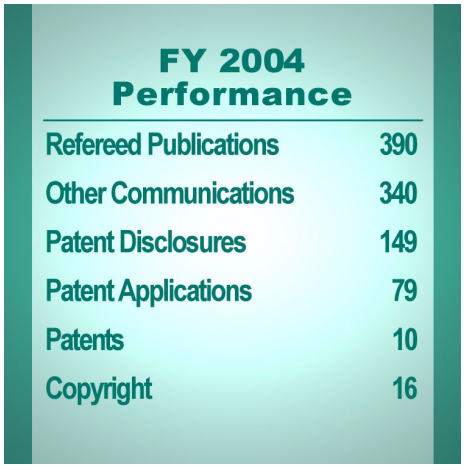

[7] DOE Order 413.2A limits LDRD research funding to not more than 6% of the Laboratories' total operating budget for the year, including non-DOE-funded work. The Order also allows funding of capital equipment for LDRD not to exceed 6% of its total capital equipment budget for the year, but Sandia's LDRD Program does not assess capital equipment. The figures provided do not include the costs of construction and capital equipment. The program is slightly less than 6% because it is planned conservatively in the previous FY.

milestones, there is a still a high level of "stretch" anticipated by LDRD participants in their research activities.

Overall, the Sandia LDRD Program is meeting its objectives and is performing well.

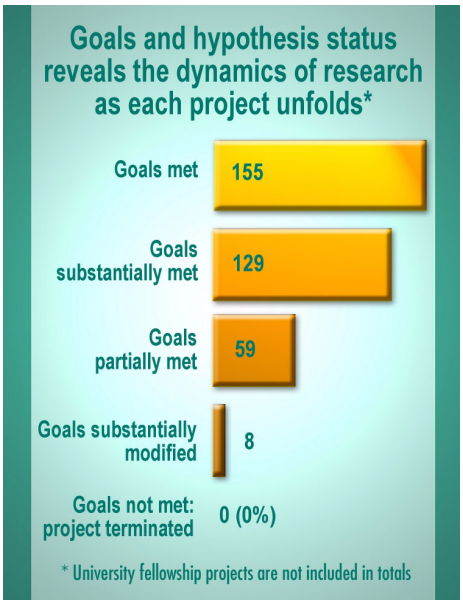

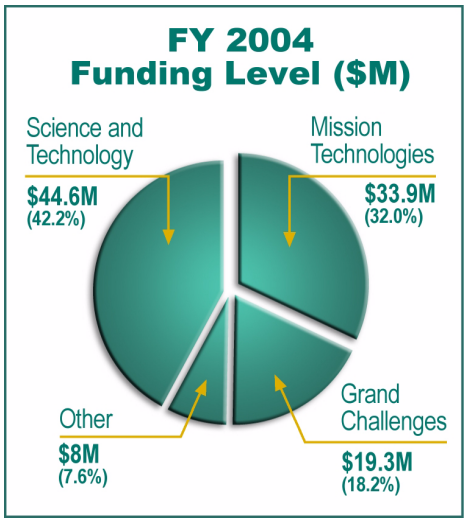

FY 2004 Program Strategy and Process

In January 2004, Sandia's Mission Council approved the organization of the FY 2004 LDRD portfolio into four categories of IAs: Science and Technology (S&T), Mission Technologies (MT), Grand Challenges (GC), and Other. Within these categories, the individual IAs are the following:

- Science and Technology Investment Areas. Advanced Manufacturing, Biotechnology, Computational and Information Sciences, Chemical and Earth Sciences, Electronics and Photonics, Engineering Sciences, Materials Science and Technology, Pulsed Power and High Energy Density Sciences
- Mission Technology Investment Areas. Differentiating Technologies, Emerging Threats, Energy and Critical Infrastructures, Nonproliferation and Materials Control
- Grand Challenges Investment Area
- Other Investment Areas. Advanced Concepts, Corporate Objectives

The Science and Technology IAs principally support the nuclear weapons mission of the Laboratories, while the Mission Technology IAs principally support other missions. However, the nature of most LDRD projects is such that multiple missions typically benefit from any given project.

The Grand Challenges IA is composed of large (greater than $1M), multidisciplinary projects that address technical areas that are vital to the core purpose of the Laboratories.

Other IAs include Advanced Concepts and Corporate Objectives. The Advanced Concepts IA supports investigations related to potential future threats to national security. Corporate Objectives includes University Collaborations, the Presidential Early Career Awards for Scientists and Engineers (PECASE), and the Seniors Council. Typically, LDRD projects in these Other IAs are late-starts, i.e., they are proposed and funded after the beginning of the FY.

The individual IAs are profiled at the beginning of each section of this report.

The process for selecting FY 2004 LDRD projects began in March 2003 with a call for proposals from each of the above IAs. In response, 975 brief ideas for proposals were submitted. The Investment Area Teams (IATs) reviewed these ideas and selected 548 for development as full proposals. The two-step idea-proposal format streamlines the process, encouraging more

ideas to be submitted and decreasing the time spent writing and reviewing unsuccessful proposals.

The proposals are reviewed for technical and programmatic merit. Technical review criteria include scientific and technical soundness, creativity and innovation, and project planning. Programmatic review criteria may include customer needs, fit within the existing technology base, competition, and potential leverage of other investments. From these proposals, 264 projects were selected by the IATs in June for funding. FY 2004 ended with 352 active projects: 174 were in their first year, 115 in their second, and 63 in their third. On average, FY 2004 projects were funded at approximately $288K, the smallest project at $12K and the largest at $3.9M.

Conclusion

The LDRD Program continues to bring extraordinary value to the Laboratories and all its customers. The innovations of the LDRD Program are the key to the future.

Innovation is a dance between "What is possible?" and "What is needed?" The reader is encouraged to read the project summaries in this report and see the dance in motion.

Additional Reading

A comprehensive discussion of DOE's and Sandia's LDRD Program management and funding sources may be found in the "Sandia National Laboratories FY 2004–2009 Institutional Plan," dated December 2003.

FY 2004 ended with 352 active projects: 174 were in their first year, 115 in their second, and 63 in their third.

FY 2004 Selected Statistics

Full-time Staff	398
Smallest Project ($K)	12
Average Project ($K)	288
Average Project (FTE)	1.13
Largest Project ($M)	3.94
1st Year Projects	174
2nd Year Projects	115
3rd Year Projects	63

Stewardship of Sandia National Laboratories' FY 2004 Laboratory Directed Research and Development (LDRD) Program

J. P. VanDevender, Vice President of Science, Technology and Engineering and Chief Technology Officer

Stockpile stewardship is the primary mission of Sandia National Laboratories. Even as we maintain a strong nuclear deterrence, the United States faces new technical challenges from the war in Iraq, global terrorism, homeland defense, energy, and the environment. Sandia's state-of-the-art scientific, technical, and engineering (ST&E) capabilities provide the basis for assuring the safety, security, and reliability of the nuclear weapons stockpile and support broader national security missions. The LDRD Program builds and adapts our ST&E capabilities in anticipation of future national security needs.

The LDRD Program is Sandia's sole source of staff-inspired R&D funding, whose purpose is to maintain and enhance the vitality of the Laboratories. It provides the rare opportunity to create innovative S&T and to develop professional leadership. It is an innovation incubator for Sandia—responsible for more R&D 100 Awards, publications, citations, patents, and royalty income per unit program funding than any other program at Sandia. These measures provide evidence of the high quality of innovations from the LDRD Program so far. Continued mission effectiveness requires continuous innovation from the LDRD Program in the future.

The LDRD Program faces multiple challenges to maintain leading-edge ST&E capabilities needed to support national security missions. We must continue to demonstrate the program's accountability in partnership with federal officials charged with LDRD oversight. This includes proper LDRD program and project planning, communication of mission relevance, and timely application of LDRD results toward appropriate mission needs. In addition, we must continue to improve the LDRD Program by enhancing our strategic vision, utilizing best management practices, and using the LDRD Program to develop the talented and dedicated workforce needed to address future challenges.

The strategic intent of the LDRD Program is rooted in the business plans for each of Sandia's strategic management units (SMUs), the strategic plans for each of the investment areas (IAs), and the corporate goals and milestones for line organizations. These documents delineate strategic intent and can trace their mission support back to the Department of

J. P. VanDevender
Vice President of Science Technology and Engineering and Chief Technology Officer
Sandia National Laboratories

The LDRD Program is Sandia's sole source of staff-inspired R&D funding....

Energy (DOE), National Nuclear Security Administration (NNSA), or Other Federal Agency (OFA) strategic plans. The Mission Council and individual IAs evaluate their LDRD portfolios on an annual basis to ensure maximum alignment with these strategic goals.

We adopt the best R&D portfolio management practices as the evidence confirms their worth. For example, the Mission Council utilizes a modification of the Stage Gate™ process for the LDRD Grand Challenges proposals. The intent is to have a fair and transparent proposal review process with clearly articulated criteria that results in the best LDRD Grand Challenges being funded.

In FY 2004, we implemented post-launch project reviews as an R&D best practice. The LDRD Program can improve and maximize potential applications of newly developed ST&E results through an objective and focused assessment of completed projects. Impacts and lessons learned from completed LDRD projects demonstrate the effectiveness of the selection process and influence an IA's future strategic direction. The simple questions "Why the initial interest?," "What was the R&D outcome?," "Who cares?," and "Where now?," asked in a very informal meeting, elicited insightful, and sometimes passionate, discussions with the principal investigators (PIs) during the last review cycle. Ready availability of this information to other SMU program managers should lead to increased innovative applications of the R&D.

Other best-practice changes included an improved proposal format and LDRD Web-based electronic submission and review process. All of these changes seek to focus and enhance LDRD activities while reducing the efforts of the PIs and IA managers.

LDRD helps to attract and retain the best scientists and engineers at Sandia and to maintain an R&D environment where staff can hone their technical skills or acquire new ones. The multidisciplinary nature of project teams serves to promote innovative applications of staff-initiated R&D. The expertise, creativity, motivation, and successes of the staff have caused LDRD to be referred to as the "the lifeblood of the Labs."[1]

Finally, good stewardship of LDRD requires proactive efforts to ensure the continuation of the program. Laboratory management is accountable for setting the LDRD targets within the 6% funding limit to ensure that current commitments can be met and that we will have the talented staff pursuing the right technical developments necessary to meet the future challenges.

LDRD helps to attract and retain the best scientists and engineers at Sandia and to maintain an R&D environment where staff can hone their technical skills or acquire new ones.

1. Quote from C. Paul Robinson, President of Sandia National Laboratories.

To that end, Sandia has been exploring options to better inform DOE, NNSA, and WFO customers about the high leverage and multiple benefits of LDRD on their programs. Often, WFO sponsors have become LDRD advocates once they have seen the leverage that LDRD has had on their programs.

Advanced Concepts

The Advanced Concepts investment area seeks solutions to future national security threats, both known and anticipated. Sandia has the opportunity to develop new tools that could fundamentally transform U.S. abilities to fight the "War on Terrorism." Advanced Concepts investments endeavor to enable exquisite situational understanding of unfolding events, to harden the homeland, and to alter perception of U.S. adversaries. Additionally, investments work toward agile, networked responses utilizing the full capabilities of the nation to deny adversaries the ability to hide plan and intention.

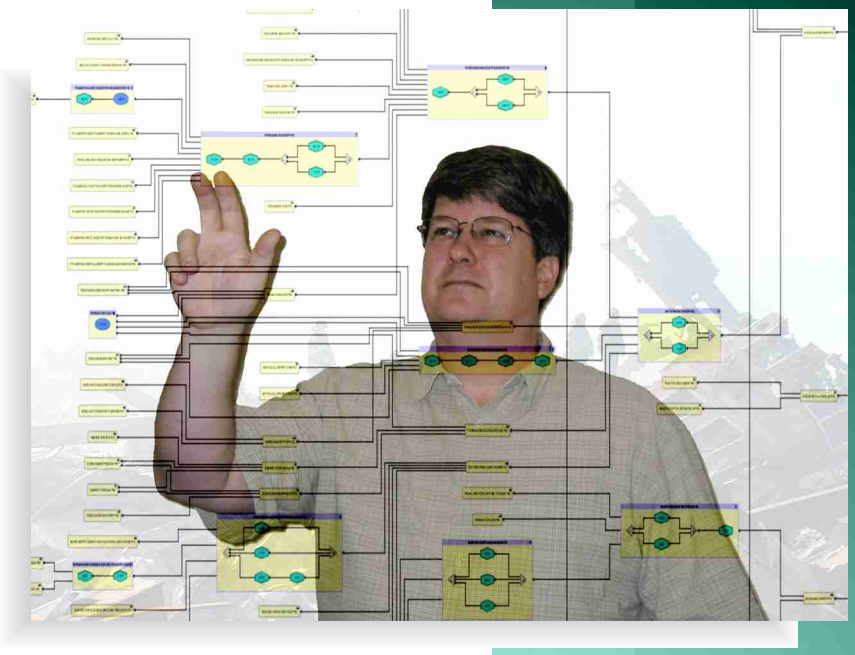

71945
"Automatic Generation of Terrorist Operation Plan Hypotheses"

As a data-intensive, knowledge-dependent, judgment-oriented operation, intelligence analysis can fall victim to human shortcomings. The "Hypothesizer" addresses the risk of human frailty with techniques for the automated generation of terrorist plans.

Leveraging existing artificial intelligence (AI) planning software for a plan-generation engine, researchers integrated a newly developed domain theory of terrorist operations that enables the generation of terrorist operation plan hypotheses. A proof-of-concept test generated a terrorist operation plan that was conceptually equivalent to a hypothetical plan developed by subject-matter experts in a previously conducted Red Team exercise. Two follow-on tasks continue research for applications in data mining, evidence extraction, and capabilities with analysts in a realistic operational test setting.

71944

Agent-Based Modeling of Middle East Terrorist Recruitment

N. M. Berry, J. D. Smrcka, J. G. Turnley, T. H. Ko, T. D. Moy

The Seldon project represents a multidisciplinary approach to developing organization software for the study of recruitment into terrorist organizations. The Seldon terrorist model combines concepts from agent-based modeling and social network analysis to create a computational model of social dynamics for terrorist recruitment. The model is based on the terrorist network model recommended by Marc Sageman.

The underlying recruitment model is based on a unique hybrid agent–based architecture that contains simple agents (individuals such as expatriates) and abstract agents (conceptual entities such as society and mosques). Interactions between agents are determined by multiple social networks that form and dissipate according to the actions of the individual. The software toolkit is used to evaluate the dynamics of social behavior and the specific dynamics associated with terrorist recruitment described by expert social scientists. This model is based on an architecture for simple adaptation to other group phenomena.

...we added new social concepts and interaction models to closely reflect how terrorist recruitment differs from the initial gang model....With these new modifications, the terrorist model permitted the user the ability to observe increased relationship development between individual agents from casual meetings to tight group formations based on similar interests.

Our work was to extend the organization software model to accommodate the concepts related to terrorist recruitment. The primary benefit of such a tool would be to provide a unique computational environment where one can evaluate the effectiveness of strategic interventions on the emergence and persistence of terrorist groups. While we used the underlying organization concepts of the Seldon toolkit, we added new social concepts and interaction models to closely reflect how terrorist recruitment differs from the initial gang model. Modifications to the Seldon model included additions for emotional behaviors and multiple levels of social networks. With these new modifications, the terrorist model permitted the user the ability to observe increased relationship development between individual agents from casual meetings to tight group formations based on similar interests. We saw the recurring meetings between individual agents as the building of bonds between the agents, thus affecting the influence agents had over each other. The terrorist model also incorporated behavioral issues associated with the happiness of the individual agents and the acceptance of the surrounding society of their presence.

The model contains two categories of agents: the individual agent—a traditional computation agent used to represent a human, and the abstract agent—a conceptual agent used to incorporate social concepts into the model. The terrorist model

has two types of individual agents: an expatriate—a foreign national who is isolated from the community and terrorist organizations, and a bridge—a foreign national who has the ability to connect an expatriate with a terrorist organization. The three types of abstract agents are the society, the mosque, and the clique. The society captures the culture in which these agents reside, encompassing societal concepts such as the willingness to accept foreigners into their world. The mosque represents the religious and social gathering place for expatriates. The clique encapsulates the group dynamics of individuals who are all close friends with one another.

The complete terrorist model permitted the user to adjust 58 different concepts and parameters, thus providing a wider range of possible outcomes based on the initial scenario. The simulation begins with no established relationship or affiliation, permitting these aspects to evolve as the simulation progresses. In its current formation, Seldon permits the user to select how the system will be initialized and to visually observe the outcome of the parameter selections.

The Seldon toolkit and terrorist model provides a unique capability that incorporates both innovation and cutting-edge research into a single software package where the innovations permit the developer to capture social norms and mores as part of the simulation in the form of abstract software agents. These agents aided in providing varied levels of granular knowledge that represent small, medium, and large societal views. The cutting-edge research was part of the desire to represent multiple social networks to explore a richer set of social interactions. While the concept of multiple social networks is not new, only a few computational systems attempt to implement this capability. The completion of this project permitted the team to explore terrorist recruitment and to develop a different architectural approach to the computational agent-based community.

Refereed

Berry, N. M., T. H. Ko, T. D. Moy, J. D. Smrcka, J. G. Turnley, and B. Wu. 2004. Emergent clique formation in terrorist recruitment. *Agent Organization: Theory and Practice Workshop* (July, San Jose, California): 10.AAAI.

Other Communications

Ko, T. H., and N. M. Berry. 2004. Agent-based modeling with social networks for terrorist recruitment. Demonstration presented at the AAAI Intelligent System Demonstration Session, July, San Jose, California.

71945

Automatic Generation of Terrorist Operation Plan Hypotheses

M. G. Stickland, G. N. Conrad, M. M. Warrant, L. S. Slater, O. H. Bray, R. L. Craft, N. D. Pattengale, P. Zhang, I. Dubicka, D. P. Miller, L. A. Cano

Intelligence analysis is a challenging activity. As a data-intensive operation, it is possible for analysts to be buried under huge volumes of data. As a knowledge-dependent operation, it can be possible for analysts to not know enough about a given subject to recognize when a given piece of data is significant. As a judgment-oriented operation, analysis can fall victim to the biases of the humans performing this work.

This project was a first step toward the creation of an automated tool concept—the Hypothesizer—that is intended ultimately to help address each of these frailties. Sandia recently researched the Hypothesizer techniques for the automated generation of terrorist plans and plan fragments that explain how given terrorist goals might be achieved in an operational context.

We decided to use the existing artificial intelligence (AI) planning software—the SIPE-2 (System for Interactive Planning and Execution) planning system developed by SRI International—as the plan-generation engine for our work, and then to develop a domain theory of terrorist operations (i.e., a knowledge base) that the SIPE-2 system could reason about to generate terrorist operation plan hypotheses. These plans are intended to provide intelligence analysts with rich, situation-specific subject matter expertise that will help them to determine what new evidence they might need to pursue to strengthen or refute a current working hypothesis.

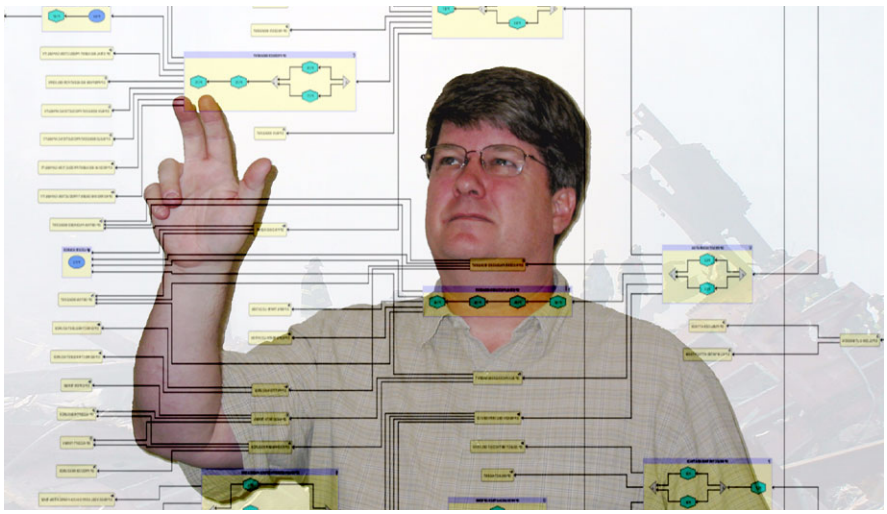

Principal investigator Michael Stickland examines the domain theory being developed by his team for their work on Automatic Generation of Terrorist Operation Plan Hypotheses.

The Hypothesizer is intended ultimately to help address some of the inherent shortcomings of human intelligence analysts. The main goal of recent work was to research techniques for the automated generation of terrorist operation plan hypotheses that explain how given terrorist goals might be achieved in an operational context.

After a comprehensive literature review, we identified several candidate techniques and technologies for plan generation. This finding meant that we probably would not need to invent a new technique, but rather would be able to leverage prior work in the field of AI planning. We determined that SIPE-2, developed at SRI International's Artificial Intelligence Center, could potentially provide the reasoning power we needed, and we acquired a license for this software to use in our research.

A secondary goal of our work was to identify the knowledge representations (e.g., entities, activities, real-world facts, etc.) that would enable generation of terrorist plans. To this end, we developed a framework for terrorist operation (task/activity) decomposition that can be used to instantiate a wide array of operational patterns in a manner that allows the planner to reuse these patterns when applicable. To prove the utility of our terrorist operations domain theory framework, we populated it with information and successfully conducted a proof-of-concept test that resulted in the automated generation of a terrorist operation plan that was conceptually equivalent to a hypothetical plan developed by subject matter experts during a previously conducted Red Team exercise.

With this success under our belts, we decided to assess the deployability of the SIPE-2 system within an operational setting. Since SIPE-2 was developed as research software, and since its user interface is implemented with CLIM (Common LISP Interface Manager), it lacks many of the user-interface features (e.g., user friendliness, modern look and feel, proper error handling, maintainability) that will be required in a nonresearch setting. To mitigate these problems, we developed a prototype JAVA™ application program interface (API) that will allow us to utilize the reasoning power of SIPE-2—programmatically and remotely controlling it from a JAVA™ client application—while providing users with the graphical-interface functionality and modes of operation that will facilitate the enhanced analytic capabilities we seek to deploy.

...[we] successfully conducted a proof-of-concept test that resulted in the automated generation of a terrorist operation plan that was conceptually equivalent to a hypothetical plan developed by subject matter experts during a previously conducted Red Team exercise.

Other Communications

Craft, R. L. 2004. The hypothesizer. Paper presented at the 2004 Intelligence Technology Innovation Center (ITIC) Knowledge Discovery and Dissemination (KDD) Conference, 23 September, Tysons Corner, Virginia.

73045

Radiation-/Geometry-Driven Jets: Proof-of-Principle Tests

R. J. Lawrence, D. S. Preece, R. A. Vesey, C. A. Hall, M. C. Grubelich, T. A. Mehlhorn, A. V. Farnsworth, Jr.

The Z-pinch machine, using a vacuum hohlraum, has been used to produce radiation-driven jets (RadJets) that are generated by differences in material density and atomic number. Based on the extensive development of high-explosive–driven conical-shaped charges (SCs), which was conducted over many years, it should be possible to use the same pulsed-radiation source to produce similar jetting phenomena that are controlled by the geometry of a hollow conical liner (high-energy-density shaped charge [HEDSC]). In this project, Sandia seeks to design and conduct two or more proof-of-principle experiments on the Z-pinch machine to demonstrate the efficacy of this latter concept.

We will perform these tests as add-on experiments to existing RadJet events and will thus take advantage of in-place expertise. Material choices, element sizing, and details of the explicit configuration, including radiation- and loading-moderator layers that will be necessary for energy management, will evolve as the design process proceeds. They will be based both on existing RadJet configurations and on parallel numerical calculations using multidimensional hydrocodes.

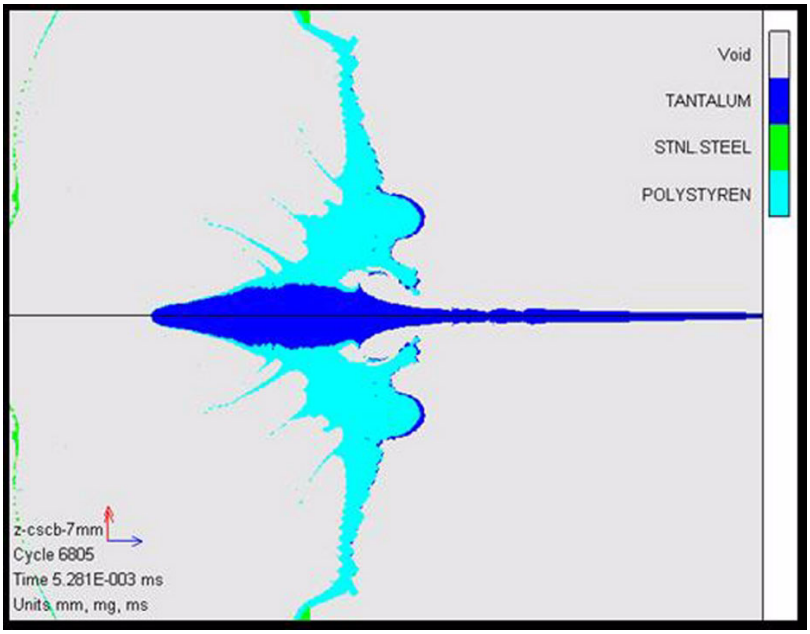

Calculated HEDSC jet. This pre-shot hydrocode calculation shows the well-formed tantalum jet at ~ 5 μs after the start of the radiation pulse.

Experimental diagnostics will include passive recovery of target blocks that will show the penetration effects of the geometry-controlled jets. Active diagnostics may include dynamic velocity measurements to gain further insight into the response of the target block to the loads produced by the jets, and/or x-ray backlighter imaging of the SC jetting phenomena.

We will consider and address specific applications for this type of jetting phenomena.

The objective of this project is to provide proof-of-principle for geometry-controlled, radiation-driven jetting phenomena, as complementary to material-controlled, radiation-driven jetting. The key to effective performance of HEDSC configurations is to provide a dynamic loading on the SC conical liner that is great enough to form a long, narrow, high-velocity jet. But for optimized penetration, the load must be small enough to keep the jet at near-normal density (i.e., the material may be partially melted but must not show any vaporization). Analysis with approximate but accepted scaling relations showed that a direct radiation load, such as that provided by a Z hohlraum, would drive the liner well beyond this limit. Thus the experimental design required energy management using both radiation and loading moderators tailored to the radiation source and the SC liner.

Using extensive one- and two-dimensional hydrocode (LASNEX and AUTODYN, respectively) calculations, we determined the dimensions of the moderators to provide the desired loading on the SC liner. We sized other elements of the test-fixture design using standard SC scaling laws. In the final target configuration, the radiation moderator is stainless steel, the loading moderator is polystyrene, and the SC conical liner is tantalum. To provide a sense of the spatial scale, the base of the SC liner has an inner diameter of 4 mm, the stand-off between the liner and the target block is 12 mm, and the length of the target block is 28 mm.

Because the experiments will be ride-on tests with the RadJet project, no active diagnostics are planned for the first several shots. For post-test examination, sectioning, and analysis, we will recover the target block with a specially designed target catcher assembly.

Other Communications

Lawrence, R. J., A. V. Farnsworth, Jr., M. C. Grubelich, P. Yarrington, and T. A. Mehlhorn. 2004. High-energy-density shaped charge (HEDSC): Proof-of-principle test on Z. Sandia Technical Report SAND2004-1541P, Sandia National Laboratories, Albuquerque, New Mexico.

76305

Systems Assessment of Water-Savings Impact of Controlled-Environment Agriculture Utilizing Wirelessly Networked SDACs

R. C. Pate, V. P. Gupta, E. E. Baynes, Jr., J. Z. Davis, N. M. Berry, P. I. Pohl

This project intersects two areas of strategic interest for Sandia. The first is ensuring water (and water-related impacts of agriculture) safety, security, and sustainability as matters of national security and global stability. The second is contributing to the accelerated development and application of smart networked Sense, Decide, Act, and Communicate (SDAC) systems to enable transformational capabilities in sensing, situational awareness, and response for national security and other dual uses. We address both interest areas by applying wirelessly networked sensor systems to facilitate assessment and future improvement of systems performance and water-use efficiency provided through controlled-environment agriculture (CEA) in arid regions. We initiated experimental investigations and systems analyses to understand and quantify operational and technical system performance, forage quality, optimization potential, and overall viability. We facilitated and enhanced experimental studies by using wirelessly networked sensor systems capable of providing a more extensible, adaptable, and higher-density spatial distribution of multimodal sensing capability than otherwise possible.

The challenge and opportunity are whether CEA can contribute more broadly and systematically to water and agricultural security and sustainability through improved systems understanding and design, adoption of improved technologies and methodologies, performance optimization, and advent of better decision-support tools. The project began to address this challenge by first quantitatively investigating the operational performance of CEA for forage production. Emphasis on forage made sense for several reasons. Irrigated forage crops are the major consumer of water in New Mexico and elsewhere in the southwestern U.S. region. Expanding livestock forage production worldwide is putting increasing strain on agricultural land and water resources. CEA offers potential orders-of-magnitude savings in required water and land usage. Forage also provides an experimental advantage because the crop production cycle is rapid (typically 10 days), thereby allowing multiple crop cycles in much shorter time than possible with other crops. Project results and experience also generally extend to other higher-value CEA applications.

We established a photovoltaically powered, hydroponic forage production greenhouse facility and populated it with both single-point and wirelessly networked multipoint sensor systems for monitoring environmental conditions. We established transportainer storage for operational supplies, and procured and received quantities of six different varieties of seed (corn, wheat, barley, oats, triticale, and sorghum) for use in the forage production operation studies. The facility began monitored forage production operations with daily on-site operational support provided by the University of Texas at El Paso (UTEP). We began forage sample collection and nutritional analysis, with technical support provided through New Mexico State University (NMSU). Forage production and sampling operations were hampered during the first month by emergence of mold growth due to a combination of the local environment, operational processes, and water-supply quality problems. We augmented the water supply and associated greenhouse water control system to allow for needed treatment for pH balance and pathogen kill. Sandia initiated and conducted wireless sensor system debugging, data collection, remote linkage, processing, and visualization efforts with partial success. Software problems continued to hamper completely successful wireless sensor system operation through recent work, but are expected to be resolved in the future. We took a considerable amount of data, along with initiation of data visualization and analysis of greenhouse system behavior. Overall assessment of greenhouse forage system operations, including nutrition content analyses, resource use, and time-varying environmental conditions, is under way.

We established a photovoltaically powered, hydroponic forage production greenhouse facility and populated it with both single-point and wirelessly networked multipoint sensor systems for monitoring environmental conditions.

Other Communications

Dye, L. 2004. Beating drought: Could wired greenhouses grow tomorrow's crops? Commentary by Lee Dye (*Dyehard Science* column) in ABCNEWS.com discussion of water as a national security and global stability issue, 15 September, ABC News, New York, New York.

Singer, N. 2004. Labs-led team tests hydroponic greenhouse method for crops to reduce possibility of future water wars: How to save millions of gallons of water a year. *Sandia Lab News* **54** (18) (3 September, Albuquerque, New Mexico).

Vorenberg, S. 2004. Greenhouse farming seen as water solution. Article in *Albuquerque Tribune*, 27 September, Albuquerque, New Mexico.

Editorial. 2004. Sandia's research may stretch "liquid gold." Editorial in *Albuquerque Tribune*, 27 September, Albuquerque, New Mexico.

78307

Climate Change Effects on International Stability

M. B. E. Boslough, J. M. Fujii, L. A. McNamara, J. A. Sprigg, M. A. Taylor, K. M. Murphy

Sandia took preliminary steps toward developing a coupled climatological/agent forecast model of climate-induced conflict. We incorporated historical climatology (severe weather events and other natural disaster data) into established macrostructural analyses. We performed a review of relevant literature on conflict arising from environmental scarcity.

Rather than simply reviewing the work that was already presented, critiqued, and expanded in our references, we actively collected data from the referenced sources, reproduced some of the work, and explored alternative models.

We also used the unfolding crisis in Darfur, in western Sudan, as our case study of conflict related to or triggered by climate change. We gathered information and developed a preliminary concept map, which can eventually lead to a system-dynamics model and possibly to an agent-based model.

Finally, we outlined a plan for implementing agents in a climate model. We defined a logical progression to the ultimate goal of running both types of models simultaneously in a two-way feedback mode, where the behavior of agents influences the climate and climate change affects the agents.

We performed a proof-of-principle project that applied the fuzzy analysis of statistical evidence (FASE) methods, developed by the Center for Army Analysis (CAA), to add weather and climate to the list of country macrostructural indicators that are used to analyze and predict instability. This pattern classification algorithm had already provided conditional probabilities of conflict based on historical data for such independent variables as youth bulge, infant mortality rate, and trade openness.

The independent variables were described in the literature by Sean O'Brien (CAA) as "oily rags" that require a spark to set the country ablaze. We aimed our preliminary analysis at determining whether natural disasters might contribute to the oiliness of the rags, provide the spark, or some combination of the two. As a preliminary analysis, we created and incorporated a natural disasters variable into the FASE analysis, resulting in a plot of the conditional probability.

Our analysis did not show a significant correlation. Taken at face value, it suggests that below-median disasters have no

discernible effect on the likelihood of conflict. Above a threshold, there is a sharp transition to a slightly higher probability of conflict. It is notable that the largest disasters in the database are associated with the highest likelihood of conflict, but data are too sparse for any definitive statement.

However, this first incorporation of disasters into the FASE analysis is suspect because it deviates from the premise of O'Brien's model. He uses macrostructural variables to forecast instability irrespective of any initiating event leading to actual conflict, whereas our initial assessment implicitly assumed that disasters were the initiating event. (Our preliminary analysis sought correlations between disasters and conflict in the same year.) Thus, our next step was to seek interactive effects of disasters in conjunction with other factors and to take a first look at the integrated effect of disasters over a period of time.

We also revisited O'Brien's model of instability using statistical regression methods for analyzing the data, which have been the most common empirical methods for this line of research. Our goal was to explore second-order effects of the independent variables on instability to more accurately and usefully model causal relationships.

These exercises demonstrated that relatively simple statistical models can generate predictions within-sample and give insight into the underlying causal structure of instability with respect to measurable macrostructural variables.

We also conducted a split-sample validation of our regression models, as O'Brien did with the FASE. We did this as an obvious follow-on exercise to properly compare the applicability of FASE with respect to more-traditional methods. However, our focus at this stage is not on forecasting so much as on understanding the underlying causal relationships in the data.

We are skeptical of purely correlative methods for modeling conflict factors, but recommend that the predicted value by countries and time frame be examined to better understand the estimated relationships between the factors and the occurrence of conflict in the context of case studies.

Finally, our preliminary development of a causal loop diagram for the Darfur region of Sudan is a case study that is amenable to dynamic simulation, which is an entirely different way of arriving at such an understanding. We believe that the best path toward understanding the relationship between climate change and conflict is through a combination of historical analysis, case studies, and coupled physical-nonphysical modeling.

These exercises demonstrated that relatively simple statistical models can generate predictions within-sample and give insight into the underlying causal structure of instability with respect to measurable macrostructural variables...[Also,] our preliminary development of a causal loop diagram for the Darfur region of Sudan is a case study that is amenable to dynamic simulation, which is an entirely different way of arriving at such an understanding.

Advanced Manufacturing

The Advanced Manufacturing investment area supports Sandia's mission by advancing the capability to fully understand and model manufacturing processes, and to develop novel production technologies. The focus is on manufacturability and rapid prototyping, both critical to present and future missions of Sandia.

Rapid-prototyping investments address Sandia's need to move quickly from concept to prototype to production. Research is directed at the need to reduce cycle time in weapons design, fabrication, and qualification to enhance homeland security and all Sandia Strategic Business Units.

Manufacturability investments strive to develop and enhance manufacturing processes as an integrated part of the design process, ensuring that products can be fabricated to meet functional requirements the first time, every time.

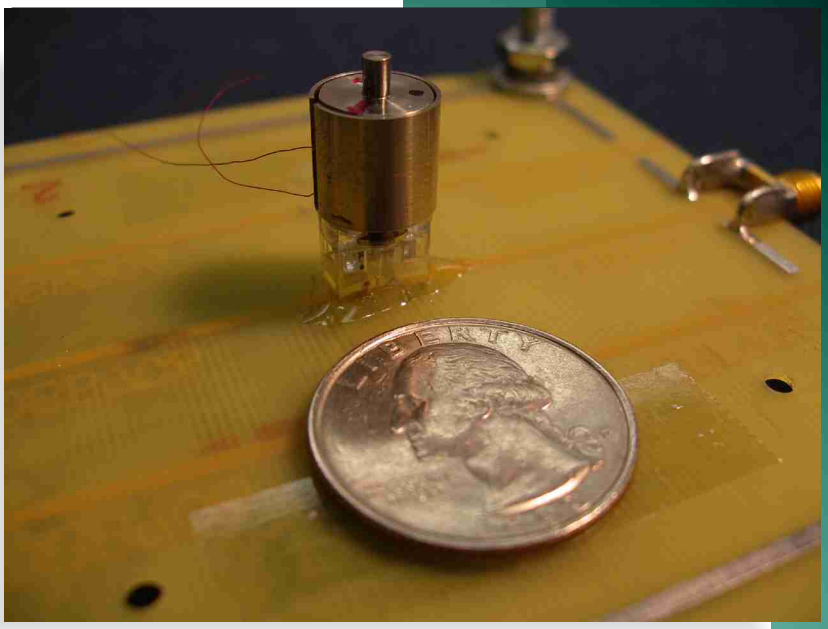

53588
"Miniature High-Power RF Components Enabled by Mesoscale Manufacturing"

Future military and consumer products require increasingly compact, high-power transmitters for functions including communications and telemetry, remote sensing, and radio-frequency (RF) identification tags. The state of the art of fabrication technology is sufficient for low-power applications. However, as power demands increase, the scale of device features must be extended. Using advanced microstereolithography (μSL) and microwire electrodischarge machining (μEDM), researchers produced a novel mesoscale RF relay for high-power applications anticipated to provide up to 10 times the power of current microscale relays. High dimensional accuracy was achieved in fabrication through the unprecedented use of Teflon™ shims. Additionally, methods and infrastructure for reliable batch assembly of mesoscale electromechanical actuators and structural parts were established. Future work will aim to improve repeatability and accuracy of the relay mechanism and to advance electrical properties through contacts with high-conductivity materials.

38605

Microfabrication with Femtosecond Laser Processing

P. Yang, J. A. Palmer, J. Guo, D. R. Tallant, M. L. Griffith, M. F. Harris, T. S. Luk, G. R. Burns

Sandia seeks to study and utilize the special characteristics of femtosecond (fs) laser processing for microfabrication. Since the ultrashort pulse significantly reduces the thermal diffusion length, material can be removed precisely with little damage to the surrounding feature volume. We will explore the basic mechanisms that control fs laser ablation, gain a science-based understanding of the process, and determine the process parameter space for laser processing of metals and glasses. We will study the effect of laser and environmental parameters on such aspects as removal rate, feature size, feature definition, aspect ratio, and material structure. We will address manufacturing requirements for component fabrication, including precision and reproducibility. Success will permit us to miniaturize multiple components, such as steel stronglinks, as well as to produce micron-size features for neutron-tube (NT) particle screens.

Another unique aspect of fs radiation is the ability to create localized structural changes. By scanning the focal point within transparent material, we will create three-dimensional (3-D) waveguides for biological sensors and optical components. We will determine and exploit the mechanisms that induce modification of the material's structure for enhanced optical performance.

This project consists of (1) mesoscale micromachining of ferrous alloys and (2) direct-write (DW) optical waveguides in the bulk glass. We made the following accomplishments:

(1) *Mesoscale micromachining of ferrous alloys*. An experimental project investigated fs laser-cut features in ferrous substrates oriented at oblique angles relative to the laser beam. We defined and measured quantifiable standards for the accuracy and precision of these features. Results show improved accuracy in terms of wall linearity and overall straightness using the statistically optimized laser parameters. This shows that the fs laser may be an effective tool for the accurate percussion drilling of undercut structures in ferrous substrates. However, other evidence suggests that the same feature would lack precision or repeatability. Based on these results, future research in this area may explore accurate, precise, deep-drilled features (with multiple passes of the beam) through programmed changes in substrate angle. Finally, the use of vacuum and secondary process gas flow does not appear

to improve precision in ferrous substrates; these findings do not address the accuracy of features generated in a vacuum environment. Furthermore, there is evidence to show that vacuum and the diminished focal-point plasma that accompanies it contribute to recast formation and incomplete material removal at low substrate velocity. We applied the results of the accuracy/precision study in bulk-micromachining mesoscale parts in 150 μm kovar substrates. We created a meso "windmill" in kovar with the optimized parameters and compared it to previous stainless-steel (SS) prototypes processed at greater fluence.

In addition, we investigated the effects of polarization on feature quality. In the nominal configuration, titanium (Ti):sapphire fs laser emissions are linearly polarized. According to Nolte, *et al.*, this condition is marked by polarization-dependent reflections from the walls of percussion-drilled holes in ferrous substrates. This leads to uneven distribution of energy intensity at the focal point and ultimately noncircular geometry at the exit. We can correct the polarization error by installing optics that continuously rotate the polarization, a technique known as *polarization trepanning*. We implemented this technique in the Sandia apparatus by installing a half-wave plate polarizer driven by a direct-current (dc) motor at approximately 500 rpm. At publication time, the last mesoscale parts micromachined with polarization trepanning were in the process of scanning-electron microscopy (SEM) characterization.

We also explored preliminary experiments on the patterning of energetic material (EM) film.

(2) *DW optical waveguides in bulk glass*. We investigated laser DW embedded waveguides and their optical properties in amorphous silica fabricated by fs laser pulses (800 nm, < 125 fs, at 1 kHz). Experimental results show that there is a narrow operating window to produce low-loss waveguides in bulk glass. Raman spectroscopy of the laser-modified glass regions shows a reduction of large network silica rings in the glass, which might contribute to the local densification and refractive index change. We will demonstrate several integrated optical devices, such as a Y coupler, directional coupler, and Mach-Zehnder interferometer, made by this technique. An angular dependence of light transmission measured between two cross-polarizers on these laser-modified regions suggests that these regions possess an optical birefringent property. In addition, the optical axes of laser-induced birefringence can be controlled by the polarization direction of the fs laser. We studied mechanisms that might contribute to the observed laser-induced

birefringence behavior. Evidence suggests that an electrostriction generated from the immense optical field associated with laser pulse could contribute to the laser-induced birefringence. We also explored subsurface machining of embedded microchannels in FORTURAN glass.

Refereed

Yang, P., D. R. Tallant, G. R. Burns, and J. Guo. 2004. Femtosecond laser-induced structural modification and birefringence in bulk glass for optical waveguide applications. *Ceramic Transactions*, accepted.

Yang, P., G. R. Burns, D. R. Tallant, J. Guo, and T. S. Luk. 2004. Direct-write waveguides and structural modification by femtosecond laser pulses. *Photonics West, Proc. International Society of Optical Engineering* **5342** (27–29 January, San Jose, California): 146–55.

Yang, P., G. R. Burns, J. Guo, T. S. Luk, and G. A. Vawter. 2004. Femtosecond laser-pulse–induced birefringence in optically isotropic glass. *J. Applied Physics* 95 (10): 5280–83.

Yang, P., J. Guo, G. R. Burns, and T. S. Luk. 2004. Direct-write embedded waveguides and integrated optics in bulk glass by femtosecond laser pulses. *J. Optical Engineering*, accepted.

Other Communications

Palmer, J. A., and M. L. Griffith. 2004. Femtosecond laser microfabrication. Paper presented at DMC 2003, 1–4 December, Washington, D.C.

Palmer, J. A., K. L. McDaniel, M. F. Harris, and R. Lumia. 2004. The effects of varying substrate angle on feature quality in femtosecond laser ablation of ferrous alloys. *SPIE—High-Power Laser Ablation 2004*, accepted.

Palmer, J. A., K. L. McDaniel, M. F. Harris, R. Lumia, and M. L. Griffith. 2004. The effects of varying substrate angle on feature quality in femtosecond laser ablation on ferrous alloys. Paper presented at SPIE—High-Power Laser Ablation 2004, 25–30 April, Taos, New Mexico.

Yang, P., G. R. Burns, T. S. Luk, J. Guo, and G. A. Vawter. 2003. Femtosecond laser-pulse–induced birefringence in glass. Paper presented at the American Ceramic Society—Glass and Optical Materials Division Meeting, 12–15 October, Corning, New York.

38606

Mesoscale Controlled Motion for a Microfluidic Drop Ejector

P. C. Galambos, J. L. Reif, D. L. Luck, D. A. Czaplewski, M. J. Braithwaite, G. E. Prevost, C. J. Atwood, M. Okandan, R. C. Givler, R. J. Shul, S. S. Mani, B. H. Jokiel, Jr.

Sandia is testing a baseline "sideshooter" ejector with parametric variations. We fabricated a SUMMiT V™ (Sandia Ultraplanar Multilevel MEMS [microelectromechanical systems] Technology V) module of ejector designs (RS349). These designs utilize banks of high-performance comb-drive actuators that rapidly push a plunger into a chamber. Liquid is thereby ejected from a hole in the top of the chamber. We modified previously tested high-performance comb drives for a longer stroke (10 mm) and bidirectional actuation (for refill)—both new features. We designed this mechanical-only system to eject drops as small as 0.5 femtoliters. Since no field or heat is applied to the liquid, virtually any liquid that does not corrode silicon (Si) can be ejected. Design parameter variations include nozzle hole size (2, 5, 10, and 20 µm diameter), piston width (7, 25, and 50 µm), and variations of sealing and filling geometries. We are developing packaging for these ejectors that is compatible with chloroform and toluene, solvents used in the gas-phase chem-lab-on-a-chip project to coat sensors. This packaging utilizes a solvent-resistant, Teflon™-filled bismaleimide (BMI) adhesive. In addition, we chose precise, rapidly positionable stages to be used to pattern the ejected drops onto the target position where the ejected drops hit.

In conjunction with this design, we used GOMA (Sandia's multiphase finite-element method [FEM] fluid mechanics code) to verify drop ejection and to size the actuators used to power the plunger. The GOMA analysis indicates that hundreds of milli-Newtons are required to eject drops. We sized the high-performance comb-drive actuators to deliver this level of force.

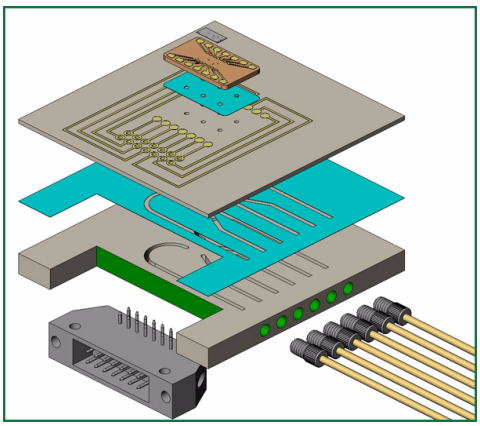

Exploded view of an ejector package.

We made significant progress in (1) drop ejection—the sideshooter effectively ejected 0.25 pl drops at 10 m/s, (2) fabrication of packaging—a compact ejector package based on a modified electromicrofluidic dual in-line package (EMDIP), and (3) development of a vision/stage system that allows precise ejector package positioning above a target.

In the vision/stage system, two orthogonal, 1 µm-precision, Aerotech stages moved the target beneath the ejector package while a third stage controlled the vertical position of the ejector relative to the target. A vision-recognition system utilized an

optical tube (100x magnification) and a charge-coupled-device (CCD) camera attached to the z-stage. This system imaged a 1 mm square area and used Sandia-developed software to recognize features in the field of view. The software commanded the stage to move precise distances relative to the feature and sent a timing signal to the ejector power supply to actuate the ejector piston and deposit a drop at the desired location.

We made the ejector package from polyethylethylene ketone (PEEK). We made the first (larger) level—flow manifold—from layers of PEEK that we laminated together using Pyrolux adhesive under moderate curing pressure and temperature (300 psi, 375°F, 1.5 hr) to form an electrofluidic package with electrical traces on the top layer and embedded fluid channels. Fluidic capillary connectors along one edge and a side-mounted electrical connector along another edge allowed connection to fluid reservoirs and the power supply, respectively. We mounted the EMDIP fan-out to the manifold, and the silicon (Si) ejector module to that, using either Pyrolux or adhesive tape. Electrical traces on top of the fan-out allow wire-bonded connection to the ejector from the fan-out. The electrical and fluid connections go from the manifold to the fan-out and from there to the ejector Si die. The fan-out consists of a flow-through channel and input/output (I/O) ports, which allows us to fill the entire fluidic package before we fill the ejector die, thereby eliminating trapped air bubbles that can interfere with system operation.

Finally, in the drop-ejection stage, we ejected 0.25 pl drops from a 10 µm nozzle using a high-force comb-drive actuator to drive a piston into the water-filled nozzle chamber and force out a drop. We applied an 80 V signal for a 12 µs pulsewidth to eject drops. We assembled the video from stroboscopic images separated by 1 µs during application of the ejection signal. The piston must travel the full stroke (about 5 µm) in 5 µs to eject a drop (approximately 1 m/s piston velocity). Drop breakoff occurred when the piston actuator hit the stop and recoiled. Approximately 35 V were required for full 4.5 µm piston travel. At 10 µs pulsewidth, the actuator did not quite attain full travel (> 3 µm instead of 4.5 µm). Piston ringing occurred when the actuation voltage was shut off.

Thus, we achieved drop ejection and developed ejector packaging, stage, optics, and image recognition. Upcoming work will involve integration of the ejector, package, and stage to produce a complete patterning system.

52523

Atomic Layer Deposition of Highly Conformal Tribological Coatings

T. M. Mayer, N. R. Moody, R. S. Goeke, T. W. Scharf, M. T. Dugger, S. V. Prasad

Tribological (friction, wear, and lubrication) issues are paramount in the performance and reliability of moving mechanical assemblies such as microelectromechanical systems (MEMS) devices. The severe geometric constraints of many micromechanical systems (high-aspect ratios, shadowed surfaces) make most deposition methods for friction and wear-resistance coatings impossible. Sandia will outline the deposition and evaluation of highly conformal, tribological coatings, deposited by atomic layer deposition (ALD), for use on surface-micromachined (SMM) and LIGA (for the German term Lithographie, Galvanoformung, und Abformung, *for lithography, electroforming, and molding) structures. ALD is a chemical vapor deposition (CVD) technique that is based on sequential introduction of gaseous precursors and selective surface chemistry to achieve controlled growth of a film one monolayer per exposure cycle.*

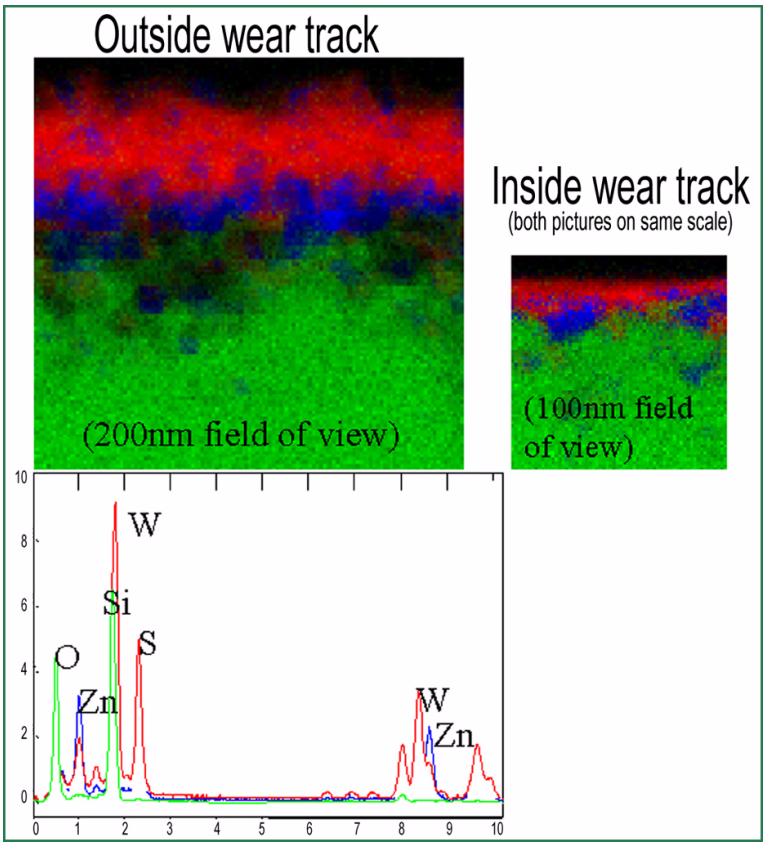

Cross-sectional TEM/x-ray spectral image maps of WS_2 film inside and outside the wear track with corresponding elemental x-ray peaks of constituents present.

Current physical vapor deposition (PVD) techniques such as sputtering and evaporation, by virtue of their line-of-sight (LOS) nature, are not capable of conformally coating high-aspect-ratio structures and shadowed surfaces. In addition, traditional CVD techniques cannot provide control of film thickness at the atomic level and are not applicable for MEMS structures due to high processing temperatures that can lead to structural problems with silicon (Si) surfaces. Thus, the development of tribological thin films by ALD will provide a method for applying solid lubricant films on MEMS structures. ALD of a wide variety of materials is possible, but there have been no studies of structural, mechanical, and tribological properties of these films. We developed processes for depositing thin (< 100 nm) conformal coatings of selected hard and lubricious films (aluminum oxide [Al_2O_3], zinc oxide [ZnO], tungsten disulfide [WS_2], and tungsten/tungsten nitride [W/WN] nanolaminates) and measured their properties. We employed new scanning-probe and nanoindentation techniques, along with detailed mechanics-based models, to evaluate these properties at smaller load regimes characteristic of microsystem operation. We emphasized deposition processes and fundamental properties of ALD material and evaluated film performance for model SMM and LIGA devices. Success will greatly expand the range of applications and long-term performance and reliability of micromechanical systems.

We developed an ALD process for the synthesis of crystalline WS_2 solid lubricant thin films grown by using tungsten hexafluoride (WF_6) and hydrogen sulfide (H_2S) gas precursors. We established a new catalytic route to promote nucleation and growth of WS_2 films on Si with native oxide, thermally grown silicon dioxide (SiO_2), and stainless-steel surfaces, which are substrates used in SMM and LIGA applications.

We made major breakthroughs in all aspects of our project. Work involved three tasks: (1) ALD film growth/kinetics, (2) tribological (friction and wear) properties of ALD solid lubricant films, and (3) mechanical properties of ALD films at the nanoscale. We developed an ALD process for the synthesis of crystalline WS_2 solid lubricant thin films grown by using tungsten hexafluoride (WF_6) and hydrogen sulfide (H_2S) gas precursors. We established a new catalytic route to promote nucleation and growth of WS_2 films on Si with native oxide, thermally grown silicon dioxide (SiO_2), and stainless-steel surfaces, which are substrates used in SMM and LIGA applications.

Initial *in situ* quartz crystal microbalance (QCM) measurements showed that WS_2 did not grow on the aforementioned substrates. However, WS_2 films nucleated readily on previously deposited zinc sulfide (ZnS) and Zn surfaces. Thus, for the nucleation and growth of WS_2 on any substrate, we first grew an ~ 3 nm layer of ZnS or Zn by sequential reaction of diethylzinc (DEZ) and H_2S, or just DEZ, respectively. During the sequential growth of ALD ZnS and

WS_2 on the 10 nm-thick SiO_2–coated QCM crystal, it was apparent that WS_2 did not initially grow on SiO_2, but growth commenced immediately on ZnS. The growth rate of WS_2 is not constant, but slows with time. However, even one cycle of ZnS growth is adequate to restore high WS_2 growth rate when its growth rate begins to slow down. This behavior indicates a catalytic effect of ZnS and Zn on WS_2 growth. While we do not fully understand the nature of this growth mechanism, we speculate that Zn present at the surface during WS_2 growth promotes adsorption of WF_6, perhaps by serving as a partial reducing agent for WF_6. The zinc fluoride (ZnF) that forms is then reduced back to Zn (or converted to ZnS) by exposure to H_2S. This catalytic action of Zn in WS_2 appears to be critical for the ALD process and may facilitate the growth of many other metal-containing films, where nucleation is impeded by low reactivity of the metal precursor.

Raman spectra and x-ray diffraction (XRD) measurements determined that the WS_2 films were crystalline, with the hexagonal (002) preferred-orientation texture typical of solid lubricant transition-metal dichalcogenides: MX2 (M=W, Mo; X=S, Se), which exhibit the easy shear basal planes necessary for low friction and wear. Thus, we determined that the films exhibit extremely low coefficient of friction (COF ~ 0.02) and low wear under high load conditions. We produced x-ray spectral imaging maps of ~ 30 nm-thick WS_2 film inside and outside the wear track at a high-normal loading condition.

We also produced W/Al_2O_3 nanolaminate films for enhanced mechanical properties. In measurements of mechanical properties of ALD films, we concentrated on modeling the nanoindenter response of nanometer-thick Al_2O_3 films on compliant substrates, adhesion and delamination of W films, and properties of W/Al_2O_3 laminates. Based on results showing high hardness for ALD W and good adhesion and fracture resistance for ALD Al_2O_3, we created 32- and 64-bilayer nanolaminates from sequential deposition of W and Al_2O_3 films to a thickness of 200 nm on Si substrates. We used Al_2O_3 as both an adhesion layer and a capping layer in both systems. Cracking and delamination were less severe in the 32-bilayer system than in the 64-bilayer system. It was also less severe than in single-layer W, but more severe than in single-layer Al_2O_3. These tests show that nanolaminates improve frictional response and film durability.

Refereed

Jungk, J. M., T. E. Buchheit, J. A. Knapp, T. M. Mayer, N. R. Moody, J. W. Hoehn, and W. W. Gerberich. 2004. Using a combined modeling-experiment approach for property determination of ultrathin ALD films. Paper presented at the 5th Global Innovations Symposium—Trends in LIGA, Miniaturization, and Nanoscale Materials, Devices and Technologies, TMS Annual Meeting, 14–17 March, Charlotte, North Carolina.

Jungk, J. M., W. W. Gerberich, T. E. Buchheit, T. M. Mayer, N. R. Moody, J. A. Knapp, J. W. Hoehn, and S. M. George. 2003. Mechanical behavior of amorphous ALD films. Paper presented at the Materials Research Society Fall Meeting, December, Boston, Massachusetts.

Mayer, T. M., T. W. Scharf, S. V. Prasad, R. S. Goeke, and M. T. Dugger. 2004. Atomic layer deposition of tungsten disulfide solid lubricant coatings. Paper presented at the AVS New Mexico Chapter Symposium, 17–18 May, Albuquerque, New Mexico.

Moody, N. R., J. M. Jungk, R. A. Wind, T. E. Buchheit, T. M. Mayer, S. M. George, and W. W. Gerberich. 2004. Mechanical performance of ALD films and nanolaminates. Paper presented at the Symposium on Mechanical Properties and Adhesion, International Conference on Metallurgical Coatings and Thin Films, April, San Diego, California.

Moody, N. R., J. M. Jungk, T. E. Buchheit, T. M. Mayer, and R. A. Wind. 2004. Tailoring ALD laminate films for dynamic toughness. Paper presented at the Materials Research Society Spring Meeting, April, San Francisco, California.

Moody, N. R., J. M. Jungk, T. E. Buchheit, T. M. Mayer, R. A. Wind, S. M. George, and W. W. Gerberich. 2004. Fracture of atomic layer–deposited tungsten films. Paper presented at the Symposium on Nanoscale Materials and Modeling—Relations Among Processing, Microstructure, and Mechanical Properties, Materials Research Society Spring Meeting, April, San Francisco, California.

Moody, N. R., T. E. Buchheit, B. L. Boyce, T. M. Mayer, and S. M. George. 2004. Mechanical performance of ALD films for microdevice coatings. Paper presented at the 5th Global Innovations Symposium—Trends in LIGA, Miniaturization, and Nanoscale Materials, Devices and Technologies TMS Annual Meeting, March, Charlotte, North Carolina.

Moody, N. R., T. E. Buchheit, B. L. Boyce, T. M. Mayer, and S. M. George. 2003. Mechanical performance of ALD films for microsystem applications. (Invited) Paper presented at the ASME Winter Annual Meeting, Symposium on Materials Issues in Small Structures, 16–21 November, Washington, D.C.

Scharf, T. W., S. V. Prasad, T. M. Mayer, R. S. Goeke, and M. T. Dugger. 2004. Atomic layer deposition of tungsten disulfide solid lubricant thin films. *J. Materials Research*, accepted.

Scharf, T. W., T. M. Mayer, S. V. Prasad, R. S. Goeke, and M. T. Dugger. 2004. Atomic layer deposition of tungsten disulfide solid lubricant coatings. Paper presented at the Society of Tribologists and Lubrication Engineers, May, Toronto, Canada.

52524

Assembly of Microsystems Using Exothermic Multilayer Thin Films

D. P. Adams, D. E. Wackerbarth, M. A. Rodriguez, C. P. Tigges, M. C. Grubelich, F. M. Hosking, K. A. Peterson, T. E. Buchheit

In this project, Sandia seeks new micro- and mesosystem assembly techniques involving energetic thin films. Energetic films consist of two or more reactive materials typically deposited as a heterostructure. If properly designed, layered materials can be stimulated in a local region to cause a self-propagating reaction (alloying) over great distances. Reactions can be ignited via a thermal impulse from some lasers, exploding bridgewires, or other mechanical methods.

Several research groups, including T. Weihs (Reactive Nanotechnologies, Johns Hopkins University), T. Barbee (Lawrence Livermore National Laboratories), and John Moore (Professor, Colorado School of Mines), are studying energetic multilayer films. Elegant work by Weihs, et al.*, demonstrates the relationship between multilayer design and propagation velocity for a few systems (nickel/aluminum [Ni/Al], niobium/silicon [Nb/Si]). Moore and his collaborators have researched combustion synthesis for many years; only recently has this group begun to investigate energetic thin films.*

For our project, microsystem assembly primarily involves joining. We intend to use the heat liberated by a self-propagating reaction to bond dissimilar parent materials. Joining via exothermic thin films holds promise for minimizing the heat load on temperature-sensitive parts of a microsystem because the reaction can be rapid (> 1 m/s). This project considers other microactuation/assembly techniques involving energetic films besides joining. For example, a large stress change resulting from a rapid exothermic reaction can be used to deflect a micromechanical switch.

Our current research on exothermic thin films intends to

(1) increase the number of known energetic material (EM) pairs that exhibit a self-propagating reaction,

(2) research techniques that pattern/machine energetic films without stimulating reactions,

(3) research ignition threshold phenomena (testing involves ultrashort-pulse lasers),

(4) characterize and improve the resultant mechanical properties of reacted films,

(5) measure stress of reacted films and determine the origin of stress,

(6) research how stoichiometric variations (away from targeted compositions) affect propagation and properties, and
(7) demonstrate joining over a number of length scales.

We studied many exothermic systems, including Ni/Ti (titanium), Co (cobalt)/Al, and Al/Pt (platinum), and selected these materials because they exhibit a self-propagating reaction. Each pair has a moderate or high heat of formation.

Tests are under way to evaluate the microstructure, purity, and mechanical properties of the three alloys (Al/Pt, Co/Al, Ni/Ti) formed as a result of a high-temperature reaction. Ni/Ti is an alloy that, in bulk form, exhibits ductility and should therefore be able to accommodate the extrinsic stress resulting from cooldown to room temperature. However, it is plagued by formation of a second monoclinic B19' structure. Al/Pt is highly energetic and forms crystallographic phases that have not been reported previously. Co/Al is the most promising alloy tested thus far, since it forms a ductile B_2 crystal structure.

We probed the dynamics of self-propagating reactions by monitoring the velocity of reactions using high-speed photography. We compared these data to analytic models that account for the experimentally determined premix thickness and other parameters such as multilayer design. We are using high-speed pyrometry to monitor the cooldown rate of films to develop a better understanding of the phases formed, including nonequilibrium Al/Pt structures.

Mechanical testing involved reacted foils and joined assemblies, including hardness and modulus testing of foils. We conducted torsional and tensile tests in concert with an examination of hermeticity on joined assemblies.

We are investigating methods that machine energetic foils into complex shapes without stimulating self-propagating reactions. For example, ultrashort-pulse laser machining appears promising for cutting EMs. We also are using this technique to determine the ignition threshold for films as a function of multilayer design.

Other Communications

Adams, D. P., and K. Archuleta. 2004. Low-stress thin-film coatings. Paper presented at the TMS Annual Symposium, March, Charlotte, North Carolina.

Adams, D. P., M. A. Rodriguez, C. P. Tigges, and D. E. Wackerbarth. 2003. Properties of reacted metal multilayers. Paper presented at the AVS 50th International Symposium, November, Baltimore, Maryland.

52526

Intelligent Interaction Control as Applied to Metrology and Assembly of Microscale Components

D. M. Kozlowski, N. A. Weir, D. G. Wilson, W. J. Prentice, T. Lemp, A. L. Ames, J. M. Bailar, P. R. Wolfenbarger, J. F. Jones, R. C. Lennox

Dimensionally inspecting microscale parts is extremely difficult. Current technology uses microscopes to optically magnify the part, and image processing to extract the dimensional relation between features. Optical measurement techniques have limitations in microscale applications for two reasons. First, they are effectively a two-dimensional (2-D) process, meaning that only the surface of the part is measured, and we obtain very limited information concerning the sidewalls of high-aspect-ratio parts. Second, optical measurements are physically limited to about 1 µm resolution and practically limited to about 2 µm resolution. It would be highly desirable to have a cost-effective way to dimensionally inspect the production quantities of microscale parts to submicron resolution.

Hard gauging is a common macroscale process because it is a cost-effective means to validate functional dimensions at production rates. A hard gauge typically consists of a precision fixture that holds the part and a variety of go/no-go "feelers" used to verify maximum and minimum material conditions. Using hard gauges, it is straightforward for a human technician to obtain 10–20 µm (e.g., less than one thousandth of an inch) validation of part dimensions. The limiting factor is the human's ability to detect the variation in force required to insert the "feelers," hence the origin of the term "feeler gauge."

It may be possible to use microscale hard gauges to economically inspect microparts to submicron resolution if a sense of feel more acute than that of a human's could be developed. Sandia is investigating the possibility of using advanced robotics to provide the ultra-acute sense of feel and manipulation required to perform microgauging. This investigation will consist of simulating microscale forces and dynamics for comparison with the data obtained through microscale gauging experiments.

Accomplishments to date focused on developing and validating simulations along with designing, integrating, and making operational an experimental test-bed. An initial study done by Purdue University found that contact dynamics and magnetism would be the dominant forces observed in the

gauging of microscale LIGA (for the German term *Lithographie, Galvanoformung, und Abformung*, for lithography, electroforming, and molding) parts. This led to identifying two main components of a microgauging simulation: the dynamic and control model of a precision robot system, and the contact dynamics of the feeler gauge insertion. The robot system must be modeled so that we may design a system that has sufficiently high fidelity for microgauging. Using the model, we predicted the required mechanical performance parameters of a robotic system. We then used these data in developing the experimental test-bed. We developed the second simulation component—contact dynamics—and validated it against published macroscale data.

The second portion of the research is to develop an experimental test-bed to demonstrate microgauging and validate the model. Based on the results of the robot model, we fabricated a robot that we believe will have sufficient fidelity for our purposes. One issue is that multiaxis force sensing of the resolution required does not currently exist. We are pursuing multiple alternatives to develop the needed force-sensing capability.

Initially, we are integrating a commercially available torque sensor with a long lever arm and restricting our work to moment sensing. We also are in the process of developing a custom multiaxis load cell fabricated from piezoresistive sensors. Another force-sensing solution that we are pursuing is to use the stick/slip piezoelectric robot actuators along with precision displacement measurements (e.g., 10 nm resolution) to determine the applied force by measuring the amount of slip in the actuator. Finally, we are exploring a collaboration to use microelectromechanical systems (MEMS) technology to develop a multiaxis force sensor on a chip.

We set up the microgauging robotic test-bed in the laboratory and completed robot motion testing. We fabricated and integrated all of the custom fixturing and tooling to support testing. We developed an adaptive control system that has a much higher performance than commercially available controllers. This control system will be able to demonstrate the feasibility (or infeasibility) of robotic microgauging.

In the very near future, we will perform initial validation experiments, the results of which we will use to reconcile differences between the test-bed and the model. Once we understand the performance characteristics of the experimental test-bed, we will attempt to evolve an ultra-acute sense of feel and manipulation. Our goal is to establish the limitations of microforce control and determine the scientific basis for the

We developed an adaptive control system that has a much higher performance than commercially available controllers. This control system will be able to demonstrate the feasibility (or infeasibility) of robotic microgauging.

limits, thus establishing the limits of microgauging using "feeler" gauges.

In parallel with the force-based microgauging research, we are collaborating with Purdue University to assess the viability of using stochastic means to gauge parts having simple geometries. Thus far, we have developed an experiment based on vibration and an analytical model. Preliminary experiments appear to validate the bulk behavior of the experiment. Future work will focus on determining the viability of using stochastic approaches for microgauging or sorting.

Refereed

Wilson, D. G., D. M. Kozlowski, W. J. Prentice, and J. F. Jones. 2004. Adaptive impedance control of stewart platforms for microgauge applications. Paper to be presented at the IEEE International Conference on Robotics and Automation, 18–22 April 2005, Barcelona, Spain.

52527

Rapid-Prototyping High-Density Circuitry (RpHdc)

D. W. Davis, J. M. Sena, P. Yang, J. M. Kelton, B. D. Chavez, M. O. Atencio

Sandia developed a new manufacturing process to integrate complex modeling, rapid-prototype stereolithography processes, and direct-write (DW) technology for the fabrication of three-dimensional (3-D), high-density circuits. This paperless manufacturing technology provides a greater flexibility for rapid development and deployment of new designs, especially for systems with weight and space restrictions.

We will conduct the research along two intertwined paths: materials and process. The materials path will be guided by both the inherent customer requirements (physical and chemical compatibilities with different materials in the fabrication process, stability of the underlying substrate, conductivity and longevity of the drawn circuit material, etc.) and the inherent limitations of stereolithography-compatible photopolymers (low glass-transition temperatures [Tgs], mechanical properties, etc.). The process studies will revolve around techniques to start, stop, fixture, and reregister stereolithography builds, as well as the mechanics of depositing the circuit materials onto the layer-manufactured substrates. We will also study techniques to embed sensors, create multilayer embedded circuits, and provide robust interconnects.

This new technology provided the ability to DW high-density conductive paths directly onto and embedded in the layers of the complex model. This technology will reduce many of the labor-extensive tasks currently required during the assembly process. Through this technology, we would also reduce the hardware required to interconnect assemblies and would combine known technologies to develop a single electrical/mechanical "design to manufacturing" process in support of rapid development and deployment of fully functional prototypes as the final product.

In upcoming work, we will strive to produce 1 mil lines and spaces on a 3-D complex model. We will also focus on combining electrical and mechanical designs into a single design package.

The rapid-prototyping high-density circuitry (RpHdc) team developed partnerships with OhmCraft and nScrypt in developing the process for DW on 3-D stereolithography

apparatus (SLA) parts. Working with these two companies, we were able to DW on SLA parts ranging in complexity from a gentle radius to those having severe transitions between structure walls. We also partnered with the University of Texas at El Paso (UTEP) to fabricate the SLA parts made with the DSM Somos ProtoTool 20L resin.

We submitted two technical advance disclosures: SD-7813/S104,548, Methods and Systems for Integration of Thermally Curable Media During Stereolithography, and SD-7758/S-104,478, Rapid Prototyping of High-Density Circuitry.

We were able to DW electrical circuits down to 1.5 mil (37 µm) in width on planar geometry over short distances.

We also were able to DW electrical circuitry anywhere on the structure of the SLA material at surprising angles. We discovered through this process that the conventional design process of using sharp corners and transitions in the structure of electronic packaging did not work well with our DW processing (e.g., aluminum cases with sharp corners). Designing the structure of our package with that in mind greatly improved our DW process, requiring less moving of the part during the writing process.

We performed thermal property testing on one of the newer SLA resins, DSM Somos ProtoTool 20L, and found it to have better characteristics than previous resins available to us.

...we were able to DW [direct-write] on SLA parts ranging in complexity from a gentle radius to those having severe transitions between structure walls.

Other Communications

Davis, D. W., J. A. Palmer, and P. Yang. 2003. Rapid-prototyping high-density circuitry. Poster presented at the Direct-Write Electronics Applications for the Military Conference, October, Newport, Rhode Island.

Palmer, J. A., P. Yang, D. W. Davis, B. D. Chavez, P. L. Gallegos, R. B. Wicker (University of Texas–El Paso), and F. R. Medina (University of Texas–El Paso). 2004. Rapid prototyping of high-density circuitry. Paper presented at the DARPA Workshop on Bridging Direct-Write Technology Dimensions, June, Seward, Alaska.

Palmer, J. A., P. Yang, D. W. Davis, B. D. Chavez, P. L. Gallegos, R. B. Wicker (University of Texas–El Paso), and F. R. Medina (University of Texas–El Paso). 2004. Rapid prototyping of high-density circuitry. Paper presented at the NNSA Future Tech Conference, May, Washington, D.C.

Palmer, J. A., P. Yang, D. W. Davis, B. D. Chavez, P. L. Gallegos, R. B. Wicker (University of Texas–El Paso), and F. R. Medina (University of Texas–El Paso). 2004. Rapid prototyping of high-density circuitry. *Rapid Prototyping and Manufacturing 2004, SME Technical Paper* **TP04PUB221** (11 May, Dearborn, Michigan): 8.

52528

Elucidating the Mysteries of Wetting

G. S. Grest, C. F. Brooks, D. R. Heine, B. J. Ash, A. M. Grillet, P. A. Sackinger

Nearly every Sandia-owned manufacturing responsibility and many technologies central to Sandia's business involve physical processes controlled by interfacial wetting. Interfacial forces, e.g., conjoining/disjoining pressure, electrostatics, and capillary condensation, are omnipresent and can surpass and even dominate bulk inertial or viscous effects, even on a continuum level. Moreover, the statics and dynamics of three-phase contact lines can exhibit a wide range of extraordinarily complicated behavior, such as contact-angle hysteresis due to surface roughness, surface reaction, or compositional heterogeneities, all of which manifest themselves in unpredictable ways when attempting to control liquid/gas motion on these length scales. These thermodynamically and kinetically driven interactions are essential to the development of new material systems such as nanocomposites, as well as to the fabrication of complex microassemblies. The focus of this project is to advance existing theoretical/computational tools and approaches and to develop and perfect pertinent experimental diagnostics for routine engineering analysis of systems and processes dominated by capillary hydrodynamic effects. We will explore a range of relevant length scales by combining atomistic-level simulations with density-functional and continuum modeling. Input from physical high-fidelity models will ensure the authenticity of the numerical simulation. We will perform experimental studies using a variety of techniques to validate the modeling work. Initial efforts will concentrate on organic systems and study the wetting and dewetting of complex processes such as adhesive bonding of microassemblies, microjoining, and complex motion of fluids traversing convoluted geometries, though the results will be applicable to a wide range of inorganic materials and biomaterials.

We implemented new experimental tools and diagnostics to measure concentration segregation during wetting. The atomistic simulations determined the wetting properties of multicomponent mixtures of polymer fluids for different chain lengths and equilibrium contact angles and compared the results for the spreading dynamics to existing continuum models. The continuum approach investigated several models for droplet spreading. In particular, the atomistic simulations both explored

the qualitative spreading behavior of multicomponent mixtures and performed detailed quantitative analysis. We extended the simulations to large droplets on the order of one million monomers to study the dependence of droplet size on the kinetics. From these simulations, we determined the dependence of the spreading rate of both the bulk droplet and the precursor foot on the radii of the initial droplet. We continue to develop and refine experimental capabilities to examine the wetting behavior of multicomponent polymer blends. We implemented a modified Wilhelmy probe technique for determining the liquid surface tensions of small amounts of polymer blends and validated it using the polypropyleneglycol (PPG)-polyethyleneglycol (PEG) blend. Using freshly drawn glass fibers as a high-surface-energy probe, we can establish the surface tension with an accuracy of 0.5 mN/m. We designed and built a continuous feed-through goniometer to study the contact angles and drop shapes during dynamic wetting using a digital video system and an interface fitting program. We confirmed the capability of confocal microscopy to study the segregation of a blend of two polymers labeled with contrasting fluorescent dyes. We imaged and quantified selective equilibrium surface segregation of one component of a blend using this technique. Contributing to the component segregation work, time-of-flight secondary ion mass spectrometry (TOF-SIMS) is developing into a quantitative technique to determine relative surface concentrations of selectively deuterated polymer blends. We found continuum simulations using natural or weakly imposed traction constraints at the moving contact line to be inappropriate since the resulting contact-angle histories did not converge as the discretization resolution improved. However, we resolved this problem by including a molecular kinetic relation between contact-angle velocity and angle. Results are in good agreement with the computer simulations.

Refereed

Heine, D. R., G. S. Grest, and E. B. Webb, III. 2004. Spreading dynamics of polymer nanodroplets in cylindrical geometry. *Physical Review E* **70** (1): 011606.

Heine, D. R., G. S. Grest, and E. B. Webb, III. 2003. Spreading dynamics of polymer nanodroplets. *Physical Review E* **68**:061603.

Other Communications

Ash, B. J., R. Giunta, A. M. Grillet, and J. A. Emerson. 2004. Wetting behavior of multicomponent polymer melts. Paper presented at the Meeting of the Adhesion Society, 14–18 February, Wilmington, North Carolina.

Grillet, A. M., B. J. Ash, C. F. Brooks, and J. A. Emerson. 2004. A multiscale approach to multicomponent wetting. Paper presented at the ASME International Mechanical Engineering Congress, 13–19 November, Anaheim, California.

Grillet, A. M., B. J. Ash, C. F. Brooks, and J. A. Emerson. 2004. Laser-scanning confocal microscopy applied to multicomponent wetting. Paper presented at the American Institute of Chemical Engineers National Meeting, 9 November, Austin, Texas.

Grillet, A. M., C. F. Brooks, D. R. Heine, P. A. Sackinger, G. S. Grest, and J. A. Emerson. 2004. Wetting behavior of polymer blends. Paper presented at the Gordon Research Conference—Adhesion, 8–13 August, Tilton, New Hampshire.

52530

Next-Generation Spindles for Micromilling

D. D. Gill, M. P. Saavedra

Many applications, including current and future weapon-surety designs, use mesoscale parts manufactured from common design materials. Conventional manufacture of these components is expensive due to the slow material removal rates (MRRs) of the submillimeter-diameter endmills used to machine the parts and the high rate of tool failure due to excessive runout in current spindle designs. State-of-the-art commercially available technology has achieved spindle speeds of 200,000 revolutions per minute (rpm), but even this speed produces unacceptably low MRRs. In this project, Sandia addressed both of these issues by creating two iterations of a design that uses diameter ratios to achieve spindle speeds in excess of 450,000 rpm and also isolates the tool shank from the spindle errors of the driving spindle to achieve submicron tool runout.

The two spindle concepts used in this study utilize a 90,000 rpm electrically driven spindle turning a 1 in.-diameter wheel that drives the 1/8 in. tool shank through friction. The first design supported the tool shank directly in an air bearing, which made alignment a simple task; however, the small area supported by the air bearing caused rapid wear of the bearing faces. The second design utilized three precision shafts supported by partial air bearings. These shafts were located in a triangular pattern surrounding the tool shank. This system had significantly more area supported by the bearing, but suffered from a difficult alignment process.

Despite these challenges, we performed machining at rotational speeds in excess of 400,000 rpm, exhibiting high MRRs and good precision. The concept was successful.

...we performed machining at rotational speeds in excess of 400,000 rpm, exhibiting high MRRs [material removal rates] and good precision. The concept was successful.

The goal of this research was to create a spindle capable of achieving rotational speeds in excess of 450,000 rpm with submicron tool runout. We must meet both of these goals to be able to economically produce mesoscale parts in common engineering materials by milling.

Current technology suffers from low MRRs due to the small tool diameter and current speed limitations (less than 200,000 rpm) of commercial spindles, which cause a low cutting speed at the outer edge of the tool. This type of machining is also expensive due to the short tool life of these small tools, which is in great part due to the excessive loading of the tool caused by runout in the tool. We created two prototype spindles. The first novel design utilized a friction wheel mounted in a 90,000 rpm

electric spindle driving a tool supported in a cylindrical air bearing. The difference in diameter between the friction wheel and tool diameter allowed the tool to achieve speeds in excess of 400,000 rpm. This design operated successfully and was used in limited machining experiments in aluminum (Al). The first-generation design suffered from the small amount of surface area in the air bearing supporting the tool shaft, which caused excessive wear, and from runout of the tool caused by bending induced by circularity errors in the driving friction wheel.

The second-generation design attempted to address the weakness of the earlier design by utilizing a novel three-cylinder rolling-element bearing. Three partial air bearings supported three precision shafts in a triangular pattern. The tool shaft was located in the middle of this triangle and was supported by all three shafts. This design greatly increased the area supported by the air bearings, so the bearing wear issues were addressed. The tool was fully supported, so we also addressed the bending. However, the loss of rigidity in the air bearings due to their shape produced a system that was difficult to align and very sensitive to air-pressure changes. Additionally, the best purchased cylinders available had significant cylindricity errors. Misalignment caused excessive rolling resistance, and the cylindricity errors caused transmittance of runout from the bearing rollers to the tool. The rolling resistance prevented this design from achieving high-speed operation. Additionally, special length tools ordered for utilization with this project were delayed and did not arrive in time for the completion of the project.

We accomplished the following:

- We built two spindle designs; experiments showed high-speed capability and a reduction in runout over the current spindle.
- We conducted machining experiments in excess of 400,000 rpm in Al.
- Excessive bearing wear prevented these designs from achieving all of the goals of the project (extensive machining analysis).

Other Communications

Pathak, J. P. 2004. Design, assembly, and testing of an ultrahigh-speed micromilling spindle. Master's Thesis, Department of Mechanical and Aerospace Engineering, University of Florida, Gainesville, Florida (June).

Ziegert, J. C., J. P. Pathak, and B. H. Jokiel. 2003. An ultrahigh-speed spindle for micromilling. *Proc.18th Annual American Society for Precision Engineering Meeting* **30** (October, Portland, Oregon): 79–82.

53588

Miniature High-Power RF Components Enabled by Mesoscale Manufacturing

J. A. Palmer, C. J. Atwood, B. A. Kast, D. J. Brandt, C. D. Nordquist, C. W. Dyck

Future military and consumer products require increasingly compact, high-power transmitters for functions that include communications and telemetry, remote sensing, and radio-frequency (RF) identification tags. The state of the art of building RF components using microelectromechanical systems (MEMS) technology is sufficient for low-power applications in the tens of watts. However, as power demands increase, the scale of device features must be extended in conjunction with material performance. This research integrates advanced microstereolithography (μSL) and microwire electrodischarge machining (μEDM) technologies to produce a novel mesoscale RF (mRF) relay for high-power applications. Sandia presents methods and infrastructure for reliable batch assembly of electromechanical actuators and structural parts less than 5 mm^3 in volume. We assembled, inspected, and characterized for electrical performance a series of mRF prototypes that consisted of a contact mechanism and actuator with return spring. The mechatronic micromanipulator assembly apparatus and epoxy-based fastening system led to durable prototypes within 4 hr (excluding a 16–24 hr cure cycle).

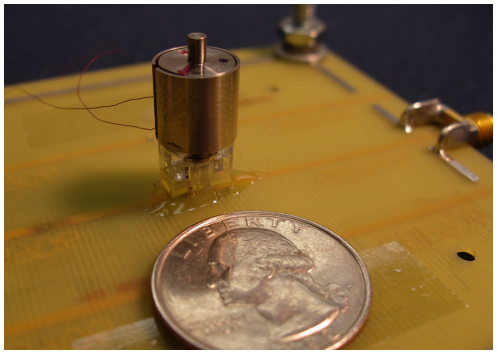

Prototype mRF relay (oblique view).

We devised methods and infrastructure for assembly of mRF relay prototypes. We assembled five mRF prototypes using an innovative mesoassembly workstation that includes a video-assisted telerobotic micromanipulator, positioning system, and assembly fixture. The fixture contains grooves and datum planes to guide and constrain mesoscale parts in desired positions and orientations. We added a containment structure to identify parts, control part slippage, and limit dust contamination. We used tools such as tweezers and vices for manipulating parts outside of the fixture. The mRF relay assembly consists of the following: a novel miniature push-type solenoid actuator with return spring, two-part housing, upper four-bar contact, and two lower contacts.

We successfully batch-fabricated the housings in two-part units by μSL. We achieved high-dimensional accuracy in μSL fabrication of the housings through unprecedented use of Teflon™ shims to maintain submillimeter gaps, and encapsulated mesoscale inserts (constructed independently from aluminum [Al] and photopolymer) to form the four-bar

contact arm grooves. The miniature push-type solenoid is significantly smaller in volume than any comparable commercial product. Prototypes demonstrated output force greater than 60 mN and stroke greater than 1 mm. This corresponds to a stiffness greater than 50 N/m. We rapidly fabricated the four-bar and lower contacts from Al by μEDM; they feature thin flexures in planar and curved configurations.

Assembly of the relay began with the separation of the housing parts within the unit. We subsequently inserted and epoxied the 0.015 in.-diameter actuator link into a hole in the four-bar contact. This operation required multiaxis telerobotic positioning of the four-bar contact within the assembly fixture. Following curing, we cut away excess epoxy from the joint. Next, we inserted the housing halves into the fixture. The groove inserts were engaged with the four-bar contact flexures, and the housing halves were ultimately mated and joined by epoxy. Although we included an apparatus for metered dispensing, we easily applied epoxy with a manual probe. We epoxied assembled actuator and relay mechanisms to RF–printed wiring boards. In the final assembly step, we epoxied fixed lower contacts into the relay through holes in the lower face of the board. However, this design failed to make electrical contact. We corrected this problem by replacing one of the fixed lower contacts with a movable pin formed from copper wire.

Prior to inserting the lower contacts, we measured the mechanism stiffness and stroke of three mRF prototypes using a force transducer. These data yielded conclusive evidence regarding the accuracy and precision of the assembly. Stroke ranged from 560 to 1650 μm compared to a design value of 800 μm, while we recorded stiffness from 17 to 334 N/m relative to a design value of approximately 105 N/m.

Electrical characterization included measurements of actuation and switching parameters, contact resistance, and RF properties. Switching with positive electrical contact occurred in less than 200 ms at an actuation voltage of 14 V dc (direct current) (less than the required limit of 24 V dc). Power dissipation was 4 W, which exceeded the required 300 mW. Contact resistance was 2.0 ohms in nominal operation. When we applied external force to the contacts, resistance was reduced to 200 milliohms or less, and to approximately 600 milliohms with up to 100 mA in the closed relay circuit. The mRF relay demonstrated RF isolation greater than 19 dB, an insertion loss greater than 9 dB, and a return loss greater than 4.5 dB from dc to 1.4 GHz.

This research successfully demonstrated a suite of integrated advanced manufacturing technologies to realize a

functional high-power mesoscale relay with measurable RF performance. Although the novel assembly process yielded robust prototypes, the prototype lot lacked accuracy and repeatability in the context of stroke and stiffness of the relay mechanism. Future work should focus on improving electrical properties through a fixed/movable contact with high-conductivity materials.

Refereed

Palmer, J. A., C. D. Nordquist, B. A. Kast, C. J. Atwood, and F. J. Livingston. 2005. Miniature high-power RF components enabled by mesoscale manufacturing. Paper submitted to the 2005 ASME International Mechanical Engineering Congress and Exposition, January 2005.

Other Communications

Livingston, F. J. 2004. Technology for mesoscopic-scale assembly of an RF switch. Thesis, Master of Science Degree, North Carolina State University, Raleigh, North Carolina (May).

67004

Rapid Prototyping to the Nanometer Scale

D. P. Adams, W. C. Sweatt, M. B. Sinclair, M. J. Vasile, T. M. Mayer

Sandia is researching new rapid-prototyping (RP) techniques that cover 30 nm–500 µm length scales in a diverse set of materials. Most commercially available RP processes are limited to large dimensions (greater than millimeters) and are restricted to a few materials.

Our approach combines focused-ion-beam (FIB) bombardment with in situ, *real-time metrology. Commercial FIB systems can control in-plane feature sizes. With beam widths of 30 nm, FIB sputtering and FIB–induced deposition are useful for defining 0.03–100 µm-wide features. To control depth and ultimately a three-dimensional (3-D) shape, our research couples FIB techniques with novel* in vacuo *metrology techniques for end-point detection and closed-loop control. These techniques are being developed for the first time at Sandia.*

These techniques should allow for more controlled prototyping of devices and components made with 10 nm–100 µm-size features.

We completed the design, simulation, and fabrication of several metrology instruments to be used during FIB processing and recently installed and tested the instruments. Two techniques will provide the ability to monitor feature dimensions in real time. This includes both asperities and ion-milled depressions of various sizes. Both instruments have vacuum-compatible designs and are being designed for use with the FEI, Inc., magnum column. We will extend techniques for eventual feedback control of the ion-beam-bombardment process. This should also provide endpoint-detection capabilities. We found that our approach is unique and filed technical advances.

These techniques should allow for more controlled prototyping of devices and components made with 10 nm–100 µm-size features. We expect the structures fabricated by FIB and controlled by these techniques to be functional prototypes (electrical, optical, mechanical, or other) and not simply clever demonstrations of shape definition.

Refereed

Adams, D. P., M. J. Vasile, T. M. Mayer, and V. C. Hodges. 2004. Focused-ion-beam milling of diamond: Effects of H_2O on yield surface morphology and microstructure. *J. Vacuum Science and Technology B* **21**:2334–43.

67005

Robust Manufacturing of Gel-Based Components for Nuclear Weapons

P. J. Cole, J. L. Lenhart, R. V. Baron, D. R. Tallant

The development of nonaqueous polymer gels is of critical importance to the Nuclear Weapons (NW) Sandia Management Unit (SMU) because they are a key constituent of a series of electrical components. A gel that is suited to this application consists of a cross-linked polymer swollen with a high-dielectric-constant solvent. Poor polymer-solvent phase behavior has been tied to the inferior mechanical properties that lead to component failures. This work sought to establish a relationship between the gel-fabrication procedure and the resulting mechanical properties, gel microstructure, and phase behavior. To develop this link, we prepared gels using one of two solvents in various proportions. In addition to confirming typical mechanical behavior for cross-linked networks, we found an impact of solvent content during gel processing. Rheological analysis of these gels, in combination with solvent extraction, shows that the screening of entanglements (physical cross-links) is changed dramatically by varying the solvent content. Furthermore, the solvent quality appears to be altered through gel-processing parameters, particularly temperature, to achieve a desired set of mechanical properties. We used neutron-scattering data, acquired with gels held at different temperatures, to identify an optimum temperature to confirm this hypothesis. We extended each of the techniques (rheological analysis, gel extraction, neutron scattering) such that it is appropriate for other gel formulations. This is particularly important as we extend this early work to network sol-gel systems that are important in this and other Sandia technologies.

We completed work associated with phase behavior and gel processing. We extended the rheological analysis technique and used it to confirm phase separation in dibutylphthalate (DBP)-based gels and homogeneity in bis(ethyl hexyl) sebacate (BEHS)–based gels. We explored the temperature range through which the phase separation occurs in DBP-based gels using neutron scattering. This permitted a temperature to be identified for future gel processing that will confirm a key hypothesis developed earlier. We fabricated gels with various effective cross-link densities by varying the solvent content. Rheological analysis and solvent extractions of these gels provided evidence that the number of effective cross-links is a

combination of chemical cross-links and physical cross-links, termed *entanglements*. While the number of chemical cross-links is determined by the gel precursor functionalities, the number of entanglements is controlled by the amount and quality of the solvent present in the gel during cure. We showed that using the solvent content to control the screening of entanglements is an effective method of altering the gel mechanical properties. Therefore, we established a link between gel processing and properties.

We showed that using the solvent content to control the screening of entanglements is an effective method of altering the gel mechanical properties. Therefore, we established a link between gel processing and properties.

67006

Meso-/Microoptical System Interface Coupling Solutions

S. A. Kemme, R. T. Mitchell, M. R. Daily, D. K. Serkland, D. Chu, J. A. Emerson, D. W. Peterson, M. Armendariz, T. Carter, S. Samora

Sandia will develop a process for flip-chip self-alignment of optical (to electrical) devices that can simultaneously support high-speed electrical transmission lines. The core technology proposed in this project is a connecting solution at the board-to-fiber interface, but will also enable self-aligned wafer-level integration of photonic components to microelectromechanical systems (MEMS). We will illustrate this process's utility in a mixed-technology demonstration, highlighting self-alignment and high-speed electrical interconnection.

We developed microsystem technology based on semiconductor fabrication techniques to combine electronic and optical functions into integrated systems. In this project, we move a step up from the microsystem and optimize the real-world-to-board connection in electronic/photonic systems, i.e., the meso-/microoptical system interface.

We fulfilled three of the four milestones defined for this year: (1) identify and compare possible solder self-align process scenarios, (2) simulate solder-process response to optimized pad layout, and (3) analyze the diffractive optical element (DOE) lens design for optimal coupling and tolerances.

We pursued an alternating-step lamination electrodeposition process through the company Surftec Technologies, Inc. This will be a layered electrodeposition buildup to create an 80/20 tin/indium (Sn/In) eutectic that we hope will have a low reflow temperature, but will still have a sufficient restoring force to precisely align the various components with the microsystem. We completed a mask and metallized substrates to be bumped by Surftec soon.

Simulations of solder evolution upon reflow indicated that a pad size of 100 µm with a bump height of 75 µm could be sufficient for die alignment and optical spacing. These solder-ball pitch and pad sizes are consistent with mainstream commercial services that use tin-lead (SnPb) and SnIn technologies.

We performed optical-ray trace simulations to illustrate the required tolerances for a nominal lens design. We based these allowed ranges on optical throughput of an apertured spot at the detector. The allowed range for the lens radius of curvature is 202–218 µm, and that for the source distance in air is 719 µm to

at least 850 µm. The fused-silica thickness can range from 870 µm to 1070 µm, and the detector distance in air may range from 0 µm to 93 µm. The most challenging aspect of optical placement is the lens lateral decenter away from the optical axis and the lens element tilt and/or face tilt on the substrate. These must stay within 5 µm and to within 2 deg, respectively, to maintain 95% efficiency.

67007

Injection Molding of Net-Shape Active Ceramic Components

P. Yang, C. B. Diantonio, A. M. Grillet, G. R. Burns, L. L. Halbleib, R. H. Moore, J. Cesarano, III, L. A. Mondy

Sandia is studying and utilizing an injection-molding technique for the fabrication of active ceramic components used in the power-supply unit of neutron generators (NGs). The new approach will significantly reduce the pressing defects and the machining-induced surface defects. Ceramics with surface defects are more susceptible to handling damage in subsequent processes. For example, more than 20% of voltage bars is lost due to cracking and chipping induced during the manufacturing processes. More importantly, by eliminating the machining processes, the net-shape–forming approach can save 18% of the touch labor cost, minimize the hazardous-waste-stream management, trim several processing steps, and make it a true lean-manufacturing process.

Fabrication of high-quality injection-molded ceramic components requires a basic understanding of the interrelationships between the powder characteristics, the thermal-rheological control of the molding compound, the pressure of material in the cavity, and tooling parameters. To date, the injection molding of ceramics has been experimental in nature. We will develop a finite-element (FE) analysis capability for the flow modeling to determine the processing and tooling parameters. Furthermore, the control of sintering shrinkage and lead loss during high-temperature processing is also critical for material performance. Because injection molding can offer the promise of high-volume, low-cost, net-shape production of micromechanical devices, establishing a knowledge base for ceramic-components fabrication will pave the road for future application development.

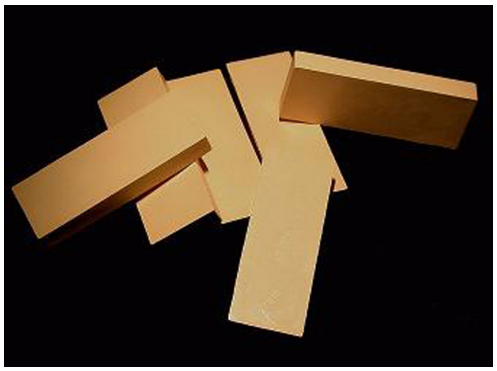

Injection-molded piezoelectric ceramics.

We focused our work on establishing basic processing capability and on understanding important processing parameters for the injection molding of ceramic components. We determined our binder system for the injection-molding process, which provides a wide organic burn-out window without creating internal defects and undesirable organic residuals in final sintered ceramics. We used the attrition milling technique to establish a consistent process for reducing the size of ceramic particles. This process is critical for controlling the final sintering shrinkage and meeting product specification. The thermal rheological behavior of the ceramic-

organic mix was characterized as a function of temperature and shear rate, using a capillary rheometer. We studied the effects of different solid loadings and the amount of surfactant on the rheological behavior. These results will help in determining the operational window for the injection-molding process. We studied the dewaxing process and organic burn-out using the master decomposition curve and the classic kinetic approaches. We successfully fabricated several injection-molded parts. We made partially molded parts injected at different shear rates and pressures to help the validation of FE modeling.

67008

Macro-/Meso-/Microsystems Integration in LTCC

K. A. Peterson, C. D. Nordquist, C. K. Ho, K. D. Patel, S. B. Rohde, B. R. Rohrer, C. A. Walker, F. Uribe

Microsystem integration involves technologies as varied as integrated digital logic, radio frequency (RF), optics, microfluidics, a host of sensors and actuators, and chemical and physical analyses. Low-temperature co-fired ceramic (LTCC) technology can meet requirements for critical microsystem elements due to its excellent high-frequency properties, nearly unlimited stacking capability, chemical inertness, and form and fit versatility. Its limitations include low thermal conductivity, special materials needs for embedded passives, and low strengths associated with the attachment of electrical leads. With new innovations, previous drawbacks to the technology can be overcome.

Microelectronic routing of electrical traces through available space on any layer has been a feature of most microelectronic-board technologies. A recent innovation using sacrificial material now makes this same routing versatility available for open volumes in a very thin multipurpose board for microsystem integration. In addition to serving as microfluidic channels for dispensing, sensing, or cooling, these volumes can integrate microelectronic and microsystem devices, as well as provide surfaces for new sensing materials in smart packages. They can also serve as temporary support for newly developed suspended structures that provide low electrical loss and low mass. The incorporation of metallic elements in the structure will permit higher-integrity leads, heat sinks for superior heat removal, and electrostatically actuated valves for microfluidic flow and pressure regulation.

Sandia will develop the capability for manufacturable, densely packed internal volumes, successfully integrating macro-, meso-, and micro- (MMM) scale features for systems. We will develop a new capability for embedded passive elements using internal volumes. We will develop integral metal elements for structural, electrical, thermal, and fluidic features required in new applications. We will characterize and implement the new structures developed previously. MMM system technology will bring together microsystems and mesoscale integrated components and present them to a macroscale world.

New developments in sacrificial volume materials (SVMs) include the following:

(1) Complex shapes for simple components—punched, blanked, laser-cut, stenciled, dispensed, written, screen-printed, and others.

(2) Evaluation of new commercial tape SVM.

(3) Evaluation of proprietary slurry SVM (obtained proactively from a commercial company).

(4) Evaluation of newly developed sacrificial paste SVM (proactive procurement).

(5) Thick-film printing to SVM, with other structure application directly to SVM also possible (thin film, etc.).

(6) Resolution (pattern) studies for solid and liquid—thickness range 0.0015–0.125 in.

These new developments are responsible for newly developed structures:

(1) Suspended thick-film features for RF, microfluidic, temperature sensing, and other applications, and

(2) Transparent hermetic viewports for microfluidic channels.

Additional LTCC innovation resulted in new devices:

(1) Micro high-performance liquid chromatography (HPLC) channels that do not fail at a pressure of 5000 psi,

(2) Smart channel using chemiresistor technology to demonstrate favorable stability, sensitivity, and performance for air, trichloroethylene, and m-xylene,

(3) Microfluidic test manifold, and

(4) Completely new functional microelectromechanical systems (MEMS) structures in LTCC that constitute additional intellectual property.

This project supported the presentation and publication of two quite different LTCC conference papers with favorable responses from industry and university contacts.

We completed one patent application and submitted three additional disclosures for technical advances.

The many new developments will require significant additional development before they can be realized in specific applications, which compose a part of the focus of additional activity.

Other Communications

Peterson, K. A., S. B. Rohde, and K. B. Pfeifer. 2003. Novel LTCC fabrication techniques applied to a rolled ion-mobility spectrometer. (Invited) *Proc. 204th Meeting of the Electrochemical Society* (12–16 October, Orlando, Florida): 16.

Peterson, K. A., S. B. Rohde, C. A. Walker, K. D. Patel, T. S. Turner, and C. D. Nordquist. 2004. Microsystem integration with new techniques in LTCC. *Proc. Ceramic Interconnect Technology: The Next Generation II (IMAPS)* (26–28 April, Denver, Colorado): 19–26.

Biotechnology

Exploring and understanding fundamental biological processes and relating them to national security applications such as bioterrorism, nonproliferation of biowarfare technologies, and energy security are the primary goals of the new Biotechnology investment area. The key to achieving success is joining faculties across technological disciplines and augmenting them with new biotechnical capabilities at the cellular/molecular level. There is a strong focus on tools to build informational and physically based system models for toxin, pathogen, signaling molecule interactions with cell membranes, and biological networks.

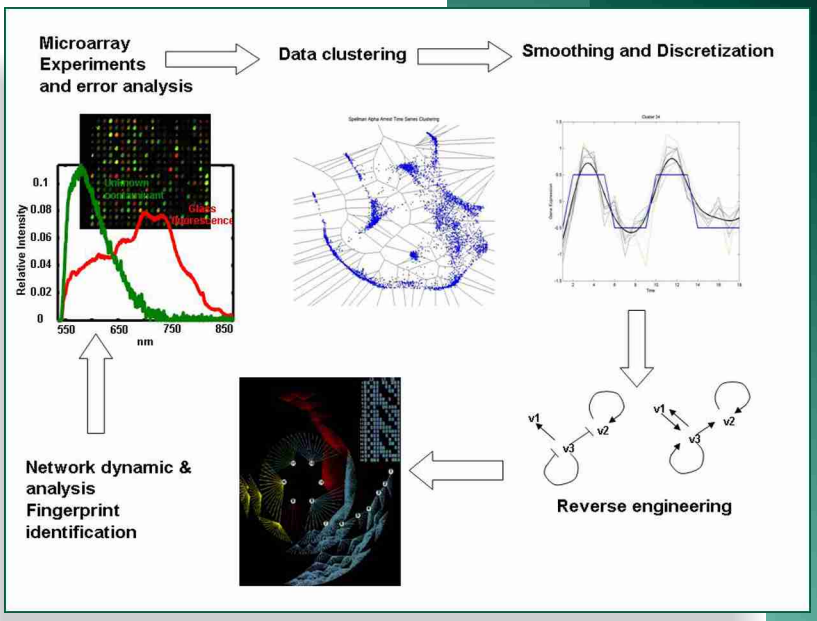

52533
"Reverse-Engineering Biological Networks: Applications in Immune Responses to Bioterrorism Threats"

Aiding the nation's defense strategy against biological warfare, researchers seek to determine the network of events, or regulatory network, that defines an immune response to a biotoxin. This understanding would enable the measurement of fingerprint elements rather than the entire immune response. To progress toward this goal, scientists developed experimental protocols and computational tools to reverse-engineer regulatory networks and to facilitate the discovery of immune-response fingerprints to biotoxins through expression levels of regulatory elements.

For the first time in the field of regulatory inference from microarray data, researchers integrated experiments, error analyses, data clustering, inference, and network analysis. Project success yielded inference algorithms and codes to enumerate and sample dynamic networks, to study dynamical robustness of modules and networks, and to analyze the network topology. Continuing research focuses on functional characterization, the determination of time trends, and the clustering of functional groups for statistically significant fingerprint genes.

38609

Physical and Electronic Changes Caused by Membrane Signaling as a Transduction Pathway in Affinity-Based Biosensors

S. M. Brozik, L. J. D. Frink, G. D. Bachand, R. C. Hughes, P. Esherick

Sandia developed a concept for integration of natural ion channels with electronically and optically addressable fluidic platforms to enable rapid, real-time measurements of single-molecule behavior. Many of the membrane functions, such as regulation of cellular potential, selective filtration, and regulation of nutrient and waste movement, are mediated by transmembrane proteins (TMPs). TMPs span the lipid bilayer, requiring hydrophobic regions that penetrate the membrane and hydrophilic regions that are exposed to the aqueous medium on either side. An important class of TMPs forms pores or channels that enable active, directional, and preferential transport of ions across the otherwise impermeable membrane in response to a specific stimulus. A good example is the serotonin type-three receptor that preferentially transports monovalent cations upon binding of serotonin to specific sites on the extracellular domain of the pentameric protein. This binding event causes the movement of 10^6 ions/s through the channel, generating an ion conductance of about 100 picosiemens (pS) compared to the leakage conductance of about 0.02 pS. With an amplification factor exceeding 10^6 and a signal-to-noise ratio (SNR) exceeding 5000, gated ion channels integrated into a sensor would have the unprecedented ability to detect single binding events. In addition, spectroscopic measurements allow us to measure fast kinetic events and the dynamics of TMPs. Molecular modeling tools are being developed to elucidate the mechanism of ion conductance at the atomic level and to understand protein-lipid interactions. As we continue to build our suite of experimental and molecular modeling tools, we are compiling structural and functional information on the serotonin receptor and gramicidin channel. This work will ultimately lead to a prototype device for sensing based on ion transport systems. The information gained from this project will enable us to exploit temporal (kinetic) information for the real-time analysis and detection of target analytes.

We focused on characterizing the serotonin protein channel and extending our experimental capabilities to the design of robust biomolecular devices. This included demonstrating controlled fabrication of high-quality nanopores upon which the protein/bilayer assembly is oriented. Our modeling efforts

focused on developing a detailed lipid model that treats head groups and charge distributions in a more precise manner.

- *Transducer development*. To create a stable via for the lipid bilayer to assemble, we first used a Bosch process in 300 µm-thick silicon (Si), resulting in irregular sidewalls. We then created a second version of the via using electron-beam lithography, which proved successful. For this device, we used 110 Si, 300 µm thick, coated with 1 µm of silicon nitride (SiN) on both sides. The through-holes in the bottom-side SiN layer ranged from 2 µm to 10 µm, and we fabricated them by depositing the positive photoresist (PR) AZ 4330 (Clariant) onto the backside of the wafer. We patterned the AZ 4330 PR using a Karl Suss MA6 contact aligner and developed it with 1:4 AZ 400K photodeveloper. We etched the exposed SiN layer in a reactive-ion etch process containing CF_4 and oxide (O_2) at 100 mTorr for 25 min.

We fabricated the topside electrodes using AZ 4330 PR, as well. Once they were patterned and developed, we defined electrodes consisting of 20 nm of chromium (Cr) and 100 nm of silver (Ag) on the top of the wafer using thermal evaporation. In addition to the Ag electrodes, we fabricated a second counter electrode from platinum (Pt). We engineered a housing device using polyetherether ketone (PEEK).

- *Molecular biology: Develop mutant $5HT_3$ (typ.) for site-specific fluorescent labeling*. The technical goal of this component of the work was to insert a 6x histidine (His)-tag at the C-terminus end of the serotonin receptor such that recombinant protein could be purified by nickel-nitrilotriacetic acid (Ni-NTA) chelate chromatography. Texas Tech University graciously provided a clone containing the 1464–base pair (bp) 5HT3 serotonin-receptor gene sequence. The overall strategy to accomplish the 6x His-tag insertion involved using site-directed mutagenesis (SDM) to create a unique BamHI restriction endonuclease site at the 3' end of the serotonin gene sequence, which would subsequently be used along with the NotI site to introduce a short deoxyribonucleic acid (DNA) oligomer containing the 6x His-tag. We fluorescently labeled serotonin-receptor agonists. The goal was to attach fluorophores with and without covalent spacers to the indole nitrogen, as it is believed that the primary amine and alcohol groups are responsible for ligand binding to the serotonin receptor. We will carry out spectroscopic studies to determine the number of labeled ligands bound to the purified receptor, thus detailing the number of receptor sites for serotonin.

- *Computational: Work up a detailed lipid model that treats head groups and charge distributions in a more precise*

way. We completed the initial investigation of a model coarse-grained lipid bilayer system and submitted two manuscripts detailing both the complexity of these model systems and the mapping of these systems onto experimental systems. In addition, we performed calculations for a simple rodlike inclusion in a lipid bilayer (a two-dimensional calculation) to demonstrate that the molecular-theory approach can capture the effect of the inclusion on both the bilayer-water interface and the local lipid tail structure in the vicinity of the inclusion.

We pursued coarse-grained models of lipid bilayers with density-functional theory (DFT) methods and performed studies on the phase space exhibited by these models. We found that both fluid and ordered lipid phases can be formed, and we enumerated the phase diagrams for these models. We investigated studies on stacks of bilayers to demonstrate their interactions. We identified zero-tension bilayers and compared their structures with molecular dynamics (MD) calculations of the same model systems at zero tension.

Refereed

Davis, R. W., E. L. Patrick, L. A. Meyer, T. P. Ortiz, J. A. Marshall, D. J. Keller, S. M. Brozik, and J. A. Brozik. 2004. The thermodynamic properties of single-ion channel formation: Gramicidin. *J. Physical Chemistry B* **108**:15364–69.

50772

Cellular Observatory: Simultaneous Time- and Frequency-Resolved Microscopy

D. W. Chandler, A. K. Luong, C. C. Hayden

Sandia seeks to build a "cellular observatory." A cellular observatory is a machine capable of monitoring multiple constituents (i.e., proteins, toxins, deoxyribonucleic acid [DNA], ribonucleic acid [RNA], etc.) within a cell in real time, as well as monitoring the local environment of those constituents (pH, viscosity, ion concentration). We will do this by developing a new type of confocal microscope system for measuring the dynamics of interactions of cellular constituents in real time. The confocal microscope and detection system will have the ability to measure the wavelength, emission time, and polarization of each detected fluorescence photon as a function of the position of laser excitation. In this manner, an image of a cell will be obtained where each pixel contains the entire fluorescence signature (lifetime and frequency spectrum) of every type of fluorescent chromophore measured in each image frame. Some cellular constituents may be tagged with multiple fluorescent chromophores to make them more detectable. We will do this with unprecedented speed, utilizing fast electronics and a high-repetition-rate laser system. The higher spectral coverage (moderate resolution over the entire visible spectrum) will enable us to monitor more species simultaneously, and the higher data accumulation rate will make it possible to take image frames fast enough to monitor real-time dynamics of cellular functions.

We studied single-molecule fluorophores for the first time with a new confocal fluorescence microscope that allows the wavelength and emission time to be simultaneously measured with single-molecule sensitivity.... At the single-molecule level, this approach makes entirely new types of temporal and spectral correlation spectroscopy possible.

We studied single-molecule fluorophores for the first time with a new confocal fluorescence microscope that allows the wavelength and emission time to be simultaneously measured with single-molecule sensitivity. In this apparatus, the photons collected from the sample are imaged through a dispersive optical system onto a time- and position-sensitive detector. This detector records the wavelength and emission time of each detected photon relative to an excitation laser pulse. A histogram of many events for any selected spatial region or time interval can generate a full fluorescence spectrum and correlated decay plot for the given selection. At the single-molecule level, this approach makes entirely new types of temporal and spectral correlation spectroscopy possible. We took simultaneous time- and frequency-resolved fluorescence measurements of single rhodamine 6G (R6G),

tetramethylrhodamine (TMR), and cyanide (Cy3) embedded in thin films of polymethylmethacrylate (PMMA).

The correlations of the fluorescence intensity, wavelength, and emission time observed in these experiments were made possible by the simultaneous measurement of the fluorescence wavelength and emission time for each single detected photon. We showed that these measurements can be made at the single-molecule level, providing entirely new ways of performing single-molecule correlation spectroscopy. The technique can be used to identify different fluorophores within a sample if the fluorescence characteristics of the individual fluorophores are well characterized under similar experimental conditions. This is critical for identification of single-molecule fluorophores because of the ubiquitous fluctuating behavior observed under single-molecule conditions. However, the time- and frequency-resolved microscope is best suited as a new tool for studying the fundamental dynamics underlying the photophysics of single molecules, such as changes in internal states of a single molecule, quenching, and resonance energy-transfer processes. Experiments on single-pair fluorescence resonance energy transfer in conjunction with the development of correlation techniques that take advantage of the multicorrelated information are under way in our laboratory.

Refereed

Luong, A. K., C. C. Gradinaru, D. W. Chandler, and C. C. Hayden. 2004. Simultaneous time- and frequency-resolved fluorescence microscopy of single molecules. *Proc. National Academy of Sciences*, submitted.

Other Communications

Gradinaru, C. C., A. K. Luong, C. C. Hayden, and D. W. Chandler. 2004. Spectrally dispersed FLIM of single molecules: Probing local environment and measuring FRET. Paper presented at Laser Science XV, October, Rochester, New York.

Hayden, C. C., A. K. Luong, C. C. Gradinaru, and D. W. Chandler. 2004. Time-resolved multispectral imaging of single molecules. Paper presented at Laser Science XV, October, Rochester, New York.

Luong, A. K., C. C. Gradinaru, D. W. Chandler, and C. C. Hayden. 2004. Time-resolved multispectral imaging of single molecules. *ACS Abstracts, Proc. American Chemical Society 228th National Meeting* (August, Philadelphia, Pennsylvania): 495.

52532

Modeling Biomembranes

M. J. Stevens, A. L. Frischknecht, S. J. Plimpton, D. Y. Sasaki, L. J. D. Frink

Understanding the properties and behavior of biomembranes is fundamental to many biological processes and technologies. Microdomains in biomembranes or "lipid rafts" are now known to be an integral part of cell signaling, vesicle formation, fusion processes, protein tracking, and viral and toxin infection processes. Understanding how microdomains form, how they depend on membrane constituents, and how they act not only has biological implications, but also will impact Sandia's effort in developing membranes that structurally adapt to their environment in a controlled manner. To provide such understanding, we seek to create physically based models of biomembranes. We will apply molecular dynamics (MD) simulations and classical density-functional theory (DFT) calculations using these models to phenomena such as microdomain formation, membrane fusion, pattern formation, and protein insertion. Because lipid dynamics and self-organization in membranes occur on length and time scales beyond atomistic MD, we will use coarse-grained models of double-tail lipid molecules that spontaneously self-assemble into bilayers. Using such a model, we have already demonstrated that the time scales of lipid diffusion and fusion intermediates are accessible to MD simulations. This model enables the study of a whole set of membrane dynamics, including those listed above. These coarse-grained models can also be used in our DFT code. DFT will provide equilibrium information on membrane structure, free energies and routes to assembly of membrane-bound proteins, and free energies of permeation for water, ions, proteins, and toxins as they traverse the membrane. We will perform experimental work to help further elucidate the fundamental organizational principles. In summary, this project will produce significant new understanding of biomembrane structure and dynamics and will build a strong foundation of physically based models for further development.

We completed a substantial amount of work in modeling lipid membranes. The foundations of our lipid modeling are now well established. We completed the characterization of a set of coarse-grained models for lipid molecules that yield fluid and gel phases. We calculated the area per lipid as a function of temperature for a range of lipid tail lengths for saturated and

unsaturated lipids. We calculated the elastic moduli. Using DFT, we calculated phase diagrams. We also observed the ripple phase in MD simulations. This was an unexpected result of the simulations, although the ripple phase is well known experimentally. We simulated two-component lipid bilayers to study microdomain formation. We found that in starting with a circular domain for a lipid type in the gel phase surrounded by a lipid type in the liquid phase, the segregated structure is stable for long simulation times. For two-component simulations starting with random distributions, the system evolves into solid and liquid domains. Interestingly, in these simulations, the solid phase is a mixture of the two lipid types. The results are consistent with our atomic-force microscopy (AFM) measurements for a phosphatidylcholine mixture. Finally, we performed initial DFT calculations of proteins in membranes.

We also observed the ripple phase in MD simulations. This was an unexpected result of the simulations, although the ripple phase is well known experimentally.

Refereed

Frischknecht, A. L., and L. J. D. Frink. 2004. Coarse-grained lipids I: A density-functional theory approach and thermodynamics of fluid bilayers. *Biophysical J.*, submitted.

Frischknecht, A. L., and L. J. D. Frink. 2004. Coarse-grained lipids II: A density-functional theory approach and thermodynamics of fluid bilayers. *Biophysical J.*, submitted.

Sasaki, D. Y. 2004. Control of membrane structure and organization through chemical recognition. *Cell Biochemical Biophysics* **39** (2) (October): 145–61.

Stevens, M. J. 2004. Coarse-grained simulations of lipid bilayers. *J. Chemical Physics*, accepted.

52533

Reverse-Engineering Biological Networks: Applications in Immune Responses to Bioterrorism Threats

J. M. Faulon, E. E. May, A. Martino, G. S. Davidson, D. M. Haaland, S. B. Martin, A. Slepoy, J. A. Timlin

Sandia's goal is to determine the network of events, or the regulatory network, that defines an immune response to a biotoxin. We anticipate that by inferring a regulatory network, we will be able to isolate a handful of specific regulatory elements that fingerprint a response. Ultimately, this work will provide the blueprint of a simple experiment where the biotoxin is characterized by measuring only the fingerprint elements rather than the entire immune response. This goal addresses the homeland security mission of the Department of Energy (DOE). Regulatory network characterization is also an explicit goal of the Genomes-to-Life (GTL) DOE program.

As a model system, we are studying a T-cell regulatory network triggered through activation of a tyrosine kinase receptor using a combination of pathway-knockout and time-series microarray experiments. Our approach comprises five steps: (1) microarray experiments, (2) data error analysis, (3) data clustering, (4) reverse-engineering, and (5) network dynamics analysis and fingerprint identification. The practical biological outcome of this work should be the discovery of immune-response fingerprints to a biotoxin in terms of expression levels of regulatory elements.

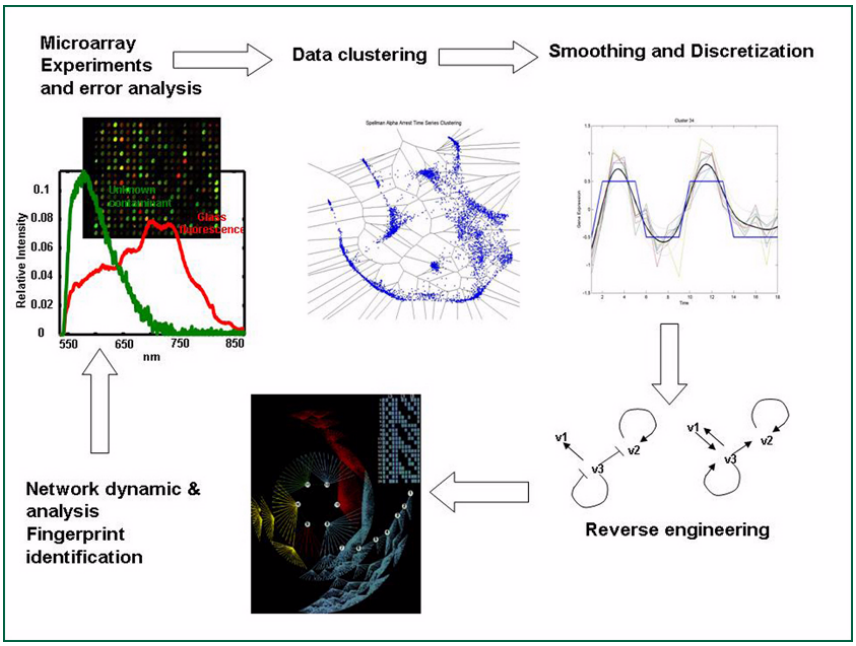

Researchers developed a suite of experimental protocols and computational tools that reverse-engineer regulatory networks given a minimum amount of data. Researchers integrated five steps: (1) microarray experiments, (2) data error analyses, (3) data clustering, (4) reverse-engineering, and (5) network dynamics analysis and fingerprint identification.

Inferring regulatory networks from microarray data is a new field of investigation that is no more than 5 years old. To the best of our knowledge, this work is the first attempt that integrates experiments, error analyses, data clustering, inference, and network analysis to solve a practical problem. While microarrays have been used with time-series experiments and gene- or pathway-knockout experiments, we are not aware of any study merging both types of experiments. The systematic approach of counting, enumeration, and sampling is new to the field of network reverse-engineering. The resulting mathematical analyses and computational tools should lead to new results on their own and should be useful to others who analyze and infer networks.

...this work is the first attempt that integrates experiments, error analyses, data clustering, inference, and network analysis to solve a practical problem.

We determined gene-expression profiles in murine CD8+ T-cells after interleukin-2 (IL-2) stimulation as a function of time. We completed careful experimental and statistical design for eight replicates each at 3 and 6 hr. The design comprised two biological replicates, two hybridization replicates, and two block-gene replicates. Statistical analysis revealed that a preponderance of genes was up-regulated compared to down-regulated. We concluded that the effect of IL-2 is greatest at earlier times before decreasing at 6 hr. We scanned a second set of mouse-microarray gene-expression slides with the upgraded hyperspectral microarray scanner to quantify the amount of green contaminant. Multivariate curve resolution (MCR) analysis of these images resulted in a previously unseen spectral component. Further investigation of this component demonstrated that it is an instrument artifact, which we corrected with a micropositioning device.

To validate our clustering and inference algorithms, we focused on the biological interpretation of a yeast regulatory network that we inferred in previous work. This dataset consists of gene-expression measurements on approximately 6000 yeast genes over 18 time points. In recent work, we used the inference algorithm to produce a set of 1000 networks matching the 18 time-point expression profiles and converted the networks produced into a minimal set of logical clauses. While the overall number of possible networks is rather large, we found the number of possible logic clauses per gene to be limited. Precisely 14% of the activation/inhibition clauses appeared in all networks, while 45% of the clauses were present in half of the networks. We also analyzed our inferred networks with our collaborator at the University of New Mexico. We discovered a module in these networks composed almost entirely of genes involved in exit from alpha-arrest.

To further restrict the search space for network inference, we studied the dynamical robustness of activation/inhibition regulatory models. We define “network dynamical robustness” as the number of perturbations that can be applied on a network without changing its equilibrium dynamics. Formally, dynamical robustness is the number of nonidentical networks having the same dynamical attractors. We systematically computed robustness on all the activation/inhibition networks up to five nodes. We found that only a few networks have robust dynamics when subjected to perturbations. In fact, the number of possible networks decreases with robustness according to a power law. We also found a predominance of robust modules in published gene regulatory networks as well as in the yeast regulatory networks that we inferred. We obtained these results using a code toolbox that we recently completed. In addition to our inference algorithms, the toolbox comprises codes to (1) enumerate and sample dynamical networks, (2) search subgraphs and functionally relevant modules in networks, (3) study the dynamical robustness of modules and networks using dynamical attractors, and (4) analyze the topology of the networks using graph algorithms (distance matrices, clustering coefficients, connected components, symmetry, and canonization).

Refereed

Faulon, J. L., S. B. Martin, and R. D. Carr. 2004. Dynamical robustness in gene regulatory networks. *Proc. 3rd International IEEE Computer Society Computational Systems Bioinformatics Conference* **3** (16–19 August, Stanford, California): 626–27.

Martin, S. B., G. S. Davidson, E. E. May, J. L. Faulon, and M. M. Werner-Washburne. 2004. Inferring genetic networks from microarray data. *Proc. 3rd International IEEE Computer Society Computational Systems Bioinformatics* **3** (16–19 August, Stanford, California): 566–69.

Timlin, J. A., M. B. Sinclair, D. M. Haaland, M. J. Martinez, M. Manginell, S. M. Brozik, J. F. Guzowski, and M. M. Werner-Washburne. 2004. Hyperspectral imaging of biological targets: The difference a high-resolution spectral dimension and multivariate analysis can make. *Proc. IEEE International Symposium on Biomedical Imaging* (Arlington, Virginia).

Other Communications

Slepoy, A., and M. Thompson. 2004. Stability of biological networks as represented in random Boolean nets. Sandia Technical Report SAND2004-4185, Sandia National Laboratories, Albuquerque, New Mexico.

Timlin, J. A., M. B. Sinclair, D. M. Haaland, and M. R. Keenan. 2004. A hyperspectral imaging system with multivariate data analysis for increased throughput. Paper presented at AOAC International, 19–23 September, St. Louis, Missouri.

Timlin, J. A., M. B. Sinclair, D. M. Haaland, M. Manginell, S. M. Brozik, and J. H. Flemming. 2004. Capabilities of hyperspectral imaging for fluorescence microscopy of cells and tissues. Paper presented at the DOE/NIBIB Imaging Workshop, Bethesda, Maryland.

52536

High-Throughput Identification of Molecular Machines Involved in Membrane Signaling and Toxin Pathways

A. K. Singh, R. Sapra, S. Chhabra, D. J. Throckmorton

Sandia seeks to develop a high-throughput method to identify protein complexes in microbial organisms. Although genes are the information repository of an organism, it is the proteins that carry out all functions. Proteins rarely act alone; they interact with other proteins to perform cellular tasks. Protein complexes are responsible for almost all biological functions, including cell signaling, transport through membranes, and biotoxin pathways. Comprehensive identification of protein-protein interaction will lead to better understanding of these functions, enabling development of improved methods of bioremediation and biosensing.

The method involves using ligand-modified magnetic beads immobilized in a 96-well microtiter plate by a magnet to selectively isolate genetically tagged (the "bait") or native proteins and associated complexes. Addressable magnetic strips allow location-specific fluidic manipulations (washing), cross-linking, and proteolysis. The purified protein complexes, bound to the magnetic beads, are then cross-linked, proteolyzed into peptides, and analyzed by mass spectroscopy (MS). We will analyze the MS data by bioinformatics software to provide identification of proteins and by constraint-based protein structure models to elucidate the topology of the complexes. We will identify the proteins to be used as bait using two-dimensional gel electrophoresis (2-D DIGE) followed by matrix-assisted laser desorption/ionization time-of-flight (MALDI-TOF) MS. These proteins will then be expressed in the native organism (Desulfovibrio vulgaris [D. vulgaris])*, as well as in* Escherichia coli (E. coli).

- *High-throughput identification of proteins and protein complexes*. We characterized the heat-shock response of *D. vulgaris* from a global proteomics perspective using 2-D DIGE technology. We visualized approximately 1500 protein spots by fluorescence imaging. After differential image analysis, we found 292 to be differentially expressed in the heat-shock-versus-control sample by ≥ twofold. We then stained the gel with Sypro, a protein dye with a limit of detection in the range of 1–10 ng to determine which protein spots contained enough material for MALDI-TOF analysis. We selected a subset of 94 spots by this method from the 292 shown to be differentially

expressed by Cy3 (green)/Cy5 (red) imaging. We subjected these spots to in-gel tryptic digestion followed by peptide mass fingerprinting by MALDI-TOF MS to identify these proteins. We identified 64 spots, representing 29 unique proteins (a given protein was sometimes identified from multiple spots). Many of the identified proteins represent homologues to proteins from other organisms known to be up-regulated by heat shock, such as heat-shock protein (HSP) 70 (dnaK) and HSP 10 (GroES). Others were proteins unique to the class of sulfate-reducing bacteria such as desulfoferrodoxin.

- *Purification of protein complexes*.

— *Using antibodies*. We observed that HSP 70 (gene dnaK) shows the highest up-regulation in response to heat shock. This has also been shown in other organisms, including *E. coli*. Using a commercial antibody against *E. coli* HSP 70 (HSP 70 from *E. coli* shows ~ 70% sequence identity to the corresponding protein from *D. vulgaris*), we pulled down HSP 70 and multiple proteins associated with it from the *D. vulgaris* cell lysate.

— *Genetic tagging of proteins in* D. vulgaris. This method of protein-complex identification relies on the use of individual proteins that are part of molecular complexes as bait proteins. This technique is a generic purification method applicable, at least in theory, to any protein. Using the recombinant deoxyribonucleic acid (DNA) technique, a genetic tag (such as a 6x Histidine [His] or Strep tag) is attached to the protein of interest. Using antibodies against the tag or other specific ligands immobilized on magnetic beads, the bait proteins and all the other proteins associated with them are isolated from the cellular contents.

Typical expression systems in bacteria are designed for heterologous or overexpression of proteins of interest. Expression of proteins at 100–1000-fold higher than native concentration can lead to false or nonspecific complexes being formed. A laboratory at the University of Missouri at Columbia recently adapted the Strep tag expression system to *D. vulgaris*, where expression is tightly regulated using a tet promoter. The constitutive expression of the tet repressor gene, which is also encoded on the expression plasmids, guarantees the repression of the promoter in the absence of the inducer. We obtained vulgaris mutant strains expressing Strep-tagged HSP 70 from that laboratory and currently are culturing them at liter-scale.

— *Exogenous method for protein-complex identification.* Many organisms, especially anaerobic bacteria or diatoms, are not easy to genetically engineer. In such cases, one high-throughput approach to isolate interacting proteins is to express

proteins from these organisms in *E. coli* using a commercial expression system such as Gateway from Invitrogen, Inc. The first step in high-throughput expression is the selection of genes to clone. *D. vulgaris* was recently sequenced and has ~ 3500 genes. Based on comparison with the genomes of other organisms such as *E. coli* and proteomics results obtained in our laboratory, we selected 96 genes involved in various stress-responses that are being used for heterologous expression in *E. coli*. We successfully cloned over 80 genes (out of 96) in an expression vector and are currently setting up a high-throughput protein-expression arrangement. After expression of the bait in *E. coli*, we will lyse the cells and use an affinity column to purify the bait.

We successfully cloned over 80 genes (out of 96) in an expression vector and are currently setting up a high-throughput protein-expression arrangement.

Refereed

Chhabra, S., S. P. Gaucher, M. Z. Hadi, and A. K. Singh. 2004. Heat-shock response in *Desulfovibrio vulgaris*: A proteomics study. Paper presented at the 5th International Symposium on the Interface Between Analytical Chemistry and Microbiology (ISIAM), 19–21 April, Richland, Washington.

Gaucher, S. P., S. Chhabra, M. Z. Hadi, and A. K. Singh. 2004. Identification and characterization of proteins involved with stress response in *Desulfovibrio vulgaris*. *Proc. 52nd American Society of Mass Spectrometry Conference on Mass Spectrometry and Allied Topics* **1** (23–27 May, Nashville, Tennessee): 643.

67010

Studies of Signaling Domains in Model and Biological Membranes Through Advanced Imaging Techniques

A. R. Burns, D. J. Frankel

Cellular membranes have complex lipid and protein structures that are laterally organized for optimized molecular-recognition and signal-transduction processes. Knowledge of nanometer-scale lateral organization and its function is of great importance in the analysis of receptor-based signaling, particularly signaling in response to toxins. In model membranes, Sandia will study in detail the chemical and physical factors that result in lateral organization of lipids and lipid-mediated protein sequestration into signaling domains. We will also map the location and follow the dynamic activity of specific membrane proteins involved in the immunological response of mast cells in collaboration with the University of New Mexico (UNM) Health Sciences Center. These studies will be enabled by our proposed development of new imaging methods that will provide both high spatial resolution and sensitivity to dynamical processes. Our technical approach will be to combine the high sensitivity and time resolution of fluorescence imaging with the high lateral resolution of atomic-force microscopy (AFM). Simultaneous fluorescence and AFM imaging allows correlation of the distribution and dynamic activity of specific biomolecules via fluorescence labeling with complete topographic information of the membrane. We successfully used AFM to image topographic features in membranes with less than 1 nm lateral and vertical resolution. We also demonstrated our ability to detect fluorescence emission from single molecules. Since most cellular signaling domains are smaller than the 200 nm diffraction limit imposed on fluorescence imaging, we also seek to develop a fluorescence imaging technique that utilizes the highly localized excitation provided by the strong near-field enhancement at a metal-coated AFM tip. Overall, our unique imaging capabilities will enable us to examine membrane structure and function with much greater detail than was previously possible and thus to provide a better understanding of cellular signaling.

We successfully established combined AFM and fluorescence imaging techniques to analyze membrane organization in both model membrane systems using multicomponent lipid bilayers and biological membranes harvested from rat basophilic leukemia (RBL)-2H3 mast cells.

In the model membrane systems, we used lipids labeled by fluorescent probes either at the head groups or tail groups to enable domain contrast in fluorescence imaging on the basis of partitioning between gel and disordered liquid phases. Correlation with nanometer-level AFM topographic information reveals that the partitioning does not always faithfully report exact gel-domain size or shape. Furthermore, we find that the fluorescence contrast decreases significantly with domain size, such that small domains observed with AFM are not observed in fluorescence images despite adequate optical resolution. We performed imaging of labeled proteins bound to membrane receptors, and the images correlated precisely with gel domains. In all cases, the complete correlation of topographic and fluorescence images provides evidence that gel-phase domains occur across both leaflets of the bilayer. To perform RBL cell-membrane AFM/fluorescence imaging, we developed a procedure for harvesting the membranes from whole, fixed cells. We labeled specific receptors and membrane-associated signaling proteins with fluorescent markers and/or fusion with green fluorescent protein. We imaged receptor clustering that occurs on immune-response activation. In addition to our imaging capabilities, we successfully acquired two-dimensional diffusion constants for labeled membrane lipids using fluorescence correlation spectroscopy (FCS) and correlated the results with membrane topography. Finally, in preliminary studies, we identified key approaches to implement near-field enhancement for subdiffraction fluorescent resolution.

Other Communications

Burns, A. R. 2004. Imaging lipid domains in supported membranes with simultaneous atomic force and fluorescence microscopy. *Biophysical J.* **86** (February): 18A.

67011

Imaging Self-Organization of Proteins in Membranes by Photocatalytic Nanotagging

J. A. Shelnutt, D. Y. Sasaki, A. K. Singh, C. J. Medforth, A. R. Burns

Sandia is developing a new nanotagging technology for detecting and imaging the self-organization of proteins and other components of membranes at nanometer resolution for the purpose of investigating cell-signaling and other membrane-mediated biological processes. We are using protein-, lipid-, or drug-bound porphyrin photocatalysts to grow in situ *nanometer-sized metal particles on proteins and membranes and then using optical and electron microscopy to detect and image the self-organization of protein-protein and membrane-protein complexes. We are initially monitoring the self-assembly of multisubunit proteins such as hemoglobin and horse-spleen ferritin, proteins that naturally bind iron-porphyrin (heme) cofactors and that can be reconstituted with analogous photocatalytically active porphyrins. By exchanging heme in these proteins with a photocatalytic tin (Sn) porphyrin, we can grow a nanoparticle at each heme site on the protein. Electron microscopy (EM) for a tagged multisubunit protein such as hemoglobin shows a symmetric constellation of a specific number of nanoparticle tags, four in the case of the hemoglobin tetramer. We are generalizing the photocatalytic nanoparticle-tagging technique by making porphyrin-drug, porphyrin-lipid, and porphyrin-protein hybrids for nanotagging of non-porphyrin-binding proteins and membrane components. We are using molecular simulations to design these hybrids and to model self-organization and cell-signaling processes. For example, a porphyrin-aspirin hybrid could be used to label and tag the pharmacologically important cyclooxygenase (COX) enzymes in membranes so that the distribution of the protein can be imaged at the nanometer scale. Our nanotagging technique may ultimately allow membrane self-organization and cell-signaling processes to be imaged in living cells. Fluorescence and plasmonic spectra of the tagged proteins can provide additional information about protein association and membrane organization.*

We developed the photocatalytic methods needed for controlled growth of metal nanotags on proteins and demonstrated these methods by the growth and EM imaging of metal nanotags on a porphyrin-modified protein (Sn hemoglobin). These tasks required extensive screening of metal complexes and solution conditions to arrive at a biologically

compatible, purely photocatalytic nanotagging system. The selected system employs the gold (Au)(I) thiourea complex, an ascorbic acid as electron donor, and a Sn(IV)-porphyrin photocatalyst. We labeled hemeproteins, including hemoglobin, ferritin, and ferrochelatase, by substituting Sn protoporphyrin for the naturally occurring heme groups. We performed metal tagging and EM imaging studies using the Sn hemoglobin; transmission-electron microscopy (TEM) images showed clusters of four Au particles, consistent with the tetrameric tetraheme structure of hemoglobin, thus validating our photocatalytic nanotagging approach for proteins. We tagged Sn-porphyrin–labeled horse-spleen ferritin with platinum (Pt) nanoparticles and are tagging ferritin with Au particles and imaging it by EM; the weak binding of Sn porphyrin to ferritin may preclude the investigation of the self-assembly of pretagged ferritin subunits until a covalent porphyrin-labeling scheme is developed in upcoming work. For covalent labeling of proteins, drugs, and lipids, we selected Sn tetrapyridylporphyrins as potential photocatalytic labels. We also investigated the use of liposomes as a membrane platform for photocatalytic nanotagging studies of membrane systems (originally a task for future work). We incorporated Sn porphyrin into the bilayer of liposomes and grew Pt nanoparticles or dendritic “nanoflowers” as nanotags on the liposomes. TEM images show circles of the Pt nanoparticles or nanoflowers with the circle diameters the same as the original liposome diameters. This result indicates that unilamellar liposomes will be satisfactory for future studies of self-organization of protein complexes, drug binding, and raft formation in membranes. We also initiated studies to develop photocatalytic methods for cadmium selenide (CdSe) nanotagging.

Refereed

Haddad, R. E., S. Jia, J. Zhang, K. M. Smith, S. Gazeau, J. Pecaut, J. C. Marchon, C. J. Medforth, and J. A. Shelnutt. 2003. Mechanism and design of molecular devices based on nickel porphyrins. *Abstracts of Papers of the American Chemical Society Meeting* **226** (September, New York, New York): U652.

Shelnutt, J. A., C. J. Medforth, E. Pereira, A. K. Singh, Y. Song, and F. B. van Swol. 2004. Controlled synthesis of dendritic platinum nanostructures. *Proc. Particles 2004* (March, Orlando, Florida): U1001.

Song, Y., S. L. Jia, R. E. Haddad, S. Hok, D. J. Nurco, N. E. Schore, J. Zhang, J. G. Ma, K. M. Smith, S. Gazeau, J. Pecaut, J. C. Marchon, C. J. Medforth, and J. A. Shelnutt. 2004. Energetics and structural consequences of axial ligand coordination in nonplanar nickel tetra(alkyl)porphyrins. *J. American Chemical Society* (June), accepted.

Song, Y., Y. Yang, C. J. Medforth, E. Pereira, A. K. Singh, H. Xu, Y. Jiang, C. J. Brinker, F. B. van Swol, and J. A. Shelnutt. 2004. Controlled synthesis of 2-D and 3-D dendritic platinum nanostructures. *J. American Chemical Society* **126** (2): 635–45.

Song, Y., Y. Yang, C. J. Medforth, E. Pereira, A. K. Singh, H. Xu, Y. Jiang, C. J. Brinker, F. B. van Swol, and J. A. Shelnutt. 2003. Controlled synthesis of 2-D and 3-D platinum dendrites using porphyrin photocatalysts. *Abstracts of Papers of the American Chemical Society Meeting* **226** (September, New York, New York): U687.

67012

Protein Microarrays for Biowarfare-Agent Detection and Characterization

A. E. Herr, V. C. Rucker, A. K. Singh, D. M. Haaland, D. C. Roe

This project is using Sandia's strengths in microfluidics, membrane-protein expression, computational analysis of ligand-binding, and hyperspectral microarray imaging to develop protein microarrays ("protein chips"). Technological means to quickly perform large-scale functional analysis are crucial to closing the information gap between genomics and proteomics. The microarray concept that we are proposing mimics the molecular machinery of the host cell by arraying proteins, ligands, antibodies, and possibly phospholipids, sugars, and oligonucleotides. Protein chips promise to be a revolutionary advance in pathogen detection by enabling high-throughput, rapid (minutes or less) detection of a broad range of dilute (pM) threat agents. The system performs a quantitative multianalyte assay using molecular recognition at bioaffinity-based binding sites. The platform also has the potential to permit fundamental analysis of bioagent-host cell binding.

Traditional immunodiagnostics have limited throughput and are restricted to screening for analyte species only known a priori. *Protein chips could overcome this hurdle by presenting chemically and spatially multiplexed capture sites (micron-scale volumes containing protein-docking sites immobilized in a support structure) for global sample analysis. Our initial work focused on arraying commercially available antibodies, including antibodies with specificity for the* Bacillus *species and for the lethal and edema toxins of* Bacillus anthracis. *We will expand work to include membrane proteins that are the binding targets of threat agents (or components thereof). We began preliminary studies that use microfluidic control to drive a fluorescently labeled analyte sample through the protein array, thus harnessing advantageous surface physics available at small length scales. We will employ hyperspectral scanning and analysis techniques developed at Sandia and also computational biology. While the concept of arrayed deoxyribonucleic acid (DNA) and proteins is not new, no high-throughput, sensitive protein chip has been demonstrated as either a general experimental platform or a biodetector.*

We developed capabilities for the high-throughput arraying of proteins and antibodies on derivatized substrates using modified techniques initially developed for DNA microarray analyses. We developed and implemented robust substrate

preparation, protein-contact printing, substrate blocking, assay incubation, substrate washing, and imaging techniques and protocols. We discovered and addressed substantial differences between DNA and protein microarray development (e.g., exquisite sensitivity of proteins to environmental conditions, importance of nonspecific protein-surface binding). Few researchers have reported on techniques for substrate surface blocking to eliminate nonspecific protein adsorption; however, we developed an effective method to address this issue. We evaluated two model systems using the protein microarray technique: (1) a protein G or protein A and antibody system using a direct detection approach, and (2) an interferon-alpha (IFN-a) and antibody system using a sandwich assay and multicolor detection. The former system allowed us to assess the performance and continue development of the protein arraying technique. We demonstrated 300 µm center-to-center spot resolution, as well as detection limits comparable with those reported in the literature (500 ng/mL protein G), using our nonoptimized system. Each microarray component has a volume of ~ 0.3 to 0.6 nL. The latter model system has enabled increased complexity and improved overall system specificity using a sandwich assay among IFN-a, biotinylated anti-IFN-a, and fluorophore-labeled streptavidin. The IFN-a system has additional significance in that a number of different cell types express IFN-a following induction by viruses, including the Ebola virus. Using the contact-printing microarrayer, we also demonstrated the ability to control the array-printing process with micron accuracy.

Both protein-antibody systems have set the groundwork for developing the biodetection system. At present, we are studying the detection capability of our system, using a suite of proteins potentially important to biowarfare-event identification. We developed microarray assays and associated response curves for six proteins (cholera toxin, diphtheria toxin, anthrax lethal factor and protective antigen, *Staphylococcus enterotoxin B*, and tetanus toxin C-fragment). Further, we investigated protein binding behavior in a complex sample matrix, namely, dilute bovine serum. We currently are extending our work to alternate assay designs, as well as investigating detection of systemic disease biomarkers. We recently began exploring alternate architectures for use with protein microarrays.

Few researchers have reported on techniques for substrate surface blocking to eliminate nonspecific protein adsorption; however, we developed an effective method to address this issue.

Refereed

Havenstrite, K., V. C. Rucker, and A. E. Herr. 2004. Array-based fluorescent profiling of proteins: Principle to practice. Paper presented at the Sandia Student Internship Symposium. 3 August, Livermore, California.

Rucker, V. C., and A. E. Herr. 2004. Antibody microarrays for unlabeled protein detection. Paper presented at the Chips-to-Hits IBC Conference, 20 September, Boston, Massachusetts.

Other Communications

Havenstrite, K., V. C. Rucker, and A. E. Herr. 2004. Array-based fluorescent profiling of proteins: Principle to practice. Poster presented at the Sandia Student Internship Symposium, 3 August, Livermore, California.

Herr, A. E., and V. C. Rucker. 2004. An overview for Beth George, DHS: Protein microarrays for biowarfare-agent detection and characterization. Sandia internal memorandum, 3 August, Livermore, California.

Rucker, V. C., A. K. Singh, D. M. Haaland, D. C. Roe, and A. E. Herr. 2004. Protein microarrays for profiling of complex samples. Paper presented at the Sandia BS&T Symposium, 26 October, Santa Fe, New Mexico.

Rucker, V. C., and A. E. Herr. 2004. Antibody microarrays for fluorescence-based analyte profiling. Paper presented at the Seminar for Physical Bioscience Division at Lawrence Berkeley Labs, 3 July, Berkeley, California.

67013

Interaction of Proteins with Lipid Films

M. S. Kent, D. Y. Sasaki, L. J. D. Frink, M. P. Sears

Understanding protein assembly at interfaces is of vital interest to a range of important technology areas at Sandia, including membrane signaling and recognition, toxin detection, mitigating the effects of toxins/biowarfare agents, and nanoscience. While techniques are well developed at Sandia to probe lipid mobility and aggregation within monolayers and bilayers, little capability currently exists at Sandia to examine protein conformations at lipid membranes. Specific issues to be addressed are protein orientation and surface density, monolayer versus multilayer adsorption, conformational changes upon adsorption including denaturization, the penetration of proteins into lipid membranes, the role of specific versus nonspecific interactions, and lateral order of crystallization. We apply neutron and x-ray scattering techniques to address these questions, along with more-traditional experimental methods and calculations using fluid/polymer density-functional theory (DFT). This combined approach allows new insights into protein-membrane interactions, enabling the design of improved biosensing techniques, inhibitors and receptors for biological toxins, and smart biomimetic systems for nanoscience initiatives. We obtained structural data on three systems: amphipathic, pore-forming peptides; synthetic helical peptides designed to adsorb to, but not penetrate, lipid membranes; and globular proteins adsorbing to lipid membranes through specific interaction sites. These techniques revealed a number of new insights such as preferred orientations upon adsorption, instability of secondary and tertiary structure upon adsorption, conditions for the insertion of peptides, and reversibility. For example, we learned that at constant pressure, the pore-forming peptide melittin penetrates the membrane upon adsorption, even at very low bulk concentrations.

These techniques [to examine protein conformations at lipid membranes] revealed a number of new insights such as preferred orientations upon adsorption, instability of secondary and tertiary structure upon adsorption, conditions for the insertion of peptides, and reversibility.

We studied helical, amphipathic pore-forming peptides (alamethicin and melittin) to focus on the process of peptide insertion into membranes. We determined the pressure-area-time behavior to supplement the structural data from the scattering techniques. We performed studies as a function of bulk peptide concentration for both alamethicin and melittin adsorbing to dipalmitoyl phosphatidylcholine (DPPC). Neutron reflection (NR) using protonated lipids and an H_2O subphase showed that little insertion occurs when the membrane is

maintained at constant area, whereas strong insertion occurs for constant membrane pressures between 30 and 35 mN/m. We also found insertion to be a strong function of bulk peptide concentration. Analogous experiments using deuterated lipids and a D_2O subphase were the most revealing, showing that, at constant pressure, melittin never adsorbs side-on to the head groups, but always penetrates the membrane upon adsorption. At constant area, some side-on adsorption appears to occur. We performed synchrotron x-ray reflection (XR) and diffraction (XRD) on the same system. Limited contrast hampered the reflectivity experiments, but the diffraction showed transient crystalline peaks. Further work is required to understand the origin of these peaks.

We studied synthetic helical peptides designed to adsorb to, but not penetrate into, lipid membranes. A colleague at the University of Delaware synthesized three helical peptides with specific amino acid sequences. For one of these, adsorption to copper (Cu)(II)-distearyl iminodiacetate (DSIDA) was studied by XR. The thickness of the adsorbed peptide layer was between 12 Å and 16 Å, in excellent agreement with the dimension of the helix adsorbed side-on. The surface density corresponded to less than half a dense-packed monolayer. The adsorption experiment was performed at constant area, and the pressure increased substantially after introducing the peptide. This may indicate that some portion of the peptide inserted into the monolayer.

We also studied globular proteins (myoglobin and lysozyme) adsorbing to crystalline- and fluid-phase lipid films by metal-ion chelation. Time-dependent NR data provided snapshots of the adsorbed layer structure during the adsorption process at 30 min intervals. We observed differences in the thickness and segment density versus time (or number of adsorbed molecules) for the cases of chelated Cu(II) and nickel (Ni)(II) ions, and we attributed these differences to the different interaction strengths. The thickness of the protein layer for high bulk concentration at early times was the same as that for low concentrations at equilibrium, indicating that the adsorbed layer structure is a function only of the number of protein molecules adsorbed. We performed experiments in which the subphase was exchanged with pure buffer after the adsorbed layer was established. These showed that adsorption was nonequilibrium for all stages of the adsorption process for myoglobin adsorbing to Cu(II)- and Ni(II)-loaded iminodiacetate (IDA). Taken together, the data appear to indicate greater denaturation for the case of chelated Cu ions. We discovered that protein adsorption disturbs the lipid crystalline packing when the membrane is

maintained at constant pressure (≤ 40 mN/m) for both Cu-IDA and Ni-IDA. Surprisingly, the disruption occurs at a very early stage of the adsorption process where little adsorbed protein can be detected by NR. This may indicate rapid denaturation after adsorption. We detected no effect on lipid packing when the membrane was held at constant area with an initial pressure of 40 mN/m.

We also developed a supported lipid bilayer system involving polyethylene glycol chains to act as spacers, and an amine group on one end to anchor to the substrate and a cholesterol group on the other end to insert into the lipid bilayer. We developed a DFT of lipid bilayers and compared it with molecular dynamics simulations.

We progressed in our development of a liposome leakage assay for selective interaction with tetanus toxin under a pH gradient, and in the synthesis of glycolipids for the selective binding of specific lectins.

Refereed

Frink, L. J. D., and A. Frischknecht. 2004. Coarse-grained lipids I: A density-functional theory approach and thermodynamics of fluid bilayers. *Biophysical J.*, submitted.

Frischknecht, A., and L. J. D. Frink. 2004. Coarse-grained lipids II: A comparison of density-functional theory and simulation. *Biophysical J.*, submitted.

Kent, M. S., H. Yim, D. Y. Sasaki, S. Satija, J. Majewski, and T. Gog. 2004. Analysis of myoglobin adsorption to Cu(II)-IDA and Ni(II)-IDA functionalized Langmuir monolayers by grazing incidence neutron and x-ray techniques. *Langmuir* **20** (7): 2819.

Kent, M. S., H. Yim, D. Y. Sasaki, S. Satija, Y. S. Seo, J. Majewski, E. Watkins, and T. Gog. 2004. Protein adsorption to lipid membranes through metal ion chelation studied by x-ray and neutron reflectivity and GIXD. Paper presented at the Workshop on Membranes, August, Argonne, Illinois.

Other Communications

Kent, M. S., H. Yim, D. Y. Sasaki, J. Majewski, and T. Gog. 2004. Analysis of myoglobin adsorption to Cu(II)-IDA and Ni(II)-IDA functionalized Langmuir monolayers by grazing incidence neutron and x-ray techniques. *Proc. American Chemical Society Meeting* (April, Anaheim, California).

Kent, M. S., H. Yim, D. Y. Sasaki, S. Satija, J. Majewski, and T. Gog . 2004. Analysis of myoglobin adsorption to Cu(II)-IDA and Ni(II)-IDA functionalized Langmuir monolayers by grazing incidence neutron and x-ray techniques. (Invited) Paper presented at the American Conference on Neutron Scattering, June, College Park, Maryland.

Kent, M. S., H. Yim, D. Y. Sasaki, S. Satija, J. Majewski, and T. Gog. 2004. Analysis of myoglobin adsorption to Cu(II)-IDA and Ni(II)-IDA functionalized Langmuir monolayers by grazing incidence neutron and x-ray techniques. Paper presented at the American Physical Society Meeting, March, Montreal, Canada.

Kent, M. S., H. Yim, D. Y. Sasaki, S. Satija, J. Majewski, and T. Gog. 2003. Analysis of myoglobin adsorption to Cu(II)-IDA and Ni(II)-IDA functionalized Langmuir monolayers by grazing incidence neutron and x-ray techniques. (Invited) Paper presented at the LANSCE User Group Meeting, October, Los Alamos, New Mexico.

Kent, M. S., H. Yim, D. Y. Sasaki, S. Satija, J. Majewski, and T. Gog. 2004. Analysis of myoglobin adsorption to Cu(II)-IDA and Ni(II)-IDA functionalized Langmuir monolayers by grazing incidence neutron and x-ray techniques. (Invited) Paper presented at the lecture series Advanced Photon Source, April, Argonne, Illinois.

67014

New Technologies for Understanding Membrane-Protein Recognition and Signaling

M. D. Leavell, A. M. Highley, K. L. Sale, P. Novak

Structural elucidation of membrane proteins is often difficult by standard techniques (e.g., x-ray crystallography and nuclear magnetic resonance [NMR]), due to the hydrophobicity of the proteins, and thus development of alternative strategies is paramount. Mass spectrometry (MS) in three dimensions (or MS3D), which combines chemical cross-linking, MS, and theoretical modeling, is a good candidate to study membrane proteins and other hard-to-study proteins, such as self-digesting proteases or aggregating proteins, due to the low concentration of sample necessary and the speed of the technique. CD69 is a vitally important membrane protein expressed on the surface of leukocytes; it is required to recognize antigens from virus- and bacteria-infected and cancer cells, thus directing the immune response. Utilizing MS3D, Sandia will study the structure of the carbohydrate recognition domain of CD69 and the conformational changes induced by antigen complexation and metal binding. We will determine the ligand binding site through chemical labeling of reactive side chains, and we will characterize the conformational changes that occur upon binding of the ligand using chemical cross-links of different lengths (molecular rulers). Dovetailed with the biological application of CD69 structural investigation is the development of new cross-linking methods and data interpretation, which will further develop and improve MS3D. Utilization of new cross-linkers will increase the accuracy of protein structures generated by MS3D.

We developed new chemistries to form the following cross-links: lysine-lysine/N-terminus, tyrosine-tyrosine, and lysine-tyrosine....In addition, we recently developed a methodology with the succinimidyl ester cross-linkers to cross-link a lysine residue to a tyrosine residue, allowing the generation of even more cross-links than with the homoreactive cross-linkers currently utilized.

We developed new chemistries to form the following cross-links: lysine-lysine/N-terminus, tyrosine-tyrosine, and lysine-tyrosine. In particular, we used the succinimidyl ester cross-linkers to cross-link the primary amine containing amino acids in ubiquitin (e.g., lysine and the N-terminus), while using the imidazole cross-linkers to cross-link tyrosine in cytochrome C. In addition, we recently developed a methodology with the succinimidyl ester cross-linkers to cross-link a lysine residue to a tyrosine residue, allowing the generation of even more cross-links than with the homoreactive cross-linkers currently utilized. We developed and tested each of these two methodologies on standard proteins (e.g., ubiquitin for the tyrosine cross-linkers and oxidized insulin-b-chain for the

lysine-tyrosine cross-linkers). As a result of this work, we filed a technical advance.

The carbohydrate recognition domain (CRD) of CD69 has been expressed in *Escherichia coli* (*E. coli*) and purified. A mass spectrum of the CRD revealed that it was of the correct molecular weight. Analysis of the protein under denaturating and buffered conditions indicates that the protein is properly folded. To improve mass spectral analysis, we developed a method for denaturation/reduction of the protein. This method improves the yield of product ions from the protein upon collision-induced dissociation, allowing localization of the cross-links. Currently, chemical cross-linking is under way to determine the structure of the CRD of CD69 in the absence of calcium. Initial studies are focusing on lysine-lysine cross-linking of the protein, followed by tyrosine-tyrosine and tyrosine-lysine cross-linking. Fortuitously, there are also three cysteines available for cross-linking, which will increase the number of cross-links and give further insight into the structure of the protein.

In addition to the developed succinimidyl ester, cross-linking chemistries have been developed to cross-link the acidic amino acids (e.g., glutamic acid, aspartic acid, and the C-terminus). We tested this chemistry with exciting results on the protein ubiquitin, and it resulted in a manuscript that we submitted to the *Journal of the American Society for Mass Spectrometry.*

Refereed

Leavell, M. D., P. Novak, C. R. Behrens, and G. H. Kruppa. 2004. Strategy for selective chemical cross-linking of tyrosine and lysine residues. *J. American Society for Mass Spectrometry,* in press.

Novak, P., G. H. Kruppa, M. M. Young, and J. S. Schoeniger. 2004. A top-down method for the determination of residue-specific solvent accessibility in proteins. *J. Mass Spectrometry* **39** (3) (February): 322–28.

Other Communications

Haskins, W. E., P. Novak, M. D. Leavell, Y. K. Light, K. L. Sale, M. M. Young, J. S. Schoeniger, and G. H. Kruppa. 2004. Top-down characterization of ligand-induced conformational changes by chemical cross-linking and Fourier-transform mass spectrometry. *Proc. 52nd American Society for Mass Spectrometry National Conference on Mass Spectrometry and Allied Topics* (May, Nashville, Tennessee): in press.

Leavell, M. D., P. Novak, W. E. Haskins, Y. K. Light, M. Z. Hadi, G. H. Kruppa, and J. S. Schoeniger. 2004. Structural characterization of MIP1a: Chemical cross-linking and top-down sequencing. *Proc. 51st American Society for Mass Spectrometry National Conference on Mass Spectrometry and Allied Topics* (May, Nashville, Tennessee): in press.

Novak, P., W. E. Haskins, M. D. Leavell, M. J. Ayson, J. S. Schoeniger, and G. H. Kruppa. 2004. Single-residue resolution of cross-link positions using ECD–FTMS. *Proc. 52nd American Society for Mass Spectrometry National Conference on Mass Spectrometry and Allied Topics* (May, Nashville, Tennessee): in press.

Chemical and Earth Sciences

Research and development in the Chemical and Earth Sciences (C&ES) investment area is key in providing solutions to a host of energy and national security challenges. Homeland security challenges are foremost, followed by longer-term infrastructure, natural resource utilization, and sustainability challenges. Chemical and Earth Sciences investments work toward ensuring the security and sustainability of natural resources, standoff detection and characterization for security and environmental applications, improving repository performance, and consequence mitigation for terrorist events. C&ES expertise aids in the advancement of multidisciplinary science and technology across core organizations, including research in combustion, chemical kinetics and dynamics, molecular simulations, mechanics and physics of earth materials, lasers, and sensors.

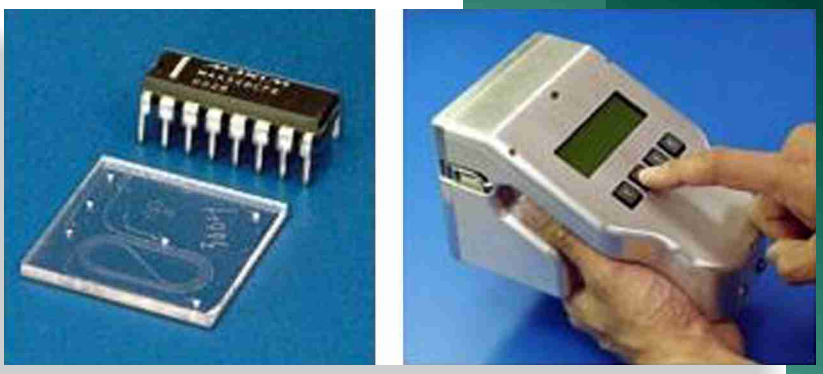

52538
"Sequestration of Pathogens on Nanoengineered Surfaces"

Recent events have heightened awareness of the vulnerability of U.S. water resources to bioterrorism. There is a critical need for both rapid-sensing and improved mitigation technologies. Scientists have developed materials that sequester pathogens based on chemical interactions, rather than on size alone. Using these materials, a preconcentrator that captures and concentrates pathogens from water streams was developed for advanced sensing in a μChemLab™ biosensor. Filtration materials that allow for lower pressures, higher flowrates, and improved efficiency relative to current ultrafiltration technology were then developed to enhance mitigation. Researchers developed the capabilities to concentrate and separate gram-positive and gram-negative bacteria through novel adsorption techniques using poly(N-isopropyl acrylamide) (PNIPAM) and polyoxometalates (POMs). Partnership research performed at Kansas State University indicated that innovative glass beads can be used in enzyme-linked immunosorbent assay (ELISA) and polymerase chain reaction (PCR)–based assays. Continuing research investigates the antiviral efficacy of polyoxoniobate, water-soluble clusters.

52538

Sequestration of Pathogens on Nanoengineered Surfaces

M. S. Kent, G. S. Chirica, M. D. Nyman, J. A. Fruetel, J. G. Curro, D. L. Huber

Recent events have heightened awareness of the vulnerability of U.S. water resources to bioterrorism. A critical need exists for both rapid sensing and improved mitigation technologies. Sandia is developing materials that sequester pathogens based on chemical interactions rather than on size alone. We will target these materials for both sensing and improved water-treatment applications. Regarding sensing, we will develop a preconcentrator for a µChemLab™ biosensor that will capture and concentrate pathogens from water streams. Regarding mitigation, we will develop filtration materials that allow for lower pressures, higher flowrates, and improved efficiency relative to current ultrafiltration technology. We focused on two materials shown previously to interact strongly with bacteria or viruses: poly(n-isopropyl acrylamide) (PNIPAM) and polyoxometalates (POMs). PNIPAM is the best-known temperature-responsive polymer, possessing a lower critical-solution temperature (LCST) at 31ºC. Our collaborators at the University of New Mexico (UNM) showed that bacteria reversibly adsorb/desorb onto PNIPAM–coated surfaces as the temperature is varied above and below the LCST. POMs are anionic, metal-oxo clusters with 6–30 metal octahedra of tungsten (W), molybdenum (Mo), niobium (Nb), vanadium (V), or tantalum (Ta), often assembled around one or two central tetrahedra. POM clusters have a charge ranging from ~ -4 to -20 and are known to interact strongly with viruses and some bacteria through electrostatic interactions. We demonstrated the ability to concentrate bacteria by adsorption to various coated media followed by release in a concentrated pulse using a surfactant.

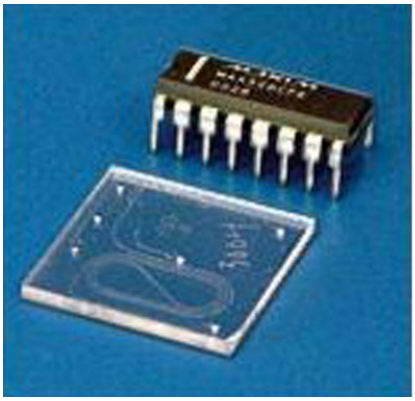

Sandia biosensors based on protein fingerprinting.

We demonstrated preconcentration for gram-positive and gram-negative species using a macroscale column and also a microcolumn that was designed for integration with the Sandia biosensor device. In further work, we demonstrated that a gram-positive and a gram-negative species can be separated by our methods. We also progressed in understanding the fundamental interactions involved in the adsorption process. We made progress in modeling the temperature transition of PNIPAM. Virus-adsorption assays and antiviral-efficacy assays were performed at Kansas State University (KSU).

We demonstrated the ability to concentrate bacteria by adsorption to a surface followed by release in a concentrated pulse using a surfactant. We demonstrated preconcentration using a macroscale column and also a microcolumn that we designed for integration with the biosensor device developed at Sandia. We accomplished this milestone for both a gram-negative species (*Cobetia marina*) and a gram-positive species (*B. atrophaeus*). For *C. marina* adsorbed to glass beads coated with octadecyltrichlorosilane, we obtained a maximum concentration factor of ~ 200. For *B. atrophaeus* in the log phase, only a small fraction of the cells were retained in the column in the first step. For clean glass beads, which present a hydrophilic surface, the peak concentration was 17x that of the input concentration. We observed a greater cell retention and a greater maximum cell concentration upon elution (a factor of 31 over input) with surfactant using PNIPAM–coated beads held at room temperature (T) (hydrophilic state) than for the hydrophilic, clean glass beads. While we performed most of the assays using deoxyribonucleic acid/ribonucleic acid (DNA/RNA) extraction and a fluorescent dye, we also developed a real-time fluorescence assay for use with the microcolumn.

We also progressed in understanding the fundamental interactions involved in the adsorption process. Our UNM colleagues completed the initial analysis of Lewis acid-based interactions—the attachment of *C. marina* to model solid surfaces. Contact-angle analysis using a nonpolar solvent (hexadecane), a polar solvent (water), and a Lewis basic solvent (formamide), and the van Oss equations for calculating van der Waals, Lewis acid, Lewis base, and polar contributions to total surface energy gave the most consistent results. We did not observe a clear relationship between any one energetic parameter and attachment of *C. marina*. However, we did observe a strong statistical correlation between attachment of *C. marina* and the hydrophobicity (i.e., van der Waals interaction) and Lewis acidity of the solid substratum, with attachment

being negatively correlated with a highly polar or basic surface. We currently are investigating whether these components can be optimized to give maximum (or, conversely, minimal) adhesion. For *B. atrophaeus*, we found that affinity depends strongly on the growth state. In the log phase, the affinity of *B. atrophaeus* for both hydrophilic and hydrophobic controls was very low. However, in the log phase, we found a strong adsorption to both hydrophilic and hydrophobic surfaces in the presence of a high salt concentration. In the late stationary phase with standard growth media, we found a very strong adsorption to both hydrophilic and hydrophobic surfaces.

In further work, we demonstrated that the abovementioned two species can be separated by our methods using multiple columns. In one experiment, we used two identical columns of PNIPAM, but held them at different temperatures (45°C and 12°C). We introduced a mixture of *C. marina* and *B. atrophaeus* in artificial seawater to the first column, and then we introduced the solution that eluted from the first column (45°C) into the second column (12°C). We found that the first column was slightly enriched in *C. marina* and that the second column was loaded nearly 100% with *B. atrophaeus*. This demonstrates that species separation can be achieved to some degree, in addition to preconcentration.

We determined the dependence of the temperature-dependent conformational transition of PNIPAM on surface density and molecular weight using density-functional theory (DFT) calculations and neutron-reflection experiments.

Virus-adsorption assays performed at KSU indicated that our coated glass beads can be used to capture viruses; the beads can also be used in enzyme-lined immunosorbent assay (ELISA) and in polymerase chain reaction (PCR)–based assays. Also, KSU began investigating the antiviral efficacy of a variety of polyoxoniobate, water-soluble clusters. Cytotoxicity studies show that the polyoxoniobates are actually less toxic than the previously investigated polyoxometalates. Initial virus-challenge tests indicate that the hexaniobate and Keggin polyoxometalates do result in a decrease in viral outgrowth.

Refereed

Mendez, S., and J. G. Curro. 2004. Integral equation theory of polymer solutions: Application to polyethylene/benzene solutions. *Macromolecules* **37** (5): 1980–86.

Mendez, S., J. G. Curro, J. D. McCoy, and G. P. Lopez. 2004. Computational modeling of the temperature-induced structural changes in poly(n-isopropyl acrylamide) with self-consistent field theory. *Macromolecules*, submitted.

Ye, Y., J. D. McCoy, and J. G. Curro. 2003. Application of density-functional theory to tethered polymer chains: Effect of intermolecular attractions. *J. Chemical Physics* **119** (1): 555–64.

Yim, H., M. S. Kent, S. Mendez, S. S. Balmurugan, G. P. Lopez, and S. Satija. 2004. Temperature-dependent conformational change of PNIPAM–grafted chains at high-surface density in water. *Macromolecules* **37** (14): 1994.

Yim, H., M. S. Kent, S. Satija, S. Mendez, S. S. Balmurugan, and G. P. Lopez. 2004. Study of conformational change of PNIPAM–grafted chains in water using neutron reflection: Molecular-weight dependence at high grafting density. *J. Polymer Science, Polymer Physics* **42** (17): 3302.

Other Communications

Curro, J. G. 2004. Molecular packing of polymers in the condensed state and the effects of confinement. (Invited) Paper presented at the University of Illinois, Department of Materials Science and Engineering, November, Urbana, Illinois.

Kent, M. S., H. Yim, S. Mendez, S. S. Balmurugan, G. P. Lopez, and S. Satija. 2004. Temperature-dependent conformational change of PNIPAM–grafted chains in water: Effects of molecular weight and grafting density. (Invited) Paper presented at the American Physical Society Annual Meeting, Montreal, Canada.

Lopez, G. 2004. Structure-property relationships for model and practical smart polymer surfaces. (Invited) *Proc. American Chemical Society Meeting, Preprints* (March, Anaheim, California).

Lopez, G. 2004. Technologies for CB defense: Smart materials, biomimetics, MEMS, and NEMS. Paper presented at the DTRA/University Strategic Partnership Workshop, 27 July, Washington, D.C.

Mendez, S., B. Subramanian, S. S. Balmurugan, G. P. Lopez, J. D. McCoy, H. Yim, M. S. Kent, and J. G. Curro. 2003. Characterization and modeling of temperature-induced structural changes of poly(n-isopropyl acrylamide) brushes. *Proc. American Institute of Chemical Engineers Meeting* (San Francisco).

Mendez, S., J. G. Curro, and J. D. McCoy. 2004. Application of self-consistent field theory to model the temperature response of tethered poly(n-isopropylacrylamide) chains. Paper presented at the American Physical Society Meeting, March, Montreal, Canada.

52539

A Combined Preconcentrator and Sensor for Live Waterborne Pathogens

E. B. Cummings, G. J. McGraw, B. H. Lapizco-Encinas, B. A. Simmons

The insulator-based electrodeless dielectrophoretic (iDEP) concentrator concept was designed to work by a sequence of physically specific interactions. (1) During collection, a moderate applied direct-current (dc) electric field dielectrophoretically traps particles in size-specific zones of the device containing a high-volume, nonuniform array of insulating posts, while other solutes and water flow unimpeded to a waste stream. (2) Trapped particles within a selected size range are released in a concentrate to a medium-volume array having a dc offset. Particles are retrapped in zones of this secondary device that are specific to the internal physique of the particles. (3) Selected particles are then released to a tertiary low-volume dielectrophoretic sieve bearing an electric-field–generated conductivity gradient to further filter and select particles that physically respond to osmolality and conductivity, a live-particle signature. (4) A sharply pulsed electric field lyses the selected cells, releasing their contents to a canonical microfluidic separation channel. This will be the first device that uses physics that occur at the microfluidics scale to take large sample volumes to small sample volumes.

Our data indicate that bacteria trap at lower field strengths than spores, which trap at lower electric-field strengths than viruses. We also demonstrated bacterial and particle trapping in plastic devices. We characterized the existing, lowest-volume concentrator stage for removal efficiency and concentration factor. We are in the process of evaluating the larger-volume stages in plastic. The final goal remains the coupling between the dielectrophoretic concentrator and a microfluidic separation channel for practical water monitors based on a wide range of separation and sensor technologies.

This will be the first device that uses physics that occur at the microfluidics scale to take large sample volumes to small sample volumes. Our data indicate that bacteria trap at lower field strengths than spores, which trap at lower electric-field strengths than viruses.

We demonstrated the separation of live and dead bacteria by achieving dielectrophoretic trapping of both live and dead cells into two distinctly separated bands. We accomplished the separation between different species of live cells. We separated gram-negative *Escherichia coli* (*E. coli*) from gram-positive *Bacillus* bacteria, and we achieved the selective dielectrophoretic trapping of mixtures of *Bacillus* bacteria. We achieved concentration of *B. subtilis* and *B. thuringiensis* spores at higher applied electric fields than those used with bacterial

cells. We accomplished selective dielectrophoretic trapping of Tobacco Mosaic Virus at higher electric fields and in the presence of an inert background of 200 nm polystyrene particles. We carried out performance characterization of our proof-of-concept devices, and we demonstrated that removal efficiencies up to 93% can be achieved for *E. coli* cells. The concentration factor obtained in our microdevice is at least one order of magnitude. We successfully started the transition from glass devices to polymeric devices. We accomplished initial testing of polymeric-based chips and obtained successful results. We demonstrated dielectrophoretic trapping and release of bacterial cells and spores. We are making plastic devices from three different materials: Z1060 (Zeonor®), T8007 (Topaz), and polycarbonate. We achieved success in polymeric substrates derived from both injection molding and hot-embossing replication technologies. Finally, our work generated a total of three publications in peer-reviewed journals, six conference presentations, and two posters. We submitted a manuscript to the *Journal of Microbial Methods* that shows bacteria removal efficiencies of 90% or greater. The selectivity between bacteria genus and species is in press in *Electrophoresis*. *Analytical Chemistry* published the live-dead bacteria separation demonstrated in previous work and featured our work on the cover.

Refereed

Lapizco-Encinas, B. H., B. A. Simmons, E. B. Cummings, and Y. Fintschenko. 2004. Dielectrophoretic concentration and separation of live and dead bacteria in an array of insulators. *Analytical Chemistry* **76** (6): 1571–79.

Lapizco-Encinas, B. H., B. A. Simmons, E. B. Cummings, and Y. Fintschenko. 2004. Insulator-based dielectrophoresis for the selective concentration and separation of live bacteria in water. *Electrophoresis* **2** (10–11) (June): 1695–1704.

53586

Geophysical Subsurface Imaging and Interface Identification

C. J. Weiss, R. S. Tuminaro, D. M. Day, P. B. Bochev

Geophysical subsurface imaging is recognized as vital for addressing the national security challenges faced by this nation. In energy security, geophysical imaging has been essential in locating oil and gas fields, thus helping to lessen this nation's dependence on foreign oil. It is also a critical technology in detecting and characterizing underground facilities, including hard and deeply buried targets (HDBTs) and subsurface contamination related to Department of Energy waste legacy issues. Geophysical imaging relies on the mathematical process called inversion. To stabilize the process, a smooth model constraint is typically imposed on the subsurface geophysical properties (conductivity, velocity, density, etc.) such that they are only allowed to vary smoothly. While such constraints can eliminate unrealistic geological models, they come with a price of reduced model resolution, seriously limiting the applicability and relevance of geophysical imaging technologies for national security concerns. Initially, Sandia will emphasize electromagnetic (EM) applications. However, the scope of the proposed methodology is much broader and is pertinent to other geophysical applications, medical imaging, and nondestructive evaluation of materials in engineering.

To address this problem, we are implementing a new type of geophysical inversion for interface identification. It will enable the location of underground structures and facilities, oil and gas deposits, and environmental-site characterization at a scale not previously possible. Construction of the interfaces will require that new optimization procedures and massively parallel linear and nonlinear solver tools be developed under the Accelerated Strategic Computing Initiatives (ASCI) program. We will use exact sequences of finite-element (FE) methods to discretize Maxwell's equations. We will extend optimal algebraic multigrid solvers to handle variable conductivity and complex coefficient matrices. To obtain reliable and sharp interfaces, we will first use smooth reconstructions of the interface for the initial topology estimate, followed by well-posed parameterization of the surfaces based on interface tracking, fictitious domains, and level-set approaches.

...we are implementing a new type of geophysical inversion for interface identification [that] will enable the location of underground structures and facilities, oil and gas deposits, and environmental-site characterization at a scale not previously possible.

We developed an FE code that assembles and solves discretizations of Maxwell's equations in the time and

frequency domains on general unstructured meshes. This was made possible, in part, by leveraging TRILINOS packages and software development and maintenance tools. This software development is centered on the notion of a discrete De Rham complex, a mathematical construct necessary for the accurate modeling and solution of EM phenomena that presently are not available in standard Sandia software libraries. Such a complex allows for a discretization of Maxwell's equations that is free of spurious modes and mimics the topological structure of the original problem. We implemented the complex for unstructured hexahedral grids. In addition to edge elements (one-forms) for discretization of the electric field, the complex provides face elements (two-forms) needed to represent currents and magnetic fluxes, and nodal elements (zero-forms) needed for the multilevel solver. These elements are required for the next stage of project development. Most notably, the multilevel solver and the application of the regularization in the inversion process both require zero-forms consistent with the definition of the one-forms used in Maxwell's equations.

We assessed the convergence properties of FE software by analyzing the accuracy of the software in recovering manufactured solutions. For those problems tested, the observed convergence behavior matches the theoretical predictions.

We developed a C++ container class that acts as an interface to FORTRAN subroutines for FE analysis. This broadens the usefulness of the FE software for geophysical applications by enabling scattered field formulations of dipole and plane-wave source excitations.

We demonstrated that the first 100 eigenvalues of the discretized curl-curl linear system used in the FE software match those found by exact methods. The convergence rate of the discrete eigenvalue estimates matches theoretical predictions and decreases quadratically with grid node spacing.

We made significant enhancements on numerical aspects of adjoint inversion methodologies. The improvements are centered on line-search, grid coarsening, and quasi-Newton optimization. We documented the details in an upcoming paper to appear in the journal *Inverse Problems.*

Computational and Information Sciences

Computational and Information Sciences investments support DOE's nuclear weapons mission, and all Sandia business units, by developing next-generation computing and information capabilities. Applications include nuclear weapons safety and reliability, design, manufacturing, electrical systems, microelectro-mechanical systems (MEMS), biotechnology, and homeland security. Recent advances in massively parallel (MP) computing technology are greatly expanding diversity and application of simulations. Growth areas include modeling complex phenomena, multiscale modeling, optimization and prediction under uncertainty, advanced architectures, and informatics. Current efforts are driving at abilities to develop system-scale modeling of nuclear weapons, to predict the reliability of micromachines, and to aid in the design process for virtual prototyping.

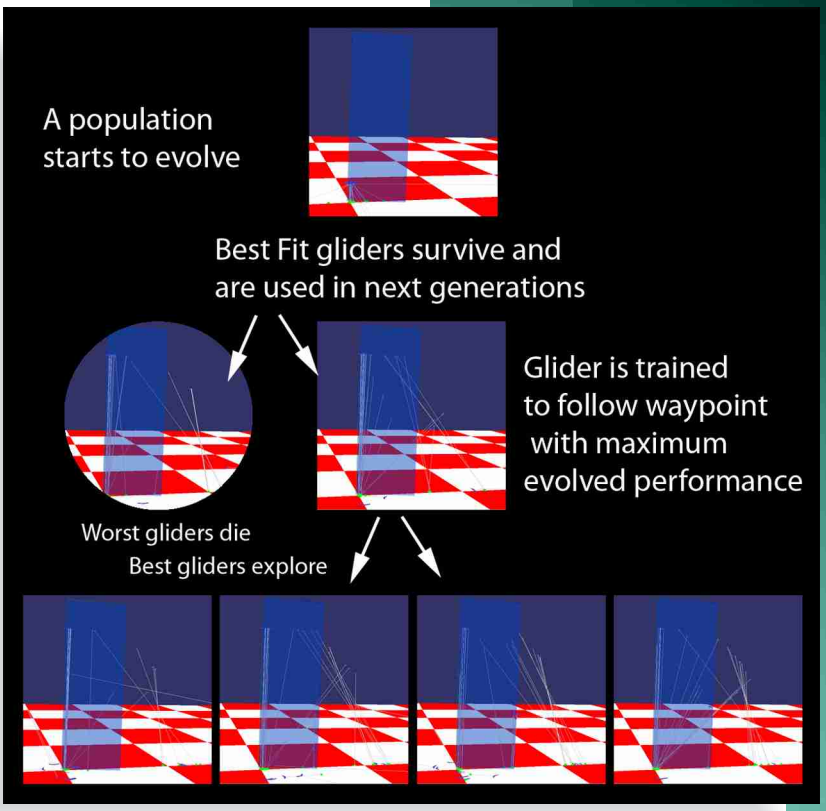

38610

"Graduated Embodiment for Sophisticated-Agent Evolution and Optimization"

Problems related to national security, ranging from urban warfare to unmanned aerial vehicle (UAV) reconnaissance, involve intelligent systems. This project developed and implemented evolutionary methods to computationally optimize the behavior of artificial intelligence (AI) agents. Researchers designed a simulation to test agents and developed a fitness function for agent evaluation. A fully object-oriented genetic programming engine was integrated with a modeling and simulation framework. A synthetic environment that ranges from a low-fidelity "toy-world" universe to high-fidelity realism was created using high-performance MP computers and state-of-the-art programming techniques.

Behavior developers are able to observe agent behaviors as they evolve and create a comprehensive behavior-system hierarchy that incorporates cognitive, instinctual, and reflexive levels of behavior and physical model attributes. Integrated tools have broad applicability for physical and non-physical modeling. Future research will drive to generate genetic programs that are competitive with human-produced results that are applicable in real-world situations.

38610

Graduated Embodiment for Sophisticated-Agent Evolution and Optimization

M. B. E. Boslough, M. D. Peters, C. R. Jorgensen, A. Breckenridge

Problems related to national security, ranging from urban warfare to unmanned airborne vehicle (UAV) reconnaissance, involve intelligent systems. In this project, Sandia developed and implemented evolutionary methods to computationally optimize behaviors by designing a representation for solutions and defining a fitness function by which they can be evaluated. Our ultimate goal is to generate genetic programs that are competitive with human-produced results and that can be used in real-world applications.

We pursued this goal by developing a modeling and simulation (ModSim) environment based primarily on the Sandia framework UMBRA, a modular ModSim system, and by building genetic programming methods that we integrated into the UMBRA ModSim framework. We developed a fully object-oriented genetic programming engine (Distributed Generic Genetic Programming [DGGP]) and integrated it with UMBRA. We developed a parallelization method that allows the code to run on a large number of processors. This uses evolutionary programming techniques to provide behavior algorithms that are evolved using high-performance massively parallel (MP) computers, providing a synthetic environment that ranges from a low-fidelity "toy world" universe to high-fidelity realism.

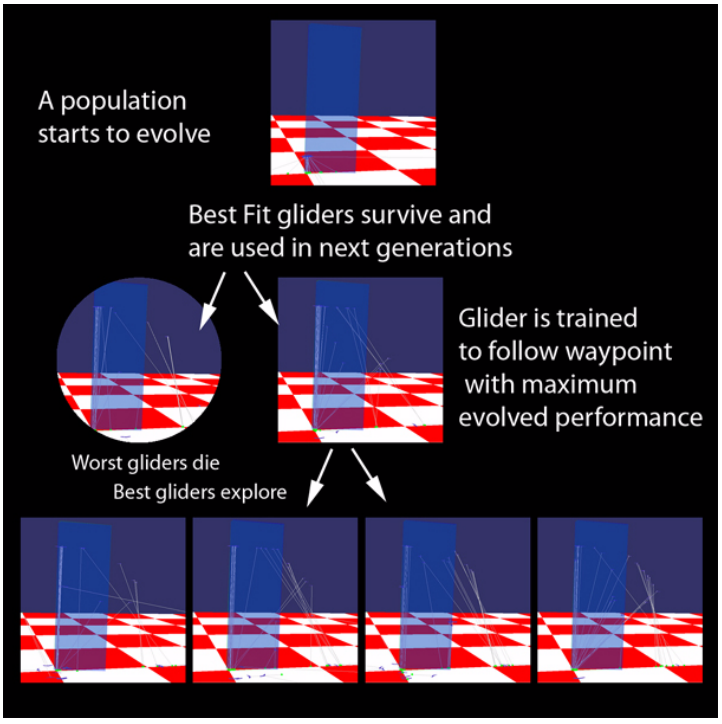

UMBRA's modeling and simulation capabilities are combined with genetic programming to visually show the results for each optimization stage as the computer evolves a segment of code to control the behavior of an autonomous glider that balances exploration with exploitation of local conditions.

The concept of "graduated embodiment" is captured by our strategy of progressive fitness evaluation through multiple levels of fidelity, using methods of staged optimization and incremental adaptation. Initial behaviors evolve in a low-fidelity universe to keep the computational requirement at a practicable level. As robust and useful behaviors develop, they can be "tuned" at a higher-fidelity, more computationally intense level.

The project exploited the fact that genetic programming possesses to some extent at least three attributes that have not yet been demonstrated by other methods of automatically generating computer programs: wide applicability, scalability, and competitiveness with human-produced results. We need these attributes to be able to automatically create computer programs to produce useful behavior algorithms.

We completed the development of a fully object-oriented genetic programming engine that can be distributed across a heterogeneous network. It was designed to be generic and applicable to a wide variety of problem domains. We integrated the DGGP code with Sandia's UMBRA ModSim framework, allowing us to take advantage of any tool or module that is developed for UMBRA. We can now use the graduated embodiment methods of incremental adaptation and staged optimization to develop behaviors using DGGP within the UMBRA framework.

The ability to use UMBRA with our genetic programming engine has many advantages over our previous stand-alone genetic programming tools. Foremost, it allows us to leverage all other projects that make use of UMBRA, and likewise allows those projects to use DGGP and the behavior algorithms that it generates. The cross-platform and parallel capabilities allow it to be used on personal computers as well as on clusters and supercomputers.

Another important aspect of the tools we developed in this project is the ability for the behavior developer to observe behaviors as they evolve. This allows genetic programming to be a more tightly iterative process and more akin to human-machine collaboration.

[An] important aspect of the tools we developed in this project is the ability for the behavior developer to observe behaviors as they evolve. This allows genetic programming to be a more tightly iterative process and more akin to human-machine collaboration.

We also developed a method for integrating behavior algorithms in a hierarchy to create a comprehensive behavior system that includes cognitive, instinctual, and reflexive levels of behavior in addition to physical model attributes. In one example of vertical integration, we implemented adaptive waypoints to provide a means of high-level guidance to

vehicles without regard to lower-level propulsion and physics or middle-level autopilot algorithms.

We showed that adaptive waypoints can be used to capture goal-oriented agent behaviors that can be transferred from one type of vehicle to another as a self-contained behavioral "building block." Each individual vehicle is guided by its own dynamic waypoint, which moves in such a way as to lead the vehicle toward its individual or collective goal.

Waypoints are coordinates in a virtual world. An entity can follow waypoints in the order they are given (e.g., read coordinates from a file). Or entities are often assigned to perform certain tasks (e.g., loiter) once they reach a certain location. Waypoints can be either user-generated or entity-generated and can be static, dynamic, or adaptive. A waypoint can be thought of as an internal representation or as part of an agent's cognitive map.

This method is needed to generalize across different conditions because of the diversity of physical environments, vehicles, locomotion abilities, and interaction dynamics with other objects. We believe that navigation strategies, such as "search-for-target," "move-to-goal," and "avoid-collision," are reusable using the method of adaptive waypoints, provided they are adjusted to suit the physical capabilities of each vehicle using graduated embodiment. By encapsulating the cognitive part of the system behavior into the waypoint, we can use behavior algorithms as building blocks for other hierarchical systems.

We expect the integrated tools that we developed for this project will have broad applicability for both physical and nonphysical (agent-based) modeling.

Other Communications

Boslough, M. B. E., A. R. Breckenridge, and M. D. Peters. 2004. Adaptive waypoints for graduated embodiment of autonomous mobile robots. Sandia Technical Report SAND2004-0006C, Sandia National Laboratories, Albuquerque, New Mexico.

Breckenridge, A. R., M. B. E. Boslough, and M. D. Peters. 2004. Position paper on scalability of evolutionary computation. *Workshop Proc. Genetic and Evolutionary Computation Conference (GECCO)* **CD** (26–30 June, Seattle, Washington).

38613

Scalable Fault-Tolerant Algorithms for Linear-Scaling Coupled-Cluster Electronic Structure Methods

M. L. Leininger, I. B. Nielsen

Coupled-cluster theory has enabled the computation of molecular properties with an accuracy often exceeding that of experiment. Despite the tremendous progress in computer architectures, the high-degree polynomial scaling of this method represents the greatest obstacle in the accurate theoretical treatment of mainstream chemical problems. Although it has long been recognized that this superlinear scaling is nonphysical, the development of efficient reduced-scaling algorithms to massively parallel (MP) computers has not been realized. Sandia is addressing this high-scaling cost of the coupled-cluster method by implementing locally correlated linear-scaling algorithms in a way that will enable the iterative solution of the nonlinear, coupled-cluster equations involving several billion unknowns, and scaling to thousands or millions of processors. Fault tolerance will be essential in allowing these distributed-memory applications to run on the next-generation advanced simulation and computing (ASC) machines, such as the Sandia Red Storm computer. We will implement the code in a modular fashion, developing general components for the distribution of large datasets across memory and disk, the solution of nonlinear equations, and the handling of faults in distributed-memory applications. This work will benefit modeling molecular structures and chemical reactions of central importance to Sandia programs in materials modeling and biochemistry. The ability to accurately describe large chemical systems is critical in validating models used in Sandia's ASC materials-aging efforts and in providing accurate scoring functions for evaluating protein ligand-binding affinities.

We addressed the following points:

- Parallel implementation of coupled-cluster doubles (CCD) and coupled-cluster single and doubles (CCSD) linear-scaling models,
- Implementation of linear-scaling perturbative triples correction to CCSD,
- Study of performance relative to conventional correlation models, and
- Implementation of fault-tolerant (FT) strategies.

These points constitute the steps required for development and implementation of a parallel FT algorithm for linear-scaling, coupled-cluster, electronic structure computations, which is the ultimate goal of this project.

We selected the local correlation model as the basis for implementing a program to perform local CCD, CCSD, and CCSD triple (T) computations. We obtained significantly reduced scaling and demonstrated the excellent performance of the algorithm by locating crossover points for the linear method versus a canonical algorithm.

We parallelized the local correlation program using a parallelization strategy that prevents communication bottlenecks and allows a coarse-grained parallelism. We demonstrated the efficiency of the parallel program by measuring the speed-up for a series of runs on a distributed-memory machine using message-passing interface (MPI).

The implementation of FT features continues to be hindered by the slow development of MPI extensions that report failures to the application and give the application an opportunity to continue running.

We implemented fault tolerance for the various steps of the code, including steps that employ replicated and distributed data arrays.

38614

Micromagnetic Suspension

L. Romero, W. E. Hart, A. A. Giunta

Friction and surface-related issues are obstacles to realizing reliable micromechanical devices. The difficulty arises since classical bearings scale poorly as one decreases the size of the system. Sandia seeks two novel types of magnetic levitation that employ arrays of permanent magnets. It is known that it is impossible to have stable levitation in a static magnetic field if the levitating body is not spinning. In one of our configurations, we achieve stable levitation with a passive (no feedback) alternating magnetic field. In the other configuration, we achieve stability by spinning the rotor.

We demonstrated the first of these concepts in electromagnetic (EM) traps for ions. However, no one has ever attempted to use similar principles to levitate objects larger than ions. The second form of levitation was demonstrated in the Levitron. Once the theory is developed for doing either of these forms of levitation, it is in principle simple to find configurations of magnets that will give stable levitation. However, these configurations can be highly sensitive to imperfections in the alignment of the system.

We will use robust optimization techniques to find configurations of magnets that yield stable levitation when they are perfectly aligned and can also tolerate imperfections in the alignment of the system. This involves finding ways of analytically characterizing the robustness of a given configuration and using optimization techniques to optimize this robustness.

We are working with others at Sandia who are planning to implement the designs we produce. The successful development of this technology will permit the design of high-speed, rotating, micromechanical devices.

We developed two theories: for spin-stabilized magnetic levitation of horizontally spinning rotors and for passive magnetic levitation in alternating magnetic fields.

We also developed codes for simulating both of these devices and for predicting the robustness of a configuration of magnets. These codes allowed us to tell how big an imperfection we could tolerate in a number of parameters in our system. For example, we came up with simple measures of how much we could tilt our system, change the mass of the top, and change the strengths of the magnets in the base. Using these

criteria, we devised an objective function that characterized the robustness of a configuration.

By minimizing this objective function, we found some configurations that were several orders of magnitude more robust than the original configurations that we initially tried.

We also looked into the effect of friction on these systems. There are some surprising effects involving what are known as *dissipation-induced instabilities*.

We gave configurations for both types of systems to our Sandia collaborator who is currently building them. We also filed technical advances for two patents.

Refereed

Bourabee, N. M., J. E. Marsden, and L. A. Romero. 2004. Tippe top inversion as a dissipation-induced instability. *SIAM J. Applied Dynamical Systems* **3**:352–70.

Romero, L. A. 2004. Passive levitation in alternating magnetic fields. *SIAM J. Applied Mathematics* **63 (**6): 2155–75.

Romero, L. A. 2003. Spin-stabilized magnetic levitation of horizontal rotors. *SIAM J. Applied Mathematics* **63** (6): 2176–94.

38615

Sensitivities for Large-Scale Simulation Codes

B. G. Van Bloemen Waanders, S. S. Collis, T. M. Smith, C. C. Ober, R. A. Bartlett

The primary objective of this research is the development and implementation of algorithms for efficient sensitivity analysis in key, large-scale partial- and ordinary-differential (PDE and ODE) equation-based simulation codes. This capability would enable the creation of a unified design environment consisting of optimization, uncertainty quantification, and error analysis techniques, in addition to the traditional forward solution. There is a growing demand for sensitivity information from the PDE/ODE simulation community to support design tools. Such tools are available in the form of powerful optimization and uncertainty quantification (UQ) algorithms that are accessible through general frameworks (i.e., DAKOTA [Design Analysis Kit for Optimization and Terascale Applications]). Without sensitivity information from the PDE simulation codes, these black-box approaches use finite-difference techniques to calculate gradient information, and this expensive approach limits optimization and other technologies from considering anything but a small number of design parameters.

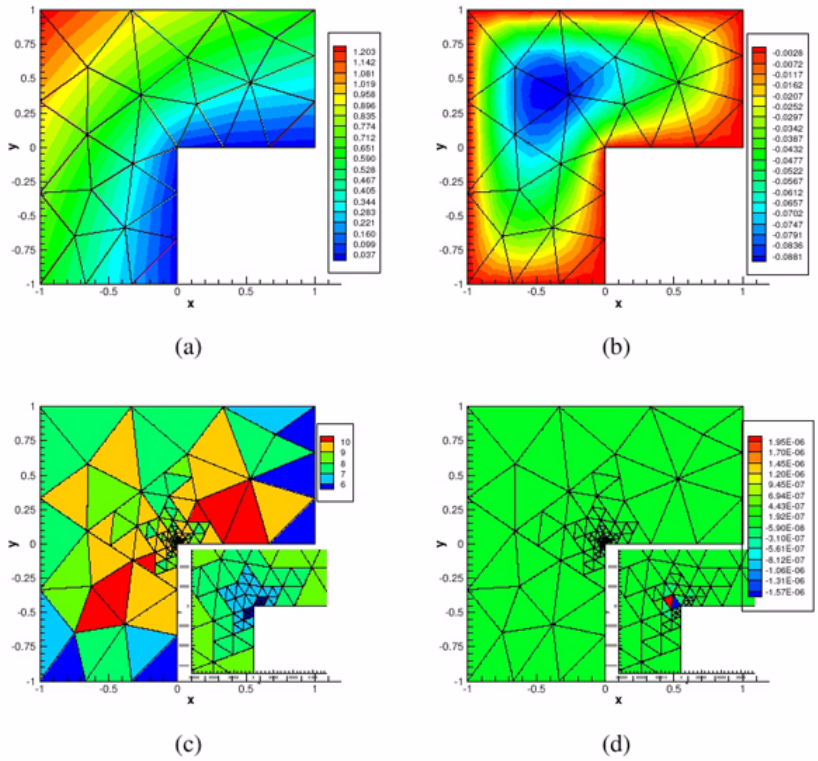

(a) *A contour plot of the primal solution on the staring mesh defined in polar coordinates.* (b) *A contour plot of the dual solution.* (c) *A plot of the final mesh where the different colors represent the order of the element.* (d) *Most of the error is concentrated at the corner.*

Among a multitude of algorithm issues, the remaining ones for this last year of the project consist of how to efficiently implement sensitivities for transient simulations and how to use sensitivity information for error estimators.

Sandia's goal is to provide general tools to the simulation community through SIERRA. We will attempt to generalize as many components as possible, such as the use of automatic differentiation tools, complex step, and the identification of sensitivity parameters. In addition, we will conduct some of our prototype design studies within the SIERRA framework.

This research resulted in key developments in the area of transient sensitivities and the use of adjoint-based error estimators. In addition, we made excellent progress toward the implementation of sensitivity information into a SIERRA compressible fluid-flow code (PREMO), utilizing hybrid automatic differentiation tools.

This research resulted in key developments in the area of transient sensitivities and the use of adjoint-based error estimators. In addition, we made excellent progress toward the implementation of sensitivity information into a SIERRA compressible fluid-flow code (PREMO), utilizing hybrid automatic differentiation tools. We developed a time-domain decomposition algorithm to calculate transient-based adjoint sensitivities. We achieved excellent results for a steady-state heat equation with promising parallel speed-up potential. We tested a red-black Gauss Seidel preconditioner, but unfortunately it did not achieve any parallel speedup. We also tested the domain decomposition algorithm in a nonlinear problem with similar success. However, additional work on parallel preconditioners is required for the algorithm to produce speedup for production codes. We developed *a posteriori* error estimators based on the adjoint formulation for a simple heat equation. The purpose of this prototyping work was specifically to demonstrate the utility of adjoint sensitivity formulations other than optimization. We used the error estimators to perform *h* and *p* adaptivity and showed an improvement in the quality of the forward solution. We developed a complete MATLAB implementation of adjoint-based Euler equations, specifically to help diagnose a difficult runtime problem in our Euler prototype code. We debugged the forward residual calculation in addition to making corrections and improvements to our rectangular mesh generator. We made significant progress toward the adjoint implementation. We developed a hybrid automatic differentiation capability to help build derivative information for both the forward and adjoint formulation. We developed special direct sensitivity algorithms to achieve real-time inversion capabilities for a Department of Homeland Security (DHS) application. We also developed a transient implementation.

Refereed

Bartlett, R. A., and B. G. van Bloemen Waanders. 2004. Hybrid symbolic and automatic differentiation methods for ANSI C++. *ACM TOMS*, to be submitted.

Bartlett, R. A., B. G. van Bloemen Waanders, and M. A. Heroux. 2004. Vector reduction/ transformation operators. *ACM TOMS* **30**:62–85.

Bartlett, R. A., S. S. Collis, M. Heinkenschloss, and B. G. van Bloemen Waanders. 2004. Time-domain decomposition iterative methods for the solution of PDE–constrained optimal control problems. Paper presented at the CSRI 2nd PDE–Constrained Workshop, May, Santa Fe, New Mexico.

Other Communications

Wilcox, L., B. G. van Bloemen Waanders, S. E. Collis, M. Gammel, and T. Warburton. 2004. Adjoint-based *a posteriori* error analysis. Sandia Technical Report, Sandia National Laboratories, Albuquerque, New Mexico (in preparation).

52540

IP Storage: A Performance and Security Study

H. Y. Chen, J. Vanrandwyk

Effective, high-performance, networked file/storage is needed to solve input/output (I/O) bottlenecks in large compute platforms. The emerging Internet protocol (IP)–based storage places message/file and storage I/O onto an Ethernet/IP network, offering block I/O performance to remote clients. Among the different flavors of IP storage, Internet small computer system interface (iSCSI) had emerged as the most promising technology, riding on the popularity of Ethernet, transmission control protocol (TCP), and IP. Thus, iSCSI is the selected technology for our research study.

In earlier work, we verified that hardware iSCSI can offer much better cost/performance ratios than Fibre Channel (FC). In fact, because the power of today's central processing unit (CPU) surpassed that required to deliver traffic at 1 Gbit/s, even software implementations of iSCSI delivered nearly identical performance, still leaving ample compute cycles for user applications. We decided to use software iSCSI to continue our study because it provides the flexibility to access tuning performance, unlike its hardware counterparts that hide their parameters in silicon.

The results of our continuation study include acquiring and applying the knowledge of tuning the Linux kernel, iSCSI, and TCP for remote access over the wide-area network (WAN). In addition, we also evaluated applications of iSCSI in cluster and parallel file systems that combine the common namespace for data-sharing and block I/O for performance to alleviate the bottleneck suffered in network file system (NFS)–based servers. In addition, we report the security options offered by iSCSI and assess its suitability in providing appropriate need-to-know and data-integrity protections to mission-critical information.

(1) *iSCSI performance tuning*. We identified the tunable parameters of iSCSI and TCP that affect the performance characteristics for local, metropolitan, and WANs. At the iSCSI level, the parameters of interest from a performance point of view are (a) command request size, (b) iSCSI command window credit amount, (c) the number of simultaneous iSCSI connections in a session, and (d) the option of sending solicited versus unsolicited data.

The command request size, the command window credit amount, and the number of simultaneous connections may impact both read and write performance. The choice of solicited

versus unsolicited data may impact write performance, but it has no impact on reads.

At the TCP/IP level, the most important parameters are the send and receive window sizes, especially in networks with a large-bandwidth delay product such as high-speed WANs. Additionally, it is also necessary to increase the buffer allocated to queue data for sending to and receiving from the network interface card (NIC) used for iSCSI to prevent iSCSI traffic from being stalled, thereby improving throughput.

We used a test control program developed for this study to benchmark the iSCSI local area network (LAN) and WAN performance. This project integrates test definition, test execution, and origination of test results and related system information.

We found that iSCSI transport can deliver FC-like LAN and WAN performance and that current state-of-the-art processors can easily achieve a gigabit line rate using software-based iSCSI solutions.

(2) *Evaluation of an iSCSI–based scalable I/O subsystem*. We partnered with Terrascale, a start-up company, to evaluate iSCSI as the transport of a block-level scalable I/O platform, TerraGRID. This I/O subsystem uses a shared-access scheduling scheme to enable Linux file systems to act as a massively parallel (MP) system. It presents a simple and elegant solution that fully harnesses commodity software components such as Linux file systems, software RAID driver, etc.

We used the same test program described above to benchmark our parallel I/O subsystem. We used a small test-bed that consists of eight I/O clients and eight I/O servers for proof of concept. The tests include baseline throughput as well as scalability verifications, where we plot the aggregate throughput as a function of the number of concurrent clients. Our system can scale up to eight clients, and the performance is limited by the throughput of the disk performance on the server machine.

We are in the process of installing TerraGRID on our 128-node InfiniBand test-bed. We believe this final test can present a more meaningful performance result regarding scalability.

Refereed

Dalgic, I., K. Ozdemir, R. Velpuri, J. Weber, H. Chen, and U. Kukreja. 2004. Comparative performance evaluation of iSCSI protocol over metropolitan, local, and wide area networks. *Proc. EEE Conference on Mass Storage Systems and Technologies* **1** (13–16 April, Adelphi, Maryland): 101–5.

52541

A Parallel Circuit Simulator for Cell Biology

R. L. Schiek, S. A. Hutchinson, E. E. May

The next revolution in biology, building on the deluge of available genomics and proteomics data, will be based on understanding the genetic and metabolic signaling pathways that define how a cell and, ultimately, an organism works. Recent work shows that the mechanisms of gene expression and the interdependence of signaling pathways in the cell can be modeled as complex electrical circuits. Cells are akin to signal processors that receive inputs (deoxyribonucleic acid [DNA] sequences or genes), process information (transcription, for example), and produce outputs (proteins).

Sandia is extending the XYCE™ circuit simulation program to create a large-scale, parallel, biocircuit simulator. This will require the development of individual circuit elements representing molecular machines and an accurate description of the coupling between elements. Synthesis will continue up the functional hierarchy to the construction of single cells and the simulation of cell cultures. Initially, we will use the tool to model cell-level responses to environmental stresses. Ultimately, we will use XYCE™'s parallel capabilities to simulate a full cell culture.

Though computationally and biologically challenging to create, such a tool will be an aid in the fundamental understanding of cellular biology and eventually will lead to models of microbial and cellular processes of interest to the Department of Energy (DOE), such as for waste remediation and energy production.

Our goals for this project involved implementing biological components within XYCE™ as analogs for cellular machinery and cellular communication, as well as identifying target unicellular and multicellular problems.

In the area of implementing biological analogs within XYCE™, we created circuit analogs for biological signal sources, enzymatic and regular reactions, repression interactions, and cellular storage. To simulate communication between cells, we developed a diffusion-limited environment within which cellular circuits can be embedded. This allows XYCE™ to simulate the interactions of many independent cells simultaneously and is a unique capability of this work within the biological pathway community.

Since existing pathway databases are very large (i.e., thousands of species and connecting pathways), manual

translation of real pathway networks into simulation net-lists is difficult and error prone. To address this, we developed an automated technique for converting databases of pathways directly into input files for XYCE™ (net-list files). While this reduces the chance of translation errors in developing a complex net-list, it also allows one to experiment with different net-list implementations, such as an all-digital or mixed-digital and analog network. Based on this effort, XYCE™ can now simulate about half of *E. coli*'s known metabolic network. Internal limits on XYCE™ prevent us from simulating the entire metabolic network, but we are working to correct this problem.

The culmination of these efforts has been an ability to conduct the largest known biological circuit simulations to date. In a multicellular study examining tissue differentiation, our simulations involved over 52,000 circuit elements and over 60,000 unknowns.

Typically, a drawback in the usefulness of computational biological modeling is the lack of kinetic and transport data. We coupled our biological circuits in XYCE™ to the optimization toolset DAKOTA (Design Analysis Kit for Optimization and Terascale Applications). This software connection allows us to use design of experiment and optimization with uncertainty techniques to define working parameter ranges for biological systems. Thus, one is able to find critical transport pathways within a biological control circuit and, most importantly, to define parameter ranges under which such control will function. This unique feature of our work strongly leverages the parallel computational abilities of XYCE™ since many large circuit simulations must be conducted to create the data needed by DAKOTA.

The culmination of these efforts has been an ability to conduct the largest known biological circuit simulations to date. In a multicellular study examining tissue differentiation, our simulations involved over 52,000 circuit elements and over 60,000 unknowns.

Refereed

May, E. E., and R. L. Schiek. 2003. Simulating regulatory networks using XYCE™. *Proc. International Conference on Systems Biology* **1** (November, St. Louis, Missouri).

Schiek, R. L., and E. E. May. 2003. Development of a massively parallel, biological circuit simulator. *Proc. IEEE Computer Society Conference on Computational Systems Bioinformatics (CSB2003)* **1** (August, Stanford, California): 620–22.

Schiek, R. L., and E. E. May. 2004. Using circuit modeling to simulate large-scale, multicellular, biological pathways. Paper presented at the Numerical Aspects of Circuit and Device Modeling Meeting, June, Santa Fe, New Mexico.

Schiek, R. L., and E. E. May. 2004. Using large-scale, multicellular pathway modeling to understand cellular differentiation. *Proc. American Institute of Chemical Engineers Annual Meeting* (November, Austin, Texas).

52542

Developing a Computationally Efficient Dynamic Multilevel Hybrid Optimization Scheme Using Multifidelity Model Interactions

J. P. Castro, G. A. Gray, P. N. Demmie, A. A. Giunta, P. D. Hough, M. A. Gonzales

With the advent of massively parallel (MP) computers, computational speed has increased tremendously. Unfortunately, the comparable scaling of numerical and model complexity in combination with overburdened machines can still result in long compute times. This problem escalates when solving an optimization problem that requires the completion of many of these computationally intensive jobs. Therefore, Sandia seeks an algorithmic approach to make the optimization calculation more computationally efficient for a wide range of applications, including earth-penetrator analysis, neutron-tube (NT) analysis, and electrical-device modeling.

The goals of this project are to develop dynamic and computational time-saving optimization algorithms by taking advantage of interactions between multifidelity models. If a system has models of different fidelities, the design space of the low-fidelity, computationally cheaper model may be used to drive the optimization. Within this design space, a set of rules or guidelines may determine the best optimization procedure. The low-fidelity design space may then be mapped to the high-fidelity design space to determine the optimum value, thus reducing the total computational time. This may be taken a step further by developing algorithms with feedback mechanisms so that the processes of determining the optimization scheme and model fidelity are done dynamically; this will be termed as dynamic multifidelity-multilevel hybrid optimization.

This project addresses three major technical challenges. First, algorithms and their corresponding feedback mechanisms must be developed for the dynamic multifidelity-multilevel hybrid optimization scheme. Second, the newly developed schemes must be integrated into DAKOTA (Design Analysis Kit for Optimization and Terascale Applications). Finally, if necessary, a convergence proof must be developed for dynamic multifidelity-multilevel hybrid optimization. Our primary goals were to refine the current multifidelity optimization capabilities into a more dynamic approach that allows for an unequal number of design variables between models of differing fidelity, to expand upon current optimization benchmark calculations and metrics, and to assess the feasibility of a convergence proof for our scheme.

Our goals were to (1) develop a limited dynamic optimization scheme for an N-fidelity level of models and a fixed (nongradient) optimization strategy that allows for an unequal number of design variables between models of differing fidelity, (2) expand upon current optimization benchmark calculations and metrics with earth-penetrator models, and (3) assess the feasibility of a convergence proof for our scheme.

We accomplished the first goal, designing a multifidelity optimization strategy, through the completion of the following tasks:

- We developed an optimization scheme that incorporates a space-mapping technique and the Asynchronous Parallel Pattern Search (APPS) method. It employs APPS to search for the optimum of the high-fidelity model and simultaneously makes strategic calls to an inner loop that optimizes over the low-fidelity model. The steps of this inner-loop procedure are the following:

(1) Map a set of high-fidelity model calculations to the low-fidelity model using space-mapping techniques.

(2) Find an optimum design point in the low-fidelity space.

(3) Reverse-map the design point to the high-fidelity space and return it to APPS as a potential best point.

There are no limitations on the number of models or the number of design variables of each model.

- We implemented our optimization scheme through modifications to the DAKOTA/APPSPACK software. We incorporated the inner loop using a tool of direct search methods called an *oracle*. Oracles are used to predict a point at which a decrease in the objective function may be observed. This point may be independent of the search pattern and can be obtained using any method.
- We execute the inner loop using a generic series of scripts and template files that can be customized easily for specific applications. First, a primary script reads a user-defined number of design variables and corresponding response values from a file created by APPS. Then, a set of space-mapping parameters is calculated via a DAKOTA least-squares calculation. Next, DAKOTA is used to calculate the optimal design variables for the “mapped” low-fidelity model. Finally, the resulting variables are reverse-mapped to the high-fidelity design space. The generation of the necessary DAKOTA input files and scripts is completely automated.

To test the APPS/space-mapping strategy, we developed a set of benchmark calculations for the responses of an earth penetrator. In this case, the displacement response is a simple

monotonic curve with the minimum occurring at the bounds, while the acceleration response is quite noisy and has many local minima. We completed a thorough set of test runs with the PRONTO code. When the latest version of the PRESTO code is released, we will complete the same set of test runs using PRESTO.

Finally, we note that the only significant algorithmic change to the APPS method is the addition of the oracle. Because the oracle point is merely an addition to the points defined by the APPS search pattern, the convergence of the DAKOTA/APPSPACK algorithm is not adversely affected. A convergence proof for the APPS algorithm already exists, and adding an oracle point does not necessitate any changes to this proof. Hence, the goal of establishing a convergence proof for our multifidelity optimization scheme has been met.

Other Communications

Castro, J. P., P. N. Demmie, A. A. Giunta, and P. D. Hough. 2003. Developing a computationally efficient dynamic multilevel hybrid optimization scheme using multifidelity model interactions. *Proc. 7th U.S. National Congress on Computational Mechanics, USACM CD-ROM Conference* **1** (27–31 July, Albuquerque, New Mexico): 260.

Giunta, A. A., M. S. Eldred, and J. P. Castro. 2004. Uncertainty quantification using response surface approximations. *Proc. 9th Joint Specialty Conference on Probabilistic Mechanics and Structural Reliability, ASCE CD-ROM Conference* **1** (26–28 July, Albuquerque, New Mexico): 1–7.

Giunta, A. A., M. S. Eldred, P. D. Hough, and J. P. Castro. 2004. Overview of surrogate-based optimization research and applications at Sandia National Laboratories. Paper presented at the Surrogate Optimization Workshop sponsored by Rice University and Exxon/Mobil Upstream Research Company, 24–25 May, Houston, Texas.

Giunta, A. A., M. S. Eldred, S. F. Wojtkiewicz, Jr., L. P. Swiler, T. G. Trucano, and J. P. Castro. 2003. Surrogate-based optimization methods for engineering design. Paper presented at the 5th Biennial Tri-Laboratory Engineering Conference, 21–23 October, Santa Fe, New Mexico.

52543

Robust Large-Scale Parallel Nonlinear Solvers for Simulations

T. G. Kolda, B. W. Bader

Sandia has a wide range of highly nonlinear phenomena models that critically depend on robust nonlinear solvers. The radiation-hardened Pentium processor simulation involves over 70,000 devices, and current solution methods are not robust because convergence depends on setting parameters that are extremely problem-dependent. Similar robustness issues occur in reacting-flow simulations for the design of chemical vapor deposition (CVD) reactors. Future goals such as predicting the dispersion of toxic chemicals in water systems or buildings and modeling weapon electrical systems in hostile environments are even more difficult and require advances in solver technology.

The issue is that nonlinear solvers based on Newton's method tend to fail when the Jacobian is singular or near-singular or when the problem is too large to effectively precondition. Sandia is doing research on two complementary approaches to address this problem: limited-memory Broyden's method and the Tensor method. Broyden's method replaces the Jacobian with an approximation that is better conditioned and that results in a Newton equation that is easier to solve. Limited-memory methods, which have been successful in optimization, allow us to extend this approach to large scale. Tensor methods are based on a higher-order model and may overcome problems with singularity in the Jacobian. They have outperformed Newton's method on small problems.

We will develop large-scale parallel versions of Broyden's method and the Tensor method to allow us to perform simulations critical to Sandia's mission. We will implement the methods in NOX, a nonlinear solver library that is part of the TRILINOS framework.

Our research focused on developing a Tensor-based algorithm that is noninvasive to the underlying linear solver. Such an algorithm would enable applications that use a Newton-based approach to freely switch to Tensor methods without additional interface requirements. We then evaluated both Tensor and Broyden algorithms designed under this project on large-scale parallel applications.

The major accomplishment for Tensor methods was the development of a novel algorithm that is independent of the underlying linear solver. Previous work on Tensor algorithms focused on using the basis functions of a Krylov iterative linear

solver to solve the approximate Tensor system. This approach is problematic since the algorithm is tied to the underlying linear algebra implementation. It is not generalizable to a library form. Our new algorithm, called a modified Bouaricha method, is completely independent of the linear solver. This breakthrough led to an algorithm that requires no more information than a Newton-based solve requires. It allows us to implement the Tensor algorithm leveraging the abstract interface to linear solvers in Sandia's nonlinear solver package, NOX, and to quickly push the algorithms into application codes.

We implemented a parallel, scalable version of the Tensor method in NOX. We tested the algorithm against Newton's method on a variety of problems in two parallel application codes: a reacting-flow code called MPSalsa, which solves the Navier-Stokes and continuity equation, and XYCE™, a circuit simulator. Results showed that as the nonlinearity increased (and thus the difficulty of the solve), the Tensor method was more robust than the standard damped Newton method. Tensor was able to solve more problems in the test set. On simple, less nonlinear problems, there was not a clear-cut winner.

The major accomplishment for the Broyden research was the development and release of a parallel version in NOX. We also tested the method on a set of problems from MPSalsa and XYCE™. Results showed that the Broyden method could outperform Newton's method with speed-ups up to 40%. The performance was not consistent, however, and on some problems, the Broyden method performed much worse. As the problems got more nonlinear (more difficult), the Broyden method became less robust. For example, in MPSalsa, we studied fluid flow in a lid-driven cavity. Below a specific Reynolds number, the Broyden method took fewer nonlinear iterations than Newton's method to converge. For simulations above this value, the Broyden's method failed to converge, while Newton's method was able to converge.

We did, however, identify one area where Broyden's method can be applied. When applications cannot supply a Jacobian matrix for a Newton's method and a direct linear solver is the only solve available, Broyden's method can approximate the Jacobian matrix. Broyden's method can be viewed as a competitor to Matrix-Free Newton-Krylov methods when an iterative linear solver is not available or desired.

The studies indicate that the two algorithms studied here are complementary to one another. For very easy nonlinear systems where all solver algorithms (Broyden, Newton, and Tensor) converge, the Broyden method can be a more efficient substitute for Newton's method. As the problem becomes more

Our new algorithm, called a modified Bouaricha method, is completely independent of the linear solver. This breakthrough led to an algorithm that requires no more information than a Newton-based solve requires. It allows us to implement the Tensor algorithm leveraging the abstract interface to linear solvers in Sandia's nonlinear solver package, NOX, and to quickly push the algorithms into application codes.

nonlinear, one could envision switching to a Newton solver and, if this fails to converge, switch to the most robust algorithm, the newly developed Tensor method.

Refereed

Bader, B. W. 2004. Tensor-Krylov methods for large-scale systems of nonlinear equations. *SIAM J. Numerical Analysis*, in review.

Bader, B. W., and R. B. Schnabel. 2004. On the performance of Tensor methods for solving ill-conditioned problems. *SIAM J. Scientific Computing*, in review.

Other Communications

Bader, B. W., and T. G. Kolda. 2004. A comparison of iterative Tensor methods for solving large systems of nonlinear equations. Paper presented at the 2004 Copper Mountain Conference on Iterative Methods, 2 April, Copper Mountain, Colorado.

Bader, B. W., and T. G. Kolda. 2004. A Tensor method for solving large-scale systems of nonlinear equations. Paper presented at the 2004 SIAM Annual Meeting, 12 July, Portland, Oregon.

Pawlowski, R. P., E. R. Keiter, R. J. Hoekstra, S. A. Hutchinson, T. V. Russo, and T. Kolda. 2004. Nonlinear solution algorithms for circuit simulation. Paper presented at the Numerical Aspects of Circuit and Device Modeling Workshop, 23–25 June, Santa Fe, New Mexico.

Pawlowski, R. P., E. R. Keiter, R. J. Hoekstra, S. A. Hutchinson, T. V. Russo, and T. Kolda. 2004. Nonlinear solution algorithms for robust circuit simulation. Paper presented at the SIAM Conference on Parallel Processing for Scientific Computing, 27 February, San Francisco, California.

52544

Development of Computational Algorithms and Inversion Capabilities for Transport/ Reaction Simulations of Chemical/Biological/ Radiological Terrorist Attack Scenarios in Support of Homeland Security

B. G. Van Bloemen Waanders, R. A. Bartlett, S. A. McKenna, K. R. Long, P. T. Boggs, J. N. Shadid, C. A. Phillips, W. E. Hart

Our nation's critical infrastructure is extremely vulnerable to chemical/biological/radiological (CBR) terrorist attacks. Sandia's goal in this project is to develop countermeasure tools using numerical transport and optimization algorithms for urban canyons, internal facilities, and water-distribution networks. In particular, we will focus on developing methods to reconstruct attack events, control fluid flow in internal facilities, strategically place sensors, optimally design the decontamination process, generate appropriate boundary conditions (BCs) for water-distribution systems, and develop a risk-assessment framework. We made significant progress in each of these areas. We developed efficient solvers to simulate a high-fidelity airport terminal model predicting chemical transport. We applied optimization algorithms to reconstruct initial conditions for fictitious CBR attacks. Most importantly, we uniquely applied these optimization algorithms to achieve real-time performance for both internal facilities and water-distribution systems. Demand-generator development examined the effect of temporal discretization of demand on flow and transport in a water-distribution network and resulted in the observation of important transport effects. Finally, we investigated combinatorial algorithms for sensor placement to consider multicriteria objectives and the inclusion of uncertainty. We found that forcing optimality in one criterion usually resulted in poor performance for other metrics, but there exist solutions that effectively compromise across all objectives. We confirmed approximately $2 million of external funding from the Environmental Protection Agency (EPA) and the Department of Homeland Security (DHS) to pursue related research topics and implement these project results into an operational setting.

We developed efficient solvers to simulate a high-fidelity airport terminal model predicting chemical transport. We applied optimization algorithms to reconstruct initial conditions for fictitious CBR attacks. Most importantly, we uniquely applied these optimization algorithms to achieve real-time performance for both internal facilities and water-distribution systems.

We made outstanding progress on all aspects of the project. For water security, we realized progress for source inversion, sensor placement, demand generation, and risk assessment. We successfully developed and tested a full-space source inversion on a medium-size dataset and achieved real-time performance.

In addition, we developed a subdomain method to address real-time performance inverting very large datasets. We developed new integer-programming models for sensor placement to (1) consider trade-offs between different objectives, (2) address robustness issues, (3) more accurately model temporal-flow effects, and (4) consider sensor placement for source inversion. We tested these models on a variety of synthetic datasets, using real-world network-flow models to test the scalability of our integer-programming formulations. We also investigated the formal complexity of a number of sensor placement models, and, in particular, we demonstrated that near-optimal solutions can be found quickly for several models.

We evaluated and tested a temporal discretization of demand on flow and transport in a full network. We examined the effect of stochastic demand time-step size on tracer transport in water-distribution networks and showed that hydraulic time-steps of less than 30 min are adequate for tracer simulation in a network.

We formulated a novel Markov Latent Effects model for application to system threat assessment, that is, to quantify the vulnerability of particular assets to attack. Additionally, we created and integrated a pre- and post-processing shell with EPANET (a hydraulics and contaminant transport code for water-distribution systems) to aid in consequence analysis, which provides estimates of customer exposure to various attack scenarios. We subsequently combined results from the threat assessment and consequence analysis to yield the risk scores of interest. We performed preliminary assessments for two different water-distribution systems in efforts to test and calibrate the models.

For air security, we demonstrated high-fidelity numerical simulation for chemical transport using efficient solver technologies. We demonstrated large-scale parallel calculations of 100,000 to 100,000,000 unknowns using from 10 to 1000 processors. These calculations consisted of transient Navier-Stokes with large-eddy simulation models. We demonstrated real-time source inversion for a steady-state simulation of a three-dimensional airport model by separating off-line and on-line calculations. We demonstrated control and decontamination processes by combining high-fidelity simulations with optimization algorithms. Finally, we took initial steps to design a production simulation code so that all our prototyping capabilities can be conducted in a common framework and avoid duplication of effort for common services.

Refereed

Berry, J., L. Fleischer, W. E. Hart, C. A. Phillips, and J. P. Watson. 2004. Sensor placement in municipal water networks. *J. Water Resources Planning and Management*, submitted.

Carr, R. D., H. J. Greenberg, W. E. Hart, G. Konjevod, E. Lauer, H. Lin, T. Morrison, and C. A. Phillips. 2004. Robust optimization of contaminant sensor placement for community water systems. *Mathematical Programming Series B*, submitted.

Laird, C. D., L. T. Biegler, and B. G. van Bloemen Waanders. 2004. Large-scale optimization for contaminant source determination in municipal drinking-water networks. *SIAM*, submitted.

Laird, C. D., L. T. Biegler, and B. G. van Bloemen Waanders. 2004. Time-dependent contamination source determination for municipal water networks using large-scale optimization. *J. Water Resources Planning and Management*, accepted.

Shadid, J. N., R. S. Tuminaro, G. L. Hennigan, K. D. Devine, and P. T. Lin. 2004. Parallel preconditioned Krylov solvers for unstructured finite-element reacting-flow solutions. *J. Computational Physics*, submitted.

Other Communications

Berry, J., W. E. Hart, C. A. Phillips, and J. Uber. 2004. A general integer-programming–based framework for sensor placement in municipal water networks. *Proc. 6th Annual Symposium on Water Distribution Systems Analysis* **1** (July, Salt Lake City, Utah).

Carr, R. D., H. J. Greenberg, W. E. Hart, and C. A. Phillips. 2004. Addressing modeling uncertainties in sensor placement for community water systems. *Proc. 6th Annual Symposium on Water Distribution Systems Analysis* **1** (July, Salt Lake City, Utah).

Laird, C. D., L. T. Biegler, B. G. van Bloemen Waanders, and R. A. Bartlett. 2004. Time-dependent contamination source determination: A network subdomain approach for very large networks. *Proc. World Water and Environmental Resources Congress 2004* **1** (July, Salt Lake City, Utah).

Lin, P. T., M. Sala, J. N. Shadid, and R. S. Tuminaro. 2004. Performance of a geometric and an algebraic multilevel preconditioner for incompressible flow with transport. *Proc. Computational Mechanics, WCCM VI/APCOM '04* **1**.

McKenna, S. A., C. Peyton, L. Yarrington, S. G. Buchberger, and R. L. Bilisoly. 2004. Modeling solute transport in distribution networks with variable demand and time-step sizes. *Proc. American Society of Civil Engineers Annual EWRI Meeting* **1** (July, Salt Lake City, Utah).

Tidwell, V. C., J. A. Cooper, and C. J. Silva. 2004. Threat assessment of water supply systems using Markov latent effects modeling. *J. Water Resources Planning and Management*, submitted.

Watson, J. P., H. J. Greenberg, and W. E. Hart. 2004. A multiple-objective analysis of sensor-placement optimization in water networks. *Proc. 6th Annual Symposium on Water Distribution Systems Analysis* **1** (July, Salt Lake City, Utah).

52546

Massively Parallel Linear Programming

C. A. Phillips, E. G. Boman, V. E. Howle, O. D. Parekh

Sandia developed a massively parallel (MP) linear programming (LP) solver. LP is the optimization of a linear objective function subject to linear constraints. Companies and universities have expended huge efforts over decades to produce fast, stable serial LP solvers. Previous parallel codes run on shared-memory systems and have little or no distribution of the constraint matrix. We have seen no reports of runs on large numbers of processors.

LPs of enormous scale arise in mitigation planning for homeland defense. Simulations of population interactions performed for the National Infrastructure Simulation and Analysis Center (NISAC) can produce graphs with 10 billion edges. Efficiently partitioning such graphs models the effective use of limited law-enforcement personnel to enforce quarantines or use of limited vaccines to contain epidemics. LPs can compute optimal strategies to attack supervisory control and data-acquisition (SCADA) networks in a new analysis system based on hidden Markov models. SCADA networks control critical U.S. infrastructure such as the power grid and natural-gas distribution. Some logistics planning applications such as commercial nuclear-waste movement and airline network analysis also require parallel LP.

A scalable LP solver will benefit the Parallel Integer and Combinatorial Optimizer (PICO) integer-programming (IP) solver. IPs are LPs with additional integrality constraints. IPs can solve resource allocation, network security, and decision-support problems (e.g., sensor placement in networks). Serial LP solves limit initial speed-up, especially for problems with difficult, large formulations.

Our parallel LP code is based on an efficient serial implementation of Mehrotra's interior-point predictor-corrector algorithm (PCx). The computational core of this algorithm is the assembly and solution of a sparse linear system. We substantially rewrote the PCx code and based it on TRILINOS, the parallel linear algebra library developed at Sandia. Our interior-point method can use either direct or iterative solvers for the linear system. To achieve a good parallel data distribution of the constraint matrix, we used a (pre-release) version of a hypergraph partitioner from the ZOLTAN partitioning library.

We developed two parallel versions of the parallel interior-point code to produce the system we now call parPCx. The first version parallelizes only the linear solver within the preexisting serial PCx interior-point code. This is the most compute-intensive part of the code and thus benefits the most from parallel solution. We developed a generic solver class that can use either direct or iterative solvers. Currently, we solve the reduced system ADA^T, though we could easily adapt the code to solve the (larger but sparser) augmented system instead. We accessed direct solvers through the Amesos package and iterative solvers through the AztecOO package. Both of these packages are in TRILINOS, Sandia's collection of compatible software packages to support parallel linear algebra.

The second version of the parallel LP code uses the same (parallel) solver class, but, in addition, we made the entire interior-point method fully data-parallel using the Epetra parallel matrix package. In this way, the constraint matrix is stored distributed across processors, enabling us to solve very large problems that will not fit on a single processor. (This version of the code is still not fully debugged.)

A crucial issue in the data distribution is how to distribute the sparse constraint matrix. We use a hypergraph model of the matrix that accurately represents the communication cost in matrix-vector multiplication. We can find a good distribution using a hypergraph partitioner. Note that we cannot use graph partitioners in this case because the constraint matrix is rectangular. Our code allows for both row and column decomposition of the matrix. Our partitioning technique is also beneficial for certain types of preconditioning.

An advantage of using the Amesos library for direct solvers is that it is easy to switch among several external sparse linear solver packages. One drawback is that we cannot modify the external solvers, which prevents us from using specialized techniques for small pivots, as is customary for interior-point methods. This leads to numerical difficulties for some types of problems. We found that we can partially avoid these problems using regularization techniques, which are nonintrusive.

As anticipated, finding effective preconditioners for iterative solvers has proved challenging. The linear systems arising in the predictor-corrector method are extremely ill-conditioned, and standard preconditioning techniques (Jacobi, incomplete Cholesky) did not work well. We generalized a class of support preconditioners. However, the linear systems from the LP iterations also are not normally symmetric diagonally dominant, where support preconditioners work well theoretically and in practice. Therefore, this type of support tree

method also did not work well, in general. We have the infrastructure to experiment with new preconditioners and have begun research on new methods, but finding effective new general preconditioning methods will require far more time and effort.

Last year we added a ramp-up capability to the core of the PICO branch-and-bound framework. This allows us to solve a single subproblem in parallel early in the solve when there are not enough independent subproblems to keep an MP system busy. This year we added ramp-up capability to the integer-programming solver within PICO. This allows us to use parallel LP solvers, especially for root solves. We began developing an Open Source Interface (OSI) for parPCx and a PICO-specific extension to this interface. This allows integration of parPCx into PICO and any other codes that use the standard OSI interface.

Other Communications

Phillips, C. A. 2004. Massively parallel mixed-integer programming: Algorithms and applications. Paper presented at the SIAM Conference on Parallel Processing for Scientific Computing, February, San Francisco, California.

59916

A Method of Evaluating Research Using New Innovation, Risk, and Impact Indicators

K. W. Boyack, G. S. Davidson

In this age of modern information availability, organizations are searching for ways to capture tacit knowledge and to use that knowledge to evaluate and select between new ideas. We are continually falling behind in our retention of knowledge due to the rapidity with which new information becomes available, and from a lack of good tools to help us retain what we have learned. Sandia seeks a method of evaluating research ideas by creating new indicators that, in essence, provide a numerical history of accumulated knowledge. These will be research community–based innovation, risk, and impact indicators that can give the researcher, administrator, or evaluator a means to quickly evaluate an idea within the context of the history of similar ideas. These indicators also will facilitate focused access to pertinent literature for those with a desire to gain more detailed knowledge and thereby improve their ideas.

The indicators and evaluation system will be made available as a tool that can be used by any Sandian. A query-based interface will enable users to find papers and research communities (sets of papers on a common subject) most related to their ideas and to see the indicator values associated with those communities. The system will also suggest higher-ranked communities that are related through citation to those returned by queries. Success in this project will have multiple impacts. On a theoretical level, it will provide data to test and evaluate theories of scientific progress and innovation. On a more applied level, this system will have great benefit to the research and development program, enabling both potential investigators and investment teams to quickly evaluate ideas in the context of global publishing. In a similar way, this system will benefit Sandia's nuclear weapons programs by providing indicators within a global context.

We did a great deal of work to generate a useful macromodel (7000 journals) of science. The purpose for doing so was to validate the methods that would be used subsequently to generate micromodels of science. We found ways to increase the local accuracy of the model through the use of VxOrd (as opposed to more-traditional hierarchical techniques) and through the reduction of local distortion by identifying and removing the distorting journals. This has application to the

micromodel in that similar distortions should occur there, and removal of those distortions will improve the accuracy of the micromodel and the resulting research communities. We also investigated the global accuracy of the macromodel and found that several different similarity types give very good global results, including the cocitation-based similarity that we propose for use with the micromodel. Thus, we found that the cocitation-based similarity will be suitable for use with the micromodel.

We also created the first micromodel (1,000,000 papers) of science using data for the year 2002. The ability to generate graph layouts on a million nodes is a significant accomplishment and has future application in bioinformatics and Department of Homeland Security (DHS) applications, as well as in our own. Initial investigations showed that the micromodel preserves both global and local structure. We ran queries to select certain papers of interest. A careful reading of the abstracts of those papers, along with the abstracts of their 20 nearest neighbors, shows that a topic focus is preserved. A clustering routine identified roughly 90,000 research communities (RCs, or clusters of papers) within this map. We calculated their placement within a discipline-based map and also calculated strong links between RCs. We also calculated static indicators for the RCs. We found that highly cited papers tend to be found in the middle of tight clusters, while uncited papers tend to be in either loose or very small and unconnected clusters.

Parsing of the conferences database took place, and we are adding these data to the SCI/SSCI data. This will allow more comprehensive maps, especially in the technology (as opposed to science) areas.

We also created the first micromodel (1,000,000 papers) of science using data for the year 2002. The ability to generate graph layouts on a million nodes is a significant accomplishment and has future application in bioinformatics and Department of Homeland Security (DHS) applications....Initial investigations showed that the micromodel preserves both global and local structure.

Refereed

Boyack, K. W. 2004. Mapping knowledge domains: Characterizing PNAS. *Proc. National Academy of Sciences* **101** (S1): 5192–99.

Boyack, K. W., and A. Backer. 2004. The growth and memory of science. *Science,* submitted.

Klavans, R., and K. W. Boyack. 2004. Identifying a better measure of relatedness for mapping the backbone of science. *J. American Society for Information Science and Technology,* submitted.

67015

Massively Parallel, Scalable Atmosphere Model

W. F. Spotz, M. A. Taylor, M. B. E. Boslough, R. C. Schmidt

Sandia seeks to develop a massively parallel (MP), highly scalable, element-based atmospheric dynamical core. A dynamical core is defined as that part of a weather or climate model that solves the primitive equations, which are the stratified Eulerian equations of fluid motion in spherical coordinates and constitute the most computationally intensive calculations in an atmosphere or ocean model. Currently, the world's fastest dynamical core runs on the Japanese Earth Simulator, which recently achieved over 26 teraflops on 5120 vector processors, at an equatorial resolution of roughly 10 km. Our objective is to compete with this in absolute-performance measures and surpass this in cost-performance measures on the next generation of proposed Department of Energy (DOE) architectures.

The Japanese dynamical core uses the spectral transform method (STM), a common production-level dynamical core that has known scalability issues. Currently, the most scalable dynamical core is the Spectral Element Atmosphere Model (SEAM), a research code developed at the National Center for Atmospheric Research (NCAR).

Element-based approaches permit new capabilities impossible for the STM, including both static mesh refinement around geographic features and dynamic refinement around moving fronts. This capability will make SEAM particularly viable for emergency-response modeling of radiological, chemical, or biological dispersions. This will be made possible by tools developed at Sandia, such as AztecOO, CHACO, and ZOLTAN. Research will consist of improving the time-stepping capability of SEAM; of applying h-, p-, and hp-refinement strategy studies to standard test cases; of applying dynamic load-balancing algorithms; and of exploring low-order and discontinuous Galerkin element alternatives to spectral elements.

We added discontinuous Galerkin spectral element capability to the shallow water (two-dimensional [2-D]) version of the code, which is sufficient to study p-refinement and quad-tree refinement strategies.

We implemented the semi-implicit semi-Lagrangian (SISL) time-stepping scheme in the shallow water version. Work has

started on adding SISL time-stepping to the primitive equation (3-D) version, but it is not yet fully debugged.

We connected SEAM to Sandia's Aztec linear solver package for solving the semi-implicit system iteratively.

We began preconditioning studies for solving the semi-implicit linear system. We found certain combinations of solvers and preconditioners to be efficient for solving the implicit time-stepping system, but an exhaustive study has not been completed.

We performed a scaling study of the explicit time-stepping version of the code on Advanced Strategic Computing Initiative (ASCI) Red, in preparation for a capability-demonstration run on Red Storm.

We explored different approaches for subgrid turbulence modeling on nonuniform grids and recommended the multiscale modeling framework of Randall and Arakawa, coupled with the one-dimensional turbulence (ODT) model of Kerstein, for high-fidelity simulations.

Other Communications

Spotz, W. F. 2004. Solution techniques for the semi-implicit formulation of the spectral element method on the sphere. Paper presented at the 2004 Workshop on the Solution of Partial Differential Equations on the Sphere, 20–23 July, Yokohama, Japan.

Taylor, M. A. 2004. Spectral element methods for atmospheric modeling. Paper presented at the 2004 External Technical Review, Computers and Information Sciences (CIS), Centers 9200 and 8900, Sandia National Laboratories, 18 August, Albuquerque, New Mexico.

67016

High-Performance Processing Architecture

K. D. Underwood, K. S. Hemmert

Processor architecture is one aspect of supercomputer design that is typically unquestioned. Commodity processors are the basis of most major supercomputer acquisitions. Even Blue Gene/L, which uses a somewhat novel approach to system design, is based on commodity embedded-processor cores. As the barriers that traditional processors face mount, it is necessary to consider the implications of alternative processor architectures for scientific codes.

Sandia is studying the impact of reconfigurable computing on supercomputers at the petaflops scale and beyond. Reconfigurable computing is defined as the use of programmable hardware to provide application-specific acceleration. It is an alternative approach to processor architecture that is receiving significant attention in the research community; however, research is currently focused on application domains and system architectures that are very different from high-end scientific computing at the petaflops scale. This project is providing insight into issues facing the integration of reconfigurable computing into future supercomputers. Specifically, we are studying the use of field-programmable gate arrays (FPGAs) to provide reconfigurable computing at the petaflops scale.

The approach is two-pronged. One focus is on actual implementations of key computational kernels associated with Sandia's applications. Application implementation using FPGAs is a time-consuming process. Instead, we are implementing a small set of kernels to investigate the characteristics of FPGAs and their interface to the system. We will use data from these implementations to support the second focus of this project: the modeling of key Sandia applications. High-level modeling with simulation is a common technique within computer architecture research. We will leverage modern architecture simulation techniques along with data from initial implementations to gain understanding of the implications of FPGAs at the petaflops scale.

We had three major objectives this year, and we met or exceeded each of them. The first goal was to complete a set of double-precision floating-point units for FPGAs. This yielded designs that dramatically exceed the performance of all single-precision floating-point units available for purchase or that have been reported in the research literature.

[Our] first goal was to complete a set of double-precision floating-point units for FPGAs. This yielded designs that dramatically exceed the performance of all single-precision floating-point units available for purchase or that have been reported in the research literature.

The second major objective was to select a set of computational kernels for implementation in FPGAs and to begin those implementations. Thus far, we have implemented and characterized three kernels (the ddot, dgemv, and dgemm routines from the Basic Linear Algebra Subroutines [BLAS] library). This characterization was published at a conference in the field and received particularly positive feedback. We selected two others: fast Fourier transforms (FFT) and sparse linear solver, with the details to be finalized and implementation to begin in upcoming work.

The final objective was to create a parameterizable simulator to model systems incorporating FPGAs. An initial version of this simulator exists, including features to model microprocessors and network interfaces.

Refereed

Underwood, K. D. 2004. FPGAs vs. CPUs: Trends in peak floating-point performance. *Proc. 12th ACM International Symposium on Field-Programmable Gate Arrays* **12** (February, Monterey, California): 171–80.

Underwood, K. D., and K. S. Hemmert. 2004. Closing the gap: CPU and FPGA trends in sustainable floating-point BLAS performance. *Proc. IEEE Symposium on Field-Programmable Custom Computing Machines* **11** (April, Napa, California): 219–28.

67017

Substructured Multibody Molecular Dynamics

P. S. Crozier, M. J. Stevens, S. J. Plimpton, R. B. Lehoucq

Sandia seeks to continue to develop, implement, and optimize substructured, multibody molecular dynamics (SMMD) for simulation of systems that are currently beyond the capability of all-atom molecular dynamics (MD). This unique simulation capability will give insights into the operation of large, complex bio- and nanosystems. For example, the number of atoms in a motor protein is too large and the dynamics too slow for study by atomistic MD. However, large parts of the motor protein move as fairly rigid bodies linked by flexible connections. The SMMD method decomposes the protein complex into atomistic, flexible-body, and rigid-body regions, depending on each region's relevant internal motion. This allows the use of conventional atomistic force fields while gaining tremendous speed-up by freezing nonessential degrees of freedom. We will develop a parallelized version of a recently proposed SMMD method, Multi-Body Order(N) Dynamics, or MBO(N)D, into our bio-MD code LAMMPS (Large-Scale Atomic/Molecular Massively Parallel Simulator). In addition, we will implement implicit solvent methods and develop a robust procedure for specifying the substructure. Overall, we anticipate that this capability will enable dynamic studies of a variety of molecular machines, e.g., kinesin motion along microtubules, deoxyribonucleic acid (DNA) polymerase, etc. Programmatically, development of SMMD will position Sandia to contribute to the Genomes-to-Life project and other bio- and nano-related projects by elucidating structure-function relationships in macromolecular systems.

We made substantial progress toward developing a user-friendly, parallelized SMMD algorithm for accelerated simulation of large, complex bio- and nanosystems. We analyzed and tested the MBO(N)D code, which we will be using for the benchmarking of our SMMD algorithm. Most of our effort focused on implementing SMMD–enabling features into our massively parallel (MP) MD simulation package LAMMPS. These new features include a simple distance-dependent dielectric implicit solvent model, the ability to exclude selected force computations that become unnecessary in the SMMD procedure, and rigid-body constraints and dynamics. Work is in progress, in collaboration with Rensselaer Polytechnic Institute, on coupling LAMMPS with YAMS (Yet Another Multibody Simulator) for multibody simulation

capability. We also explored and tested alternative MD integration schemes that could lead to faster MD simulation. The SMMD code will enable long time scale simulation of RuBisCO (ribulose bisphosphate carboxylase/oxygenase), a carbon-fixing enzyme. Our RuBisCO simulations efforts gave us the opportunity to test our SMMD code developments.

67018

Enhancing Simulation Performance on Clusters with Configurable Auxiliary Devices

C. L. Janssen, C. D. Ulmer, M. W. Sukalski, M. L. Leininger, D. C. Thompson, R. C. Armstrong

During the last decade, an important trend in supercomputing has been the transition from custom-built hardware architectures (e.g., large vector processor machines) to commodity cluster computers. While this transition has made high-performance computing (HPC) available to a wider audience of scientists at much lower cost, there is still a significant performance gap between these two types of systems. For example, Japan's custom-built Earth Simulator is nearly twice as fast as the leading U.S. cluster computer. Given cluster computing's inherent price-performance advantage and its subsequent growing rate of adoption, it is critically important to investigate means to improve its efficiency.

In this project, Sandia is examining how new commercial accelerator devices can be leveraged to increase the performance of our existing cluster computers. These accelerators feature specialized hardware that is capable of processing scientific data significantly faster than general-purpose central processing units (CPUs) by efficiently mapping a larger subset of an algorithm in hardware. The dominant commercial accelerator is based on field-programmable gate array (FPGA) technology. FPGAs can be programmed to emulate any digital hardware circuitry. As such, an FPGA can be loaded with co-processing hardware that is hand-tailored to efficiently perform complex tasks that are needed by an application.

The research performed in this project is in direct collaboration with the "High-Performance Processing Architecture" project. While both of these projects involve reconfigurable computing (RC), each project independently addresses separate key areas in this field. This project specifically examines how the multigigabit transceiver units found in modern FPGAs can be used to connect the devices directly to the cluster computer's communication and input/output (I/O) fabrics. This work is complementary to the other project, which addresses computational aspects of FPGA co-processors.

Our two main objectives were to (1) create a research environment in which we could perform RC experiments, and (2) investigate the networking potential for current FPGAs.

For the first objective, we familiarized ourselves with current state-of-the-art RC practices and surveyed the commercial market for suitable FPGA development platforms. We acquired two FPGA reference platforms and appropriate development software. Within this development environment, we explored various experiments to study the capabilities of the Virtex-II/Pro FPGA architecture. We encapsulated these experiments as a series of design tutorials. We recently participated in a field trial of Cray's XD1 RC platform. The XD1 is a cluster computer with AMD Opteron microprocessors connected by HyperTransport and an InfiniBand-like interconnect. Optional FPGAs can be connected to the interconnect communication processor. The XD1 architecture provides high-bandwidth, low-latency access between processors, memory, and FPGAs. Based on our evaluation, we acquired a single-shelf, prototype XD1 with 12 Opterons and 6 Xilinx Virtex-II/Pro FPGAs for further investigation.

The second objective focused on defining techniques by which we can integrate FPGA resources into our existing cluster computers. One method of performing this integration is to connect the FPGA resources directly to the communication fabric that a cluster uses to distribute information between its nodes. This means of integration is possible with new FPGAs, such as the Xilinx Virtex-II/Pro, which feature multigigabit network transceivers (MGTs). Our research vision is to implement a fully functional network interface in the FPGA with these transceivers to enable the FPGA to send and receive messages with other resources in the cluster. We found that data could be transferred reliably between pairs of FPGAs at high data rates. The implication of this result is that large multi-FPGA systems can be assembled easily by connecting FPGAs together through their MGTs.

We found that data could be transferred reliably between pairs of FPGAs at high data rates. The implication of this result is that large multi-FPGA systems can be assembled easily by connecting FPGAs together through their MGTs.

For our initial work with the FPGA MGTs, we targeted the Gigabit Ethernet (GigE) network standard. While GigE offers only limited performance (1000 Mbps) for cluster computers, it is a standard that is widely deployed and well understood. We implemented a network interface core for GigE in FPGA hardware that comprises two cores: OpenGigE and OpenTOE. The OpenGigE unit handles low-level packet operations such as addressing and framing. The OpenTOE unit implements the Transmission Control Protocol (TCP) in hardware, which is used to guarantee that data are transferred reliably through the network. We intend to release this work as open-source hardware after more rigorous testing is performed.

We prototyped two applications for the FPGA accelerators. The first application is an isosurfacing algorithm for

visualization. The prototype for this application transforms a raw dataset into a series of polygons that can be rendered by existing video graphics cards. This work illuminated how visualization work can be offloaded into an FPGA and placed close to the network fabric. The second application that we experimented with is pattern matching for a network intrusion-detection system (NIDS). We worked with researchers at the Georgia Institute of Technology and connected their pattern-matching core to live network data streams. In addition to providing us with a great deal of development insight, this work is of high relevance to current homeland security efforts.

67019

A Hybrid Level-Set/Particle Method for Modeling Surface Evolution During Feature-Scale Etching and Deposition Processes

L. C. Musson

In this project, Sandia explored several ideas for creating a hybrid level-set (LS)/particle method for modeling surface evolution during feature-scale etching and deposition processes. An important characteristic of these problems is that surface velocities are always normal (either positive or negative) at every point on the surface. The research was motivated by the fact that standard LS approaches have only first-order spatial accuracy, thus requiring very refined grids in regions of high curvature to maintain fidelity.

After evaluating a variety of possible strategies, we developed and tested two ideas. The first method supplements the LS method by introducing Lagrangian marker points in regions of high curvature. Once both the particle-set and the LS functions are advanced in time, minimization of certain objective functions adjusts the LS function so that its zero contour is coincident with the particle locations. Unfortunately, we found that the objective-minimization problem was unexpectedly difficult to solve, and even when a solution could be found, the acquisition of it proved more costly then simply expanding the basis set of the LS.

The second method explored can be described as a novel grid-based point-projection method. Although not an LS method, the approach has qualities that can be compared to certain aspects of the LS approach and also involves the Lagrangian movement of surface particles. A key aspect of this approach is a surface rediscretization procedure— applied at each time-step and based on a global background mesh—that acts to maintain a higher-order representation of the surface while naturally adding and subtracting surface mesh points as the surface evolves in time. This method was coded in two dimensions (2-D) and tested on a variety of surface-evolution problems by using it in the ChISELS computer code. Results demonstrated that for 2-D problems, the approach was faster and more accurate than the standard LS approach.

We explored several ideas for creating a hybrid LS/particle method for modeling surface evolution during feature-scale etching and deposition processes. After evaluating a variety of possible strategies, we developed and tested two ideas.

The first method follows from data fitting and optimization techniques. The method consists of two quadratic objective functions and a linear inequality constraint. Once both the particle-set and the LS functions are advanced in time, minimization of the objective functions adjusts the LS function so that its zero contour is coincident with the presumably more-accurate particle locations. The LS method, in spite of its lower accuracy, is retained because of its ability to handle the topological changes that particle methods cannot handle without *ad hoc* approaches and considerable user interaction. The first of the two objective functions is a least-squares fit of the LS to the particle points. This fits the zero contour but also admits a trivial solution. A second objective function is added that requires the gradient of the LS function to have a unit magnitude. To ensure that the LS function has a unique sign, a linear inequality constraint is added. The dot product of the gradient of the LS function and the gradient of the initial LS function must be nonzero and nonnegative.

Ultimately, the end goal of the hybridized method is to improve upon inaccuracies attendant to the LS method when a finite basis set is used to represent the LS function. Thus, coarser discretizations, i.e., fewer basis functions, of the LS evolution equation could be enabled and corresponding central processing unit (CPU) savings realized. As it turns out, however, the objective-minimization problem proved unexpectedly difficult to solve. Even with full Newton linearization and an analytical Jacobian matrix, solutions often could not be found. In addition to the newly written Newton solver, NOX, we used a Sandia-produced nonlinear equation solver, a part of the TRILINOS suite, with equal success. We determined that, even when a solution could be found, its acquisition proved so costly as to make it not a viable alternative to expanding the basis set of the LS.

The second method can be described as a grid-based point-projection method for surface evolution. Although not an LS method, the approach has qualities that can be compared to certain aspects of the LS approach and also involves the Lagrangian movement of surface particles.

In the first step of this approach, we discretize the evolving surface by the collection of points found by drawing a line from each mesh point in a uniform background mesh to the nearest point on the surface within each mesh cell. Based on the surface-velocity field, we then move these points, in a Lagrangian fashion, to new positions at time t + dt. Next, a local consolidation step removes redundant points and reconciles global overlaps through simple rules. Finally, we rediscretize

the surface using the same procedure described in the first step, yielding a new set of points to be advanced during the next cycle. A key aspect of this approach is how the rediscretization procedure applied at each step acts to maintain a high-order representation of the surface while naturally adding and subtracting surface mesh points as the surface evolves in time.

The second method was coded in 2-D and tested on a variety of surface-evolution problems by using it in the ChISELS computer code. Results demonstrated that for 2-D problems, the approach was faster and more accurate than the standard LS approach.

67020

Penetrator Reliability Investigation and Design Exploration (PRIDE)

M. L. Martinez-Canales, R. Heaphy, L. P. Swiler, P. J. Williams, M. L. Chiesa, T. G. Trucano, P. D. Hough

The role of modeling and simulation in weapons design raises important questions that must be credibly answered. How sensitive is the simulation to model parameters? To what extent do simulation parameters contribute to model error? How does modeling help us design a reliable weapon given specified mission uncertainties? Answering such questions using conventional tools requires excessive manpower and computational effort. The goal of this project is to integrate optimization methods and credibility metrics with uncertainty quantification (UQ) techniques in a novel way that reduces the computational expense of the overall design process, enabling the design of credible, higher-quality, more-reliable penetrators.

This project focuses on research and algorithmic development in optimization under uncertainty (OUU) problems based on earth-penetrator (EP) designs. There are three main challenges for this work:

(1) Leveraging existing small local samples, already needed by some optimization methods, to build local probability density functions (PDFs) that contribute to a Bayesian construction of a global PDF. The global PDF is vital to assessing model applicability and reliability and making probabilistic decisions.

(2) Developing a methodical design process based on multiresolution models. Using PDFs to characterize the underlying parameter and model uncertainties, as well as important model features, we are building reduced-order models that are effective and computationally inexpensive.

(3) Developing tools that not only are useful to the weapons community, but also are computationally feasible.

Sandia's strategy was to balance research in OUU and Bayesian formalism with practical design exploration. To that end, we successfully canvassed current penetrator designs, explored Bayesian formalisms and other innovative optimization approaches, conceptualized a multifidelity penetrator design and developed a small-fidelity penetrator prototype, formalized design-optimization formulations, engaged in a small design-exploration study in which general linear model analysis techniques were used, and understood performance measure choices on penetrator design. This work lays the groundwork for upcoming work.

To maximize impact to the EP programs beyond [conducting sensitivity studies on] established designs, the PRIDE team, in conjunction with penetrator experts, decided to initially focus on the Pen-X EP program. The Pen-X program is an example of an enhanced penetrator design in which a large cavity is created ahead of the penetrator by a specifically designed shaped charge. Because most design elements of the Pen-X are currently in flux, we are able to test a range of ideas being developed in this project.

To begin the penetrator study, we defined three fidelity models of the EP. The low-fidelity 30,000 finite-element model (FEM) assumes that the penetrator is a solid homogeneous cylindrical body. The penetrator body consists of a length L2, capped by two ellipsoids of major radius L1 and L3, corresponding to the radii of the nose and tail, respectively. The medium-fidelity model will include the coarse model of the penetrator case and internal blivets and a finer target mesh. The high-fidelity model includes an accurate model of the penetrator case and internals and an even finer target mesh.

We completed a small design exploration and pseudo-optimization study of the low-fidelity model acceleration response. We were interested in understanding the effect of the two variable parameters, L1 and L3, on the acceleration responses at the nose tip and aft end. We also were interested in finding the design that produces the minimum total acceleration.

A general linear model for an analysis of variance of the maximum total, vertical, and horizontal acceleration (at an aft node) versus both the nose and tail radii showed that the nose radius significantly impacted these responses more than the tail radius. The generalized linear model also detected that two designs in particular influenced the variance analysis. One of these designs corresponds to the case where the nose radius is maximally small and the tail radius is maximally large so that the penetrator nose is very blunt. This design has a minimal total acceleration at the aft node. Unfortunately, this particular penetrator design achieves poor penetration depth.

The other design flagged by the generalized linear model analysis corresponded to the case where the nose radius is maximally large and the tail radius is maximally small so that the penetrator nose is very pointy. This penetrator design had good penetration (even though it bounced off of the shaft walls) but had high lateral accelerations at the aft node. These lateral accelerations might lead to the penetrator breaking because of bending.

From these initial design exploration and pseudo-optimization studies, we learned that other performance metrics and sensitivities need to be explored.

Other Communications

Martinez-Canales, M. 2004. Improving the penetrator design process. Research highlight for the *Sandia National Laboratories California Communicator Newsletter,* Livermore, California (October). 2004-4459P.

67021

Topology Optimization for Improving Sensor Performance

K. R. Long, E. B. Cummings, B. G. Van Bloemen Waanders, P. T. Boggs

Optimal design of the geometry of a device occurs in many areas of engineering. In many problems, it is not sufficient to deform the shape of boundary surfaces; rather, we must vary the topology of the problem domain by introducing holes or islands. An example of such a problem is designing a minimum-dispersion expanding channel for use in microfluidic sensors; optimizing the shape of a channel wall without introducing new islands yields, at most, a few-percent improvement over a simple linear wall.

Level-set (LS) methods can represent changes in both shape and topology of the boundary surface. Sandia introduced a new LS method that uses a limited-memory Broyden Fletcher Goldfarb Shanno (LM-BFGS) algorithm to evolve the design variable and, along with this, developed a new method for applying boundary conditions (BCs) on the LS that preserves differentiability of objective functions, requires no explicit tracking of the zero LS or evaluation of embedded surface integrals, and is easily implemented in finite-element (FE) codes. Our new method proved to be more rapidly convergent than previously published methods. We applied it to the problem of minimizing dispersion in an expanding microfluidic channel. In our preliminary computations, we realized a reduction of a factor of 3 in our measure of the dispersion of particles in the channel outlet, many times better than what we were able to achieve by varying shape alone.

We implemented in SALINAS a homogenization method, which is appropriate for problems in structural mechanics. We developed a user interface in which an initial guess for geometry can be input through AutoCAD, and the optimized geometry is returned as an AutoCAD file. This software is being applied to optimal design of arming, fuzing, and firing (AF&F) device geometry.

We applied [our new method] to the problem of minimizing dispersion in an expanding microfluidic channel. In our preliminary computations, we realized a reduction of a factor of 3 in our measure of the dispersion of particles in the channel outlet, many times better than what we were able to achieve by varying shape alone.

We made a number of advances in algorithm development and in implementing the software infrastructure required to bring topology optimization capability to Sandia applications. Furthermore, we tested our algorithms and software on two Sandia applications: dispersion minimization in an expanding microfluidic channel, and compliance minimization in an AF&F system.

(1) We developed an accelerated LS method that uses an LM-BFGS method as a stepper rather than the traditional evolutionary partial differential equation (PDE). A prerequisite for this was the development of a new method of mapping the LS function to an approximately Boolean variable in a differentiable way. We formulated this mapping in a way that is naturally implemented in FE codes, making the application of LS BCs much simpler. We implemented these new algorithms in Sundance, a general-purpose code for solving nonlinear PDEs in parallel.

We compared the performance on the microfluidic expanding channel design problem of our LM-BFGS–based topology optimizer, the Osher-Santosa optimizer based on pseudotime evolution of the Hamilton-Jacobi equation, and a homogenization method. Our new method is significantly more efficient. For example, to produce a design yielding a factor of 3 reduction in dispersion, our method required 166 iterations to converge, while the Osher-Santosa optimizer took 400 iterations to converge to a less-satisfactory design with twice the outlet dispersion of the optimal. We were unable to solve this problem at all using a homogenization method.

The most significant challenge we have encountered in optimizing microflow geometry is the need for global optimization. At high spatial resolutions, we encounter multiple minima. Global optimization originally was part of upcoming work, but we began exploring and implementing a multilevel strategy for global optimization.

(2) While the homogenization method is not appropriate for optimizing microchannels and other nonlinear problems, it is perhaps the best choice for problems in structural dynamics. With that in mind, we introduced a simple homogenization capability into SALINAS. We tested our initial implementation by minimizing the compliance of a simple two-dimensional beam with supports carrying a centrally located load. We produced and verified different geometries by manipulating the volume constraint. We tested this capability in 2 and 3 dimensions. We initiated a preliminary study to investigate alternative geometries for a structural member in the AF&F system that has exhibited undesirable stress levels. An initial mesh dataset produced interesting shapes but was too coarse. We generated a higher-resolution discretization that will require the use of parallel resources.

To support the AF&F project and other applications of topology optimization, we developed an interface that will allow an analyst to prepare initial designs in AutoCAD, automatically apply topological optimization using SALINAS,

and return the resulting geometry back to the AutoCAD environment for post-processing. This capability will be extremely useful for many analysts, but, in particular, to microelectromechanical systems (MEMS) designers who are very interested in evaluating different geometries. Although we developed the AutoCAD interface to facilitate our work with structural topology optimization in SALINAS using the homogenization method, the interface will also be usable in problems with more complex physics that requires our LS approach. Because it uses Exodus files as an intermediary, it will be usable with most Sandia simulation codes.

Other Communications

Long, K. 2004. Sundance 2.0 and applications to topology optimization. Paper presented at the Civil and Environmental Engineering Department Seminar, Carnegie-Mellon University, 2 September, Pittsburgh, Pennsylvania.

Differentiating Technologies

Historically, the Differentiating Technologies investment area has focused on research activities that work to accelerate the development of novel sensing, microsystems, and cybersecurity technologies. Projects in the past created the opportunity for advanced, remote infrared (IR) optical sensing; novel microchip designs for sensor networks; and advanced cybersecurity counter-measures. Investments in Differentiating Technologies have been consistently successful in engaging in multidisciplinary challenges across all four Sandia Strategic Business Units. To facilitate the evolution of the LDRD program, the investment area will close, allowing new investment areas to be initiated. In 2004, Differentiating Technologies funded only one project that pursued advancements in energy and power technology for compact applications.

41674
"Microengine for Advanced Power Generation"

Operations requiring portable electronics, sensors, micro-aerial vehicles, and minirobotics systems are currently limited by the energy- and power-density capabilities of batteries. A small combustion engine using liquid hydrocarbon fuel can potentially increase both power and energy density by an order of magnitude or more. To address the issue, researchers attempted to develop a mesoscale external-combustion engine based on the Stirling cycle using LIGA-fabrication technology. Designs for both piston and rotary engines were investigated. To advance technology toward the realization of a combustion engine, a high-fidelity simulation code was developed to investigate fundamental combustion issues associated with catalytic microcombustion in channels using the spectral element approach. Temperature and scalar concentrations from the simulation were compared with the experiment. The piston design was tested as a heat pump and did not produce appreciable combustion in the compression. Due to problems with fabrication of the central shaft, the rotary design assembly was not completed.

41674

Microengine for Advanced Power Generation

B. L. Haroldsen, M. A. Hekmaty, A. M. Morales, T. N. Raber, S. Liu, A. N. Karpetis, J. H. Chen

Power sources capable of supplying tens of watts are needed for a wide variety of applications, including portable electronics, sensors, micro-aerial vehicles, and minirobotics systems. These items currently are limited by the energy- and power-density capabilities of batteries. A small combustion engine using liquid hydrocarbon (HC) fuel can potentially increase both power and energy density by an order of magnitude or more. Toward this end, Sandia is developing a mesoscale external-combustion engine based on the Stirling cycle. The engine utilizes LIGA (for the German term Lithographie, Galvanoformung, und Abformung, *for lithography, electroforming, and molding) structures fabrication technology as a means to achieve the requisite precision and miniaturization. LIGA offers the tight tolerances needed for efficient engine operation and flexibility in materials of construction, including metals, metal alloys, and ceramics for high-temperature use. LIGA also provides the potential for further scale reduction into the milliwatt regime at a later time.*

We worked on two engine designs. One is a conventionally machined piston engine, and the other is a LIGA–fabricated rotary design. We tested the piston engine as a heat pump, but not as an engine. We completed and partially assembled LIGA parts for the rotary design. However, due to problems with fabrication of the central shaft, we did not complete assembling the rotary design.

A partially assembled miniature rotary Stirling engine. We used LIGA technology to produce the critical high-aspect-ratio micromachined parts. We also developed a microcombustor under this project as a heat source for the engine.

- *Piston engine testing*. We continued testing the conventionally machined piston engine. To simplify the testing, we used a microelectric motor to drive the engine so it would function as a heat pump instead of as an engine. We measured the driving current and voltage to the motor and the pressure and temperature in the cylinder. We observed the heat-pumping effect as a temperature difference between the hot and cold ends of the engine, which increased in magnitude when we increased the engine speed or the operating pressure.

The temperature difference that we achieved in testing was limited to a few degrees. This occurred in operation at 50 Hz and 125 psi. In theory, it should have been possible to significantly increase the temperature difference by increasing the speed and the mean pressure. Our attempts to do so were unsuccessful because the jewel bearings on the piston connecting rods proved unreliable at the more stressful conditions. Furthermore, the heat-pumping effect was smaller

than expected at all conditions due to poor sealing around the pistons. The measured compression ratio was only about one-third of the ideal value. The compression improved considerably at higher speeds since there was less time for leakage past the piston. Consequently, had we been able to push the speed to several hundred revolutions per minute (rpm), it might have been acceptable. In an attempt to improve the seals, we reassembled the engine with new pistons and used two piston designs on alternating cylinders. Half the cylinders used the same metal pistons, except that we added Torlon piston rings. To make the assembly possible, we used split rings. Each piston had two rings with the splits 180 deg apart. The other cylinders used Torlon pistons, which we designed to fit more tightly than the metal pistons. Neither piston design produced appreciable improvement in the compression.

- *LIGA rotary engine*. After electroforming the first-generation LIGA Stirling engine in SU8 (ultraviolet LIGA), we designed a second-generation engine. The new design incorporated features such as enlarged via holes for faster release from the plating base, assembly-precision pinholes to stack parts to build thicker engines, and a modified Wankel engine shape. We first prototyped the second-generation design using an optimized SU8 process, and after verifying the validity of the new design, we used the LIGA process to produce 500 µm-thick nickel watts components.

We assembled the two ends of the engine individually. Unlike the earlier SU8 parts, the LIGA parts fit extremely well and turned freely. Unfortunately, we had difficulty fabricating the lobed shaft that ties the two ends together. This was a conventional machined part that was not expected to be difficult to machine. However, the machine shop scrapped several attempts and was not able to deliver a shaft before the end of the project. Consequently, the complete rotary engine has not been assembled.

- *Microcombustor.* As a first step toward characterization of combustion processes in small combustors, we took measurements of species and temperature profiles above the exit of a thin platinum/20 iridium tube operated over a range of combustion conditions in the Turbulent Combustion Laboratory (TCL), using a unique multiscalar laser diagnostic system.

This system combines line-imaging of Raman scattering, Rayleigh scattering, and two-photon laser-induced fluorescence of carbon monoxide to obtain simultaneous measurements of temperature and the concentrations of all major species with excellent spatial resolution, allowing for detailed characterization of the product stream issuing from the

microcombustor channel. We developed a high-fidelity simulation-code capability to investigate fundamental combustion issues associated with catalytic microcombustion in channels using the spectral element approach. We compared temperature and scalar concentrations from the simulation with the experiment.

Electronics and Photonics

Investments in Electronics and Photonics seek innovative ideas that build on differentiating strengths in photonics, microelectronics, and MEMS (microelectromechanical systems), and work to advance silicon and compound semiconductor science and technology. Efforts are directed toward enabling the success of small, low-power, highly integrated electronics packages called integrated microsystems. *Electronics and Photonics investments work to develop and apply semiconductor fabrication techniques to combine electronic, optical, mechanical, and chemical functions into integrated systems. The goal is to exploit the potential applications of integrated micro-systems with low cost and high reliability through new and innovative approaches to packaging, integration, and micropower systems.*

52554
"An Integrated, Stacked System-on-a-Chip"

In a miniaturized microsystem, the major difficulty is in integrating different device technologies in a small volume. Researchers developed innovative processes and materials to integrate multiple device technologies, enabling them to stack wafers and progressing toward a fully integrated system-on-a-chip that incorporates passive and active devices. Wafers are "glued" with benzocyclobutene (BCB), allowing an interconnect structure and embedded passive devices in the "glue" layer. Researchers were also able to produce through-hole vias in silicon before and after bonding, to reduce grinding effects of thinning, and to achieve wafers only 20 µm thick using a new vendor-proprietary process. Additionally, a modified bonding fixture was developed to eliminate wafer cracking caused by higher force and temperature. Continuing research pursues techniques to isolate vias from silicon and to insulate vias fabricated pre- and post-bonding. Two patents are pending.

38616

Engineered Superconductivity in Electron-Hole Bilayers

M. P. Lilly, J. L. Reno, J. A. Simmons, L. L. Stephenson, R. G. Dunn

Sandia seeks to fabricate and measure transport characteristics of an electron-hole bilayer (EHBL). Due to the strong attractive interaction between the oppositely charged carriers, this system is expected to make a transition to a superconducting state at low temperatures. We will implement the EHBL in gallium arsenide/aluminum gallium arsenide (GaAs/AlGaAs) heterostructures, where individual layers can be in close proximity to maximize the Coulomb energy. Additional critical features will be high electron and hole mobilities, low sheet densities, and independently contacted layers. Through use of bandgap engineering, we can tune these parameters to optimize the device.

The success of this project relies on the integration of four techniques: molecular beam epitaxy (MBE) crystal growth, use of undoped heterostructures, dual-side lithography, and Coulomb drag transport measurements. Since the superconducting state depends on interactions between the layers, extremely high mobility MBE heterostructures are required. To avoid problems that arise with doping bipolar systems, we implemented undoped heterostructures. The carriers are generated using self-aligned contacts in a field-effect transistor (FET) geometry; we demonstrated that this technique is consistent with high mobility and low density. In the proposed EHBL device, self-aligned contacts are needed above and below the bilayer. Our main focus was to characterize the low-density behavior of low-density electrons, improve undoped techniques, and incorporate the EBASE (epoxy bond-and-stop etch) technique with undoped double-layer heterostructures.

Our accomplishments can be divided into three categories. First, in ultralow-density single layers of two-dimensional (2-D) electrons, we have convincing transport evidence that conductions begin after a percolation threshold is reached. Second, processing advances led to reliable single- and double-layer undoped GaAs/AlGaAs structures. Finally, we demonstrated density-tunable electron-electron bilayers for the first time in undoped GaAs/AlGaAs systems and are fabricating EHBLs.

Previously, we used ultralow-density electron devices to study the interesting problem of a metal-insulator transition in 2-D. These experiments showed that the apparent metallic behavior of the resistivity (i.e., decreasing resistivity as

temperature decreases for T < 1 K) at intermediate densities can be understood using conventional scattering theory when the explicit temperature dependencies of both screening and thermal occupation are included. At the lowest density, however, these arguments fail, and other physics dominate. One possible problem with the scattering treatment is the assumption of a uniform density; it is known that inhomogeneities are important in this regime. One physically appealing concept is that of percolation. In a percolation transition, disconnected puddles of electrons connect across the samples as the density is raised, and a characteristic density dependence of the conductivity should be observed. By analyzing the density dependence of the conductivity, we show agreement with the scaling behavior predicted by a percolation transition.

To extend our successful studies of single layers to the more complicated bilayer systems, we required several advances in processing. The most important processing advance made this year was improvements to the wet-/dry-etching procedure for making self-aligned ohmic contacts. Through several iterations in cleaning procedures between steps, we improved to at least an 80% success ratio for *n*-type contacts. With our ability to make a high percentage of single-layer samples, we turned our efforts to creating undoped bilayers for the first time. We combined self-aligned *n*-type contacts for the top 2-D layer with a thinning procedure (EBASE), insulating layers, and an overlapping back gate. With these extensions of the processing, we made electron-electron bilayers.

While the ultimate goal was the fabrication and study of EHBLs, the complication of the devices pointed to the necessity of an intermediate step of making electron-electron bilayers. Using the processing described above, we created electron bilayers with good transport characteristics and several (unintentional) independent contacts. The density of each layer could be reduced to 1E10 cm^{-2}, and as high as 6E10 cm^{-2} in the top layer and 1.5E11 cm^{-2} in the lower layer. These samples were of high-enough quality to have the nu_total (ν_{total}) = 1.0 quantum hall state visible at high magnetic fields and low temperatures. This is the first time a fully undoped bilayer has ever been made, and by itself this holds promise for future fundamental studies of low-density electron bilayers.

With all of these advances in our understanding of fabricating undoped GaAs/AlGaAs structures, and of the fundamental physics effects that are important in low-density 2-D electrons, we are fabricating EHBLs to look for excitonic condensation. We will utilize all of the techniques used to make

This is the first time a fully undoped bilayer has ever been made, and by itself this holds promise for future fundamental studies of low-density electron bilayers.

electron-electron bilayers with no changes, so our chance of success is very high. While the EHBL project has faced serious technological hurdles, these have been overcome. These novel EHBL devices are positioned to contribute to our fundamental understanding of interactions and coherent states at low temperature, and several concepts are under consideration for more useful applied devices.

Refereed

Lilly, M. P. 2004. Resistivity of ultralow-density two-dimensional electrons. Paper presented at the American Physical Society Meeting, March, Montreal, Canada.

Sarma, S. D., M. P. Lilly, E. H. Hwang, L. N. Pfeiffer, K. W. West, and J. L. Reno. 2004. 2-D metal-insulator transition as a percolation transition. *Physical Review Letters*, submitted.

Other Communications

Lilly, M. P., E. Bielejec, J. A. Seamons, and J. L. Reno. 2004. Weak localization of dilute 2-D electrons in undoped GaAs heterostructures. Proc. *27th International Conference on the Physics of Semiconductors*, ed. J. Menéndez and C. G. Van de Walle. College Park, Maryland: American Institute of Physics (26–30 July, Flagstaff, Arizona).

38617

Silicon-Based RF MEMS Components

C. W. Dyck, C. D. Nordquist, M. S. Baker, J. G. Fleming, J. E. Stevens, S. E. Allen

Radio-frequency microelectromechanical systems (RF MEMS) is an enabling technology for the next generation of communications and radar systems in both military and commercial sectors. These devices have low insertion loss and low static-power consumption, are lightweight, and are capable of high levels of integration with other components. Successful development of this technology would be beneficial for frequency ranges below 10 GHz. Historically, III–V compound semiconductor material has been used for RF communications components. Sandia will design and begin fabricating prototype microdeployable antennas using actuation or fluidic approaches that allow for flexibility in deploying antenna structures when needed for operation.

We developed a high-contact-force latching relay for low-signal-frequency applications. We fabricated the latching switch in a molded tungsten (W) damascene process known as MOLTUN, which was originally developed to fabricate photonic lattice (PL) structures. Plasma-enhanced chemical vapor deposition silicon dioxide (PECVD SiO_2) is the sacrificial layer, and a grid of W-filled and polished trenches forms the mechanical structures. We accomplish electrical isolation by a PECVD silicon nitride (SiN) deposition and etch step prior to the sacrificial SiO_2 deposition.

We formed the latching switch out of a suspended W plate with two opposing thermal actuators. Each of the suspending thermal actuator arms is in tension after the release process because the W is chemical vapor deposition (CVD)–deposited at 400°C and goes into tension as it cools due to the thermal-coefficient mismatch between the W and the Si substrates. Applying a voltage between one or more combinations of bondpad pairs resistively heats and expands those springs. The springs that are opposite the heated springs contract due to built-in tension and pull the plate in the direction of the unheated springs. The switch has two pairs of opposing springs that allow it to have two degrees of freedom (2 DOF). The thermal actuation in combination with the built-in W stress results in plate displacements > 10 μm and forces > 10 mN. The switches and contacts can be patterned to accommodate mechanical stops for latching the switch plate. The high built-in stress also has the advantage that latching contact forces are

high without the need for applied signal power. Contact metals can be evaporated onto the switch sidewalls to lower the contact resistance. Angled evaporation and careful switch structural design prevent bondpads and contacts from shorting.

In an effort to extend low-loss RF MEMS technology to broadband applications at frequency ranges much greater than Ka band, we did a paper study on membrane-supported stripline technology. Planar microstrip technology is commonly used because it has low metal propagation loss and is monolithic microwave integrated circuit (MMIC)–compatible. However, microstrip performance becomes limited at Ka band frequencies by radiation losses arising from discontinuities in circuits with high dielectric constants, such as Si, gallium arsenide (GaAs), or alumina. Dispersion is also an issue due to the substrate–air-dielectric mismatch. On the other hand, an air-dielectric stripline has neither radiation loss nor dispersion and has lower metal-loss attenuation than microstrip technology. This type of technology is also MEMS–compatible for low-loss reconfigurable circuits and is readily hermetically sealed for high-reliability applications. We could use a combination of bulk micromachining and wafer bonding to obtain the upper and lower ground planes. We can fabricate the circuit elements on a thin suspended membrane made of Si-rich SiN deposited by low-pressure CVD methods. The circuit size is limited by the mechanical integrity of this membrane. High-performance static microwave circuits are possible and were demonstrated by the University of Michigan. Broadband reconfigurability requires a high-performance capacitive switch, however. The operational frequency of this technology is easily extended to greater than 100 GHz.

Currently, work is ongoing to fabricate a capacitive switch design that uses the native oxides on W and aluminum (Al) as the switch dielectric. The switch consists of a suspended Al signal line above a W shorting line that connects the two coplanar waveguide (CPW) ground lines. Separate actuation lines pull the signal line down into contact with the shorting line. The thin native-oxide dielectrics create a low-impedance path between the signal line and the ground lines, causing a reflection of the incident signal.

Refereed

Fleming, J. G. 2004. Oxide molded tungsten process for micromachining. *J. Micromachining and Microfabrication* (ASME and IEEE), to be submitted.

38619

Nanoelectromechanical Oscillators (NEMOs) for RF Filtering

J. P. Sullivan, D. A. Czaplewski, B. N. Keeler, J. R. Webster, D. W. Carr, J. R. Wendt, T. A. Friedmann, C. W. Dyck

In this project, Sandia created high-frequency and high-quality (Q) nanoelectromechanical oscillators (NEMOs) for radio-frequency (RF) signal processing, and demonstrated a possible solution to charge trapping in capacitively coupled RF microelectromechanical systems (MEMS) switches. NEMOs are defined as mechanical oscillators with critical dimensions of 50 nm or less and resonance frequencies approaching 1 GHz. Target applications for these devices include passive RF electrical filters or platforms for sensor arrays. We would expect these technologies to benefit Sandia programs in RF communications or Sandia/Department of Homeland Security (DHS) programs in chemical-, environmental-, or biological-agent sensing. The capacitively coupled RF MEMS switches have technological importance in RF electronics, reconfigurable receivers/transceivers, and radar. These technologies are important for many of the Laboratories' missions in nonproliferation, homeland security, and defense.

Our approach to achieving NEMOs with the requisite performance centered on (1) using a new, ultrahigh-modulus MEMS material, amorphous diamond (aD) (with frequency twice that of silicon [Si]), (2) using a new in-plane array of NEMOs that is easy to fabricate and permits the use of novel optical-detection schemes, (3) taking advantage of the inherent hydrophobicity of aD surfaces to enable the release of oscillator structures and to reduce surface losses, and (4) performing fundamental studies of energy dissipation in nanosized structures to understand what controls Q in this system. The approach to reduce the dielectric-charging reliability problem in capacitively coupled RF MEMS switches involved the incorporation of aD as a dissipative dielectric. We evaluated RF MEMS switch performance by performing repeated cycling of the switches while monitoring switch performance (e.g., on-off state capacitance).

We made important developments in all areas of this project, including the demonstration of RF MEMS capacitively coupled switches that show improved reliability, the development of a new electrooptic sensor structure based on a NEMO array fabricated of aD, and the demonstration of a laser

annealing process that permits integration of aD films in new technology areas.

The RF MEMS capacitively coupled switches used aD as a dissipative dielectric. The devices showed a unipolar switching response to a unipolar stimulus. This indicates the absence of significant dielectric charging, which has historically been the major reliability issue with this technology. The devices exhibited a down-state capacitance of 2.6 pF and a predicted static-power dissipation of 10 nW, making this technology promising for the development of reliable, low-power RF MEMS switches. We wrote a patent application based on this technology.

We used the aD NEMO arrays to experimentally demonstrate a laterally deformable optical nanoelectromechanical system (NEMS) grating transducer, a new device technology (patent applied). For small changes in the spacing of the NEMO array elements, lossy propagating resonant modes in the plane of the array cause a large change in the optical reflection amplitude. We measured an in-plane motion-detection sensitivity of 160 fm/$Hz^{1/2}$, exceeding that of any other optical MEMS transducer, to our knowledge. Calculations predict that this sensitivity could be improved to better than 40 fm/$Hz^{1/2}$ in future designs. In addition to having applications in the field of inertial sensors, this device could also be used as an optical modulator.

We developed an excimer-laser annealing process that permits full in-plane stress relaxation in aD films in air under ambient conditions. We used the homogenized beam of a pulsed excimer laser (248 nm, 0–300 mJ/cm^2) to irradiate aD thin films and found that it was possible to completely relieve the high average compressive stress (7 GPa) found in these films. Below a threshold fluence of 250 mJ/cm^2, Raman spectroscopy, hardness, and surface-roughness measurements before and after the laser annealing revealed only minor changes from the as-grown state, indicating that the films retained their diamondlike qualities. Above the threshold fluence, we found significant graphitization and resultant softening of the films. One significant difference between the laser-annealed and furnace-annealed films was the very high tensile stresses (~ 3 GPa) produced in films annealed near the fluence threshold under certain conditions. These high tensile stresses suggest that there is a different mechanism for stress generation in the laser-annealed films. Modeling of the laser annealing indicated that the observed stress relaxation results from a near-surface thermal spike in the film. Through appropriate control of film thickness, the temperature increase below the aD layer can be

We used the aD NEMO arrays to experimentally demonstrate a laterally deformable optical nanoelectromechanical system (NEMS) grating transducer, a new device technology (patent applied).

limited to a few hundred degrees Celsius. This permits the application of stress-reduced aD films in areas where a low thermal budget is required, e.g., integration with pre-existing complementary metal-oxide semiconductor (CMOS) electronics.

Refereed

Carr, D. W., B. E. N. Keeler, J. P. Sullivan, T. A. Friedmann, and J. R. Wendt. 2004. Measurement of a laterally deformable optical NEMS grating transducer. *Proc. SPIE Photonics West* **5346** (24–29 January, San Jose, California): 56.

Chasiotis, I., S. W. Cho, T. A. Friedmann, and J. P. Sullivan. 2003. Young's modulus, Poisson's ratio, and nanoscale deformation fields of MEMS materials. *Proc. Materials Research Society* **795** (November, Boston, Massachusetts): 461.

Chen, X., J. P. Sullivan, T. A. Friedmann, and J. M. Gibson. 2004. Fluctuation microscopy studies of medium-range ordering in amorphous diamondlike carbon films. *Applied Physics Letters* **84** (15) (April): 2823–25.

Cho, S., I. Chasiotis, T. A. Friedmann, and J. P. Sullivan. 2004. Direct measurements of Young's modulus, Poisson's ratio, and failure properties of tetrahedral-amorphous carbon for MEMS devices. *J. Micromechanics and Microengineering*, submitted.

Friedmann, T. A., J. P. Sullivan, and D. R. Tallant. 2003. Stress relaxation by excimer-laser annealing in amorphous carbon thin film. Paper presented at the Materials Research Society Conference, November, Boston, Massachusetts.

Friedmann, T. A., J. P. Sullivan, B. L. Boyce, D. R. Tallant, and P. P. Provencio. 2004. Stress relaxation by excimer annealing in tetrahedral amorphous carbon thin films. Paper presented at Diamond 2004, September, Riva del Garda, Italy.

Friedmann, T. A., J. P. Sullivan, D. A. Czaplewski, C. W. Dyck, J. R. Webster, D. W. Carr, B. E. N. Keeler, J. R. Wendt, T. E. Buchheit, I. Chasiotis, S. Cho, H. D. Espinosa, B. Peng, J. A. Carlisle, and O. Auciello. 2004. MEMS and ta-C thin films: Overview of devices. Paper presented at SMAC 2004, September, Povo, Italy.

Friedmann, T. A., J. P. Sullivan, D. R. Tallant, and B. L. Boyce. 2004. Stress relaxation of tetrahedral amorphous carbon (ta-C) thin films by pulsed excimer-laser annealing. *J. Applied Physics*, submitted.

Keeler, B. E. N., D. W. Carr, J. P. Sullivan, T. A. Friedmann, and J. R. Wendt. 2004. Experimental demonstration of a laterally deformable optical nanoelectromechanical system grating transducer. *Optics Letters* **29** (11) (June): 1182–84.

Webster, J. R., C. W. Dyck, J. P. Sullivan, T. A. Friedmann, and A. J. Carton. 2004. Performance of amorphous diamond RF MEMS capacitive switch. *Electronics Letters* **40** (1): 43–44.

Webster, J. R., C. W. Dyck, T. A. Friedmann, J. P. Sullivan, C. D. Nordquist, A. J. Carton, G. M. Kraus, and G. D. Schmidt. 2004. Development of an amorphous diamond (a-D) RF MEMS switch. *Proc. SPIE Photonics West* **5344** (18–22 January, San Jose, California): 71.

38620

Continuous-Wave Intersubband Terahertz Sources

M. C. Wanke, E. W. Young, S. Mou, M. A. Mangan, R. J. Foltynowicz, S. Samora, G. A. Vawter, C. T. Fuller, A. V. Smith, J. L. Reno

There is a general lack of compact solid-state sources between 1 and 10 terahertz (THz), a challenging spectral region lying between optical devices at high frequencies and electronic devices at low frequencies. This region is of great technological importance for higher-bandwidth space-based and short-range terrestrial communications, atmospheric sensing, and near-object analysis for chem-bio sensing. While the last few years have seen significant advances and development in ultrashort-pulsed terahertz sources, many important applications require continuous-wave (CW) sources, which remain in their infancy. Sandia is examining two approaches to terahertz generation based on intersubband transitions.

In the first approach, a quantum cascade (QC) laser simultaneously emits two mid-infrared (MIR) frequencies differing by a few terahertz. These are used to pump a nonlinear optical material to generate terahertz radiation via parametric interactions. As a specific example, we will examine difference-frequency generation by three-wave mixing in a specifically engineered intersubband transition. In general, the efficiency of the frequency mixing increases with the pump power; thus, we will examine approaches to integrate the mixing material such that it shares the same waveguide as the QC laser, where the intracavity field strength is the strongest.

Our second approach is to pursue QC lasers that operate at terahertz frequencies. This is simpler than a mixing approach and has been demonstrated by other groups over the last year with operation wavelengths spanning 70–100 µm. However, they are more difficult to design and have reliability and reproducibility issues. Currently, these lasers only operate below 90 K and are expected not to operate at high temperatures. We are exploring designs for better performance, robustness, and reliability and are testing novel designs that may have potential for higher-temperature operation.

We developed and refined the molecular beam epitaxy (MBE)–growth capabilities required for direct terahertz lasers. We used these refinements in growing many terahertz QC lasers in collaboration with the Massachusetts Institute of Technology (MIT). We significantly improved in-house design tools and are exploring many new terahertz designs. Unfortunately, we did

not complete the nonlinear modeling tools. One of the difficulties in the modeling turned out to be the lack of information on some nonlinear mixing materials in the long-wavelength range of the project; thus, we set up a terahertz time-domain spectrometer to begin looking at the optical properties of various materials. This required developing low-temperature gallium arsenide (GaAs) growth and annealing conditions to provide fast photoconductive switches and appropriate antennas. We completed this spectrometer and began material characterization. We improved many processing issues to provide higher-performance MIR lasers to be used as the pump sources for difference-frequency mixing. Some processing issues still remain, and future developments promise to improve the performance significantly.

38621

Microsystems for Chemical Signature and Reagent Delivery

R. J. Simonson, B. G. Hance, J. A. Ellison, K. S. Rawlinson, A. Robinson, A. W. Staton, R. P. Manginell

Networked systems of low-cost, small, integrable chemical sensors will enable monitoring of nonproliferation and materials control targets and chemical weapons (CW) threats. Sandia-designed prototype chemical sensor systems are undergoing extended field testing supported by the Department of Energy and other government agencies. We recently changed our efforts from extension of such systems to detection of biochemical molecules (by nitric oxide [NO] generation for use as a biomarker) to development of a high-pressure hydrogen (H) generator for very rapid chromatography (~ 2 s) for detection of chemical-warfare agents (CWAs). Use of autonomous chemical monitoring in homeland security and other high-consequence applications will demand a high level of system surety, which Sandia is uniquely positioned to provide. A required surety component will be the verification of microanalytical systems performance, which we can achieve by providing a programmable source of chemical signature(s) for autonomous calibration of analytical systems. In addition, we could use such a controlled chemical source to dispense microaliquots of derivatization reagents, extending the analysis capability of chemical sensors to a wider range of targets. We continued our development of microfabricated systems for controlled release of selected compounds (calibrants and high-pressure H, the latter to be used both as a carrier gas and as a fuel to allow gas chromatogram [GC] temperature programming) into the analytical stream of microsensor systems. To minimize pumping and valve requirements of microfluidic systems, and to avoid the degradation issues associated with the storage of dilute solutions, we developed two candidate solid-phase reservoir materials that can be patterned onto arrays of thermally activated membrane devices. We developed solid-phase reservoir films by solution-phase deposition of thermally decomposable organic salts, which provide for a pair of calibration marker compounds (one fast eluter and one slow eluter) for GC analyses.

We demonstrated the production of propene and tripropyl amine by thermal decomposition of solution-deposited tetrapropyl ammonium hydroxide on arrays of microfabricated thermal elements. The propene acts as a fast-eluting marker and

the tripropyl amine as a slow-eluting marker in GCs using microfabricated GC components. This will be a key capability in the use of H as fuel to catalytically drive temperature-programmed micro-GC systems, since the catalytically heated systems will not be as precisely temperature-controlled as resistively heated systems. This calibration capability will allow for next-generation microgas analysis systems that consume significantly lower battery power than current systems.

We demonstrated the initiation of exothermic decomposition of magnesium borohydride diammonate (MBDA) using microfabricated thermal elements. We will use this strategy to produce H carrier gas and fuel gas for the next-generation microgas analyzer.

We fabricated polysilicon microbridgewire arrays with greater than 100 elements for use as substrates in future microcalibrator and H-generator applications, to replace the 2 x 5 metal-on-silicon-nitride prototype arrays used in this project.

38622

Microfluidic Cellular-Sample Pretreatment

C. D. James, P. C. Galambos, S. M. Brozik, S. S. Mani, M. Okandan, M. M. Manginell

Sandia seeks to produce a microsystem that can rapidly detect any biological agent at low concentrations, with the primary difficulty of developing such a system being the wide range of analytes (bacterial cells, viruses, and toxin molecules) that need to be handled, collected, and then detected. Another feature that will improve speed and flexibility is the ability of the system to detect multiple agents within a single sample simultaneously. In addition, having orthogonal assay capability (for instance, one assay for identifying external protein markers and another for identifying deoxyribonucleic acid [DNA] sequences) is another feature that enhances detection specificity and reduces false positives.

Our strategy for addressing these concerns is to use microspheres as the bridge between nanometer-sized particles (DNA, toxins, antigens, etc.) and the micro-/mesoscale fluidic systems that we have already developed. We will use the microspheres as capture-and-carry tools for small-molecule-detection assays. A new addition to this project is our proposed use of dielectrophoresis (DEP) to collect and separate the microspheres based on size and polarizability properties. Our previously defined goal of cell lysis using a microdevice is now further enhanced in that we have developed a strategy for capturing and concentrating target molecules from within the cell lysate. The tagged particles will provide the surface area and specificity for capturing minute quantities of antigens, DNA/ribonucleic acid (RNA) molecules, and internal protein markers. The particles, being large in comparison to the molecules, can then be collected and separated before being sent off for analysis. Finally, real-time polymerase chain reaction (PCR) with a commercially available system will be interfaced with our microdevice in the first step of genetic identification of a particular agent.

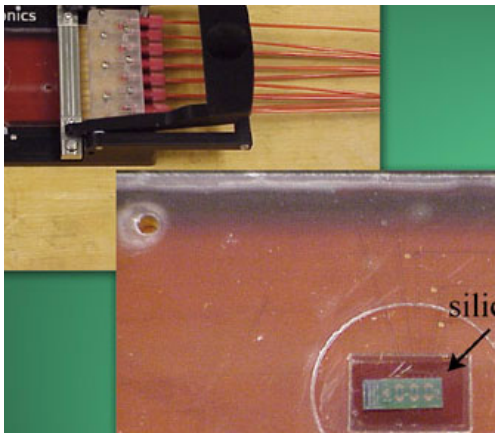

Manifold for interfacing with silicon microfludic devices.

- *Microfluidic system development*. This component of our work focuses on providing a robust interface to our surface-micromachined (SMM) fluidic devices. We used an industrial partner to develop a fluidic interface for silicon (Si)-based SMM devices. We made the manifolds from stacked layers (nine layers, total 41 mil thick) of polymer with integrated fittings. We used a pressure-dependent bonding layer to interface the backside of the Si wafer to the manifold. We tested

devices to examine the sealing pressure that they can withstand. We are pursuing other methods of producing front-end fluidics components to the Si microfluidic devices, both internally and externally.

- *Cell and particle manipulation*. The first step in processing a sample from an air collector is to separate cellular materials (spores and possibly vegetative cells) from contaminants (dust, soot, etc.). We used DEP to separate cellular particles from noncellular particles. The contaminant simulants used were 1 µm-diameter latex microspheres, and the cellular simulants were heat-killed *S. aureus* bacteria. We separated the two analytes by using different voltage frequencies to select for collecting the cellular particles and ignoring the contaminant particles. We also measured the dielectric properties of a typical dust and found that the properties indicate the particle's dielectric properties are similar to the latex microspheres. We also are characterizing metallic particles and pollen spores to determine their dielectrophoretic properties.
- *Modeling*. In conjunction with our collaborators, we developed an electrohydrodynamic model for the coupled shear, DEP, and phase-separation of latex particles in a flowing suspension. This model accounts for interparticle interactions and was validated by experimental data. The model will enable us to design devices with particle-behavior effects taken into account, a task that is needed for collecting cellular samples and rejecting large amounts of contaminant particles. We also used a commercially available simulation code to model our devices to predict the dielectrophoretic force on particles flowing in a suspension. This led to device optimization of our devices using out-of-phase voltages to increase the trapping force and to improve separation efficiency.
- *Cell-lysing*. We tested newer devices for lysing cells. These devices utilized thermally driven actuators that produce motion upon heating. Predicted forces are substantially larger (milli-Newtons) than those produced by the comb-drive actuators (tens to hundreds of micro-Newtons). We demonstrated mechanical deformation of yeast cells within our device using the actuated piston. Further experiments are necessary to examine membrane integrity after subjecting it to the mechanical stresses of the actuators. Sporylated cells are also of interest for mechanical lysis and will be the subject of future work. We can also address the pistons of the actuators electrically to provide either a direct-current electric field to help permeabilize the membrane, or an alternating-current

signal to dielectrophoretically hold the cell in place to subject it to repeated deformation.

- *PCR approach and results*. Conventional PCR systems typically require sample volumes of 50 µl; however, the output of the DNA isolated from our device is expected to be much smaller (submicroliters). To test the limits of the conventional PCR system, we attached custom synthetic oligos to 1.5 µm, streptavidin-coated, paramagnetic beads and subsequently amplified them by PCR. We used 2 µl of the conjugated bead/oligo in PCR amplification and tested total reaction volumes of 25 µl and 50 µl. PCR amplification was successful on oligos attached to microspheres in both volumes. Two options are possible for coupling PCR to our Si devices; one is to incorporate microscale PCR on the same chip used for collecting and separating the sample, and the other is to use a commercial PCR system with an array of Si devices to provide enough sample volume. Both options are feasible with our SMM technology.

Refereed

Bennett, D. J., B. Khusid, C. D. James, P. C. Galambos, M. Okandan, D. Jacqmin, and A. Acrivos. 2004. Combined field-induced dielectrophoresis and phase separation for manipulating particles in microfluidics. *Applied Physics Letters* **83** (3) (December): 4866–68.

James, C. D., M. Okandan, P. C. Galambos, S. S. Mani, D. J. Bennett, B. Khusid, and A. Acrivos. 2004. Surface-micromachined dielectrophoretic gates for the front-end device of a biodetection system. *J. Fluids Engineering*, accepted.

Other Communications

James, C. D., D. J. Bennett, B. Khusid, P. C. Galambos, M. Okandan, D. Jacqmin, and A. Acrivos. 2004. Electrohydrodynamic separation of biological and nonbiological analytes within a surface-micromachined fluidic device. Paper presented at the American Vacuum Society–ST Meeting, 17 May, Albuquerque, New Mexico.

James, C. D., D. J. Bennett, B. Khusid, P. C. Galambos, M. Okandan, D. Jacqmin, and A. Acrivos. 2004. Electrohydrodynamic separation of cellular and noncellular analytes within a surface-micromachined fluidic device. Paper presented at the Detector/Sensor Research and Technology for Homeland and National Security Meeting, 14–16 September, Gatlinburg, Tennessee.

52548

Active Photonic-Crystal Devices for Integrated Photonics and Silicon Photonics

J. G. Fleming, J. R. Wendt, W. W. Chow, P. G. Clem, G. S. Subramania, I. F. El-Kady

This project used novel silicon (Si)-based processing techniques to fabricate state-of the art three-dimensional (3-D) metallic photonic crystals (PCs) and investigated the novel properties of these structured materials. At present, Sandia is the only institution capable of fabricating good-quality samples of this sort. We successfully fabricated eight-layer tungsten (W) crystals with minimum features down to 0.35 µm in this work. In the past, there was little work on metallic systems that display a finite absorption coefficient. Initially, it was unclear whether such samples would exhibit photonic bandgap (PBG) effects since the light cannot propagate in the high-index media, the metal, and the absorption process, as thought, to possibly quench any cavity resonances. However, we successfully demonstrated that these novel materials do, in fact, exhibit PBG effects and that we can modify the absorption and emission processes by changing the physical structure of the crystals. Modeling is a critical part of this work. The imaginary component of the metallic dielectric constant causes most codes to fail. Other models treating the metals are ideal, but the properties we are interested in clearly arise from the finite absorptive and emissive properties of real metals. Also, it has been unclear how to account for the metal emission process in traditional codes. We made great strides in coming up with mathematically robust codes and models that began to take these components into account. Upcoming work will continue this progress; we will fabricate and test samples with smaller dimensions and novel structures and further refine our codes and models.

We fabricated a wide range of samples with novel structures targeted at ~ 4 µm emission and a range of samples with the Iowa state structure, but with minimum dimensions ranging from 0.35 to 1.4 µm. We looked more closely at the testing of these structures and identified ways in which this can be improved and made more reliable. In particular, we improved our ability to measure the actual temperature of the emitting sample. This new information led us to revise our theory of what is taking place in thermally excited systems. At present, we have no experimental evidence to support our initial

contention that thermal emission in excess of Planck's law has been experimentally observed in such systems.

We also developed and tested several approaches to modify the surface emission (as opposed to the PC emission) from these structures. This is of critical importance to many applications.

We made great progress on the modeling and physics aspects of this project, which is a critical portion of the work. These samples are relatively complex and require significant resources to fabricate. It is therefore critical in the long run that accurate models of the metallic PC be developed to more rapidly advance this field. However, modeling such structures is very difficult. The imaginary component of the metallic dielectric constant causes most codes to fail. Traditional models also treat the metals as ideal, but the properties in which we are interested clearly arise from the finite absorptive and emissive properties of real metals. Furthermore, it has been unclear how to account for the metal emission process in traditional codes. We made great strides in coming up with mathematically robust codes and models that begin to take these components into account. As a result, we are close to being able to accurately model the properties of these novel structures.

Refereed

Lin, S. Y. 2004. 3-D tungsten photonic crystal as an efficient light emitter. *Proc. International Symposium on Photonic and Electromagnetic Crystal Structures V, Technical Digest–PECS-V* (March, Kyoto, Japan): 4.

Lin, S. Y., and J. G. Fleming. 2004. Active metallic photonic crystals in the infrared. Paper presented at the Materials Research Society Spring Meeting, April, San Francisco, California.

52549

Co-Processing of Chalcogenide-Based Radiation-Hard Nonvolatile Memories by Sandia's MDL and BAE Systems

J. D. McBrayer, R. K. Patel, R. S. Flores, R. S. Bennett, R. McFarland, B. L. Draper, T. A. Hill, D. J. Savignon, R. D. Nasby

Radiation-hard nonvolatile chalcogenide random-access memories (C-RAMs) represent a revolution in capability for nuclear circumvention, program storage, and satellite application system designers. This technology provides an inherently radiation-hard memory cell, since the recall information is not based on stored charge but rather on a physical phase transition. It offers read speeds and densities approaching commercial dynamic random-access memory (D-RAM). It needs no refreshing and operates at voltages competitive with commercial microelectronics.

C-RAM uses the physical phase change properties of a germanium antimony telluride (Ge-Sb-Te) chalcogenide alloy as the means of storing information. Sandia wrote the information by changes in resistance due to current-induced controlled-phase transitions of the chalcogenide material. The polycrystalline state (low resistance) provides the "zero," and the amorphous state provides the "one."

We focused on designing, in Sandia's silicon-on-insulator (SOI) process, a 64K-bit C-RAM device that was similar in function to BAE Systems' chalcogenide test-characterization vehicle (CTCV) test chip. This design allows the user to provide adjustable off-chip reference and bias voltages that are critical in tuning the C-RAM's performance to fit the yielded resistance of the chalcogenide's amorphous and crystalline memory states.

We conducted work to co-process the chip between Sandia and BAE Systems. In BAE's original chalcogenide memory process, they exposed wafers to a 4 hr, 625°C temperature cycle; Sandia's CMOS-7 process exposes wafers to no more than 450°C after salicide formation. Sandia needed to assess how BAE's 4 hr, 625°C temperature anneal would affect the SOI CMOS-7 contacts. BAE currently is developing a "low-temperature" memory-bit photo/etch process and believes it will be successful. We ran four lots (short loops of 10 wafers each) of Sandia's experimental processing runs to evaluate contact survivability of a 4 hr, 625°C anneal. We evaluated contacts of varying sizes and with different interlevel dielectric (ILD) thicknesses. Contact chains consisting of larger contact

openings and thinner ILD showed no difference in contact resistance, whether or not annealed at 625°C for 4 hr. On the other hand, contact chains consisting of smaller contact openings and thicker ILD showed a significant increase in contact resistance after having been annealed. These results demonstrated that Sandia's contact survivability of BAE's 625°C anneal process depended on the contact's aspect ratio. The standard 0.4 µm-sized contacts exhibited considerable contact resistance degradation after the 4 hr, 625°C anneal. Contacts that were annealed have contact resistances ranging anywhere from 10 to 10,000 ohms, whereas contacts that were not annealed have normal contact resistances of well below 10 ohms. The tungsten plug/liner separated from the salicided surface in a transmission-electron microscopy (TEM) cross-section of a degraded (resulting from annealing) 0.4 µm contact structure. Contacts sized at 0.6 µm survive the anneal process quite well. Both nonannealed and annealed contacts have resistances well below 10 ohms. This resulted in the decision to size all contacts in the joint-process C-RAM design to 0.6 µm.

Sandia completed 80% of the circuit design and 50% of the physical layout for the joint-processed 64K C-RAM. We performed many circuit simulations to verify that a Sandia-designed sense amplifier could resolve the amorphous and crystalline states of a chalcogenide memory bit. Initially, BAE said that the resistance of an amorphous (high-resistance) bit would be equal to or greater than 500K ohms, while the resistance of a crystalline bit would be equal to or less than 100K ohms. Data from BAE's experimental "low-temperature" process runs are now yielding amorphous bits with resistances equal to or greater than 75K ohms and crystalline bits with resistances equal to or less than 40K ohms. Sandia is just now verifying that the sense amplifier design can handle these new memory-bit resistance-value ranges.

52551

Functionalized Nanoparticles for Sensor Applications

D. R. Wheeler, R. J. Simonson, M. G. Blain, S. M. Dirk, S. W. Howell

In this project, Sandia will functionalize arrays of nanoparticles with short conducting molecules that will contain sensing functionalities that will modulate their conductivity based on their interaction with analytes. We will assemble this functionalized-nanoparticles organic ligand composite material between nanogap electrodes to provide nanosized sensors.

We must achieve a number of different elements to enable the use of functionalized nanoparticles for sensor applications. The first requirement is the appropriately functionalized nanoparticle. The second is a method to assemble the particles. The third requirement is the generation of a nanogap to contain the nanoparticles.

The functionalized nanoparticles will contain two types of ligands. The first is a short nonconjugated molecule similar to the agents currently used. The other will be bifunctionalized to bridge two nanoparticles and piconjugated to dominate conduction between particles. Therefore, the bridging ligand will dramatically affect the conductivity of the nanoparticle assembly. Additionally, the use of bifunctional ligands will generate a cross-linked network of particles that will be exceptionally stable for both gas- and liquid-sensing applications.

This research is very high risk, but will generate (and has generated) intellectual property of very high value and will position Sandia to be a significant player in the realm of organic electronics and nanotechnology. The methodologies to uniquely functionalize individual electrodes in a dense array of electrodes will have a myriad of applications outside of this project. Previous sensor applications using nanoparticles have relied on a simple swelling mechanism rather than on specific analyte/receptor interaction. Finally, the realization of smaller, more versatile and robust sensor packages based on unique chemical interactions impacts all aspects of the Department of Energy and Department of Defense sensor platform and projects.

Toward the realization of our goals, we demonstrated a nonswelling-based sensing using our nanoparticle/organic conducting molecule film. We are expanding the scope of our work to further understand the sensing capabilities.

We made the following accomplishments:

- We made a series of different mesojunctions with gaps on the order of a few microns. They are the platform for initial work as well as our most easily understood devices since they rely on a large ensemble of responses.
- We optimized and standardized our synthesis of both gold (Au) and platinum (Pt) nanoparticles with sacrificial ligands and purified them to be charge free.
- Our knowledge of the assembly process progressed to the point where we built a robot that can assemble our films and generate films with very reproducible behavior.
- We demonstrated our thesis of a new sensing mechanism that is not based on a swelling of a nanoparticle film, but rather is based on the electrical modulation of the medium that connects one nanoparticle to another.
- We undertook a series of experiments to more fully understand the nature of the conduction mechanism in our organic/nanoparticle films.
- We have the second- and third-generation gaps that resulted from our collaboration with Rice University. We began work on variable-gap devices.
- Our new Sandia-designed nanogaps with reduced leakage currents will begin their fabrication run shortly.
- Numerous papers and technical advances (TAs) and patents are under way.
- *Collaborations.*

— Four Center for Integrated Nanotechnologies (CINT) proposals were submitted with our group as a primary resource. We are attempting to become a part of CINT.

— Our collaboration with Purdue University is expanding to include both experimental characterizations of our molecules and theoretical work to understand the results.

— We built a robotic assembly system that performs a layer-by-layer assembly of nanoparticles on micron-sized gaps. The robot also probes the I–V behavior of the device after each layer is deposited. This methodology ensures reproducible device fabrication.

— We assembled arrays with functionalized ligands and demonstrated sensing in aqueous phase.

— We successfully and reproducibly assembled cross-linked nanoparticle arrays between nanogaps.

— We are further characterizing polymerized nanoparticle arrays assembled on mesojunctions and nanogaps to understand the effect of silicon versus metal contacts in device behavior.

— We successfully functionalized and electrically characterized moleram devices from the collaboration with Rice

University. We fabricated a probe card to collect data more efficiently.

— We developed numerous spin-off chemistries that have had a dramatic impact on projects outside of this project.

— We submitted numerous TAs on our new chemistries and assembly techniques.

— Sandia designed nanogaps with reduced leakage currents to begin a fabrication run shortly.

— New molecules with turn-on sensing behavior are under synthetic investigation.

- *Infrastructure*.

— Our probe station with gas handling for alternating-current and direct-current measurements with probe cards is up and running.

— We achieved robotic assembly of parts.

— We implemented automated testing.

— An atomic-force microscopy (AFM) solution cell is on order for testing and fabricating improved routes to nanojunctions using our unique chemistry.

52552

Novel *In Situ* Mechanical Testers to Enable Integrated Metal Surface Micromachines

S. J. Hearne, C. W. Dyck, P. G. Kotula, M. P. De Boer, S. M. Foiles, D. M. Follstaedt, T. E. Buchheit

The ability to integrate metal and semiconductor microsystems to perform highly complex functions, such as radio-frequency (RF) microelectromechanical systems (MEMS), will depend on developing freestanding metal structures that offer improved conductivity, reflectivity, and mechanical properties. Three issues have prevented the proliferation of these systems: (1) warpage of active components due to through-thickness stress gradients, (2) limited component lifetimes due to fatigue, and (3) low yield strength. To address these issues, Sandia focused on developing and implementing techniques to enable the direct study of the stress and microstructural evolution during electrodeposition and mechanical loading. We are studying stress during electrodeposition of metal thin films by integrating a multibeam optical stress sensor (MOSS) into an electrodeposition chamber. By coupling the in situ *stress information with* ex situ *microstructural analysis, we will obtain a scientific understanding of the sources of stress during electrodeposition. These results are providing a foundation upon which to develop a stress-gradient-free thin film directly applicable to the production of freestanding metal structures. We are addressing the issues of fatigue and yield strength by developing novel surface-micromachined (SMM) tensile and bend testers, by interferometry, and by transmission-electron microscopy (TEM) analysis. The MEMS tensile tester has a "Bosch"-etched hole to allow for direct viewing of the microstructure in a TEM before, during, and after loading. This approach allows for the quantitative measurements of stress-strain relations while imaging dislocation motion and for determination of fracture nucleation in samples with well-known fatigue/strain histories. This technique facilitates the determination of the limits for classical deformation mechanisms and helps to formulate a new understanding of the mechanical response as the grain sizes are refined to a nanometer scale. Together, these studies will result in a science-based infrastructure to enhance the production of an integrated metal–semiconductor system and will directly impact RF MEMS and LIGA (for the German term* Lithographie, Galvanoformung, und Abformung, *for lithography, electroforming, and molding) technologies at Sandia.*

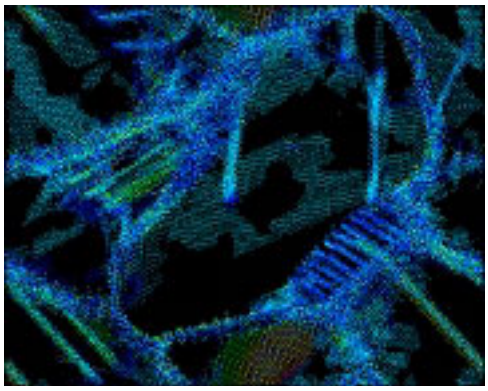

Dislocation slip bands predicted from MD simulation.

We made significant progress toward understanding the mechanisms that control stress evolution during electrodeposition of nickel (Ni) films and also toward developing a fundamental understanding of the mechanisms that control fatigue and yield in nanostructured materials.

- *Develop fatigue property-testing methodologies using interferometry.* Using a modified SUMMiT V™ (Sandia Ultraplanar Multilevel MEMS Technology V) process, we fabricated and tested $Al_{0.995}Cu_{0.005}$ thin-film structures with stiff support posts. Previous data from structures with compliant posts exhibited no plasticity. Data from the current structures indicate that this problem was resolved, and we can perform meaningful mechanical testing. We determined that hysteresis and fatigue under high-cycle loading were easily resolved with the new structure. These results demonstrate that the structure is functional and that support compliance is held to a minimum, which enables substantially high stresses in the film. New parts with thinner metal have nearly completed processing in the Microelectronics Development Laboratory to reduce the voltage level so that parts are not susceptible to arcing. We also reduced the deposition residual stress level in the new parts so that the narrowest-width devices, which will have a wider applied stress range, are more likely to remain intact.
- *Determine the effect of electroplating parameters on nucleation density and microstructure of Ni*. Based on our earlier finding that there are two distinct regions of stress during electrodeposition of Ni—the transition region (thickness < 1000 Å) and the steady-state region (thickness > 1000 Å)—we divided the study of the microstructural/stress evolution during electrodeposition of Ni according to those regions. The study of the transition region focused on expanding our understanding of island coalescence, whereas the study of the steady-state region focused on determining the dominant compressive stress-generation mechanism.

From our work in the study of the transition region, we determined that a critical issue not previously appreciated is that islands continue to coalesce after the initial contact until a planar film forms. After planarization, in the so called “steady-state region,” a new mechanism for the creation of stress becomes dominant. We found that the stress in this region can vary as much as 1 GPa, going from 0.5 GPa tension to - 0.5 GPa compression as a function of the deposition rate. It is reasonable to expect that the tensile stress in this region was induced by continual coalescence. Therefore, research focused on different possible compressive stress-generation mechanisms that would result in driving the Ni from net tensile stress into compression.

From our work in the study of the transition region, we determined that a critical issue not previously appreciated is that islands continue to coalesce after the initial contact until a planar film forms.

- *Perform molecular dynamics (MD) simulations of yield in nanograined Ni thin films*. We are using atomistic MD simulations to understand the mechanical response under deformation and annealing of the thin-film nanoscale materials. The initial simulations established a detailed methodology for performing and for analyzing the simulated microstructure.

An important question of interest is the influence of the thin-film free surfaces on the mechanical deformation. To explore this, we considered varied film thickness as well as comparison to films that have periodic boundary conditions in the directions normal to the film. The macroscopic stress-strain curves from these simulations indicate that the gross behavior does not appear to depend on the thickness, whereas similar plots of the total stored energy show that the stored energy does depend on the film thickness.

Refereed

Hearne, S. J., and J. A. Floro. 2004. Mechanisms inducing compressive stress during electrodeposition of Ni thin films. *J. Applied Physics*, submitted.

Hearne, S. J., J. A. Floro, S. C. Seel, C. W. Dyck, and T. R. Christensen. 2004. Island coalescences stress creations during thin-film growth. Paper presented at Fall AVS, November, Baltimore, Maryland.

Hearne, S. J., J. A. Floro, S. C. Seel, C. W. Dyck, and T. R. Christensen. 2004. Stress creations during thin-film island coalescences. Paper presented at the Fall Materials Research Society Meeting, December, Boston, Massachusetts.

Hearne, S. J., J. A. Floro, S. C. Seel, C. W. Dyck, and T. R. Christensen. 2004. Stress evolution during electrodeposition of Ni thin films. Paper presented at AACGE/West, 13 June, Fallen Leaf Lake, California.

Hearne, S. J., S. C. Seel, J. A. Floro, C. W. Dyck, T. R. Christensen, W. Fan, and S. R. Brueck. 2004. Stress evolution during electrodeposition of Ni thin films. Paper presented at the TMS Spring Meeting, March, Charlotte, North Carolina.

Other Communications

Hearne, S. J., S. C. Seel, J. A. Floro, C. W. Dyck, and T. R. Christensen. 2004. Stress evolution during electrodeposition of Ni thin films. Paper presented at the John Hopkins University Seminar, February, Baltimore, Maryland.

52553

Compliant Thermomechanical MEMS Actuators

M. S. Baker, T. B. Parson, T. J. Headley, R. A. Plass

Thermal actuators have proven to be a robust actuation method in surface-micromachined (SMM) microelectromechanical systems (MEMS) processes. Their higher output force and lower input voltage make them an attractive alternative to more-traditional electrostatic actuation methods. Sandia developed and validated a predictive model of thermal-actuator behavior that we can use as a design tool to customize the performance of an actuator to a specific application. We also used this tool to better understand thermal-actuator reliability by comparing the maximum actuator temperature to the measured lifetime.

Modeling thermal-actuator behavior requires the use of two sequentially coupled models—the first to predict the temperature increase of the actuator due to the applied current, and the second to model the mechanical response of the structure due to the increase in temperature. We developed these two models using MATLAB for the thermal response and ANSYS (software) for the structural response. Both models have been shown to agree well with experimental data.

In a parallel effort, we studied the reliability and failure mechanisms of thermal actuators. We measured their response to electrical overstress and electrostatic discharge and performed a study to determine actuator lifetime at various temperatures and operating conditions. We used the results from this study to determine a maximum reliable operating temperature that, when used in conjunction with the predictive model, enables us to design in reliability and customize the performance of an actuator at the design stage.

We focused on two areas: (1) improving model agreement, and (2) completing the reliability study to determine the maximum safe operating temperature.

The actuator model comprises two separate parts. First, the electrothermal model predicts the temperature increase of the actuator due to resistive heating from the applied current. We then use this temperature in the thermomechanical model to predict the structural response, including displacement and output force. We implemented the electrothermal model in MATLAB using a custom code written specifically for the actuator geometries, and performed the structural modeling using ANSYS, a commercial finite-element (FE) analysis

program. Both models are fully parametric with a combined solution time of approximately one second on a modern desktop computer. This enables rapid design evaluations needed in optimization and sensitivity analyses.

We validated the model at two stages. We compared the modeled resistance and final output displacement against measured data for several different actuator designs at different current levels. We improved model accuracy through a better understanding of material properties. Specifically, we measured polysilicon resistivity on each Sandia Ultraplanar Multilevel MEMS Technology V (SUMMiT V™) layer from room temperature up to 550°C. The increased accuracy of this property resulted in a significant improvement in model correlation.

In use, a thermal actuator is considered failed if its displacement output or its resistance changes significantly. Thus, we designed the reliability studies to measure both the displacement change and the device resistance change with device geometry, time, input power (which translates to a temperature distribution on the actuator legs), and environmental condition. These reliability studies show that the primary failure mode generating displacement output changes for thermal actuators held in direct-current conditions is in plastic deformation of the actuator legs. In dry environments, this plastic deformation has not been detected at maximum leg temperatures of ~ 450°C and is slight at ~ 500°C. Thinner and more heavily loaded thermal actuators readily deform at ~ 550°C, but more robust and lightly loaded parts do not deform as quickly. Above a ~ 600°C maximum leg temperature, all parts will plastically deform quickly. The same tests conducted in 50% relative humidity (RH) show that for the same power levels, devices will deform more quickly in wet conditions than in dry.

The expected Deal-Grove silicon oxidation rate dependencies show that the thermal-actuator resistance changes with time, current, device geometry, and varying environments. That is, in the first few hours of thermal-actuator operation, the device’s resistance increases linearly with time (oxidation reaction-rate limited), but later the resistance grows parabolically with time (diffusion-rate limited). The characteristic parabolic resistance-increase rate is related to input power and, hence, maximum leg temperature through an Arrhenius-type dependence (log of the rate is inversely proportional to 1/Temperature). Reliability studies in 50% RH conditions show the fastest reaction rates, while comparable studies of devices in dry air, dry nitrogen (~ 200 ppm of

oxygen), and hermetically sealed packages showed slower reaction rates, respectively, owing to a lack of reactive species. The inversely proportional relationship between actuator leg cross-sectional area and parabolic resistance-increase rate leads us to conclude that there is a roughly uniform oxide thickness generated on devices of different geometries under the same oxide growth conditions. Transmission-electron microscopy (TEM) cross-sectional analysis confirms the presence of high-density oxide layers on thermal actuators that show significant resistance increase during testing. These resistance changes take place over a much wider range of device leg temperatures than the plastic deformation mechanism appears to do.

By combining the predictive abilities of the model with the reliability information gained during the lifetime studies, we can build actuators with the confidence that they will perform as desired, with the needed lifetime and reliability.

Refereed

Baker, M. S., R. A. Plass, and J. Wittwer. 2004. Modeling and reliability of micromachined electrothermal actuators. To be submitted to a journal.

Messenger, R. K., M. S. Baker, T. W. McLain, L.L. Howell, and J. N. Harb. 2004. Modeling the transient response of surface-micromachined thermal actuators. *J. Micromechanics and Microengineering*, accepted.

Other Communications

Plass, R. A., M. S. Baker, and J. A. Walraven. 2004. Electrothermal actuator studies. *Proc. SPIE* **5343** (January, San Jose, California): 15–21.

Walraven, J. A., R. A. Plass, M. S. Baker, and M. J. Shaw. 2004. Failure analysis of electrothermal actuators subjected to electrical overstress (EOS) and electrostatic discharge (ESD). *Proc. International Symposium for Testing and Failure Analysis* (14–17 November, Worchester, Massachusetts).

52554

An Integrated, Stacked System-on-a-Chip

R. Chanchani, G. D. Peterson, D. J. Rieger, D. W. Peterson, D. Bethke, T. A. Fischer, D. B. Webb, M. E. Warren

In a miniaturized microsystem, the major difficulty is in integrating different device technologies in a small volume. In this project, Sandia seeks a unique concept to integrate different device technologies by stacking wafers in three dimensions (3-D). The final product will be a fully integrated system-on-a-chip, including passive and active devices made of different technologies. The uniqueness of this concept, for which we have filed a patent, is in the following:

(1) Use of benzocyclobutene (BCB) as a "glue" layer between wafers. This will allow us to incorporate interconnect structure and embedded passives within the glue layer.

(2) Use of through-hole vias in silicon (Si) with a lower aspect ratio obtained by thinning top wafers (20–125 µm thick).

We developed processes for 4 in.-diameter two-wafer stacks with electrical interconnections between them. This work involved developing new processes and modifying previous processes for wafer thinning, wafer bonding using BCB polymer, metallization of vias, and fabrication and demonstration of daisy-chain structure showing electrical interconnections between the bonded wafers.

Rajen Chanchani, Don Bethke, and Denise Webb inspect bonded wafers in the Compound Semiconductor Research Laboratory.

(1) We developed processes to stack two 4 in.-diameter wafers with electrical interconnections between them using a via daisy-chain structure. We used BCB to do the bonding. There are four 50-via daisy-chain patterns, one in each quadrant of the wafer. Some portions of the daisy-chain structure were electrically good. We developed the following processes to fabricate the two-wafer stack.

(a) *Wafer thinning (to 110 µm)*. The top wafers in the stacks were thinned at Corwil, Inc., in California. We ground them from the backside to a thickness of 110 µm, with a glass carrier attached to the topside of the wafer, using NITTO Thermal Release Tape. The original thinning process, which we developed recently, had several grinding defects ("thin spots") that resulted from air voids and dust particles entrapped between the wafer and the carrier. We developed a methodology to minimize these defects. We also thinned wafers using a new vendor-proprietary wafer-thinning process at International Wafer Services that yielded thinned wafers with fewer grinding defects.

(b) *Bonding process*. A modified bonding process, which we developed recently to obtain void-free bonding, involved using a higher force (> 2000 N) and a higher temperature (80°C–210°C). We also developed a modified bonding fixture to eliminate wafer cracking caused by the use of higher force and temperatures.

(c) *Via formation*. We developed processes to do through-hole Bosch-etched vias in Si wafers before and after bonding. The daisy-chain test pattern in each quadrant contains vias of a diameter of 75 µm, 150 µm, 300 µm, and 750 µm.

(d) *Metallization*. Prior to bonding, we metallized the bottom wafer with one-half of the daisy-chain pattern. After bonding, we removed BCB from the bottom of the vias, then metallized the top half of the daisy-chain pattern. The metal-layer sequence, deposited by evaporation, was 200 Å titanium (Ti), 30,000 Å copper (Cu), 2,000 Å nickel (Ni), and 1,000 Å gold (Au).

(2) We currently are developing techniques to isolate vias from Si. We are exploring two different techniques, one for vias made before bonding and the other for vias made after bonding.

(a) *Technique for insulating vias fabricated prior to bonding*. First, we deposited insulators like silicon dioxide (SiO_2) and silicon nitride (SiN) in vias immediately after they were Bosch-etched. Then we thinned the wafers and removed the bonded and uncured BCB from the bottom of the vias by dry etching or by a wet method using a solvent. We then hard-cured BCB and metallized the vias. We currently are improving this technique.

(b) *Technique for vias fabricated after bonding*. In this case, we can get via isolation by depositing BCB in the vias and then removing BCB from the center of the vias by either solvent or dry etching. This technique is still being developed.

(3) The uniqueness of this concept is its ability to have multiple electrical interconnect layers within the BCB (bonding) layer. We demonstrated the fabrication of two metal/BCB pair layers in the bond layers.

(4) We are exploring options for thinning wafers to less than 50 µm thickness. The through-hole via diameter depends directly on the thickness of the Si wafer. With 110 µm-thick wafers, we demonstrated minimum 75 µm-diameter vias and saw good electrical interconnection at the 300 µm via diameter. To have smaller vias, we need to thin wafers below 50 µm.

The uniqueness of this concept is its ability to have multiple electrical interconnect layers within the BCB (bonding) layer. We demonstrated the fabrication of two metal/BCB pair layers in the bond layers.

Other Communications

Chanchani, R. 2004. An overview of 3-D integration technologies—Motivation, options, and status. Paper presented at the Mini-Workshop on 3-D Integration Technologies, October, San Diego, California.

Chanchani, R. 2003. Wafer thinning and stacking. Paper presented at the 4th International Workshop on Thin Semiconductor Devices—Manufacturing and Applications, November, Munich, Germany.

Chanchani, R., D. Bethke, D. B. Webb, C. Sandoval, and G. Wouters. 2004. Integrated substrate technology. *Proc. 54th Electronic Component and Technology Conference* **2** (June, Las Vegas, Nevada): 1232–36.

52555

Micromass Spectrometer-on-a-Chip

M. G. Blain, J. G. Fleming, D. Cruz, D. E. Austin

Breakthrough improvements in microsensors for high-consequence applications, including chemical-/biological-warfare agents (CWAs/BWAs), medical diagnostics, and explosives detection, will be realized only with the development of ultrasensitive and ultraselective microfabricated detectors that are able to unambiguously identify the compound of interest. A micron-scaled mass spectrometer (MS)-on-a-chip would set the performance standard for such microdetectors. For example, the combination of a microgas chromatographic (µGC) separation column with a micromass spectrometer (µMS) detector, i.e., a µGC/MS, would provide an extremely sophisticated capability for specific and unambiguous molecular identification, which currently is not available. A µMS could also serve as a stand-alone microanalytical system in its own right. Sandia is leading the development of this breakthrough technology via this project. While development of a complete µMS system must address sample introduction, ion source, mass analyzer, ion detector, vacuum, and power subsystems, we seek here to continue our efforts to microfabricate an ~ 1 cm^2 prototype mass analyzer consisting of an array of massively parallel (MP), micron-sized cylindrical ion traps (CITs) fabricated on a silicon (Si) substrate. We designed the analyzer with an integrated Faraday detector and with the theoretical mass range for detecting biomolecules and their derivatives. Sandia has demonstrated microfabrication feasibility and built ion traps with the molded tungsten (W) process technology capability at Sandia. We will continue our collaboration with Purdue University to demonstrate functionality of an MP chip-sized array of mass analyzers operating the packaged prototype with laboratory-scale ion source, vacuum, power delivery, and (possibly) detection systems in Purdue's ion-trap laboratory. After experimental demonstration and then optimization of the micromass analyzer, we could initiate an expanded effort to incorporate sample introduction, vacuum, power, and ion source into a functional µMS system.

We fabricated the first-ever micrometer-scale ion traps using the molded W process technology at Sandia.

We fabricated the first-ever micrometer-scale ion traps using the molded W process technology at Sandia. We successfully fabricated arrays of ion traps with r_0=1 mm and r_0=1.5 mm in W; however, undersized mechanical anchors for the top end-cap electrodes caused the loss of this key trap

component during release of the silicon dioxide (SiO_2) mold and prevented ion-trapping experiments with this initial prototype. A redesigned test-chip layout fixed the trap anchor problem and implemented better radio-frequency (RF) device layout practice. In addition, we defined four trap sizes (r_0=1, 2, 5, and 10 µm) and three array sizes. We developed test protocols for the prototype CIT array. In collaboration with Purdue, we initiated designs for the RF waveform and timing diagrams and the ionization instrumentation necessary for testing of the prototype analyzers, and we expect to soon begin trapping experiments with recently fabricated traps. We defined a trap array package scheme for the arrays and are designing and building an RF circuit board. Additionally, we met goals for continued simulation of the ion-trapping characteristics and performance of an r_0=1 mm CIT. We used the expected as-fabricated trap geometry terms, including end-cap thickness, end-cap-to-ring-electrode spacing, and end-cap and ring-electrode thickness, in the simulations to further elucidate the ion-trapping characteristics and trap/eject protocols of the as-designed trap structures. We used the expected trap electrode geometries and operating RF voltages and frequencies as input boundary conditions. We calculated ion trajectories and time-dependent electric fields and confirmed ion trapping to be feasible in these traps.

Refereed

Blain, M. G., D. Cruz, L. S. Riter, D. E. Austin, G. Wu, J. G. Fleming, A. Guymon, and R. G. Cooks. 2004. Design considerations, simulation, and fabrication of an array of micron-scaled cylindrical ion trap mass analyzers. *Proc. 52nd ASMS Conference on Mass Spectrometry and Allied Topics* **A041062.pdf** (23–27 May, Nashville, Tennessee).

Blain, M. G., L. S. Riter, D. Cruz, D. E. Austin, G. Wu, W. R. Plass, and R. G. Cooks. 2004. Toward the hand-held mass spectrometer: Design considerations, simulation, and fabrication of micrometer-scaled cylindrical ion traps. *Proc. International J. Mass Spectrometry* **236** (1-3) (August): 91–104.

Cooks, R. G., L. S. Riter, A. Guymon, C. Zhang, G. Wu, H. Chen, Y. Song, Z. Ouyang, M. G. Blain, D. E. Austin, D. Cruz, and G. Patterson. 2004. New miniature ion trap mass spectrometers. *Proc. 52nd ASMS Conference on Mass Spectrometry and Allied Topics* **A040276.pdf** (23–27 May, Nashville, Tennessee).

52556

Quantum Coherence in Semiconductor Nanostructures for Improved Lasers and Detectors

J. G. Cederberg, S. K. Lyo, N. A. Modine, W. W. Chow, S. R. Kurtz, R. M. Biefeld, M. C. Phillips

Advances in atomic physics have led to demonstrating "lasing without inversion" (LWI). This novel phenomenon has brought worldwide attention, but to date has been observed only in atomic beams and doped insulators. LWI can occur when the system is quantum coherent (QC)—when scattering is sufficiently absent that carriers' wave functions retain memory of their phase. Wave-function coherence and interference can be used to generate a variety of optical phenomena, including LWI, electromagnetically induced transparency (EIT), dark-state spectroscopy, "slow light," and "stopped light."

Sandia seeks to demonstrate EIT, LWI, and other QC effects in semiconductor laser diodes. This would enable reductions in the pumping required for lasing, resulting in lower-threshold currents. We can realize this using semiconductor quantum dots (QDs) in active regions. Often referred to as "artificial atoms," QDs confine the carriers within finite volumes, thereby suppressing their scattering. Our combined resources put us in a strong position to make the transition from atomic to compound semiconductor optoelectronic systems. We completed a general treatment of QC effects in semiconductors. We performed initial evaluation of several semiconductor QD systems to evaluate the energy levels present. These results suggest that the QD systems generated are of sufficient quality to observe QC effects. We will direct optical experiments toward observation of QC effects. Theoretical efforts will support the experiments and lay the groundwork for device applications.

We made advances through our experimental efforts to observe QC phenomena in semiconductor QD structures and also tested our previous theoretical development. Our theoretical model predicts that LWI and EIT should be observed for dephasing rates of 2 x 10–12 s^{-1}, typical of what was observed at room temperature and under high-excitation conditions for semiconductor QDs. Experimentally, we performed a detailed spectroscopic evaluation of the energy levels in both indium gallium arsenide (InGaAs) and InAs QDs, which led to further optimization of QD growth conditions. We found that the energy-level spacing in InGaAs QDs is much smaller, consistent with theoretical calculations for these

structures, which limits the number of excited-state QD resonances. InAs QDs possess a very deep potential well, allowing us to resolve many excited states. We also made quantitative absorption and gain measurements for these QD systems. We compared these results with our present theory of absorption and gain in QD systems, providing further experimental validation for our theory. The absorption measurements also indicated that the waveguide geometry, with light confined in the plane of the QDs, is the preferred experimental geometry for maximizing signals of quantum coherence. We assembled the necessary apparatus for these waveguide measurements and currently are fabricating the waveguide structures. We demonstrated electrically injected InGaAs and InAs QD lasers operating at room temperature. We made the initial demonstration of an intersubband QD infrared (IR) photodetector, enabling optical schemes for observing quantum coherence that utilize only electron- or hole-energy levels. The theoretical development further targeted the experimental conditions under which LWI and EIT can be observed. We optimized the growth conditions for both InGaAs– and InAs–based QD to minimize inhomogeneous broadening of these structures.

Our efforts to demonstrate QC effects in semiconductor materials will enable optoelectronic devices with properties that are not presently possible. Our work lays the groundwork to utilize quantum coherence in semiconductor devices and opens the window to apply the concepts developed to new devices. The work performed represents an advance for the science of quantum optics and provides technical superiority for defense systems. This research aligns well with Sandia's mission. It couples the research-oriented subject of quantum optics with optoelectronics and is still in its infancy. Research in this area has the potential to create the foundation on which future Sandia technologies are built.

Our efforts to demonstrate QC effects in semiconductor materials will enable optoelectronic devices with properties that are not presently possible. Our work lays the groundwork to utilize QC in semiconductor devices and opens the window to apply the concepts developed to new devices.

Other Communications

Cederberg, J. G., M. C. Phillips, M. J. Cich, S. R. Kurtz, F. H. Kaatz, and R. M. Biefeld. 2004. InAs and InGaAs quantum dot lasers by MOCVD. Paper presented at the 12th International Conference on Metal Organic Vapor Phase Epitaxy (ICMOVPE-XII), 2 June, Lahaina, Hawaii.

Kaatz, F. H., and J. G. Cederberg. 2004. Thermal processing of InAs and InGaAs quantum dots for device integration. Paper presented at the 46th Electronic Materials Conference (EMC), 23 June, Notre Dame, Indiana.

52557

MOSFET–MEMS Integration

B. L. Draper, P. J. Resnick, W. D. Cowan, R. J. Huber, J. B. Stanley, K. B. Pfeifer, M. Okandan, A. H. Hsia, S. S. Mani, J. J. Allen, R. W. Young, M. W. Jenkins

In many microdevices and systems-on-a-chip, successful system operation depends on the detection of very small changes in capacitance, charge, or current. Because of parasitics and noise, this is very difficult to accomplish without on-chip signal processing. In still other applications, on-chip decoder and driver electronics are needed to actuate large arrays of mechanical elements.

Sandia developed a technique for building electronic and mechanical components simultaneously, eliminating many of the problems and complexities associated with previous methods of accomplishing monolithic integration. In this new technique, the elements of a simple metalorganic semiconductor field-effect transistor (MOSFET) are formed from the films and processes that we use to fabricate microelectromechanical devices, eliminating the need for extra processing. The resulting components, called SFETs (SUMMiT^{TM} [Sandia Ultraplanar Multilevel MEMS {microelectromechanical systems} Technology] field-effect transistors) have good, repeatable electrical characteristics suitable for a wide range of applications.

We also developed a set of process and device models that are useful for predicting SFET parameters and providing electrical parameters for circuit design. We used these same models to help us extend SFET operation to high voltages, allowing the devices to directly drive many traditional MEMS components such as movable mirrors and electrostatic motors.

Reliability testing shows that the SFET, and its gate oxide, in particular, behaves a little differently than classical MOSFETs, but that the technology will still provide devices capable of long life at the expected operating conditions.

We designed, fabricated, and tested several kinds of SFET digital and analog circuits. These include oscillators, logic gates, multiplexers, amplifiers, and light detectors.

We expanded our capabilities by developing a set of process and device models that are useful for predicting SFET parameters and providing electrical parameters for circuit design. We used these same models to help us extend SFET operation to high voltages, allowing the devices to directly

drive many traditional MEMS components such as movable mirrors and electrostatic motors.

In examining the reliability of the SFET, we found that the high-temperature MEMS anneals can greatly change the current-voltage characteristics of the gate oxide. A traditional reliability evaluation of the thick oxides using time-dependent dielectric breakdown tests is greatly hampered by excessive impact ionization that occurs at high voltages, so a rigorous evaluation of gate-oxide lifetime is difficult. However, the breakdown voltages are not severely impacted by the post-processing anneals. This suggests that reliable SFET-process gate oxides can be fabricated as long as the use voltage is well below the onset of impact ionization.

We generated layout and design rules based on limitations in lithography, experience gained in fabricating and testing dozens of different styles of SFETs, and computer-aided simulations.

We designed standard cell libraries, some small-scale common function blocks, and a series of test circuits; and we incorporated them into a Sandia reticle set. We used both static-ratioed logic and dynamic logic to implement functions such as simple logic gates, shift registers, level shifters, decoders, oscillators, counters, and multiplexers.

We incorporated SFETs into several MEMS fabricated at Sandia. We used them as a differential-pair amplifier on comb-drive resonators and patch-clamp arrays, as optical sensors in RS395, and as the control and drive circuitry in a mirror array that will be the basis of an adaptive optics system. The full promise of large-scale SFET–MEMS integration awaits the solution of one remaining problem: fully protecting the SFET during the processes used to release the micromechanical elements of the system.

Refereed

Draper, B. L., M. Okandan, S. S. Mani, and R. S. Bennett. 2004. A novel method of fabricating integrated FETs for MEMS applications. *Proc. IEEE J. Microelectromechanical Systems* **13** (3) (June): 500–504.

52566

Microoptical Gyroscope Via Monolithic Active/Passive Optical Integration

R. D. Kinney, T. C. Peterson, C. Alford, J. K. Kim, F. B. McCormick, G. A. Vawter, G. M. Peake, J. R. Wendt, M. J. Shaw, J. Guo, B. Salters

Technological progress in some weapons system–related application areas is dependent on the availability of small, rugged, accurate gyros (1–10 deg/hr bias uncertainty). Examples include future W87 joint test assemblies (JTAs) that will require inertial systems with volumes of a few cubic inches to minimize impact on weapons system dynamics. The gyro must withstand reentry, yet accuracy must be sufficient to allow good characterization of vehicle dynamics during reentry.

Industry has adopted optical gyros due to their superior ruggedness, reliability, and lower cost. However, attempts to miniaturize optical gyros have been thwarted by the lack of suitable microoptical components and monolithic optical integration know-how. Recently, Sandia developed the photonic elements necessary for a resonant microoptical gyro (RMOG). We individually designed an aluminum gallium arsenide (AlGaAs) distributed Bragg reflector (DBR) laser, GaAs phase modulator, and GaAs photodiode detector. The challenge now is monolithic integration of these components on a chip. Most active/passive devices use silicon (Si) optical bench techniques for integration. We seek monolithic integration where both active and passive components are fabricated simultaneously on a single chip. Monolithic integration will increase device ruggedness, reduce manufacturing complexity, and eliminate optical losses due to alignment errors. We will then couple this chip with a recently developed low-loss, multiloop silicon oxynitride (SiON) waveguide resonator to produce a high-performance RMOG.

The goal of this project is to demonstrate an RMOG produced from a monolithic photonic integrated circuit (PIC) coupled with a SiON waveguide resonator.

We completed a series of process studies to optimize silicon nitride (SiN) planar lightwave circuit (PLC) fabrication for low loss with the result that we demonstrated world-record low loss for SiN/SiO_2 (silicon dioxide) waveguides of 0.1 dB/cm at 1550 nm wavelength.

We completed a series of process studies to optimize silicon nitride (SiN) planar lightwave circuit (PLC) fabrication for low loss with the result that we demonstrated world-record low loss for SiN/SiO_2 (silicon dioxide) waveguides of 0.1 dB/cm at 1550 nm wavelength. We measured PLC waveguide crossing losses at 4% per cross. Losses at 980 nm wavelength are higher but still under evaluation. We demonstrated an indium (In)GaAs/(AlGa)As buried-grating distributed feedback (DFB) laser with 20 mW power and good side-mode suppression. The selective-

area disordering process was plagued by instability that prevented fabrication and testing of phase-modulator and photodiode devices. We are aggressively pursuing a solution employing regrowth (similar to that already used in burying DFB gratings) as a powerful method of photonic circuit integration. We expect to complete the first regrown PICs in upcoming work after a rapid development cycle for AlGaAs crystal regrowth and circuit design. We have begun developing a needed packaging technology to join two photonic chips into a common optical circuit. We demonstrated optical fiber alignment and attachment to a PLC with ultraviolet epoxy.

Refereed

Guo, J., G. A. Vawter, M. J. Shaw, G. R. Hadley, A. Jain, and C. Sullivan. 2004. Silicon nitride/dioxide planar lightwave ring resonator: Tunability and nonlinearity. *Proc. SPIE, Photonics West* (January, San Jose, California).

Vawter, G. A. 2004. Adiabatic mode converters for photonic integrated circuits and devices. (Invited) *Proc. SPIE, Integrated Optics: Devices, Technologies, and Materials VIII* **5355** (January, San Jose, California): 129.

52570

Materials Physics and Device Development for Improved Efficiency of GaN HEMT High-Power Amplifiers

D. D. Koleske, D. M. Follstaedt, A. A. Allerman, S. R. Kurtz, A. F. Wright, N. A. Missert, C. H. Seager, C. P. Tigges, A. G. Baca, R. D. Briggs, R. J. Shul, P. P. Provencio

Sandia identified gallium nitride (GaN)–based microwave-power amplifiers as critical components in our next-generation micro-synthetic-aperture radar (SAR) operating at X-band and Ku-band (10–18 GHz). To miniaturize SAR, GaN–based amplifiers are necessary to replace bulky traveling-wave tubes. Specifically, for micro-SAR development, we need to develop highly reliable GaN high-electron-mobility transistors (HEMTs), which deliver a factor of 10 improvement in power performance compared to gallium arsenide (GaAs). Despite the great promise of GaN HEMTs, problems associated with nitride materials growth currently limit gain, linearity, power-added efficiency, reproducibility, and reliability. These material quality issues are primarily due to heteroepitaxial growth of GaN on lattice-mismatched substrates. Because silicon carbide (SiC) provides the best lattice match and thermal conductivity, SiC is currently the substrate of choice for GaN–based microwave amplifiers. Obviously, for GaN–based HEMTs to fully realize their tremendous promise, several challenges related to GaN heteroepitaxy on SiC must be solved.

In this project, we plan a concerted effort to solve these materials issues through in-depth research on GaN/aluminum (Al)GaN growth on SiC. We will investigate and solve problems that limit device performance, including electron traps in GaN and AlGaN layers, dislocations, the quality of semi-insulating GaN, the GaN/AlGaN interface roughness, and surface pinning of the AlGaN gate. We will minimize the role of dislocations by leveraging our world-leadership position in growing low-dislocation GaN by transferring our patented cantilever epitaxy (CE) to SiC. We will develop predictive models of the transistor channel's two-dimensional (2-D) electron gas and surface potential through transport measurements and band structure modeling. We will also investigate charge trapping in GaN and AlGaN. To nullify surface charge, we will develop alternate methods of passivation and recessed-gate processing for HEMTs, which will require the development of nondamaging etch techniques. Constant feedback between material properties, physical understanding, and device performance will enable rapid progress.

We worked on improving the group III nitride growth conditions to improve the HEMT performance. We improved the electron mobilities from 1300 to over 1700 cm^2/Vs with sheet change near 1 x 10^{13} cm^{-2}. We achieved a better understanding of how carbon (C) is incorporated into the GaN films and how C influences the electronic properties. We also further optimized growth conditions for the aluminum nitride (AlN) nucleation layer and AlGaN capping layer. For the AlN nucleation layer, higher N to Ga ratios (V/III ratio) are preferred, while lower ratios appear to improve the surface morphology but cause cracking in the AlN and subsequent GaN layers. Lower V/III ratios lead to smoother AlGaN layers. We examined the influence of five different growth conditions and identified and quantified their influence on the HEMT device properties. We developed a method for passivating the HEMT surface using SiN to decrease the RF dispersion effects and current collapse commonly observed in unpassivated devices. Finally, we explored and modeled thermal surveying of efficient ways to cool operating devices.

52571

Leaky-Mode VCSELs for Photonic Logic Circuits

D. K. Serkland, K. M. Geib, G. M. Peake, G. R. Hadley

Leaky-mode vertical-cavity surface-emitting lasers (VCSELs) offer new possibilities for the integration of microcavity lasers to create optical microsystems. A leaky-mode VCSEL emits light horizontally, in the plane of the semiconductor wafer, which allows the light to interact with other lasers, modulators, and detectors on the same wafer. Sandia recently proposed and demonstrated the fabrication of leaky-mode VCSELs based on effective index modification but has not adequately developed it for use in applications. The goal of this project is to advance the design and fabrication of leaky-mode VCSELs to the point where we can attempt initial applications. We concentrated on overcoming previous difficulties in the epitaxial growth and fabrication of these advanced VCSELs. In subsequent years, the focus shifted to applications of leaky-mode VCSELs, such as all-optical processing circuits based on gain quenching.

The development of circuits that can process data directly in the optical domain will enable encryption and decryption of data on optical fibers at very high rates for secure communications. If we can demonstrate their feasibility during this project, such all-optical processing circuits will be of interest to the supercomputing and intelligence communities. Additionally, as time and resources permit, we intend to explore the use of leaky-mode VCSELs to achieve higher brightness sources, which are relevant to laser radar and remote-sensing applications.

We continued our earlier efforts to develop new and better methods for the fabrication of leaky-mode VCSELs. Additionally, we started work on applications of leaky-mode VCSELs to photonic logic circuits (PLCs) based on gain quenching of semiconductor lasers. Our final goal was to demonstrate an “optical diode,” in which an optical input quenches the gain of a VCSEL operating at a slightly longer wavelength.

A major accomplishment was the demonstration of a new method of fabricating leaky-mode VCSELs. The fabrication of leaky-mode coupled VCSELs requires tailoring of the effective index profile, typically achieved by performing a shallow patterned etch (2–50 nm deep) just above the cavity layers, followed by epitaxial regrowth of the top distributed Bragg

reflector (DBR). Unfortunately, when DBR regrowth is done on a typical 2 deg-miscut gallium arsenide (GaAs) substrate, the etched features do not propagate straight up from the substrate, but rather at a steep angle (beyond 45 deg) that prohibits successful fabrication of the devices. In early work, we demonstrated that regrowth on a 0 deg-miscut substrate achieved the desired vertical regrowth. However, we recently learned that the VCSELs grown on 0 deg-miscut substrates suffer from poor performance. As an alternative to epitaxial regrowth of the top DBR, we successfully demonstrated the use of a deposited dielectric DBR above the etched semiconductor surface.

We successfully fabricated and characterized leaky-mode VCSELs that employ a deposited dielectric DBR above the etched semiconductor surface. The epitaxial structure was that of a standard 850 nm VCSEL, but with only a six-period top *p*-type DBR. We oxidized a quarter-wave Al.98Ga.02As layer in the first period of the *p*-type DBR to create a current aperture. We fabricated a two-element coupled VCSEL array by etching two 3 x 4 μm rectangles to a nominal depth of 15 nm. We then deposited an eight-period silicon dioxide (SiO_2)/silicon nitride (SiN) DBR using plasma-enhanced chemical vapor deposition (PECVD). We etched the dielectric DBR to access *p*-type ohmic contacts on top of the semiconductor surface. We demonstrated in-phase and out-of-phase coupling of these two VCSELs, and we recorded output power versus current data that exhibit low-threshold currents (1.25 mA) consistent with good-quality lasers. Moreover, we recorded emission spectra above and below threshold and compared these with theoretical simulations. Spectral lines from the input optical mode and the quenched optical mode are visible.

Currently, experiments are under way to provide an optical input and to demonstrate quenching of the lasing mode, which will complete the demonstration of the “optical diode” as planned.

Refereed

Serkland, D. K., G. M. Peake, and K. M. Geib. 2004. VCSEL modulation using an integrated electro-absorption modulator. *CLEO/IQEC 2004* **Digest CD-ROM** (18 May, San Francisco, California): CTuAA2.

52575

Advanced Polychromator Systems for Remote Chemical Sensing

J. J. Allen, M. B. Sinclair, K. B. Pfeifer

The Polychromator is a microelectromechanical systems (MEMS)–based programmable diffraction grating that serves as the backbone of an infrared (IR) correlation radiometer. Applications of this device range from battlefield detection of chemical agents to remote monitoring of gaseous emissions. Deflection patterns of the individual grating elements of the Polychromator can be programmed to produce desired spectral-transmittance profiles. For remote chemical detection, IR radiation collected from a target is correlated with a series of predetermined reference spectra. The reference spectra are application-dependent and are determined using multivariate techniques to optimize the sensitivity and selectivity of chemical detection. Once programmed with a sequence of reference spectra, the Polychromator system performs real-time multivariate analysis of the collected IR radiation.

This project is to develop an advanced Polychromator, designed for fabrication within the Sandia SUMMiT™ (Sandia Ultraplanar Multilevel MEMS Technology) process, which will enable repeatable manufacture and advanced capability of the programmable grating. The goals for the new SUMMiT™ Polychromator device are superior actuation range and low-voltage operation and to have additional programmable degrees of freedom (DOFs) such as tilting of the individual beams. This more-generalized motion will enable the production of blazed profiles for enhanced sensitivity of chemical detection. In addition, the increased number of DOFs will enable greater flexibility and higher fidelity of spectral synthesis. The advanced programmable grating technology developed in this project will also enable a variety of other optical devices such as beam-steering devices and adaptive optics based on diffractive principles.

Closeup AVI of the SUMMiT™ Polychromator gratings during actuation.

- We developed a new type of optical grating element for the Polychromator system. This new optical grating element is a rotational grating, and it can be fabricated within the SUMMiT™ surface-micromachined (SMM) fabrication process. This rotational grating is 20 µm wide, and it can be rotated to any position from 0 to 19 deg. Also, the SUMMiT™ rotational grating element can be operated at a significantly reduced voltage to enable its use within a new technology for integrating electronics and SUMMiT™ devices (semiconductor

We developed a new type of optical grating element for the Polychromator system. This new optical grating element is a rotational grating, and it can be fabricated within the SUMMiT™ surface-micromachined (SMM) fabrication process.

field-effect transistor [SFET]). This new optical grating greatly enables the vision of developing the handheld Polychromator system.

- We demonstrated that, by using the concepts of Hadamard Transform Optics, the Polychromator system can also be used as a MEMS–based IR spectrometer. We showed that we can program the spectral transfer function of the Polychromator to produce a complete set of "Hadamard transform vectors." For each vector, the (single) IR detector records the associated "Hadamard weights." A simple matrix inversion then yields the desired IR spectrum. The Hadamard approach features the so-called "multiplex advantage," meaning that each sample recorded by the detector arises from many different wavelengths simultaneously reaching the detector. This has significant benefits in terms of signal-to-noise ratios (SNRs). We anticipate that the ability to directly measure IR spectra will be of great benefit for chemical sensing since it can provide an initial survey of a potentially complex target scene. We can then use the spectral information obtained in this manner to guide the subsequent correlation radiometer measurements. In addition, we believe that there will be many other applications where a rugged, handheld, fast IR spectrometer will be of interest.

Refereed

Sinclair, M. B., and K. B. Pfeifer. 2004. Chemical sensing with a MEMS–based correlation radiometer. Paper presented at the Materials Research Society Spring Meeting, April, San Francisco, California.

Sinclair, M. B., K. B. Pfeifer, M. A. Butler, S. D. Senturia, E. R. Deutsch, D. W. Youngner, and G. B. Hocker. 2004. A MEMS–based correlation radiometer. *Proc. Photonics West 2004* **5346** (January, San Jose, California): 37–47.

67022

Characterization and Application of Dielectrics with Controlled Leakage

C. W. Dyck, J. R. Webster, D. J. Dickrell, M. R. Shaneyfelt, J. P. Sullivan, J. R. Schwank, M. T. Dugger, T. A. Friedmann

Micromachined capacitive switches are ideally suited for applications such as low-loss microwave phase shifters and tunable filters for use in miniaturized synthetic-aperture radar (SAR), tags, miniaturized transceivers for autonomous sensors, and miniaturized satellite systems. They exhibit superior performance over solid-state switches in terms of static power dissipation, linearity, and signal loss, and they also have lower ohmic losses than micromachined ohmic contacting switches. Presently, these devices are limited by early failures due to buildup of surface and bulk charge during operation.

Sandia seeks to solve this problem by engineering novel dielectrics with controlled conductivity to dissipate the charge. We are studying how the dielectric composition and defect concentration affect charge trapping in conventional plasma-enhanced chemical vapor deposition (PECVD) films and amorphous diamond (aD) variants. Based on this information, we are developing the desired dielectric and leakage properties that are necessary for high-performance capacitive switches. We are studying bulk and surface charging and quantifying the relative contributions of tribocharging and charging from high electric fields. We are considering differences in static and dynamic switch behavior. Analysis techniques include capacitance-voltage (C-V) curve measurements, the use of a nanotest tribology platform, irradiation by high-energy neutral particle and charged beams, and novel microelectromechanical systems (MEMS) test structures. This information is correlated to switch performance and lifetime to select candidate films for high-capacitive-switch lifetime.

We performed high-energy electron-beam irradiation of PECVD silicon oxide (SiO), silicon oxynitride (SiON), and silicon nitride (SiN) metal-oxide-semiconductor (MOS) capacitors. Due to the timing of the availability of this radiation source, we performed electron-beam exposure in lieu of x-ray exposure. Analysis of C-V curves before and after irradiation revealed interesting properties about these PECVD films. First, all three types of films contain a large amount of charge when measured after coming directly out of the fab. This charge is substantial enough to render capacitive switches nonfunctional and has prompted us to investigate the source of this charge

buildup during the fabrication process. We currently are running short-loop lots to determine whether plasma processing is injecting charge into our dielectrics. We also plan to explore rapid thermal annealing (RTA) to reduce charge in the films after processing. Ultimately, we will have to reduce this charge buildup to have yielding switches. Second, irradiation results show that PECVD SiO_2 builds up net negative charge due to bulk oxide trapping. Typically, SiO_2 traps positive bulk charge. We also verified and are investigating this result with measurements of proton-beam–exposed films. The SiN films trap both electrons and holes, resulting in a low net-charge buildup. Surface-state charging was not significant for any of the films. In some cases, changes in charge levels within the films were difficult to detect due to the large amount of fixed charge present after fabrication. We fabricated aD MOS structures and measured C-V curves. We currently are analyzing these results before submitting the devices for irradiation.

We began our studies of bulk- and surface-charging behavior of conventional PECVD films. From these studies, we will down-select the most appropriate dielectric films for studies in upcoming work. We had two sets of Rutherford backscattering (RBS) and elastic recoil detection (ERD) measurements done on the aforementioned films. Results indicate that our latest processing methods result in repeatable films in terms of composition, and in films with relatively low hydrogen (H) content. Recent Fourier-transform infrared (FTIR) spectroscopy measurements of SiN films show that significant H is bonded to Si, which is responsible for charge trapping. SiON films have less Si-H bonding, making them more suitable for capacitive switch applications. SiO_2 films have unmeasurable Si-H bonding; however, we were not able to produce a film with reasonable enough breakdown for practical application. We will be exploring RTA to reduce the H content in the SiN and SiON films.

We fabricated capacitive switches with PECVD SiO_2, SiON, and SiN, and are developing a test chamber to evaluate the lifetime of these switches with 1 GHz signal frequencies in a controlled ambient. We also designed novel microelectromechanical systems (MEMS) test structures and fabricated some that are now awaiting testing. We are nearing completion of processing aD capacitive switches and novel test structures. We plan to characterize these devices in upcoming work.

We began studies of aD films with the NanoTest platform. Initially, we are using the platform to measure the conductivity

of the aD films. Testing consists of pressing the conductive ball on the platform into a 1 cm x 1 cm square of aD and forcing a current through the film. The backside of the samples evaporated gold for electrical connection to the bottom of the platform. The film resistivity appears to vary spatially across the sample and, in some cases, changes over the duration of the test. We currently are performing follow-on experiments to gain a better understanding of these results.

67023

Nano-G Accelerometers Using Nanophotonic Motion-Detection System

D. W. Carr, B. E. N. Keeler, J. L. Novak, G. R. Bogart

Sandia is exploring the use of laterally deformable optical nanoelectromechanical systems (NEMS) grating transducers for sensor applications. For very small changes in the spacing of the nanostructured grating elements, we observed a large change in the optical reflection amplitude, making this an ideal transducer element for detecting very small amounts of relative motion. These devices are also very sensitive to wavelength and could thus be used as tunable elements for spectrometry, as well as communications or inertial sensing. This anomalous diffraction property was predicted in a previous work; here, we experimentally verify operation of these devices and demonstrate a motion-detection sensitivity comparable to that of any other microelectromechanical systems (MEMS) transducer. As optical devices, these sensors have additional advantages over other electrical sensors, including high immunity to electromagnetic interference (EMI) and the possibility of integration with fiber optics to create a network of sensors with a single remote optical source and detector.

We completed four design runs in the fabrication area for devices that are optimized to act as mechanical transducers using optical readout.

Every design run has yielded successful devices that performed as expected. We demonstrated the noise floors required for these to be used in a nano-G accelerometer system.

We showed noise floors below 100 fm/rt Hz at low frequencies.

We designed a new balanced photodetector circuit that extends the bandwidth to much lower frequencies without the onset of 1/f noise.

We developed a coherent double-sampling technique to mitigate 1/f noise down to 1 mHz frequencies.

We developed a new fabrication process using two levels of polysilicon to make near-field–coupled gratings to be used as the transducer elements.

We developed modeling tools to predict the behavior of many types of deformable gratings.

We presented results to many potential customers and identified a new key application area of this technology in the field of seismology for nuclear test-ban treaty monitoring.

Refereed

Carr, D. W., G. R. Bogart, and B. E. N. Keeler. 2004. Femto-photonics: Optical transducers utilizing novel subwavelength dual-layer grating structures. *Proc. Hilton Head Sensors and Actuators Workshop* **1** (1 June, Hilton Head, South Carolina): 91–92.

Keeler, B. E. N., D. W. Carr, J. P. Sullivan, T. A. Friedmann, and J. R. Wendt. 2004. Experimental demonstration of a laterally deformable optical nanoelectromechanical system grating transducer. *Optics Letters* **29** (11) (June): 1182–84.

67024

Bragg Fiber Development

J. G. Fleming, S. M. Brozik, P. Esherick, S. S. Mani, G. R. Hadley

This project targets the development of a novel technology that allows light and fluids to be confined within the same microvolume. This technology will be capable of a more efficient interaction of the light with the fluid and also of a more efficient detection of any emitted light. The devices created can be arranged in arrays on-chip. One promising application of this technology will be the development of much more sensitive, miniaturized biological detectors. The technology is based on the concept of Bragg fibers. Whereas fiber-optic cables trap light in a high index of refraction medium by total internal reflection, Bragg fibers trap light in a low index of refraction medium surrounded by distributed Bragg reflectors (DBRs). This is significant, as biological fluids generally have a low index. Although proposed over 20 years ago, Bragg fibers have only recently been fabricated. Sandia was the first to demonstrate a range of structures, mirror stacks, and waveguides built using micromachining to produce the Bragg-fiber cavities. This previous work used air as the low index medium. In this project, we will use fluids as the low index medium inside the Bragg fiber. As a demonstration vehicle, this project will focus on demonstrating a Bragg-fiber microoptic/microfluidic system for optimizing the detection of fluorescent "tags" that are selectively attached to specific biological compounds. This technology also has the potential for spectroscopy and light-induced chemistry applications. This is potentially very interesting for various sensing and integrated optics applications.

We made rapid progress on the fabrication, modeling, and testing of high-Q (quality) cavities. Modeling in general also greatly advanced.

Our work on high-Q cavities led us to realize that we needed to also consider single-mode waveguides, and we successfully developed a process to fabricate such structures.

We also demonstrated the integration of these single-mode Bragg-fiber structures with two-dimensional (2-D) photonic crystals.

In terms of fluidic testing, we demonstrated the flow of fluids through the channels and the fabrication of large channels.

We now have two ways to model these structures, both of which predict similar performance. The first approach is that of

the Cal Tech group, and the second is that developed at Sandia. In general, we are now in a good position to model the addition of fluids to the Bragg fibers. Simplistic back-of-the-envelope estimates do not indicate that there should be any serious issues here, provided the optical absorption of the liquids is not too great.

Finally, in the course of our work with Cal Tech, we came across a novel resonator structure with very high Q. This structure has been termed a *Bragg onion*. It is effectively a hollow sphere with a hollow stem attached to it. This structure has now been modeled extensively and has predicted Qs in the range of 10 million.

...we came across a novel resonator structure with very high Q....This structure has now been modeled extensively and has predicted Qs in the range of 10 million.

Refereed

Fleming, J. G., and S. Y. Lin. 2004. Novel, miniature Bragg fiber structures. *Proc. International Symposium on Photonic and Electromagnetic Crystal Structures V, Technical Digest of PECS-V* **1** (March, Kyoto, Japan): 162.

Hadley, G. R., J. G. Fleming, and S. Y. Lin. 2004. Bragg fiber design for linear polarization. *Optics Letters* **29** (8) (April): 809–11.

Liang, W., Y. Xu, Y. Y. Huang, A. Yariv, J. G. Fleming, and S. Y. Lin. 2004. Mie scattering analysis of spherical Bragg “onion” resonators. *Optics Letters* **12** (4) (23 February): 657–69.

Xu, Y., A. Yariv, J. G. Fleming, and S. Y. Lin. 2003. Asymptotic analysis of silicon-based Bragg fibers. *Optics Letters* **11** (9) (5 May): 1039–49.

Xu, Y., W. Liang, A. Yariv, J. G. Fleming, and S. Y. Lin. 2004. High-quality-factor Bragg onion resonators with omnidirectional reflector cladding. *Optics Letters* **28** (18) (September): 2144–46.

Xu, Y., W. Liang, A. Yariv, J. G. Fleming, and S. Y. Lin. 2004. Modal analysis of Bragg onion resonators. *Optics Letters* **29** (5) (March): 424–26.

67025

Microwave-to-Millimeter-Wave Electrodynamic Response and RF Applications of Semiconductor Quantum Nanostructures

M. Lee, E. A. Shaner, R. G. Dunn, J. A. Simmons, S. K. Lyo, M. P. Lilly, D. R. Tibbetts, J. L. Reno

This project studies the electrodynamic properties of semiconductor quantum nanostructures in the frequency range of 0.1–150 GHz and seeks to exploit this knowledge to prototype innovative radio-frequency (RF) devices having radically superior performance resulting explicitly from quantum effects. Specifically, Sandia is working with device structures based on high-mobility, two-dimensional electron gases (2-DEGs) and quantum wells (QWs) that can be designed and fabricated from ultraclean molecular beam epitaxy (MBE)–grown III–V semiconductor heterostructures. Examples of such structures include quantum-point contacts, dots, and coupled QWs. These exhibit a range of quantum responses to electromagnetic fields, including coherent plasmon resonances, quantized conductance, and Coulomb blockade. These effects are usually marked by distinctive nonlinear response characteristics that can be used to detect and manipulate microwave and millimeter-wave signals. The peculiar advantage of quantum devices comes from the correlated, coherent, and sometimes ballistic aspects of quantum charge transport. We will continue to measure and understand the basic linear and nonlinear electrodynamic response of these semiconductor nanostructures, including the alternating-current (ac) conductivity, noise properties, and nonlinear frequency-conversion properties, about which surprisingly little is known. We will apply the knowledge gained to the design, fabrication, and testing of frequency-agile devices, principally heterodyne mixers, relevant to radar, remote sensing, and wireless communications technologies. The quantum nature of such nanostructures should allow these mixers to attain levels of sensitivity and gain bandwidth not achievable with any standard semiclassical device. This work leverages Sandia's strengths in microwave-device characterization, growth of ultrahigh-mobility 2-DEG heterostructures, and fabrication of nanoscale devices. We recently fabricated several nanostructures with quantum transport signatures evident at temperatures up to 100 K.

We made significant progress on two fronts. First, we are near completion of the assembly of all the necessary new measurement infrastructure. Second, we fabricated and made the first heterodyne frequency-mixing measurements using the quantum plasmon excitation in a grating-gated double-QW (DQW) transistor.

For measurement infrastructure, we put together a system capable of measuring direct detection and heterodyne mixing in a device at local oscillator (LO) frequencies from 75 to 147 GHz (W and F bands) and at temperatures down to 2 K. For heterodyne measurements, this system can have an intermediate-frequency (IF) bandwidth up to 20 GHz. We installed two new experimental capabilities. We used a vector network analyzer (VNA) system to measure linear response S-parameters to verify performance. We adapted the design of a grating-gated DQW transistor previously developed at Sandia as an electrically tunable direct detector of submillimeter-wave radiation to make a DQW device where the detectable frequencies are within range of our heterodyne measurement system. Using this device, we observed a quantum plasmon response at an LO frequency of 145 GHz. We showed that this device actually has two response mechanisms: a broadband bolometric response near pinch-off, and a resonant plasmon response that tunes with gate bias. We found that heterodyne mixing can be done using either response mechanism. However, the nonlinearities associated with the two mixing mechanisms are fundamentally different, with the bolometric response being almost purely square-law while the plasmon nonlinearity is both stronger and more complicated.

...we fabricated and made the first heterodyne frequency-mixing measurements using the quantum plasmon excitation in a grating-gated double-QW (DQW) transistor.

67026

Development of GaN 20–100 Watt Ku-Band Power Amplifiers for Micro-SAR

A. G. Baca, R. J. Shul, M. G. Armendariz, J. R. Wendt, C. P. Tigges, M. E. Overberg, R. D. Briggs

Gallium nitride (GaN) solid-state power amplifiers (SSPAs) are promising candidates to replace traveling-wave tubes currently used in synthetic-aperture radars (SARs). A GaN SSPA can result in 40x size reduction and a 5–7 lb weight reduction of primary components (plus secondary gains from placement) as well as 40x cost reductions. In addition, GaN SSPAs may enable further size and weight reductions in conjunction with electronically steered arrays to replace the antenna and gimbal. To be most useful for SAR and other radar applications, GaN SSPAs must operate between 20 W and 100 W at or near 17 GHz. GaN's promise derives from high breakdown field, high sheet charge, and high saturated velocity. Although SSPAs greater than 100 W exist for both gallium arsenide (GaAs) and silicon (Si) in 2 GHz communications bands (1%–2% bandwidth), SAR at 17 GHz presents extra challenges. The SSPA impedance becomes so low for GaAs and Si devices that effective broadband matching (SAR requires 15% bandwidth) with good power-added efficiency is lacking above 10 W at 17 GHz. GaN's 7x higher breakdown voltage (49x higher impedance at comparable power) alleviates these matching issues and should allow efficient SSPAs up to 100 W.

Because of favorable semiconductor properties such as high breakdown field, high quantum well (QW) sheet charge, and good thermal conductivity, the promise of GaN has been recognized for years. On-wafer power measurements indicate that GaN high-electron-mobility transistors (HEMTs) can exceed 20 W/mm power density. In spite of these impressive results, GaN HEMTs have not made their way into applications due to shortcomings in materials, reliability, packaging, and thermal management. In this project, we will work to design and build a series of high-power amplifiers, working toward a goal of achieving 100 W at 17 GHz. We will address difficult problems associated with achieving these goals, namely, thermal management, device characterization, device stabilization, power combining, and packaging.

We successfully demonstrated silicon carbide (SiC) etches for microchannel cooling. As a result, we next focused the etch effort on SiC etches for through-wafer vias to reduce ground-inductance parasitics at 17 GHz. The final substrate thickness is

intended to be greater than 100 µm, and etch chemistries in the inductively coupled plasma (ICP) have now successfully achieved these etches in approximately 4 hr. The next step is to integrate the etch process with actual thinned wafers with front-side metal; this development is under way.

We made great improvements in materials and processes for GaN/aluminum (Al)GaN HEMTs. We achieved devices with power density greater than 5 W/mm on multiple wafers. Small-periphery devices actually achieved 8 W/mm, while large-periphery devices with more heat to dissipate achieved 5 W/mm. We measured single devices at 6 W by loadpull. Several key improvements enabled these power-density results. We improved the fabrication process by developing a higher-quality silicon nitride (SiN) passivation. We improved the epitaxially grown material by means of a number of growth, test, and feedback iterations using pulsed I–V. We developed a means of growing HEMT structures with consistently greater than 800 mA/mm for I_{max} that consistently shows low levels of current collapse.

We designed and built preliminary power amplifiers at 10 GHz for devices up to 1.2 mm gate width. We also built and tested power combiners. The power amplifiers produced 2.6 W at 10 GHz. Though short of the design goal of 5 W, these amplifiers are the first building block toward achieving the higher power levels necessary for miniaturizing the front end of SARs. The power-combiner circuit showed low levels of loss when tested separately. We will undertake the next set of designs in upcoming work.

We initiated degradation studies on GaN/AlGaN HEMTs. We initiated the studies on several different epitaxial wafers with HEMT devices that we subsequently fabricated. When stressed at a 30 V quiescent condition, all wafers showed a similar type of two-step behavior. In the initial phase of degradation, the HEMTs degraded somewhat rapidly over a period of 3–4 hr. After this period, the degradation slowed markedly in a second phase of degradation that we sampled from 10 to 50 hr. The first period of degradation is short enough that it can be considered a burn-in phase. The degradation in this phase was as little as 2% and as much as 7%. The degradation on the second phase was much less and appears to extrapolate to tens of years. We stressed a few devices at 40 V, and most burned out during the test. The next step in this study is to engineer the growth of processes to produce devices that can tolerate 40 V or high drain bias stress.

We achieved devices with power density greater than 5 W/mm on multiple wafers. Small-periphery devices actually achieved 8 W/mm, while large-periphery devices with more heat to dissipate achieved 5 W/mm.

Other Communications

Baca, A. G., Y. M. Kim, P. F. Marsh, M. G. Armendariz, C. E. Sandoval, A. A. Allerman, S. R. Kurtz, M. E. Overberg, J. R. Wendt, and C. A. Sanchez. 2004. Pulse testing of GaN/AlGaN HEMTs. *Proc. Electrochemical Society Meeting* (3–8 October, Honolulu, Hawaii).

67027

Evanescent-Wave Planar Photonic Biosensor

P. Esherick, G. A. Vawter, J. Guo, D. W. Branch, M. J. Shaw

The bioterrorism threat to national security has created an increased and immediate need for effective biosensors that rapidly assess the presence and nature of a biological attack. In many cases, the only way to unambiguously differentiate between a hostile attack and a naturally occurring appearance is through the forensic analysis of deoxyribonucleic acid (DNA) sequences present in the suspect agent. While the biotechnology exists today to perform this analysis, current methods rely on polymerase chain reaction (PCR) or comparable target-amplification systems that require additional instrumentation and reagents, and, more importantly, time to carry out the procedure. A major challenge is the development of methods that do not require these sample-preparation steps. Ideally, a sensor would be able to detect a single strand of DNA containing the unique identifying base sequence and, further, would be capable of distinguishing between near matches that differ by only one base pairing, i.e., single nucleotide polymorphisms (SNPs).

Sandia seeks to combine state-of-the-art bioassay technologies with Sandia's own state-of-the-art photonics technologies to develop a compact, planar, arrayable, optically based sensor with unprecedented sensitivity. The sensor devices will employ guided-wave structures enhanced by the addition of ring-resonators. Overall sensitivity will be further enhanced by using gold (Au) or quantum-dot (QD) nanoparticles as the attached optical reporter tags to amplify the optical response, conceivably to the point of being able to detect as little as one bound DNA strand.

Of significance is that we successfully fabricated and operated a ring-resonator device. By using a resonant structure, we expect over a 1000-fold enhancement in mass sensitivity as compared to existing approaches.

We successfully designed and fabricated fully integrated high-Q (quality) micron resonators on Si substrates with very low (0.1 dB/cm) waveguide losses and observed large-resonance wavelength shifts when applying different chemicals to a window-etched 200 μm ring resonator. The evanescent sensors took advantage of Sandia's strengths in microfabrication, waveguide design, and optical science. Of significance is that we successfully fabricated and operated a ring-resonator device. By using a resonant structure, we expect over a 1000-fold enhancement in mass sensitivity as compared to existing approaches. During development, we designed and evaluated several ring-resonator designs to optimize guiding layer thickness, surface roughness, ring diameter, bending

losses, and coupler efficiency. We made considerable advances in our second-generation design that dramatically reduced waveguide losses through increasing the overall waveguide layer thickness. Moreover, we also designed balanced ring-detector circuits and a first-generation planar lightwave circuit (PLC). The PLC permits easy integration for the detection of biological agents using microfluidic approaches. The presence of a reference resonator allows our device to remove undesired background noise while actively monitoring molecular binding events. We also developed a bioconjugation approach that is compatible with antibody and oligonucleotide attachment. The attachment process can target thiols, amines, or hydroxyl groups on target proteins or oligonucleotides by shifting the pH of the attachment buffer. The process involves the application of an epoxide-based organosilane, creating a robust method for rapid covalent attachment of specific receptor films. We developed the attachment process to be compatible with the oxide surface of the evanescent waveguides. Since the process involves only two steps, it dramatically reduces preparation time and improves surface-attachment efficacy. Moreover, we developed a computational model that allows prediction of device sensitivity as well as optimization of individual device parameters and operating modes. Our computational results predict a lower detection limit of 50–100 pg/cm^2.

Refereed

Guo, J., G. A. Vawter, M. J. Shaw, G. R. Hadley, P. Esherick, A. Jain, C. R. Alford, and C. T. Sullivan. 2004. Characterization of Si_3N_4 planar lightwave circuits and ring resonator. *Proc. SPIE—The International Society for Optical Engineering* **5350** (January): 13–22.

Guo, J., M. J. Shaw, G. A. Vawter, P. Esherick, G. R. Hadley, and C. T. Sullivan. 2004. High-Q integrated on-chip micro-ring resonator. *Proc. 17th Annual IEEE/LEOS Annual Meeting* **2004** (7–11 November, Rio Grande, Puerto Rico).

67028

Passive Electronically Steerable Array (PESA) for Miniature Synthetic-Aperture Radar (Mini-SAR), Precision Guidance, and Intelligence/ Surveillance/Reconnaissance (ISR)

K. C. Branch, C. D. Nordquist, C. W. Dyck, G. M. Kraus, T. A. Plut, B. H. Strassner, II

Sandia's goal in this project is to develop an antenna system suitable for miniature synthetic-aperture radar (SAR) systems, as well as to facilitate radar use for precision guidance, tactical unmanned aerial vehicles (UAVs), and other intelligence/ surveillance/reconnaissance (ISR) applications. The proposed antenna system is a passive array constructed without expensive/complex transmit/receive modules. Instead, we insert a reflect-line phase shifter into the antenna feed path, creating a compact, low-loss, lightweight, passive electronically steerable array (PESA). We are making progress in both technology development and integration.

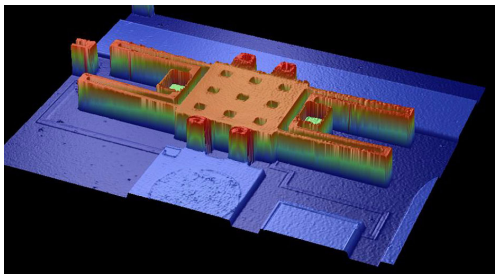

White-light interferometry image of the improved ohmic shunt switch.

Our approach focused on the antenna-array design and component development, and on the integration of both. We fabricated and tested a 2-bit reflect-line phase shifter. The reflect-line phase shifter utilizes two miniature radio-frequency (RF) devices: a Lange coupler and a microelectromechanical systems (MEMS) switch. We currently are using an ohmic switch, while a capacitive switch is under development. On average, the return loss of the 2-bit devices was greater than 10 dB, and the insertion loss was ~ 1 dB across the operating band. Additional testing indicates that 0.3 dB of the insertion loss is due to the phase-shifter launches, not the device itself. After we completed this design-build-test iteration of the phase shifters, we designed a new shunt ohmic switch to (1) move resonances outside the 15.2–18.2 GHz frequency band of operation, and (2) shorten the electrical length of the previous design. We will use this improved shunt switch in the phase shifters made for the PESA prototype.

Concurrently, we designed a 16-element array to have the following features: (1) a wide-bandwidth antenna element; (2) a modular card assembly—the array could potentially have many rows to create a two-dimensional (2-D) array; (3) scalability—the card size could be lengthened or shortened as needed; (4) combined electrical and mechanical function—the aluminum (Al) block that holds the cards together also functions as the reflector for the quasi-yagi antenna element; and (5) layout—

unlike aperture-coupled patch antennas, there is sufficient space to insert a packaged MEMS device.

The measured performance of the antenna assembly exceeded expectations. When oriented at the peak of the beam, the amplitude of the radiation pattern versus frequency was relatively flat, ~ 15 dB, across a 3 GHz bandwidth. At the center frequency, 16.2 GHz, the single-card 16-element array has low sidelobes that average ~ 25 dB below the main beam and cross-polarization isolation of at least 30 dB, all across a 3 GHz bandwidth and at ~ 90% radiation efficiency. This performance level can support ground-moving target-indication recognition in SAR images. With the success of this antenna assembly, it serves as the basis for the PESA prototype.

The measured performance of the antenna assembly exceeded expectations....This performance level can support ground-moving target-indication recognition in SAR images. With the success of this antenna assembly, it serves as the basis for the PESA prototype.

The packaging of the phase shifters and their integration into the PESA are among the key long-term challenges in this project. Ideally, we will make the phase shifters within a hermetically sealed container with little to no additional electrical lines or losses. To start, we will insert the phase shifter of the PESA prototype directly into the antenna feed assembly, and the Al ground plane for the antennas will act as a housing enclosure. This bypasses the additional losses that would be seen by commercially available packages in addition to reducing the form factor.

We made the following technical advances:

- Improved the ohmic switch design and fabrication process to have yields of ~ 90%.
- Improved the phase-shifter design to have yields of approximately 40%–50%, depending on the number of bits.
- Improved the 2-bit phase-shifter design to have an insertion loss of ~ 1.0 dB and return losses of > 10 dB.
- Collaborated with the Kansas City Plant to leverage their low-temperature co-fired ceramic (LTCC) technology for packaging.
- Designed, simulated, and constructed a broadband antenna element and array. The return loss of the 16-element array is greater than 20 dB over 3 GHz bandwidth.
- Designed an antenna-feed network that produces low sidelobe levels.
- Achieved successful “dry-fit” of phase shifters in the prototype feed network.
- Fabricated a 4-bit phase shifter with the improved MEMS switch and coupler. These devices will be used in the array prototype.
- Eliminated three yield-limiting steps in the fabrication process.

- Increased a 4-bit phase-shifter design while maintaining losses (including line transitions) in a range of 1.5–2.0 dB and a return loss of at least 12 dB across the operating band.

Emerging Threats

The diversity and rapid pace of modern warfare and antiterrorist actions require the development and application of inventive reliable technologies aimed to counter new classes of threats (e.g., chemical and biological attacks and other forms of terrorism) to homeland security. The Emerging Threats investment area supports this need through innovative ventures in sensors, communications, and intelligence systems; modeling and simulation; performance assessment and advancement in physical environments; and directed-energy and precision defeat. Sandia's mission-driven technologies are advanced further by technology development and partnership with the Department of Energy (DOE), the Department of Defense (DoD), the Department of Homeland Security (DHS), and other government agencies that broaden the application base.

67035
"Novel Processing, Affordable Motion Compensation, and Mode Multiplexing for Miniaturized Synthetic-Aperture Radar"

There is a critical need for miniaturized, affordable, synthetic-aperture radar (SAR) for both tactical unmanned aerial vehicle (UAV)–based reconnaissance and all-weather, non-global positioning system (GPS) weapon guidance. To fulfill this need, researchers are developing subsystems to facilitate a 25 lb SAR that matches or outperforms the image quality and resolution of our current 120 lb radars. New radar software architecture was fully designed, and significant progress was made on functional modules; a detailed design and simulation of a revolutionary field-programmable gate array (FPGA)–based image-formation engine was accomplished; and an innovative technique succeeded in making Sandia's autofocus algorithm significantly more tolerant of motion-measurement errors. Initial tests on raw radar data show successful results, and a patent application is in progress.

38623

Automated Visual Direction of Mobile Manipulation

R. J. Anderson, A. B. Maish, B. A. Kast, F. M. Saavedra, R. J. Anderson, T. S. Gladwell

Emergency-response personnel use mobile manipulator systems to respond to threats posed by improvised explosive devices (IEDs). Existing commercial systems are limited in their autonomous capability because they rely solely on operator interpretation of the live video images and direct operator control of the manipulator, i.e., teleoperation. In this project, Sandia focused on developing techniques to reduce the burden on the operator by digitally sampling the live video image and developing algorithms that use this information to semiautonomously control the remote manipulator system.

We demonstrated the feasibility of using statistical pressure snakes for automatic tool pickups subject to unstructured lighting conditions. We experimentally demonstrated tool pickups involving wrist camera servoing with up to 4 degrees of freedom (4 DOFs).

After completing this primary task, we investigated two other technologies critical to the utilization of visual direction of mobile vehicles: visual targeting using calibrated zoom cameras, and in situ *camera calibration.*

Visual servoing tool grab with statistical pressure snakes.

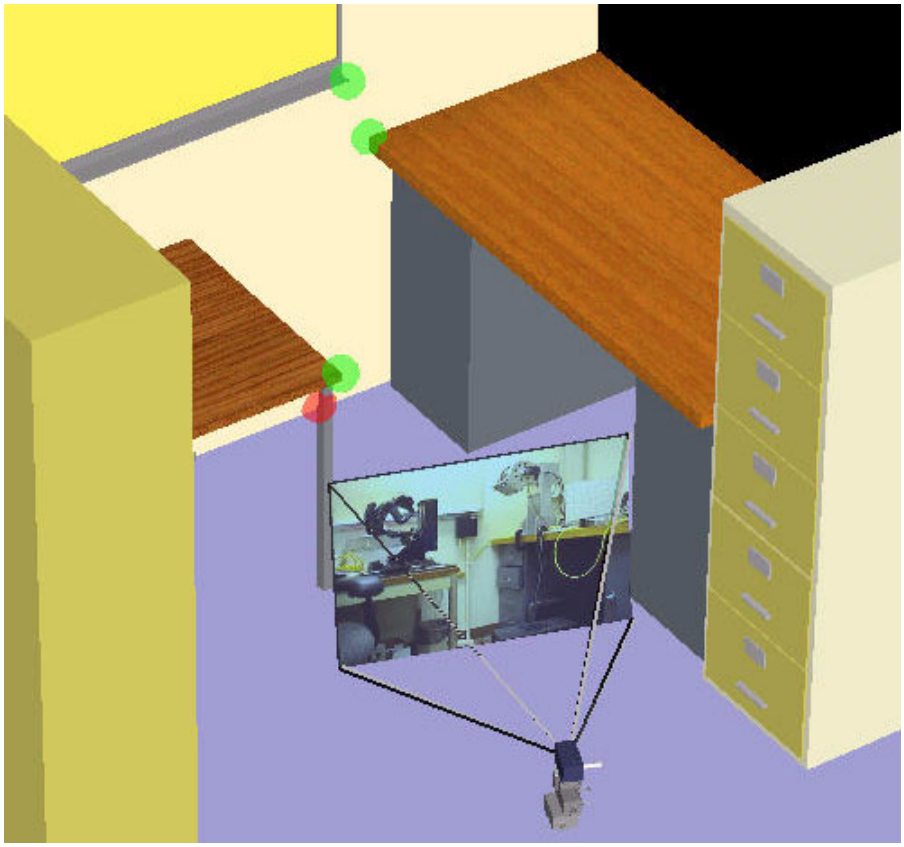

Embedded video in camera calibration.

Compact calibrated digital zoom cameras, such as the SONY-FCB-10A, recently became available commercially. These cameras solve a critical problem inherent in existing fixed-field-of-view (FOV) camera systems, namely, that they can scale to the task at hand. Previous visual targeting systems could perform tasks only on objects ranging from 4 in. to 18 in. The use of calibrated digital zoom improves the range by an order of magnitude. A new calibrated camera model has been developed that extends mobile targeting technology.

We explored three aspects of the use of video input for directing mobile robotic systems. First, we demonstrated the use of statistical pressure snakes for automating tool pickup for a mobile robot. The experiment consisted of a 6DOF robot system with a wrist-mounted camera. We designed specially made tool pickups that contained a uniquely colored rectangular block attached to a robot tool. The robot can automatically approach, align, and grab the robot tool by adjusting the robot position using visual servoing. This approach could readily accommodate the tool alignment variations in 4 DOFs (three translations and *z*-axis rotation). The snake algorithms proved to be robust in the unstructured lighting conditions typically seen by emergency-response manipulators.

Second, we demonstrated that the IED's operations could utilize live video imagery within a three-dimensional (3-D) modeling environment. Operators are often plagued with a "tunnel-vision" phenomenon, where they have the video feed but lose the context of the video. By embedding the video within a 3-D world model, we addressed this problem. The operator was able to freely move from video perspective to overview perspective.

Finally, we investigated zoom-camera calibration systems. By performing a series of fixed-camera calibrations at different zoom settings, we obtained a practical model for the zoom camera. We use an extensible markup language (XML) file to record both the normalized zoom setting and the corresponding intrinsic and extrinsic calibration terms. Linear interpolation between the settings has proven to be adequate in representing the continuously changing camera calibration matrix.

We designed specially made tool pickups that contained a uniquely colored rectangular block attached to a robot tool. The robot can automatically approach, align, and grab the robot tool by adjusting the robot position using visual servoing.

38624

Miniature Fourier-Transform Ion-Mobility Spectrometer for Real-Time Detection and Identification of Explosives and Chemical Agents

E. E. Tarver, III, A. H. Phan, K. B. Pfeifer

Ion-mobility spectrometry (IMS) is recognized as one of the most sensitive and versatile techniques available for the detection of trace levels of organic vapors. IMS is widely used for detecting contraband narcotics, explosives, toxic industrial compounds (TICs), and chemical-warfare agents (CWAs). Increasing threat of terrorist attacks, the proliferation of narcotics, Chemical Weapons Convention treaty verification, and humanitarian demining efforts have mandated that equal importance be placed on the analysis time as well as on the quality of the analytical data. (1) IMS is unrivaled when both speed of response and sensitivity must be considered. (2) With conventional (signal averaging) IMS systems, the number of available ions contributing to the measured signal amounts to less than 1%. Furthermore, the signal-averaging process incorporates scan-to-scan variations with decreasing resolution. With external second-gate Fourier-transform ion-mobility spectrometry (FT-IMS), the entrance-gate frequency is variable and can be altered in conjunction with other data-acquisition parameters to increase the spectral resolution. The FT-IMS entrance gate operates with a 50% duty cycle and so affords a seven- to tenfold increase in sensitivity. Recent data on high explosives demonstrate the parametric optimization in sensitivity and resolution of our system.

The FT-IMS entrance gate operates with a 50% duty cycle and so affords a seven- to tenfold increase in sensitivity. Recent data on high explosives demonstrate the parametric optimization in sensitivity and resolution of our system.

- Ion transmission decreased with decreasing internal diameter. The smallest tube did not transmit ions.
- There was a minimal effect on reactant ion peak intensity and resolving power, with the primary fluctuations being attributed to small changes in temperature and pressure that result from altering the drift gas-flow rate.
- The resolving powers of the large- and medium-size tubes were not significantly different, although the largest tube produced a slightly higher resolving power.
- While the observed resolving power was low compared with the theoretical maximum, these tubes did provide resolving powers similar to or better than those obtained in other small IMS tubes.
- The width of the drift rings was too large, which produced a discontinuous drift field. This discontinuous drift

field results in low ion transmission and reduced resolution power relative to that expected for tubes of this internal size.

- Temperature fluctuations as a result of varying drift gas-flow rates can cause a drift in the measured mobility constants.

We made the following recommendations:

- Of the three tubes tested, the middle size provides the best compromise among resolving power, sensitivity, and size. This tube should be used for a handheld instrument.
- In future designs, the rings of the tube should be thinner to provide a smooth electric field. A smooth electric field will aid in increasing both resolving power and sensitivity.
- Given the practical limitations of a handheld instrument, the operating temperature and voltage should be 150°C and 2000 V, respectively.

Refereed

Tarver, E. E. 2004. External second-gate Fourier-transform ion-mobility spectrometry: Parametric optimization for detection of weapons of mass destruction. *Sensors* **4**:1–13.

38627

EM Interactions with Systems to Enhance Security

R. A. Salazar, M. L. Weyn, J. M. Lundstrom, K. W. Harris, L. D. Bacon

The vulnerability of electro-explosive devices (EEDs) and their arming and firing circuits to electromagnetic (EM) radiation has long been a concern of the military and the mining industry alike. Military programs such as the Navy's "Hazards of Electromagnetic Radiation to Ordnance" and civilian investigations like those performed by the Institute of Makers of Explosives (Franklin Applied Physics Labs) produced useful guidelines for safeguarding against accidental initiation of explosives by EM radiation. Sandia's purpose in this project was to determine whether an existing radio-frequency (RF) system (e.g., existing radar) could pre-detonate improvised explosive devices (IEDs).

The purpose of this project was to determine whether an existing RF system (e.g., existing radar) could pre-detonate an IED. IEDs are a growing threat in the world. The vulnerability of EEDs and their arming and firing circuits to EM radiation are a major concern of the military and the mining industry. Military programs such as the Navy's "Hazards of Electromagnetic Radiation to Ordnance" and civilian investigations like those performed by the Institute of Makers of Explosives (Franklin Applied Physics Labs) produced useful guidelines for safeguarding against accidental initiation of explosives by EM radiation.

These studies and others produced significant progress to improve the safety of arming and firing circuitry over the last few decades. Improvement includes EEDs resistant to pre-detonation from exposure to RF energy. The initiator of an EED is either an electric match or an explosive bridgewire.

Commercial explosives often use electric matches to initiate explosives. The literature study and our testing show that radiated RF energy is much more likely to detonate electric matches. Electric matches require minimum power delivery in a minimum amount of time. The thermodynamical designs of electric matches cause them to dissipate energy. Hence, it is necessary that the power delivered overcome the dissipation rate to raise the electric-match temperature sufficiently for it to detonate. Our testing included coupling measurements to determine how much energy couples into a firing circuit as a function of frequency, geometry, and other parameters.

38629

Use of Seismic and Acoustic Responses to Assess Bomb Damage to Underground Facilities

L. C. Bartel, M. E. Kipp, J. A. Libersky, N. H. Natek, A. W. Roesler, R. E. Abbott, G. J. Elbring, D. F. Aldridge, N. P. Symons

The precise location of the weapon explosion and the resulting pressures and/or stresses within the target facility are critical for both bomb damage assessment (BDA) and battlefield planning. Simultaneous observations of seismic and acoustic waves coupled with state-of-the-art modeling offer the opportunity to determine detailed seismic- and acoustic-energy partitioning to determine detailed blast location and predict pressure and/or stress regimes within the buried facility. Weapon detonation in rock produces seismic- and acoustic-energy partitioning that is significantly different from that produced in the void of the facility. Interior detonations produce additional variations arising from possible blast venting through facility openings. Understanding and modeling of the amount of energy generated in both seismic and acoustic modes can provide critical information to determine where the blast occurred and estimate the resulting pressures and stresses within the facility and surrounding earth. Numerical simulations utilizing an existing three-dimensional (3-D) seismic-acoustic algorithm have demonstrated the capability to model these differing seismic and acoustic signatures. Sandia developed a methodology to quantify BDA through seismic and acoustic numerical simulations and analysis of field data from a weapon explosion. Utilizing an analytic solution for a whole space, we showed the potential to estimate the pressure and stress regimes in the vicinity of an exploding weapon in or near a tunnel within a complex terrain.

Movie of the simulation of a pressure time slice for an explosion in a tunnel.

Elastic waves radiating from a uniformly pressurized spherical cavity embedded in a homogeneous whole space can be described by mathematical formulae in a closed-form solution. Under this project, we developed an analytic solution in a uniform whole space for elastic waves emanating from a pressurized spherical cavity. These elastic waves can be either seismic or acoustic, depending on the medium.

When an explosive source is detonated within a soil or rock continuum, the deformations in the immediate vicinity of the source are nonlinear and irreversible. As the deformation propagates outward from the source, the amplitude decreases to the point where the soil or rock behaves in a linear fashion and

the deformations are reversible. The boundary defining the transition from nonlinear- to linear-elastic behavior is somewhat vague and arbitrary. Let us suppose, however, that we can define a spherical boundary between the nonlinear- and linear-elastic behaviors. The pressure and/or stress defined on this boundary as a function of time defines a time-dependent boundary condition (BC) for elastic-wave propagation radiating from the spherical surface. We demonstrated how the propagating elastic waves and/or acoustic pressure waves can be used to estimate the pressure and/or stress on this boundary between the nonlinear- and linear-elastic behaviors.

Using our analytic solution, we successfully showed through numerical simulations that by utilizing seismic and acoustic responses, one can estimate the pressure and stress regimes near an exploding weapon. Even though the analytic solution is for a uniform whole space, our numerical simulations show that this method may yield reasonable estimates of the pressure within a tunnel complex and the surrounding earth. Numerical simulations were of a tunnel complex with topographic relief. In addition, we applied our methodology to data obtained from an actual exploding weapon.

In addition to the work performed under this project, our analytic solution algorithm has been used to validate several Sandia nonlinear deformation codes. This validation requires that the nonlinear deformation codes be operated in the linear-elastic regime and have radial symmetry. These validations were performed for the Fossum finite-element, CTH, and Lagrangian-Eulerian ALEGRA codes.

...we successfully showed through numerical simulations that by utilizing seismic and acoustic responses, one can estimate the pressure and stress regimes near an exploding weapon.

Refereed

Aldridge, D. F., L. C. Bartel, N. P. Symons, and N. R. Warpinski. 2002. Grid search algorithm for 3-D seismic source location. *Society of Exploration Geophysicists Expanded Abstracts, Proc. 73rd Annual Society of Exploration Geophysicists Meeting* (26–31 October 2003, Dallas, Texas): 730–33.

Other Communications

Aldridge, D. F. 2002. Elastic-wave radiation from a pressurized spherical cavity. Sandia Technical Report SAND2002-1882, Sandia National Laboratories, Albuquerque, New Mexico.

38655

Free-Space Electrooptic Sampling and Remote Mapping of Electromagnetic Fields from Emitting Structures Using Femtosecond Terahertz Transceivers

S. M. Cameron, J. V. Rudd, F. J. Zutavern, T. S. Luk

New optoelectronic sensor technologies are required to remotely measure spatial and temporal distributions of free-space pulsed radiation and to probe localized electric-field and space-charge distributions in circuit and emitter structures. The ability to measure high-frequency field transients and the associated electromagnetic (EM) power spectrum is a critical diagnostic tool for assessing susceptibilities of ultra-wideband (optical/radio-frequency [RF]) signature discrimination and nonresonant (direct current [dc]-terahertz) impulse ranging of EM scattering signatures. Femtosecond terahertz transceivers based on the reciprocal behavior of optical rectification (difference mixing) and the Pockels effect in a nonlinear crystal can be used to alternatively transmit an EM interrogation waveform and to electrooptically sample a perturbed return signal from a targeted component on an optical carrier. By introducing a linearly chirped optical probe pulse for mixing with the microwave field, it is possible to encode (wavelength-division multiplex [WDM]) the temporal modulation onto the baseband optical-frequency spectrum and subsequently to decode (demultiplex) the waveform signature (frequency, time, space) in a single-shot measurement using spectral dispersion. Interaction kinematics will modify the broadcast pulse, and the resulting analysis can be used to probe the operation of an integrated circuit (IC), spatially map radiated field patterns, or interrogate carrier dynamics of an illuminated semiconductor interface. Because the electromagnetic pulse (EMP) is rectified from the intensity derivative of the optical pulse, adaptive pulse-shaping techniques can be used to produce arbitrary modulation formats to exploit coupling or enhance signatures with application to communications, tomographic imaging, and remote sensing.

We measured the radiated electric-field amplitudes (0.1–200 V/cm), power spectra, and associated radiation patterns for electron-hole plasmas from gallium arsenide (GaAs) and for surface-breakdown plasmas from aluminum (Al), glass (BK-7), silicon (Si), and germanium (Ge). We created and diagnosed these plasmas using optical fluence ranging nearly 10 orders of

magnitude (10E-7 to 10E3 J/cm^2) from a chirped-pulse regenerative amplifier laser that produces a 1 kHz train of 120 fs-wide pulses with up to 2 mJ of energy per pulse at a wavelength of 800 nm. To explore the wide bandwidth of these plasma radiation sources, we used two electric-field diagnostics. A conventional electric-field sensor (D-dot) with a 40 GHz bandwidth (calibrated to 5 GHz) and a 70 GHz sampling oscilloscope measured the low-frequency tail of the radiation spectrum. We observed the high-frequency range of the spectrum with electrooptic sampling (EOS) using zinc telluride to measure the radiated electric field with subpicosecond time resolution. We calibrated the EOS detection system by placing a dc voltage across the crystal and measuring the induced polarization rotation. The bandwidth of the electrooptic sampling is limited by the thickness of the electrooptic crystals, so we used a range of thicknesses to vary the bandwidth of the EOS measurements (0.3–1.0 THz).

Our activities included assembling an improved EOS detection system with six pump beam paths to accommodate two separate sample positions times three sample/beam geometries (one transmission and two reflection configurations). We aligned the pump and probe beam paths with path length differences of only a few hundred microns so that rapid sample and configuration changes could be made without losing the terahertz signal. Installation of new terahertz optics and a faster translation stage improved our terahertz detection sensitivity and acquisition rates by 2 orders of magnitude. We increased the bandwidth of our EOS detection system to improve our sensitivity to subtle changes in terahertz generation and initiated optical pulse-shaping experiments to determine the impact on pulsed terahertz sources.

We explored the fundamental differences between electron-hole and surface-breakdown plasmas. We characterized similarities and contrasts in radiation patterns and efficiencies for all of these plasma radiation sources. Simple models for the picosecond carrier motion in these sources were considered and compared with measurements. We demonstrated the advantages and challenges of using a kilohertz, millijoule, and short-pulse laser for plasma generation and electrooptic sampling.

We found that, despite the much lower bandwidth of the D-dot, the relative amplitudes of the two sensing technologies were in remarkable agreement. Because of its simplicity and greater sensitivity, we also used the D-dot to measure long-wavelength radiation patterns; it was particularly helpful with the preliminary alignment of the EOS apparatus.

Refereed

Zutavern, F. J., J. Van Rudd, R. T. Collins, Jr., L. A. McPherson, T. R. Nelson, T. S. Luk, and S. M. Cameron. 2004. Near-THz radiation from optically induced plasma sources. Paper presented at the International Conference on Plasma Science, June, Baltimore, Maryland.

38681

Identification of Chemical Plumes: Range-Resolved IR Lidar Enabled by New Photonic Technologies

T. J. Kulp, R. P. Bambha, D. A. Kliner, S. E. Bisson

This project supported two goal areas: (1) the development of a mid-infrared (MIR) range-resolved lidar (light detection and ranging) that employs new photonic technologies, and (2) the creation of site-differentiating technologies at Sandia that allow the fabrication of fiber-based lasers and quasi-phase-matched (QPM) nonlinear crystals.

Sandia made significant progress in both areas. The lidar work resulted in the completion of a cavity-enhanced nonlinear converter to upconvert photons from the infrared (IR) to the near-visible. The cavity successfully locked and was able to build up pump radiation at an enhancement factor of 20x. Coupling the cavity to the lidar was, however, met with difficulties associated with the narrow angular acceptance of the crystal that caused the lidar to have an extremely narrow field of view (FOV) and short depth of focus.

In response to the upconversion limitations, we decided to analyze a new alternative technology for use in the range-resolved lidar. This is an MIR avalanche photodiode array under development at DRS Infrared. We obtained a research-grade version of it and are now in the process of evaluating its performance for MIR lidar application.

We successfully completed the fiber laser and nonlinear crystal capabilities. The former effort resulted in the development of a laboratory equipped with resources to fabricate fiber lasers in-house. The crystal work led to a demonstration of our ability to fabricate QPM crystals and utilization of those crystals in a nonlinear device.

The lidar work resulted in the completion of a cavity-enhanced nonlinear converter to upconvert photons from the infrared (IR) to the near-visible. The cavity successfully locked and was able to build up pump radiation at an enhancement factor of 20x.

- *Range-resolved MIR lidar.*

— We assembled and operated a resonant cavity to enhance the pump in a nonlinear process.

— We demonstrated the ability of the resonator to enhance the pump intensity within the periodically poled lithium niobate (PPLN) nonlinear crystal by a factor of 20x. The pump used was a 1064 nm seed laser that we amplified to 0.5 W by a ytterbium (Yb)-doped fiber amplifier.

— We modified the lidar transmitter and receiver design to accommodate the narrow acceptance angle of the upconverting crystal. We formulated a transmitter to produce a focus of approximately 1 mm at a range of tens of meters. This

corresponds to the FOV of the PPLN upconverter crystal at that range.

— We identified a developmental detector technology that offers significant promise as an alternative method to upconversion for achieving the high IR sensitivity required for range-resolved MIR lidar. The avalanche photodiode (APD) achieves this without the FOV limitations affecting the upconverter. This is an APD detector under development for the Defense Advanced Research Projects Agency (DARPA) by DRS Infrared.

— We contracted with DRS Infrared to package a developmental APD array (in dewar with preamplifiers) and to conduct performance characterizations of it. We determined that the detector can achieve high internal gain (> 800x) at high bandwidth (100 MHz), allowing it to measure 3.3 μm photons at high sensitivity (10 photons noise in 10 ns), comparable to that expected of the upconverter without the FOV restrictions.

— We performed lidar performance modeling using the characteristics of the DRS Infrared APD array. Results indicate high performance comparable to that expected with the upconverter.

— We considered the APD array as the enabling technology for MIR DIAL (differential adsorption lidar system [detects and monitors lights of hydrocarbon]). (This has not previously been demonstrated.)

— We developed an alternate lidar receiver design for the APD detector using a lidar telescope and scanner developed under a previous project.

— We received the packaged developmental APD array from DRS Infrared. We assembled a diagnostic test stand to evaluate the performance of the array and to validate the measurements made at DRS Infrared.

— We assembled the lidar receiver using a near-IR (NIR) positive-intrinsic-negative (PIN) diode as the detector.

— We performed range-resolved lidar measurements at 1064 nm wavelength to demonstrate the performance of the lidar system and to benchmark the aerosol backscatter magnitude at that wavelength.

- *Fiber-laser development*. We constructed and equipped a new laboratory for fiber-amplifier development. All of the above steps are now set up in this lab. These new capabilities directly led to several funded projects and to several pending proposals.
- *Crystal development*. We demonstrated the performance of PPLN crystals fabricated in the in-house facility to create pulsed IR light for use in a MIR laser source.

49915

Critical Technology Development for Hard-Target-Defeat High-G-Tolerant Fuze and High Explosives

C. L. Smithpeter, E. J. Welle, M. W. Pilcher, P. D. O'Malley, R. McEntire

Sandia's objective is to provide a proof-of-concept demonstration for a high-speed earth-penetrating weapon. If successful, this technology could be the basis for future warheads that hold hard and deeply buried targets (HDBTs) at risk to the U.S. arsenal. Many of these targets are immune to the current arsenal. This objective is broken down into fuzing, high-explosive (HE), and penetrator technologies for high-g environments. The technical challenge for fuzing is to develop the electronics for weapon safety/function and the mechanical materials/structures to survive a high-speed impact generating in excess of 20 kg. The challenge for the HE fill is to not initiate at impact, yet to maintain integrity for reliable function at the desired time. Finally, the penetrator challenge is to provide sufficient strength to survive a 20 kg impact at high speed.

- *Fuzing*. We identified and corrected the source of a power failure in an earlier sled-track test. In the sled test of the integrated and live penetrator, the rocket sled boosted the penetrator to a supersonic speed where it impacted a multilayered concrete target. The fuze failed to detonate the weapon at the programmed time and came to rest inside a concrete target. We recovered the fuze intact after the test and read out the data. An analysis of the onboard data revealed that the high-voltage switch failed during initial impact, leaving no firing potential at the designated time. Failure analysis of the switch revealed electrical damage to the device. Testing of subsequent devices revealed processing defects that weakened the switch. We identified an alternate switch with improved quality. Shock testing of the replacement switch indicated acceptable performance for the penetrator environment. We were unable to repeat the sled-track test to achieve the objective demonstration. If we could repeat the sled-track test, we expect that the fuze would allow the weapon to function in the targeted void.
- *Explosive charge*. We successfully detonated the HE charge from the earlier sled-track test post-test. The detonation indicates that the explosives will function at the designated time during the target impact. The explosive charge in the second sled test did not initiate on impact, as expected. The integrity of

the HE could not be judged due to the breakup of the penetrator in the second layer of the target. Additional threshold testing revealed that the firing set and HE will not function if the high-voltage charge is less than 500 V. The 500 V is a conventional value for a safe “no-fire” level. Threshold testing also found that the explosives will reliably function at the intended firing level of 1000 V.

- *Penetrator.* The penetrator fabrication process matured with the hot isostatic press around a ballast. We used the ballasted penetrator in the second sled-track test, where it passed through a primary layer of concrete as expected. The penetrator path deviated in the second target, and it struck a steel panel at the back of the target and broke apart. The cause for the path deviation is uncertain. Possible causes include delivery angles, target movement, and distortion of the penetrator. The striking of the steel plate at an extreme angle exceeds the design requirements. In addition, the presence of an oblique steel plate is a test artifact required by the limited target diameter. Data from the previous tests and simulations indicate that the penetrator performance will exceed current weapons and provide an enhanced HDBT defeat capability.

52577

Immunological Basis for High-Reliability Systems Control

W. A. Amai, E. A. Walther

Software in various real-time control systems is typically reactive to error conditions as they occur, and handling these error conditions is usually solely up to the creativity and vision of the software designer or the expertise of the operator. A recent and growing body of computer immunology research focused on the security and reliability of general-purpose operating systems.

This project begins the research into using concepts and methods from computer immunology to build more robust and flexible robotic control systems. Like intrusion-prevention systems, robotic control systems must detect and respond to dangerous conditions in real time; unlike desktop systems, though, the typical causes of such problems are hardware failures, programming errors, and adverse environmental conditions. But in both contexts, such situations are deviations from normal behavior.

Work in this project focused on adapting pH, a Linux-based intrusion-prevention system, to the robot control domain. pH applies a two-phased approach to protection. First, it learns normal system behavior. Then it monitors for anomalous behavior, and, if abnormal behavior is detected, it activates autonomic responses based on the severity and type of the behavior. Such a response system is distinguished from a traditional exception-handling mechanism in its ability to detect abnormal, yet "correct," code paths, yet be able to ignore routine errors—all without operator intervention.

Recent research showed that an immune system is not only a viable and useful runtime tool, but also can serve as a diagnostic tool during development. We also demonstrated that computer immune-system concepts can be applied to smaller platforms.

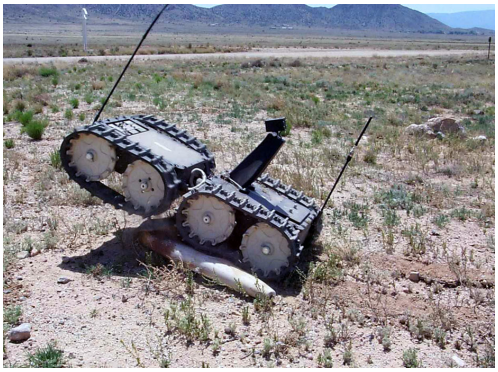

SandDragon robotic platform with an immune system implemented in the control system.

We implemented an immune system on a smaller class of platform to demonstrate the general applicability of computer immune-system concepts.

Specific accomplishments included characterizing and tuning the computer immune system on the SandDragon robotic vehicle. We updated pH to work with the latest preemptive version of the Linux kernel. Not only useful during normal vehicle operation, the immune system also proved to be beneficial as a diagnostic tool for development. We found

several control-system problems with the aid of immune-system feedback. These included problems with motor-controller communication, console output buffering, and scheduling policies. The motor controller and scheduler problems degraded system performance, while the buffering problem delayed operator feedback in some circumstances. These were all subtle problems that were brought to light by the immune system. Correction of these problems led to the achievement of a stable normal profile for the control system on the SandDragon.

To demonstrate that the computer immune-system concepts are viable on a smaller, computationally less-powerful processor, we completed the Volant robotic vehicle with a control system based on the MicroC/OS-II real-time operating system. We modified the RTOS (operating system) libraries and BIOS (operating system) code to generate a profile without user intervention, just as on the immune system on the SandDragon. We completed a handheld controller based on a personal digital assistant for driving the Volant, as well as on receiving feedback from its immune system. We demonstrated that an immune system can be implemented transparently on such a platform, and interesting profiles may be constructed even from simple control programs.

52580

Moving-Target Identification Using Ultrahigh-Range-Resolution Data

J. S. Salazar, B. K. Bray, J. A. Richards, R. J. Fogler, M. W. Koch, D. W. Harmony

This project involved the investigation of methods and development of tools for processing and exploiting ultrahigh-range-resolution (UHRR) radar data, ground moving-target indicator (GMTI) radar data, and synthetic aperture-radar (SAR) data, with an emphasis on automatic target recognition (ATR) applications.

The project enabled significant advances in Sandia's knowledge, capabilities, and software infrastructure in several radar-related fields. In particular, this project yielded numerous advances in the fields of UHRR radar, GMTI radar, and SAR.

The project enabled significant advances in Sandia's knowledge, capabilities, and software infrastructure in several radar-related fields. In particular, this project yielded numerous advances in the fields of UHRR radar, GMTI radar, and SAR. These advances center on ATR development, but also include other applications.

The primary UHRR–related accomplishments of this project are twofold. First, this project enabled Sandia researchers to develop new algorithms and techniques for application to UHRR-radar ATR. Second, Sandia researchers investigated techniques for UHRR signature stabilization, an essential processing step for UHRR–related applications. These accomplishments poise Sandia to pursue new business in UHRR data exploitation.

This project resulted in two major GMTI–related accomplishments: the development of new software tools for generating large volumes of GMTI range/Doppler imagery, and the development of new software tools for the extraction of ground-truthed target data from such imagery. The formation of large volumes of GMTI range/Doppler imagery and the reliable extraction of ground-truthed target data from this imagery are important preprocessing steps required for the development of GMTI range/Doppler ATR systems. These new tools greatly advance Sandia's capabilities in this area.

The final accomplishments of this project are related to SAR ATR. This project also enabled an investigation into the use of simulated SAR imagery for ATR development. These accomplishments will help Sandia to remain a leader in the field of SAR ATR.

Other Communications

Koch, M. W., J. S. Salazar, and D. W. Harmony. 2003. Vehicle identification using high-resolution range profiles and the sequential probability ratio test. *Proc. MSS National Symposium on Sensor Fusion and Data Fusion* **1** (2–5 June, San Diego, California): 1–19.

52581

Advanced Mobile Networking, Sensing, and Controls Using Graph Theory

J. T. Feddema, D. G. Wilson, D. Kilman, R. H. Byrne, B. P. Van Leeuwen, C. L. Lewis

This project will advance the state of communication, sensing, and control for mobile distributed systems by taking an integrated approach. Sandia will use graph theoretic methods to analyze the input/output reachability and structural controllability and observability of a decentralized system. Embedded in each node, this analysis will automatically reconfigure an ad hoc *communication network for the sensing and control task at hand. We also will use the graph analysis to create the optimal communication flow control based on spatial distribution of the network nodes. Edge-coloring algorithms tell us that the minimum number of time slots in a network is equal to either the maximum number of adjacent nodes (or degree) of the undirected graph or the maximum degree plus one. Therefore, the more spread out the nodes are, the fewer the number of time slots needed for communication and the smaller the latency between nodes. In a coupled system, this results in a more responsive sensor network and control system. We will develop network protocols to propagate this information and distributed algorithms to automatically adjust the number of time slots available for communication. In addition, we will develop information-assurance methods compatible with these protocols to support operation in an environment where adversaries may attempt to disrupt service. These protocols and algorithms must be extremely efficient and updated only as network nodes move. We will analyze the efficiency by analytical and simulation techniques and implement these algorithms on multirobot systems already in use at Sandia.*

We investigated the feasibility of solving the optimal communication and control problem by posing the problem as a convex optimization problem (linear matrix inequality), which possibly could be solved in a parallel form over the network. From our analysis, we determined that it is extremely communication-intensive to solve the linear-matrix inequality optimization in a distributed fashion and, therefore, not appropriate for real-time computation in a mobile *ad hoc* network. However, it is possible to make a conservative approximation of the solution in real time using a linearized analysis. As a result of this study, we developed design steps for creating provably stable distributed controls and evaluating

wireless communication network (WAN) protocols for cooperative robotic systems.

We used a three-step optimization process to determine the decentralized control structure that minimizes the performance metric of a specified task. The first step is to define a global performance index whose extremum produces a desired cooperative result. The second step is to partition and eliminate terms in the performance index so that only terms of local neighbors are included. This step minimizes communication among robots and improves system robustness. Rather than requiring every robot to know the position of all the other robots, each robot needs only to know the position of its nearest neighbors. Also, if a neighbor dies, a new set of nearest neighbors is selected from the remaining robots. The third step is to define a control law that is the gradient of the partitioned performance index. This control drives the system toward the local extremum of the partitioned performance index. After these three steps, we perform a connective stability analysis to determine constraints on the communication sample period and the local control gains. We use a vector Liapunov technique to ensure system stability. Finally, we evaluate the communication sample period for four different network protocols (a Time-Division Multiple Access [TDMA] linear broadcast, a TDMA polylogarithmic broadcast, a TDMA coloring algorithm, and a Collision Sense Multiple Access [CSMA] coloring algorithm) based on the network graph, which changes throughout the task.

We evaluated the initial and steady-state time required for communication in a distributed control network both analytically and through OpNet simulations. The simulations verified our communication models, allowing us to better understand the conditions under which CSMA versus TDMA protocols should be used. Our approach was tested in simulation and robotics hardware on a number of test problems. The first problem is the distribution of multiple robots along a line or curve. The second and third problems are the distribution of multiple robots in an unconstrained and constrained two-dimensional (2-D) plane. The fourth problem is the distribution of multiple robots around an elliptical curve. The fifth problem is for multiple robots to converge on the source of a plume in a plane. The sixth problem is for multiple underwater robots to converge on the source of a plume in a (3-D) volume.

Other Communications

Feddema, J. T. 2004. Communication and control of large-scale cooperative systems. *Proc. American Nuclear Society 10th International Conference on Robotics and Remote Systems for Hazardous Environments* **1** (28–31 March, Gainesville, Florida): 123–30.

Feddema, J. T., R. D. Robinett, and R. H. Byrne. 2003. An optimization approach to distributed controls for multiple robot vehicles. *Proc. International Conference on Intelligent Robots and Systems, Workshop on Control and Cooperation of Intelligent Miniature Robots* **1** (31 October, Las Vegas, Nevada): 1–16.

52582

Compact Terahertz Sources for Emerging-Threats Applications

A. Mar, J. C. Armijo, F. J. Zutavern, J. R. Wendt, G. A. Vawter

This project will develop options for compact sources of electromagnetic (EM) radiation in the so-called "terahertz gap" of the EM spectrum for covert communications and directed energy (DE). This regime is very attractive for covert applications because of the lack of readily available instrumentation and the potential compactness of highly directional transmitters. Secure communications at terahertz frequencies could employ strong absorption lines in atmospheric propagation to confine the range of potential interception, as required, for example, by the Future Combat System (FCS). The highly directional nature of terahertz radiation could also be used to enhance disruption effects on radio-frequency (RF) communications (a concept that Sandia has demonstrated at microwave frequencies) and other RF electronics. Compact and relatively inexpensive sources will also be required for large-scale deployment of terahertz-based technologies such as imaging devices for homeland defense.

Currently, terahertz research typically involves the use of large and costly laboratory femtosecond laser systems. We will develop heterodyned continuous-wave (CW) lasers and harmonic mode-locking of diode lasers to generate terahertz with compact systems of turn-key simplicity. We will combine such new compact optical sources with photoconductive semiconductor switch (PCSS) technology for terahertz generation and detection.

Terahertz technology has direct implications for many applications involving miniaturized high-voltage electronics, such as neutron generators (NGs), radars, high-power microwave (HPM) systems, lasers, and others. Imaging based on terahertz radiation (T-rays) could be used for inspection and qualification of weapon components, such as neutron tubes (NTs) and firing sets. T-rays penetrate through nonconducting materials such as those used in high-voltage potting and image materials by the variation of the complex dielectric constant. T-ray images are thus complementary to x-rays, whose image contrast is provided by the atomic number of the materials imaged.

Much etch development for interactivity reflector (ICR) fabrication has occurred at this stage of the project. This etches in the new TePla (a German company now called PVA TePla

AG) RIBETCH 160LL CAIBE system and is patterned using direct-write e-beam lithography (JEOL system). The resulting slots are ~ 1 μm deep to interact with optical mode in the the laser waveguide. We further improved vertical sidewalls using perpendicular incidence of ion beam, which is adjustable in the TePla system. We did this etch in gallium arsenide (GaAs) with no epitaxy. When we applied the same process to material grown for lasers, the etch failed in the heavily doped layers. We currently are redesigning the doping profile within the laser epitaxy to overcome this so we can successfully fabricate the ICR structure in laser material.

While ICR development continues, we are testing other devices on the first-generation mask that use only saturable absorption to achieve terahertz-frequency harmonic mode-locking. The device is ~ 300 μm long and contains a reverse-biased saturable absorber in the center of the laser cavity. This induces mode-locking at the second harmonic at ~ 280 GHz by favoring pulse collision in the centered absorber by two counter-propagating pulses. We see evidence of this effect in the optical spectra for this device. We can readily see that the laser shows a highly multimoded longitudinal mode spectra without saturable absorption, typical for such a device of this type and cavity length. When we apply reverse bias to the saturable absorber segment of the laser (~ -1 V), we see the spectra described. Most of the multiple modes are suppressed, and two lasing modes appear with a difference frequency of 267 GHz, indicating mode beating or locking at the second harmonic. Note that small residual modes at the fundamental mode spacing (~ 133 GHz spacing) are still visible at a low level.

To measure such modulation in the temporal domain, we constructed a slow-scanning autocorrelator using a quadratic detector that uses two-photon absorption, as opposed to the usual frequency-doubling approach using a nonlinear crystal. We modulated the fixed and variable delay paths in the autocorrelator at two different frequencies using a mechanical chopper and employed lock-in detection at the difference frequency to detect the quadratic signal.

We developed critical tools for optical testing of these devices, including an ultrahigh-sensitivity scanning autocorrelator. We tested colliding pulse mode (CPM) devices at the second harmonic (~ 280 GHz). This resulted in the capability to measure pulses of extremely low energy, which is appropriate for a continuous-wave (CW) pulse stream at terahertz frequencies.

To verify operation of the autocorrelator, we added a gain-switched vertical-cavity surface-emitting laser (VSCEL) to the setup. We modulate this laser using the output of a 2 GHz microwave comb generator, and it and outputs pulses of approximately 30 ps duration, as independently measured using a fast photodetector and high-speed (50 GHz bandwidth [BW]) sampling oscilloscope. We obtained a waveform from the gain-switched VCSEL, taken with a total pulse energy of only 20 fJ while still maintaining good signal-to-noise (SN)! We believe this is record sensitivity for this type of measurement. We have now measured the CPM laser using this system and obtained the waveform. Unfortunately, this signal has poor modulation depth, possibly due to detector saturation and/or incomplete mode-locking action in this particular device. Work is currently ongoing to refine this result.

Work has also begun to characterize materials for terahertz photomixing. We characterized samples of semi-insulating GaAs irradiated from 1e14 to 5e14 for carrier lifetime using a femtosecond laser–based pump-probe time-resolved reflectometer. The measurements indicate that the lifetimes were too long for terahertz photomixing, and we will next test samples with higher irradiation levels and/or low-temperature (LT)–grown GaAs.

We obtained a waveform from the gain-switched VCSEL, taken with a total pulse energy of only 20 fJ while still maintaining good signal-to-noise (SN)! We believe this is record sensitivity for this type of measurement.

52583

Understanding Communication in Counterterrorism Crisis Management

M. F. Hawley, J. D. Arnold, P. K. Barr, J. C. Forsythe, H. R. Ammerlahn, T. J. Sa, A. E. Wright, W. B. Wilcox, P. D. Hough, D. D. Djordjevich, A. S. Yoshimura, M. L. Bernard, M. M. Johnson, R. Tam

In response to terrorist attacks, multiple agencies require joint decisions under conditions of high stress. Teams with diverse membership face issues such as short time cycles, high stakes, incomplete data, and conflicting interests in these scenarios. Previous weapons of mass destruction (WMD) terrorism exercises have pointed out that communication barriers between organizations impede an effective response. For example, participant-participant and participant-machine interactions between participants playing distinct roles have a large impact on the outcome of decisions.

In the WMD Decision Analysis Center (WMD-DAC), we use distributed computer simulation and visualization tools to integrate issues surrounding terrorist attacks. Our simulations provide a means to explore WMD terrorism defense through interactive, dynamic, "what-if" computerized "war-gaming."

Traditional Department of Defense distributed simulations are based on Distributed Interactive Simulation (DIS) or High-Level Architecture (HLA). These simulations rely primarily on two communication paths: (1) electronic exchange through DIS/HLA interconnected machines running loosely coupled, federated computer models, and (2) participant-participant and participant-machine interactions between participants playing distinct roles. This second category of communications has a large impact on the outcome of decisions made as part of the simulation.

Previous to this project, participant-participant and most participant-machine interactions were not captured in these exercises. This project created the capability to capture these interactions as part of the simulation data stream and to incorporate communication measurements in our simulations. We also developed the capability to monitor the quantity and quality of interagency, participant communication during interactive simulations in WMD-DAC, thus increasing its value for WMD terrorism preparedness.

The data gathered from these communication portals is analyzed by automated and human simulation referees using established human and computer-mediated communication research methodologies to categorize individual and team interactions and behaviors and to perform sensitivity analyses.

Previous to this project, participant-participant and most participant-machine interactions were not captured in these exercises.

This allows researchers to observe, study, and increase their understanding of the relationships between interagency communication and the effectiveness of joint decisions in a high-stress environment.

We made the following accomplishments:

(1) We participated in WMD terrorism and facility protection exercises, including those hosted at Sandia through Department of Homeland Security (DHS)/Chem/Bio Countermeasures, Protective and Responsive Options for Airport Counterterrorism (PROACT), DHS and Defense Threat Reduction Agency (DTRA) BioNet, Sandia Borders Grand Challenge LDRD, and CA Site Goal 2.

(2) We enhanced the Interagency Communication Network Simulation (ICNS) by monitoring and logging participant communication through chat and e-mail/fax services provided by the Enterprise Modeling Architecture (EMA) framework.

(3) We stored communication data and metadata in the external structured query language (SQL) database for later retrieval and analysis. We wrote a post-processing interactive tool to view and query the database, allow interactive updates of Interaction Process Analysis (IPA) numbers, and provide a statistical analysis of each message by both role player and IPA.

(4) We created a prototype for speech-to-text translation in real time to be added to the EMA framework when Voice Over Internet Protocol (VOIP) and commercial-off-the-shelf (COTS) speech engine technology improves.

(5) We developed a multirole simulation that incorporates human subjects in a communications research study.

(6) We analyzed communications data gathered from the simulation by automated and human simulation referees using established human and computer-mediated communications research methodologies and post-processing sensitivity analysis tools to categorize individual and team interactions and behaviors.

Other Communications

Ammerlahn, H. R., J. Arnold, P. Barr, M. L. Bernard, D. D. Djordjevich, J. C. Forsythe, M. F. Hawley, H. Hirano, P. Hough, M. Johnson, T. Sa, R. Tam, W. B. Wilcox, A. Wright, and A. S. Yoshimura. 2004. Understanding communication in counterterrorism crisis management. Sandia Technical Report SAND2004-5390, Sandia National Laboratories, Livermore, California.

Lipkin, J., R. Tam, H. R. Ammerlahn, D. Manley, T. West, and H. Hirano. 2003. Summary and results of the joint WMD-DAC/Alameda County bioterrorism response plan exercise. Sandia Technical Report SAND2003-8650, Sandia National Laboratories, Livermore, California.

Yang, L. I., D. K. Manley, S. P. Gordon, H. R. Ammerlahn, D. D. Djordjevich, D. M. Edwards, M. E. Goldsby, M. F. Hawley, R. Tam, R. P. Tsang, and A. S. Yoshimura. 2004. Summary of the 2003 San Francisco International Airport biodefense preparation exercise. Sandia Technical Report SAND2004-2225, Sandia National Laboratories, Livermore, California.

52584

Hypervelocity Impact-Generated Flash

R. J. Lawrence, T. F. Thornhill, III, L. C. Chhabildas, T. A. Mehlhorn, J. E. Bailey, W. D. Reinhart

Kill assessment continues to be a major problem for the nation's missile defense program. A potential approach for addressing this issue involves spectral and temporal analysis of the short-time impact flash that occurs when kill vehicles intercept the target missiles. Spectroscopy will identify the materials involved in the impact event, and temporal analysis can furnish data on the target configuration. These results will, in turn, yield the information necessary for target typing, engagement analysis, and thus kill assessment.

Under this project, Sandia is providing laboratory demonstrations of the feasibility and effectiveness of this approach. We are using two major Sandia facilities, the Z-pinch accelerator, and the two- and three-stage gas guns at the Shock Thermodynamics and Applied Research (STAR) facility. They are unique in that they can achieve impact velocities at or above those associated with actual engagement scenarios.

Because of existing expertise in spectroscopy, we used experiments on the Z machine (at up to 25 km/s) to demonstrate the spectral details, including possible temperature measurements, associated with hypervelocity impact flash. Efforts on the gas guns (at velocities from 6 to 11 km/s) were used to establish diagnostic capabilities for dynamic spectroscopy at that facility and to study both basic and operational target materials.

The overall goal for this project was to provide laboratory-based proof of principle for time-resolved impact-flash spectroscopy. This technique could then be used for missile-defense kill assessment, kill-vehicle engagement analysis, and target typing. Specific goals include demonstrations of data reproducibility, material identification, and target configuration analysis.

Accomplishments in this project include the following:

- Conducted in excess of 25 experiments at the gas-gun facility that involved both basic and operational materials with single- and multilayered targets with gaps.
- Performed spectral analysis to identify many of the different materials involved in the hypervelocity impact events.
- Performed temporal analysis of the spectral data to correlate with the spaced configuration of some of the targets.

- Obtained Work for Others (WFO) support from the Department of Defense/Missile Defense Agency (DoD/MDA) for related work on impact flash for engagement analysis and target typing.

One of the goals for the project was to obtain impact-flash spectra from both depleted-uranium and high-explosive samples. We underestimated the extensive environmental and safety approvals necessary to study these hazardous materials at the gas-gun facility, so we did not meet this objective. Also, analysis of our results indicates that to establish unique spectral signal for some of the organic materials of interest (e.g., silica-phenolic) will require the extension of our spectral measurement capability from the visible into the infrared region of the spectrum.

Not only did we demonstrate the feasibility for measuring impact-flash spectra in a reproducible fashion, but the project also showed the utility of these data for material identification and target configuration evaluation, which will be essential for engagement analysis, target typing, and kill assessment in the missile-defense arena.

Other Communications

Lawrence, R. J., W. D. Reinhart, L. C. Chhabildas, and D. P. Kelly. 2004. Hypervelocity impact flash for kill assessment and engagement analysis. Paper presented at CLP Semiannual Review, Battelle Laboratories, Columbus, Ohio. SAND2004-1656P.

52585

Improving Human/System Interactions in Systems-of-Systems

S. Tucker, M. L. Bernard, M. J. Gardner, B. E. Hart, S. Tucker, M. J. McDonald, D. P. Miller

A number of applications are limited primarily by their human-system interfaces (HSIs). Unlike machines, humans are adept at conveying information between themselves using a variety of techniques, including speech, gesture, using props (tangibles), and drawing. By coupling technologies that mimic these interactions, Sandia is developing interface technologies for complex systems that are both intuitive and user-centric in design. Intuitive interfaces become more appealing with increasing system complexity, such as with large systems-of-systems (SoS) tools. While this work is useful to a variety of human-system interactions, our focus will continue to be on the development of an HSI for modeling and simulation (M&S), especially analytic and cognitive tools. To date, the capability of most M&S applications is underutilized due to the lack of tools that enable effective management by humans. The push to utilize M&S for complex analytics created tools that are usable only by specially trained modelers. This paradigm has the end-user of the analyses—the person posing the questions—needing assistance from modelers to have their questions answered. The main premise of this project is to enable a decision maker that has little familiarity with M&S to interact with simulation in a naturalistic manner similar to ways in which humans communicate ideas to others. To meet this goal, we will continue to develop a user-centric HSI prototype, based on the taxonomy of observed human interactions integrated with both two-dimensional (2-D) touch and 3-D tangible interfaces. For the M&S framework, we will use Sandia's UMBRA (a modular [M&S] system) to which we will add object-oriented containers to support the easy creation of hierarchical systems representations; we are implementing the concepts of Architectural Description Languages (ADLs) utilizing extensible markup language (XML), as well as a new graphical user interface (GUI) and scripting capabilities.

We developed our next-generation tangible interface to the UMBRA environment. This year's effort was a transition to a hardware-based method for tracking the tangible pucks. We are using a phase-space system, which uses light-emitting diodes (LEDs) and sets of crossed linear cameras. A wired system is currently operational, but we are transitioning to a radio-

frequency (RF) wireless system. The RF system allows 40 pucks to be tracked in 6 degrees of freedom (6 DOF). These pucks are tracked at 480 Hz and to submillimeter accuracy. This capability allows for the interpretation of subtle hand gestures.

We developed an UMBRA GUI extension that allows for user interaction with UMBRA simulation objects and supports High-Level Architecture (HLA) interface with remote UMBRA simulations. This interaction allows any arbitrary puck to be associated with an UMBRA object (model component) and uses the puck to modify physical characteristics of the object by performing gestures with the puck. In use, a context-specific puck menu is drawn on (and around) the puck so that the user may select from several available actions or puck functions.

Conceptually, a puck is used as if it is a wireless mouse, with a system capability that is able to track and use up to 40 pucks at once. This will allow for small-group collaboration around the display table by manipulating the simulation by manipulating the pucks.

Additionally, we are making modifications to UMBRA, including separable menu items for support of the puck menus, and implementation of XML parsers and output to support ADL to better address issues of representing entities, behaviors, and connections in more complex hierarchical SoS models.

We developed a 2-D touch-based interface that allows users to interact directly with the system by pointing and dragging directly on the different visual components in the display. This allows us to use the table for exploring cognitive models that we have developed and allows us to demonstrate this software to other people.

We are continuing our functional task analysis and taxonomy development through observations of Military Operations on Urbanized Terrain (MOUT), Logistics and Support Enterprise Model exercise observations.

Initial interactions showed that an interface that utilizes gesture (pointing) and voice recognition is more humanlike than are menuing systems. Our new focus will be on the integration of gesture and voice with the tangible interface being developed.

52586

Distributed Detection and ID Algorithm Architecture for Unattended Ground Sensors

A. B. Doser, M. E. Slinkard, D. C. Craft, W. T. O'Rourke, H. D. Nguyen

During recent years, unattended ground sensors (UGSs) have proven useful in detecting, identifying, and characterizing difficult targets (tactical UGSs, or TUGSs) and time-critical targets (Steel Eagle/RATLER). However, current research has focused on a "single-point" capability; that is, a single sensor performs most, if not all, of the system's functional capability. In the future, large arrays of low-cost, intelligent sensors will become practical because of technological advances in computing and communications driven by commercial (e.g., cell phones) as well as military (e.g., Army Future Combat System) needs. Consideration of how to effectively utilize a network of heterogeneous sensors with a distributed algorithm is a new area of research, and the design of distributed identification algorithms for such a network, considering all the factors of power usage, algorithm performance, and data-transmission failure rates, is new. In this project, Sandia will develop and demonstrate on a test-bed network of UGSs a distributed, scalable, and fault-tolerant algorithm architecture for detection, identification, and location of multiple targets traversing a large field of UGSs. We will also develop a working model of the distributed-algorithm architecture along with a cost/benefit analysis for trade-offs between local processing and data communication. The result will be a new and potentially powerful system (heterogeneous network of UGSs and detection sensors using a distributed algorithm) for data collection and analysis over wide areas, along with a new method for the combination of data from multiple UGSs. This work also introduces a new methodology for optimal design of distributed-algorithm software architectures for heterogeneous sensor networks. Possible applications for such a network and distributed algorithm include facility monitoring, traffic monitoring, and multiple ground-target tracking.

(1) We developed and designed a proof-of-concept demonstration of a detection and localization algorithm for a system of networked intelligent sensors consisting of acoustic arrays.

(2) We developed and designed a proof-of-concept demonstration of a detection and localization algorithm for a

system of networked intelligent sensors consisting of single acoustic microphones (no acoustic arrays).

(3) Corollary results indicate that the power requirements (for data processing and transmission) of the algorithms developed are feasible for a real unattended system.

(4) We held discussions with the Army Armaments Research, Development, and Engineering Center (ARDEC) and obtained and extended their target detection and counting algorithm for use with networked sensor systems. We demonstrated equivalent performance with the code for the original target set (large military vehicles), as well as detection and target counting of small quieter vehicles. We also demonstrated a capability to estimate the path of the vehicles by utilizing the extended code with networked sensor arrays.

(5) We collected data in support of the first three accomplishments with data stored for future use with follow-on research.

The principal accomplishment of this work was demonstration of the utility of networked acoustic sensors for detection and localization when utilizing distributed algorithms that were designed to utilize the capabilities of networked sensor systems. The distributed-algorithm designs help address in detail the issues of the nature of the local processing versus distributed information throughout the network.

52587

Secure Chaotic Communications

R. A. Salazar, L. L. Molina, L. D. Bacon

Sandia is developing a secure communication system based on chaos. Researchers have suggested many chaotic schemes. Our goal is to develop a robust communication system that is very secure and very robust. Most secure communication systems rely on a long sequence of nonrepeating numbers to code a message. Usually a pseudorandom generator—based on a prime number—creates the sequence. Since the pseudorandom generator is based on a deterministic equation, the sequence generated appears only randomly. Given a section of a sequence, we can determine the underlying pattern and hence the algorithm behind the sequence. We can then use this knowledge to break a coded message. As the length of the nonrepeating sequence increases, so does the difficulty to determine a pattern in the sequence. A chaotic sequence is one that never repeats, and hence is infinitely long. This aperiodic quality is the property that cryptographers refer to as a one-time pad. *The crypto community considers the use of a one-time pad to be a perfect encryption code.*

Researchers suggest many chaotic schemes, including chaotic masking, chaotic shift keying (CSK), differential chaotic shift keying (DCSK), chaotic on-off keying, and frequency hopping. Of the many schemes suggested, we consider the frequency-hopping scheme to be the most probable to meet our goal. We base this conclusion on the properties of a normal hopping system. Frequency-hopping systems are naturally spread spectrum. One advantage of a spread-spectrum signal is its low probability of intercept. Two more advantages are resistance to jamming and fading. Both of these advantages result from the increased noise caused by the increased bandwidth.

We designed a secure frequency-hopping communications system based on a chaotic sequence....The aperiodic nature of the sequence creates a high level of security by not allowing an adversary to predetermine the transmit frequencies.

We designed a secure frequency-hopping communications system based on a chaotic sequence. The system uses a chaotic equation to generate the sequence of hop frequencies. Since in principle the equation is aperiodic, the sequence of hop frequencies is also aperiodic. The aperiodic nature of the sequence creates a high level of security by not allowing an adversary to predetermine the transmit frequencies. This spread-spectrum approach forces a receiver to either know the correct receive frequency or receive with a bandwidth that is equal to the entire frequency-hopping range.

The algorithm starts with an initial value that is part of the key. A key contains information needed to decode the message. Another part of this key is a random integer used to define the number of times the nonlinear equation iterates for the first sequence. The equation (logistic) needs one parameter. This parameter determines the behavior of the sequence. The algorithm iterates on the equation the number of times defined by the key using parameters also determined by the key. The final number in the sequence maps to a frequency. The mapping may also be dynamic and change with each transmission. We will use a fixed map. The final number in the sequence is also the initial value used for the next set of iterations. The number of iterations needed for the next message is dependent upon the next desired frequency. Another mapping (or the same mapping) determines the next frequency. Hence, the algorithm iterates to the next proper frequency. If an adversary intercepted and decoded one transmission to determine the number of iterations, he would not have any other component of the key. The basic design for the system is complete.

We successfully programmed the microcontrollers needed to control the hop frequencies. Although in theory the chaotic sequence is aperiodic, real-world limitations on processors and truncation result in sequences that may actually be periodic. We completed some of the analysis needed to determine the lengths of nonrepeating sequences. We also performed some of the analysis needed to determine the distribution of the sequence. Cryptographers take advantage of message distributions to decipher coded messages.

52588

System-of-Systems Modeling and Analysis

D. J. Anderson, D. N. Shirah, A. Breckenridge, J. E. Campbell

Evaluating design concepts for a complex system of systems (SoS) involves predicting SoS performance and identifying critical operational parameters across a broad trade space, presenting a multidimensional research challenge. Even for a single system, performance is characterized by several measures of effectiveness (MOEs). For Future Combat Systems (FCSs), the SoS level is defined to be a 1000-platform unit of action (UA). Analyzing the performance of several design options of a complex SoS across external parameters and multiple MOEs generates a massive number of trade-space combinations, producing extreme computational issues.

Evaluation of performance at the SoS level is critical to achieving high-performance objectives. SoS analysis requires predicting performance at the SoS level in contrast to the traditional platform-by-platform approach. SoS analysis must examine a multitude of design and technology options to optimize mission effectiveness across wide-parameter spaces. The need exists to establish SoS performance requirements and translate these SoS requirements down to optimal or near-optimal individual platform requirements for system design and development. This challenge is further extended by the complexity presented with new technology. Prior to this research, about the only method to gain some performance knowledge at the SoS level was through traditional warfight simulation codes, which are costly and time-consuming.

The goal of this project was to develop an integrated modeling and simulation (M&S) environment that addresses the complex SoS modeling and analysis needs. The approach involved developing, enhancing, and integrating (1) state-modeling methodologies, (2) simulation objects, (3) time-step simulation methodology, and (4) experimental design and optimization for trade-space exploration. We applied the methodology to an FCS UA concept to demonstrate the approach.

Prior to this research, about the only method to gain some performance knowledge at the SoS level was through traditional warfight simulation codes, which are costly and time-consuming.

We conceived and designed an approach for comprehensive logistics treatment for SoS under this project. Actual implementation in the SoS simulation was accomplished under a separate project with the U.S. Army.

We designed, developed, and demonstrated a state-model object to serve as the basis for representing individual systems in an SoS simulation.

We designed, developed, and demonstrated a time-simulation capability, incorporating state-model objects, for detailed simulation of hundreds of interacting systems.

We developed an approach for dealing with the massive redundancy present in many SoS problems, combining scaling up existing redundancy algorithms, encapsulating redundant arrangements, and taking advantage of the identical components, subsystems, and platforms that often occur in SoS redundancy groupings.

We identified techniques for dealing with several potential sources of "singularities and nonlinearities."

We integrated state modeling with existing systems-analysis software to greatly expand its capabilities.

We modified existing software tools to simultaneously analyze and optimize multiple MOEs.

We demonstrated a variable screening technique to automatically eliminate unimportant variables in a multiobjective optimization.

We developed a new state-modeling capability that can analyze multiple MOEs for individual systems or SoS. We implemented this capability in software with an innovative new interface.

We collaborated with the Simulation and Optimization Laboratory at the University of Illinois, Urbana-Champaign, to develop robust, multiobjective optimization schemes and post-optimal procedures for selecting the best solutions based on decision-maker preferences.

We demonstrated the use of design-of-experiments for determining the best parameter settings for a genetic-algorithm–based optimization.

This project has been very successful. The SoS evaluation methodology was defined as central to the Army Evaluation Center's approach to developing test plans based on SoS performance evaluation.

Other Communications

Anderson, D. J., J. E. Campbell, and L. D. Chapman. 2004. Complex system-of-systems modeling and analysis. *Proc. Reliability, Availability, Maintainability Symposium 2004* (26–29 January, Los Angeles, California).

Anderson, D. J., J. E. Campbell, and L. D. Chapman. 2003. Evaluating a complex system-of-systems using state modeling and simulation. *Proc. National Defense Industrial Association Systems Engineering Conference* (20–23 October, San Diego, California).

52589

Eye-Safe Short-Range Standoff Aerosol-Cloud Finder

K. L. Schroder, R. P. Bambha, I. R. Shokair, T. A. Reichardt, T. P. Tooman

Because many solid objects, both stationary and mobile, will be present in an indoor environment, the design of an indoor aerosol-cloud–finding lidar (light detection and ranging) instrument presents a number of challenges. The cloud finder must be able to discriminate between these solid objects and aerosol clouds as small as 1 m in depth to probe suspect clouds. While a near-infrared (NIR) (~ 1.5 µm) laser is desirable for eye safety, aerosol scattering cross sections are significantly lower in the NIR than at visible or ultraviolet (UV) wavelengths. The receiver must deal with a large dynamic range since the backscatter from solid objects will be orders of magnitude larger than for aerosol clouds. Fast electronics with significant noise contributions will be required to obtain the necessary temporal resolution.

Previous aerosol-backscatter studies demonstrated that our plume-detection capability was limited by the acquisition of backscatter from multiple scattering events. We therefore recognized the need to limit the divergence of the laser beam and to match the detector field of view to that divergence. Rather than use a laser in an eye-safe wavelength range (> 1.4 µm), we implemented a 1064 nm Nd:YAG (neodymium:yttrium aluminum garnet) microlaser that produced 860 ps pulses, attenuating its output to the eye-safe level for the experiments. We thoroughly characterized the properties of both the laser beam and the NIR photomultiplier tube (PMT) detector so that we could apply the results obtained in this study toward the development of a practical instrument. We designed an external *f*-stop to match the 14 mrad natural divergence of the laser beam. We could then calculate the throughput of the detector and checked this value by scattering the laser pulses from a calibrated-reflectivity target surface placed at a known distance from the receiver. The number of collected photons agreed to within 10% of the theoretical return scattering signal.

We detected aerosol plumes created by a smoke generator with a well-characterized particle distribution. We used backscatter returns from this plume to calculate detection limits for more applicable plumes. With the NIR PMT and a 1.5 µm laser source providing 20 µJ pulses, we estimate a single-pulse bioaerosol detection limit of 3000 particles/l. While this

detection limit for bioaerosols is well below the desired detection range (10^5 and 10^6 particles/l), it would be much more practical to use a simpler, more-compact NIR detector (e.g., a solid-state InGaAs [indium gallium arsenide] photodiode) than to use an NIR PMT. Unfortunately the noise-equivalent power (NEP) for such an off-the-shelf packaged detector compromises the performance; we estimate a detection limit of 5e+07 particles/l for an NEP of 20 pW/$Hz^{1/2}$. Therefore, the NIR PMT (or a similarly sensitive, low-noise detector) would be required to detect the presence of a biological aerosol plume with the proposed laser source.

Our studies then focused on the true capability of the instrument to recognize aerosol plumes, differentiating the aerosol scattering from surface reflections. Because the temporally resolved signal is acquired at such a high bandwidth, we could differentiate aerosol scatter from surface scatter by the rise time of the acquired waveform. The solid-surface backscatter rise time is = 1.2 ns, and the presence of a 23 cm-thick plume located next to the surface increased the rise time to 1.375 ns. If the plume is isolated from a solid surface, for reliable detection the plume should be considerably wider than the laser pulse. For a plume ~ 0.5 m thick, the 10%–90% rise time of the aerosol backscatter was 2.25 ns, significantly longer than the corresponding rise time of the surface backscatter. However, we demonstrated similar temporal broadening of the return signal from glancing incidences off of solid targets, where the effective depth of the target is dependent on the angle of incidence on the surface as well as on the laser-beam diameter. Potentially, the plume could be differentiated from glancing incidences by measuring the amplitude as well as the temporal rise time of the return signal.

In parallel with the experimental studies, we developed a lidar performance model for performing trade studies. The model accounts for the range to the plume, the wall reflectivity, plume parameters, receiver filter characteristics (particle density, size, and index of refraction), detector noise, and A/D (analog to digital) quantization noise. We could use this model to optimize the laser/detector format, so the area of interest could be probed in the appropriate time while minimizing the chance of a false positive.

52590

Microflame-Based Detector Suite for Universal Gas Sensing

R. P. Manginell, S. K. Showalter, M. Okandan, P. R. Lewis, P. G. Clem, M. W. Moorman, D. R. Wheeler

The flame-ionization detector (FID) is the most universally applied gas-chromatography (GC) detector. In contrast, the nitrogen-phosphorous detector (NPD) is very specific for compounds containing these elements, such as chemical-warfare agents (CWAs). By combining the two detectors, a very powerful array detector system will be realized. Miniaturization of these detectors for portable applications has been hampered by the heat-transfer properties of microsystems. Sandia developed a platform that will enable both detectors; catalyst-coated microhotplates minimize heat losses on the microscale and permit catalytically stabilized combustion in this domain. This is a radically different approach from the diffusion-stabilized flames conventionally used in FID.

Because of the work that we performed in this project, device lifetime can now be measured in months, despite the aggressive microcombustion environment.

Because of the work that we performed in this project, device lifetime can now be measured in months, despite the aggressive microcombustion environment. High-temperature materials, passivation layers, and catalyst uniformity have all contributed to this success. Molybdenum disilicide ($MoSi_2$) is under evaluation since it reportedly survives to 1400°C in thin-film form. We are studying stress, resistivity, and crystal structure as a function of annealing. We fabricated several new device designs to address temperature uniformity and strength. Some designs incorporate fringe-field electrodes for further miniaturization. We developed catalyst spray coating and used it to replace micropenning for research quantities of devices. It can produce films in the proper thickness range of 10–30 µm with better than 5% tolerance.

We tested a small-volume (~ 8 µL internally) test fixture. Combustion efficiency was excellent, but signal output was noisy. We modified a conventional Varian 3400 GC/FID system to allow testing of the microFID. We optimized flow, temperature, and collector electrode location. Signal/noise (S/N) is 400:1 for 0.2 µL injections of acetone. We also studied sensitivity to dimethyl methylphosphonate (DMMP), diethyl methylphosphonate (DEMP), and carbon disulfide (CS_2); S/N for DMMP is of the same order as acetone in optimal conditions. We used this system to diagnose limitations in the small-volume fixture, as well as to predict optimized microFID designs. We will build and test a new small-volume fixture

shortly. We also demonstrated the microNPD, placing a proprietary catalyst on the microFID platform and testing in a modified scannerless range imager (SRI) system. We demonstrated high selectivity to phosphorous compounds. We also observed a third dimension to the response. The calorimetric response of the platform is excellent, providing discrimination against noncombustible gases like carbon monoxide (CO).

- We fabricated several designs for a prototype ionization detector with integrated, fringe-field electrodes, and they are in the initial testing phase. One design also has an integrated Sandia field-effect transistor (SFET) preamplifier. Integrated electrodes greatly simplify packaging requirements, demanding only miniature sample/fuel introduction channels. Another design, in progress, utilizes fringe-field or pseudo parallel-plate electrodes and microfluidic sample/fuel channels for further miniaturization. Design completion is awaiting ongoing optimization experiments.
- We evaluated the SFET preamplifier performance, showing sensitivity to 3 pA of input current. Hybrid coupling with a conventional electrometer awaits fabrication completion.
- Spray coating of catalysts is now well developed, though improvements continue for the purpose of allowing variety in catalyst formulation. We temporarily set aside MicroPen coating because, while optimal for manufacturing, research quantities of devices resulted in MicroPen clogging. Catalyst doping of microfabricated anodized alumina supports continues to make progress at a low level in this project and has promise as a future technique.
- We demonstrated both FID and NPD modes with the platform. The FID mode responds to CWAs and hydrocarbons (HCs), while the NPD strongly favors the CWA response. Together, these modes will allow for a very powerful array detector.

Flame modeling may be omitted. Testing of the microcombustor FID platform in a modified conventional FID housing is greatly aiding fundamental understanding of the microFID.

Refereed

Adkins, D. R., P. R. Lewis, G. Dulleck, and R. J. Kottenstette. 2004. Development and testing of Sandia's CWA point-detection technology. Paper presented at the 2nd Joint Conference Point Detection for Chemical and Biological Defense, 1–5 March, Williamsburg, Virginia.

Other Communications

Moorman, M. W., R. P. Manginell, and C. Colburn. 2003. A novel microcombustor for sensor and thermal management applications in microsystems. *Proc. SPIE Microfabrication* **4981** (January, Santa Clara, California): 40–50.

62827

Nonlethal Technologies for the War on Terrorism

P. D. Coleman, V. M. Hietala, M. C. Wanke, D. B. Seidel, T. Lemp, A. G. Baca

This project will establish the technical feasibility for a dramatically new method to counter elements of the terrorist threat and to affect the way we engage adversaries when lethal force is not appropriate. A nonlethal response opens a range of options for dealing with the situation by temporarily incapacitating hostiles without injury. High-frequency radio frequency (RF) has been shown to create a strong flee reaction. However, present systems designed for this RF application are based on vacuum-tube technology and, thus, are expensive, large, and fragile. Further, conventional semiconductors do not have the required power. This project seeks to build a microelectromechanical systems (MEMS)–fabricated micro-vacuum electronic source that could be arrayed to yield a robust, high-power, and relatively inexpensive alternative to present systems. These sources can find use in access denial (military and civilian use), higher-resolution synthetic-aperture radar (SAR), wideband communications, and imaging through obscurants (including clothing and epoxies used in weapons manufacturing).

The main Department of Energy (DOE) use would be in the protection of weapons and special nuclear materials, allowing for a cost-effective solution to the ever-increasing security costs. In the Department of Defense (DoD), the main use would be in nonlethal weapons.

We performed joint conflict and tactical simulations, force-on-force simulations of the effectiveness of an RF micro-vacuum device source in protecting high-value assets. The study evaluated the ability of a heavily armed attacking force with and without an RF system in place. The attackers were successful without the RF. The addition of RF shields resulted in a “win” for the security force.

We made progress in several areas toward building a first-prototype MEMS device: design and simulation of the device, testing of cathodes, and initial steps in the prototype construction.

(1) We chose a transit time oscillator (TTO) as the initial demonstration device. We will use a commercial field-emission array (FEA) for generating the working electron beam. The

cavity structure will be diffusion-bonded onto the FEA's platform.

(2) We performed extensive simulations of the TTO device using a particle-in-cell (PIC) code. We found growth to be linearly dependent on beam current and inversely dependent on beam voltage. Cavity geometry scans show that the growth rate can be enhanced using more complicated reentrant geometries.

(3) We studied the effects of loading on the instability's growth. These indicate that, for typical beam parameters available from FEAs and for simple cavity geometries, this TTO instability is weak, and that overcoming wall losses could be problematic. Thus, we will investigate alternative cathodes (cesium iodide–coated carbon fibers and carbon nanotubes). Also, we will investigate alternate oscillator designs such as split-cavity oscillators and reflex klystrons.

(4) We assembled a test-bed and tested sample FEA devices.

(5) Work is progressing on construction of the first oscillator prototype. We procured special-order FEAs to allow mounting into the prototype. Mask designs are finished, and the first build is near completion.

67029

Advancements in Sensing and Perception Using Structured Lighting Techniques and an Innovative Design Tool

D. D. Padilla, P. A. Davidson, Jr., J. J. Carlson, C. W. Wilson

There is an ever-increasing need for robust, autonomous ground vehicles for counterterrorism and defense missions. Despite nearly 30 years of government-sponsored research, it is undisputed that significant advancements in sensing and perception are necessary. Sandia seeks to develop an innovative, advanced sensing technology for national security missions serving the Department of Energy, the Department of Defense, and other government agencies. We will develop an eye-safe, robust, low-cost, lightweight, three-dimensional (3-D) structured lighting sensor for use in broad-daylight outdoor applications. The market for this technology is wide open due to the unavailability of such a sensor. Currently available laser scanners are slow, bulky and heavy, expensive, fragile, short-range, sensitive to vibration (highly problematic for moving platforms), and unreliable for outdoor use in bright sunlight conditions. Eye-safety issues are a primary concern for currently available laser-based sensors. Passive, stereo-imaging sensors are available for 3-D sensing but suffer from several limitations: computationally intensive, require a lighted environment (natural or man-made light source), and do not work for many scenes or regions lacking texture or having ambiguous texture.

Structured lighting requires image processing to isolate, or segment, a laser signal from background clutter in a camera image. Segmenting the laser signal is easy if the reflected laser light is significantly brighter than the background clutter. Under outdoor conditions, however, reflected energy from background clutter is often significantly greater than the reflected laser energy. Problems also occur when the reflective surface is highly absorptive, such as asphalt. Increasing the power is one solution that leads to eye-safety issues.

We are investigating several methods to segment the laser signal from background clutter. They include using a naturally blocked laser frequency in the absorption band, temporal differencing, spatial differencing, spectral differencing, pulsewidth modulation of the laser, and linear polarization imaging methods.

To maximize the signal-to-background clutter ratio, we investigated several potential solutions. First, we chose a laser

with a wavelength of 830 μm. At this wavelength, other various atmospheric constituents prevent a significant amount of the sun's light from reaching the Earth's surface. To increase the signal-to-noise ratio (SNR), we used a 10-bandwidth optical bandpass filter centered at the laser wavelength. Although this is the narrowest filter available at this wavelength, it is still too broad for background-clutter suppression in bright sunlight conditions. Using a filter alone is insufficient.

Next, we implemented a temporal differencing method. This method subtracts two consecutive images, one with the laser on and the other with the laser off. Although this method has been used successfully for clutter suppression, it requires a stationary or expensive high-speed camera.

We implemented a spatial differencing method that uses a spatial bandpass filter to detect the laser. In this method, we used pixels from two regions to estimate pixel values in another spatially proximate region. This method was unsuccessful in isolating the laser.

Next, we implemented a spectral differencing method that we demonstrated in audio systems, allowing discrimination of one voice in a noisy background. This method is a linear interpolation between separate spectral bands to determine the presence of light in a neighboring band. This technique exploits the fact that reflective properties of surfaces do not vary much over narrow ranges of light frequency (i.e., over a narrow spectral band). When illuminated by a broadband source such as the sun, the energy of light reflected off of a surface over one narrow band is approximately the same as that reflected from another nearby, but separate, narrow band. This method was successful.

The last method in consideration is laser pulsing. A Class IIIa eye-safe laser is limited to 5 mW of continuous optical output power. Pulsing the laser allows for an increase in the peak power output while remaining eye safe. In addition, limiting the exposure period of the camera lowers the background clutter. The overall effect is an increase in the SNR. Modern charge-coupled-device (CCD) cameras allow for manual and electronic adjustment of the sensor exposure period. We performed an experiment to validate the pulsing concept. We viewed the laser using three camera shutter speeds and three laser-power settings. As we halved the exposure, the laser power doubled to maintain the average power. The laser became readily distinguishable from the background clutter.

Implementing this technique required a video sync separator chip to determine when the shutter is open during each field of a frame. The laser is turned on during the exposure

period when the shutter is open. We made calculations to determine the maximum pulsed power that a continuous-wave laser can have and be Class I eye safe at the laser exit. For our operational parameters, the maximum power at which our laser can operate is 13 W, a vast increase in the signal. Laser pulsing provides a technique for background suppression using off-the-shelf CCD camera technology and can be used with either a stationary or a moving camera.

We are implementing the laser-pulsing technique using a 1 W, 670 nm laser. To do this, we upgraded our national television system committee (NTSC) cameras to fire-wire to eliminate the need for an image-capture board. This provides a plug-and-play capability, eliminating the need for additional project-specific hardware. In addition, fire-wire cameras offer programmable shutter speeds on the fly. Programmable shutter speeds allow the camera to serve as a sensor for structured lighting as well as for other image-processing applications. Our efforts also included porting the code from Borland C++ to MATLAB. MATLAB provides built-in image-processing libraries and libraries to utilize the full functionality of the fire-wire cameras.

67030

Biophysics of BW-Warhead Defeat with a Kinetic Interceptor

L. E. Larsen, S. MacNab, T. J. Vogler, R. P. Toth, W. D. Reinhart

Development of an effective missile defense is a high-priority national security objective. In addition, there is increasing concern about the spread of chemical and biological agents. If a missile carries a biological warfare agent (BWA), intercepting it may still result in a dangerous scattering of the infectious agent on military and civilian personnel. Thus, the intercepting vehicle must also kill the BWA. Most mechanisms (e.g., radiation) are incapable of doing so in the brief interval before the agent is scattered. To accomplish the goal of killing before scatter, Sandia is exploring the biophysics of cell-membrane disruption of BWAs by shock waves from a high-speed projectile.

High-fidelity bacterial simulants of wet plague (gram-negative), germinated anthrax (gram-positive), and sporulated anthrax will be loaded into a specially designed containment fixture and shocked by a projectile at the Shock Thermodynamics and Applied Research (STAR) gas-gun facility. The simulant will then be extracted and the survival of the bacteria versus impact velocity determined from the growth of colony-forming units. We will derive pressure and temperature from known equations of state (EOSs) and the projectile velocity. We expect that different classes of bacteria will differ in their resistance to shock loading. The spore form should be most resistant, then gram-positive vegetative forms, then gram-negative vegetative forms. There is some evidence, though, that shock loading may cause spores to clump, making them less infectious.

A systematic study of agent survival versus pressure for kPa, MPa, and GPa pressures will be the first of its kind and will be directly applicable to the design of intercept vehicles and simulations of intercept events. These results may also be important in the destruction of agent stockpiles. The technology from this project will give Sandia a unique capability for the study of BWAs and chemical warfare agents (CWAs).

A systematic study of agent survival versus pressure for kPa, MPa, and GPa pressures will be the first of its kind and will be directly applicable to the design of intercept vehicles and simulations of intercept events.

Our accomplishments are grouped into two areas: (1) simulant growth and characterization, and (2) shock-physics fixture design, verification, and experimentation.

- *Simulant growth and characterization*. We selected agent simulants for wet plague and anthrax. The simulants are nonvirulent strains of the microbes that cause those diseases.

Thus, they provide excellent fidelity as simulants. We obtained the simulant for wet plague, *Yersinia pestis* (Center for Disease Control [CDC] designation A1122), and successfully cultured it. Further, we characterized its growth history. This will allow experiments to be conducted in the same regime of microbe growth so that they are more repeatable. Finally, we used high-frequency sonic loading to rupture its cell walls. By comparison to these results, we should be able to demonstrate that cell-membrane disruption is the kill mechanism for shock loading. These experiments also showed that the microbe is only moderately susceptible to sonic loading.

- *Shock-physics fixture design, verification, and experimentation*. We designed a three-level containment system for experiments on the gas guns. Even though the agents being tested are nonvirulent, approved safety protocols require that they not be released; decontamination is necessary if they are released. We designed, built, and tested the first level, the capsule containing the microbes, in several preliminary experiments. The capsule remained sealed during the first of these but failed in the other two. We then designed and manufactured a new capsule. The secondary containment system is sealed by the projectile. The new capsule and secondary containment system both performed successfully at impact velocities of 500 m/s. Higher velocities should be possible with minor modifications to the design. Ultimately, though, a new design will be required if significantly higher velocities are needed. The tertiary confinement system consists of the catcher tank of the gas gun. Following an experiment, the tank is vented to ambient conditions through a biological filter system. A fluorescent marker is put in the bioagent sample so that leaks can be detected easily. In the event of failure of a containment level, we keep Sandia's decontamination foam in stock for cleanup. We developed procedures for preparing and loading the sample, recovering it after the shot, transporting it to the biolab, extracting the sample, and assessing kill of the simulant.

To date, we performed one experiment with *Y. pestis* at an impact velocity of 250 m/s. This velocity results in a pressure of approximately 750 MPa in the sample, a relatively low pressure. Preliminary results indicated little, if any, kill of the simulant. Experiments to be conducted in the near future will create much higher pressures and should reach a 6-order-of-magnitude kill of the simulant.

Other Communications

Vogler, T. J., L. C. Chhabildas, and L. E. Larsen. 2004. Shock defeat of biological agents. Paper presented at the Air Force Research Laboratory—Munitions Directorate, 7 June, Eglin Air Force Base, Florida.

67031

Dispersal in Urban Canyons, Source Identification, and Collateral Damage/ Mitigation Assessment

T. J. O'Hern, S. L. Ceccio

Prediction of the spread of a gas or aerosol release and its post-release effects are of obvious interest to homeland defense. Current approaches to assess tactical or asymmetric chemical-agent releases use atmospheric dispersion models linked to geographic-information-system layered datasets. One example is the Hazard Prediction Assessment Capability (HPAC) code that is currently installed and operated at Sandia for the western operations center for the Defense Threat Reduction Agency (DTRA). This tool uses recent weather data and forecasting methods to develop probability-effect maps, to define first-responder resources, and to support commander decisions to manage courses of action. The technical challenges to develop a high-fidelity, near-real-time common operating picture that reasonably represents actual field conditions are many and include the chemodynamics of complex terrain atmospheric dispersion physics. The work proposed here addresses this area by performing a feasibility study on an experimental program with analytical and computational support. The major work area is in experimental validation of dispersal and inversion codes. Sandia will study the feasibility and, if the basic concept shows promise, provide a conceptual design for a water-flow channel that could be used to acquire validation datasets, including velocity and concentration fields as a function of time, for atmospheric contaminant transport in complex urban geometries. This scale-model facility would be designed to allow data acquisition and model testing related to the inverse problem, i.e., determination of source location from distributed, sparse measurement locations. In these experiments, we would again measure the velocity field and use data from single- or multiple-concentration monitors to locate the continuous or transient source. This aspect of the project would include testing algorithms to solve the inverse problem under increasingly more-difficult flow environments.

We began this project by investigating scaling issues to show that the proposed experimental work makes technical sense, and to discuss the usefulness of data acquired in a scale model for model validation. We described these efforts in the upcoming report titled "Validation Data for Models of Contaminant Dispersal: Scaling Laws and Data Needs." The

report provides justification for the use of scale-model experiments and the usefulness of experiments in water to model air flows.

In the process of putting the report together, we held important discussions with colleagues at the Naval Research Laboratory, Los Alamos National Laboratory, Lawrence Livermore National Laboratory, Texas Tech University, Lawrence Berkeley National Laboratory, and the Department of Homeland Security. Based on these discussions, we feel that the proposed work is justified and will provide much-needed validation data. Several of the computational users have told us that they would use our data to validate their models as soon as the datasets become available.

Refereed

O'Hern, T. J., and S. L. Ceccio. 2004. Validation data for models of contaminant dispersal: Scaling laws and data needs. Sandia Technical Report SAND20045220, Sandia National Laboratories, Albuquerque, New Mexico.

67032

Weaponization of Thermobaric Explosives

A. M. Renlund, M. R. Baer, M. J. Kaneshige, R. J. Pahl

There is a growing need in the U.S. to develop energetic materials (EMs) that, when integrated into munitions, offer advantages of enhanced lethality against a variety of targets and increase the firepower of expensive precision delivery systems. Lighter and/or less-bulky munitions significantly impact the logistics burden on military actions. Increased energy density of the EMs, described either in energy per volume or energy per mass, is, however, only one consideration. The additional requirement is that the energy be released in an appropriate time domain to allow optimized coupling to the target. For enhanced lethal effects, the energy must be released either in the detonation-reaction zone or early enough in the expansion so that it couples to impulse loading or sustained high temperatures. In thermobaric explosives (TBXs), the later energy release from metal combustion is postulated to play a dominant role in enhancing lethality against soft targets like buildings and materiel and personnel in tunnels.

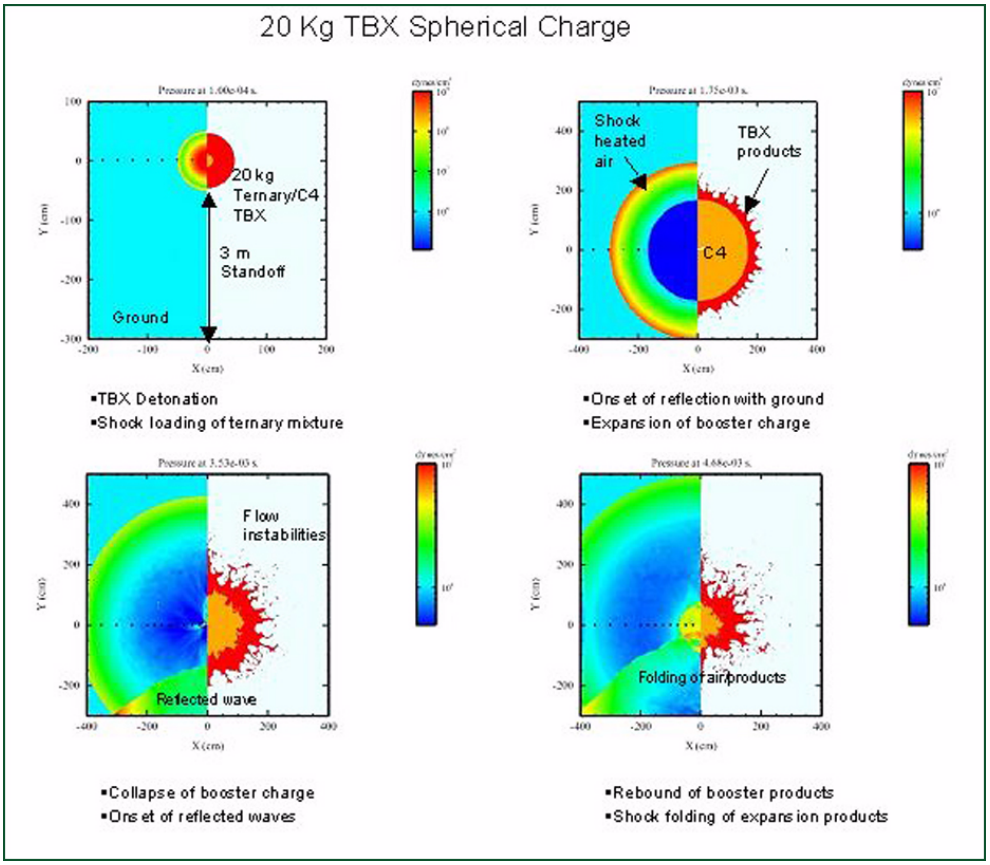

Selected time planes of the model simulation of a 20 kg spherical charge. Pressure contours are displayed on the left side and materials on the right side of each image.

In this project, Sandia focuses on specific issues related to paste materials (consisting of flake aluminum [Al], the solid explosive RDX [royal demolition explosive], the liquid monopropellant isopropyl nitrate, and a gelling agent), with a goal to understand their performance in warheadlike configurations. Initial tests and simulations will examine material dispersal of paste TBX formulations and secondary combustion of the detonation products. We will first rely on simple geometries for charges and containment tanks to help unravel the underlying physics controlling TBX performance. Later, we will examine the coupling of early explosive performance to warhead-case rupture for optimal dispersal and TBX lethality.

We designed spherical TBX charges. We tested small charges (up to 650 g) inside a containment tank, and they showed uniform and symmetric expansion. The initial tests were successful and the data were reproducible, demonstrating enhanced blast due to secondary combustion. We completed preliminary calculations of the charge expansion, and they compared very well with experiments. Sandia's analysis of plate-impact experiments performed at the Naval Surface Warfare Center demonstrated the relative insensitivity of the paste TBX to shock initiation. Initial tests also demonstrated the benefit of the paste formulation when compared to other fuel-rich explosives.

We modified a containment tank that will allow testing of larger charges and relocated it to the Terminal Ballistics Facility (or Gun Site) at Sandia. This tank has a more favorable (symmetric) geometry to facilitate modeling of the secondary combustion and shock reflections. In addition, it allows flexible access for diagnostics.

We used the CTH shock-physics analysis package to address equations of state (EOS), reactive growth to detonation, and near-field expansion of the TBX material. We applied this first-generation model to support the Sandia experimental studies in tank configurations. We applied this approach to the design of free-field tests of 20 kg spherical charges in a determination of charge standoff distance and instrumentation locations to monitor booster-rebound and ground-reflection effects.

We began studying the scale effects of TBX performance with a series of tests of 1, 2, 3, and 20 kg spherical charges. Diagnostics included free-field pressure gauges at distances up to 30 m from the charge and high-speed optical imaging. Optical records showed that the expansion remained symmetric,

but at large distances, distinct turbulence features were evident at the edges of the expansion. We postulate that this turbulence enhances the mixing of the air with the fuel-rich detonation products and is necessary for efficient secondary combustion. We will perform additional comparison shots with 1, 2, 3, and 20 kg Composition C-4 in upcoming work.

We also participated in tests with the Defense Threat Reduction Agency (DTRA) by designing and assembling our TBX materials into hardware that is more representative of a weaponized system (central booster, steel confinement). We conducted tests at a DTRA test site on Kirtland Air Force Base. These tests allowed us some direct comparisons with other materials tested by the DTRA in their tunnel test facility.

67033

Development of an Enterprise-Scale Agent-Based Autonomic Logistics Simulation Model

D. A. Schoenwald, B. Chenoweth Creel, J. Watson, C. R. Lawton, M. J. Collins, E. Starkey, B. M. Thompson, W. E. Hart, L. P. Swiler

Sandia is focused on the development of a general-purpose enterprise-scale logistics-support-system modeling capability to address requirements of the Department of Defense (DoD) community. The model will incorporate various optimization strategies that assist both customers and contractors/ manufacturers in meeting performance metrics, managing risk, and minimizing costs. Since the "best" logistics support system will change over time, both the model and the optimization capabilities must be capable of addressing the time-dependent nature of the problem. One of the biggest factors driving the need for logistics system models is the large-scale nature of many military and commercial systems and the associated costs. These systems typically contain thousands of parts from hundreds of different suppliers, all with different manufacturing schedules. By multiplying the number of parts per system by the number of systems that may be deployed over the production cycle, one can see that potentially millions of parts may need to be tracked worldwide. Therefore, this model will be capable of handling such a large volume of parts and systems with the ability to update their status regularly. This model will be able not only to track such data but also to analyze them and to quickly deliver reliable information to support the design and operation of the logistics system and deal with unexpected events (war, labor disputes, natural disasters, etc.). This implies the ability to do fast and dependable optimization of the model for a variety of design questions and what-if scenarios. Finally, the model will be accurate in its portrayal of the status and location of all systems and resources, as well as in its prediction of resource-usage and equipment-performance metrics.

We accomplished several tasks that position the project well for implementing a realistic DoD weapons system enterprise model. These tasks focused primarily on building the model such that it will be a general agent-based weapons logistics model that is not tied to any particular application but is capable of simulating a range of applications with only input-file modifications. First, we chose an architecture for the agent-based model. Second, we completed the high-level design of the model. This includes flow charts and task descriptions for each major unit of code. Third, we coded much of the software

in C++ so that we could run a small-scale test problem. Fourth, we ran a small-scale test problem consisting of one part in two states (repaired and broken) with a supply and repair chain of one squadron, one base, one supply and repair point, and one original equipment manufacturer (OEM). We sufficiently tested this problem to show that the high-level design and written code are working correctly. Fifth, we completed much of the parallelization effort, with only the load balancing and implementation on the target cluster (a 70-node Linux cluster) remaining. Finally, we did initial work on the optimization strategy. Here, the two biggest subtasks were agreement on several cost criteria and general strategy to pursue. The cost criteria are a combination of inventory and transportation costs along with maintenance of a certain level of weapons system availability. The general strategy will be that of discrete optimization with a future path toward stochastic optimization. Much of this strategy depends on a surrogate-based approach that will estimate the model at various operating points.

- *Basic agent structure*. The agents in this model will be the sites. That is, the squadrons, bases, depots, OEMs, etc., represent the agents since this is where the decision making takes place. All sites will be represented by the construct SiteAgents, which are composed of a number of objects. The basic design includes the following:
  - Requesters and Providers, which communicate in Arenas to set up transactions with other SiteAgents.
  - A Warehouse to manage the inventory of parts.
  - A Resource Manager to keep track of support equipment, personnel, and their current status.
  - The set of possible Actions the SiteAgent may take.
  - Squadrons that need some additional logic to handle the plane flights and generate the demand for parts.
  - Arenas, which are “bulletin boards” where Providers post availability and Requesters look to find appropriate Providers. These Arenas will be set up according to the specified supply and repair chains.

A Shipper (or perhaps more than one, depending on simulation complexity) handles the actual movement of parts from one site to another. Requesters and Providers will communicate with the Shipper to send out parts.

The Resource Manager keeps track of the support equipment and personnel at a site. The resources are separated into at least two categories: available and unavailable. When an Action has possession of some resources, the resources are in use and therefore are unavailable. If we allow for support equipment to break or personnel to work only during certain

shifts, we may want to divide the unavailable category to separate the different reasons that resources may be unavailable in addition to being in use.

Since needed resources may not be available at the time a request arrives, the Resource Manager also must track the pending requests. These requests are arranged in a priority queue based on arrival time and some sort of importance ranking. (Getting a grounded weapons system ready again might take precedence over a routine supply action, even if the request came in later.)

Refereed

Schoenwald, D. A., D. C. Barton, and M. A. Ehlen. 2004. An agent-based simulation laboratory for economics and infrastructure interdependency. *Proc. 2004 American Control Conference* **2** (June, Boston, Massachusetts): 1295–1300.

67034

Mobile-Node Authentication in a Wireless *Ad Hoc* Environment

J. T. Michalski, M. D. Torgerson, B. P. Van Leeuwen, A. J. Lanzone

In hostile ad hoc *wireless communication environments, such as battlefield networks, end-node authentication is critical. In a wired infrastructure, this authentication service can be performed by a centrally located "authentication certificate generator" such as a certificate authority (CA). This centralized approach to authentication will not work in hostile and mobile environments with time-critical applications such as command and control because of dynamic and unpredictable connectivity and routing. There is a need for a secure, resilient, and distributed approach to mobile-node authentication.*

Either current mechanisms used in ad hoc *communications assign a preshared key (shared by all participating parties) or each node retains a collection of individual keys for communication with other nodes. Both approaches allow for a single compromised node to jeopardize the entire node community.*

In this research, Sandia is developing a protocol to facilitate the implementation of a distributive CA for the purpose of providing a secure distributed means of node authentication. This protocol design will address authentication for critical time-sensitive communications in a mobile ad hoc *wireless environment while providing protection from single-node-system compromise. We will develop and test the protocol using a communication simulator to provide useful mobile scenarios and gather important statistics to test its scalability and performance.*

- *Define wireless threat model*. We developed a threat model that defines threats to node authentication in an *ad hoc* wireless environment. The threat model examines threats against both a centralized CA and a distributed CA. This threat model will be the basis for our research. We will continue to refine this threat model throughout this research.

A threat model is important because it helps define the scope of the protocol and avoid so-called "design creep," ensuring that the protocol does only what it needs and nothing more. The threat model also provides the authentication-protocol designers with a means in which to test components of the protocol against adversary and environmental stressors.

- *Identify cryptographic authentication components and identify wireless supporting attributes*. Our team identified

some of the authentication components needed to support the authentication framework. We also developed some associated wireless attributes that are providing an efficient and streamlined approach in supporting the authentication process. Some of the developed attributes are as follows:

— *Group-cast certificate request*. The group-cast method of information request is more scalable and efficient than broadcast forms of the same request. A broadcast request requires each node that receives the broadcast process to forward the request, even when the receiving node does not have the capability of providing part of the answer. With the group-cast method, only nodes that are associated with the "group" address are asked to process and potentially forward the request.

— *Selectable outreach*. How far the initial request is propagated is selectable as described:

- *Default mode*. In this mode, the initial reach of the request can be limited to a user-defined broadcast domain. This allows for a very rapid response to an initial request.
- *Sparse CA scenario mode*. In this mode, the reach capability can be extended to encompass multiple broadcast domains over a widely dispersed geographical area.

— *Redundant and stale request detection.* The design of the protocol provides a means for a receiving node to determine whether the incoming certificate request is an original or is redundant; all redundant requests are discarded. The protocol also provides a means for mobile nodes forwarding requests to "time-out" a request after a preselected amount of time.

- *Map the interactions of selected wireless protocol attributes with authentication functions*. We designed the wireless "group-cast certificate request" attribute to map directly to the "certificate request function" that resides within the authentication process. This is the first step in the node-authentication process. We designed the wireless "selectable outreach "attribute to map directly with the "K share request value" that resides within the authentication process. The K value refers to the number of partial share certificates associated with the number of nodes participating in the distributed CA generation process.

We designed the wireless "response function" to map directly to the "certificate generator response" mechanism that will be associated with the certificate generation-response process.

- *Create movement algorithm for wireless* ad hoc *nodes*. In a mobile environment, the movement of nodes can have a detrimental impact on the communications. For this research,

we identified and implemented a movement algorithm to provide an appropriate stressor to the communication process. The algorithm is based on a random-location-generation process that selects the starting positions of each node. A separate vector is then plotted along which each node can travel. When nodes reach the end of the vector, a new randomized vector is plotted.

We identified, designed, and are continuing to investigate additional *ad hoc* wireless attributes to determine their interaction and impact as part of a developing protocol.

67035

Novel Processing, Affordable Motion Compensation, and Mode Multiplexing for Miniaturized Synthetic-Aperture Radar

G. R. Sloan, T. P. Bielek, P. G. Ortiz, A. D. Sweet, T. J. Kim, A. W. Doerry, M. W. Holzrichter, D. F. Dubbert

A critical need exists for a miniaturized, affordable synthetic-aperture radar (SAR) for both tactical unmanned aerial vehicle (UAV)–based reconnaissance and all-weather, non-global positioning system (GPS) weapon guidance. Consequently, Sandia has been steadily developing the needed subsystems to facilitate a 25 lb SAR that maintains or improves upon the performance (image quality and resolution) of our current 120 lb radars. At present, the phase 1a "miniSAR" hardware set is essentially complete. The continuing goal of this project is to provide an equally innovative control, motion-measurement, and image-formation architecture that fully exploits the new hardware's capability and integrates the state-of-the-art subsystems into a fully functional, highly agile radar.

For this project, we will do the following: (1) develop and implement a highly modular, easily modified software architecture for miniSAR; (2) study and develop optimal miniSAR image-formation algorithms and approaches, for both processor- and hardware-based implementations; (3) develop miniaturized field-programmable gate-array (FPGA)–based image-formation hardware; (4) investigate the viability of using a smaller, lower-quality inertial measurement unit (IMU) by enhancing Sandia's autofocus algorithm; and (5) develop and implement a miniSAR–compatible ground moving-target indicator (GMTI) mode.

We made significant progress on both the primary (software architecture) and secondary (FPGA–based image formation and autofocus enhancements) tasks. We fully designed the new radar software architecture and made significant progress on the functional modules. We successfully completed a detailed design and simulation of a revolutionary FPGA–based image-formation engine. We successfully developed a valuable enhancement to Sandia's autofocus algorithm (patent in progress).

Sandia is developing novel control/image-formation algorithms and some of the associated hardware to support next-generation synthetic-aperture radar (SAR), including Sandia's high-profile SAR miniaturization effort. Michael Holzrichter and April Sweet are shown with the "miniSAR" hardware.

The accomplishments of this project can be grouped into three primary areas: (1) software architecture, (2) FPGA image engine, and (3) motion measurement.

- *Software*.

(1) We completed a detailed study of the relative merits of polar format (PF) and overlap subaperture (OSA) image-formation algorithms from a miniSAR perspective. This study indicates that there are clear advantages to using the PF approach.

(2) We developed and successfully tested the core signal-processing code for a new algorithm.

(3) We designed and implemented the infrastructure of a novel software architecture that is highly modular and extensible.

(4) We benchmarked the high-risk, time-critical software computations and processes that will interface directly with the new miniSAR hardware.

(5) We began developing the functional software modules that will integrate the miniSAR hardware set and facilitate the initial miniSAR demonstration. (This effort is currently about 30% complete). Some specific accomplishments include the following:

(a) We defined and formalized a set of more than 200 parameters to configure and control the radar.

(b) We designed an agile communication/interface scheme (based on shared memory and interrupts) for the five boards on the miniSAR cPCI (compact peripheral component interface) backplane.

(c) We completed the radar control infrastructure.

(d) We developed and tested real-time control modules (waveform-synthesizer updates, motion-measurement updates, etc.).

- *Motion measurement*. We developed an innovative technique (initial proof-of-concept) to make Sandia's autofocus algorithm significantly more tolerant of motion-measurement errors. Initial tests on raw radar data showed successful results. A patent application is in progress.
- *FPGA image formation*.

(1) We completed several conceptual designs for an image engine and performed a study to determine the needed FPGA logic resources. (The study indicated that a single large FPGA is adequate.)

(2) We designed, implemented, and successfully tested a scaled-down, simplified image former (two-dimensional fast Fourier transform [FFT] with corner-turn function) in FPGAs. While not fieldable in a high-performance SAR, the successful effort was valuable as a first step toward validating concept viability.

We developed an innovative technique (initial proof-of-concept) to make Sandia's autofocus algorithm significantly more tolerant of motion-measurement errors. Initial tests on raw radar data showed successful results. A patent application is in progress.

(3) We designed and successfully simulated a full-scale FPGA–based image engine.

Refereed

Sloan, G. R., and D. F. Dubbert. 2004. Affordable, miniaturized SAR for tactical UAV applications. *Proc. SPIE Defense and Security Symposium* **5409** (13 April, Orlando, Florida): 74–83.

Other Communications

Doerry, A. W. 2004. Autofocus correction of excessive migration in synthetic-aperture radar images. Sandia Technical Report SAND2004-4770, Sandia National Laboratories, Albuquerque, New Mexico.

Dubbert, D. F., G. R. Sloan, and A. W. Doerry. 2004. FPGA's role in the development of SARs. *Wireless Design and Development* **12** (N3) (March): 16–20.

67036

Coilgun Technology Demonstration Test-Bed

R. J. Kaye, G. A. Mann, E. D. Reedy, Jr.

Induction coilguns, which use electromagnetic force (EMF) without a sliding electrical contact instead of chemical propellant, are capable of launching projectiles of interest to the Department of Defense (DoD). Technical issues that remain include (1) lifetime of coils that make up the gun barrel, (2) integrity of the coil's mechanical structure, (3) demonstration of repetitively fired coils with thermal management, and (4) robustness of fire/control systems. The objective of this project is to design a coilgun coil capable of repetitive-firing and test that design at loads consistent with a DoD application for lifetime data. This work is in collaboration with the National High Magnetic Field Laboratory (NHFML) at Florida State University and Los Alamos National Laboratory.

The key accomplishment of recent work was the development of a 120 mm bore, nested-helix coil design with active heat-transfer mechanisms for repetitive operation in a coilgun at the mechanical, electrical, and thermal stresses.

The key accomplishment of recent work was the development of a 120 mm bore, nested-helix coil design with active heat-transfer mechanisms for repetitive operation in a coilgun at the mechanical, electrical, and thermal stresses.

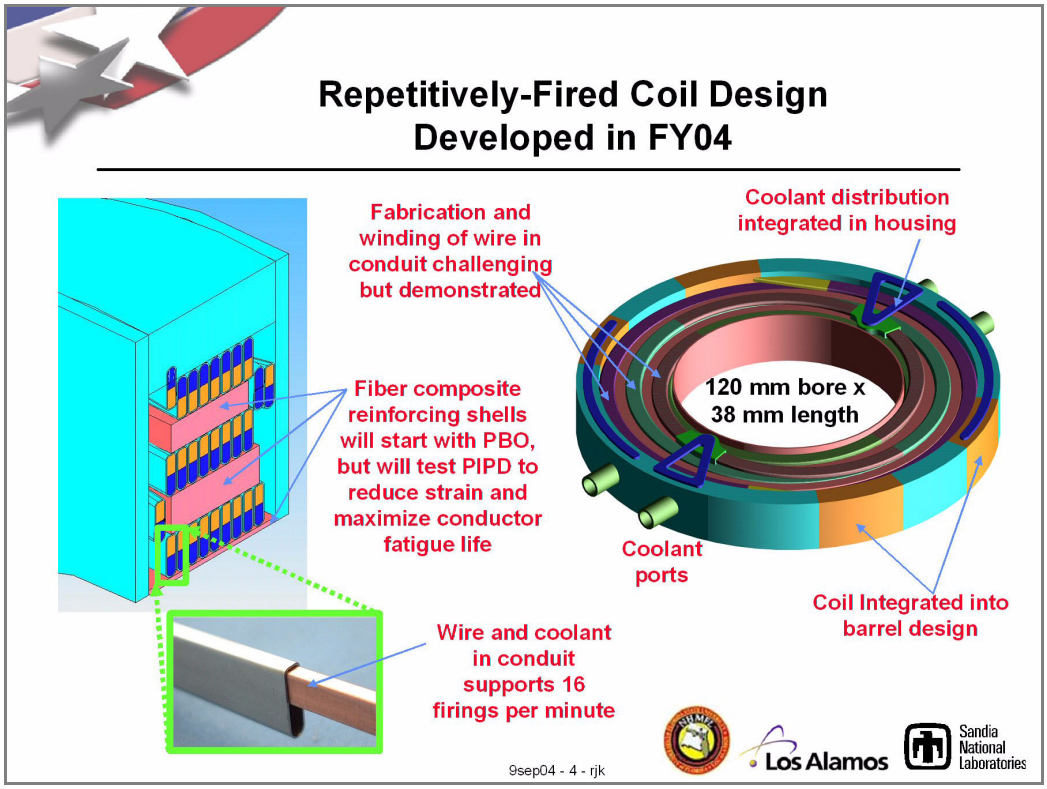

The repetitively fired coil design incorporates wire and coolant in a conduit structure well coupled to PBO composite shells. The integration of all the coil's components in the compact structure was demonstrated in the CAD model.

While the magnetic field intensity of 30 Tesla is modest compared to the state-of-the-art, nondestructive 100 Tesla magnetic field coils currently being developed, the 120 mm bore, nested-helix coil's size, geometry, and 16-shot/minute repetition rate take this design beyond the current art for repetitive coils. The design concept also has applicability in the development of repetitive high-field coils for materials science studies. The concept has matured through three design phases, with progress documented at each phase review.

Specific accomplishments in the coil design are as follows:

(1) We developed a new (atypical of common magnet practice) concept of wire-in-conduit conductor for magnets permitting high heat transfer at required repetition rates with good mechanical coupling to the coil support structure.

(2) We characterized and improved poly(p-phenylene-2,6-benzobisoxazole (PBO)-filament-wound/epoxy composites to a very high (95%) packing fraction for the reinforcement of the winding layers. Composites with 200 GPa modulus at 20°C demonstrated 10,000-cycle fatigue-life at 3.5 GPa tensile stress, significantly extending the current art. We found the effect of thermal cycling of composites to be negligible, permitting alternative construction options. The evaluation of higher-modulus fiber is pending in upcoming work.

(3) We demonstrated integration of the coil components (conductor windings, reinforcing shells, coolant distribution channels and manifolds, electrical feeds) in a 40 mm-long structure in a parametric-based computer-aided design (CAD) model with sufficient details to proceed with development/demonstration of the fabrication process.

(4) Thermal, electromagnetic, mechanical, and system analyses of the coil design demonstrated the stress conditions, material-property requirements, and potential coil performance, and identified the need to increase the elastic modulus of the fiber composite reinforcing the winding to minimize conductor strain.

(5) We demonstrated the ability to produce, insulate, and edge-wind the wire-in-conduit conductor into a multilayer winding, eliminating the need for a typically weak, layer-to-layer conductor splice.

(6) Characterization of the strain-controlled fatigue-life of highly ductile conductor metals suggests alternatives to copper to maximize conductor and coil lifetime. Data will significantly extend the extremely limited information in the literature.

(7) Characterization of the electrical breakdown and resistance properties of ethylene-glycol/water coolant in the

geometry and materials of the coil design demonstrated its suitability for operation.

(8) Characterization of the electrical breakdown strength of conductor insulation (film-served polyimide insulation with PBO/Kevlar-epoxy composite buffer) under compressive stress is encouraging for the anticipated mechanical and electric stresses that exceed the current magnet art.

(9) We designed the test metrics, conditions, diagnostics, and protocol for evaluation of the prototype coils.

(10) The coilgun's firing system senses the projectile position and energizes each barrel coil at the appropriate time. Radar appears promising to locate the projectile in the gun with immunity to environmental conditions as an alternative to previously used optical techniques. We developed a firing system concept for hardware and software to provide adaptive control during launch using the real-time feedback of the projectile diagnostic.

Refereed

Kaye, R. J. 2004. Operational requirements and issues for coilgun EM launchers. *IEEE Transactions on Magnetics, Proc. 12th Electromagnetic Launch Technology Symposium* (26–28 May, Snowbird, Utah): in press

67037

Enhanced Perception for Remote 3-D Mapping of Unknown Indoor and Outdoor Environments

C. L. Lewis, G. A. Laguna

A robotic vehicle's ability to simultaneously localize and accurately map its surroundings is crucial to its autonomy and an enabling technology for future Department of Energy and Department of Defense minimally manned systems' applications. Localization and mapping provide essential feedback to the operator for area intelligence, surveillance, reconnaissance, and remote crisis response. Robotic three-dimensional (3-D) mapping technology provides enhanced situational awareness by permitting a virtual "fly-through" of denied environments. While Sandia has vital experience with 3-D sensing technologies such as scanning-laser range finders and structured lighting sensors, 3-D sensors have not yet been integrated onto our robotic vehicles. In this project, we seek to integrate the most advanced laser range finders and video sensors onto several robotic vehicles and incorporate the simultaneous localization and mapping (SLAM) algorithms recently developed by Thrun, Fox, Konolige, and Lowe onto the vehicle's embedded computer. These algorithms use probabilistic state-estimation techniques (particle filters) that combine measurements from multiple sources to simultaneously estimate map features and the robot's location. This work will provide the capability to robotically generate 3-D maps of both indoor and outdoor environments. These automatically generated maps will be transmitted to a remote-operator control station where they will be displayed in real time in the Sandia-developed UMBRA (a modular modeling-and-simulation system) graphical environment. Once this technology is proven on a single vehicle, we will employ new research in classification and feature-extraction technologies to facilitate cooperative 3-D map generation by a swarm of mobile vehicles using an ad hoc *communications network.*

We integrated a SICK (company name) laser scanner onto a robotic vehicle. In addition, we evaluated an outdoor structured-lighting sensor. This sensor is under development in a separate project and promises to enhance our outdoor performance at a reduced weight and power cost. Using the SICK laser scanner, we collected a number of datasets for characterization. These datasets included scanner data, navigational data, and video streams. Combining the scanner

and navigational data, we generated 3-D maps offline of a building at Sandia. We then displayed these maps in the environment using a derivative of the rapid-world-modeling toolset that provides a virtual fly-through of the data. We investigated different scan-matching approaches. Our datasets include both 2-D and 3-D data. Most SLAM algorithms operate in two dimensions to form the map that may itself be 3-D. With our data, we are able to demonstrate localization in two dimensions using particle-filtering techniques.

Refereed

Little, C., and R. R. Peters. 2004. Simulated mobile self-localization using 3-D range sensing and an *a priori* map. *Proc. IEEE Conference on Robotics and Automation* (18–22 April 2005, Barcelona, Spain), submitted.

67038

A Modular Micromagnetic Accelerometer in Support of the mTalon Vision

R. A. Kellogg, J. K. Brotz, B. P. Engler, B. Jokiel, Jr., J. M. Schare, V. I. Bateman, T. Lemp

The micromagnetic accelerometer (microaccelerometer) is an open-loop inertial sensor that uses giant magnetoresistive (GMR) magnetic sensors to detect the displacement of a magnet-embedded sense mass. The open-loop design is desired for its simplicity, and the magnetic approach permits simultaneous low-g and high-g measurement capabilities. High device sensitivities are possible due to low self-noise. This is achieved using low-damped single-crystal silicon (Si) and optimized mechanical and electronic designs. In recent work for the micromagnetic accelerometer, Sandia focused on modeling, application identification, design, fabrication, and preparation for assembly and testing.

We modeled the microaccelerometer's electromagnetic (EM) and mechanical characteristics to identify performance capabilities and system requirements for design and construction. We targeted an operational range of 10–200 Hz (with potential down to 1 Hz) using multiple devices having resonance configurations from 100 to 2000 Hz. Performance calculations account for GMR-sensor Johnson, thermomechanical, and preamp noise sources and show that 20 ng/root-Hz to 5000 ng/root-Hz noise floors are expected for micro-g through 20-g sensing configurations. Based on these performance levels, we concluded that battlefield and underground facilities (UGF) monitoring and oil and gas exploration are appropriate target applications.

The prototype microaccelerometer design, currently under fabrication, accommodates structural, magnetic, and GMR-sensor material property and assembly variables using a matrix of spring geometries and sensor configurations. We chose single-crystal Si for the structural components and are processing it using deep reactive-ion milling at Litton Systems, Inc. We are incorporating bonded NdFeB (neodymium iron boride) magnets into the Si sense mass. Wafers containing arrays of bridge-configured GMR sensors, to form differential detectors, were fabricated by NVE, Inc.

We are investigating an assembly method for joining the Si sense-mass die to the GMR-sensor die. We submitted designs, and fabrication is under way to produce test die for bonding experiments. A low-temperature tin (Sn)/indium (In) eutectic

(135°C) solder will be used to join die that are aligned to within 1 μm in a Karl Suss bonder. To allow free motion of the sense mass die, we will maintain die separation with electroplated gold (Au) standoffs.

To evaluate the microaccelerometer performance down to micro-g acceleration conditions, we must establish a low-noise test capability. We acquired components of such a test system, which include a vibration-isolation base, a low-noise EM shaker, a high-sensitivity acceleration reference, and a low-signal data-acquisition/vibration controller.

In summary, we carefully designed the microaccelerometer to optimize its performance and facilitate fabrication and assembly. Fabrication is nearing completion, and we made preparations for assembly and testing.

67039

MICROFUZE Integration

A. W. Roesler, E. J. Welle, J. J. Calderone, R. McEntire, S. H. Kravitz, R. J. Shul, A. S. Tappan, S. M. Harris

The primary mission of a weapon fuze is to provide system-safety enablement and subsequent control of weapon-detonation events. Within this architecture, a fuze must integrate inputs from various environmental sensors and, if the preset conditions for weapon function are met, supply the required initiation stimulus for detonation. Evolving mission scenarios for future Department of Defense (DoD) and Department of Energy (DOE) weapon platforms, such as hard and deeply buried target (HDBT) defeat and "smart bullets," will soon outpace the capabilities of today's fuze technologies. Targeting buried assets and meeting tomorrow's battlefield engagements will require advanced fuzing architectures and technologies characterized by "intelligent" function under multiple, high-gravity (G) impacts. Achieving increased fuze functionality in a size constraint implicit with high-G survivability implies novel system architectures, incorporation of new concepts in munitions safety, and the realization of miniaturized integrated components based on emerging processes and technologies. The MICROFUZE, or "Fuze-on-a-Chip," established the novel fuzing technologies necessary for enabling a microelectromechanical systems (MEMS)–based miniature fuze. Groundbreaking technical progress was made through demonstration of a multilayer deep reactive-ion etched (DRIE) mechanical safe and arm (S&A) device that allows out-of-plane motion and responds to two separate high-G mechanical environments, low-voltage microinitiation technologies, and the innovative processing and detonation characterization of an explosive train on the MEMS size scale. Sandia seeks to integrate the previously developed microinitiator and explosive-train technologies with the MEMS mechanical S&A device to enable a true MEMS fuze. The project will culminate in the successful firing and detonation of an artillery shell, under field-test environments, resulting in the first fully integrated MEMS device to ever accomplish such a feat.

Our recent research and development (R&D) objectives included (1) evaluation of the MICROFUZE S&A functionality in a gun-launched spinning round to confirm proper response to the combined environments of setback shock and spin, (2) integration of explosives into MEMS structures using inkjet

explosives processing and demonstration of a MEMS-enabled microenergetic firetrain, and (3) assessment of MICROFUZE compliance with MIL-STD-1316E and incorporation of additional safety features into a second-generation S&A device necessary to meet all safety requirements. We emphasized field testing of the MICROFUZE to provide essential data for iterative process maturation based upon lessons learned. The tests, which should be completed shortly, provide evaluation of the first-generation MICROFUZE. The development of a glass frit-bonding process overcame serious setbacks caused by limitations of the previously developed fusion-bonding technique, which allows these tests to still be conducted in the near future. In the area of microenergetic firetrain development, we investigated explosive deposition utilizing inkjet printing. Targeted deposition of Sandia-formulated alumina (density surrogate for silver azide) ink into reactive-ion etched (RIE) silicon cavities created material structures with volumes comparable to the primary explosive component of MICROFUZE, and identified printing parameters for optimal filling of MEMS–processed cavities. We will optimize motion-controlled deposition of silver azide in upcoming experiments to allow wafer-level integration of this primary explosive with MICROFUZE devices. Finally, we completed concepts for new MICROFUZE designs that incorporate safe-separation arming-delay features, and they are currently in fabrication. These designs look to use mechanical escapement features to delay arming up to 1 s after setback to fulfill all safety requirements of MIL-STD-1316E. Hardware should be in-hand soon, and we will test it to compare and quantify the obtained arming delays. We will perform these arming-delay tests on a newly developed centrifuge with *in situ* video recording.

67041

Analysis of Technology Impacts on Operations in Complex Environments

M. J. McDonald, B. P. Van Leeuwen, S. Tucker, E. P. Parker, F. J. Oppel, III

There are currently no effective analysis tools to support the evaluation of technology impacts on operations in complex physical environments such as facility security, homeland security (HS), and military operations in urban terrain (MOUT). A major reason for this is that the physical complexity of urban environments requires variable fidelity modeling capabilities to address issues such as building geometries and physical affects, secure network communications with limited range due to manmade obstructions, civilian and combatant populations, traffic flows, and utility infrastructures against the proposed technologies.

The main product of this project will be a unique capability to assess technology impacts in urban environments by focusing on specific measures of effectiveness such as casualty rates, fratricide rates, and time-to-successful-completion. This capability will be useful to technology developers as well as to military and security technology decision makers.

A key aspect of this project will be to perform technology impact analyses addressing realistic scenarios after each model-development phase to identify needs for new model development. Key technical issues expected include development of tractable representations, efficient dynamic resource federation, computational efficiency, and general complexity issues.

This project builds upon a significant suite of codes, tools and models that Sandia has already assembled. Sandia-developed codes include models for secure ad hoc *communication, sensor network phenomena, and unmanned air and ground vehicles. Applicable commercial codes that Sandia is expert at using include communications codes (OPNET), Department of Defense (DoD)–preferred terrain-editing tools (Terrex), human-motion simulators (DI-Guy), and High-Level Architecture (HLA) federation design codes. We will use existing urban and Department of Energy (DOE) facility terrain models for initial analyses. In addition, this project identified emerging Sandia codes for crowd-behavior modeling, information cognition, and automated planning, as well as new higher-resolution DoD terrain standards that we plan to specifically leverage as they become available.*

Results, both in capabilities developed and in analytical findings, are significant. Specific accomplishment highlights include the following:

- We completed three build, execute, and analyze spirals and two ancillary model federation tests where only one spiral had been initially planned.
- We developed a new modeling approach to seamlessly thread event-based simulation substeps into a discrete-time simulator.
- We developed new *ad hoc* networking algorithms that push beyond current network-size limits and provide verified multicast radio communications.
- Our analysis provided concrete examples that show the benefits of analyzing and designing network technologies in close association with the military or system-level objectives.
- DOE physical-security experts joined the team and helped to develop scenarios that optimally push our technologies forward in valid and useful ways.

Our analysis provided concrete examples that show the benefits of analyzing and designing network technologies in close association with the military or system-level objectives.

67042

CBW Cloud Knockdown and Neutralization

R. G. Betty, D. A. Lucero, J. E. Brockmann, M. D. Tucker

Chemical/biological warfare (CW/BW) cloud knockdown and decontamination following a CW/BW attack are necessary to protect lives, minimize impact to infrastructure, and allow timely restoration of operations. Preliminary estimates based on the challenge presented to a knockdown spray system and the necessary spray concentration based on our initial testing and modeling indicate that a cloud knockdown-and-decontamination system is feasible.

Sandia will perform model-based analysis in the early stages of development and proof-of-concept. We will experimentally calibrate the models we plan to use. A spray chamber with diagnostics to measure spray drop-size distributions and concentration is available to perform model development, validation, and calibration. Electrostatically charged drops should enhance the collection of small particles, and we will investigate them experimentally. Methods are available to generate monodisperse drops for benchtop testing and model development. The use of models will enable parametric evaluation of possible approaches and play a role in scaling the process.

We will assess various CW/BW cloud knockdown-and-decontamination deployment systems for force protection at a stand-alone facility such as an airbase. Knockdown approaches that will be considered include ground-based knockdown systems, fan-assisted systems, and aircraft knockdown. We will recommend optimum knockdown approaches, based on feasibility and efficiency of achieving cloud knockdown and decontamination.

Outdoor cloud knockdown-and-neutralization technologies developed through this project will be important in maintaining critical military operations. Additionally, aerosol science and decontamination elements of these technologies may be applied in future projects exploring response and restoration following terrorist attacks against a civilian population, or hazmat response to large-scale industrial incidents. Whether functional in military or civilian scenarios, the overall benefit of successful cloud knockdown and decontamination is an increased response-and-recovery capability by enabling intelligent countermeasures and thus maintaining critical military, infrastructure, or industrial operations.

Model development and concept development proceeded well. We used a Gaussian plume model to estimate the challenge presented to our conceptual mitigation methods. We compared these results to Hazard Prediction and Assessment Capability (HPAC) calculations and found them to be in reasonable agreement. The plume-modeling results indicate that protection of a specified area in the plume path may be achieved using a spray-dispersion system upwind of the area to be protected. The scheme entails use of a sprayed neutralizer dispersed from a fixed location into the path of the contaminant-laden plume so that the plume motion itself would produce the means to mix the neutralizing spray drops into the plume so that facilities and people downwind of the dispersion location would be exposed to a neutralized plume. We conceptualized two spray-deployment schemes in which drops of sprayed neutralizer solution would be mixed into the plume as it passed. The first is to use large fans to draw upwind air through a spray stream, which would produce a high-velocity flow of well-mixed air and drops that would expand downwind. A series of these devices placed perpendicular to the plume's travel direction would generate a decontaminated zone downwind of the sprayers that would protect people and facilities. The second scheme uses an array of sprays in a balloon-supported curtain to saturate the plume as it passes through the curtain. This idea would produce the same result. Other possibilities include ground- or tower-mounted sprays to produce the same effect as a curtain.

Modifications of the decontamination formulation included investigation of alternative surfactants and select solvents. We assessed surface tension, chemical-agent stimulant solubility, and decontamination efficacy with the ultimate goal being the development of a formulation that demonstrates effective agent-capture efficiency. We developed modified formulations that exhibit a decrease in surface tension (relative to standard DF200) of ~ 31%; theoretically, this improvement should increase the agent-capture efficiency.

Preliminary chamber testing indicates a knockdown and neutralization of stimulant-agent concentrations ranging from 2 to 4 orders of magnitude. We collected results following the use of standard DF200 deployed from electrostatic spray (ESS) nozzles in the charged state. We will evaluate the modified formulations in chamber tests conducted in upcoming work. Pending verification of initial chamber results, we will submit a technical advance outlining the concept and design of an optimized cloud-knockdown spray system.

Preliminary chamber testing indicates a knockdown and neutralization of stimulant-agent concentrations ranging from 2 to 4 orders of magnitude.

67043

Assessment of Biokillers in EDS for Biological-Agent Destruction

P. J. Crooker, D. A. Layne, G. M. Buffleben, R. W. Bradshaw, B. A. Simmons, J. R. Ross, D. F. Golling, T. J. Shepodd

Treatment systems that can neutralize biological agents are needed to mitigate risks from novel and legacy biohazards. Sandia performed tests with Bacillus thuringiensis *and* Bacillus stearothermophilus *spores in a 190-liter, 1 1/2 lb trinitrotoluene (TNT)-equivalent–rated explosive destruction system (EDS) to evaluate its capability to treat and destroy biological agents. We conducted five tests using three different agents to kill the spores. We operated the EDS in steam-autoclave, gas-fumigation, and liquid decontamination modes. The first three tests used EDS as an autoclave, which uses pressurized steam to kill the spores. We performed autoclaving at 130°C–140°C for up to 2 hr. We also performed tests with chlorine dioxide at 750 ppm concentration for 1 hr and 10% (vol) aqueous chlorine-bleach solution for 1 hr. All tests resulted in complete neutralization of the bacterial spores based on no bacterial growth in post-treatment incubations. We demonstrated explosively opening a glass container to expose the bacterial spores for treatment with steam, and this could easily be done for chlorine dioxide gas or liquid bleach.*

All tests resulted in complete neutralization of the bacterial spores based on no bacterial growth in post-treatment incubations.

The EDS using any of the three treatments examined in these tests is effective for killing *B. thuringiensis* (a relative of anthrax) and *B. stearothermophilus* spores. The use of spores in these tests is important since spores are the most resilient form of a microbe and are therefore the hardest to kill. While all three agents worked well, each has its advantages and disadvantages.

Using the EDS as an autoclave worked well and required no additional chemicals since it uses steam for the killing agent. It is important to ensure that all interior parts of the vessel reach autoclave temperatures. This includes sampling ports and feed-throughs in the door. While this was achieved in these experiments by wrapping the feed-throughs with heating tape, we believe that a redesign of the sampling system and other feed-throughs, as well as an improved thermal design covering heating and insulation, would optimize this option.

A bleach solution was also effective as a killing agent. Added advantages to this technique are that bleach is a cheap and readily available chemical. A significant asset of the EDS is its ability to safely contain the agent until analytical tests can confirm the agent’s destruction, but the corrosive effects of the

bleach limit the ability to contain the disinfectant for extended periods of time without damaging the EDS vessel. We believe this drawback can be overcome with techniques like buffering the disinfectant solution to maintain a high pH, passivating the surface of the vessel, and/or changes to the materials of construction; however, these would require additional study that is beyond the scope of this project.

Chlorine dioxide was effective at killing the spores. As a gas, it was able to permeate through all the internal volumes of the vessel without rotation. The high solubility of chlorine dioxide in water ensures that spores in aqueous solutions are killed, as demonstrated in this test. The use of chlorine dioxide in this test was achieved by generating the gas *in situ*, but for field-deployed vessels it will be more practical to use a commercial generator to make the gas and pump it into the EDS vessel. Since venting chlorine dioxide may be an issue in some locations, it will be necessary to vent through scrubbers to remove the gas. Liquids from the vessel are likely to outgas chlorine dioxide for an extended time and will therefore need to be collected in drums protected with scrubbers. The chlorine dioxide will likely cause the same pitting problems seen in the test using bleach and needs to be addressed.

Based on the results with the test vessel, extending EDS technology for treatment and complete neutralization of biological agents can be successfully performed. Common killing agents and methods such as steam autoclaving, liquid bleach, and chlorine dioxide are compatible with the EDS technology platform. However, each method has different process requirements and trade-offs for implementation into the EDS. The next step to advance the EDS technology for use with biological agents requires further conceptual and detailed engineering and design. Depending on the process, engineering can include developing designs to provide process reagents, improving thermal control, and improving sampling system hardware and materials of construction.

Other Communications

Didlake, Jr., J. E. 2004. Expanding explosive destruction system capabilities. Paper presented at the 12th Global Demil Symposium and Exhibition (NDIA), 20 May, Dallas, Texas.

Didlake, Jr., J. E. 2004. Processing lewisite munitions in the explosive destruction system. Paper presented at CWD 2004, 27 May, St. Petersburg, Russia.

67044

Adaptive-Force-Feedback Surface Control

D. K. Kholwadwala, J. W. Wheeler, B. Hassan, P. C. Galambos, D. L. Keese, B. R. Rohrer, G. L. Benavides

Sandia is developing a system to allow surface adaptation based on microelectromechanical systems (MEMS) technology. The proposed system consists of an array of small balloons that can be inflated and deflated with MEMS valves based on information provided by MEMS pressure transducers. The use of MEMS components allows a large number of small balloons to be placed close together with minimal hardware. We designed the balloons to inflate primarily in one direction, i.e., they change length, not diameter. We designed the controller to regulate the pressure in each balloon to create a surface with the desired profile. Applications for this system include adaptive airfoils for unmanned aerial vehicles (UAVs).

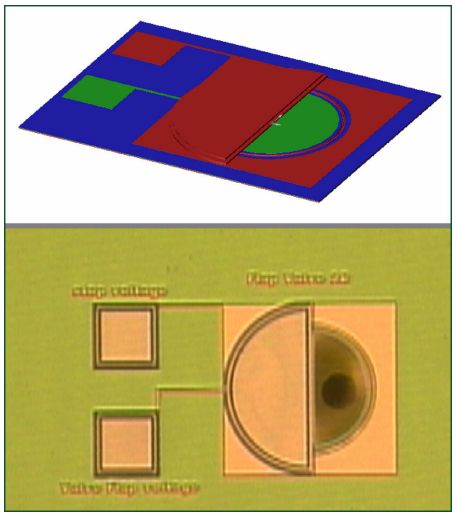

(top) *Flat-valve schematic, and* (bottom) *actuating schematic. The Bosch through-hole is 33 µm in diameter.*

The enabling technology for this system is the design and fabrication of the MEMS components. We developed and tested a number of MEMS valves and pressure transducers.

We designed and fabricated three types of valves. The most developed design is a flap valve that opens under a pressure difference. This valve can be held closed with an electrostatic force against a small pressure difference but is best used as a check or pressure-relief valve. We characterized these valves, and the results compare reasonably with theory. The other types of valves are disk-in-cage and slider valves. These can be held closed against a pressure difference and used as control valves. Each type of valve allows flow through a Bosch-etched through-wafer hole. The valve mechanism (flap, disk, or slider) is surface micromachined on the top surface of the MEMS die over the holes. The valves can be placed in an array on a die and packaged to allow precise flow control in two directions.

We also fabricated and tested a number of MEMS pressure transducers. They consist of various shapes and sizes of diaphragms that deflect under a load, causing a change in resistance across the device. Preliminary tests showed relatively linear pressure-versus-resistance profiles in the desired working range (0–15 psi).

In a parallel effort, we developed a non-MEMS prototype to demonstrate balloon and controller performance. The prototype consists of small solenoid valves, thin-film pressure transducers, and an array of silicon rubber balloons. The system is controlled by a personal computer through a data-acquisition

board. We designed the balloons with ribs around the circumference to resist radial ballooning.

67046

High-Capacity Earth-Penetrator Instrumentation

M. E. Partridge, B. J. Welch, J. M. Bowen, T. L. Martinez, M. Arviso

Our current ability to collect critical engineering data during full-scale earth-penetrator tests does not meet the demands of the Robust Nuclear Earth Penetrator (RNEP) and other proposed penetrator weapon systems. Specifically, sample rates are insufficient for the component-level data required, and the number of measurement signals supported is inadequate. To allow the development of these weapon systems to proceed with the necessary testing data, Sandia is developing a shock-hardened data recorder system with new approaches for measurement sampling, data-storage capacity, and data upload. Although with vastly greater capability than current designs, the instrumentation must remain compact and extremely rugged. The design would be capable of withstanding more than 20,000 G acceleration for tens of milliseconds.

Our current penetrator-instrumentation designs record a maximum of 12 channels at 30,000 samples per second per channel, with a 500 ms record time. Engineers supporting early RNEP tests have requested more than 48 channels at rates of at least 100,000 samples per second. The proposed design will meet their needs with 64 channels sampled at a maximum of 150,000 samples per second per channel and tens of seconds of recording time.

The proposed work includes the design, prototyping, and construction of a flight-qualified unit and its testing on board a rocket-sled–propelled penetrator into a concrete target. We completed and flight tested the analog section of the design, and we completed and assembled, but have not tested, a bench prototype of the digital section.

We completed the analog section of the design and flight-tested it as part of the advanced penetrator nonvolatile (AdPen-NV), a penetrator instrumentation design. The flight tests uncovered an unanticipated vulnerability to shock that is currently being investigated. The design includes a programmable sample rate and anti-alias filter frequency, and programmable gain, bias, and offset. In addition to its role as a test-bed for these signal-conditioning capabilities that are required in the High-Capacity Penetrator (HiCapPen), this approach allowed early evaluation of the operational capability that the final HiCapPen design will provide. The capabilities evaluated include interface features for system integration, the

associated automated product test equipment, and overall functionality of the penetrator instrumentation.

Following detailed evaluation of two programmable logic devices from different manufacturers, we selected an appropriate device and then completed the initial logic design. We completed and assembled a bench prototype design, but we have not yet tested it. We completed draft firmware for the microcontroller that was selected.

Because the design nature requires a large memory capacity of as much as 2 GB, one challenge has been to efficiently transfer the data from the penetrator instrumentation into a laptop computer. We developed and breadboarded an approach that is expected to allow a transfer rate of > 10 MB/s. We also started development of the user-interface software that, in addition to accomplishing the data extraction, will be used to configure the system and perform state-of-health tests.

67047

Systems Analysis of Networked Sensors

J. A. Rohwer, B. McDaniel, J. E. Stamp, K. J. Smart, D. Kilman, M. T. Oswald

Dense clusters of miniaturized self-similar wireless sensors are an evolution of current sparse, heterogeneous, wireless sensor clusters. Dispersed in large quantities, the nodes assist each other in the transmission of data by means of an ad hoc*, multihop, wireless mesh network. A sensor network is designed and deployed for a set of system requirements. To achieve reliable, error-free data transmission, the wireless sensor network (WSN) must allow for, and adapt to, time-varying traffic and channel conditions. Specific areas of interest are communication channel models for link gain margins, fading, and interference. These physical imperfections must be included in network simulations.*

Choosing sensor architectures appropriate for a given mission is a systems-engineering challenge, whose solution is a function of time-varying environments, restrictive logistical issues, and demanding sensing requirements. To provide the reliability, adaptability, and scalability that are required of a real-world working sensor network, internode communications must be thoroughly analyzed.

The ultimate goal of such an analysis is to provide a sensor network of the appropriate topography, number, and density to meet predefined, application-specific requirements while simultaneously minimizing energy consumption, latency, and detection. To meet this challenge, Sandia seeks to develop a set of analytical tools. The development of this analytical capability will allow for the solution of the optimal method of dynamically tuning sensor density, bandwidth, modulation, and sleep time for a given application, while accounting for communication channel disturbance, as noted above. This work will serve to create simulation infrastructure capable of accurately modeling sensor networks. The purpose of such an infrastructure is to provide rapid feedback to developers to help guide the choice of system settings, deployment constraints, and real-time optimization capabilities for a given network design, and to identify areas of improvement in network radio design.

WSNs are routinely proposed as solutions for complex applications. Current research addresses complex network designs based on standard architectures. The simulation spaces are well defined, and the results are impressive. The limitation of the published algorithms is that current technology does not

support efficient, low-power hardware implementation of the complex signal-processing algorithms and network protocols.

Our research is driven toward advanced sensor-network architectures that are required for large-scale, efficient sensor networks. We developed a new architecture, a WSN framework, to specifically address complex, heterogeneous networks. Systems analysis through modeling and simulation (M&S) will support the advanced architecture and lead to future design activities.

We developed a new architecture, a WSN framework, to specifically address complex, heterogeneous networks.

A major contribution to the recent milestones was an analysis of commercial and government radios for potential use in a sensor network. This task is an important first step. The demanding scope of unattended ground sensor (UGS) applications requires robust communications. Commercial radios are designed for home and office applications. Thus, designing a UGS system around a commercial radio imposes severe operational limitations.

We reviewed common radios such as 802.11, 802.15, and cordless and cellular telephones, along with original equipment manufacturers (OEM) radios such as the MaxStream and XETI. We also analyzed, tested, and compared the Army Research Lab's Blue Sensor Radio with the commercial and OEM network radios. Each radio has various advantages and disadvantages. This commercial-radio trade study provides a baseline for M&S activities.

Through field testing, we compared radio technologies included in the radio trade study. We tested the MaxStream, XETI, and Ember radios in open and mountainous regions. We measured and compared the performance of the radios.

We completed a comprehensive review of commercially available M&S tools, along with Sandia's in-house capabilities. The tools ranged from the commercially supported OPNET (operating network) to free academic simulation tools. The review catalogues tools and their capabilities as the starting point for future simulations.

The Battle Damage Assessment (BDA) White Paper addresses the UGS application and outlines operational and system requirements for an air-delivered WSN. This application is one focus of future simulation work. This application requires advanced technology to deal with a complex and changing communication environment and provides an application context to exercise the analysis and design tools.

We conducted a comprehensive review of power-management algorithms. Successful power management in a WSN requires optimization of the protocols that affect energy consumption on each node and the aggregate effects across the

network. We analyzed, simulated, and optimized a sleep protocol for an energy-efficient WSN. We developed a method for determining the optimal sleep time, providing reference data that spans several orders of magnitude.

The WSN framework is based on role management with heterogeneous sensor nodes. Important considerations include the energy budget and node classification for role distribution. We included a performance margin for uncertain future conditions such as node failures, situational changes, mission modification, or security compromise. We based role assignment on an adaptive network architecture that supports sensing activities for an array of situational evolution, provided these are reasonable within the overall system budget. If performance improvements outweigh energy costs, then the system transitions to the new operating point.

We incorporated the research, analysis, and framework into systems simulations focusing on energy management, latency, and self-organization of large-scale, heterogeneous networks. The framework provides a general, abstract starting point for simulation. The effects of different radio technologies and sleep protocols are considered to yield a high-fidelity model that is robust in capturing the wide range of applications. In future activities, we will begin to apply these network design and analysis tools against prototypical system environments and performance requirements.

Refereed

Oswald, M. T., J. A. Rohwer, and M. A. Forman. 2004. Analysis of power management and system latency in wireless sensor networks. *Proc. SPIE Defense and Security Symposium, SPIE Digital Wireless Communications VI* **5440** (12–13 April, Orlando, Florida): 134–44.

Smart, K. J. 2004. Network radio trade study report. Sandia Technical Report SAND2004-3846, Sandia National Laboratories, Albuquerque, New Mexico.

Other Communications

Jones, L. A. 2003. Battle damage assessment using ordinance delivered and dispersed sensor networks. Internal unpublished report (23 November).

Oswald, M. T., K. J. Smart, L. S. López, J. A. Rohwer, J. E. Stamp, and D. Kilman. 2004. Multimission requirements and an optimization framework for wireless unattended ground sensor networks. Paper presented at the 1st Annual IEEE Communication Society Conference on Sensor and *Ad Hoc* Communication and Networks, 4–7 October, Santa Clara, California. SAND2004-2463C.

67048

Deployable Object Tracker for NMD Flights

A. D. Niese, T. A. Pitts, W. J. Zubrzycki, R. O. Nellums, J. V. Sandusky, M. W. Koch, D. L. Davidson, J. C. Gilkey

Sandia seeks to develop a system capable of completely characterizing the relative kinematic and dynamic properties of a deployed object from a remote platform with no contact or impact to any of the target objects. Specifically, this project seeks to advance three-dimensional laser radar (3-D LADAR) to focus on applications related to national missile defense (NMD) concerns in space-based deployments. The proposed system will have the ability to track multiple objects in the field of view. We will use the technique of scannerless range imaging (SRI) (scannerless 3-D LADAR) to acquire the data. This technique uniquely provides high-speed, high-resolution 3-D imaging.

Sandia has significant experience and a leadership position with scannerless 3-D LADAR. Sandia sensors are currently operating at the LADAR range facility of Eglin Air Force Base and the Non-Acoustic Underwater Imaging Facility of the Naval Coastal Systems Station; these sensors flew on STS-97 for the Structures Directorate of the National Aeronautics and Space Administration (NASA) Johnson Space Center. While all of these sensors are capable of high-resolution imagery, none of these sensors have the ability to identify objects, characterize the object, and report updated kinematic and dynamic data. This project will develop the ability to perform object tracking and characterization.

The advantages of such a system are that it does not require cooperation from the target, and it can operate at extended ranges. The functionality of such a system is twofold. First, it can be used to characterize and improve the deployment of known objects. Second, it can be utilized to characterize unknown objects and then to categorize these objects into classes. Ultimate success will culminate in a final (staged) demonstration where data are acquired for multiple objects deployed simultaneously, and the dynamics of these objects are determined in near real time.

We achieved an initial understanding of the scene. This is a very crucial step. The scene dynamics and optical environment (Scene Albedo) directly impact the system requirements. We chose to understand the potential applicability of LADAR for the intercept event in addition to the deployment event. Some of the more-challenging aspects of intercept include the event time

scales. At the closing velocities, the relative frame times and shutter time must be very short—in excess of 100,000 frames per second and shutter speeds < 1 μs. We developed several algorithm concepts for target dynamic analysis. One approach includes a 6-degree-of freedom (6DOF) registration process with a by-product of 6DOF parameters.

We made additional advancements and came to understand actual national needs, and we developed both interim and long-term solutions. In fact, research completed under this project led to the development of a new capability applicable to the NMD program that will be implemented on an upcoming flight.

...research completed under this project led to the development of a new capability applicable to the NMD program that will be implemented on an upcoming flight.

67049

Continuous-Flow Detector for Rapid Pathogen Identification

G. J. Fiechtner, A. K. Singh, E. B. Cummings, B. A. Simmons

Sandia is developing a low-power, portable detector for the rapid identification of pathogens such as Bacillus anthracis *and smallpox. Based on our recent successful demonstration of the continuous filter/concentrator inlet, we believe strongly that the inlet section will enable differentiation between viable and nonviable populations, between types of cells, and between pathogens and background contamination. Selective, continuous focusing of particles in a microstream enables highly selective and sensitive identification using fluorescently labeled antibodies and other receptors such as peptides, aptamers, or small ligands to minimize false positives. Processes such as mixing and lysing will also benefit from the highly localized particle streams. The concentrator is based on faceted prisms to contract microfluidic flows while maintaining uniform flowfields. The resulting interfaces, capable of high throughput, serve as high-, low-, and bandpass filters to direct selected bioparticles to a rapid, affinity-based detection system.*

The proposed device is superior to existing array-based detectors as antibody-pathogen binding can be accomplished in seconds rather than tens of minutes or even hours. We are designing the system to interface with aerosol collectors under development by the national laboratories or commercial systems. We designed the focused stream so that it can be interrogated using diode lasers to differentiate pathogens by light scattering. Identification of particles is done using fluorescently labeled antibodies to tag the particles, followed by multiplexed laser-induced fluorescence (LiF) detection (achieved by labeling each antibody with a different dye).

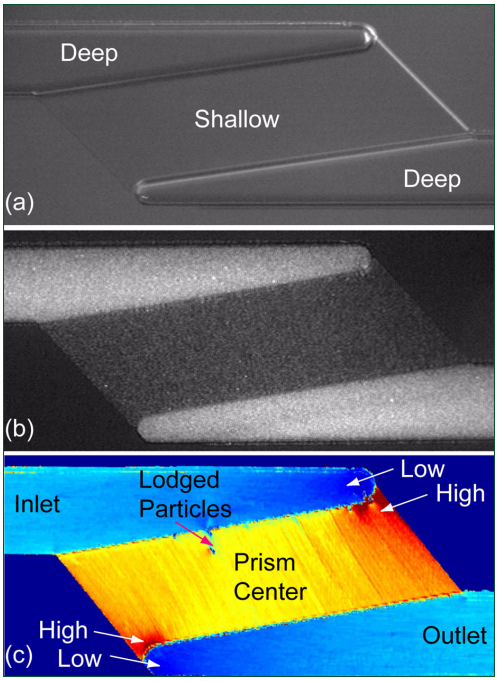

(a) *A microchannel constructed using a two-level wet etch in glass. The deep regions have a depth of 50 mm, while the shallow regions have a depth of 5 mm.* (b) *Fluorescence image of 200 nm polystyrene beads flowing in the microchannel.* (c) *Speed field obtained from PIV measurements.*

We demonstrated two types of selective pathogen filter/concentrators that can operate continuously, without the need to implement trap-and-release methods. The first selective concentrator uses single, insulating ridges to construct a voltage-addressable flow splitter in which desired pathogens can be forced selectively to flow into an output port of choice. We showed in a borosilicate glass microchip that *B. subtilis* can be switched to a central outlet simply by increasing the voltage to affect particles using dielectrophoresis. The second continuously operating, selective concentrator relies on serial sequences of ridges to focus particles to a concentrated stream in which particles exit a wide channel in single file along a side

The proposed device is superior to existing array-based detectors as antibody-pathogen binding can be accomplished in seconds rather than tens of minutes or even hours.

wall. Finally, we showed that these continuous designs can also be operated in a trap-and-release mode, if desired.

We tested designs using numerous types of particles, including polystyrene latex beads (diameters of 5, 3, 1, 0.5, and 0.2 μm), *E. coli*, *B. subtilis*, and *B. cereus*. We found filter behavior to be a strong function of particle diameter and type. Designs that deflect 1 μm particles at a given operating voltage do not deflect 200 nm beads; in addition, we found that designs that readily concentrate *B. subtilis* deflect 3 μm beads, but only after tripling the applied potential. We also replicated and tested structures in polymeric, thin-film substrates—an important step for the ultimate mass production of inexpensive sensors.

The successful demonstration of the filter/concentrators prompted us to move up the design of subsequent diagnostic microchannel sections. We designed and constructed mixers to mix either micron-sized bacteria or molecules. We designed these to match a wide range of filter fluid velocities. We developed substantial intellectual property, yielding filed patents and technical advances.

Refereed

Barrett, L. M., A. J. Skulan, G. J. Fiechtner, A. K. Singh, and E. B. Cummings. 2004. Dielectrophoretic filter/concentrators based on insulating ridges. *Analytical Chemistry* (American Chemical Society), to be submitted.

Barrett, L. M., A. J. Skulan, G. J. Fiechtner, B. A. Simmons, E. B. Cummings, and A. K. Singh. 2004. Dielectrophoretic particle deflection using corrugated insulating ridge arrays. *Analytical Chemistry* (American Chemical Society), in preparation.

Fiechtner, G. J., A. J. Skulan, L. M. Barrett, B. A. Simmons, E. B. Cummings, and A. K. Singh. 2004. Continuous particle filtration and concentration by multigradient dielectrophoresis. Paper presented at the International Mechanical Engineering Congress and Exposition, November, Anaheim, California.

Skulan, A. J., L. M. Barrett, G. J. Fiechtner, A. K. Singh, and E. B. Cummings. 2004. Experimental and numerical investigation of electrokinetic fields over faceted, isotropically etched ridges in insulating substrates. *Analytical Chemistry* (American Chemical Society), in preparation.

71943

Simulating Human Behavior for National Security

M. L. Bernard, P. R. Wolfenbarger, R. L. Waymire, M. L. Bernard, D. H. Hart, P. G. Xavier, J. B. Rigdon

In this research and development effort, Sandia is focusing on what we believe is a significant technical gap in existing modeling and simulation (M&S) capabilities: the representation of human behaviors. In particular, we are developing models that will realistically represent intra- and intergroup interactions between virtual humans and human-controlled avatars as they interact with their environment. We are conducting research to enhance our existing cognitive models to include sociologically plausible behaviors most important for representing human interactions. This work will integrate, and thus leverage, multimillion-dollar past investments to include UMBRA (a modular M&S system) and the Cognitive Modeling Framework to build an M&S capability that will serve as the technical foundation for subsequent national security analysis and security-personnel training. Through this large-scale development and integration effort, we intend to achieve a scalable capability allowing us to model large numbers of virtual humans and their interactions with high-fidelity cognitive modeling of key personnel or smaller numbers of participants. Development of computationally efficient code will allow us to run many instantiations of our model in a Monte Carlo fashion and provide the resultant body of outputs to optimization algorithms enabling state-space searches in support of national security applications. We anticipate that the technical foundation developed by this project will serve as the basis for assessments of proposed security enhancements and/or new technologies that will aid in the generation of recommendations for security strategies. We envision that the capabilities generated by this project will serve as the technical foundation for next-generation training tools for Department of Energy (DOE) response forces and Department of Defense (DoD) military personnel.

The intent of this project is to demonstrate an initial virtual human-interaction modeling capability. We began the process of simulating human behavior in a manner that produces lifelike characteristics and movement, as well as creating the framework for models that are based on the most current experimental research in cognition, perception, physiology, and cognitive modeling. Our first major milestone was a

"strawman" or transition implementation whose architecture and components are mostly simplified, but that still enable simulated human models to sense each other, react to each other, and move about in a simulated three-dimensional (3-D) environment. We reached this milestone with an initial demonstration notional scenario showing security forces clearing an office environment of adversaries and innocent bystanders. For geometry, appearance, and motion of simulated humans, our prototype utilizes an integration of Boston Dynamics' DI-Guy™ into Sandia's UMBRA simulation framework.

We also met the second and third milestone: action generation and the cognitive model modification, respectively. In addition, we developed a preliminary action-generation or motor-level cognition model that transforms abstract actions generated by high-level cognition to actions that can be carried out by a simulated physical human model. Our work has yielded models of perceptual, spatial, and motor functioning and memory that will be embedded in upgrades to the cognitive framework, undertaken by the next-generation intelligence system (NGIS) Grand Challenge project in upcoming work. The next main objective is to upgrade our initial implementation for simulating humans by developing extensible simulation components that are compatible with the upgraded cognitive simulation architecture and that replace several *ad hoc* components currently used.

Our first major milestone was a "strawman" or transition implementation whose architecture and components are mostly simplified, but that still enable simulated human models to sense each other, react to each other, and move about in a simulated three-dimensional (3-D) environment.

72715

Compact Ultrabright Multikilovolt X-Ray Sources for Advanced Material Studies, 3-D Nanoimaging, and Attosecond X-Ray Technology

A. Mar

Experimental evidence and the corresponding theoretical analyses have led to the conclusion that the system composed of xenon (Xe) hollow-atom states, which produce a characteristic Xe(L) spontaneous emission spectrum at λ @ 2.9 Å and arise from the excitation of Xe clusters with an intense pulse of 248 nm radiation propagating in a self-trapped plasma channel, closely represents the ideal situation sought for amplification in the multikilovolt region.

The key innovation that is central to all aspects of the work in this project is the controlled compression of power to the level (~ 10^{20} W/cm^3) corresponding to the maximum achieved by thermonuclear events. Furthermore, since the x-ray power that is produced appears in a coherent form, an entirely new domain of physical interaction is encountered that involves states of matter that are both highly excited and highly ordered. Moreover, these findings lead to the concept of "photon-staging," an idea that offers the possibility of advancing the power compression by an additional factor of ~ 10^9 to ~ 10^{29} W/cm^3. In this completely unexplored regime, γ-ray production (w_γ ~ 1 MeV) is expected to be a leading process. A new technology for the production of very highly penetrating radiation would then be available.

The Xe(L) source at w_x ~ 4.5 keV can be applied immediately to the experimental study of many aspects of the coupling of intense femtosecond x-ray pulses to materials.

In a joint collaboration, the University of Illinois–Champaign group and Sandia plan to explore the following areas: (1) anomalous electromagnetic (EM) coupling to solid-state materials, (2) three-dimensional (3-D) nanoimaging of solid matter and hydrated biological materials (e.g., interchromosomal linkers and actin filaments in muscle), and (3) EM pulse (EMP) generation with attosecond x-rays.

We examined the coupling of fast x-ray lasers to solids in two stages: initially, with readily performed screening studies utilizing foils to examine the gross response, and subsequently, with more-detailed experimental analyses. We examined titanium (Ti) foils and studied plastic foils. We performed some analysis of the interaction and constructed film packs for

sufficiently thin foils. We observed a strengthening of the radiative coupling to the solid over what we conventionally predicted. We also extended the single-pulse measurements to evaluate the ability to produce attosecond x-ray pulses with a length < 100 attoseconds for studies of EMP generation. On a single pulse, we observed 60 eV saturated spectral width, supporting the observation of 30 attoseconds. The limit was established at 10 attoseconds. We have EMP data that could lead to the development of a new technology for attosecond-pulse measurement, but the results above superseded the need for this technique. The results show sensational power scaling with high-energy efficiency and extraction coupled to high bandwidth. Projections for this type of laser-area peak powers well above the power levels of inertial confinement fusion (ICF) simulators.

The results show sensational power scaling with high-energy efficiency and extraction coupled to high bandwidth.

The Xe(L) system at $\lambda \sim 2.9$ Å exhibits all of the canonical attributes of a saturated amplifier. The key observables [1,2] are (1) sharp spectral narrowing, (2) the detection of a narrow directed beam ($\delta\theta_x \cong 200$ μrad), (3) an increase in the amplitude of the emission and the development of an intense output ($\geq 10^6$ enhancement), and (4) the observation of deep spectral hole-burning on the inhomogeneously broadened spontaneous emission profile. Experimentally determined by two methods, line narrowing and signal enhancement, the observations for several single-vacancy 3d→2p transitions indicate a range of values for the effective linear gain constant given by $g_L \cong 25–100$ cm^{-1}. It is shown that this result stands in clear conflict with the corresponding upper bound estimated with conventional theory from prior spectroscopic studies of $g_L \cong 40–80$ cm^{-1}. Overall, the observed values deviate substantially from expectations scaled to the spectral density of the measured Xe(L) spontaneous-emission profile; they are systematically too high. The most extreme example is the strongly saturated Xe^{32+} transition at $\lambda = 2.71$ Å, a case that fails to reconcile the measured signal strength with the corresponding theoretically predicted value by a factor exceeding 10^3. The paradox is resolved with the Ansatz that the amplification is governed principally by the saturated gain g_s, not the conventionally described small signal (linear) value g_L. This interpretation is supported by the observation of deep spectral hole-burning, the signature of strong saturation, that occurs uniformly across the spectrum of the spontaneous emission profile; the effective amplification exhibits an anomalously weak dependence on the spectral density. One clear manifestation of the saturation is the recording of high spectrally resolved x-ray yields that cause gross structural

damage to material in the film plane of the spectrometer. The behavior of the amplifier can be best described as a system that undergoes explosive supersaturated amplification. The source of this exceptionally strong amplification can be traced to the dynamically enhanced radiative response of the excited Xe hollow-atom states located in the clusters that are mode-coupled to the plasma waveguide forming the amplifying channel.

74795

Magnetophoretic Bead Trapping in a High-Flowrate Biological Detection System

C. D. James, P. C. Galambos, M. M. Hopkins, L. E. Rohwer

This project produced significant advancements toward the development of a novel high-throughput biodetection system. The primary areas of investigation were the capture of targets from a real-world sample, the concentration of captured targets using a novel microfluidic device, and the development of magnetic microspheres to serve as capture-and-carry chaperones for concentrating/separating targets and in back-end detection. In the first task, Sandia investigated using the magnetic microsphere chaperones as magnetic stirrers. We conducted mixing tests using different methods of mixing and determined that the magnetic mixing of the sample increased hybridization speed and efficiency. The second task was to develop methods for producing a prototype polymer-based microfluidic device for trapping magnetic particles. Early experiments demonstrated significant trapping forces being generated with currents on the order of several hundred milliamps. We also examined the trapping efficiency as a function of distance from the electromagnet, fluid-suspension properties, and magnetic-field gradient. We will fabricate the second-stage prototype using embossing of polymers and printing of silver nitrate onto substrates. This will enable the rapid production of roll-to-roll fabricated polymer microfluidic devices. The final task is to investigate the development of a magnetic microsphere, with target-specific surface functionalizations, and internal "bar-codes" in the form of quantum-dot (QD) assemblies. The unique mix of QDs located within the microsphere will serve as identification for the particular surface functionalization, thus enabling rapid target identification. We will detect target presence using a second fluorophore bound to all targets.

We also addressed smaller components of the project's ultimate goal: discussing options for producing a wet-electrostatic precipitator (WESP) with modified design requirements to meet portable specifications, performing calculations to determine appropriate mixing and hybridization conditions, and investigating possibilities for an orthogonal assay for back-end detection.

This project produced significant advancements toward the development of a novel high-throughput biodetection system.

- *Sample collection*. We are investigating the use of WESP technology for collecting samples to be analyzed. One of our objectives is to develop a system compatible with operation

in an aircraft, specifically to collect and monitor the air for biological threats (infectious disease and biowarfare agents). We are working with Turbosonic Technologies to design a downsized WESP that can be powered on an airborne aircraft. We are also addressing other design criteria for sample-collector operation.

- *Magnetic mixing*. This task is focused on developing protocols and methods for determining the effect of mixing on binding rate and reaction velocity. We examined four different methods of mixing: passive diffusion, pipette-based mixing, vortexing, and rotating-magnetic-field–based mixing. We used a standard streptavidin-biotin reaction, which has extensively characterized kinetics. Initial results indicated problems with vortexing that may have damaged the binding molecules. The rotating magnetic field worked the best in terms of having the shortest time required to achieve maximum binding.
- *Model development for bead-target interaction*. This task proceeded concurrently with the magnetic mixing, but without addressing a particular mixing method. Given assumptions on the type of target (e.g., it is much smaller than a bead), and assuming a local superposition principle for the flowfield, we developed a model to help understand the major contributing factors for bead-target interaction (e.g., hybridization rates). The practical questions that can be addressed with this framework include the effects of the number of beads, capture radii, bead size, target size, mixing speed, detection probabilities, etc.

The first step in this task laid out a foundation for the fluid dynamics problem (computation of the bead-capture radii). Using these results, we developed a framework for relating the volume of the sample searched to the previously mentioned parameters. This included calculating a variety of example scenarios that relate to the probability of a hybridization event occurring to the bead size, target size, and mixing speed. Finally, we coupled the hybridization model to the other components of the overall sensor system, including the magnetic trapping device, to give overall sensor-system efficiency.

- *Magnetic trapping*. The magnetic-trapping effort focused on two subtasks: experimental data with first-generation prototypes, and investigation of fabrication techniques for producing the second-generation prototype. The first-generation magnetic-trapping device utilizes machined polymethylmethacrylate (PMMA) substrates for producing a single-fluid channel with a fluid inlet and outlet. We manually placed different diameter wires and affixed them into the

channel to serve as an electromagnet. We sealed the channels with polydimethylsiloxane and a glass cover. We examined trapping efficiency (magnetically induced velocity) of 8 µm-diameter magnetic beads as a function of the wire diameter and the distance from the electromagnet. We also conducted trapping in different fluid suspensions with different conductivities and pH levels (bile, blood, and urine stimulant buffers).

The second-generation prototype used embossing to produce channels in thin (~ 200 µm-thick) polymer substrates. We accomplished the printing of a silver nitrate solution onto the substrates using the Robocaster system and a custom-made inkjet printing system. Once printed, the films are heated, leaving a thin conductive film of silver (Ag). The films show good adhesion to several substrates, including glass and Kapton, and film conductivities are usually within 1 order of magnitude of bulk Ag.

- *Microsphere development*. Our technology will depend on the development of a novel magnetic microsphere that contains both custom surface chemistry and internal fluorophores for identification. Our first task in developing the microspheres was to characterize commercially available QDs for use as internal fluorophores within our magnetic microspheres. We examined quantum efficiency and fluorescence lifetime for streptavidin-coated cadmium selenide (CdSe)/zinc sulfide (ZnS) QDs. We found that the surface coatings significantly affected the fluorescence lifetime behavior.

Other Communications

Derzon, M. 2004. Design approaches to a portable diagnostic system. Paper presented at Research, Technologies and Applications in Biodefense, 18–20 September, Washington, D.C.

75441

TPV Energy Scavenging for Hypervelocity Vehicles

J. G. Fleming, A. R. Ellis, M. C. Wanke

There is currently interest in potential ways to convert the considerable heat generated on surfaces of hypervelocity vehicles into useful power. A potential approach to this problem could employ thermal photovoltaic (TPV) energy conversion. The principle behind TPV is that thermal energy emitted by a heated source is converted directly into electrical energy though the use of narrow-bandgap photovoltaic cells. Typically, the heat source is chemical, concentrated solar, or nuclear energy. In this project, Sandia will consider scavenging thermal energy from the heated surfaces of hypervelocity vehicles. This approach may be attractive for several reasons: (1) it is relatively simple, (2) it has no moving parts that might be affected by centrifugal forces, and (3) it would reduce the overall heat load on the vehicle. There are two figures of merit for TPV systems: efficiency and energy density. It is possible to achieve high efficiencies using textured tungsten (W) or Er_2O_3 emitters. Recent work on W photonic crystals showed that they also can be an efficient emitter of relatively narrow-band thermal energy and may be attractive for this application.

We built a test stand to compare the emission from photonic bandgap (PBG) materials to that of other emitters at multiple temperatures. We built the system in a vacuum chamber to reduce W PBG oxidation at high temperatures, and it is composed of a heater, a detector, and a set of heat shields. The ceramic heater incorporates a sample plate with k-type thermocouples to measure emitter temperature. We mounted the gallium antimonide (GaSb) TPV detector to a large metal heat sink to reduce performance-robbing heat buildup in the detector. The heat sink also has a k-type thermocouple so that the detector temperature can be monitored. The detector is 8 in. above the heater, and in this space there are three heat shields above the heater and five collimating shields before the detector to reduce absorption of stray radiation. We placed additional heat shields around the sides of the heater to block indirect radiation from reaching the detector.

We made voltage measurements across a 150-ohm resistor in parallel with the GaSb detector. We compared the PBG data to that of polished silicon (Si) and Si coated with high-temperature blackbody paint (an approximate blackbody). We

made measurements at temperatures between 300°C and 1000°C.

We also investigated the emissivity of the W photonic lattice in more detail. In particular, we made more careful measurements of the temperature of the sample and determined that the sample temperature had been underestimated in earlier work. At this point we believe, within experimental error, that the emissivity of this structure is high, but less than one.

Energy and Critical Infrastructures

The multitude of issues that contribute to international conflict impacting the U.S. demands a holistic approach to enhancing the surety of critical infrastructure and related environmental-quality issues. The Energy and Critical Infrastructures investment area addresses possible conflict mitigation through inventive approaches to making clean, affordable energy and water available in the U.S. and worldwide, with particular emphasis on areas where tensions are high.

Investments in Energy and Critical Infrastructures strive for advancements and innovation in energy systems analysis and operation to enhance and explore solutions to energy and water security; improved nuclear systems; resource conservation and environmental protection; and global infrastructure security and sustainability.

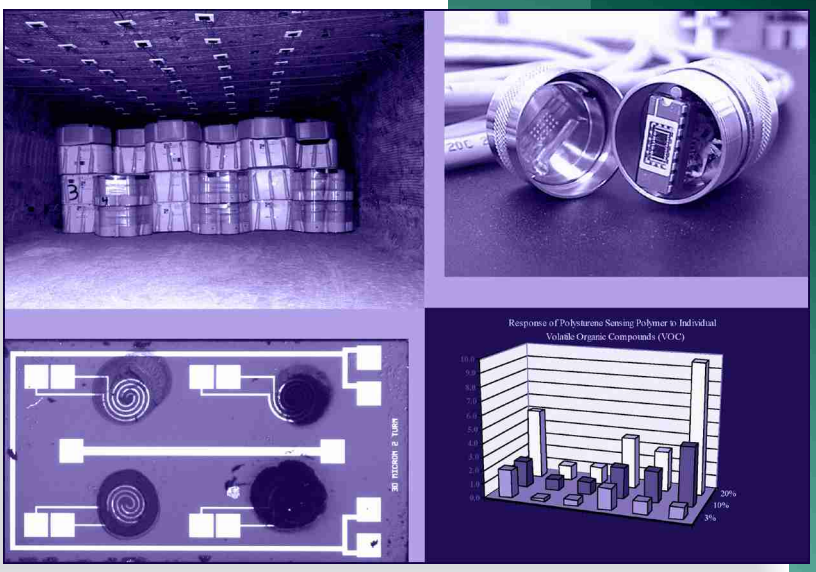

38677
"Potential Application of Microsensor Technology in Radioactive-Waste Management—with Emphasis on Headspace Gas Detection"

Waste characterization is probably the most costly part of radioactive-waste management. An important part of this characterization is the measurement of headspace gas in waste containers to demonstrate compliance with the Resource Conservation and Recovery Act (RCRA) or transportation requirements. Traditional chemical analysis methods are expensive and time-consuming and increase human exposure to hazardous environments. Focus is on advancements toward developing techniques that enable quick, *in situ*, and real-time detections of headspace gas compositions.

Scientists determined that preconcentrators are needed for chemiresistor sensors to meet desired detection limits. They also developed various volatile organic compound (VOC) preconcentrators that reduce detection limits by 2 orders of magnitude. Techniques advancing performance and sensitivity of sensor polymers were created. Inverse models that enable identification of VOCs based on sensor-array responses were produced, and a method for eliminating VOC interference of sensor readings was developed.

38662

Natural-Gas Production Problems: Solutions, Methodologies, and Modeling

J. C. Lorenz, J. M. Herrin, B. W. Arnold, S. P. Cooper, W. A. Olsson, J. F. Holland

Natural gas is a clean fuel that will be the most important domestic-energy resource of the 21st century. Ensuring a stable supply is essential for our national energy security. Sandia's research will maximize the extractable volume of gas while minimizing the environmental impact of surface disturbances associated with drilling and production. We are developing a system for comprehensive evaluation and modeling of the total gas system within a basin, focusing on problematic horizontal fluid-flow variability. This will be accomplished through extensive use of geophysical, core (rock sample), and outcrop data to interpret and predict directional flow and production trends. Side benefits will include a first-order approximation of probable carbon dioxide (CO_2) flow patterns during sequestration (injection and storage) of this greenhouse gas, and reduced environmental impact of drilling due to a reduced number of required wells for resource extraction.

We will accomplish these results through a cooperative and integrated systems approach involving industry, government, academia, and a multi-organizational team within Sandia. We will receive extensive core data, production data, maps, seismic data, coal desorption analyses, production analyses, and engineering studies, as well as equipment and staff for obtaining geophysical data and samples from industry.

Ultimately, this approach will provide innovative ideas and technologies to reduce the overall environmental impact of drilling. More importantly, the products of this research will not be location-specific, but can be extended to other areas of gas production throughout the Rocky Mountain area. Thus, this project has the potential to grow into a continuing program designed to solve problems associated with natural-gas production at developing sites or at old sites under redevelopment.

Ultimately, this approach will provide innovative ideas and technologies to reduce the overall environmental impact of drilling. More importantly, the products of this research will not be location-specific....

We made final interpretations of the geophysical logs that measure fractures and *in situ* stresses, concluding that the present-day maximum horizontal *in situ* stress trends normal to the majority of subsurface natural fractures in the basin. The local exceptions, where fractures and stresses are parallel, are poor candidates for drilling since hydraulic fractures would be ineffective and since the stresses would tend to close fracture apertures, as production causes pressure drawdown.

We interpreted these local exceptions to the common fracture and stress orientations to occur along north-south–trending wrench fault systems, observed in proprietary industry seismic lines, that were not recognized previously within the basin and that have only been inferred, not proven, to exist at the western basin margin.

In addition, the field data show that the background east-west fracture trends that are pervasive across the basin are significantly disrupted by the imposition of secondary fracture sets in the vicinity of local structures. These structures seem to have compound geologic histories, having apparently formed over blind thrusts that domed the overlying strata and deep-seated faults that provided access for laccolithic intrusions.

The tectonic modeling of the basin shows that the thick ductile layer, the Pierre shale, that underlies the reservoir strata of interest has a significant influence on the deformation behavior, which creates fracturing and controls stresses in the reservoir strata. We simulated the stress distributions and magnitudes in the reservoir strata during tectonic deformation and compared them to the observed fractures in outcrop and in the subsurface.

We modeled the differing mechanical properties of the different layers of strata and their different depths of burial across the basin to explain their different observed strain-accommodation responses. Conjugate fractures can be explained by deeper burial, where the overburden stress becomes a more significant part of the total stress, whereas vertical extension fractures are present in the same strata where they are less deeply buried and where the overburden stress is less. The puzzling simultaneous formation of igneous dikes (vertical, indicating a horizontal minimum stress) and sills (horizontal, indicating a vertical maximum stress) has been explained by the different mechanical properties of different layers of strata: Coals, in which the sills are found in most cases, have a high Poisson’s ratio. Thus, the depth at which the vertical overburden stress exceeds the horizontal stress in coals is significantly depressed, and sills can form in coals at the same time that dikes form in the related strata.

Geostatistical techniques have been used to assess the observed variations in production trends. In certain areas, there is an affinity in production characteristics between wells along northwest-southeast trends, meaning that new wells have a higher probability of being successful if drilled northwest or southeast of an existing good producer, or northeast or southwest of a poor producer. In other areas, the affinity between production characteristics of adjacent wells is poor in

all directions, implying a high degree of geological heterogeneity.

We can use these conclusions to plan for more efficient and more environmentally friendly well placements. Minimizing the number of poor producers decreases the number of well pads needed to be cut into the land while increasing the economic return of the play as well as the efficiency of resource recovery.

Other Communications

Arnold, B. W., J. M. Herrin, and P. M. Basinski. 2004. Statistical and geostatistical analyses of coal-bed methane production in the Raton Basin, New Mexico and Colorado. (Abstract) *Proc. American Association of Petroleum Geologists Annual Convention* (18 April, Dallas, Texas).

Basinski, P. M., and J. C. Lorenz. 2004. CBM geological overview, Southern Raton Basin, NM, and CO. *Houston Geological Society Bulletin* **15** (8 March, Houston, Texas): 5.

Cooper, S. P., P. M. Basinski, R. Larson, J. M. Herrin, R. G. Keefe, and J. C. Lorenz. 2004. Natural fracture patterns within the Raton Basin of Colorado and New Mexico. *AAPG Bulletin* **88** (supplement) (April, Dallas, Texas).

Cooper, S. P., W. A. Olsson, J. C. Lorenz, P. M. Basinski, R. Larson, J. M. Herrin, and R. G. Keefe. 2004. Controls on natural fracture variability in the southern Raton Basin of Colorado and New Mexico. *Abstracts AAPG Rocky Mountain Section Meeting* (10 August, Denver, Colorado).

Herrin, J. M., P. M. Basinski, J. C. Lorenz, S. P. Cooper, and R. Larson. 2004. Gas and water production trends of the Raton Basin coal-bed methane play, northeastern New Mexico. *Proc. Geological Society of America Annual Meeting, Program with Abstracts* (7 November, Denver, Colorado).

Herrin, J. M., P. M. Basinski, J. C. Lorenz, S. P. Cooper, C. A. Rautman, and B. A Arnold. 2003. Integrating geologic and hydrologic information to identify coal-bed methane sweet spots in the Southern Raton Basin, New Mexico. *Proc. American Association of Petroleum Geologists Mid-Continent Section Meeting* (12 October, Tulsa, Oklahoma).

Lorenz, J. C., S. P. Cooper, B. A. Arnold, J. M. Herrin, P. M. Basinski, and R. Larson. 2004. Geologic controls on coal-bed methane production domains within the southern Raton Basin of New Mexico. *Proc. Geological Society of America Annual Meeting, Program with Abstracts* (7 November, Denver, Colorado).

38665

Time-Domain Reflectometry for Remote, Real-Time Water-Quantity/-Quality Monitoring of Perennial and Ephemeral Streams

V. C. Tidwell, J. D. Roberts, L. M. Desonier, J. R. Brainard, D. S. Ruby

Thousands of acre-feet of water go unutilized in New Mexico every year because of inadequate stream gauging, costing the state millions in lost economic development. Sandia proposes time-domain reflectometry (TDR) as a remote, real-time method for monitoring the quantity and quality of perennial and ephemeral stream flows. TDR operates by propagating an electromagnetic pulse (EMP) down a transmission line while monitoring the returned signal. The pulse is susceptible to reflection by dielectric discontinuities (i.e., air-water and water-sediment interfaces) and attenuation by clays and salts. Thus, with one method, we can measure simultaneously, and at numerous locations across the channel, the depth of water, depth of scour, sediment load, and salinity.

Development of this monitoring system began in the laboratory where we conducted tests to evaluate, calibrate, and optimize the TDR sensor for this application. We conducted controlled experiments under static conditions using sand tanks and under simulated stream conditions using the Sediment Erosion Flume at Sandia-Carlsbad. We also designed, tested, and optimized a remote-monitoring package, including photovoltaic (PV)/battery power, telemetry, Web-based data management/visualization, and analysis software. In cooperation with the United States Geological Survey (USGS), we conducted field-testing of the full TDR monitoring package on two perennial rivers. One site was located on the Rio Grande near the Central Bridge in Albuquerque, New Mexico, while the other site was located on the Paria River near Lee's Ferry, Arizona.

Recent efforts focused on field-testing the TDR stream-monitoring system and evaluating the integrated sensor/power/data telemetry unit.

- *Field studies*. We established a permanent monitoring site on the Rio Grande in Albuquerque at the Central Bridge. This site corresponds to one of the USGS's permanent gauging stations. The installed instrumentation package consists of a TDR cable tester, multiplexer, data logger, cellular modem, and multiple probes. Power is supplied by a 75 W PV module, fitted with a sealed battery (4-day storage), charge controller, and

lightning arrester. This sensor package is interfaced with a material-monitoring system (MMS) for managing, storing, and analyzing the TDR data. Integrated into the MMS is the inverse modeling software for real-time, automated analysis of the TDR traces. Results from the MMS are available for display on the Web.

TDR monitoring of the Rio Grande proceeded continuously for 9 months. Hourly measurements included stream stage, aqueous conductivity, and channel depth at seven locations. To evaluate the accuracy of the TDR-monitoring system, we compared measured data to independently measured stream stage data by the USGS, continuous conductivity probe readings, and hand-measured channel depth. We found TDR stream-stage measurements to be within ± 0.88 cm of the USGS gauge; TDR conductivity was within ± 11% of conductivity probe measurements, while channel-depth measurements were within ± 0.36 cm of hand-measured depths. River-channel measurements also showed continuous movement of sand waves (10–16 cm amplitude with a 2–3 hr frequency) and sand bars (> 16 cm on > 2 month frequency) across the TDR probes. Such information can be used to continuously calculate the active bed load being conveyed downstream by the river under different flow regimes.

One deficiency identified with this sampling effort was the length of the TDR probes (16 cm). Longer probes are problematic because of their susceptibility to damage by floating debris and the susceptibility of signal attenuation by elevated conductivity levels in the river. To address this issue, we made efforts to design a probe that self-adjusts its position to optimally measure stream stage or channel depth. The probes have a measuring interval of 1 m and are pneumatically driven. The cost for such a system is comparable to that of a conventional stream-gauging unit.

We installed an additional TDR stream-gauging unit on the Paria River near Lee’s Ferry, Arizona, at a site that we established with the cooperation of the USGS. The instrumentation package is similar to that described above. Continuous operation of this unit has proceeded for 5 months, collecting data at 15 min intervals. At this site, we measured only stream stage and aqueous conductivity. We drew comparisons between the measured TDR data and independent USGS stream-stage data and conductivity-probe measurements. Results appear comparable to those given above. However, one difficulty encountered at this site has been the periodic silting in the probes and USGS gauge as the result of heavy storm flows.

Refereed

Tidwell, V. C., and J. R. Brainard. 2004. Laboratory evaluation of time-domain reflectometry for continuous monitoring of stream stage, channel profile, and aqueous conductivity. *Water Resources Research* (American Geophysical Union), submitted.

Other Communications

Brainard, J. R., V. C. Tidwell, and A. K. Coplen. 2003. Monitoring stream stage, sediment transport, and salinity with time-domain reflectometry. Paper presented at the Fall Meeting of the AGU, 9–13 December, San Francisco, California.

Tidwell, V. C., and J. R. Brainard. 2004. Laboratory evaluation of time-domain reflectometry for continuous monitoring of stream stage, channel profile, and aqueous conductivity. Sandia Technical Report SAND2004-5397, Sandia National Laboratories, Albuquerque, New Mexico.

Tidwell, V. C., and J. R. Brainard. 2003. Time-domain reflectometry as a continuous and real-time method for stream monitoring. Paper presented at the Sediment Monitoring Instrument and Analysis Research Workshop, Federal Interagency Subcommittee on Sedimentation, 9–11 September, Flagstaff, Arizona.

Young, C. A. and V. C. Tidwell. 2003. Breakout session 3: Bed material and bed topography data needs, uncertainty, and new technology. *Proc. Sediment Monitoring Instrument and Analysis Research Workshop, Federal Interagency Subcommittee on Sedimentation* **1** (9–11 September, Flagstaff, Arizona): 10–24.

38668

Functionalized Nanoelectrode Arrays for *In Situ* Identification and Quantification of Regulated Chemicals in Water

W. G. Yelton, K. B. Pfeifer, D. J. Muron, M. J. Kelly, W. Einfeld

Most chemical species that currently are regulated by the national water-quality standards, and other compounds, such as endocrine disrupters, that are under consideration for regulation, are redox-active species that can be identified and quantified by electrochemical techniques. Standard microelectrodes and even commercial nanoband electrodes require the addition of extra chemicals to condition the water before analysis and so are not useful for most real-time, in situ *sampling. They require trained personnel and cannot be used either for distributed remote analysis in a water system or in a dipstick mode for on-site testing of drinking water. An array of suitably functionalized nanoelectrodes could be incorporated into a small, integrated sensor system that can identify many species rapidly and simultaneously under field conditions without chemical addition with signal-to-noise ratios (SNRs) up to 103-fold greater than conventional electrodes. Sandia will investigate the use of functionalized nanoelectrodes as a sensor-array system for rapid, noncontaminating field analysis. The self-assembled template for these arrays will consist of conducting nanoelectrodes, whose diameter, length, and surface-area density can be systematically controlled. Chemical selectivity can be provided by chemical alteration of the metal nanoelectrode surfaces. Electrochemical deposition of a range of different metals to functionalize the nanoelectrodes will produce different current/voltage relationships from electrode elements in the array as the analytes of interest are subjected to electrochemical analysis. Enhanced selectivity and sensitivity for specific metals, such as heavy-metal industrial pollutants and radioactive nuclides, can be conferred by electrodeposition of thin organic conducting polymers containing functional groups, such as crown ethers, that selectively bind and preconcentrate the metals of interest for redox sampling.*

- *Determined detection parameters and characteristics of lead (Pb2+) in water.* We used several nanoelectrode designs in this study to determine the greatest sensitivity for a target analyst; we focused mainly on the silver (Ag) working electrode and the Ag quasi-reference (AgQRE) electrode. Through a series of experiments, we found that Ag is much more effective when testing for limits of detection of Pb2+. For

the detection analysis, we used subtractive anodic stripping voltammetry (SASV). We created a two-electrode system using an Ag working electrode and an AgQRE electrode where we utilized Ag mesh as the counter electrode. With low levels of conductive salt, we were unable to detect Pb2+ in the range of 5 nM to 35 nM.

- *Developed high-speed transient potentiostat for high-density nanoelectrode arrays*. We developed a small, portable, high-speed transient potentiostat that can measure the current from nanoelectrode arrays with a time resolution on the order of microseconds. The device has 21 control functions and can be demonstrated in the "slow" mode for cyclic voltammetry and SASV, or in the "fast" mode for transient measurements. We demonstrated the system in the cyclic voltammetry and SASV modes and found favorable comparison to commercial hardware. We performed calibrations to allow conversion between internal hex values and real voltages from the system. We described the system architecture and the "firmware" in the system controller along with the control functions. We developed actual nanoelectrode arrays (200 nm Ag electrodes, 10 µm pit) using a 0.5 mM Pb2+, 10 mM potassium chloride (KCl) solution, with no agitation and a sampling head and potentiostat; they are complete and show promising results.

A major advantage of employing an array of nanoelectrode ensembles is the selectivity for high-priority analytes that can be realized by chemical modification of the nanoelectrode surfaces. We can chemically treat individual nanoelectrode elements within an array to provide a working electrode surface with enhanced specificity and sensitivity for priority-analyte processes that permit measurements of Pb2+, As3+, and As5+ ionic species in water sources.

The goals of this project required the development of nanoelectrodes that permit measurement of electroactive species in high-resistivity water, i.e., without adding chemicals to increase conductivity. In a standard cell configuration where a counter electrode is placed far from the working (nano) electrodes, our analysis required lower-than-standard additions of conductive salts; but in an analysis using a "sandwich" nanoelectrode design, the ohmic drop between electrodes was extremely minute, allowing analysis without conductive salts. Most of our standardizing for an analytical protocol first involved the use of commercial electrodes with the same geometric area as our nanoelectrode arrays. This work progressed to the nanoelectrode array for both the 1.4 µm- and the 10 µm-spaced electrodes. The biggest problem we had using these arrays was the polymethylmethacrylate (PMMA) polymer

We developed a small, portable, high-speed transient potentiostat that can measure the current from nanoelectrode arrays with a time resolution on the order of microseconds.

insulator film that swelled and delaminated during some of the study. We based our selection of PMMA as the insulating layer on its nature as a lithographic material that would permit pattern processing. To engineer more reliability and continued use into the arrays, the insulator should be patterned from a robust oxide that would allow physical polishing or cleaning at high potentials that impacted the weakly adherent polymer films. Chemically functionalized films would require replacement after fouling or stripping and reapplication of a fresh film.

38673

Water Desalination

T. E. Hinkebein, M. L. Phillips, D. L. Moore, J. D. Pless, J. L. Krumhansl, L. Evans, J. E. Miller, J. A. Voigt, T. M. Nenoff

Sandia's research in this project will use a combination of forward osmosis (FO) and precipitation to treat seawater. The selection of a "designer" solute for the osmosis process would allow the process to focus on the removal of salt rather than on the removal of water. The resulting process has the potential for significant cost savings. The new perspective for the water desalination and purification team focuses on the removal of salt from saline waters through the use of FO and a designer solute. By focusing on the use of FO to remove salt from the water, two important drawbacks associated with reverse osmosis (RO) may be avoided: high-pressure costs and membrane fouling. The FO process is predicated on the identification of a designer solute. This material must provide a high osmotic potential and be compatible with the chosen membrane. The membrane for our process must meet three criteria. It must be nonreactive with the osmotic agent; it must be stable at the temperature of the osmotic agent; and the flux across the membrane must be maximized, preferably with near-100% selectivity.

We developed a novel method/process for an energy-efficient, environmentally friendly method for desalinating inland brackish waters.

This project examined two novel methods for desalinating water: an FO process and an ionic sequestration process. The need for fresh water has increased exponentially during the last several decades due to the continual growth of human population and industrial and agricultural activities. Yet existing resources are limited or of lower quality. This unfavorable situation requires the development of new, long-term strategies and alternative technologies for desalination of saline waters.

We developed a novel method/process for an energy-efficient, environmentally friendly method for desalinating inland brackish waters. This process can be applied to either groundwater or produced waters (i.e., coal-bed methane–produced waters). Using a set of ion-exchange and sorption materials, our process effectively removes anions and cations in separate steps. We chose the ion-exchange materials because of their specific selectivity for ions of interest and for their ability to work in the temperature and pH regions necessary for cost and energy effectiveness.

For anion exchange, we focused on hydrotalcite, layered clay. For cation exchange, we developed an amorphous silica material that has enhanced cation (in particular for Na+)

selectivity. In the case of produced waters with high concentrations of Ca_2+, we included a lime-softening step.

We based the FO project on the premise that a "designer" solute in combination with an osmotic membrane could customize an aqueous stream to allow for ultra-energy-efficient desalination. We found that the process is mechanically feasible, but is unlikely to result in significant cost savings except under very specific circumstances involving highly fouling feed streams or very concentrated brine feeds. This process may also have application in settings where lower-quality waste heat is available.

We adapted and used a cost model to evaluate the economics of these processes. Benchmark costs for brackish-water reverse osmosis (BWRO) were $0.70 to $2.65 per 1000 gal (gallons) of treated brackish water, varying system size, pretreatment and disposal options, etc. An increase in unit water cost of up to $3/kgal may be required in cases where zero discharge is the only option for disposal.

We used the Water Treatment Estimation Routine, WaTER, developed by the U.S. Department of the Interior, Bureau of Reclamation, to develop cost estimates for a BWRO system using conventional RO technology, the FO process, and the DESAL® process. The estimated water cost of $1.16/kgal generated by the WaTER program for a BWRO system with high (95%) recovery is within the reported range of cost for BWRO systems. The cost analysis of the FO process using RO as the separation step clearly indicates a doubling in water cost over that of the BWRO results ($2.22/kgal versus $1.16/kgal). The cost for using FO as a pretreatment alone is about $0.60/kgal. This was due primarily to the low water flux of 6 gal./ft^2/day used for analyzing the FO system. If the FO flux is increased to 10 gal/ft^2/day (17 l/m^2/hr), the unit water cost drops to about $0.44/kgal.

For the ionic sequestration approach, the analysis revealed that discarding resin rather than regenerating resin is more expensive. Conventional chemical regeneration costs about $3.75/kgal. Thermal regeneration and reuse of resin is not well characterized, but we developed an optimistic cost estimate of $2.34/kgal. Not included in this estimate are additional manufacturing costs, resin handling during the thermal regeneration step, and any possible cost benefit for recycling of waste streams. A possible alternative approach that would yield lower costs is thermal regeneration with hot water at temperatures of 100°C or less. Experimental work is required to determine the validity of this approach for the ion exchangers developed under this project.

Other Communications

Pless, J. D., J. L. Krumhansl, J. A. Voigt, D. L. Moore, M. L. Phillips, A. Sattler, and T. M. Nenoff. 2004. Desalination of brackish ground waters and produced waters using *in situ* precipitation. Sandia Technical Report SAND2004-3908, Sandia National Laboratories, Albuquerque, New Mexico.

Pless, J. D., J. L. Krumhansl, J. A. Voigt, D. L. Moore, M. L. Phillips, and T. M. Nenoff. 2004. Synthesis and characterization of ion-exchange materials for the desalination of brackish waters. Paper presented at the 228th ACS National Meeting, 22–26 August, Philadelphia, Pennsylvania.

Pless, J. D., J. L. Krumhansl, J. A. Voigt, D. L. Moore, M. L. Phillips, A. Sattler, and T. M. Nenoff. 2004. Desalination of brackish waters using ion-exchange media. Paper presented at the 228th ACS National Meeting, 22–26 August, Philadelphia, Pennsylvania.

38674

Revolutionary Systems for Catalytic Combustion and Diesel Catalytic Particulate Traps

J. Cesarano, III, R. M. Ferrizz, P. O. Witze, J. N. Stuecker, J. E. Miller

Diesel-particulate emission (soot) is a global problem, but current technologies for meeting looming regulations are costly and failure-prone. NOx (oxides of nitrogen) formation from methane combustion in electric-power plants is also an environmental concern, but materials and catalyst reliability issues have prevented the application of catalytic combustors that circumvent NOx formation. Sandia seeks to utilize a commercially viable, scalable, direct ceramic fabrication technique as a basis for creating revolutionary systems for diesel-particulate trapping and destruction and for catalytic methane combustion. Traditional fabrication techniques are limited to producing "honeycomb"-structured extrudates and foams. Our technique is not only more flexible in terms of the shape of the ceramic product, but it also allows a broader range of materials (and catalysts) to be used.

Our design is a three-dimensional (3-D) cross-hatched mesh, formed from alternating layers of precisely spaced rods, similar to "Lincoln logs." Direct fabrication inherently ensures that the rods meld together and form a strong bond upon sintering. The sintered meshes will have controlled porosity in three dimensions, but no line-of-sight pathways. This macrostructure ensures adequate tortuosity and a high surface-to-volume ratio while maintaining predictable permeability and low-pressure drop. The incorporation of, or fabrication from, a catalytically active material will allow efficient combustion of methane without NOx formation. Similarly, the structures will trap soot particles that will then be catalytically combusted, thereby extending the life of the trap indefinitely.

Research challenges include efficient particle trapping with low-pressure drop, catalyst design for severe combustion environments, mechanical and chemical stability, flow and filtration simulation for optimizing designs, and real-time performance characterization. Our expertise in ceramic processing, catalysis, engine diagnostics, and modeling uniquely positions us to overcome these challenges to create "real-world" systems with broad impact in clean-energy utilization.

Sandia seeks to utilize a commercially viable, scalable, direct ceramic fabrication technique as a basis for creating revolutionary systems for diesel-particulate trapping and destruction and for catalytic methane combustion.

Work focused on demonstrating the usefulness of our lattice supports for catalytic reactions and for development of

materials and structures for self-regenerating diesel particulate traps. We successfully demonstrated the usefulness of advanced catalytic reactors and also succeeded in demonstrating the individual components necessary for a self-regenerating diesel-particulate trap. The project ended before a completely assembled prototype device could be tested. We submitted four patent applications. This project was selected by Sandia as an "LDRD Success Story," included in the "Sandia National Laboratories OVERVIEW" brochure, and highlighted as a cover story for the magazine *TechComm*, a publication of the Technology Ventures Corporation.

This project was selected by Sandia as an "LDRD Success Story," included in the "Sandia National Laboratories OVERVIEW" brochure, and highlighted as a cover story for the magazine TechComm, *a publication of the Technology Ventures Corporation.*

- *Catalytic reactions*. Data acquired previously proved that supports made with our Robocast lattice geometry improve catalyst performance by increasing turbulent flow and improving mass transfer of the reactants to the catalytic reaction sites. In recent work, we developed catalysts and supports for two potentially important reactions. We developed iron (Fe)/potassium (K) catalysts, applied them to our lattices, and used them to demonstrate their effectiveness for the dehydrogenation of butene. This important reaction is used to produce synthetic rubber. This reaction is exothermic and can be problematic because "hot spots" can develop within the reactor. Our lattice supports demonstrated the ability to dissipate heat quickly to maintain temperature uniformity throughout the reactor. We also developed lattice supports with nickel (Ni) luminate and demonstrated their utility in the extremely important "syngas" reaction that produces carbon monoxide (CO) hydrogen from methane. These by-products are used in everything from diesel fuel to plastics. Current approaches to the production of syngas use noble metal- or Ni-containing catalysts. These materials deactivate at high temperatures and over time and have a tendency to form reaction-inhibiting coke. Our Ni-hexaaluminate lattices proved to inhibit the formation of coke and remain stable, even at temperatures greater than 800°C.
- *Diesel-particulate traps*. Our goal was to develop materials and methods for trapping soot from an exhaust stream with a lattice structure that also was catalytically active on its surface. The idea is to catalytically combust the soot into carbon dioxide (CO_2) and water as soon as the lattice traps the soot particles. In principle, there would be no need to replace the trap because it would be self-cleaning. Part 1 of this endeavor was to develop a catalyst that can combust soot at temperatures less than 400°C. We developed a cesium (Cs)-vanadate (V) material that may be useful; however, the presence of V in exhaust streams may not be environmentally desirable. Therefore, we developed an alternative Cs/copper (Cu)/

molybdenum (Mo) material and showed it to combust soot at 330°C in preliminary tests.

In parallel, we developed materials and processes for fabricating lattice traps that are electrically resistive and can be electrically heated to temperatures as high as 800°C. We successfully developed silicon carbide (SiC) lattices and zirconia/metal composites. Preliminary diagnostic testing indicates that our lattices may be able to trap submicron soot particles, even though the spacing between the rods is several hundred microns. This result seems to substantiate our original hypothesis proposed at the beginning of this project. The next step is to apply the appropriate catalyst to our electrically heated lattices, assemble the device into a prototype package, and test the prototype on a diesel engine with diagnostics for capture efficiency and pressure drop. This test remains to be completed.

- *Spin-offs related to lattices*. We implemented collaborations with the City of Albuquerque Transportation Department and Caterpillar, Inc., for testing materials and trap performance in city buses and on diagnostic diesel engines. A collaboration with the University of Illinois to study the usefulness of our lattices as biomedical bone scaffolding is ongoing.

Refereed

Ferrizz, R. M., J. N. Stuecker, J. E. Miller, and J. Cesarano. 2004. Monolithic supports with unique geometries and enhanced mass transfer. *Industrial and Engineering Chemistry Research*, accepted.

Stuecker, J. N., J. Cesarano, J. E. Miller, R. M. Ferrizz, and J. E. Mudd. 2004. Advanced support structures for enhanced catalytic activity. *Industrial and Engineering Chemistry Research* **43**:51–55.

Other Communications

Cesarano, J., J. N. Stuecker, D. D. Gill, and M. P. Saavedra. 2003. Robocasted lattices for porous bone scaffolds: A case study. Paper presented at the Pacific Coast Meeting of the American Ceramic Society, October, Oakland, California.

Ferrizz, R. M., J. E. Miller, J. Cesarano, and J. N. Stuecker. 2003. Monolithic supports with unique geometries and enhanced mass transfer. Paper presented at NLCat 2003, Oak Ridge, Tennessee.

Ferrizz, R. M., J. N. Stuecker, J. Cesarano, and J. E. Miller. 2004. Monolithic supports with unique geometries and enhanced mass transfer. Sandia Technical Report SAND2004-0152, Sandia National Laboratories, Albuquerque, New Mexico.

Stuecker, J. N., R. M. Ferrizz, J. E. Miller, and J. Cesarano. 2004. Application of Robocast monoliths to catalyst systems. Paper presented at the Symposium of the Western States Catalysis Club, February, Provo, Utah.

Stuecker, J. N., R. M. Ferrizz, J. E. Miller, L. R. Evans, and J. Cesarano. 2004. Robocast monoliths for catalyst supporters and diesel particulate traps. Paper presented at the Exposition on Advanced Ceramics and Composites, January, Cocoa Beach, Florida.

38677

Potential Application of Microsensor Technology in Radioactive-Waste Management—With Emphasis on Headspace Gas Detection

Y. Wang, H. Gao, M. L. Thomas, R. C. Hughes, P. I. Pohl, C. K. Ho, C. R. Bryan

Measurements of headspace gas in waste containers or in waste-disposal facilities are generally required for the demonstration of compliance with the Resource Conservation and Recovery Act (RCRA) or transportation requirements, as well as for an operational safety concern. The existing methods for such measurements are time-consuming and expensive and increase workers' exposure to hazardous environments. Therefore, a reliable, real-time, in situ *gas-detection technique is highly desirable. Sandia-developed H_2 and volatile organic compound (VOC) microsensors are expected to have a wide range of applications in radioactive-waste management. This project focused on (1) testing the long-term stability of both H_2 and VOC microsensors and making necessary improvements, (2) optimizing the ability of VOC microsensors for the discrimination of individual VOCs that are present in transuranic wastes, and (3) studying the feasibility of using microsensors as a screening tool to discriminate two populations of waste drums according to a prespecified total VOC concentration limit.*

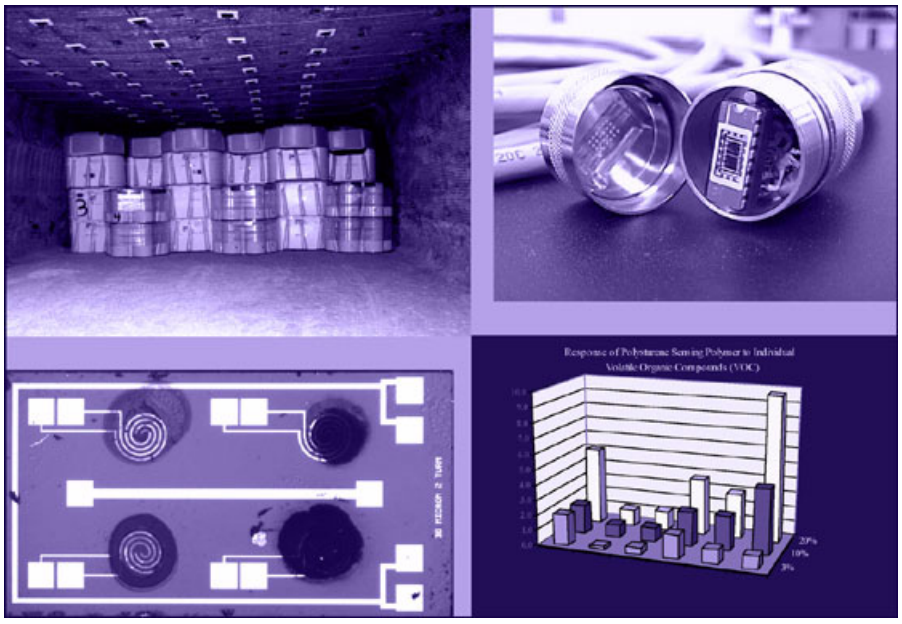

Waste characterization is a costly part of radioactive-waste management. Polymer-based microsensors developed in this project allow us to have real-time and in situ *monitoring of volatile organic compounds (VOCs) in radioactive wastes.* (a) *Transuranic wastes disposed in the Waste Isolation Pilot Plant in Southern New Mexico, which requires extensive measurements of VOCs in waste-container headspace.* (b) *Microsensor package.* (c) *Conductive sensing polymer films deposited onto a microfabricated circuit.* (d) *Differential responses of a sensor polymer to different VOCs.*

Waste characterization is probably the most costly part of radioactive-waste management. An important part of this characterization is the measurement of headspace gas in waste containers to demonstrate the compliance with RCRA or transportation requirements. The traditional chemical-analysis methods, which include all steps of gas sampling, sample shipment, and laboratory analysis, are expensive and time-consuming, and increase workers' exposure to hazardous environments. Therefore, an alternative technique that can provide quick, *in situ*, real-time detections of headspace gas compositions is highly desirable. The objective of this project is to bridge the technical gap between the current status of microsensor development and the intended applications of these sensors in nuclear-waste management. The major results are summarized below:

- We conducted a literature review on the regulatory requirements for headspace gas sampling/analysis in waste characterization and monitoring. We identified the most relevant gaseous species and the related physiochemical environments. We found that preconcentrators might be needed for chemiresistor sensors to meet desired detection limits.
- We conducted a long-term stability test for a polymer-based chemiresistor sensor array. We observed significant drifts over the time duration of one month. Such drifts should be taken into account for long-term *in situ* monitoring.
- We explored several techniques to improve the performance of sensor polymers. We demonstrated that freeze deposition of black carbon (BC)-polymer composite can effectively eliminate the so-called "coffee ring" effect and lead to a desirable uniform distribution of BC particles in sensing polymer films. We determined the optimal ratio of BC/polymer. We showed that ultraviolet (UV) irradiation improves sensor sensitivity.
- From a large set of commercially available polymers, we selected five polymers to form a sensor array that was able to provide optimal responses to six target VOCs. We performed a series of tests on the response of the sensor array to various VOC concentrations. We observed linear sensor responses over the tested concentration ranges, although the responses over a whole concentration range are generally nonlinear.
- We developed inverse models for identifying individual VOCs based on sensor-array responses. A linear solvation energy model is particularly promising for identifying an unknown VOC in a single-component system. We demonstrated that a sensor array such as the one we developed is able to discriminate waste containers for their total VOC

We demonstrated that a sensor array such as the one we developed is able to discriminate waste containers for their total VOC concentrations and therefore can be used as a screening tool for reducing the existing headspace gas-sampling rate.

concentrations and therefore can be used as a screening tool for reducing the existing headspace gas-sampling rate.

- We fabricated various VOC preconcentrators using Carboxen 1000 as an absorbent. We conducted extensive tests to obtain optimal configurations and parameter ranges for preconcentrator performance. We showed that use of preconcentrators can reduce the detection limits of chemiresistors by 2 orders of magnitude. We also evaluated the life span of preconcentrators under various physiochemical conditions.
- We evaluated the performance of palladium (Pd) film–based H_2 sensors in the presence of VOCs. We observed the interference of sensor readings by VOCs, which can be attributed to the interference of VOCs with the H_2-O_2 reaction on the Pd alloy surface. This interference can be eliminated by coating a layer of silicon dioxide (SiO_2) on a sensing film surface.

Our work demonstrated a wide range of applications of gas microsensors in radioactive-waste management. Such applications can potentially lead to a significant cost saving and risk reduction for waste characterization.

Our work demonstrated a wide range of applications of gas microsensors in radioactive-waste management. Such applications can potentially lead to a significant cost saving and risk reduction for waste characterization.

52591

Beyond Nanoparticles—Attack on a Chemical "Holy Grail"

R. A. Kemp, J. E. Miller, J. T. Moore

One of the "Holy Grails" set by the Department of Energy in energy-related catalysis chemistry is the direct and selective partial oxidation of hydrocarbons (HCs) using molecular oxygen rather than expensive alternatives such as peroxides or nitrous oxide (N_2O). A key commodity chemical produced in ~ 12 billion lb/yr capacity is propylene oxide (PO). PO is currently produced by multistep processes that use environmentally unfriendly reagents or produce co-products. We seek to expand Sandia's technical base and expertise by attacking this problem by use of homogeneous catalysis. Molecular-level control of catalysts is the ultimate in catalyst design—despite years of effort in industry and academics, no heterogeneous catalyst system has yet directly produced PO in high-enough conversion and selectivity to be commercially implemented. One key feature of this project is the design of a catalytic cycle in which each step of the cycle has literature precedent using middle-to-late transition metals. However, combining these assorted reactions into a rational catalytic cycle will require the correct combination of metals and ligands. If we are successful, the potential impact on both Sandia's scientific reputation and licensing revenues could be enormous—there are many examples of commercially produced, partially oxidized organic products. However, the most significant impact if we are successful would be in energy savings due to the improved efficiencies of partial-oxidation processes, as well as the learnings that might be applied to other partial-oxidation routes. Our success will significantly enhance Sandia's expertise and experience in catalysis.

If we are successful, the potential impact on both Sandia's scientific reputation and licensing revenues could be enormous...[T]he most significant impact ...would be in energy savings due to the improved efficiencies of partial-oxidation processes....

Recent accomplishments focused mainly on synthetic chemistry. We made tremendous progress in developing models of the fundamental steps in our proposed catalytic cycle to convert propylene to PO. It appears that we are on the right track in identifying the proper metals and ligands that will accomplish this important transformation. To arrive at an optimal catalyst system more quickly, we took the approach of focusing synthetic efforts on two ligand systems: the pincer-type ligand coordinated to late-transition metals, and the salen-type ligand coordinated to middle-late metals. We prepared a wide variety of pincer-type ligands that contain –PR2 groups, -NR2 groups, -SR2, and –OPR2 groups. Changing these groups

and attaching to the metals allowed us the opportunity to understand which ligand systems will allow the metal hydrides to add oxygen to form metal hydroperoxides. We also changed the sizes of the R groups attached. We developed procedures to follow these oxygen-insertion reactions by solution nuclear magnetic resonance (NMR), either at atmospheric pressure or at higher pressures. We synthesized late-transition metal hydrides (Pd, Pt) using the pincer ligands. Oxygenated products were formed, and we are in the midst of determining the selectivity to desired products. A graduate student at Washington State University has been working on this project, examining the individual steps in the catalytic cycle, including the insertion reactions of CO into metal-hydroxide bond to form metal-acid complexes. We also prepared a large number of complexes using the salen ligand system with middle, first-row transition metals. These complexes can be diamagnetic or paramagnetic, depending on the metal used. We believe we have synthesized a (salen)Co-H complex; however, the reaction with oxygen is not clean. This led us to believe that the better systems with salen may be the second- and third-row metals, due to stronger metal-H bonds, allowing for more selective reactions to occur. We believe strongly that we are well on track for understanding all of the individual steps in our proposed catalytic mechanism.

Our accomplishments in the late-transition metals–pincer ligands include the following:

(1) Prepared (pincer)Pd-H complexes that directly insert O_2 to form hydroperoxides,

(2) Reacted these complexes with O acceptors, such as olefins like cyclohexene, or with R3P, and observed O atom transfer,

(3) Observed the insertion of CO into a (pincer)Pd-OH species to yield an acid complex (as opposed to a formyl complex), and

(4) Observed the decarboxylation of the (pincer)Pd-COOH complex to liberate CO_2.

We concentrated more on the pincer complexes of the late-transition metals due to the promising results seen in recent work. We anticipate that most of the future work, as well, will be done with these complexes, although we will continue to investigate the salen ligand system.

Refereed

Smythe, N. A., K. L. Cetto, K. I. Goldberg, and R. A. Kemp. 2004. Insertion of O_2 into a Pd-H bond to form a stable Pd-OOH complex. *Organometallics*, submitted.

Other Communications

Moore, J. T., K. I. Goldberg, and R. A. Kemp. 2004. Synthesis of homogeneous olefin epoxidation catalysts. Paper presented at the 227th National Meeting of the American Chemical Society, 28 March–1 April, Anaheim, California.

52592

Advanced Proton-Exchange Materials for Energy-Efficient Fuel Cells

C. J. Cornelius, M. R. Hibbs, C. H. Fujimoto, G. S. Grest, D. Ingersoll

The goal of this project is to utilize modeling and experiments to design novel proton-exchange membrane (PEM) materials (that require little to no water for proton conduction. Achieving this goal would enable fuel-cell operation to potentially reach an operating temperature of 200ºC. The technical approach being utilized is to alternate block copolymers containing acid and base functionality to force self-assembly that should be more proton-conductive. Additionally, these links are to provide additional mechanical integrity, while modeling will provide molecular insight for understanding how to potentially improve this PEM system. Additional work included the development of a novel polymer electrolyte for inclusion and replacement of Nafion® within anode and cathode electrodes. These intrinsically microporous poly(arylene-ether) ladder polymers provide a route to control the permeability of hydrogen, oxygen, water, and electrons within a membrane electrode assembly (MEA) while simultaneously reducing the interfacial resistance created from bonding the catalyst layer to the PEM. These materials are based on 3,3,3',3'-tetramethyl-1,1"-spirobisindane-5,5',6,6'-tetrol (3MSBIT) and 2,3,5,6-tetrafluorophthalonitrile (4FPN) that we synthesized and characterized in our labs.

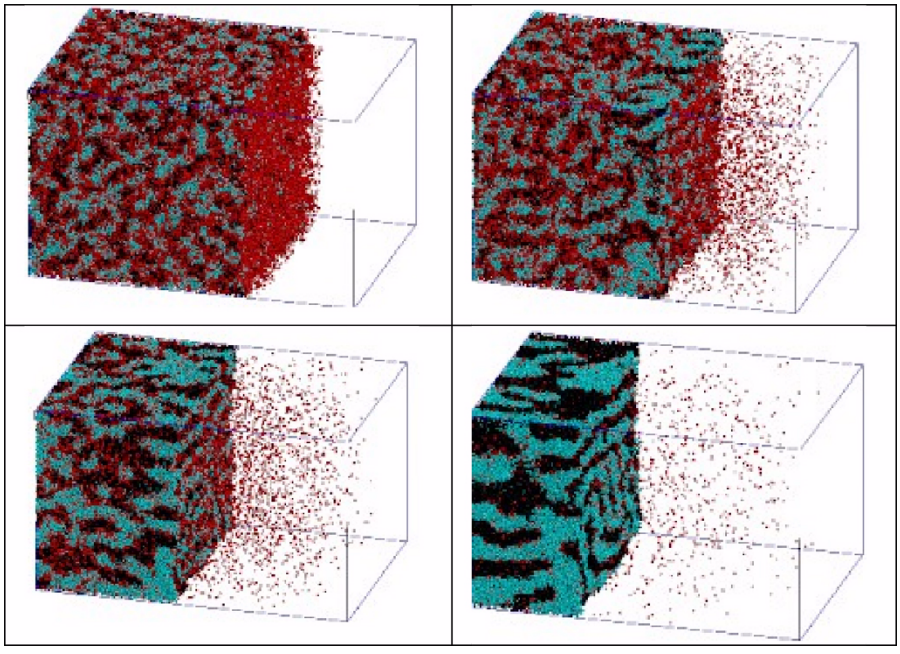

Perspective view of the evaporation process. The four figures are before evaporation, and after 30%, 60%, and 92% of the solvent has been evaporated.

The decomposition temperature of this ladder polymer was 490ºC at 5 wt.% weight loss, a glass-transition temperature (Tg) of 390ºC, and a surface area of > 700 m^2/g, which are good basic properties of the parent material. Additional studies evaluating the ideal permselectivity for O_2/N_2, CO_2/CH_4, H_2/CH_4 reveal that this polymer has properties that exceed the upper-bound separation characteristics observed for glassy and rubbery polymers. This suggests that these may be used as highly permeable and selective H_2/CH_4 membranes, and the high H_2 solubility in these materials warrants investigation as a possible H_2 storage material.

Characterization of first-generation materials is nearly complete, and we currently are making second-generation materials. We developed testing equipment to evaluate the proton conductivity of PEM materials at high temperatures, acquired a fuel-cell test station for testing PEM materials in a hydrogen and methanol fuel cell, and established a collaboration with Clemson University to understand PEM structure-property relationships via small-angle neutron scattering (SANS) and small-angle x-ray scattering (SAXS). We added morphology characterization using atomic-force microscopy (AFM) and transmission-electron microscopy (TEM) as new tasks to assist in the understanding of observed microphase separation and predicted systems. We continued efforts for the synthesis, characterization, and testing of high-temperature PEM materials at elevated temperatures. Additional discoveries include the role of interfacial resistance in the MEA on power production in non-Nafion®-based PEM, and ways to reduce this interfacial resistance utilizing non-Nafion®-based inks used in the electrode. We developed and are pursuing a new family of microporous polymers to reduce the interfacial resistance while simultaneously increasing oxygen, water, and hydrogen transport within the electrode composite that consists of ionomer and platinum (Pt) catalyst. This new electrolyte may be enabling for other non-Nafion®-based PEM materials.

Refereed

Hibbs, M. R., and C. J. Cornelius. 2004. Sulfonated random and block copolyimides. Paper presented at the Electrochemical Society Meeting, October, Honolulu, Hawaii.

Tsige, M., and G. S. Grest. 2004. Molecular dynamics simulation of solvent-polymer interdiffusion: Fickian diffusion. *J. Chemical Physics* **120** (6) (February): 2989–95.

Tsige, M., and G. S. Grest. 2004. Molecular dynamics study of the evaporation process in polymer films. *Macromolecules* **37** (12): 4333–35.

52593

Alanate-Hydride Fuel-Cell Demonstration Project

K. J. Gross, D. E. Dedrick, J. P. Chan, S. Spangler, M. P. Kanouff, K. D. Stewart

An entirely new class of light-weight reversible hydrides was recently discovered—the alanates. These titanium (Ti)-doped sodium aluminum hydride ($NaAlH_4$) materials have reversible hydrogen (H)-storage capacities of up to 5 wt.%, making them nearly 4x lighter than commercial metal hydrides. For this reason, they have been considered a breakthrough for the onboard H storage for fuel-cell vehicles. This project is the first to demonstrate the use of alanates for the generation of electrical power and the first demonstration of a hydride-powered, high-temperature, proton-exchange membrane (PEM) fuel cell. Because the kinetics of H uptake and release by the alanate improves with elevated temperatures, Sandia tested several novel concepts to develop a stand-alone power system. A major focus of this work was on the modeling, design, construction, and testing of an integrated fuel-cell/H-storage system that eliminates the need of complicated heat-transfer systems and media. After extensive modeling efforts, we built a proof-of-concept system that employs integrated fuel-cell stack and hydride beds that balance the generation of fuel-cell-waste heat with the endothermic release of H from the alanates.

This project is the first to demonstrate the use of alanates for the generation of electrical power and the first demonstration of a hydride-powered, high-temperature, proton-exchange membrane (PEM) fuel cell....We performed experiments on this system, and results surpassed our expectations.

This project successfully met its goals, which entailed demonstrating a proof of concept and entirely new approach to electrical-power systems through the integration of a fuel cell with the H-storage system. To our knowledge, this was the first demonstration of any fuel cell running on H from alanates. We successfully completed the following tasks:

(1) *Novel integrated approach to system thermal balance*. We used a unique engineering design based on integrating fuel-cell stacks with hydride-storage beds to develop an autonomous power-delivery system.

(a) We used a total-system model that incorporated fuel-cell-waste heat generation, composite-hydride desorption enthalpies, and system thermal conductivities to design a composite hydride system that was thermally matched with a high-temperature fuel cell.

(b) We used the results of the modeling to construct a proof-of-concept demonstration system.

(c) We performed experiments on this system, and results surpassed our expectations. The high-temperature PEM fuel-

cell stack ran for more than an hour on H generated from the integrated alanate H-storage system.

(2) *Modeling of heat and power generation for a typical demand cycle*.

(a) We investigated modeling of the power-demand cycles for typical applications as an initial step to determine an appropriate size of the demonstration system.

(b) We tested and modeled a commercial fuel cell (1000 W).

(c) This modeling helped to define the operable pressure and temperature ranges of the H-storage materials as well as the waste-heat requirements to provide a steady generation of H.

(3) *Composite hydrides for cold start-up*.

(a) We used the Sandia database of the thermodynamic properties of classic hydrides to evaluate and select the best interstitial hydride to be used in combination with the alanates.

(b) We measured absorption and desorption rates for the composite materials.

(c) We incorporated these data, combined with the thermodynamic data from the first task, into a system model to proportion the hydrides versus alanates. We determined an optimum combination for this pilot system to be a mass ratio of 1.0 traditional hydride mass unit to 1.8 alanate mass units. This would provide us with 10–20 min of start-up time.

(4) *Kinetics designed for rapid fill*. We evaluated the use of composite materials for rapid fill as well as for cold start-up. Heat released from the low-temperature hydride increases the temperature of the system, improving the kinetics of absorption of the high-temperature hydride. Experimental work confirmed our assumption that the recharging rate could be enhanced by using the two materials, but only when the materials are in separate gas-handling sections of the same bed. This allows for the necessary benefit of heat transfer while independently maintaining control of the charge state of each material.

(5) *H-power milestone*. The final product was a fully integrated set of the composite alanate-hydride beds and fuel-cell stack.

(a) This system is intended to simulate a stand-alone “power-pack” for a variety of portable power applications.

(b) We designed the test unit, which is available to test more advanced complex hydrides, amides, and other H-storage materials as they become available.

Because this is an entirely new regime of temperatures, pressures, and operating configuration for the fuel-cell system as we know it, there is a great amount of learning, innovation, and advancements in performance that will be generated from future work on this novel integrated system approach. We

believe that a working experimental/demonstration platform is needed to address the many questions and state-of-the-art concepts that this new technology will generate. Sandia and its partners are in a unique position to move forward quickly with scientific and technical developments that this demonstration has proven possible.

52595

Real-Time Discriminatory Sensors for Water-Contamination Events

P. R. Lewis, D. R. Adkins, A. Robinson, C. D. Mowry, R. P. Manginell, W. Einfeld, D. R. Wheeler, S. M. Dirk, K. S. Rawlinson

America's water-distribution systems are vulnerable to contamination through either malicious intent or accidental events. Online methods such as free available chlorine, total organic carbon, and conductivity sensors can quickly determine state changes in the system (assuming good baseline information is available). However, current methods of organic sample collection/analysis are costly, slow, and useful primarily for imposition of fines, not for the protection of consumers. Mitigation steps need to be performed immediately following detection of contaminants in the water system, not days or weeks after the sample is collected. Sensors that identify specific contaminants would allow water-system operators options to address the problem by suspending water flow in the parts of the system where contamination has been detected. Real-time identification of the contaminant(s) would be helpful in determining effective mitigation methods and procedures, as well as in providing timely notification of the water-utility customers. The gas-phase μChemLab™ developed by Sandia can detect volatile organic carbons (VOCs) and semivolatile organic carbons (SVOCs) via gas-phase sampling. This unique Sandia-developed detection system has uses for cost-efficient determination of environmental contaminants such as toxic industrial compounds (TICs), as well as for chemical contaminants that might be introduced through malevolent anthropomorphic actions. We will adapt this versatile device for use as a small-footprint, low-cost, reliable, sensitive, and quickly deployable water sensor. We demonstrated purge and trap (P&T) as well as solid-phase microextraction (SPME) in proof-of-principle experiments with this device with contaminants of regulatory concern. We also analyzed chemical weapon (CW) hydrolysis products. Required changes to the system would include sizing to meet the required form factor, a front-end condensed-phase sampling system, analyte-specific coatings/separation methods, possible derivatization methods, and calibration standards. Coupled with this is the need for field testing and determination of system reliability/stability in a condensed-phase analysis system.

This unique Sandia-developed detection system has uses for cost-efficient determination of environmental contaminants such as toxic industrial compounds (TICs), as well as for chemical contaminants that might be introduced through malevolent anthropomorphic actions.

We developed a bench-scale data collection and analysis system for testing that we can further miniaturize to produce a

portable testing unit. We are investigating the use of a cheap programmable integrated circuit (PIC) processor to handle the majority of the heating, timing, valve control, and data-collection functions for the system. We will perform analysis and user interface with a portable computer. We demonstrated the front-end testing and collection apparatus for the μChemLab™ platform. We performed collections out of water onto a miniature preconcentrator (PC), separated them on a microfabricated gas-chromatography (GC) column, and detected them on one of our surface acoustic-wave (SAW) detectors. We performed these collections using P&T collection of trihalomethanes (THMs, four regulated compounds) out of water. We also demonstrated the solid-phase extraction of a CW simulant from water using a commercial microextraction syringe as well as a Sandia-developed microextraction channel apparatus. THM work indicated that we have a detection limit of hundreds of nanograms for VOCs. The detection limits for SVOC materials are appreciably lower. We demonstrated separation of THM components using microfabricated components. We performed development and testing on larger-capacity PCs, to be used in conjunction with the standard PC hardware, to allow collection and focusing of the VOC materials. This will allow us to achieve the desired detection limits (larger-capacity PC) while maintaining sharp peak shapes (standard PC) for the chromatography. We developed and tested an automated system for the use of commercial SPME fibers. Unfortunately, the power requirements preclude the use of this apparatus in a portable device; however, it may have applications in the future to an emplaced sensor system.

52596

Advanced High-Efficiency Direct-Cycle Gas Power-Conversion Systems for Small Special-Purpose Nuclear-Power Reactors

S. A. Wright, M. F. Young, M. E. Vernon, G. E. Naranjo, P. S. Pickard, E. J. Parma, Jr., P. H. Helmick

Nuclear-power systems are receiving increasing attention as the enabling technology for new and challenging Department of Energy, National Aeronautics and Space Administration (NASA), Department of Defense, commercial space, and terrestrial applications. The key factor in this interest is the ability of closed-Brayton-cycle (CBC) systems to efficiently produce electricity. This project examines the systemwide coupling issues between nuclear reactors and CBC power-conversion systems. The project has three major tasks. The first task consists of developing a dynamic system model for the reactor and the closed-loop power-conversion system. The second task focuses on developing, fabricating, and operating a low-cost CBC electrically heated test loop that Sandia will use to verify the dynamic system model. The third task consists of examining alternative advanced dynamic power-conversion systems that might prove useful for terrestrial or space-based power-conversion systems.

Our major accomplishments include the following:

(1) We developed and implemented systems models in a state-the-art simulation code (SIMULINK), and developed and tested control algorithms for the coupled reactor and CBC system in these models.

(2) We published and presented two research papers describing the dynamic model.

(3) Five abstracts and papers were accepted for publication.

(4) We operated an open-cycle commercial gas turbine (Capstone) to determine the operational and design conditions to modify the Capstone C-30 gas turbine to make a closed-loop test-bed.

(5) We placed an order with Barber-Nichols, Inc., to design, manufacture, assemble, and perform acceptance tests on a modified open-cycle gas turbine so that it can operate as a closed-system test loop.

(6) We modeled and compared the performance curves of the open-cycle system with actual measurements of the Capstone C-30 gas turbine unit.

(7) We opened and modified the Capstone C-30 gas-turbine housing to operate in a closed-system loop.

(8) We developed the power, volume, and cooling requirements for Sandia's test lab and issued a contract with a physical plant to make facility modifications that provide adequate power and water cooling.

(9) We acquired a Cooperative Research and Development Agreement (CRADA) with Northrup-Grumman Space Technologies (NGST) to collaborate with us in the development of a dynamic systems model for a nuclear electric-propelled spacecraft and other related activities.

(10) We analyzed a variety of thermodynamic advanced/alternative power-conversion systems for both space and terrestrial applications with the intent of developing test programs for the closed test loop, to determine and validate alternative and innovative closed-cycle systems that may operate with other gas fluids such as CO_2, to evaluate the use of heat-pipe–cooled reactors in gas dynamic power-conversion systems, and to study the temperature distributions within reactors that may be coupled to gas dynamic systems.

We acquired a Cooperative Research and Development Agreement (CRADA) with Northrup-Grumman Space Technologies (NGST) to collaborate with us in the development of a dynamic systems model for a nuclear electric-propelled spacecraft and other related activities.

Refereed

Lipinski, R. J., S. A. Wright, D. J. Dorsey, C. D. Peters, N. Brown, J. Williamson, and J. Jablonski. 2004. A gas-cooled-reactor closed-Brayton-cycle demonstration with nuclear heating. *Space Technology and Applications International Forum—STAIF 2005, Proc. AIP Conference*, accepted.

Wright, S. A. 2003. Application of a digital-controlled reactor architecture to space reactors. *Proc. American Nuclear Society Winter Meeting, American Nuclear Society Transactions* **89** (November, Washington, D.C.): 540.

Wright, S. A., and R. D. Beets. 2003. Application of a digital-controlled reactor architecture to space reactors. *Proc. American Nuclear Society Winter Meeting, American Nuclear Society Transactions* **89** (November, Washington, D.C.): 542.

Wright, S. A., and S. Stout. 2004. Temperature distributions in LMR fuel pin bundles as modeled by COBRA-IV-I. *Space Technology and Applications International Forum—STAIF 2005, Proc. AIP Conference*, accepted.

Wright, S. A., and T. J. Sanchez. 2004. Dynamic modeling and control of nuclear reactors coupled to closed-loop Brayton cycle systems using SIMULINK. *Space Technology and Applications International Forum—STAIF 2005, Proc. AIP Conference*, accepted.

Wright, S. A., R. Fuller, R. J. Lipinski, K. Nichols, and N. Brown. 2004. Operational results of a closed-Brayton-cycle test-loop. *Space Technology and Applications International Forum—STAIF 2005, Proc. AIP Conference*, accepted.

Wright, S. A., R. J. Lipinski, T. Pandya, and C. Peters. 2004. Proposed design and operation of a heat-pipe reactor using the Sandia National Laboratories annular core test facility and existing UZrH fuel pins. *Space Technology and Applications International Forum—STAIF 2005, Proc. AIP Conference*, accepted.

52597

Securing Mobile Code

C. L. Beaver, W. D. Neumann, H. E. Link, W. E. Anderson, R. C. Schroeppel, P. L. Campbell, L. G. Pierson

If software is designed so that it can issue functions that will move that software from one computing platform to another, the software is said to be "mobile." There are two general areas of security problems associated with mobile code. The "secure host" problem involves protecting the host from malicious mobile code. The "secure mobile code" problem, on the other hand, involves protecting the code from malicious hosts. Sandia's work focused on the latter problem.

We found three distinct camps of opinions regarding how to secure mobile code: (1) those who believe that special distributed hardware is necessary, (2) those who believe that special distributed software is necessary, (3) and those who believe that neither is necessary.

In the distributed software camp, we examined some commonly proposed techniques including JAVA™, D'Agents, and Flask. For the specialized hardware camp, we proposed a cryptographic technique for "tamper-proofing" code over a large portion of the software/hardware life cycle by careful modification of current architectures. This method culminates in decrypting/authenticating each instruction within a physically protected central processing unit (CPU), thereby protecting against subversion by malicious code.

Our main focus was on the camp that believes that neither specialized software nor hardware is necessary. We concentrated on methods of code obfuscation to render incomprehensible an entire project or a data segment on which a project depends. We focused on a method called "white-boxing." We put forth some new attacks and improvements on this method and demonstrated its implementation for various algorithms. We also examined cryptographic techniques to achieve obfuscation and created a new application to digital-signature algorithms. We further examined in detail general theoretical models of obfuscation. We considered the need for formal models to obtain provable security and the progress made in this direction thus far.

Finally, we tackled the problem of verifying remote execution. We invented some methods of verifying remote exponentiation computations and some insight into generic computation checking.

- *Analysis and improvement of white-boxing techniques*. A system intended to run on a malicious host is, by definition, not a black box because the adversary is able to view the program's execution and any intermediate results. The white-box attack context was introduced by Chow *et al*. as a setting where the adversary is not only allowed to make such observations about the software, but is also able to examine and alter the software arbitrarily. They implement in this context a white-box data encryption standard (DES) algorithm. Ideally, a white-box encryption function would be as difficult to analyze as a black box. Their implementation does lend itself to some analysis, however, and a key can be extracted easily. We built upon their ideas to create a similar white-box version of DES that is much less vulnerable to direct analysis. We also applied these ideas to create a white-box implementation of triple-DES and AES (Advanced Encryption Standard).
- *Proof-of-concept demonstration for white-boxing*. We demonstrated that a software agent given a decrypt-only obfuscated DES function was able to verify the origin of messages bearing a message authentication code (MAC). This MAC was a DES–encrypted hash code for the message that, when decrypted by the agent, could be compared to the message hash, and which only the originator of the message (being the only party privy to the encryption key itself, or being the only party with an encrypt-only obfuscated DES function for that key) could have generated. Because the key cannot be extracted from the obfuscated function, and because the decrypt-only function could not be used to generate a valid MAC, the system was able to use DES for MAC verification instead of more expensive public/private key signature generation.
- *Trusted hardware solution*. We proposed a cryptographic technique for tamper-proofing code over a large portion of the software/hardware life cycle by careful modification of current architectures. This method culminates by decrypting/authenticating each instruction within a physically protected CPU, thereby protecting against subversion by malicious code.
- *Development of remote signature capability protocol*. We developed a protocol that allows a remote host to aid a client (e.g., low-power client) in performing a digital-signature operation. Our protocols provide a mechanism for the originator to refute a signature that it did not intend the host to sign, but maintains accountability of the originator to stand by a valid signature; hence, nonrepudiation is retained.
- *Analysis of formal security proofs for obfuscation*. To obtain provable security, we need to construct a formalized

model of obfuscation. The first effort to initialize a formal investigation into obfuscation models came from Barak, *et al*. They show in general that it is impossible to construct an all-purpose program obfuscator. Following this work, several alternative models were proposed, some constructing secure obfuscated programs. We examined these papers and researched obfuscation models that may lend themselves to security proofs.

- *Development of methods for verifiable remote computing*. We developed algorithms for performing a modular exponentiation (or elliptic curve multiply) remotely and verifiably on one or several host machines. We also investigated methods for verifying generic remote computations. Such algorithms, if they can be carried out, require a lot of overhead, and we developed some improvements, greatly reducing the amount of data that would need to be stored.
- *Literature search on specialized software approaches to securing mobile code*. We investigated methods for securing mobile code that require specialized hardware, including the JAVA™, D'Agents, and Flask platforms.

52598

Novel Catalysts for Hydrogen Fuel-Cell Applications

S. M. Thornburg, W. A. Steen, M. J. Kelly, R. L. Jarek, J. E. Miller, E. N. Coker

Catalysts in hydrogen (H) fuel-cell applications have had to rely heavily on high concentrations of platinum (Pt). The high cost and scarce supplies of Pt are important barriers to the commercialization of fuel cells, given the present requirements of almost 25 g per cell for automotive applications. A more inexpensive and readily available catalyst would aid the development of fuel-cell–powered vehicles. Small differences in particle size have been shown to affect catalytic activity for clusters of a few dozen atoms. However, traditional catalyst characterization techniques, where testing and synthesis are separate steps, make it difficult to determine the optimal particle size.

Sandia will use laser-ablation mass spectrometry to generate a range of cluster sizes of known mass, whose adsorption of H and carbon monoxide (CO) molecules will be measured in vacuo. *This unique approach is a rapid and parallel method to provide fundamental data that will test the catalyst chemistry prior to synthesis. We will also investigate non-Pt catalysts (e.g., tungsten [W]) and alloys of Pt with other metals (e.g., ruthenium [Ru]). We will then design supported catalysts using the optimal cluster size, thereby significantly decreasing the total amount of metal required and potentially yielding catalysts that are more resistant to CO deactivation. We will then test optimum catalyst designs for electrolytic efficiency and resistance to CO poisoning by electrochemical measurements of fuel-oxidation processes, and will test promising electrodes in a prototype fuel cell. This research has the potential for dramatic reductions in the cost of fuel-cell electrodes.*

The prime objective of this project is to develop novel H-oxidation electrocatalyst materials that contain reduced Pt content compared to traditional catalysts. Our approach is to (1) use fundamental materials science (experimental and modeling) to identify optimum nanocluster chemical and physical catalyst configurations, (2) develop flexible synthesis techniques to fabricate supported catalyst structures, and (3) verify electrochemical performance in half cells and ultimately in laboratory fuel cells.

- *Optimized catalyst configuration*

— *Laser-ablation Fourier-transform mass spectrometer (FTMS)*. We are using laser ablation combined with high-resolution mass spectrometry (MS) to produce catalyst clusters and evaluate gas-phase oxidation processes. We tested the quadrupole ion guide and Pt laser-ablation system in a simplified configuration that has no mass selection capability, except that heavier ions arrive at the detector later than lower-mass ions. We also confirmed the effect of the cooling gas pulse that produces heavier clusters. We measured the energy of the positive ions produced by laser ablation by positive biasing of electrodes to observe which clusters were repelled and at what voltage. All of the ions produced have less than 40 eV of energy, which should be readily cooled by additional ion-neutral impacts. Integration of the quadrupole ion guide and laser-ablation system into the FTMS is complete.

— *Theoretical modeling*. Mathematical convergence issues delayed our expected progress on identifying candidate cluster calculations. A new software code, Jaguar, was recently used to benchmark the density-functional theory (DFT)–level chemisorption calculations of atomic oxygen to Pt(111) clusters containing up to 28 atoms in a three-layer configuration (William Goddard, Cal Tech). Calculations of the Pt6 structure confirmed results of Yang, *et al*., 1997, that the planar structure is more stable than a near-octahedral one. Calculations on this type of system are currently under way on this n=6 Pt cluster as the experimental methods produce structures down to this size.

- Electrocatalyst synthesis efforts focused on optimizing the control of the Pt cluster size, and particularly on narrowing the distribution of cluster size. This advancement permits performance characterization as a function of discrete cluster size. To this end, we prepared clusters with an average size ~ 0.96 nm (from extended x-ray absorption fine structure [EXAFS]) with very narrow size distribution. The ability to tune this size exists through (1) the loading of Pt cluster-precursor into the microporous host, and (2) the precise calcination temperature employed during decomposition of the cluster-precursors. Studies of catalyst properties as a function of the temperature at which the catalyst was carbonized (to convert a supporting polymer into a conductive carbon [C] matrix) revealed optimal carbonization temperatures between 600°C and 800°C.

- *Electrochemical testing*. As scheduled, we performed electrochemical testing of multiple Pt/C electrocatalysts to determine the kinetics of H_2 oxidation and the effective electroactive surface area. We discovered that the carbonization

step is critical to H_2 oxidation kinetics, with temperatures ~ 700°C yielding electrocatalyst materials that have nominally the same conductivities as industry standards. We expended great effort to identify a suitable way to evaluate the electroactive surface area before adopting a CO stripping voltammetry procedure. Furthermore, we performed rotating-disk electrode H_2 oxidation studies to better assess charge transfer and any mass-transport kinetic limitations.

Overall, we completed development on the sophisticated MS–based techniques needed to fabricate and test base catalyst structures and the flexible synthesis fabrication methods needed to generate the resulting optimized cluster configurations.

Refereed

Coker, E. N., W. A. Steen, M. J. Kelly, I. C. Abraham, and J. E. Miller. 2004. Novel, size-controlled Pt cluster electrocatalysts for H_2 fuel cells. *American Chemical Society, Div. Fuel Chem.* **49** (2) (February): 681–82.

Other Communications

Coker, E. N. 2004. Novel fuel-cell electrocatalysts based on noble metal-exchanged Zeolites. Paper presented at the 27th Annual British Zeolite Association Meeting, July, St. Andrews, Scotland.

Coker, E. N. 2004. The development of novel electrocatalysts for hydrogen-powered fuel cells. Paper presented at the Graduate Seminar, University of New Mexico Chemical and Nuclear Engineering Department, 21 September, Albuquerque, New Mexico.

Coker, E. N., W. A. Steen, J. E. Miller, M. J. Kelly, and I. C. Abraham. 2004. Preparation, characterization, and modeling of novel platinum-on-carbon catalysts with controlled cluster size for application in PEM fuel cells. Paper presented at the 13th International Congress on Catalysis, July, Paris, France.

Coker, E. N., W. A. Steen, J. E. Miller, M. J. Kelly, and I. C. Abraham. 2003. Synthesis of novel platinum/carbon catalysts for use in hydrogen fuel cells. Paper presented at the 4th National Laboratory Catalysis Conference, October, Oak Ridge, Tennessee.

Coker, E. N., W. A. Steen, M. J. Kelly, I. C. Abraham, and J. E. Miller. 2004. Novel, size-controlled Pt cluster electrocatalysts for H_2 fuel cells. *Proc. 228th American Chemical Society National Meeting* **1** (August, Philadelphia, Pennsylvania).

Kelly, M. J., D. Ingersoll, W. A. Steen, E. N. Coker, I. C. Abraham, and J. E. Miller. 2004. Electrochemical oxidation of d-glucose at noble metal and binary metal catalysts for fuel-cell applications. Paper presented at the 205th Electrochemical Society Meeting, May, San Antonio, Texas.

Steen, W. A., E. N. Coker, M. J. Kelly, I. C. Abraham, and J. E. Miller. 2003. Platinum/carbon catalysts for use in hydrogen fuel cells—Synthesis and characterization. Paper presented at the 15th Rio Grande Symposium on Advanced Material, October, Albuquerque, New Mexico.

Steen, W. A., E. N. Coker, M. J. Kelly, I. C. Abraham, and J. E. Miller. 2004. Synthesis and characterization of H_2 fuel-cell electrocatalysts with optimized cluster size. Paper presented at the 205th Electrochemical Society Meeting, May, San Antonio, Texas.

Steen, W. A., E. N. Coker, M. J. Kelly, J. E. Miller, and I. C. Abraham. 2004. Synthesis and characterization of Pt-based electrocatalysts for H_2 fuel cells. Paper presented at the 18th Annual Western States Catalysis Club Meeting, February, Provo, Utah.

Steen, W. A., E. N. Coker, M. J. Kelly, J. E. Miller, and I. C. Abraham. 2004. Synthesis and characterization of Pt-based electrocatalysts for H_2 fuel cells. Paper presented at the Research Seminar, University of New Mexico Chemical and Nuclear Engineering Department, March, Albuquerque, New Mexico.

52606

Linking Optimization and Simulation in Critical-Infrastructure Systems

D. A. Jones, C. E. Davis, J. A. Lloyd, M. A. Turnquist, C. A. Phillips, L. K. Nozick

This research focused on the development of specialized algorithms to identify optimal strategies for decision making in complex interconnected infrastructure systems under dynamic and rapidly changing conditions. This research has two key features. The first is its emphasis on networks (graphs of nodes and arcs) as an overarching modeling architecture to represent infrastructure components, the interaction between interdependent infrastructures, the condition of supporting information-system components, and the movement of commodities and individuals through these systems. The second key feature is the emphasis on integrating optimization and simulation methods for system-performance estimation and investment optimization.

Sandia developed a critical-infrastructure (CI) modeling approach based on characterizing the uncertain evolution of the condition and capacity of those networks over time using Markov and semi-Markov processes. Depending on the performance measure of interest, these processes are either treated analytically or simulated. These analytical calculations and simulations form the basis for investment optimization. As a complement to these analysis tools, we developed a model of malicious intruders in infrastructure systems because they are an important source of potential disruption in these systems. We created the modeling tools based on Markov processes in network models to represent the progress of intruders attempting to penetrate the security of an infrastructure system and simulation as an effective method to represent the variety in attackers. The tools created as a result of this research provide the capability to understand the impact of system intruders and to optimize the steps taken to thwart their advances. Our objective during the remainder of this project is to apply these tools to the air transportation system. Clearly, this is a critical national infrastructure system. Intruders do pose a clear danger to the system, and optimizing our actions to thwart their advances is of tremendous importance.

The tools created as a result of this research provide the capability to understand the impact of system intruders and to optimize the steps taken to thwart their advances.

The objective of this project is to research and develop optimization-based models to work in conjunction with simulations of CI interdependencies. The purpose of the optimization models is to identify optimal strategies for

decisions made in complex interconnected infrastructure systems under uncertain and dynamic conditions, especially in response to failures (whether natural, accidental, or malicious). The goals of the effort are to identify optimal strategies for mitigating vulnerabilities and to develop effective strategies to restore functionality in the aftermath of a failure, in the event that a failure occurs.

A cornerstone of this project is network-based modeling. Networks (graphs of nodes and arcs) can represent capacities of components in infrastructure systems and their evolution over time, the condition of supporting information-system components, location and condition of an intruder in a system, etc. Network-based models also represent significant opportunities to integrate simulation and optimization.

In early work, we developed an approach to modeling CI networks that is based on modeling uncertain evolution of the condition and capacity of those networks over time using Markov and semi-Markov processes. Those Markov and semi-Markov processes are simulated over time, and those simulations form the basis for an optimization of investment. Therefore, this approach enables a combined simulation/optimization analysis to produce strategies for most effectively mitigating vulnerabilities and restoring functionality after some disruption.

In recent work, we focused attention on modeling an important source of potential disruptions in infrastructure systems—those created by malicious intruders intending to create system failures. We created a framework based on Markov processes in network models to represent the progress of intruders attempting to penetrate the security of an infrastructure system. This work complements earlier efforts by creating understanding of the instigation of disruptions, whereas earlier work focused on restoring system functionality after a disruption.

Our development of network-based models of intruders in infrastructure systems focused on two key questions:

(1) For a given infrastructure system, can we estimate the probability of success for a malicious intruder as a function of some basic system characteristics and parameters, and characterization of the intruder's level of knowledge and skill?

(2) If so, can we estimate the probable benefit of various types of "system hardening" as a basis for cost-benefit evaluation of potential system modifications and/or investments?

The basis for our analysis is a representation of the system of interest as a network of nodes and arcs. Nodes represent

system assets, and arcs represent opportunities for intruders to move within the system. Several previous researchers also used graph-based methods to represent attackers or defenders in security analyses, and a few used Markov Decision Processes (MDP) for situations in which the attack path is probabilistic. We also used MDP tools for analyzing the strategy of system intruders, but our work is based on a different type of state representation for the system, and our objective is somewhat different from previous studies—the optimization of investments in system security.

Work to date also sets the stage for upcoming work—focusing on the application of these concepts to airport security. The air transportation system is obviously a CI, and hub airports are both vital to its functioning and points of vulnerability in the system. Optimization of efforts to reduce the vulnerability of airports to penetration by malicious intruders can pay very significant security benefits, and airports appear to be a very important and appropriate application domain for the tools we have developed thus far.

Refereed

Nozick, L. K., M. A. Turnquist, D. A. Jones, and C. R. Lawton. 2004. Investments to improve performance of interdependent infrastructures. Paper presented at the CORS/INFORMS International Conference, May, Banff, Alberta, Canada.

Nozick, L. K., M. A. Turnquist, D. A. Jones, J. R. Davis, and C. R. Lawton. 2004. Assessing the performance of interdependent infrastructures and optimizing investments. *International J. Critical Infrastructure Systems*, accepted.

Nozick, L. K., M. A. Turnquist, D. A. Jones, J. R. Davis, and C. R. Lawton. 2004. Assessing the performance of interdependent infrastructures and optimizing investments. *Proc. 37th Hawaii International Conference on System Sciences* **37** (January, Honolulu, Hawaii): 54–60.

Turnquist, M. A., L. K. Nozick, D. A. Jones, C. E. Davis, and C. R. Lawton. 2004. Physical security and vulnerability at airports. Paper presented at the INFORMS National Conference, October, Denver, Colorado.

53591

Hydrogen Futures Dynamic Simulation Model

T. E. Drennen, P. H. Kobos, D. J. Borns, S. A. Jones, P. S. Pickard, J. O. Keller, A. E. Lutz

The overall goal of this project is the creation of a high-level dynamic simulation model of the integrated hydrogen (H) enterprise by key sector, including H production, distribution, storage, and consumption. When completed, the model will allow the user to explore various technology options for each component of a complete H system, tracking both the costs of the delivered H and the key environmental effluents that might result (e.g., carbon [C], nuclear waste, etc.). This tool will allow policy, corporate, and research and development (R&D) decision makers to gain a much better understanding of the future H enterprise, the implications of alternative enterprise configurations, and a strategic understanding of where R&D investment might have the greatest impact on making the H enterprise successful.

H has the potential to become an integral part of our energy transportation and heat and power sectors in the coming decades and offers a possible solution to many of the problems associated with a heavy reliance on oil and other fossil fuels. We developed the Hydrogen Futures Simulation Model (H_2Sim) to provide a high-level, internally consistent, strategic tool for evaluating the economic and environmental trade-offs of alternative H production, storage, transport, and end-use options in the year 2020. Based on the model's default assumptions, estimated H production costs range from $0.68/kg for coal gasification to as high as $5.64/kg for centralized electrolysis using solar photovoltaics **(**PV). This basic result does not change if carbon capture and sequestration costs are added ($0.16/kg). This result is fairly insensitive. For example, coal prices would have to more than triple or the assumed capital cost would have to increase by more than 2.5x for natural-gas reformation to become the cheaper option. Alternatively, natural-gas prices would have to fall below $2/MBtu to compete with coal gasification. The electrolysis results are highly sensitive to electricity costs, but electrolysis becomes cost-competitive with other options only when electricity drops below $0.01/kWhr.

Delivered H costs are likely to be double the estimated production costs due to the inherent difficulties associated with storing, transporting, and dispensing H due to its low volumetric density. H_2Sim estimates distribution costs ranging

from $1.37/kg (low distance, low production) to $3.23/kg (long distance, high production volumes, carbon sequestration). Distributed H production options, such as on-site natural gas, would prevent some of these costs.

H_2Sim compares the per-mile driving costs (fuel, capital, maintenance, license, and registration) of existing internal-combustion engine (ICE) vehicles ($0.55/mile), hybrids ($0.56/mi), and electric vehicles ($0.82–$0.84/mi) with 2020 fuel-cell vehicles (FCVs) ($0.64–$0.66/mi), FCVs with onboard gasoline reformation (FCVOB) ($0.70/mi), and direct-combustion H hybrid vehicles (H_2Hybrid) ($0.55–$0.59/mi). The results suggest that while the H_2Hybrid vehicle may be competitive with ICE vehicles, it will be difficult for the FCV to compete without significant increases in gasoline prices, reduced predicted vehicle costs, and stringent C (carbon) policies, or unless they can offer the consumer something existing vehicles cannot, such as on-demand power, lower emissions, or better performance.

Refereed

Baker, A. B., T. E. Drennen, S. A. Jones, W. Kamery, A. E. Lutz, and J. Rosthal. 2004. The hydrogen futures simulation model (H_2Sim), a first-year progress report: Overview, results, and initial observations. Paper prepared for peer review panel of H_2Sim, Sandia National Laboratories, Albuquerque, New Mexico.

Drennen, T. E., and J. E. Rosthal. 2004. The hydrogen futures simulation model (H_2Sim): Pathways to a hydrogen future. *Frontiers in Environmental Valuation and Policy*, accepted.

Other Communications

Drennen, T. E., A. B. Baker, W. Kamery, and P. H. Kobos. 2003. Pathways to a hydrogen economy: The hydrogen futures simulation model. Paper presented at the North American Association of Energy Economist's Annual Meeting, October, Mexico City, Mexico.

64811

Agent-Based Control of Distributed Infrastructure Resources

L. R. Phillips, H. E. Link, R. B. Smith, L. A. Weiland, M. A. Cook

Sandia's goal in this project is to demonstrate that a coalition of software agents can successfully operate a distributed infrastructure utility. We selected the electric-power MicroGrid (an interconnected set of microsources—generators of < 100 kW capacity—disconnected from the main grid) as our target application. The meaning of the word "successful" is not well defined, but is related to a set of liveness and safety properties that define what it means to operate safely, effectively, and efficiently. We will consider the agents successful if they can maintain operation for an extended period of time and deal correctly with unforeseen circumstances. We made progress this year in defining how a MicroGrid should work, which is not an easy task because there are no functional MicroGrids. (There are operational groups of microsources, but they generally operate in close proximity to one another and are connected to the main grid, thus effectively acting as mini-power-plants rather than as cooperating independent entities.) Our understanding of the operation of electric-power devices from which a MicroGrid could be constructed has increased greatly over the past year to the extent that we now have two models of the MicroGrid: one low-resolution and one high-resolution. We now understand that the regime of the agent is inhibitory: The agent's job is to prevent the MicroGrid from attempting to satisfy certain loads (that would overload some elements) by dropping them, to prevent lines from transmitting power (that would burn them out) by opening breakers, and to prevent generators from responding to load variations to better distribute power flows. The agent framework is operational, and we expect to demonstrate agents observing the (simulated) MicroGrid, comparing these (simulated) sensor readings with their own internal models, finding discrepancies between the two, and deciding what, if anything, they need to do about what they observe.

We made progress this year in defining how a MicroGrid should work, which is not an easy task because there are no functional MicroGrids.

- *Constructed a high-fidelity MicroGrid simulation*. We implemented a simulated MicroGrid. It is our intent that the agents created for the project will receive data from and emit commands to this simulation. A reasonably accurate model of a MicroGrid is needed so that the agent activities are relevant to actual MicroGrid operation. We are simulating a MicroGrid situated on an isolated military camp composed of four tents:

headquarters, communications, kitchen, and hospital. This is a true MicroGrid because it is not connected to any outside utility power.

- *Constructed a low-fidelity MicroGrid simulation*. The low-fidelity simulation is a matrix-based load-flow calculator that returns the current on each transmission line given the loads, the sources, and a transmission network.
- *Resolved several discrepancies between the two MicroGrid models*. Some examples and test cases produced glaring differences that were resolved; the two simulators now produce similar answers.
- *Defined appropriate control regime for agents*. Groups of small generators in current use are normally configured with a single load-following generator and any number of fixed-output generators running at near-optimum. Note that two or more load-following generators cannot be interconnected in an unconstrained way since their closed-loop controllers would beat against each other. This constraint limits the options available, especially when load fluctuations exceed the ability of the single allowed load-follower to respond. The agents ought to allow some dynamic behavior, e.g., it should be possible to exert control such that two generators can run at a lower level and respond to load variance larger than a single generator can accommodate. We are also examining the relationship between the stochastic properties of the load and the inferred constraints on the generator(s). Note that this grid configuration represents a single point of failure; if we take out the load-following generator, we will likely impact the entire grid. Without the load-following generator, there is no means to adapt to the resulting (or any other) generation/load imbalance. The options for such a situation might include:

(1) Black out, reassign the load-follower role, and restart.

(2) All tents island, convert to the load-following mode, reassign the load-following role, and regroup.

(3) One generator with sufficient capacity switches over to the load-following mode.

Any of these might be effective in certain circumstances. We determined that this is the kind of decision the agents should make, depending on the criticality of the loads involved, whether transmission lines will be overloaded, and so forth, and that this is where the agents will be effective, as opposed to the millisecond-level stability regime. Our understanding at this time is that individual devices can function in a stable manner in all but the worst conditions; what is missing is some actionable concept of how the MicroGrid as a whole is performing that the agents will provide and act on.

- *Developed an optimizing strategy for determining the best grid behavior.* We constructed an optimization framework based on transmission cost to enable us to assign generating levels to sources in an efficient manner (in essence, to dispatch economically).

We will use these elements in conjunction with agents observing the high-fidelity simulator to enable the agents to decide how the MicroGrid should be running, send control and inhibitory signals to bring that situation about, predict the behavior of the transmission grid, condition the high-fidelity simulator to execute the commands, observe the high-fidelity simulator, discover and report discrepancies between the internal and external representations, and finally, react as appropriate to observed discrepancies.

67050

Biological-Security Decontamination Technology—Reducing the Threat of Infectious-Agent Spread

R. G. Betty, J. M. Bieker, M. D. Tucker

Currently, there are no highly integrated response capabilities to outbreaks of extremely infectious agricultural diseases. These diseases, introduced either intentionally or naturally, could have a catastrophic impact on the U.S. economy. Through the combination of enhanced biosecurity decontamination remediation and validated inactivation verification methodology, Sandia seeks to provide important technologies for incorporation as components of a robust response capability. Because of the potentially devastating economic impact that could result from the spread of infectious agricultural diseases, the proposed capability components will promote critical-infrastructure (CI) protection and greater border security.

We will develop biosecurity-decontamination technologies that will reduce the threat of infectious-agent spread to plants, animals, and humans via surfaces inherent to an agricultural environment. In addition to ensuring wide-spectrum decontamination efficacy and low corrosivity, we will address biodegradability issues.

Through partnership with Kansas State University, we will develop rapid verification of loss of pathogenic inactivity (inactivation) methodology. This enhanced technology will enable rapid assessment of contamination following an intentional event, and will also be extremely useful in routine assessment of agricultural environments.

Our primary effort in future work will be a demonstration of both decontamination and viral inactivation detection technologies of the foot-and-mouth virus (FMDv) developed through this project. Utilizing the decontamination technology developed for enhanced detergency in the presence of heavily loaded organic environments, the field test will serve as both a test for the decontamination technology and a validation of the rapid viral inactivation methodology on an actual live infectious agent. The demonstration will likely be held at the Department of Homeland Security's Plum Island facilities.

This enhanced technology will enable rapid assessment of contamination following an intentional event, and will also be extremely useful in routine assessment of agricultural environments.

We progressed in development of a biosecurity decontamination technology with demonstrated increased detergency, capable of infectious-agent decontamination in the presence of heavy organic loads. We achieved the increase in

detergency by using alternative surfactants and detergency builders. Initial tests indicate a treatment-dependent increase in detergency, as measured by changes in surface reflectance of selected surfaces (polypropylene, anodized steel, and butyl rubber) following soil application and exposure to various formulations. Decontamination efficacy data are based on treatment exposure times of 15 and 60 min.

During the first few months of the project, we assessed a variety of surfactant chemistries in spore-kill efficacy tests. We explored the effectiveness of alternative cationic surfactants, as well as anionic surfactants, anionic/nonionic surfactant combinations (i.e., mixed micelle systems that can form highly stable micelles), or cationic/nonionic combinations. We made progress in developing a preliminary biosecurity decontaminant by the selection of a surfactant that demonstrated increased activity against biological pathogen simulants and characteristic soil microorganisms. The surfactant is a cationic surfactant mix of ethyl and benzyl quaternary alkyl ammonium chlorides. The surfactant properties include an established synergistic effectiveness against a broad spectrum of biological pathogens, including algae, fungi, viruses, and bacteria. This characteristic makes this surfactant applicable for use in an agricultural environment where broad-spectrum microorganisms are often prevalent. The use of a specific cationic surfactant, low levels (< 4%) of oxidizer and oxidizer activator, carbonate, solvents, and added detergent builders combine to provide increased detergency. Additionally, the Food and Drug Administration permits this surfactant for use in no-rinse food-contact sanitizers at no more than 200 ppm, per 21 CFR part 178.1010. This fact will be leveraged in further development of Sandia decontamination technologies as applicable to the food-processing industry.

We developed a repeatable methodology for determining the effectiveness of various disinfectants against bovine coronavirus (BCV). The gold-standard assays in the cell-culture system correlate (in most cases) with the integrity of viral ribonucleic acid (RNA). We are validating this correlation to develop field-use verification of loss of infectivity following remediation of an affected area. We use serological assays to study the effect of various disinfectants on structural and capsid proteins. This work used BCV as a viral model; in theory, any infectious virus could be used in its place with the change of the cell-culture system, polymerase chain reaction (PCR) primers, and antibodies for serological assays. Results verifying loss of viral infectivity using this tool resulted within 2–3 hr (for sample preparation and analysis) of sample collection following

remediation and are much faster than the gold-standard cell-culture assays (2–3 days). These methodologies and enhanced assays demonstrate broad capabilities and could potentially be targeted and developed for any infectious-disease biosecurity threat.

Specifically, we evaluated a variety of diverse disinfectants, including Sandia-developed formulations (DF-200 and its modifications), Virkon® S (potassium peroxymonosulfate), and common chemicals such as ethanol and bleach, for corona- and orthomyxo-virus disinfection effectiveness. We determined the efficacy of the various test disinfectants using *in vitro* cell-culture systems in human rectal tumor (HRT) or Madin-Darby Canine Kidney (MDCK) cells, respectively. Results thus far indicate that DF-200 and its modifications and bleach are highly effective for inactivating these viruses, while Virkon® S and ethanol are much less effective. Additionally, we evaluated the effect of the various disinfectants on viral targets, including viral RNA and structural proteins. Virkon® S and ethanol have no effect on degrading viral RNA; however, DF-200, its modifications, and bleach were highly effective at degrading viral RNA and protein. We are conducting all of these assays in the presence of organic challenge (soil, feces) as well as on the various test surfaces. We submitted a technical advance using the degradation of the viral RNA following treatment with disinfectants as a molecular tool for rapid verification of loss of infectivity.

Other Communications

Bieker-Hawkinson, J. M., R. D. Oberst, and S. Kapil (Kansas State University, Manhattan, Kansas). 2004. Disinfection of coronavirus and orthomyxoviruses in liquid and on solid surfaces by various disinfectants. Poster presented at the 47th Annual Conference of American Association of Veterinary Laboratory Diagnosticians, 21–27 October, Greensboro, North Carolina.

Bieker, J. M., J. W. Anderson, R. D. Oberst, and S. Kapil (Kansas State University, Manhattan, Kansas). 2004. Verification of complete inactivation of highly infectious respiratory viruses. Poster presented at the 47th Annual Biological Safety Conference, 17–20 October, San Antonio, Texas.

Bieker, J. M., R. G. Betty, J. W. Anderson, R. D. Oberst, and S. Kapil (Kansas State University, Manhattan, Kansas). 2004. Detection of bovine coronavirus in farm soil samples. Poster presented at the 23rd Meeting of the American Society for Virology, 10–14 July, Montreal, Canada.

67051

Consequence Management, Recovery, and Restoration after an Intentional Contamination Event

J. D. Roberts, S. C. James, V. C. Tidwell, D. Wall

The fate of contaminants after a terrorist act is a major concern, and waterways are particularly vulnerable to such an event. Contaminants could be introduced directly into a water system (municipal or general) or indirectly (radiological dispersal device [RDD]) from aerial dispersion, precipitation, or improper cleanup techniques that may wash contamination into storm water drains, sewer systems, rivers, lakes, and reservoirs. Most radiological, chemical, and biological contaminants have an affinity for sediments and organic matter in the water system. If contaminated soils enter waterways, a plume of contaminated sediments could be left behind, subject to remobilization during the next storm event. Or contaminants could remain in place, thus damaging local ecosystems. Suitable planning and deployment of resources to manage such a scenario could considerably mitigate the severity of the situation. First responses must be prearranged so that cleanup efforts do not increase dispersal and exacerbate the problem.

Interactions among the sediment, contaminant, and water cycle are exceedingly complex and poorly understood. This research focuses on developing a risk-based model that predicts the fate of intentionally introduced contaminants in surface-water systems. Achieving this goal requires integrating sediment transport with contaminant chemical reactions (sorption and desorption) and surface-water hydrodynamics. Sandia is leveraging its existing state-of-the-art capabilities in sediment-transport measurement techniques, hydrochemistry, high-performance computing, and performance-assessment modeling to accomplish this task. In addition, we calculated the basis for the physical hydrodynamics using the Environmental Fluid Dynamics Code (EFDC), an Environmental Protection Agency (EPA)–sponsored public-domain model. The results of this effort will enable systems analysis and numerical simulation that allow the user to determine both short-term and long-term consequences of contamination attacks on waterways as well as to help formulate preventive and remedial strategies.

Time-history EFDC results for bed topography. The channel bend has 11.5 m entrance and exit lengths, a central angle of 180°, a 4 m inner radius, and a 1 m width. The channel was adjusted to a slope of 0.002.

We accomplished the following:

(1) Evaluated, validated, and selected the EFDC for use in consequence-management modeling,

(2) Performed a literature review describing the fate of radiological contaminants in the environment,

(3) Built sediment erosion and transport algorithms based on unique Sandia-developed devices and began implementing them into the EFDC code,

(4) Generated a representative grid of the Pecos River for further evaluation of the model, and

(5) Submitted a paper describing the initial results.

Early in this research effort, we focused on selecting and evaluating a hydrodynamic computer code that will underlie a risk-analysis framework that can model and visualize the time-history migration patterns of contaminants introduced into surface-water and sedimentary environments. Modeling efforts revolved around correctly predicting sediment erosion and transport, as they are critical in determining contaminant fate. We performed model evaluation and validation against noncohesive sediment erosion and transport experiments carried out in a 180°C meander bend using existing model formulations. Concurrent with this activity were efforts to assemble data on factors that influence the short- and long-term effects of radiological contaminants released into the environment. In the end, Sandia will have a unique and distinct capability to assess surface-water contamination that should prove vital to national security.

In the end, Sandia will have a unique and distinct capability to assess surface-water contamination that should prove vital to national security.

- *Model selection*. EFDC is the best choice of existing models because (1) it has the same or similar hydrodynamic capabilities of other leading models; (2) it can represent inflows and has been modified to simulate near-shore areas (includes wetting and drying capabilities); (3) in addition to salinity and thermal transport, it can simulate multisize sediment transport and the transport of equilibrium-partitioning toxic contaminants (in water and sediments); (4) it is EPA–sponsored and nonproprietary; and (5) it can simulate nutrient cycling. (The model has 20 state variables for simulating water-column eutrophication and 26 state variables for simulating sediment biogeochemical processes.) These characteristics provide the framework for addressing nutrient loading and also provide options for applying the model to other water-quality or toxic parameters (West Consultants, Inc., 1996).
- *Model evaluation*. The evaluation and validation of the EFDC model required comparison to a detailed and well-documented set of physical experiments. We selected results of a study published by Yen and Lee (1995), hereafter referred to as YL, because of their detailed measurements of bed topography and sediment sorting in a channel bend subject to unsteady flow conditions.

In our evaluation, we used EFDC to model noncohesive sediment transport in the curved waterway used by YL and compared the results to YL's experimental data. To maximize model efficiency and accuracy, we assessed the number of sediment-size classes required to reach a converged solution, including an evaluation of effective sizing techniques. The YL dataset consists of contour plots of bed topography that demonstrate erosion and transport as well as size ratios that demonstrate sediment sorting. We created comparative plots using EFDC model outputs and demonstrated a positive correlation.

- *Radiological contaminant fate in the environment*. The Chernobyl accident of 1986 served as an inadvertent, massive experiment enabling us to assemble field data on factors that influence the short- and long-term environmental distribution of radionuclides. The radionuclides that escaped Chernobyl included 60Co, 90Sr, 134Cs, 137Cs, 239Pu, 240Pu, and 241Am, which also represent those most likely to be incorporated into an RDD. Since the accident, hundreds of research papers were published on the environmental behavior of the radionuclides, including studies of migration and environmental mobility in numerous matrices, such as soils, river and lake sediments, coastal waters, and other surface waters.

In general, Cs (cesium) and the actinides are strongly associated with particulate matter, including clay minerals and organics, and therefore their mobilization in the environment depends heavily on the mobility of sediments.

Refereed

James, S. C., P. L. Shrestha, and J. D. Roberts. 2004. Selecting the number of size classes and technique for calculating effective particle size for noncohesive sediment modeling efficiency. Abstract to be presented at the World Water and Environmental Resources Congress 2005, Anchorage, Alaska, submitted.

James, S. C., P. L. Shrestha, and J. D. Roberts. 2004. Selecting the number of size classes and technique for calculating effective particle size for noncohesive sediment modeling efficiency. *J. Estuarine, Coastal, and Shelf Science*, submitted.

Other Communications

James, S. C. 2004. Stochastic sediment transport modeling for risk assessment. (Invited) Paper presented at New Mexico Tech University, 2 February, Socorro, New Mexico.

James, S. C. 2003. Stochastic sediment transport modeling for risk assessment. (Invited) Paper presented at the University of New Mexico, 4 December, Albuquerque, New Mexico.

67052

Fully Integrated System-Dynamics Toolbox for Water Resources Planning

V. C. Tidwell, O. H. Paananen, H. D. Passell, L. A. Malczynski, J. L. Krumhansl

Water resources planning within a public-mediated context is quickly becoming the norm rather than the exception. Unfortunately, supporting tools are lacking that interactively engage the public in the decision-making process and integrate over the myriad values and physical processes that influence water management. To support Sandia's efforts to develop such a tool, we are creating a modular and generic resource-planning "toolbox."

The technical challenge lies in the integration of the disparate systems of hydrology, ecology, climate, demographics, economics, policy, and law, each of which influences the supply and demand for water. Specifically, these systems, their associated processes, and, most importantly, the constitutive relations that link them must be identified, abstracted, and quantified. In this way, the toolbox will form a collection of process modules and constitutive relations that the analyst can "swap" in and out to model the salient features of the subject watershed, thus allowing "transportability" of the tool. We will develop this toolbox, with all of its modules, within the common computational platform of system dynamics linked to a geographic information system (GIS), allowing analysis of spatially distributed data.

This resource-planning toolbox will provide Sandia with a unique tool for assisting local, national, and international water managers in resource planning. We can also use the toolbox to bring conflicted parties together to jointly explore solutions to complex problems, which could lead to reduced tension over shared resources in regions of the world of strategic importance to the U.S. Additionally, development of this toolbox and interactive modeling environment will position Sandia as a clear leader in the integrated modeling of water resource systems. This toolbox will also provide the technical foundation and framework for creating an interactive, icon-driven, system-dynamics modeling application for commercial distribution, and thus represents an important intellectual-property development for Sandia's corporate water initiative.

Efforts focused on developing a solid and coherent framework for creating an integrated system-dynamics modeling toolbox for water resources planning. We organized

efforts according to four specific activities: team building, model architecture formulation, problem conceptualization, and development of strategic external relationships.

- *Team building*. Foundational to this effort is the idea of integrating the myriad of processes important to water resources planning. The first step toward this goal involved the assembly of a multidisciplinary team of water experts including hydrologists, biologists, economists, aquatic chemists, lawyers, and policy analysts. Team members represent multiple institutions, including Sandia, the University of New Mexico, New Mexico Tech, and the University of Arizona.
- *Model architecture*. We built the system-dynamics toolbox within a modular framework. We created, organized, and maintained generic process modules within the toolbox. Key to this modular framework is the ability to easily swap modules into and out of watershed-specific models. To facilitate this mode of modeling, we established strict protocols for creating process modules. We created a detailed naming convention to avoid similarly named variables, which prevent swapping of modules. We also constrained the structure of the modules to ease identification of the inputs and outputs to and from the module. We also created "plugs" that network the generic modules within watershed-specific models. Finally, we established protocols for documenting modules and for model version control.
- *Problem conceptualization*. There are many processes important to modeling the balance between water supply and water demand. As such, it became clear that some sense of focus and purpose was needed in our toolbox-development initiative. Toward this end, we decided to organize the toolbox development according to a series of unifying issues.

Our first issue is water banking. There are a number of examples of water banks, some that work and some that do not. In other cases, stakeholders are apprehensive about the potentially undesirable results of water banking. We are creating a model to allow one to evaluate the unintended consequences of water banking, to explore the economic efficiency of different market systems, and to understand how third-party effects and different policy/institutional structures constrain the trading of water.

The water-banking model tracks the balance of water in the Rio Grande, the alluvial aquifer, and the irrigation conveyance system. Demands are calculated individually for irrigated agriculture, municipal, and industrial users. Demands are influenced by population growth and by local and regional economic indices. Irrigators project their expected profits and

then decide at what price they are willing to buy or lease water. Various market structures are allowed to connect potential buyers and sellers. Institutions and physical infrastructure constraints are also applied so that unphysical or illegal trades are prevented. We can also explore leasing of water for instream and riparian uses with the model. We then evaluate the consequence of a particular lease in terms of its influence on instream flows, regional economic benefit, water quality, and distribution of water consumption among and across different irrigators (i.e., pecans versus alfalfa), municipalities, and industrial uses. To test the resulting modules and integrated model, we are making comparisons with historical data taken from the Elephant Butte Irrigation District.

- *Strategic partnerships and technology transfer.* The ultimate goal of this effort is to develop a water-planning tool for use by local, state, federal, and international water agencies. Toward this end, we made efforts to expose potential end-users to the technology and to develop strategic partnerships. Two noteworthy efforts to date include meetings with the New Mexico Interstate Stream Commission and the Center for Advanced Decision Support for Water and Environmental Systems (CADSWES) at the University of Colorado.

Refereed

Cockerill, K., H. D. Passell, and V. C. Tidwell. 2004. Cooperative modeling: Building bridges between science and the public. *J. American Water Resources Association*, submitted.

Tidwell, V. C., and H. D. Passell. 2004. Whole-basin multisystem modeling on the Rio Grande. Paper presented at the Identifying Technologies to Improve Regional Water Stewardship Workshop, University of New Mexico, 21–22 April, Albuquerque, New Mexico.

Other Communications

Tidwell, V. C. 2004. System-dynamics modeling to support community-based water planning: An application to the Middle Rio Grande. Paper presented at the University of Arizona, Graduate Seminar Series, Hydrology and Water Resources Department, 26 February, Tucson, Arizona.

Tidwell, V. C., A. M. Michelsen, J. Aparicio, and H. D. Passell. 2004. The Rio Grande/Rio Bravo—A river of change. *Water Resources IMPACT, J. AWRA* **6** (3) (May): 14–17.

Tidwell, V. C., and H. D. Passell. 2003. Supporting regional water planning with community-based decision modeling. Paper presented at the American Water Resources Association Annual Conference, 2–5 November, San Diego, California.

Tidwell, V. C., K. Cockerill, and H. D. Passell. 2003. System-dynamics modeling and its role in community-based water planning. Paper presented at the New Mexico Water Research Symposium, 13 August, Socorro, New Mexico.

67053

Predicting System Performance of Proton-Exchange-Membrane Fuel Cells: Computational Modeling with Experimental Discovery and Validation

K. S. Chen, M. A. Hickner, D. R. Noble, C. J. Cornelius, D. Ingersoll

Hydrogen (H)-fed proton-exchange-membrane fuel cells (PEMFCs) are rapidly emerging as a viable technology for generating clean, alternative power for automotive and stationary applications. Several key technical issues must be addressed, however, before PEMFCs can be used to power our automobiles or homes. First, liquid water produced by cathodic oxygen (O)-reduction reaction must be carefully managed to obtain optimal performance in a PEMFC at high current loads—sufficient water is needed to maintain proton conductivity, whereas too much liquid water can result in "flooding" in the gas diffusion layer (GDL), which prevents O from reaching reaction sites and causes performance deterioration. Second, the pore structure and associated wetting (hydrophilic/hydrophobic) property in GDL must be well characterized since they strongly affect O/water transport. Third, platinum (Pt)-catalyst activity decreases over time due to "poisoning" by carbon monoxide (CO) or other contaminants. Finally, polymer membrane degrades over time due to mechanical and thermal stresses. Though various piecemeal numerical treatments for PEMFCs have been reported in the literature, they lack models that incorporate the essential phenomena and that can be used to simulate PEMFC performance at practical operating conditions.

Sandia seeks to develop first-principle–based or phenomenological computer models to tackle these outstanding research challenges. We will carry out experiments for phenomenological discovery and model validation. Our objective is to develop an integrated PEMFC performance model by taking advantage of infrastructure in GOMA (a Sandia-developed finite-element [FE] code). Specifically, we propose to formulate a constitutive model for proton conductivity and to validate it using experimental data. We will develop phenomenological models to simulate (1) transports of H/air in flow channels and GDLs, proton/water in membrane, and liquid water in cathode GDL; (2) H-oxidation/O-reduction reactions in catalyst layers; (3) liquid-water droplet growth and removal from the cathode-GDL/flow-channel interface; and (4) Pt-catalyst activity reduction and polymer-membrane

degradation. We will perform visualization experiments and current-distribution measurements to validate the models.

We focused our efforts on investigating, experimentally and computationally, the key phenomena of liquid-water droplet growth and removal from the GDL/gas-flow-channel interface in the cathode, developing a phenomenological model for liquid-water transport in uniformly hydrophobic diffusion media, formulating a new constitutive model for predicting proton conductivity, and developing a baseline PEMFC performance model. More specifically, we accomplished the following: (1) fabricated a transparent PEMFC visualization cell; (2) carried out experiments under realistic operating conditions to visualize growth and breakup of liquid-water droplets at the interface between the cathode GDL and flow channel; (3) developed simplified and FE models for predicting the instability diagram for droplet removal; (4) performed experiments to measure proton conductivity of Nafion® 117 using electrochemical impedance spectroscopy over a wide range of water contents and temperatures; (5) formulated a new constitutive model for predicting proton conductivity and validated it using data from literature as well as our own measurements; (6) developed an analytical performance model for an idealized PEMFC; and (7) completed a phenomenological model for liquid-water transport through uniformly hydrophobic diffusion media and studied the fundamental roles played by a commonly used, but poorly understood, microporous layer in PEMFCs. In addition, we made significant progress on the development of a GOMA-based, phenomenological, baseline PEMFC performance model. Work is also ongoing to examine the effects of the microporous layer on water management by combining the uniformly hydrophobic diffusion-medium model with a membrane model. Finally, we set up the apparatus and are making progress in measuring the hysteresis of contact angles between the water droplet and the cathode GDL surface.

...we made significant progress on the development of a GOMA-based, phenomenological, baseline PEMFC performance model.

Refereed

Chen, K. S., and M. A. Hickner. 2004. A new constitutive model for predicting proton conductivity in polymer electrolytes. *Proc. IMECE '04: 2004 International Mechanical Engineering Congress and Exposition*, accepted.

Noble, D. R., and K. S. Chen. 2004. Elucidating water-droplet removal in polymer-electrolyte fuel cells. *Proc. IMECE '04: 2004 International Mechanical Engineering Congress and Exposition*, accepted.

Pasaogullari, U., C. Y. Wang, and K. S. Chen. 2004. Liquid water transport in polymer electrolyte fuel cells with multilayer diffusion media. *Proc. IMECE '04: 2004 International Mechanical Engineering Congress and Exposition*, accepted.

Other Communications

Chen, K. S., M. A. Hickner, and D. R. Noble. 2004. Elucidating water transport in polymer electrolyte fuel cells. Paper presented at the 2004 AIChE Spring Meeting, 25–29 April, New Orleans, Louisiana.

Hickner, M. A., K. R. Grossarth, K. S. Chen, and D. R. Noble. 2004. Liquid water droplet instability and removal at the GDL/gas flow channel interface. Paper presented at the Fuel Cell Gordon Research Conference, 25–30 July, Bristol, Rhode Island.

67054

Optimal Allocation of Terrorist Countermeasures Using Risk-Based Systems Pathways Analysis

M. L. Young, L. Shyr, M. J. Berg, R. A. Jung, M. A. Minton, F. J. Schelling, Jr., R. L. Craft, B. J. Smith, L. M. Chavez

This effort explored concepts that could enable the cost-benefit analysis of candidate countermeasures (CMs) for the reduction of risks related to terrorist attacks. Sandia focused on developing an approach that would enable the analysis of CMs that could be implemented at any point along an attack path, including attack planning and preparation through consequence mitigation. We examined risk reduction as a possible measure of CM benefit. We investigated attack graphs as a central analysis tool for estimating relative risk over an attack option space of concern. This effort produced a high-level systems view of the problem space, a scenario analysis process, a prototype attack-graph tool, and a prototype CM analysis tool. In addition, we developed an example analysis of a hypothetical radiological dispersal device (RDD) scenario as well as a concept for a generic event sequence that would enable the analysis of alternative event models.

This effort explored concepts that could enable the cost-benefit analysis (CBA) of candidate CMs for the reduction of terrorist attack–related risks. We focused the effort on developing an approach that would enable the analysis of CMs that could be implemented at any point along an attack path, including attack planning and preparation through consequence mitigation. We selected risk reduction as the measure of CM benefit. We investigated attack graphs as a central analysis tool for estimating relative risk over an attack option space of concern.

We selected the attack-graph approach as a candidate tool for the assessment of risk reduction achieved via CM implementation for a number of reasons. We developed the attack-graph approach to model the adversarial actions required and the alternatives available for achieving specific outcomes. We can generate relative likelihood values for alternative paths through an option space based on a comparison of attribute values assigned to individual activities and related adversarial preferences. Because attack graphs are not constrained to the single hierarchical tree structure of traditional logic models, they can be used to create less-constrained models of adversarial actions and potential consequences.

We developed GAME, a prototype attack-graph tool, to support the analysis needs of this effort. GAME utilizes algorithms developed for the calculation of quality-of-service metrics for network-routing protocols to provide modeling and analysis capabilities required for this application and unavailable in any other attack-graph tool. New capabilities provided by the GAME tool include algorithms that enable the analysis and ranking of paths based on an analysis of multiple attributes, both the minimization and maximization of attributes in a single analysis, and the ability to analyze nonadditive metrics. In addition, GAME immediately eliminates paths from consideration that exceed user-defined limits for adversarial preferences, significantly improving the efficiency of the analysis algorithm.

The application of attack graphs to the analysis of the entire pre- and post-consequence attack path presents a number of challenges. One concern is that attempts to model the myriad of alternatives available to an adversary could quickly result in a combinatorial explosion of possible attack paths. In addition, many preconsequence activities are not inherently sequential, and the sequence in which activities occur may define future constraints or opportunities along a path. We proposed a segmented approach to the attack-graph problem that could enable the generation of limited-scope attack graphs that could simplify the use of attack graphs for the analysis of the entire attack path.

A wide array of information will be required to produce defensible estimates for risk reduction achieved through CM implementation. An efficient, cost-effective analysis tool must include effective strategies for knowledge management, preservation, and retrieval. We outlined a prototype database structure as well as a concept for and prototype of a CM database and analysis tool. The tool provides a structure for the automated retrieval and analysis of CM information based on a generic event sequence.

This effort produced a high-level systems view of the problem space, a scenario analysis process, and prototype attack-graph tool, database structure, and CM analysis tool. In addition, we developed an example analysis of a hypothetical RDD scenario as well as a concept for a generic event sequence that would enable the analysis of alternative event models. The prototype attack-graph tool provides a number of needed analysis capabilities that were previously unavailable in attack-graph tools.

The development of a comprehensive approach to CM CBA within the context of the complete pre- and post-consequence

event path represents a formidable task. We concluded that a multiyear effort would be required to detail a comprehensive approach and to develop a software package that would automate the analysis process.

Other Communications

Young, M. L., R. L. Craft, F. J. Schelling, Jr., L. Shyr, M. A. Minton, R. A. Jung, M. J. Berg, and B. J. Smith. 2004. Optimal allocation of terrorist countermeasures using risk-based systems analyses. Sandia Technical Report SAND2004-4675, Sandia National Laboratories, Albuquerque, New Mexico.

67055

Silicon Field-Emission Electric Propulsion Arrays (FEEP) Powered by Orbital Nuclear Reactors

S. H. Kravitz, R. X. Lenard

Sandia seeks to fabricate field-emission electric propulsion (FEEP) microthrusters to demonstrate silicon (Si)-based thrusters powered by solar or nuclear energy. FEEPs are operational electric thrusters based on space-proven liquid-metal ion sources operating with indefinite lifetimes, high propellant efficiency (approaching 100%), and high electrical efficiency ~ 95%. We demonstrated overall electric-to-jet efficiency of indium (In)-FEEPs > 85%. Single devices are tediously machined and hand-assembled. Current configurations of FEEPs reach 10^{-3}–10^{-6} thrust levels.

With microelectromechanical systems (MEMS) technologies, fabricating emitters in Si with precise and small tolerances is now possible. Large-scale fabrication of millions of emitters with very close spacing, using very strong materials whose properties can be accurately predicted, will develop a thruster array producing Newtons of force! Such thrust could be used to power space tugs that could slowly move objects in orbit. This power source could be used to rescue defective satellites or move vehicles to higher orbit after achieving low-earth orbit.

In early work, we will design and build an initial prototype of a 10 x 10 thruster array. This size will be capable of meeting thrusts in the micro-Newton level. In later work, we will test, modify, and scale our design, and, finally, we will build and test an array of 100,000 thrusters covering an entire 6 in. Si wafer.

Thrusters made from single-crystal Si can be used as a structural component of a spacecraft. Because the engines are on the outside of the craft, the interior can be used for mission payload and for fuel storage. A design based on individual emitter/extractor electrode pairs enables beam collimation and on-thruster thrust vector control (TVC) at low mass. TVC on NASA's DS-1 spacecraft weighed three times the ion engine.

Large-scale fabrication of millions of emitters with very close spacing, using very strong materials whose properties can be accurately predicted, will develop a thruster array producing Newtons of force!

We met most of our goals. Because of the need to design a much more complex and individually addressable device, our modeling and design work has delayed assembly of our first device. We completed all of the modeling, design, test jigs, and fabrication planning. We developed numerical codes to model FEEP thrusters. We ordered all the custom parts, began fabrication and assembly of the piece parts, and will fabricate

the device. We established a working relationship with the Austrian Research Center to surface prepare, wet, and fill with In propellant and test completed devices. We designed a 5 x 5 array of individually addressable emission thrusters so that measurements of voltage start-up and thrust can be separately tested. All parts will be made of either single-crystal Si or Pyrex so that we can assemble them using anodic bonding rather than adhesives. We designed a fuel tank and emitter so we can accomplish the tungsten wetting treatment and fill the tank before bonding the tank bottom in place. We found two methods to create aspect ratios higher than 20:1, by (1) back-filling larger holes to decrease their diameter, and (2) creating planar spiral paths that wick into vertical holes. We wrote several technical advances for new intellectual property that we created.

We completed all the individual piece parts. The Si emitter is not etched as deeply as requested, but we will still be able to use these parts with modification to the assembly process. The emitter must be lapped to its correct thickness and then we will begin assembly on the FEEP system. We designed adapters and manufactured them to allow testing at the Austrian Research Center. Work is also proceeding to provide wetting of tungsten surfaces with liquid In.

Other Communications

Lenard, R. X., and S. H. Kravitz. 2004. Progress in microengineered machine systems field-emission thrusters at Sandia National Laboratories. *Proc. International Astronautical Congress* (3–8 October, Vancouver, B.C., Canada).

Lenard, R. X., S. H. Kravitz, and M. Tamar. 2004. Recent advances in silicon-based field-emission thrusters. *Space Technology Applications international Forum* (13 February 2005, Albuquerque, New Mexico).

67056

Advanced Fuel-Cell Reactor for the Direct Cogeneration of Electricity During Selective Partial Oxidation of Hydrocarbons

A. H. McDaniel, W. A. Steen, S. F. Rice, R. E. Loehman, J. E. Miller

A fuel cell operates on the principle that either hydrogen (H) or hydrocarbon (HC) fuels be completely oxidized to water and carbon dioxide (CO_2) while generating electricity. The idea of an advanced fuel-cell reactor is to control oxidation to produce H or other valuable oxygenated HCs in addition to electricity. The proposed electrocatalytic membrane reactor will make novel use of fossil fuels directly in solid-oxide fuel cells (SOFCs), and, at the same time, address the broader needs of energy security by replacing more-conventional, less-efficient fuel reformer and selective oxidation processes. Sandia focused on realizing these objectives by combining expertise in materials advanced diagnostics. Activities include synthesis and evaluation of novel, low-temperature, ion-conducting membranes activated for selective oxidation of HCs. The project involves challenging materials development, catalyst formulation, and processing issues, as well as advanced diagnostics and experimentation. The main objective is to prototype the reactor concept for a select class of partial-oxidation reactions and thereby provide Sandia with a unique position in an area that has not been exploited for SOFC applications. Unlike existing Department of Energy (DOE) projects targeting auxiliary power, the SOFC-like concept for combined chemical production and electrical generation is an emerging field.

We designed and assembled two perfectly mixed reaction vessels and the accompanying flow system to investigate the catalytic and electrochemical behavior of SOFC membranes. We incorporated turbulent, subsonic gas jets into the designs in lieu of mechanical agitation to achieve mixing. The reactors (one hot-wall, the other cold-wall) consist of small enclosed volumes with pairs of opposing gas-injection nozzles located such that efficient mixing may be accomplished, a means to support and heat the SOFC membrane, electrical and thermocouple feedthroughs, and windows for optical access. The accompanying flow system comprises fluid- and thermal-control systems such that gas residence times between 50 and 5000 ms, pressures between 200 and 750 Torr, and continuous-stirred, batch, or fed-batch operating modes can be achieved. Depending on the experiment, we accomplish membrane

heating by using resistive heating elements (cold-wall) or by insertion of the reactor core into a furnace (hot-wall).

We outfitted the jet-stirred reactors (JSRs) with three main diagnostics: (1) a modulated effusive source mass spectrometer (MS), (2) a pulsed-laser surface Raman capability, and (3) a means to perform electrochemical measurements including impedance spectroscopy. We interfaced the MS to either JSR using a crimped capillary to continuously extract gases from within the reactor. We modulated the effusive source and accomplished ion detection via lock-in amplification. The pulsed-laser surface Raman diagnostic uses optical fibers to couple the excitation beam into, and scattered light out of, the JSR. The scattered light was filtered, dispersed, and recorded onto a charge-coupled device (CCD) array. We executed electrochemical measurements with a commercial potentiostat equipped with data collection and analysis software.

In the catalyst-development task, efforts focused on the partial oxidation of methane to synthesize gas and methane to H. We based initial formulations on modifications to the nickel (Ni)/yttria-stabilized zirconia (YSZ) system by adding alkali-, alkali-earth, and selective lanthanide and transition metals. The goal was to optimize the activity of the material and increase the stability of Ni against deactivation by coking. We explored various methods such as ball milling, wet impregnation, and co-precipitation to synthesize anode powders. We accomplished nonelectrochemical characterization in a conventional packed-bed reactor operating at temperatures between 673 K and 1173 K. We measured gas compositions exiting the reactor by gas chromatography (GC), allowing methane conversion and selectivity, and the H_2/CO ratio, to be determined.

Catalytic activity tended to correlate with preparation methods rather than Ni loading, with co-precipitated samples behaving similarly and more reactive than other methods. Wet-impregnated materials were the least active. As anticipated for the baseline Ni/YSZ material, the degree of deactivation correlated with Ni loading and was accompanied by a significant degradation in selectivity and H_2/CO (molecular hydrogen/carbon monoxide) ratio. Catalysts modified with calcium (Ca), magnesium (Mg), and manganese (Mn) were most promising for mitigating the effects of coking. In addition, Ni/barium oxide/aluminum oxide (Ni/BaO/Al_2O_3) catalysts that were produced using high-temperature calcination created crystalline hexaaluminate material, which showed no deactivation or coke buildup during tests. Further modification of these materials is required to impart sufficient electrical conductivity for use as an SOFC anode.

Paramount to the success of this project is the ability to rapidly synthesize viable electrochemical stacks (anode-electrolyte-cathode) for experimental characterization. We contracted this task to Ceramatec, a private firm proficient at screen-printing and tape-casting ceramic materials. While Sandia personnel will be responsible for identifying and synthesizing alternative anode formulations and ion conductors, Ceramatec will fabricate test cells. We fabricated two cell types: (1) a tab of YSZ with coatings and current collectors on one side, and (2) an electrochemical stack sealed to the end of a YSZ tube. We will use one-sided cells primarily to investigate the inherent catalytic properties of the anode material or the nonfaradic electrochemical modification of catalytic activity. We will use the electrochemical stack sealed to a YSZ tube to perform more conventional fuel-cell experiments; in this configuration, the JSR becomes an air-breathing SOFC.

67057

New Hydrogen-Storage Material: Metal-N-H System

W. Luo, E. E. Ronnebro, S. M. Sickafoose, K. D. Stewart, K. J. Gross, S. Spangler

FreedomCAR (Cooperative Automotive Research) hydrogen (H)-storage goals for the future of H-powered transportation are 6–10 wt.% gravimetric system capacities operable at near proton-exchange-membrane fuel-cell (PEMFC) temperatures (80°C). Great advances have been made with metal-hydride systems in the last few years, essentially doubling capacity. However, today's best hydrides will not meet one or the other of the required goals; for example, titanium (Ti)-doped sodium alanate $NaAlH_4$ (4 wt.%, at 125°C) and catalyzed MgH_2 (7.4 wt.% at 300°C). What is required is an "out-of-the-box" approach to achieve H-storage material with even higher capacity.

Amides, rather than hydrides, offer a unique opportunity to explore novel H-storage systems. For example, the Li-N-H (lithium-nitrogen-hydrogen) system contains up to 11% H (Li_3NH_4). Recently, a group at the National University of Singapore reported that the Li-N-H system can reversibly store ~ 7 wt.% H in the temperature range of 255°C–285°C. While these temperatures are still high, not much is known about this system. It is essential that the thermodynamic properties and reaction kinetics be characterized. Beyond this, Sandia would like to try to destabilize this material through doping, as we have done with the alanates. If successful, elemental doping should enable the tailoring of these materials to allow lower-temperature operation.

We recently validated the first step of this reaction. We measured desorption isotherms of $LiNH_2$-LiH at three temperatures and calculated the reaction enthalpy, which is very close to the value reported by Chen (from the National University of Singapore).

Since the operating pressure is too low and the temperature is too high to use this material for onboard H-storage application, we successfully developed and tested a new material that improves the operating conditions significantly, compared with the one reported by Chen. We measured the desorption isotherms of the newly developed material at three temperatures. According to the van't Hoff plots, this material can have pressure of three bars at 100°C, which is very promising for H-storage application.

We filed a patent application.

Refereed

Luo, W. 2004. ($LiNH_2$-MgH_2): A viable hydrogen-storage system. *J. Alloys and Compounds*, in press.

Other Communications

Luo, W. 2004. Toward a viable hydrogen-storage system for transportation application. *J. Alloys and Compounds, Proc. International Symposium on Metal-Hydrogen Systems* (6 September, Krakow, Poland).

67058

Intrusion Detection for Wireless Networks

J. Vanrandwyk, D. Kilman, E. D. Thomas, E. J. Lee, R. P. Custer, T. J. Toole

Sandia began developing an intrusion-detection architecture for wireless networks. We wrote tools and prototype code specific to the IEEE (Institute of Electrical and Electronics Engineers) 802.11b standard wireless networks that are currently most popular. Our intent is to develop an architecture and prototype software that can be transitioned easily to intrusion-detection and monitoring in networks based on future wireless technologies.

We wrote visualization tools to look at wireless networks in novel ways. Some of our prototype software enhances the commercial and open-source software already available for wireless intrusion detection and monitoring. We studied the radio-frequency (RF) layer of the 802.11b protocol, looking for ways to detect and mitigate attacks at that layer. We are investigating how to physically locate devices in a wireless network to disable attacks or possibly control access to the network. Much of this work is ongoing.

Wireless networks are being deployed rapidly with attention often paid to the integrity and confidentiality of the data being transmitted, but without proper intrusion-detection or monitoring on those same networks. We anticipate that this research will give Sandia and other national labs within the Department of Energy (DOE) the confidence to deploy wireless networks when using our architecture as a guide. This work could potentially provide input for a "best-practices" guide to monitoring infrastructure wireless networks in the Department of Homeland Security (DHS), other federal agencies, and even private organizations. We plan to test some of our tools on Sandia networks as we stand up some of our own wireless networks.

Our research differs from other wireless intrusion-detection research in that it will focus on infrastructure networks as opposed to ad hoc *networks. This project looks in depth at the hard-to-understand RF layer of wireless protocols, attempts to use a wireless device's location in new ways, and gives a picture (literally) of wireless networks not seen before.*

We wrote visualization tools to look at wireless networks in novel ways....This work could potentially provide input for a "best-practices" guide to monitoring infrastructure wireless networks in the Department of Homeland Security (DHS), other federal agencies, and even private organizations.

We found visualization tools to be missing from the existing software base. We developed several visualization tools to aid in viewing wireless networks in new ways. These tools allowed

us to see currently identified attacks in a new format and to look for attacks not currently detected.

We found that adequate software exists to detect attack signatures in wireless networks. But we cannot record wireless traffic, and post-analysis of traffic is quite limited. We built a framework for capturing, disassembling, and displaying characteristics of wireless-network packets. We wrote prototype tools to collect both session data and individual packets from wireless networks. Current work is exploring the problem of aggregating data from multiple wireless-network sensors. Our work in this area has made hardware/software incompatibilities in the wireless area very apparent.

We began studying the RF layer of the 802.11b protocol and how denial-of-service (DOS) attacks work against the RF layer. We simulated DOS attacks using network-simulation software to discover ways to mitigate these types of network attacks.

We also studied wireless-device–locating techniques. Once we discover that a wireless device is attacking our network or that one of our wireless devices has been compromised, we need to locate that device. We studied several methods for locating wireless devices used by the mobile-phone industry that are gaining popularity in the wireless computing arena; these include analysis of time of arrival (TOA) and signal strength.

We developed a set of usage scenarios applicable to lab use of wireless networks. We developed these scenarios in such a way that other government and private-entity wireless networks should be described by this set of scenarios. Following our development of wireless-network usage scenarios, we drew a network diagram that encompasses the physical and logical components of a typical infrastructure wireless network.

To ensure that our architecture and tools can be extended to work with future wireless-network technologies, we conducted a brief survey of current and future wireless technologies. In that survey, we looked at various IEEE standards that outline wireless packet communications. We focused on those standards related closely to the IEEE 802.11 standard and Internet Protocol (IP) networking. Our survey included the frequency spectrum used, the method of RF modulation, the typical use of the equipment based on the standard, and typical usable distance, among other things.

67059

Membranes for H_2 Generation from Nuclear-Powered Thermochemical Cycles

T. M. Nenoff, T. J. Garino, A. Ambrosini, P. S. Pickard

Sandia seeks to develop high-temperature, robust ceramic membranes for thermochemical cycles that are being considered for hydrogen (H) production. Our project will initially review the cycles being considered by Department of Energy (DOE) nuclear energy (NE) and energy efficiency (EE) and identify where membrane separations have the potential to improve cycle efficiency or complexity. We will then focus on developing membranes able to perform separations under extreme conditions, thereby allowing for the economically viable chemical production of H_2. Earlier studies identified over 100 possible reaction cycles that produce H_2 at high temperatures. Of the cycles identified as the most promising, many require the removal of O_2 or H_2 to push reaction equilibriums in favorable directions. A leading candidate cycle is the sulfur-iodine (S-I) cycle, based on projected high efficiencies (about 50%). To push this process forward, we use a stable membrane to remove O_2 from the first reaction, and then we use another membrane to remove the purified H_2 from the third reaction. The demanding conditions of high temperature, the oxidizing environment of the decomposed H_2SO_4, and the separations of the competing similarly sized compounds require (1) development of the separations module, (2) advanced materials research for membranes and membrane sealants (to avoid leakage at edges), and (3) testing under realistic conditions.

Recent work focused on three major research areas: (1) materials synthesis/characterization, (2) conductivity apparatus design/build/testing, and (3) bench-scale reactor design/build. Synthesis results from the hydrothermally derived Perovskites (sodium/niobium/titanium,zirconium [Na/Nb/Ti,Zr]) and solid-state synthesized Perovskites include new and traditional compositions. Characterization techniques include powder x-ray diffraction (XRD), themogravimetric analyzer and differential thermal analyzer (TGA/DTA), thermal analyses under various gases and temperatures, scanning-electron microscopy/energy-dispersive x-ray (SEM/EDX), elemental analyses, and conductivity measurements. We are using an in-house, high-temperature, four-probe, ionic conductivity measurement device on Perovskites samples for testing.

We ran thermal studies to get information on oxygen stability and oxygen adsorption/desorption. To determine oxygen stoichiometry, we reduced samples under 5% H_2/N_2 at 1000°C until weight loss stabilized, usually at about 14%. For absorption/desorption, we ran multiple-cycle TGA on the single-phase samples. First, we cycled the temperature three times between 50°C and 850°C under an O_2 atmosphere. This was followed by cycling between O_2 (high pO_2) and argon (Ar) or helium (He) (low pO_2) atmospheres at a constant temperature of 850°C. We created a graph that shows the weight change as the temperature is cycled between 50°C and 850°C, under a constant flow of O_2 gas. It describes an easily reversible temperature-swing adsorption/desorption of oxygen. The graph also illustrates the reversible weight change as a function of oxygen partial pressure, by cycling the gas between O_2 and Ar or He at a constant temperature of 850°C. This implies that the material can transport oxygen across a membrane by pressure differential. We ran XRD studies before and after thermal study samples to confirm retention of the structure.

Our most promising phase to date is the double-substituted Perovskite $La_{0.1}Sr_{0.9}Co_{1-x}Mn_xO_{3-}$. In addition, we ran experiments with yttrium-stabilized zirconium (YSZ, also used in conductivity measurements) as a baseline material and an initial Sandia octahedral molecular sieve (SOMS)–derived Perovskite (Na/Nb,Ti/O). Under the same TGA/DTA experimental conditions, the YSZ and the niobate phase underperform the cobalt (Co) phase ($La_{0.1}Sr_{0.9}Co_{0.7}Mn_{0.3}O_{3-}$) in oxygen desorption studies by an order of magnitude.

- *Conductivity.* We designed and built a four-point conductivity test instrument. We began measurements on samples of synthesized materials as well as on standard materials (YSZ) for comparison. We machined-pressed and heat-treated powder samples into bars nominally 2 mm x 2 mm x 20 mm. We then wrapped platinum (Pt) wires around the bars at four places, both ends and just inside each end. We used conducting paint (silver [Ag]-palladium [Pd]) to ensure good electrical contact between the wires and the sample. We placed the samples in a tube furnace under controlled temperature and atmosphere. We are making measurements in the 400°C–800°C range. We connected a direct-current (dc) source to the wires at the ends of the sample and measured voltage drop across the other two wires with a voltmeter. We then simply determined the conductivity from the current, voltage, and geometry. The initial measurements for each sample were done in air. We measured materials with high conductivity (comparable to that

of the YSZ reference material) in other pO_2 atmospheres (e.g., ultrahigh-purity [UHP] Ar and 3% H in Ar) to determine whether the conductivity is ionic or electronic; ionic conductivity will be independent of the oxygen pressure, while electronic conductivity will scale with it. For materials of interest, we will also perform alternating-current (ac) measurements (impedance spectroscopy) to learn more details about the mechanism of conductivity.

67060

Microfabricated BTU Monitoring Device for System-Wide Natural-Gas Monitoring

A. Robinson, R. P. Manginell, M. Moorman

The natural-gas industry is seeking automation of pipeline processes and distribution. Development of an inexpensive monitoring device for gas heating value in British thermal units (BTUs) is desirable for pipeline system analysis and gas accounting. As natural gas is billed by the BTU and sold by the cubic foot, improved distributed analysis will produce more equitable trade between buyers and sellers. Unaccounted for (UAF) gas content will be reduced, and billing will become more timely and accurate. A 10% improvement in UAF gas accounting will benefit the industry by about $45 million annually (market analysis, 2001). Industrial users will benefit, as well, through continuous feedback of physical gas properties during use. This addresses a critical need for turbine operators to reduce pollution while improving power-generation efficiency.

For market acceptance, the monitoring system must be low cost. Widespread implementation will occur only below a threshold cost of approximately $5000 per instrument. This unit cost can be achieved by using microfabricated analytical components. To achieve this goal, Sandia is developing a BTU monitoring instrument using existing and modified microfabricated components. The instrument will consist of a silicon (Si) gas chromatography (GC) microcolumn in conjunction with a micropellistor (catalytic combustor) array. Thermal-conductivity sensing will provide sensor diagnostics and surety. Microfabrication techniques allow these components to be manufactured in production quantities at a low per-unit cost.

Sandia micropellistor technology is concurrently being developed for low-precision (± 5% BTU), stand-alone, natural-gas monitoring. We will achieve accuracy of ± 0.1% BTU through preseparation of the compounds using Sandia's novel microfabricated GC (µGC) columns. This combination will allow for continuous calorimetric determination with a 1–2 min cycle time. An instrument with these devices can replace month-long sample tank collections at remote natural-gas production wells, as well as provide near-real-time data at pipeline switching and metering stations, turbine generators, and other industrial user sites.

We will achieve accuracy of ± 0.1% BTU through preseparation of the compounds using Sandia's novel microfabricated GC (µGC) columns....An instrument with these devices can replace month-long sample tank collections at remote natural-gas production wells....

We broke our work down into two major tasks for concurrent development. The first involved tailoring Sandia's μGC columns to spatially separate a plug injection of natural gas into its individual constituents. The second task was to tailor Sandia's microhotplate pellistor to respond to natural-gas compounds found in pipelines, with emphasis placed on rapid response to chromatography-type transient exposures.

Development of the natural-gas separation task began with testing the separation ability of multiple Sandia μGC columns. These included columns with wall-coated stationary phases and packable columns containing commercially available chromatography beads. Wall-coated columns were inadequate, but we achieved success with several packable columns. We found a class of high-surface-area porous polymer beads (Haysep) to provide excellent separation, according to carbon number for methane (C1) through pentane (C5). However, isomers of butane and pentane were not completely resolved. With a moderate degree of overlap, separation of C1–C5 can be performed isothermally at 125°C within 70 s. Taking a conservative estimate of the C4–C5 composition of natural gas, the peak overlap of isomers will generate a systematic error in the calculated BTU value of no more than 0.01%. To further improve the separation, we began developing a hybrid column, commercially known as a PLOT (porous-layer, open-tube) column. This type of column offers the best combination of high-surface-area, stationary-phase beads attached only to the walls, leaving an open tubular path down the center. This minimizes the pressure drop, allowing longer columns for more efficient separations. We filed a technical advance for microfabricating such a column with a novel method of producing the high-surface-area stationary phase directly from the walls. This column will find application in the analysis of natural gas, refinery gas, halogenated methanes, and toxic industrial chemicals.

As noncombustible components (carbon monoxide [CO], carbon dioxide [CO_2], and N_2) of natural gas do not contribute to the heating value, their presence is important only from a volumetric standpoint during the injection. However, for certain applications, it is desirable to separate and analyze these compounds with a universal detector. We found a bead packing that was too retentive for butane to be excellent at separating, in order of elution, air, CO, water, CO_2, acetylene, ethylene, ethane, and propane. With the needs of natural-gas analysis in mind, we developed a schematic whereby these compounds could be separated alongside much heavier compounds (C12) in a flow-switching, dual-column system. A 10-port switching

valve would allow all compounds to share the injector and a single detector.

We made several advances in developing the micropellistor as a chromatography sensor. The pellistor responded to low-level, steady-state exposures of natural gas in flow conditions typical of microcolumns. It was then shown to rapidly respond to chromatography injections of whole (unseparated) natural-gas samples and acetone vapors. The response of the detector was much faster than the 4 Hz speed of the data-acquisition system in use at the time. We have since acquired a 100 Hz system. The limit of quantification, found at a peak height-to-noise ratio of 3, was 0.03% in air.

We made several improvements to the micropellistor device. To promote robustness and stability at high temperatures, we added dielectric overcoats and a better metal-adhesion layer to the microhotplate membrane. New catalyst-coating techniques produced films of greatly increased quality and uniformity. Catalyst spraying through a shadow mask onto devices at an elevated temperature led to a denser catalyst coating that showed improved resilience to cracking and spalling. In addition, we determined the sensitivity stated above using a 1% catalyst coating. A 10% catalyst coating can now be applied successfully, and these devices show a much-enhanced response to HC exposures.

Other Communications

Robinson, A. L., W. Einfeld, M. Moorman, R. P. Manginell, and J. A. Ellison. 2004. Microfabricated BTU monitoring device for natural-gas analysis. Paper presented at the Center for Process Analytical Chemistry Summer Institute, July, Seattle, Washington.

67061

"Tunable" Ion Conductors for Low-Temperature Oxide-Based Fuel Cells

T. M. Nenoff, T. J. Garino

This project focuses on the synthesis and characterization of "tunable" Perovskite ceramics with resulting controlled strength and temperature of dielectric constants and/or with ionic conductivity. Traditional methods of synthesis involve high-temperature oxide mixing and baking. Sandia seeks a new methodology of synthesis involving the (1) low-temperature hydrothermal synthesis of metastable porous phases with "tuned" stoichiometry and element types, and then (2) low-temperature heat treatment to build exact stoichiometry Perovskites, with the desired vacancy concentrations. This flexible pathway can lead to compositions and structures not attainable by conventional methods. We will then study these materials by high-temperature oxide melt solution calorimetry and conductivity measurements to better delineate stability and stoichiometry/bulk conductivity relationships. This, in turn, will lead to a predictive model for the possible extent of (sometimes metastable) substitutions.

Recent work consisted of three major research areas: (1) Sandia octahedral molecular sieves (SOMS) and novel SOMS synthesis/characterization, (2) SOMS–derived Perovskite synthesis/characterization, and (3) conductivity-apparatus design/build/testing. Results from the SOMS (sodium/niobium/titanium,zirconium [Na/Nb/Ti,Zr]) and Perovskite syntheses include traditional compositions now made from both alkoxides or oxides (allowing for future commercial scale-up). Furthermore, we extended the phase space to include Na/Nb, vanadium (V), antimony (Sb), tantalum (Ta)/Ti, Zr, cerium (Ce), and germanium (Ge). The reactions produced either SOMS, hexaniobate, or direct Perovskite phases. We also ion-exchanged europium (Eu), barium (Ba), strontium (Sr), and lanthanum (La) cations into SOMS and synthesized new various compositions. Characterization techniques include powder x-ray diffraction (XRD), scanning-electron microscope/energy-dispersive x-ray (SEM/EDX), thermal and elemental analyses, conductivity measurements, and some calorimetry. We are using an in-house, high-temperature, four-probe, ionic conductivity measurement device on Perovskites samples for testing. Calorimetry experiments with the University of California at Davis are ongoing; initial work focused on end members for (1) SOMS

and Perovskite materials, and (2) solid-solution series of Ti and Zr-substituted SOMS and Perovskite.

First, there is a large selection of pure SOMS phases that are synthesized hydrothermally—some from oxide reactants, some from alkoxide reactants. Also, there is a list of Perovskite phases that have been synthesized. These phases are either synthesized directly by low-temperature hydrothermal methods, or by heat treatment of SOMS metastable phases. The hexaniobate phase is a polyoxoanion precursor phase to SOMS. The 6° and 69-2B phases are recurring unidentified precursor or impurity phases. Furthermore, with a focus on the need for an eventual synthetic reaction process that can be commercialized, we developed a hydrothermal method for synthesizing the SOMS and Perovskites with oxide reactants.

- *Calorimetry.* The defect chemistry of many Perovskites is controlled by a series of charge-coupled ionic substitutions. In this project, we are measuring the energetics of substitutions, such as the variations on SOMS and Perovskites, by high-temperature oxide melt solution calorimetry. One study has been with the end member SOMS phase $Na_2Nb_2O_6{\cdot}H_2O$, and its comparison with the solid solution of the $Na_2Nb_{2-x}M_{4+x}O_{6-x}(OH)_x{\cdot}H_2O$ family of materials; we synthesized various stoichiometries. Upon heating, $Na_2Nb_2O_6{\cdot}H_2O$ converts to $NaNbO_3$ Perovskite. The exothermic enthalpy for the latter reaction suggests that $NaNbO_3$ Perovskite is energetically favorable and that the microporous phase $Na_2Nb_2O_6{\cdot}H_2O$ is metastable, even under its synthesis conditions. This stability relation is consistent with the ease of conversion of the microporous phase to its Perovskite counterpart upon extensive heating.
- *Conductivity.* We designed and built a four-point conductivity test instrument. We began measuring samples of synthesized materials as well as standard materials (yttria-stabilized zirconia [YSZ]) for comparison. We machine-pressed and heat-treated powder samples into bars nominally 2 mm x 2 mm x 20 mm. We then wrapped platinum (Pt) wires around the bars at four places, both ends and just inside each end. We used conducting paint (silver [Ag]-Pt) to ensure good electrical contact between the wires and the sample. We then placed the samples in a tube furnace under controlled temperature and atmosphere. We made measurements in the 400°C–800°C range. We connected a direct-current (dc) source to the wires at the ends of the sample and measured voltage drop across the other two wires with a voltmeter. We then determined the conductivity simply from the current, voltage, and geometry. The initial measurements for each sample are

done in air. Materials with high conductivity (comparable to that of the YSZ reference material) will be measured in other pO_2 atmospheres (e.g., ultrahigh-purity [UHP] Ar and 3% hydrogen in Ar) to determine whether the conductivity is ionic or electronic: Ionic conductivity will be independent of the oxygen pressure, while electronic conductivity will scale with it. For materials of interest, we will also perform alternating-current (ac) measurements (impedance spectroscopy) to learn more details about the mechanism of conductivity.

Refereed

Xu, H., A. Navrotsky, M. D. Nyman, and T. M. Nenoff. 2004. Thermochemistry of framework titanosilicates, $A_2TiSi_6O_{15}$ (A=K, Rb, Cs). *J. American Ceramic Society,* accepted.

Xu, H., A. Navrotsky, M. D. Nyman, and T. M. Nenoff. 2004. Thermochemistry of niobated-based microporous phases $Na_2Nb_{2-x}MxO_{6-x}(OH)_xH_2O$ (M = Ti) and their dehydrated Perovskites. *J. Materials Research Society,* accepted.

Xu, H., M. Nyman, T. M. Nenoff, and A. Navrotsky. 2004. The prototype Sandia octahedral molecular sieve (SOMS) $Na_2Nb_2O_6{\bf .}H_2O$: Synthesis, structure, and thermodynamic stability. *Chem. Mater.* **16**:2034–40.

67062

Nuclear Nanobatteries: On-Board Power for Independent MEMS Devices

J. A. Crowell, C. Muñoz, R. W. Olsen, R. A. Causey, F. P. Doty, D. A. Chinn, D. F. Cowgill

Size reductions of microelectromechanical systems (MEMS) have not been matched by similar reductions of their power supplies, limiting the potential for independent microsystems. Radionuclides, which have energy densities 3 to 5 orders of magnitude greater than chemical batteries, may offer a solution that can be integrated into these devices.

Sandia will demonstrate a solid-state, microscale, radionuclide-powered battery with power sufficient to drive MEMS devices. We leveraged Sandia's ongoing research into p-*conjugated materials (PCMs) to produce candidate heterojunctions. These materials offer good radiation hardness and wide choice of materials and properties.*

We produced a series of heterojunctions of various compositions by spin-casting the PCMs on an electrode-coated substrate, then vapor-depositing a second metal electrode.

At a minimum, we seek junctions that exhibit rectifying behavior: a nonlinear current-voltage relationship like a diode—as opposed to a linear current-voltage relationship like a resistor. Testing of the earliest devices revealed shorted or failed (linear) junctions. However, two developments have produced heterojunctions with favorable electrical characteristics.

One of these developments was the production of "bulk" heterojunctions (use of a single layer of blended PCM with single-walled carbon nanotubes (CNTs) sandwiched between dissimilar metal electrodes). The other development was the discovery of a novel solvent system that allowed us to filter troublesome particulate impurities from our heterojunction materials before spin-casting.

Initial testing of the devices consisted of measuring the current versus applied voltage. In addition, we measured the photovoltaic characteristics of the devices. An initial test of a single device with an electron-beam source failed to show the expected open-circuit voltage. Further tests are currently under way.

[We discovered]...a novel solvent system that allowed us to filter troublesome particulate impurities from our heterojunction materials before spin-casting.

We fabricated and tested numerous heterojunction devices made of PCMs. We produced PCM heterojunctions of various compositions and three distinct configurations.

Testing of the earliest devices revealed shorted or failed (linear) junctions. Heterojunctions produced by two developments, however, exhibited favorable electrical characteristics.

In one of these developments, we produced “bulk” heterojunctions by a process that involved the use of a single layer of blended PCM with single-walled CNTs sandwiched between dissimilar metal electrodes. These heterojunctions exhibited superior performance as compared with the bipolymer heterojunctions that we produced initially.

In the other development, we discovered a novel solvent system that allowed us to filter troublesome particulate impurities from our heterojunction materials. This discovery resolves a long-standing problem plaguing the fabrication of polymer electronics.

Devices fabricated to date have been qualified as junctions by I-V testing: measuring the resultant current versus applied voltage. Shorted junctions exhibit a linear current versus voltage response, while functional heterojunctions exhibit the nonlinear response of a diode.

Another qualifying test is observing photogenerated voltage across the junction (solar-cell action). Mechanisms of solar-cell operation are similar to a betavoltaic, with the source of charge separation being photons instead of fast electrons. By depositing a bulk heterojunction film on an indium-tin-oxide (ITO)–coated glass substrate and then depositing aluminum (Al) top contacts, we can test the film as a solar cell. Monitoring the open-circuit voltage and short-circuit current in the dark and then exposing them to ambient room light will give indications of solar-cell performance. Devices tested in this fashion exhibited an open-circuit voltage of up to 0.5 V.

These tests indicate that our heterojunction development effort was successful in producing a functional rectifying junction that should function as a betavoltaic.

A key test of these devices is to measure voltage and current produced by exposure to an accelerated electron beam. This will allow us to characterize the devices with a fast monoenergetic electron source, over varying electron energies and incident angles. We assembled a 20 keV electron-beam testing apparatus for this purpose. This apparatus has proven problematic, although an initial test of one device has been performed. That test failed to generate the expected open-circuit voltage. We are still investigating the cause of that failure.

Significant advances continued in the development of device configurations and material compositions. The attachment of electrical leads initially presented difficulties.

Placement by hand of the wire lead developed concentrated pressure against the thin-layered structure, depressing the surface electrode down into the polymer layer until it shorted against the opposing electrode. An arrangement of tape as a cushioning layer over part of the device resolved this problem.

67063

Integrated Tunable Light Sources for Miniature Sensors

R. P. Bambha, S. E. Bisson

Sandia is investigating the development of infrared (IR) light sources for sensor applications based on difference-frequency mixing in waveguides fabricated in periodically poled lithium niobate (PPLN). We expect these devices to be key components in the development of miniature gas sensors that will be useful for the energy industry as well as for first responders at disaster sites. The effort involves modeling, fabrication, and testing of waveguides. We made significant progress in all of these areas. We developed numerical models that allowed us to design masks for the fabrication of PPLN and for the diffusion of waveguides. We set up equipment to perform the diffusion processes and are now prepared to begin fabricating devices. We developed an optical measurement setup for launching the input lasers into waveguides and characterizing the conversion efficiency.

We developed numerical models based on the finite-element method (FEM) to allow us to simulate the diffusion processes used in the fabrication. The diffusion model generates a profile of the proton concentration in the lithium niobate (LiNb) wafer that is related to the index-of-refraction change that occurs as a result of the exchange of hydrogen (H) atoms for Li atoms in the lattice. We then used the FEM to solve Maxwell's equations for the complicated index-of-refraction profile resulting from the diffusion process. An eigenmode solution for the structure gives us the effective index of refraction and the electric field distribution of the mode. We used the effective index of refraction to design waveguides that we could use for difference-frequency mixing in three wavelength ranges: ~ 3300 nm, ~ 3500 nm, and ~ 4300 nm. The model allows us to investigate the effect of proton dose, waveguide width, temperature, and diffusion time on the waveguide modes. We are then able to predict the poling period necessary for quasi-phase-matching the pump, signal, and idler waves.

Given the results of our modeling, we had PPLN fabricated with periods suitable for use in our desired wavelength ranges. We also had diffusion masks deposited on LiNb wafers to allow us to do initial waveguide-fabrication experiments. We investigated two diffusion-mask materials: silicon dioxide (SiO_2) and tantalum (Ta). Unfortunately, the quality of the initial diffusion masks was very poor, and we decided to go

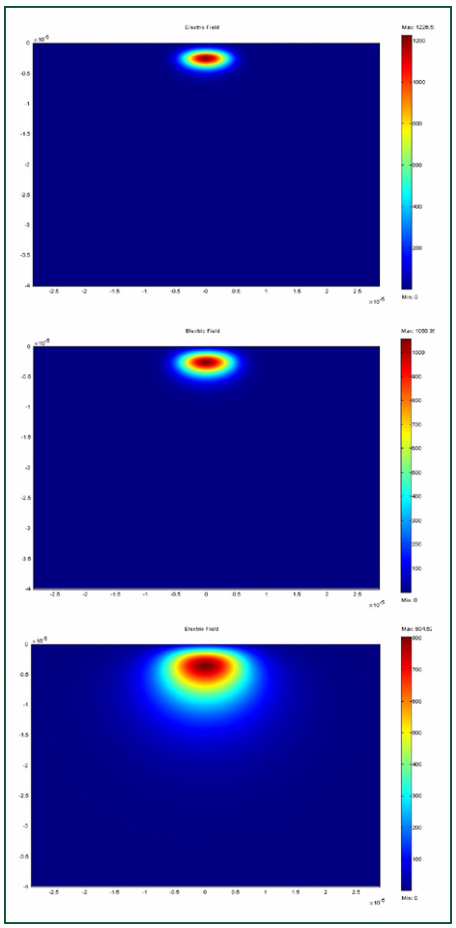

Electric field solution for the lowest-order mode for fields at (top) *1064 nm,* (middle) *1570 nm, and* (bottom) *3302 nm wavelength in a 16 mm-wide waveguide.*

through another mask-fabrication run prior to attempting fabrication runs.

We developed an apparatus for each of the three diffusion processes used in fabricating waveguides. For the first diffusion step, proton exchange, we designed and fabricated a benzoic acid bath that is suspended in a silicone-oil constant-temperature bath. We procured a horizontal tube furnace for the annealing step. We will perform the reverse proton-exchange step in a crucible furnace with a stirring mechanism that we designed.

We developed an optical setup to launch a pump beam (1064 nm) and a signal beam (1530–1630 nm) into a waveguide chip and to collect and measure the mid-IR difference frequency generated at the output.

69143

Design and Fabrication of Advanced Device Structures for Ultrahigh-Efficiency Solid-State Lighting

A. J. Fischer, A. A. Allerman, J. R. Wendt, K. H. Bogart, D. D. Koleske, R. J. Shul, M. H. Crawford

Solid-state lighting holds the promise of white lighting for general illumination with greater than 50% efficiency and extremely long lifetimes of 50,000 hr or more. One significant hurdle to achieving these unprecedented efficiencies is the problem of light extraction. The majority of the photons generated inside the high-index semiconductor of a light-emitting diode (LED) cannot escape the chip due to total internal reflection. Significant improvements in LED efficiency are possible by using a photonic lattice (PL) to improve light extraction. Although we investigated many advanced device geometries, including resonant-cavity LEDs, we quickly down-selected to a PL etched into an indium gallium nitride (InGaN) LED as the most promising approach to improved light extraction.

Sandia demonstrated electrical operation of InGaN/GaN multiple quantum-well LEDs with an incorporated PL. We used electron-beam lithography to define nanometer-scale PL features. We etched a triangular lattice of holes into the top surface of InGaN LEDs using reactive-ion etching (RIE). We implemented a variety of PL configurations into InGaN LEDs with hole diameters ranging from 200 nm to 250 nm and lattice constants ranging from 270 nm to 340 nm. We measured PL dimensions using atomic-force microscopy (AFM) measurements with high-aspect-ratio cantilever tips. The typical hole depth was measured to be ~ 100 nm, where the holes had a sidewall angle of ~ 75 deg with respect to the plane of the LED. We significantly modified far-field LED emission patterns due to the presence of the PL. LEDs with an incorporated PL demonstrated emission up to 1.5x brighter than the planar-control LEDs without PLs.

Although it is more challenging to fabricate PLs in GaN–based LEDs, GaN is the most technologically relevant material system since it can emit light across the whole visible spectrum. Initial problems with etching into the *p*-type GaN surface prompted the use of an NPN (negative-positive-negative) structure with *n*-GaN on the top such that a PL could be etched into the *n*-type material. We used electron-beam lithography to define a triangular lattice of holes in the etch mask and RIE to

etch holes in the *n*-type GaN. We used AFM with a special high-aspect-ratio tip as a nondestructive method to characterize the PL dimensions. We investigated a wide range of hole diameters and lattice constants. We found that very small hole sizes (< 100 nm) are achievable, but this was typically achieved only for shallow hole depths (< 50 nm). For PLs incorporated into InGaN LEDs, the hole diameters ranged from 200 nm to 250 nm, and lattice constants ranged from 270 nm to 340 nm. We measured the typical hole depth to be ~ 100 nm where the holes had a sidewall angle of ~ 75 deg with respect to the plane of the LED.

We fabricated LEDs emitting at 460 nm with and without an incorporated PL for comparison. The LEDs with an incorporated PL showed light emission that is 1.5x brighter than control LEDs. The NPN device structure necessitates the use of a tunnel junction that adds to the device forward voltage. Thus, PL LEDs with a tunnel junction had forward voltages in the range of 4–5.5 V at 33 A/cm^2, while control LEDs without a tunnel junction had voltages near 3.5 V at 33 A/cm^2. It is clearly desirable to fabricate PL LEDs without tunnel junctions since increased forward voltage will reduce the overall efficiency. The far-field radiation patterns were also strongly modified compared to LEDs with no PL. The emission patterns are not well understood at this point and are the subject of future investigations.

This work represents a significant improvement in light extraction and demonstrates that a PL can be used to improve the efficiency of InGaN LEDs.

The LEDs with an incorporated PL showed light emission that is 1.5x brighter than control LEDs....This work represents a significant improvement in light extraction and demonstrates that a PL can be used to improve the efficiency of InGaN LEDs.

Refereed

Wierer, J. J., M. R. Krames, J. E. Epler, N. F. Gardner, M. G. Crawford, J. R. Wendt, J. A. Simmons, and M. M. Sigalas. 2004. InGaN/GaN quantum-well heterostructure light-emitting diodes employing photonic crystal structures. *Applied Physics Letters* **84**:3885.

72599

Develop a System-Dynamics Modeling Framework for Assessing Factors that Influence Water Resource Consumption

H. D. Passell, P. H. Kobos, L. A. Malczynski, G. C. Newman, L. A. McNamara, V. C. Tidwell, J. G. Turnley

This project will create a pioneering, science-based, technical approach for integrating and simulating the impact that disparate hydrological, climatological, ecological, legal, and policy-level factors have on water resource consumption anywhere in the world. Current "state-of-the-art" water resource modeling at Sandia simulates for decision makers the effects of various physical processes on water supply in the Middle Rio Grande (MRG) region. This project will develop an additional technical module that will integrate other decision-impacting variables—in addition to the physical ones—into the calibrated MRG model. This project provides the missing component for development of the first fully integrated, comprehensive modeling approach that will (1) enhance capabilities to more effectively manage scarce water resources for use in direct human consumption, industry, agriculture, energy production, and environmental cleanup; (2) lay a foundation for understanding and integrating factors that control consumption of other resources, including fossil fuels and electricity; and (3) lay a foundation for developing tools that can help avert or resolve regional and international conflict over resource scarcities and other issues.

The technical challenges associated with this effort are focused on (1) collecting new and disparate sets of physical/nonphysical data on water use, water policy, cost-benefit relationships, and consumption patterns; and (2) developing functional relationships among them all that can be directly integrated into the dynamic-simulation framework that already exists for the MRG model. The existing water model offers a unique medium for integrating and then calibrating nonphysical variables against the physical processes already represented. This approach will ultimately have applications to an array of issues much broader than water or energy consumption. It will be applied to avoidance and resolution of civil and political conflict and de-escalation of terrorism, and it will be useful in risk-assessment and planning applications for various federal agencies, including the Department of Homeland Security.

We partially met one major goal: the effort to build a functioning model of the transfer of water rights from agricultural to urban uses in the MRG, and the integration of that model into the existing MRG water-balance model. We failed to build a model of the transfer of water rights because data on water rights turned out to be unavailable. However, the transfer of water rights was really only a surrogate for the transformation of agricultural land to urban uses, so we sought other data that would allow us to model that transformation. Data for that exercise were also sorely lacking, but we acquired enough to build a model reflecting the system.

The second major accomplishment was to develop a method for modeling nonphysical processes as they relate to physical ones. In this case, the physical process was the transformation of land use from agriculture to urban; the nonphysical process encompassed the economic, social, and cultural decisions that people made that allowed the physical transformation to take place. We made great progress in this effort and established a method for integrating the physical and nonphysical processes in one model.

72600

Develop a Cooperative Water-Management Process, Creating a System-Dynamics Model of Water Resources in the Lower Rio Grande Basin

H. D. Passell, M. L. Ennis, G. C. Newman, J. R. Brainard, V. C. Tidwell

Internationally shared surface-water and groundwater resources are an increasing source of conflict in the world. Averting and resolving these conflicts calls for a unified package of technical decision-support tools. The Rio Grande along the U.S.–Mexico border is a prime example of an internationally shared water resource stressed by population growth and conflict over international water treaties. U.S. congressional interest in the region is high, with draft legislation to evaluate transboundary groundwater resources. Looming regional drought threatens to exacerbate existing scarcities.

In this project, Sandia will wage peace by developing the technical tools and processes required for system-dynamics (SD) modeling of water resources in internationally shared river basins. Sandia will apply these tools and processes to the Lower Rio Grande Basin from Ft. Quitman (near El Paso) to the Gulf of Mexico. SD modeling allows the simulation of alternative water-management strategies and is invaluable for helping managers, stakeholders, and policy makers understand complex relationships inherent in water-resource systems. SD models built among multiple agencies and stakeholders from both sides of a border can become transparent trusted tools for transboundary users, and can therefore provide an effective tool for collaborative transboundary resource management.

This project will involve technical collaboration between U.S. and Mexican scientists to develop both the process and the model for jointly managing the shared resource. The overall technical challenge is to build a model that includes distinct, yet interconnected, geographic/political/ecological regions involving multiple complex feedbacks across multiple scales. This includes integration of data collected over multiple jurisdictions with different sampling techniques and quality standards, and from different temporal and spatial scales; development of a thorough understanding of water uses and legal constraints along both sides of the long border; development of compatible modeling approaches among institutions, and integration of model components into a single model; and integration into a single model of the complex

In this project, Sandia will wage peace by developing the technical tools and processes required for system-dynamics (SD) modeling of water resources in internationally shared river basins.

hydrological, ecological, demographic, and political systems in multiple sections of a large, international region.

We will create an SD water-resource planning model for the Lower Rio Grande Basin from Fort Quitman (near El Paso) to the Gulf of Mexico. This model will be the largest of its kind, encompassing 1170 river mi. and a 149,000 mi.^{2} watershed. This model will cover an area about 10x larger than the area covered in Sandia's existing Middle Rio Grande (MRG) model. Specific details of the proposed research and development (R&D) include development of a complex SD model at a geographic scale heretofore not attempted; model development with highly uncertain data; integration of data collected over multiple jurisdictions with different sampling techniques and quality standards and from different temporal and spatial scales—all collected for differing purposes; integration of data across diverse technical disciplines, including hydrology, land uses, ecology, demographics, etc.; and integration of model components developed in three different institutions throughout the basin. This project will construct or derive empirical equations or probability distribution functions for parameters to be used in the analyses, combine the various sources of information and equations into the SD framework, and calibrate the resulting model with historical data.

The benefits of developing this SD model of the Lower Rio Grande are numerous. This model will be the first complete, science-based water-resource dynamics model that incorporates data across international and intranational boundaries. Shared surface-water and groundwater resources are an increasing source of concern for national security, environmental cleanup, and energy security. Averting and resolving these issues calls for a unified package of technical decision-support tools. The Lower Rio Grande offers the best opportunity to complete a major shared river and groundwater system model. The water-stressed border region has the fastest-growing human population in North America and has serious water-related national security concerns for energy production and environmental cleanup.

This model will be the largest of its kind, encompassing 1170 river mi. and a 149,000 mi.^{2} watershed....This model will be the first complete, science-based water-resource dynamics model that incorporates data across international and intranational boundaries.

72716

Energy-Systems Analysis Framework and Modeling

S. A. Jones, M. M. Valdez, L. E. Klebanoff, K. B. Vanderveen, G. W. Kuswa, J. V. Zuffranieri, A. E. Lutz, K. L. Stamber, J. D. Brewer, T. H. Karas, O. H. Paananen, D. J. Borns

The U.S. relies on a national energy system and infrastructure that has "evolved" with limited systemwide management over the past century under varying policy, market, and environmental forces. Overall, it presently meets our energy needs reliably and inexpensively. However, growing concerns over impacts on the environment, physical and economic security, system reliability, and long-term sustainability may require changes in the way energy is produced, transported, stored, and used. Investments will be made in energy infrastructure because of near-term needs, yet their impact will last for decades because of the high cost and long lifetime of energy infrastructure. Public policy influences infrastructure investments and funds energy research and development programs. Decisions based on a systemwide perspective, rather than on a narrow scope of concern, will permit more optimized solutions.

Additional understanding of, and insight into, the murky issues and complex trade-offs associated with our evolving energy system can help improve the quality of decisions and strengthen our national security. Policies that are robust over a range of future scenarios are ideal, given the difficulty in predicting the future. Furthermore, analyses that consider the human element, which affects things like public preferences and the policy-making process, can assist in making effective policies and decisions.

Sandia's goal in this project is to develop and implement a framework for energy systems analysis.

Initially, work focused on evaluating Sandia's capabilities, national needs, and opportunities in energy systems analysis and on developing a framework for contributions. We made the following accomplishments:

- Developed background papers on several topics and identified key questions, disagreements, and analysis of projects worth pursuing. Topics included sustainability, the intersection of power and water, natural gas, oil dependence, energy security, nuclear power, and critical infrastructures.
- Evaluated internal capabilities and identified external models and agencies involved in energy systems analysis.

- Held a meeting with a diverse group of policymakers, modelers, analysts, and scholars to explore ways in which the relationships between modelers and policymakers in the energy and environment fields (with an emphasis on energy) could be made more productive for both. A Sandia report documents the meeting results and suggests 20 guidelines to help modelers improve the relationship, followed by 10 guidelines to help policymakers toward the same goal.
- Compiled a library containing more than 400 records on energy topics and created an EndNote® database to facilitate search, retrieval, and insertion of appropriate references in project documentation.

As per the project plan, we then selected a topic to demonstrate a more holistic framework for energy systems analysis. The analysis will evaluate the impacts of a transition to a natural-gas–based hydrogen economy by 2050 on these diverse metrics: energy cost, energy security, the environment, sustainability, reliability, and safety.

Refereed

Karas, T. H. 2004. Modelers and policymakers: Improving the relationships. Sandia Technical Report SAND2004-2888, Sandia National Laboratories, Albuquerque, New Mexico.

Other Communications

Borns, D. 2004. Oil dependency: Relationship between agriculture and oil. Presentation at Sandia National Laboratories, April, Albuquerque, New Mexico.

Brewer, J. D. 2004. Nuclear energy for electricity generation: Current conditions and future directions. Presentation at Sandia National Laboratories, May, Albuquerque, New Mexico.

Jones, S. A. 2004. Natural gas: Potential implications for the U.S. Presentation at Sandia National Laboratories, October, Albuquerque, New Mexico.

Kuswa, G. W. 2004. A single metric for comparing energy systems (surety). Presentation at Sandia National Laboratories, August, Albuquerque, New Mexico.

Kuswa, G. W. 2004. Communication: How do we engage and influence policymakers and the public? Presentation at Sandia National Laboratories, June, Albuquerque, New Mexico.

Kuswa, G. W. 2004. Links between energy supplies and water needs to produce energy. Presentation at Sandia National Laboratories, May, Albuquerque, New Mexico.

Kuswa, G. W. 2004. Sustainability and energy surety. Presentation at Sandia National Laboratories, April, Albuquerque, New Mexico.

Paananen, O. H. 2004. Energy security: Definitions and issues. Presentation at Sandia National Laboratories, April, Albuquerque, New Mexico.

75443

A Mathematical Method for Quantifying the Effectiveness of Management Strategies

J. A. Cooper, C. J. Tamez, J. M. Covan

Large complex teams (e.g., National Nuclear Security Administration [NNSA] labs) must achieve sustained productivity in critical operations (e.g., weapons and reactor development) while maintaining safety for involved personnel, the public, and physical assets, as well as security for property and information. This requires informed management decisions that depend on trade-offs of factors such as the extent of personnel protection, potential accident impacts, and degree of information and physical asset protection. All of these interact (and potentially interfere) with each other and must be weighed against financial resources and implementation time. Existing risk-analysis tools can successfully treat physical response, component failure, and routine human actions. However, many "soft" factors involving human motivation and interaction among weakly related factors remain problematic. Sandia is developing a more effective tool for quantifying these trade-offs and helping make rational choices. This tool will measure potential improvements in safety, security, and productivity as a function of resources expended. We will prioritize potential approaches, preclude the most likely and damaging impediments, and cost-effectively guide the apportionment of resources. We intend to sense and interpret data in real time, react, and respond to changing conditions. Operational safety and security conditions are significantly influenced by "latent effects," which are pre-occurring influences that can affect personnel performance and motivation. One example of these is that an atmosphere of excessive fear can suppress open and frank disclosures, which can in turn hide problems, impede correction, and prevent lessons learned. Another is that a cultural mindset of commitment, self-responsibility, and passion for an activity is a significant contributor to the activity's success. Specifically, we developed a tool for personnel interchanges, a game theory model for demonstrating the potential effects of management decisions on personnel performance, a model for assessing team performance, and a model for assessing operational safety.

We constructed high-level mathematical models for personnel, management, team performance and assessment, and organizational performance and operation surety. We decomposed the operational factors into analyzable chained

latent-effects structures. We determined input categories for these structures and developed a structured expert elicitation guideline to help obtain particular input values. We combined these values using soft aggregation analysis to obtain scores for each module. We determined importance and sensitivity metrics to rank the inputs in terms of contribution to overall value and overall payoff for improvements to particular inputs. The intent of the personnel model was to test a vehicle for communication between management and personnel regarding personnel performance and assessment. The model has five modules: "self-awareness" continues to "personal culture," then to "team interaction," all of which contribute to "execution," which then results in a "performance" metric. Feedback is derived through "lessons learned," which also provides a measure of "prognosis." The results have appropriate mathematical properties. We developed guidance on the meaning of the numeric values. We currently are testing this model on a selection of managers and staff members, where each is entering his view of what the scores should be. This provides an opportunity for discussing differences, which helps each better understand the other's views. We also ranked all inputs (based on the values entered by each individual) on the basis of "importance" (contribution to the overall result) and "sensitivity" (most effective impact, if improved). These rankings provide further opportunities for discussion. We developed a "game theory" demonstration to simulate the effects of human motivation on overall results. We ran a computer simulation of this game and compared the results to a Markov latent-effects analysis to help validate the latent-effects approach.

Refereed

Cooper, J. A., and R. D. Robinett, III. 2004. Productivity/reward game demonstration. *Proc. 22nd International System Safety Conference* **1** (August, Providence, Rhode Island): 178–86.

Cooper, J. A., R. Pedersen, S. Camp, and R. D. Robinett, III. 2004. Managing safety into high-consequence operations (with supporting analysis). *Proc. 22nd International System Safety Conference* **1** (August, Providence, Rhode Island): 193–99.

76306

Inactivation of Avian Influenza (Bird Flu) with Sandia-Developed Decontamination Formulations

G. S. Brown, J. M. Bieker

The objective of this research is to validate various disinfectants (Sandia DF200d, bleach, ethanol, Virkon® S) for efficacy against highly pathogenic avian influenza to enhance the ability to rapidly contain the current outbreak in Asia (avian influenza, H5N1). A secondary objective is to develop a rapid means of verification of the viral inactivation. Sandia recently developed an enhanced diagnostic capability to rapidly determine the inactivation (loss of infectivity) of various pathogens after exposure to various disinfectants. This is considered enhanced as the results of loss of infectivity can be achieved within a 4 hr period with increased sensitivity, while gold-standard cultivation methodology typically requires 3–5 days for demonstration of complete loss of infectivity (viability). This is a novel approach based on thorough understanding of disinfectant mechanism of action on various structural components, including structural proteins and genomic and subgenomic nucleic acid material of the viral target. The experimental design is to initially assess the efficacy of the test disinfectants using an in vitro *cell-culture system (Madin-Darby canine kidney [MDCK] cells for influenza). After we determine the* in vitro *loss of infectivity using MDCK cells, we evaluate the samples using molecular- or serological-based assays. Negative results using these assays correlate with negative cytopathic effect in an* in vitro *system based on the functionality of the specific target (i.e., viral ribonucleic acid [RNA], structural proteins, etc.). Our results show degradation of viral RNA and viral structural proteins (receptor binding proteins, nucleocapsid proteins) that are vital to successful viral infection and are the first demonstration for alternative uses of clinical diagnostic tools for potential field-use application following remediation. All results are validated with an* in vitro *cell-culture system and internal control assays to negate carryover of inhibitors (for integrity of nucleic acid experiments).*

Preliminary studies for determining the efficacy of the test disinfectants against influenza after 1 min of exposure demonstrated 10% bleach and 12.5% DF200d; both produced complete loss of viral infectivity of influenza H1N1 *in vitro* against MDCK cells and produced complete degradation of

viral RNA as demonstrated by reverse transcriptase polymerase chain reaction (RT-PCR). The study also showed that Virkon® S was ineffective as a disinfecting agent against influenza H1N1. Additionally, we demonstrated that a 70% ethanol solution, which normally is used for disinfection of biosafety cabinets in biohazard microbiology laboratories, resulted in loss of infectivity in an *in vitro* system (MDCK cells) but left viral RNA intact. To assess challenge level and exposure time effects for the test disinfectants, we used reduced concentrations for exposure times up to 30 min to determine *in vitro* efficacy and retention of viral RNA integrity. Influenza challenged with 1.25% DF200d and 1% bleach showed no *in vitro* signs of infectivity after 30 min, but 35% ethanol was not effective as demonstrated by cytopathic effects and hemagglutination reaction evaluated with poultry red blood cells, which is the verification for positive infection of MDCK culture. Only the 1.25% DF200d resulted in complete degradation of the viral nucleic acid for all exposure times evaluated (1, 15, and 30 min).

79943

GeSi–Strained Nanostructure Self-Assembly for Nano- and Optoelectronics

J. A. Floro

Sandia grew coherent pits in strained germanium silicon (GeSi) epilayers on Si (001) substrates using molecular beam epitaxy (MBE). The MBE growth chamber recently was plagued by inconsistent results stemming from an unknown contamination source somewhere in the process stream. In this project, we made an intensive effort to locate and eliminate the contamination. We made a breakthrough toward the end of the project and are now able to consistently grow very high quality quantum-dot molecules (QDMs) and quantum-pit structures suitable for high-resolution characterization to determine the fundamental origins of strain-driven pit formation.

We made a breakthrough...and are now able to consistently grow very high quality quantum-dot molecules (QDMs) and quantum-pit structures suitable for high-resolution characterization....

Strained GeSi alloy films grown epitaxially on Si (001) form QDs (quantum dots) under conditions of high adatom mobility. In a special range of deposition parameters, with somewhat limited adatom mobility, our previous work showed that fourfold-symmetric QDMs can be self-assembled; that is, four QDs form in close proximity, elastically bound by a central pit (or quantum antidot) in the center of the structure.

Our primary goal was to better characterize the shape and structure of the pits themselves, which are key to understanding how the subsequent QDM evolves. However, to make progress, we first had to overcome a persistent problem in the MBE chamber used to form QDMs. The MBE yielded inconsistent results compared to those obtained in previous work, and we attributed this problem to an unknown source of contamination within the film process flow.

A Texas A&M student systematically examined various aspects of the process flow. He showed that the extensive chemical cleaning process used to prepare the Si substrates was not the problem. He replaced both the Ge and Si deposition sources in case of contamination, but this did not solve the issue. He repaired a cryopump and completely cleaned and baked the chamber, including using a new hydrogen (H) scrub approach during bakeout to better remove residual hydrocarbons, to attain ultrahigh vacuum of the highest quality, which helped partially. He used full-size wafers to eliminate the issue of whether our substrate plate (used to hold smaller pieces) was the origin of the contamination. While this was not the case, the use of the full wafer did ultimately provide the solution.

In the course of the investigation, we found that the central portion of the large wafer still exhibited contamination problems in the form of nonintrinsic “macropits” and excessively high densities of QDMs. However, toward the edge of the wafer, we found good, low-density arrays of QDMs without any macropit formation. The only possible difference between center and edge is the distribution of temperature, which we found to vary by only about 5% between the positions measured. The hottest regions showed the greatest defect density, suggesting that these regions were too hot. By deliberately lowering the temperature of our thermal clean and buffer growth, we completely suppressed macropit formation and grew some of the highest-quality arrays of QDMs that we have ever seen.

It is still not entirely clear why the temperature profile is so important. The recipe being used for the thermal clean and buffer growth is about 2 yr old, so clearly something has changed. One possibility is that, for some reason, the H partial pressure during GeSi growth is higher than in the past and, at the high temperatures in recent use, leads to etching of the wafer surface via silane creation. Another possibility is surface carbide precipitation, which can lead to pit formation during Si buffer growth. We submitted samples earlier this summer for secondary ion mass spectrometry (SIMS) and Auger analysis, but results are still not in.

With the contamination problem solved, we grew a set of samples at the end of the summer for detailed atomic-force microscopy measurements of the morphology, which are currently under way.

Refereed

Floro, J. A., J. L. Means, J. L. Gray, N. Singh, R. Hull, D. Elzey, P. Sutter, and C. H. Lam. 2004. Heteroepitaxial self-assembly of higher-complexity structures by combining growth control with nanopatterning. (Invited) Paper presented at the Fall 2004 Materials Research Society Meeting, 29 November–3 December, Boston, Massachusetts.

Engineering Sciences

The Engineering Sciences investment area supports Sandia's national security mission by advancing core engineering disciplines through increasing the understanding of phenomenology, developing first-principles–validated models, and advancing application in computational tools. Engineering Sciences investments seek to support and advance technologies critical to advanced weapons concepts and homeland security. Researchers and scientists in Engineering Sciences strive to integrate experimentation, simulation, and test activities necessary for physics discovery and validation and to push efforts in quantification and optimization. Engineering Sciences investments encompass the core engineering disciplines that make advancement and innovation possible in thermal transport and aerosciences; electromagnetics and electrical engineering; material, fluid, and solid mechanics; and structural dynamics.

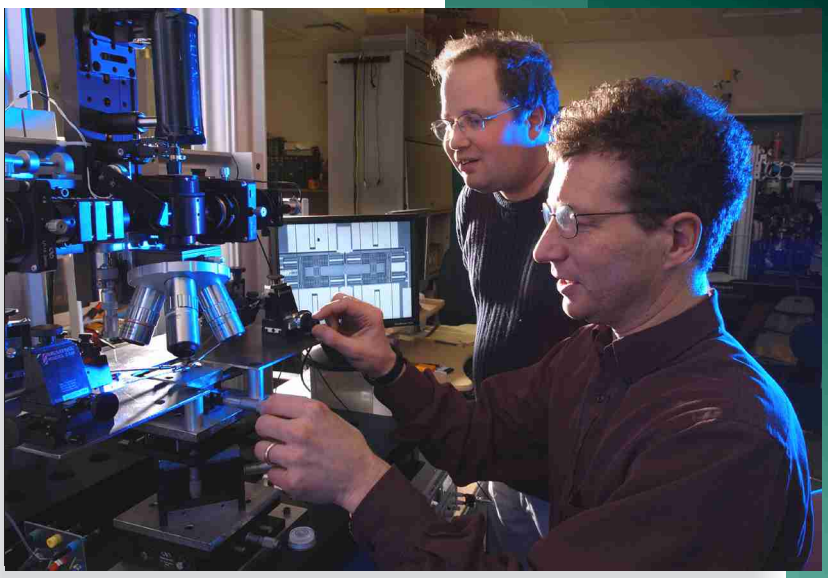

38686
"High-Fidelity Frictional Models for MEMS"

Understanding the mechanical and structural responses of materials and systems supports reliability, performance, and manufacturing. A focus on contacting and sliding surfaces in polysilicon micro-electromechanical systems (MEMS) is aimed at determining how and why MEMS-scale friction differs from friction on the macro scale. Researchers developed novel sensitive metrology to make accurate MEMS-scale measurements. The new measuring accuracy enabled the discovery of a new phenomenon, presliding tangential displacement (PSTD), that is not described by a classical coefficient of friction. The phenomenon appears to depend on the specific spatial features of contacting surfaces, load level, the nature of the contacting surfaces, and time-dependent behavior of specific coating materials. During the course of research, scientists implemented adhesion and junction models in simulations to directly predict frictional response of a sliding asperity, developed grid-level models for friction in polysilicon micromachines, and performed detailed characterization of polysilicon topography to create multi-asperity contact models.

38684

A Robust, Coupled Approach for Atomistic-Continuum Simulation

J. A. Zimmerman, G. J. Wagner, S. Aubry, C. J. Kimmer, R. E. Jones, P. A. Klein, E. B. Webb, III, J. J. Hoyt

With the growing focus on predictive modeling and simulation, Sandia must develop the capability to model deformation and failure in multiple-scale settings. The goal of our project was to develop a robust approach for coupled atomistic-continuum simulation, capable of both quasi-static and finite-temperature/dynamic analyses. Sandia did not previously possess this simulation capability.

We formulated and implemented an atomistic-to-finite-element (FE) coupling method for quasi-static analysis. The formulation assumes that an FE mesh covers all parts of the computational domain, while regions of interest in the domain are also covered with an atomistic crystal, and this formulation uses a hyperelastic formulation to compute the stress response of the continuum based on a Cauchy-Born constitutive model. Our formulation boasts mechanisms designed to treat the overlapping atomistic and continuum domains, including cross terms that naturally appear in the equilibrium equations and bond density corrections to the Cauchy-Born rule. We performed verification simulations on our implemented coupling approach. These simulations consisted of the free-surface relaxation for one-dimensional (1-D), 2-D, and 3-D crystals in which atoms interact via multineighbor pair potentials.

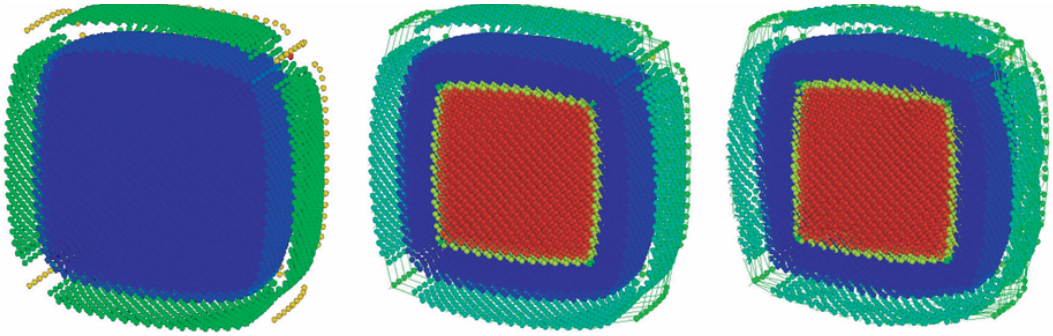

One-half of a 3-D cube modeled with (a) *pure atomistics,* (b) *coupled atomistics continuum using a hexahedral element mesh, and* (c) *coupled atomistics continuum using a tetrahedral element mesh. Displacements are magnified by a factor of 200.*

In our effort to quantify how time and spatial averaging play a role in defining continuum variables calculated from atomistic properties, we performed molecular dynamics (MD) simulations of transient and steady-state heat flow to assess temperature and heat-flux expressions derived from a formalism developed by R. J. Hardy and analogous expressions originating from statistical mechanics. These simulations enabled us to define minimum-sized "windows" in time and space that are necessary for atomistic-continuum correspondence and that are used to estimate thermodynamic material properties such as thermal conductivity.

Finally, we developed an expression for a continuum temperature field that is derived by projecting the fine-scale portion of the atomic kinetic energies onto the coarse-scale grid of the overlapping continuum. We performed atomistic simulations to understand the optimum ratio of element size to atomic spacing needed for expected continuum behavior.

We formulated and implemented an atomistic-to-FE coupling method for quasi-static analysis. The formulation assumes that an FE mesh covers the entire computational domain, while regions of interest are also covered with an atomistic crystal, and the formulation uses a hyperelastic formulation to compute the stress response of the continuum based on a Cauchy-Born constitutive model. Our formulation boasts mechanisms designed to treat the overlapping atomistic and continuum domains, including cross terms that naturally appear in the equilibrium equations and bond density corrections to the Cauchy-Born rule.

We performed verification simulations of free-surface relaxation for 1-D, 2-D, and 3-D crystals in which atoms interact via multineighbor pair potentials.

We performed surface-relaxation simulations for a 3-D cube of face-centered-cubic (FCC) crystal that contains 32,000 atoms.

We performed MD simulations of transient and steady-state heat flow to assess expressions for temperature and heat flux developed by R. J. Hardy. We simulated a rectangular cross section of a copper (Cu) rod containing 160,000 atoms with an initial temperature of ~ 300 K and constant heat-flux boundary conditions in the x (long) direction. The transient and steady-state behaviors of Hardy's expressions can be better understood by examining their binned distributions down the long direction of the crystal, for temperature and heat flux in the *x* direction. While both the instantaneous and time-averaged curves show an evolution to a linear distribution of temperature, the spatial

fluctuations are absent for the time-averaged distribution. The slope of the time-averaged distribution is estimated to be 0.179 ± 0.002 K/Å. The fluctuations in heat flux greatly overwhelm the expectation value for the instantaneous calculation. However, the time-averaged distribution reveals an evolution to a constant heat flux of nearly equal magnitude and opposite sign for the two halves of the crystal, calculated to be 0.20866 ± 0.01 nW/Å^2. This value is within its uncertainty of the prescribed heat flux of 0.20924 nW/Å^2. Assuming Fourier's Law as the longtime behavior of the system, we estimate thermal conductivity to be 11.65 ± 0.69 W/(m K).

We developed an expression for a continuum temperature field by projecting the fine-scale portion of the atomic kinetic energies onto the coarse-scale grid of the overlapping continuum. In this expression, the ratio of the continuum grid to the atomic spacing dictates the smoothness and overall behavior of the continuum temperature field. We performed simulations in a long strip of FCC Cu in which a constant heat flux and uniform temperature gradient along the rod are created after a steady state has been established. The results showed that the time-averaged expression for nodal temperature exhibits good behavior provided that the element size is sufficiently larger than the underlying atomic spacing.

Refereed

Aubry, S., D. J. Bammann, J. J. Hoyt, R. E. Jones, C. J. Kimmer, P. A. Klein, G. J. Wagner, E. B. Webb, III, and J. A. Zimmerman. 2004. A robust, coupled approach for atomistic-continuum simulation. Sandia Technical Report SAND2004-4778, Sandia National Laboratories, Livermore, California.

Klein, P. A., and J. A. Zimmerman. 2004. Coupled atomistic-continuum simulation using arbitrary overlapping domains. *J. Computational Physics*, to be submitted.

Klein, P. A., and J. A. Zimmerman. 2004. Formulation for quasi-static, coupled, atomistic-continuum simulation. *Proc. 6th International Conference for Mesomechanics, Multiscaling in Applied Science and Emerging Technology: Fundamentals and Applications in Mesomechanics* **1** (June, Patras, Greece): 514–21.

Zimmerman, J. A., and E. B. Webb, III. 2004. Evaluating thermomechanical continuum variables in atomistic simulation. *Proc. 6th International Conference for Mesomechanics, Multiscaling in Applied Science and Emerging Technology: Fundamentals and Applications in Mesomechanics* **1** (June, Patras, Greece): 530–37.

Zimmerman, J. A., E. B. Webb, III, J. J. Hoyt, R. E. Jones, P. A. Klein, and D. J. Bammann. 2004. Calculation of stress in atomistic simulation. *Modeling and Simulation in Materials Science and Engineering* **12** (4) (June): S319–S332.

Zimmerman, J. A., and P. A. Klein. 2004. Coupled atomistic-continuum analysis of nanowires and nanofilms. Paper to be presented at the 11th International Conference on Fracture, March 2005, Turin, Italy, submitted.

38685

Microscale Rarefied-Gas Dynamics and Surface Interactions for EUVL and MEMS Applications

D. J. Rader, T. W. Grasser, J. R. Torczynski, W. M. Trott, J. N. Castaneda, M. A. Gallis

Momentum and heat transfer to surfaces immersed in noncontinuum transitional (rarefied)-gas flows continues to be an active area of research. Gases exhibit noncontinuum effects when the characteristic length scale of the system becomes comparable to the gas mean-free path. Thus, rarefaction becomes important either when system length scales become small (e.g., microelectromechanical systems [MEMS]) or when gas pressures become low (e.g., semiconductor manufacturing). To predict momentum and heat fluxes, it is essential to understand the details of the gas-surface interaction; unfortunately, despite considerable effort, reliable interaction mechanisms are still lacking. Only two relevant experimental studies are found in the literature, and these two studies present limited data that are not in complete agreement. A combined experimental/modeling study is under way to better understand the critical role of gas-surface interaction in rarefied-gas flows. Sandia will make extensive, well-characterized experimental measurements of heat flux, gas density and/or temperature profiles, and aerosol forces in a quiescent transition-regime gas between two parallel plates. We will conduct tests with a broad range of diagnostics for a variety of gases (monatomic and polyatomic) using carefully controlled, well-characterized surfaces of different types (metals, ceramics) and conditions (rough, smooth). We will compare the experimental results to modeling predictions to identify areas of model strength and weakness. We will pay particular attention to validating current gas-wall interaction models and to developing new models, if needed. This work will have immediate benefit for extreme ultraviolet lithography (EUVL) particle protection work and will help validate rarefied-gas model performance.

Measurements of gas-density profiles and heat flux can now be made under identical conditions, eliminating an important limitation of earlier studies.

We built and demonstrated an experimental facility that can be used to determine thermal accommodation coefficients from measured interplate gas-density profiles and from the pressure-dependence of heat flux between two parallel plates. Measurements of gas-density profiles and heat flux can now be made under identical conditions, eliminating an important limitation of earlier studies. We demonstrated the application of electron-beam fluorescence to measure gas-density profiles,

although additional work is needed to improve the accuracy of the data. We inferred heat flux between the plates from temperature-drop measurements. The use of high-precision thermistors and the careful control of experimental conditions allow the heat-flux measurements to be made with great precision.

We specifically designed the vacuum test chamber to accommodate all of the control systems and diagnostics needed to provide simultaneous heat-flux and gas-density-profile measurements between two parallel 14.25 cm-diameter plates. We inferred heat flux between the plates from temperature-drop measurements between precision thermistors embedded near the exposed surface of each plate and those immersed in an adjacent water plenum. We inferred gas-density profiles from the fluorescence intensity of the gas illuminated with a tightly collimated electron beam. We met two particularly challenging design requirements: (1) to provide pressure isolation between the electron gun and the main chamber, and (2) to provide two temperature-controlled, movable plate assemblies. The high degree of accuracy required for this project placed severe requirements on control and measurement subsystems. Consequently, we selected state-of-the-art components for controlling system pressure, flowrate, plate alignment, plate temperatures, and plate positions. We selected high-precision, high-accuracy, state-of-the-art components for measuring system pressure, temperature, and fluorescence intensity. The present test chamber and supporting subsystems represent a significant investment in staff time, materials, and equipment.

We operated the system with both monatomic (helium [He] and argon [Ar]) and diatomic (nitrogen [N]) gases coupled with 304 stainless-steel (SS) plates with a standard milled surface. We analyzed the resulting heat-flux and gas-density-profile data using analytic and computational models. The results revealed that a simple Maxwell gas-surface-interaction model is adequate to represent all of the observations. Based on this analysis, we determined the thermal accommodation coefficients for 304 SS coupled with Ar, N, and He to be 0.88, 0.80, and 0.38, respectively, with an estimated uncertainty of $\pm$ 0.02.

Other Communications

Rader, D. J., W. M. Trott, J. R. Torczynski, M. A. Gallis, J. N. Castaneda, and T. W. Grasser. 2004. Microscale rarefied-gas dynamics and surface interactions for EUVL and MEMS applications. Sandia Technical Report SAND2004-5329, Sandia National Laboratories, Albuquerque, New Mexico.

38686

High-Fidelity Frictional Models for MEMS

E. D. Reedy, Jr., M. J. Starr, H. Sumali, M. P. de Boer, A. D. Corwin, F. Bitsie, B. R. Antoun, R. E. Jones

Frictional losses play a dominant role in microsystem performance and reliability, but are not yet well-enough understood to enable the high-fidelity modeling and simulation needed for weapon-component design and qualification. Surface interactions, currently treated in a global sense using classical friction laws, are insufficient for microelectromechanical systems (MEMS) in which single asperities and their interplay with interfacial roughness are the primary energy-dissipation mechanisms. First, Sandia will construct three-dimensional (3-D) computer models of the interface on the basis of surface topography, constitutive frictional relations for the asperity contacts, and surface interactions due to van der Waals forces. Second, we will evaluate and optimize novel MEMS friction test structures to explore a wide pressure-velocity space and develop necessary metrologies that yield information on slip for nanometer displacements. This will allow us to resolve microsecond time frames and enable the determination of velocity and stick-slip effects over many orders of magnitude. Third, we will model the frictional response at the mesoscopic scale. This modeling/experimental approach will allow us to connect frictional response across the length scales and will form the basis for microdomain-aware contact algorithms to be incorporated into the evolving multiphysics SIERRA code infrastructure. Successful completion of the project will yield validated grid-scale models for MEMS interfaces that accurately treat dissipation mechanisms.

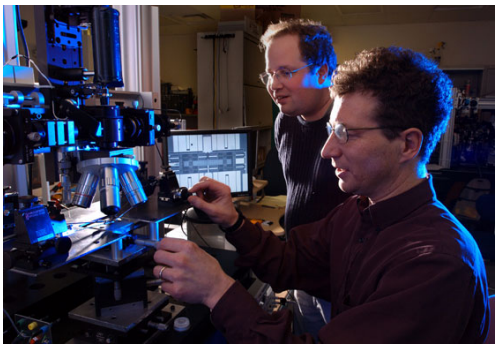

Maarten de Boer and Alex Corwin investigate friction at the microscale using a recently developed nanotractor actuator fabricated using the Sandia Ultraplanar Multilevel MEMS Technology (SUMMiT V^{TM}) process.

We continued an effort aimed at determining how and why MEMS-scale friction differs from friction on the macroscale. We used a newly developed MEMS nanotractor actuator to make MEMS-scale measurements. This device is distinguished by its ability to generate both very low and very high forces in both the tangential and normal directions. We developed increasingly sensitive metrology during the course of this work, with an ultimate, Moiré-based capability to measure in-place displacements with an accuracy of ± 1 nm. This capability enabled us to discover an entirely new phenomenon that cannot be described by a classical coefficient of friction.

We also implemented an adhesion model and a junction model in PRESTO, Sandia's transient dynamics finite-element

We developed increasingly sensitive metrology...with an ultimate, Moiré-based capability to measure in-place displacements with an accuracy of ± 1 nm. This capability enabled us to discover an entirely new phenomenon that cannot be described by a classical coefficient of friction.

(FE) code, to enable asperity-level simulations. The junction model includes a tangential shear traction that opposes the relative tangential motion of contacting surfaces. We used an atomic-force microscope (AFM)–based method to measure nanoscale, single-asperity friction forces as a function of normal force. We used these data to determine the parameters of the junction model. We performed illustrative simulations that demonstrate the use of the junction model in conjunction with a mesh generated directly from an AFM image to directly predict the frictional response of a sliding asperity.

Finally, we studied grid-level, homogenized models. We would like to perform an FE analysis of a MEMS component, assuming nominally flat surfaces, and to include the effect of roughness in such an analysis by using homogenized contact and friction models. We made AFM measurements to determine statistical information on polysilicon (poly-Si) surfaces with different roughnesses, and we used these data as input to a homogenized, multiasperity contact model (the classical Greenwood and Williamson model). There are two extensions of the Greenwood and Williamson model: One incorporates the effect of adhesion, while the other modifies the theory so that it applies to the case of relatively few contacting asperities.

We did not anticipate the discovery of the presliding tangential displacement (PSTD) phenomenon when this study began. This phenomenon cannot be described by a classical coefficient of friction, and for small nanoscale sliding distances, Amonton's law does not apply. This is our most important finding. PSTD can determine the operation of some MEMS devices. For example, the operation of the nanotractor, with its 40 nm step size, cannot be predicted on the basis of measured static and dynamic friction coefficients. We developed a simple two-dimensional model to help us understand the mechanics of PSTD. This model suggests that PSTD is a cascade of small-scale slips with a roughly constant number of contacts equilibrating the applied normal load. PSTD appears to depend not only on the specific spatial features of the contacting surfaces, but also on the load level. We do not yet fully understand this phenomenon. It depends on the nature of the contacting surfaces (i.e., octadecyltrichlorosilane [OTS]-coated versus perfluoroactyl-trisdimethylaminosilane [FOTAS]-coated), and there are indications of time-dependent behavior for OTS-coated materials.

Refereed

Corwin, A. D., and M. P. de Boer. 2004. Effect of adhesion on dynamic and static friction in surface micromachining. *Applied Physics Letters* **84** (13) (March): 2451–53.

de Boer, M. P., D. L. Luck, W. R. Ashurst, R. Maboudian, A. D. Corwin, J. A. Walraven, and J. M. Redmond. 2004. High-performance surface-micromachined inchworm actuator. *J. Microelectromechanical Systems* **13**:63–74.

Flater, E. E., A. D. Corwin, M. P. de Boer, and R. W. Carpick. 2004. *In situ* wear studies of surface-micromachined interfaces subject to controlled loading. *Wear,* submitted.

Other Communications

de Boer, M. P. 2004. Microelectromechanical systems (MEMS) problems requiring miniaturized solutions. Paper presented at the Gordon Research Conference on Tribology, 27 June–2 July, Bristol, Rhode Island.

Starr, M. J., H. Sumali, J. M. Redmond, E. E. Flater, and R. W. Carpick. 2004. Analysis of contact forces using AFM data of polycrystalline silicon surfaces. *Proc. SEM X* **1** (7–10 June, Costa Mesa, California): 525.

38687

Soot Formation, Transport, and Radiation in Unsteady Diffusion Flames

C. R. Shaddix, S. P. Kearney, L. G. Blevins, R. W. Schefer, T. C. Williams, K. A. Jensen

Fires pose the dominant risk to the safety and security of nuclear weapons, nuclear transport containers, and Department of Energy and Department of Defense facilities. The thermal hazard from these fires results primarily from radiant emission from high-temperature flame soot. Therefore, it is necessary to understand the local transport and chemical phenomena that determine the distributions of soot concentration, optical properties, and temperature to develop and validate constitutive models for large-scale, high-fidelity fire simulations. In this project, Sandia is devoted to obtaining the critical experimental information needed to develop such constitutive models. We employed an array of laser diagnostics and novel extractive measurement techniques in both steady and pulsed laminar diffusion flames of methane, ethylene, and JP-8 surrogate burning in air. For methane and ethylene, we investigated both slot-flame and co-annular-flame geometries, as well as normal and inverse diffusion-flame geometries. For the JP-8 surrogate, we investigated co-annular normal diffusion flames. We successfully measured soot concentrations, polycyclic aromatic hydrocarbon (PAH) laser-induced fluorescence (LiF) signals, hydroxyl radical (OH) LiF, acetylene and water-vapor concentrations, soot-zone temperatures, and the velocity field in both steady and unsteady versions of these various flames. In addition, we measured the soot microstructure, soot dimensionless extinction coefficient (Ke), and the local radiant-heat flux. Taken together, these measurements compose a unique, extensive database for future development and validation of models of soot formation, transport, and radiation.

We seek to perform a daunting list of advanced diagnostics in a challenging environment of low- to high-soot concentrations and transient flame phenomena. After a focused measurement campaign, we successfully gathered the data that we desired from all but one of the originally proposed measurement techniques. We constructed both gas-fueled and liquid-fueled co-annular burners with identical dimensions and optimized their performance. The liquid-fueled burner utilized a compact, capillary-force vaporizer that sent a jet of vaporized fuel into a heated cylindrical fuel tube. We created pulsed

flames by using a loudspeaker at the base of the fuel tube for the gas burner and by using a model-airplane piston assembly attached to a sidearm of the fuel tube for the liquid burner. We obtained steady operation of the liquid burner with kerosene and JP-8 surrogate by providing some nitrogen dilution of the fuel vapor. We established "inverse" diffusion flames (with the positions of fuel and air switched) on the previously investigated slot burner, and we measured soot and OH concentrations, PAH fluorescence signals, near-infrared (NIR) radiation from soot, and total radiation in the normal and corresponding inverse slot flames for both methane and ethylene fuel. These measurements demonstrated for the first time that soot and PAH levels are somewhat lower in inverse flames, as is the soot radiation. In pulsed flames, the PAH levels are substantially higher in the inverse flames than in the normal flames, as a consequence of vortical roll-up on the fuel side of the flame sheet. We documented these results in a manuscript that was accepted for publication by the Combustion Institute, and we presented these results at the biennial International Symposium on Combustion.

We used particle image velocimetry (PIV) to measure the transient flowfield in both steady and pulsed flames and explicitly showed, for the first time, the vortex roll-up on the air side of the flame sheet (in normal diffusion flames). These measurements also recorded the transient inlet velocity field for the different flames investigated; this information is required for modeling the investigated flames. We obtained accurate soot-field measurements in all of the canonical flames using Nd:YAG (neodymium:yttrium-aluminum-garnet) laser sheet excitation of laser-induced incandescence (LII). We obtained NIR soot-field radiation from these flames using an 850 nm bandpass filter in front of an intensified charge-coupled device (ICCD) camera, and we measured local, total radiant emission in radial profiles across the flames using a fast-response thermopile with an attached light-pipe. We used a thermophoretic transmission-electron microscopy (TEM) grid-sampling probe to capture soot aggregates at different flame positions for analyzing soot morphology and microstructure. We measured the Ke of soot (an important optical property for interpreting laser-extinction measurements and predicting soot radiation) for all of the flames, using a transmission-cell reciprocal nephelometer (TCRN). These measurements showed that the lightly sooting methane flames had a Ke that was substantially lower than that for ethylene flames, and especially for kerosene flames. Also, the soot in the slot-burner flames showed lower Ke values than the soot in the co-annular flames.

These measurements demonstrated for the first time that soot and PAH [polycyclic aromatic hydrocarbon] levels are somewhat lower in inverse flames, as is the soot radiation.

We measured the soot-field temperatures with the technique of planar, two-color pyrometry, using a large cube beamsplitter and two ICCDs mounted at a right angle on an optical breadboard. We calibrated these measurements with the use of a high-temperature blackbody. We attempted to implement filtered Rayleigh scattering (FRS) for full-field temperature measurements, but we found the signals to be too low, probably because of poor performance of the injection-seeded Nd:YAG laser. We also successfully made tunable diode laser (TDL) measurements of acetylene and water-vapor profiles in the slot flames. The acetylene measurements, in particular, are important for generation and validation of chemical models of soot inception and surface growth.

Refereed

Shaddix, C. R., T. C. Williams, L. G. Blevins, and R. W. Schefer. 2004. Flame structure of steady and pulsed sooting inverse jet diffusion flames. *Proc. 30th International Symposium on Combustion* **30** (July, Chicago, Illinois): 1100–1106.

Other Communications

Williams, T. C., C. R. Shaddix, L. G. Blevins, and R. W. Schefer. 2004. Flame structure of steady and pulsed sooting inverse jet diffusion flames. *Proc. Western States Section of the Combustion Institute* **Paper 04S-51** (Spring, Davis, California).

52537

Coupled Solid-Fluid-Mechanical-Computational Modeling of Fracture and Fragmentation in Geomaterials, such as Hard and Deeply Buried Targets (HDBTs)

R. A. Regueiro, A. F. Fossum, D. S. Preece, R. P. Jensen

Modeling fracture and fragmentation in geomaterials due to various loading and environmental conditions is a challenging problem and requires the latest in experimental constitutive modeling and in computational-solution-method technology. At Sandia, current geomaterial constitutive models and computational methods are incapable of predictively modeling the transition of continuous rocklike material to fragmented rock material within the context of coupled solid-mechanics and fluid-mechanics physics. To address this need, we seek to develop a physically based geomaterial constitutive model and computational method that can predictively model this transition. The constitutive-modeling effort will leverage experimental investigations of the fundamental mechanisms of rock penetration.

Two problems that would be better understood with such a modeling capability are the defeat of hard and deeply buried targets (HDBTs) and the long-term performance of deep geologic nuclear-waste repositories. It would be useful to be able to predict the behavior of these buried structures when subjected to extreme dynamic-loading conditions such as high-velocity-penetration events, explosive blasts, or seismic events. Presently, the mechanics of rock penetration are poorly understood, and there are no empirical data that can be used to forecast long-term performance (over thousands of years) of deep geologic nuclear-waste repositories. Obtaining approval of the Nuclear Regulatory Commission (NRC) becomes difficult if the Department of Energy is restricted to using existing methodologies.

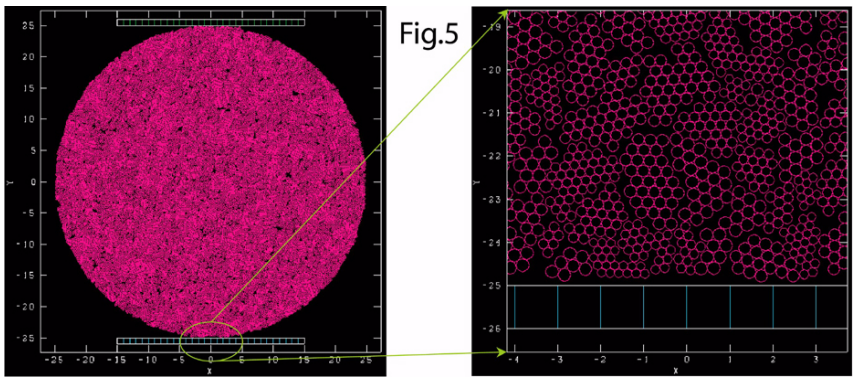

Demonstration of the two-dimensional (2-D) macroparticle algorithm implemented to grow macroparticles from seed microparticles within a 2-D shape, a circle.

In addition to modeling the defeat of HDBTs and the long-term performance of nuclear-waste repositories, the resulting computational analysis tool will be useful for understanding fracture and fragmentation in geomaterials such as concrete, rock, frozen soil, and heavily overconsolidated clay encountered in tunneling construction, oil and natural-gas production, and depleted reservoirs used for subsurface sequestration of greenhouse gases.

Our main accomplishments were an implicit numerical integration of the Sandia Geomodel and a demonstration of a macroparticle discrete-element method (DEM).

An implicit integration is needed for a more-robust numerical solution when checking for the onset of localization and post-localization response. First, we verified that the consistent tangent functions and exhibits quadratic convergence. To do this, we allowed free movement in the orthogonal direction that does not have prescribed axial or shear displacements. Essentially, this is a plane-stress compression and constrained shear loading. We ran this problem in a fully three-dimensional setting to give the problem unconstrained degrees of freedom (DOFs). The test had two parts—compression and shear, and we verified that the global residual vector converged quadratically for both loadings.

Second, we compared an implicit integration implementation to an existing explicit (forward Euler) integration implementation of the same model in the SIERRA codes (Fossum & Brannon, 2004). The problem is a plane-strain, one-element, loading/unloading to 2.5% compressive strain. We applied a 20 MPa confining pressure. We ran the explicit algorithm in 5000 steps and the implicit algorithm in 80 steps. The material properties were the same as for the first example (Salem limestone, Fossum & Brannon, 2004). For this one-element test, the implicit algorithm ran more quickly than did the explicit algorithm, but as the number of elements grew, the combination of local and global implicit iterations was slower than for the explicit algorithm. Perhaps the use of an implicit local algorithm to solve for stress and internal state variables in conjunction with an explicit solver for the governing equations could be faster than using an explicit algorithm for both local and global iterations (i.e., not being concerned about instabilities in numerical integration of the constitutive-model equations due to too large a time-step). For research purposes, however, we want a robust iterative solver (i.e., implicit) to simulate prebifurcation and postbifurcation constitutive response.

We used a macroparticle DEM to grow arbitrary polygonal shapes from seed microparticles in two dimensions and arbitrary polyhedral shapes in three dimensions. The interparticle constitutive relations between the microparticles that compose the macroparticle dictate the overall constitutive response of the macroparticle. Such macroparticles could be grown once the continuum bifurcation model and finite-element (FE) implementation predicted fragment dimensions. In essence, the macroparticle composed of microparticles (circles in two dimensions and spheres in three dimensions) would replace the fragments determined by the FE solution. These macroparticles could then further fragment into submacroparticles based on their microparticle interparticle strengths. This could be one approach to a one-way–coupled DEM/finite-element method (FEM) approach, and it could potentially be more computationally efficient than a two-way approach that would treat each fragment as a discrete element (DE) meshed with FEs, thus relying on the continuum bifurcation model to further fragment a fragment. For the macroparticle approach, the choice of seed microparticle size is important, assuming these particle radii are fictitious, i.e., not radii of the inherent microstructural particles that possibly constitute the material, such as sand particles of sandstone.

Refereed

Foster, C. D., R. A. Regueiro, A. F. Fossum, and R. I. Borja. 2004. Implicit numerical integration of a three-invariant, isotropic/kinematic hardening cap plasticity model for geomaterials. *Computer Methods in Applied Mechanics and Engineering*, accepted.

Regueiro, R. A., C. D. Foster, A. F. Fossum, and R. I. Borja. 2004. Bifurcation analysis of a three-invariant, isotropic/kinematic hardening cap plasticity model for geomaterials. *GulfRocks 2004: Rock Mechanics Across Borders and Disciplines, ARMA/NARMS 04-520* **CD-ROM** (1–5 June, Houston, Texas).

53585

Novel Diagnostics for Rarefied Flows in MEMS Applications

C. J. Bourdon, A. D. Gorby, M. A. Gallis, S. P. Kearney

Until recently, the inability to make in situ *measurements within microscale devices under rarefied and compressible flow conditions has made it impossible to improve and validate computational models of such flows, where the geometric scale can approach the mean-free path of the gas molecules at ambient conditions. Quantities such as tangential-momentum accommodation coefficients, thermal-accommodation coefficients, electric wall-potential effects, and wall-roughness effects have all been either inferred from external bulk flow measurements or derived implicitly or explicitly from direct-simulation Monte Carlo (DSMC) or molecular dynamics (MD) simulations, respectively. Estimates of these coefficients and effects can vary as much as 50% for common materials under controlled conditions, and the effect of compressibility is still largely unknown. A more reliable estimate of these properties is critical to accurate models of wall slip, aerodynamic damping, and micropropulsion, all of which are important to Sandia.*

The lack of established techniques for studying microflows under rarefied and compressible conditions has resulted in a dearth of experimental data, and thus a general lack of understanding of this important flow regime. Consequently, there is a need for the development of diagnostic tools for accurate, nonintrusive in situ *measurements within microdevices. This project focused on developing a seedless, nonintrusive diagnostic technique for deducing velocity information and estimating the tangential-momentum accommodation coefficient within microsystems with dimensions in the range of a few to tens of microns. We focused on an experimental technique called* Raman Excitation plus Laser-Induced Electronic Fluorescence (RELIEF) *to accomplish this goal. These experiments will be accompanied by a thorough examination of existing analytical slip models and DSMC simulations of the microchannel flows. We will then compare the experimental results with DSMC computations to judge the performance of current computational models and to provide accurate data on surface accommodation.*

We made significant progress toward developing a working RELIEF system for examining rarefied-gas effects and microscale gas flows. RELIEF is a velocity-measurement technique that operates by first Raman-exciting (RE) diatomic

oxygen molecules in a tagging region. After a short time delay, it uses the laser-induced electronic fluorescence (LIEF) technique to track the displacement of the oxygen molecules. We significantly modified the RELIEF system from its original configuration to increase the sensitivity of the detection system, reduced the background-fluorescence intensity, and significantly decreased the spatial, temporal, and frequency alignment requirements. Because the quantum efficiency of the RELIEF technique is quite low and molecular diffusion rates at low pressures are quite large, we developed a nonlinear fitting technique that fits the experimental data to an analytical solution of the diffusion equation to increase the accuracy of the velocity measurements. This displacement-measurement technique is approximately five times more accurate than a traditional centroid method, given expected measurement parameters. This technique employs a nonlinear fitting algorithm to fit the experimental data to an analytical solution of the diffusion equation.

Our first attempt at building an operational RELIEF system from existing equipment helped to determine the primary attributes that a RELIEF system must have to function at high efficiency. By monitoring the forward-propagating coherent anti-Stokes Raman-scattering (CARS) signal generated at the beam focus, we determined that Raman excitation of oxygen molecules was occurring in the first-generation system. Because the first-generation RELIEF system was difficult to align and because it contained several features that led to inefficient signal generation and collection, we recently redesigned the entire system. We replaced the dye laser with a Raman conversion cell to simplify the spatial, temporal, and frequency alignment of the system. We purchased a narrow-band Excimer laser to eliminate ground-state fluorescence generation that masks the RELIEF signal, and we designed and purchased a new detection system to significantly increase the efficiency of RELIEF signal collection.

67064

Ray Model of High-Frequency Cavity Scarring

L. K. Warne, H. G. Hudson, J. D. Kotulski, R. E. Jorgenson

The development of high-frequency (HF) electromagnetic (EM) sources leads to an interest in and a requirement to understand the performance of systems subjected to short-wavelength coherent radiation. Interaction with these systems is usually a two-step process: Radiation enters the system interior (cavity) and then couples to interior antennas or circuits. These frequencies are usually beyond what numerical simulations can handle directly.

In recent years, Sandia analyzed cavity-interaction problems using concepts that were developed in quantum mechanics (the approach to the classical limit). Given that the cavity is irregularly shaped, the eigenfunctions (modes) are assumed to be normally distributed. Microwave and optical experiments show that deviations from this simple assumption exist when the cavity boundary is of sufficient regularity to support periodic ray trajectories. This is called scarring. *Weapon cavities are typically more complex than the simple shapes studied in these experiments, but we do not know to what extent these deviations persist as the boundary becomes more complex.*

Because statistical tails of upset or damage events are of interest when assessing safety or reliability of components, it is of interest to capture cavity field scarring (or hot spots) when calculating coupling to interior cables.

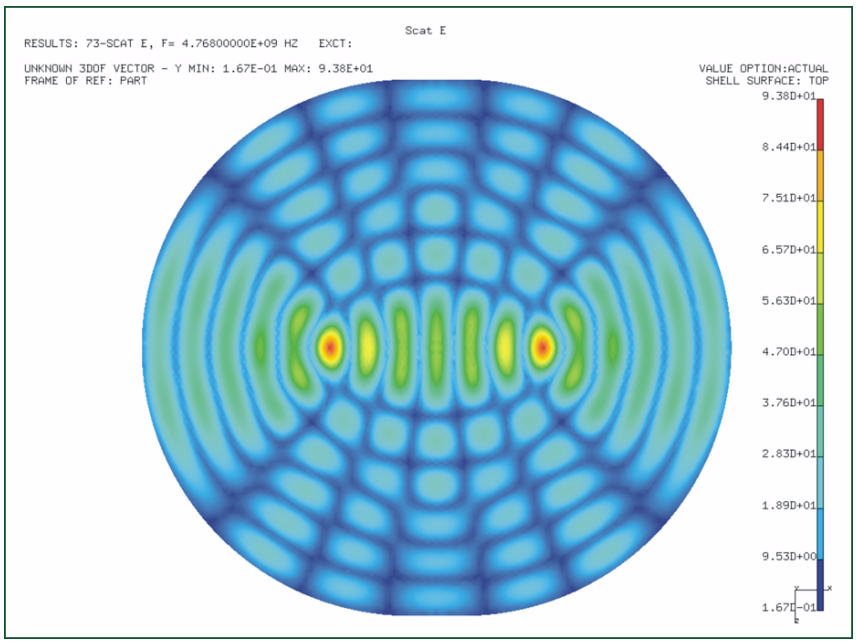

Example of stadium scarring.

We proposed using a modification of HF ray techniques to examine the connection between boundary topology and scarring (localized modal field enhancements).

Successful completion of this project will provide a means to model HF EM problems that are beyond the range of current simulations. The theory developed will provide an understanding of modal field enhancements from boundary geometry that would allow better facility designs (mode-stirred chambers). The theory would allow better interpretation of probe measurements and predictions of EM compatibility, covering the entire range of typical EM requirements. Finally, the theory would provide underpinning and possible modifications for EM field-level controls in explosives-handling facilities (V curve).

We sought to use a modification of HF ray techniques to examine the connection between boundary topology and scarring (localized modal field enhancements, or hot spots). We first selected typical but canonical geometries to focus the effort. In two dimensions, we selected the rectangle (stable), the circle (conditionally stable with curved boundary), the ellipse (stable bouncing ball and whispering gallery), and the stadium (unstable).

We used exact solutions for the stable two-dimensional (2-D) geometries to examine quantities of interest and as test cases for comparison with HF boundary-layer approximations. We verified the Poisson eigenvalue spacing distributions for these stable geometries. We compared the eigenfunction distributions to boundary-layer solutions for the stable modes. Although eigenfunction amplitudes in separable geometries exhibit periodic regularities, we nevertheless demonstrated the amplitude distributions over the entire cavity to be Gaussian. We investigated the quality-factor distribution, which is quite narrow in the rectangle (with nearly unit aspect ratios), in the curved-wall geometries and found that it exhibited a form of beta distribution. Comparisons with a boundary-layer analysis showed that this broad distribution resulted from the whispering-gallery modes confined near the boundary.

We set up a ray-tracing algorithm for arbitrary boundary shapes in two dimensions. This allowed us to determine periodic-orbit eigenvalues. We also determined and checked stability exponents for various periodic orbits against available laser-cavity formulas for certain orbits. These stability exponents are required to determine scar amplitudes in unstable geometries.

We ran the boundary-element code EIGER on 2-D geometries as numerical experiments to compare with the HF models. We verified the eigenvalue spacing distribution for the even modes in the stadium to be Wigner (or Rayleigh). We verified eigenfunction distributions over the entire cavity and over limited sections away from scars to be Gaussian. We verified these statistics both spatially and over mode numbers. We examined deviations from Gaussian statistics associated with bouncing-ball modes.

We investigated a scar theory for time-harmonic fields. The idea involved is a generalization of the boundary-layer construction for stable modes. In the stable case, a single solution in the localized mode region decays away from the region. Transverse propagation in the unstable scar region requires two solutions to be present with a random-phase coefficient between them to account for return from the chaotic region of the cavity.

We applied the scar theory to the stadium cavity. However, we found that the theory needed to be modified to account for smaller radii of curvature and interior foci. We currently are modifying the descriptions of HF modes that include arbitrary curvature to the unstable case using the random-phase reflection criterion. We hope that this new form of the scar model will yield accurate predictions compared to the numerical experiments that we accumulated.

Refereed

Warne, L. K., K. S. H. Lee, W. A. Johnson, and R. E. Jorgenson. 2004. An improved statistical model for cavity antenna impedance in an electrically large cavity. *IEEE AP*, submitted.

67065

New Smart Material to Address Issues of Structural Health Monitoring

P. M. Chaplya

Nuclear weapons/storage facilities may benefit from in situ *structural health-monitoring systems. Appending health-monitoring functionality to conventional materials has been only marginally successful. Sandia seeks to create a new material that will include a health-monitoring function similar to a nervous system of a living organism. Suppose that each material grain contains a nanosize sensor that can communicate with the neighboring sensors. A loss of a sensor and/or a communication link may indicate developing structural defects, thus prompting for maintenance and avoiding catastrophic failure. A technology to create such a material does not exist. However, recent progress in micro-/nanotechnology allows us to envision this new smart material.*

This study will evaluate the feasibility of creating new materials with embedded health-monitoring functions. We will first explore new methods of damage detection based on the assumption that the distributed nanosensors exist (i.e., what properties should be measured?). This will identify requirements for the nanosensors (i.e., how will the properties be measured?). Next, we will design the necessary nanosensors (i.e., what are the manufacturing and embedment techniques?). Concurrently, we will develop data-processing algorithms applicable to prognostics and health management (i.e., how will the available data be used?).

Although the ultimate goal of this project is to create a fundamentally new material from scratch, developing a macroscale prototype using existing technology may be advantageous. For example, silicon micromachined sensors (or even smaller carbon nanotube–based devices) may be embedded into a polymer or a concrete. The prototypes may find their applications in civil engineering structures such as nuclear weapons-/waste-storage facilities.

Our goal was to evaluate the feasibility of a new smart material that includes self-sensing health-monitoring functions similar to the nervous system of a living organism. We also evaluated the state of the art of general sensor networks and their application in dense-data–collection techniques for validation of numerical methods and material-parameter identification.

Each grain of the envisioned material contains sensors that are connected in dendritic manner similar to networks of neurons in a nervous system. Each sensor/neuron can communicate with the neighboring grains. Both the state of the sensor (on/off) and the quality of the communication signal (speed/amplitude) should indicate not only a presence of a structural defect, but also its nature. That is, a failed sensor may represent a through-grain crack, while a lost or degraded communication link may represent an intergranular crack. A technology to create such material does not exist. While recent progress in the fields of microelectromechanical systems (MEMS) and nanotechnology allowed us to envision these new smart materials, it is unrealistic to expect creation of self-sensing materials in the near future. Our survey of nanotechnology, MEMS, communication, sensor networks, and data-processing technologies indicates that it will take 10 to 15 years for the technologies to mature enough to make self-sensing materials a reality.

Recent advances in the field of nanotechnology demonstrated that nanotubes (NTs), nanorods, and nanoparticles of carbon, boron and other materials have remarkable mechanical and electrical properties. Record strength-to-weight ratios, ballistic conductivity, and sensing capabilities (i.e., piezoresistance and piezoelectricity) have been reported. The first transistors, sensors, and actuators were made from NTs and other nanomaterials. However, nanomaterials are notoriously difficult to manipulate into useful geometries. Nanomanufacturing processes often produce bundles or random networks of nanostructured materials. Samples of the material are then manipulated with advanced microscopy tools to measure properties or to create a single device. This is a laborious and time-consuming process. An often-overlooked analogy between the manufactured bundles of NTs is their similarity to the dendritic structure of neural networks with a great quantity of interconnects that may act or serve as initiation sites for artificial neurons in a self-sensing material's nervous system. To accelerate the development of self-sensing materials, future research should concentrate on naturally occurring dendritic nanostructures.

While self-sensing materials with subgrain-size sensors (scale of micrometers) remain in the realm of basic research, mesoscale (millimeters to centimeters) sensors and their networks are in the state of mature research and have begun to find their way into commercial applications. Macroscale (centimeters to decimeters) sensors and their networks are commercially available from various sources. The majority of

applications that employ sensor networks are driven by the needs of the Department of Defense. Widespread adaptation of sensor networks has been limited by the sensor's high cost of design, development, and deployment, and also by a lack of reliable long-term power sources. Solutions to both of these drawbacks require significant investments driven by real-life applications. Possible applications for sensor networks include dense-data–collection techniques for validation of numerical methods and material-parameter identification. For example, an array of distributed wireless macroscale sensors can record the structural response of soils and reinforced concrete during explosives loading. Another example is an array of surface-mounted microsensors that can record the modal response of nuclear weapon components. The collected data would be used to validate existing numerical codes and to help identify new physical mechanisms that must be included to improve Sandia's computational models.

67067

Noncontact Surface Thermometry for Microsystems

S. P. Kearney, L. M. Phinney, T. W. Grasser, J. R. Serrano

Future Sandia systems will include microelectromechanical systems (MEMS) components playing critical roles. We currently are designing and evaluating the discriminating microswitch (DMS), nonvolatile memory, vertical-cavity surface-emitting lasers (VCSELs), and microsensors for near-term applications. Characterization of thermal-energy transport in these devices is necessary for understanding their performance in normal environments and their response to abnormal environments. Although quantitative temperature measurements are essential for implementing MEMS technology into engineered systems, Sandia's capability in this area traditionally has been lacking.

In this project, Sandia is cultivating state-of-the-art diagnostics for microscale surface-temperature measurements. These diagnostics are noncontact in nature, offer submicron resolution, minimize indirect heating, and apply to most materials. Microsurface Raman scattering and microthermoreflectance are complementary techniques that we are pursuing. Both methods utilize a low-power-probe laser of arbitrary wavelength.

Analysis of Raman phonon spectra is a robust technique for probing most any nonmetallic surface. Temperature, stress, and dopant information potentially can be obtained from the peak location, linewidths, and relative line intensities of the probed material's Raman signature.

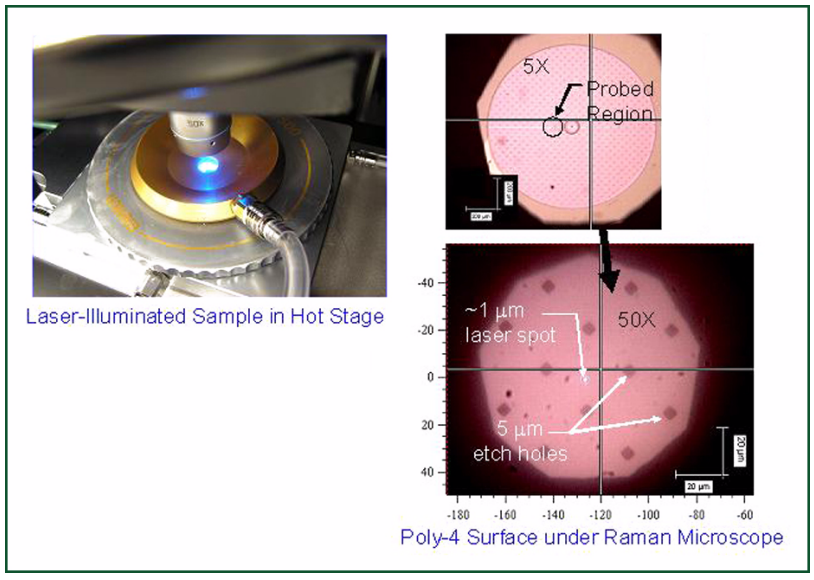

Summary of Raman characterization experiments of SUMMiT V™–fabricated parts.

Our accomplishments include (1) specification and acquisition of a high-resolution Raman instrument, (2) characterization of the Raman phonon spectrum of polysilicon (poly-Si) materials from Sandia's SUMMIT V^{TM} (Sandia Ultraplanar Multilevel MEMS Technology V) microfabrication process, (3) acquisition of the first-known spatially resolved temperature profiles from working microthermal actuators, (4) construction of a microthermoreflectance system, and (5) a collaboration with Georgia Tech, where the stress-dependent properties of Si and poly-Si MEMS materials were investigated.

We characterized the temperature-dependent properties of the Raman spectrum of SUMMIT V^{TM} materials. The results show that the Stokes- (red) shifted first-order phonon peak is a robust indicator of temperature. We measured a temperature coefficient of 0.024 cm^{-1}/K for the Stokes peak position for both SUMMIT V^{TM} poly-Si and bulk crystalline Si. This measurement proved repeatable over many different repeat runs, and we used the result to measure the spatially resolved temperature profile of microscale joule-heated thermal actuators for the first time.

We are considering joule-heated thermal actuators for nonvolatile-memory applications in Sandia's Defense Programs systems. The small spatial dimensions (3 µm width) make temperature and/or stress probing of these actuators exceedingly difficult with conventional contact probes or with infrared (IR) imaging. We mapped the temperature profile in five separate actuator scenarios with 1 µm spatial resolution and better than 10 K precision. These Raman-measured-device temperature fields are the first of their kind, and we used the experimental data to validate computational models. These application-specific measurements result from a collaboration with others at Sandia who are investigating the utility of thermal actuators under a second project.

We are collaborating with a colleague at Georgia Tech who is an expert on experimental microscale heat transfer; this collaboration leverages his expertise with the Raman-development efforts at Sandia. He is performing a systematic evaluation of the impact of material stress and doping on measured Raman spectra.

The Georgia Tech group utilized a Raman microscope with a four-point bending stage to test both doped and undoped poly-Si films over a material stress range of ± 400 MPa. Their results showed that stress-induced effects are second order when compared to temperature-induced shifts in Si-based materials in the temperature and stress range of interest to Sandia. They also

We mapped the temperature profile in five separate actuator scenarios with 1 µm spatial resolution and better than 10 K precision. These Raman-measured-device temperature fields are the first of their kind, and we used the experimental data to validate computational models.

found that boron-doped poly-Si material has a measurable impact on the temperature dependence of the Stokes-shifted Si Raman peak. They reported that other materials, such as gallium nitride (GaN), have increased stress-dependent Raman properties, and we will investigate the possibility of using Raman for a combined temperature and stress measurement under this project.

While Raman methods are robust over a wide range of semiconductor materials, they typically fail when the surface in question is a metal, where shallow-probe laser penetrations often render Raman scattering ineffective. As a complement to the Raman diagnostic, we are cultivating microscale reflectance thermometry or "thermoreflectance" for MEMS applications. Thermoreflectance methods exploit the small, temperature-dependent reflectivity of semiconductor surfaces and metallized coatings for noncontact thermometry. Thermoreflectance data can be simpler to interpret than Raman spectra, and their ability to resolve thermal transients is potentially superior to Raman. The chief disadvantage of thermoreflectance is the very low reflectivity changes that must be detected. We constructed a helium neon (HeNe)-laser–based thermoreflectance system. We are also considering simple modifications to our Raman microscope, which will convert it to a thermoreflectance facility.

Planned efforts for upcoming work include characterization of our thermoreflectance diagnostic and thermometry of metallized samples, investigation of advanced Raman techniques for improved spatial-temporal resolution, and application of our diagnostic tools to other materials of interest to Sandia, including GaN or other III-V semiconductors.

Refereed

Kearney, S. P., M. S. Baker, and L. M. Phinney. 2004. Raman temperature characterization of joule-heated microthermal actuators. *J. Heat Transfer,* in preparation.

67068

High-Speed Interferometric Deformation Measurements

B. D. Hansche, P. L. Reu, R. O. Nellums

A number of converging factors are driving the need for noncontact dynamic measurements. These include the development and validation of detailed structural models that need experimental data for comparison and the design and testing of microelectromechanical systems (MEMS) with parts such as gears and accelerometer reaction masses that exhibit dynamic motion. Laser Doppler vibrometry (LDV) is one technique to measure velocity, but is limited to a single point at a time. Wide-area measurement of out-of-plane motion has proven more difficult, leaving a strong need for a noncontact measurement technique that provides quantitative data on a dense spatial grid—a velocity "image."

This project involves the significant extension of LDV techniques from a single-point method into a wide-field measurement. Typically, an LDV uses a probe beam focused to a single point, and the returned Doppler-shifted beam is interferometrically measured, resulting in a heterodyned-difference frequency proportional to the object velocity. For typical structural mechanics velocities, this frequency is in the tens of megahertz, requiring the use of fast diode detectors. This limits the technique to single-point measurements, with velocity images built up by scanning the probe beam. This can take several minutes for a velocity image of an object in steady-state vibration and is impossible for transient events. In this project, Sandia is extending this measurement into a parallel detection system, measuring thousands of velocities simultaneously. We will accomplish this by using optical modulation to heterodyne the signal down to frequencies at which a conventional video system can directly respond to the Doppler frequencies. In addition to modulation of the signal, we are using joint time-frequency analysis (JTFA) techniques with sub-Nyquist sampling to significantly expand the bandwidth of the video system and increase the velocity bandwidth detectable by the system.

We conducted an extensive literature search to determine the state of the art for wide-field LDV measurements. We discovered a number of techniques, including strobed interferometry, iodine filtering, arrays of high-speed photodiodes, and complementary metal-oxide semiconductor (CMOS) camera techniques. All of these displayed significant

drawbacks that encouraged the development of the current project's proposed methods.

We assembled a preliminary wide-field LDV system using a gated microchannel plate and a Phantom 4 digital camera (up to 6000 Hz frame rate). Initial experiments for heterodyning in the image domain failed due to lack of brightness in the microchannel plate. We installed an electrooptic modulator to modulate the illumination beam. Experiments are under way to compare modulation of various beam combinations. We are now using a faster, more-sensitive Phantom 7 digital camera (up to 50 kHz frame rate). We attempted fiber-optic illumination, but it was unsuccessful.

We conducted experiments, both with and without laser modulation, to begin developing signal-processing techniques. A constant-velocity system with spatial-velocity gradients (i.e., a rotating plate) and a time-varying harmonic-velocity system (i.e., a pendulum) provided well-controlled velocity fields. We successfully demonstrated the use of both fast Fourier transform (FFT) and JTFA techniques to discriminate frequencies (hence, velocities, since $V=F\lambda/2$) both spatially and temporally. We suggested other analysis techniques, including wavelet decomposition, and they are under preliminary study.

A practical implementation of this technique will depend on measuring megahertz signals at kilohertz sampling rates. We demonstrated sub-Nyquist sampling techniques with "velocity unwrapping" for these simple velocity fields. Aliasing of the various higher-frequency components of the modulated image stream remains a severe problem, and techniques to combat it are under development.

67069

Fundamentals of Nanofluidics

R. H. Nilson, S. K. Griffiths

Nanoscale transport plays an important role in a broad range of engineering applications including thin-film flows, membrane filtration, colloidal particle motion, microfabrication, and electrokinetic (EK) transport in chip-based devices for detection of chemical and biological species. Despite this broad importance, there currently exists no reliable means for simulating flow in domains of micron scale to nanometer scale. Traditional continuum models fail to account for the molecular-scale physics of structured fluid layers adjacent to solid surfaces, while molecular-scale simulations alone cannot address the submicron- to micron-scale domains of interest in most applications.

In this project, Sandia is developing multiscale models of flow and transport within submicron channels by combining density-functional theory (DFT) with classical continuum mechanics. We are using DFT to compute structured fluid- and ion-density profiles based on Lennard-Jones, Coulombic, and hard-sphere interactions. These DFT profiles provide the basis for calculation of fluid-transport properties, surface-slip velocities, and EK driving forces that are then used to solve the continuum transport equations. We will utilize analytical integration of the DFT equations over molecular-sized layers to derive compact constitutive models or wall functions that can be used to incorporate nanoscale physics into any continuum fluid dynamics code.

We developed a hybrid continuum/DFT model that includes preliminary models of the physics essential to nanoscale flows.

(1) We extended our existing DFT model to include an arbitrary number of charged or uncharged molecular species. Also, in addition to Lennard-Jones attractions and hard-sphere repulsions, we now include Coulombic interactions among charged ionic species. We also improved our modeling of molecular repulsions using a second-order formulation that provides good agreement with Monte Carlo calculations and molecular dynamics (MD) simulations. We extensively tested these new aspects of our DFT model by comparison with published results.

(2) We implemented a preliminary model that yields the local fluid viscosity in terms of integral averages over the surrounding DFT density profile. The functional relationship that we currently employ is an extension of the Chapman-

Enskog formulation based on recent comparisons (Sigurgeirsson and Heyes, 2003) between continuum models and MD simulations. This model should provide good agreement between our nanoflow simulations and MD simulations, a topic we intend to pursue in upcoming work. We also plan to implement more complex viscosity models that incorporate the structure of the surrounding density field as well as the local average density.

(3) For use in conjunction with DFT, we developed a continuum model of channel flows driven by pressure and electric-field forces. Inputs to the model include fluid-viscosity and ion-charge distributions based on DFT. In addition to this hybrid DFT/continuum modeling, we also used this classical continuum model to explore the effects of double-layer overlap on the performance of EK pumping devices.

(4) We used a coupled DFT/continuum model composed of the preceding three building blocks to perform preliminary simulations of pressure-driven Poiseuille flow in nanochannels as well as electroosmotic flows driven by an applied electric field.

Upcoming work will center on development and verification of constitutive models describing fluid-transport properties and surface boundary conditions. We also will explore practical implications of our modeling, with an emphasis on EK flows.

67070

Simulating Self-Assembly and Growth of Biological Nanostructured Materials

P. A. Klein, P. J. In't Veld, D. R. Noble, D. J. Holdych, T. D. Nguyen, M. J. Stevens

Self-assembly of biomolecules is a promising avenue toward development of new materials. Engineering principles for micro- and nanofabrication can be discovered from the study of molecular self-assembly phenomena in nature. Biological tissues serve as model factories for the production of macromolecular structures, where the processes of molecular self-assembly and macroscopic growth are integrated in robust systems that display self-healing and adaptivity. Growth occurs as nutrients, amino acids, and enzymes undergo mass transport and react to increase tissue mass. At the molecular scale, there is considerable understanding of the reactions for self-assembly of tissue components such as collagen. There is less understanding of the thermodynamic driving forces and of how these forces interact with growth processes to form multicellular tissue. These processes are also influenced by mechanics at the continuum scale.

In this project, Sandia will study the processes of self-assembly and growth in collagen from the macromolecular to the continuum scale. The mathematical description of growth constitutes a highly complex system that requires mixture theory with coupled diffusion-reaction and mechanics and that differs significantly from classical continuum formulations of closed systems.

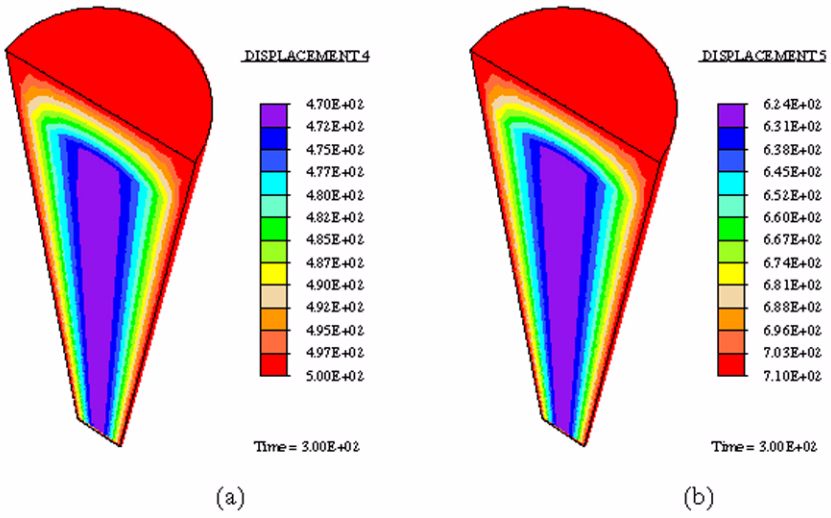

Growth of collagenous phase: (a) *Concentration of extra-cellular fluid at the end of 150 s.* (b) *Concentration of solid collagenous phase at the end of 150 s.*

We will develop and validate the models with collaborators at the University of Michigan, where they have the capability for growing in vitro *tendon constructs and characterizing their microstructure and mechanical response. This project provides the opportunity to uncover fundamental principles in the extension of characteristics of biological systems to the development of new engineering materials, and for Sandia to extend its leadership in computational and engineering science to a pioneering role in biotechnology.*

The work for this project is divided into three areas. At the coarse scale, we established the theoretical foundation that describes the phenomenon of growth for a multiphysics treatment in the setting of mixture theory, tightly coupling transport, and growth/resorption with mechanics. In comparison to standard theories for continuum solids, the formulation applies to systems that are open with respect to mass, admitting changes to the mass of the system that result not only through an overall increase in the size of the system, but also through changes in the relative concentration of its constituents. We revised the description of species transport in the continuum formulation to make it better suited for describing conditions in collagen.

Previously, we described all species motion with respect to the solid phase. In the revised view, we still describe the fluid motion with respect to the solid, while we describe the motion of the remaining species with respect to the fluid. This description of the motion of chemical species in the fluid, due in part to advection with the fluid and diffusion with respect to it, is better suited for determining the driving forces and mobilities associated with each contribution to the total transport. The coarse-scale formulation requires information about the structural properties of collagen and the transport through the collagen structure. We are investigating these areas in the other tasks. We performed lattice-Boltzmann (LB) simulations to study fluid transport through the solid phase. We simulated two-dimensional (2-D), pressure-driven Stokes flow through a periodic hexagonal cell for a Newtonian fluid to obtain the permeability of fibers (groups of fibrils) as a function of the volume fraction occupied by the fibrils. We also modified the LB code to incorporate moving solid boundaries, conditions intended to represent deformations imposed on the tissue during growth. These calculations provide information to the coarse-scale continuum in two ways. First, the permeability calculated for the fibers is needed in the coarse-scale formulation to describe the mobility of the fluid with respect to the solid.

Second, the flowfield through the fiber network is used to calculate the dispersion of species traveling with the fluid. This dispersion tensor is needed by the coarse-scale formulation to describe how species traveling with the fluid move relative to it. Once the implementation of the revised coarse-scale formulation is complete, we will compare predictions of species transport from the coarse-scale formulation, using the calculated permeabilities and dispersion tensors, with direct simulations of transport through a fiber network. At the molecular scale, we are investigating the structure of the triple-helix collagen molecule itself to understand not only its structural properties and the origins of its stability, but also how the molecules interact leading to self-assembly of fibrils. We developed a formalism to investigate the mechanical behavior of collagen fibrils through course-grained molecular dynamics (MD) simulations. Proposed structures for collagen fibrils taken from the literature serve as starting points for the construction of our initial configuration. We assume that a Lennard-Jones bead approximates each helical turn and assume some cross-linking morphology. We can then relax the models to see the final stable configuration and subject it to deformation to study the stress-strain response.

The purpose of the exercise described above is to demonstrate our capability of constructing and deforming collagen fibrils by means of molecular simulations. The current approach by no means is the final version of our model; however, it provides a starting point from which we can develop a final model. This final model will include a study of the needed degree of cross-linking in both the shell and the core collagen strands, a study of system size, and deformations in directions other than along the principal chain axis.

67071

A Low-Power, Ultrafast-Current Transient Measuring Device

P. Rossi, F. J. Zutavern, R. J. Foltynowicz, J. P. Sullivan, M. Armendariz

Sandia studied the feasibility of an innovative device to sample 1 ns low-power single-current transients with a time resolution better than 10 ps. The new concept explored here is to close photoconductive semiconductor switches (PCSSs) with a laser for a period of 10 ps. The PCSSs are in series along a transmission line (TL). The transient propagates along the TL, allowing one to carry out a spatially resolved sampling of charge at a fixed time instead of the usual time-sampling of the current. We proved that the fabrication of such a digitizer was feasible but very difficult.

Single-pulse transient digitizers currently are available only in the 5 GHz regime. We seek to develop a digitizer that consists of a number of extremely fast switches placed along the TL and to connect these switches to independent readout channels that work in parallel and that consist of "traditional" relatively low-speed charge integrators. Our goal is to achieve a 10 ps time resolution in digitizing a 1000 ps transient time range.

Such fast switches were invented by D. H. Auston and consist of two TLs fabricated on a semi-insulating substrate and separated by a tiny gap. The substrate then becomes conductive when illuminated by a laser pulse of suitable frequency, power, and duration.

We found two switch geometries that were practical: a linear design and a star-pattern design. We examined the basic notion of our linear transient digitizer with a small-scale four-channel prototype, including a gold TL fabricated on a gallium arsenide (GaAs) substrate in coplanar geometry. The prototype also included a black resist mask superimposed on the circuit. This mask, opaque to the laser light, features a few openings above the PCSSs that allow the laser light to go through and close the switches without shorting the remaining circuit. This mask allows a tremendous simplification of the project: with it, the laser beam can simply shine uniformly on the whole circuit, and standard methods used to manufacture integrated circuits (ICs) can be employed.

We found that to avoid damage to the masks, laser average and peak-power densities should be kept below ~ 1 TW/cm^2, which is ~ 100x larger than those required to close the PCSSs. We also performed studies to evaluate the effect of the black

plastic DARC 300 (the most successful of the three we tried) on the attenuation of the signal, which we also showed to be negligible.

Photoconductive switches look adequate as the basic building blocks of a 100 GHz digitizer. Their switching time is tunable in a range from 0.5 to 10 ps, and current mode-locking (ML) lasers have enough power to drive a hundred such Auston switches. We studied two possible TL geometries. A linear geometry with a single TL and many pickup electrodes is suitable for digitizing low-current signals (down to 100 μA), but with a number of samples that can hardly exceed 10, due to the substantial signal degradation that each pickup electrode implies. A star configuration can handle 100 time samples, but the initial signal cannot be smaller than 10 s of mA. This latter configuration might not be suitable for ion-beam–induced charge experiments, where signals scarcely exceed a few mA. As for inertial confinement fusion (ICF) explosions, their energy should be adequate also for a star geometry.

Other Communications

Rossi, P., and B. Doyle. 2004. A low-power ultrafast-current transient measuring device. Paper presented at the Engineering Sciences External Review, Sandia National Laboratories, 5 August, Livermore, California.

67073

A Capillary Valve for Microfluidic Systems

M. P. Kanouff, P. E. Rahm, B. M. Rush, E. B. Cummings

Microfluidic systems are becoming increasingly complicated as the number of applications grows. The use of microfluidic systems for chemical- and biological-agent detection requires that a given sample be subjected to many process steps, which requires microvalves to control the position and transport of the sample. Each microfluidic application has its own specific valve requirements, and this has precipitated a wide variety of valve designs. Each of these valve designs has its strengths and weaknesses. The strength of Sandia's proposed valve design is its simplicity, which makes it easy to fabricate, easy to actuate, and easy to integrate with a microfluidic system. It can be applied to either gas-phase or liquid-phase systems. This novel design uses a secondary fluid to stop the flow of the primary fluid in the system. The secondary fluid must be chosen based on the type of flow that it must stop. A dielectric fluid must be used for a liquid-phase flow driven by electroosmosis, and a liquid with a large surface tension should be used to stop a gas-phase flow driven by a weak pressure differential.

We carried out experiments that investigated certain critical functions of the design. These experiments verified that the secondary fluid can be reversibly moved between its "valve-opened" and "valve-closed" positions, where the secondary fluid remained as one contiguous piece during this transport process. The experiments also verified that when Fluorinert™ is used as the secondary fluid, the valve can break an electric circuit. We found it necessary to apply a hydrophobic coating to the microchannels to stop the primary fluid, an aqueous electrolyte, from wicking past the Fluorinert™ and short-circuiting the valve. We used a simple model to develop valve designs that could be closed using an electrokinetic pump (EKP) and reopened by simply turning the EKP off and allowing capillary forces to push the secondary fluid back into its stowed position.

The experiments demonstrated that the position of a dielectric fluid can be controlled in a microchannel and used to break an electric circuit.

The experiments demonstrated that the position of a dielectric fluid can be controlled in a microchannel and used to break an electric circuit. They also demonstrated that this secondary fluid remains intact so that it can be moved reversibly between a stowed position and a position where it can stop a flow. We found that the wetting behavior of the secondary fluid plays an important role. Here, the secondary

fluid is said to wet the channel walls when the interface between the primary and secondary fluids makes a contact angle less than 90 deg, as measured on the secondary fluid side. If the secondary fluid did not wet the channel walls, the primary fluid wicked along sharp corners in the channel past the secondary fluid, resulting in a short circuit for electric current to flow past it. By making a hydrophobic coating on the interior surfaces of the channel, the secondary fluid, Fluorinert™, did not wet the walls. We did not detect an electrical short circuit under these conditions. However, when the secondary fluid wets the walls, it cannot be completely withdrawn from the main channel, where a small chunk is left behind.

We used a simplified model to develop designs for the capillary valve that could be actuated with an EKP, i.e., they could be actuated with an electrical signal. But the experiments showed that the contact angle may not always be constant, which could defeat designs that rely on capillary forces to hold and move the secondary fluid. If the capillary forces do not work, other methods could be used to control the position of the secondary fluid. These include electrowetting, electrocapillary, and dielectrophoretic methods. Finally, another method that could be used is a reversible EKP to shuttle the secondary fluid into and out of the stowed position.

We identified several other applications of immiscible liquids in microchannels in this work. One is a method for mixing and transporting reagents in microchannels with low dispersion. The reagent mixture is “sandwiched” between two plugs of Fluorinert™, and the assembly is pushed along the channel with a pressure gradient. The combination of the motion and the near-shear-free interfaces bounding the ends of the reagent mixture results in a recirculating flowfield within it that produces accelerated mixing therein. A second application is for a dielectrophoretic process, where Fluorinert™ is partially extruded from a side channel into a main channel, thereby forming a constriction. When combined with an electric field, the constriction creates gradients in the field that can be used to dielectrophoretically trap particles depending on their size and other characteristics. Such an application could be used to sort particles so that subsets of them could be subjected to further analyses. This would be a unique implementation of dielectrophoresis, where the size of the constriction and, hence, the degree of particle trapping, could be adjusted during the process.

Grand Challenges

The Grand Challenges investment area seeks innovative, high-risk, outrageous ideas with the potential to dramatically impact national-level concerns, and to create the technologies and processes required for the twenty-first century. Grand Challenges investments engage labwide multidisciplinary research teams that establish critical mass, in participation and funding, to focus on world-class research.

41193 "Biomicrofuel Cell"

A biomicrofuel cell would provide power by harvesting energy from the environment, making it possible to realize unprecedented lifetimes in a variety of self-sufficient microsystems. Biomicrofuel cell technology would provide power by directly oxidizing carbohydrate fuels (sugars). Carbohydrate fuels have high-energy density, are readily available in foodstuffs, and can even be harvested from the surrounding environment.

In 2004, researchers advanced the understanding of carbohydrate fuel electrochemistry, creating new technology for improved catalysts for carbohydrate fuels and characterization of a novel polymer electrolyte membrane. Advanced system architectures that produce long-lived, electronic-grade power, and increased power density and lifetime were achieved. Major new capabilities were also established in enzyme engineering. Scientists were able to uncover enzymatic catalysts on high-surface-area electrodes that would enable high-power densities. In tests, sustained power was demonstrated for over 400 hr without power degradation, a record for biofuel cells. Research resulted in 11 technical advances, 4 of which are in patent application.

41193

Biomicrofuel Cell (BMFC)

C. A. Apblett, P. L. Dolan, R. P. Muller, S. Chhabra, P. M. Baca, C. Schmidt, J. V. Volponi, M. M. Manginell, M. A. Hickner, B. A. Simmons, C. H. Fujimoto, K. R. Zavadil, C. J. Cornelius, C. L. Staiger, R. A. Kemp, J. L. Novak, D. Ingersoll, M. J. Kelly, S. H. Kravitz, S. M. Brozik, S. K. Eisenbies, J. H. Flemming, A. R. Straumanis

Sandia's vision in this project is to provide long-lived power by directly oxidizing carbohydrate fuels (sugars) in a microfuel cell. Carbohydrate fuels have high-energy density, are readily available in foodstuffs, and can even be harvested from the surrounding environment (plants and animals). Success in this venture would extend mission lifetimes for sensored microsystems beyond those achievable with current battery technologies because the fuel (energy) can be obtained locally rather than carried in, and would enable new solutions for a variety of national security applications. Our accomplishments include a deeper understanding of carbohydrate-fuel electrochemistry, establishment and demonstration of new capabilities to develop improved catalysts for carbohydrate fuels (both metal- and enzyme-based), improvement and characterization of a novel polymer electrolyte membrane (PEM), demonstration of advanced system architectures that include power-management circuitry for production of long-lived, electronic-grade power, and increased power density and lifetime.

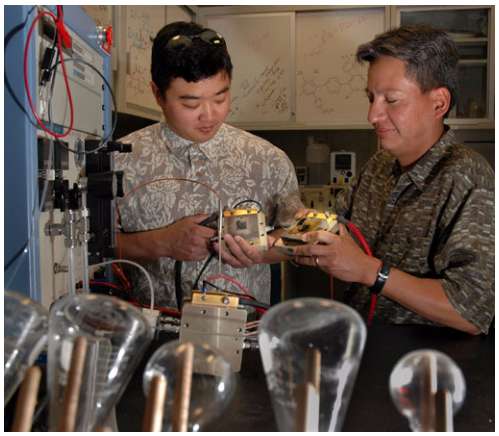

Cy Fujimoto, left, *and Chris Cornelius hold a test microfuel cell with the Sandia membrane. Next to Fujimoto is a microfuel test station.*

This project demonstrated excellent progress both programmatically and technically. Technical efforts concentrated on demonstrating higher power and longer life when running on glucose solutions, establishing methods for the discovery of better catalysts (both metallic and enzymatic), and performance characterization of our new PEM material. We made significant accomplishments in each of these areas.

We improved initial power output with glucose solutions by about 5x to 13 mW/cm^2. More importantly, we demonstrated sustained power of 1.5–2 mW/cm^2 over 400 hr without power degradation, a record for biofuel cells. Improved understanding of catalyst poisoning mechanisms and fuel-cell operation enabled this dramatic lifetime improvement over any biofuel cells reported in the literature. We implemented the lifetime-enhancement protocol with power-management circuitry that requires less than 400 µW of power overhead. This circuitry is also designed to provide electronic-grade power from a stack of six fuel cells. The circuitry involved could be reduced to a single application-specific integrated circuit (ASIC) chip,

...we demonstrated sustained power of 1.5–2 mW/cm^2 over 400 hr without power degradation, a record for biofuel cells. Improved understanding of catalyst poisoning mechanisms and fuel-cell operation enabled this dramatic lifetime improvement over any biofuel cells reported in the literature.

consistent with the long-term vision of a miniature BMFC (biomicrofuel cell) power source.

We made a major investment in catalyst discovery capabilities. A high-throughput combinatorial electrochemical screening capability was put in place to explore optimum noble metal compositions and revealed several new binary and ternary compositions that look promising for direct-glucose fuel-cell applications. We initiated membrane electrode assembly (MEA) optimization efforts involving some of these new compositions, and they are continuing. We also established major new capabilities in enzyme engineering. Earlier enzyme work involved only native glucose oxidase (Gox) strains (i.e., those found in nature) and indicated that significant performance gains might be possible through enzyme engineering. Such techniques can be effective in increasing activity, electron transfer, and pH and thermostability ranges. To pursue this course, three major capabilities must be in place: methods (1) to induce the mutations, (2) to screen the mutations for desirable properties, and finally, (3) to produce significant quantities of the most promising mutation strains. We successfully used both rational redesign (directed at specific pre-identified sites in the deoxyribonucleic acid [DNA] sequence) and random iterative mutagenesis (also called *directed evolution*) to induce the mutations. The rational redesign process successfully produced 1200 Gox mutants, some of which appear to have higher activity, according to calorimetric screening methods. We demonstrated a more quantitative electrochemical screening method, but we must develop instrumentation for high-throughput use. Work is under way to produce tens of milligrams of a chosen mutant enzyme, sufficient to produce several fuel-cell electrodes. Another important accomplishment was the successful demonstration of enzymatic catalysts on high-surface-area electrodes, showing a path to high-power densities for this approach.

Recently, we further enhanced and characterized the new PEM developed earlier. The poly(phenylene)s synthesized via Diels-Alder condensation resulted in polyelectrolytes that could be post-sulfonated in a controllable manner with chlorosulfonic acid. The aryl backbone resulted in a tough, rigid rod material, indicated by its high glass-transition temperature (Tg) and inherently high thermochemical stability. This type of high-Tg material possesses physical properties that are attractive in high-temperature fuel-cell applications. This could prove to be a very significant development for the general fuel-cell community.

The technical accomplishments cited above resulted in 11 technical advances, 4 of which are currently included in patent applications, and 11 papers and presentations.

Refereed

Cornelius, C. J., and C. H. Fujimoto. 2004. Sulfonated Diels-Alder polyphenylenes in hydrogen-based PEM fuel cells. Paper presented at the 15th North American Membrane Society Annual Meeting, 26–30 June, Honolulu, Hawaii.

Cornelius, C. J., and C. H. Fujimoto. 2004. Sulfonated Diels-Alder polyphenylenes: Synthesis and properties of a novel polyelectrolyte. Paper presented at the 15th North American Membrane Society Annual Meeting, 26–30 June, Honolulu, Hawaii.

Other Communications

Apblett, C. A., D. Ingersoll, E. Matteo, D. Maricle, and S. Sarangapani. 2004. A direct glucose microfuel cell. Paper presented at the 205th Meeting of the Electrochemical Society, 9–13 May, San Antonio, Texas.

Cornelius, C. J., and C. H. Fujimoto. 2004. Physical properties of sulfonated Diels-Alder polyphenylenes: Applications for PEM fuel cells. Paper presented at the 227th ACS National Meeting, 28 March–1 April, Anaheim, California.

He, L., D. Perahia, C. H. Fujimoto, and C. J. Cornelius. 2004. The correlation between molecular and phase structure in highly ionic polymer. Paper presented at the American Physical Society Meeting, 22–26 March, Montreal, Quebec, Canada.

Kelly, M. J., D. Ingersoll, W. A. Steen, E. N. Coker, I. C. Abraham, and J. E. Miller. 2004. Electrochemical oxidation of d-glucose at noble metal and binary metal catalysts for fuel-cell applications. Paper presented at the 205th Meeting of the Electrochemical Society, 9–14 May, San Antonio, Texas.

Volponi, J., B. Simmons, D. Ingersoll, and A. Walker. 2004. Bioreforming fuels for a biofuel cell. Paper presented at the 205th Meeting of the Electrochemical Society, 9–13 May, San Antonio, Texas.

41194

Augmented Cognition: Next-Generation Intelligent Systems

P. D. Heermann, D. E. Small, J. S. Wagner, J. H. Ganter, D. P. Gallegos, J. C. Forsythe, N. M. Berry, K. W. Larson, P. G. Xavier, R. F. Martinez, B. D. Farkas, P. C. Reeves, A. Backer, A. E. Speed, M. L. Bernard

In this project, Sandia will develop the capability to dramatically improve understanding in the exploding national security data (text/image) environment by significantly increasing the ability to detect and interpret hidden, meaningful patterns in complex environments. Analysts in areas vital to national security (such as weapons surveillance and safety and security) are bombarded with obscure cues/data within diverse, multifaceted situations; they must effectively integrate those cues and data into actionable information. The human ability to recognize patterns in context, and thereby understand them, will be replicated via development and validation of software/hardware instantiations of computational representations of human perception and thinking/cognition. Resulting capabilities will be broadly extensible; in this project, we will demonstrate and validate these on a focused set of applications.

We will deliver these capabilities by accomplishing three goals and measurable objectives: (1) perceptive systems—establish and validate revolutionary visual object recognition by computational representation of the primate ventral stream (the objectives being object discrimination, invariance, and spatial recognition, feature/shape recognition, and feature-vector recognition), (2) cognitive systems—establish and validate context-based understanding by developing computational science–based (psychologically and physiologically) models of how humans think (the objectives being an accurate cognitive model, accurate automated knowledge capture, and superior human performance of context-based understanding), and (3) systems engineering—establish and validate an extensible computational systems engineering/infrastructure for a cognitive collective with visual object recognition (the objectives being core, multiagent, and next-generation intelligent systems [NGIS] architecture development). This project is directed at a challenging class of complex applications for which integration of object recognition and contextual understanding is required. We will conduct a demonstration showing the synergy of integrated perceptive and cognitive systems for situation awareness in a

secure facility, which has broad Department of Energy (DOE) and national security applications.

We conducted work along three technical tracks: perceptive systems, cognitive systems, and systems engineering. We defined an integrated demonstration and created a first-look business plan/transition strategy, and a successful External Advisory Board review was completed. We made the following accomplishments:

- *Perceptive systems*. We completed initial development of the ROCIT algorithm in both MATLAB and C++.

We did an extensive literature search for appropriate datasets and the accompanying methodologies to test algorithm performance in relatively uncontrolled settings, including variation in illumination, scale, rotation, cluttered background, and occlusion of the principal target. The only dataset and methodology found was the FERET (facial-recognition technology) face-identification test from the late 1990s, which tests illumination changes with slight scale, object rotation, and translation. We designed and built the SCALO dataset and methodology to evaluate visual object-recognition algorithms with systematic variation in scale, clutter, affine rotation, lighting, and occlusion.

We conducted an extensive search for the best available visual object-recognition technology for the general application in uncontrolled environments, and identified the recently developed SIFT algorithm from the invariant interest point paradigm in computer vision as the current state of the art. We acquired the SIFT algorithm for the purposes of benchmark testing.

We conducted an extensive benchmark test using the Rank-Order Coding implementations of ROCIT and SpikeNET, as well as the SIFT algorithm. The FERET test, with a repeatable methodology, allowed direct comparison to prior algorithms for face identification. ROCIT and SpikeNET both performed better than late-1990s algorithms for face identification. SIFT, however, performed better than both ROCIT and SpikeNET in both the FERET and SCALO tests.

- *Cognitive systems*.

— Accurate Cognitive Model: upgraded semantic and contextual episodic memory.

— Accurate Automated Knowledge Capture: developed knowledge-capture infrastructure, derived key concepts, and made concept associations.

— Superior Human Performance of Context-Based Understanding: compared current to past transactions, and compared and contrasted the semantic memory of models.

— Implemented methods for automatic capture of the knowledge to derive a semantic memory model for an individual.

— Implemented initial capabilities to automatically capture the knowledge to derive a contextual memory model for an individual.

— Implemented methods for comparing the current and past transactions of an individual.

— Implemented capabilities to compare the semantic memory models of different individuals.

- *Systems engineering*.

— Core software architecture.

- Completed the conceptual design, upgraded the cognitive framework initial design, exported the current implementation to UMBRA 4, and completed the semantic memory, the spatial-temporal memory, and the contextual/episodic recall episodic acquisition.
- Developed a cognitive world model and perceptual synthesis interface and updated the cognitive collective.

— Agent software architecture.

- Completed the selection of an underlying agent framework, a cognitive-agents system design, and an embedded cognitive framework in agents.
- Began initial interactive multiple cognitive agents.

- *Integrated demonstration*. The goal for this portion of the project was to integrate the synthetic perceptive capabilities with the cognitive framework. We identified a physical-security variation of the “big data” problem as an ideal situation in which to perform this integration. This problem is one currently faced at many DOE and other secure sites and becomes more compelling as unmanned ground sensors proliferate; it has applications to military operations in urban terrain (MOUT) environments and to other big data problems. We created a software demonstration of a cognitive model of a physical-security expert attending to sensor data as a series of attack forces breached the external perimeter of the facility and moved toward an attractive target within the facility. We intended that the simulation act as a test-bed for integration problems, as we plan to develop a prototype of this system in an actual facility in upcoming work.

Refereed

Bauer, T., and R. G. Abbot. 2004. Automated knowledge elicitation: Current technology and future research. Paper presented at the Cognitive Systems Workshop, 29 June–1 July, Santa Fe, New Mexico.

Bauer, T., Z. Benz, and J. Kimmel. 2004. Automated knowledge capture for deriving individual cognitive models. Chapter in *Cognitive Systems: Human Cognitive Models in Systems Design*, accepted.

Forsythe, J. C. 2004. Atypical, but practical applications for cognitive modeling. Paper presented at the Human Factors and Ergonomics Society Meeting, 20–24 September, New Orleans, Louisiana.

Forsythe, J. C., and P. G. Xavier. 2003. Cognitive models to cognitive systems. Chapter in *Cognitive Systems: Human Cognitive Models in Systems Design*, accepted.

Forsythe, J. C., M. L. Bernard, and T. Goldsmith. 2004. *Cognitive systems: Human cognitive models in systems design*. Book to be published by Lawrence Erlbaum.

Forsythe, J. C., P. G. Xavier, and A. E. Speed. 2004. Dynamic model of human context recognition and understanding. Paper presented at the Cognitive Systems Workshop, 29 June–1 July, Santa Fe, New Mexico.

Other Communications

Farkas, B. D., A. I. Gonzales, J. J. Jones, and P. C. Reeves. 2004. ROCIT: A visual object-recognition algorithm based on a rank-order coding scheme. Sandia Technical Report SAND2004-2129, Sandia National Laboratories, Albuquerque, New Mexico.

Speed, A. E. 2004. Dynamic context discrimination: Psychological evidence for the Sandia cognitive framework. Sandia Technical Report SAND2004-4567, Sandia National Laboratories, Albuquerque, New Mexico.

50065

TALON

F. T. Mendenhall, K. T. Malone, D. A. Wiegandt, F. J. Oppel, III, M. D. Ladd, S. M. Deland, K. T. Stalker, L. J. Ellis, R. L. Williams, M. R. Ackermann, J. B. Woodard, J. R. Yoder, M. C. Reineke, L. G. Stotts, M. B. Murphy, J. W. Hampton, V. C. Hindman, J. J. Carlson, D. P. Gallegos, P. R. Bryson

The fundamental hypothesis of this project is that sensor networks provide a robust system solution for many problem classes, from intelligence collection to military force protection, Department of Energy (DOE) asset protection, Department of Homeland Security (DHS) ports and border security, and countless others. To focus the effort appropriately, Sandia chose to consider the problem of detection, classification, and tracking of a diverse set of mobile ground targets using heterogeneous unattended ground sensing, adaptive communications, and long-lived efficient network and sensor management. Furthermore, we expect that sensor networks will lead to significant improvement in capability over existing solutions. We tested and continue to test this hypothesis by exploring the collaboration and multisensor data fusion enabled by local networking to address the target set and range of environments of interest.

- *Network communications*. A solid understanding of radio-frequency (RF) propagation and local-area network (LAN) performance is critical to the viability of sensor networks and is a critical need in a number of Sandia sensor network programs, including TALON. We accomplished the following:
  - — Dramatically improved network performance in all environments.
    - Included packet-level collision avoidance.
    - Included improved timeout and overall timing.
    - Included radio-level acknowledgments and failure assessment.
    - Included better power handling via point-to-point mechanisms.
    - Included packet-by-packet control of radio behaviors.
  - — Achieved understanding of propagation effects of environments.
  - — Achieved understanding of propagation effects of short-range connectivity between a device and a network node.
  - — Achieved multichannel networking capability with improvements made with high throughputs.

— Built in adaptive capabilities for future use.
- Found that variable transmit powers are possible for future use. (Radio hardware change is necessary.)
- Found that variable data rates are possible for future use. (Radio hardware change is necessary.)

— Currently are negotiating three follow-on projects via the external interest of our network.

- *Advanced networked systems-level optimization analysis*. The TALON optimization project developed the ability to optimize the performance of a network of wireless sensors based on the results of full, physics-based simulations of vehicle traffic around facilities of interest. This capability builds on prior work done in UMBRA, a Sandia-developed three-dimensional (3-D) modular simulation framework, for other aspects of the TALON project. These include high-fidelity wireless-communications modeling and multiple modes of sensing (imaging, acoustic, seismic, magnetic, and passive infrared [PIR] sensors).

We developed methods of interfacing with and using a variety of optimization techniques, including stochastic, gradient-based, and hybrid methods, for the UMBRA framework. Until this point, UMBRA was primarily a stand-alone modeling and simulation (M&S) environment. The capabilities of the DAKOTA (Design Analysis Kit for Optimization and Terascale Applications) toolkit are also now available in UMBRA.

Another major accomplishment was the construction and implementation of a realistic, multicomponent fitness function.

Overall, the capabilities developed during the TALON optimization project give Sandia the capability to simulate and optimize the performance of a sensor cluster relative to a specific scenario.

- *Global tracking*. We performed three tasks: (1) developed tracking algorithms to track multiple targets constrained on a road network over a large geographical area, (2) investigated information architectures to optimize network efficiency while minimizing power usage, and (3) extended the M&S toolkit to design and analyze sensor networks to evaluate tracking performance.

We made progress in assessing four different tracking algorithms: (1) imaging-processing algorithm, (2) graph theory approach, (3) particle-filter algorithm, and (4) rule-based or expert-system approach.

An information architecture study examined the trade-offs of sensor network efficiency against sensor density, network protocols, and power consumption.

Overall, the capabilities developed during the TALON optimization project give Sandia the capability to simulate and optimize the performance of a sensor cluster relative to a specific scenario.

- *Image sensor studies*. This TALON effort supported field data collection in the area of thermal imaging of ground targets, field testing of algorithms, and to some extent, the development of algorithms to exploit the thermal image data.

This TALON study was instrumental in helping Sandia obtain $10 million in imager programs.

Our accomplishments consisted of technical data collections of thermal data against ground targets. Our signal-processing people then evaluated these collections and analyzed and tested the resulting algorithms in MATLAB against real data from the field data collections. We published a SAND report on the technical design of unattended ground sensors for tactical intelligence applications.

Other Communications

Ackermann, M. R., J. J. Carlson, M. W. Edenburn, S. M. Deland, F. T. Mendenhall, K. Seager, K. T. Stalker, L. G. Stotts, and D. A. Wiegandt. 2004. TALON local area network (LAN) sensor systems report. Sandia Technical Report SAND2004-3423, Sandia National Laboratories, Albuquerque, New Mexico.

Berry, N. M., J. T. Feddema, J. H. Gauthier, M. J. McDonald, F. T. Mendenhall, F. J. Oppel, E. P. Parker, and B. P. Van Leeuwen. 2004. TALON LDRD program report: Wireless networks of unattended ground sensors. Sandia Technical Report SAND2004-2742, Sandia National Laboratories, Albuquerque, New Mexico.

55079

Near-Real-Time Characterization for Assured HDBT Defeat

D. R. Gardner, D. A. Dederman, E. R. Hoover, M. E. Bukaty, S. Hostetler, J. M. Opalka, T. W. Pfeifle, M. T. Oswald, E. P. Chael, R. J. Franco, M. E. Gonzales, J. T. Hollenshead, R. J. Fogler, R. T. Gilchrist, R. E. Abbott, D. F. Aldridge, K. T. Stalker, N. P. Symons, G. C. Bessette, D. J. Frew, W. H. Rutledge, G. J. Elbring, L. S. Costin, P. Yarrington, L. C. Bartel, B. P. Engler

Sandia's goal in this project is to perform research and development on key technologies for an aerially deployed system of seismic sensors, sources, and penetrators that will improve the survivability and effectiveness of our nation's earth-penetrating weapons (EPWs) against hard and deeply buried targets (HDBTs) through rapid site characterization and aim-point selection.

The project involves several high-risk technical challenges. One of these is to obtain adequate resolution of the near surface of the HDBT site with a sparse, irregular array of seismic sources and sensors. The arrays used in this project will be much sparser and more irregular than those used in geotechnical engineering applications. This project is exploring both seismic-imaging and seismic-detection methods.

Another high-risk technical challenge is to correlate penetration data with the seismic velocity map. The velocity map is developed from elastic material properties (e.g., the shear modulus), while penetration events are governed by nonlinear elastic-plastic material properties such as yield strength. We will require methods to integrate penetration data with seismic velocity maps to develop a composite description of target material properties and their spatial distribution in the near-surface layer.

Other challenges include shock-hardening of componentry such as geophones and global positioning system (GPS) electronics, emplacing seismic sensors near the surface in a variety of soils, collecting accelerometer data from more deeply buried probes, and forming efficient ad hoc *data-collection networks. Addressing these challenges requires a multidisciplinary systems approach and will draw on Sandia's expertise in seismic imaging, air-deployed sensors and sensor networks, earth penetrators, and modeling and simulation, and will enhance Sandia's capabilities in these areas.*

Success of the project will provide the technological basis for increasing our confidence that an EPW can defeat a targeted HDBT. The project has important potential extensions

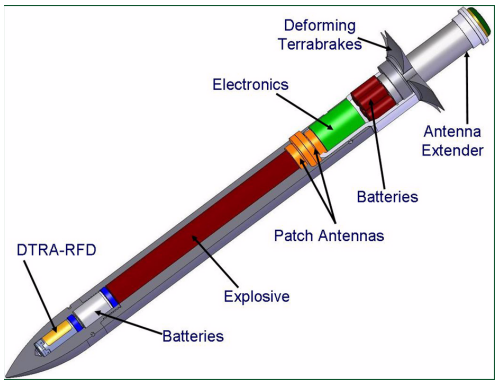

Design of the separable penetration probe.

to precision engagement, bomb-damage assessment (BDA), mineral exploration, water-resource management, and reservoir engineering.

We refined the guiding concept of operations to involve smaller sensor darts that remain near the surface and larger, more deeply penetrating, separable penetration probes that collect penetration data. *Ad hoc* networks collect seismic and deceleration data and transmit them to a remote site where the penetrability map is constructed.

We validated the Zapotec code for normal and oblique penetration into homogeneous concrete targets. We validated Zapotec for normal penetration into targets containing an inclusion with contrasting properties embedded just below the concrete surface. The impact with the inclusion imparts significant lateral accelerations to the penetrator. We evaluated the PENCURV code for scoping calculations using the complex-targets test data.

We modeled sensor-dart impacts with trees of varying sizes. Preliminary results suggest that even at heavily forested sites, most of the darts will survive to impact the ground.

We modeled sensor-dart impacts with trees of varying sizes. Preliminary results suggest that even at heavily forested sites, most of the darts will survive to impact the ground.

We field-tested seismic sources to determine the explosive charge needed for an adequate signal-to-noise ratio (SNR) for the seismic imaging.

We explored the sensitivity of seismic imaging to various parameters and events, such as noise, incomplete data, velocity contrasts, layer thickness, and random source/receiver deployment patterns. Using synthetic and local field data, we determined the resolution limit of the sparse, random, surface-wave tomography method for isolated inclusions. We began exploring detection methods to complement the imaging methods.

We determined the range requirements for the network radio for the darts and probes. We studied differential carrier-phase GPS accuracy as a function of terrain and ground foliage. These studies guided the selection of the radio and the GPS for shock testing.

We successfully formed an *ad hoc* radio network using the TALON Pleiades sensors from the “Terrorist Activity Location, Observation, and Neutralization (TALON)” project with custom software modifications (no hardware modifications were used) and measured its baseline performance.

We developed a prototype design for the sensor dart and completed an electronics packaging estimate. We developed a new terra brake design to keep the dart at or near the surface in geologies with a wide and representative range of properties.

The prototype was drop-tested at the Antelope Tuff and Antelope Lake sites at the Tonopah Test Range. The terra brake functioned as designed to keep the dart at or near the surface in softer targets.

We developed potting methods for critical electronic components for the dart and probe. We determined the maximum accelerations that the components could sustain in laboratory shock tests. Based on these tests, we selected the electronic components (e.g., geophones) for the dart and probe for drop testing at Tonopah. All the critical components survived the drop tests.

We designed and built six hand-emplaced units for the sensor darts. These units provide a test-bed for the validation of software and hardware for the development of an air-deliverable sensor dart. These units also will be used for a geophone ground coupling test with air-delivered sensor darts. The units performed as designed at a local Sandia field-test site.

We developed a prototype design for the penetration probe and drop-tested the separable prototype at the Antelope Tuff and Antelope Lake sites at Tonopah. The prototype separated into the fore- and aft-bodies, and the aft-body remained near the surface, as designed.

We studied data transmission between the fore-body and aft-body of the penetration probe. We designed an extender to elevate the radio antenna to ensure network communications.

Other Communications

Broyles, T. P. 2004. An evaluation of the PENCURV model for penetration events in complex targets. Sandia Technical Report SAND2004-3482, Sandia National Laboratories, Albuquerque, New Mexico (July).

Gardner, D. R. 2004. Rapid, near-surface geologic site characterization for HDBT defeat. Paper presented at the 2nd Worldwide Underground Facilities Conference, 20–22 September, McLean, Virginia. SAND2004-4651P.

Gardner, D. R., G. J. Elbring, R. J. Fogler, and D. J. Frew. 2004. An air-deployed sensor system for rapid, near-surface site characterization. Paper presented at the Conference on Research and Development on Finding, Characterizing, and Assessing Underground Facilities, 2–4 June, Chantilly, Virginia. SAND2004-2355C.

55086

Prompt Global Response

J. M. Macha, D. E. Outka, D. D. Stokebrand, R. B. Bond, J. A. Galloway, J. R. Phelan, J. A. Emerson, R. D. Tucker, M. A. McWherter-Payne, J. B. Christensen, M. S. Howard, D. W. Kuntz, R. E. Loehman

Prompt global response (PGR) is providing an exceptional opportunity for Sandia to become a leader in hypersonics technologies. We made significant progress toward our objectives:

(1) Technical investments in a next-generation flight computer indicate applications across many of Sandia's future, advanced systems concepts.

(2) Development has begun on navigation, guidance, and control (NG&C) algorithms that use advanced carrier-phase processes.

(3) Materials science projects are continuing that will develop thermal protection systems (TPS) to facilitate the high-temperature, long-duration missions.

We are pursuing this technical focus in a context that emphasizes the creation of new national hypersonic system capabilities. The national need for a global presence and prompt strike continues to be reaffirmed in the Defense Science Board study completed recently on strategic strike. This effort has received favorable reception from organizations such as the Defense Advanced Research Projects Agency (DARPA), the National Aeronautics and Space Administration (NASA), Strategic Command (STRATCOM), and other Department of Defense (DoD) organizations. This support is reflected in the positive response from our External Advisory Board with membership from these national organizations. Sandia's previous experience in the field of hypersonics, coupled with an acknowledged continuing investment reflected in PGR, allowed us to become active participants in two externally funded programs. Other national program opportunities are also being pursued with the Strategic Navy and the Army Space and Missile Defense Command.

PGR is already having an impact on Sandia and the nation's capability in hypersonic technologies. One of the best examples is reflected in the NG&C progress. Not only is PGR making technical advancements; it also is building a breadth of capability embodied in a cadre of new staff members. We are teaming some of our newest staff with our most senior engineers to address this challenging technical task. PGR is also expanding teaming throughout the Laboratories between

technology-focused developers and systems designers. Key team members were also invited to join Integrated Product Development teams and other government leadership groups.

We made the following technical accomplishments:

- *Limiting performance of conventional TPS materials and design concepts*. We completed an extensive comparative analysis to determine the maximum achievable performance using available TPS materials and conventional design concepts. The analyses showed that our targeted performance in terms of reentry velocity and glide range is not possible without developing and employing new materials and aeroshell designs.
- *Assessment of current NG&C capability and exploration of advanced concepts*. GPS provides a low-cost means to provide error-correcting updates to an inertial navigation system. However, GPS may be unavailable during war due to satellite destruction or, more likely, to jamming of the GPS signal near targets. We assessed the feasibility of two non-GPS methods of providing the aiding updates. We completed conceptual designs that included system requirements, candidate hardware components, and preliminary link analyses.
- *Preliminary vehicle shape/trajectory optimization*. We completed definition of a new vehicle geometry, a generalized-maneuvering reentry-vehicle sensitivity study, and a preliminary vehicle energy-management study. The new geometry is characterized by an aerodynamic database developed exclusively using parabolized Navier-Stokes (N-S) computational-flow dynamics (CFD). In addition, we developed a method to bridge the aerodynamic coefficients from the continuum regime to free molecular flow.
- *Requirements and possible concepts for a deployable payload*. We made good progress in defining the requirements for a deployable payload. We defined a set of performance attributes and then used them to evaluate a large number of vehicle concepts. We began flight testing two competing prototypes.
- *Preliminary design of a baseline PGR vehicle*. We completed the preliminary design of a baseline vehicle suitable for a hypothetical PGR operational scenario. We based the design on technologies requiring a “moderate” level of development such that a prototype could be flown on a demonstration mission in a 2–3 yr time frame. The design includes all necessary flight systems and electronics and provides a reasonable payload volume.

55087

Winning the War: A Systems Approach to Defending Our Borders

C. A. Pura, H. R. Ammerlahn, M. J. McDonald, R. G. Hillaire, L. Shyr

The goal of this project is to develop and evaluate the tactical and strategic systems-level performance of security architectures and concepts of operation (CONOPS) deployed to protect the U.S. border system. Sandia is developing a system-of-systems (SoS) simulation that captures air-, land-, and sea-based border ports of entry (POEs), technologies, commodity and person flows, and policies, as well as their relationships and interdependencies. We are designing the Borders Security/Flow Simulation to provide a basis for the following types of analyses:

- *Evaluation of enhanced or alternative security systems and measures in the context of the SoS in which they would be deployed.*
- *Technology cost/benefit analyses—Quantify the added security benefit of deploying sensor technologies and their capital and operational costs.*
- *CONOPS development—Characterize and model the interdependencies among the various components of the borders security components to support development of tactical and strategic concepts of operation.*
- *Information requirements—Explore potential impacts of new information or more extensive integration of existing information.*
- *Interdependencies among components—Identify and exploit interdependence and intercommunication among the borders security components.*

A key aspect of this project is to establish the feasibility of developing an extensive and comprehensive simulation of border operations, capturing measures of security effectiveness and flow-based economic impacts in a way that can be used to perform meaningful and far-reaching analyses. The methodology and software framework used reflects an SoS approach to characterize and model threat, detection, delay, and response elements. The software framework provides the basis for modeling U.S. POEs, including land crossings, airports, and seaports. This dynamic simulation will support analysis of the effectiveness of technology and the impact on operation due to changes in technology, detection limits, procedures, and policies. Input parameters that reflect threat conditions, facility layouts, and other environments can be

The Customs and Border Protection (CBP) inspector's dilemma: Where is the source?

changed dynamically to evaluate the impact on POE operations.

- *Specification development and analysis—Issued simulation-specific guidelines*. Much of the systems-engineering work performed so far has focused on developing a rigorous set of process and equipment specifications. Specifications developed for this project simulation serve dual roles. First, they are a record of all pertinent information on a topic that was uncovered as a result of open-source research and on-site visits. Second, they provide the information needed to create the appropriate numerical models for the borders simulation. To accomplish these goals and ensure that the specifications are uniform in content and layout, we wrote a set of specification guidelines. We created these guidelines as a collaborative effort between the systems-analysis team and the software-implementation team to ensure that the resulting documents contain the information needed by both parties.
- *Framework—Developed an engine for entity management in arbitrary regions*. We addressed the first technical challenge identified, Entity Management and Communication Infrastructure, through the development of a prototype engine for managing synthesis, movement, and state evolution of large numbers of entities within arbitrary regions. This capability is based on a network-flow paradigm—entities (pedestrians, trucks, cargo, personally owned vehicles [POVs], etc.) that flow through a hierarchical network representation of the border system.

  Each node in the network represents a component of the borders security system—a sensor, a human inspector, a collection of sensors with a defined purpose (super sensor), or a POE. As these entities move from node to node, the entity interacts with the node and is routed, based on that interaction, to the next node in the network. Paths within the network are enforced by routing constraints.

  The engine supports rapid adaptation to new regions and dynamic addition and removal of nodes during simulation, and it inherently supports computation decomposition for parallel execution.
- *High-fidelity pedestrian modeling*. We developed two approaches (high and medium fidelity) to pedestrian modeling through a proof-of-principle stage for pedestrian modeling. The high-fidelity approach uses a commercial tool called DI-Guy™ (developed by Boston Dynamics, Inc.) to simulate human behavior in custom model elements and human motion. The medium-fidelity approach replaces the DI-Guy™ characters

with solid geometric objects and, to the extent possible, uses the human-behavior models from the high-fidelity approach.

For both approaches, general challenges in modeling human motion concerned imposing the logic of the facilities (e.g., waiting in lines and moving through inspection points) upon the people models. People models moved along straight paths between points indicated by the queuing models. It is noteworthy that, in addition to position information, attribute data are associated with (or computationally carried by) the simulated people and can be queried by the various sensor models in computing their responses as the simulated people move through the facility.

For the higher-fidelity model, an ancillary challenge comprised integrating the commercial tool, which was not originally designed to be used for this type of analysis, into the modeling environment in a way that best supported the modeling needs. In addition, we developed initial advanced approaches to provide the simulated people with some freedom of motion between points so that, for example, they would respond appropriately before bumping into one another.

- *Models—Modeled San Ysidro land crossing*. We developed a midfidelity, composite model of the San Ysidro POE in San Diego, California. The San Ysidro land crossing processes pedestrians and POVs and is the busiest land crossing in the U.S. This model includes the following:
  - Representation of the pedestrian flow through the port, including interaction with human inspectors and x-ray scanners.
  - Representation of the POV primary and secondary inspection, including human inspector, license plate, and radiation-detection technologies. We can introduce threat and nuisance sources into the simulation and can perform sensitivity analyses on detector thresholds and throughput delay based on detector alarms.

Other Communications

Horschel, D. S. 2004. Using systems-level modeling and simulation to analyze the U.S. ports of entry. Paper presented at Balancing Security and Mobility: A Symposium on Innovative Approaches to Transportation Security, May, Cambridge, Massachusetts.

Horschel, D. S., and H. R. Ammerlahn. 2004. Homeland security: A systems approach to defending our borders. Paper presented at the White House Office of S&T Policy Briefing, April, Washington, D.C.

Horschel, D. S., and M. J. McDonald. 2004. Homeland security: A systems approach to defending our borders. Paper presented at the American Association of Port Authorities Briefing, February, Washington, D.C.

Horschel, D. S., C. Pura, H. R. Ammerlahn, and R. Macklin. 2004. Homeland security: A systems approach to defending our borders. Paper presented at the Accenture Briefing, April, Reston, Virginia.

Horschel, D. S., C. Pura, H. R. Ammerlahn, and R. Macklin. 2004. Homeland security: A systems approach to defending our borders. Paper presented at the DHS S&T Briefing, April, Washington, D.C.

Horschel, D. S., C. Pura, H. R. Ammerlahn, M. J. McDonald, and R. Macklin. 2004. Homeland security: A systems approach to defending our borders. Paper presented at the Department of Homeland Security S&T Briefing, June, Washington, D.C.

Horschel, D. S., C. Pura, H. R. Ammerlahn, M. J. McDonald, and R. Macklin. 2004. Homeland security: A systems approach to defending our borders. Paper presented at the U.S. Coast Guard Briefing, June, Washington, D.C.

Horschel, D. S., C. Pura, H. R. Ammerlahn, M. J. McDonald, and R. Macklin. 2004. Homeland security: A systems approach to defending our borders. Paper presented at the U.S. Customs and Border Protection, June, Washington, D.C.

Horschel, D. S., M. J. McDonald, and R. Macklin. 2004. Homeland security: A systems approach to defending our borders. Paper presented at the Department of Homeland Security S&T Briefing, February, Washington, D.C.

Horschel, D. S., M. J. McDonald, and R. Macklin. 2004. Homeland security: A systems approach to defending our borders. Paper presented at the U.S.–VISIT Briefing, February, Washington, D.C.

Pura, C., and H. R. Ammerlahn. 2004. Sandia's borders grand challenge LDRD. Paper presented at the DOE/NNSA Annual Program Review, August, Las Vegas, Nevada.

Shyr, L., H. R. Ammerlahn, R. Hillaire, M. J. McDonald, B. Rigdon, C. Pura, and D. S. Horschel. 2004. System modeling of port of entry for security and operational evaluation. Paper presented at the IEEE Boston Chapter Meeting on Homeland Security Technology, April, Boston, Massachusetts.

Materials Science and Technology

The Materials Science and Technology investment area supports Sandia's national security mission by developing novel materials and materials-processing concepts to enhance our ability to steward the nuclear weapon stockpile and to mitigate national security threats. Materials Science and Technology invests in the understanding of aging and reliability phenomena to advance integrated microsystems, and in improving materials and processes for advanced product fabrication based on fundamental understanding, process modeling, and process control.

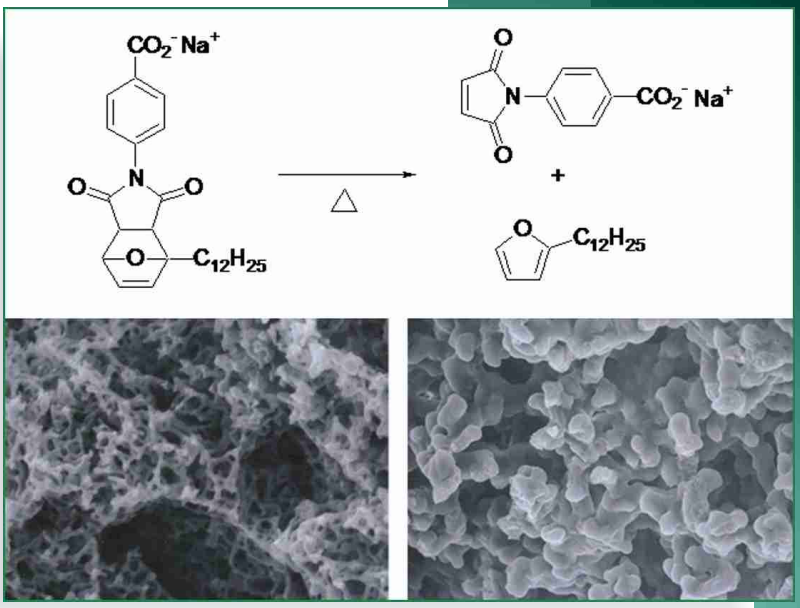

52699 "Thermally Cleavable Surfactants"

Surfactants are molecules that have the ability to self-assemble into a variety of supramolecular structures. These structures, and the nature of the oil-water interface they possess, are used in diverse laboratory and industrial processes, including the synthesis of advanced materials. A major problem with the use of surfactants is removal after use and the recovery of segregated materials. Surfactant removal is specifically important with materials like ceramics, polymers, and inorganic nanocrystals. To solve this problem, researchers developed two novel approaches to surfactant removal that exploit weaklinks in the molecule itself: thermal degradation and metathesis depolymerization. The integration of a cleavable linkage allows for the removal of the surfactant molecules through the formation of hydrophilic and hydrophobic sections. Scientists have been able to incorporate a cleavable linkage into a range of surfactants that function as removable templates. Observations indicate that the surfactants degrade upon initiation of the appropriate trigger and lose their surface-active properties, resulting in successful removal.

38688

The Basics of Aqueous Nanofluidics: "Interphase" Structure and Surface Forces

P. J. Feibelman, K. Leung, D. L. Huber, B. C. Bunker

To understand flow through narrow pores, biomaterial properties, micromachine operation, and other key nanofluidic phenomena, we need to learn how the unexpectedly strong forces, measured as far as tens of nanometers from water-solid interfaces, are mediated by near-surface water structure. Using ab initio *calculations and a suite of incisive experiments, Sandia will identify and characterize icelike, clathratelike, and possibly other arrangements of water molecules in the "interphase" adjacent to ice-nucleating, hydrophobic, and intermediate surfaces. The measurement techniques, including infrared (IR) spectroscopy, interfacial-force microscopy (IFM), and contact-angle studies, will illuminate the relationships among interphase structure and energetics, mechanical properties, and hydration forces. Our theoretical efforts will target an explanation of how templates produced by strong short-range interactions nucleate near-surface ordering of water molecules. For this purpose, we will develop and deploy a computational scheme in which the near-surface transition region is described by a classical water potential, specifically designed to reproduce the* ab initio *phases and properties of bulk water, while an* ab initio *description of the immediate surface vicinity provides a boundary constraint amounting to a template. After initial work in which we develop and validate novel experimental and theoretical methods, we will apply theory and experiment concurrently to a set of representative cases, including a silver iodide (AgI) surface (epitaxy with ice), a clean metal, and a self-assembled-monolayer (SAM)–covered (oily) surface. We will thus learn the microscopic underpinnings of the relationships among hydration-force strength, surface chemistry (e.g., hydrophilicity), and physics (e.g., epitaxial match).*

(1) We discovered that the half-dissociated wetting layer is *not* the low-energy configuration of the first water layer on ruthenium (Ru)(0001). Energy versus concentration of dissociated water molecules shows a minimum at about 40% dissociated, in excellent agreement with new x-ray photoelectron spectroscopy (XPS) measurements (from Lund, Sweden). The Bjerrum defects in the optimal structure should make proton transport facile in the wetting layer.

(2) We computed oxygen (O)(1s) and Ru(3d) core electron binding energy shifts for various wetting structures to help interpret the Lund XPS data.

(3) We analyzed oxygen-deuterium (O-D) stretch-band data from Sum Frequency Generation experiments conducted in Berlin, Germany. Although the data do provide information on the O-O (oxygen-oxygen) distance distribution in a wetting layer, they contain essentially no information on the concentration of dissociated water molecules, despite claims by the experimental study's authors.

(4) We accurately estimated entropy of the wetting layer on Ru(0001), the configurational contribution, using arguments similar to those of Pauling for three-dimensional (3-D) ice; we roughly estimated the vibrational term using a Debye model; and we published estimates of Debye temperature. Results show that the sum is a few meV/molecule, which is not enough to play a major role in determining whether wetting is thermodynamically favored at ~ 150 K, where experiments previously were done.

Using a Debye model and the arguments similar to those of Pauling for 3-D ice, we accurately estimated the entropy of the wetting layer on Ru(0001), the configurational contribution. We published estimates of the Debye temperature.

(5) We determined the binding energy of argon (Ar)/ Ru(0001) to estimate the contribution of Van der Waals forces to wetting by water, whose polarizability is similar to that of Ar. The result was ~ 24 meV, which is about 40 meV smaller than experiment. This is a large percentage error, but is not prohibitive on an absolute scale, if our goal is structural predictions using density-functional theory/general gradient approximation (DFT/GGA). Importantly, water resides much closer to the metal than Ar because of the lone-pair interaction with the metal. There, the Van der Waals error should be smaller because forces are more "chemical," i.e., determined by wave-function overlap and less "dispersive."

(6) We computed the energies and structures that correspond to scanning-tunnel microscopy (STM) images of water on palladium (Pd)(111) taken by researchers at Lawrence Berkeley National Laboratory. Energetics showed little preference for intact water molecules as against edge-dissociated cluster structures. Collaborators (in Madrid, Spain, and Lyon, France), however, used DFT/GGA (meta-) stable structures together with a Green's function code to simulate STM images for the various arrangements. These images made clear that the undissociated structures agree with the experimental images, and the dissociated ones do not. Thus, STM is a valuable tool for analyzing wetting structures that are determined by kinetic barriers and not thermodynamic preference.

(7) We computed the free-energy profile of glycine tautomerization in water (between the zwitterion and a neutral form glycine) using *ab initio* molecular dynamics (AIMD). We found that the reaction pathway proposed in the experimental literature does not describe the reaction-free energy. Another "neutral form" glycine conformation must be involved.

(8) We investigated single-file water conformation in a narrow carbon nanotube (CNT) using AIMD. We found that water evaporates from the tube interior, in contrast to classical force-field predictions, despite comparable treatment of water-NT (nanotube) interaction. The difference is attributed to subtleties in water-water interaction and edge charges on NTs. Currently, we are refining the quantitative treatment of the water-NT interaction.

(9) We used the IFM to probe interactions between functionalized surfaces immersed in water as a function of separation distance. Surfaces investigated included the following:

(a) *Passive SAMs such as polyethylene oxide (PEO)*. IFM results indicated that such surfaces are capable of generating repulsive hydration forces associated with the formation of an ordered water layer having a viscosity 107x greater than that of bulk water.

(b) *Optically switching monolayers*. We used IFM measurements to probe the photoactivated opening and closing of rings in tethered spiropyrans that result in the creation of charged surface sites that control electrical double-layer interactions.

(c) *Thermally switching monolayers*. We used IFM results to characterize the inverse-temperature phase transition in thin films of poly(n-isopropylacrylamide) that result in substantial changes in the hydrophobic-hydrophilic character of a surface and promote reversible adsorption and desorption of proteins.

Refereed

Bunker, B. C., B. I. Kim, J. E. Houston, R. Rosario, A. A. Garcia, M. Hayes, D. Gust, and S. T. Picraux. 2004. Direct observation of photoswitching in tethered spiropyrans using the interfacial force microscope. *Nano Letters* **3**:1723–27.

Cerda, J. I., A. Michaelides, M. L. Bocquet, P. J. Feibelman, T. Mitsui, M. Rose, E. Fomin, and M. Salmeron. 2004. Novel water overlayer growth on Pd(111) characterized with STM and DFT. *Physical Review Letters* **93**:116101.

Feibelman, P. J. 2004. Effect of high-viscosity interphases on drainage between hydrophilic surfaces. *Langmuir* **20** (4): 1239–44.

Feibelman, P. J. 2004. What the stretch frequency spectrum of D_2O/Ru(0001) does and does not mean. *Chemical Physics Letters* **389** (1-3): 92–95.

Feibelman, P. J., and A. Alavi. 2004. Entropy of H_2O wetting layers. *J. Physical Chemistry B* **108** (38): 14362–67.

Leung, K., and S. B. Rempe. 2004. *Ab initio* molecular dynamics study of formate ion hydration. *J. American Chemical Society* **126** (1): 344–51.

Weissenrieder, J., A. Mikkelsen, J. N. Andersen, P. J. Feibelman, and G. Held. 2004. Experimental evidence for a partially dissociated water bilayer on Ru(0001). *Physical Review Letters*, accepted.

Other Communications

Bunker, B. C. 2003. Integrated biomolecular systems: Integration issues. (Invited) Paper presented at the LANSCE 6th User Group Meeting, 19 October, Los Alamos, New Mexico.

Bunker, B. C. 2004. Interfacial issues in bio-integration. (Invited) Paper presented at the Materials Research Society Spring Meeting, 12 April, San Francisco, California.

Cerda, J. I., A. Michaelides, M. L. Bocquet, P. J. Feibelman, and M. Salmeron. 2004. An STM study of water on Pd(ll1): Experiment and theory. Paper presented at the 1st NanoSpain Workshop, 9–12 March, San Sebastian, Spain.

Feibelman, P. J. 2004. Vibration spectra and the structure of water adlayers. (Invited) Paper presented at the 11th International Conference on Vibrations at Surfaces, 6–10 June, Bar Harbor, Maine.

Feibelman, P. J. 2004. What the stretch frequency spectrum of D_2O/Ru(0001) does and does not mean. Paper presented at the March American Physical Society Meeting, 22–26 March, Montreal, Canada.

Feibelman, P. J. 2003. Why water wets precious metals. (Invited) Paper presented at the National AVS Symposium, 2–7 November, Baltimore, Maryland.

Held, G., J. Weissenrieder, A. Mikkelsen, J. N. Andersen, and P. J. Feibelman. 2004. Partial dissociation of water on ruthenium 0001. Paper presented at the International Vacuum Congress, IVC-16, 28 June–2 July, Venice, Italy.

Leung, K., and S. B. Rempe. 2004. *Ab initio* molecular dynamics study of glycine tautomerization in water. Paper presented at the American Chemical Society Spring Meeting, 28 March, Anaheim, California.

Thayer, G. E., A. K. Boal, B. I. Kim, J. E. Houston, and B. C. Bunker. 2004. Measurements of interfacial water properties as a function of surface functionalization using the IFM. Paper presented at the AVS 51st Annual Symposium, 19 November, Baltimore, Maryland.

38689

Design, Synthesis, and Characterization of Soft-Matter Nanolayer Superlattices

A. M. Morales, P. J. Cole, J. R. McElhanon

Recently, birefringent polymer nanolayer superlattices that displayed enhanced reflectivities were reported in the literature. These superlattices consisted of alternating nanolayers of isotropic polymethylmethacrylate (PMMA) and either birefringent polyester or birefringent syndiotactic polystyrene (PS). We determined the reflectivities of the p- *and* s-*polarized light from the superlattices by the indices of refraction of the nanolayers. However, as reported, these superlattices are passive materials. Once fabricated, the optical properties cannot be changed in response to the reflected light or to a trigger signal. Sandia's goal in this project was to modify by organic chemistry the composition of one of the nanolayers to include photochromic molecules that could change the indices of refraction of that set of nanolayers when triggered by an external signal. This change in refractive indices will change the overall reflectivity and the value of the Brewster angle, thus enabling optical switching. We successfully synthesized photoswitchable polymers by appending azobenzene dies to the PMMA nanolayers. The azobenzene functionality undergoes a trans-cis photoisomerization that changes the refractive index of the material. We incorporated the modified PMMA into superlattices prepared by spin-casting and characterized their optical activity. We designed and fabricated a modified coextruder that allows the rapid production of soft-matter superlattices.*

We successfully synthesized photoswitchable polymers by appending azobenzene dies to the PMMA nanolayers. The azobenzene functionality undergoes a trans-cis photoisomerization that changes the refractive index of the material.

We developed the capability to characterize superlattices by combining cross-sectioning techniques usually used for biological specimens and imaging them with an atomic-force microscope (AFM) operating in tapping mode. The biological cross-sectioning techniques allowed us to cross-section the soft organic superlattice without the scratching, smearing, and distorting typically observed when standard metallographic cross-sectioning techniques are used. Imaging with a tapping-mode AFM enabled us to examine the fragile organic superlattice without mechanically destroying the organic layers and without having to subject the sample to the vacuum collapse experienced when using scanning-electron microscopy (SEM). This imaging capability allows us to measure the thickness of individual superlattice layers and relate the layer thickness to the observed optical properties.

We fabricated doped and undoped superlattices by spin-casting alternating layers of PS and PMMA. We fabricated the spun samples from individual films that were spun, floated, and then collected. After we made each layer, we floated and collected the sample on the stack, and then annealed the stack to adhere the layers together. This allowed us to fabricate superlattices made up of alternating PS and PMMA. We designed and built a nanolayer coextruder, which brings together two or more polymers into a layered structure with continuous layers of controlled thickness. We modified the coextrusion process with the generalized multilayer coextrusion process to meet the requirements of this project, as well as to improve the performance of the process. Commercial and Sandia synthesized polymers can be coextruded into superlattices. We characterized the superlattices optically.

38690

Photocontrol of Nanointeractions in Microsystems

N. S. Bell, G. M. Jamison, T. M. Long, W. J. Thomes, Jr., M. Piech, L. Jiang, S. Lin

The manipulation of physical interactions between structural moieties on the molecular scale is a fundamental hurdle in the realization and operation of nanostructured materials and high-surface-area microsystem architectures relying on such nanointeraction-based phenomena as self-assembly, fluid flow, and interfacial tribology. Conventional nanointeraction control strategies typically involve the tailoring of material structures either during synthesis or through invasive post-synthesis processing with no opportunity for real-time, remote modulation of intermolecular and/or interparticle forces. By contrast, Sandia's research focuses on the reversible phototuning of such interactions through the introduction of photosensitive molecular structures into the material system. This new material strategy provides optical actuation of nanointeractions impacting behavior on both the nano- and macroscales with the potential for impact in directed nanostructure formation, microfluidic rheology, and tribological control.

The work identified organic structures possessing known photophysical effects with a high probability for influencing target interaction processes, e.g., physical entanglement, hydrophobicity/-philicity, local electrostatic charge, or pH changes. Their incorporation into polymeric chemistries will allow their application to inorganic colloids as photoactive surfactants to enable the photoactuated control of interparticle nanointeractions to reduce the defect content of colloidal crystal arrays (artificial opals). Primary demonstration of successful nanointeraction control will be provided by zone refining of assembled colloidal crystals. A successful demonstration will provide proof that colloidal crystal arrays can be used to form complete photonic bandgaps (PBGs) by eliminating defects that currently prevent bandgap development.

Conventional nanointeraction control strategies typically involve the tailoring of material structures....By contrast, Sandia's research focuses on the reversible phototuning of such interactions through the introduction of photosensitive molecular structures into the material system.

We conducted experiments that focus on the identification and examination of organic structures possessing known photophysical effects that have a high probability for influencing target interaction processes, e.g., physical entanglement, hydrophobicity/-philicity, local electrostatic charge, or pH changes. Their incorporation into polymeric

chemistries allows their application to inorganic colloids as photoactive surfactants. In our study, we synthesized photoswitchable molecules with chemically binding deposition to silicon (Si)-wafer substrates. We tested the response of the materials using contact-angle measurements and characterization of the surface-energy parameters of the photoswitchable films. We used these parameters to predict changes in wetting behavior for the surfaces against known solvent parameters, and allowed for screening of the effect of these films for additional study. Extension of these fundamental findings can also provide optically tuned microfluidic rheology and tribological control useful in a range of microsystems with an impact on Department of Energy Defense Programs technologies for stockpile safety and security.

This project was successful in the synthesis of colloidal particles functionalized with photoreversible organic moieties to provide photocontrol of the state of particle agglomeration. The functionalized particles developed for this purpose are coated with polymer layers that contain PMMA polymers doped with benzospiropyran molecules. These molecules can be switched from a nonpolar closed form (benzospiropyran) to the open, zwitterionic form (merocyanine) through exposure to ultraviolet (UV) light at 330 nm wavelength. They can be reversibly switched to the closed form by exposure to heat and/or visible light at 540 nm wavelength. The cycles of exposure and return lead to reversible states of aggregation in the system. In nonpolar solvents such as toluene, we observed reversible aggregation/deaggregation.

We studied the aggregation and deposition of the photocontrolled particles on derivatized substrates. We used confocal microscopy with 1 μm particles to determine the affinity of particles in the switched form to undergo agglomeration, and to test the dynamics of switching to restructure the aggregate. The aggregation mechanism remains to be determined, but we did not observe crystallization upon switching.

This project was successful in the synthesis of colloidal particles functionalized with photoreversible organic moieties to provide photocontrol of the state of particle agglomeration.

38691

Electrochemically Deposited Alloys with Tailored Nanostructures for LIGA Micromachines

D. C. Dibble, J. J. Kelly

The performance of LIGA (for the German term Lithographie, Galvanoformung, und Abformung, *for lithography, electroforming, and molding) micromachines is directly linked to the mechanical, magnetic, and tribological properties of the electrodeposited alloys used in component fabrication. Surface-active compounds are used in the electrodeposition process to control grain nanostructure, composition, and internal stress of the alloy. Additives dramatically alter these properties and can greatly enhance the mechanical strength of the component, or they may contribute to undesirable effects such as fracture embrittlement. Additives for electrodeposition processes are empirically developed. More importantly, there is little, if any, physicochemical understanding of the relationship between additive structure and electrochemical action. Sandia seeks to develop the science base needed for the rational development of alloy-deposition processes in LIGA using additives and other advanced electrodeposition techniques, such as pulsed-current electrodeposition. To such effect, we will develop nanoscale diagnostics that can be performed* in situ *during electrodeposition. We will use these diagnostics to characterize in detail the electrodeposits at the nanometer scale. We will clearly focus the efforts of such an investigation on improving process conditions and facilitate them by a close collaborative effort between fundamental surface science and electrochemical engineering methods.*

Our previous work resulted in a significant amount of image data detailing the surface evolution of nickel (Ni) during electrodeposition with and without additives present in the electroplating solution. The majority of our work centered on extracting quantitative information from these raw data to evaluate the various proposed theories of surface growth relevant to the length and time scales examined. In particular, for several experiments we determined the local growth rate (or velocity) for each location in a volume derived from sequential topographical data at the same surface location during Ni electrodeposition. These local velocities in part depend on the local geometry, such as the local slope, curvature, or relative surface height, and may change with time and over-potential.

Various growth models are proposed in the literature that are differentiated primarily by aspects of surface geometry and velocity emphasized. In many cases, a physical origin for these surface velocities was proposed. The direct measurement of these surface velocities allows us to identify the dominant physical phenomena controlling the formation of electrodeposited microstructure and also gain insight into the mechanism by which additives are able to modify this microstructure.

We found that the local surface curvature, and thus the chemical potential of the surface, is the strongest indicator of future growth velocity. The surface curvature is also the geometry most affected by the grain-refining and stress-reducing additive saccharin. Our measurements indicate that saccharin is a weakly inhibiting additive with preferential bonding to regions of high surface curvature. Saccharin does not appear to impede Ni mobility at low over-potentials, even at relatively high concentration. Simulations of surface growth indicate that surface crystallinity must be included in accurate modeling of surface morphology evolution.

Refereed

Dibble, D. C., A. A. Talin, and J. J. Kelly. 2003. The effect of saccharin on electrodeposited nickel: An *in situ* SPM study. Paper presented at the 204th Meeting of the Electrochemical Society, 16 October, Orlando, Florida.

Dibble, D. C., N. Bartelt, and J. J. Kelly. 2004. *In situ* scanning probe microscopy and the modification of nickel growth with additives. Paper presented at the 2004 Gordon Research Conference on Electrodeposition, 11 August, New London, New Hampshire.

38692

Nanostructured Materials for Directed Transport of Excitation Energy

M. B. Sinclair, J. A. Floro, D. Y. Sasaki

An extremely desirable functionality for nanostructured materials is the ability to efficiently activate or interrogate structures within a nanoscale device using optical energy. However, given the packing densities obtainable with nanofabrication, direct focusing of incident optical energy onto individual nanostructures is impractical. Sandia's research in this project will determine how energy-transfer phenomena can be harnessed to provide this functionality. Energy transfer is the process by which excitation energy resulting from absorption of photons can become delocalized and move from the site where the photon was absorbed. Energy transfer plays a prominent role in the photosynthetic process, where "light-harvesting antennas" efficiently absorb sunlight and deliver the excitation energy to the photosynthetic reaction center. The antennas comprise arrays of absorbing organic chromophores that are coupled via near-field electromagnetic (EM) interactions. The coupling between the chromophores allows the excitation energy to hop from site to site until it becomes trapped at a low-energy site where it is utilized. In this context, energy-transfer networks can loosely be thought of as "lenses" that "focus" optical energy onto a desired site. In addition to initiating chemical, structural, or electrical processes, one can envision energy-transfer networks that are used for efficient interrogation of the state of selected nanostructural units. In this case, absorbed optical energy is delivered to a fluorescent nanostructure whose emission properties depend on the local state or environment. We will fabricate and characterize both organic and metallic nanoarrays for energy transfer. We will fabricate energy-transporting arrays of organic chromophores using Langmuir-Blodgett techniques, crystal growth, and lipid bilayers. We will fabricate metallic nanoparticle arrays for plasmonic energy transport using self-assembly on suitably prepared insulating substrates.

We observed anomalously low optical reflectivities (less than 1%) for structures composed of either ultrathin silicon (Si) or germanium (Ge) films on oxidized Si substrates. The discontinuous semiconductor films are only a few tens of nanometers thick, yet they reduce the reflectivity of the oxidized Si by 2 orders of magnitude. The wavelengths associated with this strong absorption subtend most of the

visible spectrum, so that the films appear visually to have a deep blue coloration. *In situ* monitoring of reflectivity during the thin-film deposition in combination with *ex situ* microscopy pointed toward a correlation between very low reflectivity with the onset of island percolation. We attempted to increase the film thickness coinciding with the onset of percolation by changing the thin-film deposition temperature. Between room temperature and a few hundred degrees Celsius, we deposited both Si and Ge as amorphous thin films with microstructural length scales that did not vary with the deposition temperature. For the amorphous films with microstructures smaller than optical wavelengths, we successfully modeled the experimentally measured reflectivity spectra using classical multilayer thin-film optics. The effectiveness of the classic optics, which assumes flat continuous films, in capturing the reflectivity behavior indicates that there is not a strong correlation between the microstructure at percolation and the low reflectivity observed. At higher temperatures, both Si and Ge were deposited as polycrystalline films, and we again found the onset of percolation (almost an order of magnitude thicker than the amorphous films) to coincide with the weakest reflectivity. Unsuccessful modeling of films with larger microstructures (e.g., films deposited at higher temperatures) demonstrated that light absorption and scattering by small particles is a more appropriate representation than using thin-film optics. We determined from modeling that the low reflectivity was due to the exceptionally strong absorption of the amorphous semiconductor thin films and to the thickness of the less strongly absorbing polycrystalline films. Our initial hope of using these films for antireflection coatings because of the low reflective will not be pursued because of the strong absorption. However, by depositing the thin films on the oxidized Si substrate, the absorptance of the ultrathin semiconductor films increases by more than 50% compared to a freestanding film, which could be useful for improving the efficiency of thin-film photovoltaics.

38693

Modeling Local Chemistry in the Presence of Collective Phenomena

N. A. Modine, M. E. Chandross

Confinement within the nanoscale pores of a Zeolite strongly modifies the behavior of small molecules. Typical of many such interesting and important problems, realistic modeling of this phenomenon requires simultaneously capturing the detailed behavior of chemical bonds and the possibility of collective dynamics occurring in a complex unit cell (672 atoms in the case of Zeolite-4A). Classical simulations alone cannot reliably model the breaking and formation of chemical bonds, while quantum methods alone are incapable of treating the extended length and time scales characteristic of complex dynamics. Sandia developed a robust and efficient model in which a small region treated with the Kohn-Sham density-functional theory (DFT) is embedded within a larger system represented with classical potentials. We applied this model in concert with first-principles electronic-structure calculations and classical molecular dynamics (MD) and Monte Carlo (MC) simulations to study the behavior of water, ammonia, the hydroxide ion, and the ammonium ion in Zeolite-4A. Understanding this behavior is important to the predictive modeling of the aging of Zeolite-based desiccants. In particular, we studied the absorption of these molecules, interactions between water and the ammonium ion, and reactions between the hydroxide ion and the Zeolite cage. We showed that interactions with the extended Zeolite cage strongly modify these local chemical phenomena, and thereby proved our hypothesis that capturing both local chemistry and collective phenomena is essential to realistic modeling of this system. Based on our results, we identified two possible mechanisms for the aging of Zeolite-based desiccants.

We developed an algorithm for localizing the electronic structure of oxide materials (such as Zeolites) that is both more efficient on Sandia's parallel computers and significantly easier to use.

We accomplished all of our project milestones with the exception of the implementation of a moving quantum mechanical region that would track phenomena of specific interest. This proved to be problematical due to discontinuities in the energy of the system that arise when atoms are added to or removed from the quantum mechanical region. We continued to investigate possible approaches to overcoming this issue. Otherwise, we were successful on both the software development and materials science fronts.

We developed an algorithm for localizing the electronic structure of oxide materials (such as Zeolites) that is both more

efficient on Sandia's parallel computers and significantly easier to use. Another important part of refining the algorithms and their implementation was the systematic reduction of memory usage. This proved to be critical to the simulation of large systems such as the full Zeolite-4A unit cell. We identified and eliminated two particularly severe memory hot-spots. We refined and simplified the integration of the SOCORRO electronic-structure code with the large-scale atomistic/molecular massively parallel simulator (LAMMPS) classical MD code. We obtained purely quantum mechanical results for the absorption of water for a hierarchy of models containing up to a full unit cell of Zeolite-4A. We used the comparison of these results with the results of our mixed quantum/classical model to refine the quantum/classical coupling and the classical potentials used in the model. These results also clearly demonstrated that neither reduced model cells treated with quantum mechanical methods nor a purely classical approach is adequate to accurately model this system.

On the materials science front, we identified and investigated two possible mechanisms for the reduced capacity of Zeolite-based desiccants after aging in the presence of water and ammonia. In the first proposed mechanism, ammonium ions substitute for the sodium ions located in the eight oxygen rings of the Zeolite structure. The large ammonium ions then block the diffusion of water through these rings. Calculations showed that the presence of an ammonium ion does indeed increase the energy of a water molecule as it moves through the window. In the second proposed mechanism, hydroxide ions created by the reaction of water and ammonia catalytically hydrolyze bonds in the Zeolite framework, leading to degradation of the Zeolite. We explored a mechanism for this process.

Other Communications

Modine, N. A., M. E. Chandross, and E. Jaramillo. 2003. Multiscale modeling of absorption in zeolite-4A. Paper presented at the Materials Research Society Meeting, 1 December, Boston, Massachusetts.

39017

Solution-Based Nanoengineering of Materials

J. A. Voigt, E. D. Spoerke, B. C. Bunker, J. Liu, L. J. Criscenti, Z. R. Tian, R. T. Cygan

Solution-based synthesis is a powerful approach for creating nanostructured materials. Although there have been significant recent successes in its application to fabricating nanomaterials, the general principles that control solution synthesis are not well understood. The purpose of this project is to develop the scientific principles required to design and build unique nanostructures in crystalline oxides, II/VI semiconductors, and other materials using solution-based molecular self-assembly techniques. The ability to synthesize these materials in a range of different nano-architectures (from controlled morphology nanocrystals to surface-templated three-dimensional [3-D] structures) will provide new opportunities for the development of interactive interfaces for optics, electronics, and sensors. Sandia continued to use the homogeneous precipitation of zinc oxide (ZnO) in aqueous solution as the model system for most of the work. We emphasized (1) improving and extending molecular simulations of organic cation and anion adsorption on ZnO surfaces, and (2) applying "bio-inspired" growth modifiers to the development of processing strategies to produce controlled multimaterial nanostructures. The modeling work provided a realistic picture of ligand adsorption on the various ZnO growth surfaces and gave insights into the control of morphology. For the multimaterial synthesis work, we explored the use of engineered synthetic peptides to regulate the synthesis of cadmium sulfide (CdS) semiconductor nanocrystals and their integration into ZnO-based heterostructures.

(1) *Molecular simulations*. We used the adsorption of ethylene diamine and citrate onto different zincite surfaces using classical molecular dynamics (MD) simulations to test our ability to computationally predict the experimental results of ZnO growth studies. First, we prepared molecular models of the (001), (001-bar), and (100) zincite surfaces and the two adsorbates, which are protonated according to known or predicted pKs for aqueous conditions at 25°C and pH 7. To better design our surfaces, we used a revised multisite complexation **(**MUSIC) model with the bond lengths in the ZnO crystal structure. Then, we used 3-D MD simulations to examine the energetics and geometries of both aqueous and adsorbed citrate and ethylene diamine. We examined adsorption

onto the (001-bar) surface, although ZnO crystal growth is assumed to occur in the (001) direction. The most intriguing result from the present molecular modeling study is our success in matching the experimental result that citrate binds much more strongly to the (001) zincite surface than to either the (001-bar) or (100) surfaces. The experiments demonstrate a strong growth inhibition on the (001) surface leading to a more platy ZnO morphology.

The most intriguing result from the present molecular modeling study is our success in matching the experimental result that citrate binds much more strongly to the (001) zincite surface than to either the (001-bar) or (100) surfaces.

(2) *Growth studies*. We applied the versatility of peptide chemistry to create a series of multifunctional molecules whose structures are based on a "tree" model. The branches of the tree consist of a dendritic arrangement of amino acids such as cysteine, histidine, or lysine that interact strongly with metal ions such as Cd or Z, primary constituents of semiconductors such as CdS and ZnO. The trunk and roots of the tree model comprise more structurally functional amino acids such as strongly charged aspartic acid or the bioderived dihydroxyphenylalanine (DOPA) commonly found in adhesive proteins of aquatic creatures like mussels.

Our studies show that a peptide whose branches are made from cysteine and whose roots comprise aspartic acid makes an excellent capping agent for the aqueous synthesis of blue-emitting fluorescent CdS nanocrystals. Interestingly, substitution of histidine for cysteine into that same molecule produces yellow-emitting fluorescent CdS nanocrystals. We believe these differences are due to the differences in the capping ability of the peptide, and demonstrate one form of applicable control that these versatile peptide compounds may exert over the synthesis of semiconductors and their properties.

The same molecular tree motif was useful in creating ZnO, CdS heterostructures. We showed the bioderived DOPA molecule to have a particular adhesive affinity for ZnO. We also showed that films of peptides with DOPA roots and cysteine branches may be adhered to hexagonal ZnO rods grown off of glass surfaces. The high cysteine density in this adherent film has a strong affinity for Cd and was shown to direct the growth of CdS nanocrystals on ZnO crystals. In other cases, the use of lysine in the branched element of this molecular design, coupled with the use of DOPA in the roots of the molecule, allowed us to create highly amine-functionalized ZnO surfaces. This approach allows us to consider functionalization of ZnO surfaces in much the same way that aminosilanes were applied to silica-based surfaces and that aminothiols were used to aminate gold surfaces. This amine functionalization provides a valuable chemical handle on semiconducting ZnO surfaces, which already shows promise in sensor applications and

multicomponent materials assembly using biological microtubules.

Refereed

Liu, J., G. Cao, Z. R. Tian, H. Shang, and J. A. Voigt. 2004. Solution-based synthesis of oriented one-dimensional nanomaterials. *Advanced Materials*, submitted.

Spoerke, E. D., J. C. Voigt, and B. B. McKenzie. 2004. Engineered peptides for directed nanomaterial synthesis. Paper presented at the Materials Research Society Fall Meeting, 29 November–3 December, Boston, Massachusetts.

Tian, Z. R., J. A. Voigt, J. Liu, B. McKenzie, M. J. McDermott, M. A. Rodriguez, H. Konishi, and H. F. Xu. 2004. Complex and oriented ZnO nanostructures. *Nature Materials* **2** (12): 821–26.

Tian, Z. R., J. Liu, J. A. Voigt, H. Xu, H. F. Zhao, and B. McKenzie. 2003. Oriented titania-based nanotubes: Synthesis and application. Paper presented at the Materials Research Society Fall Meeting, 1–5 December, Boston, Massachusetts.

Voigt, J. A., and J. Liu. 2004. Growth of large arrays of oriented nanostructured films. Paper presented at the American Physical Society March Meeting, 24–26 March, Montreal, Canada

Other Communications

Criscenti, L. J., R. T. Cygan, and J. A.Voigt. 2003. Molecular modeling of the adsorption of anionic and molecular species to zincite surfaces. Paper presented at the Fundamentals of Molecular Modeling and Simulation Meeting, 6–11 July, Keystone, Colorado.

Voigt, J. A., Z. R. Tian, L. J. Criscenti, J. Liu, R. T. Cygan, T. J. Boyle, P. G. Clem, M. J. McDermott, and D. L. Moore. 2003. Nanoengineering of extended ZnO film structures. Paper presented at the Materials Research Society Fall Meeting, 1–5 December, Boston, Massachusetts.

Voigt, J. A., Z. R. Tian, L. J. Criscenti, R. T. Cygan, J. Xu, and J. Liu. 2004. Chemical synthesis: New bottom-up approach for 3-D nanostructures. Paper presented at the Materials Research Society Spring Meeting, 12–16 April, San Francisco, California.

52531

Assembly and Actuation of Nanomaterials Using Active Biomolecules

G. D. Bachand, R. P. Manginell, M. P. De Boer, S. J. Hearne, B. C. Bunker, C. M. Matzke

The formation and function of living materials are fundamentally different from those of synthetic materials and devices. While synthetic materials tend to have static structures and are not capable of adapting to changing environmental conditions, living systems utilize energy to create, heal, reconfigure, and dismantle materials in a dynamic, nonequilibrium fashion. Sandia's goal in this project is to organize and reconfigure functional assemblies of nanoparticles using strategies that mimic those found in living systems. Our first strategy, active assembly of nanostructures, involves the application of principles similar to those used by diatomaceous algae in assembling their silica shells to assemble nanowires and interconnects via manipulation of gold (Au) nanoparticles. We used microfluidic channels and self-assembled monolayers (SAMs) to demonstrate guided kinesin-based transport of microtubules (MTs) in microfluidic platforms. In addition, we built a surface plasmon resonance instrument to evaluate the interaction between kinesin and various SAM chemistries. We also demonstrated and characterized transfer of particles by MTs being transported by kinesin. Our second strategy, responsive reconfiguration of nanostructures, involves the use of kinesin and MTs to mediate the optical properties of nanocrystal quantum dots (nQDs) by modulating the spacing among particles, thus mimicking the strategy used by fish to change the color of their skin. We developed several methods for synthesizing, functionalizing, and linking nQDs in conjunction with Los Alamos National Laboratory (LANL). We demonstrated the ability to induce fluorescence resonance energy-transfer (FRET) events using nQDs, fluorescent dyes, and Au nanoparticles organized on MT scaffolds. Lastly, we designed, fabricated, and calibrated microcantilever-based microelectromechanical systems (MEMS) devices for measuring the forces associated with MT polymerization. Overall, we developed several key enabling technologies. Experiments planned for upcoming work are aimed at demonstrating the ability to create and reconfigure synthetic nanostructures using biomimetic processes that direct energy consumption to single molecules.

Video showing microsphere transport.

We demonstrated the ability to induce fluorescence resonance energy-transfer (FRET) events using nQDs, fluorescent dyes, and Au nanoparticles organized on MT [microtubules] scaffolds.

Our work focused on the following five areas:

(1) Incorporating nQDs, kinesin, and MTs into fluidics platforms,

(2) Demonstrating and characterizing particle transport using optical methods and MEMS devices,

(3) Investigating the formation of single nanowires or arrays of parallel nanowires with metal nanoparticles,

(4) Characterizing the optical properties and conductivity of metal nanowires, and

(5) Studying the aggregation/dispersion of nQDs in solutions containing motor proteins and MTs.

Overall, we made excellent progress.

We developed microfluidic platforms for guiding the transport of MTs and nanoparticles. The platforms consisted of microfluidic channels with silicon oxide (SiO) floors and Au sidewalls. We functionalized sidewalls with thiol-based SAMs with a range of functional groups. Of the different functional groups tested, only polyethylene oxide–based SAMs resisted kinesin absorption and efficiently guided MT transport. In several cases, SAMs successfully guided MT transport, but did not resist kinesin adsorption. To further investigate such interactions, a surface-enhanced plasmon resonance system was developed at LANL for measuring kinetic rates of protein adsorption to SAMs. System characterization demonstrated the ability to measure time-resolved adsorption of a submonolayer of protein. This system currently is being used to characterize kinesin adsorption to the SAMs and to correlate adsorption with MT guiding.

To characterize nanoparticle transport by MTs, we evaluated the behavior of MT-tethered cargo when interacting with other MTs with homologous functionality. Fluorescent, streptavidin-coated microspheres were bound to biotinylated MTs. We then evaluated the ability to transfer an attached microsphere from one MT to another MT during kinesin transport. We observed six distinct events in these experiments: (1) no microsphere transfer, (2) microsphere transfer, (3) MT breaking, (4) forcible release of the microsphere, (5) bending of MT with no transfer, and (6) MT aggregation. The degree of biotinylation and temperature significantly affected the rate of microsphere transfer.

LANL evaluated three alternate methods for linking nQDs to MTs: (1) surface exchange of TOP/TOPO (tri-octylphosphine/tri-octylphosphine oxide)–coated nQDs with thiol-containing molecules, (2) polymer amphiphiles to form an outer shell with exposed carboxylic acid groups, and (3) amphiphilic phospholipid block co-polymers for encapsulating

nQDs in a micelle complex. The quantum yields of the nQDs prepared by these methods ranged from 5% to 57%, with the highest yield for micelle-encapsulated nQDs. We evaluated covalent cross-linking of these functionalized nQDs to MTs. Initially, we used fluorescently tagged proteins with comparable sizes to nQDs to develop cross-linking methodologies and demonstrated kinesin-based transport. More recently, we pursued the ability to covalently link nQDs to MTs.

We performed optical characterization of nQD-coated MTs in conjunction with LANL. We assembled three types of composites at Sandia: (1) MTs functionalized with nQDs, (2) MTs co-functionalized with rhodamine dye and nQDs, and (3) MTs co-functionalized with nQDs and Au nanoparticles. Analyses performed at LANL demonstrated that the transfer rate between nQDs (donor) and TRITC (tetramethyl rhodamine isothyocyanate) (acceptor) was ~ 0.5 ns, with FRET efficiency ~ 16%. We observed rapid, strong quenching for MTs co-functionalized with both nQDs and Au nanoparticles. Overall, these experiments demonstrated the ability to achieve FRET using nQDs, fluorescence dyes, and Au nanoparticles organized on MT scaffolds.

We fabricated microcantilever beams for measuring the mechanical forces produced during MT polymerization using the SUMMiT V^{TM} (Sandia Ultraplanar Multilevel MEMS [microelectromechanical systems] Technology V) process. We calibrated the Moiré gauge attached to the sensor using a stepper motor and found it to have an accuracy of measurement of ± 1 nm, and a force resolution of ± 1 pN. We subsequently will measure the polymerization forces of MTs with these microcantilever devices.

Refereed

Bachand, G. D., S. B. Rivera, A. K. Boal, J. Gaudioso, J. Liu, and B. C. Bunker. 2004. Assembly and transport of nanocrystal CdSe quantum-dot nanocomposites using microtubules and kinesin motor proteins. *Nano Letters* **4** (5): 817–21.

Bachand, G. D., S. B. Rivera, A. K. Boal, J. M. Bauer, S. J. Koch, R. P. Manginell, J. Liu, and B. C. Bunker. 2003. Developing nanoscale materials using biomimetic assembly processes. *Proc. Materials Research Society Symposium* **782** (Fall, Boston, Massachusetts): A1.1.1–A1.1.8.

Bauer, J. M., A. K. Boal, S. B. Rivera, R. G. Manley, G. D. Bachand, J. Liu, R. P. Manginell, and B. C. Bunker. 2004. Nanoscale transport and assembly with motor proteins and microtubules. Paper presented at Hilton Head, 6–10 June, Hilton Head Island, South Carolina.

Boal, A. K., S. B. Rivera, G. D. Bachand, and B. C. Bunker. 2004. Stability of chemically covalent cross-linked microtubules. Paper presented at the Materials Research Society Spring Meeting, 12–16 April, San Francisco, California.

Boal, A. K., S. B. Rivera, G. D. Bachand, B. C. Bunker, J. M. Bauer, and R. P. Manginell. 2004. Engineered microchannels for active nanomaterials assembly. Paper presented at the Materials Research Society Spring Meeting, 12–16 April, San Francisco, California.

Boal, A. K., S. B. Rivera, G. D. Bachand, B. C. Bunker, J. M. Bauer, and R. P. Manginell. 2004. Monolayer engineered microchannels for motor protein transport platforms. Paper presented at the American Chemical Society Spring Meeting, 28 March–1 April, Anaheim, California.

Bunker, B. C., G. D. Bachand, A. K. Boal, S. B. Rivera, J. M. Bauer, R. P. Manginell, and D. L. Huber. 2004. Interfacial issues in bio-integration. Paper presented at the Materials Research Society Spring Meeting, 12–16 April, San Francisco, California.

Bunker, B. C., G. D. Bachand, A. K. Boal, S. B. Rivera, T. Headley, J. Gaudioso, R. P. Manginell, and J. M. Bauer. 2003. Nanoparticle transport using microtubules and motor proteins. Paper presented at the American Vacuum Society 50th International Symposium, 2–7 November, Baltimore, Maryland.

Edwards, J. M., S. B. Rivera, A. K. Boal, N. Miller, B. C. Bunker, and G. D. Bachand. 2004. Exploring microtubule stabilization using chemical cross-linking and thermostable tubulin. Paper presented at the American Chemical Society Spring Meeting, 28 March–1 April, Anaheim, California.

Koch, S. J., S. B. Rivera, A. K. Boal, J. M. Edwards, J. M. Bauer, R. P. Manginell, J. Liu, B. C. Bunker, and G. D. Bachand. 2004. Active and dynamic nanomaterials based on active biomolecules. Paper presented at the American Physical Society Meeting, 22–26 March, Montreal, Quebec, Canada.

Liu, J., G. D. Bachand, B. C. Bunker, A. K. Boal, and S. B. Rivera. 2003. Active assembly of dynamic and adaptive materials based on motor proteins and microtubules. Paper presented at the World Congress on Medical Physics and Biomedical Engineering, 23–30 August, Sydney, Australia.

Rivera, S. B., J. M. Bauer, S. J. Koch, J. M. Edwards, and G. D. Bachand. 2004. Kinesin from *Thermomyces lanuginosus* displays novel kinetic properties and fast velocities at high temperature. Paper presented at the 48th Annual Meeting of the Biophysical Society, 14–18 February, Baltimore, Maryland.

52698

Decomposition of Contaminants Using Photochemically Active Nanoparticles

K. F. McCarty, D. H. Morse, T. Zifer, R. A. Kemp, T. J. Boyle, D. R. Jennison, B. A. Simmons

The decomposition of hazardous biological (viruses and bacteria) and nonbiological (nerve agents, hydrogen sulfide [H_2S], hydrocyanic acid [HCN]) compounds can be realized using a new class of photochemically active nanoparticles that have been fine-tuned for decontamination applications. Several metal oxides (titanium dioxide [TiO_2], zinc oxide [ZnO], iron oxide [Fe_2O_3], tungsten trioxide [WO_3]) demonstrate the ability to destroy contaminants upon exposure to ultraviolet (UV) light; however, to make them of practical use, improvements in their activity is necessary. These materials work by photoactivating water and oxygen to create highly reactive species (e.g., OH•) that readily decompose the compounds described above. Sandia's approach is to develop highly photoactive, doped nanomaterials using novel synthetic routes. In this project, we will link materials-synthesis studies to understanding the underlying physical mechanisms of these reactions through the use of in situ *microscopy and spectroscopy. We will couple these efforts to first-principles calculations examining the advantages of likely dopants, followed by a study of reaction processes and statistical mechanical modeling of the reaction dynamics after a material/dopant is selected. In this manner, we will unravel the complex interrelationship between nanostructure, composition, and photochemical activity. Directed by this understanding, we will use sol-gel and surfactant-based supramolecular self-assembly techniques to engineer optimized nanostructures with specified compositions. We will verify the photochemical activity of these improved materials by testing. The ultimate outcome of this work will be the development of a new class of highly active materials for wide-ranging decontamination applications.*

The ultimate outcome of this work will be the development of a new class of highly active materials for wide-ranging decontamination applications.

We developed new methods to synthesize doped TiO_2. We researched two approaches—coating TiO_2 nanoparticles with metals (a "core-shell"), and coating particles with TiO_2 (a "shell-core"). Using the former approach, we successfully deposited fine lanthanide metal particles on TiO_2 nanoparticles. We synthesized a TiO_2 shell on silver (Ag) nanoparticles using the latter approach. Most importantly, photocatalytic testing established that the lanthanide-doped materials exhibited activity with visible light. While synthesizing metal lanthanide

nanoparticles proved to be difficult, we did successfully implement a procedure to make nanoparticles of lanthanide oxides.

We also substantially improved our capability to test materials for the photocatalytic activity. We completed the assembly and testing of a powerful test reactor. The computer-controlled system enables the simultaneous evaluation of eight materials under exquisitely controlled and characterized conditions. We can test activity in both the UV and visible light regimes. Our second major achievement was developing the ability to test the biocidal action of the photocatalysts to kill cells. We developed a procedure to quantify the biocidal activity of photocatalysts to deactivate *Escherichia coli* (*E. coli)* cells. Initial tests established that TiO_2 nanoparticles readily kill *E. coli* cells.

Our materials development was aided by efforts to understand the underlying physical mechanisms using first-principles electronic-structure calculations and *in situ* microscopy. We continued to study how nitrogen doping causes TiO_2 to adsorb light in the visible region. Based on our calculations, we submitted a detailed picture for publication. Finally, we successfully imaged the process of photocatalysis occurring on a surface. We used low-energy electron microscopy (LEEM) to image the adsorption and photocatalytic oxidation of trimethlyacetic acid (TMA) on the TiO_2(110) surface. Both the adsorption and decomposition of the TMA, which caused large contrast changes, occurred uniformly across the surface. Atomic steps on the substrate appeared to play no special role.

We completed the assembly and testing of a powerful test reactor. The computer-controlled system enables the simultaneous evaluation of eight materials under exquisitely controlled and characterized conditions.

Refereed

Jennison, D. R. 2004. Density-functional study of N-doped TiO_2. *Physical Review B*, submitted.

McCarty, K. F., and N. C. Bartelt. 2004. Crystal growth rate limited by step length—The case of oxygen-deficient TiO_2 exposed to oxygen. *J. Crystal Growth* **270**: 691.

52699

Thermally Cleavable Surfactants

B. A. Simmons, T. Zifer, K. Rahimian, G. M. Jamison, J. R. McElhanon, L. A. Domeier

Surfactants are molecules that have the ability to self-assemble into a variety of supramolecular structures. These structures, and the intrinsic amphiphilic nature of the oil-water interface they possess, have been used in numerous laboratory and industrial processes, including the synthesis of advanced materials. A major problem associated with the use of surfactants is their subsequent removal after use and the recovery of segregated materials. Sandia successfully developed two novel approaches to surfactant removal using thermally degradable surfactants and metathesis depolymerization that contain weaklinks that are internal to the molecule itself. The thermal degradation is based on a reversible Diels-Alder reaction, which has already found utility at Sandia in the preparation of removable encapsulants, foams, adhesives, and dendrimers. The metathesis depolymerization degradation is based on a catalyzed alkane ring-forming reaction of the surfactant that is widely used in polymer science.

Surfactant removal becomes very significant in the realm of extended mesoporous nanosized structures, such as ceramics, polymers, inorganic nanocrystals, and polymer-ceramic composites. The present technique of material recovery is typically a combination of centrifugation, calcination, and solvent washing that destroys the desired architecture and functionality of the synthesized material. We believe that the incorporation of a cleavable linkage would solve this problem by allowing for the removal of the surfactant molecules through the formation of a hydrophilic and hydrophobic section. In this project, we successfully synthesized a wide range of cleavable surfactants that will function as removable templates. We determined that all of the surfactants synthesized behave as traditional amphiphiles, and we characterized their static and dynamic properties. Observations indicate that the surfactants degrade upon initiation of the appropriate trigger and lose their surface-active properties. We utilized these surfactants in proof-of-concept experiments that involve emulsion polymerizations using these labile assemblies as scaffolding agents.

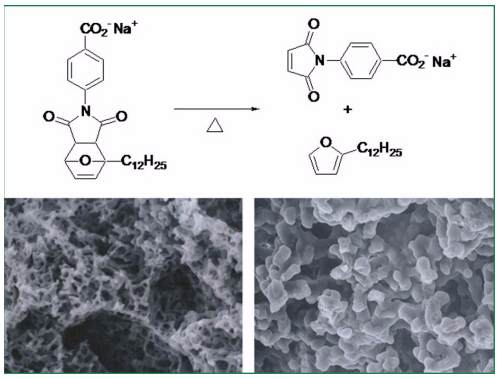

Sandia researchers are developing a novel class of surfactants based on the Diels-Alder reaction that undergo degradation at elevated temperatures. The top image is a molecular schematic of such a surfactant, the process by which it degrades, and the resulting fragments. The lower images are electron micrographs of polymer monoliths synthesized with these new surfactants.

Sandia successfully developed two novel approaches to surfactant removal using thermally degradable surfactants and metathesis depolymerization that contain weaklinks that are internal to the molecule itself.

Our activities included two independent synthetic routes for the incorporation of a cleavable linker to be incorporated within a surfactant molecule. We used these two synthetic routes to

prepare and analyze both monomeric and dimeric (Gemini) cleavable surfactants. These cleavable linkers are based on Diels-Alder thermally degradable linkages and Grubbs catalyzed ring-forming depolymerization.

The Diels-Alder surfactant linkage consists of a diene and dienophile adduct situated between the hydrophilic and hydrophobic moieties of the surfactant. We synthesized five Diels-Alder–based surfactants consisting of four monomeric variants and one Gemini surfactant. We determined structural characterization for all surfactants by ^{1}H nuclear magnetic resonance (NMR). These surfactants form aqueous micellar aggregates above a critical micelle concentration, as indicated by dye micellization, dye solubilization, and surface-tension measurements. We completed the initial characterization of dynamic and static surfactant behavior and determined the micelle shape and size through small-angle neutron scattering. When exposed to elevated temperatures, typically in the range of 80°C–95°C, the surfactants lose their surface-active properties and disassociate into oil and water-soluble components. We used these surfactants in the emulsion polymerization of porous materials as proof-of-concept experiments.

We also synthesized and characterized two surfactants that can undergo a variation of metathesis depolymerization. These surfactants possess a cleavable element that is susceptible to a catalyst that essentially transforms the hydrophobic tail section of the surfactant molecule into alkane rings. We fully characterized the micellar solutions formed by these surfactants and their susceptibility to catalytic degradation. After we added a small amount of the catalyst to a surfactant solution, NMR results indicated the formation of alkane rings and a decrease in surfactant molecule concentration. We verified this degradation through surface-tension and small-angle neutron-scattering experiments.

Refereed

Simmons, B. A., J. R. McElhanon, T. Zifer, G. M. Jamison, K. Rahimian, T. M. Long, D. Wheeler, D. A. Loy, and S. R. Kline. 2004. Thermally cleavable surfactants based on furan-maleimide Diels-Alder adducts. (Invited) Paper presented at Los Alamos National Laboratory, Los Alamos, New Mexico.

Other Communications

Simmons, B. A., J. R. McElhanon, T. Zifer, D. A. Loy, G. M. Jamison, T. M. Long, K. Rahimian, D. R. Wheeler, and W. R. Even. 2004. Thermally cleavable surfactants based on furan-maleimide Diels-Alder adducts. Paper presented at the 227th ACS National Meeting, 28 March–1 April, Anaheim, California.

52700

Transition-Metal Catalyzation of Complex-Hydride Absorption/Desorption Reactions

E. H. Majzoub, S. Spangler, K. J. Gross, D. R. Tallant

Sandia focused this investigation on the enhanced hydrogen (H) sorption kinetics present in titanium (Ti)-doped sodium aluminum hydride ($NaAlH_4$). Competing models developed for the rate-limiting step of H sorption include surface enhancement of H dissociation due to the presence and dispersion of Ti on aluminum (Al) surfaces, and possible bulk effects such as lowering of nucleation barriers and interfacial free energies, allowing phase transitions to occur more rapidly between the decomposition products of $NaAlH_4$.

Previous studies determined that substitution of Ti on lattice sites of Na and Al in bulk $NaAlH_4$ is unlikely due to total energy considerations and x-ray diffraction (XRD) data from single crystals of $NaAlH_4$ exposed to Ti during growth. This does not rule out the possibility of defect-induced stability for Ti substitution. Previous first-principles work also showed that defect structures involving Ti can be stable, such as Ti on an Al site, with an H vacancy.

A combination of experiments will determine which, and possibly if both, mechanisms are responsible for the enhanced kinetics. We will use H sorption experiments using well-known catalysts such as H dissociators to determine the dissociation efficiency of Ti dopants, yielding information on surface kinetics models. In addition, Raman spectroscopy of both single crystals and doped and undoped powders of $NaAlH_4$ will directly probe the Al-H bond strength and Al coordination in these materials. This will give direct information on defect structures that may be present in doped alanates. This work will also be useful for other compounds where Al-H coordination is needed.

We will determine which of the kinetics enhancement models offers the greatest increase in sorption kinetics, and whether it is possible to carry over these enhancements to related hydrides.

Diffraction data from single crystals grown as both pure and "Ti-exposed" samples show that there is no incorporation of Ti in bulk $NaAlH_4$ during slow crystal growth. This answers one of the main questions regarding the action of Ti in the enhanced kinetics of this material. The negative results of this experiment are in full agreement with first-principles calculations of total energies of structures with Ti substituted on Na or Al sites in

$NaAlH_4$. The energy penalty required for Ti substitution without other defect structures is of the order of 1.5 eV or greater. This indicates that the Ti is either in other stable compounds or perhaps on the surface of the decomposition products and the mechanism may not be bulk substitution.

We performed a full-polarization Raman-spectra analysis and observed all Raman active modes; they appear to be in agreement with first-principles calculations. This work will guide future experiments on doped materials to help distinguish between known and unknown modes that appear in the Raman spectra of powders.

We used nuclear magnetic resonance (NMR) experiments in conjunction with XRD to determine stable Ti compounds forming in doped alanates prepared by solution and solution-free techniques, as well as mechanically milled and unmilled materials. We conclusively demonstrated the differences between compounds formed in mechanical milling ($TiAl_3$) and solution-mixed samples prepared in tetrahydrofuran (THF), where Ti-Al colloids are the probable reaction products. NMR spectra indicate that Al-O coordination in solution-mixed samples of THF could correspond to nanoparticle formation of Ti-Al colloids. XRD of these materials indicates an extremely fine particle size or amorphous structure in solution-doped samples (in THF), consistent with the NMR and literature data.

First-principles calculations are investigating phase stability of stable Ti-compounds, which we will test through future sorption experiments.

Refereed

Herberg, J., R. Maxwell, and E. H. Majzoub. 2003. Investigation of Ti-doped $NaAlH_4$ by solid-state NMR. *Proc. Materials Research Society, Materials and Technology for Hydrogen Economy* **801** (November, Boston, Massachusetts): 147–52.

Majzoub, E. H., R. Stumpf, S. Spangler, J. Herber, and R. Maxwell. 2003. Compound formation in Ti-doped sodium aluminum hydrides. *Proc. Materials Research Society, Materials and Technology for Hydrogen Economy* **801** (November, Boston, Massachusetts): 153–58.

Ozolins, V., E. H. Majzoub, and T. J. Udovic. 2004. Electronic structure and Rietveld refinement parameters of Ti-doped sodium alanates. *J. Alloys and Compounds* **375** (1) (July): 1–10.

52701

Quantification of Environments and Surfaces Within Micropackages

S. M. Thornberg, M. S. Kent, D. E. Peebles, R. A. Plass, M. R. Keenan, K. R. Zavadil, D. R. Tallant

Maintaining the integrity of the internal atmosphere of a hermetic device is essential for long-term component reliability because it is within this environment that all internal materials age. As the size of microelectromechanical systems (MEMS) packages decreases with miniaturization, characterization of the internal surfaces and gases becomes increasingly difficult. This project seeks to develop the tools necessary for these characterizations.

Sandia conducted directed aging experiments on FOTAS (perfluorooctyltris(dimethylamino)silane) films on silicon (Si). To study local displacement of the self-assembled monolayer (SAM) due to degradation, we developed a multianalytical technique investigation of the adsorption of FOTAS on Si. We also developed methods for mapping SAM coatings on MEMS devices using photoluminescence (PL) from fluorescent taggants. Initial tagging experiments successfully showed coverage differences. Finally, we developed techniques for gas-sampling MEMS devices that have internal volumes of 30 nl and for performing multiple residual gas analyses (RGA) from the same gas sample. We gas-sampled and analyzed several 30 nl MEMS packages.

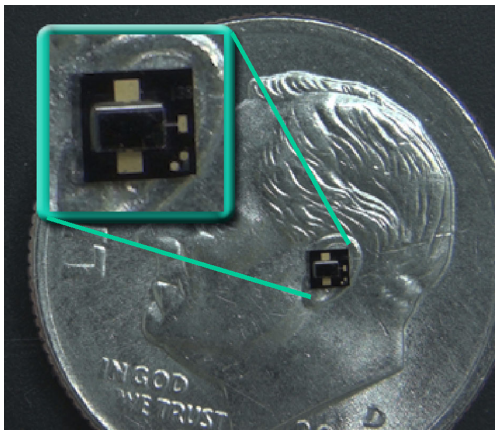

The 30 nl internal-volume MEMS device.

- *Directed aging experiments*. We conducted directed aging experiments on FOTAS films on Si. We induced specific aging-relevant chemical changes in the SAM. In one experiment, an electric field drove water into the SAM, simulating loss of package hermeticity. Results demonstrated that directed aging experiments can be conducted that yield useful chemical information concerning reliability and aging mechanisms in MEMS materials.
- *Chemical signatures and multivariate spectral analysis*. We developed a multianalytical technique investigation of the adsorption of FOTAS on Si to study local displacement of the SAM due to degradation. The results of our measurements show the contact angle and three separated time-of-flight secondary ion mass spectrometry (TOF-SIMS) spectral components plotted as a function of exposure time of clean Si to FOTAS under Sandia's standard SAM deposition conditions. The data show that the surface energy (contact angle) is strongly correlated to two distinct chemical signatures: the

fluorinated pendant chain of the FOTAS molecule and the higher-order FOTAS fragments. Clearly, FOTAS fragmentation is coverage-dependent, and ion yields depend significantly on which molecular species are bound to the surface near the FOTAS molecules.

- *SAM mapping using fluorescent taggants*. We developed methods for mapping SAM coatings on MEMS devices using PL from fluorescent taggants. Taggants are bound either directly or through an intermediary ((3-glycidoxypropyl)-trimethoxysilane, or GPS) to a Si surface. The intermediary occupies surface areas not covered by the SAM coating and bonds to the fluorescent taggants. GPS does not exhibit detectable PL; however, we observed PL from the taggant.
- *Nanoliter MEMS package gas sampling*. Gas sampling of MEMS provides a clear indication of the hermeticity of the device as well as the atmosphere within which the internal components age. Typical transistor metal cans (e.g., TO-5 type) and large MEMS devices have an internal volume of tenths of a milliliter or more. We previously developed and demonstrated gas-sampling methods for smaller-sized MEMS packages having internal volumes as low as 3 ml. Recently, we developed techniques that allow us to gas-sample MEMS devices having internal volumes 2 orders of magnitude lower, 30 nl, and to develop a method for performing multiple RGA from the same gas sample. We gas-sampled and analyzed several 30 ml MEMS packages. The method of breaking the package in the specially designed manifold and introducing the gas into the RGA via a pulsed valve gives solid analytical signals. The raw data are presented with no filtering or averaging, which shows a signal-to-noise ratio (SNR) of approximately 10. We can adjust several parameters (e.g., pulse duration, RGA gain, vacuum throttle valve) to increase the SNR even more.

We made excellent progress in surface analyses and gas sampling and analysis. We anticipate great insight into MEMS state-of-health through the information generated from these techniques.

We made excellent progress in surface analyses and gas sampling and analysis. We anticipate great insight into MEMS [microelectromechanical] state-of-health through the information generated from these techniques.

Refereed

Knorovsky, G. A., M. R. Keenan, K. R. Zavadil, D. O. MacCallum, J. A. Ohlhausen, R. A. Plass, B. M. Nowak-Neely, I. C. Abraham, D. E. Peebles, and S. M. Thornberg. 2003. Unified characterization of surfaces and gases in MEMS devices. *Proc. IMAPS 5th Topical Technology Workshop on MEMS* (November, Boston, Massachusetts).

Other Communications

Ohlhausen, J. A., K. R. Zavadil, D. E. Peebles, and S. M. Thornberg. 2004. Advanced surface characterization of MEMS devices: From release to packaging. *Proc. IMAPS Conference and Exhibition on Ceramic Interconnect Technology* **1** (April, Denver, Colorado).

Ohlhausen, J. A., K. R. Zavadil, D. E. Peebles, and S. M. Thornberg. 2004. Analysis of TOF-SIMS spectral series and spectral image series using AXSIA. Paper presented at the 17th Annual SIMS Workshop, May, Westminster, Colorado.

Zavadil, K. R., J. A. Ohlhausen, D. E. Peebles, and S. M. Thornberg. 2004. Advanced surface characterization of MEMS devices: From release to packaging. Paper presented at the Ceramic Interconnect Technology Conference, 26–28 April, Denver, Colorado.

52702

Assembly of Ordered Electrooptical and Bioactive Materials and Composites

C. J. Brinker, F. B. Van Swol, B. A. Simmons

The discovery of intrinsic metal-like conductivity in conjugated polymers represents a significant milestone in polymer chemistry and materials science, as recognized by the 2000 Nobel Prize Award in Chemistry. This project addresses several key issues related to the performance and utility of conductive polymers. Sandia's objectives are to do the following:

(1) Develop new methods to assemble ordered conducting materials on multiple length scales. We will explore both self-assembly and directed nucleation and growth approaches to produce oriented and aligned polymer nanostructures and microstructures.

(2) Establish fundamental structure-property relationships of nanostructured conjugated polymers. We will investigate films in which conjugated polymers and polymer-nanocrystal composites are confined to ordered structures with one-dimensional (1-D), 2-D, or 3-D connectivity and separated by either insulating or semiconducting walls. Such composites are ideal model systems in which to test and understand the role of nanostructuring in determining charge and energy-transport properties.

(3) Integrate the new materials/structures with microelectronic/microfluidic devices. This strategy holds the promise for inexpensive electronic/optical devices. We will also develop microarrays of such materials for quantitative and high-sensitivity detection of chemical and biological agents. This research will not only contribute to our new strategy thrust in complex functional materials, it will also have a positive impact on the Department of Energy's missions in energy and national security.

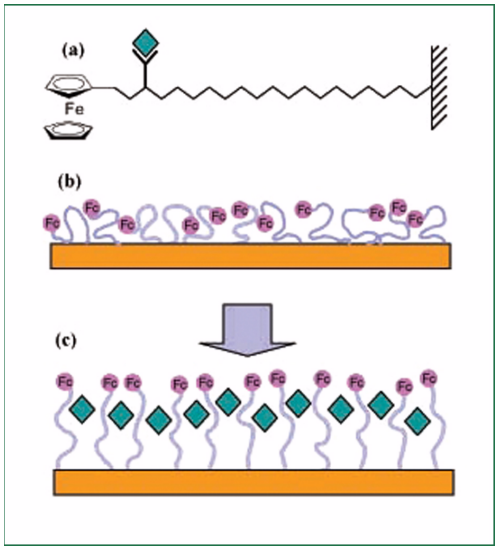

Attomolar and label-free electrochemical detection of biomolecules.

We used water-in-oil microemulsions to synthesize cadmium sulfide (CdS) nanoparticles with controlled particle size and crystal structure. We extended this technique to spin-coating the precursors onto a substrate to better control nucleation and growth. We used uniform nanoparticles to produce self-assembled, ordered nanocrystal arrays that have potential for electronics and energy applications. Initial experiments on a metal-insulator-metal capacitor fabricated with an ordered 3-D gold nanocrystal/silica array as the "insulator" demonstrated collective coulomb blockade behavior

This research will not only contribute to our new strategy thrust in complex functional materials, it will also have a positive impact on the Department of Energy's missions in energy and national security.

below 100 K and established the current-voltage scaling relationship for a well-defined 3-D array of coulomb islands. For the first time, highly ordered cubic polymerizable polyphenylenevinylene (PPV)/silica nanocomposites were fabricated using this surfactant as both the structure-directing agent and the monomer in the evaporation-induced self-assembly (EISA) process. We also developed a new reagentless electrochemically bioaffinity assay. The surface chemistry of the self-assembled monolayers (SAMs) can be tailored to selectively bind chemical or biological agents without labeling. We demonstrated reliable, selective detection of toxic heavy metal (mercury) down to the 5 ppq (10^{-9} ppm) level, 8 orders of magnitude lower than commercial instruments. We further showed that we can perform selective protein detection down to the 0.01 ppq level, pushing toward single-molecule detection with a simple instrument and without any labeling technique. We obtained detailed understanding of the molecular mechanisms that will enable us to expand this technique to a wide range of chemicals and bioagents. The molecular chains switch from a parallel conformation to a perpendicular conformation upon binding, causing a change in the chemical environment around the ferrocene groups. The change causes a shift of formal oxidation potential. The zero-background approach contributed to the extreme high sensitivity of this technique. Finally, we are developing new coarse-grain lattice-modeling techniques and a dissipative particle-dynamics method to calculate the surface energy, morphology, and structure of self-assembled materials.

Refereed

Tian, Z. R., J. A. Voigt, J. Liu, B. McKenzie, and H. Xu. 2003. Large oriented arrays and continuous films of TiO_2-based nanotubes. *J. American Chemical Society* **125**: 12384.

52703

Advanced Packaging/Joining Technology for Microsystems

C. V. Robino, J. R. Michael, G. A. Knorovsky, E. A. Holm

It is generally agreed that current microelectronics packaging technologies are inadequate for potential microsystems applications. Additionally, the capability to join microelectromechanical systems (MEMS) components into complex three-dimensional (3-D) assemblies will be necessary for stockpile applications. Two complementary new technologies have been identified—micron-scale high-energy-density (HED) fusion welding and focused-ion-beam deposition joining (FIBDJ)—that can jointly address these key microsystem needs. At the micron scale, materials properties that dominate joining response differ appreciably from those at macroscopic sizes. This project will identify and quantify the materials properties/process interactions that control microscale joinability in HED welding and FIBDJ.

Sandia is studying microscale HED welding with concurrent experimental and modeling approaches. We are developing techniques for producing the fine-scale beams and are characterizing these power sources spatially, temporally, and in terms of energy transfer. Previous modeling showed that melt ejection may preclude joining at < 100 µm beam diameters, but did not incorporate the effect of surface tension. Model improvements are incorporating this effect and are using molecular dynamics (MD) simulations to provide surface tensions. We are using Surface Evolver (SE) and GOMA simulations to guide experiments and to determine whether recoil pressure can be used to aid coalescence. Expected results are quantitative mechanistic descriptions of microscale fusion welding and definitions of microscale weldability.

We are evaluating FIBDJ as an alternative approach. Experiments include characterization of operating parameters, joint geometry, energy transfer, and development of microstructure and properties. Modeling is aiding the interpretation of microstructural evolution and its relation to FIBDJ processing. We are using the models to derive quantitative mechanistic descriptions of micron- and submicron-size FIBDJ connections and to optimize processing. We expect residual stress and distortion to be a key issue in both processes and will address them in the latter stages of the project.

We used SE to examine the conditions under which coalescence can be expected in microscale-fusion butt welds, and we constructed a processing diagram that describes the stability of liquid ligaments in terms of joint size and liquid volume. Based on these calculations, an analysis of the SUMMiT V™ (Sandia Ultraplanar Multilevel MEMS Technology V) design rules for MEMS device gaps will nearly always require the addition of filler material. These calculations further demonstrate the utility of SE for analyzing coalescence problems and can provide guidance needed for joint design at high-surface-area/-volume ratios.

We produced a variety of fusion joints in LIGA (for the German term *Lithographie, Galvanoformung, und Abformung*, for lithography, electroforming, and molding)–related and other parts. We also added micromanipulation capabilities to the scanning-electron microscope (SEM) that will be useful for experiments in which we plan to add filler material.

We conducted laser-beam and electron-beam (EB) coalescence experiments and are comparing them with model estimates. Techniques for characterizing the energy distribution in the EB via Faraday cup measurements are under way, providing increased knowledge of the heat-source dimensions and distributions and allowing for better modeling of the heat source. We further refined our previously developed melt/drill model for microlaser welds by adding surface tension, and we brought a newly acquired short-pulse laser online to better validate the additional predictions that have been made relative to drilling/welding thresholds.

We experimentally explored operating parameter ranges for FIBDJ and developed procedures for bridging joint gaps as large as 2 μm, although the procedures developed are relatively time-consuming. This difficulty, coupled with the limited availability of the FIB, restricted the production of mechanical test joints envisioned in our original MEMS test-die design; however, we identified alternative (and less time-consuming) procedures using the existing die. Our work demonstrated the significant role of gas dynamics in the FIBDJ process, and we constructed a preliminary kinetic Monte Carlo deposition model. The precursor density (or layer thickness) is distributed over the substrate surface and is limited by a precursor saturation level. The model allows three different options for the distribution of the saturation density: (1) flat, in which the precursor saturation density is constant over the entire surface; (2) distributed, in which the precursor saturation density is user-specified and remains constant during one left-to-right round of the FIB; and (3) Bernoulli, in which the precursor saturation

Our work demonstrated the significant role of gas dynamics in the FIBDJ process, and we constructed a preliminary kinetic Monte Carlo deposition model.

density depends on the shape of the substrate surface in a Bernoulli-like manner, simulating higher densities for deeper surface dips. This model, while still preliminary and qualitative, indicates that the organometallic gas density plays a very important role. Consequently, more detail in tracking gas-density changes will be required in subsequent developments.

We identified alternate deposition species (to reduce nonmetallic content of the deposits) early in the project year; however, we abandoned that approach and are now exploring the utility of deposition at higher substrate temperatures, which required the purchase of a hot-stage facility for the FIB.

Refereed

Knorovsky, G. A., D. O. MacCallum, and V. V. Semak. 2003. On the possibility of microwelding with laser beams. *J. Physics D: Applied Physics* **36** (17) (September): 2170–74.

Other Communications

Knorovsky, G. A., and D. O. MacCallum. 2003. Microwelding with a Nd:YAG Q-switched laser: A progress report. Paper presented at the DOE IMOG Subgroup on Joining Meeting, December, Amarillo, Texas.

Knorovsky, G. A., D. O. MacCallum, and B. M. Nowak-Neely. 2004. Scanning electron beam micro-to-nano welding. Paper presented at the American Welding Society Annual Convention, April, Chicago, Illinois.

52705

Magnetostrictive Elastomers for Actuators and Sensors

D. L. Huber, J. E. Martin, R. A. Anderson

There is a need for soft actuators that have a much larger response than piezoelectrics and that can respond in microseconds. Applications include artificial muscles in robots and stress/strain sensors based on permittivity or permeability changes. Sandia showed theoretically that large magnetostrictive effects can be obtained from composites of magnetic nanoparticles in an elastomer, if the nanoparticles have been preorganized into chainlike agglomerates using magnetic fields. Such magnetostrictive elastomers (MEs) have a magnetic permeability that increases rapidly with compression, and so contract in a magnetic field, provided the particles are spaced by a soft matrix. This effect should be especially large for nanoparticles, where calculations show that the stresses should be comparable to that of human muscle. "Latched" MEs could also be made with particles having large magnetic remanence. A short magnetic pulse magnetizes the particles causing permanent composite contraction without further power consumption until an opposing coercive pulse removes the magnetization, thereby releasing the contraction. One challenge in realizing MEs is preventing contact between magnetic nanoparticles during chaining. The most effective method of precoating the nanoparticles with a thin layer of low-modulus elastomer is through a surface-initiated polymerization, wherein an initiating group covalently linked to the surface is used to grow polymers in situ, *forming a defect-free coating. MEs should have wide application as large strain actuators and as soft sensors for robotic fingertips. We expect strains that are 10x–100x that of piezoelectrics, and stress-response times limited only by the inductance time of the coil.*

MEs [magnetostrictive elastomers] should have wide application as large strain actuators and as soft sensors for robotic fingertips....We made excellent progress in theory, modeling, and experiments designed to understand and evaluate the potential of MEs.

We made excellent progress in theory, modeling, and experiments designed to understand and evaluate the potential of MEs. These composites consist of magnetic particles in an elastomer. The magnetic particles are formed into assemblies by magnetic fields. The structures can be particle chains, particle sheets, or more complex three-dimensional (3-D) particle assemblies, as described in Martin, *et al*., *J. Chem. Phys*. **118**, 1557–70 (2003). In conventional magnetostrictive materials, the strain is due to the effect of spin alignment on atomic interactions within the magnetic material. The strain in MEs is due to the dipolar interactions between particles, and particle

deformations make a negligible contribution to the effect. The degree to which these dipolar interactions can be altered by an applied field is strongly dependent on the structure of the particle assemblies, as described in the isomorphic language of electrostriction in Martin and Anderson, *J. Chem. Phys*. **111** 4273 (1999).

We completed extensive experimental measurements of magnetostriction in a variety of composite materials having a range of particle loadings and structures. We discovered that, contrary to theoretical expectations, the magnetic field can be thought of as increasing the elastic modulus of these materials. We demonstrated a material that exhibits negative magnetostriction. We also showed that these materials can be designed to exhibit magnetoresistance of several orders of magnitude. We found that using complex magnetic-field processing can greatly enhance magnetostriction in these materials, and that some such materials exhibit significantly enhanced mechanical properties. We proposed and investigated theoretical models of field-driven structural instabilities in these composites and developed a method of creating very high susceptibility nanocomposites.

Refereed

Huber, D. L. 2004. Synthesis, properties, and applications of iron nanoparticles. *Angewandte Chemie*, accepted.

Huber, D. L., E. L. Venturini, P. P. Provencio, R. J. Patel, and J. E. Martin. 2004. Synthesis of highly magnetic iron nanoparticles suitable for field structuring using a beta-diketone surfactant. *J. Magnetism and Magnetic Materials* **278** (3): 311–16.

Martin, J. E., E. L. Venturini, and D. L. Huber. 2004. Giant magnetic susceptibility enhancement in field-structured dipolar nanocomposites. *Physical Review B*, accepted.

Other Communications

Huber, D. L., J. E. Martin, E. L. Venturini, and P. P. Provencio. 2004. Synthesis and properties of highly magnetic nanoparticles and their composites. (Invited) Paper presented at Particles 2004, March, Orlando, Florida.

52739

Experimental and Computational Study of Liquid-Solid Transition in Tin

J. Davis, S. M. Foiles

The behavior of materials under dynamic high-pressure conditions is directly relevant to stockpile stewardship and is of scientific interest. In particular, there is a programmatic need for improved understanding of dynamic solidification behavior under high pressures. The purpose of this project is to study the solidification transition in tin (Sn) under isentropic compression. A decrease in funding reduced the scope of the project and delayed completion of some milestones.

Sandia developed a new empirical potential and began large-scale molecular dynamics (MD) simulations of solidification in Sn using this potential. Work is ongoing to characterize solidification kinetics under a variety of conditions. We continued preliminary analyses of previous experiments on ramp-wave compression of liquid Sn and continue to work on improving the experiment design. Upcoming work will investigate the equation-of-state (EOS) for Sn and attempt to develop a continuum-level model for kinetics of the solidification process that incorporates results from MD simulations.

The goal of this work is to develop future capability and expertise in a novel area of MD characterization that is of high interest to stockpile stewardship, beyond the scope of existing programmatic work; the latter focuses on obtaining experimental data rather than on understanding those data. The results will also improve the fundamental understanding of solidification processes, aiding both the prediction of material behavior under dynamic loading and the modeling of more-traditional processes such as welding and soldering.

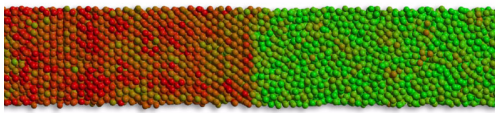

Initial atom configuration for MD (molecular dynamics) simulation of liquid-solid interface (red is solid, green is liquid).

We developed an entirely new empirical interatomic potential for Sn that fits the *ab initio* results obtained recently and is thus suitable for simulating the thermodynamics of both the liquid phase and high-pressure solid phase, as well as the kinetics of the interface between the two phases. Efforts to develop such a potential with existing central force approaches such as the embedded atom method (EAM) could not describe both the BCT (body-centered tetragonal [a solid state]) and liquid phases. Thus, we needed to develop a new form for the interatomic interactions. We computed the static structure factor of molten Sn using the new interatomic potential. We can then

compare this to the results obtained earlier, based on *ab initio* calculations as a test of the quality of the potentials.

MD simulations of liquid-solid interfaces using the new potential are in progress. These simulations determine kinetic coefficients for the solidification process as a function of temperature, pressure, and crystal orientation. The predicted solid-liquid coexistence line can also be obtained. These indicate lower solidification pressure than experiment, but correctly reproduce the experimental pressure derivative of the melt curve. Work is ongoing to characterize the kinetic coefficients for a variety of conditions.

We executed two experiments on the Z Accelerator to study isentropic compression of molten Sn. Due to technical experimental issues, however, neither produced much usable data. We completed further preliminary analyses of velocity profile measurements from earlier experiments, and these show additional evidence of a slow solidification transition without reliance on any particular model for the EOS of Sn.

We used the backward integration and minimization technique in the new analysis. We used two time-resolved velocity measurements, one from a sapphire/sapphire interface representative of the Lagrangian coordinate at the front of the liquid Sn sample, and the other from the Sn/sapphire interface at the back of the liquid sample, to initialize backward-integration calculations of the longitudinal stress history at the front surface of the first sapphire layer (at its interface with the aluminum drive panel). We then iterated the second calculation to find values for parameters of the Sn isentrope that minimize the difference between computed stress histories over a given range in stress.

The tin isentrope was represented by Lagrangian sound speed as a quartic function of pressure, with an initial guess for the parameters obtained by a fit to the existing model for liquid Sn. We looked at the results for three different samples at different temperatures. One sample was thicker than the other two, and it resulted in a significantly different isentrope (outside the error bounds due to uncertainty in sample thickness) above 10 GPa. This indicated violation of the centered-wave assumption required for backward integration, which would occur for time-dependent behavior such as a nonequilibrium solidification transformation. Ongoing work will compare various existing EOSs against results from the *ab initio* MD simulations.

58907

Active Photonic Nanostructures

M. B. Sinclair, J. G. Fleming, P. G. Clem, S. Y. Lin, J. C. Barbour, T. J. Boyle, G. S. Subramania, N. S. Bell

Photonic crystals (PhCs) are periodically modulated dielectric structures that alter the flow of electromagnetic (EM) energy in many profound and potentially useful ways. Photonic bandgaps (PBGs), transmission resonances, restricted or enhanced densities of state, and modified spontaneous emission rates are all features of photonic lattices (PLs). In general, the PhCs demonstrated to date are entirely passive components; there are no means to alter, turn on, turn off, or modulate the unique photonic properties of these structures. The goal of the research in this project is to integrate these passive Phc structures with active materials to provide "active" functions such as optical amplification, lasing, light switching and steering, optical logic, chemical sensing, etc. In addition to greatly expanding the functionality of PhCs, incorporation of active materials will offer new opportunities for investigating the novel physics arising from the strong modification of the photonic density of states and photonic band structures as they impact electron-photon interactions. Sandia is exploring a number of approaches to the "activation" of PhCs, including fabricating the PhCs from active materials such as light-emitting materials, nonlinear optical materials, piezoelectric, or electromechanical materials. Fabrication efforts include both top-down lithographic approaches and bottom-up self-assembly methods. Another approach involves doping of PhC structures such as high-quality (Q) resonators with optically active materials such as quantum dots (QDs) or rare-earth ions. Another approach involves integrating the PhCs with active layers of light-emitting, piezoelectric, or electromechanical materials. In addition, we are investigating energy-transfer processes for use as a means to couple energy into and out of PhCs. This project is a collaboration between Sandia and Los Alamos National Laboratory and draws upon the demonstrated strengths of these institutions in PhC structures, colloidal QDs, energy transfer in composite nanomaterials, nanomechanics, and self-assembly.

Our efforts to develop active photonic nanostructures were successful in a number of important areas. Each of the accomplishments listed here provides us with another tool to use toward our ultimate goal of integrating active optical materials with photonic nanostructures to enable a new class of

optical devices. We demonstrated that we can tune the spectral positions of photonic microcavity resonances in a controlled and repeatable fashion. We established both coarse-tuning and fine-tuning methodologies. Such resonance tuning is essential for proper integration with active materials and to ensure that these photonic devices operate at desired wavelengths. In addition, we demonstrated that the light extraction from a light-emitting diode (LED) can be significantly enhanced by fabrication of PL arrays directly on a LED. This achievement has the potential to significantly impact future solid-state lighting programs. We demonstrated optical pumping of nanocrystalline QDs using an energy-transfer scheme in which a semiconductor quantum well (QW) is optically pumped with subsequent nonradiative energy transfer to a nearby monolayer of QDs. Extension of this technique to electrically injected QWs would enable electrical pumping of nanocrystalline QDs and potentially lead to wide-ranging technological applications. We developed the ability to fabricate high-quality colloidal crystals. The optical properties (i.e., width and amplitude) of the stop-bands of these crystals rival the best found in the literature. We also developed the process flow for fabricating fluorescent Yablonovite crystals using a combination of e-beam lithography and energetic neutral atomic-beam etching. In addition, we developed a new materials-patterning technique, solution stamping nanolithography (SSNL), and used a similar soft lithography to pattern substrates at 200 nm linewidths for assembly of magnetic nanoparticles. We demonstrated epitaxial materials stamping with yttrium-barium-copper oxide (YBCO), a high-temperature superconductor. We achieved large-area line patterns and micron-size patterns.

...we demonstrated that the light extraction from a light-emitting diode (LED) can be significantly enhanced by fabrication of PL arrays directly on a LED. This achievement has the potential to significantly impact future solid-state lighting programs.

Refereed

Achermann, M., M. A. Petruska, S. Kos, D. L. Smith, D. D. Koleske, and V. I. Klimov. 2004. Energy-transfer pumping of semiconductor nanocrystals using an epitaxial quantum well. *Nature* **429** (6992) (10 June): 642–46.

Subramania, G. S., S. Y. Lin, J. R. Wendt, and J. M. Rivera. 2003. Tuning the microcavity resonant wavelength in a two-dimensional photonic crystal by modifying the cavity geometry. *Applied Physics Letters* **83** (22) (1 December): 4491–93.

Other Communications

Subramania, G. S., S. Y. Lin, J. R. Wendt, and J. M. Rivera. 2003. Tuning microcavity resonant wavelength in a 2-D photonic crystal by modifying cavity geometry. Paper presented at the Materials Research Society Meeting, December, Boston, Massachusetts.

67074

Electrochemically Switchable Materials for (Bio)Microfluidics

K. R. Zavadil, M. Farrow, G. E. Thayer, M. Okandan, B. C. Bunker

Homeland security needs require the development of a new generation of microfluidic devices that can concentrate, separate, and sense a variety of viral, bacterial, and toxic agents. The key enablers are functional materials that are capable of being programmed to perform a wide variety of operations on complex biological samples and that are compatible with nanoscale architectures. This project addresses electrochemical means of controlling the transport of relevant species using binding or complex formation between host molecules and analyte guest molecules. Sandia demonstrated the synthesis of several stable host molecules based on beta-cyclodextrin (B-CD) that form complexes with metallocence molecules like ferrocene. Many biomolecules can be modified to incorporate a ferrocene ligand and, as a result, be transformed into a suitable guest molecule. We showed the stable binding of modified B-CD molecules to gold (Au) electrodes. We demonstrated electrochemically controlled complex formation between these host molecules and derivatives of ferrocence in aqueous electrolytes. A combination of electrochemical techniques and atomic-force microscopy (AFM) shows that binding functionality can be maintained and monitored in aqueous electrolytes over a practical range of potentials for sensing. These accomplishments represent the first step in meeting the longer-term project goals of developing electrochemically switchable surface functionality for microfluidic sensing applications. These project goals are aligned with the development of multifunction biosensing devices by providing a class of materials and assembling technologies suitable for device integration and use.

We synthesized thiolated B-CD for multidentate covalent bonding to Au surfaces. We successfully synthesized two variants of this host molecule: one analog that has five to seven of its primary hydroxyl groups replaced with sulfhydryl groups, and the second analog for which all seven primary hydroxyl groups are replaced with flexible alkylsulfide chains. The sulfide groups extending from the base of the CD ring provide a set of strong covalent bonds between the molecule and an Au electrode surface. The benefit to using the flexible alkylsulfide chains is a potentially more efficient packing of host molecules on the electrode surface produced by conformational changes in

the bound molecule. We conducted nuclear magnetic resonance (NMR) characterization of this alkylsulfide analog at key steps in the synthesis to ensure by-product purity.

We demonstrated attachment of these host molecules to Au electrode surfaces. We used infrared (IR) reflection absorption spectroscopy to confirm that characteristic vibrational modes specific to each analog were present for coated electrodes. We also determined the presence of these molecules using electrochemical techniques. We also used cyclic voltammetry to evaluate the extent of B-CD coverage at the surface. This experiment involves probing the anodic current generated during the oxidation of two iron-containing probe anions: (1) ferrocene carboxylate, which is electroactive at both Au and B-CD-coated Au surfaces, and (2) ferrocyanide, which is active only at the Au surface. Ferrocyanide provides a measure of the degree to which the host molecule blocks access to the surface and, therefore, to the host coverage. The ferrocene confirms that the molecule responsible for blocking access to the underlying Au is the B-CD host. We used this electrochemical technique to aid in optimizing solvents and deposition times to ensure host molecule activity and stability. We find that using water:dimethyl formamide mixtures with deposition times of 2–4 hr produces optimized binding of ferrocene derivatives with the thiolated analog of B-CD. We investigated ethanol:chloroform solvent mixtures at elevated temperatures for deposition of the alkylsulfide analog of B-CD.

We demonstrated the binding of ferrocene derivatives to the B-CD host molecule on electrode surfaces using electrochemical techniques coupled with AFM. We developed a technique where equilibration of the surface complex can be observed and measured by controlled electrolyte transfers and anodic stripping of the guest from the host site. The resulting quantity of charge shows that nearly saturation coverages of the guest-host complex are possible on Au. AFM measurements show that alkylsulfided host molecules do not deposit epitaxially onto the oriented Au(111) electrode surfaces used, but rather deposit in clusters. Evidence does exist from AFM measurements for epitaxial domain formation for the thiolated analog. The existence of ordered domains creates an opportunity to image the lateral dimension of the host-guest complex formation process under electrochemical control. We find correct height dimensions off the Au surface, indicating that single molecular layers have covalently bonded. Electrochemical AFM measurements show that the host molecule films are stable over the potential range necessary for controlling complex formation.

These accomplishments demonstrate that this project is steadily progressing toward developing electrochemically switchable surface functionality that can be implemented into microfluidic-based sensors for various missions of the Department of Energy and the Department of Homeland Security. This project is developing the scientific knowledge and capabilities necessary to design functional engineered surfaces and to define their viability at the micro- and nanoscale device levels.

67075

Modeling of Friction-Induced Deformation and Microstructure

S. V. Prasad, C. C. Battaile, R. E. Jones, J. R. Michael, D. J. Bammann, N. R. Moody, J. J. Kelly, E. B. Marin

The objective of this project is to model friction-induced microstructure in ductile materials and validate results with experimental measurements. Sandia designed and built a rotary stage module for the linear friction tester to facilitate friction measurements on single-crystal surfaces in specific crystallographic directions. We procured nickel (Ni) single crystals and established optimum conditions for electropolishing their surfaces without introducing any surface damage. For the first time, we are able to make friction tracks on (100) single-crystal surface in <100> and <110> crystallographic directions with utmost precision, as evidenced by electron backscatter diffraction (EBSD) imaging. We used focused-ion-beam (FIB) microscopy to prepare cross sections parallel to the friction tracks and EBSD analysis to understand the friction-induced microstructure and deformation. We observed the development of fine-grained equiaxed recrystallized substructure right below the friction surface in both <100> and <110> directions. The plastically deformed zone underneath the recrystallized structure extended much deeper for the <110> wear direction than for <100>. Preliminary nanoindentation tests on Ni and diamondlike carbon (DLC)–coated Ni showed that the DLC film elastic modulus was significantly less than that for Ni, but hardness was substantially higher. More importantly, the coefficient of friction measured in a single-pass nanoscratch test was much less for the DLC–coated sample than for the Ni, indicating a substantial benefit may be gained by using hard coatings.

For the first time, we are able to make friction tracks on (100) single-crystal surface in <100> and <110> crystallographic directions with utmost precision....

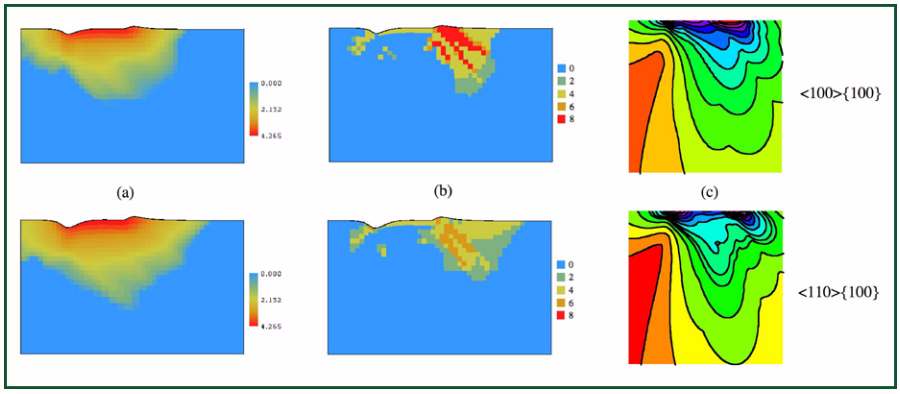

Finite-element analysis of (a) *the plastic strain (on a log scale),* (b) *number of active slip systems underneath a 1/8 in.-diameter sliding Si_3N_4 cylinder, and* (c) *numerical elastic analysis of the maximum resolved shear stress underneath unit normal and 0.8 frictional point loads.*

We initiated the development of a modified Hertzian contact analysis for sliding plastic contact. We conducted nonlocal crystal plasticity simulations to derive a preliminary statistical volume element formulation, which was implemented into Sandia's PRESTO and ADAGIO analysis codes. We will integrate the effects of recrystallization explicitly into this formulation. Preliminary phenomenological modeling of the characteristics of the recrystallized microstructure, based on results from theory and simulation, demonstrate qualitative agreement with empirical data.

We established optimum conditions for electropolishing Ni surfaces to avoid subsurface damage induced by mechanical polishing. We expanded our friction characterization capabilities by designing and fabricating a new module that enabled friction measurements in specific crystallographic directions on single-crystal surfaces with an accuracy of ± 0.5°. We made friction tracks on null single-crystal surface in <100> and <110> crystallographic directions, and on null surface in <211> direction at a normal load of 100 mN with a silicon nitride (Si_3N_4) ball in unidirectional linear mode. We specifically chose these three crystallographic combinations to gain a fundamental understanding of the role of interacting slip systems on subsurface deformation. To minimize the environmental effects on friction, we conducted the 1000-cycle friction experiments in dry nitrogen atmosphere. We used FIB microscopy to prepare cross sections parallel to the friction tracks and performed EBSD to map out friction-induced microstructure and deformation. We observed significant differences in both the extent of subsurface deformation and the friction forces of the three crystallographic combinations. This can be understood by analyzing the friction orientations this way: heavy subsurface damage leads to rapid and extensive recrystallization, which in turn could explain the observed decrease in friction coefficient (0.8–0.3).

We used nanoindentation and nanoscratch techniques to evaluate the strength, friction, and adhesion of Ni sulfamate on silicon (Si), with and without a DLC coating, at small loads characteristic of microsystem operation. The DLC–coated films exhibited lower elastic modulus, higher hardness, and lower friction coefficient. We performed numerical elastic stress analyses using friction conditions relevant to the experiments, and local finite-element simulations using an Asaro latent hardening model, to predict the relative responses of Ni to <100> null and <110> null wear. Both approaches qualitatively reproduce the "lobes" in the subsurface deformation state, and

the higher damage underneath the <110> track on the null surface seen in the experiments, further supporting the hypothesis that slip-system interaction could be responsible for the observed differences in subsurface damage between the different wear track orientations. We developed a nonlocal crystal plasticity model to simulate the formation of misoriented dislocation cells beneath the sliding contact surface. It will be used to develop an evolution equation for a local variable representing this phenomenon.

Refereed

Michael, J. R., and S. V. Prasad. 2004. FIB preparation of samples for EBSD: Applications to wear studies of MEMS materials. Paper presented at Microscopy and Microanalysis 2004, August, Savannah, Georgia

67076

Reversible Antibody Trapping for Selective Sensor Devices

D. L. Huber, B. C. Bunker, J. E. Houston, G. D. Bachand, R. P. Manginell, S. M. Brozik

For homeland security, Sandia needs to develop compact sensors that can selectively detect low concentrations of a wide range of potential biological agents. The most sensitive and selective materials for binding and detecting bioagents are antibodies. Many sensor technologies rely on tethered antibodies for interacting with biospecies. Unfortunately, each antibody is selective to only one antigen. As antibody-antigen complexes form, active sites are consumed, limiting use to one analysis cycle. This project involves studying concepts for producing antibody monolayers that can be regenerated and reused. The baseline concept involves using Sandia's "reversible protein trap" to adsorb and release highly selective antibody monolayers. The protein trap consists of a microhotplate onto which a thermally activated polymer (PNIPAM [poly n-isopropylacrylamide]) film is tethered. The hotplate is used to switch PNIPAM between a room-temperature phase that repels proteins and a higher-temperature phase that adsorbs proteins (in this case, antibodies). The scientific component of the proposed work will involve using surface-sensitive Fourier-transform infrared (FTIR), interfacial-force microscopy (IFM), and neutron-scattering measurements to determine (1) the extent and kinetics of antibody adsorption on activated PNIPAM versus solution conditions (e.g., competition with other proteins), (2) surface concentrations and orientations of the antibodies, (3) antibody-antigen interactions versus monolayer structure, and (4) the extent and kinetics of release of antibody-antigen complexes from deactivated PNIPAM films, allowing the surface to be refreshed with the same or a different antibody. The technical component of the work will involve integrating the reversible protein trap into Sandia's highly mass-sensitive shear horizontal surface acoustic-wave (SAW) sensors to make a compact device in which selective capture, sensing, and release functions are all performed in the same location. This investigation of concepts for using switchable, "nonselective" surfaces to adsorb monolayers of highly selective agents will impact a wide range of evolving on-chip separation and sensor systems.

The viability of the previously developed protein trap as a highly selective adsorbing layer for biosensors depends on the

ability of the protein trap to capture an antibody film. The antibody film then needs to remain active, enabling it to capture antigens of interest such as specific bacteria or virus particles. We demonstrated the feasibility of the overall project concept by performing adsorption experiments with tobacco mosaic virus (TMV) and two antibodies (nonspecific Rabbit immunoglobulin G [IgG] and TMV-specific TMV-IgG). We monitored component adsorption using ellipsometry. The IgG adsorption experiments demonstrate that the active polymer film in the protein trap (PNIPAM) can be thermally programmed to reversibly adsorb and release antibodies. The TMV adsorption experiments show that the TMV-IgG remains active when attached to its PNIPAM host. While we observe slight TMV adsorption on bare PNIPAM, we see no adsorption when the PNIPAM is covered with rabbit IgG. We do observe extensive TMV adsorption when the TMV-IgG is present. Surprisingly, it appears that adsorption of the TMV to TMV-IgG interferes with the ability of TMV-IgG to be released by the PNIPAM. This is presumably because the TMV is bound by multiple antibodies, forming a complex that interacts more strongly with PNIPAM than individual antibodies.

We performed neutron-reflectivity measurements at the Los Alamos Neutron Science Center (LANSCE) neutron-scattering facilities at Los Alamos Laboratory using a special temperature- and fluids-controlled sample cell that we designed and built for compatibility with the LANSCE beam line. Preliminary results were encouraging, in that we could observe the PNIPAM phase transition and antibody adsorption. However, surface-roughness effects (since corrected) created sufficient interference with the neutrons to prevent us from obtaining data of sufficient quality to monitor antibody orientations that control TMV binding.

67077

Correlated and Comprehensive Analytical Techniques for Homeland Defense

P. G. Kotula, L. N. Brewer, J. A. Ohlhausen, T. T. Borek, III, D. R. Tallant, B. L. Doyle, M. R. Keenan, A. J. Antolak, S. M. Sickafoose, J. A. Timlin

Sandia's multipart project seeks to select and obtain a weaponized/nonweaponized simulant of anthrax and to analyze the same specific region of simulant material with multiple analytical techniques. In parallel, we will characterize the range of analytical techniques with simple test specimens and with multivariate statistical analysis (MSA) tools that we will develop to augment our Automated eXpert Spectral Image Analysis (AXSIA) software. Additionally, and most importantly, we will develop and test new algorithms for multiple correlated analyses. The outcome will be a comprehensive and correlated analytical protocol as well as tools for performing analysis of bio- or other agents.

We can group the analytical techniques included into three categories: bulk methods (gas/liquid chromatography with mass spectrometry and laser-induced breakdown spectroscopy); surface methods (x-ray photoelectron spectroscopy [XPS], auger electron spectroscopy, and time-of-flight secondary ion mass spectrometry [TOF-SIMS]); and microanalytical methods (electron, x-ray, and particle-excited x-ray microanalysis, infrared [IR], Raman and visible spectroscopy).

The analytical data-analysis method, which is based on MSA, will build on the previously developed AXSIA software to read new data types, perform calculations optimized for new analytical techniques, and perform correlated analyses.

Successful analysis of a 4 Gb tomographic spectral image. This represents the first step in correlated data analysis.

We made significant progress. We analyzed data from new analytical techniques, developed and implemented new MSA techniques, and developed a new test sample.

We acquired and analyzed spectral image and series data from several analytical techniques: particle-induced x-ray (PIXE) emission, x-ray fluorescence (XRF), XPS, electron energy-loss spectrometry (EELS), gas chromatography with mass spectrometry (GCMS), and visible spectroscopy (with hyperspectral scanner). The samples analyzed were simple and native to the analysts and their techniques and facilitated more rapid progress.

We developed, tested (on several of the techniques above), and implemented new algorithms. The original MSA approach

The outcome will be a comprehensive and correlated analytical protocol as well as tools for performing analysis of bio- or other agents.

provided a spectrally simple view of large and complex spectra series and images. This is not, however, always a good way to look at data where there are comparable signal levels in all of the channels. To solve this problem, we developed a new approach based on maximizing spatial simplicity. We applied this approach to the techniques above. Additionally, we made progress in adding equality constraints to the multivariate curve resolution (MCR) algorithms. In this case, known spectral shapes can be set as a constraint for a calculation. In addition to the new algorithms, we made progress in migrating our software and algorithms from a stand-alone application into a complete analysis and visualization program in the MATLAB environment.

We developed a new test specimen that contains gamma-irradiated *Bacillus thuringiensis* (nonviable) spores mixed with inorganic particulates. We analyzed this specimen with both x-ray microanalysis and TOF-SIMS.

Refereed

Keenan, M. R., and P. G. Kotula. 2004. Multivariate statistical analysis of EEL-spectral images. *Microscopy and Microanalysis* **20** (2) (Augusts, Savannah, Georgia): 874–75.

Kotula, P. G., M. R. Keenan, and J. R. Michael. 2004. Tomographic spectral imaging with a dual-beam FIB/SEM: 3-D microanalysis. *Microscopy and Microanalysis* **10** (Suppl. 2) (August, Savannah, Georgia): 1132.

Kotula, P. G., M. R. Keenan, R. P. Grant, and P. F. Hlava. 2004. Multivariate statistical analysis of wavelength and energy-dispersive x-ray spectral images. *Microscopy and Microanalysis* **10** (August, Savannah, Georgia): 118–19.

Oliver, J. M., J. R. Pfeiffer, Z. Surviladze, S. L. Steinberg, K. Leiderman, M. L. Sanders, C. Wofsy, J. Zhang, H. Fan, N. Andrews, A. Bunge, T. J. Boyle, P. G. Kotula, and B. S. Wilson. 2004. Membrane receptor mapping: The membrane topography of Fc(epsilon)RI signaling. Book chapter in *Subcellular Biochemistry* **37**: 3–34.

Wilson, B. S., S. L. Steinberg, K. Liederman, J. R. Pfeiffer, Z. Surviladze, J. Zhang, L. E. Samelson, L. H. Yang, P. G. Kotula, and J. M. Oliver. 2004. Markers for detergent-resistant lipid rafts occupy distinct and dynamic domains in native membranes. *Molecular Biology of the Cell* **15** (6) (June): 2580–92.

Other Communications

Kotula, P. G., M. R. Keenan, and J. A. Ohlhausen. 2004. Multivariate statistical analysis of x-ray and ion spectral images. Paper presented at the NIH/NIBIB DOE Meeting on Optical Imaging Technology, 11 February, Bethesda, Maryland.

Kotula, P. G., M. R. Keenan, J. A. Ohlhausen, D. K. Melgaard, D. E. Peebles, J. A. Timlin, D. R. Tallant, T. T. Borek, S. M. Sickafoose, B. L. Doyle, A. Antolak, and G. A. Poulter. 2004. Comprehensive and correlated analytical techniques for homeland defense (CATHODE): Bio-forensics analytical technique development at Sandia. Paper presented at the Gordon Research Conference on Chemical and Biological Terrorism Defense, 20 January, Rancho Santa Barbara, California.

67078

Development of High-Energy-Density Dielectric Materials for Integrated Microsystems

B. A. Tuttle, A. W. Roesler, V. K. De Marquis, J. A. Voigt, P. G. Clem, J. Cesarano, III, M. A. Rodriguez, E. L. Venturini, G. A. Samara

Next-generation surety systems require compact, highly integrated microsystems to improve device functionality, miniaturization, and performance. Capacitors are by far the largest components in these systems; therefore, the greatest increase in volumetric device efficiency can be gained by reducing capacitor size. In the last 3 years, dramatic developments in dielectric science have been reported that can enable 2x–100x size reduction in capacitor size over state-of-the-art (SOA) commercial materials. Sandia investigated two new dielectric-materials families as alternatives to SOA $\varepsilon r' \sim 1100$ dielectrics: (1) specially formulated lead lanthanum zirconate titanate (PLZT) dielectrics, and (2) novel relaxor dielectrics such as $CaCuTiO_3$ (CCTO). Our goal is to develop these new materials for high field applications and then integrate them into microsystems using direct-write technologies.

We developed a direct-write aerosol-spray deposition system that resulted in integrated PLZT dielectric layers that have 50% greater electrical breakdown field than SOA Department of Energy Defense Programs (DOE/DP) capacitors. The expected factor-of-two decrease in SOA capacitor size is significant, as Sandia component engineers would implement capacitors with only a 30% reduction in size into their systems immediately. An important scientific accomplishment was to definitively demonstrate that the origins of the dielectric response of CCTO are extrinsic in nature and can be explained by a semiconductor grain/insulting grain-boundary barrier-layer capacitor model. Further, Sandia materials scientists made significant advances on the microstructural development and control of defect chemistry of these complex CCTO materials. Systematic oxygen partial pressure studies demonstrated reversible changes of dielectric constant over 2 orders of magnitude—consistent with the barrier-layer model. From these fundamental studies, we fabricated CCTO materials with dielectric constants in excess of 100,000 that were temperature stable over 100°C temperature intervals.

An important scientific accomplishment was to definitively demonstrate that the origins of the dielectric response of CCTO are extrinsic in nature and can be explained by a semiconductor grain/insulting grain-boundary barrier-layer capacitor model.

We investigated the influences of temperature, pressure, and niobium (Nb) and iron (Fe) doping on the dielectric properties of CCTO. The results revealed new features not seen before and shed much light on the physics of this material. Highlights of the work are as follows. The unusual dielectric relaxation response of CCTO is indeed extrinsic and can be understood quantitatively in terms a capacitive barrier-layer model, as for an inhomogeneous semiconductor, consisting of semiconducting grains and insulating grain boundaries. We determined the energetics and kinetics of the main (low-temperature [T]) relaxation process. Two thermally activated regimes related to different conduction processes in the CCTO grains control the dynamics. It is suggested that these two regimes result from the emission of electrons from two energy levels associated with the processing-induced oxygen vacancy. We also discovered a higher-T relaxation process that is determined by grain-boundary conduction. Both Nb and Fe doping lead to lower dielectric constant in the temperature-insensitive region and to lower dielectric loss, but Fe doping causes the more dramatic effects. In particular, 3 at.% Fe makes CCTO an intrinsic very-low-loss dielectric and removes the anomalous dielectric constant (w,T) response. It is suggested that the intrinsic behavior is due to carrier compensation in the grains. Specifically, Fe-produced holes from Fe^{3+} substitution of Ti^{4+} ions compensate the conduction electrons attributed to oxygen vacancies. The intrinsic nature of the response for the 3 at.% Fe sample allowed us to determine the intrinsic value of dielectric constant (» 75 at low Ts) and its temperature dependence for the first time.

We fabricated PLZT ceramics using both conventional mixed-oxide and chemically prepared powder processing. Chemical preparation of PLZT 12/70/30 powders, using Sandia's patented process, resulted in a 200°C decrease in sintering temperature. Dielectric properties of the low-firing temperature chemically prepared dielectrics were equivalent to properties of higher-firing temperature conventionally processed ceramics. We developed an aerosol-spray deposition system that is fully computer-automated and provides linear translational-deposition motion control along two axes. Process modifications resulted in deposition of high-quality platinum (Pt) electrodes and PLZT dielectric layers that can withstand 50% greater electric fields than those deposited by manual airbrush deposition. High-quality PLZT dielectric layers can be deposited as demonstrated by a thick-film single-layer PLZT film of 20 μm thickness that had a measured energy density of 2.6 J/cm^3. We direct-write–deposited device structures ranging

from 0.02 cm^2 to 20 cm^2 in area. A systematic phase study resulted in the fabrication of PLZT ceramics that exhibited the following nanoscale features: anti-ferroelectric (AFE) commensurate phases, AFE in commensurate phases, polar nanodomains, antipolar nanodomains, field-enforced AFE to ferroelectric (FE) behavior and relaxor phases. A particularly intriguing set of materials is one with materials that are above their relaxor transformation temperature for device operating temperatures. Sandia fabricated such PLZT materials that had dielectric constants of 2000 to 3000, were relatively insensitive to temperatures over a 100°C temperature range, and could withstand fields of 200 kV/cm. We also investigated doping PLZT with silver (Ag), which we found to reduce the sintering temperature, thus minimizing PLZT/alumina package interactions. An additional benefit of Ag doping is that it lowers the dissipation factor of the material (DF < 0.006) over a temperature range greater than 100°C. Future work will determine which of the aforementioned nanoscale phase structures leads to the highest energy-density PLZT materials.

Refereed

Grubbs, R. K., E. L. Venturini, P. G. Clem, J. J. Richardson, and G. A. Samara. 2004. Pressure study of complex perovskites: $Pb(Sc0.5Nb0.5)O_3$ and $CaCu_3Ti_4O_{12}$. Paper presented at Fundamental Physics of Ferroelectrics, 8–11 February, Williamsburg, Virginia.

Other Communications

Grubbs, R. K., E. L. Venturini, P. G. Clem, J. J. Richardson B. A. Tuttle, and G. A. Samara. 2004. Dielectric and magnetic properties of $CaCu_3Ti_4O_{12}$: Influence of temperature, pressure, and doping. *J. Applied Physics*, to be submitted.

Tuttle, B. A., D. P. Williams, P. G. Clem, and J. Cesarano, III. 2004. Integrated resistor and capacitor fabrication for next-generation microelectronics. (Invited) Paper presented at the 204th Annual Meeting of the Electrochemical Society—ACERS Electronics Division, 13–17 October, Orlando, Florida.

Williams, D. P., and B. A. Tuttle. 2004. High-energy-density capacitors formed via aerosol deposition. Paper presented at the Center for Dielectric Studies Spring Meeting, 17–18 May, Albuquerque, New Mexico.

Williams, D. P., and B. A. Tuttle. 2004. Integrated high-energy-density PLZT-based capacitors. Paper presented at the 106th Annual Meeting of the American Ceramic Society, 18–21 April, Indianapolis, Indiana.

Williams, D. P., and B. A. Tuttle. 2004. Integrated high-zirconia-content PLZT dielectrics for high-energy pulse discharge applications. *Proc. HiTEC 2004: International High-Temperature Electronics Conference and Exhibition* **1** (17–20 May, Santa Fe, New Mexico): 124–28.

Williams, D. P., B. A. Tuttle, and P. G. Clem. 2004. Fabrication and characterization of integrated PLZT thick-film capacitors. Paper presented at the 15th Annual Rio Grande Symposium, 27 October, Albuquerque, New Mexico.

Williams, D. P., B. A. Tuttle, J. Cesarano, III, and M. Rodriguez. 2004. Robocast high zirconia content $(Pb,La)Zr,TiO_3$ dielectrics. *Proc. 204th Annual Meeting Electrochemical Society, ACERS Electronics Division Meeting* **24** (13–17 October, Orlando, Florida): 207–12.

Williams, D. P., B. A. Tuttle, R. K. Grubbs, and P. G. Clem. 2004. Fabrication and characterization of integrated PLZT thick-film capacitors formed via aerosol deposition. *Proc. 2004 IMAPS Ceramic Interconnect Meeting* **4** (26–28 April, Denver, Colorado): 137–42.

67079

Nanolithography-Directed Materials Growth and Self-Assembly

J. W. P. Hsu, J. A. Voigt

The goal of this project is to integrate nanotechnology and inorganic materials growth/assembly for potential applications in bio-/chemical sensing, optoelectronics, catalysis, and novel microsystems. To include these inorganic materials in microdevices and microsystems, they need to be positioned on the substrates in a controlled and predetermined fashion. Sandia's approach to this goal is from "bottom-up" rather than "top-down," in which conventional optical and electron-beam lithography function. We adapt soft nanolithography techniques to selectively modify the growth surfaces chemically with organic molecules to enhance or inhibit crystal nucleation, which in turn determines the final spatial organization of inorganic crystals. Another method, which we call solution stamping nanolithography *(SSNL), is to selectively print inorganic sol-gel precursors on the substrate that we then convert to polycrystalline oxides or metals. Both of these approaches are purely additive (i.e., depositing materials only where they are desired) and avoid contaminating the pristine nature of substrate surfaces. In the first case, we use the chemically patterned surfaces as templates for nanocrystal growth in aqueous solutions. In addition to spatial selectivity, we can control the crystal orientation through the different chemical or physical structure of the patterned surfaces. Crystal morphology and hierarchical structures can be tuned through solution chemistry and growth conditions. We successfully demonstrated the approach described above in selective growth of zinc oxide (ZnO) nanorods on silver (Ag) surfaces. In principle, this approach is applicable to a wide variety of inorganic crystals and substrates, depending on the desired applications. We will gain new insight into crystal growth and self-assembly processes at the nanometer scale.*

We successfully (1) established soft nanolithography capabilities, (2) chemically modified metal surfaces with spatially selectivity using the soft nanolithography capabilities, (3) demonstrated spatial and orientation control of ZnO crystal growth on Ag surfaces using the chemically modified metal surfaces, and (4) developed SSNL, an additive method to print sol-gel precursors in desired patterns.

(1) We established the capabilities to make polydimethylsiloxane (PDMS) elastomeric stamps with micron-

and submicron-size relief structures. These stamps can be inked with molecules that form self-assembled monolayers (SAMs); stamping the molecules on surfaces forms chemical patterns (microcontact printing [mCP]). In SSNL, we ink the PDMS stamps with sol-gel precursors and print patterns on appropriate substrates, which then undergo conventional sol-gel processing. Alternatively, we can coat these samples with thin gold (Au) films for making Au patterns on metal and semiconductor surfaces (nanotransfer printing [nTP]). We are now using mCP and nTP for this and other projects.

(2) We used ellipsometry, Fourier-transform infrared spectroscopy (FTIR), and scanning-electron microscopy (SEM) to characterize the chemical patterns that are formed by mCP on the surfaces. We devoted substantial effort to optimizing the mCP process so that we can obtain a uniform and dense coverage of SAM molecules on surfaces while maintaining submicron feature sizes.

(3) The patterned SAM layer acts to inhibit ZnO nucleation, resulting in ZnO nanorods growing selectively in predetermined regions of the surface. We found that ZnO nanorods grow preferentially c-axis normal to Ag surfaces when surrounding regions are covered with mercaptoalkanoic acids ($HSCnH_2nCOOH$). We achieved excellent selectivity with virtually no nanorods grown on the SAM regions. The density of nanorods inside the patterned Ag areas is substantially higher than that of nanorods grown on unpatterned Ag. Furthermore, we can control the average density with patterns over 2 orders of magnitude! In addition, by tuning the feature size and solution chemistry, we are making progress toward growing isolated individual nanorods on lattices.

(4) Using SSNL, we succeeded in printing copper (Cu) and yttrium-barium-copper oxide (YBCO) high-temperature superconductor precursor solutions on silicon (Si), glass, $LaAlO_3$ substrates. We found that solution chemistry is very important since the quality of printing depends strongly on the wetting/dewetting of the solution on the PDMS stamps and on the substrate. With experimentation, we succeeded in making Cu patterns with sizes ranging from 300 nm to 50 μm with judicious tuning of solution chemistry. We also found that we can utilize dewetting to make nanometer-size features. Pyrolysis and reduction processes need to be optimized. High-temperature superconducting properties of printed lines are comparable to spun-on films when the line thickness is large, but are degraded when the printed lines are too thin. This will need to be optimized through solution composition.

Refereed

Hsu, J. W. P., Z. R. Tian, N. C. Simmons, C. M. Matzke, J. A. Voigt, and J. Liu. 2004. Directed spatial organization of zinc oxide nanorods. *Nature Materials*, submitted.

Other Communications

Hsu, J. W. P., Z. R. Tian, N. C. Simmons, C. M. Matzke, J. A. Voigt, and J. Liu. 2004. Spatial organization of ZnO nanorods on surfaces via organic templating. (Invited) Paper presented at SPIE's International Symposium on Optics East, 25–28 October, Philadelphia, Pennsylvania.

Hsu, J. W. P., Z. R. Tian, N. C. Simmons, C. M. Matzke, J. A. Voigt, and J. Liu. 2004. Surface chemical route to control ZnO nucleation on metals and gas. Paper presented at the Workshop on Frontiers of Epitaxial Engineering, 2–5 May, Moab, Utah.

Tian, Z. R., J. W. P. Hsu, J. A. Voigt, J. Liu, J. Xu, C. M. Matzke, and B. McKenzie. 2004. Patterning and alignment of crystalline nanostructures using modified surfaces. Paper presented at S04 Materials Research Society Meeting, 13–15 April, San Francisco, California.

Voigt, J. A., and J. Liu. 2004. Growth of large arrays of oriented nanostructured films. Paper presented at the APS March Meeting, 24–26 March, Montreal, Quebec, Canada.

67080

Development of a Novel Technique to Assess the Vulnerability of Micromechanical System Components to Environmentally Assisted Cracking

D. G. Enos, S. H. Goods, S. J. Glass, K. R. Zavadil, J. J. Kelly

Microelectromechanical systems (MEMS) will play an important functional role in future Department of Energy weapon and homeland security applications. If these emerging technologies are to be applied successfully, it is imperative that the long-term degradation of the materials of construction be understood. Unlike electrical devices, MEMS devices have a mechanical aspect to their function. Sandia will subject some components (e.g., springs) to stresses beyond whatever residual stresses exist from fabrication. These stresses, combined with possible abnormal exposure environments (e.g., humidity, contamination), introduce a vulnerability to environmentally assisted cracking (EAC). EAC is manifested as the nucleation and propagation of a stable crack at mechanical loads/stresses far below what would be expected, based solely on the materials' mechanical properties. If not addressed, EAC can lead to sudden, catastrophic failure. Considering the materials of construction and the very small feature size, EAC represents a high-risk environmentally induced degradation mode for MEMS devices. Currently, the lack of applicable characterization techniques prevents the needed vulnerability assessment. The objective of this work is to address this deficiency by developing techniques to detect and quantify EAC in MEMS materials and structures under atmospheric conditions relevant to the anticipated service conditions. Our activities focused on the construction of a test apparatus and test specimen (and associated sensor) design. We designed and assembled a first-generation test system and verified its proper function. This system includes the mechanical testing apparatus, as well as a gas exposure system that allows precise control of the exposure environment (gaseous contaminants, temperature, and relative humidity). We made several attempts to instrument test specimens with crack-detection sensors using photolithographic techniques, but were unsuccessful due to metal redeposition issues. We also assembled a high-precision, direct-current potential drop (DCPD) system to facilitate crack detection. Proof-of-concept work for this system is in progress, along with the design and construction of additional instrumented samples.

Our initial goal was to establish a mechanical test method and demonstrate the feasibility of this approach for evaluating the environmental cracking susceptibility of MEMS materials, focusing first on high-sulfur LIGA (for the German term *Lithographie, Galvanoformung, und Abformung*, for lithography, electroforming, and molding) material. We selected the three-point-bend test, as defined in American Society for Testing Materials (ASTM) C1421 and E399, as the basis for the initial mechanical test system. We had to make a number of simplifications to the test technique itself to the size scale of the materials being evaluated. Another aspect of the test system is environmental control—the ability to "dial in" specific combinations of aggressive species (e.g., hydrogen sulfide, chloride, etc.), temperature, and humidity level. The system constructed utilizes permeation tubes (tubes that emit a contaminant at a known rate) combined with a complex flow-control system to maintain a constant concentration of aggressive species as well as humidity level. We are conducting proof-of-concept testing utilizing high-sulfur nickel (Ni) formed through the LIGA process. We utilized post-production thermal processing to alter the grain size and grain-boundary contaminant level to produce material with a range of susceptibilities to EAC. Initial experiments are focusing on measuring the basic mechanical properties for the LIGA material, which we will then compare to values obtained via other means. We are developing crack-length sensors and incorporating them into the test samples. We attempted to produce these sensors by using a spun-coated SU-8 photoresist as the insulator, but failed to produce a usable device. Presently, we are exploring an alternative resist (Paralene) and improved sample-preparation techniques, along with the implementation of DCPD, a classical means for crack-length detection.

67081

3-D Optical Sectioning with a New Hyperspectral Deconvolution Fluorescence Imaging System

D. M. Haaland, H. D. Jones, J. A. Timlin, M. B. Sinclair, G. S. Davidson, B. K. Ford, T. L. Sounart, G. D. Jones, G. D. Bachand

This project includes designing, building, and applying a novel hyperspectral deconvolution fluorescence microscope for three-dimensional (3-D) diffraction-limited optical sectioning of cells and subcellular organelles, 3-D monitoring of microfluidic processes, and investigation of molecular motors. Sandia is developing data-analysis methods to deconvolve the hyperspectral image (HSI) data and to rapidly extract 3-D concentration distribution maps of all emitting species. The imaging system has many advantages over current confocal imaging systems: simultaneous monitoring of numerous highly overlapped fluorophores, immunity to autofluorescence or impurity fluorescence, enhanced sensitivity, and dramatically improved accuracy and dynamic range. Combining our patented multivariate curve resolution (MCR) analysis with the deconvolution of HSIs can improve both spectral and spatial deconvolution processes. The system can make rapid survey scans of large areas, followed by detailed 3-D composition maps of small targeted volumes at high spatial and temporal resolutions. Efficient data compression in both the spatial and spectral dimensions will allow personal computers to perform quantitative analysis of HSIs of the size > 10 Gb without loss of image quality. The new imaging system will be an enabling technology for numerous applications, including (1) 3-D composition mapping analysis of multicomponent microfluidic processes such as mixing, dispersion, and chemical syntheses of materials, (2) quantitative analysis and co-localization of molecular motors in 3-D, and (3) examinations of the binding of functionalized lipid vesicles to specific cells and the release and/or internalization of the vesicle contents. This challenging project, when successful, will make Sandia a major player in advanced spectral imaging techniques for materials research, sensor technology, and biotechnology. Realization of this new system will position us for future homeland security, Genomes-to-Life (now Genomics:GTL), and National Institutes of Health projects.

This challenging project, when successful, will make Sandia a major player in advanced spectral imaging techniques for materials research, sensor technology, and biotechnology.

We completed the design of the 3-D HSI system. All parts for the imager are now being assembled into a complete system. The new design includes true confocal imaging that uses a

newly constructed high-throughput, high-image-quality prism-imaging spectrometer and a sensitive charged-coupled device (CCD) camera with electron multiplier gain. We also completed the bulk of the control software for the system. Characterization of the new X-Y positioners demonstrated a fivefold improvement in the spatial background noise compared to our earlier 2-D HSI system. We selected spatial deconvolution algorithms and wrote software in MATLAB to implement the deconvolution in 3-D. We tested and successfully applied the software to the deconvolution of 2-D two-color images of microtubule fibers with spatially defined regions of fluorescent organic dyes and nanocrystal quantum dots (QDs). We prepared fluorescent biobeads by coupling fluorescently labeled streptavidin protein with silane-functionalized silica microspheres. These biobeads, when coupled with fluorescently labeled molecules and cast in thin polymer films, can serve as a model for protein-membrane interactions and will be used to further test and characterize the hyperspectral system. The MCR software used for spectral deconvolution was tested with simulated data including realistic spectral and spatial images with real spectral noise obtained from repeat 2-D images. These studies identified excess noise due to nonuniform velocity of the original positioners and discovered correlated errors in the CCD detector. We devised methods to reduce the detrimental effect of correlated errors on the analyses. We noticed systematic instrument artifacts with our 2-D HSI system due to a slight rotation of the CCD camera relative to the imaging spectrometer slits and due to keystone distortion of the image on the CCD detector. Since these problems are also possible with the 3-D system, we developed methods to measure, quantify, and correct the instrument artifacts generated by these distortions.

Refereed

Haaland, D. M., J. A. Timlin, M. R. Keenan, H. D. T. Jones, C. L. Stork, D. K. Melgaard, and M. B. Sinclair. 2004. New approaches for understanding multivariate curve resolution applied to hyperspectral images. (Invited) Paper presented at the Federation of Analytical Chemistry and Spectroscopy Societies Meeting, 3–7 October, Portland, Oregon.

Other Communications

Haaland, D. M. 2004. Multivariate curve resolution applied to the analysis of hyperspectral images. (Invited) Paper presented at the Naval Research Laboratories, May, Washington, D.C.

Haaland, D. M., J. A. Timlin, D. K. Melgaard, M. R. Keenan, M. H. Van Benthem, and M. B. Sinclair. 2004. Spectroscopy and chemometrics: A personal vision for the future. Paper presented at the Pittsburgh Conference, Bomem-Michelson Award Address, March, Chicago, Illinois.

Haaland, D. M., J. A. Timlin, M. B. Sinclair, M. R. Keenan, C. L. Stork, and M. M. Werner-Washburne. 2003. Multivariate curve resolution for analysis of hyperspectral images. Paper presented at the Eastern Analytical Symposium, November, Somerset, New Jersey.

Haaland, D. M., J. A. Timlin, M. B. Sinclair, M. R. Keenan, M. H. Van Benthem, M. J. Martinez, and M. M. Werner-Washburne. 2004. Improved microarray analysis and multifluorophore imaging with hyperspectral image analysis. Paper presented at the 2nd New Mexico Workshop on Computational Cell Biology: Microscopy, Membrane Biology and Modeling for Biosignaling Research, January, Santa Fe, New Mexico.

Haaland, D. M., J. A. Timlin, M. B. Sinclair, M. R. Keenan, M. H. Van Benthem, M. J. Martinez, and M. M. Werner-Washburne. 2003. Multivariate curve resolution for analysis of hyperspectral images. (Invited) Paper presented at the Federation of Analytical Chemistry and Spectroscopy Societies Meeting, 19–23 October, Ft. Lauderdale, Florida.

Haaland, D. M., J. A. Timlin, M. R. Keenan, H. D. T. Jones, C. L. Stork, and M. B. Sinclair. 2004. Multivariate analysis of hyperspectral images for biotechnology applications. Paper presented at the 9th Annual Conference on Chemometrics in Analytical Chemistry, September, Lisbon, Portugal.

Haaland, D. M., J. A. Timlin, M. R. Keenan, H. D. T. Jones, C. L. Stork, D. K. Melgaard, and M. B. Sinclair. 2004. Multivariate analysis of hyperspectral images for biotechnology applications. (Invited) Paper presented at the Meeting of the American Chemical Society, 22–26 August, Philadelphia, Pennsylvania.

Haaland, D. M., J. A. Timlin, M. R. Keenan, M. H. Van Benthem, M. B. Sinclair, M. J. Martinez, and M. M. Werner-Washburne. 2003. Methods to improve the efficiency of the quantitative analysis of hyperspectral image data. Paper presented at the Federation of Analytical Chemistry and Spectroscopy Societies Meeting, October, Ft. Lauderdale, Florida.

Haaland, D. M., J. A. Timlin, P. G. Kotula, A. R. Burns, M. B. Sinclair, M. H. Van Benthem, M. R. Keenan, M. J. Martinez, A. D. Aragon, and M. M. Werner-Washburne. 2004. Bio-imaging at Sandia National Laboratories. Paper presented at the DOE/NIBIB Imaging Workshop, February, Bethesda, Maryland.

Timlin, J. A., D. M. Haaland, and M. B. Sinclair. 2004. A hyperspectral imaging system with multivariate data analysis for increased throughput. Paper presented at the 118th AOAC Annual Meeting and Exposition, September, St. Louis, Missouri.

Timlin, J. A., D. M. Haaland, and M. B. Sinclair. 2003. Hyperspectral imaging and multivariate data analysis for biological and biomedical applications. Paper presented at the CENSSIS Research and Industry Collaboration Conference, November, Boston, Massachusetts.

67082

The Science of Solutes: Transition Metals in LIGA Nickel

A. A. Talin, D. L. Medlin, S. H. Goods, S. M. Foiles, E. Marquis, J. J. Kelly

All engineered materials contain solutes, whether intentional (alloying elements) or unintentional (impurities). Although solutes control both the processing and the properties of most alloys, material and process models almost never include their effects. In this project, Sandia makes the first concerted effort to include realistic solute effects in mesoscale material models. Novel LIGA (for the German term Lithographie, Galvanoformung, und Abformung, *for lithography, electroforming, and molding)-fabricated nickel (Ni)-manganese (Mn) electrodeposits are prime candidate materials for stockpile microsystems applications that require high strength and ductility. Incorporating small amounts of transition metal (TM) dopants in LIGA Ni dramatically suppresses recrystallization and grain growth, preserving the fine-grained as-deposited microstructure throughout subsequent processing. How TMs do this is unknown; nucleation inhibition (via subgrain pinning), enhanced twinning (via decreased stacking fault energy), and growth inhibition (via boundary drag) have been proposed. We shall use state-of-the-art* ab initio *simulations to characterize the energetics and kinetics of solute segregation and boundary/solute equilibrium for realistic subgrain, twin, and grain boundaries. Using the resulting thermodynamic and kinetic parameters, a three-dimensional (3-D) digital kinetics model will simulate boundary motion in realistic, multiscale Ni polycrystals containing various TMs. By comparing subgrain, twinning, and grain-growth processes, this model will determine recrystallization retardation and texture development mechanisms for a spectrum of Ni-TM alloys. A suite of annealing experiments and mechanical tests will elucidate grain growth, twinning, recrystallization, texture development, and properties for these alloys to guide and validate the simulations. The resulting insight into solute effects will enable improved materials design for LIGA alloys and will greatly extend the realism and utility of Sandia's material process modeling capabilities.*

...Sandia makes the first concerted effort to include realistic solute effects in mesoscale material models....The resulting insight into solute effects...will greatly extend the realism and utility of Sandia's material process modeling capabilities.

We established experimental capabilities and prepared and analyzed a suite of experimental samples that will form the basis for further study. In parallel, we established computational

capabilities, and we performed atomic-scale simulations to determine a basic set of physical parameters upon which subsequent models will rely. Specifically, we set up a dedicated cell to produce Ni electrodeposits with varying Mn, sulfur (S), and oxygen (O) concentrations. Using this cell, we prepared a series of electrodeposited Ni-Mn films with varying Mn concentration and characterized their recrystallization temperatures and textures. In addition, we prepared and characterized a series of arc-melted, ultrapure NiMn alloys. Using these materials, we established the relationship between plating conditions, annealing temperature, and texture of Ni and NiMn electrodeposits. In addition, we measured both yield strength and annealed grain size for <110> and <100> NiMn electrodeposits. To begin to connect the continuum results to atomic and microstructural models, we examined grain boundaries in NiMn electrodeposits using a 3-D atom-probe microscope (3DAP). We used *ab initio* electronic structure calculations of the energetics of Mn, tungsten (W) and niobium (Nb) impurities in bulk Ni to determine the excess volume and the modulus-interaction key parameters in continuum models of impurity-defect interactions. We also computed the interaction of Mn impurities with several grain boundaries, finding qualitative agreement with 3DAP observations. To capture the effects of solutes on grain-boundary motion, we developed a new 3-D digital kinetics (3DDK) approach based on cellular automata (CA) models; we developed a numerical diffusion model and verified it for model diffusion systems. As a first step to modeling the effect of twinning on microstructural evolution, we developed a twinning model that takes a 3-D grain structure and forms twins according to user-input parameters.

Refereed

Janssens, K. G. F., E. A. Holm, and S. M. Foiles. 2004. Introducing solute drag in irregular cellular automata modeling of grain growth. *Proc. 2nd International Conference on Recrystallization and Grain Growth* **I** (29 August–3 September, Annecy, France).

Talin, A. A., S. H. Goods, J. J. Kelly, S. Spangler, E. A. Marquis, and G. Lucadamo. 2004. X-ray–based analysis of dilute, electrodeposited nickel-manganese alloys. *Proc. IMECE 2004, ASME International Mechanical Engineering Congress* (13–19 November, Anaheim, California).

67083

Novel Gel-Based Technology for Sensors and Weapons

J. L. Lenhart, P. J. Cole

This project focuses on developing a fundamental understanding of the mechanisms that control the volume phase transition in nonaqueous-based polymer gels, and to relate this solvent—polymer partitioning—to the gel microstructure and mechanical properties. The research will have two applications. First, this work will provide the scientific foundation necessary to launch Sandia into sensor development for chemical and biological agents, a likely new arena relevant to homeland defense initiatives. Second, this research is essential for developing materials to use in electronics applications.

A gel is a cross-linked polymer highly swollen by solvent. Mechanically, the solvent creates a "soft solid," which is easily deformable, yet still recovers from deformation due to the elastic nature of the permanent cross-links in the polymer. While polymer gels have potential use in a variety of emerging technical applications, including drug delivery, biomedical implants, artificial muscles, food and cosmetics, separation systems, display devices, batteries, and optical devices to name a few, of particular interest to Sandia are gel applications in sensors and electronic devices. Typically, the solvent loading in a gel is high (> 30%), and in some uses, the loading approaches 90%. While varying solvent types and loading provide a wealth of potential applications, the high solvent loading invokes unique materials challenges because the gel properties are largely determined by solvent–polymer partitioning. A key scientific question that remains unanswered is the relationship between this phase behavior and the desired gel properties. We will utilize a combination of scattering and rheology to link the gel chemistry and physics to the phase behavior, microstructure, and material properties.

We began rheological and neutron-scattering studies on the gel systems. Neutron scattering proved useful for detecting phase separation, and we identified the phase boundary of gel systems. We determined that the current gel formulation exhibits phase separation in the use range of typical weapons, which is detrimental to device performance. We designed a new gel with improved polymer–solvent miscibility and performance. We conducted a combination of rheology, scattering, and swelling experiments to investigate the impact of solvent quality and loading on the gel properties. We used the

knowledge gained from this study to design improved gel materials for electronic applications. We also started to investigate the role of gel processing on the gel phase boundary. Preliminary results indicate that processing temperature has only minimal impact on the phase diagram. We initiated theoretical modeling to link the neutron scattering to the gel microstructure. For sensor applications, we started investigating mechanisms to increase the volume shrinkage kinetics in polymer gels by increasing the gel surface-area-to-volume ratio. This allows the solvent to transfer rapidly to the gel surface and increases the polymer collapse rate in the gel. We explored porous polymer gels to increase the surface area.

Other Communications

Lenhart, J. L., P. J. Cole, and R. Hedden. 2004. Polymer gels with broad temperature performance. *Proc. American Chemical Society, ACS Polymer Preprints* **45** (1) (March, Anaheim, California): 555–56.

67084

Coupled Nanomechanical Oscillator Arrays for the Study of Internal Dissipation in Nanoscale Structures and Collective Behavior in Large Systems

J. P. Sullivan, D. A. Czaplewski, B. E. N. Keeler, W. Pan, N. A. Modine, D. W. Carr, J. R. Wendt, T. A. Friedmann

Controlling energy dissipation in nanostructured materials is a fundamental materials issue for Sandia's future micro- and nanosystems. The goal of this project is to understand internal dissipation in structures of nanoscale dimensions. We developed a new approach to achieve this goal—the study of large arrays of coupled nanomechanical oscillators combined with theoretical calculations aimed at identifying atomistic mechanisms of dissipation. This research is directly relevant to the nanomechanics thrust area of the newly established Center for Integrated Nanotechnologies (CINT), which is part of the nation's investment in nanotechnology. An important practical application of this research is the development of nanomechanical resonators for homeland security applications (e.g., sensors).

Technical aspects of this project include development of a means to measure oscillators at low temperatures where dissipation due to tunneling states and ballistic phonon transport become important. In addition, we will develop a new theoretical approach that combines large-scale classical force-field techniques together with first-principles quantum mechanical calculations to identify the dissipative defects, such as the ubiquitous tunneling states defects in amorphous materials. The large system of coupled nanomechanical elements provides a unique experimental platform for understanding major problems in solid-state and statistical physics. Coupled oscillator arrays, which resemble two-dimensional (2-D) ball-and-spring models, can be used to study disorder-induced localization in 2-D systems and stochastic resonance and nonlinear effects in coupled systems. Specifically, we will examine localization of vibrational modes of the array at intentionally introduced defects and coupling of these modes to mechanical noise leading to mode amplification (stochastic resonance) or the emergence of complex phenomena in the case of bistable oscillator arrays, which are a mechanical analog to biological neural networks.

We obtained exciting results in the understanding of internal dissipation in disordered materials using mechanics

measurements on small structures and theoretical simulations at the atomic scale. We fabricated micro- and nanomechanical structures out of amorphous carbon (C) to study the intrinsic internal dissipation in a model amorphous solid material. Analysis of these structures revealed a remarkably dispersionless dissipation over several orders of magnitude. This indicates the existence of a dissipation process that is independent of time scale from milliseconds to hundreds of nanoseconds and insensitive to length scale from 1 m to less than 1 μm. This dispersionless dissipation has been explained as arising from the existence of a wide spectrum of dissipative defects operative over a large distribution of time scales. The flat distribution of defect relaxation energies and the magnitude of the dissipation are remarkably similar to the dissipation observed in nearly all amorphous materials, indicating that dissipation in disordered materials is very similar, despite large variations in material systems.

Using theoretical simulations of internal dissipation in another disordered system, amorphous silicon (Si), we found that internal dissipation in the presence of disorder can be 2 orders of magnitude larger than that found in a well-ordered system (crystalline Si). The theoretically determined internal dissipation in amorphous Si follows an approximate linear scaling with oscillator frequency, which is the expected behavior for intrinsic internal dissipation processes.

We also designed, fabricated, and tested the first-generation coupled oscillator structures. We fabricated oscillator arrays containing 100 elements (10 x 10) by combining electron-beam lithography and reactive-ion etching (RIE). The rigid elements of the oscillator arrays consisted of suspended tungsten (W) islands, and the spring elements consisted of thin, 500 nm-wide ligaments of tetrahedral amorphous C. We used finite-element (FE) linear elasticity modeling to identify resonant modes of the arrays and measured these resonance modes using interferometric light scattering in vacuum; we quantified the mode shapes using scanning laser Doppler vibrometry in air. We also used FE modeling to predict the expected response for coupled oscillator arrays containing defined defects (e.g., mass disorder) and will use it to guide the development of the next-generation coupled oscillator arrays.

Current findings have important implications for the utilization of nanoscale oscillators in Sandia’s future electronics or sensor platforms.

Refereed

Czaplewski, D. A., J. P. Sullivan, T. A. Friedmann, D. W. Carr, B. E. N. Keeler, and J. R. Wendt. 2004. Mechanical dissipation in tetrahedral amorphous carbon. *J. Applied Physics*, accepted.

Sullivan, J. P. 2004. The micro- and nanomechanics of amorphous diamond. (Invited) Paper presented at Texas Tech University, November, Lubbock, Texas.

67085

Precisely Controlled Picoliter Vessels with Rapid Sample Preparation for Trace Biotoxin Detection

C. R. Ellis, E. S. Lee, L. A. Domeier, P. M. Dentinger, C. Muñoz, B. A. Simmons, R. V. Davalos

This project explores the synthesis and characterization of novel microstructures for discrete, controllable sample management in microsystems. Large, synthetic analogues of natural vesicles will enable control over microsamples and microreactions in ways that were previously unattainable. These containers are formed, loaded, moved, and fused to conduct picoliter reactions with exquisite precision. As containers, vesicles are made of an engineerable wall material capable of being selectively permeated, yet when sealed, they prevent samples from escaping. As substrates, vesicles are ideal for low reagent volumes and fast surface-dominated reactions required in the preparation of any assay. The applications abound: in biochemistry as a platform for the study of molecular dynamics (MD), in chem/bio threat detection as a dilution-free conveyance and preparation motif, and in medicine as an accurate and local drug-delivery technique. Predicated on the paradigm of electrical control, we envision a system boasting vesicle electroformation from lipid primitives, membrane permeation and loading of analytes using electroporation, container fusion with electrical mediation, and vesicle control with electrokinesis. The first steps are embodied in this project.

Sandia's objectives are (1) to synthesize vesicles capable of withstanding electrical and mechanical stressors, (2) to develop an embedded vesicle formation technique, (3) to increase our ability to permeate vesicle membranes for sample loading and unloading, (4) to confine and trigger metered reactions within these vesicles, and (5) to demonstrate chip-based movement, filtering, and sensing control over individual vesicles.

We devoted our initial efforts to formulating robust large vesicles for individual capture and electroporation. We developed new chemistry and procedures to repeatedly generate such stable liposomes and used a vesicle characterization apparatus designed, built, and improved for sensitive electrical stimulus and sensing of electroporation. We proficiently demonstrated the formation of photopolymerized large liposomes and their subsequent storage for weeks. Also, we repeatedly captured 10 µm vesicles using hydrostatic suction

and monitored reversible electroporation by measuring impedance spectra during pulse delivery.

We established a variety of vesicle interrogation and formation techniques that culminated in successful, reproducible vesicle electroporation. Discrete, on-chip liposome electroporation is a technique that has never before been achieved.

Our approach to vesicle formation evolved through four strategies: (1) hydration, (2) rehydration, (3) evaporation, and (4) electroformation. While we currently use evaporative formation for electroporation tests, we anticipate progressing to electroformation since this latter technique has been shown to be very effective at producing vesicle populations with large diameters. We investigated a variety of membrane constitutions, comprising different phospholipids, cholesterol additives, and varying degrees of ultraviolet (UV) polymerization. The polymerizable phospholipid DIYNE PC (1,2-bis(10,12-tricosadiynoyl)-sn-glycero-3-phosphocholine) is a necessary ingredient for membrane strengthening. We found the cross-linking step to be very sensitive to both formation and storage temperature prior to UV exposure; however, the formed vesicles are quite stable subsequent to photopolymerization. Evaporation-formed vesicles, measuring up to 10 μm in diameter, may be stored refrigerated for weeks without breakdown. We entrapped three different dyes in these vesicles for visualization of vesicle lysis and membrane permeation due to electroporation. We captured the most robust vesicles, polymerized DIYNE PC:Cholesterol (10:1 mole ratio), at a 6 μm microhole using hydrostatic suction, whereas all other formulations re-extrude through the hole. These polymerized vesicles may also be centrifuged and resuspended for easy washing of excess dye.

We developed a test platform to investigate membrane behavior by trapping and delivering electrical pulses to single vesicles while sensing transmembrane impedance. This platform incorporates a replaceable silicon (Si) chip with a supported silicon nitride (SiN) membrane in which a microhole is patterned. A manifold seals around this chip and interfaces with a four-electrode geometry paramount in acquiring true transmembrane potentials. Single vesicles are pulled to the microhole, sensed with small voltages (200 mV), and pulsed with larger voltages (1–5 V). Electrical impedance data and supporting, concurrent fluorescence evidence show that vesicle membranes permeate and reseal at lower voltages and break down with large pulses. Impedance data show progressive

permeation as greater pulse amplitudes are applied, with recovery between pulses to higher (less permeated) impedances. When compared to expected impedance results, the data are evidence of reversible electroporation.

Positive results from forming, capturing, and electroporating vesicles provide sound evidence for feasibility of compartmentalized reactions in a microsystem. In upcoming work, it is our principal goal to study and optimize the response of synthetic vesicle walls to external stimuli. Research is under way to quantify an individual vesicle's membrane response upon exposure to shear, electrical, and chemical stressors.

Refereed

Lee, E. S., C. M. Muñoz, B. A. Simmons, C. R. B. Ellis, and R. V. Davalos. 2004. Feasibility study on the use of temperature-dependent liposomes for variable concentration profiles in drug delivery applications. *Proc. ASME IMECE,* accepted.

70799

Developing the Foundation for Polyoxoniobate Chemistry: Highly Tunable and Exploitable Materials

M. D. Nyman, T. M. Alam, F. R. Bonhomme, M. A. Rodriguez

The first ~ 70 years of polyoxometalate (POM) research was dominated by polyoxotungstates, polyoxomolybdates, and more recently, polyoxovanadates. Many POM geometries and compositions have been reported and used (1) in a diversity of applications, including virus/protein binding, catalysis, and electrooptic and electrochromic materials; and (2) as building blocks for nanostructured materials. In 2002, Sandia reported a general synthetic procedure for polyoxoniobates, thus beginning a new branch of POM chemistry that impacts both fundamental understanding and applications of POMs. Even more intriguing, these polyoxoniobates differ significantly from other POMs in that they display much higher surface charges and base-stability rather than acid-stability. These different properties of the polyoxoniobates present the opportunity for new applications such as nuclear-waste processing and improved performance for metal and virus binding.

The purpose of our research is to develop the foundation for polyoxoniobate chemistry so that it may become an expanded class of functional materials similar to the other POMs. We will execute this by first understanding the mechanisms of polyoxoniobate formation using in situ *nuclear magnetic resonance (NMR) techniques. Synthesis of new polyoxoniobates will be guided by the NMR studies, as will synthesis of solid-solutions between the polyoxoniobate family and the other POM families. Development of these solid solutions will yield POMs with highly tunable properties, including charge and pH stability. In these studies, we also seek to understand the fundamental differences among the POM families. Additionally, we will use this project to develop* ab initio *structure determination from x-ray powder data as an integral part of the capabilities of the Center for Integrated Technologies (CINT) and Sandia.*

Execution of this work will allow Sandia to take the lead in establishing polyoxoniobate chemistry, explore avenues for new and improved POM applications, and become one of the few U.S. institutions with ab initio *structure determination from powder diffraction as a core capability.*

Execution of this work will allow Sandia to take the lead in establishing polyoxoniobate chemistry, explore avenues for new and improved POM applications, and become one of the few U.S. institutions with ab initio *structure determination from powder diffraction as a core capability.*

We made tremendous progress and set new directions for expanding our scope of focus and range of impact. In synthetic

efforts, we determined how to nanoengineer 0-dimensional (0-D), 1-D, and 2-D materials from polyoxoniobate building blocks. We incorporated phosphate and germanate into polyoxoniobate chemistry as the tetrahedral core atoms. Phosphate gave the first lacunary polyoxoniobate cluster. From this investigation, we learned the chemical mechanism by which we can control formation of lacunary clusters. Lacunary clusters (meaning incomplete) are particularly exciting because they have pockets for binding cationic species as well as especially high negative charges. These characteristics have excellent potential for nuclear-waste processing and virus/pathogen binding, mitigation, and sequestration.

In the NMR task, we investigated the behavior of basic niobium-oxo species in solution and examined how they transform as a function of pH and temperature. This gives insight into how to build new heteropolyniobate species. Within the scope of this project, we developed a suite of new NMR tools to measure the structure and activity of water species at interfaces. This is critical as we utilize and manipulate materials of diminishing dimensions with the expanding interest in nanoscience and understanding how nanomaterials are constructed, how they function, and how they fail, break down, or transform. We also established collaboration with the National High Magnetic Field Laboratory to develop new multiple quantum NMR techniques and provide the first 93Nb structural characterizations for a series of polyoxoniobate compounds. In the structure determination from the x-ray powder data task, we used this method integrated with other analytical methods to determine the structure of lead maleate (Trimol), an important plastics and explosives modifier material.

Refereed

Alam, T. M., M. Nyman, B. R. Cherry, J. M. Segall, and L. E. Lybarger. 2004. Multinuclear NMR investigations of the oxygen, water, and hydroxyl environments in sodium hexaniobate. *J. American Chemical Society* **126** (17) (May): 5610–20.

Alam, T. M., M. Nyman, G. P. Holland, B. R. Cherry, and J. M. Segall. 2004. High-speed ^{1}H MAS NMR studies of water on polyniobate surfaces. Paper presented at the American Chemical Society National Meeting, March, Anaheim, California.

Holland, G. P., B. R. Cherry, and T. M. Alam. 2004. Distribution effects on ^{1}H double-quantum MAS NMR spectra. *J. Magnetic Resonance* **167** (1): 161–67.

Nyman, M., F. Bonhomme, T. M. Alam, J. B. Parise, and G. M. B. Vaughan. 2004. $[SiNb_{12}O_40]_{16-}$ and $[GeNb_{12}O_40]_{16-}$: New highly charged keggin ions with sticky surfaces. *Angewandte Chemie International Edition* **43** (21) (May): 2787–92.

Other Communications

Alam, T. M., M. Nyman, G. Holland, B. Cherry, and J. Segall. 2004. High-speed ^{1}H MAS NMR investigations of hydroxyl and water environments in polyniobate materials. Paper presented at the 45th Annual Experimental Nuclear Magnetic Resonance Conference, April, Pacific Grove, California.

Gan, Z., H. Kwak, T. M. Alam, R. Vold, and G. Hoatson. 2004. A new representation of multiple quantum NMR. *NHFML Annual Reports*.

Nyman, M. 2004. Lacunary to linked—new developments in heteropolyniobate chemistry. (Invited) Paper presented at the International Symposium on Polyoxometalate Chemistry, November, Kanagawa, Japan.

Nyman, M. 2004. Polyoxo-niobate chemistry unveiled. (Invited) Paper presented at the NSF Materials Chemistry Workshop, October, Denver, Colorado.

Nonproliferation and Materials Control

The Nonproliferation and Materials Control investment area intends to reduce our vulnerability to threats from nuclear, biological, and chemical weapons of mass destruction. Investments seek to develop a collective of capabilities and products that will empower the continuing development of organized system-level responses to national security challenges. Research focuses on technological evolutions in advanced monitoring systems and sensors, security systems and technologies, detection systems and satellites, vulnerability assessment, intelligence technologies, virtual global presence, and global awareness.

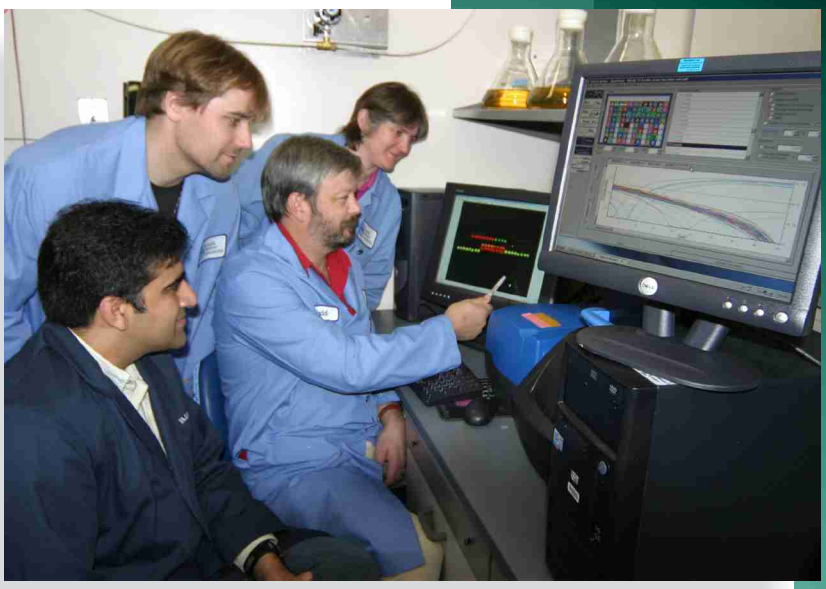

52714
"Detecting the Toolmarks of Genetic Engineering in Bioweapons Strains"

Incidence of infection by naturally occurring strains of biowarfare agents is low; however, it is important to discern the difference between infection by a natural background strain and one enhanced by genetic engineering. Viral vectors are the genetic-engineering tools used to alter an organism, and traces of their use are left in the modified organism. These toolmarks take the form of genetic elements such as multiple cloning sites. By detecting these toolmarks, scientists can discern the difference between naturally occurring and genetically modified bacteria.

To achieve the goal of toolmark detection, researchers created a microarray system that detects nonspecific evidence of genetic engineering in bacterial systems. They developed and validated the methodologies for detecting toolmarks from both replicative and integrated vectors in both gram-negative and gram-positive bacterial hosts. Scientists extended the goals of the project and also devised a methodology for detecting toolmarks by real-time polymerase chain reaction, providing an alternative to microarray hybridization.

38722

Agile, Microsystems-Enabled Receiver

C. D. Nordquist, M. V. Pack, S. Coffee, T. Lemp, C. Sanchez, A. Muyshondt, I. C. Reines, G. R. Sloan, P. S. Finnegan, F. Austin, IV, C. L. Goldsmith, A. G. Baca, G. M. Kraus, T. A. Plut, C. W. Dyck

The goal of this project is to develop and integrate radio-frequency (RF) microelectromechanical systems (MEMS) and gallium nitride (GaN) device technologies to create an agile receiver front-end. The module consists of a MEMS transmit/receive (T/R) switch, a MEMS tunable filter, and a GaN low-noise amplifier (LNA), providing significant advantages over existing radar front-ends. The low loss of the RF MEMS elements will allow tunable filters and T/R switches to precede the LNA without significantly degrading the noise figure, facilitating both jammer protection and real-time adaptivity. The GaN LNA offers high dynamic range and natural immunity to overload damage, eliminating the need for a separate limiter. The module, interconnected via monolithic and multichip-module (MCM) techniques, will be several times smaller than current radar front-ends.

Realizing these advances presents formidable technical challenges in electronic materials, processing, and devices. To achieve optimum performance, the RF MEMS components require careful design, well-controlled processing, and detailed characterization. The GaN transistors present challenges in materials growth, device processing and testing, and thermal management. Finally, the integration of these novel technologies into a single module will require accurate component characterization and electrical design. Once these challenges are met, the module will provide lower loss and higher power than existing packages much larger in size.

Sandia intends to integrate the resulting receiver module with an advanced GaN power amplifier, producing circuitry that will comprise a miniaturized, fully integrated T/R function for multiple applications: synthetic-aperture radar (SAR), fuzes, tags, active phased arrays, and communications. The jammer resistance, signal agility, ultraminiaturization, and high-power density offered by such a module are essential facilitators for next-generation precision-guidance and reconnaissance radars. Some specific, high-impact applications include modulation-agile covert communications, multiplatform tags, fuze upgrades, and mini-SARs for reconnaissance (satellites/unmanned aerial vehicles [UAVs]) and precision guidance (weapons).

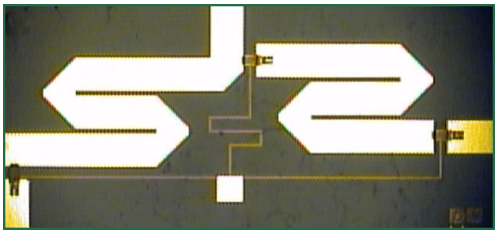

Microscope image of the MEMS–enabled T/R switch.

We realized all of the subcomponents of the agile front-end and designed the receiver module. The subcomponents are an

RF MEMS T/R switch, an RF MEMS–enabled tunable filter, and a GaN LNA. All of these components showed excellent performance, translating into good performance for the agile front-end.

We demonstrated an X-band (8–12 GHz) RF MEMS T/R switch with less than 1.5 dB of loss in the receive state and greater than 65 dB of isolation in the transmit state. The 4.2 mm x 1.9 mm die uses three individual metal-contacting RF MEMS devices. Additional improvement is possible with further tuning, but the improved switches will not be fabricated for this project. While this switch is not as fast as a solid-state T/R switch or circulator, it can still be switched in less than 20 μs, allowing its use in low-pulse-repetition-frequency applications. We circumvented the power-handling limitations of RF MEMS devices by designing the T/R switch network such that all of the RF MEMS switches are open during the high-power transmit pulse, enabling its use in moderate-power radar systems.

We realized two specific RF MEMS–enabled filters for this project. The first filter is a state-of-the-art 10.7–15.5 GHz band-hopping two-pole filter with a 15% bandwidth, a tuning range of 38%, and a passband loss of 2 dB. This filter occupies a die area of 2.2 mm x 1.5 mm and utilizes two RF MEMS capacitive switches. The second filter improves upon this design using microstrip technology and a three-pole combline design. This filter has four tuning states ranging from 8.2 GHz to 11.3 GHz with a 1 GHz bandwidth and a passband loss ranging from 4.4 dB to 6 dB, which can be improved to about 2 dB with layout and processing optimization. The 2.85 mm x 2.15 mm die utilizes six capacitive switches to achieve the filter tuning in a compact area. These filters represent state-of-the-art tunable filter performance.

The final component required to demonstrate the agile front-end is the GaN LNA. Characterization of Sandia's GaN high-electron-mobility transistor (HEMT) technology indicates a noise figure of 0.6 dB at 10 GHz, which is comparable to commercially available gallium arsenide (GaAs) HEMT technology. However, GaN technology has the benefit of increased dynamic range and robustness, providing for a more survivable radar system. An X-band (8–12 GHz) hybrid single-stage GaN LNA demonstrates 11 dB of gain and a noise figure of 1.5 dB at 10 GHz. We completed a balanced design for improved gain flatness and noise figure, but will not fabricate this design under this project.

To achieve the circuit demonstrations described above, this project advanced the state of Sandia's RF MEMS and GaN

technologies. We dramatically improved the reproducibility, yield, and reliability of Sandia's RF MEMS devices. We also improved the performance of the GaN transistor, with progress in epitaxial growth, passivation, and processing.

The receiver module is fabricated on a 38 mm x 51 mm duroid printed circuit board (PCB). While the circuit components occupy an area of only 15 mm x 23 mm, the connectors determine the PCB size. The individual dies are assembled onto the ground plane into cavities cut in the duroid PCB and connected via wirebonding. We fabricated and assembled several different designs with various combinations of the three components. While yield issues prevented testing of the module, it should have a noise figure of about 2.5 dB without the filter in front of the LNA and about 7 dB including the filter. With further improvements in the MEMS and GaN technologies, the receiver noise figure can drop even further, to 1.5 dB without the filter and to about 3.5 dB with the filter. This module provides a building block for future microsystem–enabled RF and microwave systems.

We dramatically improved the reproducibility, yield, and reliability of Sandia's RF MEMS devices. We also improved the performance of the GaN transistor, with progress in epitaxial growth, passivation, and processing.

Refereed

Kraus, G. M., C. L. Goldsmith, C. D. Nordquist, C. W. Dyck, P. S. Finnegan, F. Austin, IV, A. Muyshondt, and C. T. Sullivan. 2004. A widely tunable RF MEMS end-coupled filter. *Proc. IEEE MTT-S International Microwave Symposium* **1** (June, Fort Worth, Texas): 429–32.

Nordquist, C. D., A. Muyshondt, M. V. Pack, P. S. Finnegan, C. W. Dyck, I. C. Reines, G. M. Kraus, T. A. Plut, G. R. Sloan, C. L. Goldsmith, and C. T Sullivan. 2004. An x-band to ku-band RF MEMS switched coplanar strip filter. *IEEE Microwave and Wireless Components Letters* **14** (9) (September): 425–27.

Nordquist, C. D., C. L. Goldsmith, C. W. Dyck, G. M. Kraus, P. S. Finnegan, F. Austin, IV, and C. T. Sullivan. 2004. An x-band RF MEMS tuned combline filter. *Electronics Letters* (Stevenage, United Kingdom: Institute of Electronics Engineers Publishing), submitted.

Yuan, X., S. Cherepko, J. C. M. Hwang, C. L. Goldsmith, C. D. Nordquist, and C. W. Dyck. 2004. Initial observation and analysis of dielectric-charging effects on RF MEMS capacitive switches. *Proc. IEEE MTT-S International Microwave Symposium* **1** (June, Fort Worth, Texas): 1943–46.

Other Communications

Dyck, C. W., C. D. Nordquist, and G. M. Kraus. 2004. RF MEMS technologies fabricated using low-temperature processing. *Proc. SPIE Photonics West* **5342** (January 2005, San Jose, California): 42–50.

Dyck, C. W., T. A. Plut, C. D. Nordquist, P. S. Finnegan, F. Austin, IV, I. C. Reines, and C. L. Goldsmith. 2004. Fabrication and characterization of ohmic contacting RF MEMS switches. *Proc. SPIE Photonics West* **5342** (January 2005, San Jose, California): 79–88.

Nordquist, C. D., C. W. Dyck, G. M. Kraus, C. L. Goldsmith, T. A. Plut, F. Austin, IV, P. S. Finnegan, I. C. Reines, A. J. Carton, K. L. Gass, M. V. Pack, W. D. Cowan, A. Muyshondt, G. R. Sloan, and C. T. Sullivan. 2004. RF MEMS for reconfigurable filters at Sandia National Laboratories. Paper presented at the IEEE MTT-S International Microwave Symposium, June, Fort Worth, Texas.

Nordquist, C. D., C. W. Dyck, G. M. Kraus, T. A. Plut, I. C. Reines, M. V. Pack, A. Muyshondt, G. R. Sloan, C. T. Sullivan, P. S. Finnegan, F. Austin, IV, T. Lemp, G. Schmidt, and C. L. Goldsmith. 2003. RF MEMS for reconfigurable microwave circuits: A switched filter example. Paper presented at the Sandia Labs/Kansas City Plant Joint RF Conference, 18 November, Albuquerque, New Mexico.

52706

Development of a High-Throughput Microfluidic Integrated Microarray for the Detection of Chimeric Bioweapons

J. A. West, B. J. Kirby

Genomic analysis tools have recently become indispensable for evaluating gene expression in a variety of experiment protocols. Two of the main drawbacks to this technology are the labor- and time-intensive process for sample preparation and the relatively long times required for target/probe hybridization. To overcome these two technological barriers, Sandia developed a microfluidic chip to perform on-chip sample purification and labeling, integrated with a high-density gene array. We performed sample purification using a porous polymer monolithic material functionalized with an oligo d(T) nucleotide sequence for the isolation of high-purity messenger ribonucleic acid (mRNA). These purified mRNAs can then be rapidly labeled using a covalent fluorescent molecule that forms a selective covalent bond at the N7 position of guanine residues. These labeled mRNAs can then be released from the polymer monolith to allow for direct hybridization with oligonucleotide probes deposited in microfluidic channels. To allow for rapid target/probe hybridization, we printed the high-density microarrays in microchannels. The channels can accommodate array densities as high as 4000 probes. When oligonucleotide deposition is complete, these channels are sealed using a polymer film that forms a pressure-tight seal to allow sample reagent flow to the arrayed probes. This process will allow for real-time target-to-probe hybridization monitoring using a top-mounted charge-coupled-device (CCD)/fiber-bundle combination. Using this process, we performed a multistep sample preparation of labeled target/probe hybridization in less than 30 min. These results demonstrate the capability to perform rapid genomic screening on a high-density microfluidic microarray of oligonucleotides.

Our results demonstrate the feasibility of fabricating high-density gene-array chips with the capability of performing rapid genomic profiling. The chips are simple to use and easily customizable, allowing for the rapid alteration of probe content. In addition, the entire assembly is miniaturized and can be packaged in a hand-held portable platform for field analysis of biological agents.

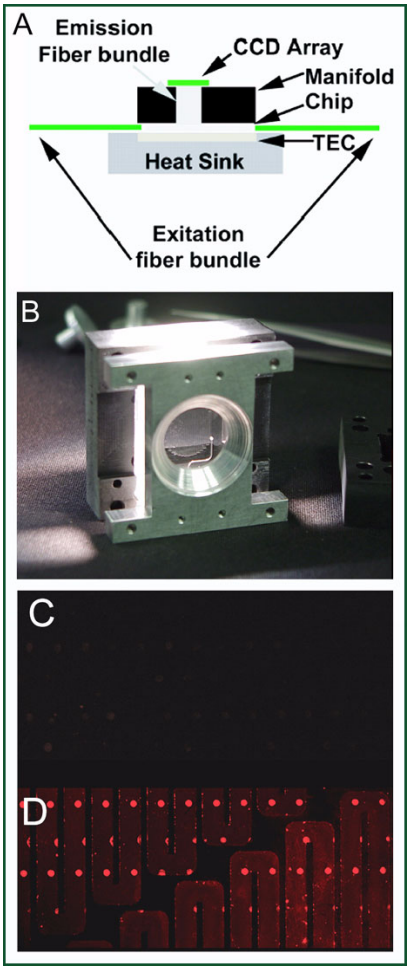

Design, fabrication, and use of the microfluidic gene-array platform. We designed a manifold to incorporate the use of an excitation source, emission light collection using a CCD camera, and a thermocycling apparatus (a). *We fabricated the manifold and associated parts to house the microfluidic chip and associated optics* (b). *Using this system to perform on-chip hybridizations, we found mRNA labeled with Alexa fluor 647 annealed to the nonfluorescent spotted microfluidic gene array* (c) *in less than 20 min* (d).

- *Microfluidic microarray platform*.

(1) We fabricated a microfluidic microarray device with integrated sample-preparation areas.

(2) We wrote software that allows individually addressable microchannel locations to be spotted with deoxyribonucleic acid (DNA) probes for a high-density microarray (up to 4000 probes).

(3) We constructed a polymer monolith for oligo trapping.

(4) We integrated color CCD and fiber optics for fluorescence detection.

- *Enhancing device performance*.

(1) We optimized a labeling strategy to greatly reduce sample-labeling times.

(2) We performed hybridization of mRNAs in a sealed microfluidic device in less than 20 min.

(3) We trapped and eluted mRNA in less than 2 min using a sealed microfluidic device.

We demonstrated a first-generation integrated microfluidic high-density microarray platform (up to 4000 probes) that has the ability to house rapid sample preparation, hybridization, and detection of genomic samples. This allows sample preparation of less than 30 min, including direct labeling of mRNA, trapping of mRNA with porous monolith, and elution with mRNA for hybridization. Most importantly, this device demonstrates the hybridization of mRNA in a microfluidic channel in less than 20 min.

Most importantly, this device demonstrates the hybridization of mRNA in a microfluidic channel in less than 20 min.

Other Communications

West, J. A., K. W. Hukari, G. A. Hux, and T. J. Shepodd. 2004. Microfluidic gene arrays for rapid genomic profiling. *Proc. SPIE Conference* (26 October, Philadelphia, Pennsylvania).

West, J. A., K. W. Hukari, T. J. Shepodd, and G. A. Hux. 2004. A high-density microfluidic microarray platform for rapid genomic profiling. *Proc. Micrototal Analysis Systems (MicroTAS 2004)* **2** (26 September, Malmo, Sweden): 514–17.

West, J. A., R. M. DeVay, and M. Shultz. 2004. Development of a microfluidic microarray for the rapid detection of toxicogenomic signatures. *The Toxicologist* **78** (March, Baltimore, Maryland): 390.

52708

Zero-Power Radio Receiver

R. W. Brocato, E. J. Gurule, G. A. Wouters, M. A. Montaño, J. R. Wendt, E. J. Heller, G. Omdahl

The final product proposed for this project is a radio receiver that is completely passive, requiring no operating power. This receiver will be a much more sophisticated version of the zero-power (ZP) crystal-set radios that were used decades ago. Its construction will leverage developments in Sandia's state-of-the-art capabilities in microfabrication. The modern ZP radio receiver will make use of completely passive electronic components with the centerpiece being a surface acoustic-wave (SAW) correlator.

The SAW correlator required for this radio receiver will make use of a long, precisely selected code at a given frequency to serve as a "key." Previous work demonstrated "key" lengths of 127 bits, or 1038 unique combinations. We will use significantly longer codes here to effectively narrow the receiver bandwidth even more. The radio energy from this "key" can then be used to turn on a transistor switch used to power a standard radio transceiver or other electronic device.

Since the ZP radio receiver requires no operating power, it is ideal for use in waking up remote-sensing systems that may be left dormant for weeks or months at a time. The entire radio receiver will consist of an antenna, input matching network, a SAW correlator, a passive peak-detection circuit, and a field-effect transistor (FET) switch. It can be built in a small button-sized volume (minus the antenna) and could potentially receive signals transmitted via satellite.

Since the ZP radio receiver requires no operating power, it is ideal for use in waking up remote-sensing systems that may be left dormant for weeks or months at a time.

The problem of building a radio receiver that operates without direct-current (dc) electrical power has been around for as long as radio has existed. Some of the earliest available radio receivers, referred to somewhat confusingly as "crystal-set" radios, used a very simple circuit with a germanium-diode detector (the "crystal") to demodulate fairly strong amplitude-modulation (AM) radio stations. Early radio users did not have readily available low-cost dc power supplies or batteries and thus needed to use a passive radio. Though modern users may not have the same battery constraints as in the past, they may need a radio receiver that can remain dormant for months or years.

The basic principle behind both the crystal-set and other ZP radio receivers is that they use a high-Q [quality] circuit to selectively receive a signal. These receivers then use a

demodulator to transform a very small impedance into a high impedance. The high-Q circuit selectively receives the appropriate portion of radio spectrum from the entire spectrum, and the demodulator efficiently converts a small amount of energy at a low voltage and a high frequency into a slightly smaller amount of energy at a much higher voltage with a low frequency. Both of these elements are the keys to making an efficient ZP receiver. A modern ZP receiver includes the following elements: a very high Q circuit to select frequency, a detector to demodulate a desired signal from a radio-frequency (RF) carrier signal, and a signal processor to further refine the demodulated signal.

The special component that provides the requisite high Q-factor is the SAW correlator. A SAW correlator combines the narrowband, high Q-factor operation of a bandpass filter with a coded reception scheme that further enhances the Q-factor by the use of coding gain. The SAW correlator effectively enables the reception of a very narrow band of signals while still using a broad bandwidth to transmit the signal. The SAW correlator is a completely passive device. It uses the electromagnetic energy in the input RF wave to convert to an acoustic wave that is subsequently used in a matched filter. The SAW correlator's Q-factor is directly proportional to the code length of the device. Therefore, it is important to maximize the code length of the correlator. The ideal ZP receiver consists of a very long SAW correlator connected directly to an antenna on one end and a highly efficient, demodulating detector on the other end.

We devised, built, and tested ZP radio receivers suitable for a variety of different applications. The SAW correlators built for the various ZP radios exhibited very good levels of performance. However, true ZP radio performance is adequate only in high-signal-level applications. Improvements to passive demodulator/ detectors are needed to improve the low-signal-reception capabilities of the ZP radio. We obtained significant improvements in radio performance by using very low-power detectors and amplifiers. The current SAW correlator–based radios suitable for a wide range of applications are very low powered receivers, possibly lower than any other comparable technology. True ZP radio receivers based on SAW correlators are very viable but need improved passive detectors to achieve high levels of sensitivity.

Refereed

Brocato, R. W., E. J. Heller, J. R. Wendt, E. J. Gurule, G. Omdahl, C. Gibson, J. Smith, and D. W. Palmer. 2003. Ultrawideband communication using a SAW correlator zero-IF architecture. *Proc. IEEE Topical Conference on Wireless Communication Technology* **1** (15–17 October, Honolulu, Hawaii): s27p04.

52709

Completely Passive Microwave Tag

R. W. Brocato, J. D. Blaich, G. A. Wouters, E. J. Gurule, J. R. Wendt, E. J. Heller, G. Omdahl

This project will build a completely passive, radar-readable tag to work at frequencies of 1 to 5 GHz. Recent advancements in Sandia's surface acoustic-wave (SAW) microfabrication capabilities indicate that it is possible to build a SAW–based, completely passive tag that will work with low-power microwave radars. This expands on previously developed SAW correlators. The tag size will be 1 mm^3, minus the antenna.

A SAW correlator delivers a frequency-modulated impulse signal when stimulated with a properly phase-coded signal at the correct frequency. The impulse signal from a receiving SAW correlator can be used to drive a second SAW correlator. The impulse response of the second SAW correlator can be another unique code that will be transmitted back to the exciting radar. The principle is similar to that used in a microwave corner reflector, but the advanced coding capability of the SAW correlator enables use of a complex and unique code. The returning signal will appear as a unique, very wideband, and very discrete signature to the tracking radar. The return signal may also be below the background-noise level, but can still be highly detectable due to its spread-spectrum, coded nature.

A passive microwave tag should enable low-cost, long-term tagging and tracking of objects from low-power, ground-based radars. This can enable tracking of goods within a facility without the vulnerabilities of current passive-tag–based systems. This can also have applications for vehicle- or people-tracking in homeland defense, nonproliferation, and security applications. The final milestone will be a fieldable, passive tag of immediate use in one or more Sandia system applications.

We generated both a general methodology and some specific examples of completely passive microwave tags. We used SAW devices to provide both identification and sensing tags at different frequencies. We optimized SAW correlators for identification-related applications and developed SAW filters for a variety of different sensing applications.

The specific focus of this work can be called *passive remote tag sensing*. Passive remote tag sensing is the ability to wirelessly either identify a tag or measure some physical property from a tag without using additional direct-current (dc) power at the tag. It requires the careful sensing and retransmission of the original radio-frequency (RF) signal sent

from an interrogation device. The interrogation device can be thought of as a radar, though it differs greatly from aviation radars. The basic principle is that an interrogation device will send an RF signal and will receive a response from any tags in the vicinity.

Since it is generally essential to differentiate one particular tag of interest from any other tags that might be in the vicinity, the tag must either respond to any general interrogation with a unique code, or the interrogation must be specific to the tag of interest. For general interrogation, each tag must be encoded, typically with phase coding, to provide a unique signature to the general interrogation pulse. In addition, each interrogation device must be able to distinguish between all coded tags of interest within range. For specific interrogation, we designed the tags to respond to different narrow-frequency bands, and the interrogator can select the tag of interest by changing the interrogation frequency. We accomplished both the frequency and code space separation in the tag by means of SAW devices. SAW filters provide narrow-band frequency separation and thus are well suited to specific interrogation. SAW correlators provide a coded response to a general interrogation or a general response to a specific interrogation. As a consequence of these properties, SAW filters are useful for remote sensing, and SAW correlators are useful for tag identification.

Consider first a SAW filter–based passive remote-sensing application. Each sensing arrangement will consist of (1) a small radio transmitter sending out a short burst of RF waves, (2) a SAW–based tag both receiving and modifying a portion of that signal, and (3) a receiver to pick up the transmitted and modified pulse. A SAW–based sensor tag is a frequency-selective device that responds to the sensor-impedance load connected to its output port. Amplitude variations in the received signal correlate to the sensor impedance. The sensor impedance can then be measured back at the receiver. A proper application of a narrow-band SAW filter enables clear reception and measurement of the sensor impedance.

For SAW–based identification systems, we use a SAW correlator for the central part of the tag. A SAW correlator is a frequency- and code-selective device that can respond in two different modes. In a specific interrogation mode, the correlator responds with a noncoded pulse only in response to the correct frequency signal with the correct code transmitted from the interrogator. The transmitter sends a coded interrogation pulse that is received and processed into a frequency-modulated pulse by the tag. The desired correlator responds only to the correct frequency signal with the correct code. This is referred to as

specific interrogation, since the interrogator controls the code and must select which correlator it wishes to respond. The correlator responds to the specific interrogation by outputting a modulated pulse at the same frequency as the input signal. The SAW correlator is an acoustic device, just like the SAW filter, and it delays its output pulse until after all undesirable radar signals have died away. All SAW correlators within range of a given transmitter and with a center frequency set to that of the transmitter will respond to that interrogation. However, only the correlator with the matching code to the one transmitted will respond with a correlation peak. All other correlators will respond with pseudorandom noise. Because these two responses are easily differentiated, only the specifically selected correlator can be deemed to have responded.

Refereed

Brocato, R. W., E. J. Heller, J. R. Wendt, J. D. Blaich, G. A. Wouters, E. J. Gurule, G. Omdahl, and D. W. Palmer. 2004. UWB communication using SAW correlators. *Proc. IEEE Radio and Wireless Conference (RAWCON)* **1** (19–22 September, Atlanta, Georgia): T4B.5.

52710

Security Coatings for Multichip Modules

R. A. Neiser, Jr., A. C. Hall, D. J. Cook, D. A. Hirschfeld

Sandia's goal in this project was to develop tamper-resistant coatings for multichip modules (MCMs) used in military electronics. Much of the current edge that exists for the U.S. military is reliant on sophisticated electronics. Protecting this valuable technology is becoming an increasingly important consideration in battlefield deployment and foreign military sales of military equipment. The central task of this project was to develop a coating system that could be applied to MCMs. Currently available tamper-resistant coatings are limited in number. The proposed solution offers a number of advantages over existing technology. Effective tamper-resistant coatings must provide good protection to the electronic parts while not affecting their functionality. The coatings must also be relatively inexpensive and easy to apply. Furthermore, the coating process should have sufficient flexibility to accommodate different board compositions, geometries, chip sizes, and operating conditions (e.g., temperature and humidity ranges, vibrations, and accelerations). Our approach was to synthesize a number of candidate coating materials, apply them to test coupons, and evaluate their performance.

We evaluated four coating materials: three different ceramic powders and a ceramic rod. We also designed and built a new type of electronic test vehicle (the STV3) that offers some advantages over our previous test vehicles for this project. In addition, we conducted a study to evaluate a new technique for improving the adhesion of the coatings to MCMs.

We placed a contract with an outside firm to manufacture two of the proposed coating materials that were not readily available commercially. When they arrived, we applied these two materials under a wide variety of processing conditions; however, it proved impossible to develop an acceptable coating with either of these two materials.

We applied a third proposed coating material, which was available commercially, to the Sandia-designed electronic test vehicle. The STV3 remained functional after the coating was applied, and the coating performed well in several evaluation tests.

We conducted a study to determine whether an alternate application process could be used to produce tamper-resistant coatings. We produced a process map that showed that a wide range of conditions could be used to produce coatings.

However, the operating conditions damaged the microelectronics, so this process should not be considered for this application.

We also performed work to increase the adhesion of the coating to the microelectronic circuit board and explored an alternate bonding approach. We conducted experiments with a number of materials applied at different processing conditions to investigate this alternative approach. The results of the experiments showed that thick coatings could be rapidly applied to this bonding material and suggest that the use of this new approach could improve the bond strength of the tamper-resistant coatings while simultaneously improving process economics.

52711

Detailed Modeling and Simulation of Contaminant Transport in Architectural Spaces

C. E. Hickox, Jr., G. H. Evans, W. S. Winters, Jr., J. E. Brockmann, M. J. Martinez, D. K. Gartling

This project addresses the modeling and simulation of contaminant transport in interior architectural spaces. Geometries of interest can range in scale from offices and conference rooms to large public spaces such as airport terminals, shopping malls, and arenas. The work is motivated by concerns about the risks associated with the possibility of attacks on buildings with chemical and biological (C/B) agents. In this regard, it is noted there are two important applications for this endeavor: mitigation of the effects of attacks with C/B agents to reduce the risk of exposure to individuals, and decontamination of exposed structures. Sandia's goals in this project are to (1) develop a multizone simulation capability, (2) link multizone simulations with computational fluid dynamics (CFD) simulations, (3) determine effective CFD simulation strategies for the prediction of contaminant transport, (4) develop simplified modeling approaches to improve the efficiency of CFD simulations, and (5) validate predictions through comparisons with existing experimental data.

- We developed a multizone code, NETFLOW, to the point where it is now a viable resource for the prediction of contaminant transport in complex interior spaces, and we documented the application of NETFLOW to contaminant transport studies performed in the German Village Exercise at the U.S. Army Dugway Proving Ground. Contaminant concentrations predicted with NETFLOW are shown to be in good agreement with experimental data. Furthermore, we elucidated the sensitivity of predicted results to atmospheric conditions and the mass of contaminant released.
- We developed two approaches for the coupling of multizone and CFD simulations and applied them to model problems. We based one approach on an explicit coupling and a control-volume CFD modeling strategy. A complementary approach uses an implicit coupling with a finite-element–based CFD simulation.
- We performed a simplified CFD simulation, based on inviscid flow theory, for a two-room enclosure. The results

indicated that further modifications of this approach are needed to produce more-realistic results.

- We compared laminar and turbulent transport via CFD simulations for several model rooms. We observed significant differences among some of the modeling approaches. Additional studies will be required to determine which approaches most accurately represent the transport of contaminants in rooms.
- We gave initial consideration to the application of the SIERRA CFD code FUEGO to simulations of contaminant transport in rooms.
- We compared some initial CFD simulations with the limited data available to validate the flow within a model room.

Ad hoc measurements of velocity fluctuations in a conference room at Sandia demonstrated the variability of velocity at discrete locations and indicated the possible need to consider such fluctuations in predictive methods for contaminant transport.

Other Communications

Winters, W. S., and B. M. Rush. 2004. Application of NETFLOW to the 911-bio consequence management ACTD German village exercise. Sandia Technical Report SAND2004-3099, Sandia National Laboratories, Albuquerque, New Mexico.

52712

Content-Based Video and Image Indexing System

T. D. Russ, J. C. Garrison, M. R. Muguira

Video and image data are knowledge-rich sources of information, but their utility for current and future systems is limited without autonomous methods for understanding and characterizing their content. The proposed system addresses this issue by exploiting the spatial and temporal information available in video imagery to gain scene understanding. This will allow video imagery to be organized by spatial objects that may include faces, and by targets identified by the motion signatures associated with their objects, and/or even by the interactions between objects that occur in a sequence of images. This information can then be used to autonomously characterize video data and/or provide content-specific information to a number of systems that seek information from images and video. Such capabilities may benefit systems dedicated to the detection of insiders, alarm patterns, unauthorized activities in material-monitoring applications, etc. A direct benefit of this approach is the ability to browse and perform query-based searches for useful and interesting information after video data have been acquired and stored. These searches can provide a tremendous benefit for use in intelligence agency, government, military, and Department of Energy site investigations.

A direct benefit of this approach is the ability to browse and perform query-based searches for useful and interesting information after video data have been acquired and stored. These searches can provide a tremendous benefit for use in intelligence agency, government, military, and Department of Energy site investigations.

In earlier work, we established the system architecture and initial algorithms to enable the searching of video information from an archive of video sequences. Because the initial algorithms for object segmentation and object tracking were somewhat simplistic and would not enable the implementation of motion-based recognition with success, we devoted efforts to improving these foundational algorithms in recent work.

The first task was to move the video storage component into C++, the same platform as the video processing and searching components. This improved the interface between the different system components. In the next task, we sought to improve the quality of the object segmentation being performed by the video archiving unit. Previously, the video archiving system identified pixel-intensity changes from a background model or a previous image frame. However, when objects in motion are similar in appearance to the background model, insignificant changes are not detected, resulting in broken objects or objects with holes that do not accurately represent object characteristics. The

ability to obtain coherent object descriptions was important to our ultimate task of being able to recognize objects and their motions by observing their spatiotemporal profiles. We looked at a number of strategies to address this problem. Our initial strategies included using (1) more-sophisticated background models, (2) intensity-based scene-segmentation approaches, (3) motion edges as a cue to bound moving regions, and (4) improved connected-component algorithms. Of these, improved background models and connected-component algorithms were the most beneficial. Our previous background model was sensitive to temporally local changes in pixel intensities, even using individual pixel means and variances to determine a separate change threshold for each pixel, and a statistical background update model did not completely remove this sensitivity. Transitioning to a mode-based (maximum gray-level to occur over time) approach for estimating the background enabled a noticeable improvement in performance. The computational cost associated with this approach was minimal, thus still enabling approximate real-time processing capability. We implemented a quasi-connected-component labeling algorithm developed at the University of Colorado at Colorado Springs to obtain connected objects from pixel-change images with minimal holes and broken objects. Connecting components were computed at a reduced image resolution using a parent image generated by accumulating information from a hysteresis-thresholded pixel-change image. Because of the computational load associated with connected-component analysis, we devoted some effort to a fast-connected-component (FCC) analysis algorithm, but did not complete this task.

We also developed tracking algorithms, another key component needed to realize motion-based recognition. Again, we investigated multiple approaches, including an object-cluster tracking algorithm, the KLT (Kanade-Lucas-Tomasi) feature-based tracking algorithm, and a Hausdorff edge-based tracking algorithm. The vision behind investigating multiple approaches is that gross object characteristics could be used to obtain an initial correspondence that can be refined with feature-match scores (i.e., points or edges). To accommodate large interframe motions, we adopted a multiresolution pyramid scheme. This enabled larger search regions to be explored without incurring the associated cost of examining every pixel within the defined search window.

This project enabled the investigation and resolution of many issues related to video analysis and processing. We did not achieve our ultimate goal of motion-based recognition;

however, we laid a solid foundation for enabling this capability in the future. Currently, the system can store video in a compressed manner, process video for objects, track objects, and compute object and motion characteristics that can be searched. The next steps for system development consist of identifying patterns in motion that can be interpreted as events, and defining algorithms that can recognize objects and motion events.

52713

Bioaerosol Collection and Concentration for Microseparations-Based Detectors

K. Wally, E. B. Cummings, M. P. Kanouff, D. J. Rader, C. R. Ellis

The ability to detect biological agents is vital to national security and homeland defense needs, spurring development of compact systems for sensitive field detection of these agents. A universal challenge for these systems is the efficient autonomous collection and selective concentration of highly dispersed threat agents for detection against the enormous background of benign particles. The challenge is even greater when the goal is concentrated liquid microsamples for input to liquid-based microanalysis and detection systems. A general approach is to follow a two-stage strategy of aerosol collection followed by post-collection concentration to microsample levels. The greater the ability of the collection stage to separate and concentrate, the less the demand placed on the post-collection concentration stage. Conversely, the greater the capabilities of the concentration stage, the more tolerant to the performance of the collection stage. These twin considerations guided our development activities as we worked to perfect Sandia-proprietary collection and concentration technologies for this purpose. In the area of aerosol collection technology, we are pursuing a strategy of focusing and inertial separation via aerodynamic particle size to achieve initial concentration and separation sufficient to allow impingement collection into mere microliters of liquid collection solution. We are exploiting our microfluids and electrokinetic flow capabilities to attempt direct micro-impingement collection into open microchannels of collection fluid. Such an approach minimizes otherwise large evaporation losses and provides minimal input volume to burden subsequent post-collection concentration stages. In the area of post-collection particle concentration in liquid, we pursued a strategy of exploiting dielectrophoretic phenomena to concentrate and selectively sort particles. Our unique approach uses arrays of passive dielectric microstructures rather than arrays of electrodes. For concentration of solubles, such as biotoxin proteins, we are considering a variety of physical, electrical, and chemical means.

Our unique approach uses arrays of passive dielectric microstructures rather than arrays of electrodes.

Through refinement of the opposed-flow virtual cyclone (OFVC) microseparator technology, we developed a highly effective means to continuously separate the respirable (1–10 µm particle diameter) fraction of particles from aerosol samples and to deliver those respirable particles in an extremely focused

stream (line or spot) for impingement collection, deposition collection, real-time laser interrogation, etc.

With the direct microimpinger development, we demonstrated a rudimentary ability to impinge a highly focused stream of respirable particles directly into a microfluidic collection and transport system. In the course of this microimpinger work, we encountered the phenomenon of the capture and trapping of microparticles (< 10 μm particle diameter) in (on) the free surface of a collection liquid due to surface-tension forces. This phenomenon obtains for microparticles if impinging at any velocities less than extremely high velocity (i.e., 100 m/s, "hurricane" wind velocity). Although the existence of this surface-tension particle-trapping phenomenon might have very nearly scuttled the concept of direct microimpingement, we were able to demonstrate the feasibility of microdroplet bombardment as a means of wetting and submerging microparticles trapped by surface tension. Practical implementation needs further development.

With the invention and development of the corduroy dielectrophoretic design methodology (CDDM) for the dielectrophoretic concentration and/or sorting of particles, we produced a world-class technology that significantly advances the state of the art. One can anticipate that this development is likely to achieve significant recognition and, ultimately, important application in the field of microfluidics. Easy to engineer and intuitive, the technique incurs little or no added costs and achieves great performance improvements compared to the previous state of the art. As its inventors have remarked, "The ability to make a two-obstacle automatic and high-throughput particle spectrometer that requires only a single dc [direct-current] power supply is truly remarkable, and certainly exceeds our wildest hopes at the start of this project."

With respect to unmet expectations, an initial objective of this was to demonstrate an integrated "front-end" system capable of the collection, preconcentration, and selective transport of aerosolized biological agents from dilute atmospheric concentrations to microliter liquid concentrations for interfacing with micro-Total Analysis Systems (μTAS), such as Sandia's μChemLab™, for identification of bioagent bacteria and spores. Although our work demonstrated, to a greater or lesser extent, individual needed "front-end" technologies, we were not able to achieve our goal of an integrated demonstration before the project ended. However, each of the technologies (inertial microseparator, direct microimpingement, dielectrophoretic corduroy concentrator/

With the invention and development of the corduroy dielectrophoretic design methodology (CDDM) for the dielectrophoretic concentration and/or sorting of particles, we produced a world-class technology that significantly advances the state of the art.

sorter) should, independently, prove greatly useful in a variety of additional applications.

Other Communications

Wally, K., E. B. Cummings, C. R. B. Ellis, M. P. Kanouff, and D. J. Rader. 2004. Bioaerosol collection and concentration for microseparations-based detectors. Sandia Technical Report, Sandia National Laboratories, Albuquerque, New Mexico (in preparation).

52714

Detecting the Toolmarks of Genetic Engineering in Bioweapons Strains

T. W. Lane, P. Lane, J. S. Brennan, R. Sapra, Y. K. Light

Although the incidence of infection by naturally occurring strains of biowarfare agents is low, it is important to discern the difference between infection by a natural background strain and by an unusual strain that may have been enhanced by genetic engineering. A number of vectors exist for the cloning and expression of genes in important taxa such as Bacillus. *These are the genetic engineer's tools used to alter an organism, and traces of their use can be left modified in the organism. These toolmarks take the form of genetic elements such as exogenous promoter sequences, antibiotic resistance genes, and multiple cloning sites. By detecting these, one can discern the difference between a naturally occurring strain of an organism like* B. anthracis *and one that has been genetically modified.*

A finite but growing number of vectors exist for Bacillus. *Sandia seeks to analyze the toolmarks left behind by genetic modification by each of these vectors, then developing polymerase chain reaction (PCR) and hybridization technologies to detect these modifications. These toolmarks can be predicted by modeling and then verified experimentally. There may be multiple ways of detecting a given vector, and many vectors may share the same toolmarks. It will not then be necessary to experimentally verify each vector. The end product of this work will be an integrated assay in a microarray architecture designed to detect genetically engineered pathogens. This work would be carried out in* B. cereus, *a strain closely related to* B. anthracis. *The techniques will be applicable to other organisms.*

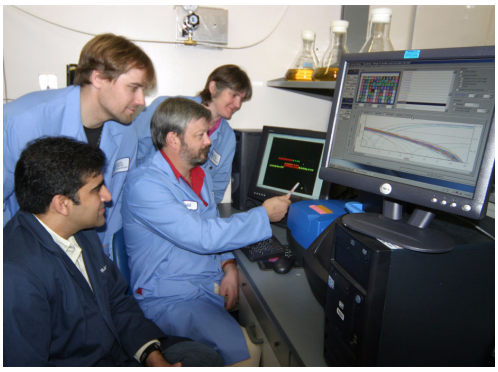

Sandia Researchers Todd Lane (seated), *Pamela Lane, Rajat Sapra, and Jim Brennan examine data from a microarray experiment designed to detect genetically engineered microorganisms.*

We created a microarray system for the detection of nonspecific evidence of genetic engineering in bacterial systems. We developed and validated methodologies for detecting toolmarks from both replicative and integrated vectors and in both gram-negative and gram-positive bacterial hosts. We also devised a primer set and methodology for detecting toolmarks by real-time PCR. We tested both the PCR and microarray methods with a variety of plasmids in different bacterial species.

We developed a microarray method for the detection of nonspecific evidence of genetic engineering. Using the custom microarray spotter that we built earlier, we spotted microarrays containing 60 base oligonucleotides corresponding to each

toolmark. We developed and validated methodologies for the labeling and hybridization of target deoxyribonucleic acid (DNA) to the arrays. We also developed and validated methodologies for the isolation and amplification of DNA from both integrated and replicative plasmids from single bacterial colonies for hybridization to the toolmark microarray. We tested these methodologies against a variety of integrated and replicative plasmids in both gram-negative and gram-positive bacterial hosts. We extended the goals of this project by creating a primer set that can be used in conjunction with real-time PCR to detect toolmarks. This gives us an alternative to microarray hybridization as a methodology for toolmark detection.

52716

Joint Authentication/Encryption

T. J. Draelos, W. E. Anderson, R. D. Miller, C. L. Beaver, M. D. Torgerson, R. C. Schroeppel

In this project, Sandia addresses three primary issues associated with systems that perform both encryption and data authentication:

(1) Combine encryption and data-authentication operations. For example, during encryption, hash the internal state of the cipher instead of the entire message for authentication. In some cases, authentication would be free with encryption.

(2) Minimize the size of the authentication tag. The bandwidth overhead of data authentication can often be a problem, especially for small messages.

(3) Explore efficient software and hardware implementations of joint encryption/authentication algorithms.

We invented a new paradigm for authenticated encryption, where the internal state of the cipher is used for authentication. One of the algorithms, ManTiCore4 (MTC4), which is based on cryptographic hash functions, is provably secure against combined chosen plaintext/ciphertext attacks. Because of the hash-function construction, MTC4 supports variable encryption block sizes up to twice the hash output block length and trivially supports variable key lengths. When using the largest encryption block size, the time to encrypt and authenticate a message is a small multiple of the time it would take to hash the entire message. This class of ciphers also has encryption properties similar to the cipher-block-chaining (CBC) mode, yet the encipherment and authentication mechanisms can be parallelized and/or pipelined. We also invented a more general construction for using the state of a block cipher as an authenticator.

- *Develop very high speed integrated circuit (VHSIC) hardware description language (HDL) implementation of authenticated encryption algorithms.* We developed VHSIC HDL code for the MTC4, RMTC4 (Reduced ManTiCore4), Pepper, and CS (Cipher State)-AES (Advanced Encryption Standard) authentication encryption algorithms to simulate and prepare for a hardware implementation.
- *Incorporate algorithms into Sandia's cryptographic software library.* We developed C and C++ software to test the functionality and performance of our authenticated encryption algorithms.

- *Conduct research on shorter authentication tags*. We did not make any advances on the size of the authentication tags. One can simply shorten the size of the authentication tag with a corresponding reduction in its security.
- *Prove facts about information revealed in authentication tags*. We developed proofs of security regarding data privacy and integrity for the MTC4 algorithm.
- *Pursue acceptance of best algorithms into standards bodies*. We submitted the CS-AES algorithm specification to the National Institute of Standards and Technology (NIST) as a candidate for an authentication encryption standard.

We submitted the CS-AES algorithm specification to the National Institute of Standards and Technology (NIST) as a candidate for an authentication encryption standard.

Refereed

Anderson, W. E., C. L. Beaver, T. J. Draelos, R. C. Schroeppel, and M. D. Torgerson. 2004. ManTiCore: Encryption with joint cipher-state authentication. *Proc. 9th Australasian Conference on Information Security and Privacy* **LNCS 3108** (July, Sydney, Australia): 440–53.

52717

Ultrahigh-Temperature Ceramics for Hypersonic Vehicle Applications

R. E. Loehman, S. J. Glass, P. G. Kotula, D. W. Kuntz

Re-entry vehicles require control surfaces with sharp leading edges if they are to be maneuverable at hypersonic velocities. Low-radius leading edges are subject to much greater aerothermal heating than blunt edges, such as in the space shuttle, and thus will reach temperatures that may exceed 2000°C during re-entry. Available thermal-protection materials will not survive such extreme temperatures, and new materials are required for advanced thermal-protection systems.

The goal of this project is to develop more heat-resistant thermal-protection materials based on zirconium diboride (ZrB_2) and hafnium diboride (HfB_2). Those compounds and composites in which they are the primary constituent are referred to as ultrahigh-temperature ceramics *(UHTCs) because they have some of the highest melting points known, above 3200°C. Previous attempts to make these UHTCs have shown mixed results, and the properties obtained have been inconsistent.*

The specific objectives of this project are to (1) develop improved processing for HfB_2– and ZrB_2–based UHTCs, (2) develop a database of reliable UHTC physical and mechanical properties, (3) determine the relation between UHTC microstructure and properties using advanced electron microscopic analysis, (4) simulate realistic thermal histories using computational modeling that incorporates reliable properties data, and (5) determine the origin and type of failure for UHTCs subjected to realistic stresses and feedback to improve processing. Sandia is using the results to gain an understanding of the performance-limiting features of the UHTC specimens, which in turn is helping us to make better UHTCs.

We previously described the processing of high-quality ZrB_2 and HfB_2 ceramics. We developed methods to make high-quality test specimens, typically as cylinders up to 6 cm in diameter. We recently concentrated on measuring UHTC properties and characterizing microstructures.

We made substantial progress toward our goal of learning how to make superior UHTCs and then determining the properties needed to make intelligent design decisions. We made ZrB_2–silicon carbide (SiC) and HfB_2–SiC UHTCs with excellent properties in compositions as low as 2 vol.% SiC.

Previous attempts by others to make thermal-protection materials in those systems required 20% SiC. We demonstrated a wider range of compositions than was previously known, which gives designers more options in optimizing thermal-protection systems for hypersonic re-entry applications.

We made the UHTCs by pressing powders at 2000°C and 5000 psi in a vacuum hot press. We made the different UHTC compositions as cylindrical billets 3 in. in diameter and 1 ½ in. high, which for the HfB_2 specimens weigh more than 400 g. One of the outstanding scientific issues in processing the UHTCs is why at least 2% of additives such as SiC or WC are required to achieve full density. That result suggests the UHTCs densify by a liquid-phase sintering mechanism, but until now there has been no evidence for such a mechanism. If we understood the densification mechanism, we might be able to devise a pressureless sintering process that would allow us to make bigger parts much more cheaply, and possibly with better high-temperature properties.

If the UHTCs densify by a liquid-phase sintering mechanism, we would expect to find evidence of second phases on the grain boundaries in the dense ceramics. Previous attempts using scanning- and transmission-electron microscopy (SEM/TEM) did not show any residual grain-boundary phases, and thus the role of the additives and how they affected the densification were unclear. Our recent microstructural analysis using high-resolution electron microscopy coupled with Sandia's spectral-image analysis technique provided the first evidence of grain-boundary phases in the UHTCs. We observed very narrow silicate grain-boundary phases some tens of nanometers thick, and we determined their compositions and locations. Although much more extensive analysis will be required before we can be definitive, results so far suggest that oxide impurities in the SiC additives react at 2000°C to make a small amount of liquid that promotes densification. Softening of such phases could explain the falloff in strength above 1200°C observed by others in their UHTCs.

We determined the thermal diffusivities of the ZrB_2– and HfB_2–based UHTCs as a function of composition from room temperature to 2000°C. We measured the heat capacities and the expansion coefficients of the ZrB_2 compositions, which allow us to compute their thermal conductivities. We will measure the heat capacities of the HfB_2–based UHTCs in upcoming work. We found that the thermal-diffusivity and thermal-conductivity data for both families of ceramics are in a moderate range and somewhat below the values for SiC. The thermal-transport values for the ZrB_2–SiC and HfB_2–SiC

composites follow a rule-of-mixtures relation using the data for the pure components.

We measured the mechanical properties of the ZrB_2– and HfB_2–based UHTCs to determine the relationships among properties, microstructure, and processing. We measured the fracture toughness for ZrB_2–SiC with SiC contents of 5, 10, and 20 vol.% SiC using the chevron-notch technique. This method is more difficult than the popular diamond-indent technique, but it gives much more reliable results for multiphase ceramics such as these UHTCs. We obtained room-temperature fracture-toughness values of 5.1 to 6.2, with no systematic dependence on composition. These values are quite good, particularly for ceramics that have not been optimized for their mechanical properties. It is worth noting that these values are about 50% higher than the ones reported this year by the National Aeronautics and Space Administration (NASA) Ames Research Center Thermal Protection Materials and Systems Branch group for their HfB_2–20% SiC material.

These [room-temperature fracture-toughness] values are quite good....[and] are about 50% higher than the ones reported this year by the...NASA Ames Research Center Thermal Protection Materials and Systems Branch group for their HfB_2–20% SiC material.

Refereed

Loehman, R. E., H. P. Dumm, B. Gauntt, P. G. Kotula, R. Tandon, and D. Zschiesche. 2004. Preparation, microstructures and thermomechanical properties of HfB_2–SiC and ZrB_2–SiC ultrahigh-temperature ceramics. *Proc. 2004 National Space and Missile Materials Symposium* (July, Seattle, Washington).

52718

Leveraging Robotic Planning for Physical-Security Analysis

P. G. Xavier, J. B. Rigdon, T. H. Peters, S. E. Jordan, M. K. Snell, R. R. Peters

*Physical-security analysis against terrorists attempts to estimate a minimum probability of system effectiveness, PE. The assumed model is PE = PI * PN, where PI is the probability of interruption (detecting adversaries in a timely sense) on a path through a graph modeling the site, and PN is the probability that the security forces neutralize the adversary force in combat, given timely detection. Current tools find only PI-minimizing paths, and there is no guarantee that such a path will result in the minimal PE. PN estimates are based on labor-intensive, human-in-the-loop simulations.*

This project brings together path-planning and vulnerability-analysis expertise to better estimate the minimum PE. The basic idea is to develop approximation models for the PE for which best (minimizing) paths can be found by applying or extending robot path/trajectory planning techniques. These models should identify lower PE candidate paths than the best PI paths because they consider attrition.

Sandia is developing an approximation model, associated planning algorithms, and a planning tool for finding best paths based on minimizing the PE for a key adversary—a designated adversary team member whose purpose is to personally commit the act of theft or sabotage that is the main goal of the adversary mission.

In recent work, the baseline prototype planning tool became functional, and we demonstrated its use. Subsequent enhancements enabled (1) application to multiple-adversary attack analysis based on disrupting the key defender; (2) interactive, geometry-aware modification of underlying three-dimensional (3-D) spatial path networks; and (3) finding optimal conditional plans that take into account probability of detection (P_d) and probability of effectiveness given detection.

Our accomplishments this year built on previous work. Briefly, our previous accomplishments can be summarized as follows: (1) We developed a theoretical framework for estimating system effectiveness PE(K) against a designated adversary entry team member K (the key adversary). Our model takes into account barriers (delay and detection), alarms, multiple-guard patrol and response patterns, and attrition. Our framework includes a series of problems with increasingly

relaxed assumptions, and we have been developing algorithmic approaches to finding paths that approximately minimize PE(K) with respect to them. (2) We finalized an algorithmic approach for the basic problem of planning a key-adversary entry path to its goal, while minimizing exposure with respect to a particular set of guard trajectories; the basic idea is to "lift" the problem into space-time. (3) We began implementing the system architecture for a deliverable prototype, including a basic graphical user interface (GUI) design, an ability to read site-model data files, 3-D representation, etc. (4) We developed an algorithmic approach that enables the optimal adversary plan to account for P_d.

In recent work, we continued developing the prototype. An important development was the implementation of a highly modular search framework, beginning with a small graph-based search library designed for easy integration with any underlying graph data structure and with lazily constructed state-space graphs. This effort resulted in a functional prototype tool that included an implementation of our algorithm for the basic problem, and we demonstrated this capability.

We then proceeded to enable application to multiple-adversary attack analysis. The first enhancement enabled accounting for individual guard contributions to path cost (system effectiveness) as a function of time. The second enhancement consisted of two methods for finding candidate secondary (and tertiary, etc.) adversary unit paths to disrupt a given response unit. Thus, a user can apply the tool to find trajectories for an adversary team member to disrupt the guard that is the key defender with respect to the key adversary's planned trajectory. In addition, the user interface was enhanced with input from analysts to enable interactive editing of the underlying 3-D spatial path network that automatically conforms to site and terrain geometry. The path network is automatically adapted to account for barrier models just before path planning takes place.

Finally, we implemented and integrated an algorithm into the prototype for finding conditional plans that take into account P_d and probability of effectiveness given that detection has occurred. We demonstrated the enhanced prototype tool, the implementation of which builds on our modular search framework. The prototype tool runs on personal computers running either Linux or Windows, and we produced documentation for it.

We also worked out theoretical but implementable extensions that build on this new capability to relax problem

assumptions and to make the software more generally applicable when implemented.

We are preparing two patent/technical advance disclosures.

Other Communications

Jordan, S. E., M. K. Snell, P. G. Xavier, R. R. Peters, T. H. Peters, and J. B. Rigdon. 2004. Leveraging robotic planning for physical-security analysis: LDRD project final report. Sandia Technical Report, Sandia National Laboratories, Albuquerque, New Mexico (in preparation).

52720

Ultralightweight Telescope with MEMS Adaptive Optic for Distortion Correction

O. B. Spahn, G. D. Grossetete, W. D. Cowan, A. J. Grine, D. J. Dagel, S. S. Mani, C. A. Boye, D. P. Adams

Sandia continued to improve the mirror figure. We employed processes common to SUMMiT V™ (Sandia Ultraplanar Multilevel MEMS Technology V), such as chemical-mechanical polishing (CMP), to modify the final mirror figure. We also made a concentrated effort on actuator design, fabricating, and testing several types of actuators for their suitability for adaptive-optics applications. We implemented advances in both the actuator design and the mirror figure in novel mirror-array designs. We implemented several of such mirror arrays with varying degrees of design aggressiveness and therefore risk, and are currently in the process of fabricating them. The mirror arrays represent the state of the art in terms of number of elements, complexity of motion, and available stroke.

We also conducted studies of system requirements for optical microelectromechanical systems (MEMS), as well as a review of other potential applications. A collaboration with the Air Force Research Laboratory (AFRL) emerged as a result of these activities, among others.

Continued work on mirror surfaces yielded information on CMP of the top layer of polysilicon (poly4). We found that CMP was able to reduce surface roughness from 2–4 nm to 1.2 nm and reduce the topography from 70 nm to 10 nm while not affecting print through (20 nm in all cases). We obtained a global mirror curvature of 0.8 m for 500 µm mirrors with a standard process as well as 0.2 µm CMP of poly4, whereas thickened poly4 (by 0.2 µm) with the addition of 0.2 µm CMP resulted in a curvature of 0.4 m.

We explored several actuator designs. We fabricated zipper actuators and measured their deflections. We measured vertical displacement in these structures as large as 6–7 µm for an applied bias of 100 V. We also designed and fabricated lifter actuators. We observed vertical displacement of 4.5 µm at 40 V. Advanced designs with predicted displacements in the 10–20 µm range currently are being fabricated.

Furthermore, we designed and fabricated several arrays of mirrors. These incorporate 91 hexagonal piston/tip/tilt mirrors arranged in a hexagonal array. We will package them in a 256-pin PGA (pin grid array) and test them in an adaptive optic test-bed at the AFRL. An expected stroke of 10 µm using the lifter

actuators represents the state of the art in surface-micromachined optical MEMS mirrors. Other more-aggressive actuator designs using both zippers and lifters are expected to reach displacements of 20 μm.

52721

Modeling Signals from Earth-Penetrating Nuclear Weapons for Remote Kill Assessment

P. L. Dreike, D. E. Carroll, A. V. Farnsworth, Jr., G. D. Cable

Sandia seeks to develop algorithms that will evaluate the yield and penetration of an earth-penetrating nuclear weapon from optical and possibly electromagnetic pulse (EMP) signatures measured remotely. Knowledge of the yield and penetration performance of the weapon gives a good indication of the likely damage to a deeply buried hard target.

Light and EMP signals are produced in the air, so it is necessary to model the coupling of nuclear energy from below ground to the air. We used generic energy sources to model nuclear energy produced by some device and then used two shock-physics codes to model the transfer of shock energy and ejection of dirt into the air. High-speed photographs were available of the fireball produced by a shallow-buried event. We found that the shape and history of the fireball could be reproduced with both codes. We then post-processed the code outputs of material density, pressure, and temperature to compute optical signals as a function of time and viewing angle. It was not possible to reliably determine the optical output of the actual fireball for comparison with the modeled output. We subsequently used one of the codes to model the fireballs produced by one low-yield and one high-yield weapon. We believe that we made a credible model for the light signals that would be produced by buried nuclear events.

Other Communications

Dreike, P. L. 2004. Production of high-frequency EMP signals by earth-penetrating nuclear weapons. Sandia Technical Report SAND2004-0468 (Classified), Sandia National Laboratories, Albuquerque, New Mexico.

Dreike, P. L., G. D. Cable, A. V. Farnsworth, Jr., and D. E. Carroll. 2004. Final report on modeling signals from earth-penetrating nuclear weapons for remote-kill assessment. Sandia Technical Report SAND2004-5265 (Classified), Sandia National Laboratories, Albuquerque, New Mexico.

Farnsworth, Jr., A. V., G. D. Cable, and P. L. Dreike. 2004. Codes for generation of nuclear detonation optical signals from hydrodynamic calculation outputs. Sandia Technical Report (OUO–Limited Distribution), Sandia National Laboratories, Albuquerque, New Mexico (in preparation).

52723

Novel Micropreconcentrators for CW, Explosives, and Water Surety

R. P. Manginell, R. J. Kottenstette, M. P. Siegal, S. K. Showalter, R. J. Shul, D. R. Adkins, P. R. Lewis, S. S. Sokolowski, M. Moorman

Chemical preconcentrators (PCs) are often placed at the entrance to analytical detection systems for the purpose of accumulating analytes of interest out of a large gas-sample volume. Sandia is developing a microfabricated PC that possesses a thermally isolated, three-dimensional (3-D), chemical-adsorbent support zone. As compared with earlier planar microfabricated PCs, the 3-D PC (3DPC) has 300x–1000x the available adsorbent coating area, depending on the specific design. The measured collection capacity for semivolatile compounds on sol-gel adsorbents increased by an order of magnitude compared with the planar PC. Lithographically defined gas-flow constrictions within the 3-D support improve the mass transfer of analytes into and out of the adsorbent, so that while the transient electrothermal response of the 3DPC can be 2 orders of magnitude longer than the planar PC, due to the added support mass, desorbed analyte peak widths are only a factor of 2 wider. Steady-state power consumption of the electrically heated 3-D support is as little as 50% greater than the planar device via thermal isolation of the 3-D support by a thin (1 µm) silicon nitride (SiN) membrane.

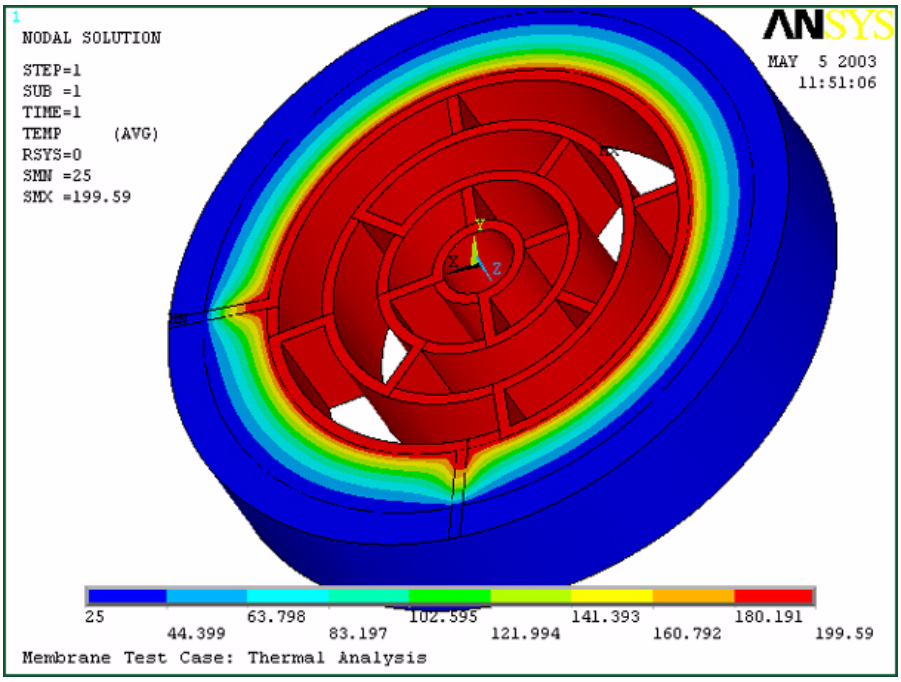

Silicon lattice exhibits complete temperature uniformity at steady-state 3-D PC temperature and 7.1 V potential on wiring.

We implemented two basic designs, one with flow perpendicular to the device surface and one with parallel flow; both designs permitted sample flow through the adsorbent bed. We evaluated a variety of techniques for applying adsorbent coatings to the 3-D support. We also applied several adsorbents, including laser-ablated nanoporous carbon (C), sol gels, and conventional PC packing materials, and tested them against chemical warfare agents (CWAs), explosives, and toxic industrial chemicals (TICs).

The status of our milestones for the design, fabrication, coating, testing, and modeling of two basic 3DPC designs is described below. We compare their performance with the planar PC and conventional PCs, as observed using downstream flame-ionization detectors (FIDs) and surface acoustic-wave detectors (SAWs).

- *Evaluate the connection of micropacked PC and/or solid-phase microextraction (SPME) with the 3DPC for focusing*. We omitted this milestone as both 3DPC designs are capable of direct use without SPME for most applications.
- *Attempt direct preconcentration of water contaminants, possibly toluene 2,4 di-isocyanate, on the 3DPC. Other contaminants may be used instead if deemed more relevant. We will consult with water-quality/-surety experts to make this determination.* We tested a variety of contaminants, including TICs and trihalomethanes (THMs). The device performs well against all of these, showing direct preconcentration of water contaminants and industrial contaminants.
- *Determine the best methods/materials for coating based on the same issues as in previous work.* We evaluated several methods of coating with several materials. For example, nanoporous C coatings and packing with commercial coatings provided excellent performance for TICs and THMs.
- *Demonstrate the testing of both PCs with microanalytical components*. We successfully tested the PCs with microfabricated SAW detectors and micro-gas chromatograph (micro-GC) columns.
- *Improve the strength/weight ratio of both basic PC designs while retaining the appropriate thermal characteristics*. The purpose is to improve desorption characteristics. Modeling based on the first designs pointed to improved designs. These designs are currently in process and should have superior mechanical strength and preconcentration performance.

Refereed

Manginell, R. P., P. R. Lewis, D. R. Adkins, R. J. Kottenstette, D. R. Wheeler, S. Sokolowski, D. Trudell, J. Byrnes, M. Okandan, J. M. Bauer, and R. G. Manley. 2004. Recent advancements in the gas-phase microChemLab. *Proc. SPIE Optics East Lab on a Chip*, accepted.

Other Communications

Manginell, R. P., P. R. Lewis, D. R. Adkins, R. J. Kottenstette, D. R. Wheeler, S. Sokolowski, D. Trudell, J. Byrnes, M. Okandan, J. M. Bauer, and R. G. Manley. 2004. Advancements in the gas-phase microChemLab. *Proc. Electrochemical Society*, accepted.

Sokolowski, S. S. 2004. Microfabricated three-dimensional preconcentrators. Masters thesis, University of New Mexico, Albuquerque, New Mexico.

52724

Ion-Mobility Spectrometer/Mass Spectrometer

D. E. Austin, E. S. Varley, D. E. Hunka

Sandia currently has no capability to interface our state-of-the-art ion-mobility spectrometer (IMS) systems (micro-IMS systems, Explosives Detection Personnel Portal, Explosives Detection Vehicle Portal, the Materials Access Area [MAA] Checkpoint, and Fourier-transform IMS) to a mass spectrometer (MS). We are building an IMS/MS (ion-mobility spectrometer/mass spectrometer) system that will improve the IMS trace detection of explosives and chemical/biological (C/B) materials. IMS detectors can quickly identify explosives or chemical agents from the location of the peaks in the IMS spectrum, but they do not provide information regarding the actual mass number of the species (ion) responsible for each peak. A typical spectrum has many peaks, and most of them are unidentified. Combining IMS with mass spectrometry allows a determination of the molecular makeup of the material that produces these peaks to reduce false alarms, improve detection limits, and develop multivariate analysis techniques for the quantitative discrimination of mixtures. Although we experienced several equipment failures, the interface between the instruments is nearly complete and operational. After extensive ion trajectory simulations, we modified the interface design to allow sufficient ion transmission into the MS. These modifications are now complete. We also spent some time updating the control software of the MS to allow single-computer control of the combined instrument. This control software is, in and of itself, a valuable asset, as researchers at other labs have expressed interest in purchasing what we develop. In addition, we rewired and remounted the IMS to accommodate the new interface design.

...the control software of the MS....is, in and of itself, a valuable asset, as researchers at other labs have expressed interest in purchasing what we develop.

Our work focused on testing and optimizing the interface between the IMS and the MS, including addressing issues of combined instrument control and data acquisition, improving ion transmission between instruments, and developing a versatile system for easy interchange between IMS instruments.

We performed numerous computer simulations of ion-transmission behavior and discovered some problems with the original interface design. As a result, we completely redesigned, fabricated, and rebuilt the interface, resulting in significant improvement in ion transmission into the MS.

We explored options to improve the vacuum compatibility between the two instruments, and we modified the interface to facilitate easy exchange of IMS instruments.

Efforts of other groups (universities and industry) to create and implement a single control system for IMS/MS instrumentation have been unsuccessful. We are developing all-new control software using LabVIEW architecture, which we believe will circumvent the difficulties experienced by previous groups and allow single-computer control of our IMS/MS system.

52725

Cryptographic Assurance of Execution Correctness and Confidentiality

L. G. Pierson, J. M. Eldridge, E. L. Witzke, K. W. Insch, T. D. Tarman, P. L. Campbell, P. J. Robertson

Current computing architectures are "inherently insecure" because they are designed to execute any *arbitrary sequence of instructions. This key to success is also a vulnerability, as malicious code can easily be substituted and executed. Also, programs that attempt to protect data from disclosure are fraught with difficulty since the keys and instructions used by the program to encrypt its data can be inspected and reverse-engineered. As a result, these programs are subject to subversion by malicious code.*

Can cryptographic means be introduced into this architecture to restrict the execution of arbitrary instruction sequences to a single intended sequence of instructions? Furthermore, can cryptographic methods be incorporated that protect software-based encryption keys from disclosure, yet still allow cryptographic computations using these data?

Sandia's goal is to produce a cryptographic method of "tamper-proofing" trusted code over a large portion of the software life cycle. We developed a technique called "faithful execution" to cryptographically protect instruction sequences from subversion.

We studied earlier implementations of faithful execution in a JAVA™ virtual machine prototype and applied the lessons learned to prototype a system for securing code that operates in a configurable soft-core processor implemented in a field-programmable gate array (FPGA). The prototyped system for cryptographically ensuring the execution correctness of programs demonstrated the viability of this technique for the protection of high-consequence applications.

When perfected and incorporated into a single tamper-resistant application-specific integrated circuit (ASIC), these techniques may also enable greatly improved protection of computer-controlled critical infrastructures.

We developed a technique called "faithful execution" to cryptographically protect instruction sequences from subversion....When perfected and incorporated into a single tamper-resistant application-specific integrated circuit (ASIC), these techniques may also enable greatly improved protection of computer-controlled critical infrastructures.

We developed a processor that can execute code correctly even if an adversary owns the processor. The cryptography embedded in the processor guarantees both the integrity and the confidentiality of the code: the adversary cannot determine the sequence of instructions, nor can the adversary change the instruction sequence in a goal-oriented way; and code modification is detected and mitigated before execution.

In initial work, we focused on the detailed design of a cryptographic system to protect instruction-stream confidentiality and sequence authenticity while coping with the complexities of variable-length instructions, conditional branches, subroutines, interrupts, caches, instruction pipelines, etc. To simplify this difficult problem, we chose, in recent work, to prototype these protections for a "reconfigurable embedded hardware processor" in a programmable logic device (PLD). We developed a hardware design to protect the instruction stream delivered to an Altera NIOS processor compiled into a state-of-the-art PLD. The prototype consists of software that enables us to perform the cryptographic "shrink-wrapping" of a simple software application and to demonstrate its protected execution on the reconfigurable hardware prototype.

Our recent approach differs from previous attempts in three ways. First, we use a "chaining" encryption/authentication mode. This detects instruction reordering. Second, we add redundant information. This detects intra-instruction bit manipulation. Third, the cryptographic protection is extended all the way into the central processing unit (CPU) module. This eliminates the need for a "trusted program loader" and reduces the volume to be protected from tampering to just the CPU chip.

The approach pioneered in this work can be tailored to provide transparency (authentication only) and nontransparency (encryption and authentication), and the approach can be used with exportable algorithms.

After simulating a simplified (JAVA^{TM}) version of such a processor, we implemented our approach on a "real" hardware processor. This step required resolution of difficulties presented by discrepancies between fetch width and instruction size, cryptographic separation of code and data, and protection through interrupt cycles.

Using this prototype system, we demonstrated the viability of this concept for protecting high-consequence applications. We engaged student effort to "red team" this system. We incorporated the results of this "red teaming" effort into improvements in the security of the system design. Two major variations of the secure processor design emerged: one for protection of "legacy" code, which may include certain unwise (less secure) programming practices, and another that precludes the execution of these unwise programming practices. We analyzed and documented trade-offs regarding the cost/complexity/processing/memory overhead and the robustness against cryptoanalytic attack associated with the cryptographic design parameters. We identified several approaches for reducing the cryptographic processing overhead and for

improving the secure processor's performance. The cryptographically assured processor technique is ready to be experimentally applied to specific applications to further explore the trade-offs between robustness against subversion for high-consequence applications and the processing overhead associated with accomplishing such security.

- When perfected and incorporated into a single tamper-resistant ASIC, these techniques may also enable greatly improved protection of computer-controlled critical infrastructures.

Refereed

Pierson, L. G., P. L. Campbell, J. M. Eldridge, P. J. Robertson, T. D. Tarman, and E. L. Witzke. 2004. Secure computing using cryptographic assurance of execution correctness. *Proc. 38th IEEE International Conference on Security Technology* (11–14 October, Albuquerque, New Mexico).

Other Communications

Campbell, P. L., L. G. Pierson, J. M. Eldridge, P. J. Robertson, and E. L. Witzke. 2004. Stateless and stateful implementation of faithful execution. Sandia document 5227374, Sandia National Laboratories, Albuquerque, New Mexico.

Pierson, L. G., P. J. Robertson, P. L. Campbell, J. M. Eldridge, and E. L. Witzke. 2004. Final report: Cryptographic assurance of execution correctness LDRD. Sandia Technical Report, Sandia National Laboratories, Albuquerque, New Mexico (in preparation).

52726

Characterization, Performance, and Optimization of PVDF as a Piezoelectric Film for Advanced Space Mirror Concepts

J. W. Martin, M. C. Celina, R. A. Assink, G. D. Jones, T. Dargaville, P. M. Chaplya, D. M. Mowery

Sandia is involved in the selection and lifetime prediction of smart materials for use in novel adaptive optics (polymer-based mirrors) with improved sensitivity and resolution for future satellite-based remote reconnaissance systems such as those needed to support nonproliferation programs. The materials being evaluated are lightweight, thin piezoelectric polymer films based on polyvinylidene fluoride (PVDF), which deforms in response to charge deposition. With optimized electrode configuration and control systems, we can achieve a perfect paraboloidal-shaped mirror with adjustable focal point. To minimize overall weight, we will not enclose the mirror; instead, the mirror will be directly exposed to the low-earth-orbit (LEO) environment. Environmental degradation due to large thermal cycling, atomic oxygen (AO), the complete unattenuated solar irradiance, micrometeoroids, and charged particles is unavoidable. This study focuses on the performance features of various polymers and changes expected in the piezoelectric properties of PVDF–based materials.

During this project, we gained extensive knowledge and experience with the fundamental features of various PVDF–based materials. This allowed us to conceive, design, and implement more-specific experiments to determine the most suitable material for use in the space environment. These experiments included testing the magnitude of actual electromechanical responses of custom-made bimorphs over the temperature range of -100ºC to +130ºC, instead of relying on less-informative physical property measurements, such as d33. We also conducted more-complex accelerated-aging exposures, measuring the erosion rates of test specimens exposed to AO and vacuum ultraviolet (VUV) radiation, in collaboration with NASA Glenn. Based on these studies, it was possible to limit the range of available polymers to the two most promising materials, a PVDF homopolymer (homo-PVDF) and a P(VDF-TrFE) copolymer with low (20%) comonomer content. The homo-PVDF has the highest melting point of all the polymers examined, reasonable retention of piezoelectric properties at high temperatures, and good radiation resistance; however, the homo-PVDF has relatively limited electromechanical efficiency

at cryogenic temperatures due to a pronounced glass-transition (Tg) temperature at -40ºC. In comparison, the P(VDF80-TrFE20) copolymer has properties similar to the homo-PVDF, as well as superior low-temperature performance due to a more subtle low-temperature Tg. This copolymer also has the advantage that it can be solution-processed and that an optically smooth surface is more easily obtained when cast onto an appropriate substrate. The erosion rates of both polymers due to AO/VUV exposure are at the upper end of the range for organic materials and pose a significant limitation to the lifetimes of the polymers. Additional protection strategies, such as internal inorganic fillers or protective coatings, should be considered. As a positive feature, the piezoelectric responses appear largely unaffected by the exposure to AO/VUV due to the bulk of the material remaining unchanged.

Through contacts at NASA Glenn and Boeing, we were invited to participate in active material evaluation experiments on the outside of the International Space Station as part of the upcoming MISSE-6 mission. Preparation for these experiments involved designing novel, small, robust excitation and sensing experiments capable of remotely recording piezoelectric response. Challenges included finding a suitable, space-qualified power supply and data logger. Results from the MISSE-6 experiment, with plans for monitoring the piezoelectric performance over a period of 8 months in space, will offer the ultimate validation of ground testing and performance qualification for the real space environment.

Through contacts at NASA Glenn and Boeing, we were invited to participate in active material evaluation experiments on the outside of the International Space Station as part of the upcoming MISSE-6 mission.

Refereed

Celina, M. C., T. R. Dargaville, J. W. Martin, R. L. Clough, R. A. Assink, and D. M. Mowery. 2004. Optimization of piezoelectric PVDF polymers for adaptive optics in space environments. *J. AIAA*, submitted.

Dargaville, T. R., M. C. Celina, and P. M. Chapyla. 2004. Evaluation of piezoelectric PVDF polymers for use in space environments, part I: Temperature limitations. *Smart Materials and Structures*, submitted.

Other Communications

Celina, M. C., T. R. Dargaville, J. W. Martin, R. L. Clough, R. A. Assink, and D. M. Mowery. 2004. Optimization and characterization of piezoelectric PVDF polymers for adaptive optics in space environments. *Proc. National Space and Missile Materials Symposium* **CD** (21–25 June, Seattle, Washington).

Celina, M. C., T. R. Dargaville, J. W. Martin, R. L. Clough, R. A. Assink, and D. M. Mowery. 2004. Optimization of piezoelectric PVDF polymers for adaptive optics in space environments. *Proc. 45th AIAA Structures, Structural Dynamics and Materials Conference* **CD** (19–22 April, Palm Springs, California).

Dargaville, T. R., M. C. Celina, P. M. Chapyla, and R. A. Assink. 2004. Evaluation of piezoelectric PVDF polymers for use in space environments. *Proc. 45th AIAA Structures, Structural Dynamics, and Materials Conference* **CD** (19–22 April, Palm Springs, California).

67086

Adaptive Optics and Phase-Diversity Imaging for Responsive Space Applications

M. W. Smith, B. F. Clark, D. V. Wick

Phase-diversity imaging is an established technique for deriving optical-phase information from measurements of intensity. The work conducted under this project concerns the use of phase diversity to improve image restoration for aberrant optical systems. All previous implementations of phase-diversity imaging of which we are aware used defocus to introduce phase diversity. Because of its rotational symmetry, defocus diversity is effective in improving the quality of image restorations only for even-order aberrations such as spherical aberration and astigmatism. However, simple defocus diversity fails to improve the quality of image restorations for odd-order aberrations such as coma.

In this work, Sandia explored the use of nonquadratic and rotationally nonsymmetric phase diversity versus standard defocus diversity. We explored various types of nonquadratic phase diversity using numerical simulations. We optimized the types and amounts of phase diversity for specific types and amounts of aberrations, using channel capacity as a metric. We performed simulated image reconstructions. The simulations proved the central hypothesis of the investigation, which is that nonquadratic and rotationally nonsymmetric phase diversity are superior to simple defocus diversity in improving the quality of image restorations for odd-order aberrations such as coma. We designed and assembled a benchtop optical system that incorporates an active optic as a means to introduce phase diversity. While we did not obtain high-quality results with the benchtop system, we did complete a variety of characterization tests.

We laid out the following milestones for the numerical simulations: (1) decide between scalar or vector diffraction calculations for the forward model, (2) determine the type of nonquadratic phase diversity to use for handling odd-order aberrations, (3) incorporate the effects of finite spectral bandwidth into the point-spread function (PSF) and modulation-transfer function (MTF) calculations, (4) create software to view the PSF and MTF results, (5) create software to optimize channel capacity as a function of phase diversity, (6) get diffraction-limited images from the benchtop system to use as input to the simulations, (7) optimize channel capacity for the specific aberrations of the benchtop system, (8) create

inversion software to handle nonstationary PSFs, (9) compare results from the model calculations to measurements from the benchtop system, (10) perform phase-diverse image reconstructions using images from the benchtop system, and (11) document the results.

We laid out the following milestones for the breadboard system: (1) evaluate commercial microelectromechanical systems (MEMS) mirrors and pick the most suitable one, (2) complete the optical design of the benchtop system both for diffraction-limited imaging and with intentional aberrations introduced, (3) acquire the benchtop hardware, (4) assemble the benchtop hardware, (5) verify diffraction-limited imaging and acquire diffraction-limited test images, (6) implement and verify phase diversity, (7) acquire phase-diverse images and compare the results to simulations for different conditions, and (8) document the results.

Although we met the numerical simulations and breadboard-system milestones, we were unable, despite repeated and diligent efforts, to demonstrate diffraction-limited imaging with the breadboard system. We also made efforts to quantify the type and amount of aberration that existed in the as-built system, but the results were inconclusive and not wholly repeatable. It was therefore not possible to make a precise and quantitative comparison between calculations and measurements of the PSF and the MTF. Consequently, we did not meet some of the milestones.

We did, however, complete extensive numerical calculations and simulations. The bottom line of the results is that generalized phase diversity can improve the channel capacity of an aberrant optical system by almost 30% in certain cases, although it produces almost no improvement in other cases. A central hypothesis of this project was that some type of generalized, nonquadratic phase diversity would be superior to simple defocus (or quadratic) phase diversity when it comes to compensating for odd-order aberrations such as coma. The numerical simulations confirmed this hypothesis. On the other hand, cutting aberrations in half produces a greater increase in channel capacity than does collecting phase-diverse images. The overall conclusion of this work is that while phase diversity does have some utility when it is used to enhance the MTF of an aberrant optical system, there is probably more to gain by using active optics to compensate directly for aberrations. The traditional role for phase diversity is, in fact, to diagnose aberrations and provide feedback control to active optics.

The bottom line of the results is that generalized phase diversity can improve the channel capacity of an aberrant optical system by almost 30% in certain cases....

Other Communications

Smith, M. W. 2004. Use of adaptive optics to implement nonquadratic phase-diversity imaging. *Proc. SPIE Annual General Meeting* **5524** (August, Denver, Colorado): 66–77.

Smith, M. W., and D. V. Wick. 2004. Comparison of different modes of phase-diversity imaging with adaptive optics. *Proc. Air Force Maui Optics and Supercomputing (AMOS) Conference* (13–17 September, Wailea, Hawaii).

67087

Infrastructural Development for Flexible Network of Devices

T. Q. Thai, W. A. Amai, Z. L. Lovelady, J. Z. Liang, D. C. Locke, S. A. Mulder, A. Phan, D. L. Smythe, N. S. Rattan

This is a classified report.

67088

Monolithic Reconfigurable Radio-Frequency Microelectromechanical Systems (RF MEMS) Antennas

L. M. Feldner, C. T. Rodenbeck, B. H. Strassner, II, C. W. Dyck, C. D. Nordquist

A critical requirement of many miniature systems is the ability to sense and/or transmit electromagnetic (EM) energy for communications or remote sensing. This is accomplished using radio-frequency (RF), microwave, or millimeter-wave antennas, which can be fabricated monolithically with other electrical/mechanical components to yield a new class of reconfigurable antennas capable of multiband operation, adaptive beam forming, jamming/interference mitigation, polarization diversity, low probability of detection/interception communication, and direction-of-arrival estimation. This project combines Sandia's growing expertise in RF microelectromechanical systems (MEMS) research and solid background in microwave radar, RF tag, and communication system design to develop revolutionary integrated antenna technologies.

Realizing these advances requires a substantial research and development effort addressing critical RF/microwave antenna- and system-design issues in conjunction with sophisticated MEMS processing and integration technologies. We will integrate RF MEMS switches and phase shifters with novel antenna topologies to realize physically reconfigurable radiating elements and feed structures in addition to monolithic electronically scanned antenna arrays. Successful fabrication of the first completely integrated monolithic reconfigurable electronically scanned antenna array will demonstrate the level of technological maturity appropriate for further programmatic development in the future. Specific antenna-design goals will emphasize miniaturization, low power consumption, radiation efficiency, and amenability to monolithic and hybrid microsystem integration.

Our work is highly synergistic with other RF MEMS, RF/microwave hybrid miniaturization, and wireless sensor work at Sandia. For example, our project will continue to leverage ongoing Sandia work in RF MEMS switch and phase-shifter development and miniature synthetic-aperture radar (SAR) antenna development, and we plan to collaborate with a Sandia group that is analyzing networked sensors.

We developed, investigated and down-selected a number of innovative antenna architectures based on their potential for integration into monolithic/hybrid microsystems.

We developed a reconfigurable aperture-coupled triangular microstrip patch antenna on a 20-mil quartz substrate bonded to a 10-mil alumina substrate. A common ground-plane aperture eliminates the need for vias, and 10 monolithic RF MEMS capacitive switches enable 5 digitally reconfigurable frequency bands. Full-wave EM models predict a 1.5 GHz 2:1 voltage standing-wave ratio (VSWR) bandwidth tunable from 31 to 39 GHz, and a 4.9 dBi element gain. Array studies using this antenna element are currently under way.

Our processing-development studies indicate that gold-gold (Au-Au) diffusion-bonding techniques can be used to successfully integrate the quartz and alumina substrates. We are fabricating prototype monolithic triangular microstrip patch antenna designs on quartz/alumina substrates and will obtain measured results in upcoming work. We currently are developing a novel antenna measurement that will enable simultaneous backside wafer probing and monolithic antenna-pattern measurements.

We designed Ka-band distributed MEMS transmission line (DMTL) phase shifters and fabricated them using capacitive RF MEMS switches on 10-mil alumina. We obtained good switch yield (99%), but a layout error led to poor return loss and insertion-loss measurements of 6 dB. The 3-bit phase shifter yielded measured phase shifts of 60 deg, 180 deg, and 240 deg at 35 GHz; however, the most significant bit showed some dispersion (time delay changing with frequency) due to the reactance of the capacitive stubs changing over frequency.

We specifically designed a quasi-yagi radial end-fire antenna for wireless sensor-network applications. This antenna provides pattern reconfigurability at distinct azimuthal angles (six or eight beams, depending on design). Each state has an impressive 2.5 GHz (43%) bandwidth and 7 dBi of gain centered in the 5.8 GHz ISM (industrial, scientific, and medical) band. We are optimizing prototype end-fire elements to operate in both C-band (5.8 GHz) and Ku-band (16 GHz). We designed radial end-fire array architectures in both bands, and prototyping is under way. Initial prototype arrays will integrate commercial solid-state switch die with the antenna substrate to realize the switched-beam antenna function.

We also investigated electrically small antennas and antenna-miniaturization techniques. We designed a dual-band Koch fractal planar inverted f-antenna (PIFA) to operate at both the 2.4 GHz and 5.8 GHz ISM bands, requiring a 50% smaller

ground plane than a conventional dual-band PIFA. Investigations into ultrahigh-frequency (UHF)/L-band electrically small antenna designs are under way. We used commercial full-wave EM simulators to design and characterize antennas prior to prototype fabrication.

67089

Next-Generation 3-D Inspection System for Facility Monitoring

J. J. Carlson, T. H. Ko, M. R. Muguira, C. Q. Little

Sandia seeks to develop a next-generation, three-dimensional (3-D) inspection system for facility and material monitoring. The system will include components for detection, tracking, classification, and assessment. Our approach involves the integration of two pre-existing 3-D sensing technologies developed at Sandia. We will combine these technologies, 3-D video motion detection (3DVMD) and laser mapping (LAMA), to continuously maintain real-time, high-fidelity 3-D models of both static and dynamic components of monitored areas. We will use LAMA, a structured light sensor, to accurately monitor the 3-D physical characteristics of static, or stationary, components. The 3DVMD will monitor dynamic components and will provide real-time estimates of the shape, location, and motion of humans and moving objects. The combination of these two Sandia-developed technologies provides a unique capability currently unavailable in other 3-D–sensing technologies. We will develop analysis capabilities to process the 3-D sensor data and to identify activities or conditions that could signify potential threats (e.g., unauthorized intrusions into a restricted space, structural changes in facilities, material movement). We will also develop and implement a revolutionary, self-calibrating 3DVMD algorithm. Self-calibration will dramatically extend the practicality and usability of the 3DVMD system, especially in potentially hazardous environments. We will also develop an interactive 3-D visualization capability. This capability will allow remote, interactive inspection of a monitored area (via Internet, satellite, or telephone links) using a 3-D computer model of the area that is rendered from actual sensor data.

We selected the monitoring application to be the main display area of Sandia's Cooperative Monitoring Center. We initially installed a four-camera system, with cabling to a nearby lab, where a computer workstation is set up. We installed a 3DVMD system. We experimented with a fish-eye lens system for area monitoring, as well. We are developing software to enable a distributed computer system to move beyond the four-camera system, to expand the area of coverage as well as improve the resolution of area coverage. We completed the first phase of a self-calibration system that allows the camera parameters, critical to rapid and even remote

calibration, to be done. We will expand the camera installation to upwards of 20 cameras to facilitate monitoring of a much larger area. We will merge 2-D and 3-D techniques in data gathering. At that point, we will demonstrate a full distributed system (for an *n*-camera system). We will also demonstrate a rapid deployment of a camera system, with the goal of setup time, including calibration, to be less than 1 hr. During that time, we will also work to improve and expand the detection algorithms for monitoring both static and dynamic components of the area under surveillance.

67090

Risk-Assessment Metatool

A. M. Bouchard, W. D. Henry, L. J. Whittet, G. C. Osbourn

Sandia is developing a risk-analysis metatool—a tool that will enable analysts at both the site and enterprise levels to combine and analyze data from multiple other tools on demand. We will design this metatool to rapidly generate new analyses that were never considered when the original tool was built. Such a capability could be extremely powerful in times of urgent need, such as after 9/11, and have a high impact on Sandia's homeland security mission. The key to importing new file formats and generating new calculations on the fly is the innovative self-assembling software (SAS) technology under development at Sandia. This technology will provide a mechanism for the user to specify his intentions at a very high level (e.g., equations or English-like text), and the code will self-assemble, taking care of the implementation details. Before this project began, we had developed a proof-of-concept demonstration showing self-assembling execution sequences (code) and self-assembling data structures, but only within an isolated environment. Early in this project, we developed (invented) a significant amount of new infrastructure to go from the proof-of-concept stage to the capabilities required for the metatool. Specifically, we designed and implemented the capability to import files from the Joint Conflict and Tactical Simulation (JCATS) or any other text files. We designed the SAS infrastructure to construct new statistical analyses on the JCATS or other tabular data, and we expect to complete implementation in upcoming work. We will then also provide the capability to import files from a second risk-analysis tool. We will also develop an intuitive, highly user-friendly interface to support the rapid development of risk analyses, combining JCATS and the new data. Although the goal of this project is to develop a risk-analysis metatool, the cutting-edge SAS technology that we develop could have far-reaching impact in the software development arena in general.

We completed requirements, analysis, design, and some implementation of software, specifically in the following areas:

(1) We obtained requirements and priorities from Sandia vulnerability analysts on what types of data and analyses we should focus on first. JCATS is a combat (conflict) simulation in which "good guys" fight "bad guys." Current technology does not provide a querying capability, so personnel often spend hours or days analyzing the data by hand. The first version of

the metatool will enable users to import multiple JCATS files and create new analyses on the fly.

(2) We developed a conceptual design of a user interface to support these functions. The user will be able to store many files (a batch of JCATS runs, for example) together in a "binder" (analogous to a three-ring binder). To define an analysis, the user will be able to drag and drop columns, rows, or cells of data onto an analysis-builder interface, and specify functions to be performed (mean, count, etc.) as well as constraints (after time t, using weapon x, etc.) The metatool will self-assemble the code to perform the analysis and display the results. The user can name and save the analysis. Then, the metatool will examine the contents of every binder and insert a link to this analysis into any binder that has the appropriate types of files. This interface is expandable as we support files from other tools in the upcoming years. Those files can be added to the binders, and analyses involving data from multiple tools will also be linked to the appropriate binders.

(3) We developed a conceptual design of the SAS machinery to accomplish the data import and analyses. In particular, we designed the high-level building blocks from which all new file-import and analysis code will be self-assembled.

(4) We implemented code to import JCATS files and store the data in the SAS data structures.

(5) We completed the detailed design and some implementation of the SAS building blocks and machinery.

67091

Featureless Spread-Spectrum Waveform Design and Processing

G. B. Haschke, R. M. Holman, D. D. Kiffer, C. R. Collins, D. D. Cox, R. M. Axline

Many benefits accompany the use of spread-spectrum waveforms for radio-frequency (RF) over-the-air links. These waveforms support communications, radar, and geolocation applications. Most direct-sequence, spread-spectrum (DSSS) waveforms are generated by mixing a low-rate digital message signal against a higher-rate digital pseudonoise code. One important benefit of this waveform type is that, if the spreading bandwidth is large, an eavesdropping adversary finds it difficult to determine that the DSSS waveform is on the air.

But standard DSSS waveforms contain features (e.g., constant amplitude) and periodicities (e.g., constant chip rate) that an adversary can exploit to detect the presence of the waveform, even when DSSS signal energy is small relative to noise in the channel. Sandia seeks to develop a new method for designing spread-spectrum waveforms that are essentially featureless. That is, these waveforms, although they will reliably deliver information to a suitable receiver, will be indistinguishable from Gaussian noise.

For waveforms to develop, information will be encoded into both the amplitude and the phase of the waveform. In this work, we will develop and evaluate several different waveform design approaches. In a parallel effort, we will develop a new receiver algorithm to allow the new waveforms to be demodulated and decoded by a digital receiver.

We must address several significant challenges in this work. First, current spread-spectrum transmitters need not operate in an amplitude-linear mode; however, our technical approach may require a transmitter that is approximately linear. It would be desirable to be able to implement such a transmitter in a miniaturized hand-held radio. Second, although the companion receiver algorithm may be able to "run" on a reasonably sized airborne or ground-station signal processor, it should not be overly complex. That is, the receiver algorithm must be feasible to implement.

One important benefit of this waveform type is that, if the spreading bandwidth is large, an eavesdropping adversary finds it difficult to determine that the DSSS waveform is on the air.

We made the following accomplishments:

- Developed a new methodology for designing DSSS waveforms that are devoid of the periodicities found in traditional DSSS modulation and, therefore, are significantly less vulnerable to standard exploitation methods.

- Performed an autocorrelation analysis of the new featureless waveforms. The analysis indicates that the new waveforms are suitable for use either as preamble sequences or as data-spreading sequences in a digital communications system.
- Completed the design of a receiver detection algorithm and prototyped it in MATLAB. The algorithm, based on the fast correlation technique, was developed via simulation in MATLAB.
- Assembled a prototype transmitter and receiver. The transmitter employs an arbitrary waveform generator, a custom up-converter, a power amplifier, and an antenna. The receiver uses a custom down-converter and a commercial data-acquisition system to supply a digital signal to a workstation hosting MATLAB.
- Successfully detected signals transmitted over an RF link. These tests validate the MATLAB simulation results and confirm the utility of the waveforms.
- Performed a vulnerability analysis showing that the modulation technique is significantly more immune to second-order spectral detection methods as compared to traditional spread-spectrum modulation.
- Strengthened the infrastructure at Sandia required to demonstrate the feasibility of novel communication waveforms.

Other Communications

Axline, Jr., R. M., D. D. Cox, G. B. Haschke, C. R. Collins, R. M. Holman, D. Kiffer, and V. Hindman. 2004. Global personnel recovery system (GPRS) and diamond LDRD single-transponder demo. Sandia Technical Report, Sandia National Laboratories, Albuquerque, New Mexico (in preparation).

67092

Tracking Slow-Moving Objects in a GPS–Denied Environment

J. L. Novak, T. D. Osborn, M. R. Muguira, J. R. Podgorski, R. E. Abbott, J. T. Feddema

There currently are many solutions to tracking objects that move relatively fast, such as fixed-wing aircraft, through the use of the global positioning system (GPS) and/or inertial measurement units (IMUs). Unfortunately, tracking the movement of slower objects remains a problem in situations where the GPS is not available. In this project, Sandia focuses on developing geophysical approaches to position determination that eliminate requirements for radio-frequency or optical contact with known reference beacons. The integration of geophysical and microsystems computer models suggests that geolocation is possible if an object is moving slowly.

Our work focused on using variations in the local gravitational field. We developed simulations using closed-form solutions that analyze these geophysical signals, add appropriate noise levels, and then compute a location based on an iterative technique. We are using these simulations to determine the boundary conditions under which geolocation can be performed, and to ascertain the types of sensing and signal-processing technologies required to implement a fieldable microsystem.

67093

Optical Communications

V. M. Hietala

Sandia is exploring the feasibility of a unique optical-communication method. The project has two primary tasks: (1) a proof-of-concept system demonstration of the proposed technique, and (2) a study of the necessary custom components for eventual realization. In recent work, we emphasized the system-feasibility demonstration. In upcoming work, we will move toward the study of components for realization.

We made significant progress in completing the proof-of-concept system demonstration. This included the move from storage, installation, and setup of a suitable telecommunication system by Sandia's Advanced Networking organization as well as the configuration and testing of a variety of optical and electronic components. We completed a simple demonstration with good results. We have not yet demonstrated actual data transport due to equipment limitations. The proper equipment is now in place, and additional optical components have been received to demonstrate operation in a more realistic test-bed. We began the study of special custom optical components for realization, and the study is ongoing. The objective of this component study is to primarily identify methods for realization.

67094

A Unique Vibration-Based Miniature Power Generator for National Security Applications

R. A. Kellogg, J. G. Fleming, B. Jokiel, Jr., S. K. Frederick, J. M. Schare, R. J. Shul, T. Lemp

The microgenerator is an energy-scavenging system intended to collect ambient vibrations and convert them to usable electrical energy. Sufficient electrical energy is desired to power a microelectronic system having potential modes of operation, including the collection of sensor data, the storage of data while in sleep mode, and the transmission of stored data. The microgenerator's basis of operation, for transducing mechanical to electrical energy, utilizes the changing magnetic induction in a planar coil. This is produced by the relative motion of a spring-mounted magnet array. Inductive operation favors a low mechanical impedance and enhanced coupling to vibration sources. The incorporation of planar coils facilitates fabrication and provides a low-profile form factor. Sandia's work for the micromagnetic accelerometer focused on modeling, application identification, design, fabrication, and preparation for assembly and testing.

We modeled the microgenerator's mechanical and electromagnetic characteristics to guide component design, materials selection, and fabrication specifications. Models show that the microgenerator will best function mechanically as a high-pass filter, thus allowing maximal transduction near its resonance frequency and above. A device resonance of ~ 30 Hz is anticipated using single-crystal silicon (Si) as the structural material.

Modeling of the microgenerator has been vital to examining interfaces for driving a useful electrical load. Performance calculations for the prototype design consider electric and magnetic material properties and component dimensions, each of which is dictated by currently available fabrication techniques. As such, we are currently using bonded neodymium iron boron (NdFeB) magnets with a partial Permalloy magnetic return path and aluminum (Al) planar coils. A quantitative analysis of the prototype for a 30 Hz excitation frequency and 2 mm drive amplitude shows that an output current of 1.6 µA and 1.2 V amplitude may be expected. This low output voltage favors the use of single-wave rectification, with one diode drop, to transfer power to a capacitor over that of a full-wave rectifier with two diode drops. This holds true up to 4.9 V amplitude, at which point the full-wave rectifier becomes more efficient.

Battery technology is unfavorable for interfacing to the microgenerator, given charging and voltage requirements. Research shows that a system furnishing 1.6 μA needs to offer at least 2.4 V of rectified voltage to have useful applications. Higher voltages should be achievable using a coil with more turns and lower resistance combined with increased magnet field strengths.

To establish a baseline for the microgenerator performance objectives, we reviewed various data-transmission methods and their power requirements. One low-power approach includes radio-frequency (RF) burst communication at 915 MHz using frequency-shift keying. A data rate of 38.4 kbps is realizable at 8.6 mJ per byte. Using a 1000 μF capacitor for energy storage with a 25% depth of discharge, about 23 bytes of information could be sent. Considering the present microgenerator performance, it would take approximately 20 min to harvest this much energy and execute the transmission event. Occasional RF transmission typically accounts for approximately 10–20% of the circuit power consumption when overhead, leakage, sampling, and processing factors are considered. This would mean that 200 min would be required to repeat an RF transmission event unless more power is made available.

Fabrication of the prototype microaccelerometer is under way. We used single-crystal Si for the structural components based upon previous successes in producing high-aspect-ratio components. Scheduling challenges with deep reactive-ion milling dictated consideration of an alternative fabrication resource in the near term. Anticipating the next construction phase of the microaccelerometer, we are investigating an assembly method for joining the Si/magnet array die to the coil die. We submitted designs, and fabrication is in progress to produce test die for bonding experiments. We will use a low-temperature indium/tin (In/Sn) eutectic (135°C) solder to join die that are aligned to within 1 μm in a Karl Suss bonder. To allow free motion of the magnet array, we will maintain die separation electroplated gold (Au) standoffs.

To evaluate the microgenerator performance, we must establish a test capability reflecting real-world vibration inputs. We acquired portable data-acquisition (DAQ) equipment to study and record various vibration sources, including structures, vehicles, and aircraft. Vibration profiles for these sources may then be reproduced under laboratory conditions.

In summary, we carefully modeled and designed the microgenerator with materials properties and fabrication limitations in mind to optimize its performance and facilitate

construction. As fabrication continued, we made preparations for assembly and testing.

67095

Image Georectification Using Digital Elevation Model Shadows

J. P. Kern, M. P. Wilson, J. A. Mercier, C. L. Walker

Sandia is pursuing an approach to orthorectify overhead reconnaissance images using a synthetic shadow image produced from a digital elevation model (DEM) of the area of the image and the solar position. We model the image formation using a perspective transformation, with parameters initially estimated by an assumed sensor position or a preliminary warp of the image to the DEM shadow map. We then refine the transformation parameters using an optimization algorithm that maximizes the cross-correlation between the warped image and the DEM shadow map. The warped image is derived from the forward, ground-to-sensor perspective transformation. The approach has the advantage of not requiring user-selected ground-control points (GCPs), which can be a laborious procedure. A statistical measure of the goodness of the match over the whole scene between the synthetic and real images is used instead. The method offers the possibility of an automated procedure requiring little, if any, user intervention.

Although the method is general, we demonstrated that with our simple model, which incorporated the terrain elevation information directly in the transformation, we can obtain fairly good orthorectification of Multispectral Thermal Imager (MTI) satellite images. The forward-frame camera perspective model is not adequate for the orthorectification of push-broom sensors. We developed the framework for a push-broom model but did not implement it yet. We believe that this improved model, which more accurately mimics the image-formation process of the MTI sensor, can provide much better orthorectification than we obtained with the forward-frame camera model. A number of less-critical refinements to the basic technique might lead to enhanced performance. These include improved shading algorithms and more extensive investigations into optimization calculations.

We developed and implemented methods and algorithms to support automated orthorectification and geocoding of overhead reconnaissance imagery. The approach matches an enhanced image of an area and synthetic shadow maps derived from DEMs of the area and the known solar angles at the time of data collection. We used standard “hill shade” algorithms to generate the DEM shadow maps. We considered a number of techniques for deriving shadows from real images. We finally

adopted a simple multispectral-image-enhancement technique using the first-principle component of the covariance of the visible and near-infrared bands. This eliminated the necessity of computing binary or m-ary shade images derived from the raw image and the shadow-map image.

We developed a camera perspective model transformation that forms a synthetic image of the synthetic shadow image and the actual known terrain elevations for each point using the DEM. We investigated a few similarity measures to compare the real image and the synthetic image and settled on cross-correlation as the most satisfactory initial measure. The camera model that we initially modeled is based on the well-known perspective transformation matrix. This transformation maps each ground point, (x, y, z), to an image point, (u, v). The parameters or coefficients of this perspective matrix define the camera's external orientation (EO) consisting of its location (x0, y0, z0) and pointing direction (roll, pitch, yaw) along with a scale factor. It is different from traditional image-to-image registration transformations in that the z-coordinate of the ground point is also included. Given the image coordinates of a number of ground points, the image is resampled or interpolated to produce a warped image. We compare this image with the synthetic shadow map by cross-correlation, which calculates the average product of the intensities of both images. We implemented optimization algorithms that searched the EO parameter space to find a point that produced a warped image with the highest cross-correlation with the shadow map. The resulting warped image is thus orthorectified.

Although the method is general, we applied it to MTI data for testing. The MTI is a push-broom sensor and, as such, does not exactly match the frame camera perspective model. Additional modifications to our model are required for push-broom sensors. We developed these modifications but did not yet implement them. This requirement consists of developing an inverse transform in which an actual sensor element line is projected to the ground. This ground-projection point is then corrected to account for the actual DEM surface. We investigated a number of refinements of our basic approach such as imaging small subsections of the ground points. These results revealed the inadequacy of the unmodified frame camera model.

We initially investigated the effects of sensor characteristics and the requirements for using a spherical earth model in using the DEM. We found that MTI images theoretically could be orthorectified to within a pixel. We initiated a final error investigation using operator-chosen GCPs in the original image

and the DEM shade map. However, we did not complete a statistical analysis of error across a number of images.

67096

Vulnerability Assessment of State-of-the-Art Microelectronics

J. J. Clement, S. Montague, J. L. Etzkin, J. M. Green, E. I. Cole, Jr.

There are significant challenges in performing vulnerability assessment (VA) of current and projected future generations of microelectronic devices. Sandia's overall goal in this project is to develop novel techniques for evaluating vulnerabilities in these devices.

We explored several potentially promising VA methodologies for very advanced microelectronic devices. We attempted one potential approach and ultimately abandoned it because we determined that our analysis equipment was not appropriate for the task. This redirected us to a potentially much more powerful (less brute-force) approach involving a combination of electrical measurement and optical inspection techniques.

67098

Nonlinear Optical Detection of Biological and Chemical Aerosol Agents Using Femtosecond Lasers

T. R. Nelson, J. Urayama, B. W. Atherton, T. S. Luk, E. A. Disch, T. A. Pitts

Nonlinear spectroscopy using ultrashort-pulse lasers is a promising technique to remotely obtain information about physical parameters in bioaerosol or chemical plumes, including estimation of size distribution, refractive index, and composition spectroscopy. The unique combination of wavelength diversity, coherent bandwidth, and impulsive coupling attributes characteristic of femtosecond laser technology provides the potential for capable and robust next-generation standoff detection in aerosol and topographic measurement environments using new signature paradigms that employ both temporal and spectral discrimination. Active broadband imaging technology will enhance scene contrast by noncooperative conversion to reflectance independent of ambient light conditions and will allow estimation of aerosol size distribution properties using multispectral elastic backscatter and wavelength-dependent extinction in the laser-radar inverse equation. Adaptive pulse shaping of the bandwidth can be used to customize molecular excitation conditions for a broad range of applications, including quantum coherent control of molecular vibrations, continuum generation for multitrace gas analysis, and random frequency hopping to avoid detection by threat warning systems. Propagation control strategies employing short-pulse laser pulses can be used to controllably generate intensity at range to initiate nonlinear spectroscopic processes by exploiting optical nonlinear effects such as multiphoton-excited fluorescence, stimulated Raman scattering, and laser-induced plasma breakdown in aerosol droplets. It is possible to enhance backscatter signatures for improved collection and achieve spectral specificity in chromophores using near-infrared (NIR) lasers with reduced atmospheric-transmission losses. The internal focusing properties and spatially resonant microcavity modes with an individual aerosol droplet excited by a femtosecond pulse will further enhance nonlinear optical conversion and reduce corresponding thresholds for signal generation in the power-dependent cross section. Sandia is conducting proof-of-principle laboratory experiments to evaluate the feasibility of nonlinear remote sensing. We will use

the calibrated experiments of surrogate systems to baseline performance models and assess operational capability.

We conducted calibrated laboratory experiments to identify and measure candidate nonlinear aerosol signatures in well-characterized surrogates (riboflavin, tryptophan) using multiphoton-excited fluorescence, including two-photon–excited fluorescence from riboflavin and three-photon fluorescence from tryptophan, and using a NIR (800 nm) pump wavelength. In addition, we performed measurements at extended range in the field, measuring the two-photon fluorescence from riboflavin, to illustrate the feasibility of the production of a nonlinear signature at extended range. We measured hyper-Raman signatures, which represent a new class of nonlinear signature for spectroscopic discrimination, in the laboratory in tryptophan, generated near 400 nm, using an 800 nm pump wavelength. We constructed a calibrated adaptive pulse shaper using a spatial light modulator and used the shaper in preliminary experiments to explore quantum coherent control strategies for nonlinear signature generation. These experiments incorporated phase-only masks across the bandwidth of the excitation laser pulse. The results of these experiments demonstrated an enhancement of ~ 300% in the measured two-photon absorption coefficients at 8000 nm for common two-photon–absorbing materials of interest. Experiments to assess the fluorescence yield of these transitions are ongoing. We are developing a model to include the potential impact of pulse shaping on nonlinear signature generation, including multiphoton fluorescence, stimulated Raman, and coherent anti-Stokes Raman scattering (CARS) signal generation.

The results of these experiments demonstrated an enhancement of ~ 300% in the measured two-photon absorption coefficients at 8000 nm for common two-photon–absorbing materials of interest.

In recent experiments, we began to explore the phenomenon of third-harmonic generation (THG) in air using femtosecond lasers. Initial experiments indicate a conversion efficiency of as high as 10^{-3} for 800 nm (third harmonic = 266 nm) femtosecond laser pulses. This is significant because of the potential for the remote generation of ultraviolet (UV) radiation, which still allows access to linear excitation cross sections without the need for the propagation of UV light through the atmosphere. We performed experiments examining the pump-wavelength dependence of the third-harmonic conversion efficiency. These experiments indicate a strong wavelength dependence; for a fixed intensity, the conversion efficiency for 1.5 μm pump wavelengths is approximately a factor of 3–4 greater than at 800 nm. We performed follow-up lab experiments using the generated third-harmonic light to excite multiple biological materials. These experiments successfully allowed for the

simultaneous measurement of tryptophan, nicotinamide adenine dinucleotide **(**NADH), and riboflavin signatures, using one NIR laser source. The data demonstrated a resonant energy transfer between tryptophan and NADH, suppressing the tryptophan fluorescence and producing a blue-shifted NADH fluorescence spectrum. As the pump wavelength was tuned from 800 nm to 1225 nm, the third harmonic was no longer resonant with the tryptophan absorption, thus shifting the NADH fluorescence red to ~ 450 nm. We are developing system-performance models based on these laboratory measurements.

67099

Polymer Electronic Devices and Materials

D. L. Barton, D. A. Chinn, G. R. Anderson, F. L. Lucero, C. A. Zimmerly, P. M. Baca, R. W. Olsen, F. P. Doty, S. M. Dirk, D. R. Wheeler, K. Rahimian, T. M. Berg, T. A. Ulibarri

This project launched the development of a polymer electronics core competency at Sandia to support several Strategic Business Unit (SBU) microsystems integration issues. We successfully collected the expertise that existed throughout the laboratories and made significant progress toward the development of a useful technology for large-scale, complex devices applicable to the current needs of Sandia and its customers.

We initiated a systematic process to address the critical materials issues and develop the infrastructure for device processing and device and material characterization. The issues are as follows:

(1) The need for high-mobility charge carriers in semiconductors and high-conductivity conductors,

(2) Materials that can be processed or deposited as needed by the application,

(3) Pure materials that can yield consistent, predictable performance, and

(4) Air-stable materials for applications that cannot guarantee hermetic packaging.

To support these issues, we focused our efforts in the following areas:

(1) Creating highly conducting and processible nonmetals or "synthetic metals" using dopants and nanoparticles

(2) Creating bulk heterojunctions with high "mobility" or high "charge collection efficiency" materials for nuclear nanobatteries and for ionizing radiation detection

(3) Gaining an understanding of junctions between dissimilar conducting polymers and between heterojunctions in the bulk on a nanoscale

(4) Making solutions that are "spin-castable" and "ink-jettable"

(5) Making materials that are air stable under moderate fields over long periods

(6) Creating materials that stop ionizing radiation so it can be measured

(7) Measuring conductivity and carrier densities of numerous polymers and blends using four-point-probe (van der Pauw) and Hall-effect methods.

(8) Determining how molecular weight and purity affect conductivity, mobility, and absorbance

(9) Characterizing the bandgap and work functions of select materials through the use of ultraviolet and visible spectroscopy to allow us to understand the device physics of fabricated junctions.

- *Polymer device fabrication and fluid formulations for process compatibility.* We developed an inkjet printing system and polymer device fabrication infrastructure and process flows that allowed us to fabricate an array of devices that range from test structures for materials evaluation to multilayer, complex polymer circuits and sensors. This activity area also includes the development of fluid formulations for inkjet and spin-cast processing. The results range from advanced filtering techniques to milling and preparation of suspensions, as well as to converting suspensions to solutions (especially for polymer conductor materials like polyethylene dioxythiophene [PEDOT] and polypyrrole [PPY], which are difficult to ink-jet dispense). Other aspects include molecular-weight separation techniques, purification of materials, and solution development for process compatibility with previously deposited layers. We also developed retreatment techniques for surfaces for process compatibility and the resulting material quality control.
- *Materials development*. Most laboratories work with a single material. Based on customer needs, we began working with numerous materials. Another advantage of having expertise in numerous pi-conjugated materials is that future complex devices will require multiple functions. Each material works best in certain applications. The literature is very inconsistent on material properties due to factors such as different synthesis techniques, different solvents, and different measurement techniques.

To bring order to the literature and to help us design and fabricate devices, we are collecting data on the following relevant materials (listed to convey the broad range of materials being evaluated for different applications).

- *Polymers*.

  PPV family—MEHPPV, D1PPV

  Polythiophenes—linear PT, regioregular poly 3 hexyl thiophene, RRP3HT

  RRP3HT (from several sources for comparison)

  Polyanilines—linear PANI, methyl PANI, N-methyl PANI

  Polypyrrole—linear PPY powders and suspensions

  Polyethylene dioxythiophene—PEDOT suspensions

  Polyethylnylene—PY

Polyfluorine—PF
Polyacetylene—substituted PA
Polyphenylene sulfide—PPS
A new STAR polymer from EIC Laboratories

- *Nanoparticles*.
  C60
  As-made single-wall nanotubes SWNT
  Purified/open-ended single-wall nanotubes PSWNT
  Substituted or functionalized C60
  Surface-modified nanotubes
- *Dopants*.
  BARF—boron tetra(3,5 trifluoromethyl phenylene) sodium salt (Sandia-developed)
  Iodine
  HCl

Some of the other materials-development activities included soxhlet extraction, synthesis of highly pure D1PPV, evaluation of composites for bulk heterojunctions, solution processing with solvents, nanotube modification, monomer deposition polymerizing after pattern dispensing and interface smoothing, evaluation of differences in PPY formulations and resulting material conductivity, and an evaluation of the relative conductivity of PEDOT, PPY, and carbon nanotube (CNT)–modified films.

We paid particular attention to the use of carbon nanoparticles to increase the conductivity of conducting polymers. Phase segregation was a problem with as-made nanoparticles because the graphitic carbon surface does not wet with polymer solutions. Single-walled NTs (nanotubes) promise better electrical properties than do multiwalled NTs, but require a metal catalyst to form. To make the NTs more soluble, as well as remove some of the metals, we applied the following chemical treatments. To modify the surface, we modified carbon nanoparticles by hydrogenation and treated the nanoparticles with perchloric and concentrated sulfuric acid. We tested the resulting films via simple resistivity-measurement techniques with the best films (lowest resistivity) evaluated with four-point-probe measurements and Hall-effect measurements. The results showed significant differences in the resistivity and the solution processibility of the materials.

- *Devices*. In addition to the materials-development activities, we had good results fabricating a number of test devices. We fabricated many Schottky diode arrays with a five-layer, all-inkjet process. The arrays are the first completely free inkjet-processed polymer memories that have been made.

We fabricated other devices such as a solar cell/betavoltaic battery (conceptually proven to be viable), a position-sensitive radiation detector (fabricated, tested, and reported on), synthetic metals, polymer antennas, and several types of test chips.

Other Communications

Doty, F. P., D. A. Chinn, C. M. Muñoz, R. W. Olsen, A. J. Antolak, and D. H. Morse. 2004. Fast neutron radiography detectors based on organic semiconductors. Paper presented at the SPIE 49th Annual Meeting, 2–6 August, Denver, Colorado.

67101

Small Circuits for Cryptography

T. J. Draelos, W. E. Anderson, C. L. Beaver, R. D. Miller, M. D. Torgerson, R. C. Schroeppel

There are applications where a small circuit is needed to perform encryption or authentication and speed is less critical. A serial approach to cryptographic processing of information can reduce circuit size. This can also reduce power needs and may help with the total energy required per operation. All of these positive attributes of small circuits will enhance the security of sensors and communication in unattended, battery-operated, resource-constrained settings. The design of small cryptographic circuits will allow information security to be embedded in sensors for nonproliferation and materials-control monitoring and for military and homeland defense applications.

Sandia will develop small circuits for important cryptographic primitive operations such as the following:

- *Encryption with the new Advanced Encryption Standard (AES) cipher,*
- *Hashing with the Secure Hash Algorithm (SHA-1),*
- *ManTiCore and cipher-state (CS) authenticated encryption with algorithms developed under another project,*
- *Serpent cipher, and*
- *Public-key cryptography operations.*

Our focus is on small serial implementations of algorithms as opposed to large parallel ones. As such, we will explore the use of tiny cryptographic circuits, recognizing the typical trade-off between size and speed.

Listed by milestones, the following describes our accomplishments:

- *Research and select cryptographic primitives for small circuits*. We selected the following cryptographic primitives on which to conduct research and development of small circuits:
  - *AES*.
  - *CS-AES*. The CS mode of the AES, developed in another project. We submitted the CS-AES algorithm to the National Institute of Standards and Technology (NIST) as a proposed mode for the AES.
  - *SHA-1*.
  - *MTC4, RMTC4, Pepper*. The ManTiCore algorithms, MTC4, RMTC4, and Pepper, developed in another project. These algorithms utilize a hash algorithm, such as SHA-1, as a cryptographic primitive.

- *Serpent*. The Serpent cipher was a candidate for the AES and is recognized as the most hardware-friendly encryption algorithm of the AES candidates.
- *Public-key cryptography primitives*. RSA (Rivest, Shamir, and Adleman), Diffie-Hellman, and selected elliptic-curve operations are important for public-key encryption, authentication, and exchange.

- *Provide a family of specifications for each selected algorithm suitable for a trade space of speed versus size*. We focused on minimizing the circuit needed for the AES. We developed and tested Verilog hardware-description-language (VHDL) code for a family of AES circuits on a field-programmable gate array **(**FPGA) development board. Our smallest circuit is one-third the size of the smallest "other" AES circuit, with sufficient speed for most applications.

We also implemented CS-AES, SHA-1, MTC4, RMTC4, and Pepper in VHDL. Work to minimize the circuits for these algorithms is ongoing.

- *Perform theoretical performance analysis of circuits*. We replaced the theoretical performance analysis expected for this project by the ability to perform an empirical performance analysis with the purchase and utilization of FPGA development boards.

Our smallest circuit is one-third the size of the smallest "other" AES circuit, with sufficient speed for most applications.

67102

Analysis of Multichannel Internet Communication

C. E. Nove, C. O. Rogers, S. Y. Goldsmith, R. F. Maclin

Sandia is evaluating a novel method that employs machine-based learning to identify messages related to other messages. This technique may enable an analyst to identify and correlate a small number of related messages from a large sample of individual messages. The classic machine-learning techniques of decision trees and naïve Bayes classification are seeded with few (or no) messages of interest and "learn" to identify other related messages. We evaluated and generalized the performance of this approach and these specific learning techniques.

We evaluated the utility of applying three active-learning techniques to the problem of searching large amounts of captured conversation data. This approach differs from the traditional machine-learning paradigm, since it starts with a very small amount of information (or none at all) and proceeds incrementally instead of learning all at once beforehand with a large batch of data. The three techniques tested using this approach were naïve Bayes with seed messages, naïve Bayes with no seeds, and decision tree with seed messages.

This approach differs from the traditional machine-learning paradigm, since it starts with a very small amount of information (or none at all) and proceeds incrementally instead of learning all at once beforehand with a large batch of data.

None of the three approaches was clearly the best; each outperformed the others on two out of the six datasets. However, we can offer observations on why some topics were easier than others. One characteristic of topics that were better retrieved is a unique vocabulary. Topics with specialized technical language are easier to identify than conversational exchanges. Another characteristic is a sufficiently narrow focus. One test dataset contained conversations on two distinguishable facets of a single topic, and this often caused learning to occur in two separate runs. A third characteristic is a good seed, which applies of course only to the seeded-Bayes and decision-tree methods. Finding a seed that is representative of the dataset can substantially improve the results of the search process.

We evaluated messages solely on the basis of the words found in the messages. Applying these active-learning methods using a greater number of attributes, such as user IDs, phrases, word proximity, and word frequencies, may provide better discrimination of conversations of interest.

67104

Receiver for Ultralow-Power Wake-Up and Command

J. A. Payne, S. J. Leslie, K. W. Plummer, R. W. Brocato, M. B. Murphy, J. A. Payne, K. T. Stalker, M. D. Sena, R. Chanchani, R. C. Ghormley, II

There is a broad range of electronic military systems that are infrequently used but that must be available to a remote operator at a moment's notice. Instead of constantly powering these large devices, Sandia aims to create an ultralow-power wake-up and command radio-frequency (RF) receiver to allow a connected device to remain off until needed. This receiver, called the "LDRD receiver" herein, will allow, for example, a remote inaccessible video camera to achieve a useful life of months rather than days. The chosen approach addresses not only RF aspects of the receiver, but power and packaging issues as well. This project successfully field-tested a brassboard version of the receiver at a range of 3 mi with an equivalent power consumption of 20 µW. Miniaturization of the brassboard demonstration platform is on track with the identification of chip-scale–packaged components and miniature batteries. A secondary goal of this effort is to implement a solar-trickle–charged secondary battery. Brassboard field tests of this hybrid power system showed considerable promise for a receiver lifetime limited only by the wear-out life of the battery. Our work has a twofold emphasis: (1) to miniaturize the LDRD receiver, and (2) to add a transmit capability to form an ultrasmall, low-power transceiver. This transmission capability, along with a simple analog-to-digital converter, will add basic remote-sensing capability for low-rate data such as temperature, switch positions, or host-device status.

This receiver...will allow, for example, a remote inaccessible video camera to achieve a useful life of months rather than days.

We made the following accomplishments:

- *Evaluated and rejected surface acoustic-wave (SAW) correlator wake-up receiver for use in LDRD transceiver.* Our original proposal focused on milestones leading toward the completion of a brassboard consisting of two receivers: a SAW correlator wake-up receiver and a frequency-shift–keyed (FSK) command receiver. Previous Sandia work in the SAW-correlator area focused on applications where ample transmit power is available. A sensitivity measurement was performed, and the correlator was found to need at least -10 dBm of RF power to function. We proposed a front-end low-noise-amplifier architecture for the SAW correlator having a

combined RF gain of 57.5 dB and a quiescent current drain of 22 mA at 3 V. This addition would allow the device to be used with remote wake-up signals, but requires more power than is needed for the FSK command receiver. For this reason, we will not integrate the SAW correlator wake-up receiver into the miniaturized LDRD receiver in upcoming work.

- *Designed and tested FSK wake-up and command receiver.* The RF circuitry consists of an FSK transceiver and microcontroller. Sensitivity is -97 dBm for 100 kb/s data (Manchester encoded). A transmit power of up to +10 dBm is available for upcoming transceiver applications. We field-tested this circuitry and showed it to have the sensitivity necessary for remote wake-up. We performed the test with both a test transmitter and the LDRD receiver brassboard located near the ground and found that propagation losses were bounded by free space and two-ray propagation models.
- *Designed and tested new antenna*. We tested several antennas for use with the LDRD receiver. We found that a folded dipole antenna had about twice the bandwidth and similar gain to a standard dipole. Field tests performed with each antenna also showed similar link performance with each antenna.
- *Designed a solar-recharged battery.* We explored microphotovoltaic systems for use with the LDRD receiver. Such an approach will allow a system lifetime limited only by the charge-discharge life of the battery. This approach is particularly important during miniaturization activities because the battery begins to dominate the size budget for applications > 1 month. The challenge in a microphotovoltaic system is the efficient conversion of highly variable photovoltaic-cell voltage to a usable battery-charge voltage. We used special ultralow quiescent current regulators with a solar array of 1.75 x 2 in. to charge a 20 mAh battery in 2 hr during a solar irradiance of 1000 W/m^2. This daytime-charge rate easily supplies the current necessary to charge the battery for continuous receiver operation 24 hr a day.

67105

Extraordinary Optical Transmission Through Patterned Subwavelength Apertures

D. W. Peters, C. E. Lanes, S. A. Kemme, G. R. Hadley, I. F. El-Kady

Light propagating through a subwavelength aperture can be dramatically increased (by hundreds) by applying texture to the metal around the hole. Moreover, light that would typically diverge uniformly when passing through an unpatterned subwavelength hole can be directed into a narrow beam by utilizing a specific pattern around the aperture. While the increased transmission and narrowed angular emission appear to defy far-field diffraction theory, they are consistent with a fortuitous plasmon/photon coupling.

Sandia explored the transmission and emission from such a surface, with the goal of optimizing structure parameters and extending research from the visible regime into the infrared (IR). Results indicated the ability to tailor the emission and transmission characteristics. We also demonstrated the ability to optimize a structure for maximum transmission.

We performed numerical simulations using commercial and Sandia-developed code. Algorithm development performed under this project will add to Sandia's numerical toolset and will be available for future numerical simulation needs.

In this project, we focused on two issues: (1) tunability of the transmission and emission spectra through the manipulation of structure parameters, and (2) optimization of emission and transmission properties of patterned apertures.

We studied the tailorability of transmission and emission characteristics using in-house and commercial software packages. We modified a scalar Helmholtz equation–based finite-difference-method code to properly model the boundary conditions necessary in such a structure. This code will be available for other projects in the future. We showed that the transmission and emission peaks could be moved in the spectrum by adjusting structure parameters. Shifting from the visible to the IR is not merely a linear scaling of the device sizes since metal properties vary considerably across this range. We investigated these properties and the appropriate structure parameters needed in different wavelength regimes. Optimization of these parameters led to increased transmission and emission.

We now have a greater understanding of the mechanisms that affect the emission and transmission through patterned

apertures in thin metal films. This knowledge could be applied to application areas such as near-field microscopy.

Refereed

Peters, D. W., I. El-Kady, S. A. Kemme, and G. R. Hadley. 2004. Surface plasmon-assisted transmission and emission from subwavelength-patterned apertures. *Proc. DOMO Conference*, accepted.

67107

Reconstruction Algorithm Development and Assessment for a Computed Tomography–Based Spectral Imager

B. K. Ford, J. S. Salazar, M. P. Wilson, D. E. Bodette, R. L. Bilisoly, C. L. Grotbeck

Within the field of remote sensing, multiplexed imaging (MI) spectrometers offer distinct advantages over standard scanning systems. Potential benefits include increased data-collection rates; spatial, spectral, and temporal co-registration; and improved signal-to-noise ratios (SNRs). Offsetting these benefits are the complexity and inaccuracy of computational methods required to reconstruct the three-dimensional (3-D) (x, y, l) object cubes.

Sandia is looking at the complex relationships between the design and calibration of an MI spectrometer and the accuracy and usefulness of associated object-cube estimates. We focused our investigations on the rotating-prism chromotomographic spectrometer (CTS); however, developed techniques may be generally applied to the larger class of instruments. The CTS acquires multiple, dispersed images of remote targets while rotating its prism between images. The prism rotation provides different angular projections of the 3-D (x, y, l) object on the 2-D (x', y') detector array. Knowledge of the optical-transfer function is used to reconstruct a spatial and spectral estimate of the object from this set of projection images.

We concentrated our efforts on the establishment of required infrastructure for CTS simulations, reconstructions, and data analysis. To this end, we generated a range of scene and target data consistent with various configurations and potential mission spaces of the CTS technology. In addition, we generated and compiled a set of reconstruction algorithms used to reconstruct estimates of hyperspectral datacubes from these simulated datasets. This work included developing algorithms to refine reconstructions based on filtered-image constraints. In preparation for an upcoming sensitivity analysis, we developed task-based measures of reconstruction quality (TMRQs). We based these TMRQs on three specific criteria: (1) spectral accuracy of datacube reconstructions, (2) variations in bulk classification due to reconstruction artifacts, and (3) reductions in detectability of point targets due to reconstruction errors. These TMRQs will eventually provide system engineers and end-users with a direct link between system-performance specifications and the desired mission utility.

We completed scene specification for all required scene simulations and received the vast majority of these scenes from SciTec, Inc. An ongoing contract with this company allows us to generate additional scenes and targets as required. We also received a set of higher-spatial- and spectral-resolution imagery from Photon Research Associates. This delivery marked the completion of all originally planned scene simulations.

In addition to creating simulated scene data, SciTEc provided us with sets of single-point and extended (covering multiple pixels) targets. The temporally varying targets are embedded within the various scenes to test our evolving TMRQs. Material maps were provided for the same purpose.

We completed programs to generate CTS images from scene-simulation data. These programs assume a theoretically derived system-transfer function that is perfectly known. We utilized a previously developed algorithm to incorporate ray-trace models exported from the optical design program Zemax.

We also completed programs that take the CTS images and reconstruct estimates of their corresponding datacubes. We showed that significant improvements in reconstruction accuracy can be obtained by utilizing auxiliary filtered images. Filtered-image constraints greatly reduce reconstruction artifacts associated with standard reconstruction algorithms while improving our TMRQs.

We selected a set of TMRQs for assessing reconstruction quality in terms of mission utility. These TMRQs are based upon three separate mission-based criteria: (1) spatial- and spectral-reconstruction accuracy, (2) bulk material classification, and (3) target detection and identification. For the first TMRQ, we are specifically interested in how accurately spectra are reconstructed at each ground sample. While this is an important parameter for assessing strict reconstruction accuracy, it does not hold the answers to questions most likely posed by end-users. Specifically, it does not include any information regarding how the data will be used or, better yet, whether or not the data are accurate enough to meet specific mission requirements.

To this end, we looked at two possible mission scenarios. The first involves the need to perform bulk classifications on all materials within the scene. This would correspond to fairly general classes such as vegetation, water, and bare soil. We are interested in quantifying the difference between bulk classification using data collected by a “standard hyperspectral instrument” (no reconstruction required) and a CTS. The CTS data will inherently be corrupted by reconstruction artifacts. We selected the algorithm used for classification. The method of

quantifying changes in bulk classification is nearly complete and is being tested. The second mission scenario assumes a need to detect/identify point targets against a cluttered background. Thus, the associated TMRQ is based upon the relative proportions of true positives, true negatives, false positives, and false negatives.

We began laying the groundwork for an upcoming sensitivity analysis. Currently, we are developing programs to simulate platform motion. While the full analysis of this error source is scheduled for future work, we are developing programs to apply an existing jitter model to CTS datasets. Soon, we will begin the process of adding varying amounts of modeled noise to simulated CTS imagery. This SNR study will represent our first sensitivity analysis using our developed TMRQs.

67108

Power-Combining Techniques for Solid-State Power Amplifiers

B. H. Strassner, II, A. Ganti, C. P. Tigges, G. A. Wouters

Efficient high-power radio-frequency (RF) amplifiers are a key component in a variety of Sandia satellite, radar, and communication systems. Current technologies have restrictive efficiency limits at high frequencies, which result in inadequate output power, excessive system-power dissipation, and/or large size. Key to achieving high-efficiency power amplifiers is the realization of high-efficiency power combiners. Unfortunately, there is no known design method for these power combiners, especially when required for high bandwidths as with many Sandia applications. In this project, Sandia addressed the development and computer optimization of very high-efficiency broadband RF power combiners.

We achieved prototype nine-port power combiners with exceptional simulated performance (i.e., ~ 90% efficient) as compared to all known literature.

We achieved prototype nine-port power combiners with exceptional simulated performance (i.e., ~ 90% efficient) as compared to all known literature. These power combiners should be an enabling component for miniature high-performance solid-state power amplifiers (SSPAs). We obtained these results by custom optimization techniques/software, an approximately one-year computer simulation time, an intelligent combiner geometry choice, and, admittedly, a bit of luck.

Computer optimization of the combiner structure greatly limited the project schedule. Therefore, we were unable to demonstrate an actual amplifier using these new advanced power combiners.

We chose to bypass the originally planned test structures at lower test frequencies and move directly into a structure useful for a moderate power SSPA for Sandia's synthetic-aperture radar (SAR) program (15.2–18.2 GHz with eight input ports). This resulted in a somewhat increased risk in realization as well as in increased numerical complexity (i.e., simulation time) of the power combiner. Fortunately, we achieved an excellent power-combiner structure.

We chose to use a proven commercial electromagnetic (EM) field solver as the computational engine. Our task then became to select a suitable seed geometry and an optimization technique for the power combiner. We considered a variety of seed structures along with suitable parametric geometric models. We then applied a variety of optimization techniques to these models, from which certain structures eventually evolved.

We also completed a survey of single-chip SSPAs that cover the frequency range of Sandia's Ku-band SAR system. Further, we identified the two best candidates and confirmed component operation per manufacturer specifications. These commercial SSPAs along with our nine-port power combiner should readily allow for the realization of an SSPA with over 30 W output power for Sandia's SAR application.

67109

Dispersive Diffractive Optical Elements for the Infrared

S. A. Kemme, T. R. Carter, S. Samora, D. W. Peters, C. L. Grotbeck, J. R. Wendt

Sandia will develop two new diffractive optical element (DOE) technologies: (1) a broad wavelength-band effective antireflection (AR) structure, and (2) a design tool to encode polarization and dispersion information into a unique diffraction pattern.

The first technology is an antireflective layer that may be etched into the DOE surface. For many wavelengths of interest to the remote-sensing communities (e.g., 1.9–2.5 µm), transmissive silicon (Si) DOEs are ideal. However, a significant portion of light (30% from each surface) is lost due to Fresnel reflection at the Si/air interfaces. To address this issue, we will implement a subwavelength, surface-relief structure that acts as an effective antireflective coating and is tolerant to varying wavelengths and angles of incidence.

The second DOE component technology is a design tool to determine the optimal DOE surface-relief structure that encodes the light's degree of polarization and dispersion into a unique spatial pattern. Many signals of interest have unique spatial, temporal, spectral, and polarization signatures. The ability to determine the degree of polarization and disperse the signal into a unique diffraction pattern would result in improved signal-detection sensitivity with a simultaneous reduction in the false alarm.

Success of these technologies is highly dependent on the quality of fabrication. Sandia has state-of-the-art fabrication capabilities: e-beam feature definition, precision etching of several materials, and advanced modeling tools to predict realistic DOE performance.

These proposed DOE technologies address Sandia's Nonproliferation and Materials Control Strategic Business Unit's call for global virtual presence and technologies for international security.

We numerically investigated the effect of a binary grating etched into Si. Rigorous coupled-wave analysis models the orders reflected and transmitted from the grating and is used to model the effect of the grating over a wide range of grating periods, from subwavelength to much larger than the wavelength. We began fabricating this subwavelength optical component. With this numerical design tool, we identified a

broad wavelength and angular band and a triangular profile that performs well as an effective antireflective coating.

We first defined the optical birefringence and dispersion of the subwavelength photonic device with the goal that the two polarizations (TE [transverse electric] and TM [transverse magnetic]) could be completely separated into two angular ranges. We developed a numerical design code that calculates the effective index versus wavelength for two polarizations (dispersion and birefringence). We developed the fabrication conditions for nanoscale photonic structure in gallium arsenide (GaAs) with newly installed chemically assisted reactive ion-beam etching (CAIBE) equipment. We achieved a well-controlled vertical feature with an aspect ratio of 10. We designed a subwavelength device with greater than 0.35° angular dispersion for the wavelength range of interest and for the two polarizations. This device is under fabrication and will be ready for testing in upcoming work.

Refereed

Kemme, S. A., D. W. Peters, T. R. Carter, S. Samora, D. S. Ruby, and S. H. Zaidi. 2004. Inadvertent and intentional subwavelength surface texture on microoptical components. *Proc. SPIE Photonics West* **5347** (January, San Jose, California): 247–54.

Other Communications

Kemme, S. A., D. W. Peters, T. R. Carter, S. Samora, and J. J. Hudgens. 2004. Subwavelength structures for micropolarizers and LO applications. Paper presented at the HAVE Forum, September, Lexington, Massachusetts.

67111

Atmospheric Propagation of Terahertz Radiation

R. J. Foltynowicz

Terahertz technologies have been proposed as solutions to many current problems such as remote sensing of bio-chem (biological-chemical) agents and explosives, covert terrestrial and space-based communications, and cold-body tracking. While the promise for terahertz looms large, there are many issues that need to be resolved for full exploitation of this frequency range. Some address the technical immaturity of the technology in this frequency range, including the lack of compact, tunable sources, detectors, and other standard optical components. Besides the hardware problems, there are three very fundamental issues: (1) What is the atmospheric transparency in the terahertz frequency range? (2) How do we separate desired signals from the thermal blackbody-background created by any warm object present in the terahertz? (3) What are the signatures of materials between 0.1 and 10 THz? In this work, Sandia will address the first question regarding the atmospheric transmission to determine in what instances the other two should be examined. In the field of atmospheric terahertz propagation, there exists a wealth of simulated transmission spectra. These programs are based on experimental data; the peak positions of molecular absorption are accurate; and the absorption coefficients at the peak positions are thought to be fairly accurate. However, the background absorption coefficients between the absorption lines are empirical and of unknown accuracy. For many of our applications, such as cold-body tracking, the transmission windows are very important; thus, verifying this information is of critical importance to applications of interest to Sandia.

We made significant progress in recent work. We completed our literature study on the state-of-the-art experimental and theoretical knowledge base on the atmospheric propagation of terahertz radiation. We pinpointed experimental gaps in this database and also pinpointed transmission windows at different altitudes. We constructed a bibliography of the best experimental and theoretical literature on this topic. We acquired the fast atmospheric signature code (FASCODE) and FASCODE for the environment (FASE) atmospheric radiation codes that we will use to enhance our understanding of our measured data. We used the results from Siegel's published calculations on Mauna Kea (14,000 ft) using Airhead Software

to validate our copy of the FASE radiation code. We successfully reproduced Siegel's results from 0 to 500 GHz. In addition, we completed our experimental plan that will test the radiation codes and expand our knowledge base on terahertz propagation through the atmosphere. The most significant accomplishment was completing the building of the terahertz time-domain spectrometer.

The most significant accomplishment was completing the building of the terahertz time-domain spectrometer.

67113

High-Confidence Estimation of Relative Event Locations from Space-Based Sensors

K. M. Simonson, E. A. Shields, M. M. Moya, F. R. Tanner, S. Drescher, R. L. Schmidt, R. D. Wickstrom, E. N. Reckase

The ability to measure the relative positions of different events is a critical part of the intelligence, surveillance, and reconnaissance (ISR) mission. For long-range sensors with limited capability for absolute geolocation, accurate relative positioning is generally achieved only for events that occur simultaneously. This project will enable accurate and precise estimation of the relative locations of events that are not temporally coincident.

Sandia's technical approach in this project builds on recent advances in statistics-based methods for image cross-registration. A newly developed Sandia technique for registration is unique in providing a well-defined measure of the statistical uncertainty associated with the solution. Poor solutions are automatically recognized, minimizing the opportunity for errors to propagate. We successfully extended statistical registration to subpixel levels of precision. In addition, a rigorous statistical characterization of a specific sensor and all of its data-collection modes is well under way. This latter work allowed us to demonstrate high-confidence registration solutions that are based on scene features rather than sensor artifacts.

We successfully extended statistical registration to subpixel levels of precision.

Our research advanced along two tracks: image registration and sensor characterization. We obtained excellent results on each track.

We made the following accomplishments:

- *Image registration.*

(1) We extended a Sandia-developed registration technique based on cross-correlation of whitened image subregions ("chips") to subpixel levels of precision. This technique was the subject of an earlier technical advance (SD-7315/S-100,138).

(2) We developed a new edge-based method for image registration that automatically chooses chips based on the statistical distribution of the metric used to determine match quality. For some sensors, this approach will prove to be more robust (than correlation-based registration) to residual sensor artifacts, allowing for registration that is based solely on scene content. We are filing a technical advance for the new edge-based registration technique.

(3) We defined a robust statistical technique for estimating six-parameter affine transformations describing the spatial relationship between two sensor frames taken at different times. From this information, an event observed at a specific pixel location in the first frame can be tied to a well-defined confidence region for the corresponding location in the second frame.

These elements together provide the mathematical framework for high-confidence measurement of the relative locations of events that are not temporally coincident, a critical technology requirement for the success of the project.

- *Sensor characterization.*

(1) We developed a preliminary sensor model that incorporates contributions from all known signal and noise (deterministic as well as random) sources. This model is based on a physical understanding of the sensor along with supporting data.

(2) We outlined a protocol for experiments and data collections that can be used to estimate the magnitude of each of the contributing terms as a function of measurable quantities.

The goal of the sensor-characterization task is to develop a robust algorithm for automated processing of sensor data, which provides output frames that are minimally influenced by sensor artifacts.

67114

Critical-Infrastructure System-of-Systems Assessment Methodology

J. M. Depoy, R. C. Parks, G. B. Varnado, J. M. Phelan, P. L. Campbell, T. M. Torres, G. D. Wyss, J. E. Stamp

Physical-security and cyber systems (process-control systems, communications, Internet, data storage, information technology [IT] enterprises) are tightly integrated in critical-infrastructure (CI) facilities. However, we lack a security-assessment method that facilitates security analysis of this cyber-/physical-security system integration. Current assessment methods view the CI facilities as tightly bounded systems rather than as the complex system-of-systems they have become. In addition, lessons learned from recent CI assessments that included both physical and cyber components point out the need for integrated assessment methods to identify potentially critical problems, introduced by physical and cyber integration.

Sandia will create an integrated methodology for assessing CI by leveraging existing assessment methods used for physical- and cyber-security analysis. We will investigate possible points of interface between current assessment methods and identify the corresponding interactions between physical and cyber systems. We will also develop new methods or subprocesses to support the assessment of critical interplay between physical and cyber elements. A key source of incompatibility among risk-assessment methods in the past has been the use of inconsistent risk metrics to support this integrated assessment methodology. This combined methodology will allow rapid assessment of CI vulnerabilities due to the dynamic nature of the threats we face. To address this problem, we seek to develop a risk-assessment methodology with automated tools that accounts for the integration of physical and cyber elements in CI systems to analyze vulnerabilities, understand the interdependencies between the two systems, and allow decision makers the ability to understand the trade-offs associated with security upgrades.

One important task for this project was to research existing risk-analysis methods within the cyber computer-security domain, the physical-security domain, and other relevant domains to identify the methods germane to extension, modification, or hybridization for developing an integrated physical- and cyber-security assessment capability.

Another important task is to identify critical interfaces and points of interaction among physical, information/IT, personnel,

and operational interfaces. We are considering the following four bounding cases for our physical/cyber analysis:

(1) Physical-only attack—adversary attacks commodity-delivery-system components using only physical means.

(2) Cyber-only attack—adversary manipulates cyber-controlled commodity-delivery-system components using only cyber means.

(3) Cyber-enabled physical attack—adversary uses cyber system to disable cyber-controlled physical-protection elements to facilitate a physical attack on commodity-delivery-system components.

(4) Physically enabled cyber attack—adversary gains physical access to cyber-control components to facilitate manipulation of cyber-controlled commodity-delivery-system components.

These bounding cases help to identify those critical assets required to meet mission objectives and, of those assets, the ones that are physical/cyber interface points.

We are evaluating various tools for helping to identify these interfaces. To date, we have analyzed fault trees, event trees, attack diagrams, influence diagrams, and state-space tools using specially developed example infrastructure and automation systems.

Other tasks include refinement of the definitions for consequence, threat, and vulnerabilities within the context of the integrated risk-assessment methodology, and identification of meaningful metrics to calculate integrated risk values (based on the new definitions for risk variables). These tasks are in progress.

Refining current tools to help visualize system characteristics is an ongoing task; in conjunction with the identification of interface points, we are evaluating and modifying various tools to provide the information required. We are using object models to represent the systems and the cyber/physical interfaces.

Also, we are developing a draft methodology that will be applied to case studies in future work. A framework for the methodology will be complete at the end of the fiscal year.

Finally, we will propose preliminary architectures for automating the methodology. This is ongoing, and we have already identified portions of the methodology for automation, specifically the planning and scoping portions of the methodology, which are done up front in any assessment.

67115

Dynamic Vulnerability Assessment

C. L. Nelson, S. E. Jordan, C. L. Allen

With increased terrorist threats in the past few years, it is no longer feasible to feel confident that a facility is well protected with a static security system. Potential adversaries often research their targets, examining procedural and system changes, to attack at a vulnerable time. Such system changes may include scheduled sensor maintenance, scheduled or unscheduled changes in the guard force, facility-alert-level changes, sensor failures or degradation, etc. All of these changes impact the system effectiveness and can make a facility more vulnerable. Currently, a standard analysis of system effectiveness is performed approximately every 6 months using a vulnerability-assessment tool called ASSESS (Analytical Systems and Software for Evaluating Safeguards and Systems). New standards for determining a facility's system effectiveness will be defined by tools that are currently under development, such as ATLAS (Adversary Time-Line Analysis System) and NEXTGEN (Next-Generation Security Simulation). Although these tools are useful to model analyses at different spatial resolutions and can support some sensor dynamics using statistical models, they are limited in that they require a static system state as input. They cannot account for the dynamics of the system through day-to-day operations. Sandia's emphasis in this project was to determine the feasibility of dynamically monitoring the facility security system and performing an analysis as changes occur. Hence, the system effectiveness is known at all times, greatly assisting time-critical decisions in response to a threat or a potential threat.

A need exists to determine the effectiveness of a facility's security system on a dynamic basis. Although a vulnerability analysis (VA) is generally performed biannually on a system, the system effectiveness changes continually. This may be due to sensor failures, degradation of sensors over time, removal or replacement of certain safeguards, guard-shift changes, unexpected absences of members of the guard force, maintenance schedules, etc. When changes are made to the physical-protection system, a new VA is executed, providing immediate results that could greatly influence the placement or movement of security forces and/or assets. For this project, we developed a proof-of-concept simulation of a system that could detect changes in the security system and automatically produce new VA results. This required accessing and manipulating data

files and performance values that are created or maintained by existing VA tools to produce results on an as-needed basis. The analysis algorithms used in this simulation were from the “Outsider Analysis” tools in ASSESS. As long as the data are accessible, algorithms from ATLAS or NEXTGEN could also be used. The simulation shows that system effectiveness could be updated dynamically as system changes occur.

67116

Inflatable Antenna with Adaptive Actuators

H. Sumali, J. E. Massad, J. W. Martin, P. M. Chaplya

High resolution in antennas for monitoring the movement and proliferation of weapons of mass destruction (WMD) demands large apertures. Current large-aperture antennas are heavy and very expensive to launch. Sandia is developing a shape-controlled deployable reflector that has the following features: (1) lightweight, membrane-based, (2) compactly folded or rolled before launch and then deployed on orbit, and (3) actively shape-controlled to steer its beam.

We learned from Sandia's National Space Programs department that foldable or rollable flexible reflectors are more robust against damages from meteorites and have deploying advantages over inflatable reflectors. Because of this knowledge, we modified the goal of this project to include developing a foldable, rollable, or otherwise deployable reflector rather than an inflatable reflector.

We developed a theory for calculating the shape of the actuated reflector bimorph as a function of actuation voltage distribution. To validate our actuation theory, we performed a finite-element (FE) calculation. The result is within a difference of 2% from the corresponding theoretical simulation. We also developed a theory to determine the voltage distribution that is required to achieve a desired shape.

We fabricated a bimorph of piezoelectric polyvinylidene fluoride (PVDF) with an adhesive layer in the middle. We developed techniques to attach the voltage control lines and the ground to the PVDF pads using a very small amount of silver epoxy.

To actuate an 8 x 8 PVDF segmented membrane array, we created a high-voltage (± 150 V) actuation system. This consisted of a multiplexing "sample-and-hold" amplifier (HV257DB1) that we controlled using digital and analog output boards (National Instruments PXI) and LabVIEW software. The LabVIEW software controls and synchronizes the digital control output lines and the corresponding voltage input into the chip to independently set and maintain a specified control voltage. The outputs are updated at a user-selectable rate to ensure that there is little or no voltage drop on the PVDF pads. We successfully tested the software and the voltage control system.

Refereed

Sumali, H., J. E. Massad, P. M. Chaplya, and J. W. Martin. 2004. Deflection control of a corner-supported plate using segmented in-plane actuators. *Proc. 2004 ASME International Mechanical Engineering Congress and Exposition*, accepted.

Sumali, H., J. W. Martin, J. M. Redmond, and P. M. Chaplya. 2003. Shape control of a flexible mirror and experiment with an electron gun. *Proc. 2003 ASME International Mechanical Engineering Congress and Exposition* **1** (15–21 November, Washington, D.C.): CD-ROM.

Other Communications

Massad, J. E., H. Sumali, P. M. Chaplya, and J. W. Martin. 2004. Deflection model for corner-supported plates with segmented in-plane actuators. *Proc. SPIE Smart Structures and Materials* **1** (5383) (14–18 March, San Diego, California): 309–19.

67117

Data-Driven Dynamic Models of Conflict

L. A. Malczynski, P. H. Kobos, L. A. McNamara, G. A. Hendrickson

In this project, Sandia investigates the factors that lead countries into conflict. Specifically, political, social, and economic factors may offer insight as to how prone a country (or set of countries) may be for intercountry or intracountry conflict. Largely methodological in scope, this study examines the literature for quantitative models that address or attempt to model conflict both in the past and for future insight. The analysis concentrates specifically on the system dynamics paradigm, not the political science mainstream approaches of econometrics and game theory. The application of this paradigm builds upon the most sophisticated attempt at modeling conflict as a result of system-level interactions. This study presents the modeling efforts built on limited data and working literature paradigms and provides recommendations for future attempts at modeling conflict.

System dynamics modeling, the chosen methodological approach upon which the research is based, is intended to develop a useful abstraction of real socioeconomic systems, focusing on the relationships that link concepts together, and to use this abstraction to simulate the development and behavior of the interrelated elements over time. We relied upon previous work to develop useful abstractions of conflict and tried to operationalize those abstractions using a system dynamics software tool.

In some sense, this research is a defense of the methodology—system dynamics—applied to the specific problem domain of international conflict. Past attempts have not become part of the mainstream methodologies used by scholars of international relations. That mainstream is occupied by econometric and game theoretic approaches. However, the widespread availability of quantitative international datasets has not triggered a move toward system dynamics approaches to modeling international conflict. Interestingly, the international relations area of research never widely adopted system dynamics as an analytical tool. This lack of popularity likely stems from the prevalence of contradictory findings in the mainstream quantitative international relations literature on conflict (Beck, 2000), as well as from a backlash to prior efforts (i.e., the Limits-to-Growth model). System dynamics is not taught in international relations programs, as are econometrics and game theory.

The current modeling attempts demonstrated the complexity in format and time coverage available in the quantitative international relations datasets. Additionally, this research explored and developed a modeling methodology for conflict largely as a proof of the concept. The literature offers a multitude of variables purportedly explaining why conflict arises. The final modeling efforts demonstrate the need to further develop the methodological connection between variables that may affect conflict in a modeling environment.

We believe that the data collection, hypothesis selection, and software issues related to building an interactive model in this study highlight the state of the art with respect to system dynamics modeling applied to conflict modeling. Future analysis could examine additional causal links among military spending, the application of technology, demographic-transition issues, sector-specific resource distribution, and other factors that affect relative levels of conflict.

73207

Microoptical Radar (MOR) Facial-Recognition Project

R. D. Habbit, Jr., J. V. Sandusky, T. A. Pitts, A. D. Niese, C. Q. Little, K. O. Wessendorf, T. D. Russ, R. O. Nellums, R. B. Taplin, M. W. Koch, D. J. Savignon, S. K. Dunlap

Sandia seeks to improve security at U.S. points of entry, such as airports and borders, and at critical U.S. facilities, and to move the bad-actor identification process abroad through the development of next-generation three-dimensional (3-D) biometric identification. The fundamental enabling technology will be microoptical radar (MOR) technology coupled with advanced recognition algorithms. We will focus on the use of facial recognition (FR) to address (1) the "9-11 terrorist security problem" by autonomous identification of known terrorists and criminals at points of entry and critical facilities, and (2) the U.S. security-screening problem by helping to identify frequent "good actor" entrants to improve the screening of unknowns and increase the flow of commerce. The recognition problem applies to many applications in which a person or automated process is attempting to identify an object from imagery taken from a distance, such as target recognition and intrusion detection.

Recent news articles illustrated the poor performance of commercial 2-D systems and emphasized the difficultly in FR. We expect that the use of 3-D geometric facial images from MOR will improve performance to acceptable levels. Our approach requires two key technology advances: (1) a small image sensor to unobtrusively capture subcentimeter-resolution 3-D images of moving subjects, and (2) new algorithm constructs to utilize the 3-D information.

For the sensor development, we will specifically address the challenge of high-resolution Flash MOR technologies at the single-pixel level and address the readout challenges of the multipixel, complex, high-speed, low-noise, mixed-mode MOR application-specific integrated circuit (ASIC). We will also examine the utility of 3-D information for FR and evaluate its sensitivity to certain parameters. This will enable 3-D FR sensitivities to be considered during the MOR research and development phase. We expect to demonstrate the feasibility of Flash MOR and 3-D FR algorithms.

Research and discussions continue to highlight the importance of this work for homeland security applications (FR), national security applications (space dominance), and

scientific dominance (space exploration). In all cases, this development will be a key enabling technology, and there continue to be no close alternatives.

- *3-D FR algorithm development*. We focused on improving algorithms for facial segmentation (i.e., removing hair and extraneous clothing), on improving algorithms for facial registration and matching, on integrating different components of the 3-D FR software system, and on performing a preliminary system analysis. Although the target goal is 3-D FR, we are developing the expertise to address the more general problem of 3-D object recognition. We also made significant improvements in algorithm operating speeds by porting the code to Linux.
- *MOR sensor development*. We submitted the higher-resolution pixel architecture (PIX-2) for fabrication. We submitted the readout-integrated-circuit (ROIC) feasibility demonstration ASIC 3 months ahead of schedule. We utilized and developed advanced modeling techniques to accelerate development by minimizing the number of fabrication runs. Since the requirements for MOR designs are so challenging, one side benefit of this project will be the experience gains and efficiency improvement in Sandia's ASIC design and modeling capabilities.

Early test results indicate the design functions; however, there appears to be some unexpected parasitic capacitance in the device. We identified the source of the problem, are modifying the designs, and will resubmit the designs in upcoming work according to the planned schedule for fabrication. As a result of this finding, we made improvements to the modeling-and-design implementation process.

The current die will continue into full die testing for further design investigation as planned.

In addition to the direct MOR sensor work, we developed a new approach for capturing 3-D data at 1500 nm (a key operating wavelength for the MOR) using newly developed electrooptical materials. This work, if successful, will provide additional data to further the MOR sensor development and algorithm development. As a side benefit, it offers an interim solution for present 3-D sensor needs.

Other Communications

Boehnen, C., and T. D. Russ. 2004. A fast multimodal approach to facial feature detection. *Proc. Workshop on Applications in Computer Vision* (January 2005, Breckenridge, Colorado).

Russ, T. D. 2004. 3-D facial recognition. Paper presented at the INMM Workshop on Safeguards and Security Technologies for the 21st Century, March, Albuquerque, New Mexico.

Russ, T. D., M. W. Koch, and C. Q. Little. 2004. 3-D facial recognition: A quantitative analysis. Paper presented at the INMM Annual Conference, July, Orlando, Florida.

Russ, T. D., M. W. Koch, and C. Q. Little. 2004. 3-D facial recognition: A quantitative analysis. *Proc. IEEE Carnahan Conference on Security Technology* (October, Albuquerque, New Mexico).

74760

Automatic-Target-Recognition Algorithms for Uncooled Thermal Imagery

K. T. Malone, G. B. Haschke, M. W. Koch

The ability to automatically recognize targets from uncooled thermal imagery is critical to fielding security systems employing uncooled thermal imagers. Typically, the quality of imagery from uncooled thermal imagers is significantly less than that of their cooled counterparts. This degradation can cause problems in algorithms developed for cooled thermal imagery. Thus, new algorithms tailored specifically for uncooled imagery are necessary for good performance. Sandia is investigating automatic target recognition (ATR) algorithms that are based on three stages: focus of attention, feature extraction, and feature matching. The focus-of-attention stage searches the raw image for moving groups of pixels. If a target is detected, image features are extracted from the appropriate portion of the image. We then compare these features to an existing library of templates.

We collected imagery from three target vehicles at six aspect angles and two imager distances. The algorithm performed very well on imagery from all three vehicles.

The ATR algorithm developed for this project consists of three stages: focus of attention, feature extraction, and feature matching. The focus-of-attention phase is based on previous work done in the field of synthetic-aperture radar (SAR). This stage utilized pixel motion, quantization, and binary morphology to determine a region of interest in the raw thermal image. The target was typically located with three horizontal and six vertical pixels of the correct location.

We selected edge features as appropriate target features for reasons of robustness to intensity variations and minor physical variations in the target. Feature-extraction complexity was also an issue in feature selection. We extracted edge features from a region of an image and matched them to a library of templates using the Hausdorff distance.

We tested the algorithm using data collected during an earlier project. We collected imagery from three target vehicles at six aspect angles and two imager distances. The algorithm performed very well on imagery from all three vehicles. As expected, recognition performance for the smaller vehicle was slightly lower than the that of the two larger vehicles, and performance decreased as the distance to the target increased. A limited brute-force search over location and scale was necessary to compute the best registration for the extracted region of interest. The overall results of this effort are very promising. Future efforts are necessary to determine the recognition

performance as the target set grows and to study the robustness of the algorithm to target occlusion and clutter.

80835

Vulnerability Analysis for SCADA

J. E. Stamp, M. J. Berg, R. P. Custer, E. J. Lee, R. C. Parks

Sandia has extensive field experience in assessing the cyber security of supervisory control and data acquisition (SCADA) systems. Our experience has been that the state of SCADA security is almost uniformly poor in fielded systems, which is of considerable concern for our national critical infrastructure. This project addresses several classes of vulnerabilities in SCADA and automation systems. Our hypothesis is that typical elements in SCADA have significant vulnerabilities that will strongly degrade the cyber security of the overall automation system.

We examined and analyzed vulnerabilities for end devices, protocols, communications, and master stations in the context of a representative model of an operational SCADA system. In this case, we evaluated a programmable logic controller; among its security vulnerabilities, a particular cause for concern included its unsecured in-band management. We used the Ethernet/industrial protocol application protocol, common in automation systems, in the test system. We showed how a hypothetical adversary could alter SCADA messaging to cause undesired control actions, given that the protocol had no encryption, signing, or other security services. Finally, we found that the master station had several important vulnerabilities, including some in the SCADA master software and others in the operating system environment. Overall, the key findings of this project reinforce the hypothesis that security for SCADA systems is hobbled by inadequate security features on the parts of its constituent hardware and software. In the field, the poor security state of SCADA equipment exacerbates inherent problems with security in the modern technology environment.

The key findings of this project reinforce the hypothesis that security for SCADA systems is hobbled by inadequate security features on the parts of its constituent hardware and software.

81209

Randomness Complexity and Cryptography

M. D. Torgerson

As we rely more and more on digital communications, the privacy and security of our electronic data are essential. Sensitive military, financial, and personal information must be kept hidden from prying eyes, and we must ensure that honest parties can communicate securely and privately, even in the presence of malicious adversaries who will do anything to thwart their efforts. This goal of secure and private communication is the essence of cryptography. In this research, Sandia will concentrate on an interleaving set of research questions that all contribute to this goal by using tools from the theory of derandomization.

We will explore the applications of unconditional pseudorandom generators. Can such tools be used in improving the security and/or efficiency of cryptographic protocols? Already, in work by Barak, Ong, and Vadhan, it is shown how to reduce the number of rounds in so-called witness-indistinguishable interactive proofs *by using techniques from derandomization. Can such approaches be applied to practical cryptosystems, resulting in concrete performance gains? In light of the surprising efficacy of derandomization in hardness amplification, these are natural questions that we will answer in this research.*

While much of modern cryptography relies on complexity-theoretic assumptions, recent breakthroughs have been made in constructing cryptographic algorithms in the so-called bounded storage model *(BSM) that do not rely on any complexity-theoretic assumptions. We will investigate the development of efficient cryptographic protocols for the BSM.*

Some known protocols in the BSM place a very large storage burden on the honest parties. A major advantage of the limited-access model is its practical viability. We will investigate this natural extension to the BSM to develop efficient alternatives to less-efficient protocols from the bounded storage paradigm.

The notion of “hardness” is fundamental to the study of cryptography. To be useful, a cryptographic primitive must be resistant to adversarial manipulations. In particular, the difficulty to recover secret information must be beyond the capabilities of the adversary. The study of hardness amplification, in essence, investigates methods of combining smaller hard primitives into larger harder primitives.

This research continues to explore the possibility of building session-key generation protocols in the BSM. We obtained preliminary results, both upper and lower bounds, but there is much more to understand. There appears to be an intimate connection to two-source extractors (i.e., extractors that recover nearly perfect randomness from two imperfect sources, in contrast to extractors that recover nearly perfect randomness from one imperfect source and one [small] truly random source) that are notoriously difficult to construct explicitly.

This research has also led to advancements in the parallel complexity of algebraic operations through the development of extremely fast parallel algorithms for basic algebraic operations over finite fields of characteristic 2. For example, we showed how to multiply field elements, perform field exponentiation, perform division of polynomials with remainder, and perform iterated multiplication of field elements in uniform constant-depth (unbounded fan-in) circuits that have AND, OR, and PARITY gates (and, in some cases, MAJORITY gates). The functions computable by such circuits are known to be a subset of logarithmic-space, and therefore these results also give very small space algorithms for all these problems. We are seeking improvements and extensions for these results.

This research has also led to advancements in the parallel complexity of algebraic operations through the development of extremely fast parallel algorithms for basic algebraic operations over finite fields of characteristic 2.

81354

System Study: Adaptive Optics for Weapon, Reconnaissance, and Military Space Applications

J. A. Palmer, W. D. Cowan, D. E. Lewis, M. W. Smith

Adaptive optics (AO) describes a group of emerging optical technologies. In its most common application, AO provides a means for programmed correction of wavefront aberrations due to factors such as atmospheric distortion in next-generation military assets, including multiple-target acquisition, laser communication and tracking systems, airborne laser radar (ladar), and terminal guidance for penetrating munitions. AO can also include advanced microoptoelectromechanical systems (MOEMS) for hyperspectral imaging (HSI) in electrooptic sensors, beam steering, and pulse forming/phase locking in directed-energy weapons. The objectives of this project are as follows: (1) perform a detailed survey of potential Sandia customers for AO, (2) determine which Sandia products/ technologies can benefit most from AO integration, and (3) discuss how Sandia resources should be allocated in a large-scale AO research effort.

The traditional application for AO is wavefront correction with macroscale deformable mirrors in terrestrial telescopes. However, in this study, Sandia recognizes that AO can also include MOEMS for HSI in electrooptic sensors, beam steering, and pulse forming/phase locking in directed-energy weapons.

The following is a synopsis of broad and high-value AO research in which Sandia may become involved in the future. This information is based on conference presentations from external entities such as Lockheed Martin Corporation and the U.S. departments of Defense and Homeland Security.

- *Beam steering*. All electronic AO beam steering is useful to replace bulky conventional gimbal systems and liquid-crystal scanning mechanisms that attenuate beam power. Potential application areas include infrared countermeasures (IRCMs) for commercial aircraft, and hand-held/airborne ladar target-acquisition systems.
- *Laser communication*. Atmospheric turbulence, clouds, and, in the case of moving aircraft, supersonic bow shock and airfoil boundary-layer effects cause beam spreading, attenuation, scattering, and phase perturbations in laser communication systems. AO can be useful in providing active wavefront correction (referred to as *coherent channel compensation*) in this scenario.

- *Directed-energy weapons*. Certain directed-energy weapon designs rely on the emissions from arrays of smaller lasers. AO may be useful in phase matching the emissions from individual array elements.

Based on the customer inputs received as a part of this study, we recommend that future AO research and development at Sandia be led by cross-functional product realization teams within the Microsystems Engineering Sciences Applications (MESA) initiative. We illustrate this recommendation in the following example. A practical high-value AO project in the near term is AO–based electronic beam steering for unmanned aerial vehicle (UAV) ladar platforms. This project may be managed by customers in one area of Sandia. Microsystems design and fabrication may be conducted through MESA facilities by resources from other areas in Sandia. Performance simulation may be led by MESA resources from still another Sandia area. Packaging and systems integration may be led by MESA experts from some of the same areas that are performing other project tasks identified here. Although this example is not complete, it emphasizes the need for a coordinated approach facilitated by MESA.

Pulsed Power and High Energy Density Sciences

Pulsed Power and High Energy Density Sciences invests in innovations that lead to the development of next-generation pulsed power and high-energy-density science and technology that will facilitate the resolution of important nuclear weapon and national security issues. Investments strive to develop experimental and computational capabilities that address stockpile stewardship, emerging threats, basic science, industrial competitiveness, and future energy production. Specific applications and missions include advancements in inertial confinement and high-yield fusion, hostile nuclear environment survivability, dynamic properties of shocked materials in nuclear weapon operations, electromagnetics, and innovation that improves and advances the development of pulsed-power technology.

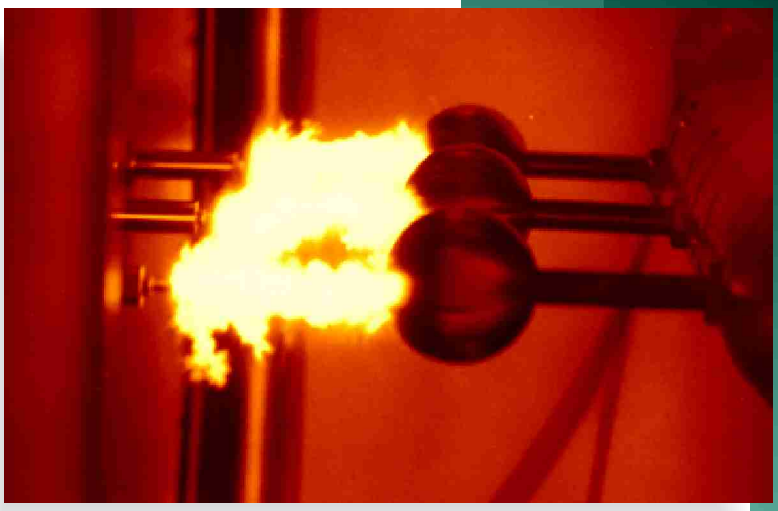

67121
"Model for Channel Resistance in Water Breakdown"

Water-breakdown switches are an integral part of the pulse compression schemes used in pulsed-power machines. The electrical properties of the switch are determined from breakdown channel radius, length, and conductivity. One of the traditional models for water breakdown overestimates channel resistance requiring the use of empirical substitutes. Building on the traditional model, researchers incorporated change in channel conductivity with temperatures to create a more complete model. An accurate water-breakdown switch model based on physical principles would allow simulations to be conducted in the design of future higher-amplitude pulsed-power machines. This advance would yield circuit models that can be implemented in existing circuit simulations of pulsed-power machines. Comparisons with simulations thus far indicate that final switch resistance is underestimated in the new model. Further investigation of material properties, initial channel conditions, and more accurate extractions of resistive fall levels are required before a final conclusion is reached.

39670

Simulations of Intense Petawatt Laser Pulses with Dense Z-Pinch Plasmas

R. B. Campbell

Over the past 3 years, Sandia has used LSP (Large-Scale Plasma simulation code) for studying beam propagation and fast-igniter physics. We made good progress in the areas of laser-plasma interaction, transport of relativistic electron beams in solid-density plasma, and the generation of energetic ion beams from the backside of exploded foils.

The Z-machine experiment is renowned for attaining ultra-intense x-ray pulses, which can be used to obtain high densities. There is now considerable interest in using short laser pulses to study laser-plasma interactions in an as-yet unexplored parameter regime. Sandia is pursuing a modification of the Z-Beamlet laser facility to enable a near-term high-energy petawatt (HEPW) capability for high-energy radiography and fast-ignition physics. The combination of an HEPW laser and an inertial confinement fusion (ICF) fuel-compression facility (Z) will be unique within the National Nuclear Security Administration (NNSA) community. In keeping with Sandia's paradigm of science-based stockpile stewardship, simulation must be an integral part of utilizing such a facility to its full potential and designing and understanding experiments carried out in this new physics regime.

The specific knowledge areas that will benefit from these simulations include ICF, weapons physics, weapons effects, high-pressure dynamic material properties, and basic light-matter interaction physics.

We submitted a technical advance describing a foil with a vacuum gap that is quite effective in keeping the hot electrons radially contained.

In this project, Sandia modified LSP, a simulation code, to allow a laser injection with Gaussian radial profile in both the full-wave and paraxial approximation. We incorporated the Lee Moore Desjarlais (LMD) equation of state (EOS) for different materials, as well as a dynamic model for the average Z of the plasma, based on Thomas-Fermi theory coupled with the QEOS (Quotidian equation of state). We performed a study to determine whether in the laser-plasma interaction timescales we needed to have models to follow the detailed atomic states and ionization and recombination processes. A desirable characteristic that beams of laser-produced energetic particles should possess is that they be radially collimated. We submitted a technical advance describing a foil with a vacuum gap that is quite effective in keeping the hot electrons radially contained.

The transport laser–produced relativistic electrons through solid-density foils formed the basis for the bulk of the simulation work and were pursued in both two dimensions

and three dimensions, with important differences noted. Later in the study, we began to include the full laser-plasma interaction physics along with the transport with a good bit of success.

We used the modified LSP code to simulate the petawatt GEKKO/PW experiments at the Institute of Laser Engineering (ILE) in Osaka, Japan. We began an extension of this work that involves the integration of the explicit laser-plasma interaction and hot-electron generation with the transport of the hot electrons through halo and core plasmas. Sandia recently performed some ion plume measurements on the LULI (laboratoire pour l'utilisation des laser intense) laser. We simulated these shots with LSP in a multiple-scale approach. The signals of electron, ion, and net current from the simulation exhibit many of the characteristics of the measurements.

Refereed

Campbell, R. B., J. S. DeGroot, T. A. Mehlhorn, D. R. Welch, and B. V. Oliver. 2003. Collimation of petawatt laser–generated relativistic electron beams propagating through solid matter. *Physics of Plasmas* **10** (10): 4169–72.

Campbell, R. B., R. A. Vesey, S. A. Slutz, T. A. Mehlhorn, J. S. DeGroot, and D. R. Welch. 2003. Simulations of petawatt laser–generated electron beams in precompressed fast-ignition hot-spot plasmas. *Proc. IFSA Conference (ANS Press)* **700** (7–12 September, Monterey, California): 461.

Campbell, R. B., T. A. Mehlhorn, D. R. Welch, J. S. DeGroot, and T. L. Marshall. 2003. Particle-in-cell simulations of intense relativistic electron beams propagating through solid-density plasma. *Proc. 11th International Conference on Emerging Nuclear Energy Systems* (September, Albuquerque, New Mexico): 260.

MacFarlane, J. J., I. E. Golovkin, P. R. Woodruff, D. R. Welch, B. V. Oliver, T. A. Mehlhorn, and R. B. Campbell. 2003. Simulation of the ionization dynamics of aluminum irradiated by intense short-pulse lasers. *Proc. 2003 IFSA Conference (ANS Press)* **700** (7–12 September, Monterey, California): 457.

Welch, D. R., B. V. Oliver, D. V. Rose, R. B. Campbell, and T. A. Mehlhorn. 2002. Hybrid particle-in-cell simulation of intense laser-plasma interaction. *Proc. 11th International Conference on Emerging Nuclear Energy Systems* (September, Albuquerque, New Mexico): 269.

Welch, D. R., B. V. Oliver, J. J. MacFarlane, R. B. Campbell, and T. A. Mehlhorn. 2003. Hybrid simulation of energetic electron-beam propagation in solid-density aluminum. *Proc. 2003 IFSA Conference (ANS Press)* **700** (7–12 September, Monterey, California): 398.

Other Communications

Campbell, R. B., R. Kodama, T. A. Mehlhorn, K. A. Tanaka, and D. R. Welch. 2004. A simulation of heating compressed fast-ignition cores by petawatt laser–generated electrons. *Physical Review Letters*, submitted.

Campbell, R. B., T. A. Mehlhorn, and D. R. Welch. 2004. Progress on simulating the GEKKO/PW experiments. Paper presented at the Internal Japanese Fast-Ignition and High-Field Physics Workshop, January, Kurashiki, Japan.

52737

Development of an Efficient Large-Aperture High-Damage-Threshold Sol-Gel Diffraction Grating

P. K. Rambo, R. S. Broyles, J. Schwarz, B. D. Thurston, C. S. Ashley, I. C. Smith

A high-energy (< 3 kJ) petawatt laser at Sandia's Z-Beamlet facility could have applications toward fusion research, advanced radiography, and fundamental physics. Such a laser will require large-aperture, high-damage-threshold gratings for use in pulse compression. Existing gold (Au)-coated gratings have 95% efficiency and damage at laser fluences above 0.5 J/(cm^2) for 0.5 ps pulses, requiring meter-scale optics to reach the 1 kJ level. New multilayer dielectric gratings promise improved damage thresholds and efficiencies, but are at a prototype stage, with scalability being a key question. Sol-gels and aerogels exhibit high-laser-damage thresholds in the nanosecond regime, but little has been done to examine behavior for shorter pulses. Similarly, sol-gels can have gratings written into them. Sandia seeks to coat a high-damage-threshold mirror with sol-gel, which can be done up to the meter scale with a simple dip or meniscus coater. If the sol-gel is appropriately photosensitive, we can apply ultraviolet (UV) light with an interference pattern on it to the sol-gel to create a permanent periodic modulation to its index of refraction. Since the substrate is a mirror, this periodic structure will act as a double-pass transmission grating for a wavelength that has another use, with the whole structure used as a reflection grating. Optimization of the key variables should allow us to obtain high efficiency in conjunction with high-damage threshold, allowing us to use the gratings in a pulse compressor. This technique is a novel improvement over existing grating architectures that require large-aperture etching, a difficult task to achieve uniformly.

Previous work focused on concept validation, specifically two key elements that impact the proposed mirror-backed volume-phase grating (VPG) development: design (modeling) and achievable index modulations (chemistry). Recent work also addressed these along with laser damage testing.

- *Design*. We based initial design efforts around *s*-polarized incident beams on the mirror-backed gratings, allowing for the thinnest multilayer dielectric (MLD) mirror coatings and VPG layers, as desired for fabrication purposes with MLD and sol-gel films. However, we needed experimental

verification of the design concept, and a sol-gel approach was in development. After discussions with commercial dichromated gelatin (DCG) grating vendors, we made design modifications because the VPG thicknesses for sol-gels were too low for DCG, and the desired top antireflection (AR) layer was not applicable. To fabricate prototypes, we applied previous design methods to *p*-polarized operation. Since the grating-use angle is near the VPG layer's Brewster angle (i.e., the angle where *p*-polarized reflections vanish), multiple reflections and etalon effects are reduced such that no AR layer is required. Furthermore, the *p*-polarized VPG layer is thicker and more suited to the DCG medium. In addition, we developed designs that used a small tilting (slant) of the VPG fringes with respect to the mirrored substrate to allow the off-Littrow incidence angles. Two vendors helped with fabrication: one with the complex MLD mirror coating and one with the gelatin VPG top layer. We made prototypes with up to 88% diffraction efficiency.

- *Chemistry and index modulation*. Development of high-/low-index modulation materials using sol-gel coatings continued, focusing on ultralow refractive-index (n) silica aerogel films as the low-*n* component (thickness 1–10 µm, n = 1.05–1.10) and various high-*n* oxides (n > 1.6) as infiltrants into the highly porous aerogel. We previously demonstrated that aerogel porosity may be exploited for infiltration with ZrO_2 (n = 1.8) and TiO_2 (n = 2.2), with zirconia-infused films showing full infiltration and titania partial. Recently, we modified the titania synthesis procedure for full infiltration. Similar epoxide synthetic routes successfully produced hafnia coatings (n = 1.6–1.8), which historically exhibit high-laser-damage thresholds. We used a new synthetic approach to prepare alumina coatings (n = 1.7) specifically to demonstrate patterning using selective dewetting techniques.

Investigations continued on selective dewetting as a process to pattern the aerogel into hydrophobic or hydrophilic regions by UV/ozone treatment such that direct subsequent high-*n* film deposition to specified regions is possible. We demonstrated that the water contact angle on aerogel could be reversibly varied from 160 to 15 deg by controlling surface methylation and UV/ozone treatment. Overcoating of hydrophilic-/hydrophobic-patterned aerogel films with high-*n* films showed poor patternability for epoxide-derived films (due to amphiphilic nature of ethanol solvent) and excellent patternability for alumina films (aqueous synthetic process). We subsequently developed a new aqueous process for zirconia, titania, and hafnia, resulting in significant patternability

We...developed a new aqueous process for zirconia, titania, and hafnia, resulting in significant patternability improvements.

improvements. While material options now exist for low- (n = 1.05–1.4) and high- (n = 1.6–2.2) index coatings, further investigations are needed to optimize and increase the obtainable resolution using this technique for VPG structures.

- *Damage testing*. Material science issues require that short-pulse-laser damage of sol-gels/aerogels be investigated for the proposed gratings. We constructed a compact damage-testing setup with a vacuum vessel at the sample to allow studies under intended-use environments. The setup characterizes the fluence (J/cm^2) involved in damage for given pulsewidths and employs two sensitive *in situ* damage-detection methods: optical scatter of a probe laser by damage via a dark field setup, and particle detection from the laser plasma generated during damage via microchannel plates. Both techniques are complemented by *ex situ* microscope inspection.

To benchmark the approach, the damage tester measured the laser-induced-damage threshold for fused silica, with the result of 2.7 J/cm^2 at 800 fs at 1053 nm being in agreement with other published data. By comparison, the result for silica aerogel was 1.0 J/cm^2, which is lower than one might expect from previous modeling.

Other Communications

Ashley, C. S., S. T. Reed, E. D. Branson, P. K. Rambo, and I. C. Smith. 2003. Aerogel composite diffraction gratings for high-laser-damage-threshold applications. Paper presented at the 7th International Symposium on Aerogels—ISA7, 2–5 November, Alexandria, Virginia.

Schwarz, J., L. Ruggles, P. K. Rambo, and J. Porter. 2004. Highly sensitive method for measuring the onset of damage using a microchannel plate. Paper presented at the Boulder Damage Symposium XXXVI, 20–22 September, Boulder, Colorado.

52738

Laser Triggering of Water Switches in Terawatt-Class Pulse-Power Accelerators

J. R. Woodworth, G. S. Sarkisov, D. L. Johnson, D. E. Bliss

Sandia is studying the use of lasers to command trigger high-voltage water switches. The jitter in self-breaking water switches limits the peak power and timing accuracy in a number of high-voltage accelerators. We previously demonstrated water breakdown using focused laser beams at 1064, 532, and 355 nm. The lowest breakdown threshold of 110 J/cm^2 or 14 GW/cm^2 occurred at 532 nm.

In recent experiments, we demonstrated low-jitter laser triggering of a 3 mm water gap pulse-charged to 170 kV in 250 ns. We achieved a command-triggering jitter below 2 ns using 85 mJ of focused green laser energy at 532 nm. We also demonstrated a command jitter of 4.7 ns using 112 mJ of focused infrared (IR) laser energy at 1064 nm. We designed and are beginning construction of a 2 MV laser-triggered water-switching test-bed for upcoming experiments.

In early work, we demonstrated that water breakdown could be achieved by focusing relatively modest amounts of laser radiation into the water at 1064 nm, 532 nm, and 355 nm, with the lowest breakdown threshold being observed at 532 nm. We previously demonstrated low-jitter triggering of a laboratory-scale (180 kV) water switch and began assembly of a 2 MV water-switch test facility.

Recently, we constructed a switch-triggering test-bed consisting of a mini-Marx that applied an ~ 180 kV pulsed voltage with an ~ 300 ns rise time across a water switch with a 3 mm gap. The optical access designed into this system allowed us both to focus a laser beam between the water-switch electrodes and to perform time-resolved optical diagnostics of the arcs produced.

In its self-breaking mode, our 180 kV water switch had a jitter of about 25 ns. Using a laser with an ~ 7 ns pulse length, we demonstrated laser triggering of this gap with 89 mJ of green (532 nm) laser energy with a 1 sigma jitter of less than 2 ns. The gap could also be triggered by 113 mJ of IR (1064 nm) laser energy with a jitter of 4.7 ns. The laser-triggering process could cause the switch to break down with low jitter to about 70% of the switch's self-break voltage. We also attempted triggering with a short-pulse laser (0.15 ns pulse length), but were unable to obtain consistent triggering, even with ~ 200 mJ of green laser energy. This suggests that a

relatively “long” pulse length is beneficial to the triggering process.

Our optical diagnostics suggested that a three-stage process is responsible for the triggering. First, the focused laser beam produces a long string of point plasmas, possibly by vaporizing and ionizing impurities or microbubbles that are still present in the deionized, degassed water of our switch. Second, these point plasmas expand and cool rapidly, merging into a long, nearly continuous gas column between the switch electrodes. Third, because this vapor column is highly overvolted by the voltage between the water-switch electrodes, it breaks down rapidly with low jitter.

On the basis of the successful triggering results listed above, we are designing and fabricating a 2 MV laser-triggered water-switch test facility to be used in our final work. This test facility will operate near the voltages and currents used in a variety of pulsed-power machines supporting research in flash radiography and inertial confinement fusion.

Other Communications

Woodworth, J. R., D. A. Chalenski, D. L. Johnson, G. Sarkisov, and J. R. Blickem. 2004. Laser-triggered water switching. Paper presented at the 31st IEEE Conference on Plasma Science, 28 June, Baltimore, Maryland.

53590

Electrical Conductivity of Metal Alloys

T. K. Mattsson, S. E. Rosenthal, K. R. Cochrane, M. P. Desjarlais

Present knowledge of material properties at extreme conditions is mostly founded on measurements, few of which do not require complex modeling as part of the interpretation. Accordingly, measured numbers are often intertwined with modeling assumptions. Recent advances in the field of density-functional theory (DFT) offer a new paradigm for this class of problems. Fundamental properties of matter, such as the variation of pressure and electrical conductivity with density and temperature, can be calculated without fitting to experimental data. Work according to this principle has already substantially improved the fidelity of Sandia's advanced modeling codes; aluminum (Al) is now described correctly at temperatures and pressures adequate to pulsed-power and high-energy-density research. The success of modeling Al at a new level of accuracy puts the focus on the need to also describe more complex materials in similar detail. Stainless steel (SS) is such a material; the complexity lies in its being an alloy of transition metals, whose electronic structure is fundamentally different from those of simple metals like Al. SS is also of high importance to the design and function of the accelerator since it is the material of choice for magnetically insulated transmission lines (MITLs). We will model SS from first principles, exploring the phase diagram in regions important to Sandia, as well as calculate the electrical conductivity at these conditions.

The QMD simulations resulted in knowledge of the equation of state (EOS) of steel at more than 100 points in phase-space....

We made significant progress regarding our atomistic understanding of steel as well as our macroscopic modeling capability.

We continued the validation of *ab initio* results for SS and expanded the range of densities and temperatures in calculations. Quantum molecular dynamics (QMD) calculations are routinely made over 2–3 orders of magnitude in density (0.1–15 g/cc) and between 300 and 90,000 K in temperature.

The QMD simulations resulted in knowledge of the equation of state (EOS) of steel at more than 100 points in phase-space, comprising the QMD–EOS. We calculated the electrical conductivity for many points in phase-space. We also made an initial study of carbon (C) impurities both as an impurity in bulk iron (Fe) and in SS in the wavelength division multiplex (WDM) region.

Although constituting a significant effort in high-performance computing, the QMD points are not enough to cover the necessary area of phase-space for macroscopic simulations applications. We therefore made wide-range lower-level modeling for EOS as well as conductivity.

For conductivity, we used a database of experimental and QMD results to construct an analytical LMD (Lee Moore Desjarlais) model. The resulting model was implemented in SESAME format and is currently employed in ALEGRA simulations.

For EOS, we modified the soft-sphere EOS to include temperature-dependent parameters and fitted the new model to the QMD–EOS. The model EOS interpolates between QMD points very well. The model EOS also extrapolates the EOS to regions where more basic models are valid, for example, at low and high density.

To obtain a model of wide-enough validity for Sandia's pulsed-power research, we merged the soft-sphere model with the currently used EOS table (SESAME 4272). The resulting EOS modifies 4272 in the warm-dense-matter regime, is thermodynamically consistent, and is manifestly consistent with the conductivities.

We used the new conductivity models for SS in simulations of the exploding wire experiments with the ALEGRA code. Results for voltage collapse in exploding wires agree quantitatively with experiments, reproducing the collapse to nanosecond accuracy.

We recently implemented the new EOS in ALEGRA; initial simulations confirm that the 4272 SESAME table is a good EOS for SS, as changes are not significant using the new model.

Refereed

Mattsson, A. E., P. A. Schultz, M. P. Desjarlais, T. R. Mattsson, and K. Leung. 2004. Designing meaningful density-functional theory calculations in materials science—A primer. *Modeling and Simulation in Materials Science and Engineering*, accepted.

Other Communications

Desjarlais, M. P. 2004. Quantum molecular dynamics calculation of electrical and thermodynamic properties for high-energy-density physics. (Invited) *Proc. DPP 2004*, *Physics of Plasmas*, to be submitted.

Desjarlais, M. P., and T. R. Mattsson. 2004. Predictive simulations of warm-dense matter: Magnetic flyer plates and exploding wires. *Science*, to be submitted.

Mattsson, T. R., and M. P. Desjarlais. 2004. Equation of state and electrical conductivity of stainless steel. Sandia Technical Report SAND2004-5253, Sandia National Laboratories, Albuquerque, New Mexico.

67120

Efficient Implicit Multigroup Radiation Calculations

T. A. Brunner

Radiation transport is an important part of many high-energy-density physics (HEDP) simulations. Because of the short timescales of the radiation transport compared with the other physics, robust, fully implicit methods must be used. Since the radiation solve typically dominates the total runtime of a solution and limits the time-step, it is critical that the transport methods in the code run as efficiently as possible with a time-step that is as large as possible.

Both nonlinear and linearized diffusion methods solve large linear systems. Typically, each group has been solved one at a time and outer iterations performed to converge the intergroup coupling. The convergence of this scheme can be slow. The ALEGRA code now has the capability to create one large multigroup matrix, but the performance of this new method is dependent on the preconditioner used in the iterative Krylov solver. Sandia will develop several preconditioners for this scheme and test them on a wide variety of physical problems. When possible, we will develop the preconditioners so that they can be applied to both linearized and nonlinear systems.

Some simulations, such as those of wire-array implosions, do not require the full accuracy of implicit Monte Carlo (IMC), but need more accuracy than diffusion. The spherical harmonics approximation shows promise in a structured-mesh explicit formulation, but it must be extended to be practical for HEDP simulations. Our collaborator at the University of Michigan will develop an implicit, unstructured-mesh, spherical-harmonics capability within ALEGRA.

We wrote the diffusion package so that the material properties have an abstract interface. This allows the different parameters needed by the different phases of the Multi-Approximation Method (MAM) to work in conjunction while reusing as much code as possible.

While we were doing the data-abstraction work, we re-examined the various approximations in the old linearized method and found them to be rather limiting. The new diffusion package has the ability to keep the group-to-group coupling that was ignored in the old package. This allows for larger time-steps, but the matrix solution is more expensive. We have already completed one preconditioner for the multigroup matrix

and have written up the new diffusion methods in a theory document.

Upon further analysis, we decided that the MAM probably will not improve the speed of the IMC simulations greatly. Time-steps may be improved, but the cost of doing an IMC time-step is roughly proportional to the length of the time-step. This, combined with the limitations of the diffusion package outlined above, indicated that we should focus our effort on making the diffusion package as efficient as possible. We postponed this work and will use the multigrid in group ideas from the MAM to develop preconditioners for the diffusion solves.

An automated verification program currently works. More work needs to be done to flesh out the verification problems to fully test all features of the code.

Collaborators have begun work on the implicit spherical-harmonics solver. We completed a one-dimensional implicit spherical-harmonics code that shows some promising features.

All methods currently in the code have detailed theory documents.

67121

Model for Channel Resistance in Water Breakdown

L. K. Warne, R. E. Jorgenson, J. M. Lehr

Water-breakdown switches are an integral part of the pulse-compression schemes used in pulsed-power machines. The electrical properties of the switch are determined from breakdown channel radius, length, and conductivity.

A physics model for water breakdown was introduced by Martin based on the gas-breakdown model of Braginskii. This model tends to overestimate channel resistance, and discrepancies have led to the use of empirical substitutes.

The Braginskii model postulates that the channel conductivity remains constant (its value is an empirical input to the model), and the channel resistance varies over time because of shock expansion of the channel. There are alternative models, such as those proposed by Rompe and Weizel and Vlastos, based on a postulated constant channel radius (again, an empirical input to the model) and a time-varying conductivity as a result of channel heating.

Because the large density of water impedes channel expansion in Martin's model, Sandia believes the resulting increase in channel temperature and consequent increase in channel conductivity must be taken into account. We proposed to incorporate the change in channel conductivity with temperature into Martin's model. This should both improve correspondence with experiment and eliminate the need for empirical conductivity input. We also proposed comparing resulting predictions with existing PITHON and Z20 data.

An accurate water-breakdown-switch model based on physical principles would allow simulations to be conducted in the design of future higher-amplitude, pulsed-power machines. This research effort has the potential to yield simple circuit models that can be implemented in existing circuit simulations of pulsed-power machines.

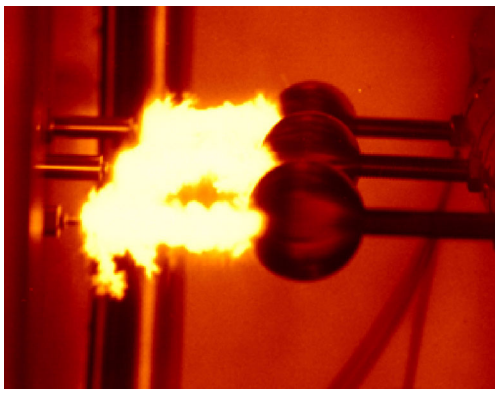

Underwater breakdown across a switch in one of Sandia's pulsed-power machines. Experimental, analytical, and numerical techniques are being applied to understand the resistive-fall phase of the arc, which is a key issue for the development of pulsed-power systems for nuclear-weapon and fusion-energy programs.

We expected the large density of water to impede expansion and result in higher temperatures than in gases; therefore, we proposed to more accurately model the channel expansion and heating.

We used electrical conductivity, heat transfer, and radiation parameters from the literature to set up a lumped model for the water-channel expansion. We first examined power-law behaviors of the system to get a feel for the evolution of the channel. We ran numerical simulations of the lumped model for

a ramp current drive, a sinusoidal current drive, and a fixed-voltage drive. Constant-voltage drives resulted in substantial delays in the resistive fall (< 100 ns). This time delay is supported by experimental data after the streamer propagation delay is removed. For the current drives, reasonable variations in the assumed initial conditions (channel radius, temperature, and pressure) did not result in substantial changes at intermediate (10 ns) or late times (100 ns).

We used ALEGRA to run one-dimensional (1-D) radial simulations of the channel expansion for ramp current drives. Importantly, the radial profiles show reasonably constant density and temperature in the channel region at intermediate times (10 ns) and only relatively small variations (50%) at late times (100 ns), implying that a lumped model may be a reasonable approximation. Surprisingly, in these initial runs, the radial expansion agreed with the lumped-model predictions, even though the water material properties (in the ALEGRA database) were slightly different from those used in the lumped-model runs. Other quantities, such as temperature, density, and pressure, also agreed with the lumped-model results during the initial phase of expansion, but exhibited more of a plateau level at later times than the lumped model. We are reaching temperatures on the order of 25 eV, which are higher than those typically reported in gas breakdown. The density in the channel quickly falls from that of water to a few percent of water. Pressures of approximately 1 Mbar are reached at early time.

Comparisons with PITHON and SatPro data indicate that the final resistance of the switch is being underestimated in these simulations (more so in the lumped model than in the ALEGRA model). Thus, the more complete model of the channel and the resulting higher temperatures are resulting in much-reduced resistance levels versus Martin's model. We need further investigation of the material properties and initial channel conditions, and more accurate extraction of resistive fall levels from the experiments before we reach a final conclusion on plateau switch-resistance levels.

- *Water breakdown*.

(1) We examined channel radius from Martin's model.

(2) We examined water electrical conductivity, thermal conductivity, and radiative transfer models from the literature.

(3) We set up and explored power-law and numerical solutions to a lumped model of the water channel.

(4) We performed preliminary comparisons with PITHON and SatPro switch data.

(5) We ran ALEGRA 1-D simulations of the water-channel expansion and compared them with lumped-model results.

We used ALEGRA to run one-dimensional (1-D) radial simulations of the channel expansion for ramp current drives. Importantly, the radial profiles show reasonably constant density and temperature in the channel region at intermediate times (10 ns) and only relatively small variations (50%) at late times (100 ns), implying that a lumped model may be a reasonable approximation.

67122

Embeddable Shock Physics Sensors

T. A. Friedmann, M. D. Knudson, R. E. Setchell, T. J. Vogler, R. J. Hickman, J. Davis

Sandia is developing miniaturized embeddable sensors for use in Z experiments to measure the velocity, stress (both longitudinal and transverse), and temperature histories of propagating compression waves in materials. Currently, observations of shock and compression experiments at Z are limited to optical techniques. For opaque materials, this provides information only at material interfaces, and wave interactions at these interfaces must be taken into account. To directly obtain measurements of dynamic compression behavior within a material sample, ways must be developed to embed small, nonperturbing sensors into materials of interest and of electrically measuring the material response. This approach provides challenges both for the sensor design and for recording the generated signal in the extreme electromagnetic environment of Z. The sensors must be capable of nanosecond temporal resolution with inherently (very) large electrical noise rejection. We expected that data generated from these sensors will allow for the determination of material equation-of-state (EOS) data and strength that can be used to validate models of materials behavior under extreme dynamic pressure environments.

We met our early milestones involving planning, testing, and fabricating sensors. We electrically evaluated these sensors under static and dynamic conditions, and they appear appropriate for further testing in gas-gun experiments. We currently are fabricating targets for gas-gun experiments. These targets consist of gauges embedded into aluminum (Al) discs and have been largely fabricated. Namely, we embedded the gauges on the face of one disc and are diffusion-bonding them together for the future gas-gun experiments. We also made a preliminary assessment of the noise environment on Z.

We fabricated the manganin (stress) and thin-film thermocouple (temperature) sensors using pulsed-laser deposition (PLD). We made static calibrations of the thin-film thermocouple gauge in an oven and found good agreement with bulk thermocouples. Using a short-pulse excimer laser to directly heat the thermocouple, we characterized the dynamic response of the thin-film thermocouple gauges and found ~ 10–20 ns risetimes for the temperature response. The measured response agrees reasonably well with finite-element

modeling (FEM) calculations of the time and temperature profile, increasing confidence that the measured gauge response both is fast and accurately records the dynamic temperature profile. The measured resistivity of the thin-film manganin gauge was within 10% of the bulk value. These gauges appear ready for insertion into target materials for gas-gun experiments.

We chose Al as the test material due to its well-characterized response to shock. To obtain Al discs with the required surface finish and flatness to fabricate thin sensors (~ 250 Å thickness) with electrical continuity, we diamond-turned Al discs (~ 70Å rms) followed by further mechanical polishing to reduce the surface roughness to an acceptable level (< 20 Å rms). We sandwiched the thin-film gauges between insulating dielectric layers of alumina oxide capped with an Al film for bonding purposes. We will cap the target assembly with another Al disc by diffusion bonding. Once we achieve this bonding, the targets will be ready for gas-gun experiments.

We are looking at the noise response of commercial thermocouples in Z. Initial results for an unshielded commercial thermocouple (the worst case) reveal an expected high noise level. With proper shielding, this signal can be reduced significantly to near mV levels.

Corporate Objectives

Training and acquiring the next generation of outstanding scientists and engineers ensures a progressive future and guarantees the continuance of Sandia's exceptional reputation as a leader in science and technology. Corporate Objectives investments create the opportunity for collaboration with universities to create new science and engineering technologies, to employ complementary resources and skills for achieving common goals, and to recruit and guide top students for Sandia's work force.

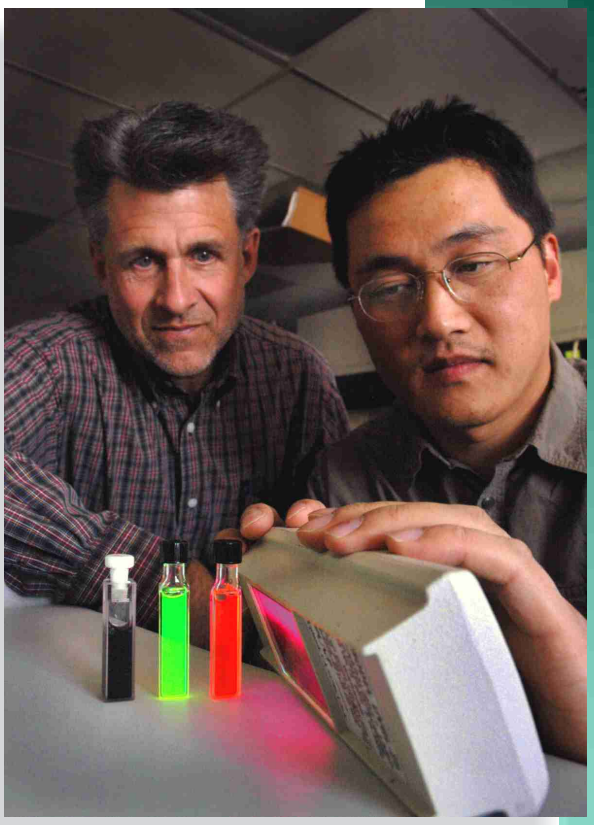

69163
"New Self-Assembled Nanocrystal Micelles for Biolabels"

The ability of semiconductor nanocrystals (NCs) to display multiple (size-specific) colors simultaneously during a single, long-term excitation holds great promise for their use in fluorescent bio-imaging. The main challenges of using NCs as biolabels are achieving biocompatibility, low nonspecific adsorption, and no aggregation. Functional groups that can be used to further couple and conjugate with biospecies are also required.

To alleviate these challenges, researchers assisted by top students at the University of New Mexico, invented a new method of synthesizing water-soluble and biocompatible NCs. The novel water-soluble metal and semiconductor NC-micelles preserve the optical properties of the original hydrophobic NCs. New semiconductor NCs emit the same color and exhibit equal photoluminescence (PL) intensity and lifetime. Research also indicates that the water-soluble semiconductor NC-micelles are biocompatible and exhibit no aggregation in cells.

38717

Nanoscale Energetic Materials by Inverse Micellar Synthesis

A. S. Tappan, S. G. Thoma, B. L. Abrams, S. P. Maharrey, R. Behrens, Jr., W. M. Trott, J. P. Wilcoxon, S. M. Woessner

Sandia is investigating inverse micellar synthesis (IMS) as a technique for preparing nanoscale energetic materials (nano-EMs). Particle sizes of materials such as metals, oxidizers, and composite mixtures can be precisely controlled by this technique, and this synthesis can result in particles as small as a few nanometers. The lower limits of useful particle size of aluminum (Al) for EM formulations are being realized as the surface-area-to-volume ratio is increased, thus increasing the ubiquitous surface coating of nonenergetic Al oxide. Inverse micellar synthesis allows for pure Al particles to be synthesized and should allow them to be passivated against oxidation by a coating of a compound that would contribute to the energy release. By careful selection of the passivation layer, composite EM energy densities twice that of high-melting explosive (HMX) are possible. Of particular importance are the precise control and enhancement of chemical energy release in overcoming dissipative processes at the small length scales characteristic of microelectromechanical systems (MEMS) devices for future components.

Characterization of these materials is critical to understanding the enhancement to EM performance and the mechanisms of this enhancement. We will use standard analysis techniques, such as standard safety tests, electron microscopy, calorimetry, light scattering, and chromatography, to characterize the chemical and physical properties of these materials. We will use Fourier-transform ion-cyclotron resonance mass spectrometry (FTICR–MS) as an analysis technique for these nanoparticles.

We will examine the characterization of the performance of EMs formulated with nano-EMs by shock studies, using a line-imaging optically recording velocity interferometry system (ORVIS) to observe reactive-wave growth and to evaluate the contribution of the nanoscale material to this reactive-wave growth.

We developed the first synthesis of nano-boron (n-B) via thermal decomposition. We discovered that we could add ligating agents to control the growth and form dispersed n-B clusters. We developed a synthesis of Al/B alloyed clusters using Al seed clusters. In this method, Al clusters made by either inverse micelle or thermal decomposition methods serve

as “seeds” to catalyze the thermal decomposition of the B precursor.

We investigated the role of the titanium (IV) (Ti[IV]) catalyst in the synthesis of n-Al and n-B. By varying the type of Ti(IV) catalyst, we discovered that we could tailor the size of the final n-Al. Thermal decomposition of iron (Fe) carbonyl in the presence of n-Al clusters with a mean size of 20–25 nm resulted in clusters with an Al/Fe core/shell-type structure. We investigated the deposition of a variety of other metals from inverse micelle and organometallic sources to reduce the oxidation sensitivity of n-Al.

We demonstrated the cross-linking of n-Al clusters to form a metallic gel via intercluster cross-linking. The resulting metallic microgel allowed the samples to be harvested easily for thermal analysis. In harvested samples, we observed qualitative oxygen stability of our B-passivated Al nanoclusters. We performed comparative thermal analysis on Al versus Al-B samples. Calorimetry measurements on these samples indicated a sharper onset of oxidation in the samples that contained B. This indicates that the B may play a role in passivating the Al from oxidation until a critical temperature is reached.

We tested the new annular reflectron time-of-flight (ToF) mass spectrometer. We tested the ToF system with the cesium (Cs) iodide clusters, and we can now obtain spectra of high-mass clusters quite readily out to ~ 2000 Daltons. We completed ToF/FTICR coupling and measurements of the same clusters. We obtained increased cluster-size transmission efficiency in coupled mode. We have now demonstrated the initial goal of obtaining rapid ToF mass spectra up to 5000 Daltons with nominally < 1 Dalton resolution and can transfer these cluster ions with high efficiency for successful high-mass accuracy measurement by FTICR and subsequent unambiguous compositional analysis. Due to challenges in developing this technique and the difficulty in preparing a suitable Al nanocluster/solvent system, we could not perform it on Sandia-synthesized n-Al.

We analyzed wave profiles in nanoscale EMs using velocity interferometry. We made our measurements on formulations of sensitized, gelled nitromethane containing commercially available n-Al. We chose this liquid explosive to maximize intimate contact with the n-Al. We evaluated the effect of 10% n-Al on shock-induced wave profiles in nitromethane and compared these results to nitromethane containing nonreactive Al hydroxide of the same particle size.

We determined the essential features of the impact-induced wave profile using single-point velocity interferometry system

for any reflector (VISAR) measurements. In all cases, we observed an initial nonreactive shock state. After a few hundred nanoseconds, this shock compression state was followed by a high-amplitude reactive wave generally consistent with previously observed shock-to-detonation profiles in homogeneous explosives. In our experiments, however, the reactive wave displayed a discernible ramplike increase in material velocity rather than the prototypical jump state identified with homogeneous initiation. These experiments suggested an enhancement in time to reaction with the material containing n-Al; however, shot-to-shot variations of impact velocity made it impossible to draw firm conclusions.

The spatially resolved line-imaging ORVIS results produced significant additional insight. The image data clearly revealed a two-dimensional structure to the reactive wave with reaction occurring most rapidly toward the edges of the sample. This observed structure contributes to some degree to the apparent ramplike reactive wave seen in the single-point VISAR measurements. In these tests, reaction clearly occurred most rapidly in the sample containing n-Al versus gelled nitromethane alone and gelled nitromethane containing nonreactive Al hydroxide.

Other Communications

Wilcoxon, J. P., S. M. Woessner, and A. S. Tappan. 2003. Synthesis of aluminum and boron nanoclusters by inverse micelle and thermal decomposition methods. Paper presented at the Fall Meeting of the Materials Research Society, 1–5 December, Boston, Massachusetts.

38718

Modeling of Rock Penetration

L. S. Costin, R. D. Hardy, D. J. Frew, D. J. Holcomb, A. F. Fossum

The objective of this project is to develop a basic understanding of the mechanics of rock penetration that will lead to enhanced modeling capabilities to support the design of new penetrator systems. In its initial conception, the project had four principal tasks: (1) to develop an understanding of the physical mechanisms of rock deformation during penetration, (2) to develop a constitutive model for rock behavior during penetration, (3) to conduct intermediate-scale dynamic tests to validate the model, and (4) to integrate the experimental and constitutive modeling results with other ongoing efforts to develop an enhanced dynamic penetration-simulation capability. Sandia made significant progress in developing a constitutive model that incorporates some, but not all, of the important behaviors. Laboratory work resulted in key data on rate sensitivity and other effects that we incorporated into the model, resulting in good agreement between model results and ballistic penetration experiments. We are exploring new analytical approaches to understanding the penetration process. We leveraged work from other projects to collect unique datasets on near-field rock conditions before and after full-scale penetration experiments. We plan to test our modeling concepts further by conducting a unique set of experiments in large rock blocks to simulate early stages of the penetration process. We will also conduct additional detailed laboratory tests to resolve some remaining issues with the numerical modeling approach. The expected outcomes of this project are (1) a greatly enhanced constitutive model that can simulate the rock response during penetration, and (2) an enhanced understanding of the deformation mechanics involved in rock penetration that will lead to greater analytical capability for engineering applications (i.e., a method for determining a penetrability index, like the S number, but more physically based).

We followed two primary approaches: the development of a realistic, constitutive model for geomaterials, and the design of an experimental approach to study penetration from the target's point of view.

We completed the Sandia GeoModel to the point that it incorporates most of the physics thought to influence the penetration process. Using this model, we performed three-dimensional (3-D), nonlinear, transient dynamic finite-element

(FE) penetration simulations to determine which features have the most influence on penetration-depth calculations. We made a baseline penetration calculation with a representative set of material parameters evaluated from measurements made from laboratory experiments conducted on a familiar sedimentary rock. Then, a sequence of perturbations of various material parameters allowed an assessment to be made of the main penetration effects. We calculated the cumulative probability distribution function by using an advanced reliability method that makes use of this sensitivity database, probability density functions, and coefficients of variation of the key controlling parameters for penetration-depth predictions. We drew the following conclusions from more than 30 penetration FE analyses:

(1) From the standpoint of predicting penetration, the most important physics features represented in the rock model, in order of importance, are (a) pressure sensitivity of yield, (b) the coefficient of friction between the penetrator and the rock, (c) ubiquitous rock jointing, (d) strain-rate sensitivity, and (e) pore collapse.

(2) When the important physics features are included in the model, the material parameters representing the physics that are most sensitive deterministically, in order of importance, are (a) strain-rate sensitivity, (b) ubiquitous rock jointing, (c) the coefficient of friction between the penetrator and the rock, (d) porosity, and (e) pressure sensitivity of yield.

(3) Penetration depth increases with increasing striking velocity. If the striking velocity is too low, the penetrator will ricochet off the target.

To validate the modeling results, we developed a new experimental method. Using explosive line charges placed in a central borehole, we loaded cylindrical specimens in a manner equivalent to an increment of penetration, allowing the measurement of the associated strains and accelerations and the retrieval of specimens from the more-or-less-intact cylinder.

Results show clearly that the deformation zone is highly concentrated near the borehole, with almost no damage occurring beyond one-half a borehole diameter. This implies that penetration is not strongly influenced by anything but the material within a diameter or so of the penetration. For penetrator tests, target size should not matter strongly once target diameters exceed some small multiple of the penetrator diameter. Penetration into jointed rock should not be much affected unless a discontinuity is within a similar range. These conclusions are somewhat counter to conventional wisdom in the penetrator community. However, recent penetration

experiments using varying target diameters demonstrated that the results were insensitive to target size, confirming the predictions based on the present work.

Accelerations measured at several points along a radius from the borehole are consistent with highly concentrated damage and energy absorption. At the borehole wall, accelerations were an order of magnitude higher than at half a diameter, but at the outer surface, eight diameters away, accelerations were as expected for propagation through an elastic medium. Accelerations measured at the outer surface of the cylinders increased significantly with cure time for the concrete targets. As strength increased, we observed less damage near the explosively driven borehole wall consistent with the lower energy absorption expected and observed for stronger concrete. As it is the energy-absorbing properties of a target that ultimately stop a penetrator, we believe this may point the way to a more readily determined and equivalent of the S (index of penetrability) number.

Other Communications

Fossum, A. F. 2004. Rock penetration: Finite-element sensitivity and probabilistic modeling analysis. Sandia Technical Report SAND2004-3926, Sandia National Laboratories, Albuquerque, New Mexico.

Holcomb, D. J., A. F. Fossum, G. Gettemy, R. D. Hardy, D. Bronowski, R. Rivas, and D. Preece. 2004. Geomechanics of penetration: Experimental and computational approaches. Sandia Technical Report SAND2004-5211, Sandia National Laboratories, Albuquerque, New Mexico.

41726

Direct Simulation of Solid-Fluid Systems

B. K. Cook

Numerous important industrial and natural processes are dominated by the interaction of particles (or a cemented particulate matrix) with neighboring particles and a surrounding fluid. For example, in the petroleum industry, sanding is a billion-dollar problem that results from the erosion of sand from an oil-bearing sandstone formation during production. Our understanding of the discontinuous physics underlying these processes and our associated predictive capabilities have been limited by continuum modeling approaches and difficult-to-perform experimental studies. An alternate approach is to simulate these systems at the grain scale. However, until recently, the direct simulation of these three-dimensional (3-D), dynamic solid-fluid systems proved computationally intractable.

Rapid increases in parallel-based computational resources, combined with the development of efficient and robust modeling schemes, are marshalling in an exciting era of simulation-based discovery into the behavior and prediction of the dynamics of particle-fluid systems. Leveraging these developments, Sandia will develop an unprecedented computational capability for the dynamic simulation of the coupled solid and fluid phases, fully resolving the interaction of individual solid particles (and particle assemblages) with other solid particles and the surrounding fluid. This project focuses on the refinement and efficient implementation of a numerical scheme that uses the lattice-Boltzmann (LB) and discrete-element methods (DEM) to solve the underlying governing equations for the fluid and solid phases, respectively. We are developing a powerful simulation environment to enable the computational exploration of solid-fluid physics.

We are collaborating with researchers from the Massachusetts Institute of Technology (MIT). In addition to the aforementioned fossil-energy applications, the DEM is useful for understanding and modeling the mechanics that govern the behavior of materials undergoing large deformations, which is important for many Defense Programs (DP) problems such as penetration, shock-structure interaction, and blast damage.

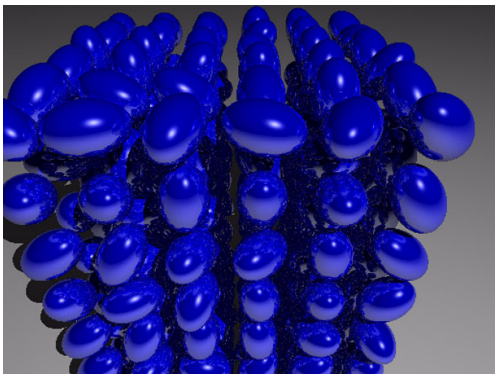

A visualization of an array of interacting ellipsoids in a DEM simulation.

We significantly improved previous work on the representation and contact methods for pseudo-ellipsoids in DEM simulations, in which we approximated functional ellipsoidal shapes by three arcs rotated around a central axis.

Extending upon the algorithms developed for these pseudo-ellipsoids, which were limited by axial symmetry, we developed a new contact-detection algorithm for contact between general ellipsoids, which exhibit C-infinity continuity along the surface and are not necessarily axially symmetric. We showed empirical convergence and demonstrated computational cost (Johnson, *et al*., 2004). This advance allows for the practical simulation of a large set of interacting ellipsoidal particles, which could not have been tractably computed using previous contact schemes.

...we developed a new contact-detection algorithm for contact between general ellipsoids, which exhibit C-infinity continuity along the surface and are not necessarily axially symmetric. We showed empirical convergence and demonstrated computational cost....

We continued to develop a 3-D DEM simulation environment building upon the .NET framework formulated earlier. Alongside the architectural implementation of this simulator framework, we also made progress in the development of powerful algorithms for decreasing computational load throughout the DEM simulation pipeline. One of our objectives was to validate the code's resolution of expected behavior based on multibody dynamics theory. The integration of rigid-body motion in 3-D space is a nontrivial task that is aggravated by the discrete temporal nature of the simulations. The straightforward update of the rotation matrix over time through successive matrix multiplications can lead to error accumulation. Matrix updates can also lead to singular matrices or to "gimbal lock," which results from the alignment of two of the three axes of rotation. This problem is typically solved through the use of quaternions, which offer nonsingularity under rotation and ease of renormalization between time-steps to avoid orthogonality losses. Leveraging these advantages, a recently proposed DEM integration scheme based on the rotation matrix update and the assumption of small angular displacement was improved through the reparameterization of the rotation matrix as a quaternion. This new integration scheme results in a more efficient algorithm with superior accuracy.

We had anticipated completing large-scale simulation studies, but were delayed by the additional research required to improve the ellipsoidal representation and to implement and verify the rigid-body integration scheme. The simulation framework now exists to refocus our attention in subsequent work on the hypothesis that particle shape strongly influences bulk behavior in granular systems through particle contact interactions.

Other Communications

Johnson, S. M. 2004. Survey of rigid-body rotation integration algorithm for use in discrete element methods. Internal MIT publication, in preparation for journal publication.

Johnson, S. M., J. R. Williams, and B. K. Cook. 2004. Contact detection between axially asymmetric ellipsoids for discrete element modeling. *Proc. 7th International Conference on Computational Structures Technology.*

42461

Support–Active Site Interactions in Heterogeneous Catalysts

R. A. Kemp, A. G. Hascall

To rationally synthesize heterogeneous catalysts, it is imperative to comprehend the function of the various components of the catalyst. It is of utmost importance to know how a support interacts with the active site of the catalyst. In fact, in the catalysis world, this lack of fundamental understanding of the relationship between active site and support is the single largest reason catalysis is considered an "empirical" or "black-box" science rather than a well-understood one. In this study, Sandia will look at an industrially important catalyst system with an eye toward explaining what features define the active site. Along with the interest in understanding the catalyst in a fundamental sense, we also have the very real possibility of significantly affecting the technology and economics of ethylene oligomer production. In this work, we will prepare novel ethylene oligomerization catalysts, which are normally homogeneous, inside the pores of nano- and mesoporous materials. We also will be preparing these catalysts with new ligands attached in place of phosphines that are normally used. The overall purpose of the study will be to understand the effects that steric and electronic constraints can have on growing oligomer chains. If possible, we wish to limit oligomer growth at defined lengths by using the steric constraints imposed by the pore walls of the nano- or mesoporous supports of the new supported homogeneous catalysts that we prepared. In the future, understanding the relationship between support and active site should and will certainly lead to faster development and implementation of advanced catalysts.

We continued our work in attempting to prepare new, well-defined homogeneous catalysts for the oligomerization of ethylene to *a*-olefins, and to graft the catalysts onto porous supports. We investigated the use of complexes of chelating stable carbene ligands, which occupied most of our current efforts. These ligands should give advantages over traditional phosphine-based ligands in ease of synthesis of the ligands, stability of the catalysts, particularly in the protic environment of a porous silica support, and, we hope, greater activity. In particular, we attempted to prepare carboxylate-functionalized carbene ligands, which would form C-O chelating complexes, analogous to the phosphine-carboxylate chelate complexes of

nickel (Ni) that are used as ethylene oligomerization catalysts in the Shell Higher Olefins Process (SHOP).

As precursors to carbene ligands, we prepared carboxylic acid–substituted imidazolium salts, by hydrolysis of the corresponding imidazolium esters. Deprotonation of the carboxylic acids leads to the formation of novel imidazolium carboxylate zwitterions. Conversion of the zwitterions based on imidazolium acetic acid to carbenes was not successful, possibly due to the presence of the protons to the carboxylate group, which would be expected to be acidic, and may be deprotonated in preference to the imidazolium C_2 proton, leading to complications in trying to synthesize carbenes. For this reason, we prepared an imidazolium carboxylate based on isobutyric acid, i.e., the analogous compound with methyl groups in the *a* position. When we treated this carboxylic acid with excess silver oxide (Ag_2O), we removed the carboxylic, as well as an imidazolium proton, to give a silver carbene complex. The silver complex can be transmetallated to give other metal complexes, which might be catalytically useful. To date, we have prepared palladium and rhodium complexes of the novel, chelating carbene-carboxylate ligand. Future work will attempt to structurally characterize these new complexes by x-ray crystallography. In addition, work currently is in progress to prepare complexes with this ligand of Ni, which would be analogues of the SHOP catalyst, and to explore their catalytic activity.

Refereed

Hascall, A. G., and R. A. Kemp. 2004. Functionalized heterocyclic carbene complexes of Ni as catalysts for ethylene oligomerization. *Organometallics*, submitted.

Hascall, A. G., and R. A. Kemp. 2004. Functionalized heterocyclic carbene complexes of Ni as catalysts for ethylene oligomerization. Paper presented at the 227th National Meeting of the American Chemical Society, 28 March–1 April, Anaheim, California.

Hascall, A. G., and R. A. Kemp. 2004. Heterocyclic carbene complexes of Ni as catalysts for ethylene oligomerization. Paper presented at the Gordon Research Conference on Inorganic Chemistry.

Hascall, A. G., and R. A. Kemp. 2004. Heterocyclic carbene complexes of Rh as catalysts for ethylene oligomerization. *Organometallics*, submitted.

42483

An Analysis of the Automotive Industry as a Source for Weapon Components and Manufacturing Processes

R. J. Steichen

The automotive industry sector has many characteristics and technology requirements that are common to those required for management of the nuclear weapons (NW) stockpile. Automotive components have performance requirements for lifetime, reliability, temperature, thermal cycle, mechanical shock, and others that are similar to those required for weapons systems. To address these requirements, the automotive industry invests in research to design and develop new components and solutions to improve performance and reduce cost.

In this project, Sandia investigates technology areas of interest and opportunities to access capabilities and technologies that would be beneficial for weapons programs and the Department of Energy (DOE) mission.

We completed the analysis and verified it by improved research interactions with the automotive sector. Successful synergistic relationships primarily focused on fundamental research needs. Research areas, such as the Advanced Strategic Computing Initiative (ASCI) and hydrogen (H) science, are tied to NW technology needs.

The DOE Freedom Car Initiative, developing technologies to support an H economy, builds on Sandia's H capabilities for weapon systems. Technologies encompass H-storage materials, catalysts, membranes, sensors and microsystems, fuel cells, modeling and simulation, batteries, and others.

As a result of this analysis, we are initiating collaborative projects with major automotive manufacturers that include H fuel management, nanomaterial catalysts for fuel cells, and battery technologies.

As a result of this analysis, we are initiating collaborative projects with major automotive manufacturers that include H fuel management, nanomaterial catalysts for fuel cells, and battery technologies.

46070

High-Speed Micro-EDM

G. L. Benavides, S. P. Moylan

When two electrodes are in close proximity in a dielectric liquid, application of a voltage pulse can produce a spark discharge between them. Some of the energy in the discharge is transferred to the electrodes and results in the heating of highly localized regions of the electrodes. If the regions are heated above their melting temperature, molten droplets or vaporized material may be ejected from the electrodes. Pulsed application of the voltage results in repeated breakdown of the dielectric and material removal, and consequently to a continuous machining process called electrical discharge machining *(EDM). Since material removal is controlled by the melting/vaporization temperature of the electrode materials, EDM has proven to be enormously beneficial for machining complex shapes in hard materials that are difficult to fabricate by conventional means. A variant of the EDM process is micro-EDM, so called because it utilizes low discharge energies (~ 10^{-9}–10^{-5} J) to remove small volumes of material. Spark erosion by micro-EDM provides significant opportunities for producing small features and microcomponents such as nozzle holes, slots, shafts, and gears in hard alloys and advanced ceramics; very rapidly solidified micropowders; and colloidal suspensions. If the speed and precision of micro-EDM processes can be significantly enhanced, they have the potential to be used for a wide variety of micromachining applications, including fabrication of microelectromechanical systems (MEMS) components. It is these topics that constitute the core of this research.*

Micro-EDM complements and is compatible with other microsystem technologies developed for the Microsystems and Engineering Sciences Applications (MESA) program. In this project, Sandia seeks to develop the technology to increase the throughput of the micro-EDM process (i.e., high speed) and to uncover the science behind the process. Micro-EDM, as well as other microsystem technologies, promises to keep our NW stockpile safe, secure, and reliable.

This project is progressing well in several different directions. We drilled holes with diameters of 150 mm in a variety of metals using the experimental setup designed specifically for this project. We completed preliminary experiments and determined that applied voltage has the largest impact on cutting speed when compared to pulse duration, pulse

frequency, and any combinations thereof. Additionally, we varied the method of positioning the tool electrode—vibrating the tool at different frequencies and amplitudes—and showed a noticeable impact on machining times. This fact indicates that positioning the tool using gap conditions as feedback—a more directed, less-arbitrary method than simply vibrating the tool by a sine wave—should further increase cutting speeds.

A major limitation of micro-EDM is that tools show an appreciable amount of wear throughout the cutting process. An effort to understand and quantify the amount of wear is under way. We took optical microscope pictures of the tool after several intervals of the machining process. These pictures show that tools eventually evolve into the same bullet shape, regardless of their starting shape or the cutting conditions. Machine settings do have an impact on the rate of tool wear. This relationship appears to be nonlinear and will be specifically diagnosed in the near future.

We collected and studied debris formed during the micro-EDM process. The debris, in the form of spherical particulates, has a bimodal size distribution. The smaller particles are only tens of nanometers in diameter and stay in solution with the liquid dielectric. The larger particles eventually fall out of solution and are collected, cleaned, and investigated. Particles produced at discharge energies of 47 mJ have diameters of approximately 2 mm. While the particle diameters are on the order of micrometers, they are nanocrystalline in nature. The reason for this grain refinement appears to be the rapid melting and resolidification of the material. Literature indicates that amorphous particles are possible, but have yet to be observed.

46686

Microexternal-Combustion Engine: The P3 Engine Prototype

C. A. Apblett

A microelectromechanical systems (MEMS)–based micropower-generation system was under development at Washington State University and supported by this project. The power system consisted of individual dynamic microheat engines, each producing electrical power and contributing to the power output of the overall system. An individual engine converts thermal to mechanical energy through a novel thermodynamic cycle, and mechanical to electrical energy by straining a thin-film piezoelectric membrane. This work focused on the design of a single individual engine, fabricating the engine, and measuring the engine's thermal efficiency and power-generation capability. Sandia gave particular attention to factors affecting resonant operation of the engine, controlling the state of the working fluid, and initial implementation of a grooved wicking structure to promote more efficient heat addition. A unique aspect of this work is that the engine concept is not based on a scaled-down version of an existing macroscale engine. Because we designed this engine to be implemented strictly on the microscale, it is not subject to some of the major design challenges facing scaled-down engines, namely, friction losses, sealing issues, complex fabrication, and external conversion of mechanical to electrical energy.

Because we designed this engine to be implemented strictly on the microscale, it is not subject to some of the major design challenges facing scaled-down engines, namely, friction losses, sealing issues, complex fabrication, and external conversion of mechanical to electrical energy.

One severe limitation to operating the engine quickly is the fact that there is no thin layer of liquid available for evaporation during the heat-addition process of the cycle. The proximity of the heater relative to the liquid-vapor interface is quite close, which is a poor configuration for evaporative heat transfer. The only two heat paths to the interface are through the silicon (Si) and through the vapor. In each case, the path is exceedingly long, greatly compromising speed and power consumption. The method we used to address this issue is the use of a radial grooved wicking structure to pump liquid from the area of the engine containing the liquid phase onto the evaporator (heater). The capillary grooved structures can wick liquid from the reservoir onto the heater, which in this case is a serpentine shape so we can see what is going on in a few of the channels. The horizontal serpentine is a resistance thermometer. These channels are 50 µm wide by 5 µm high and, because of the poor aspect ratio, the liquid does not fill the entire channel, but rather

only the 90 deg angle formed by the surface of the Si and the sidewall. We currently are sending out a mask containing 300 channels rather than the 24 we currently have. With this structure, the liquid phase can properly wet the heater surface and allow for good thermal contact between the heater surface and the membrane.

Preliminary calculations show that wicking the desired volume and evaporation each will happen on the order of a millisecond time scale consistent with operation in the hundreds of hertz. Later, we will work on a more detailed model coupling the thermo and fluidic behavior. This is something that has never been done. Capillary grooves have been used for years in microheatpipes but have never been integrated into a thermopneumatic actuator.

A big challenge will be cooling the surface during heat rejection to promote wicking into the channel, which is beyond the scope of our research.

Refereed

Whalen, S., M. Thompson, D. Bahr, C. Richards, and R. Richards. 2004. Design, fabrication, and testing of the P3 micro heat engine. *Sensors and Actuators A* **104** (3) (15 May): 290–98.

47795

Lipid Membranes on Nanostructured Silicon

D. Y. Sasaki

Sandia is developing dynamic, nanocomposite materials that combine the self-organization and molecular dynamics (MD) of lipid membranes with a nanotextured silicon (Si) wafer. The goal of this project is to understand how these structures can be assembled and how their interfacial interactions dictate unique physical and mechanical behavior through the confinement of phases in the membrane. We assembled biphasic lipid membranes on the nanostructured Si surface and imaged the surface using in situ *tapping-mode atomic-force microscopy (AFM). The membrane could be readily observed to span the ridges of the structure. Fluorescence recovery after photobleaching (FRAP) experiments found that on the microscale, those same structures exhibit anisotropic lipid mobility that was coincident with the Si substructure. The results showed that while the lipid membrane maintains much of its self-assembled structure in the composite architecture, the Si substructure indeed influences the dynamics of the molecular motion within the membrane.*

For the fluorescence microscopy studies, we used both vesicular and bicelle structures to generate the membrane-fused materials. We prepared the vesicular structures by extrusion or sonication using egg-phosphatidylcholine (egg-PC) doped with 1.0% of fluorescent-labeled phosphatidylethanolamine (PE) lipid. We fused the lipid bilayers to the substrate surfaces by incubating the lipid vesicles with either oxidized planar or the nanostructured Si. The nanostructured Si had a line pattern with a pitch of ~ 360 nm, depths of 200 nm, and linewidths of ~ 100 nm. We successfully prepared homogeneous lipid bilayer films on both surfaces, as evidenced by homogeneous fluorescence covering the substrates.

The FRAP experiments consisted of photobleaching a small area of the bilayer with intense light over a short period of time, then following the recovery of the fluorescence in that area as the peripheral lipids permeate and exchange positions with the photobleached lipids. If the nanostructured Si surface strongly interfaces with the supported lipid membrane, the observed fluorescence recovery should be anisotropic. Furthermore, the anisotropy on the patterned surface should significantly slow the total recovery time.

We photobleached the membrane using the maximum intensity of a confocal instrument. On the planar Si,

fluorescence recovery was complete in 30 min and proceeded isotropically, as expected. In comparison, recovery of the bilayers supported on the grooved Si took significantly longer with incomplete recovery after 90 min. In addition, the recovery was anisotropic, with the fluorescence recovery parallel to the grooves much faster than that perpendicular to the grooves, indicating greater mobility of the lipids in the direction of the grooves.

We successfully formed supported lipid bilayers prepared with bicelles, using two-component membranes of 1,2-diheptanoyl-sn-glycero-3-phosphocholine (DHPC) and 1,2-dipalmitoyl-sn-glycero-3-phosphocholine (DPPC) at a molar ratio of 1:2.8. Bicelles are disc-shaped lipid membrane structures that utilize the lamellar bilayer structure favored by long-chain PC (16–18 carbons) lipids combined with the high-curvature structures, such as would be found at the edges of a lipid bilayer, favored by short-chain PC (6–8 carbons) lipids. The two lipids should naturally phase-separate, as their chain lengths are considerably different in size. Those phases will tend to be gel-like for the long-chain lipids and fluidlike for the short-chain lipids. The supported membranes formed by fusion of bicelles to planar and textured Si readily formed as detected by fluorescence microscopy.

In situ AFM images of the 2.8:1 DPPC/DHPC bilayers on both planar and nanostructured Si yielded a number of interesting observations. We performed imaging with a Nanoscope III Multimode (Veeco Instruments) in phosphate-buffered water in tapping mode. On the planar substrate, the supported lipid membrane exhibited a biphasic structure of small 100 nm domains consisting of taller lipids embedded in a continuous fluidlike phase of smaller molecules. The taller domains were 13–17 Å above the fluid-phase areas, consistent with the height difference between DPPC and DHPC. Holes found in the bilayer allowed a measurement from the top of the membrane surface to the Si substrate of 55–60 Å. The images were stable with time, and the bilayer seemed to be robust to the scanning of the AFM.

On the nanostructured Si surface, we found the lipid membranes to span over the valleys between the raised line structures. This set of images is the first of a free-standing lipid membrane in a nanostructured surface. Topographic imaging of this unique composite structure finds that the membrane sags in between the lines to a depth of around 40 nm. At the nanoscale, this might look like a canopy draped over a repeating set of ridges where the canopy sags approximately one-fifth to the depth of the channel. The AFM images were not able to

distinctly resolve the fluid from the gel-like domains of the two-component membrane, but further efforts are continuing.

Refereed

O'Brien, M. J., P. Bisong, L. K. Ista, E. M. Rabinovich, A. L. Garcia, S. S. Sibbett, G. P. Lopez, and S. R. J. Brueck. 2003. Fabrication of an integrated nanofluidic chip using interferometric lithography. *J. Vacuum Science Technology B* **21** (6) (November): 2941–45.

49769

Resin Infusion Between Double Flexible Tooling

J. A. Ruffner

Resin infusion between double flexible tooling (RIDFT) is a novel composite manufacturing technology that has the potential for substantial cost savings and was the motivating factor behind this project collaboration with Florida State University (FSU). Composite fabric is placed between two flexible silicone membranes and then secured into a fixture. Resin is then infused under a vacuum until it wets the entire fabric. The membranes are then drawn over a male mold (the desired final product shape) by applying a vacuum. The use of a single-sided mold provides a substantial cost savings over the conventional resin transfer molding (RTM) processes that require both male and female molds. In addition, the molds are not subjected to high processing pressures and subsequently can be fabricated using less expressive materials and processes. The potential for cost savings is even greater in the production of large component parts (several feet in size). The RIDFT process lends itself to the incorporation of reconfigurable tools that can conform to different geometries, thus reducing tooling requirements and development-cycle times. Because the infusion of resin is done between translucent silicone diaphragms, ultraviolet (UV) curing processes can be used. However, this limits the RIDFT process to line-of-sight geometries.

The successful development of this technology could provide Sandia with a better understanding of RIDFT techniques, in-mold painting techniques, and coating processes that are important for a variety of Defense Programs (DP) and commercial applications. Potential DP applications include robot vehicle bodies, target/decoy shells, and re-entry bodies. Potential military and commercial applications include structural members for satellites, hatch covers, doors, panels, and light-weight members for robot arms.

Recent work concentrated on the assessment of in-mold coating by the co-infusion of the resin and coating materials. We also conducted an assessment to ascertain the viability of using UV lamps to cure photo-initiated resins for the rapid production of components using the RIDFT process.

The project further developed the RIDFT process for in-mold coating (IMC) and the incorporation of UV curing. We demonstrated that IMC is possible by co-infusing the resin and

the coating material. We successfully implemented UV curing, reducing curing times by a factor of 20 when compared with thermal curing while improving the mechanical properties of the resulting components.

(1) We investigated the RIDFT process with the view of shortening production cycle times using UV light curing. This work successfully incorporated a UV curing system into the RIDFT process. The resulting laminates not only exhibited consistent mechanical and thermal mechanical properties, but also had properties that were comparable to thermally cured composite laminates made using the same settings. We performed experiments that determined the best exposure time was 90 s. A shorter time (60 s) resulted in incomplete curing, and a longer time (120 s) resulted in laminates with inferior properties. We made a comparison between the tensile properties of the UV-cured and the methyl ethyl ketone peroxide (MEKP)–cured laminates. We found that there was no significant difference between the tensile strengths of the UV-cured (90 s) and the MEKP–cured laminates. However, the Young's modulus differed considerably between the two. The UV laminates had a higher Young's modulus (83%) than the MEKP laminates. A comparison of the cure times yielded a factor of 20:1 in favor of UV curing (based on a curing time of 90 s).

(2) The goal was to create a procedure for producing composite parts with a decorative finish to meet the customer's specifications by co-infusing the resin and the coating material in a single process without opening the mold. Preliminary results of IMC assessment studies of RIDFTed components indicated that co-infusion was possible. However, a problem that we encountered since we investigated the paint (DuPont Imron 5000) is that it interacted negatively with the separation layer, allowing the paint to seep through and mix with the resin. Material selection should continue to determine a more suitable separation-layer material.

We successfully implemented UV curing, reducing curing times by a factor of 20 when compared with thermal curing while improving the mechanical properties of the resulting components.

Refereed

Chiu, P., and O. I. Okoli. 2004. In-mold coating of composites manufactured by the resin infusion between double flexible tooling process by means of co-infusion. *Composites Part A*, accepted.

Chiu, P., O. I. Okoli, and H. P. Wang. 2004. In-mold coating of composites manufactured by the resin infusion between double flexible tooling process by means of co-infusion. *Proc. 7th International Conference Flow Processes in Composite Materials* (7–9 July, University of Delaware, Newark, Delaware): 189–94.

Nwabuzor, A. O., and O. I. Okoli. 2004. UV curing of composites manufactured by the resin infusion between double flexible process. *J. Materials Science*, accepted.

Toro, N., O. I. Okoli, and H. P. Wang. 2004. In-mold coating of composites manufactured with the resin infusion between double flexible tooling process. *J. Reinforced Polymers and Composites*, accepted.

Other Communications

Nwabuzor, A. O., and O. I. Okoli. 2004. Development of the resin infusion between double flexible tooling process: Incorporation of ultraviolet curing technique. Paper presented at ACMA Composites 2004, 6–8 October, Tampa, Florida.

Toro, N., and O. I. Okoli. 2003. In-mold coating of composites manufactured with the resin infusion between double flexible tooling process. Paper presented at CFA Composites 2003, 1–3 October, Anaheim, California.

49772

Studies on the Disbonding Initiation of Interfacial Cracks

E. D. Reedy, Jr.

There is a continuing trend toward smaller feature sizes in flip-chip assemblies. Consequently, there is an increasing interest in the nucleation and growth of small-scale disbonds. Traditional fracture-mechanics approaches typically assume a relatively large, preexisting disbond. In contrast, this project is aimed at predicting initiation phenomena. Disbond initiation often occurs at stress-free edges and corners. Such edges and corners induce high-stress concentrations. Indeed, within the context of elasticity theory, interface edges and corners generate singular stresses similar to those found at a crack tip, though less severe in intensity. As such, a "fracture-mechanics-like" approach can be employed. A material parameter—a critical interface-corner stress-intensity factor—can be defined and used to predict the initiation of a disbond at an interface. Sandia applied this approach to quantify the critical stress-intensity factor at interfacial corners in underfill-bonded tensile butt joints. Results showed a close correlation with interfacial fracture toughness data for a propagating crack as measured with a double-cantilever-beam specimen. Current testing is to characterize subcritical crack initiation under cyclic loading. This effort includes examining the fatigue lifetime of interfaces in a flip-chip–type geometry. In these tests, we are using acoustic emission techniques to identify when a crack initiates. We are assessing both mechanical and thermal-loading conditions.

We successfully characterized monotonically loaded, adhesively bonded butt joints that contain interfaces relevant to microelectronic packages.

We successfully characterized monotonically loaded, adhesively bonded butt joints that contain interfaces relevant to microelectronic packages. We found a nearly linear correlation between interfacial toughness (propagation) and interface corner toughness (initiation). In other work, we studied the variation in butt-joint strength with the strength of interfacial molecular interactions. Results show a linear increase in the critical free-edge stress-intensity factor with increasing levels of molecular bonding. We also developed and tested modified tensile butt-joint specimens to compare the effect of different types of interfacial discontinuities on crack nucleation. The three new geometries tested incorporated a stress-free corner, an embedded edge, and an embedded corner. A comparison of joint-failure loads showed an inverse relationship between the order of the stress singularity for a particular interfacial

geometry and the overall joint strength. The interfacial strength of an adhesive joint exhibits a predictable behavior that depends significantly on the severity of the order of the dominant singularity, ranging from a crack tip (0.5) to the stress-free edge (0.27). We also completed preliminary fatigue testing of the standard butt-joint geometry and mechanical loading of the flip-chip specimens, and successfully used new acoustic emission-detection equipment to detect crack initiation.

Refereed

McAdams, B. J., and R. A. Pearson. 2004. Initiation and propagation of delaminations at the underfill/passivation interface relevant to flip-chip assemblies. *IEEE Transactions on Device and Materials* **4** (2) (June): 169–75.

Other Communications

Pearson, R. A., and B. J. McAdams. 2004. Initiation and propagation of delaminations at the underfill/passivation interface in flip-chip assemblies. *Proc. 9th International Symposium on Advanced Packaging Materials: Processes, Properties, and Interfaces* **1** (24–26 March, Atlanta, Georgia): 260–63.

50396

Compliant Membranes for MEMS Microphones

W. K. Schubert

The objective of this project is to investigate compliant membranes for the development of a microelectromechanical systems (MEMS) microphone using Sandia's Ultraplanar Multilevel MEMS Technology V (SUMMiT V™) fabrication process. The microphone is a dual-backplate capacitive microphone that utilizes electrostatic-force feedback. The microphone consists of a diaphragm and two porous backplates, one on either side of the diaphragm. This forms a capacitor between the diaphragm and each backplate. As the incident pressure deflects the diaphragm, the value of each capacitor will change, thus resulting in an electrical output. We use feedback in this device by applying a voltage between the diaphragm and the backplates. This voltage creates an electrostatic force, which balances the incident pressure keeping the diaphragm stationary.

We designed a MEMS capacitive microphone utilizing a compliant diaphragm to be fabricated with the SUMMiT V™ process. Before fabrication, we simulated the design using finite-element method (FEM) analysis to verify the various performance metrics of the device. In addition, we verified the successful fabrication of the device by passing the SUMMiT V™ design rules.

We fabricated the microphone at Sandia up to the backside cavity etch and release steps. Upon completion of the SUMMiT V™ process, we fabricated the three layers (bottom backplate, diaphragm, and top backplate). The remaining steps of the process included a backside through-wafer deep reactive-ion etch (DRIE) and the final release by etching the sacrificial oxide. These steps were completed at the University of Florida (UoF), thus completing the fabrication of the MEMS microphone.

Once the device was fabricated, we tested and characterized the microphone. First, we measured the capacitance of the device as the bias voltage was swept, verifying the release of the diaphragm. After this initial testing, we measured the frequency response and the linearity of the microphone. We conducted these experiments in an acoustic waveguide, where we placed the microphone and a reference microphone in a known sound-pressure field. The predicted values of all properties of the microphone were within 25% of the

experimentally measured values, including frequency response of 204 mV per Pa.

The microphone demonstrated a linear response up to the designed value of 160 dB. The initial frequency-response measurements were over the limited range of 300 Hz–6.4 kHz due to the current limitations of our experimental setup. In the future, this range will be extended out to 20 kHz.

The MEMS capacitive microphone was fabricated at Sandia and post-processed at the UoF. We packaged the microphone and completed initial testing. The microphone demonstrates a flat frequency response, a linear response up to the designed limit, and a sensitivity that is close to the designed value. Further characterization and interface-circuit development is under way. Sandia is an essential partner in this project by providing access to and training for the SUMMiT V™ process.

50717

Multiscale Experimental/Numerical Study

J. A. Zimmerman

Lightweight and miniaturized weapons systems are driving the use of new materials in design, such as microscale materials and ultralow-density metallic materials. Reliable design of future weapon components and systems demands a thorough understanding of the deformation modes in these materials that comprise the components and a robust methodology to predict their performance during service or storage. Traditional continuum models of material deformation and failure are not easily extended to these new materials unless microstructural characteristics are included in the formulation. For example, in LIGA (for the German term Lithographie, Galvanoformung, und Abformung*, for lithography, electroforming, and molding) nickel (Ni) and aluminum-silicon (Al-Si) thin films, the physical size is on the order of microns, a scale approaching key microstructural features. For a new potential structural material, cast magnesium (Mg) offers a high stiffness-to-weight ratio, but the microstructural heterogeneity at various scales requires a structure-property continuum model. Processes occurring at the nanoscale and microscale develop certain structures that drive material behavior. The objective of this work is to understand material characteristics in relation to mechanical properties at the nanoscale and microscale in these promising new material systems. Sandia's research will employ tightly coupled experimentation and simulation to study damage at various material size scales under monotonic and cyclic loading conditions. We will accomplish experimental characterization of nano-/microdamage by novel techniques such as* in situ *environmental scanning-electron microscopy (SEM), 1 MeV transmission-electron microscopy (TEM), and atomic-force microscopy (AFM). New simulations to support experimental efforts will include modified embedded atom method (MEAM) atomistic simulations at the nanoscale and single-crystal micromechanical finite-element (FE) simulations.*

This work will advance our understanding and analysis capabilities in applying new materials and microsystems to weapons programs supported by the Department of Energy.

- In situ *fatigue damage of cast Mg*. We used the environmental scanning-electron microscope (ESEM) to track the growth of fatigue cracks *in situ*. Recent work, resulting in two publications, focused on qualitative mechanistic characterization of low- and high-cycle fatigue in cast Mg.

Work concentrated on quantitative characterization of small cracks growing under high-cycle fatigue conditions. Two key findings are noteworthy. First, we identified changes in crack growth rates with various microstructural features. Second, we quantified the effect of large-scale porosity on microstructural fatigue crack growth rate. We discovered that the fatigue crack growth rate for microstructurally small cracks depends on overall porosity level, even when the cracks do not directly interact with this porosity, but rather the porosity alters the "nominal" stress level.

- *Atomistic simulations of face-centered cubic (FCC) materials*. We used atomistic simulations to investigate the stability and structure of gold (Au) nanowires under their own surface stresses. We published key findings in three journal articles. Atomistic simulations with MEAM potential reveal that, for wires with a <100> initial crystal orientation and null side surfaces, surface stresses induce phase transformation from an FCC structure to a body-centered tetragonal (BCT) structure for very small nanowires and reorientation from an FCC <100> nanowire into an FCC <110> nanowire for relatively larger wires. In embedded atom method (EAM) and surface embedded atom method (SEAM) simulations, surface stresses induce yielding and reorientation from an FCC <100> nanowire into an FCC <110> nanowire below critical sizes. The difference in the instability mechanisms and the final structures is rooted in the differences in the unstable stacking fault energy and orientation dependence of electron density in the potentials. The existence of the BCT phase is confirmed by first-principle calculations.
- *Properties of thin films for microelectromechanical systems (MEMS)*. Gold/chromium/silicon (Au/Cr/Si) devices find use in optics, electronics, chemical and biological sensing, microactuation, and fabrication process monitoring applications. Arrays of Au/Cr/Si microcantilevers subject to isothermal hold conditions exhibit dimensional instability as a function of time measured through change in curvature. We performed characterization in the temperature range of 50°C–225ºC, and we observed, for example, drastic and nonintuitive changes in curvature for specimens annealed in air at 225ºC for less than 24 hr. The changes observed will influence design performance as well as device reliability. This work was published in two journal articles.

...we identified changes in crack growth rates with various microstructural features [and]....quantified the effect of large-scale porosity on microstructural fatigue crack growth rate. We discovered that the fatigue crack growth rate for microstructurally small cracks depends on overall porosity level, even when the cracks do not directly interact with this porosity....

Refereed

Diao, J., K. Gall, and M. L. Dunn. 2004. Atomistic simulation of the structure and elastic properties of gold nanowires. *J. Mechanics and Physics of Solids* **52** (9) (September): 1935–62.

Diao, J., K. Gall, and M. L. Dunn. 2004. Surface-stress–driven reorientation of gold nanowires. *Physical Review B* **70**:075413.

Diao, J., K. Gall, and M. L. Dunn. 2003. Surface-stress–induced phase transformation in metal nanowires. *Nature Materials* **2** (October): 656–60.

Gall, K., G. Biallas, H. J. Maier, P. Gullet, M. F. Horstemeyer, and D. L. McDowell. 2004. *In situ* observations of low-cycle fatigue damage in cast AM60B magnesium in an environmental scanning-electron microscope. *Metallurgical and Materials Transactions* **35** (1) (January): 321–31.

Gall, K., G. Biallas, H. J. Maier, P. Gullet, M. F. Horstemeyer, D. L. McDowell, and J. Fan. 2004. *In situ* observations of high-cycle fatigue mechanisms in cast AM60B magnesium in vacuum and water vapor environments. *International J. Fatigue* **26** (1) (January): 59–70.

Gall, K., N. West, K. Spark, M. L. Dunn, and D. Finch. 2004. Creep of thin-film Au on Au/Si microcantilevers. *Acta Materialia* **52** (8) (May): 2133–46.

Zhang, Y., M. L. Dunn, K. Gall, J. W. Elam, and S. M. George. 2004. Suppression of inelastic deformation of nanocoated thin-film microstructures. *J. Applied Physics* **95** (12) (June): 8216–25.

52727

Predictive Accelerated Aging of Microsystems: The Science of Dormancy

M. T. Dugger, B. Jokiel, Jr., K. A. Klody, T. J. Skousen, J. A. Ohlhausen, M. A. Duesterhaus, J. A. Walraven, D. M. Tanner, J. V. Cox, R. A. Plass

Qualification of microsystems for defense applications is critically dependent on our ability to build confidence in their performance by accurately predicting the evolution of their behavior over time in the stockpile. Understanding the effects of dormant storage on device performance is the greatest challenge we face to ensure reliable operation of devices over required stockpile service life. In this project, Sandia seeks to establish a device-level predictive capability for aging and reliability of packaged microsystems for defense applications. The effort is weighted toward experimental exploration in early work, but will include more modeling as the project progresses. We will package surface-micromachined (SMM) surety devices (e.g., the discriminating microswitch and nonvolatile memory) with diagnostic structures in packages with optically transparent lids to facilitate quantitative measurements of performance. We will use various packaging technologies to produce a range of realistic gaseous environments in the packages. We will subject packages to accelerated aging and stress tests to explore dormancy and operational environment effects on reliability and performance. We will make functional tests and quantitative measurements (adhesion, friction) without opening the packages. We will perform quantitative measurements in situ *where possible. Device tests and post-test analyses of surface composition, morphology, and gas composition will identify failure modes and underlying physical mechanisms relevant to defense microsystems. We will then use controlled experiments combined with simulations to determine the kinetics of specific degradation phenomena and build age-aware constitutive models that capture their dependence on environmental parameters. We will integrate knowledge from this and existing studies into a toolset that we will apply to predict the behavior of packaged microsystems after dormant storage. We will validate failure mechanisms identified by simulation using diagnostic structures and prototype devices exposed to environments to produce known changes to interface behavior.*

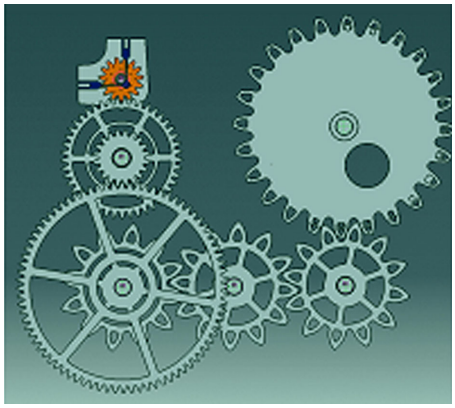

Rigid-body dynamics model.

We demonstrated the ability to hermetically package prototype weapon devices and diagnostic structures. Gas

analysis indicates the presence of hydrocarbon and fluorocarbon gases that we subsequently determined to come from die-attach adhesive. We developed a test for die-attach materials to ensure that they will not contaminate package environments, and it will likely become part of any microelectromechanical systems (MEMS) packaging qualification.

We modified our dormancy module to incorporate flaps that we can then invert to permit chemical examination of both contacting surfaces. To examine cleaning effectiveness, we used ultraviolet (UV)-ozone or oxygen plasma to remove monolayers from coated structures. We used time-of-flight (ToF) secondary ion mass spectrometry (SIMS) and spectral image analysis to highlight differences. UV-ozone effectively removed the monolayer from exposed surfaces, but left material in narrow gaps. The oxygen plasma cleaned hidden surfaces more effectively, but also left some monolayer under the flaps. This suggests that deeply buried interfaces may not be effectively cleaned by oxygen plasma, and hence may be more susceptible to degradation during aging.

We also made significant progress in identifying contaminants on surfaces and their impact on interface behavior. We chemically identified an adsorbate on MEMS die after packaging and determined that it can increase the force required to separate two structures by shear. Contaminate adsorption appears to be associated with defects in the monolayer.

Our aging study of surety-like MEMS attempts to accelerate aging by exposing devices to controlled temperature, humidity, and atmosphere. We chose temperatures of 100°C, 200°C, and 300ºC, and water concentrations of 500 and 2000 ppmv in nitrogen, representing the package environment. For each temperature and humidity setting, we tested for three time intervals using about 30 packages each to ensure a good statistical sample and to include bare silicon (Si) for surface analysis.

In the failure data for the microengine-driven gear train, each data point represented about 15 devices. For the rotational actuator exposed to 300ºC, we observed mean times to failure of 31 hr for the samples exposed to 2000 ppmv water, and 196 hr for those at 500 ppmv water. This indicates a strong link to moisture and is the first step in developing a model. Future tests will take place at lower temperatures and longer time intervals. Failure analysis is under way for these devices and will include measurement of adhesion energy and friction using diagnostic

We developed a test for die-attach materials to ensure that they will not contaminate package environments, and it will likely become part of any microelectromechanical systems (MEMS) packaging qualification.

devices. Bare Si exhibited metallic contamination that increased in concentration with time.

Development of a device model addressed a MEMS gear train since small actuation forces made it more vulnerable to aging, which we qualitatively observed. Finite-element (FE) results implied that the mesh density needed to capture contact stresses would make a complete finite-element model (FEM) intractable. FE analyses also indicated the potential for adhesion to be an important factor in the gear-hub interaction.

Flexure of the gears/hubs is not significant, so we uncoupled the dynamics and deformations of the system using a rigid-body dynamics model (RBDM) of the gear train. We can apply the gear-hub force and orientation to the FEM to evaluate contact stresses and contact area. A tilted-gear contact model illustrates that in real devices we must account for asperity contact. The nominal contact stresses provide upper bounds for experimental studies.

AutoCAD geometry was the starting point for the RBDM, with additional features progressively added. A recent model uses simplified contact to define the gear-hub interaction, where actual tolerances will allow the gear to wobble in-plane, and constant friction coefficients are used to model friction forces.

Refereed

Romig, Jr., A. D., M. T. Dugger, and P. J. McWhorter. 2003. Materials issues in microelectromechanical devices: Science, engineering, manufacturability, and reliability. *Acta Materialia* **51** (19) (25 November): 5837–66.

Wiehn, J. S., and M. T. Dugger. 2003. Aging effects on the structure and performance of monolayer surface treatments for MEMS. Paper presented at IMAPS, 20 November, Boston, Massachusetts.

Other Communications

Dugger, M. T. 2004. The role of materials and interfaces in the performance and reliability of microsystems. Paper presented at a seminar at Texas Instruments, 30 August, Dallas, Texas.

Dugger, M. T. 2004. Tribology and mechanics of microsystem materials. Paper presented at a seminar at the University of Arizona, 18 February, Tucson, Arizona.

Dugger, M. T., J. S. Wiehn, and D. E. Peebles. 2003. Effects of operation, processing, and storage environments on the performance and structure of monolayer lubricants for MEMS. Paper presented at the Materials Research Society Fall Symposium, 1 December, Boston, Massachusetts.

Dugger, M. T., J. S. Wiehn, J. A. Ohlhausen, and D. E. Peebles. 2004. Effects of processing and storage conditions on the tribological behavior of monolayer lubricants for MEMS. Paper presented at the American Chemical Society National Meeting, 28 March, Anaheim, California.

52728

Surety and Accountability Enhancements for Storage Containers

J. W. O'Connor

As world politics change and treaties result in reductions of fielded nuclear weapon (NW) systems, a need for handling warheads exists, whether a weapon is in a fully assembled state in the stockpile or in a partially disassembled configuration. Large quantities of surplus warheads are expected from stockpile reductions, yet an insufficient number of storage assets exist to support a large-scale draw-down; existing shipping-container inventories are inadequate. Sandia successfully designed and produced a one-quarter-scale prototype container incorporating a wireless inventory-management system (IMS), a user-controlled viewing window, and a fiber-optic viewing system. The development efforts culminated with an interactive demonstration displaying the advanced capabilities of the container system.

We will perform research and development that will demonstrate advanced concepts applied to weapon-inventory and accountability needs. The overarching goal would be to provide a new design alternative, specifically for weapon storage, and to lay the foundation for a lightweight and inexpensive container paradigm. The challenge involves the production of a high-quality prototype container with advanced inventory-management features, including advanced communication capabilities, while maintaining a manufacturing cost of about $2,000 per container.

We focused on developing a prototype quarter-scale container that incorporated an IMS, an electronic viewing window, and an optical viewing system. We centered development of the IMS on the use of commercial off-the-self (COTS) wireless-communication packages known as "motes." To demonstrate the container system's capabilities, we developed an interactive demonstration to allow users to test wireless functionality between the prototype container and a base station.

In addition to the IMS functionality, the demonstration allowed users to control an electronic viewing window via the use of a personal digital assistant (PDA). One function of the PDA enabled users to wirelessly set a viewing window in the container structure to an "inventory" state (transparent) or a "privacy" state (opaque). The "inventory" state allowed users to view the serial number of a scaled-down mock nuclear warhead

inside the container, as would be performed on a real weapon during a Department of Defense inventory.

Our accomplishments demonstrate the concepts that provide the basis of a highly capable, yet low-cost weapon-storage container, and set the stage for a final year of advanced communications development and implementation.

Our accomplishments demonstrate the concepts that provide the basis of a highly capable, yet low-cost weapon-storage container, and set the stage for a final year of advanced communications development and implementation.

52729

Nuclear-Safety Weaklinks for Thermal and Mechanical Environments

A. C. Hall, S. J. Glass, K. Eras, K. Rahimian

Weaklinks, stronglinks, and barriers are key components of the Enhanced Nuclear Detonation Safety (ENDS) theme. The ENDS theme provides design guidance for nuclear detonation safety implementation. A weaklink is a detonation-critical element that fails predictably, passively, and irreversibly at abnormal environment levels (i.e., accident environments) well below the failure levels of the weapons safety-critical components (i.e., stronglinks and barriers).

This project focused on developing two materials that could be used to design weaklinks for abnormal thermal and mechanical environments. Sandia is studying a novel polymeric system (polyvinylalcohol [PVA]/silver nitrate [$AgNO_3$]) for thermal weaklink applications. At 150°C, this material undergoes an irreversible chemical reaction that results in its resistivity decreasing by over 5 orders of magnitude. It becomes irreversibly conductive. We are exploring engineered stress profile (ESP) glass for mechanical (shock or crush) weaklink applications. ESP glass is a specific glass composition that has been treated by multiple ion exchanges so that it fractures at a highly predictable stress level.

Much of this development effort focused on understanding the material properties and behavior of ESP glass and PVA/$AgNO_3$ that affect weaklink performance (chemical reactions, initiation temperatures, fragmentation behavior, etc.). However, we also worked to investigate materials properties and behavior that could affect the reliability of a component or a system built using these materials. These experiments included radiation exposures (high-dose gamma-ray and neutron environments) to provide initial radiation-hardness determinations.

We focused on demonstrating weaklink concepts using a specially designed model firing set. It has provisions for inserting prototype weaklinks in various locations within the critical firing circuitry. We monitored the performance of the firing set using resistive "dummy" loads instead of actual detonators. Using this tool, we demonstrated that fracture of ESP glass can significantly change the behavior of a capacitive circuit and that PVA/$AgNO_3$ can be used to create short circuits in the firing set.

...we demonstrated that fracture of ESP glass can significantly change the behavior of a capacitive circuit and that PVA/$AgNO_3$ can be used to create short circuits in the firing set.

We focused on further characterizing and understanding the materials science of PVA/$AgNO_3$ films and ESP glass. We worked with a model firing set to conduct proof-of-concept tests of potential weaklink implementations. We completed neutron exposure of ESP glass and PVA/$AgNO_3$ and began initial testing to explore incorporating PVA/$AgNO_3$ and/or ESP glass into weaklink capacitors.

Development of PVA/$AgNO_3$ films included preparing prototype weaklinks using PVA/$AgNO_3$, long-term thermal-aging experiments, and exploration of other metallic salts that could be used to prepare similar polymeric systems.

We further studied the fracture behavior of ESP glass. Specifically, we explored joining technologies that allow fractures to be propagated from one piece of ESP glass to another. We successfully demonstrated that fractures can be transferred from one piece of ESP glass to another.

We gave ESP glass and PVA/$AgNO_3$ samples an acute neutron exposure using Sandia's Annular Core Research Reactor. Both materials survived the neutron exposure. Macroscopic fracture behavior of the glass appears to be unchanged, and the PVA/$AgNO_3$ did not convert to silver.

We designed and constructed a model firing set, capable of firing War Reserve (WR)-like detonator systems using WR-like components. We used this firing set to test prototype ESP glass and PVA/$AgNO_3$ weaklinks. This testing demonstrated that thermal weaklinks based on PVA/$AgNO_3$ can significantly change a firing signal when exposed to abnormal environment conditions. It also demonstrated that fracture of an ESP glass dielectric material placed between the plates of a capacitor will cause arcing/shorting of the capacitor plates.

Our efforts resulted in a further understanding of both potential weaklink materials and proved initial proof-of-concept for a new thermal and mechanical weaklink.

Refereed

Glass, S. J. 2003. Microstructural characterization of porous or partially sintered ceramics using nuclear magnetic resonance (NMR). Paper presented at the 5th International Meeting of the Pacific Rim Ceramic Societies, 29 September–2 October, Nagoya, Japan.

Glass, S. J. 2003. Nuclear magnetic resonance (NMR) characterization of the surface area and porosity of partially sintered ceramics. Paper presented at the International Conference on the Characterization and Control of Interfaces for High-Quality Advanced Materials, 24–26 September, Kurashiki, Japan.

Glass, S. J., and R. Tandon. 2003. Residual stresses in glasses and ceramics. Paper presented at the Residual Stress Summit, 10–11 December, Los Alamos, New Mexico. SAND2003-4518A.

Glass, S. J., and R. Tandon. 2003. Strength and fragmentation of stressed glass. Paper presented at the 5th International Meeting of Pacific Rim Ceramic Societies, 29 September–2 October, Nagoya, Japan.

Kooi, J. E., S. J. Glass, and J. J. Mecholsky, Jr. 2003. Fractal analysis of crack branching in ion-exchanged glasses. Paper presented at the 15th Rio Grande Symposium on Advanced Materials, 27 October, Albuquerque, New Mexico.

Kooi, J. E., S. J. Glass, R. Tandon, and J. J. Mecholsky, Jr. 2004. Crack-branching density in ion-exchanged glass. Paper presented at the Rio Grande Symposium on Advanced Materials, 25 October, Albuquerque, New Mexico.

Mecholsky, Jr., J. J., J. E. Kooi, and S. J. Glass. 2004. Fractal analysis of crack branching in ion-exchanged glasses. Paper presented at the 28th Conference and Expo on Advanced Ceramics and Composites, 25–30 January, Cocoa Beach, Florida.

Tandon, R., and S. J. Glass. 2004. Fragmentation in a residually stressed system. Paper presented at the 28th Conference and Expo on Advanced Ceramics and Composites, 25–30 January, Cocoa Beach, Florida.

Tandon, R., S. J. Glass, and A. C. Hall. 2003. Fragmentation-enabled weaklink utilizing a self-stressed system. Paper presented at the 25th Aging, Compatibility, and Stockpile Stewardship Conference, Lawrence Livermore National Laboratory, 18–20 November, Livermore, California.

Other Communications

Glass, S. J. 2004. Glass fracture: Can we control it? Paper presented at the Advanced Materials Lab Seminar, Sandia National Laboratories, 4 August, Albuquerque, New Mexico.

Kooi, J. E., S. J. Glass, and R. Tandon. 2004. Fractal analysis of macroscopic crack branching in ion-exchanged glass. Paper presented at the Sandia Student Symposium, Sandia National Laboratories, 2 August, Albuquerque, New Mexico.

Rygel, J., S. J. Glass, and R. Tandon. 2004. Determination of stress in ion-exchanged glass and its effect on fragmentation. Paper presented at the Sandia Student Symposium, Sandia National Laboratories, 2 August, Albuquerque, New Mexico.

52730

Advanced Packaging Technology for Optical Firesets

B. Jokiel, Jr., K. A. Klody, L. S. Weichman, D. W. Peterson

Sandia performed technology and process development to integrate and package a fiber-optic, microelectromechanical systems (MEMS), photocell system. Technologies and processes developed are aimed strictly at enabling microoptical firesets using some type of MEMS locking element. We discussed a variety of different system architectures that may be considered for optical firesets. Our work consisted of prototypes for two different system architectures. One prototype is an in-line shutter-type system where we use a discriminating MEMS device to gate light between an input optical fiber and an output optical fiber. The second prototype is a more-sophisticated out-of-line system using a MEMS mirror to redirect light to a photocell. Processes developed and discussed include optical alignment, hermetic laser welding and sealing, and precision die placement. The processes developed fulfill the main project goal, which was to generate a toolbox of processes that we can use to create a variety of different systems requiring MEMS, optical fiber, and photocell alignment and integration.

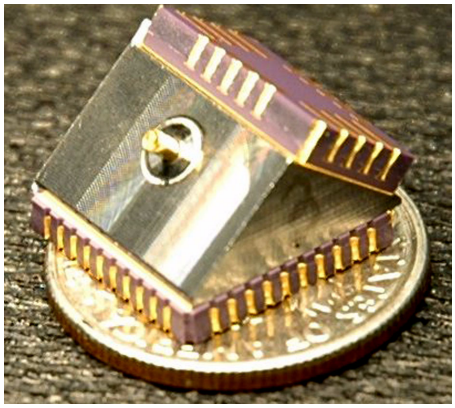

Defense Message System 6 V system on a dime.

Our final milestones included the following:

(1) Transfer MEMS requirements to the design organization,

(2) Complete nonfunctional mock-ups,

(3) Document packaging technology, and

(4) Deliver 10 technology demonstrators.

We previously concentrated on an in-line shutter system. We decided that we would focus on developing the assembly processes to realize an out-of-line system. We used a design and tolerancing analysis performed as the basis to determine the MEMS mirror shape, size, and placement. Others at Sandia designed and fabricated a discriminating MEMS mirror system that would work in conjunction with our packaging system.

We created an aluminum mock-up and Kovar test devices to perfect the hermetic ferrule welding processes. We ordered the photocells. The first MEMS devices of the new packaging-friendly design were delivered. We “mocked-up” the basic components, which were in-house.

We documented packaging technology throughout the project.

We proved the design and assembly technologies to be achievable and realizable, but were unable to build a working

prototype because of time constraints; consequently, we were unable to deliver the 10 technology demonstrators. However, the basic processes and components are ready to finish this part of the project with Defense Programs (DP) funding under the Defense Message System (DMS) project.

At the end of this project, we are able to (1) place active elements of MEMS devices in specific locations within a package; (2) assemble and hermetically seal fiber-optic ferrules of varying size and geometry using a low-melting-point glass; (3) polish the fiber optics; (4) design and create packaging systems that require multiple components produced in various manufacturing technologies; (5) successfully actively and passively align MEMS, photocells, and fiber-optic subcomponents; and (6) weld and hermetically seal different subcomponents together to create composite packaging systems that are suitable to WR and DP applications.

Other Communications

Jokiel, Jr., B., and D. W. Peterson. 2003. Realization of packaging solutions for MEMS devices with optical and electrical interconnects. *Proc. IMAPS 5th Topical Workshop on MEMS, Related Microsystems, and Nanopackaging* (16–20 November, Boston, Massachusetts).

52731

Miniature Transmitter Filter for JTA Using LIGA Technology

M. A. Forman, M. Armendariz, E. J. Garcia, D. M. Skala, M. T. Oswald, R. A. Renn, A. M. Morales

Sandia developed a low-loss LIGA (for the German term Lithographie, Galvanoformung, und Abformung, *for lithography, electroforming, and molding)–micromachined conductor-backed coplanar waveguide (CPW). The 517 µm lines are the tallest uniplanar LIGA–fabricated microwave transmission lines to date, as well as the first to be constructed of copper (Cu) rather than nickel (Ni). The conductor-backed micromachined CPW on quartz achieves the lowest measured attenuation of CPW line to date at 0.064 dB/cm at 15.5 GHz.*

In LIGA–micromachined CPWs, the electric field is confined primarily to the space between the signal and the ground lines. This geometry distributes the surface current over the full height of the metal, reducing ohmic losses relative to standard CPW while simultaneously drawing the electric field out of the substrate, reducing dielectric loss. The reduced interaction between the propagating fields and the substrate minimizes dispersion, radiation loss, and the excitation of substrate modes. Additionally, the ability to fabricate microwave structures with variable thickness adds an additional design parameter, increasing design flexibility.

The 517 µm lines are the tallest uniplanar LIGA–fabricated microwave transmission lines to date, as well as the first to be constructed of copper (Cu) rather than nickel (Ni). The conductor-backed micromachined CPW [(coplanar wave guide)] on quartz achieves the lowest measured attenuation of CPW line to date at 0.064 dB/cm at 15.5 GHz.

We fabricated a conductor-backed CPW using the LIGA–micromachining process. In the LIGA process, we fabricated structures with near-vertical sidewalls by means of deep x-ray lithography (DXRL), electrodeposition of metal, and mechanical grinding. This process enables the creation of thick structures or molds with near-vertical sidewalls based on two-dimensional (2-D) patterns.

In LIGA–micromachined CPW, the electric field is confined primarily to the space between the signal and the ground lines. This geometry distributes the surface current over the full height of the metal, reducing ohmic losses relative to standard CPW while simultaneously drawing the electric field out of the substrate, reducing dielectric loss. The reduced interaction between the propagating fields and the substrate minimizes dispersion, radiation loss, and the excitation of substrate modes.

- *Design*. With our primary goal being to create a low-loss transmission line, we selected the conductor and substrate to minimize loss. The selected metal is Cu, with a conductivity of 5.8e7 S/m, which is higher than the traditionally used Ni, with a

conductivity of 1.0e7 S/m. The selected dielectric is GE-124, a clear fused quartz, with a relative permittivity of er = 3.75 and a loss tangent of tand = 0.0004. To maximize compatibility with existing in-house manufacturing techniques, the quartz wafer is selected to have a height of h = 1.0 mm and a diameter of d = 100 mm.

The height of the transmission line is set at t = 500 μm. Similarly, the gap between conductors is set to be s = 300 μm to reduce the likelihood of long beams of acrylic polymethylmethacrylate (PMMA) buckling due to expansion during the processing. With the given conductor, substrate, and geometry constraints, we use the full-wave finite-element (FE) electromagnetic simulator, Ansoft HFSS, to solve for the remaining dimensions. The final CPW has a center-conductor width of w = 250 μm, a signal-ground separation of s = 300 μm, and a ground-conductor width of g = 850 μm. The line has a simulated characteristic impedance of Zo = 52, an effective relative permittivity of ere = 1.614, and a guided wavelength of 18.9 mm at 20 GHz.

- *Measurements*. We characterized three transmission lines with lengths of 1.875 cm, 2.345 cm, and 4.220 cm on an Agilent 8510C network analyzer using a Cascade Microtech probe station with ACP40-A GSG probes. We measured two-port s-parameters from 1 to 20 GHz and extracted line parameters from s-parameters using previously published techniques.

The measured characteristic impedance of the three lines is approximately 55 ohms at 20 GHz and is within 3 ohms, or 5.7 %, of the simulated value. Characteristic impedance as a function of frequency varies between lines by 3 ohms at most. The measured relative effective permittivity for the three lines is between 1.585 and 1.655 at 20 GHz, and is within 0.04, or 2.5 %, of the simulated value of 1.614. Relative effective permittivity as a function of frequency varies between the lines at most by 0.070. Variation in measurements between lines is believed to be due to variations in fabricated dimensions due to nonuniform etching and grinding, as well as randomly distributed defects in the sidewalls.

We extracted attenuation from measured s-parameters using two independent methods, one that employs a transmission-line lumped-element model and another that employs an ABCD-matrix conversion. We used the difference in values for each method to generate ranges for the points plotted on the graph. Measured attenuation is 0.050 dB/cm at 10 GHz and 0.064 dB/cm at 15.5 GHz. Measured data agree within 0.01 dB/cm of simulations that include the measured sidewall irregularities.

Recent electroplating experiments eliminated sidewall irregularities; we believe that the second iteration of the circuitry will achieve the simulated ideal loss levels, yielding CPW with loss on the order of comparable microstrip transmission lines.

52732

Novel and Robust Environmental Sensing Devices (ESDs)

J. A. Mitchell, N. S. Finch, J. W. Franklin, S. M. Wooden, R. C. Clemens, T. Lemp

Sandia is developing novel environmental sensing device (ESD) prototypes using microelectricomechanical systems (MEMS) technologies. Research and development in this project is associated with novel design development, fabrication, packaging, and testing of MEMS ESDs. We are primarily targeting low-G (3 Gs to 15 Gs) applications using LIGA (for the German term Lithographie, Galvanoformung, und Abformung*, for lithography, electroforming, and molding) designs that tether shuttle masses to specific combinations of folded flexure beams and novel bistable beam designs. We are also investigating damping mechanisms, including eddy-current damping, which is a fluidless approach that has the potential to circumvent longstanding issues associated with fluid damping in ESDs. The project is also exercising and pushing LIGA fabrication technologies associated with multimaterial systems development.*

Our primary focus was been on the design, fabrication, packaging, and testing of ESDs using the LIGA technology. We successfully developed four ESD concepts: (1) a low-G accelerometer/acceleration switch, (2) a bistable acceleration switch, (3) an eddy-current–damped acceleration switch, and (4) an X-wing design synthesizing the first two designs.

- *Low-G accelerometer/acceleration switch*. We successfully fabricated and subsequently packaged this device for switch-closure testing and accelerometer measurements in a centrifuge. As an accelerometer, the giant magnetoresistive (GMR) sensors in the package successfully detected the appropriate G levels developed by the centrifuge. As an acceleration switch, we found the tethered mass to be highly undamped, which prevented successful switch closure due to undamped vibrations against the electrical contacts.
- *Bistable acceleration switch*. This design exploits the bistable nature of a system of flexure beams that we use to tether a shuttle mass. The concept aims to significantly increase the contact force of interaction between the tethered mass and electrical spring contacts so that contact chatter is significantly reduced, thereby lowering electrical-contact resistance and obtaining a clean switch closure. The design relies on the placement of a shuttle stop at the low point in the force-

deflection curve of the tether springs. In centrifuge testing, we successfully demonstrated the mechanism to close at the appropriate G-setpoint and open at the appropriate reset value, validating *a priori* modeling/design analyses.

- *Eddy-current–damped acceleration switch*. Eddy-current damping is widely used in macroscopic devices, and we pursued this approach as a novel way of adding damping to our MEMS ESD designs. This approach has a potential benefit in that it may provide a nonfluid damping mechanism, alleviating longstanding issues with thermal expansion and leakage of fluid from the ESD. However, some technical challenges exist, and the project is addressing those. Device design is more complex and requires a fairly sophisticated understanding of eddy currents and their modeling so that damping levels can be predicted *a priori*. To achieve useful levels of damping, eddy-current–damped systems often use an array of magnets that set up a static magnetic field that is cut by a moving conductor. We did some preliminary modeling (static magnetic fields induced by magnetic array) and plan to do more in upcoming work. LIGA fabrication also posed challenges and created an environment for innovation.

Areas of innovation and research in the LIGA processes include the following:

(1) Thin high-aspect-ratio (HAR) insulator on metal development,

(2) Development and molding of bondable neodymium iron boride (NdFeB) into HAR structures,

(3) 78/22 nickel iron (NiFe) improvements and characterization for LIGA electrodeposition,

(4) Protection of NdFeB–molded LIGA structures through the release process,

(5) Self-aligned LIGA electrical contacts with break-away alignment structures, and

(6) The creation of repeating metal/insulator/NdFeB structures in X and Y (array of magnets).

- *X-wing development*. This device combines the features of the GMR accelerometer capability with a novel tethering system for the shuttle mass that has bistable force-deflection curve characteristics. We submitted the design to the fabrication facility.

52733

Advanced Neutron Monitors for JTA and Stockpile Monitoring

N. Mascarenhas, W. R. Dunkel, J. Peel, D. A. Sunnarborg, J. S. Zaha, C. M. Cuppoletti

In this project, Sandia will evaluate two prototype directional neutron-detector concepts for use in joint test assembly (JTA) and stockpile monitoring.

We completed the construction of the two prototype directional neutron detectors and tested the segmented fiber-detector prototype using a 14 MeV controlatron source, which exhibited a directional response.

We completed the fabrication of the multi-anode photomultiplier (MAPMT) tracking detector and completed software to read the detector data-acquisition system. We completed preliminary data-analysis software and currently are analyzing the data from the MAPMT detector.

We calibrated the detector for tracking using cosmic-ray muons. We used a light-emitting diode (LED) to verify fiber/photomultiplier (PMT) operation and calibrate light collection in the fibers. We also performed an energy calibration using 3 MeV protons at the Sandia/Lawrence Livermore National Laboratory (LLNL) proton accelerator.

We are studying angular resolution and background with the detector and working to optimize detector performance.

We made the following accomplishments:

(1) Evaluated optical readout technologies with experimental results and evaluated a single-photocathode PMT detector.

(2) Completed the MAPMT detector. We developed software to read out the data-acquisition electronics and for data analysis. An optimization study is now in progress.

(3) Performed a three-dimensional (3-D) calculation of neutron-proton transport in a segmented scintillator detector using MCNPX. (MCNPX is the 3-D Monte Carlo radiation transport code, which includes the capability to do charged-particle tracking.)

(4) Conducted experiments with thin-plate detectors. We tested several thin-plate detectors (100 µm, 400 µm, and 800 µm). However, results do not indicate angular sensitivity.

(5) Studied the angular response of segmented fiber detectors. Optimization remains to be done. We evaluated fibers encapsulated in an aluminum (Al) absorber. We demonstrated directional response with near- and far-field detectors. We

began studying the response of the “far-field” MAPMT detector and developed software to reconstruct neutron-proton recoil tracks in the detector. We are evaluating the directional response. Work is in progress to optimize the angular response and to identify ways to suppress the backgrounds.

(6) Studied optical transport in fibers. We conducted a Monte Carlo study of the light collection from round and square fibers. Light collected from round fibers shows a radial nonuniformity. Square fibers are a better choice for our detector. A 1 MeV electron-equivalent particle results in 65 photoelectrons collected per fiber.

(7) Measured angular response and x-ray sensitivity to demonstrate feasibility. This is mostly completed; x-ray sensitivity and optimization remain to be done. We measured the response using a 14 MeV D-T neutron generator (a controlatron). We tested the detector with a controlatron in a cave shielded for neutrons using boron-loaded polyethylene. The detector shows a directional response to neutrons. There is a large gamma-ray background at this location from neutron capturing in the 10B (boron 10). Occasionally, x-rays are produced in the controlatron, in addition to neutrons. The detector has performed in this background.

(8) Performed LIGA (for the German term *Lithographie, Galvanoformung, und Abformung*, for lithography, electroforming, and molding) fabrication experiments and determined dimensional parameters of LIGA fabrication with fluor-loaded polymethylmethacrylate (PMMA) scintillator parts. This work is in progress. We are investigating the fabrication of a prototype detector using LIGA.

Other Communications

Peel, J., and N. Mascarenhas. 2004. Developing a directional neutron detector for 14 MeV neutrons. Poster presented at Summer Intern Symposium, Sandia National Laboratories, 3 August, Livermore, California.

52797

Design and Control of the Magnetic Properties of Nanoparticles

B. A. Simmons

Magnetic spinel ferrite nanoparticles, MFe_2O_4 (M = Mn, Mg, Zn, Co, Fe, etc.), have great potential in detecting bioagents. A crucial component in the applications of magnetic nanoparticles for biodetections is the surface chemistry. Understanding and controlling the effects of surface chemistry on magnetic properties has become increasingly important for the technological applications of magnetic nanoparticles such as high-density magnetic storage media, medical imaging, and drug delivery. For practical implementation in biomedical applications of nanoparticles, the surfaces of the nanoparticles have to be modified with biocompatible ligands and/or polymer matrices that also serve as drug-carrying vehicles. Once internalized, the surfaces of nanoparticles are inevitably encapsulated with biological ligands that are associated with the body's defense system.

Furthermore, the shapes of the nanocrystals can be controlled into either spherical or cubic during the nanoparticle formation. Critical magnetic properties such as coercivity are closely related with the surface chemistry of nanoparticles. Coercivity has to be considered together with the surface pinning of magnetic moments and the resulting surface anisotropy. The surface magnetic disorder and pinning originate from missing coordinating oxygen atoms around surface metal cations. When the coordination of surface metal cations has a closer similarity to the coordination symmetry of the metal cations in the core of a nanocrystal, the surface anisotropy should be lower. Compared to the curved topology of spherical nanocrystals, the flat surfaces of cubic nanocrystals enable the surface metal cations to possess a more symmetric coordination and fewer missing coordinating oxygen atoms. Therefore, the surface anisotropy should be much smaller in cubic nanocrystals than the one in spheres. Clearly, the surface anisotropy shows dominance in determining the coercivity over the core anisotropy. A comparison of the magnetic properties possessed by spherical and cubic nanocrystals offers rich insights into the fundamentals of nanomagnetism.

We made direct correlations between the magnetic properties of nanoparticles and the surface chemistry.

We made direct correlations between the magnetic properties of nanoparticles and the surface chemistry. To understand the influence of surface interactions upon the magnetic properties of magnetic nanoparticles, the surface of

manganese ferrite, $MnFe_2O_4$, we systematically modified nanoparticles with a series of parasubstituted benzoic acid ligands (HOOC-C_6H_4-R; R= H, CH_3, Cl, NO_2, OH) and substituted benzene ligands (Y-C_6H_5, Y = COOH, SH, NH_2, OH, SO_3H). The coercivity of magnetic nanoparticles decreases up to almost 50% upon the coordination of the ligands on the nanoparticle surface while the saturation magnetization has increased. The percentage coercivity decrease of the modified nanoparticles with respect to the native nanoparticles strongly correlates with the crystal field-splitting energy (CFSE) *f´* evoked by the coordination ligands. The ligand inducing the largest CFSE results in the strongest effect on the coercivity of magnetic nanoparticles. The change on magnetic properties of nanoparticles also correlates with the specific coordinating function group bound onto the nanoparticle surface. The correlations suggest the decrease in spin-orbital couplings and surface anisotropy of magnetic nanoparticles due to the surface coordination. Such surface effects clearly show the dependence on the size of nanoparticles.

In addition, we studied the interactions between magnetic nanoparticles and living cells. Magnetic cobalt spinel ferrite nanoparticles, $CoFe_2O_4$, were conjugated to oligonucleotides and delivered into African green monkey kidney cells, CV-1, and human cervical cancer cells, HeLa, through transfection using Lipofectamine. Confocal microscopy studies indicate that transfected $CoFe_2O_4$-oligonucleotide conjugates are localized within the cell. The $CoFe_2O_4$-oligonucleotide conjugates have not shown any adverse effects on cell growth, even 250 hr post-transfection. Cellular movement in buffer solution synchronized with a moving magnet demonstrates the feasibility of using $CoFe_2O_4$ nanoparticle-oligonucleotide conjugates for magnetic manipulation of cells.

Refereed

Han, M., C. R. Vestal, and Z. J. Zhang. 2004. Quantum couplings and magnetic properties of $CoCrxFe_2$-xO_4 ($0 < x < 1$) spinel ferrite nanoparticles synthesized with reverse micelle method. *J. Physical Chemistry B* **108** (2): 583–87.

Song, Q., and Z. J. Zhang. 2004. Shape control and associated magnetic properties of spinel cobalt ferrite nanocrystals. *J. American Chemical Society* **126** (19): 6164–68.

Vestal, C. R., and Z. J. Zhang. 2003. Effects of surface coordination chemistry on the magnetic properties of $MnFe_2O_4$ spinel ferrite nanoparticles. *J. American Chemical Society* **125** (32): 9828–33.

Vestal, C. R., and Z. J. Zhang. 2003. Synthesis and magnetic characterization of Mn and Co spinel ferrite-silica nanoparticles with tunable magnetic core. *NanoLetters* **3** (12): 1739–43.

52977

Flow Control and Mixing in Microfluidic Devices

A. C. Sun, C. J. Bourdon

In collaboration with the University of Colorado, Sandia is studying flow control and mixing in microfluidic devices. As one means of microfluidic flow control, we considered electroosmosis both to control the liquid flowing through the channels and as a pumping technique. We utilized living radical photopolymerization (LRPP) to produce polymeric microfluidic devices. LRPP allows for excellent control of microchannel geometry and can be used to chemically modify the surfaces of the channels by attaching charged species or other functional groups. This ability allows us to modify the zeta potential of the surface and, in turn, manipulate the electroosmotic flow in the channel. With LRPP, we can also change the dimensions of the channels. With these considerations, we focused on developing a model that takes into account step changes in both zeta potential and cross section.

For mixing, we are investigating porous polymer plugs as well as hydrodynamic focusing. We fabricate porous polymer plugs using photopolymerization to polymerize a monomer/salt paste. After polymerization, we wash the plug with deionized water to dissolve the salt. The resulting porous structure disrupts the laminar nature of microfluidic flow and promotes mixing. The hydrodynamic focusing mixer uses a side channel, with an inlet and outlet, to constrict the flow through the microfluidic channel. By constricting the flow, the overall diffusion length decreases and the characteristic mixing time decreases.

To simulate flows in electroosmotic pumps, we used GOMA, a software program developed at Sandia. GOMA allows us to simulate channels with complex zeta potential and geometry configurations. Our specific problem investigates three-dimensional (3-D) flow in an electroosmotic channel where specific channel walls have a zeta potential of the opposite sign compared with the rest of the walls in the channel. By examining the flow streamlines within the channel, we see that near the walls with the opposite sign there is a recirculating flow profile. If all four walls within a specific section of the microfluidic channel have an opposite sign, a recirculating flow occurs along each wall. This channel configuration could be useful for hydrodynamic focusing where a liquid stream is

constricted when it passes through the channel region with the opposite zeta potential.

Mixing is typically a slow process on microfluidic devices. Our research group focused on developing two techniques to reduce the mixing length in microfluidic flows. The first technique uses porous polymer plugs. We performed experiments to determine the effectiveness of the plugs. Typical results show that mixing in a porous polymer plug is 5x more effective than by diffusion alone. Currently, we are focusing on manipulating the parameters of the porous polymer plugs to maximize mixing while minimizing the pressure drop. Recent experiments focused on porous polymer plugs made with a salt-crystal size range of 75–106 µm. The size of the salt crystals determines the final size of the pores in the porous polymer plugs. For flowrates between 10 and 50 µl/min, the extent of mixing is between 3x and 5x better than a similar microfluidic channel without a plug. We determine the extent of mixing by comparing the concentration profile of a solute before and after the porous polymer plug.

Future experiments will focus on different salt-crystal size ranges, plug lengths, and fluid velocities. In addition to experiments, we developed a correlation that will serve as a design tool for fabricating porous polymer plugs.

The second technique uses hydrodynamic focusing to constrict fluid streams in microfluidic devices. We also modeled this problem using GOMA. The simulations allow us to determine useful mixer configurations. Typical results show that the greater the constriction of the mixing streams, the more effective the mixer is. This problem has a characteristic dimensionless group that is a modified form of the Peclet number. The Peclet number describes a ratio between the characteristic diffusion time and the characteristic convection time. The modified form we use includes two geometry parameters. One parameter describes the height of the channel, and the other describes the distance between the inlet and outlet of the side channel. For smaller height values, the overall diffusion length decreases, causing an increase in mixing. For longer side-channel inlet/outlet distance, we compress the main stream for a longer amount of time, allowing for an increase in mixing. Simulations also predict that, for certain dimensionless groups and flowrate ratios, solute from the main has enough time to diffuse into the side channel. The solute that leaves through the side-channel outlet decreases the final solute concentration in the outlet of the main stream. We intend to further investigate this problem to determine useful configurations that we can build and test.

We performed experiments to determine the effectiveness of the [porous polymer] plugs. Typical results show that mixing in a porous polymer plug is 5x more effective than by diffusion alone.

Refereed

Brotherton, C. M., and R. H. Davis. 2004. Electroosmotic flow in channels with step changes in zeta potential and cross section. *J. Colloid Interface Science* **270** (1) February: 242–46.

Brotherton, C. M., and R. H. Davis. 2003. Flow control and mixing in microfluidic devices. Paper presented at the Gordon Research Conference on Microfluidics, August, Big Sky, Montana.

Simms, H. M., B. T. Good, C. M. Brotherton, K. S. Anseth, R. H. Davis, and C. N. Bowman. 2004. *In situ* fabrication of macroporous polymer networks by living radical photopolymerization and leaching within microfluidic devices. *Lab-on-a-Chip*, submitted.

53464

Atomic-Scale Scanning-Tunneling Microscopy Measurements of Nucleation and Growth of Ge/Si Alloy Structures

B. S. Swartzentruber

One of the key issues in the development of nanoscale technology is the fundamental understanding of the kinetics involved in their formation and stability. Often self-assembly (or self-organization) is the proposed route to forming desirable nanoscale structures in parallel. Self-assembly is driven by a system's desire to reach equilibrium tempered by activation barriers that control the kinetics or time scale of pattern formation. Once understood, the trade-off between kinetics and thermodynamics can be used to control the nanostructure morphology.

Sandia's goal in this work is to determine and measure the fundamental atomic-scale processes responsible for the formation and stability of germanium/silicon (Ge/Si) alloy structures on Si(001). The Ge/Si(001) material system is of technical interest because its electronic properties make it useful for optoelectronic devices. In addition, it is a model system for the self-assembly of quantum-dot (QD) structures with a length scale that is tunable through the atomic-percent of Ge in the alloy. Because of the size mismatch between Ge and Si (Ge is 4% larger than Si), lattice strain relief provides much of the driving force for pattern formation. However, little is known about how the strain affects the kinetics of mass transport and Ge incorporation into the Si lattice.

We previously exploited our *in situ*, elevated-temperature scanning-tunneling microscopy (STM) capability to investigate growth dynamics during Ge/Si(100) QD self-assembly. We found that pyramid clusters are more stable than hut clusters. During *in situ* extended-growth temperature anneals, hut clusters are consumed by pyramid clusters during Ostwald ripening of the island ensemble. We also investigated wetting-layer evolution during growth. Surprisingly, we identified surface morphologies for which nanometer-scale features are very stable during longtime (several hours) anneals. We are investigating whether this anomalous stability is related to the layer-to-island transition. We also find that submilliliter deposition at T = 500°C results in Ge dissolution into the Si surface, as evidenced by the appearance of a characteristic 2xn surface reconstruction.

In upcoming work, we will continue our investigation into Ge QD self-assembly. We will focus particularly on evolution of the wetting layer during growth. We are particularly interested in the anomalous stability of nanometer-scale features and their relationship to the layer-to-island transition and the development of the self-assembled architecture. We have nearly completed the initial dataset spanning growth temperatures in the range of 400°C–550°C and growth rates of 0.01–0.15 ml/min for Ge coverages less than about 3 ml. We will investigate the stability (at the subnanometer scale) of the various morphologies encountered during wetting-layer growth via growth-temperature annealing. Also, by further investigating Ge interdiffusion during growth, we hope to elucidate the role of surface steps in this process. Recently, Hannon, *et al*., pointed out the essential role of surface steps in Ge/Si interdiffusion during submilliliter deposition at T = 750°–900°C. The role of surface steps in Si/Ge intermixing at the substantially lower temperatures used in our investigations is not clear.

53465

Micro-/Nanoscale Thermomechanical Manufacturing

A. C. Sun

Microelectromechanical systems (MEMS) will continue to face large barriers to market if the prohibitive costs and cycle times of production are not reduced. Soft lithographic techniques, such as hot-embossing nanoimprinting, hold the promise to meet the stringent requirements of accurate nanometer-size features while allowing for the rapid, agile, and inexpensive manufacturing of microsystems. In the hot-embossing process, a micromachined silicon (Si) master is heated and pressed into a thermoplastic polymer layer atop a Si substrate. The applied heat and force transfer the master pattern in a negative relief replica in the polymer sample, resulting in feature sizes as small as 10 nm over areas > 1000 cm^2. At present, the widespread usage of nanoprint manufacturing is limited by the lack of understanding of the transport of the polymer during printing. This problem is particularly acute when the nanoscale heat and mass transport properties of the polymer are not known. The lack of fundamental materials science knowledge limits the ability to tailor fabrication methods to final feature design.

Experiments and computer simulations provided insight for greater understanding of the initial stages of polymer deformation during hot-embossing manufacturing (HEM). Research at Sandia focused on computer simulations with GOMA. For the simulations to match preliminary experimental data, the GOMA models developed point to HEM producing a viscosity gradient in the polymer. We presented the simulations at the American Society of Mechanical Engineering (ASME) International Mechanical and Engineering Congress and Exposition (IMECE) 2003.

New experiments on polymer deformation modes in HEM followed the modeling research. Analysis of replicated features produced from controlled imprinting at temperatures just below and above the glass-transition temperature (Tg) of a standard polymer for short imprint times suggested an area of high strain and possible shear-thinning behavior occurring adjacent to Si master features. Dual polymer peaks form in cavities at characteristic lengths from master sidewalls and deform upward and away from the master sidewalls, eventually filling the cavity geometry or merging into one polymer peak that fills the cavity geometry.

Fabrication research demonstrated proof-of-concept for HEM as a viable microfabrication tool in patterning thermally sacrificial polymers. HEM imprinted patterns into a sacrificial layer of polynorbornene (PNB). After overcoating the patterned PNB, applied heat decomposed the sacrificial material, resulting in enclosed channels with suspended post structures.

Fabrication research demonstrated proof-of-concept for HEM as a viable microfabrication tool in patterning thermally sacrificial polymers.

Refereed

Rowland, H. D., and W. P. King. 2004. Polymer deformation and filling modes during microembossing. *J. Micromechanics and Microengineering*, in press.

Rowland, H. D., J. L. Charest, T. L. Wright, and W. P. King. 2003. IMECE2003-41838 transport during hot-embossing micromanufacturing studied via stylus profilometry and SEM. *Proc. 2003 ASME International Mechanical Engineering Congress, Heat Transfer* (November, Washington, D.C.): 8.

White, C. E., T. Anderson, C. L. Henderson, H. D. Rowland, and W. P. King. 2004. Microsystems manufacturing via embossing of photodefinable thermally sacrificial materials. *Proc. SPIE, International Society of Optical Engineering* **5374** (May): 361–70.

53587

Evolution of Near-Surface Scalar Concentrations Through a Compact Cylinder Array Embedded in the Atmospheric Surface Layer

E. S. Hertel, Jr.

Gas dispersion and plume development in the urban atmosphere have become topics of increasing significance because of their direct effect upon the many people who reside in or near large urban areas. Research studies in this field are concerned with gaining a better understanding of the physical mechanisms involved in plume dispersion and developing more-accurate models to predict plume behavior to enhance public safety and health. Many issues that are directly related to public safety and health surround the topic of gas dispersion. Accidental gas leaks from a chemical laboratory are possible. Gas releases with the intent to harm, as in biological warfare (BW) or chemical warfare (CW), are also a concern.

With the harmful effects of pollution in cities, possible accidental gas leaks, and threats of BW/CW, improved characterizations of near-surface plumes are needed to better address these challenges. In light of these growing concerns, Sandia conducted detailed experiments of near-field plume dispersion through a compact uniform array of cylindrical barrels. We intend that results from the study both benefit the physical understanding of near-field plume behavior in the presence of surface-mounted obstacles and provide information that will aid in the development of models used to predict dispersion in urban environments. To truly understand the physical nature of plume development through an array of surface-mounted obstacles, it would be necessary to analyze many different parameters such as the effects of thermal stability, source height, source geometry, obstacle layout, source location, flow conditions, etc., on the plume.

We continued our data analyses and conducted a detailed analysis of sonic anemometer data to better understand the flow physics within and immediately above the barrel array.

We plan to use our high-resolution dispersion data to validate a dispersion model created at the University of Utah.

53681

Design of Biospecific Surfaces to Control Specific Cellular Responses

S. M. Brozik

Cell substrates with micro- and nanoscale chemical and mechanical topographies provide an excellent tool for in vitro *tissue- and cellular-engineering studies. Since cell sizes are on the order of tens of microns and many cell features are on the order of nanometers, a substrate for cellular growth presenting topographies on these same scales can impact cellular response, including morphology and adhesion. While traditional micromachining techniques and electron-beam lithography can create these features, they cannot produce the large-area samples required for robust biological studies. In addition, they are not effective in processing samples made of implantable polymer materials such as biodegradable tissue scaffolds and biologically inert polymers, and they require photoresists and other chemicals that can damage living cells. A technique of hot embossing, where a master is replicated by pressing it into thermoplastic at an elevated temperature, can pattern polymer substrates with features of micro- and nanoscale accuracy over a large area rapidly and inexpensively without the need of any cell-damaging chemicals. In addition, the polymers are receptive to chemical patterning via soft lithography, a technique that utilizes a flexible rubber stamp to selectively deposit chemicals such as self-assembled monolayers (SAMs) and proteins. These techniques combined result in a methodology that can be used to pattern substrates of appropriate materials that elicit specific cellular responses. These substrates can be utilized for large-scale cellular-engineering studies as well as tissue-engineering constructs.*

A rigorous understanding of cell-surface interactions is important for lab-on-a-chip, tissue engineering, and the design of implanted biomedical devices. The micron-scale topography and chemistry of a surface can modulate the morphology, alignment, and biochemical function of adherent cells. Extensive research investigated the use of silicon (Si) micromachining to generate cell-culture substrates with micron-scale topography. Numerous groups use microcontact printing to generate chemical micropatterns on cell substrates, but have not combined it with micromachining to further modulate cell-substrate interaction. Increasingly, biomicroelectromechanical systems (bio-MEMS) devices use selective biochemical functionalization and polymer cell substrates to enhance

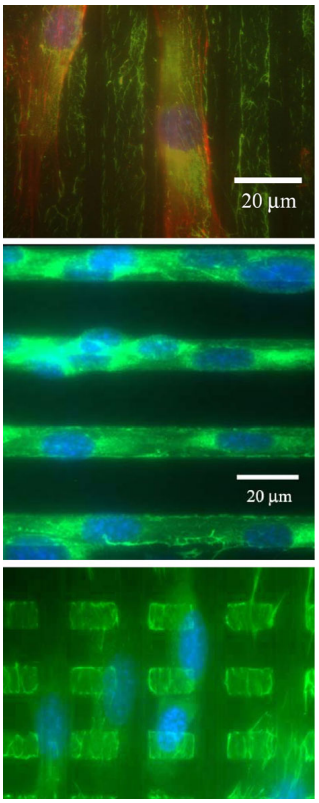

Immunofluorescent-stained osteoblasts on various substrates (blue: DNA; green: fibronectin; red: vinculin, on left image only). Top, *osteoblasts align and elongate to the mechanical grooves (running vertically) uniformly coated with fibronectin.* Center, *osteoblasts align and elongate to the 10 µm-wide fibronectin lanes (running horizontally) on a mechanically smooth surface. The 20 µm-wide spaces between lanes are functionalized with nonadhesive tri-ethylene C42glycol. No bridging of lanes occurs, even though the spacing is below a normal cell diameter.* Bottom, *when presented with a combination of the mechanical grooves (running vertically) and fibronectin lanes (running horizontally), osteoblasts preferentially align to and elongate along the mechanical grooves.*

functionality and improve biocompatibility over Si. Our work addresses the need to bring non-Si materials into bio-MEMs and seeks to combine micromachining with micropatterning techniques.

We (1) developed hot embossing to form three-dimensional (3-D) microtopography on polymer cell substrates, (2) combined this technique with microcontact printing of biomolecules, and (3) investigated the response of osteoblast cells on these engineered substrates. We previously used hot embossing to create microtopographies that influence cell alignment and morphology. Here, we further enhance functionality of the embossed substrates by creating an independent geometry of protein patterns via microcontact printing

We can see the immunofluorescence staining of cells (blue: deoxyribonucleic acid [DNA], green: fibronectin) grown on various mechanochemical substrates. Cells align along mechanical grooves (8 µm wide, 16 µm spaces, 4 µm deep) with a uniform fibronectin covering. Similarly, cells align along fibronectin lanes (10 µm wide) patterned on a smooth surface with tri-ethylene glycol (nonadhesive) lanes (20 µm wide) separating them. On these surfaces, cells remain constrained to fibronectin lanes. Remarkably, when microgrooves and fibronectin lanes are presented in an orthogonal pattern, cells preferentially align to the microgrooves. As the spacing of the fibronectin stripes increases (groove width/spacing is held constant), osteoblasts bridge long distances of nonadhesive tri-ethylene glycol domains to maintain their alignment to the grooves. We observed osteoblasts bridging a space of ethylene glycol as large as 50 µm. We quantified cell alignment via image analysis. The mechanical grooves alone induce over 80% of cells to align with a fairly tight grouping, whereas the fibronectin lanes alone induce 97% of cells to align with an extremely tight grouping. When we combine the two patterns orthogonally, over 67% of cells align to the mechanical grooves, only a slight reduction when compared to a substrate with only grooves. Osteoblasts maintained alignment to the grooves as we increased fibronectin lane spacing up to 100 µm.

The combination of microcontact printing and hot-embossing techniques provides an enabling tool to manufacture substrates with unlimited configurations for controlling cell adhesion and alignment. This approach provides a robust, mechanochemical strategy to elicit specific cellular behaviors.

The combination of microcontact printing and hot-embossing techniques provides an enabling tool to manufacture substrates with unlimited configurations for controlling cell adhesion and alignment. This approach provides a robust, mechanochemical strategy to elicit specific cellular behaviors.

Refereed

Charest, J. L., L. Bryant, A. Garcia, and W. P. King. 2004. Hot embossing for micropatterned cell substrates. *Biomaterials* **25**:4767–75.

54211

Nanomagnetic Films

M. W. Jenkins

Recent advances in chemical synthesis allow the fabrication of molecular nanomagnets. Micro- and nanodevices that could be enabled by nanomagnets will require a reproducible process for creating thin films. The instability of these nanomagnets at high temperatures precludes the use of many established thermal techniques for depositing thin films. Recent work on the development of nonthermal laser techniques for the deposition of thin films of the molecular magnet manganese12-acetate (Mn12) led to the ability to create quality films of molecular magnets. Preliminary results in work on patterning these films were also encouraging and may allow studies of hybrid materials made of a layer of nanomagnets in close proximity to metallic, semiconducting, or superconducting layers. These studies could generate greater understanding of the effects of localized magnetic fields on electron transport in metals, having possible applications in quantum computing and magnetic storage.

Many standard film-deposition techniques involve thermal evaporation of the film material. The thermal instability of Mn12 molecular magnets makes these techniques impractical for the production of films. We worked on the development of other techniques for the deposition of thin films of Mn12. One technique used is pulsed-laser deposition (PLD). This technique involves making a compressed pellet of the Mn12 powder and ablating it with a laser. We used two laser systems: a nitrogen (N) laser, with energy around 2 mJ, and an excimer laser, with energies ranging from 200 to 400 mJ. The purpose for using different systems is to determine the optimum laser energy, pulsewidth, pulse frequency, etc., for the creation of high-quality films that maintain the molecular and magnetic properties of the starting material. The deposited films are characterized using x-ray photoelectron spectroscopy (XPS), superconducting quantum interference device (SQUID) magnetometry, electron-spray ionization–mass spectrometry (ESI–MS), and atomic-force microscopy (AFM). We use XPS and ESI–MS to compare the chemical makeup of the deposited films to that of the starting material. The SQUID measurement allows comparison of the magnetic properties of the films to that of the starting material. We use AFM to determine the roughness and homogeneity of the films. We found that using lower energies with the N laser and using lower pulse rates are

critical for better-quality films with less fragmentation. SQUID magnetization data indicate that the magnetic properties of the starting material are conserved, but we also see evidence for the creation of a new magnetic phase. We currently are examining this new phase in more detail.

We also are exploring other methods of depositing and patterning films. We showed that a simple technique of dipping a silicon (Si) substrate into a solution of Mn12 yields very thin films with high smoothness.

We showed that a simple technique of dipping a silicon (Si) substrate into a solution of Mn12 yields very thin films with high smoothness.

Refereed

Kim, K., D. M. Seo, J. Means, V. Meenakshi, W. Teizer, H. Zhao, and K. R. Dunbar. 2004. Mn12-acetate film pattern generated by photolithography methods. *Applied Physics*, accepted.

Means, J., V. Meenakshi, R. V. A. Srivastava, W. Teizer, A. A. Kolomenskii, H. A. Schuessler, H. Zhao, and K. R. Dunbar. 2004. Films of Mn12-acetate deposited by low-energy laser ablation. *J. Magnetism and Magnetic Materials*, accepted.

Other Communications

Kim, K., D. M. Seo, J. Means, M. Viswanathan, and W. Teizer. 2004. A simple way to pattern Mn12-acetate thin films. *Bulletin APS*.

Means, J., R. V. A. Srivastava, V. Meenakshi, W. Teizer, H. Zhao, K. R. Dunbar, A. A. Kolomenskii, and H. A. Schuessler. 2004. Pulsed-laser deposition of Mn12-acetate films using a nitrogen laser. *Bulletin APS*.

54213

A Multiscale Approach to Modeling Carbon Nanotube–Reinforced Composites

J. W. Foulk, III, D. C. Hammerand

Carbon nanotubes (CNTs) represent one member of a significant new class of materials, those whose nanoscale dimensions provide access to unprecedented levels of material tailoring. CNTs have nearly half the density, 5x the tensile modulus, and 20x the tensile strength of conventional silicon carbide (SiC) fibers. In addition, CNTs can be metallic or semiconducting and can store molecules larger than water within their hollow centers. The desire to incorporate these traits into more-tractable materials gives rise to what are known as multifunctional materials*, i.e., composites whose constituents consist of CNTs and thereby require the development of multiscale, multiphysics models. The focus of the present research is on the development of such multiscale models for predicting the mechanical properties of CNT–reinforced composites.*

Discrete modeling in the form of ab initio *calculations and molecular dynamics (MD) are used to provide individual CNT thermomechanical properties as well as insight into nanotube-matrix interaction and adhesion, but remain computationally limited to individual nanotubes and small time scales. As such, information obtained from such calculations is incorporated into continuum-level properties that readily lend themselves to use in micromechanics calculations. Thus, analytic and computational micromechanics techniques are employed to capture microscale effects such as CNT–polymer interaction and bonding, CNT orientation, and nanotube clustering. Sandia's initial focus was on developing modified analytic micromechanics techniques to address issues such as the hollow geometry of CNTs, and on understanding the effects of the orientation of CNTs, between CNTs and matrix, and clustering of CNTs. Analytic solutions first provide ready access to parametric studies, but more importantly, serve as a baseline for numerical studies. Computational micromechanics in the form of finite-element (FE) simulations will confirm prior analytical work and extend efforts to capture the effects of the weak bonding along CNT/matrix boundaries through a cohesive zone approach.*

We focused on developing single- and two-step composite-cylinders approaches to modeling CNT–reinforced composites, and on the comparison of these results with FE modeling. In the

two-step approaches, we apply the composite-cylinders technique to an individual CNT to represent the nanotube as a solid effective "nanofiber." This then allows for the clear calculation of an Eshelby tensor and, hence, the use of either the Mori-Tanaka or generalized self-consistent techniques in the second step. In the single-step approach, we apply a modified composite-cylinders approach using the hollow center of the nanotube, the ring of graphitic carbon of the single-wall nanotube, and the matrix. We found the single-step and two-step Mori-Tanaka methods to yield identical results, while the two-step self-consistent method proved significantly different at higher volume fractions. In all three cases, the CNT composite properties transverse to the CNT alignment were matrix-dominated to volume fractions as high as 60%. This, as shown in parametric studies, is a result of the large relative difference in stiffness between the CNTs (~ 1 TPa) and the matrix (~ 3 GPa). We found FE simulations to be in remarkable agreement with the two-step Mori-Tanaka; the single-step approaches in the volume fractions range as high as 70% and across the entire spectrum stiffness, considered in the aforementioned parametric studies.

We conducted parametric studies on the effects of the interphase thickness and stiffness, which demonstrated that even moderate stiffness increases or decreases make large impacts on the transverse properties. We observed that the thickness dictates the volume fraction at which dramatic changes in transverse properties are noticed. Large interphase thicknesses result in low-transition volume fractions, while small interphase thicknesses result in higher-transition volume fractions. FE simulations of several cases considered in the parametric study observed identical behavior.

We also made an effort to incorporate the effects of clustering. We quantified and simulated clustering using Dirichlet tessellation in conjunction with an *n*-phase Mori-Tanaka technique. We observed that while clustering does not impact properties parallel to the fiber direction, clustering does augment transverse moduli. We observed that initial increases in CNT volume fraction within clustered arrangements have an increasingly stronger effect on the transverse properties. We conducted FE simulations on identical test cases; they also yielded increases in the transverse properties. Micromechanics predictions for clustering indicated a 9% increase in transverse stiffness, while FE simulations indicated a 13% increase in transverse properties. In addition to focusing on highly aligned systems, we also considered randomly oriented composites. Although the effective properties compare well with

experiments, one should note that the “quasi-isotropic” properties associated with randomly oriented composites are only a fraction of the moduli along the fiber direction of highly aligned systems.

Refereed

Lagoudas, D. C., and G. D. Seidel. 2003. A micromechanical study on the clustering effect of carbon nanotube–reinforced composites. Paper presented at the ASME Winter Conference, 16–22 November, Washington, D.C.

Lagoudas, D. C., and G. D. Seidel. 2004. Effective elastic properties of carbon nanotubes and carbon nanotube–reinforced composites. Paper presented at the AIAA SDM Conference, 19–22 April, Palm Springs, California.

Lagoudas, D. C., and G. D. Seidel. 2004. Micromechanics of load transfer in carbon nanotube composites. Paper presented at the 41st Annual Meeting of the Society of Engineering Science, 10–13 October, Lincoln, Nebraska.

Other Communications

Lagoudas, D. C., and G. D. Seidel. 2004. Effective mechanical properties of carbon nanotube composites. (Invited) Talk presented at NASA LaRC, 29 June, Hampton, Virginia.

Seidel, G. D., and D. C. Lagoudas. 2004. Effective elastic properties of carbon nanotubes and nanocomposites. (Invited) Talk presented at Sandia National Laboratories, 22 August, Albuquerque, New Mexico.

57300

Integrated Superhard and Metallic Coatings for MEMS

M. P. De Boer

Sandia seeks to integrate new materials, as coatings and structural materials, into polysilicon (poly-Si)-based microfabrication technology. Specifically, we will pursue two classes of new materials: superhard materials and metals. We will make a special effort to develop processes that integrate materials at the microstructure release step because such processes would afford a wider class of materials and a greater degree of flexibility to device engineers. Consequently, processes will have to allow conformal deposition.

We will choose superhard ceramic materials with the following properties: wear resistance, hydrophobicity, lubricity, and chemical and thermal inertness. The single-source silicon carbide (SiC) chemical vapor deposition (CVD) technique, which we pioneered for the realization of SiC–coated microelectromechanical systems (MEMS) and for SiC–based MEMS, appears very promising, based on our work to date. For MEMS applications, we must optimize the electrical properties of SiC and develop the selective etch processes.

Integrating metals offers special opportunities for realizing devices such as microrelays and microchemical reactors. Standard metal-deposition techniques suffer from being line-of-sight. One way to circumvent this problem is to use galvanic displacement techniques, which exploit the reducing behavior of elemental Si toward noble metal ions in aqueous solutions containing fluoride ions. In such solutions, upon simple immersion, the surface of Si dissolves and the cations deposit as the corresponding metal.

In the aforementioned deposition processes, little is known about the tribological properties of the resulting materials in thin-film forms. Therefore, we will also characterize both ceramic and metallic films using surface analytical techniques in our laboratory and specially designed test microstructures. These surfaces may be hydrophilic, and hence additional surface modification may be necessary to alleviate stiction.

[We] successfully demonstrated hydrophobic coatings for metallic overlayers in MEMS [and] investigated tribology of metallic overlayers by nanoindentation methods.

- *Successfully demonstrated hydrophobic coatings for metallic overlayers in MEMS; investigated tribology of metallic overlayers by nanoindentation methods*. We were able, for the first time, to successfully integrate this functionalization scheme with copper (Cu) plating and a microstructure release process. We used dodecanethiol-coated cantilever beam arrays

to find the apparent work of adhesion of the film. Measurements on several different arrays yielded an average detachment length of about 1100 μm, or a work of adhesion of about 3 $\mu J/m^2$.

- *Demonstrated very low adhesion (less than 6 $\mu J/m^2$) for polycrystalline SiC (poly-SiC) films*. These structures can be released and dried in air. We also showed that adhesion does not increase strongly in moist environments.
- *Demonstrated very high fracture stress of 23 GPa for poly-SiC films*. We investigated the fracture of poly-SiC films using a micrometer-sized fracture tester fabricated by micromachining techniques. A moving shuttle tethered to the substrate carries a series of SiC cantilever beams varying in length; the beams are bent in-plane until fracture. We calculated the fracture strain of SiC films from the deflection of bending beams using nonlinear beam theory and determined it to be 3.3%, which corresponds to a fracture stress of 23.4 GPa. These values are significantly higher than those for polycrystalline Si (2.6% and 4.2 GPa). In addition, we observed the crack propagation in the poly-SiC films to be transgranular.
- *Showed that both the residual stress and the strain gradient of poly-Si films can be tailored by process control*. We characterized the residual strain of amorphous and poly-SiC films deposited using 1,3-disilabutane single precursor as a function of deposition temperature ranging from 700°C to 850°C. We used SiC microstrain gauges and cantilever beam arrays fabricated by micromachining to characterize directly the average residual strain and strain gradient. The residual strain of SiC films changes from compressive to tensile as the deposition temperature increases. We also found the strain gradient to depend on the deposition temperature, and it can be adjusted between positive and negative values to fabricate flat, curling-up, and curling-down micromechanical structures. The released cantilever beams curve up when the film is deposited at 750°C, but curve down for 800°C deposition temperatures. We found the lowest strain gradient of 36 m^{-1} for a deposition temperature of 800°C.

Refereed

Ashurst, W. R., M. B. J. Wijesundara, C. Carraro, and R. Maboudian. 2004. Tribological impact of SiC encapsulation of released polysilicon microstructures. *Tribology Letters*, accepted.

Carraro, C., L. Magagnin, and R. Maboudian. 2002. Selective metallization of Si micromechanical devices. (Invited) *Electrochimica Acta* **47** (16) (21 June): 2583–88.

Fritz, M. C., C. Carraro, and R. Maboudian. 2001. Functionalization of scanning-force microscopy cantilevers via galvanic displacement technique. *Tribology Letters* **11**:171–75.

Gao, D., C. Carraro, V. Radmilovic, R. T. Howe, and R. Maboudian. 2004. Fracture of polycrystalline 3C-SiC films in MEMS. *J. Microelectromechanical Systems*, accepted.

Gao, D., M. B. J. Wijesundara, C. Carraro, and R. T. Howe. 2003. High-modulus poly-SiC technology for RF MEMS. *Proc. 12th International Conference on Solid-State Sensors and Actuators, Transducers '03* **1** (June, Boston, Massachusetts): 1160–63.

Gao, D., M. B. J. Wijesundara, C. Carraro, R. T. Howe, and R. Maboudian. 2003. Characterization of residual strain in SiC films deposited using 1,3-disilabutane for MEMS application. *J. Microfabrication, Microlithography and Microsystems* **2**:259–64.

Gao, D., M. B. J. Wijesundara, C. Carraro, R. T. Howe, and R. Maboudian. 2004. Transformer-coupled plasma etching of 3C-SiC films using fluorinated chemistry for MEMS applications. *J. Vacuum Science and Technology B* **22** (2) (March): 513–18.

Gao, D., R. T. Howe, and R. Maboudian. 2003. High-selectivity etching of 3C-SiC films using HBr-based transformer-coupled plasmas. *Applied Physics Letters* **82** (11) (24 March): 1742–44.

Gao, D., W. R. Ashurst, C. Carraro, R. T. Howe, and R. Maboudian. 2004. Silicon carbide for enhanced MEMS reliability. *Technical Digest, Proc. 2002 Solid-State Sensor and Actuator Workshop, Hilton Head '04* **1** (June, Hilton Head, South Carolina): 192–95.

Magagnin, L., C. Carraro, and R. Maboudian. 2003. Adhesion evaluation of immersion plating copper films on silicon by microindentation measurements. *Thin Solid Films* **434** (1) (June): 100–105.

Magagnin, L., C. Carraro, and R. Maboudian. 2002. Gold deposition by galvanic displacement on semiconductor surfaces: Effect of substrate on adhesion. *J. Physical Chemistry B* **106** (2): 401–7.

Magagnin, L., R. Maboudian, and C. Carraro. 2001. Selective deposition of thin copper films onto silicon with improved adhesion. *Electrochemical and Solid-State Letters* **4** (1) (January): C5–C7.

Magagnin, L., V. Bertani, P. L. Cavallotti, R. Maboudian, and C. Carraro. 2002. Selective deposition of gold nanoclusters on silicon by a galvanic displacement process. *Microelectronic Engineering* **64**:479–85.

Stoldt, C. R., C. Carraro, D. Gao, W. R. Ashurst, R. T. Howe, and R. Maboudian. 2002. A low-temperature CVD process for silicon carbide MEMS. *Sensors and Actuators A* **97-98** (April): 410–15.

Stoldt, C. R., M. C. Fritz, C. Carraro, and R. Maboudian. 2001. Micromechanical properties of SiC thin films grown by single-source CVD. *Applied Physics Letters* **79** (3) (16 July): 347–49.

Stoldt, C. R., M. C. Fritz, W. R. Ashurst, D. Gao, and R. Maboudian. 2004. Novel low-temperature CVD process for SiC MEMS. *Proc. 11th International Conference on Solid-State Sensors and Actuators* **1** (June, Munich, Germany): 984–87.

Valente, G., C. R. Stoldt, C. Carraro, and R. Maboudian. 2004. Theoretical and experimental study of the chemisorption of 1,3-disilabutane on the Si(100) surface. *J. Chemical Physics* **118** (13) (April): 6089–97.

Valente, G., M. B. J. Wijesundara, R. Maboudian, and C. Carraro. 2004. Single-source chemical vapor deposition of 3C-SiC films in an LPCVD reactor, part II: Reactor modeling and chemical kinetics. *J. Electrochemical Society* **151** (3): c215–c219.

Wijesundara, M. B. J., C. R. Stoldt, C. Carraro, R. T. Howe, and R. Maboudian. 2002. Nitrogen doping of 3C-SiC films grown by single-source chemical vapor deposition. *J. Thin Solid Films* **419** (1) (November): 69–75.

Wijesundara, M. B. J., D. Gao, R. T. Howe, C. Carraro, and R. Maboudian. 2003. Nitrogen doping of polycrystalline 3C-SiC films grown using 1,3-disilabutane in a conventional LPCVD reactor. *J. Crystal Growth* **259** (1) (November): 18–25.

Wijesundara, M. B. J., G. Valente, R. T. Howe, A. P. Pisano, C. Carraro, and R. Maboudian. 2004. Single-source chemical vapor deposition of 3C-SiC films in an LPCVD reactor, part I: Growth, structure, and chemical characterization. *J. Electrochemical Society* **151** (3): c210–c214.

57307

Microscale Separations of Biological Compounds Using Novel Polymeric Separations Materials

A. K. Singh

In this project, Sandia is developing and characterizing a novel class of materials that potentially improve the efficacy of chemical separations in microanalytical systems used for detection of chemical and biological agents. The research and development will be performed at the University of Montana (UM). We will develop methods for the analysis of compounds using specialized chromatographic materials known as "pseudostationary phases." These materials are easily introduced into microfabricated channels, enable high-performance chemical separations, and provide a high degree of chemical diversity.

As pseudostationary phases for electrokinetic chromatography (EKC), amphiphilic polyelectrolytes have been shown to provide significant advantages over conventional micellar pseudostationary phases. These novel polymeric phases may play an important role in the development of miniaturized instruments for the selective determination of a variety of chemical compounds. We previously developed, characterized, and studied a variety of polymeric structures as pseudostationary phases. This project will apply these materials to the analysis of specific target biomolecules and classes of biomolecules, as well as continued development of novel polymeric materials with potentially improved performance, selectivity, and commercial viability.

We used two polymeric pseudostationary phases that were shown to provide high-performance separations and selectivity different from sodium dodecyl sulfate (SDS) micelles to separate amino acids and peptides. Amino acid separations are important in many areas of chemistry and biochemistry. We comprehensively reviewed the large body of work on the use of capillary electrophoretic methods for amino acid analysis and their applications. Peptides play many important roles in living systems. Additionally, their separation and analysis are important tools for protein characterization.

We studied the effects of the changes in the selectivity of the pseudophases on the separations and the performance of the polymers for the separation of derivatized amino acids and peptides. Additionally, we used the polymers in combination with laser-induced fluorescence (LiF) detection to achieve very

good sensitivity for derivatized amino acids. This, to our knowledge, is the first report of the successful use of polymeric pseudophases with LiF detection, and there are challenges unique to this approach.

We synthesized two polymers for this study. The first polymer is dodecy/allylglycidyl ether-sulfonate-siloxane (DAGESS) with 85% of the silicon (Si) centers modified with allylglycidyl ether-sulfonate and the remainder modified with dodecene. We prepared it by modifying polymethylhydro-siloxane having a nominal molecular weight of 1500 g/mol with dodecene and allylglydidyl ether in the presence of platinum divinyl complex as a catalyst. We then modified the epoxy functionalities with sodium sulfite and sodium bisulfate in ethanol to produce the hydrophilic sulfonate functionality. Relative to SDS micelles, this polymer is not much more resistant to solvation cavity formation, is less able to interact with basic compounds, and displays much stronger interaction with acidic compounds. The polymer has a nominal molecular weight of 5400 g/mol.

The second polymer (LMAm-27) is a copolymer of 2-acrylamido-2-methyl-1-propane sulfonic acid (AMPS) and lauryl methacrylamide with 73 mole percent AMPS and 27 mole percent lauryl methacrylamide. It was synthesized by free-radical polymerization of a mixture of AMPS and lauryl methacrylamide in THF-water (80:20). This polymer is significantly more resistant to cavity formation, less able to interact with basic compounds, and better able to interact with acidic compounds than SDS micelles. The molecular weight of this polymer is estimated to be 3×10^5 g/mol.

We achieved separations of 14 naphthalene-2,3,-dicarboxaldehyde (NDA)–derivatized amino acids using both polymer systems. We observed excellent efficiency, peak shape, and selectivity with both systems, particularly when LiF detection was used. Not all of the amino acids are resolved on either system. Both polymers are compatible with LiF detection, although there remains significant background. We greatly reduced this background when the polymers were washed with ether, implying that low levels of fluorescent impurities were responsible for at least part of the signal. It is also possible that some of the background is the result of scattering from polymer aggregates and cannot be eliminated. Even with the background and associated noise, the average estimated detection limit (S/N=3) for the amino acids on either system is 1×10^{-8} M.

We also investigated the DAGESS polymer and compared it to SDS for the separation of five oligopeptides. These relatively

...we used the polymers in combination with laser-induced fluorescence (LiF) detection to achieve very good sensitivity for derivatized amino acids. This, to our knowledge, is the first report of the successful use of polymeric pseudophases with LiF detection....

small peptides range in molecular weight from 698 to 877 g/mol. They do not have significant electrophoretic mobility and are not separated in the buffer system without added pseudophase. The results of the separations with SDS and DAGESS show that SDS clearly outperforms the polymeric phase for this separation, with better efficiency, selectivity, and resolution. Higher concentrations of the polymer did not significantly improve the separation.

Refereed

Palmer, C. P., and J. P. McCarney. 2004. Developments in the use of soluble ionic polymers as pseudostationary phases for electrokinetic chromatography and stationary phases for electrochromatography. *J. Chromatography A* **1044** (1-2): 159–76.

Pandey, S., R. A. Redden, A. E. Hendricks, K. A. Fletcher, and C. P. Palmer. 2003. Characterization of the solvation environment provided by dilute aqueous solutions of novel siloxane polysoaps using the fluorescence probe pyrene. *J. Colloid and Interface Science* **262**:579–87.

Schulte, S., and C. P. Palmer. 2003. Alkyl-modified siloxanes as pseudostationary phases for electrokinetic chromatography. *Electrophoresis* **24**:978–83.

57308

Friction in Micromachine Interfaces

B. R. Antoun

Understanding and controlling friction in micromachine interfaces is critical to the reliability and operational efficiency of microelectromechanical systems (MEMS). The relatively high adhesion forces and friction forces encountered in these devices often present major obstacles to the design of reliable MEMS devices. Using surface-micromachining (SMM), Sandia is designing arrays of microstructures and testing them to examine the adhesion characteristics, static friction behavior, and dynamic friction response. We are also emphasizing the control and actuation of the test structures and the modeling of the dynamic response and contact mechanics at the interface. Specifically, the purpose of this research is to fabricate and test MEMS devices to obtain insight into the effect of surface topography, material properties, surface chemical state, environmental conditions, and contact load on the static and dynamic characteristics of the contact interface.

We effectively eliminated several shortcomings of previous adhesion studies of MEMS and measured the true pull-out force under different environmental testing conditions.

We designed an SMM test structure specifically for studying the sidewall adhesion characteristics of MEMS devices. We investigated the dependence of adhesion on contact load under quasi-static loading conditions. We found that the adhesion force is linearly dependent on the contact load due to the increase of the real contact area and the decrease in separation distance of the noncontacting asperities. We also obtained insight into the relative contributions of van der Waals and capillary forces to the measured adhesion force and apparent work of adhesion. We effectively eliminated several shortcomings of previous adhesion studies of MEMS and measured the true pull-out force under different environmental testing conditions. The experimental methods developed enable the isolation of the van der Waals component of the adhesion force and the determination of the contributions of contacting and noncontacting asperities to the total adhesion force. We performed a complete parametric study of sidewall adhesion and established a set of solid experimental methods for this study.

We designed a second test structure for testing the static and dynamic friction characteristics, as well as the wear properties of MEMS devices. Initial data from these devices show that we will gain insight into the effect of contact load and environmental conditions on the friction behavior. The experiments will also take into account the relatively high

adhesion forces in MEMS devices (that can be on the same order of magnitude as the external normal loads) to obtain a more thorough understanding of the contact mechanics at the interface.

Refereed

Shannon, T. J. 2004. An experimental study of sidewall adhesion in microelectromechanical systems. Master of Science Thesis, Plan II, University of California, Berkeley, California.

Shannon, T. J., and K. Komvopoulos. 2004. An experimental study of sidewall adhesion in microelectromechanical systems. *J. Microelectromechanical Systems*, accepted.

57309

Lipid Microarray Biosensor for Biotoxin Detection

A. K. Singh

Sandia is developing a microarray biosensor for simultaneous detection of multiple biological toxins such as botulinum, tetanus, cholera, and ricin. The biosensor consists of a silicon (Si) or glass microchip on which arrays of lipids containing receptors have been deposited using photolithographic patterning, followed by vesicle fusion and a dry liftoff. We will expose the chip to samples containing toxins and transduce the binding of toxin to the receptor into a fluorescence signal using a secondary fluorophore-labeled antibody in a "sandwich" assay or employing a fluorophore-labeled toxin in a competitive assay followed by detection with a charge-coupled device (CCD).

Artificial lipid bilayers, supported on a sensor surface, that contain the membrane receptors mimic cells that are invaded by these bacterial toxins and viruses and, hence, can be used as sensitive probes for detecting them. We patterned lipid arrays on a Si substrate using a novel polymer-based dry liftoff technique that is suitable for patterning biological molecules. Conventional liftoff involves removal of the photoresist layer by organic solvents and, hence, is unsuitable for chemically sensitive or biological materials. Our dry liftoff technique uses a conformal Parylene layer, a vapor-phase–deposited inert polymer, that is photolithographically patterned using standard ultraviolet-sensitive photoresists, and dry etching in a reactive-ion etch (RIE) chamber using oxygen plasma. The Parylene layer acts as a template to physically pattern subsequently deposited lipid bilayers by contact-induced vesicle fusion. Parylene is then peeled from the substrate, and the result is a geometrically confined region, the negative tone of the Parylene pattern, of immobilized lipid bilayers.

We developed a technique to create micron-sized patterns within microfluidic channels for multiplexed biosensor applications and cell studies. The arrays used to demonstrate the technique consist of ganglioside-populated supported lipid bilayers (SLBs) located within microfluidic channels. To pattern the SLBs, we used a polymer liftoff technique. Microfluidic connections to independent channels allowed the preparation of lipid domains with different compositions on a single device. We incubated channels with the patterned polymer with lipid vesicles, which formed SLBs with sizes in

the 1–50 μm range. We imaged the deposited lipids by epifluorescence and showed that lipid-domain formation was achieved in all exposed areas. We observed lipid domains in all feature sizes and noted no significant spreading after removal of the polymer coating. The deposited lipids and gangliosides are functional, as shown by the effective toxin binding. We performed detection by epifluorescence using an upright microscope with water-immersion objectives and a CCD camera.

We performed binding assays to determine the limit of detection and binding specificity for the SLB arrays. We used concentrations from 1 mg/mL to 100 ng/mL in successive dilutions and took epifluorescence images to assess the detection limit. In the 1–500 μg/mL range, fluorescence intensity varied linearly with concentration. Concentrations above 1 mg/mL showed no increase of fluorescence intensity due to saturation of available binding sites. The lowest detectable concentration was 83 nM for cholera toxin B (CTB) and 18 nM for tetanus toxin c (TTC). Lower concentrations of either fragment could not be discerned as patterns or recovered after image processing.

We ran specificity assays to incubate the toxin fragments and a nonspecific protein with both types of gangliosides. We observed low cross-reactivity by comparing the fluorescence intensities to the assays with the specific gangliosides. Any binding observed was higher than the nonspecific binding of these toxin fragments to the bare Si substrate. We expected low cross-reactivity, as it has been shown that the binding specificity of the toxins is related to the number of sialic residues present in each of the gangliosides. We also performed nonspecific binding assays on both types of ganglioside-containing domains by incubating them with fluorescently labeled bovine serum albumin (BSA). We observed low binding mostly on the areas with no patterned lipid. We expected this patterning behavior, as BSA adsorbs onto Si surfaces and is used frequently as a blocker for nonspecific adhesion of analytes.

- *SLB patterning within microfluidic channels*. We used a microfluidic approach to deposit SLBs of different compositions in separate channels of a Si microchip. We coated Si substrates with etched trenches with Parylene and etched 2–50 μm features into the polymer. We attached a slab of poly(dimethyl-siloxane) (PDMS) containing microfluidic connections to the top of the device by noncovalent surface adhesion. This cover gave a seal to prevent cross-contamination between the channels filled with different lipid compositions

and the flexibility to remove it after lipid patterning for subsequent incubation with targeted analytes. We delivered lipid vesicle solutions containing either ganglioside GM1 or GT1b into the reservoirs and flowed them into each channel. The total volume needed to fill a single reservoir and channel was ca. 150 nL. In this way, we obtained microarrays of SLBs containing different gangliosides on a single chip. The patterns obtained within the microfluidic channels were of micron size, as opposed to previously reported lipid arrays that had larger dimensions.

We used the microfluidic substrates containing patterned SLB arrays with different lipid compositions to segregate toxin fragments from binary mixtures. We optimized the mixture pH to 6.5 to allow specific fragment binding to the corresponding gangliosides and segregation from the binary mixture, with low nonspecific binding. Incubation of the patterned microfluidic substrates with a single-toxin-fragment concentration yielded results similar to those obtained with planar substrates.

57310

Advanced Manufacturing Techniques Using Rapid Prototyping

J. A. Palmer, B. D. Chavez

The focus of this project is the use of the three-dimensional (3-D) systems Viper™ si2 stereolithography apparatus (SLA) rapid-prototyping (RP) machine for direct manufacturing of mesoscale parts (with features on the order of microns to millimeters) and assemblies in a variety of applications of interest to Sandia. Major efforts included research in advanced ProtoTool™ composite stereolithography (SL) resin material in support of Sandia's Rapid-Prototyping of High-Density Circuitry (RPHDC) project. We demonstrated an innovative dual-use junction-box structure with encapsulated circuitry and pilot devices. This work resulted in a technical advance application. Furthermore, we used the Viper™ machine to fabricate innovative mesoscale housings for Sandia's mesoscale RF Relay (mRF) project. In addition to discrete parts, joint research advanced to a documented design for a novel multiprocess, multimaterial SLA platform that moves beyond the capabilities of current systems. A design patent is pending.

We demonstrated an innovative dual-use junction-box structure with encapsulated circuitry and pilot devices. This work resulted in a technical advance application.

We performed trials to evaluate the composition and material properties of ProtoTool™ 20L composite SL resin. Trials included the following: (1) determination of the percentage of glass filler-material present, (2) inspection of the resin microstructure, (3) evaluation of the thermal curing parameters, (4) tensile testing of cured material specimens, and (5) testing of compatibility with conductive inks. Results indicated the resin to be 60% filled with glass microspheres 10–30 µm in diameter. When heated at a linear rate, we observed the glass transition temperature (Tg) of the ultraviolet (UV)-cured resin material to be 94.8°C, approximately 5°C less than the nominal value of 100°C. The average coefficient of thermal expansion (CTE) for the UV-cured material above Tg was 122 ppm per degree Celsius, 27% greater than the nominal value. We observed stress relief in the uncured ("green") and cured material at 50.3°C on average. We experimentally determined the tensile strength of the cured resin to be 9650 psi with a 3% elongation at failure. Cured-resin substrates maintained their integrity when we applied silver-filled Hereus ink traces and cured it at 120°C. We observed no leaching or diffusion of the ink into the substrate. Research in the area of high-temperature composite resins and encapsulation techniques led to space-saving monolithic parts for the Sandia

MicroHound Program. A powerful demonstration of this technology was in the Sandia RPHDC project. This effort culminated in a novel low-voltage electrical distribution box fabricated by SL with the ProtoTool™ resin. We encapsulated pilot devices within structural members and successfully applied circuit traces comprising cured Hereus ink.

The Viper™ si2 SLA machine incorporates a high-resolution build mode with a 75 µm (3 mil) beam diameter and 50 µm (2 mil) build layer thickness. Using this capability, collaborators at the University of Texas at El Paso successfully demonstrated batch fabrication of mRF switch housings. We achieved high-dimensional accuracy in fabrication through the unprecedented use of Teflon™ shims to maintain submillimeter gaps, and encapsulated mesoscale inserts (constructed independently from aluminum and photopolymer) to form the four-bar contact arm grooves.

Finally, we filed a patent application documenting the partnership's efforts to design an advanced multimaterial SLA with integrated direct-write dispensing capability. We will develop a prototype in upcoming work.

Other Communications

Palmer, J. A., P. Yang, D. W. Davis, B. D. Chavez, P. L. Gallegos, R. B. Wicker, and F. R. Medina. 2004. Rapid prototyping of high-density circuitry. *Proc. SME RAPID 2004* (10 May, Dearborn, Michigan): CD-ROM.

Wicker, R. B., A. V. Ranade, F. R. Medina, and J. A. Palmer. 2004. Practical considerations for microstereolithography of embedded microchannels. *Proc. SME RAPID 2004 Conference* (10 May, Dearborn, Michigan): CD-ROM.

57311

Robust Hermetic Packaging Techniques for MEMS Integrated Microsystems

A. D. Oliver

In this project, Sandia seeks to develop thin-film packages for chip-level encapsulation of microelectromechanical systems (MEMS) devices. These chip-level packages are intended to be hermetic and capable of maintaining a high level of vacuum.

Thin-film packaging is relevant to MEMS because nearly 75% of the cost of MEMS devices is in the packaging. This research has the potential to reduce the cost by a factor of 10. It will also make the MEMS devices easier to integrate into the next assembly, which has been a monumental hurdle in the past. This project is a collaboration between Sandia and the University of Michigan (UM).

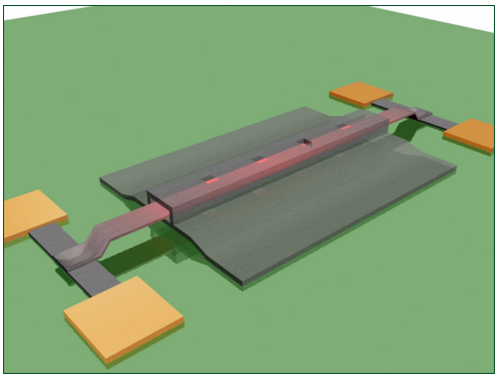

Pirani (vacuum) gauge.

We developed a packaging technology that employs a thick nickel (Ni) film to vacuum-seal a MEMS structure at the wafer level. The package is fabricated in a three-mask process by electroplating a 40 µm-thick Ni film over an 8 µm sacrificial photoresist that is removed prior to package sealing. Implementation of electrical feedthroughs in this process requires no planarization. The large release channel enables an 800 x 800 µm package to be released in less than 3 hr. We investigated several mechanisms, based on localized melting and lead/tin (Pb/Sn) solder bumping, for sealing the release channel. We also developed Pirani gauges integrated with this package, which we used to establish the hermeticity of the different sealing technologies, and measured a sealing pressure of approximately 1.5 Torr. Our work differs from previous Pirani gauges in that we utilize a novel doubly anchored structure that stiffens the structural membrane while not substantially degrading performance to measure fine leak rates. UM transferred this Pirani gauge design to Sandia, and it was fabricated in Sandia's SUMMiT V™ (Sandia Ultraplanar Multilevel MEMS Technology V) surface-micromachining (SMM) project.

We developed a micropackage technology and Pirani (vacuum) gauges. For the micropackages, we developed a packaging technology that uses a thick Ni film to vacuum-seal a MEMS structure at the wafer level. We fabricated the package in a three-mask process by electroplating a 40 µm-thick Ni film over an 8 µm sacrificial photoresist that is removed prior to package sealing. The large fluidic access port enables an 800 x 800 µm package to be released in less than 3 hr.

...nearly 75% of the cost of MEMS devices is in the packaging. This research has the potential to reduce the cost by a factor of 10.

Implementation of electrical feedthroughs in this process requires no planarization. We performed device release after the formation of the first-level package. We investigated several mechanisms, based on localized melting and Pb/Sn solder bumping, for sealing low-fluidic-resistance feedthroughs.

In the area of Pirani gauges, we designed and fabricated a new type of SMM polysilicon (poly-Si) Pirani gauge that is designed to monitor pressure in micropackages. This gauge can measure absolute pressure from greater than 760 Torr to less than 10 mTorr. The gauge utilizes a distinctive double-heat-sink design to maximize dynamic range while maintaining adequate pressure sensitivity (~ 1 x 10^3 (K/W)/Torr). A distinctive feature of this gauge is that it achieves high performance using a widely available foundry process. We can integrate this sensor with other devices on the same substrate and package it to measure leak rates several orders of magnitude smaller than traditional helium (He) leak testing. UM transferred the design of this device to Sandia, and we investigated these devices as a possible diagnostic device in a national security application.

Other Communications

Stark, B. H., J. Chae, A. Kuo, A. D. Oliver, and K. Najafi. 2004. A high-performance surface-micromachined Pirani gauge in SUMMIT V™. Abstract to be presented at the MEMS 2005 Conference, 30 January–3 February 2005, Miami, Florida.

59034

3-D Large-Eddy Simulation of Turbulent Flow Based on One-Dimensional Turbulence Modeling

R. C. Schmidt

Sandia seeks to develop and demonstrate a fundamentally new approach to large-eddy simulation (LES) turbulence modeling based on the recently developed one-dimensional turbulence (ODT) model of Kerstein. We developed two distinct types (or families) of formulations: LES/ODT and ODT/LES.

In the LES/ODT modeling approach, we used the standard three-component ODT model to directly calculate the unclosed subgrid terms in a traditional "volume-balance"-type LES formulation. However, in the ODT/LES approach, we introduced revised ODT equations that, when spatially filtered, have strong similarities to the classic LES turbulence equations. Also, in contrast to the LES/ODT approach, a separate LES momentum equation is not solved.

We tested both approaches against experimental and direct numerical simulation (DNS) data for the problem of isotropic turbulence decay in a periodic box. We showed that both approaches could accurately simulate the spatially filtered data. However, when comparing the statistics of the ODT–resolved turbulent fluctuations with the DNS and experimental data, differences between the modeling approaches become apparent. Results from the ODT/LES approach show a consistent representation of both the three-dimensional (3-D) spatially filtered LES turbulent energy spectrum and the 1-D turbulent energy spectrum, whereas an artificial "dip" appears near the LES Nyquist limit in the LES/ODT for the 1-D turbulent energy spectrum. However, in general, we showed the cost of the LES/ODT approach to be significantly less than the ODT/LES method.

This project successfully developed and demonstrated a fundamentally new approach to LES [(large-eddy simulation)] turbulence modeling based on the recently developed ODT [(one-dimensional turbulence)] model of Kerstein.

This project successfully developed and demonstrated a fundamentally new approach to LES turbulence modeling based on the recently developed ODT model of Kerstein.

Initial work led to the recognition that several different model formulations were viable, each with the possibility of having certain advantages and/or disadvantages. As a result, we explored two distinct types of formulations: LES/ODT and ODT/LES. In each case, three sets of orthogonal 1-D lines are embedded in the 3-D mesh such that they cross at the center of each LES-scale control volume. However, in the LES/ODT modeling approach, we use the standard three-component ODT

equations without modification, and use ODT as a means of defining a model for the unclosed “subgrid” terms in a traditional “volume-balance”-type LES formulation. In the ODT/LES approach, we introduced revised ODT equations that account for the effect of each term in the DNS momentum equations. When spatially filtered, the ODT/LES equations have strong similarities to the classic LES turbulence equations. Therefore, in contrast to the LES/ODT approach, a separate LES momentum equation does not need to be solved.

We tested both approaches against experimental and DNS data for the problem of isotropic turbulence decay in a periodic box. We showed that both approaches could accurately simulate the spatially filtered data. However, when comparing the statistics of the ODT–resolved turbulent fluctuations with the DNS and experimental data, differences between the modeling approaches became apparent. The ODT/LES approach demonstrated a consistent representation of both the 3-D spatially filtered LES turbulent energy spectrum and the 1-D turbulent energy spectrum, whereas an artificial “dip” appears near the LES Nyquist limit in the LES/ODT simulations for the 1-D turbulent-energy spectrum. However, this apparent advantage is balanced by the fact that, in general, the cost of the ODT/LES approach is shown to be significantly greater than the LES/ODT method.

In the ODT/LES approach, we also demonstrated the utility of a 1-D ODT closure model denoted EMC (ensemble mean closure). This model introduces a 1-D eddy viscosity, local to the ODT–resolved space, which accounts for the transport of momentum due to eddy events not resolved on the ODT grid. This enables ODT to play the role of an intermediate-scale closure model that captures spatial and temporal velocity fluctuations not resolved on the LES field, but only down to user-defined cutoff. We modeled turbulent transport occurring below this cutoff using an eddy-viscosity approach consistent with and derived from the ODT model itself. For high-Reynolds-number flows, this was a very effective and cost-effective way of extending the dynamic range of the simulated flow while avoiding the cost of resolving the smallest scales of motion.

Although results for the canonical turbulent channel flow were not completed, progress made during this work suggests strongly that both the LES/ODT and the ODT/LES approaches are viable methods that could be more generally applied to a variety of turbulent-flow problems of interest to Sandia.

Other Communications

McDermott, R., A. R. Kerstein, R. C. Schmidt, and P. J. Smith. 2004. ODT subgrid closure for LES: Deterministic limits and effects of stochastic dynamics. Paper presented at the LANL Workshop on Fluid Turbulence Cascade Dynamics: Fundamentals and Modeling, 16–19 August, Santa Fe, New Mexico.

McDermott, R., R. C. Schmidt, A. R. Kerstein, and P. J. Smith. 2003. Subgrid closure for large-eddy simulation using one-dimensional turbulence. Paper presented at the APS Division of Fluid Dynamics 56th Annual Meeting, 23–25 November, East Rutherford, New Jersey.

McDermott, R., R. C. Schmidt, A. R. Kerstein, and P. J. Smith. 2003. Subgrid closure for large-eddy simulation using one-dimensional turbulence. Paper presented at the Workshop on LES & SGS Modeling for Turbulent Mixing and Reactive Flows, 8–9 December, California Institute of Technology, Pasadena, California.

61046

Photonic Encryption Using All-Optical Logic

J. D. Tang, P. J. Robertson, R. C. Schroeppel

With the build-out of large transport networks utilizing optical technologies, more and more capacity is being made available. Innovations in dense-wave division multiplexing (DWDM) and the elimination of optical-electrical-optical conversions have brought on advances in communication speeds as we move into 10 Gb Ethernet and above. Of course, there is a need to encrypt data on these optical links as the data traverse public and private network backbones. Unfortunately, as the communications infrastructure becomes increasingly optical, advances in encryption (done electronically) have failed to keep up. This project examines the use of optical logic for implementing encryption in the photonic domain to achieve the requisite encryption rates.

To realize photonic encryption designs, technology developed for electrical logic circuits must be translated to the photonic regime. Sandia examined symmetric self-electrooptic effect devices (S-SEEDs) and how discrete-logic elements can be interconnected and cascaded to form an optical circuit. Because there is no known software that can model these devices at a circuit level, we modeled the functionality in PSpice. PSpice allows modeling of the macro characteristics of the devices in context of a logic element as opposed to device-level computational modeling. By representing light intensity as voltage, "black-box" models are generated that accurately represent the intensity response and logic levels in both technologies. By modeling the behavior at the systems level, one can incorporate design tools and a simulation environment to aid in the functional design. Each model takes certain parameters (reflectance, intensity, input response) and models the optical-ripple and time-delay characteristics. Demonstration circuits show how these logic elements can be used to form NAND, NOR, and XOR functions. We also performed cryptanalysis of a serial, low-gate-count demonstration algorithm suitable for scrambling/encryption using S-SEEDs.

We were successful in building PSpice models of optical logic and simulating their logic functionality.

We were successful in building PSpice models of optical logic and simulating their logic functionality. We modeled a family of Boolean logic elements, including the NAND, NOR, and XOR functions. The basic building block of logic was the SEED, which we modeled using a basic p-i-n photodiode represented as a capacitor in parallel with a current source.

Using the SEED models, we built a circuit that modeled symmetric SEED-switching behavior. Measured data and modeled results showed an agreement of 7 ps switching time, which was a result of capacitive, inductive, and optoelectronic behaviors on the actual device. We also characterized the behavior of SEED models in cascaded arrangements, as necessary for an optical logic circuit. We continued examining stream ciphers for optical communications systems and filed a technical advance regarding the development of low-gate-count, serial, cascadable encryption algorithms. We wrote a simulator in the C language that examined the statistical randomness of the cipher-text output as a simple proxy for encryption strength.

62269

Nanoporous-Carbon Adsorbers for Chemical Microsensors

M. P. Siegal, W. G. Yelton

Chemical microsensors rely on partitioning of airborne chemicals into chemically selective films to collect and measure trace quantities of hazardous vapors. Polymer sensor coatings in use today are typically slow to respond and difficult to apply reproducibly. The objective of this project is to produce a durable sensor-coating material based on graphitic nanoporous-carbon (NPC), a new material first studied at Sandia, for collection and detection of volatile organic compounds (VOCs), toxic industrial chemicals (TICs), chemical-warfare agents (CWAs), and nuclear processing precursors. Preliminary studies using NPC films on exploratory surface-acoustic-wave (SAW) devices and as a µChemLab™ membrane preconcentrator suggest that NPC will outperform existing, irreproducible coatings for SAW sensor and µChemLab™ preconcentrator applications. Success in this project will provide a strategic advantage for the development of a robust, manufacturable, highly sensitive chemical microsensor for public health, industrial, and national security needs. We use a line-of-sight physical deposition process to grow NPC films at room temperature with negligible residual stress and that we can deposit onto nearly any substrate material to any thickness. Controlled deposition yields reproducible NPC density, morphology, and porosity without any discernible variation in surface chemistry. We demonstrated NPC coatings > 20 µm thick with density < 5% that of graphite.

We determined NPC networks as a function of mass density. We optimized NPC structure for SAW-device microsensor sensitivity. We measured record-breaking adsorption for various analyte gases, including VOCs, TICs, and nuclear processing precursors. We proposed and validated a simple model to predict the adsorption behavior of any coating on a SAW device in low concentrations. Only analyte selectivity via NPC–doping was not accomplished, although we proposed alternate routes based on the results from this project.

NPC growth by pulsed-laser deposition (PLD) is more complex than first believed. It now appears that serendipity played a role in first discovering NPC and its tremendous potential as a chemical gas adsorbent. Many PLD parameters are critical to the growth of controlled NPC. The laser-energy

density used to ablate pyrolytic graphite controls the carbon-cluster sizes used for NPC film growth. If the clusters are too large, the resulting film "grains" are not well connected and cannot support an acoustic wave in SAW devices; we showed that SAW sensor sensitivity is directly related to the film acoustic loss. If the clusters are too small, they deposit in a manner that precludes the development of sufficient surface area for analyte adsorption. A laser-energy-density range exists to ablate ideally sized carbon clusters. Furthermore, the laser beam must be homogeneous; laser-induced defects in the optics create inhomogeneous beams that lead to mixed-structure NPC films with reduced cluster connectivity.

Transmission-electron microscopy (TEM) performed on high-functioning microsensor NPC film material identifies two nanostructural features that help explain the superb chemical adsorption in NPC. First, 1–2 nm voids exist throughout the material. While such voids are similar in size to fullerenes, such molecules are not identified in the images; rather, they likely represent the smallest possible structures that curved graphene sheet fragments can make to enclose small volumes. Second, and perhaps more importantly, the interplanar spacing between graphene sheet fragments increases with decreasing density. Molecular intercalation into graphite is well known; expanding the spacing between graphene sheets should improve analyte diffusion into and out of the film.

We compared NPC coatings for SAW devices directly with several commonly used polymer coatings for a wide range of analytes. In all cases, NPC outperformed every polymer coating by multiple orders of magnitude in terms of SAW signal response and predicted analyte limits-of-detection (LODs). These results are revolutionary. Furthermore, NPC is stable at higher temperatures than any of the polymers, leading to significantly longer working lifetimes, especially in preconcentrator applications that require the coating to be heated to purge the analyte into another sensor device.

We demonstrated that every SAW coating material obeys a power-law functionality of mass adsorbed versus analyte concentration in the ambient. This new understanding of SAW microsensor-device behavior enables extrapolation of device performance to levels well below those measured in the laboratory. Extrapolation of analyte data from every polymer coating tested suggests that such devices will not be able to achieve LODs < 10–1000 ppm, depending on the analyte. However, NPC–coated SAW data suggest LODs < 1 ppb for all but one analyte tested, and even for trichloroethylene, NPC–

We compared NPC coatings for SAW devices directly with several commonly used polymer coatings for a wide range of analytes. In all cases, NPC outperformed every polymer coating by multiple orders of magnitude in terms of SAW signal response and predicted analyte limits-of-detection (LODs). These results are revolutionary.

coated SAW LODs are 1000x lower than any polymer-coated SAW tested.

Refereed

Siegal, M. P., D. L. Overmyer, D. R. Tallant, and W. G. Yelton. 2002. Nanoporous-carbon films for microsensor applications. *Applied Physics Letters* **80** (21) (27 May): 3940–42.

Siegal, M. P., D. L. Overmyer, W. G. Yelton, and A. W. Staton. 2004. Nanoporous carbon for chemical microsensors. Paper presented at the Specialist Meeting for Amorphous Carbon, September, Povo-Trento, Italy.

Siegal, M. P., W. G. Yelton, D. L. Overmyer, and P. P. Provencio. 2004. Nanoporous-carbon films for gas microsensors. *Langmuir* **20**:1194–98.

Siegal, M. P., W. G. Yelton, D. L. Overmyer, and P. P. Provencio. 2003. Nanoporous carbon for chemical microsensors. Paper presented at the Electrochemical Society Meeting, October, Orlando, Florida.

Yelton, W. G., M. P. Siegal, D. L. Overmyer, and A. W. Staton. 2004. Nanoporous carbon: A revolutionary new material for chemical gas microsensors. Paper presented at the Electrochemical Society Meeting, May, San Antonio, Texas.

Other Communications

Siegal, M. P., W. G. Yelton, P. P. Provencio, A. W. Staton, and D. L. Overmyer. 2004. Nanoporous carbon for gas microsensors: Correlating growth structures with performance. Paper presented at the Electrochemical Society Meeting, October, Honolulu, Hawaii.

Yelton, W. G., M. P. Siegal, A. W. Staton, and D. L. Overmyer. 2004. Exploring the limits of detection of nanoporous-carbon SAW coatings. Paper presented at the Electrochemical Society Meeting, October, Honolulu, Hawaii.

65559

Direct Single-Ion Machining of Nanopores

D. M. Follstaedt, T. A. Friedmann, A. K. Norman

Sandia seeks to use individual high-energy heavy ions to directly produce nanometer- and possibly subnanometer-size pores in membranes, through "Coulomb explosions" (also known as electronic sputtering*). The ultimate goal of this research is to understand the combination of ion-solid interaction physics and materials science that controls the diameter and depth to which nanopores can be spontaneously produced by individual ions in ultrathin membranes. There currently are numerous Sandia applications for membranes with a highly controlled array of nanopores, or even a single nanohole, where this pore diameter approaches or even goes below 1 nm.*

We cleaved mica films as thin as 18 nm. This material came the nearest to forming a nanopore with the 5 nm-diameter pits on the surface. Based on our results and recent new information, we can identify promising candidate materials for nanopore formation.

We ion-irradiated thin materials with 374 MeV Au+25 or 241 MeV I+19 with flux rates of 5 x 10^3 ions/cm^2 or greater to achieve ion fluences ~ 10^8 ions/cm^2. Such ions have high electronic-energy losses in oxides (depositing 20–35 keV/nm of track length), and we expect them to produce detectable tracks in oxides. To identify tracks, we tilted the specimens ~ 30 deg from normal and examined them in the transmission-electron microscopy (TEM), using underfocusing to image voids or surface pits, and using diffraction contrast to image strain fields. We did not detect tracks in amorphous silicon nitride (SiN), silicon dioxide (SiO_2), and carbon (C) films; the reasons are not currently understood. Following initial discussions with world experts, we focused on oxides as the best candidates for nanopore formation. Tracks detected in the following crystalline materials are summarized.

- *Sapphire (hexagonal aluminum oxide [Al_2O_3])*. We observed pits ~ 5 nm in diameter at the entrance and exit points on either side of the thin material, along with evidence for piled-up material on the surface. The pits appear to be connected by a low-density track line. Both gold (Au) and iodine (I) produced tracks.
- *Quartz (hexagonal SiO_2)*. We did not detect surface pits in irradiated quartz, perhaps because stronger diffraction contrast obscured them. With diffraction, we detect strain fields

in the material around the track, perhaps due to displaced atoms from the track center. There is evidence that the center is amorphous.

- *Muscovite mica (monoclinic, $K_2O.3Al_2O_3.6SiO_2.2H_2O$).* We cleaved mica to as thin as 18 nm. Au irradiation produced surface pits ~ 5 nm in diameter on either side of the film. These results suggest that if mica could be cleaved to 10 nm or less thickness, nanopores might be formed by joining the pits on both sides. The sputtering of material to form surface pits may be aided by the weak bonding of the easily cleaved mica atomic planes. Tracks in mica also showed diffraction contrast.

We collaborated with Lawrence Livermore National Laboratory (LLNL) to use the molecular dynamics (MD) calculations they developed to simulate displacements in thin films by high-energy ions. Such simulations show that a low-density ion track is formed ~ 7 ps after the ion passes, but that the material reforms, leaving only shallow pits (a few atomic layers deep) and piled-up material on the surface. In this aspect, our results with sapphire and mica verify the results of the MD simulation. However, the simulations use simple Lennard-Jones interatomic potentials with only one type of atom; we need additional theoretical work to simulate the irradiation of oxides.

Recent discussion with theorists at the International Conference of Ion-Beam Modification of Materials (Bringa, M. Toulemende–CAEN, France) indicate that a “thermal spike” model, in which the track is modeled as it is rapidly heated to melting and possible vaporization, is being validated. This and our results above led us to identify promising materials for future work. (1) Cleaving mica even thinner to connect surface pits may yield nanopores. (2) High-energy ions in Au have very high energy losses (65 keV/nm), and nanoholes have been found with lower-energy ions. (3) Energy losses are also high in zinc (Z), which melts and vaporizes at relatively low temperatures (420°C and 906°C, respectively). Attaining the vaporization temperature is thought to produce holes at the track. (4) Holes have been formed in tin oxide (SnO_2) with energy loss of 47 keV/nm. We can understand the SnO_2 results by using cylindrical heat-flow codes for the thermal spike. Such codes could be useful for guiding future work.

Refereed

Follstaedt, D. M., A. K. Norman, P. Rossi, B. L. Doyle, F. D. McDaniel, and E. M. Bringa. 2004. High-energy ion tracks in thin films. Paper presented at Ion-Beam Modification of Materials 2004, 6–10 September, Asilomar, California.

66170

Investigation of the Effects of Intense Pulsed Particle Beams on the Durability of Metal-to-Plastic Interfaces

T. J. Renk, P. P. Provencio

Sandia's unique pulsed-power capability was originally developed to simulate the effects of nuclear explosions on weapon components and to investigate nuclear fusion for power generation. In recent years, we showed that exposure to pulsed-power beams can improve the wear durability of metal surfaces. The cyclic heating and cooling caused by such beams (1e9 K/s) leads to grain refinement, dispersal of second-phase particles, and formation of metastable phases, all of which can lead to durability improvements. In some applications where counterfaces exist between metals and polymers, it is desired to reduce wear of both the polymer and the metal surfaces by either hardening the surfaces, reducing the friction between the counterface surfaces, or both. In the case of polymers, hardening can be produced by promoting cross-linking of the polymer. The understanding of the effects of pulsed-power beams on the wear durability of these surfaces will contribute to our understanding of the wear durability of similar materials used in various defense applications.

An opportunity exists to work with outside partners who are investigating the durability of the materials used in artificial hip joints. The materials to be investigated include metal (titanium [Ti] and cobalt-chromium-molybdenum [Co-Cr-Mo] alloy) and ultrahigh-molecular-weight polyethylene (UHMWPE). The objectives include improvement of the abrasion resistance of the UHMWPE and reduction of friction wear of the contact surface between UHMWPE and the metal counterface. We will investigate biocompatibility by producing a doped thin-film coating. We will use ion beams to produce thin films and surface alloying of the metals. We will use electrons beams to cross-link the UHMWPE.

These experiments will broaden our experience base of working with different materials in repetitive high-energy pulsed power (RHEPP-1) and will contribute to the durability of components used in national security missions.

We made the following accomplishments:

(1) We conducted pulsed ion-beam treatment at RHEPP-1 at Sandia to modify the surface properties of UHMWPE polyethylene, Co-Cr-Mo, and Ti-6Al-4V alloys. DePuy Orthopedics provided the UHMWPE, the Co-Cr-Mo, and one

type of Ti alloy. We attempted several treatment levels on the UHMWPE and also performed treatment with electron beams. Only the lowest-dose ion treatment left the UHMWPE bulk properties unaffected. At present, new samples have been treated at this lowest dose and returned to DePuy for wear analysis. We subjected the Co-Cr-Mo and Ti alloy provided by DePuy to ion-beam treatment, and no property improvement occurred. However, we coated Ti-6Al-4V samples provided by Alvarado Orthopedics with a hafnium (Hf)-rich coating and beam-treated them to produce a surface-alloyed layer. We subjected this Hf/Ti surface to pin-on-disk analysis that demonstrates substantial wear improvement over the untreated Ti-6Al-4V. Cell-culture tests also indicated improved biocompatibility. This Hf/Ti layer looks to have commercial potential. In addition, we began deposition and modification of nanolaminate ceramic coatings on Co-Cr-Mo substrates.

(2) We performed electron-beam treatment of UHMWPE. DePuy analyzed the resulting treated surfaces and found that significant decreases in bulk properties occurred, even at treatment levels lower than were predicted as optimum by pretreatment modeling. Higher-dose ion-beam treatment also caused a decline in bulk property performance. This is an unexpected result because both ion- and electron-beam treatments were assumed to be a surface process. Further investigation is necessary to understand this effect.

66450

Advanced Techniques for Multiobjective Discrete Optimization

J. E. Campbell, S. H. Jacobson, G. K. Kao

A wide variety of real-world, practical applications can be modeled as discrete optimization problems. Many of these problems are intractable and require specialized algorithms and heuristics to obtain even near-optimal solutions in a reasonable amount of computing time. Two common characteristics of difficult, real-world optimization problems are (1) hundreds or even thousands of decision variables that result in a massive decision space, and (2) the need to optimize multiple objective functions.

Large input spaces are common to many problems such as maximizing system performance or minimizing logistics footprint. While such problems often have large numbers of input variables, many of these variables may have little effect on optimization objectives. Furthermore, variables that do affect key objectives may do so only in limited regions of their ranges. The result often is a massive input space in which promising search regions are extremely small. To address this issue, Sandia will examine adaptive-learning techniques that can help focus an optimization search on promising areas of the decision space. The approach will examine techniques to focus optimization searches on input regions that are likely to contain useful solutions.

To address the second problem area, the need to optimize multiple objectives, this research will examine algorithms for obtaining Pareto optimal solutions and procedures to understand the trade-offs between these solutions. We can then use such results for post-optimality analysis to obtain sets of the "best of the best" Pareto optimal solutions. Given that discrete optimization problems cover a wide range of applications, the research conducted in this area has numerous potential applications.

This work seeks to fill an important need for optimization techniques that can be applied to complex systems of systems such as future combat systems (FCSs). FCS performance is evaluated in terms of several measures of effectiveness (MOEs). Optimizing FCS performance across multiple MOEs and multiple platform families presents a challenge that is beyond currently used optimization techniques.

One of our accomplishments was a comprehensive literature review of several discrete multiobjective optimization

algorithms. The survey covered traditional methods ranging from variations of hill-climbing algorithms to evolutionary algorithms and summarized hybrids of such methods. In addition, a large portion of the survey focuses on artificial intelligence (AI) techniques. The survey also includes a general discussion of potential directions in combining the use of AI and combinatorial optimization algorithms.

We developed several test examples that represent typical multiobjective optimization problems of interest to Sandia. In their current form, these test problems are deterministic. However, they can and will be modified to represent stochastic multiobjective optimization examples.

We began to evaluate and compare simulated annealing, tabu search, and genetic algorithm (GA) methods in solving multiobjective example problems. These studies have three objectives: (1) to evaluate and compare the performance of the algorithms under different parameter settings, (2) to explore the use of AI methods to fine-tune algorithm control parameters as the optimization proceeds, and (3) to identify broad problem characteristics that might influence the algorithm selection or help establish ranges of algorithm control parameters.

A final area of research involves the initial examination of methods for identifying and eliminating decision variables that have little or no effect on optimization objectives. We used a combinatorial optimization problem with two objective functions as a test case. The selected optimization technique was a GA. We created the initial population of solutions by a stratified sampling scheme that ensured coverage of the input space. Following the first generation, we calculated partial rank correlations between input variables and the two objective values. We automatically eliminated any input variables with correlations less than a predefined cutoff value, thereby reducing the chromosome length, and then allowed the optimization to continue. The result was that the size of the input decision space was reduced by several orders of magnitude between the first and second generations of the optimization search. While results of this effort are preliminary, they certainly indicate the potential benefits of adaptive schemes to focus the optimization search on promising regions of the decision space.

66809

Nonradioactive Safety and Performance Issues with Supercritical Water Reactor (SCWR) Safety Technologies

J. V. Zuffranieri

The next generation (Generation IV) of nuclear-reactor designs will need to feature enhanced safety, a substantially lower cost of electricity, and minimized waste streams to enhance sustainability. The use of supercritical light water as a coolant in a direct-cycle reactor design offers thermal-efficiency improvements of over 33% above current operating plants, along with considerable plant simplification.

This project will help to identify issues associated with accident scenarios in future supercritical water (SCW) nuclear-reactor designs that involve loss-of-coolant and loss-of-flow transients. In a single-phase compressible fluid, a critical flow is achieved when the velocity of the exiting fluid is equal to the sound speed in that medium, and a pressure discontinuity exists at or outside the pipe exit. This precludes any change in back-pressure being transmitted upstream of the exit, and there exists a maximum flowrate. In a two-phase fluid, however, a maximum flow occurs when the kinetic-energy dissipation-per-unit volume in each phase is equal. This occurs when the momentum and frictional pressure losses attain a maximum at a given area and is determined by the local phase velocities and local void fraction. Two-phase critical flow, therefore, is fundamentally different from single-phase flow; it is suspected that a critical flow of a supercritical fluid will act differently from either a single-phase or a two-phase system due to highly nonlinear property variations.

Experimental design modifications to the SCW loop are currently under way. Key modifications include a separate flow channel designed to equip a heater rod simulating a nuclear fuel pin and the optical access necessary for turbulent velocity and density measurements.

The heater rod being developed will provide 50 kW of power in 1 m lengths, providing a surface heat flux of 1500 kW/m^2, which is slightly higher than what is expected in prototypical reactors. The design will include 16 thermocouples equally spaced in the 1 m heated length providing axial cladding temperatures and surface heat fluxes near the optical window. Due to the high operational temperatures and pressures, we dealt with thermal-expansion issues in the design. Compressing a seal-bearing ring welded to the heater rod

between two flanges will seal one end of the heater rod. The other end of the heater rod will be freely supported in the tube and cooled to allow power and thermocouple wires to be extracted at low temperature and high pressure.

We designed a test section that contains two orthogonal sapphire windows with a 2 cm^2 view area. This will allow optical access for measuring fluctuating velocities and densities in the radial direction from the boundary layer of the heater rod wall to the bulk fluid. To make optical access feasible, we chose a square flow channel. This permits flat optical windows that will not disrupt flow and allows for easy index of refraction corrections with measuring instrumentation.

We will obtain velocity information with a particle image velocimetry (PIV) and a laser Doppler velocimetry (LDV) system, and a Rayleigh-scattering method will provide information on density fluctuations. PIV and Rayleigh-scattering equipment is already on hand, and the LDV system selection is currently under way. We built a low-temperature and -pressure experiment to test the capabilities of the LDV system; it gives us the ability to test laser-beam alignments before making the actual measurements.

66810

Radiation Performance Issues with Advanced Coolants for Next-Generation Reactor

J. V. Zuffranieri

Proposed nuclear-reactor designs in the Generation IV programs have great potential to produce safer and cheaper electricity. One such design, the supercritical water reactor (SCWR), combines two proven technologies: a thermal nuclear-fission heat source and an SCW turbine cycle. Many obstacles remain in the effort to design and implement such reactors, including material choice. To determine proper materials for the construction of an SCWR, one must understand the corrosive properties of SCW in a radioactive environment.

The University of Wisconsin, in collaboration with Argonne National Laboratory and Notre Dame Radiation Laboratory, is studying the neutron radiolysis effects of SCW. This work will determine the radiolytic decomposition rates of water into different species, the critical hydrogen (H) concentration of the water (the concentration at which radiolytic decomposition is just suppressed), and G-values of different reactions. Temperature range will be from room temperature to approximately 500°C with an operating pressure of 25 MPa.

Sandia collected data by running high-pressure water into the apparatus, where it was heated to a specific temperature, exposed to radiation, and recovered for analysis. The radiolysis occurs at the far end of the apparatus, which is inserted into a beam port in the University of Wisconsin Nuclear Reactor, next to the core. We analyzed a sample by extracting gases from the water and running them through a mass spectrometer.

Before we could proceed with the experiment, we had to perform a rigorous safety analysis to ensure that there were no neutronic, activation, reactivity, or thermal-hydraulic issues. We did the neutronic analysis with a reactor model using the Monte Carlo N-particle (MCNP) neutronics code, which among other things gave a flux profile as a function of energy and position. We used this to predict the activation of the different pieces inside the apparatus that would be subject to high neutron fluxes. It also calculated the reactivity worth of the experiment to ensure that it would not be out of the technical specifications for reactor experiments. The thermal-hydraulic analysis guaranteed that the tubing and other aspects of the system would not fail, and determined the best conditions for limiting heat transfer out of the SCW. We presented the safety analysis, and the Reactor Safety Committee approved the project.

Following approval, initial testing showed that temperatures could be maintained in the irradiation section within desired variation (~ 0.1°C) and that the radiolysis gases that formed gave signals that were well above the noise rate. To prove that we were seeing real radiolysis signals, we ran an experiment to determine the H_2 formed in N_2-saturated water. This experiment gave expected results as well as some initial data on radiolysis rates above 300°C. Subsequent experiments included using N_2O to scavenge aqueous electrons by looking for the N_2 formed, using deuterated alcohol to scavenge for H+ atoms, and adding different concentrations of H to determine the critical H concentration as a function of temperature. We took significant data for all experiments, but more are needed before we can make a report on the results.

In addition to collecting data, we made an effort to redesign and update the MCNP model for the reactor and the experiment. In the process of doing so, we determined that the gamma dose in the irradiation volume was significant enough that the radiolysis occurring was far from pure neutron radiolysis. While some data are useful with a full nuclear-reactor spectrum of neutron and gamma radiation, we also need results for G-values due to pure neutron radiolysis. This prompted an effort to design a removable gamma shield for the irradiation section.

The project is proceeding with continued data collection, optimization of scavenging agents, and design of the gamma shield.

67118

MEMS/Fuze Diagnostic Extraction in High-G Environments

M. E. Partridge, T. L. Martinez, R. R. Lockhart, A. Mittas

To demonstrate microelectromechanical systems (MEMS) devices and miniature fuze components in flight tests of opportunity, we need a means for including these devices in the tests without interfering with the tests' primary purpose. Sandia seeks a diagnostic extraction system that would be compact, shock-hardened, and readily integrated into the test vehicle. This self-contained system would provide whatever stimulus a particular device required for normal operation, plus acquire data to verify that the operation was performed properly. In addition to recording the acceleration environment, the system could generate stimulus based on the environment or other timing factors that would be part of the intended final application of the device under test. Diagnostic data for the devices could include optical and/or electrical monitoring techniques and be recorded to maximize the benefit from each test opportunity.

This diagnostic capability would also benefit the Sandia Intelligent Penetrating Fuze (SIPE) development programs, which require extensive high-G testing for environment characterization and functional evaluation in these environments. Testing the multievent functions needed for SIPE programs requires data-sampling capabilities unattainable with the current penetrator instrumentation recorders. The self-contained diagnostic extraction system includes telemetry with associated timing and functionality measurements and a high-quality, three-axis-acceleration, data-gathering capability.

We reviewed with MEMS/fuze researchers candidate systems that could be supported using the MEMS/Fuze Diagnostic Extraction System (MDES) and identified several candidates. However, the majority of these candidates were not mature enough to be considered for near-term integration into a flight test. One system, the M2CDU (Monolithic Micro Capacitive Discharge Unit) system, was approaching maturity and would be ready for flight testing by the end of the year. This system contains a MEMS accelerometer and miniaturized CDU, a fireset component. Based on the stimulus and diagnostic measurement requirements of the M2CDU, and considering the needs of the other candidate systems, we began developing a prototype instrumentation system. Schematics are complete; we printed and assembled the circuit boards and

completed the programmable logic design. Development of the microcontroller firmware is still in draft stage, with a change in approach from using assembly language to C. Delays in the firmware development resulted in delaying the flight test until upcoming work, but we did complete an initial system integration.

Mechanical design of the unit under test housing for the M2CDU is complete and has started for the instrumentation housing. This flight test will rely on an existing penetrator design, with the flight dedicated to this initial test of the MDES. Following successful results from the flight test, we will begin mechanical design of housings that can be incorporated into the aft end of a penetrator flight-test vehicle, a location that permits integration as a “free-ride” package in otherwise unused void space.

67716

Smart Detectors of Enrichment of Bioaerosols

D. A. Kliner

We successfully implemented the TAOS technique in the mid-IR.

Rapid detection of bioaerosols is required for monitoring and protection of critical facilities and for damage assessment and cleanup following a bioagent release. Existing detect-to-warn bioaerosol triggers are sensitive but lack adequate specificity (i.e., high false-positive rate). To address this problem, Sandia is investigating two approaches to real-time optical detection of bioaerosols: laser-induced fluorescence (LiF) and two-dimensional angular optical scattering (TAOS). The LiF technique utilizes an ultraviolet (UV) laser beam to excite the fluorophores (tryptophan, etc.) commonly found in biological aerosol particles. The resulting fluorescence is dependent on the aerosol's composition and thus can be used to characterize the aerosols. The TAOS technique also utilizes a laser beam, but with this technique, the angular dependence of the elastically scattered light is detected and used as a characterization parameter. The angular variation of scattered light intensity is a function of the particle's size, shape, surface texture, and composition. Thus, with the help of an image-processing routine, the angular distribution of the scattered light can be used to differentiate bioagents from the background environment.

For both of these techniques, we will tune the wavelength of the laser source for increased sensitivity as well as specificity. For LiF, a shorter wavelength source could greatly improve the signal-to-noise ratio (SNR). To this end, we will make efforts to shift the excitation wavelength from 266 nm to 220 nm. In addition, we will investigate the use of two wavelengths (on and off absorption) in the hope of increasing the specificity of the device even further. As for TAOS, shifting the source into the infrared (IR) increases the sensitivity of TAOS to differences in molecular structure. Currently, the thinking is to shift into the 3–5 µm window, where atmospheric absorption is low and background noise from blackbody radiation would not overwhelm the signal.

We successfully implemented the TAOS technique in the mid-IR. Our initial experiments utilized a state-of-the-art developmental laser system and focal-plane-array (FPA) IR camera. We used a mid-IR type-II interband cascade laser to generate light at a wavelength of 3.4 µm, with optical powers reaching 40 mW. The laser emission was elastically scattered off of flowing aerosol droplets and detected with an indium

antimoide (InSb) FPA IR camera. The 50 μm-diameter droplets were composed of a mixture of D_2O and H_2O. Altering the ratio of the mixture led to a change in the complex refractive index that was evident in the TAOS patterns. Using Mie theory, we extrapolated the single-particle absorptive properties and compared them with known IR absorption spectra and absorption cross sections.

In addition, we simultaneously collected TAOS patterns over a solid angle approaching 2p at two mid-IR wavelengths from the same aerosol particle. Since the two TAOS patterns were collected simultaneously, the particle's orientation and morphology will be identical for both scattering events, thereby allowing the absorption-based variations in the patterns to be prominent. The two laser sources were optically pumped gallium antimonide (GaSb)–based semiconductor lasers with type-II indium arsenide (InAs)/InGaSb quantum well (QW) gain regions emitting at 3.9 mm and 5.1 mm with a peak power of ~ 0.4 W and pulse duration of 100 ms. We used an ellipsoidal reflector to collect the scattered light at both wavelengths, but farther down the optical train, a dichroic mirror separated the two wavelengths, after which the scattering light at each wavelength was independently detected. This technique distinguished between droplets composed of pure H_2O and droplets composed of 25% D_2O/75% H_2O since D_2O has an absorption band at around 3.9 mm. Such an approach provides a rough sketch of a particle's absorption spectrum in the mid-IR at a rate limited by the readout speed of the detector. Future experiments will gravitate toward biological aerosols where the wavelengths in the dual TAOS pattern-collection scheme will be selected so that they are on/off an absorption band of a known biowarfare-agent simulant. We will run sensitivity and specificity tests to determine the ability to pick out this agent from background aerosols.

We investigated the LiF technique in the deep UV (DUV). Initial experiments used the third harmonic from a neodymium:yttrium aluminum garnet (Nd:YAG)–pumped dye laser to excite LiF in tryptophan particles. Our findings support the belief that shifting the excitation wavelength from 266 nm to 220 nm will greatly improve SNR (better than a factor of 10) due to an increase in the absorption cross section of tryptophan at this lower wavelength. In the future, we will measure the fluorescence spectra of tryptophan aerosol particles following DUV excitation at wavelengths between 210 and 250 nm. We will use this dataset to determine the optimal on/off wavelengths for distinguishing tryptophan-based biological

aerosols from known interferents polycyclic aromatic hydrocarbons (PAHs).

Refereed

Aptowicz, K. B., Y. L. Pan, and R. K. Chang. 2004. Two-dimensional angular optical scattering (TAOS) of single aerosol particles in the visible and mid-infrared. Paper presented at the 2004 Scientific Conference on Obscuration and Aerosol Research, 21–25 June, Aberdeen Proving Ground, Maryland.

Aptowicz, K. B., Y. L. Pan, R. K. Chang, and B. V. Bronk. 2004. Large-angle two-dimensional angular optical scattering (LA TAOS) in the mid-infrared of single aerosol particles. Paper presented at the 2nd Joint Conference on Point Detection for Chemical and Biological Defense, 1–5 March, Williamsburg, Virginia.

Aptowicz, K. B., Y. L. Pan, R. K. Chang, R. G. Pinnick, S. C. Hill, K. Gurton, R. L. Tober, and B. V. Bronk. 2003. Two-dimensional angular optical scattering patterns in the mid-infrared of microdroplets: On and off absorption. Paper presented at the 2003 Joint Service Scientific Conference on Chemical and Biological Defense Research **5269** (17–20 November, Towson, Maryland): 168–71.

Aptowicz, K. B., Y. L. Pan, R. K. Chang, R. G. Pinnick, S. C. Hill, K. Gurton, R. L. Tober, and B. V. Bronk. 2004. Two-dimensional angular optical scattering patterns of aerosol particles in the mid-infrared: Measurements designed to obtain particle absorption. *Proc. 2003 SPIE Photonics East* (27–31 October, Providence, Rhode Island).

Aptowicz, K. B., Y. L. Pan, R. K. Chang, R. G. Pinnick, S. C. Hill, R. L. Tober, and B. V. Bronk. 2004. Two-dimensional angular optical scattering patterns in the mid-infrared of microdroplets: On and off absorption. *Optics Letters* **29** (17) (September): 1965–67.

Other Communications

Aptowicz, K. B., and R. K. Chang. 2004. Elastic light scattering and laser-induced fluorescence, optical techniques for bio-aerosol enrichment. Paper presented at a seminar, Sandia National Laboratories, 29 June, Livermore, California.

68063

Computational Studies of JP-8 Diffusion Flames with Detailed Chemistry and Particulate Formation

J. C. Hewson, S. R. Tieszen

This research focuses on the computational study of hydrocarbon (HC) diffusion flames with emphasis on the modeling of complex chemical kinetics and detailed transport for fuels of practical industrial interest. The work provides knowledge necessary for modeling and analysis of fire environments to support Sandia's weapon-safety mission and Sandia's role as a national security laboratory.

The initial stage of our research examined soot formation in one-dimensional (1-D), counterflow methane (CH_4) diffusion flames with various oxidizer inlet compositions. The present work concentrates on modeling the flame structure and pollutant formation characteristics of diffusion flames using practical aviation fuels such as JP-8. We model JP-8 as a six-component surrogate blend of well-known HCs that together mimic the thermophysical properties of the parent fuel. We model the chemistry of the surrogate blend with a large, semidetailed kinetic mechanism consisting of 260 species participating in 7001 gas-phase reactions. To validate this mechanism, we examine lean, nonsooting counterflow diffusion flames using the surrogate mixture, as well as its individual constituent species, as fuels. We compare individual numerical solutions and calculated extinction limits with experimental data in an ongoing validation process. We also extended the present counterflow model to account for soot formation and to predict soot dynamics in JP-8 surrogate flames via a sectional aerosol dynamics submodel. Although the solution of a counterflow JP-8 surrogate flame is tractable on a single processor, a significant reduction in computational time was realized through the parallelization of the counterflow flame model on a distributed-memory system. The solution of a coflow JP-8 surrogate flame is intractable on a single processor due to memory constraints, and work is under way to implement the coflow model on a distributed-memory system.

The initial stage of this project entailed the evaluation of the chemical kinetic model for a JP-8 surrogate fuel in the counterflow configuration. We used a six-component mixture of HCs to computationally simulate real JP-8 fuel, which is composed of many hundreds of individual components. We selected these six components for their ability to reproduce key

physical and chemical characteristics of JP-8 fuel while limiting the complexity of the chemical-kinetic model. With six components, the chemical-kinetic model contained a somewhat reduced 221 gaseous species and 5032 reactions.

We conducted predictive simulations by coupling a code to simulate the counterflow configuration in which the experimental data are available, with an arc-length continuation method that allows a wide range of boundary conditions to be efficiently computed along with extinction limits. We obtained reasonably good agreement between the simulations and the measured temperature profiles and extinction limits for each of the single-component n-dodecane, iso-octane and methylcyclohexane flames. We also observed good agreement in the comparison between the predictions and measurements with the surrogate, and the agreement of the predictions with actual JP-8 fueled flames is even better. We completed the first stage of this research and will continue with further evaluation of the chemical-kinetic model as other measurements, such as species concentrations, become available to better characterize the model.

Future efforts will concentrate on the computational study of a steady, sooting coflow JP-8 surrogate diffusion flame. For sooting flames, the coflow diffusion flame configuration provides geometry more amenable to certain measurements. An essential part of this study will be the parallel implementation of the coflow model on a distributed-memory system to allow simulations with the large chemical-kinetic models required for JP-8 and similar real fuels. We identified the breakdown of the computational effort and the priorities for the parallelization strategy and will spend the bulk of the computational effort forming the nonlinear residual vector, forming the Jacobian, and iteratively solving the resulting sparse linear system. The parallelization of the iterative solver employs a stripwise decomposition of the physical grid and a local preconditioning operation on each domain. We identified an initial implementation of the parallel coflow model X, and the model is currently undergoing evaluation and refinement. Initial simulations model a sooting, ethylene coflow flame, and are geared toward assessing the functionality of the parallel code and obtaining baseline scaling measurements. Once complete, these initial efforts will transition to the modeling of a sooting, coflow JP-8 flame on a distributed-memory parallel system.

Refereed

Cooke, J. A., M. Belluci, M. D. Smooke, A. Gomez, A. Violi, T. Faravelli, and E. Ranzi. 2003. Computational and experimental study of a JP-8 surrogate, and its components in counterflow diffusion flames. *Proc. Combustion Institute* **30** (April 2004).

69145

Molecular Simulation of Beta-Amyloid (A-beta) Peptide Interaction with Phospholipid Membranes

A. P. Thompson

Sandia focused on the use of molecular simulation to probe the interaction of beta-amyloid (A-beta) peptides with phospholipid membranes. Recent experimental work by our collaborator at the University of Maryland led to a hypothesis that the binding of an oligomeric form of A-beta with cell membranes leads to neurotoxicity associated with Alzheimer's disease. However, fundamental information required for the development of effective treatments, such as the nature of the oligomeric species and the driving force for the peptide-membrane binding, remains unknown. We use molecular dynamics (MD) simulation as a means to gain this information. Because the time scales for MD (~ 10 ns) are not sufficient to observe entire peptide folding processes, we use the simulations in an iterative process that incorporates the experimental data of our collaborator.

We constructed various molecular-level models of A-beta peptide species (fragments and full monomers) in water. Instead of starting with peptide-membrane interactions directly, we first examined the self-interaction of the A-beta peptide. Experimental work by our collaborators, using hydrogen-deuterium isotope exchange electrospray ionization mass spectrometry (HX-MS), showed that residues 5–19 are significantly protected from exchange in fibril-containing samples, indicating that this is a key region for the self-aggregation process. Results from free-energy perturbation simulations involving two solvated peptide fragments confirmed the hydrophobically driven association in this region, as well as the lack of association between the N-terminus regions. We also built and equilibrated molecular models of hydrated phospholipid membranes for use in future work. Finally, we planned to incorporate a parallel tempering feature into Sandia's MD program LAMMPS; however, the main code developers had already added such a capability, and it is available in the latest release (LAMMPS 2003). We are currently migrating to that version of the code.

69146

Nanoscale Testing of Deformation and Fracture in Engineering Materials

N. R. Moody

This project is a joint research project between Sandia and Washington State University. There currently are few experimental testing methods that can assess nonlinear deformation and fracture phenomena on the micrometer and submicrometer length scales. Those that exist often are not verified using a second experimental approach. Nanoindentation techniques have been developed to probe failure modes, including film fracture and delamination, but these tests are difficult to verify without resorting to other indentation or scratching techniques. Therefore, we are applying a study that allows for the development of testing using an independent technique (bulge testing and blister testing) to materials systems of interest to film-substrate systems that we can use as models for components in the stockpile. We performed additional testing in materials that exhibit nonlinear deformation and shear band formation under high stresses. Because both systems, nanoindentation and bulge testing, can be carried out in aqueous environments that are environmentally aggressive, we will perform testing correlation under various thermochemical environments to ensure the robust nature of the experimental procedure. We are comparing the results of all of these tests to simulations in projects supported in the Accelerated Strategic Computing Initiative (ASCI) program to show applicability of the testing methods to future verification of simulations for life-cycle engineering.

We quantified piezoelectric film fracture on platinum (Pt) films, and the stress at failure during bulge testing was approximately an order of magnitude greater than for the indentation testing. Bulge testing shows that film fracture occurs during the point of largest applied tensile stresses to the oxide films. Indentation testing to fracture in lead zirconate titanate (PZT) films suggests that the crystallization process in which the amorphous film is heat-treated to develop the piezoelectric phases weakens the film (from applied tensile stresses at fracture of 3.4 to 1.6 GPa). Bulge testing results exhibit fracture at an order-of-magnitude-lower applied stresses. If the thicker Pt and thinner PZT layers lead to lower residual stresses, the nanoindentation results are about a factor of 2 higher than the bulge test results. This suggests that the differences are caused by both the residual stress differences

between the two systems and the flaw density sampled by the two tests since the bulge tests sample lengths of millimeters, while the indentation tests sample lengths of micrometers. We tested the aluminum oxide (Al_2O_3)–aluminum (Al) system with thermal oxides using indentation and will test it using bulge testing of different-sized volumes to study the sample volume effects (which should separate the flaw density issue). We extended an analysis of the fracture behavior during indentation from the initial method of measuring a stress at film fracture to now extend to a stress intensity fracture at film fracture. These results on two different Al substrates demonstrate the ability to resolve film properties between oxides grown on a 99.99% pure Al substrate versus a commercially available 1100 Al alloy.

We observed yield points during nanoindentation of 180 nm-thick PZT films on 500 nm of Pt. We used these yield points to determine the stress at fracture, 3.6 GPa for the amorphous film and 1.6 GPa for the crystalline film. However, bulge testing of these films showed a stress at failure of approximately 130 MPa when we tested films with a residual stress of 100 MPa. Increasing the tensile residual stress in the film lowers the strength of the film. Therefore, if the stress in the film used for nanoindentation was lower (e.g., 20 MPa), the strain-at-failure difference between the indentation and bulge testing would be about a factor of 2 different. We observed similar behavior in Al_2O_3–Al, and it was possible to measure the stress intensity at film fracture for different alloys and at different oxide thicknesses. We carried out additional work to identify individual slip systems around indentations in face-centered cubic (FCC) metals, as this will be a major system to explore in upcoming work.

Refereed

Bahr, D. F., A. L. Olson, K. R. Morasch, M. S. Kennedy, D. R. Marek, and A. Alamr. 2003. Fracture in thin oxide films. *Materials Research Society 2003 Fall Meeting—Thin-Films Stresses and Mechanical Properties X* **795** (Boston, Massachusetts): 55–63.

Bahr, D. F., K. A. Nibur, K. R. Morasch, and D. P. Field. 2002. Probing hydrogen—Deformation interactions using nanoindentation. *Hydrogen Effects on Material Behavior and Corrosion Deformation Interactions* **1** (Moran, Wyoming): 165–72.

Cordill, M. J., N. R. Moody, and D. F. Bahr. 2004. Quantifying improvements in adhesion of platinum films on brittle substrates. *J. Materials Research* **19** (6) (June): 1818–25.

Kennedy, M. S., M. Zosel, C. D. Richards, R. F. Richards, D. F. Bahr, and K. W. Hipps. 2003. Optimization of film stresses in composite piezoelectric membrane microgenerators. *Proc. Materials Research Society 2003 Fall Meeting—Thin Films: Stresses and Mechanical Properties X* **795** (Boston, Massachusetts): 503–8.

Nibur, K. A., and D. F. Bahr. 2004. Identifying slip systems around indentations in FCC metals. *Scripta Materialia* **49**:1055–60.

Other Communications

Nibur, K. A., D. F. Bahr, and B. P. Somerday. 2003. Hydrogen effects on dislocations around indentations. *TMS Letters* **1**:1–2.

69148

Nanocrystal-Polymer Composites for High-Luminous-Efficiency LEDs

L. E. Rohwer, J. E. Martin, B. L. Abrams, S. M. Woessner, J. P. Wilcoxon, S. G. Thoma

The goal of this project is to develop quantum dots (QDs) that can be encapsulated without aggregation and that have an efficient conversion of ultraviolet (UV) excitation light into white light. Some materials exhibited improved quantum efficiency (QE) over previous materials, but results were mixed.

(1) A previous blue-emitting cadmium sulfide (CdS) sample had QE=60.5%; the recent blue-emitting sample gave 37.8%.

(2) Previous white-emitting CdS QDs gave QE=15.8%; the recent yellow-white QDs gave 19.8%.

(3) Previous blue-green–emitting cadmium selenide (CdSe) QDs gave QE=33%; recent QDs gave 29.7%.

QDs are susceptible to spectral shifts and luminescence quenching by the local environment, making encapsulation challenging. Previously, we encapsulated the blue, alkyl thiol-functionalized CdS QDs synthesized in epoxy with minimal reduction of QE (60.5% to 56.9%). We encapsulated amine-functionalized CdS and CdSe QDs in silicone and organically modified silanes (ormosils). The QEs of CdS QDs encapsulated in ormosil ranged from 7% to 9%. We measured the QE of CdS QDs in silicone to be 4.8%.

We developed time- and frequency-domain methods of measuring fluorescence lifetimes to gain insight into QD luminescence as a function of surface stabilizer, solvent, and encapsulant. Blue QD samples exhibited exponential decay with lifetimes ranging from 2.7 to 5.5 ns. We found white-emitting QDs to have longer lifetimes (~ 500 ns) and to exhibit stretched exponential decays. Encapsulated QDs also exhibited stretched exponential decay, and we observed power-law decays for some QDs.

We fabricated blue and blue-green QD light-emitting diodes (LEDs) with luminous efficiencies of 9.8 and 16.6 lm/W, respectively. The blue-green value outperforms incandescent lamps by 10%, and the blue value is 78% better than achieved previously, but serious problems remain; after 3 months, conversion efficiency for a blue QD–LED decreased 34%, probably due to oxidation of the QDs. Direct thermoluminescence measurements showed that the QE of CdS drops by a factor of 3 at 200°C.

- *Evaluate the encapsulation of QDs in thiol-functionalized siloxanes*. We will vary the carbon (C) chain lengths and the ratio of inorganic to organic constituents.

We found that alkyl thiols added to the CdS QD surface broaden the spectral-energy distribution, producing white emission. The long chain-length alkyl thiols bind more strongly to the surface, resulting in the broadest spectral-energy distribution and sharpest absorption peaks. Spectral broadening occurs most rapidly with hexadecane thiol. We developed a measurement system for measuring the thermal stability of CdS and CdSe QDs in solution and encapsulants. We did not investigate the encapsulation of QDs in thiol-functionalized siloxanes.

- *Demonstrate the direct synthesis of QDs in an encapsulating matrix*. We will investigate a series of potential encapsulants (methacrylates, styrenes, and siloxanes). In addition to the standard characterization techniques, we will use time-resolved laser spectroscopy and QE measurements to monitor the stages of the gelation process.

We encapsulated amine-functionalized CdS and CdSe QDs in ormosils, resulting in a higher concentration of CdSe in encapsulant (thin-film and bulk form), white emission from orange-emitting CdS, and higher QD thermal stability compared to epoxy and silicone. We attempted direct synthesis in silicone and ormosils and did not investigate methacrylates and styrene encapsulants.

We developed both frequency- and time-domain capabilities for measuring fluorescence lifetimes. Each system has 100 ps time resolution, and lifetime measurements from both methods agree. Using lifetime measurements, we found that white-emitting CdS QDs have 100x slower lifetimes than blue-emitting CdS QDs and exhibit stretched exponential decay. We measured the maximum QE of blue to be 37.8% for blue-emitting CdS QDs and 19.8% for yellow-white CdS QDs.

- *Fabricate QD light sources using commercial near-UV LEDs*. Our past efforts used standard 5 mm lead frame packages and a molded epoxy dome into which we injected the QDs. We will redesign the packages to reduce the near-UV leakage and maximize the absorption of LED light by the QDs. Our goal is to raise the luminous efficiency to 7 lm/W for a blue LED.

We fabricated and increased the luminous efficiency of blue QD LEDs by 78% through improvements in packaging (from 5.5 lm/W to 9.8 lm/W). We fabricated blue-green QD LEDs with a luminous efficiency of 16.6 lm/W.

- *Investigate visible emitters based on silicon (Si) or germanium (Ge) dots*. Deposition of visible light-emitting

We developed both frequency- and time-domain capabilities for measuring fluorescence lifetimes.

atoms such as terbium (Tb) or europium (Eu) to such near-UV absorbing dots, followed by passivation using oxygen (O), could create a new class of white-light phosphors.

In very old samples from previous work, (2–5 yr), significant broadening of the photoluminescence (PL) occurred, producing white emission. This indicates that these small clusters also undergo the structural rearrangements and changes in PL found in the CdS(Se) systems, but much slower, perhaps due to the weaker surface ligation by the nonionic surfactants used in the older samples. It is unlikely that thiols will be useful for binding these hydride-terminated surfaces, but preliminary results indicate that alkyl amines or cyanides may be useful to enhance and broaden the white PL observed in the old samples. Initial attempts at doping with manganese (Mn) and deposition of zinc sulfide (ZnS) did not result in energy transfer from the Si to the Mn, likely due to the severe lattice incompatibility of ZnS and Si or Ge.

Refereed

Abrams, B. L., J. P. Wilcoxon, S. G. Thoma, and P. P. Provencio. 2004. Chromatographic investigation of size, shape, and luminescence of semiconductor nanoclusters synthesized by inverse micelles. *Langmuir*, in preparation.

Rohwer, L. E. S., and J. E. Martin. 2004. Subnanosecond lifetime measurements using inexpensive LED light sources. *J. Luminescence*, to be submitted.

Thoma, S. G., A. Sanchez, P. P. Provencio, B. L. Abrams, and J. P. Wilcoxon. 2004. Synthesis and optical properties of blue-emitting CdSe nanoclusters. *Nanoletters*, in preparation.

Thoma, S. G., B. L. Abrams, A. Sanchez, and J. P. Wilcoxon. 2004. Synthesis and encapsulation of semiconducting nanoclusters in amine-functionalized ormosils. *Chemistry of Materials*, in preparation.

Other Communications

Abrams, B. L., J. P. Wilcoxon, S. G. Thoma, and L. E. S. Rohwer. 2003. Quantum dots for solid-state lighting applications: Effects of photoluminescent thermal quenching. Paper presented at the Materials Research Society Fall Meeting, 1–5 December, Boston, Massachusetts.

Abrams, B. L., L. E. S. Rohwer, J. P. Wilcoxon, and S. G. Thoma. 2004. Temperature effects on quantum dots for solid-state lighting applications. Paper presented at the Materials Research Society Spring Meeting, 12–16 April, San Francisco, California.

Abrams, B. L., L. E. S. Rohwer, J. P. Wilcoxon, S. M. Woessner, and S. G. Thoma. 2003. Photoluminescent thermal quenching of encapsulated CdS and CdSe quantum dots for solid-state lighting applications. Paper presented at the 203rd Meeting of the Electrochemical Society, 12–17 October, Orlando, Florida.

Rohwer, L. E. S., B. L. Abrams, J. P. Wilcoxon, and S. G. Thoma. 2004. Development of solid-state light sources based on II–VI semiconductor quantum dots. *Light-Emitting Diodes: Research, Manufacturing and Applications VIII, Proc. of SPIE Photonics West*, edited by Steve A. Stockman, H. Walter Yao, and E. Fred Schubert, **5366** (January, San Jose, California): 66–74.

Rohwer, L. E. S., B. L. Abrams, S. G. Thoma, and J. P. Wilcoxon. 2004. Solid-state light sources based on encapsulated quantum dots. Paper presented at the 1st International Workshop on Nano- and Bioelectronics Packaging, 22–23 March, Atlanta, Georgia.

Thoma, S. G., B. L. Abrams, L. E. S. Rohwer, A. Sanchez, J. P. Wilcoxon, and S. M. Woessner. 2003. Encapsulation of nanoparticles for the manufacture of solid-state lighting devices. *Proc. SPIE International Symposium (Microelectronics, MEMS, and Nanotechnology)* **5276** (December, Perth, Australia): 202–12.

Wilcoxon, J. P., B. L. Abrams, and S. G. Thoma. 2004. Chromatographic investigations of the size, shape, and chemical interface dependent optical properties of direct- and indirect-type semiconductor nanocrystals. Paper presented at the National American Chemical Society Meeting, 28 March–1 April, Anaheim, California.

Wilcoxon, J. P., S. M. Woessner, B. L. Abrams, S. G. Thoma, and L. E. S. Rohwer. 2004. New synthetic strategies for nanosize phosphors based upon semiconductor quantum dots. Paper presented at the Materials Research Society Spring Meeting, 12–16 April, San Francisco, California.

69149

Outstanding Challenges for AlGaInN MOCVD

J. R. Creighton, A. A. Allerman, M. J. Russell, K. Cross, G. T. Wang, C. C. Mitchell, D. D. Koleske

Solid-state lighting is a promising new energy-efficiency technology that could potentially double the energy efficiency of lighting. To achieve this potential, substantial improvements in luminous efficiency and reductions in cost for the light-emitting diodes (LEDs) must be achieved. Metal-organic chemical vapor deposition (MOCVD) is one of the most costly and technically difficult steps in fabrication of LEDs and is identified in solid-state lighting technology roadmaps as a critical-path item. This project will examine three outstanding challenges in aluminum gallium indium nitride (AlGaInN) MOCVD. The first challenge is to more accurately measure the temperature during the MOCVD with in situ *emissivity-corrected pyrometry (ECP). Sandia will investigate novel approaches using ultraviolet-visible (UV-vis) and mid-infrared (MIR) wavelengths and new emissivity-correction pyrometry systems. The second challenge involves improving the reproducibility and control of* p-*type doping using magnesium (Mg). We will improve our understanding of ammonia-Mg gas-phase chemistry and adduct formation and will use this knowledge to develop processes that avoid gas-phase adduct formation, which should lead to improved reproducibility of Mg doping. The third challenge involves improved nucleation processes to reduce dislocation densities. AlGaInN films are grown on lattice-mismatched substrates (sapphire) that generate a large density of threading vertical defects. We will base the improved nucleation process on a study of the growth nucleation and surface reconstruction in the initial layers. We identified innovative approaches to meet these challenges based on a fundamental understanding of the physics and chemistry of the MOCVD processes.*

- *Accurate temperature measurement for III-nitrides*. We designed and tested on a reactor mockup a multiwafer, dual-wavelength, emissivity-correcting pyrometer for group-III nitride MOCVD. This system simultaneously measures the reflectance (at 405 nm and 550 nm) and emissivity-corrected temperature for each individual wafer, with the platen signal entirely rejected. We planned to install the system on one of our Veeco MOCVD reactors, but upon opening the reactor chamber, we were unable to remove the original arbor (to be replaced with a modified part) from the drive shaft. We ordered new parts and rescheduled the installation for upcoming work.

- *Reproducible magnesium (Mg) doping*. We measured the $MgCp_2$ (bis-cylopendienyl magnesium) + NH_3 (ammonia) adduct condensation phase diagram from 70°C–110°C at typical MOCVD concentrations. Results indicate that it requires temperatures approaching 100°C to prevent adduct condensation, a somewhat higher temperature range than our previous extrapolation had indicated. The phase diagram does follow the expected $MgCp_2$ and NH_3 concentration dependencies. At the highest temperatures, there is also some evidence for a new, irreversible chemical-reaction pathway forming another solid product that might possibly destroy this whole approach. If this new reaction is happening in parallel to the normal adduct condensation equilibrium, it may represent a serious problem. If the new reaction requires adduct condensation as a first step, this approach should still work.

We tested a method of heating the reactor walls to ~ 100°C and designed a heated inlet flange. Complete system testing will take place in upcoming work.

- *Low-dislocation-density GaN (gallium nitride)*. We installed and qualified a new commercial Veeco reactor. After the reactor was qualified, we conducted growth experiments to improve the GaN quality using a delayed recovery technique. The delayed recovery growth conditions favor the formation of large GaN nuclei on the surface, followed by promoting lateral growth to bend dislocations near the sapphire GaN interface. Using this technique, we reduced the dislocation densities determined from x-ray diffraction (XRD) from 2×10^9 cm^{-2} to 4×10^8 cm^{-2}. The reflectance waveforms measured on the new Veeco reactor were similar in appearance to previously measured waveforms on the high-speed rotating-disk reactor.

We also developed a model to simulate reflectance waveforms for GaN growth on sapphire. We based the model on detailed studies of nucleation layer evolution, analytical models to describe three-dimensional (3-D) island growth and coalescence and modifications to the virtual interface model. We measured these details using reflectance measurements and atomic-force microscopy images of paused growths. The model includes (1) temperature dependence of the optical constants for GaN and sapphire; (2) low-temperature nucleation layer growth and annealing; (3) nucleation layer decomposition kinetics and roughening; (4) high-temperature 3-D island growth, followed by coalescence of the islands to form a smooth surface; and (5) wavelength of light used for the reflectance.

Refereed

Wang, G. T., and J. R. Creighton. 2004. Complex formation between magnesocene ($MpCp_2$) and NH_3: Implications for *p*-type doping of group II-nitrides and the Mg memory effect. *J. Physical Chemistry A* **108** (22): 4873–77.

Other Communications

Koleske, D. D., M. E. Coltrin, K. C. Cross, C. C. Mitchell, A. A. Allerman, J. J. Figiel, and M. J. Russell. 2003. GaN nucleation layer evolution on sapphire. Paper presented at the AVS 50th International Symposium, 2–7 November, Baltimore, Maryland.

Koleske, D. D., M. E. Coltrin, K. C. Cross, M. J. Russell, and A. A. Allerman. 2004. Using optical reflectance to quantify GaN evolution on sapphire. Paper presented at the Electronic Materials Conference, 23–25 June, Notre Dame, Indiana.

Wang, G. T., and J. R. Creighton. 2003. Complex formation between magnesocene ($MgCp_2$) and NH_3: Origin of the “memory effect.” Paper presented at the AVS 50th International Symposium, 2–7 November, Baltimore, Maryland.

69150

Nanoporous Polymeric Materials for Chemically and Spatially Multiplexed Sensing of Bioagents

R. Shediac, V. C. Rucker, K. Havenstrite, B. A. Simmons, A. E. Herr

Sandia seeks to develop a novel fabrication approach for high-surface-area, nanoporous polymeric materials for numerous microdevice applications, including chemical-/biological-agent sensing, size-based sorting and filtering of molecules, microfluidic mixing, and chromatography. Preliminary results indicate that reactive-ion etching (RIE) of a variety of polymers generates high-aspect-ratio features with significant sidewall and surface roughness. We will exploit the resulting high surface area to enable enhanced immobilization of biomimetic recognition elements. RIE is particularly well suited for the fabrication of high-density microarrays of discrete, plasma-induced roughened sites, thereby providing a method for high-throughput, multi-analyte sensing while simultaneously enabling improved surface-reaction yields, increased immobilization efficiencies, and optimized array sensitivity. We will use this on-chip multiplexed immunoassay to analyze pathogens, toxins, and cytokines. In another application, we will exploit the plasma-generated nanoporous polymer microstructure as a porous membrane that can act as a front-end filter for separating target analytes in real-world samples such as cell lysates, blood, and contaminated water. Another potential application for RIE of polymers is microfluidic mixing, in which we will pattern plasma-roughened regions within polymeric microfluidic channels to create pressure gradients that will enhance mixing in electrokinetically driven miniaturized devices. We plan to use RIE to fabricate polymeric microchannels and to exploit the generated roughness within the channels as an in situ *fabricated porous high-surface-area stationary phase for electrochromatography of peptides and proteins.*

We used RIE to pattern proteins on the surfaces of polymethylmethacrylate (PMMA), the cycloolefin polymer Zeonex, and polycarbonate (PC). We used a low-pressure oxygen plasma to anisotropically etch 25–30 µm-deep features into polymer substrates. We significantly roughened etched polymer surfaces, which were significantly more hydrophilic than were unetched regions. On RIE–patterned PMMA and Zeonex substrates, proteins selectively bind to etched regions, but they bind selectively to the native, unetched regions on PC

surfaces. We patterned antibodies on etched PMMA and Zeonex surfaces and demonstrated direct immunochemical assays for the detection of protective antigen and cholera toxin.

We demonstrated that using an oxygen plasma for RIE of a variety of polymers generates features with significant surface roughness. We proposed that the resulting chemically altered, high-surface-area porous polymer microstructure would enable enhanced immobilization of biomimetic recognition elements.

We selected the polymers investigated in this study on the basis of chemical compatibility, biocompatibility, processability, and optical properties. We found that etch resistance is dependent on polymer structure, with network polymers exhibiting faster etch rates than amorphous polymers. Under the same processing conditions, etch rates for PMMA, PC, polyetherimide (PEI), and the cycloolefin Zeonex were 0.60 μm/min, 0.25 μm/min, 0.18 μm/min, and 0.18 μm/min, respectively.

For the patterned polymer substrates used in this study, we etched approximately 30 μm-deep holes in an array using a stencil mask. We used fluorescence imaging to study the protein adsorption characteristics of RIE–patterned polymer surfaces. We observed that polyclonal immunoglobulin (IgG) labeled with a fluorophore binds differentially to etched and unetched regions of RIE–patterned polymer substrates. Except for PEI, the background fluorescence from the polymer substrate itself was negligible. In the case of patterned PMMA and Zeonex, the fluorescently labeled IgG selectively binds to etched areas, whereas in the case of PC, the protein localizes in the native, unetched areas. We patterned antibodies on etched PMMA and Zeonex surfaces and successfully performed direct immunochemical assays for the detection of protective antigen and cholera toxin.

We used several surface-characterization techniques to elucidate the protein adsorption mechanism. Water-contact-angle measurements indicate that etched polymers are more hydrophilic than is the native polymer. Scanning-electron microscopy (SEM) and atomic-force microscopy (AFM) demonstrate that PMMA and Zeonex etched surfaces exhibit more surface roughness than does etched PC. Fourier-transform infrared spectroscopy (FTIR) indicates that extensive chemical modification occurs when PMMA and Zeonex surfaces are reactive-ion–etched to depths of 30 μm, whereas we observed no significant differences between the FTIR spectra of native and etched PC. We sent out samples of RIE–patterned PMMA, Zeonex, and PC for analysis by x-ray photoelectron

spectroscopy (XPS) and time-of-flight secondary ion mass spectrometry (ToF–SIMS).

69151

Evolutionary Complexity for Protection of Critical Assets

M. E. Chandross, C. C. Battaile

The protection of critical assets from the threat of reverse engineering is of extreme concern for most sensitive technologies. While physical technologies can be protected through destructive means (e.g., injecting foams into hard drives or intentionally bombing downed aircraft), the protection of software assets can be much more subtle and difficult. Any critical asset can be lost or captured during service, but software is also susceptible to compromise through other avenues, such as cyber attacks and software-license violations. Recent developments in adaptive genetic software led to codes that evolve fitness according to externally imposed criteria, such as the ability to perform addition or comparison of numbers. Occasionally, the evolutionary path taken by these codes produces algorithms that are efficient, yet extremely complex for the solution of these trivial problems. Until now, these solutions have been a mere curiosity. Sandia seeks to encourage and exploit the complexity of evolved code to create critical software components that retain their functionality, yet are impossible to reverse-engineer.

Even the most trivial piece of code can thus be converted into one that takes hundreds of manhours to understand. After proof-of-concept with relatively simple software, we can use this idea not only to obfuscate large codes, but also to add additional protection to critical physical assets through the obfuscation of component and systems designs.

The goal of this project was to investigate whether or not it is feasible to take a complex function and use genetic programming methods to obfuscate it, rendering it difficult or impossible to reverse-engineer. We found that genetic programming will, in general, create obfuscated functions just by the very nature of the method. Even a simple function, such as $2x^3$, can easily be transformed into a long expression that is difficult to understand. However, the applicability of the method seems to end here. Attempts at using genetic programming to generate exact matches to complex functions have generally been unsuccessful. Even with large populations and long iteration times, genetic programming can, in general, arrive only at approximate solutions. Thus, it would seem that the best course is to genetically engineer complicated versions of simple functions and use these to build up obfuscated

versions of more-complex ones. We found that this method results in unacceptable performance. An obfuscated version of $x^3 + x^2 + x$ calculated 200 million values in 79 s, compared to 6 s for the unobfuscated version. We deemed this to be unacceptable. Using the optimization features of the compiler resulted in both versions taking only 1.0 s, but resulted in all obfuscation being removed (i.e., the resulting assembly code was identical). We therefore think that this method is inappropriate for generating obfuscated codes for protection of critical assets.

69152

Nanomechanical Stochastic Resonators

D. W. Carr, R. H. Olsson

Sandia developed a framework for understanding how stochastic resonance and related phenomena can impact sensor system design, especially with respect to inertial sensing systems. We designed an optically coupled mechanical device that is bistable and can readily switch between +1 and -1 states, depending on the presence of an applied external force. Upon entering such a state, the system is reset to zero, and a new state can be entered. By counting the number of switches into the two states, an analog measure of the applied force can be achieved. In the presence of noise, this system will display stochastic resonance.

We can show that uncoupled arrays of such devices could serve very well to give accurate measures of an applied force with a very high signal-to-noise ratio (SNR). The real advantage gained is that this threshold system produces a very large signal for a single-state transition. As a result, the electronics required to read out the signal are much simpler and lower noise than those that would be required to measure a typical analog-type sensor.

We developed a theoretical device that can be implemented in existing technologies and that would display all of the benefits of stochastic resonance. We [then] fabricated this device.

We developed a theoretical device that can be implemented in existing technologies and that would display all of the benefits of stochastic resonance.

We fabricated this device, which consists of a structure with a large suspended plate coupled to grating transducers that are used to make changes in the optical reflectance in the presence of an applied force. Additionally, there are electrodes that enable the tuning of the spring constant. By feeding back an optically reflected signal into these electrodes, we can make a bistable switching system. We have not yet tested this device, but will have results very soon.

We also showed where the real advantage of stochastic resonance can present itself in our sensor systems. Theoretically, the greatest advantage will occur in large arrays of structures. If each structure generates a large signal, this can be a superior manner in which to generate a large SNR, as compared to merely making a single large sensor.

69153

Augmented Musculature Device

B. R. Rohrer, T. D. Pankretz, G. A. Johnston, D. K. Kholwadwala

Sandia seeks to develop an augmented musculature device (AMD) that assists the movements of its wearer. It could be applied directly to aiding military and law enforcement personnel, the neurologically impaired, or those requiring any type of cybernetic assistance. As proposed, the AMD consists of a collection of artificial muscles, each individually actuated and strategically placed along the surface of the human body. Well-fitted, heavy-duty nylon clothing would provide a framework for attaching the artificial muscles to the body.

The actuators that would be used by the AMD are known as "air muscles" and operate pneumatically. They are commercially available from several vendors and are relatively inexpensive. They have a remarkably high force-to-weight ratio—as high as 400:1 (as compared with the 16:1 ratio typical of direct-current [dc] motors). They are flexible and elastic, even when powered, making them ideal for interaction with humans.

We developed four generations of AMD prototype. The first generation was a proof-of-concept mockup in which air muscles were directly attached to an articulated mannequin. The second generation consisted of a frame, stitched of nylon webbing. We based the third generation on a motocross protective jacket, which provided fabric coverage and support to the entire upper body. The fourth generation used a ballistic vest as a platform and proved to provide the most stable attachment points and the least impairment to arm movement.

- *Homemade suit*. The first implementation of the AMD consisted of tubular webbing (used in climbing) sewn together to make adjustable straps. We then attached muscles to the webbing, extending to a collar, a chest strap, and wrist straps. This completely homemade suit was less effective than we had hoped. The flimsy nature of the tubular webbing allowed for the desired range of movement but lacked the necessary support for the muscles, causing the suit to slide on the body. Other flaws included the restriction caused by the Velcro on the adjustable straps: although permitting the desired adjustability, the Velcro could not withstand the expanding forces without shifting in undesired directions. Although not a total success, this first suit emphasized the need for longer muscles and for the muscles to work in groups. Structurally, the suit needed to be more secure,

enabling the muscles to pull in unison to keep the harness in place.

- *Pressure suit*. Learning from the first suit, our next direction was toward a pressure suit to solve the structural stability problem. Pressure suits are used by motocross riders to prevent overextension; the suits are formfitting, with molded plastic on the shoulders, the forearms, and the spine. Initially, the plastic protectors served to help attach the muscles to the suit, and the spine helped to provide leverage (excellent in preventing chocking). The suit gave the muscles greater range of motion, but efficiency was lost when the fabric sleeves slid up the arm and defeated the effort of the muscles. Additionally, there was difficulty putting on the suit with its long sleeves. In an attempt to correct the problem of the sliding sleeves, we removed them. We took two different approaches to create a type of fixed sleeve and used both molding foam and leather.
- *Ballistic vest*. The ballistic vest, in combination with the leather sleeves, solved the problems posed by previous attempts at the AMD. It provides stable shoulder support for the muscles, has Velcro to fasten it securely around the waist, is easy to put on, and is comfortable to wear. Special one-way snaps covering the vest keep the muscles in place and allow muscle attachment at virtually any point in the front or in the back. This has minimized slippage due to the stability of the vest. To completely solve the problem of muscles falling off the shoulders, we sewed fabric to the shoulders, which neatly keeps the muscles in place. This, in combination with the leather sleeves, allowed for optimal arm movement.

We based each suit on a wooden dummy rigged with muscles. We drilled holes in the dummy with eyelets placed on key muscle groups, based on the human anatomy. This dummy predicted where muscles would need to be attached on the suit to obtain the desired movement.

69154

Biomolecular Decision-Making Processes for Self-Assembly

G. C. Osbourn, A. M. Bouchard

The brain is often identified with decision-making processes in the biological world. In fact, single cells and single macromolecules (proteins) also make simple decisions. These decision processes are essential to survival and to the biological self-assembly and self-repair processes that we seek to emulate. How do these tiny systems make effective decisions? How do they make decisions in concert with a cooperative network of other molecules or cells? How can we emulate the decision-making behaviors of small-scale biological systems to program and self-assemble microsystems? To answer these questions, Sandia will theoretically propose, model, simulate, and categorize decision mechanisms that can be exhibited by nonequilibrium systems. We will compare our results against existing biological data to further identify the crucial features and possible commonalities of decision making exhibited by small biological systems.

Biochemical reactions taking place in living systems that map different inputs to specific outputs are intuitively recognized as performing information processing. Conventional wisdom distinguishes such proteins, whose primary function is to transfer and process information, from proteins that perform the vast majority of the construction, maintenance, and actuation tasks of the cell (assembling and disassembling macromolecular structures, producing movement, and synthesizing and degrading molecules). We examined the computing and decision-making capabilities of biological processes in the context of the formal model of computing known as the *random-access machine* (RAM), which is equivalent to a Turing machine (Minsky, 1967). When viewed from the RAM perspective, we were able to show that many of these dynamic self-assembly processes—synthesis, degradation, assembly, movement—do carry out computational operations. We also showed that the same computing model is applicable at other hierarchical levels of biological systems (e.g., cellular or organism networks as well as molecular networks). We performed stochastic simulations of idealized protein networks designed explicitly to carry out a numeric calculation. We explored the reliability of such computations and developed models of error-correction strategies (algorithms) employed by living systems. Finally, we identified

a representative set of real examples of dynamic self-assembly processes that occur in living systems and described the RAM computer programs they implement. By viewing the processes of living systems from the RAM perspective, a far greater fraction of these processes can be understood as computing and decision-making processes than recognized previously by the scientific community.

Refereed

Bouchard, A. M., and G. C. Osbourn. 2004. Dynamic self-assembly and computation: From biological to information systems. Paper presented at the Bio-ADIT Conference, 29–30 January, Lausanne, Switzerland.

Other Communications

Bouchard, A. M., and G. C Osbourn. 2004. Dynamic self-assembly in living systems as computation. *Natural Computing J.*, submitted.

69155

Light-Powered Nanovehicle Propulsion

J. A. Shelnutt, G. D. Bachand, C. J. Medforth

Having verified that nanoscale metallic vehicle bodies could be constructed, Sandia's goal was to develop a reliable synthesis of these nanovehicles and install a mechanism for powering these structures using biological motors, which could be activated and driven by visible light energy. The propulsion system was to be constructed entirely by self-assembly and could be powered by a photocatalytic process already partially built into the nanovehicle. Thus, the nanovehicles would be composed of both natural biological components (ATPase, kinesin-microtubules) and biomimetic components (platinized liposomes, photosynthetic membrane) as functional units. We originally envisioned the vehicle's body to be composed of a surfactant liposome coated with joined platinum (Pt) nanoparticles; however, instead of the expected nanoparticles, we were able to grow dendritic disklike Pt sheets 2 nm thick and of controlled diameters (10–200 nm) on the liposomes. A hydrogen-evolving artificial photosynthetic system in the liposomal bilayer could generate a pH gradient across the membrane to drive the synthesis of adenosine triphosphate (ATP) by employing ATP-synthase incorporated in the membrane. ATP could be used to fuel the molecular motor (kinesin) attached to the vehicle. For its synthesis, we need only light, storable ADP, phosphate, and an electron donor to be used by ATP-synthase. These nanovehicles could potentially respond to chemical gradients, light intensity, and field gradients in the same manner in which magnetic bacteria navigate. The cargo might include decision-making and guidance components, drugs and other biological and chemical agents, explosives, catalytic reactors, and structural materials.

We made unilamellar liposomes, which were completely enclosed with dendritic Pt or palladium (Pd) sheeting in large numbers. However, we have not yet gained sufficient control over the synthesis to be able to make these nanovehicles exclusively. We showed that these Pt spheres have good structural stability since the nanostructures seen in transmission-electron microscopy (TEM) images have survived the stresses of drying during TEM sample preparation. However, in the absence of a method of producing monodisperse suspensions of the nanovehicles, we have not been able to complete the follow-on task of developing the propulsion system for these nanovehicles. Because the

unilamellar liposomal membrane apparently remains intact, we see no reason why ATPase cannot be inserted into the membrane. However, we do not yet know if the Pt is deposited inside the membrane or on the inner or outer surface. This is crucial to the operation of the nanovehicle because it determines whether a usable pH gradient can be developed across the membrane. Thus, our efforts show some progress toward installation of a propulsion system and no insurmountable barriers to completing that task to make functional nanovehicles, given sufficient funds and time. We accomplished our goal of showing the feasibility of making light-powered nanovehicles.

We accomplished our goal of showing the feasibility of making light-powered nanovehicles.

69156

System-Dynamics Modeling to Assist Regional Water Planning: Modeling the Nonmarket Value of Water

V. C. Tidwell, H. D. Passell

Fresh water is central to the vitality of our society; however, current demands are increasingly being met through unsustainable practices. As such, improved management of our finite supplies is needed; unfortunately, establishing such practices is complicated by the differing values placed on water by the disparate sectors of our society (municipal, industrial, agricultural, environmental). Integrated modeling tools are needed to assist in regional water planning and to facilitate public involvement in the decision process. Sandia takes a novel approach to community-mediated water planning, employing a cooperative modeling process formulated within a system-dynamics decision framework.

Society values water for many different uses, from basic life support to economic, aesthetic, cultural, and instream/environmental applications. In some cases, these values can be directly quantified as with economic valuation; in other cases, quantifying worth can be difficult. Nevertheless, these diverse value systems are playing an increasing role in establishing management plans that are acceptable both publicly and politically. For this reason, valuation methodologies must be researched and implemented within the water-planning process.

We will pursue this work cooperatively with the University of Arizona and the National Science Foundation Science and Technology Center for the Sustainability of Semi-Arid Hydrology and Riparian Areas (SAHRA). SAHRA is a multi-institutional, multidisciplinary research program to improve understanding of the hydrologic cycle, provide improved tools for decision makers, and raise the level of hydrology literacy.

The purpose of this research is to develop a decision-support model to assist water agencies and decision makers in the management and long-range planning of water resources. Unique aspects of this work include the system-dynamics approach to modeling that allows the integration of a broad range of factors into the decision model as well as provides a vehicle for engaging stakeholders in the decision process. Key to such decisions, but rarely quantified, are nonmarket factors (i.e., metrics that cannot easily be quantified in terms of dollars and cents). Early studies addressed many nonmarket valuation issues. The first of these considered nonmarket pressures

influencing water transfers. Although the economy plays a role, other factors are reasoned to modify the price at which transfers occur (e.g., ease of transfer, attitudes toward abandoning of rights). We developed causal relations, while currently making an effort to formulate these relations into quantitative models.

Second, we explored nonmarket valuation of instream recreational value for Aravaipa Creek Wilderness, a tributary to the San Pedro River, along with a colleague at the University of New Mexico. We quantified dollar estimates of consumer surplus per recreation-visitor-day. Results compared well with other nonmarket recreational value research and will be useful as avitourism research within SAHRA gets under way elsewhere in the San Pedro River system.

Third, we researched nonmarket valuation of "ecosystem services," the most controversial and probably most important element of riparian valuation. We developed conceptual models of several key riparian services. Key model issues identified include the trade-off between urban/agricultural demands and instream flows affecting both aquatic and riparian habitat.

Upcoming work will focus on the continued development of a riparian valuation package for implementation within a system-dynamics modeling context. Currently, we are pursuing modeling in a fully generic manner, by identifying cause-and-effect relations and then developing integrated models to quantify key system processes, feedback, and time-delayed responses.

Refereed

Weber, M., and R. Berrens. 2004. Value of instream flow and remote recreation in the Sonoran Desert. *J. Water Resources Planning and Management*, submitted.

Other Communications

Weber, M., and R. Berrens. 2004. Value of instream flow and remote recreation in the Sonoran Desert. Paper presented at the Arizona Hydrological Society Annual Meeting, 15–17 September, Tucson, Arizona.

69157

Interactive Water-Quality Modeling to Assist Regional Water Planning

V. C. Tidwell

While freshwater supplies are finite, demand has tripled since 1950. This growing disparity between supply and demand necessitates difficult decisions that often directly impact groundwater levels and stream flows and that may result in unexpected impacts on water quality, socioeconomic value, and the riparian ecosystem. Unfortunately, making these decisions is complicated by the differing values placed on water by the different sectors of our society (industrial, agricultural, environmental, municipal). While many models serve water-resources managers in day-to-day operations, there is a lack of integrated modeling tools to assist in regional water planning and to facilitate public involvement in the decision process. Sandia takes a novel approach to community-mediated water planning, using a cooperative modeling process formulated within a system-dynamics decision framework.

Water quality often limits the potential uses of scarce water resources in semiarid and arid regions. Consequently, changing water quality, particularly nutrient levels, is often an important concern with many water-resource decisions. Increasing nutrient loads may result in eutrophication of reservoirs and increased riparian vegetation and transpiration. To best manage water quality, one must understand the sources and sinks of both solutes and water to the river system. Therefore, modeling will also need to include biological uptake both within the river and within the shallow groundwater of the riparian corridor. Incorporating these processes and feedback is paramount to modeling and evaluating the water-quality dynamics that may result from changing land-use practices, watershed/range management, and reservoir operations.

Our efforts focused on developing a conceptual framework for modeling geochemical dynamics in semiarid watersheds. We developed a basic understanding of the principal chemical and physical processes and identified the key sources and sinks. To help improve our understanding and provide a quantitative basis for evaluating our model, we performed water-quality sampling throughout the Middle Rio Grande. Data collection involved winter and summer synoptic sampling from Del Norte, Colorado, to Fort Quitman, Texas. Sampling demonstrated that the primary source of water for the Rio Grande is runoff from the San Juan and Sangre de Cristo mountain ranges and that

water quality, both salinity and nutrient concentrations, degrades with distance downstream. Dissolved organic carbon (DOC) concentrations gradually increase with distance downstream, but inorganic nitrogen (N) concentrations are more variable due to localized surface-water inputs from both agricultural and urban/wastewater sources. Below these localized inputs, ammonium and phosphate are quickly removed or converted to other N or phosphorus (P) species in the river during both summer and winter, whereas nitrate concentrations decrease more slowly. Exchange between surface water, the hyporheic zone, and the riparian corridor results in the net removal of nitrate from the river. We compared measured concentrations of three nutrients (DOC, nitrate, and ammonium) to concentrations calculated using a simple conservative mass balance equation to identify regions where instream processes are occurring. Results indicate that net consumption is a significant process during the summer for all nutrients, whereas net production is more common in river reaches during the winter. While conservative mixing relationships do not fully account for changes in stream chemistry, river discharge does appear to be an important control on nutrient uptake rates. Recent sampling results indicate that nutrient concentrations in agricultural drains are highly variable and that nutrient loading from these point sources is complicated by significant variations in drain discharge. Recent sampling also was an opportunity to observe the dynamics controlling stream-water chemistry during a monsoon season. Based on these results, we updated our conceptual geochemical model and began work on the nutrient model framework. We are now ready to quantify the model and compare it against the acquired data in a more robust manner.

Other Communications

Oelsner, G., J. Hogan, P. Brooks, S. Mills, J. Villinski, and H. Lacey. 2003. Water and solute sources along a 1000-km reach of the Upper Rio Grande. Paper presented at the 3rd Annual Meeting, SAHRA, 14–17 October, Tucson, Arizona.

Oelsner, G., P. Brooks, J. Hogan, H. Lacey, D. McDonnell, and J. Villinski. 2004. Quantifying nutrient sources and cycling along the Upper Rio Grande. Paper presented at the 2004 New Mexico Water Research Symposium, 10 August, Socorro, New Mexico.

Oelsner, G., P. Brooks, J. Hogan, H. Lacey, S. Mills, and J. Villinski. 2004. Quantifying nutrient sources and cycling along the Upper Rio Grande. Paper presented at the 14th Annual El Dia de Agua, 3 March, Tucson, Arizona.

69158

Microbe-Exuded Polymers and the Enhanced Corrosion of Carbonate Materials

R. T. Cygan, M. S. Kent

Cation binding by polysaccharides is observed in many environments and is important for predictive environmental modeling and many industrial- and food-technology applications. The complexities of these organo-cationic interactions are well suited to predictive computer molecular modeling studies for investigating the roles of conformation and configuration of polysaccharides on cation binding. In this study, Sandia chose alginic acid as a model environmental polysaccharide and modeled representative disaccharide subunits and polymers. We investigated the ability of subunits to bind calcium (Ca) and extended these findings to modeling polymer interactions with Ca ions.

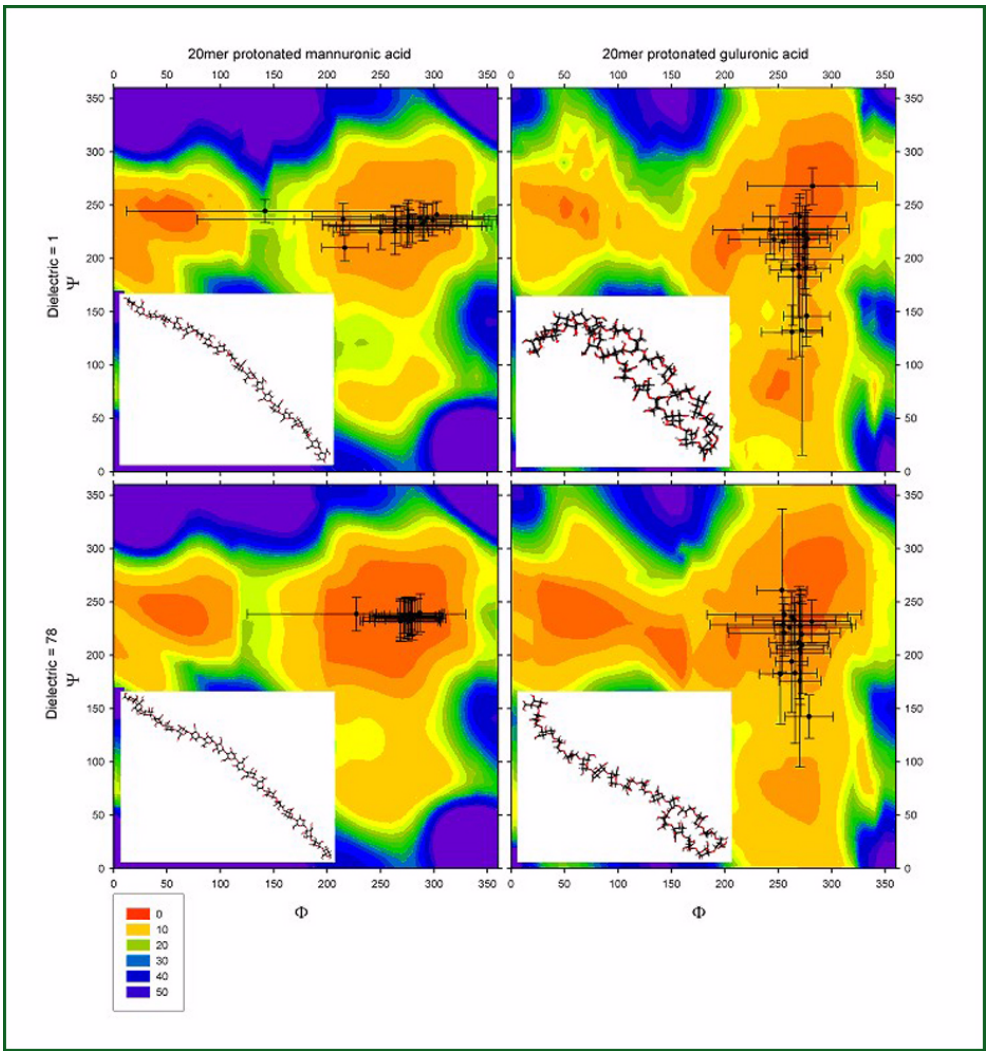

Potential energy map of alginate dimers and the molecular dynamics (MD)–derived structures of alginate polymers.

We found torsion angles (phi and psi) of the ether linkage between various monomeric subunits to consistently have two energy-minima conformations for all representative dimer subunits, including mannuronic (M)-M, guluronic (G)-G, and M-G linkages. We attributed cation binding by alginic acid to the alpha 1-4 linkage between G monosaccharides and the ability to form tetradentate complexes about cations. Our theoretical studies indicate that some conformations of M-G disaccharides have a higher binding energy than G-G disaccharides and may play a heretofore underdeveloped role in cation binding by alginic acid.

In terrestrial environments, polysaccharides are the second most abundant organic species following humic substances and can range from 5% to 30% of the total organic matter. Many of these polysaccharides are produced in microbial biofilms—thin films of microorganisms, including bacteria, Archaea, cyanobacteria, algae, fungi, and lichens—growing on surfaces in an excreted layer of polysaccharide. The functionally diverse polysaccharide chemical structures vary by microorganism, growth stage, nutrient abundance, and other environmental stimuli. The three-dimensional (3-D) structure of gelled biofilms is maintained by polysaccharides cross-linked by cations. The polysaccharides generally comprise a variety of sugars and often contain functional groups (such as carboxylic acids) that can interact with the cations. The specific cation-binding effects of polysaccharides depend on polysaccharide conformation and configuration, cation type, ligand functionality, acidic moieties, and pH.

This investigation applies the predictive capability of molecular modeling methods to explore the effects of conformation and configuration of the constituent dimers of a model polysaccharide on molecular stability, Ca binding, and polymer conformation. The ability to model and predict cation binding as determined by polysaccharide structure is desirable for a variety of industrial applications that require the dissolution of metal-bearing minerals, and is important for understanding cation binding in the environment and geochemical modeling. We selected alginic acid as a model environmental polysaccharide due to its well-characterized chemistry and demonstrated presence in the environment. It is a straight-chain, hydrophilic, colloidal, polyuronic acid composed of G and M acid residues configured in poly-G, poly-M, or alternating GM blocks, and which is capable of chelating aqueous cations. Natural polysaccharides are produced from a variety of biological sources and exhibit chemical and

functional diversity, depending on the organism that produces them.

We used a detailed molecular-level approach to understand the complex chemical contributions in conformation analysis and cation-binding determinations. We used energy optimization and molecular dynamics (MD) methods to obtain chemical insights that may be difficult, if not impossible, to obtain experimentally and ultimately to broaden the understanding of these interactions. We used the consistent valence force field (CVFF) energy force field to evaluate the potential energy of each conformation based on the torsional variation of the linking ether of the alginate dimer. We developed a computer algorithm to obtain a potential energy map based on the full exploration of the torsion phi-psi angles with resolution of 1–10 deg increments. Additionally, we used implicit solvation using a variable dielectric constant to assess the impact of water on the conformation behavior. We mapped the energy values three dimensionally to identify two to three unique energy minima configurations. MD simulations (constant-temperature [NVT] ensemble) for the various alginate dimers indicate the possible transitions and energy barriers among the conformers at room-temperature conditions. We also completed several preliminary MD simulations of the various water-solvated dimers interacting with a calcite cleavage surface. These calculations involve periodic simulation cells of approximately 5000 atoms. We will significantly expand this latter effort in the next phase of the project.

We found the energy minima associated with the dimer conformations to exist at temperature by dynamic modeling with a global energy minimum for all disaccharides at phi = 274.1 ± 7.2 deg, psi = 227.2 ± 4.8 deg. We observed similar conformations to be most stable when the disaccharides were modeled with Ca ions and as larger (20-unit) polysaccharide chains. We therefore predict that alginic acid *in situ* will commonly exist with this conformation.

Refereed

Perry, T. D., R. T. Cygan, and R. Mitchell. 2004. Molecular mechanics of the conformation and configuration of alginic acid subunits and polymers. *J. American Chemical Society*, to be submitted.

69159

Nerve-Cell Function and the Development of Cognitive Networks

R. Behrens, Jr., R. J. Bastasz

Sandia's intent in this project was to explore the potential to create new types of experiments to probe the development of nerve-cell function and nerve-cell interactions, and how they lead to memory and cognitive function. The basic idea was to place nerve-cell networks onto the surface of silicon (Si) substrates that can be probed and stimulated via electrical circuitry integrated into the Si surface. The cell network would be enclosed to provide an in vitro *medium. We envisioned interspersing small-diameter holes in the Si surface in the regions of the nerve-cell networks that would allow fluids to flow through the Si layer and to be injected into a high-resolution mass spectrometer (MS) for analysis of constituent neurotransmitters, hormones, peptides, and proteins. This would provide the capability to monitor the chemical signatures of nerve-cell growth and interaction as a function of time and location in the network. Thus, the development of memory effects in the network could be monitored and its ability to respond to stimuli could be examined to understand the emerging properties of the nerve-cell network.*

In our initial review of the neuroscience literature, it became apparent that the major challenge in developing this research idea of relating nerve-cell function to cognition was not an experimental one, but one of understanding cognition and how this is related to higher-level mental activity.

We examined the feasibility of developing a new type of experimental capability that will create new methods to understand how the molecular basis of nerve-cell function is integrated and leads to the development of cognitive networks that are the basis for brain function. We evaluated the following areas: (1) modeling of biological systems to identify one or more classes of neuronal cells amenable to the objectives of this study; (2) neural-cell adhesion, directed growth, detection of neurotransmitters and proteins, diffusion rates of these molecules; (3) methods for fabricating neuronal microarrays; (4) nanospray methods for the MS–analysis target molecules: (5) cell stimulus methods; (6) data collection and analysis methods; and (7) modeling issues.

We conducted a literature search to address each area outlined and drew two broad conclusions:

(1) It is feasible to grow nerve cells in culture and monitor the chemical and electrical processes that control their interactions. Recent publications also show that the location of nerve cells and the growth of neuronal interconnections between nerve cells can be controlled and directed.

(2) Detection of the spatiotemporal features of the neurotransmitters involved in neuronal signaling is more easily addressed using photosensitive molecular probes to tag the molecules of interest and broad-field or confocal microscopy to measure their spatial and temporal behavior. The need for spatially resolved MS is not required to monitor the physicochemical reaction processes that control signaling in the neuronal network.

In our initial review of the neuroscience literature, it became quite apparent that the major challenge in developing this research idea of relating nerve-cell function to cognition was not an experimental one of examining the behavior of neurons, but one of understanding cognition and how this is related to higher-level mental activity. It became clear after reviewing the literature from the fields of neuroscience, psychology, and cognitive neuroscience (e.g., work of Kandel, Edelman, Fuster) that a fundamental understanding of concepts associated with higher-level mental function and cognition was required before any reasonable attempt could be made to develop new experiments that would relate nerve-cell function to cognition.

To illustrate this problem, we pose the simple question, How does one perceive that a tulip is a flower? The research project that we would like to develop would provide insight into how the operation of the nerve cells involved in visualizing and perceiving a tulip as a flower behave and help to accomplish this task.

To tackle this problem, we devoted considerable effort to reviewing seminal works in the areas of theoretical psychology, cognitive neuroscience, and the neurobiology of the central nervous system to obtain an understanding of the main issues underlying higher-level mental function and cognition.

Once we obtained a better understanding of the general issues of cognitive neuroscience, it became apparent that current understanding of how the visual sensory pathways convert visual information from the physical world into perceptions in our phenomenological world is quite advanced. We used this topic as a guide for creating concepts for the research program we would like to develop. We also used it to evaluate the efficacy of these concepts, striving to determine whether or not they will provide new insight and understanding

of how nerve-cell function is related to cognition and higher-level mental function.

We are using current understanding of the neuronal processes involved in processing information in the visual pathway to create perceptions to evaluate each aspect of creating an artificial nerve-cell array that can be used to probe the underlying physicochemical processes that control the behavior of nerve cells and relate their behavior to the development of cognition.

69160

Ultrahigh-Gain Fusion Concept

J. R. Schendel, S. A. Slutz

A brief all-source assessment of foreign research in ultrahigh-gain fusion has identified a new high-energy-density physics (HEDP) concept that has been untried in the U.S. This potentially revolutionary concept could provide insight into the possibility of ultrahigh-gain fusion and could lead to major unforeseen advances in pulsed-power–driven high-yield (HY) fusion, thereby accelerating progress toward this goal. This understanding would also enhance the reputation of Sandia's work on high-energy-density science. A full understanding of this HEDP concept could prevent technical asymmetries between the U.S. and others, while also eliminating potential vulnerabilities.

By combining two recurring themes in the scientific literature, ultrahigh-gain fusion could occur. This combination should enhance the burn efficiency substantially. This combination could also provide a path for achieving HY in a slightly different way and accelerate Sandia's goals for HY fusion. The results of this study conclude that this approach is technically feasible.

We completed a review of foreign work in the concept of ultrahigh-gain fusion. The review led us to a complete overview of the foreign research that included a conclusion not initially considered. This conclusion explains many aspects of the foreign research.

We also concluded a review of foreign theoretical work. This review indicates a density-related criterion to sustain fusion burn that we were unable to verify with our calculations. Initial calculations at Sandia showed a different criterion, but for a different physical situation. We recently finalized the Sandia calculations that will investigate the various criteria; these calculations show slightly different criteria for the sustenance of fusion burn.

We also performed a second set of calculations that involved a second concept that showed some promise.

Other Communications

Schendel, J. R. 2004. Ultrahigh-gain fusion. Paper presented at the JAEIC Working Group, 30 September, Washington, D.C.

69161

Nanofluidic Devices for Rapid Detection of Virus Particles

P. L. Gourley

A nanodevice that could quickly detect and identify virus particles would play a critical role in fighting bioterrorism and in helping to contain the rapid spread of disease. Such detection requires new devices to quickly screen for the presence of tiny pathogens. To develop such a device, Sandia fabricated nanochannels to transport virus particles through ultrashort laser cavities. These channels are about 100x smaller than previous laser microcavities used for studying biological cells. The small virus size (~ 20–100 nm) requires new spectroscopic techniques for detection and differentiation. We investigated intracavity quantum photonics using direct pathogen-supported lasing modes and indirect modulation of the modal noise in stimulated emission from the laser cavity. We used Bacillus megaterium *virus since it is relatively large, ~ 100 nm. The virions were flowed through the laser cavity. The bacteria did modulate the noise spectrum of the cavity modes as measured with a spectrum analyzer in the frequency range 0–100 KHz, but we observed no evidence of directly supported lasing modes. We also performed coherent and incoherent light-scattering measurements to determine the magnitude of the scattered intensity. We performed the measurements in flow channels, cuvettes, and with high-resolution laser-scanning confocal microscopy. The results were in reasonable agreement with our finite-difference (FD) time-domain calculations. Those calculations show that the transition from Rayleigh to Mie scattering from small particles occurs near 200 nm. Since the viruses exist in the Rayleigh limit where the scattering is more isotropic, they act primarily as a loss mechanism to modulate the cavity lasing modes as observed in the experiments. The scattering loss is predicted to scale quadratically with virus size and should be tested in future experiments.*

Sandia fabricated nanochannels to transport virus particles through ultrashort laser cavities. These channels are about 100x smaller than previous laser microcavities used for studying biological cells.

- We designed a mask set for nanometer-scale channels to be fabricated by lithography for transporting submicron organelles, pathogens, and macromolecules through laser cavities.
- We performed inductively coupled etching experiments on glass. We determined limits of mask selectivity, etch chemistry, and etch rates for 10–1000 nm channel structures.
- We compared Ar+ milling and CHF_3 etching and determined conditions for optically smooth surfaces.

- We fabricated nanochannels to transport virus particles through ultrashort laser cavities.
- We performed flow experiments using bacterial virions. We observed modulation of the noise spectrum of the bare cavity modes and ruled out the possibility of direct virion-supported lasing modes.
- We performed coherent and incoherent light-scattering measurements to determine the magnitude of the scattered intensity from virions and other nonbiological submicron particles.
- We carried out FD time-domain calculations to determine the transition from Rayleigh to Mie scattering near 200 nm.
- We predicted that virions act primarily as a loss mechanism to modulate the cavity lasing modes as observed in the experiments.
- We predicted that the scattering loss scales quadratically with virion size.

69162

Solution Behavior of PEO: The Ultimate Biocompatible Polymer

J. G. Curro, A. L. Frischknecht

Poly(ethylene oxide) (PEO) is the quintessential biocompatible polymer. Due to its ability to form hydrogen (H) bonds, it is soluble in water and yet is uncharged and relatively inert. It is being investigated for use in a wide range of biomedical and biotechnical applications, including the prevention of protein adhesion (biofouling), controlled drug delivery, and tissue scaffolds. PEO has also been proposed for use in novel polymer hydrogel nanocomposites with superior mechanical properties. However, the phase behavior of PEO in water is highly anomalous and is not addressed by current theories of polymer solutions. The effective interactions between PEO and water are very concentration dependent, unlike other polymer/solvent systems, due to water-water and water-PEO H bonds. An understanding of this anomalous behavior requires a careful examination of PEO/water mixtures on the molecular level. Sandia will perform massively parallel (MP) molecular dynamics (MD) simulations on PEO in water. We will use a new method developed at Sandia to extract the so-called Flory chi parameter, *a measure of the interactions, as a function of concentration and temperature. We will also examine the H bond network and its effects on the phase behavior. Based on our improved understanding, we will develop new theoretical models of PEO/water-solution behavior with predictive capability. This work will enable better design of PEO coatings and gels for a wide variety of biological and materials applications. Ultimately, it will shed light on many scientific questions involving macromolecule-water interactions, including protein folding. We will also examine the influence of an applied electric field on the structure and phase behavior of aqueous PEO solutions and melts.*

We performed MD simulations on PEO liquids with and without partial charges. We performed corresponding polymer reference interaction site model (PRISM) calculations on PEO liquids without charges. We found very good agreement of the pair correlations between the theory and simulation. Furthermore, when the charges were turned on, MD simulations showed large changes in the packing relative to the uncharged case. This is in contrast to earlier calculations on poly(dimethyl siloxane).

We developed an analytical theory to describe the thermodynamics of polymer solutions in the presence of an electric field. Of particular interest was to see if an electric field could shift the coexistence curve. We modified the Flory-Huggins theory by including an electric-field term in the free energy. Shifts in the phase diagram were related to concentration fluctuations between solvent and polymer having different dielectric constants. We found concentration fluctuations to be small except near the critical point. Therefore, our theory predicts that indeed the coexistence curve can be shifted by an applied external field in the neighborhood of the critical point. MD simulations are under way to test this prediction.

We developed an analytical theory to describe the thermodynamics of polymer solutions in the presence of an electric field.

69163

New Self-Assembled Nanocrystal Micelles for Biolabels

H. Fan, C. J. Brinker, T. J. Boyle

The ability of semiconductor nanocrystals (NCs) to display multiple (size-specific) colors simultaneously during a single, long-term excitation holds great promise for their use in fluorescent bio-imaging. The main challenges of using NCs as biolabels are achieving biocompatibility, low nonspecific adsorption, and no aggregation. In addition, functional groups that can be used to further couple and conjugate with biospecies (proteins, deoxyribonucleic acids [DNAs], antibodies, etc.) are required. In this project, Sandia invented a new route to the synthesis of water-soluble and biocompatible NCs. Our approach is to encapsulate as-synthesized, monosized, hydrophobic NCs within the hydrophobic cores of micelles composed of a mixture of surfactants and phospholipids containing head groups functionalized with polyethylene glycol (-PEG), carboxylate (-COOH), and amine ($–NH_2$) groups. PEG provided biocompatibility, and we used the other groups for further biofunctionalization. The resulting water-soluble metal and semiconductor NC micelles preserve the optical properties of the original hydrophobic NCs. For semiconductor NCs, they emit the same color; they exhibit equal photoluminescence (PL) intensity under long-time laser irradiation (one week); and they exhibit the same PL lifetime (30 ns). The results from transmission-electron microscopy (TEM) and confocal fluorescent imaging indicate that water-soluble semiconductor NC micelles are biocompatible and exhibit no aggregation in cells.

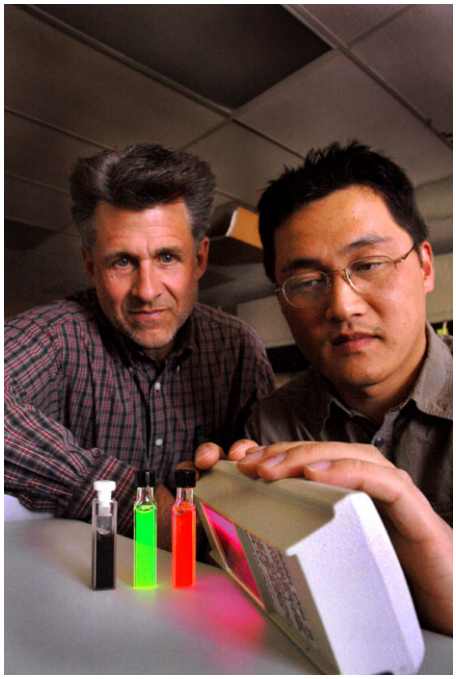

Jeff Brinker (left) *and Hongyou Fan observe satisfactory fluorescence by their well-trained nanocrystals in water solution. The dark vial holds gold nanocrystals; the orange and green are semiconductor nanocrystals.*

We have the preliminary results of the synthesis of new self-assembled NC micelles for biolabels. Our concept is to consider monosized, organically passivated NCs as hydrophobic molecules that, if introduced into aqueous media containing amphiphilic surfactants or phospholipids, can be incorporated into the hydrophobic micellar interior to create a water-soluble NC micelle. The uniform NC size and self-assembled monolayer (SAM)-like nature of its surface result in the formation of monosized NC micelles composed of an NC core and a hybrid bilayer shell with precisely defined primary- and secondary-layer thicknesses. To achieve biocompatibility, we used phospholipids to encapsulate gold (Au) and cadmium selenide (CdSe)/cadmium sulfide (CdS) NCs. In studying the ultraviolet-visible (UV-vis) spectra of alkanethiol-stabilized Au

Sandia invented a new route to the synthesis of water-soluble and biocompatible NCs.

Ncs and those water-soluble Au NC micelles prepared by using different surfactants and phospholipids (C8/GC8-lipids), we observed no difference in the position and width of surface plasmon resonance bands (~ 520 nm). This suggests that after encapsulation the water-soluble Au NC micelles remain monodisperse in water.

Based on the successful results from the encapsulation of Au NCs (model system), we applied the same concept to the synthesis of water-soluble semiconductor NCs. We first synthesized CdSe/CdS core-shell–structured Ncs using Oleylamine as the stabilizing agent in a thermal process. We performed encapsulations by using cetyltriethylammonium bromide and lipids. We confirmed the formation of individual CdSe/CdS NC micelles (as opposed to aggregated dimers, trimers, etc.) by UV-vis spectroscopy, where we observed no difference in the position or width of the absorbance bands at ~ 480 nm and ~ 590 nm. Studies of photostability of these water-soluble NC micelles under long-time laser irradiation show that these NC micelles exhibit no loss of PL intensity in water for at least a week.

We measured the PL lifetime of surfactant-/lipid-encapsulated CdSe/CdS NC micelles in comparison to hydrophobic CdSe/CdS and organic dye (Rhodamine B). The Rhodamine B persistence is only slightly longer than the instrumental bandwidth. The loge plots of the persistence curves from the CdSe/CdS in toluene and C8-lipid encapsulated NCs water solutions are similar, and both are nearly linear, with a (1/e) relaxation constant of about 30 ns. In comparison, Rhodamine B has a much shorter lifetime of ~ 1.5 ns.

We invented a new method of synthesizing water-soluble NCs through encapsulation of hydrophobic NCs into surfactant/lipid micelles. The resulting water-soluble metal and semiconductor NC micelles preserve the optical properties of the original hydrophobic NCs. For semiconductor NCs, they emit the same color; they exhibit equal PL intensity under long-time laser irradiation (1 wk); and they exhibit the same PL lifetime (30 ns). The results from TEM and confocal fluorescent imaging indicate that water-soluble semiconductor NC micelles are biocompatible and exhibit no aggregation in cells.

Refereed

Fan, H. 2004. Self-assembly and integration of ordered, robust, three-dimensional gold nanocrystal/silica arrays. (Invited) Paper presented at Particles 2004, March, Orlando, Florida.

Fan, H., K. Yang, D. M. Boye, T. Sigmon, K. J. Malloy, H. Xu, G. P. López, and C. J. Brinker. 2004. Self-assembly of ordered, robust, three-dimensional gold nanocrystal/silica arrays. *Science* **304**:567–71.

69164

Rapid Detection of Biothreat Agents Based on Cellular Machinery

T. W. Lane, R. W. Gantt

Sandia will address rapid and sensitive identification of biological agents in a complex background. We will use the specificity of the cellular transcriptional machinery to detect and identify bacterial bioterror agents in a background of other organisms. Bacterial cells contain ribonucleic acid (RNA) polymerases that transcribe genes into mRNA (messenger RNA) for translation into proteins. RNA polymerases recognize regulatory elements (promoters) upstream of the gene. Promoters are, in many cases, recognized by the polymerases of one species only.

We will engineer a plasmid (circular self-replicating deoxyribonucleic acid [DNA]) for Escherichia coli (E. coli) *that contains promoters from target species* (Bacillus cereus [B. cereus]) *and* Pseudomonas aeruginosa [P. aeruginosa]). *We will fuse individual promoters to different reporter genes. We will fuse the* B. cereus *promoter to GFP (green fluorescent protein), and the* P. aeruginosa *promoter to YFP (yellow fluorescent protein). We will mix the indicator strain (carrying the plasmid) with the target strain and lyse the two. The cellular machinery from both cells mixes and produces the appropriate color protein (green for* B. cereus, *yellow for* P. aeruginosa).

One advantage of this system over polymerase chain reaction (PCR) is that it is not dependent on the presence of specific primer sites but instead on required pieces of cellular machinery that are difficult to alter by genetic engineering (RNA polymerases); GFP fusions can be detected at a single-cell level. Our limit of detection would depend on the bulk lysis volume. The method could be adapted to a microfluidic system, limiting the lysis volume and increasing sensitivity. In a microfluidic system, we should readily detect approximately 10–50 organisms.

We identified a set of transcription factors (MxiE and IpgC) in the pathogen *Shigella flexneri* (*S. flexneri*) that were necessary for the expression of a series of genes including the gene virA. These genes were found only in *S. flexneri* and not in the closely related species *E. coli*. We obtained a plasmid containing a fusion of the virA promoter region to a GFP reporter gene. It was reported in the literature that when this plasmid was introduced into shigella, GFP was produced if the transcription factors MxiE and IpgC were present in the cell.

We decided to use this virA::GFP fusion plasmid as our test plasmid to see if we could detect the presence of the transcription factors. We cloned the genes encoding MxiE and IpgC into *E. coli* expression vectors so that they could be overexpressed in *E. coli*. We grew strains of *E. coli* containing the expression vectors to mid-log phase and induced expression. We then harvested these cells and added them to cells from a mid-log culture of the strain containing the virA::GFP fusion. We then lysed the cell mixture and monitored the production of GFP in a fluorometer for several hours. We carried out a similar experiment in which the virA::GFP fusion strain was mixed with *S. flexneri* treated with Congo Red, which induces expression of MxiE and IpgC. That mixture was also lysed, and we monitored the production of GFP in the same manner as above. We were unable to detect production of the GFP fusion protein in lysates containing Congo Red–grown *S. flexneri*, which indicated a severe limitation of this technique as a means of detecting and identifying bacterial agents.

69165

Patterning Quantum-Dot Arrays Using DNA Replication Principles

G. D. Bachand, K. K. Crown

The convergence of nanoscience and biotechnology has opened the door to the integration of a wide range of biological molecules and processes with synthetic materials and devices. A primary biomolecule of interest has been deoxyribonucleic acid (DNA), based on its role as information storage in living systems, as well as its ability to withstand a wide range of environmental conditions. DNA also offers unique chemistries and interacts with a range of biomolecules, making it an ideal component in biological-sensor applications. The primary goal of this project was to develop methods that utilize in vitro *DNA synthesis to provide spatial localization of nanocrystal quantum dots (nQDs). To accomplish this goal, Sandia addressed three specific technical objectives: (1) attachment of nQDs to DNA nucleotides, (2) demonstration of the synthesis of nQD–DNA strands in bulk solution, and (3) optimization of the ratio of unlabeled to nQD–labeled nucleotides to produce extended nQD–DNA strands. We successfully attached DNA nucleotides to nQDs using the biotin-streptavidin linkage. Initially, we demonstrated synthesis of 450 nm-long, nQD–coated DNA strands using a circular DNA template and the polymerase chain reaction (PCR) method of DNA amplification.*

We successfully attached DNA nucleotides to nQDs using the biotin-streptavidin linkage.

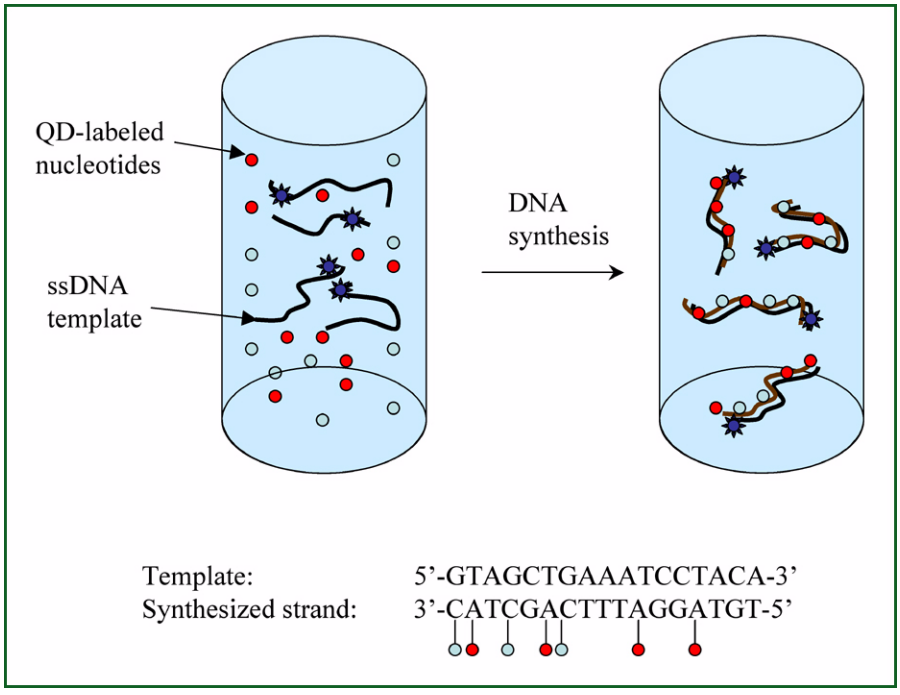

Strategy for patterning QDs (quantum dots) using DNA replication.

To increase the length of the nQD–DNA strands, we varied and evaluated the ratio of unlabeled to nQD–labeled DNA nucleotides. We also modified the PCR amplification methodology such that nQD-DNA strands would be synthesized in a "one-step" process. These modifications enabled the synthesis of 2 µm-long, linear nQD–DNA assemblies, which were characterized by epifluorescence microscopy. In summary, proof-of-principles experiments demonstrated the successful synthesis of patterned nQD arrays using DNA replication technologies. Continued development of this technology will enable rapid, spatial patterning of semiconductor nanoparticles with nanometer resolution, as well as optically active probes for DNA and other biomolecular analyses.

We focused on demonstrating the synthesis of patterned arrays of nQDs using DNA templates and *in vitro* replication technologies. We addressed three specific technical objectives: (1) attachment of nQDs to DNA nucleotides, (2) demonstration of the synthesis of nQD–DNA strands in bulk solution, and (3) optimization of the ratio of unlabeled to nQD–labeled nucleotides to produce extended nQD–DNA strands. Overall, we made excellent progress.

In terms of the first technical objective, we successfully developed a methodology for coupling nQDs to deoxycytidine DNA nucleotides (dCTPs) using biotin-streptavidin linkage. We purchased both the biotinylated dCTP and streptavidin-coated nQDs from commercial vendors. In the first step, we prepared varying ratios of streptavidin-coated nQDs to biotinylated dCTP (e.g., 1/16,000, 1/19,000, and 1/50,000) in a solution of 20 mM Tris-HCl (pH 8.4), 50 mM KCl, and 5 mM $MgCl_2$**.** We then incubated samples at room temperature for 30 min with gentle shaking. Subsequent experiments demonstrated successful coupling of biotinylated dCTPs to nQDs.

The second objective focused on demonstrating nQD–DNA synthesis in bulk solution. We utilized a circular DNA plasmid that contained the coding sequence for a monomeric kinesin as the DNA template in these experiments. The synthesis strategy exploited the PCR method of DNA amplification to synthesize the nQD–DNA strands. Based on the size of an individual DNA nucleotide (i.e., 3.4 Å), the predicted size of the amplified nQD–DNA strands should have been approximately 450 nm. Epifluorescence microscopy confirmed the synthesis of nQD–DNA strands using this method. We observed short (less than 1.0 µm in length), irregular arrays of nQDs by fluorescence microscopy, while control samples without DNA templates, oligomer primers, and/or nQD-dCTP did not show any similar

types of nQD assemblies. We also separated nQD-DNA samples by agarose gel electrophoresis and confirmed the synthesis of 1.3 kilobase nQD–DNA strands that fluoresced under ultraviolet light. Thus, these initial experiments successfully demonstrated the ability to synthesize nQD–DNA strands using *in vitro* DNA replication techniques.

The final technical objective was to optimize the ratio of unlabeled to nQD–labeled nucleotides to produce extended linear strands of nQD–DNA. We adjusted the PCR methodology, starting concentration of DNA template, and ratio of streptavidin-coated nQD–dCTPs to unlabeled dCTPs to achieve this goal. We evaluated five ratios of streptavidin-coated nQD–dCTPs to unlabeled dCTPs: 1:10, 1:20, 1:30, 1:40, and 1:520. Based on the modifications, we expected nQD–DNA strands of 2 μm in length using the selected 5869-base pair DNA template. Epifluorescence microscopy demonstrated the synthesis of linear nQD–DNA strands of ~ 2 μm in length. These linear assemblies were most prevalent in samples in which the ratios of streptavidin-coated nQDs to biotinylated dCTP and streptavidin-coated nQD–dCTPs to unlabeled dCTPs were 1/50,000 and 1:520, respectively.

In summary, we achieved our critical technical objectives. Key methodologies and proof-of-principle experiments established a core technology for synthesizing patterned arrays of nQDs using DNA templates and replication techniques.

69166

Adaptive Algorithms for Use in the Rejection of Periodic Disturbances of Unknown Frequency

E. S. Hertel, Jr.

Sandia is studying the development and use of new adaptive algorithms for use in the rejection of periodic disturbances of unknown frequency. The particular area of application involves problems encountered in active noise cancellation and vibration control. The topics to be explored involve the application of adaptive cancellation algorithms to systems with resonant modes as well as the pursuit of more globalized cancellation. This involves the use of multi-input, multi-output, adaptive disturbance-rejection algorithms. Exploration of various higher-order input/output configurations will build upon research already begun at the University of Utah. Also, we will examine the cancellation of disturbances consisting of rapidly time-varying frequency.

We investigated algorithms for the rejection of periodic disturbances through an active noise-control (ANC) system. Both the algorithms and the ANC system were developed at the University of Utah. The algorithms were designed for the rejection of periodic signals of unknown frequency. They require that the plant P(jw) be known, where P(jw) consists of the dynamics from the control sources to the error sensors, including analog-to-digital converter forward scattering (ADCs), digital-to-analog converter forward scattering (DACs), amplifiers and filters, and any delay effects from propagation through the air. P(jw) was identified by the method of empirical transfer function estimate (ETFE). We then used this estimate to explore the robustness and the performance of the adaptive disturbance-rejection algorithms through both single-channel and multichannel ANC experiments.

One measure of the performance of the algorithms was the attenuation of the error signal observed by engaging the controller. In the case of a single-channel ANC, we observed an attenuation of 97%. Multichannel cancellation allows for the establishment of “quiet zones” in which the disturbance is considerably suppressed. We explored both square (m=n) and nonsquare plant configurations (m≠n), where P(jw) is an m x n matrix with m and n defined as the number of error sensors and control sources, respectively. In the case where m < n, we observed as much as 97% attenuation of the error. When m > n, one has more error sensors than canceling loudspeakers. Since

the behavior of the system is such that cancellation occurs mainly in the vicinity of the error sensors, we attained a slightly decreased attenuation of 93%. In addition, we investigated noise disturbances consisting of harmonically related components. We observed a 97% attenuation of the error signal when the disturbance consisted of a fundamental and second harmonic component.

A crucial component in the rejection of periodic disturbances of unknown frequency is frequency estimation. A phase-locked loop approach to online frequency estimation was shown to work in conjunction with the disturbance-rejection algorithms through both single-channel and multichannel experiments. Also, we explored the ability to track time-varying disturbances. We varied the disturbance frequency from 180 Hz to 205 Hz in 6.5 s, and a mean tracking error of 0.68 Hz resulted while we observed excellent attenuation results. The ability to deal with disturbances of time-varying amplitude was an inherent quality of the adaptive algorithms being explored. The thorough investigation of the case of unknown frequency but known plant laid the foundation for the exploration of the case of known frequency but unknown plant. This naturally leads to the novel investigation of the case where both the frequency and plant are unknown.

We effectively designed, simulated, and implemented systems for the control of 5- and 6-degree-of-freedom robot manipulator arms. This included parameterization of the robot, trajectory planning, calculation of the kinematic angles needed to accomplish a given endpoint, and feedback controller design.

We effectively designed, simulated, and implemented systems for the control of 5 and 6 degree-of-freedom robot manipulator arms.

69168

Property-Based Testing for Cybersecurity Assurance

N. A. Durgin

Property-based testing is a technique for testing the security of programs. Secure means conforming to a security policy. The analyst doing the testing first specifies the properties for which he/she wishes the program to conform. The program is then instrumented, based on the specification of the properties. Consider the execution of the program as a state machine, where the state of the program changes as each instruction is executed. Relevant changes affect only those portions of the state used in the properties. The instrumentation produces output whenever such a change occurs. The program is then executed under control of another program called the test-execution monitor *(TEM). The TEM is given the properties, and whenever the execution enters a state forbidden by the specified properties, the TEM reports a security error.*

These properties are written in a little language called TASpec that has constructs designed to aid testing. These include (1) location specifiers, which specify specific places in the program where the properties hold, or where the state of the executing program will change; (2) assertion statements, which assert that a certain property now holds; (3) retraction statements, which assert that a certain property no longer holds; and (4) temporal relationship operators, which specify whether something occurs before or after something else, or should occur and hold for the rest of the execution.

One goal of this project was to produce a library of properties that the analyst can extract, instantiate against the program under test, and use. Sandia succeeded in developing properties for several common problems, notably buffer overflows, race conditions, and inadequate authentication.

The second goal was to determine how well TASpec could be integrated with a model-checking language. We examined the model-checking language LTL because that language is being used in an allied project, and we hoped to be able to apply our work to a tool that had been checked using that model.

Sandia succeeded in developing properties for several common problems, notably buffer overflows, race conditions, and inadequate authentication.

The research began with an examination of other testing and specification languages. During this phase, it became clear that some of TASpec's predicates and temporal operators were not well specified, so we focused on that. We compared the language with the specification patterns used for finite-state

specifications at Kansas State University that summarize features of specification languages. For concreteness, we focused on LTL. This led to us define certain terms, like “until,” more precisely, and derive ways to express other forms of “until” in TASpec.

Consider “until” as an example. If one writes “A until B,” does that mean A holds until B holds, and from that point on A can no longer hold; or does it mean that, after B, it is immaterial whether or not A holds? We refined the definition of “until” in TASpec and showed how to express the alternate form in terms of TASpec operators.

This led us to consider the relationship between model-checking and property-based testing. During high-assurance development, the design of the software is tested using a technique called “model checking.” We construct a model of the software, write desired properties in a specific model-checking language, and validate the model using automated tools. A project being done at the National Aeronautics and Space Administration (NASA) is using the LTL language to validate a model of a software system. The next step would be to verify that corresponding properties hold in the implementation, leading us to ask if the properties expressed in LTL could be translated, or somehow mapped, into properties expressed in TASpec. So we examined the LTL constructs and showed how many can be translated into TASpec.

The next phase was to produce a library of properties that a testing analyst can extract, instantiate against the program under test, and use. This is important because most analysts will not be skilled in writing properties using TASpec. Further, certain properties (e.g., a property to test for buffer overflow) will be used over and over. Creating such a set of properties would also demonstrate the completeness of the TASpec language, or show deficiencies that should be remedied by altering or expanding the language. In this phase, we examined a collection of common vulnerabilities in programs and developed specifications for several common problems.

69170

Self-Assembled Ordered Carbon-Nanotube Arrays and Membranes

M. P. Siegal, W. G. Yelton

Imagine free-standing flexible membranes with highly aligned arrays of carbon nanotubes (CNTs) running through their thickness, perhaps with both ends of the CNTs open for highly controlled nanofiltration, or CNTs at heights uniformly above a polymer membrane for a flexible array of nanoelectrodes or field-emitters. How about CNT films with incredible amounts of accessible surface area for analyte adsorption? These self-assembled crystalline nanotubes (NTs) consist of multiple layers of graphene sheets rolled into concentric cylinders. Tube diameters (3–300 nm), inner-bore diameters (2–15 nm), and lengths (nanometers–microns) are controlled to tailor physical, mechanical, and chemical properties. Sandia seeks to grow and characterize NT arrays and explore their exciting functionality for Sandia applications. Thermal chemical vapor deposition (CVD) growth in a furnace nucleates from a metal catalyst. Ordered arrays grow using templates from self-assembled hexagonal arrays of nanopores in anodized-aluminum oxide (AAO). Polymeric binders can mechanically hold the CNTs in place for polishing, liftoff, and membrane formation.

The stiffness and the electrical and thermal conductivities of CNTs make them ideally suited for a wide variety of possible applications. Large-area, highly accessible gas-adsorbing carbon (C) surfaces, superb cold-cathode field emission, and unique nanoscale geometries can lead to advanced microsensors using analyte adsorption, arrays of functionalized nanoelectrodes for enhanced electrochemical detection of biological/explosive compounds, or mass ionizers for gas-phase detection. Materials studies involving membrane formation may lead to exciting breakthroughs in nanofiltration/ nanochromatography for the separation of chemical and biological agents. With controlled nanofilter sizes, ultrafiltration will be viable to separate and preconcentrate viruses and many strains of bacteria for "downstream" analysis.

This ambitious project had three main goals. First, we were to fabricate AAO templates from the deposition of thick aluminum (Al) films on silicon (Si) substrates. Second was the determination of spacing methods for the growth of CNTs on a substrate surface. Many potential applications require

significant spacing between individual CNTs. Third was the growth of CNT arrays in AAO templates, to be followed by CNT membrane fabrication.

No other group has reported the growth of several-micron-thick Al films on any substrate, due to the development of high residual stress and rough film morphology, not to mention using them for conversion into AAO. However, we learned to grow such thick, mirror-smooth films by using a thin adhesion layer, rare-earth doping, and unique radio-frequency (RF) sputter-deposition conditions that greatly lower the kinetic energy of the depositing species, effectively eliminating the development of residual stress. This room-temperature, stress-free physical deposition of Al has many other potential applications to create AAO templates for extremely high-aspect-ratio CNTs and nanowires of other materials. In addition, we extended the method to other elemental films, such as C for nanoporous-C growth for sensor applications, boron (B) for thick films for neutron detection, and tungsten (W) and iridium (Ir) metals for various other projects.

No other group has reported the growth of several-micron-thick Al films on any substrate....However, we learned to grow such...films....

In addition, we showed that stress-free Al films can be anodized very uniformly and that the lateral dimensions of pore development are not dependent on the thickness of the Al film. This provides independent control of the template length for CNT/nanowire growth from other growth parameters controlling diameters, spacings, etc. A new project and other new collaborations have already resulted from this achievement alone.

We identified two complementary methods to control the spacing between CNTs on a substrate surface as a function of growth conditions without any additional processing. Combined, they yield more than 4 orders-of-magnitude of control over CNT areal site density. The first method shows that the site density varies with the heat of formation of the hydrocarbon gas using during CNT growth by CVD. The second method demonstrates that the site density decreases with increasing residual stress of the metal catalyst/diffusion barrier layers. This latter method is possible only by our understanding the mechanism to relieve metal stress during sputter deposition, as described above.

We only partially completed the final major milestone. For the first time, we electrochemically deposited nickel metal catalysts into AAO templates grown on Si substrates. Previously, only bulk AAO templates were used because of the inability (which we have overcome) to grow thick, mirror-smooth Al films. Initial studies of CNT growth into these templates are promising, but are incomplete at this time.

Clearly, this also prevents our attempt to create free-standing CNT membranes. Given how close the project came to full fruition, it is likely that these final milestones will be achieved shortly after the end of this project.

Refereed

Siegal, M. P., and D. L. Overmyer. 2004. Controlling the site density of carbon nanotubes on a substrate surface via growth methods. Paper presented at the Electrochemical Society Meeting, May, San Antonio, Texas.

Siegal, M. P., D. L. Overmyer, and F. H. Kaatz. 2004. Controlling the site density of multiwall carbon nanotubes via growth conditions. *Applied Physics Letters* **84** (225) (21 June): 5156–58.

69189

Chemical Cross-Linking and Mass-Spectrometry Studies of the Structure and Dynamics of Membrane Proteins and Receptors

J. S. Schoeniger, W. E. Haskins, M. D. Leavell, P. Novak, P. Lane, R. B. Jacobsen, Y. K. Light, M. Z. Hadi, J. Hong, N. L. Wood, M. J. Ayson

Membrane proteins (MPs) are of compelling interest because of their role as receptors for viruses and cell-signaling molecules. Traditional structural biology tools (x-ray and nuclear magnetic resonance [NMR]) do not work well for most MPs. Thus, it is difficult to obtain the structures necessary to produce effective countermeasures for threat such as autoimmune deficiency syndrome (AIDS), smallpox, or potential bioagents such as peptide bioregulators. The Interfacial Bioscience Grand Challenge (IBIG) project previously created integrated analytical and computational tools that allow the development of new approaches to problems in membrane biology. Specifically, Sandia demonstrated that chemical cross-linking and probes of protein surface reactivity, combined with modern mass-spectrometry (MS) methods, can be used to measure interatomic distances in MPs.

The results of IBIG indicated that it may be possible to use MS3D (MS in three dimensions) methods to probe dynamics and conformational changes in the protein structure, and to derive the structure of protein-protein complexes. We used the protein rhodopsin as a test system for development of analytical and modeling methods. We used x-ray data and computational modeling of rhodopsin to test our hypotheses and also began to test these methods against other mammalian proteins, such as human glycine receptor.

Our work allowed us to begin to resolve three significant issues that arose regarding the discovery and interpretation of cross-links in MPs. First, the exact residues that are cross-linked may be ambiguous. We implemented new MS methods able to resolve them (Fourier-transform mass spectrometry with electron capture dissociation [FTMS/ECD], quadrupole time-of-flight tandem MS [QToF/MS/MS]). Second, the presence or absence of cross-links is due to a combination of residue reactivity and interresidue distances. We developed quantitative pulse-chase methods for mapping the reactivity of individual cysteine and lysine residues to allow this to be accounted for. Finally, there is substantial controversy over the interpretation of observed cross-links and their relation to interresidue

distances. We developed and are testing a new model and experimental strategy that relates the rates of cross-link formation to interresidue distances.

The MS3D method for measuring distance constraints between residues in protein involves exposing the proteins to cross-linking reagents, proteolytically digesting them, and then identifying cross-linked peptides using liquid chromatography (LC)/MS. The focus of our work was to apply this method to a model MP, rhodopsin, to enable MS3D to be implemented as a means for measuring structure and conformational changes in MPs.

Previous work carried out under the IBIG Grand Challenge project established basic infrastructure and methods for MS3D. We discovered multiple cross-links that formed between residues in rhodopsin. However, many of these cross-links were ambiguous, and we could not resolve the residues involved using standard MS techniques. We implemented a newly developed MS method, QFTMS/ECD, to resolve which residues were cross-linked in the large peptides produced by CNBr digest of rhodopsin. We were the first to demonstrate that this technique could resolve such covalent cross-links. Recently, we also showed that combined tryptic/CNBr digests of cross-linked rhodopsin can be assigned despite their inherent complexity, and we implemented data-dependent MS/MS (tandem MS) techniques on our QToF instrument, which allows unambiguous assignment of smaller cross-linked species and very high sensitivity.

The presence or absence of cross-links between residues on rhodopsin must be explained in terms of the distance between residues on rhodopsin as well as their intrinsic reactivity. We developed methods to explore the impact of both of these factors. Systematic comparison of all observed cross-links with the interresidue distances in the crystal structure, taking into account side-chain mobility using molecular dynamics (MD) and Monte Carlo (MC) methods, allowed us to establish that all observed cross-links are compatible with the x-ray structure, ruling out the idea that they require substantial distortion of the structure to form. We also developed a pulse-chase method for measuring the pseudo-first-order rate constants for the reactivity of lysine and cysteine residues with cross-linkers. We demonstrated this method on model peptides, and applications to rhodopsin are under way.

Review comments by others indicate that, while one part of the structural biology community is enthusiastic about our approach, another part of the community does not believe cross-

link formation to be informative about structure. To satisfy these criticisms, we developed a new paradigm for interpreting cross-link formation in terms of structure. Previously, the observation of a cross-link was taken to imply a certain distance constraint between the reacting atoms. We developed a simple kinetic model based on polymer theory that shows that the relative rate of reaction of cross-linkers in a homologous structural series can be related to the distance between the alpha carbons of the reacting residues, in a manner similar to the way that fluorescence resonance energy measurements are used to measure distances in proteins. Experiments are currently under way to validate this theory in test peptides and refine experimental strategies for measuring cross-linking reaction rates.

...we developed a new paradigm for interpreting cross-link formation in terms of structure.

Refereed

Fujii, N., R. B. Jacobsen, N. L. Wood, J. S. Schoeniger, and R. K. Guy. 2004. A novel protein cross-linking reagent for the determination of moderate-resolution protein structures by mass spectrometry (MS3-D). *Bioorganic and Medicinal Chemistry Letters* **14** (2) (January): 427–29.

Novak, P., W. E. Haskins, M. D. Leavell, M. J. Ayson, M. M. Young, J. S. Schoeniger, and G. H. Kruppa. 2004. Single-residue resolution of cross-link positions using ECD-FTMS. Paper presented at the American Society for Mass Spectrometry Conference, May, Nashville, Tennessee.

69190

Toxin Studies Using an Integrated Biophysical and Structural Biology Approach

J. S. Schoeniger, P. Lane, J. M. Gaudioso, A. L. Slade, A. R. Burns, J. S. Brennan

The clostridial neurotoxins (botulinum and tetanus) are among the most toxic substances in the world. Botulinum toxins (BoNTs), in particular, have a history of association with state-sponsored biowarfare and bioterrorism and are Center for Disease Control (CDC) category A bioterror agents. For these neurotoxins to destroy cell function, they must breach the cellular membrane and enable a catalytic domain to enter the cytosol, where it destroys the activity of proteins responsible for the vesicle transport of neurotransmitters. A basic understanding of the molecular mechanism of cell-membrane penetration by BoNTs is still lacking and is needed to facilitate effective countermeasures against its use as a bioterror agent. The goal of this project is to develop tools to characterize the mode of binding, insertion, pore formation, and translocation of the catalytic domain of clostridial neurotoxins on model cell membranes. These tools are designed to yield complementary information at the macro- and nanoscale. The use of model membranes will allow precise control of the factors affecting membrane interactions.

Currently, it is believed that clostridial neurotoxins act first through recognition of gangliosides on the cell surface, followed by internalization via lysosome formation. The lysosome's pH is then lowered via proton pumps triggering the injection of the toxin's light chain into the cell and catalyzing the disruption of neurotransmitter transport. Sandia made efforts to clarify some issues in the first part of this process that involve ganglioside recognition/membrane binding of the neurotoxin and the pore formation driven by pH change. We examined tetanus toxin binding and subsequent pore-formation studies on lipid membranes through a combination of lipid vesicle (liposome) leakage studies and atomic-force microscopy (AFM) imaging of supported lipid bilayers.

Cell membranes are a complex mixture of lipids, steroidal molecules, proteins, and gangliosides. In an effort to elucidate the mechanism of tetanus toxin binding and permeation through the membrane, we developed a simple yet representative model that consisted of the ganglioside GT1b incorporated into a bilayer of cholesterol and DPPC (dipalmitoylphosphatidyl choline). The bilayers were stable over time, yet sensitive to the

binding and activity of whole toxin. We used liposome-leakage studies at constant and gradient pH to elucidate the effect of pH on the toxin's membrane binding and permeation capability. Additionally, topographic imaging via *in situ* AFM provided detailed characterization of the toxin's binding location and pore-formation activity.

For the leakage studies, we prepared Texas Red (50 mM) encapsulated liposomes (50% DPPC/cholesterol, 200 nm diameter), with and without GT1b, by extrusion. We placed the liposomes in either pH 7 or pH 4 HEPES/MES (N-[2-Hydroxyethyl]piperazine-N′-[2-ethanesulfonic acid]/2-[N]-Morpholino]ethanesulfonic acid) citrate buffer and added whole tetanus toxin (*Clostridium tetani*) at concentrations between 8 and 166 nM. The fluorescence intensity of Texas Red was constant within the pH range of 4–7. We monitored dye leakage via fluorescence over a time period of 33 min. To generate the pH gradient, we added 0.1N HCl after an initial incubation time of 10 min with the toxin. We then collected the fluorescence after the HCl addition. In control experiments, the liposomes, both with and without GT1b, leaked only 4% of the entrapped dye over the experimental time.

In the presence of whole toxin (83 nM), the dye release was greatest in experiments with the pH gradient from 7 to 4, with a 35% release of the total entrapped. At constant pH 7, we observed less but still significant membrane leakage at 22% of entrapped dye, whereas at pH 4 only 8% was released. These results suggest that the toxin binds to the membrane surface at pH 7, and its pore-forming activity increases with the lowering of solution pH. However, at low initial solution, pH binding and permeation were inhibited.

We successfully obtained AFM images of a 10% GT1b/45% DPOPC (dipalmitoleoylphosphatidylcholine)/45% DPPC-supported lipid bilayer on mica incubated with a tetanus toxin C fragment at pH 7. The 3-D image shows that the protein tends to bind in the fluid-phase areas of the DPOPC, where we also observed pore formation to occur. We are progressing toward imaging of whole toxin on GT1b/cholesterol/DPPC bilayers with the pH gradient to monitor toxin superstructure formation and pore generation in the membrane.

We successfully obtained AFM images of a 10% GT1b/45% DPOPC (dipalmitoleoylphosphatidylcholine)/45% DPPC-supported lipid bilayer on mica incubated with a tetanus toxin C fragment at pH 7.

Refereed

Hibbard, A. E., A. Slade, and D. Y. Sasaki. 2004. Elucidating the binding and penetration of tetanus neurotoxin to lipid membranes. Paper presented at the International Symposium on Securing High-Consequence Pathogens and Toxins, 1–6 February, Albuquerque, New Mexico.

Hibbard, A. E., A. Slade, and D. Y. Sasaki. 2004. Investigation of tetanus toxin adsorption and disruption of lipid membranes via leakage studies. Paper presented at the 228th ACS National Meeting, 22–26 August, Philadelphia, Pennsylvania.

Slade, A., A. E. Hibbard, C. M. Yip, and D. Y. Sasaki. 2004. High-resolution imaging of tetanus toxin on lipid bilayers via *in situ* scanning probe microscopy. Paper presented at the 228th ACS National Meeting, 22–26 August, Philadelphia, Pennsylvania.

69191

Top-Down Structural Studies

G. H. Kruppa, J. Hong, A. M. Highley, P. Novak, C. C. Langley

High-throughput protein-structure determination efforts rely on multidimensional nuclear magnetic resonance (NMR) and x-ray crystallographic methods. These methods provide detailed, high-resolution protein structures. However, x-ray crystallography requires single crystals of a protein, which are often difficult or impossible to grow. NMR requires milligrams of protein, which must be soluble in an NMR-compatible solvent system, and NMR investigations are currently limited to proteins of ~ 30 kDa or less. Membrane proteins are particularly difficult to study by either technique.

Intramolecular chemical cross-linking followed by mass spectrometric analysis was recently shown to have potential as a new method for obtaining distance constraints in proteins. The advantages of this method, known as MS3D*, include the ability to work with small amounts of protein without the need for single crystals. Initial experimental results from the protein structure group of the Interfacial Biosciences Grand Challenge Project (IBIG) show that cross-link–based distance constraints can be obtained for rhodopsin, a membrane protein with seven transmembrane helices.*

Despite the initial report indicating the potential of MS3D, current methods are labor-intensive, and the number of distance constraints reported using this method remains small. Several publications indicate that the cross-linking chemistry may be difficult to optimize, and the method is further complicated by the difficulty of using proteolytic digestion and high-pressure liquid chromatography–mass spectrometry (HPLC–MS) to localize the cross-links. During the IBIG project, Sandia published and submitted for patent a whole-protein approach, the top-down method, using Fourier-transform MS (FTMS). This method allows us to optimize cross-linking chemistry and to localize the cross-links using MS^n *fragmentation analysis rather than proteolytic digestions. We will develop this method as a protein-structure determination tool and improve its data throughput. If successful, it can be used to determine membrane protein structure using the MS3D method.*

We pursued two principal hypotheses. The first is that multiple chemical approaches for forming covalent cross-links within proteins would be useful for defining structural constraints and obtaining structural information about the protein. The second is that FTMS of intact cross-linked protein

proteins, followed by fragmentation of the proteins within the FTMS (so-called “top-down methods”) could be used to optimize these cross-linking chemistries and identify cross-linked amino acids within the proteins, avoiding complex and time-consuming sample-preparation steps.

We partially proved the first hypothesis, in that cross-linking chemistries between acid groups on proteins were implemented with ubiquitin as the target protein. However, efforts to synthesize cross-linking reagents for arginine residues were unsuccessful. We successfully demonstrated the top-down approach for acid-acid and tyrosine-tyrosine cross-linking.

We developed methods that allow the specific chemical cross-linking of acidic amino acids in protein to each other. We found that di-hydrazide cross-linkers in the presence of excess carbodiimides (EDC) at low pH (5.5) form cross-links between glutamate, aspartate, or C-terminal residues. At the higher pHs customarily used (pH 7), we found that competing reactions involving lysine-acid cross-links complicate analysis. We optimized the cross-linking conditions for ubiquitin by electrospray FTMS of the intact internally cross-linked protein monomers. We used fragmentation of the protein in the FTMS with near-infrared (NIR) multiphoton dissociation and/or sustained off-resonance irradiation collision-induced dissociation (SORI-CID) to identify the exact residues cross-linked. We used cross-linkers of varying length, allowing the derivation of limits on distance constraints between residues in ubiquitin.

After determining effective methods for alkylating arginine reagents, we attempted to synthesize di-di-keto reagents as homobifunctional arginine cross-linking reagents. However, it proved impossible within the time scope of this short project to find selective oxidation conditions needed to make these reagents from available starting materials.

69192

Molecular Dynamics of Membrane Proteins

M. J. Stevens, P. S. Crozier

Understanding the dynamics of the membrane protein (MP) rhodopsin (Rho) will have broad implications for other MPs and cellular-signaling processes. Rho is a light-activated G-protein coupled receptor (GPCR). When activated by ligands, GPCRs bind and activate G-proteins residing within the cell and begin a signaling cascade that results in the cell's response to external stimuli. More than 50% of all current drugs are targeted toward G-proteins. Rho is the prototypical member of the class A GPCR superfamily. Understanding the activation of Rho and its interaction with its G-protein can therefore lead to a wider understanding of the mechanisms of GPCR activation and G-protein activation. Understanding the dark-to-light transition of Rho is fully analogous to the general ligand binding and activation problem for GPCRs. This transition is dependent on the lipid environment. The effect of lipids on MP activity in general has had little attention, but evidence is beginning to show a significant role for lipids in MP activity. Using the large-scale atomistic/molecular massively parallel simulator (LAMMPS) program and simulation methods benchmarked under the Interfacial Biosciences Grand Challenge (IBIG) project, Sandia will perform the all-atom molecular dynamics (MD) simulations of MPs.

We performed a 150 ns simulation of Rho after isomerization of the retinal molecule. We compared our final structure to experimental measurements of the LUMI (lumirhodopsin) state. The analysis of the long simulation of Rho after isomerization shows that significant structural changes occur in the 150 ns period. The isomerization results in some of the seven transmembrane helices to undergo tilt-and-kink angle changes that are well beyond their fluctuation range in the equilibrium dark state. One of the key structural changes is the motion of the ionone ring of retinal, which is consistent with cross-linker experiments. We observed a strong energetic transition to occur at 70 ns after isomerization. The majority of the energy of this transition involved breaking the salt bridge between Glu 113 and the protonated Schiff base. Raman spectroscopy shows that the protonated Schiff base stretching modes are indicative of very different Schiff-base environments in agreement with our results.

We compared simulations of isolated helices against the corresponding intact Rho simulation from the level of the entire

helix down to the structural details of the individual residues that make up the helices. These relatively long-time-scale simulations showed that helix characteristics slowly evolve and require a long time to equilibrate. In all seven Rho transmembrane helices, we observed very substantial structural differences between the isolated helix simulations and the intact Rho simulation. The observed differences are due to the unraveling of the untethered ends in the isolated helix simulations and the effects of the rest of the Rho molecule beyond the helix in question, which plays a key role in maintaining helix secondary structure through disulfide bridges, hydrogen-bonding networks, and nonbond interatomic interactions. It does not appear possible to use isolated helix simulations to predict MP helix structures, even if simulated in a native-like lipid environment. We demonstrated that expensive all-atom simulations of idealized individual transmembrane helices give little useful information about native helix conformations. The rest of the protein, with its tertiary structure, is required to enforce the helix secondary structure. Solvent matching alone is a necessary, yet insufficient, condition for tilt-and-kink angle determination or for proper folding.

A key aspect of membranes is control of the electrostatic potential. Ion channels control the ion concentration on both sides of the membrane. The potential gradient that results is fundamental to biomembranes. Because of limitations in the time- and length-scales accessible to all-atom simulations, MD was not used to explicitly model the transmembrane potential gradient. Biologically relevant potential gradients require an ion:lipid ratio on the order of 10^5 atoms—historically too many. A straightforward solution to the periodicity problem is to simulate more than one bilayer per unit cell, which was considered too computationally expensive. We implemented this approach, which allows for full three-dimensional periodicity and an all-atom representation of the transmembrane potential with no continuum approximations.

Refereed

Crozier, P. S., M. J. Stevens, and T. B. Woolf. 2004. Rhodopsin photoisomerization simulation results: The 150 ns after forced cis-trans transition. To be submitted to a journal.

Jang, Y., P. S. Crozier, M. J. Stevens, and T. B. Woolf. 2004. How environment supports a state: Molecular dynamics simulations of two states in bacteriorhodopsin suggest lipid and water compensation. *Biophysical J.* **87**:129–45.

Sachs, J. N., P. S. Crozier, and T. B. Woolf. 2004. Atomistic simulations of biologically realistic transmembrane potential gradients. *J. Chemical Physics*, submitted.

Other Communications

Crozier, P. S., M. J. Stevens, J. S. Schoeniger, and T. B. Woolf. 2004. Comparison between isolated rhodopsin helices simulations and intact rhodopsin simulation. To be submitted to a refereed journal.

69193

Model-Building Codes for Membrane Proteins

K. L. Sale, T. W. Hunt, D. N. Shirley, J. M. Faulon, A. Slepoy

Integral membrane proteins (MPs) are essential components of the cell membrane that participate in many important cellular processes, such as cell intoxication and pathogenesis, energy transduction, cell signaling, mediation of senses, and immune recognition. Approximately one-third of the proteins encoded by a typical genome are MPs, and approximately 70% of current pharmaceuticals are thought to act on MPs. Yet despite their obvious importance, in contrast to over 27,000 soluble proteins structures, the structures of fewer than 75 integral MPs have been solved. Given the instability of MPs in environments lacking phospholipids, their tendency to aggregate, and protein abundance, expression, and purification issues, it is unlikely that generating high-resolution structural data from traditional methods such as x-ray crystallography and nuclear magnetic resonance (NMR) will yield a significant increase in the number of solved MP structures in the near future.

The Interfacial Biosciences Grand Challenge (IBIG) project supported the development of algorithms for modeling the geometry of transmembrane helical bundles and new approaches to protein side-chain packing. In this project, Sandia built on the successes demonstrated under IBIG by developing and validating an integrated set of software tools for MP modeling. Our goal was to develop methods to model transmembrane proteins using a set of sparse distance constraints, thus leveraging the many recent advances in techniques for measuring distances within protein in their native environment, including chemical cross-linking combined with mass spectrometry (MS3D), which we developed for MPs under IBIG; site-directed spin labeling combined with electron paramagnetic resonance (SDSL-EPR); and fluorescence resonance energy transfer (FRET). We combined these low-to-moderate-resolution structural data with constraints derived from analysis of existing MP structures, such as structural rules derived from helix-helix interactions in known structures, to determine the structure of the transmembrane spanning protein domain. Since this produces only a backbone-level structure, our final goal was to develop methods for adding the amino acid side-chains.

We developed a two-step approach to modeling the transmembrane-spanning helical bundles of integral MPs using

sparse distance constraints such as those derived from chemical cross-linking, dipolar EPR, and FRET experiments. The combination of these two steps provides a rapid method for searching the immense conformational space of helical bundles. In step one, using an algorithm we developed as part of IBIG, we explored the conformational space of MP folds matching a set of distance constraints to provide initial structures for further refinement using local conformational searches. Depending on the number of distances, the error on each distance, and the manner in which the distances connect the transmembrane helices, this step reduces the number of possible helix arrangements from on the order of 10^{11} to on the order of 10^{2} structures, which is a reasonable number for further refinement.

Our published algorithm for this first step (Faulon, J. L., *Protein Science* **12**:1750 [2003]) generates helix arrangements by mapping helices onto a library of helix templates, which we generate following a procedure outline by Bowie (Bowie, J. U., *Protein Science* **8**:2711 [1999]). Bowie's procedure is stochastic, and thus does not guarantee that all solutions are constructed. To overcome this pitfall, we developed a deterministic algorithm, which enumerates all transmembrane protein folds within a given root-mean-square deviation (RMSD). Precisely, the algorithm enumerates all folds, each being a provided RMSD apart from all the others and each matching a given set of distance constraints. Again, the end result is a set of distinct protein conformations, which can be scored and further refined.

In step two, we refined these structures against a custom penalty function that incorporates both measures derived from statistical analysis of solved MP structures and experimental distance constraints. Our complete scoring function includes a penalty for violations of experimental distance constraints and penalties for measures such as interhelix tilt angles and distances, helix tilt with respect to the membrane normal, helical bundle-packing density, and side-chain to side-chain packing preferences being outside the range observed in our statistical analysis of solved MP structures.

A requirement for the utility of our scoring function as a tool for refining helical bundles was for low scores to represent "good" structures and for the score to increase as the structure gets "worse." To test this, we used six known MP structures for which we generated a set of 5000 decoy bundles spanning a wide range of RMSD from the native bundle and showed that the total penalty distinguishes helical bundles that are close to the native bundle from those that are far from the native bundle.

We developed a two-step approach to modeling the transmembrane-spanning helical bundles of integral MPs using sparse distance constraints....[that] provides a rapid method for searching the immense conformational space of helical bundles.

This validation of the scoring function allows us to accomplish the structural refinement step by performing rigid-body translations and rotations of the individual helices until the total penalty is minimized. To this end, we implemented both an MC–simulated annealing routine and Sandia's asynchronous parallel pattern search (APPS) routine to perform the function minimization. Using a set of only 27 distance constraints extracted from the literature, we were able to use our two-step approach to successfully recover the structure of dark-adapted Rho to within 3.2 Å of that determined by x-ray crystallography.

This two-step approach results in a helical bundle consisting of only backbone atoms to which the amino acid side-chains must be added. We developed the theory and computational methodology for side-chain placement onto protein backbones using discrete rotamer libraries and the full-scale atomistic CHARMM22 force field with implicit solvent. Methods for searching the vast conformational space of protein side-chains include algorithms for branch-and-bound search with a dead-end elimination algorithm as a preconditioner. The methods and algorithms are embodied in an object-oriented C++ software application called CENTIPEDE. Our initial studies indicate that the full-force-field method produces more accurate results than popular methods currently in use.

Refereed

Brown, W. M., J. L. Faulon, K. L. Sale, J. S. Schoeniger, and M. M. Young. 2004. Deterministic algorithm for constrained enumeration of transmembrane protein folds. *Biocomputing 2005, Proc. Pacific Symposium* (PSB 2005), submitted.

Gray, G. A., T. G. Kolda, K. L. Sale, and M. M. Young. 2004. Optimizing an empirical scoring function for transmembrane protein structure determination. *INFORMS J. Computing* **16** (4) (Fall): 13.

Sale, K. L., J. L. Faulon, G. A. Gray, J. S. Schoeniger, and M. M. Young. 2004. Optimal bundling of transmembrane helices using sparse distance constraints. *Protein Science* **13** (10) (October): 2628–38.

Other Communications

Gray, G. A., J. L. Faulon, T. G. Kolda, K. L. Sale, J. S. Schoeniger, and M. M. Young. 2004. Optimal bundling of transmembrane helices using sparse distance constraints. Paper presented at IPAM, Program in Proteomics: Sequence, Structure and Function, Spring, Los Angeles, California.

Gray, G. A., K. L. Sale, J. L. Faulon, and M. M. Young. 2004. An empirical scoring function for the optimal bundling of transmembrane helices. Paper presented at the AWM Workshop, SIAM Annual Meeting, July, Portland, Oregon.

Gray, G. A., K. L. Sale, J. L. Faulon, J. S. Schoeniger, and M. M. Young. 2004. An integrated computational experimental approach to the transmembrane protein structure determination problem. Paper presented at the UCLA Bioengineering Department Colloquium, April, Los Angeles, California.

Sale, K. L., and G. A. Gray. 2004. Optimal bundling of the transmembrane helices of integral membrane proteins using sparse distance constraints. Paper presented at the 5th Biennial Structural Biology Symposium, 23–24 January, Tallahassee, Florida.

Sale, K. L., G. A. Gray, J. L. Faulon, J. S. Schoeniger, and M. M. Young. 2004. Optimal bundling of the transmembrane helices of integral membrane proteins using sparse distance constraints. *Biophysical J., Proc. Biophysical Society 48th Annual Meeting* **86** (14–18 February, Baltimore, Maryland): 1334.

69198

Poroelastic-Wave Propagation on the Earth Simulator

D. F. Aldridge, B. G. Van Bloemen Waanders, D. F. Aldridge, N. P. Symons, U. Hetmaniuk, L. C. Bartel

Sedimentary rocks, soils, and certain man-made materials (e.g., concrete) consist of a solid framework surrounding a microscopic pore/fracture system saturated with fluids. The fluid phase may exist in gaseous (air, methane) and/or liquid (water, oil) state. Theoretical, numerical, laboratory, and field experiments indicate that propagation of deformational waves through a porous solid is significantly affected by the presence of saturating fluid. In particular, the ability of a viscous fluid to migrate through a spatially connected pore/fracture geometry is an important mechanism for attenuation and dispersion of seismic waves in typical earth materials. In turn, measurements of seismic attenuation/dispersion may be used to infer the presence, distribution, and properties of fluids contained within geologic media. Successful solution of this inverse wave-propagation problem requires robust numerical modeling tools for simulating wave propagation (the forward problem) through a porous, fluid-saturated body.

Accurate poroelastic-wave-propagation modeling and inversion capability is of great interest to the petroleum industry for oil and natural-gas exploration, production, and/or reservoir-monitoring purposes.

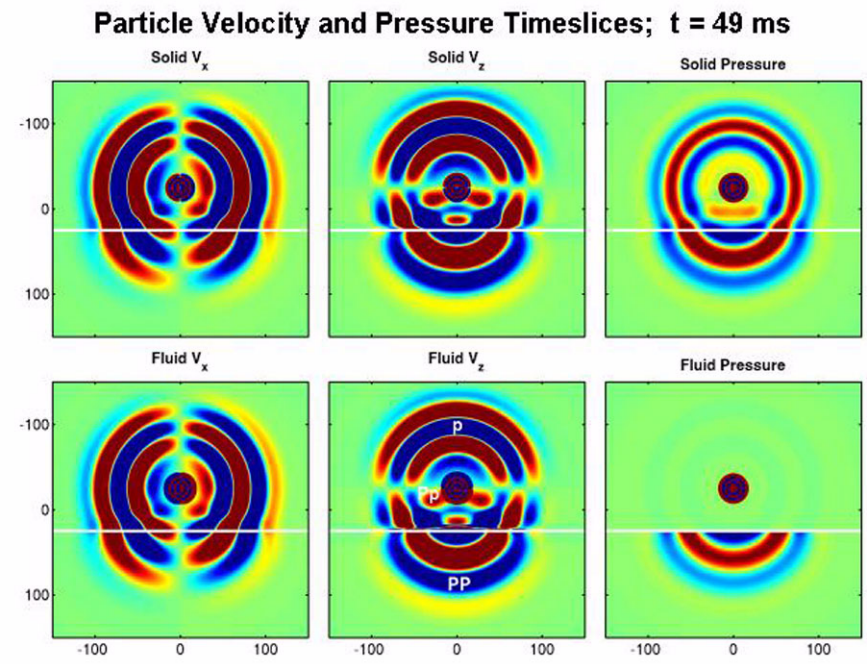

Reflected/refracted poroelastic wavefield at time t = 49 ms after source explosion.

Furthermore, numerous applications involving remote detection and characterization of subsurface fluids and flow will also benefit from poroelastic simulation tools and modeling expertise. These include sequestration of carbon dioxide within depleted petroleum reservoirs or saline aquifers, migration of environmental contaminants within the shallow subsurface vadose or saturated zones, exploration for deep hydrological resources, earthquake hazard assessment associated with fluid-controlled fault rupture, and determination of rock porosity for evaluation of subsurface weapon penetrability.

Three-dimensional (3-D) wave propagation within a realistic heterogeneous poroelastic medium may be numerically simulated with an explicit, time-domain, finite-difference (FD) algorithm. A system of 13 coupled, first-order, linear, nonhomogeneous partial differential equations (PDEs) is solved for the particle velocity vector components, stress tensor components, and pressure associated with solid and fluid constituents of the composite porous medium. This is a computationally demanding task requiring a massively parallel implementation to investigate large-scale earth models or broadband wave propagation within reasonable execution times.

We derived a favorable system of 13 coupled, first-order, nonhomogeneous PDEs governing 3-D linearized (e.g., infinitesimal deformation) wave propagation in a fluid-saturated porous solid from fundamental principles of continuum mechanics. The derivation technique utilizes a volume-averaging approach to develop expressions governing phase-averages of the particle velocity vector components, stress tensor components, and pressure associated with solid and fluid constituents of the composite medium. We discretized these equations in space and time and implemented an explicit, time-domain, FD numerical solution scheme in both serial and MP computational environments. All FD operators are centered and constructed on temporally and spatially staggered grids with second-order and fourth-order accuracy in the respective discretization intervals. We used staggered spatial and temporal storage schemes for the 13 poroelastic wavefield variables. Utilization of staggered grids, as well as high-order FD operators, constitutes state-of-the-art practice in current seismic-wave-propagation algorithms. The resulting numerical solution scheme possesses high accuracy, in the sense of reducing FD numerical dispersion noise to an acceptable level, provided grid intervals are sufficiently fine.

We stored material parameters characterizing the poroelastic medium at the four corners of the basic grid cell (i.e., coincident with the solid compressional stress components and the fluid pressure). We used 1-D and 2-D linear interpolations to estimate values at neighboring particle velocity and shear stress locations, respectively. We amalgamated all of the numerous poroelastic medium parameters into eight stored 3-D fields. Hence, a grand total of 21 3-D fields are required to store all dependent variables and medium parameters. The floating-point arithmetic operation count associated with this O(2,4) staggered-grid FD scheme is approximately 300 operations per grid cell per time-step. Operation counts for analogous isotropic elastic and acoustic algorithms are 140 and 43, respectively. Hence, poroelastic wave-propagation simulations will require about 2.1x and 7.0x times longer than equivalent-sized elastic and acoustic simulations, respectively. This highlights the need for a massively parallel (MP) algorithm implementation to treat large-scale earth models (requiring large 3-D grids) or broadband wave propagation (requiring very fine gridding) in reasonable run times.

Although the parallel algorithm is currently operative (ahead of the original intended schedule), there are numerous algorithmic issues that require significant additional attention to create a robust and flexible poroelastic modeling tool. These include (1) absorbing boundary conditions (BCs), (2) stress-free surface BC, (3) body and surface source implementations, (4) improved seismic-energy receiver and timeslice display implementations, and (5) derivation and study of numerical dispersion and stability criteria. We also need a superior module for constructing 3-D poroelastic models.

We conducted preliminary validation of forward-modeling algorithms by simulating 3-D wave propagation in an earth model relevant to subsurface petroleum reservoir characterization. This model consists of a methane-saturated sandstone overlying a water-saturated sandstone. In accordance with theoretical predictions, fast and slow compressional (P) waves diverge from a small explosive source and subsequently reflect and refract at the fluid boundary. Particularly noteworthy are mode conversions between fast and slow P waves and shear (S) waves at the gas/water contact.

Finally, we developed a prototype poroelastic inversion algorithm utilizing the simultaneous analysis and design (SAND) methodology to evaluate various numerical solution strategies and to characterize the level of complexity associated with large-scale material property inversions. This algorithm

restricts the problem to one spatial dimension and solves the inversion equations in the frequency domain using a finite-element approach and a biconjugate gradient algebraic solver. We demonstrated successful recovery of the applied body force function using three noise-free, synthetic, solid-/fluid-displacement data.

Refereed

Aldridge, D. F., L. C. Bartel, and N. P. Symons. 2004. Velocity-stress-pressure algorithm for 3-D poroelastic wave propagation. *Expanded Abstracts, Society of Exploration Geophysicists International Exposition 74th Annual Meeting* **1** (10–15 October, Denver, Colorado).

69239

Development of Microreformers for Fuel Cells

D. Ingersoll, K. E. Waldrip, K. Norman

The goal of this project is to develop a biomass-derived, hydrocarbon (HC)-powered microfuel processor capable of driving an existing microfuel cell. Steam reforming as a fuel-processing method is preferred, as it has the highest theoretical efficiency and potential H_2 selectivity compared with other HC-reforming methods and has already been demonstrated for use in methanol reforming. The use of microchannel reactors will demonstrate the feasibility of fuel processing on the microscale. Sandia will model the proposed microfuel processor on a bench-top-scale steam-reforming system and will build it using commercially available microreactors, parts, and catalysts. Of the various biomass-derived HCs available, glucose and ethanol show promise in bench-scale steam-reforming experiments. We analyzed the cost of producing glucose and ethanol from commercial starch sources and cellulosic biomass to determine the preferred fuel.

- *Fuel-cost analysis.* A variety of biomass-related carbohydrates, including ethanol, methanol, sorbitol, glucose, glycerol, and ethylene glycol, are candidates for steam reforming. While the reforming of less-reduced compounds like glucose is likely to be more practical, ethanol is also of interest because it can be obtained via fermentation of glucose and other sugars. Bench-scale steam reforming of ethanol yielded nearly stoichiometric conversion rates. Steam reforming of glucose converted ~ 50% of the available hydrogen (H) under direct steam-reforming conditions. The H_2 selectivity increases to ~ 60% in a dual-reactor system where glucose is first hydrogenated to sorbitol. We conducted a fuel-cost analysis to understand the relative cost effectiveness of glucose and ethanol. We determined corn starch and cellulosic biomass to be the most desirable sources of glucose and ethanol. Starch is a biopolymer of glucose; it is broken down into glucose via dilute acid or enzymatic saccharification. The glucose can then be converted to ethanol via fermentation. Glucose and ethanol can be obtained from cellulose, another biopolymer of glucose, via a similar process, though the cellulose must first be separated from the remaining plant matter. We examined the process design and economic analyses of obtaining ethanol and glucose from starch and cellulosic biomass. The economic models generally included all energy and material costs incurred in producing ethanol. We considered processes from feedstock

storage and handling, enzyme production costs, equipment costs, and waste-water treatment. The design suggested for obtaining ethanol from biomass was dilute acid hydrolysis (to liberate cellulose), followed by simultaneous enzymatic saccharification and fermentation. A sugar stream containing primarily glucose is an intermediate in the process of producing ethanol, so the cost of obtaining glucose from biomass can also be evaluated. We determined that the cost of ethanol fuel is an order of magnitude more than glucose fuel from any source. Future projections indicate that a drop in price due to more cost-effective enzymes will benefit both products equally, and the cost ratio of ethanol and glucose is expected to remain similar. It is clear that glucose is a much more cost-effective fuel. While the bench-scale processes show larger conversion factors for ethanol than for glucose, it is hoped that miniaturization of the process will make glucose more competitive. We hope to exploit the advantages of microscale reforming, including reduced surface-to-volume ratio, reduced heat- and mass-transfer rates, and control of reactant residence time over the surface catalyst to make glucose steam reforming more competitive with ethanol processing.

We determined that the cost of ethanol fuel is an order of magnitude more than glucose fuel from any source.

- *Process design*. While we chose glucose as our H_2 source due to its cost-effectiveness, the experimental setup outlined below will enable reforming of ethanol as well. We purchased a commercially available reactor from IMM (Germany) with 100 µm channels. We designed the gas-phase microreactor with mixer and internal heating/cooling to operate under our desired initial reforming conditions of 50 atm and 520 K. We also purchased a Hitachi L-6000 dual-plunger reciprocating HPLC pump for driving the liquid stream. We will determine the composition of the effluent gas using residual gas analysis/mass spectrometry (RGA-MS). We will accomplish pressure and flow control of the RGA-MS with digital and manual flow controllers. With the exception of the microreactor, assembly of the remaining components is under way. Manufacturing and assembly of the microreactor by IMM is nearly complete, and we expect delivery soon.

Other Communications

Norman, K., D. Hirschfield, D. Ingersoll, and D. H. Doughty. 2004. Micro reforming of glucose for hydrogen production. Paper presented at the Student Intern Symposium, 2 August, Albuquerque, New Mexico.

73185

Superhydrophobic Surface Coatings for Microfluidics and MEMS

F. B. Van Swol, T. L. Sounart, J. E. Houston, A. K. Singh, E. B. Cummings, D. J. Rader

Superhydrophobic (SH) surfaces exhibit high-contact angles, which leads to rolling and bouncing of liquid droplets, cavitation, and self-cleaning of particle contaminants. Sandia seeks to develop the understanding of the fundamental surface phenomena that underlie SH behavior. In addition, we will exploit the rough porous structure of a novel, synthetic SH surface for aerosol collection, its self-cleaning properties for particle concentration, and its slippery nature to enhance the performance of fluidic and microelectromechanical systems (MEMS) devices. To accomplish these goals, our approach relies on a combination of experiments (atomic-force microscopy [AFM], small-angle x-ray scattering [SAXS], neutron reflectivity, particle imaging velocimetry [PIV]), synthesis (e.g., ultraviolet [UV]/ozone for patterned surfaces), and modeling (molecular and dissipative particle dynamics, density-functional theory [DFT]).

Deformation of a simulated water drop as it impacts a superhydrophobic surface.

Neutron-reflectivity (NR) experiments were performed at Los Alamos Neutron Science Center (LANSCE) to probe the nature of the synthetic, aerogel-like SH films/water (H_2O and D_2O, both vapor and liquid) interface. The NR experiments clearly established that SH films submerged in water do not exhibit water penetration into the film, and SH films in contact with water vapor do not undergo capillary condensation. Fitting the NR data allows the determination of the water interfacial profile. Although the intrinsic SH film roughness makes this type of analysis difficult, the fitted interfacial profile rules out a smooth interface that touches only the outermost asperities of the film. The data are consistent with a water interface that penetrates larger valleys more deeply and bridges smaller ones. We also observed an interfacial structure in our DFT calculations. We developed a UV/ozone procedure in which, by increasing UV exposure times, the macroscopic contact angle varies continuously from ~ 160° to 0° due to a successive change in surface chemistry, while maintaining surface roughness. NR experiments of treated films with smaller contact angles (e.g., 0°) find the expected water penetration, but surprisingly also indicate that there exists a small deeply buried zone that, although porous, remains inaccessible to water.

The UV/ozone procedure provides an unprecedented approach to optically defining wetting with lithographic control—important for directing rolling droplets and effecting mixing in capillaries.

We showed the "self-cleaning" action of rolling droplets on SH surfaces to be a very efficient means to collect and transport anthrax simulant spores—few or no spores were left behind in contrast to previous collection strategies. Molecular dynamics (MD) modeling was developed to study bouncing and rolling nanodroplets. Our results provide the first detailed insight into droplet motion and deformation. We find that the contact time of a bounce is independent of impact velocity, but with a significantly smaller coefficient of restitution than observed experimentally with millimeter-sized larger drops. Simulated rolling droplets larger than the capillary length reach a terminal velocity that confirms rolling as opposed to sliding. We performed flow visualization experiments but, due to limitations in confirming/defining the position of the solid/liquid interface, we have not yet confirmed the magnitude of the slip velocity. Using interfacial-force microscopy (IFM), we observed cavitation upon the approach of two SH surfaces under water. This cavitation phenomenon is macroscopic (separation distances on the order of 1 mm) and was not observed previously; it may, however, be vital for operation/performance of living systems. We initiated modeling studies (both DFT and MD) to help understand the cavitation. We performed the MD simulations for liquid confined to a slit capillary with an SH patch and then studied cavitation as a function of capillary width, patch size, and meniscus curvature.

We showed the "self-cleaning" action of rolling droplets on SH surfaces to be a very efficient means to collect and transport anthrax simulant spores....

Other Communications

Van Swol, F. B. 2004. Superhydrophobic surfaces: Liquids on the move. Paper presented at ICAM, April, Santa Fe, New Mexico.

74545

Determining Explosive Ignition Criteria for Miniaturized Devices

A. M. Renlund, E. S. Hafenrichter, R. J. Pahl

Sandia conducted experiments to investigate the critical temperature of explosives at small scales and relatively high heating rates. At bulk scales, explosives ignited thermally (either by electrical bridgewires or laser absorption) can be characterized by a critical temperature. Critical temperatures are scale-dependent and can be thought of as the temperature at which the energy balance between chemical-energy release and thermal conduction reverses to promote thermal runaway within the explosive. For traditional low-power systems, heat conduction is always a dominant factor leading to ignition, and ignition times are often in the millisecond regime. Modern higher-power diode lasers and component miniaturization can lead to localization of energy deposition to smaller explosive volumes and may allow high temperatures to be achieved before substantial heat losses with faster ignition times. Therefore, the following questions arise: (1) Is a critical temperature a sufficient description of ignition thresholds? or (2) Is there also a critical volume that must be heated to that temperature to ignite and lead to sustained explosive combustion?

This work focused on delivering large rates of energy to relatively small areas of an explosive in a short period of time. We accomplished this by designing a laser detonator that allowed high-power light from a laser diode to be focused into relatively small spot sizes on the surface of the explosive. We used a fiber-coupled 65 W laser diode for all experiments. We connected the fiber from the laser to the laser detonator via an SMA-905 connector. We used focusing optics in the laser detonator to produce a specific spot size on the surface of the explosive. All experiments used 20 µm mean-particle-size BNCP (bis[5 nitrotetrazolato]pentaaminecobalt[III] perchlorate) explosive mixed with 1% carbon black pressed to a nominal density of 1.55 g/cc, an explosive configuration that is known to be sensitive to the 808 nm light emitted from the high-power laser diode.

We characterized the ignition of the explosive by using six diagnostic fibers that we potted into the SMA-905 connector around the laser delivery fiber. We routed these pick-up fibers to various photodetectors. By monitoring the signal from these photodetectors, one is able to directly measure ignition delay by

detecting light that is emitted and absorbed by the explosive when it begins to react.

We controlled the power density delivered to the explosive by manipulating the power delivered by the laser, as well as the spot size produced by the focusing optics. We varied the spot-size diameter from 40 μm to 200 μm and the power density from 50 kW/cm^2 to 4.5 MW/cm^2.

In addition to the experiments, we constructed a simple model to describe the dependence of ignition time on spot size and laser-energy deposition rate for comparison with data. The model uses a three-dimensional (3-D) Monte Carlo radiation heat-transfer approach, including scattering effects. We used the model to calculate temperature as a function of time for various depths into the explosive. We then compared those data to experimental measurements to determine whether the critical temperature of the explosive was affected by either spot size or heating rate.

Comparisons of the experimental data with the numerical data suggested that the critical temperature was not significantly affected by spot size over the studied region, as experiments with identical power density but different spot size yielded essentially identical results. Likewise, the rate of heating appeared to have little impact on the critical temperature, as the model predicted a nearly identical critical temperature for various power densities when spot size was held constant.

These data suggest that even at relatively small ignition scales, critical temperature does not vary significantly, given a sufficient heating rate. Furthermore, if a critical volume exists, it is much smaller than the volume of material heated in the present experiments, even with the smallest spot size of 40 μm (only twice the diameter of the mean particle size of the explosive).

74546

Quantum Squeezed Light for Probing Mitochondrial Membranes and Study of Neuroprotectants

P. L. Gourley

Sandia developed a new biomicroelectromechanical systems (bio-MEMs) nanolaser technique for measuring characteristics of small organelles. We initially applied the method to study mitochondria, a very small (500 nm–1.0 µm) organelle containing the respiration apparatus for animal cells. Because the mitochondria are so tiny, it has been difficult to study them using a standard light microscope or flow cytometry techniques. We used a recently discovered nanooptical transduction method for high-speed analysis of submicron organelles. This ultrasensitive detection of submicron particles uses nanosqueezing of light into photon modes imposed by the ultrasmall organelle dimensions in a submicron-laser cavity. We measured mitochondria spectra under normal conditions and under high-calcium-ion-gradient conditions that upset membrane homeostasis and lead to organelle swelling and lysis, similar to that observed in the diseased state. We compared the measured spectra with our calculations of the electromagnetic modes in normal and distended mitochondria using multiphysics finite-element methods (FEMs).

Sandia developed a new biomicroelectromechanical systems (bio-MEMs) nanolaser technique for measuring characteristics of small organelles.

Mitochondrial organelles are very tiny particles as small as the wavelength of light. Detection and analysis of these ultrasmall particles require new spectral-imaging techniques with high sensitivity. Our novel idea is to use nanosqueezing of spontaneous light emitted through a cell flowing at high speed in a biocompatible semiconductor microcavity. This quantum squeezing allows even tiny organelles to generate a large spectral signal that can be detected easily. We rapidly recorded and analyzed the spectral images (hyperspectra) in a newly devised biolaser INCEPTOR (intracellular protein transduction by optical resonance) spectral imager/analyzer. The laser light is spatially, spectrally, and temporally analyzed within seconds using efficient image-recognition software. This method extracts critical biological information from the lasing hyperspectra, including the membrane integrity, intracellular protein density and uniformity, and organelle size and shape. To our knowledge, we may have the first-ever capability to probe individual mitochondria and the pharmacokinetics of the membrane permeability transition. Our work is distinguished from that in other laboratories that rely on light-scattering

techniques to study respiring mitochondria. Because the total and angular scattering intensity is a strongly oscillating function of organelle size, variations in size can lead to ambiguities in the scattering measurements. Our technique avoids this ambiguity in relative scattered light intensity by relying instead on spectral measurements. With further development, a biolaser developed for tiny organelles could rapidly determine the effects of neuroprotectants like cyclosporin A on mitochondria. This analysis could be very useful for rapid, front-end screening of pharmaceuticals. The entire testing process could be completed in minutes. One objective of a future study would be to carefully characterize cyclosporin inhibition of Ca_2+– induced mPT in isolated mitochondria. The results could then be used to directly compare the effects of native cyclosporin with newly developed cyclosporin analogs capable of crossing the blood-brain barrier.

- We obtained lasing spectra from mouse, rat, and human mitochondria, showed that organelles support lasing modes, and showed that the number of photon modes decreases with organelle/cell size.
- We observed inhibited spontaneous emission and proved quantum optic enhancement of lasing efficiency.
- We proved that calcium swelling of mitochondrial membrane can be detected and quantified with this method.
- We carried out finite-element parametric studies on eigenfrequency dependence on sphere radius and dielectric contrast in the cavity, calculated the effect of osmostic swelling on frequency, and showed good agreement with experimental measurements.
- We performed the first biolaser experiments with cyclosporin A on mitochondria, showing initial evidence of the neuroprotective effect.

Refereed

Gourley, P. L., P. Chen, R. G. Copeland, J. D. Cox, J. K. Hendricks, A. E. McDonald, D. Y. Sasaki, M. E. Keep, and J. R. Karlsson. 2004. Nanosqueezed light for probing mitochondrial membrane swelling and study of neuroprotectants. *Proc. Photonics West, Conference on Microfluidics, BioMEMS, and Medical Microsystems* **SPIE 5345** (edited by P. Woias and I. Papautsky) (January, San Jose, California): 51–60.

74547

Characterization of a New Class of Surface-Micromachined Pumps

P. C. Galambos

This project addresses continued research to develop novel surface-micromachined (SMM) pumps based on Sandia's SUMMiT™ (Sandia Ultraplanar Multilevel MEMS [microelectromechanical systems] Technology) five-level polysilicon fabrication process and SwIFT™ (SUMMiT™ with Integrated Fluidics Technology). In SwIFT™, extra silicon nitride (SiN) films are added to the SUMMiT™ process to allow transparent electrically insulating channels with arbitrarily located embedded electrodes and built-in micromachines to be fabricated. At the microscale, pumping methods based on inertia, such as are common at the macroscale, are ineffective because of the dominance of viscous forces (Reynold number < 1 typically). Our novel pumps utilize viscous forces to move fluids with a modified Couette flow configuration. These on-chip pumps (flow passage < 10 µm deep) are powered by on-chip electrostatic actuators such as the torsional ratcheting actuator (TRA) and drive fluid through SMM channels in a highly integrated, complete, chip-scale, microfluidic system.

We will perform detailed experimental investigation of the performance of these devices, including generation of pump-performance curves; characterization of filling and leaking pressures; the effect of hydrophobic versus hydrophilic drying; and the movement of particles (beads) in the generated shear field, possibly leading to particle fractionation in the outlet fluid stream (device channel). We expect these experimental results to demonstrate the usefulness and efficiency of this pump for powering on-chip microfluidics, which have potential applications in the areas of chemical-/biological-warfare–agent detection and µTAS (Micro Total [chemical] Analysis Systems). Also, based on past experience with SMM microfluidics, we expect the experimental results to surprise us and to point to fruitful new areas of research. These experiments are the evaluation step in which we will determine whether these pumps really work and provide the key input to necessary changes in the system design.

In this project, we focused on characterizing second-generation viscous drag and gear pumps. The second-generation combined pump/actuator devices had improved TRAs with higher force per applied voltage and more-effective

ratchet stops, as well as fewer dimple cut guides in the pump housing to reduce friction. Since pump friction, flowrate, and pressure drop are all related to pump size, we coupled smaller-diameter pumps with the higher-force actuators to allow more effective operation. In short, we sized up the actuation force and sized down the force required to pump fluid to achieve smooth pump operation, as compared to the previous pump designs in which the pump actuator was too small for the pump and only achieved intermittent pump actuation. We demonstrated more effective pumping as a result of these design changes. We generated a first pump curve for this class of SMM pumps. Specifically, we generated a pump curve (pressure versus flow) for a signal of 30 V at 10 Hz with zero back pressure and at a slight vacuum. This curve represents a minimum-pressure, maximum-flowrate operating point. At zero back pressure, we generated a 6 nl/s flow. Since a typical SMM channel has a volume of 1 nl or less, this flowrate is more than sufficient for many SMM pumping applications. Thus, we characterized redesigned SMM pumps, demonstrated improved performance, and generated the first pump curve for this type of pump.

Our primary accomplishment was generation of the first pump curve (pressure versus flowrate) for this class of SMM micropump.

Our primary accomplishment was generation of the first pump curve (pressure versus flowrate) for this class of SMM micropump. We generated the pump curve for the crescent gear-pump design on RS415. This module contained second-generation viscous drag, spiral, and gear-pump designs. The designs were actually redesigns based on the results from testing the first-generation micropump designs from RS275. This earlier testing revealed that the actuator (first-generation TRA) was underpowered relative to the pump, primarily as a result of friction in the pump housing. As a result, we improved the actuator in the second-generation design (second-generation TRA—higher force per volt and better ratchet stops) and reduced the pump size. In addition, we reduced the area of the rubbing surfaces in the pump. These changes resulted in more effective pumping for all pump designs and the generation of a pump curve for the gear pump.

In addition to the pump curve generated for the gear pump, initial characterization of the spiral and viscous drag pumps indicates that the redesigned pumps operate more robustly than the previous first-generation pumps. However, we have not yet done enough testing to generate a pump curve for these designs. Further characterization work will focus on more gear-pump testing at higher back pressures, generation of pump curves for spiral pump and viscous pump designs, and the investigation with a design-of-experiments matrix of failure modes possibly

related to electrostatic charge buildup or glue out-gassing during pump/tubing assembly.

Refereed

Haik, Y., J. Hendrix, M. Kilani, P. C. Galambos, and C. J. Chen. 2004. Characterization of micropumps for biomedical applications. *Proc. Nanotech 2004* **1** (7–11 March, Boston, Massachusetts): 521.

Kilani, M., P. Galambos, Y. Haik, and C. J. Chen. 2004. Surface-micromachined viscous spiral pump. *Proc. Nanotech 2004* **1** (7–11 March, Boston, Massachusetts): 560.

Other Communications

Galambos, P. C. 2004. A surface-micromachined gear pump. *Proc. New Mexico AVS Symposium* **40** (17 May, Albuquerque, New Mexico): 21

74548

Risk of Biological Terrorism to Water-Distribution Systems

S. J. Altman, L. K. McGrath, C. A. Souza

The goal of this research is to position Sandia as an expert on the transport of biological agents through water-supply distribution systems. Water-distribution systems are highly vulnerable to terrorism because there is virtually an infinite number of access sites to the system downstream of the treatment sites. We seek to answer the following questions: (1) Do biofilms enhance or reduce the initial risk of toxic exposure to a host of biological agents? (2) If agents are used in a drinking-water system, do biofilms add a latency dose that will remain in the pipelines even after shocking with chlorine or other typical cleaning methodologies? (3) What effect does a biofilm have on restoration and remediation activities after an attack has been carried out?

This research will result in a basic physical understanding of behavior that can be used to improve the fidelity of risk assessments. We will conduct laboratory-scale experiments to better understand (1) under what conditions colloids will be adsorbed and desorbed onto/from biofilms, (2) the effects of biofilms on biocolloid transport, and (3) what effect a biofilm has on restoration and remediation activities (latency effects). At the conclusion of this study, we will have a greater understanding of how important biofilms are in controlling biocolloid transport, and how much remediation is needed to ensure that water users will not be contaminated after a terrorist attack. If the knowledge gained from this research shows that the biofilms play a significant role in transport of biocolloids through the water-distribution systems, this research could lead to technologies applicable to the Department of Homeland Security, the Environmental Protection Agency/National Homeland Security Research Center, and/or the American Water Works Association Research Foundation.

Our primary accomplishment was the successful growth of biofilms in an annular reactor. This experiment was the first step in determining when we will achieve maximum biofilm growth in our experimental apparatus and how to grow reproducible biofilms. To do this, we had to select a biofilm organism (*Pseudomonas fluorescens*), culture the organism, measure cell counts of the organism through different plate-counting methods, acquire and learn how to use the annular

reactor (the apparatus in which we will conduct our transport experiments), and sample and measure biofilm concentrations. Based on this experimental setup, we wrote a draft test plan for transport experiments.

In addition to growing biofilms, we conducted our first settling experiment using polystyrene microspheres as our surrogate for the pathogen. The one extreme flow regime in a water-distribution system is stagnant water. Thus, the purpose of the settling experiments is to determine the time it would take for a pathogen to contact a biofilm under stagnant conditions. To conduct this experiment, we had to successfully measure concentrations of 1 µm-diameter polystyrene microspheres with fluorescence spectrophotometry.

In addition to the above experiments, we accomplished the following: (1) visualized the biofilm organism (*Pseudomonas fluorescens*) and 1 µm-diameter polystyrene microspheres with a confocal laser-scanning microscope; (2) selected the "pathogen" organisms (*Cryptosporidium parvum* and *Bacillus cereus* [as a surrogate for *B. anthracis*]); and (3) conducted an extensive literature review of an overview of biofilms, biofilms in water-distribution systems, interactions of other agents with biofilms, use of annular reactors for water-distribution-system–related experiments, etc.

In addition to growing biofilms, we conducted our first settling experiment using polystyrene microspheres as our surrogate for the pathogen.

74759

Explicit and Implicit Measures in Human Aversive Classical Conditioning

P. B. Merkle

The neuroscience research community has found that associative learning is implicated in higher-level cognitive processes in some forms of classical conditioning. An ongoing debate concerns attention and awareness as necessary for trace, but not delay eye-blink conditioning (Clark and Squire, 1998; Lovibond and Shanks, 2002). In previous studies, Sandia investigated human classical fear conditioning as dependent on working memory (Carter, et al.*, 2003). Subjects executed an n-back task, requiring tracking an item one or two back in a sequentially presented list while simultaneously being tested for their ability to associate auditory cues with shocks under a variety of conditions (single-cue versus differential; delay versus trace; no task versus zero-back, one-back, and two-back). We found that the larger the cognitive demands on the system, the less likely it is that conditioning occurs (for delay versus trace, single versus differential, and for increasing working memory load). A post-experimental questionnaire showed positive correlation between conditioning and awareness for differential trace-conditioning extinction. We hope to extend these studies in three ways in this project. (1) We will look at subject comparison of simultaneous trace and delay conditioning using functional magnetic resonance imaging (fMRI) to elucidate brain structures that show activity during both trace and delay conditioning as well as those that show activity during one but not the other. (2) We will examine masked delay conditioning compared to unmasked delay conditioning using fMRI as a means to identify structures specifically involved in establishing conditioning when subjects are aware of the stimuli that predict a shock (unmasked) compared to when they are not aware (masked). (3) We will perform single-trial analysis of correlations between subjective shock expectancy, skin conductance, and electroencephalogram (EEG) responses during conditioning.*

We seek to address the neural representation of explicit and implicit knowledge. Our experimental approach involved using blood oxygen-level dependence functional magnetic resonance imaging (BOLD fMRI) to ascertain the neural substrate underlying contingency awareness during delay and to trace human aversive conditioning. We randomly assigned four abstract images to one of four trial types: delay CS+

(conditional stimulus), trace CS+, or one of two unpaired baseline stimuli (CS-) during concurrent aversive delay and trace conditioning. We reinforced CS+ trials with a mild electric shock (US [unconditional stimulus]) 50% of the time. We acquired 44 slice-tilted axial images using a 3T head-only scanner. We asked subjects to indicate their shock expectancy by pressing one of three buttons (shock, unsure, or no shock). We then used skin conductance (SC) and expectancy responses for each trial as parametric regressors of conditioning. We analyzed 14 subjects as the conjunction of trace and delay conditioning and reinforced and nonreinforced trials. Results comparing hemodynamic activity for CS+ > CS- trials replicate the majority of activity demonstrated by human fMRI studies of aversive conditioning. Bilateral middle frontal gyrus (dorsolateral prefrontal cortex [DLPFC]) BOLD responses were correlated with accurate online shock expectancy to differing degrees that reflected the subject's ability to accurately describe the CS/US relationship using a second assessment of explicit knowledge (post-experimental questionnaire). These results are consistent with previous imaging work in the related areas of cognitive reassessment and working memory. Para-hippocampal and amygdala BOLD responses correlated with the amplitude of normalized SC responses on each trial in a manner reflecting the strength of conditioning (as measured by the average CS+, CS-SC response difference).

- We completed data acquisition and basic analysis for trace/delay comparison.
- We completed data acquisition for specific masked versus nonmasked conditioning.
- We completed preprocessing and confirmation for the previous goal.
- We completed expectancy and trial-by-trial CS value analysis for the first goal.
- We completed basic analysis for the second goal.

We found significant effects of interest in our research to meet the first goal. We also completed data acquisition and preprocessing for the second goal. Preliminary analysis for the second goal indicates interesting trends.

Other Communications

Carter, R. M., J. P. O'Doherty, B. Seymour, C. Koch, and R. J. Dolan. 2004. Activity covaries with explicit knowledge of CS/U.S. contingency in human aversive conditioning. *Society for Neuroscience 2004* (online), Program No. 369.4, accepted.

75442

Assessment of Advanced Pulsed-Power Fusion Concepts

T. A. Mehlhorn, B. V. Oliver, R. A. Vesey, C. J. Garasi, S. A. Slutz, D. R. Welch, M. E. Cuneo, D. B. Sinars, R. B. Campbell, A. C. Robinson, M. R. Lopez, D. L. Hanson

The primary purpose of this project was to perform a preliminary assessment of a number of recently proposed advanced pulsed-power fusion concepts that could revolutionize the field and possibly lead to a fast track to fusion for weapons effects, material testing, and fusion energy. The common theme of these advanced concepts is that none of them relies on the symmetric implosion of a spherical *inertial confinement fusion (ICF) capsule or on traditional hot-spot ignition. Rather, these advanced concepts utilize strong magnetic fields and novel heating methods in a variety of geometries. All of these concepts leverage the simplicity, efficiency, and cost-effective advantages of pulsed-power–driven Z-pinch systems for producing high-fusion yields for both defense and energy applications.*

Sandia obtained the results of the preliminary theoretical, computational, and experimental assessment of the feasibility of the following four fusion concepts:

(1) Utilizing enhanced heating of Z-pinch ions by molecular hydrodynamics (MHD) turbulence,

(2) Developing advanced liner-implosion concepts,

(3) Developing magnetized fast-ignition (FI) concepts, and

(4) Developing magnetized cluster-fusion concepts.

We identified and documented the key physics issues and technical risks of each concept and proposed a priority order for further theoretical, computational, and experimental research and development. We also performed a preliminary evaluation of the requirements for full computational modeling and for performing proof-of-concept experiments. In addition to this physics evaluation, we began developing a technology maturation strategy for pulsed-power–driven fusion systems that defines the requirements on fusion output as a function of application.

We made significant progress in studying the underlying physics of the four proposed fusion concepts.

(1) *Utilizing enhanced heating of Z-pinch ions by MHD turbulence*. We investigated a new mechanism for converting magnetic energy to soft x-ray radiation during the stagnation phase of dynamic Z-pinches and converting part of the

magnetic energy into ion thermal energy via the viscous damping of nonlinearly saturated MHD turbulence. Equipartition of the ion thermal energy to the electrons and the eventual stopping of electrons in the dense pinch material resulted in soft x-ray production. We made a preliminary investigation and assessment of the proposed mechanism. The primary assumptions in the proposed model are the expected spectra of MHD instabilities, the saturation amplitudes of such instabilities, and the critical wavelengths for ion heating.

(2) *Developing advanced liner-implosion concepts*. The initial results from a study of advanced Z-pinch linear-implosion experiments on the Z Facility show great promise. A diagnostic and hardware development strategy is necessary to assess the scaling of this concept.

(3) *Developing magnetized FI concepts*. Simulations of the Z dynamic hohlraum (DH) concept employed on Z refurbishment (ZR) suggest that compression of capsules to several hundred grams/cm^3 is possible. We examined some initial FI simulations with cores compressed with ZR at peak densities of about 100 g/cm^3. We generated plots of performance as measured by Q=Efus/Edep where Efus is the fusion energy released from the core and halo, and Edep is the energy from the petawatt (PW) laser that is deposited in the core. We performed LSP (a three-dimensional [3-D] implicit electromagnetic particle-in-cell [EM PIC] code) simulations of FI core heating at two laser-energy levels, 2 kJ and 18 kJ at 100 g/cm^3. We generated estimates of heating performance in Q space if the core density is increased to 300 g/cm^3, assuming the trapping efficiency of the hot electrons is the same as for the lower density. At the higher density, a Q of about 0.1 is possible with the 2 kJ system, and if four beamlines are fitted with dielectric gratings, a total of 18 kJ is available and may yield a core Q of approximate unity. The encouraging performance of the higher core density suggests that additional study of these cases should be pursued.

(4) *Developing magnetized cluster-fusion concepts*. We examined the generation and confinement of a plasma filament in an external magnetic field via numerical simulation using the LSP hybrid plasma physics code. We utilized a three-stage numerical process whereby the plasma distribution function is followed from the initial stages of the Coulomb explosion of individual atomic clusters driven by a short-pulse high-intensity laser through the merging of individual cluster plasmas to the confinement of the fully formed hot plasma filament. We calculated the evolution of the plasma filament in various applied magnetic field strengths to estimate confinement times.

We also developed a White Paper and associated plot that describe the required fusion yield and equivalent neutron yield versus pulsed-power repetition rate for a variety of potential fusion applications.

While we made excellent progress in the preliminary assessment of each of these concepts, we do not have sufficient information to accomplish the comparison with the baseline ICF concepts initially planned for this project.

75513

Developing Algorithms for Predicting Protein-Protein Interactions from Experimental Constraints

D. C. Roe, K. L. Sale

Although it is now feasible to sequence entire genomes, there is still a large gap in obtaining functional information from these deoxyribonucleic acid (DNA) sequences. This project addresses this gap by developing a new technology to go from primary DNA sequence to protein structure and function. This technology will extend the computational portion of Sandia's mass spectrometry in three dimensions (MS3D) technology, currently a combined computational/experimental technique being developed to generate low-resolution models of folded proteins, into a tool for understanding how proteins interact or "dock" with each other. The protein-protein docking problem, essential in understanding protein function, is a large unsolved problem that is related to protein folding, but in practice has its own unique algorithmic challenges. Purely computational approaches to this protein-protein docking problem require highly accurate three-dimensional (3-D) structures to be solved using x-ray crystallography (a slow experimental procedure) as a starting point. By taking an approach that combines computational docking with more readily available experimentally derived structural constraints from chemical cross-linking experiments, we may be able to perform these docking calculations on less-accurate protein homology models that can be relatively quickly generated computationally from their amino acid sequences. If successful, this tool will greatly speed and expand the number of protein-protein models that can be generated for a given proteome—a result that would have numerous applications in both the pharmaceutical and biodefense communities. The goal of this project is to evaluate the feasibility of this approach and to develop a prototype protein-protein docking software tool that performs the docking calculations given a set of experimentally derived constraints.

We created a database of 182 structurally unique protein-protein complexes whose solved structure is in the Protein Data Bank.

We created a database of 182 structurally unique protein-protein complexes whose solved structure is in the Protein Data Bank. This database will be used for our feasibility studies. We completed a survey of possible interprotein cross-links for all protein complexes in our database by calculating the distance between cross-linkable amino acid pairs for which cross-linkers are available (C-C, K-K, C-K, C-D, D-D, D-E, and E-E). On

average, there are 27 possible cross-links between two proteins comprising each complex using all the cross-linkers, whereas the average number of possible cross-links for each individual probes were 0.7, 5.6, 1.7, 1.5, 5.3, 5.7, and 6.8, respectively. This study shows that there should be sufficient cross-links available so that, when used within our docking codes, they will provide sufficient data to at least determine the protein-protein binding site and probably to get a rough approximation of the relative orientations of any two proteins in a complex. (The docked orientations are not exactly determined with three cross-links because the probes are highly flexible.) Based on this survey, we can justify further exploration of cross-linking combined with protein-protein docking.

We also compared the complexed protein structures in our database to their uncomplexed structures. Our initial study, in agreement with smaller studies in the literature, showed that a large portion of the modification to the protein structures upon complex formation (i.e., protein-protein docking) was due to conformational changes in side chains rather than from alterations to the protein backbone. We concluded from this study that a major challenge in predicting correct protein-protein docking structures would be in correctly positioning these side chains. This is especially true when the starting point is homology-modeled protein structures, for which initial side-chain positions are frequently unknown. To address this problem, we decided to explore initial algorithms for placing and evaluating side chains in protein-protein structures. These side-chain-placement algorithms would be the final step of a protein-protein docking tool that would start by using experimental constraints to identify one or several initial orientations of one protein with respect to the other, and then use side-chain searching to optimize and evaluate each possible protein orientation to identify the correct one. We started with Sandia's PDock software that was being developed for peptide-protein docking, and adapted it to the side-chain-placement problem for protein-protein structures. The code uses a combined discrete/continuous optimization of side-chain positions by starting with a rotamer library to sample all positions, and then performing a local minimization of the conformation using Sandia's Coliny optimizers. All side chains are scored using the AMBER molecular force field with a generalized Born electrostatics model for solvation. We divide the calculation into two parts—side-chain–main-chain interactions, which is an order N problem (N=number side chains), and side-chain–side-chain interactions, which is of order N^2. We are comparing a Boltzmann model of side-chain

positions, where the free energy of binding is calculated directly from a partition function with contributions from all the rotamers, to a more traditional score based on solving the combinatorial problem of identifying the set of side-chain rotamers that produce the lowest overall energy. For the latter problem, we are using integer program solvers being developed as part of Coliny. We completed integration and adaptation of these codes to fit the side-chain-placement problem and will test them on the database of protein-protein structures during upcoming work.

75514

Instrumentation Development for Real-Time Brain-Wave Monitoring

L. F. Anderson, M. K. Alam, R. A. Salazar

Brain-wave monitoring is traditionally done in a hospital or laboratory setting with many large instruments and huge amounts of hard disk space devoted to storing large files of brain-wave data. These data files are eventually analyzed for patterns of concern. Advances in signal processing and microelectronics over the last decade have paved the way for the realization of portable "real-time" monitoring of brain waves and detection of physiological stressors of personnel while in a crisis situation on field assignments. Sandia's plan is to develop the sensors, signal processing, and portable instrumentation package to issue an alert of a potential problem with personnel while involved in dangerous activities.

The relevance to national security issues includes real-time brain-wave monitoring of military personnel in battlefield situations, or special agents on assignment in foreign countries.

Homeland security issues would include monitoring personnel in key positions, such as nuclear-power-plant workers, air-traffic controllers, and emergency and search-and-rescue workers.

We envision that ultimately a system would include a sensor-detection mechanism, transmitter, receiver, microprocessor and associated memory, and audio and/or visual alert system. If successful in prototyping, the device could be considered for eventual implementation in application-specific integrated circuit (ASIC) form or as a fully integrated complementary metal-oxide semiconductor (CMOS) microsystem.

We began developing a dedicated computer workstation that has now been built and will double as a hardware/software development system and demonstration tool for present and future software development. The hardware design completed for the Sandia prototype includes high-gain amplifiers with high-order filtering for the front-end interface between the electrodes and the analog-to-digital (A/D) converters.

The University of Florida (UFL) collaborator's existing brain-wave software will now run on the workstation using input data files recorded from patients at the collaborator's facilities at UFL and the University of New Mexico (UNM). These raw data files are presently recorded with a Nicollet BMSI-6000 system that amplifies, filters, and digitizes the

analog input. We can now use the electroencephalogram (EEG) files as the source of stimulus input with signal injection after the A/D converter interface for the development of the Sandia prototype and to validate correct functionality of that prototype.

A trip to UFL was successful in addressing multiple concerns. The UFL collaborators demonstrated their algorithm's detection capabilities using prerecorded patient-scalp electrode data files. They have a version running on a desktop personal computer (PC) written in C++ with graphics that uses prerecorded patient data to predict seizures. We discussed simplifications to the software for a Sandia version that will run in real time with fewer electrodes (5 to 8 pairs, as compared with ~ 20), a simplified algorithm, and an output to warn of impending seizure. Also discussed was the ability to re-create analog output generated from patient data to drive the new Sandia prototype. UFL agreed to fabricate a system for getting the raw data output, presently recorded with a Nicollet BMSI-6000 system, for testing the new Sandia prototype after the A/D interface.

The accomplishments above are steadily moving the project closer to resolving recognized challenges to researchers in the past. These efforts, together with the selection of an appropriate microcontroller and software development package, have been of critical importance. Sandia's familiarity and hands-on experience with resolution of these types of engineering challenges have been, and will continue to be, of critical importance in resolving issues that have stymied biomedical engineering researchers for two decades.

The Sandia team has had multiple telephone conversations with the algorithm author at Arizona State University (ASU) and the medical collaborators at both the UNM Hospital and UFL/Gainesville to address concerns with the suitability of scalp electrodes. Each stated that the clarity of scalp electrodes has proven suitable for the detection of the brain signal as evidenced by the existing analog recording they currently use to further verify the predictive capability of the existing algorithm. The collaborators have researched alternative technical approaches for signal detection in the event that scalp electrodes are unsuccessful and have promising results that they plan to publish soon.

75786

Maximally Autonomous Autodirective Antenna Array Technology

R. A. Bates

Antennas are the critical link between the relatively controlled domain of radio-frequency (RF) guided waves and the difficult-to-predict and deleterious radiated propagation environment, passively filtering signal energy with respect to operating frequency, polarization state, and direction. All undesired signals are noise to a receiving system and directly reduce system performance. Simply directing antenna response toward a desired source and away from interference sources results in significant improvements, enhancing received signal-to-noise (S/N). The effective bandwidth available to all users in a shared environment also increases.

Sandia will explore technology that addresses the significant and high-value goal of implementing a class of practical antenna solutions that use automatic electrical-array pointing with minimal loading on the original target system. Target tracking of aircraft or vehicles in intelligence applications requires quantitative understanding of electrical-switching latency times. Antenna beam-steering properties must be subject to network algorithm control.

Applications for steered-beam antennas exist in intelligence ground-sensor applications and re-entry vehicle (RV) flight testing. RV communications with stationary communications satellites requires dynamic control of the antenna beam. Missions such as unmanned aerial vehicles (UAVs) and national missile defense (NMD) applications, along with nanosatellite constellations, distributed remote-sensing networks or personal communications where emitter power, space, and cost limitations are more the focus. Many of these applications demand more performance improvement than can be offered through enhancements in other, more exhaustively addressed areas of RF communications research such as error coding, modulation techniques, or amplifier-efficiency improvement.

76069

Miniaturized Electronic Steerable-Array Synthetic-Aperture Radar

K. W. Sorensen, P. A. Dudley, D. F. Dubbert, B. C. Brock, S. E. Allen, K. C. Branch, M. Armendariz, A. G. Baca, D. C. Sprauer, C. D. Nordquist, A. W. Doerry, C. W. Dyck, R. S. Flores, G. R. Sloan, D. D. Chu, B. L. Burns, R. W. Brocato, P. J. Robertson, D. V. Campbell, G. A. Vawter, R. Chanchani, M. J. Rightley, B. Jokiel, Jr., B. L. Tise

The MESASAR (Miniature Electronically Steerable-Array Synthetic-Aperture Radar) project plans to demonstrate a revolutionary leap in integrated radar technology by concentrating a full radar exciter and receiver into a single 2 x 2 x 1 in. module, known as FIRE *(fully integrated radar element). The effort is based on the exploitation of MESA technologies that exist, are under development, and are proposed. The module fully integrates digital waveform generation, digital receiver processing, radio-frequency (RF) up/down-conversion, RF power amplification, and optical (single-fiber) input/output. The FIRE module will directly facilitate both unprecedented miniaturization (e.g., SAR 1/10th the weight of Lynx) and novel systems with unprecedented scalability (numbers of FIRE modules) and agility (multiple simultaneous beams and modes).*

The military, intelligence, and security arms of the government have recently expressed a critical need to greatly enhance the ubiquity and persistence of both tactical and strategic surveillance capabilities/assets. The radar applications facilitated by the FIRE module would have immediate high impact. Examples include the following: (1) providing all-weather, day/night sensors on smaller unmanned aerial vehicles (UAVs); (2) facilitating next-generation (hyperconcurrent) radar modality on larger UAVs and space-based assets; and (3) enabling all-weather precision guidance for next-generation munitions. In addition, FIRE technology would greatly benefit the capabilities of radar fuzes, advanced communication systems, tags, and other related systems.

We can group our accomplishments into two primary areas: (1) FIRE module system design and technology roadmap development, and (2) FIRE module application studies.

- FIRE module system design accomplishments include the following:

(1) We completed a high-level system design of the FIRE module. We determined both the corresponding specifications

for each subsystem and the required interfaces. Specific studies included the following: (a) high-level mechanical design (size, weight, layout), (b) high-level thermal analysis and proposed cooling approaches, and (c) an integrated packaging approach.

(2) We completed a detailed assessment of the best technology options for the realization of each subsystem/integrated circuit (IC). In each instance, the team analyzed the trade-offs between commercial off-the-shelf (COTS) procurement versus custom design, and industry versus MESA fabrication. Furthermore, for each selected technology, we made a detailed evaluation of the current maturity inside and outside Sandia. The end result yielded two primary products. The first product is a detailed assessment that identifies the technology readiness level of each subsystem and whether each subsystem will be COTS–procured, MESA–fabricated, or Sandia-designed and industry-fabricated. The second product is a detailed roadmap for the required schedule/budget to design, develop, and fabricate each subsystem.

Some of the specific studies performed and documented assessed the following technologies and subsystems: (a) RF MEMs phase shifters, (b) gallium-nitride (GaN) solid-state power amplifier, (c) silicon-germanium (SiGe) up-/down-converter custom microwave IC, (d) SiGe digital-waveform synthesizer custom IC, (e) SiGe digital-receiver custom IC, (f) integrated substrate packaging technology, and (g) custom photonic IC for optical module interface. Taken together, these studies provide a detailed roadmap and estimate for the development of the FIRE module and associated technologies.

- FIRE module system application accomplishments include the following:

(1) We performed a preliminary study that indicated FIRE technology could facilitate the practical implementation of tomographic SAR (synthetic-aperture radar), by providing multiple radar phase centers under the length of an aircraft wing. This novel imaging technology yields individual images at specific elevation slices. We believe that such a capability could provide foliage peek-through as well as true three-dimensional (3-D) imagery.

(2) We performed a preliminary study that indicated FIRE technology could facilitate larger, scalable electronically steered arrays (ESAs) with unprecedented simultaneous mode/beam capability. (Unlike traditional ESAs, each FIRE module provides an independent phase center that can act either in concert with other modules or independently.)

(3) We performed a study that characterized multiple versions of FIRE–based radars and compared their performance

to current systems. The study indicated that FIRE technology would greatly enhance both strategic and tactical systems.

76070

Full-Earth-Monitoring Sensor MESAWorks

T. A. Fischer, T. D. Osborn, S. K. Dunlap, D. J. Savignon, K. S. Rawlinson, R. K. Patel, M. W. Brown, M. P. Napier, K. R. Lanes, L. J. Krumel, J. A. Galloway, D. D. Fleming, C. C. Colmenero, W. J. Landaker, M. J. Leatherwood, P. E. Dodd, D. Bethke, D. D. Chu, R. Chanchani, R. S. Flores, B. Jokiel, Jr., J. A. Felix, J. R. Schwank, K. P. Lamppa, M. J. Rightley, D. B. Webb, D. A. Dixon, R. R. Kay, R. L. Akau, C. C. Wong

The Full-Earth-Monitoring Sensor (FEMS) MESAWorks evaluation constitutes an exploration of the applicability of microsystem technologies to the development of high-spatial-resolution staring-array-sensor systems. These next-generation sensor systems would have substantial benefit to the nuclear-proliferation-awareness mission. As resolution increases, however, such real-time imaging systems require exponential improvement in data-processor throughput. Commercial high-performance signal processors can meet this challenge, but are susceptible to radiation-induced upset, and conventional packaging methods conflict with the limited launch mass and volume required of satellite-mounted sensors. Extant and nascent microsystem technologies enable the conceptualization of compact, high-capability-density data processors that will meet throughput requirements. The application of Sandia radiation-effects expertise to a commercial gate-array technology will lead to the creation of a radiation-hardened processor that could be made using standard commercial fabrication processes and for which circuits could be configured using well-honed commercial design tools. Adoption of a modular processor architecture enables both scalability and maximum reuse in subsequent implementations. The development of a FEMS incorporating a radiation-hardened, modular, extensible data-processor architecture would fundamentally improve the system paradigm for space-based infrared (IR) surveillance sensors and improve surveillance system architecture on the whole by moving more of the data processing onto the sensor. A voluminous data downlink would thus be replaced with a much smaller processed-information downlink. The FEMS processor is a high-leverage investment with multiple, diverse opportunities for inclusion in systems demanding high-reliability and high-processing throughput within a small volume.

The purpose behind this project was to evaluate the opportunities for the creation of superior space-based IR

staring-array sensor systems. We developed a new architecture that exploits MESA technologies to accomplish a paradigm shift from voluminous data downlink in excess of 100 Mb/s to a much smaller information downlink that could be as low as 10 Kb/s. We evaluated seven MESA (Microsystems and Engineering Sciences Applications) technologies with possible system relevance:

- *Advanced packaging*.
  High-density integrated substrate technology (HDIST)
- *Radiation-hardened processors*.
  Chalcogenide via array
  Hardened-by-design modified commercial field-programmable gate array (FPGA) (processor core)
- *Power management*.
  Radiation-hardened point-of-load power converter
- *Thermal management*.
  Microfluidic convective cooler
  Joule-Thomson microcryogenic cooler array
  Thermal interface materials (TIMs)

A data processor with reduced volume and improved reliability requires at minimum advanced packaging and a radiation-hardened processor core. A sample layout performed on HDIST showed that all of the functional elements of a data-processing node could be packaged on a 6.6 cm^2 substrate, about 6x smaller than for a printed wiring board, and were superior to all other available high-density interconnects. We found that the Chalcogenide via array increases estimated power requirements tenfold and removed it from consideration, but the hardened-by-design modified commercial FPGA is estimated to have similar performance to off-the-shelf chips at about half the gate density, which is more than adequate for FEMS.

State-of-the-art synchronous dynamic random access memory (SDRAM)–based FPGAs such as those envisioned for the FEMS data processor have operating voltages near 1.0 V, but currents up to 20 A. The complete processor module will therefore consume up to 200 A. Currents of this magnitude are difficult to distribute, and for this reason we considered the use of point-of-load (POL) power conversion to supply each FPGA submodule locally from a higher voltage, hence lower current. Commercial POLs are not radiation-hard, but the radiation-hardened controller for a suitable POL could be made at Sandia.

The power consumption of the cryocooler is about 40% of total system power and a good target for improvement. However, calculations for the Joule-Thomson array based on literature values demonstrated that the cooling efficiency would

We developed a new architecture that exploits MESA technologies to accomplish a paradigm shift from voluminous data downlink in excess of 100 Mb/s to a much smaller information downlink....

be insufficient to compete with off-the-shelf cryocoolers for advanced FEMS.

We considered microfluidic convective coolers for thermal management of processor module waste heat, but determined less-exotic methods using passive heat spreaders to be adequate. Similarly, advanced TIMs are promising for improved thermal management, but are not required for near-term FEMS integration; in far-future evolutions, this sort of technology could become vital.

In summary, we chose three technologies as applicable to a near-term implementation of a FEMS:

- High-density integrated substrate technology (dense interconnect),
- Hardened-by-design commercial FPGA (processor core), and
- Radiation-hard POL power converter (local processor supply).

Conceptual integration of these elements yields 30x reduction in data-processor volume and 8.5x reduction in data processor mass. These savings in volume and mass enable the processor to be integrated into the main sensor unit, with the benefit of reducing integration issues with the satellite system.

Other Communications

Chanchani, R., D. T. Bethke, D. B. Webb, C. Sandoval, and G. Wouters. 2004. Integrated substrate technology. *Proc. 54th Electronic Components and Technology Conference* **2** (1–4 June, Las Vegas, Nevada): 1232–36.

78132

Deciphering the Genetic Regulatory Code Using an Inverse Error Control Coding Framework

E. E. May, W. M. Brown, J. Watson, W. E. Hart, A. M. Johnston

Sandia found that developing a computational framework for reconstructing error control (EC) codes for engineered data and ultimately for deciphering genetic regulatory coding sequences is a challenging and uncharted area that will require advances in computational technology for exact solutions. Although exact solutions are desired, computational approaches that yield plausible solutions would be considered sufficient as a proof of concept to the feasibility of reverse-engineering EC codes and the possibility of developing a quantitative model for understanding and engineering genetic regulation. Such evidence would help move the idea of reconstructing EC codes for engineered and biological systems from the high-risk/high-payoff realm into the highly probable/high-payoff domain. Additionally, this work will impact biological sensor development and Sandia's ability to model and ultimately to develop defense mechanisms against bioagents that can be engineered to cause catastrophic damage. Understanding how biological organisms are able to communicate their genetic messages efficiently in the presence of noise can improve our current communication protocols, a continuing interest of Sandia and the Department of Energy (DOE).

Toward this end, project goals include the following:

(1) To develop parameter estimation methods for n *for block codes and for* n, k, *and* m *for convolutional codes. We will use methods to determine the EC code parameters for the gene regulatory sequence.*

(2) To develop an evolutionary computing (GA [genetic algorithm]) computational framework for near-optimal solutions to the algebraic-code-reconstruction problem. We will test the method on engineered and biological sequences.

We used information theory, cryptographic analysis, and evolutionary computing methods to achieve the goals of this project.

Our primary goal was to develop an evolutionary computing framework for determining near-optimal solutions for the reconstruction of algebraic EC codes in systematic form. We developed algorithms for the code-reconstruction problem and used the algorithms to study the fitness landscape of the

(7, 4) Hamming code. The fitness landscape contains neighborhoods with multiple local maxima. The overall fitness landscape appeared surprisingly regular. Landscape studies helped determine the most viable fitness coefficients for the cost function of our GA. The optimal cost function weights the number of zeros in the syndrome matrix of a candidate code significantly higher than the number of nonzero terms in the parity matrix of the code. As the coefficients in the cost function approach optimal values, the (7, 4) code's fitness landscape forms three distinct regions. The majority of codes fall in the 0.5 fitness range, followed by the ~ 0.67 range. Very few codes fall in the ~ 0.84 range, and only one code (the solution) has a fitness value of 1. Exploration of the fitness landscape also suggested that modifications of candidate solutions in integer space may prove an effective approach for exploring neighborhoods. We used the reconstruction algorithms to develop a parallel GA that uses local search to find the optimal code for a set of codewords.

The secondary objective was to develop parameter estimation methods for key EC code values such as the number of information bits, codeword length, and memory length for convolutional codes. Expanding the modified entropy approach, we applied the entropy algorithm to codebooks with multiple code configurations to gain insight into codeword length approximation methods. The value of *k* (number of information bits) in the current algorithm is bounded by log_2 (number of codewords in codebook) for binary codes. Additionally, errors in codewords can distort results. For codebooks composed of concatenated codes (a sequence is composed of two codewords produced by two different codes), the coding parameter for the larger code (larger *k*) masks the *k* value of the smaller code. Further investigation continues into a more robust and extendable approach for code parameter estimation for a generic sequence set.

In addition to parameter estimation for generic binary codebooks, we explored EC coding characteristics of genetic sequences. We investigated more decisive linearity measures for biological sequences. We developed a biological channel capacity model using a relay channel framework to represent deoxyribonucleic acid (DNA) transmission via genetic replication. Using the relay channel framework, we found that channel capacity for eukaryotic organisms is less for the entire genome than for the effective genome, suggesting the presence of EC codes of rates less than (n-1)/n as we originally believed. We also used the relay channel model to perform a cursory study of the relationship between channel capacity and cellular

aging and death. The model investigates the correlation between the number of times genomic DNA is replicated in an organism's lifetime and the capacity of the replication channel. The reduction in capacity over replication time suggests the necessity of significant EC in the long-term transmission of DNA.

Refereed

May, E. E. 2004. Error-control codes and the genome. (Invited) Book chapter in *Genomics and Proteomics Engineering* (IEEE), in review.

May, E. E., A. M. Johnston, J. P. Watson, W. E. Hart, and D. C. Schmidt. 2004. Deciphering the genetic error-control code. *IEEE Engineering in Medicine and Biology Magazine's* special issue on Communication Theory, Coding Theory, and Molecular Biology, submitted.

Schmidt, D. C., and E. E. May. 2004. Visualizing ECC properties of *E. coli* K-12 translation initiation sites. *Proc. Workshop on Genomic Signal Processing and Statistics* (May, Baltimore, Maryland).

Other Communications

May, E. E. 2003. Coding theory and protein synthesis. Paper presented at the MIT Center for Bits and Atoms' Avogadro-Scale Engineering Workshop, November, Boston, Massachusetts.

78783

Generalized Continuum Models for Inelasticity in Solids: Formulation of Theories and Variational Methods for Computation

R. A. Regueiro, K. K. Garikipati

Classical continuum theories of inelasticity in solids break down when the deformation occurs at scales of a micron and below. In polycrystalline materials, for instance, microstructural features such as grain boundaries, dislocation clusters, microvoids, and microcracks introduce length-scale effects that are not represented in the classical theories. However, length scales embedded in additional degrees of freedom (DOFs) associated with generalized continua can be introduced on a physically and mathematically rigorous basis. Therefore, these theories are capable of modeling the influences of microstructure. Such models have gained prominence over the past decade. They are being applied actively to model strain localization associated with material softening, large stresses ahead of atomically sharp cracks, grain size effects, grain rotation and breakage, and the influence of asperities in contact or friction. The most widely used of such theories introduces length scales via first and higher gradients of some inelastic strain measure. There is a large range of these theories, and not all of them are equivalent. Fundamental physical, mathematical, and numerical questions remain on (1) the order of strain gradients, (2) the place of higher-order derivatives in governing equations, (3) inelastic strain-gradient dependence in yield functions and flow rules, and (4) the application of additional boundary conditions. In this project, we will work with a class of generalized continuum inelasticity models of interest to Sandia researchers. The length scales in these models arise from the density of geometrically necessary dislocations and the disclination density. They are represented by appropriately defined tensors. We will critically examine the models in context of the four issues raised above. We will take recourse to experimental data in addition to mathematical analysis. In particular, we will draw heavily from dislocation theory. We seek to develop vector finite-elements and discontinuous Galerkin methods to solve initial and boundary value problems using these models.

We made two accomplishments.

(1) We completed the numerical formulation of a strain-gradient–enhanced plasticity model using vector finite-element methods (FEMs). We presently are working on the two-

dimensional (2-D) problem for classical plasticity wherein the plastic strain is interpolated from DOFs carried along element edges. The corresponding DOFs are scalars, while the interpolation functions are vectors. The base element that we used is the four-node quadrilateral with bilinear shape functions for displacements. The numerical formulation can reproduce the correct solution for shear deformation arising from a single slip system with no contribution from plastic strain gradients. Next, we will include the plastic strain-gradient effects. To our knowledge, this will be the first implementation of vector FEMs for strain-gradient plasticity problems. We anticipate that the vector treatment will result in a more accurate representation of the incompatibilities associated with strain-gradient plasticity.

(2) We continued work on discontinuous Galerkin formulations for strain-gradient damage theories and completed a detailed study of a recently proposed discontinuous Galerkin formulation for a class of strain-gradient damage models. This included analytical and numerical studies of convergence rates.

80838

Molten Salt-Based Growth of Bulk GaN and InN

K. E. Waldrip, D. Ingersoll, F. M. Delnick, J. L. Krumhansl

The realization of widespread implementation of both high-power solid-state electronics such as high-electron-mobility transistors (HEMTs) for applications like synthetic-aperture radar (SAR), and visible light-emitting diodes (LEDs) for high-brightness, high-efficiency lighting applications, is stifled by, among other things, poor material quality. The best way to improve the material quality is to grow epitaxial layers on high-quality native gallium nitride (GaN) and indium nitride (InN) substrates. However, a process that is capable of manufacturing bulk GaN has not yet emerged; those processes currently being explored suffer from extremely high process pressures (4,000–45,000 atmospheres) resulting from the unfortunate combination of high melting points and high-equilibrium vapor pressures of nitrogen over the solid phase at high temperatures encountered in this materials system. For InN, the overpressures are much higher. In conjunction with slow kinetics, both the manufacturability and scalability of these processes may ultimately be limited, and the cost of such processes is potentially prohibitive when one considers the impact on a high-volume, low-cost commodity such as LEDs for the purpose of reducing the amount of energy spent for lighting in the U.S. and the world.

Sandia met three milestones to investigate the possibility of using a molten salt-based approach to grow GaN and InN:

(1) Measured the solubility of GaN in lithium chloride (LiCl) versus temperature,

(2) Made a decision point for dissolution and precipitation, and

(3) Constructed an electrochemical apparatus.

(1) Solubility of GaN in LiCl investigations by inductively coupled plasma–mass spectrometry (ICP–MS) are under way. Although there are some difficulties inherent in the analysis method, it is becoming increasingly convincing that these problematic events (described below) are conspiring to produce a lower-bound estimate of the solubility for the data collected to date. If this is correct, then the solubility is at least as high as was predicted theoretically, and could be a factor of 10 higher.

The analysis approach involves extracting samples of GaN–saturated molten salt from the vessel at various temperatures. The salt is quenched to room temperature, and an amount of the

salt/GaN solution is scraped from the extraction tube and weighed. (The first problem is that it collects water during the weighing process, which ultimately leads to a lower-bound measurement of the GaN content. This can be resolved by doing the scraping and weighing in a dry room, or by measuring the Li concentration and calculating a Ga/Li ratio.) Then water and a few drops of HNO_3 are added to the salt mixture, and it is weighed again. If necessary, we make secondary dilutions from this primary solution, inject them into the ICP–MS, and analyze them for Ga and Li for a final Ga/Li ratio. There exists some scatter in the data, and the solubility appears to be somewhat constant with temperature; this is probably attributable to the GaN segregating out of solution once it is in water. The LiCl dissolves in water, but the GaN does not; and we must find a way to keep the GaN from agglomerating and giving spurious results. The scatter in the data is considerably reduced upon filtering the diluent with a 0.2 µm filter, which again would produce a lower-bound estimate of the true GaN concentration in the LiCl. Even after filtering out GaN agglomerates, the measured concentration lies above the theoretical solubility curve even at lower temperatures. The fact that the solubility is somewhat constant with temperature could be due to the limited solubility of GaN in the water at constant temperature (25°C). Experiments are in progress to determine whether this explanation is true.

(2) The second milestone was to decide whether to continue with the dissolution and precipitation phase of the project on the basis of the results of the first milestone. The decision is that this does, in fact, appear to be much more promising an approach than was originally thought. At this time, the GaN concentrations in LiCl at 800°C–950°C appear to lie in the 10–50 ppm range, corresponding to a growth rate of ~ 50–100 µm/hr. This is high enough to begin trying to grow bulk crystals and start learning what the problems will be.

We made a first attempt to measure the solubility of InN in LiCl at high temperature (650°C is considered to be a high temperature for this material), but we found that the InN decomposed. We will continue with these experiments in LiCl–potassium chloride (KCl) eutectic at 350°C–3500°C.

(3) In constructing an electrochemical apparatus, we acquired two glove boxes. Vacuum, process-and-purge gas supply/return, thermocouple, coaxial, and additional alternating-current (ac) power bulkhead feedthroughs were added to the first glovebox. The second glovebox will receive similar treatment. We acquired quartz and alumina vessels (> 2.5 in. I.D. [inside diameter]) and custom-built “top hats” for

electrical/gas feedthroughs into the electrochemical cell. Furnaces and controllers are standing by, ready for use for the project. A small leak is present in the glove box after all the feedthrough installations, but we expect to resolve that issue shortly.

Appendix A: Project Number/Title Index

Project Number	Title	Page Number
38605	Microfabrication with Femtosecond Laser Processing	41
38606	Mesoscale Controlled Motion for a Microfluidic Drop Ejector	44
38609	Physical and Electronic Changes Caused by Membrane Signaling as a Transduction Pathway in Affinity-Based Biosensors	77
38610	Graduated Embodiment for Sophisticated-Agent Evolution and Optimization	116
38613	Scalable Fault-Tolerant Algorithms for Linear-Scaling Coupled-Cluster Electronic Structure Methods	119
38614	Micromagnetic Suspension	121
38615	Sensitivities for Large-Scale Simulation Codes	123
38616	Engineered Superconductivity in Electron-Hole Bilayers	168
38617	Silicon-Based RF MEMS Components	171
38619	Nanoelectromechanical Oscillators (NEMOs) for RF Filtering	173
38620	Continuous-Wave Intersubband Terahertz Sources	176
38621	Microsystems for Chemical Signature and Reagent Delivery	178
38622	Microfluidic Cellular-Sample Pretreatment	180
38623	Automated Visual Direction of Mobile Manipulation	231
38624	Miniature Fourier-Transform Ion-Mobility Spectrometer for Real-Time Detection and Identification of Explosives and Chemical Agents	233
38627	EM Interactions with Systems to Enhance Security	235
38629	Use of Seismic and Acoustic Responses to Assess Bomb Damage to Underground Facilities	236
38655	Free-Space Electrooptic Sampling and Remote Mapping of Electromagnetic Fields from Emitting Structures Using Femtosecond Terahertz Transceivers	238
38662	Natural-Gas Production Problems: Solutions, Methodologies, and Modeling	332
38665	Time-Domain Reflectometry for Remote, Real-Time Water-Quantity/-Quality Monitoring of Perennial and Ephemeral Streams	335
38668	Functionalized Nanoelectrode Arrays for *In Situ* Identification and Quantification of Regulated Chemicals in Water	338
38673	Water Desalination	341
38674	Revolutionary Systems for Catalytic Combustion and Diesel Catalytic Particulate Traps	344
38677	Potential Application of Microsensor Technology in Radioactive-Waste Management—With Emphasis on Headspace Gas Detection	348

Appendix A: Project Number/Title Index

Project Number	Title	Page Number
38681	Identification of Chemical Plumes: Range-Resolved IR Lidar Enabled by New Photonic Technologies	241
38684	A Robust, Coupled Approach for Atomistic-Continuum Simulation	434
38685	Microscale Rarefied-Gas Dynamics and Surface Interactions for EUVL and MEMS Applications	438
38686	High-Fidelity Frictional Models for MEMS	441
38687	Soot Formation, Transport, and Radiation in Unsteady Diffusion Flames	444
38688	The Basics of Aqueous Nanofluidics: "Interphase" Structure and Surface Forces	493
38689	Design, Synthesis, and Characterization of Soft-Matter Nanolayer Superlattices	497
38690	Photocontrol of Nanointeractions in Microsystems	499
38691	Electrochemically Deposited Alloys with Tailored Nanostructures for LIGA Micromachines	501
38692	Nanostructured Materials for Directed Transport of Excitation Energy	503
38693	Modeling Local Chemistry in the Presence of Collective Phenomena	505
38717	Nanoscale Energetic Materials by Inverse Micellar Synthesis	701
38718	Modeling of Rock Penetration	704
38722	Agile, Microsystems-Enabled Receiver	572
39017	Solution-Based Nanoengineering of Materials	507
39670	Simulations of Intense Petawatt Laser Pulses with Dense Z-Pinch Plasmas	684
41193	Biomicrofuel Cell (BMFC)	473
41194	Augmented Cognition: Next-Generation Intelligent Systems	476
41674	Microengine for Advanced Power Generation	164
41726	Direct Simulation of Solid-Fluid Systems	707
42461	Support–Active Site Interactions in Heterogeneous Catalysts	710
42483	An Analysis of the Automotive Industry as a Source for Weapon Components and Manufacturing Processes	712
46070	High-Speed Micro-EDM	713
46686	Microexternal-Combustion Engine: The P3 Engine Prototype	715
47795	Lipid Membranes on Nanostructured Silicon	717
49769	Resin Infusion Between Double Flexible Tooling	720
49772	Studies on the Disbonding Initiation of Interfacial Cracks	723

Appendix A: Project Number/Title Index

Project Number	Title	Page Number
49915	Critical Technology Development for Hard-Target-Defeat High-G-Tolerant Fuze and High Explosives	243
50065	TALON	480
50396	Compliant Membranes for MEMS Microphones	725
50717	Multiscale Experimental/Numerical Study	727
50772	Cellular Observatory: Simultaneous Time- and Frequency-Resolved Microscopy	80
52523	Atomic Layer Deposition of Highly Conformal Tribological Coatings	46
52524	Assembly of Microsystems Using Exothermic Multilayer Thin Films	50
52526	Intelligent Interaction Control as Applied to Metrology and Assembly of Microscale Components	52
52527	Rapid-Prototyping High-Density Circuitry (RpHdc)	55
52528	Elucidating the Mysteries of Wetting	57
52530	Next-Generation Spindles for Micromilling	60
52531	Assembly and Actuation of Nanomaterials Using Active Biomolecules	510
52532	Modeling Biomembranes	82
52533	Reverse-Engineering Biological Networks: Applications in Immune Responses to Bioterrorism Threats	84
52536	High-Throughput Identification of Molecular Machines Involved in Membrane Signaling and Toxin Pathways	88
52537	Coupled Solid-Fluid-Mechanical-Computational Modeling of Fracture and Fragmentation in Geomaterials, such as Hard and Deeply Buried Targets (HDBTs)	447
52538	Sequestration of Pathogens on Nanoengineered Surfaces	107
52539	A Combined Preconcentrator and Sensor for Live Waterborne Pathogens	111
52540	IP Storage: A Performance and Security Study	126
52541	A Parallel Circuit Simulator for Cell Biology	129
52542	Developing a Computationally Efficient Dynamic Multilevel Hybrid Optimization Scheme Using Multifidelity Model Interactions	131
52543	Robust Large-Scale Parallel Nonlinear Solvers for Simulations	134
52544	Development of Computational Algorithms and Inversion Capabilities for Transport/Reaction Simulations of Chemical/Biological/Radiological Terrorist Attack Scenarios in Support of Homeland Security	137
52546	Massively Parallel Linear Programming	140

Appendix A: Project Number/Title Index

Project Number	Title	Page Number
52548	Active Photonic-Crystal Devices for Integrated Photonics and Silicon Photonics	183
52549	Co-Processing of Chalcogenide-Based Radiation-Hard Nonvolatile Memories by Sandia's MDL and BAE Systems	185
52551	Functionalized Nanoparticles for Sensor Applications	187
52552	Novel *In Situ* Mechanical Testers to Enable Integrated Metal Surface Micromachines	190
52553	Compliant Thermomechanical MEMS Actuators	193
52554	An Integrated, Stacked System-on-a-Chip	196
52555	Micromass Spectrometer-on-a-Chip	199
52556	Quantum Coherence in Semiconductor Nanostructures for Improved Lasers and Detectors	201
52557	MOSFET–MEMS Integration	203
52566	Microoptical Gyroscope Via Monolithic Active/Passive Optical Integration	205
52570	Materials Physics and Device Development for Improved Efficiency of GaN HEMT High-Power Amplifiers	207
52571	Leaky-Mode VCSELs for Photonic Logic Circuits	209
52575	Advanced Polychromator Systems for Remote Chemical Sensing	211
52577	Immunological Basis for High-Reliability Systems Control	245
52580	Moving-Target Identification Using Ultrahigh-Range-Resolution Data	247
52581	Advanced Mobile Networking, Sensing, and Controls Using Graph Theory	249
52582	Compact Terahertz Sources for Emerging-Threats Applications	252
52583	Understanding Communication in Counterterrorism Crisis Management	255
52584	Hypervelocity Impact-Generated Flash	258
52585	Improving Human/System Interactions in Systems-of-Systems	260
52586	Distributed Detection and ID Algorithm Architecture for Unattended Ground Sensors	262
52587	Secure Chaotic Communications	264
52588	System-of-Systems Modeling and Analysis	266
52589	Eye-Safe Short-Range Standoff Aerosol-Cloud Finder	268
52590	Microflame-Based Detector Suite for Universal Gas Sensing	270
52591	Beyond Nanoparticles—Attack on a Chemical "Holy Grail"	351
52592	Advanced Proton-Exchange Materials for Energy-Efficient Fuel Cells	354

Appendix A: Project Number/Title Index

Project Number	Title	Page Number
52593	Alanate-Hydride Fuel-Cell Demonstration Project	357
52595	Real-Time Discriminatory Sensors for Water-Contamination Events	360
52596	Advanced High-Efficiency Direct-Cycle Gas Power-Conversion Systems for Small Special-Purpose Nuclear-Power Reactors	362
52597	Securing Mobile Code	365
52598	Novel Catalysts for Hydrogen Fuel-Cell Applications	368
52606	Linking Optimization and Simulation in Critical-Infrastructure Systems	372
52698	Decomposition of Contaminants Using Photochemically Active Nanoparticles	514
52699	Thermally Cleavable Surfactants	516
52700	Transition-Metal Catalyzation of Complex-Hydride Absorption/Desorption Reactions	518
52701	Quantification of Environments and Surfaces Within Micropackages	520
52702	Assembly of Ordered Electrooptical and Bioactive Materials and Composites	523
52703	Advanced Packaging/Joining Technology for Microsystems	525
52705	Magnetostrictive Elastomers for Actuators and Sensors	528
52706	Development of a High-Throughput Microfluidic Integrated Microarray for the Detection of Chimeric Bioweapons	576
52708	Zero-Power Radio Receiver	578
52709	Completely Passive Microwave Tag	581
52710	Security Coatings for Multichip Modules	584
52711	Detailed Modeling and Simulation of Contaminant Transport in Architectural Spaces	586
52712	Content-Based Video and Image Indexing System	588
52713	Bioaerosol Collection and Concentration for Microseparations-Based Detectors	591
52714	Detecting the Toolmarks of Genetic Engineering in Bioweapons Strains	594
52716	Joint Authentication/Encryption	596
52717	Ultrahigh-Temperature Ceramics for Hypersonic Vehicle Applications	598
52718	Leveraging Robotic Planning for Physical-Security Analysis	601
52720	Ultralightweight Telescope with MEMS Adaptive Optic for Distortion Correction	604
52721	Modeling Signals from Earth-Penetrating Nuclear Weapons for Remote Kill Assessment	606
52723	Novel Micropreconcentrators for CW, Explosives, and Water Surety	607

Appendix A: Project Number/Title Index

Project Number	Title	Page Number
52724	Ion-Mobility Spectrometer/Mass Spectrometer	610
52725	Cryptographic Assurance of Execution Correctness and Confidentiality	612
52726	Characterization, Performance, and Optimization of PVDF as a Piezoelectric Film for Advanced Space Mirror Concepts	615
52727	Predictive Accelerated Aging of Microsystems: The Science of Dormancy	730
52728	Surety and Accountability Enhancements for Storage Containers	733
52729	Nuclear-Safety Weaklinks for Thermal and Mechanical Environments	735
52730	Advanced Packaging Technology for Optical Firesets	738
52731	Miniature Transmitter Filter for JTA Using LIGA Technology	740
52732	Novel and Robust Environmental Sensing Devices (ESDs)	743
52733	Advanced Neutron Monitors for J TA and Stockpile Monitoring	745
52737	Development of an Efficient Large-Aperture High-Damage-Threshold Sol-Gel Diffraction Grating	686
52738	Laser Triggering of Water Switches in Terawatt-Class Pulse-Power Accelerators	689
52739	Experimental and Computational Study of Liquid-Solid Transition in Tin	530
52797	Design and Control of the Magnetic Properties of Nanoparticles	747
52977	Flow Control and Mixing in Microfluidic Devices	749
53464	Atomic-Scale Scanning-Tunneling Microscopy Measurements of Nucleation and Growth of Ge/Si Alloy Structures	752
53465	Micro-/Nanoscale Thermomechanical Manufacturing	754
53585	Novel Diagnostics for Rarefied Flows in MEMS Applications	450
53586	Geophysical Subsurface Imaging and Interface Identification	113
53587	Evolution of Near-Surface Scalar Concentrations Through a Compact Cylinder Array Embedded in the Atmospheric Surface Layer	756
53588	Miniature High-Power RF Components Enabled by Mesoscale Manufacturing	63
53590	Electrical Conductivity of Metal Alloys	691
53591	Hydrogen Futures Dynamic Simulation Model	375
53681	Design of Biospecific Surfaces to Control Specific Cellular Responses	757
54211	Nanomagnetic Films	760

Appendix A: Project Number/Title Index

Project Number	Title	Page Number
54213	A Multiscale Approach to Modeling Carbon Nanotube–Reinforced Composites	762
55079	Near-Real-Time Characterization for Assured HDBT Defeat	483
55086	Prompt Global Response	486
55087	Winning the War: A Systems Approach to Defending Our Borders	488
57300	Integrated Superhard and Metallic Coatings for MEMS	765
57307	Microscale Separations of Biological Compounds Using Novel Polymeric Separations Materials	769
57308	Friction in Micromachine Interfaces	772
57309	Lipid Microarray Biosensor for Biotoxin Detection	774
57310	Advanced Manufacturing Techniques Using Rapid Prototyping	777
57311	Robust Hermetic Packaging Techniques for MEMS Integrated Microsystems	779
58907	Active Photonic Nanostructures	532
59034	3-D Large-Eddy Simulation of Turbulent Flow Based on One-Dimensional Turbulence Modeling	781
59916	A Method of Evaluating Research Using New Innovation, Risk, and Impact Indicators	143
61046	Photonic Encryption Using All-Optical Logic	784
62269	Nanoporous-Carbon Adsorbers for Chemical Microsensors	786
62827	Nonlethal Technologies for the War on Terrorism	273
64811	Agent-Based Control of Distributed Infrastructure Resources	377
65559	Direct Single-Ion Machining of Nanopores	789
66170	Investigation of the Effects of Intense Pulsed Particle Beams on the Durability of Metal-to-Plastic Interfaces	792
66450	Advanced Techniques for Multiobjective Discrete Optimization	794
66809	Nonradioactive Safety and Performance Issues with Supercritical Water Reactor (SCWR) Safety Technologies	796
66810	Radiation Performance Issues with Advanced Coolants for Next-Generation Reactor	798
67004	Rapid Prototyping to the Nanometer Scale	66
67005	Robust Manufacturing of Gel-Based Components for Nuclear Weapons	67
67006	Meso-/Microoptical System Interface Coupling Solutions	69
67007	Injection Molding of Net-Shape Active Ceramic Components	71

Appendix A: Project Number/Title Index

Project Number	Title	Page Number
67008	Macro-/Meso-/Microsystems Integration in LTCC	73
67010	Studies of Signaling Domains in Model and Biological Membranes Through Advanced Imaging Techniques	91
67011	Imaging Self-Organization of Proteins in Membranes by Photocatalytic Nanotagging	93
67012	Protein Microarrays for Biowarfare-Agent Detection and Characterization	96
67013	Interaction of Proteins with Lipid Films	99
67014	New Technologies for Understanding Membrane-Protein Recognition and Signaling	103
67015	Massively Parallel Scalable Atmosphere Model	145
67016	High-Performance Processing Architecture	147
67017	Substructured Multibody Molecular Dynamics	149
67018	Enhancing Simulation Performance on Clusters with Configurable Auxiliary Devices	151
67019	A Hybrid Level-Set/Particle Method for Modeling Surface Evolution During Feature-Scale Etching and Deposition Processes	154
67020	Penetrator Reliability Investigation and Design Exploration (PRIDE)	157
67021	Topology Optimization for Improving Sensor Performance	160
67022	Characterization and Application of Dielectrics with Controlled Leakage	213
67023	Nano-G Accelerometers Using Nanophotonic Motion-Detection System	216
67024	Bragg Fiber Development	218
67025	Microwave-to-Millimeter-Wave Electrodynamic Response and RF Applications of Semiconductor Quantum Nanostructures	220
67026	Development of GaN 20–100 Watt Ku-Band Power Amplifiers for Micro-SAR	222
67027	Evanescent-Wave Planar Photonic Biosensor	225
67028	Passive Electronically Steerable Array (PESA) for Miniature Synthetic-Aperture Radar (Mini-SAR), Precision Guidance, and Intelligence/ Surveillance/Reconnaissance (ISR)	227
67029	Advancements in Sensing and Perception Using Structured Lighting Techniques and an Innovative Design Tool	275
67030	Biophysics of BW-Warhead Defeat with a Kinetic Interceptor	278
67031	Dispersal in Urban Canyons, Source Identification, and Collateral Damage/Mitigation Assessment	281
67032	Weaponization of Thermobaric Explosives	283

Appendix A: Project Number/Title Index

Project Number	Title	Page Number
67033	Development of an Enterprise-Scale Agent-Based Autonomic Logistics Simulation Model	286
67034	Mobile-Node Authentication in a Wireless *Ad Hoc* Environment	289
67035	Novel Processing, Affordable Motion Compensation, and Mode Multiplexing for Miniaturized Synthetic-Aperture Radar	292
67036	Coilgun Technology Demonstration Test-Bed	295
67037	Enhanced Perception for Remote 3-D Mapping of Unknown Indoor and Outdoor Environments	298
67038	A Modular Micromagnetic Accelerometer in Support of the mTalon Vision	300
67039	MICROFUZE Integration	302
67041	Analysis of Technology Impacts on Operations in Complex Environments	304
67042	CBW Cloud Knockdown and Neutralization	306
67043	Assessment of Biokillers in EDS for Biological-Agent Destruction	308
67044	Adaptive-Force-Feedback Surface Control	310
67046	High-Capacity Earth-Penetrator Instrumentation	312
67047	Systems Analysis of Networked Sensors	314
67048	Deployable Object Tracker for NMD Flights	317
67049	Continuous-Flow Detector for Rapid Pathogen Identification	319
67050	Biological-Security Decontamination Technology—Reducing the Threat of Infectious-Agent Spread	380
67051	Consequence Management, Recovery, and Restoration after an Intentional Contamination Event	383
67052	Fully Integrated System-Dynamics Toolbox for Water Resources Planning	386
67053	Predicting System Performance of Proton-Exchange-Membrane Fuel Cells: Computational Modeling with Experimental Discovery and Validation	390
67054	Optimal Allocation of Terrorist Countermeasures Using Risk-Based Systems Pathways Analysis	393
67055	Silicon Field-Emission Electric Propulsion Arrays (FEEP) Powered by Orbital Nuclear Reactors	396
67056	Advanced Fuel-Cell Reactor for the Direct Cogeneration of Electricity During Selective Partial Oxidation of Hydrocarbons	398
67057	New Hydrogen-Storage Material: Metal-N-H System	401
67058	Intrusion Detection for Wireless Networks	403

Appendix A: Project Number/Title Index

Project Number	Title	Page Number
67059	Membranes for H_2 Generation from Nuclear-Powered Thermochemical Cycles	405
67060	Microfabricated BTU Monitoring Device for System-Wide Natural-Gas Monitoring	408
67061	"Tunable" Ion Conductors for Low-Temperature Oxide-Based Fuel Cells	411
67062	Nuclear Nanobatteries: On-Board Power for Independent MEMS Devices	414
67063	Integrated Tunable Light Sources for Miniature Sensors	417
67064	Ray Model of High-Frequency Cavity Scarring	452
67065	New Smart Material to Address Issues of Structural Health Monitoring	455
67067	Noncontact Surface Thermometry for Microsystems	458
67068	High-Speed Interferometric Deformation Measurements	461
67069	Fundamentals of Nanofluidics	463
67070	Simulating Self-Assembly and Growth of Biological Nanostructured Materials	465
67071	A Low-Power, Ultrafast-Current Transient Measuring Device	468
67073	A Capillary Valve for Microfluidic Systems	470
67074	Electrochemically Switchable Materials for (Bio)Microfluidics	534
67075	Modeling of Friction-Induced Deformation and Microstructure	537
67076	Reversible Antibody Trapping for Selective Sensor Devices	540
67077	Correlated and Comprehensive Analytical Techniques for Homeland Defense	542
67078	Development of High-Energy-Density Dielectric Materials for Integrated Microsystems	545
67079	Nanolithography-Directed Materials Growth and Self-Assembly	549
67080	Development of a Novel Technique to Assess the Vulnerability of Micromechanical System Components to Environmentally Assisted Cracking	552
67081	3-D Optical Sectioning with a New Hyperspectral Deconvolution Fluorescence Imaging System	554
67082	The Science of Solutes: Transition Metals in LIGA Nickel	558
67083	Novel Gel-Based Technology for Sensors and Weapons	560
67084	Coupled Nanomechanical Oscillator Arrays for the Study of Internal Dissipation in Nanoscale Structures and Collective Behavior in Large Systems	562
67085	Precisely Controlled Picoliter Vessels with Rapid Sample Preparation for Trace Biotoxin Detection	565

Appendix A: Project Number/Title Index

Project Number	Title	Page Number
67086	Adaptive Optics and Phase-Diversity Imaging for Responsive Space Applications	618
67087	Infrastructural Development for Flexible Network of Devices	621
67088	Monolithic Reconfigurable Radio-Frequency Microelectromechanical Systems (RF MEMS) Antennas	622
67089	Next-Generation 3-D Inspection System for Facility Monitoring	625
67090	Risk-Assessment Metatool	627
67091	Featureless Spread-Spectrum Waveform Design and Processing	629
67092	Tracking Slow-Moving Objects in a GPS–Denied Environment	631
67093	Optical Communications	632
67094	A Unique Vibration-Based Miniature Power Generator for National Security Applications	633
67095	Image Georectification Using Digital Elevation Model Shadows	636
67096	Vulnerability Assessment of State-of-the-Art Microelectronics	639
67098	Nonlinear Optical Detection of Biological and Chemical Aerosol Agents Using Femtosecond Lasers	640
67099	Polymer Electronic Devices and Materials	643
67101	Small Circuits for Cryptography	647
67102	Analysis of Multichannel Internet Communication	649
67104	Receiver for Ultralow-Power Wake-Up and Command	650
67105	Extraordinary Optical Transmission Through Patterned Subwavelength Apertures	652
67107	Reconstruction Algorithm Development and Assessment for a Computed Tomography–Based Spectral Imager	654
67108	Power-Combining Techniques for Solid-State Power Amplifiers	657
67109	Dispersive Diffractive Optical Elements for the Infrared	659
67111	Atmospheric Propagation of Terahertz Radiation	661
67113	High-Confidence Estimation of Relative Event Locations from Space-Based Sensors	663
67114	Critical-Infrastructure System-of-Systems Assessment Methodology	665
67115	Dynamic Vulnerability Assessment	667
67116	Inflatable Antenna with Adaptive Actuators	669
67117	Data-Driven Dynamic Models of Conflict	671
67118	MEMS/Fuze Diagnostic Extraction in High-G Environments	800

Appendix A: Project Number/Title Index

Project Number	Title	Page Number
67120	Efficient Implicit Multigroup Radiation Calculations	694
67121	Model for Channel Resistance in Water Breakdown	696
67122	Embeddable Shock Physics Sensors	698
67716	Smart Detectors of Enrichment of Bioaerosols	802
68063	Computational Studies of JP-8 Diffusion Flames with Detailed Chemistry and Particulate Formation	805
69143	Design and Fabrication of Advanced Device Structures for Ultrahigh-Efficiency Solid-State Lighting	419
69145	Molecular Simulation of Beta-Amyloid (A-beta) Peptide Interaction with Phospholipid Membranes	808
69146	Nanoscale Testing of Deformation and Fracture in Engineering Materials	809
69148	Nanocrystal-Polymer Composites for High-Luminous-Efficiency LEDs	812
69149	Outstanding Challenges for AlGaInN MOCVD	817
69150	Nanoporous Polymeric Materials for Chemically and Spatially Multiplexed Sensing of Bioagents	820
69151	Evolutionary Complexity for Protection of Critical Assets	823
69152	Nanomechanical Stochastic Resonators	825
69153	Augmented Musculature Device	826
69154	Biomolecular Decision-Making Processes for Self-Assembly	828
69155	Light-Powered Nanovehicle Propulsion	830
69156	System-Dynamics Modeling to Assist Regional Water Planning: Modeling the Nonmarket Value of Water	832
69157	Interactive Water-Quality Modeling to Assist Regional Water Planning	834
69158	Microbe-Exuded Polymers and the Enhanced Corrosion of Carbonate Materials	837
69159	Nerve-Cell Function and the Development of Cognitive Networks	840
69160	Ultrahigh-Gain Fusion Concept	843
69161	Nanofluidic Devices for Rapid Detection of Virus Particles	844
69162	Solution Behavior of PEO: The Ultimate Biocompatible Polymer	846
69163	New Self-Assembled Nanocrystal Micelles for Biolabels	848
69164	Rapid Detection of Biothreat Agents Based on Cellular Machinery	851
69165	Patterning Quantum-Dot Arrays Using DNA Replication Principles	853
69166	Adaptive Algorithms for Use in the Rejection of Periodic Disturbances of Unknown Frequency	856

Appendix A: Project Number/Title Index

Project Number	Title	Page Number
69168	Property-Based Testing for Cybersecurity Assurance	858
69170	Self-Assembled Ordered Carbon-Nanotube Arrays and Membranes	860
69189	Chemical Cross-Linking and Mass-Spectrometry Studies of the Structure and Dynamics of Membrane Proteins and Receptors	863
69190	Toxin Studies Using an Integrated Biophysical and Structural Biology Approach	866
69191	Top-Down Structural Studies	869
69192	Molecular Dynamics of Membrane Proteins	871
69193	Model-Building Codes for Membrane Proteins	874
69198	Poroelastic-Wave Propagation on the Earth Simulator	878
69239	Development of Microreformers for Fuel Cells	882
70799	Developing the Foundation for Polyoxoniobate Chemistry: Highly Tunable and Exploitable Materials	568
71943	Simulating Human Behavior for National Security	321
71944	Agent-Based Modeling of Middle East Terrorist Recruitment	28
71945	Automatic Generation of Terrorist Operation Plan Hypotheses	30
72599	Develop a System-Dynamics Modeling Framework for Assessing Factors that Influence Water Resource Consumption	421
72600	Develop a Cooperative Water-Management Process, Creating a System-Dynamics Model of Water Resources in the Lower Rio Grande Basin	423
72715	Compact Ultrabright Multikilovolt X-Ray Sources for Advanced Material Studies, 3-D Nanoimaging, and Attosecond X-Ray Technology	323
72716	Energy-Systems Analysis Framework and Modeling	425
73045	Radiation-/Geometry-Driven Jets: Proof-of-Principle Tests	33
73185	Superhydrophobic Surface Coatings for Microfluidics and MEMS	884
73207	Microoptical Radar (MOR) Facial-Recognition Project	673
74545	Determining Explosive Ignition Criteria for Miniaturized Devices	886
74546	Quantum Squeezed Light for Probing Mitochondrial Membranes and Study of Neuroprotectants	888
74547	Characterization of a New Class of Surface-Micromachined Pumps	890
74548	Risk of Biological Terrorism to Water-Distribution Systems	893
74759	Explicit and Implicit Measures in Human Aversive Classical Conditioning	895

Appendix A: Project Number/Title Index

Project Number	Title	Page Number
74760	Automatic-Target-Recognition Algorithms for Uncooled Thermal Imagery	676
74795	Magnetophoretic Bead Trapping in a High-Flowrate Biological Detection System	326
75441	TPV Energy Scavenging for Hypervelocity Vehicles	329
75442	Assessment of Advanced Pulsed-Power Fusion Concepts	898
75443	A Mathematical Method for Quantifying the Effectiveness of Management Strategies	427
75513	Developing Algorithms for Predicting Protein-Protein Interactions from Experimental Constraints	901
75514	Instrumentation Development for Real-Time Brain-Wave Monitoring	904
75786	Maximally Autonomous Autodirective Antenna Array Technology	906
76069	Miniaturized Electronic Steerable-Array Synthetic-Aperture Radar	907
76070	Full-Earth-Monitoring Sensor MESA Works	910
76305	Systems Assessment of Water-Savings Impact of Controlled-Environment Agriculture Utilizing Wirelessly Networked SDACs	36
76306	Inactivation of Avian Influenza (Bird Flu) with Sandia-Developed Decontamination Formulations	429
78132	Deciphering the Genetic Regulatory Code Using an Inverse Error Control Coding Framework	913
78307	Climate Change Effects on International Stability	38
78783	Generalized Continuum Models for Inelasticity in Solids: Formulation of Theories and Variational Methods for Computation	916
79943	GeSi–Strained Nanostructure Self-Assembly for Nano- and Optoelectronics	431
80835	Vulnerability Analysis for SCADA	678
80838	Molten Salt-Based Growth of Bulk GaN and InN	918
81209	Randomness Complexity and Cryptography	679
81354	System Study: Adaptive Optics for Weapon, Reconnaissance, and Military Space Applications	681

Appendix B: Awards/Recognition List

Awards/Recognition	*Project Number*	*Project Title*
R&D 100 Award, R&D Magazizne	**26517**	Parallel Repartitioning for Optimal Solver Performance
R&D 100 Award, R&D Magazizne	**27328**	A Revolution in Lighting: Building the Science and Technology Base for Ultraefficient Solid State Lighting
Best Processing Technical Paper Award, ACMA Composites 2004 Convention	**49769**	Resin Infusion Between Double Flexible Tooling
Institute of Electronic and Electrical Engineers (IEEE) Fellow for his Contribution to Advanced Packaging Technologies and to the Electronic Profession in 2003: Rajen Chanchani	**52554**	An Integrated, Stacked System-on-a-Chip
2004 William D. Ashman Award: Rajen Chanchani		
American Welding Society Fellow Award: C. V. Robino	**52703**	Advanced Packaging/Joining Technology for Microsystems
RTAM/SME Dick Aubin Distinguised Paper Award	**57310**	Advanced Manufacturing Techniques Using Rapid Prototyping
Cosslett Award for Best Invited Paper at the 2003 Microscopy and Microanalysis Meeting, Microbeam Analysis Society: D. P. Adams	**67004**	Rapid Prototyping to the Nanometer Scale
Fellow of the Society of Tribologists and Lubrication Engineers: Somuri Prasad	**67075**	Modeling of Friction-Induced Deformation and Microstructure
Best Techniques Paper of 2003 from *Journal of Microscopy and Microanalysis*: "Automated Images: A Powerful New Microanalysis Tool"	**67077**	Correlated and Comprehensive Analytical Techniques for Homeland Defense
2004 Bomem Michaelson Award from the Coblentz Society: David Haaland	**67081**	3-D Optical Sectioning with a New Hyperspectral Deconvolution Fluorescence Imaging System

Appendix B: Awards/Recognition List

Awards/Recognition	*Project Number*	*Project Title*
Materials Research Society Medal: C. J. Brinker	**73185**	Superhypdrophobic Surface Coatings for Microfluidics and MEMS
DOE Basic Energy Sciences Chunky Bullet Competition Award	**74546**	Quantum Squeezed Light for Probing Mitochondrial Membrances and Study of Neuroprotectants

Appendix C: Project Performance Measures

		Performance Statistics (Number of)										Project Qualitative Assessment		
Project Title	Project #	Refereed Publications	All Other Reports and Publications	Patent Disclosures	Patent Applications	Patents	Copyrights	Students	Post-docs	Permanent Staff Hired*	Awards	New Non-LDRD-Funded Projects†	% Milestones Completed	Goals Status**	Hypothesis Status***
Microfabrication with Femtosecond Laser Processing	38605	4	4	1						1			95%	1	7
Mesoscale Controlled Motion for a Microfluidic Drop Ejector	38606			1	1			2		1			80%	3	7
Physical and Electronic Changes Caused by Membrane Signaling as a Transduction Pathway in Affinity-Based Biosensors	38609	1						3					90%	2	7
Graduated Embodiment for Sophisticated-Agent Evolution and Optimization	38610		2	1				3		1			95%	2	6
Scalable Fault-Tolerant Algorithms for Linear-Scaling Coupled-Cluster Electronic Structure Methods	38613												100%	1	7
Micromagnetic Suspension	38614	3		2									100%	1	7
Sensitivities for Large-Scale Simulation Codes	38615	3	1		2			3	1	1			100%	1	6
Engineered Superconductivity in Electron-Hole Bilayers	38616	2	1					1					70%	2	7
Silicon-Based RF MEMS Components	38617	1											20%	3	8
Nanoelectromechanical Oscillators (NEMOs) for RF Filtering	38619	11		2	2			2	2				70%	1	7
Continuous-Wave Intersubband Terahertz Sources	38620							1		2			70%	3	7
Microsystems for Chemical Signature and Reagent Delivery	38621			1				1					75%	4	7
Microfluidic Cellular-Sample Pretreatment	38622	2	2	1				2					75%	2	8
Automated Visual Direction of Mobile Manipulation	38623						1						75%	2	6
Miniature Fourier-Transform Ion-Mobility Spectrometer for Real-Time Detection and Identification of Explosives and Chemical Agents	38624	1				1		4		2			100%	1	6
EM Interactions with Systems to Enhance Security	38627												100%	1	7
Use of Seismic and Acoustic Responses to Assess Bomb Damage to Underground Facilities	38629	1	1					1					95%	1	6

Appendix C: Project Performance Measures

		Performance Statistics (Number of)										Project Qualitative Assessment		
Project Title	Project #	Refereed Publications	All Other Reports and Publications	Patent Disclosures	Patent Applications	Patents	Copyrights	Students	Post-docs	Permanent Staff Hired*	Awards	New Non-LDRD-Funded Projects†	% Milestones Completed	Goals Status**	Hypothesis Status***
Free-Space Electrooptic Sampling and Remote Mapping of Electromagnetic Fields from Emitting Structures Using Femtosecond Terahertz Transceivers	38655	1											90%	1	8
Natural-Gas Production Problems: Solutions, Methodologies, and Modeling	38662		7					1					100%	1	6
Time-Domain Reflectometry for Remote, Real-Time Water-Quantity/-Quality Monitoring of Perennial and Ephemeral Streams	38665	1	4	1				1					100%	1	6
Functionalized Nanoelectrode Arrays for *In Situ* Identification and Quantification of Regulated Chemicals in Water	38668				12			2					100%	1	6
Water Desalination	38673		3										100%	1	6
Revolutionary Systems for Catalytic Combustion and Diesel Catalytic Particulate Traps	38674	2	5		4			2	1		3		80%	3	7
Potential Application of Microsensor Technology in Radioactive-Waste Management—With Emphasis on Headspace Gas Detection	38677			2				1		9			100%	1	6
Identification of Chemical Plumes: Range-Resolved IR Lidar Enabled by New Photonic Technologies	38681									1			75%	3	9
A Robust, Coupled Approach for Atomistic-Continuum Simulation	38684	6							1				90%	1	7
Microscale Rarefied-Gas Dynamics and Surface Interactions for EUVL and MEMS Applications	38685		1										80%	2	6
High-Fidelity Frictional Models for MEMS	38686	3	2					2	1				85%	2	6
Soot Formation, Transport, and Radiation in Unsteady Diffusion Flames	38687	1	1						1				90%	2	9
The Basics of Aqueous Nanofluidics: "Interphase" Structure and Surface Forces	38688	7	9										90%	2	6
Design, Synthesis, and Characterization of Soft-Matter Nanolayer Superlattices	38689							1					100%	1	6
Photocontrol of Nanointeractions in Microsystems	38690				1								60%	3	7
Electrochemically Deposited Alloys with Tailored Nanostructures for LIGA Micromachines	38691	2		1									55%	3	7
Nanostructured Materials for Directed Transport of Excitation Energy	38692			1				2	1				70%	3	7

Appendix C: Project Performance Measures

		Performance Statistics (Number of)											Project Qualitative Assessment		
Project Title	Project #	Refereed Publications	All Other Reports and Publications	Patent Disclosures	Patent Applications	Patents	Copyrights	Students	Post-docs	Permanent Staff Hired*	Awards	New Non-LDRD-Funded Projects†	% Milestones Completed	Goals Status**	Hypothesis Status***
Modeling Local Chemistry in the Presence of Collective Phenomena	38693		1										80%	1	6
Nanoscale Energetic Materials by Inverse Micellar Synthesis	38717		1	1					1				70%	2	7
Modeling of Rock Penetration	38718		2					1					75%	2	7
Agile, Microsystems-Enabled Receiver	38722	4	4							1			90%	2	6
Solution-Based Nanoengineering of Materials	39017	5	3					1	1				100%	1	6
Simulations of Intense Petawatt Laser Pulses with Dense Z-Pinch Plasmas	39670	6	2	1									95%	1	6
Biomicrofuel Cell (BMFC)	41193	2	5	11	3			2	4	1			90%	2	7
Augmented Cognition: Next-Generation Intelligent Systems	41194	6	3	5			3	3	1	3			95%	2	7
Microengine for Advanced Power Generation	41674								2				75%	3	8
Direct Simulation of Solid-Fluid Systems	41726		2					1					70%	3	7
Support–Active Site Interactions in Heterogeneous Catalysts	42461	4							1				75%	3	7
An Analysis of the Automotive Industry as a Source for Weapon Components and Manufacturing Processes	42483												100%	1	7
High-Speed Micro-EDM	46070												80%	2	7
Microexternal-Combustion Engine: The P3 Engine Prototype	46686	1											100%	1	6
Lipid Membranes on Nanostructured Silicon	47795	1						1	1				90%	2	6
Resin Infusion Between Double Flexible Tooling	49769	4	2					3			1		100%	1	7
Studies on the Disbonding Initiation of Interfacial Cracks	49772	1	1					1					90%	1	7
Critical Technology Development for Hard-Target-Defeat High-G-Tolerant Fuze and High Explosives	49915												90%	3	7

Appendix C: Project Performance Measures

		Performance Statistics (Number of)											Project Qualitative Assessment		
Project Title	Project #	Refereed Publications	All Other Reports and Publications	Patent Disclosures	Patent Applications	Patents	Copyrights	Students	Post-docs	Permanent Staff Hired*	Awards	New Non-LDRD-Funded Projects†	% Milestones Completed	Goals Status**	Hypothesis Status***
TALON	50065		2				2						90%	2	7
Compliant Membranes for MEMS Microphones	50396												100%	1	9
Multiscale Experimental/Numerical Study	50717	7											100%	1	7
Cellular Observatory: Simultaneous Time- and Frequency-Resolved Microscopy	50772	1	3		1			2		1			95%	1	6
Atomic Layer Deposition of Highly Conformal Tribological Coatings	52523	10		1				1	1	1			95%	2	6
Assembly of Microsystems Using Exothermic Multilayer Thin Films	52524		2		2			1					90%	1	7
Intelligent Interaction Control as Applied to Metrology and Assembly of Microscale Components	52526	1						1		1			90%	4	7
Rapid-Prototyping High-Density Circuitry (RpHdc)	52527		4	2									71%	3	7
Elucidating the Mysteries of Wetting	52528	2	4						1				100%	1	7
Next-Generation Spindles for Micromilling	52530		2					1					88%	3	7
Assembly and Actuation of Nanomaterials Using Active Biomolecules	52531	12						1	2				90%	2	6
Modeling Biomembranes	52532	4											90%	2	7
Reverse-Engineering Biological Networks: Applications in Immune Responses to Bioterrorism Threats	52533	3	3					1	1				100%	2	7
High-Throughput Identification of Molecular Machines Involved in Membrane Signaling and Toxin Pathways	52536	2		1				1	1				90%	1	6
Coupled Solid-Fluid-Mechanical-Computational Modeling of Fracture and Fragmentation in Geomaterials, such as Hard and Deeply Buried Targets (HDBTs)	52537	2						1					75%	3	7
Sequestration of Pathogens on Nanoengineered Surfaces	52538	5	6	1				3	3				90%	1	6
A Combined Preconcentrator and Sensor for Live Waterborne Pathogens	52539	2		1					1				100%	1	7

Appendix C: Project Performance Measures

		Performance Statistics (Number of)										Project Qualitative Assessment		
Project Title	Project #	Refereed Publications	All Other Reports and Publications	Patent Disclosures	Patent Applications	Patents	Copyrights	Students	Post-docs	Permanent Staff Hired*	Awards	New Non-LDRD-Funded Projects†	% Milestones Completed	Goals Status**	Hypothesis Status***
IP Storage: A Performance and Security Study	52540	1											90%	3	6
A Parallel Circuit Simulator for Cell Biology	52541	4						1					100%	1	7
Developing a Computationally Efficient Dynamic Multilevel Hybrid Optimization Scheme Using Multifidelity Model Interactions	52542		4										90%	2	7
Robust Large-Scale Parallel Nonlinear Solvers for Simulations	52543	2	4						1				100%	1	6
Development of Computational Algorithms and Inversion Capabilities for Transport/Reaction Simulations of Chemical/Biological/Radiological Terrorist Attack Scenarios in Support of Homeland Security	52544	5	7		2			4		1	2		100%	1	6
Massively Parallel Linear Programming	52546		1										65%	3	7
Active Photonic-Crystal Devices for Integrated Photonics and Silicon Photonics	52548	2		2		1				2			90%	2	8
Co-Processing of Chalcogenide-Based Radiation-Hard Nonvolatile Memories by Sandia's MDL and BAE Systems	52549												70%	3	7
Functionalized Nanoparticles for Sensor Applications	52551			4	2			1	2				50%	2	6
Novel *In Situ* Mechanical Testers to Enable Integrated Metal Surface Micromachines	52552	5	1										85%	3	7
Compliant Thermomechanical MEMS Actuators	52553	2	2										100%	1	6
An Integrated, Stacked System-on-a-Chip	52554		3	1	1						2		75%	2	6
Micromass Spectrometer-on-a-Chip	52555	3						1					90%	1	7
Quantum Coherence in Semiconductor Nanostructures for Improved Lasers and Detectors	52556		2						1				50%	2	7
MOSFET–MEMS Integration	52557	1		3	2	1		2					95%	1	6
Microoptical Gyroscope Via Monolithic Active/Passive Optical Integration	52566	2		1				1		1			85%	3	7

Appendix C: Project Performance Measures

		Performance Statistics (Number of)										Project Qualitative Assessment		
Project Title	Project #	Refereed Publications	All Other Reports and Publications	Patent Disclosures	Patent Applications	Patents	Copyrights	Students	Post-docs	Permanent Staff Hired*	Awards	New Non-LDRD-Funded Projects†	% Milestones Completed	Goals Status**	Hypothesis Status***
Materials Physics and Device Development for Improved Efficiency of GaN HEMT High-Power Amplifiers	52570							1					90%	1	7
Leaky-Mode VCSELs for Photonic Logic Circuits	52571	1						1					90%	2	7
Advanced Polychromator Systems for Remote Chemical Sensing	52575	2		1	1			1					100%	1	6
Immunological Basis for High-Reliability Systems Control	52577							3					75%	4	6
Moving-Target Identification Using Ultrahigh-Range-Resolution Data	52580		1										95%	2	7
Advanced Mobile Networking, Sensing, and Controls Using Graph Theory	52581		2					2					90%	3	6
Compact Terahertz Sources for Emerging-Threats Applications	52582												80%	2	7
Understanding Communication in Counterterrorism Crisis Management	52583		3					4					98%	1	6
Hypervelocity Impact-Generated Flash	52584		1										95%	2	6
Improving Human/System Interactions in Systems-of-Systems	52585												60%	3	7
Distributed Detection and ID Algorithm Architecture for Unattended Ground Sensors	52586												100%	1	7
Secure Chaotic Communications	52587												100%	1	7
System-of-Systems Modeling and Analysis	52588		2					2		2			100%	1	6
Eye-Safe Short-Range Standoff Aerosol-Cloud Finder	52589												80%	2	9
Microflame-Based Detector Suite for Universal Gas Sensing	52590	1	1	2	2	1		2		1			95%	1	6
Beyond Nanoparticles—Attack on a Chemical “Holy Grail”	52591	1	1					3	1				90%	2	7
Advanced Proton-Exchange Materials for Energy-Efficient Fuel Cells	52592	3			1			1	1				90%	1	7
Alanate-Hydride Fuel-Cell Demonstration Project	52593			1				1					100%	1	6

Appendix C: Project Performance Measures

		Performance Statistics (Number of)										Project Qualitative Assessment		
Project Title	Project #	Refereed Publications	All Other Reports and Publications	Patent Disclosures	Patent Applications	Patents	Copyrights	Students	Post-docs	Permanent Staff Hired*	Awards	New Non-LDRD-Funded Projects†	% Milestones Completed	Goals Status**	Hypothesis Status***
Real-Time Discriminatory Sensors for Water-Contamination Events	52595												100%	1	7
Advanced High-Efficiency Direct-Cycle Gas Power-Conversion Systems for Small Special-Purpose Nuclear-Power Reactors	52596	7					1	6					100%	1	7
Securing Mobile Code	52597							1					100%	1	7
Novel Catalysts for Hydrogen Fuel-Cell Applications	52598	1	10	2				2	1				50%	3	7
Linking Optimization and Simulation in Critical-Infrastructure Systems	52606	4											100%	1	7
Decomposition of Contaminants Using Photochemically Active Nanoparticles	52698	2						1	2				100%	1	7
Thermally Cleavable Surfactants	52699	1	1	2	2			1	2				100%	1	7
Transition-Metal Catalyzation of Complex-Hydride Absorption/Desorption Reactions	52700	3											83%	2	9
Quantification of Environments and Surfaces Within Micropackages	52701	1	3		1			5	1				100%	1	7
Assembly of Ordered Electrooptical and Bioactive Materials and Composites	52702	1		1				3	3				100%	1	6
Advanced Packaging/Joining Technology for Microsystems	52703	1	2					1	1	1	1		92%	2	7
Magnetostrictive Elastomers for Actuators and Sensors	52705	3	1					2					100%	1	6
Development of a High-Throughput Microfluidic Integrated Microarray for the Detection of Chimeric Bioweapons	52706		3	3	2		1	3					95%	1	7
Zero-Power Radio Receiver	52708	1		2	1								100%	1	6
Completely Passive Microwave Tag	52709	1		2	2								100%	1	6
Security Coatings for Multichip Modules	52710							2					100%	3	8
Detailed Modeling and Simulation of Contaminant Transport in Architectural Spaces	52711		1										90%	1	7
Content-Based Video and Image Indexing System	52712												80%	3	7

Appendix C: Project Performance Measures

		Performance Statistics (Number of)										Project Qualitative Assessment		
Project Title	Project #	Refereed Publications	All Other Reports and Publications	Patent Disclosures	Patent Applications	Patents	Copyrights	Students	Post-docs	Permanent Staff Hired*	Awards	New Non-LDRD-Funded Projects†	% Milestones Completed	Goals Status**	Hypothesis Status***
Bioaerosol Collection and Concentration for Microseparations-Based Detectors	52713		1	1	1		1						90%	1	6
Detecting the Toolmarks of Genetic Engineering in Bioweapons Strains	52714			1									100%	1	6
Joint Authentication/Encryption	52716	1		2							1		100%	2	6
Ultrahigh-Temperature Ceramics for Hypersonic Vehicle Applications	52717	1						2					100%	1	7
Leveraging Robotic Planning for Physical-Security Analysis	52718		1	2				1					90%	1	6
Ultralightweight Telescope with MEMS Adaptive Optic for Distortion Correction	52720			1				1		1			80%	2	6
Modeling Signals from Earth-Penetrating Nuclear Weapons for Remote Kill Assessment	52721		3										75%	2	6
Novel Micropreconcentrators for CW, Explosives, and Water Surety	52723	1	2	2	2			2	1	1			100%	1	6
Ion-Mobility Spectrometer/Mass Spectrometer	52724								1				80%	3	7
Cryptographic Assurance of Execution Correctness and Confidentiality	52725	1	2	1	1			4					95%	1	8
Characterization, Performance, and Optimization of PVDF as a Piezoelectric Film for Advanced Space Mirror Concepts	52726	2	3						1				90%	1	6
Predictive Accelerated Aging of Microsystems: The Science of Dormancy	52727	2	4					2	1				90%	2	7
Surety and Accountability Enhancements for Storage Containers	52728							3					100%	1	7
Nuclear-Safety Weaklinks for Thermal and Mechanical Environments	52729	9	3	4	2	2		1					95%	1	7
Advanced Packaging Technology for Optical Firesets	52730		1										95%	3	6
Miniature Transmitter Filter for JTA Using LIGA Technology	52731			4		1		1					90%	1	6
Novel and Robust Environmental Sensing Devices (ESDs)	52732							1					85%	2	7
Advanced Neutron Monitors for JTA and Stockpile Monitoring	52733		1					2					90%	2	6

Appendix C: Project Performance Measures

		Performance Statistics (Number of)											Project Qualitative Assessment		
Project Title	Project #	Refereed Publications	All Other Reports and Publications	Patent Disclosures	Patent Applications	Patents	Copyrights	Students	Post-docs	Permanent Staff Hired*	Awards	New Non-LDRD-Funded Projects†	% Milestones Completed	Goals Status**	Hypothesis Status***
Development of an Efficient Large-Aperture High-Damage-Threshold Sol-Gel Diffraction Grating	52737		2		3			2	1				80%	3	7
Laser Triggering of Water Switches in Terawatt-Class Pulse-Power Accelerators	52738		1					1					90%	2	6
Experimental and Computational Study of Liquid-Solid Transition in Tin	52739												75%	3	7
Design and Control of the Magnetic Properties of Nanoparticles	52797	4											100%	1	6
Flow Control and Mixing in Microfluidic Devices	52977	3						1					100%	1	7
Atomic-Scale Scanning-Tunneling Microscopy Measurements of Nucleation and Growth of Ge/Si Alloy Structures	53464							1					85%	2	7
Micro-/Nanoscale Thermomechanical Manufacturing	53465	3						1					75%	2	6
Novel Diagnostics for Rarefied Flows in MEMS Applications	53585												60%	3	7
Geophysical Subsurface Imaging and Interface Identification	53586												100%	1	8
Evolution of Near-Surface Scalar Concentrations Through a Compact Cylinder Array Embedded in the Atmospheric Surface Layer	53587												100%	1	6
Miniature High-Power RF Components Enabled by Mesoscale Manufacturing	53588	1	1	1				1					100%	2	6
Electrical Conductivity of Metal Alloys	53590	1	3					1	1				100%	1	6
Hydrogen Futures Dynamic Simulation Model	53591	2	1				1		1				95%	1	6
Design of Biospecific Surfaces to Control Specific Cellular Responses	53681	1						1					100%	1	7
Nanomagnetic Films	54211	2	2					1			3		100%	1	7
A Multiscale Approach to Modeling Carbon Nanotube–Reinforced Composites	54213	3	2					1					80%	3	6
Near-Real-Time Characterization for Assured HDBT Defeat	55079		3					5	1	1			90%	2	8

Appendix C: Project Performance Measures

		Performance Statistics (Number of)										Project Qualitative Assessment		
Project Title	Project #	Refereed Publications	All Other Reports and Publications	Patent Disclosures	Patent Applications	Patents	Copyrights	Students	Post-docs	Permanent Staff Hired*	Awards	New Non-LDRD-Funded Projects†	% Milestones Completed	Goals Status**	Hypothesis Status***
Prompt Global Response	55086							3	1				75%	2	8
Winning the War: A Systems Approach to Defending Our Borders	55087		12	1				2					85%	3	7
Integrated Superhard and Metallic Coatings for MEMS	57300	21		2	2			1	1				100%	1	6
Microscale Separations of Biological Compounds Using Novel Polymeric Separations Materials	57307	3						2					90%	1	6
Friction in Micromachine Interfaces	57308	2						1					90%	1	7
Lipid Microarray Biosensor for Biotoxin Detection	57309							1					90%	1	7
Advanced Manufacturing Techniques Using Rapid Prototyping	57310		2	2							2		100%	1	7
Robust Hermetic Packaging Techniques for MEMS Integrated Microsystems	57311		1					1					99%	1	6
Active Photonic Nanostructures	58907	2	1	1				1	2				90%	2	7
3-D Large-Eddy Simulation of Turbulent Flow Based on One-Dimensional Turbulence Modeling	59034		3										90%	2	6
A Method of Evaluating Research Using New Innovation, Risk, and Impact Indicators	59916	3											90%	1	7
Photonic Encryption Using All-Optical Logic	61046												95%	2	7
Nanoporous-Carbon Adsorbers for Chemical Microsensors	62269	5	2	1									90%	2	6
Nonlethal Technologies for the War on Terrorism	62827												90%	2	7
Agent-Based Control of Distributed Infrastructure Resources	64811							1		1			66%	4	7
Direct Single-Ion Machining of Nanopores	65559	1						1					70%	2	8
Investigation of the Effects of Intense Pulsed Particle Beams on the Durability of Metal-to-Plastic Interfaces	66170												100%	1	8
Advanced Techniques for Multiobjective Discrete Optimization	66450							1					80%	2	7

Appendix C: Project Performance Measures

		Performance Statistics (Number of)											Project Qualitative Assessment		
Project Title	Project #	Refereed Publications	All Other Reports and Publications	Patent Disclosures	Patent Applications	Patents	Copyrights	Students	Post-docs	Permanent Staff Hired*	Awards	New Non-LDRD-Funded Projects†	% Milestones Completed	Goals Status**	Hypothesis Status***
Nonradioactive Safety and Performance Issues with Supercritical Water Reactor (SCWR) Safety Technologies	66809												45%	3	7
Radiation Performance Issues with Advanced Coolants for Next-Generation Reactor	66810												100%	2	7
Rapid Prototyping to the Nanometer Scale	67004	1			2			1			1		100%	1	7
Robust Manufacturing of Gel-Based Components for Nuclear Weapons	67005												100%	1	7
Meso-/Microoptical System Interface Coupling Solutions	67006												90%	3	7
Injection Molding of Net-Shape Active Ceramic Components	67007							1		1			100%	1	7
Macro-/Meso-/Microsystems Integration in LTCC	67008		2	3	1								100%	1	7
Studies of Signaling Domains in Model and Biological Membranes Through Advanced Imaging Techniques	67010		1						1				95%	1	6
Imaging Self-Organization of Proteins in Membranes by Photocatalytic Nanotagging	67011	5		5	1			2	1				80%	2	7
Protein Microarrays for Biowarfare-Agent Detection and Characterization	67012	2	4	2				1	1				90%	2	7
Interaction of Proteins with Lipid Films	67013	4	5					2	1				100%	1	7
New Technologies for Understanding Membrane-Protein Recognition and Signaling	67014	2	3						1				75%	3	7
Massively Parallel, Scalable Atmosphere Model	67015		2							1			85%	2	6
High-Performance Processing Architecture	67016	2							1				100%	1	7
Substructured Multibody Molecular Dynamics	67017												70%	2	7
Enhancing Simulation Performance on Clusters with Configurable Auxiliary Devices	67018												90%	2	7
A Hybrid Level-Set/Particle Method for Modeling Surface Evolution During Feature-Scale Etching and Deposition Processes	67019												80%	2	8
Penetrator Reliability Investigation and Design Exploration (PRIDE)	67020		1										95%	2	7

Appendix C: Project Performance Measures

		Performance Statistics (Number of)											Project Qualitative Assessment		
Project Title	Project #	Refereed Publications	All Other Reports and Publications	Patent Disclosures	Patent Applications	Patents	Copyrights	Students	Post-docs	Permanent Staff Hired*	Awards	New Non-LDRD-Funded Projects†	% Milestones Completed	Goals Status**	Hypothesis Status***
Topology Optimization for Improving Sensor Performance	67021		1										95%	2	7
Characterization and Application of Dielectrics with Controlled Leakage	67022							1	1				90%	2	7
Nano-G Accelerometers Using Nanophotonic Motion-Detection System	67023	2		1	1								90%	2	7
Bragg Fiber Development	67024	6		1		1							90%	2	6
Microwave-to-Millimeter-Wave Electrodynamic Response and RF Applications of Semiconductor Quantum Nanostructures	67025			1	1			1	1				85%	2	7
Development of GaN 20–100 Watt Ku-Band Power Amplifiers for Micro-SAR	67026		1										75%	2	7
Evanescent-Wave Planar Photonic Biosensor	67027	2											70%	2	7
Passive Electronically Steerable Array (PESA) for Miniature Synthetic-Aperture Radar (Mini-SAR), Precision Guidance, and Intelligence/Surveillance/Reconnaissance (ISR)	67028												90%	3	7
Advancements in Sensing and Perception Using Structured Lighting Techniques and an Innovative Design Tool	67029			1				2					95%	1	6
Biophysics of BW-Warhead Defeat with a Kinetic Interceptor	67030		1					1					85%	3	7
Dispersal in Urban Canyons, Source Identification, and Collateral Damage/Mitigation Assessment	67031	1											100%	1	7
Weaponization of Thermobaric Explosives	67032												100%	1	7
Development of an Enterprise-Scale Agent-Based Autonomic Logistics Simulation Model	67033	1						1	1				80%	2	7
Mobile-Node Authentication in a Wireless *Ad Hoc* Environment	67034												100%	1	7
Novel Processing, Affordable Motion Compensation, and Mode Multiplexing for Miniaturized Synthetic-Aperture Radar	67035	1	2	1	1			1					80%	2	7
Coilgun Technology Demonstration Test-Bed	67036	1											100%	1	7
Enhanced Perception for Remote 3-D Mapping of Unknown Indoor and Outdoor Environments	67037	1											90%	2	7

Appendix C: Project Performance Measures

		Performance Statistics (Number of)										Project Qualitative Assessment		
Project Title	Project #	Refereed Publications	All Other Reports and Publications	Patent Disclosures	Patent Applications	Patents	Copyrights	Students	Post-docs	Permanent Staff Hired*	Awards	New Non-LDRD-Funded Projects†	% Milestones Completed	Goals Status**	Hypothesis Status***
A Modular Micromagnetic Accelerometer in Support of the mTalon Vision	67038												80%	3	7
MICROFUZE Integration	67039			2				1					90%	1	7
Analysis of Technology Impacts on Operations in Complex Environments	67041						4	2		2			100%	1	7
CBW Cloud Knockdown and Neutralization	67042							2					70%	3	7
Assessment of Biokillers in EDS for Biological-Agent Destruction	67043		2	1									100%	1	6
Adaptive-Force-Feedback Surface Control	67044			1				1		1			95%	2	7
High-Capacity Earth-Penetrator Instrumentation	67046							2		1			95%	2	7
Systems Analysis of Networked Sensors	67047	2	2										95%	2	7
Deployable Object Tracker for NMD Flights	67048							1		1			90%	1	7
Continuous-Flow Detector for Rapid Pathogen Identification	67049	4		7	4				1				100%	1	6
Biological-Security Decontamination Technology—Reducing the Threat of Infectious-Agent Spread	67050		3	1				2					80%	4	7
Consequence Management, Recovery, and Restoration after an Intentional Contamination Event	67051	2	2					1					100%	1	7
Fully Integrated System-Dynamics Toolbox for Water Resources Planning	67052	2	4										90%	2	7
Predicting System Performance of Proton-Exchange-Membrane Fuel Cells: Computational Modeling with Experimental Discovery and Validation	67053	3	2					2	1				90%	2	7
Optimal Allocation of Terrorist Countermeasures Using Risk-Based Systems Pathways Analysis	67054		1										90%	2	7
Silicon Field-Emission Electric Propulsion Arrays (FEEP) Powered by Orbital Nuclear Reactors	67055		2	2									90%	3	7
Advanced Fuel-Cell Reactor for the Direct Cogeneration of Electricity During Selective Partial Oxidation of Hydrocarbons	67056								1				65%	3	7

Appendix C: Project Performance Measures

		Performance Statistics (Number of)											Project Qualitative Assessment		
Project Title	Project #	Refereed Publications	All Other Reports and Publications	Patent Disclosures	Patent Applications	Patents	Copyrights	Students	Post-docs	Permanent Staff Hired*	Awards	New Non-LDRD-Funded Projects†	% Milestones Completed	Goals Status**	Hypothesis Status***
New Hydrogen-Storage Material: Metal-N-H system	67057	1	1		1								100%	1	6
Intrusion Detection for Wireless Networks	67058							8					40%	3	8
Membranes for H2 Generation from Nuclear Powered Thermochemical Cycles	67059							2	2				90%	2	7
Microfabricated BTU Monitoring Device for System-Wide Natural-Gas Monitoring	67060		1	1				1					90%	2	6
"Tunable" Ion Conductors for Low-Temperature Oxide-Based Fuel Cells	67061	3			1				2				90%	2	7
Nuclear Nanobatteries: On-Board Power for Independent MEMS Devices	67062			1									80%	2	7
Integrated Tunable Light Sources for Miniature Sensors	67063												75%	1	7
Ray Model of High-Frequency Cavity Scarring	67064	1											70%	2	7
New Smart Material to Address Issues of Structural Health Monitoring	67065												100%	1	6
Noncontact Surface Thermometry for Microsystems	67067	1						1	1				90%	1	7
High-Speed Interferometric Deformation Measurements	67068			1									95%	2	7
Fundamentals of Nanofluidics	67069												100%	1	7
Simulating Self-Assembly and Growth of Biological Nanostructured Materials	67070								2	1			90%	1	8
A Low-Power, Ultrafast-Current Transient Measuring Device	67071		1		1								90%	2	6
A Capillary Valve for Microfluidic Systems	67073							1					100%	1	7
Electrochemically Switchable Materials for (Bio)Microfluidics	67074												95%	1	7
Modeling of Friction-Induced Deformation and Microstructure	67075	1						1			1		100%	2	7
Reversible Antibody Trapping for Selective Sensor Devices	67076							2	2				100%	1	6

Appendix C: Project Performance Measures

		Performance Statistics (Number of)										Project Qualitative Assessment		
Project Title	Project #	Refereed Publications	All Other Reports and Publications	Patent Disclosures	Patent Applications	Patents	Copyrights	Students	Post-docs	Permanent Staff Hired*	Awards	New Non-LDRD-Funded Projects†	% Milestones Completed	Goals Status**	Hypothesis Status***
Correlated and Comprehensive Analytical Techniques for Homeland Defense	67077	5	2				1			1	2		85%	2	7
Development of High-Energy-Density Dielectric Materials for Integrated Microsystems	67078	1	8					2	3				95%	1	6
Nanolithography-Directed Materials Growth and Self-Assembly	67079	1	4	1				1					100%	1	7
Development of a Novel Technique to Assess the Vulnerability of Micromechanical System Components to Environmentally Assisted Cracking	67080												75%	3	7
3-D Optical Sectioning with a New Hyperspectral Deconvolution Fluorescence Imaging System	67081	1	11		1	2				1	1		85%	2	7
The Science of Solutes: Transition Metals in LIGA Nickel	67082	2							2				100%	1	8
Novel Gel-Based Technology for Sensors and Weapons	67083		1										100%	1	6
Coupled Nanomechanical Oscillator Arrays for the Study of Internal Dissipation in Nanoscale Structures and Collective Behavior in Large Systems	67084	2							2	1			100%	1	7
Precisely Controlled Picoliter Vessels with Rapid Sample Preparation for Trace Biotoxin Detection	67085	1		2	1			1					100%	1	7
Adaptive Optics and Phase-Diversity Imaging for Responsive Space Applications	67086		2	1									70%	3	6
Infrastructural Development for Flexible Network of Devices	67087												100%	1	7
Monolithic Reconfigurable Radio-Frequency Microelectromechanical Systems (RF MEMS) Antennas	67088												100%	1	7
Next-Generation 3-D Inspection System for Facility Monitoring	67089							5					100%	1	7
Risk-Assessment Metatool	67090												85%	2	7
Featureless Spread-Spectrum Waveform Design and Processing	67091		1								1		100%	1	6
Tracking Slow-Moving Objects in a GPS–Denied Environment	67092			1	1					1			55%	2	8
Optical Communications	67093												90%	1	7

Appendix C: Project Performance Measures

		Performance Statistics (Number of)										Project Qualitative Assessment		
Project Title	Project #	Refereed Publications	All Other Reports and Publications	Patent Disclosures	Patent Applications	Patents	Copyrights	Students	Post-docs	Permanent Staff Hired*	Awards	New Non-LDRD-Funded Projects†	% Milestones Completed	Goals Status**	Hypothesis Status***
A Unique Vibration-Based Miniature Power Generator for National Security Applications	67094												80%	3	7
Image Georectification Using Digital Elevation Model Shadows	67095												90%	2	6
Vulnerability Assessment of State-of-the-Art Microelectronics	67096							1					80%	2	7
Nonlinear Optical Detection of Biological and Chemical Aerosol Agents Using Femtosecond Lasers	67098									1			100%	1	6
Polymer Electronic Devices and Materials	67099		1	1	1			7	2				85%	1	7
Small Circuits for Cryptography	67101												100%	1	7
Analysis of Multichannel Internet Communication	67102							4					100%	2	8
Receiver for Ultralow-Power Wake-Up and Command	67104												100%	1	6
Extraordinary Optical Transmission Through Patterned Subwavelength Apertures	67105	1											90%	2	6
Reconstruction Algorithm Development and Assessment for a Computed Tomography–Based Spectral Imager	67107												90%	2	7
Power-Combining Techniques for Solid-State Power Amplifiers	67108												70%	1	8
Dispersive Diffractive Optical Elements for the Infrared	67109	1	1	2									90%	3	7
Atmospheric Propagation of Terahertz Radiation	67111												100%	1	7
High-Confidence Estimation of Relative Event Locations from Space-Based Sensors	67113			1				1					100%	1	7
Critical-Infrastructure System-of-Systems Assessment Methodology	67114							1					96%	2	7
Dynamic Vulnerability Assessment	67115									2			100%	1	6
Inflatable Antenna with Adaptive Actuators	67116	2	1	1						1			95%	4	7
Data-Driven Dynamic Models of Conflict	67117												75%	3	6

Appendix C: Project Performance Measures

		Performance Statistics (Number of)										Project Qualitative Assessment		
Project Title	Project #	Refereed Publications	All Other Reports and Publications	Patent Disclosures	Patent Applications	Patents	Copyrights	Students	Post-docs	Permanent Staff Hired*	Awards	New Non-LDRD-Funded Projects†	% Milestones Completed	Goals Status**	Hypothesis Status***
MEMS/Fuze Diagnostic Extraction in High-G Environments	67118							1					85%	3	8
Efficient Implicit Multigroup Radiation Calculations	67120							1					50%	2	8
Model for Channel Resistance in Water Breakdown	67121												80%	1	7
Embeddable Shock Physics Sensors	67122												90%	2	7
Smart Detectors of Enrichment of Bioaerosols	67716	5	1					1					80%	3	7
Computational Studies of JP-8 Diffusion Flames with Detailed Chemistry and Particulate Formation	68063	1						1					100%	1	7
Design and Fabrication of Advanced Device Structures for Ultrahigh-Efficiency Solid-State Lighting	69143	1											83%	1	6
Molecular Simulation of Beta-Amyloid (A-beta) Peptide Interaction with Phospholipid Membranes	69145												80%	3	7
Nanoscale Testing of Deformation and Fracture in Engineering Materials	69146	5	1					2					100%	1	6
Nanocrystal-Polymer Composites for High-Luminous-Efficiency LEDs	69148	4	8	1					2				75%	3	8
Outstanding Challenges for AlGaInN MOCVD	69149	1	3		1								64%	2	7
Nanoporous Polymeric Materials for Chemically and Spatially Multiplexed Sensing of Bioagents	69150			1	1								50%	3	6
Evolutionary Complexity for Protection of Critical Assets	69151												85%	2	10
Nanomechanical Stochastic Resonators	69152												75%	3	8
Augmented Musculature Device	69153			1				1					100%	1	7
Biomolecular Decision-Making Processes for Self-Assembly	69154	1	1	1									85%	2	6
Light-Powered Nanovehicle Propulsion	69155								1				60%	3	7
System-Dynamics Modeling to Assist Regional Water Planning: Modeling the Nonmarket Value of Water	69156	1	1					1					90%	2	7

Appendix C: Project Performance Measures

		Performance Statistics (Number of)										Project Qualitative Assessment		
Project Title	Project #	Refereed Publications	All Other Reports and Publications	Patent Disclosures	Patent Applications	Patents	Copyrights	Students	Post-docs	Permanent Staff Hired*	Awards	New Non-LDRD-Funded Projects†	% Milestones Completed	Goals Status**	Hypothesis Status***
Interactive Water-Quality Modeling to Assist Regional Water Planning	69157		3					1			1		95%	2	7
Microbe-Exuded Polymers and the Enhanced Corrosion of Carbonate Materials	69158	1						1					95%	2	7
Nerve-Cell Function and the Development of Cognitive Networks	69159												100%	2	8
Ultrahigh-Gain Fusion Concept	69160		1										95%	2	8
Nanofluidic Devices for Rapid Detection of Virus Particles	69161							1					90%	2	9
Solution Behavior of PEO: The Ultimate Biocompatible Polymer	69162												95%	2	6
New Self-Assembled Nanocrystal Micelles for Biolabels	69163	2		1				1					100%	1	7
Rapid Detection of Biothreat Agents Based on Cellular Machinery	69164									1			100%	1	10
Patterning Quantum-Dot Arrays Using DNA Replication Principles	69165			1									75%	2	6
Adaptive Algorithms for Use in the Rejection of Periodic Disturbances of Unknown Frequency	69166							1					100%	1	7
Property-Based Testing for Cybersecurity Assurance	69168							3					100%	3	7
Self-Assembled Ordered Carbon-Nanotube Arrays and Membranes	69170	2		1				1					75%	2	6
Chemical Cross-Linking and Mass-Spectrometry Studies of the Structure and Dynamics of Membrane Proteins and Receptors	69189	2							3	1			80%	2	8
Toxin Studies Using an Integrated Biophysical and Structural Biology Approach	69190	3						1	3				70%	3	7
Top-Down Structural Studies	69191												70%	3	8
Molecular Dynamics of Membrane Proteins	69192	3	1					1		1			75%	2	6
Model-Building Codes for Membrane Proteins	69193	3	5										90%	1	6
Poroelastic Wave-Propagation on the Earth Simulator	69198	1											70%	2	8

Appendix C: Project Performance Measures

		Performance Statistics (Number of)										Project Qualitative Assessment		
Project Title	Project #	Refereed Publications	All Other Reports and Publications	Patent Disclosures	Patent Applications	Patents	Copyrights	Students	Post-docs	Permanent Staff Hired*	Awards	New Non-LDRD-Funded Projects†	% Milestones Completed	Goals Status**	Hypothesis Status***
Development of Microreformers for Fuel Cells	69239		1					1					100%	1	7
Developing the Foundation for Polyoxoniobate Chemistry: Highly Tunable and Exploitable Materials	70799	4	4					3	4	1			100%	2	8
Simulating Human Behavior for National Security	71943												100%	1	7
Agent-Based Modeling of Middle East Terrorist Recruitment	71944	1	1				1						100%	1	6
Automatic Generation of Terrorist Operation Plan Hypotheses	71945		1										85%	2	8
Develop a System-Dynamics Modeling Framework for Assessing Factors that Influence Water Resource Consumption	72599							1	1	3			80%	4	8
Develop a Cooperative Water-Management Process, Creating a System-Dynamics Model of Water Resources in the Lower Rio Grande Basin	72600							1		2			90%	2	6
Compact Ultrabright Multikilovolt X-Ray Sources for Advanced Material Studies, 3-D Nanoimaging, and Attosecond X-Ray Technology	72715												90%	2	7
Energy-Systems Analysis Framework and Modeling	72716	1	8					1					80%	2	7
Radiation-/Geometry-Driven Jets: Proof-of-Principle Tests	73045		1										85%	2	7
Superhydrophobic Surface Coatings for Microfluidics and MEMS	73185		1	1				4	2	1	1		100%	1	7
Microoptical Radar (MOR) Facial-Recognition Project	73207		4	3				2		1			90%	2	7
Determining Explosive Ignition Criteria for Miniaturized Devices	74545												80%	2	8
Quantum Squeezed Light for Probing Mitochondrial Membranes and Study of Neuroprotectants	74546	1		1				2			1		100%	1	6
Characterization of a New Class of Surface-Micromachined Pumps	74547	2	1	2	1			2					100%	1	6
Risk of Biological Terrorism to Water-Distribution Systems	74548												80%	2	7
Explicit and Implicit Measures in Human Aversive Classical Conditioning	74759		1					1			1		100%	1	6

Appendix C: Project Performance Measures

		Performance Statistics (Number of)											Project Qualitative Assessment		
Project Title	Project #	Refereed Publications	All Other Reports and Publications	Patent Disclosures	Patent Applications	Patents	Copyrights	Students	Post-docs	Permanent Staff Hired*	Awards	New Non-LDRD-Funded Projects†	% Milestones Completed	Goals Status**	Hypothesis Status***
Automatic-Target-Recognition Algorithms for Uncooled Thermal Imagery	74760												90%	2	7
Magnetophoretic Bead Trapping in a High-Flowrate Biological Detection System	74795		1	2				2					100%	1	7
TPV Energy Scavenging for Hypervelocity Vehicles	75441												60%	4	8
Assessment of Advanced Pulsed-Power Fusion Concepts	75442												95%	2	8
A Mathematical Method for Quantifying the Effectiveness of Management Strategies	75443	2											98%	1	7
Developing Algorithms for Predicting Protein-Protein Interactions from Experimental Constraints	75513												95%	2	7
Instrumentation Development for Real-Time Brain-Wave Monitoring	75514												100%	1	7
Miniaturized Electronic Steerable-Array Synthetic-Aperture Radar	76069												90%	2	7
Full-Earth-Monitoring Sensor MESAWorks	76070		1					2					100%	2	8
Systems Assessment of Water-Savings Impact of Controlled-Environment Agriculture Utilizing Wirelessly Networked SDACs	76305		4					5					80%	3	7
Inactivation of Avian Influenza (Bird Flu) with Sandia-Developed Decontamination Formulations	76306												50%	3	7
Deciphering the Genetic Regulatory Code Using an Inverse Error Control Coding Framework	78132	3	1										80%	2	7
Climate-Change Effects on International Stability	78307							2			1		97%	1	7
Generalized Continuum Models for Inelasticity in Solids: Formulation of Theories and Variational Methods for Computation	78783							1					100%	1	7
GeSi–Strained Nanostructure Self-Assembly for Nano- and Optoelectronics	79943	1						1					70%	3	7
Vulnerability Analysis for SCADA	80835												100%	1	6
Molten Salt-Based Growth of Bulk GaN and InN	80838							1					97%	1	7
Randomness Complexity and Cryptography	81209							1					100%	1	7

Appendix C: Project Performance Measures

		Performance Statistics (Number of)											Project Qualitative Assessment		
Project Title	Project #	Refereed Publications	All Other Reports and Publications	Patent Disclosures	Patent Applications	Patents	Copyrights	Students	Post-docs	Permanent Staff Hired*	Awards	New Non-LDRD-Funded Projects†	% Milestones Completed	Goals Status**	Hypothesis Status***
System Study: Adaptive Optics for Weapon, Reconnaissance, and Military Space Applications	81354												90%	2	7
		391	339	149	79	10	16	289	103	65	26	0			

† Identification of new non-LDRD-funded projects is now completed in the fiscal year following the annual report.

* Permanent Staff Hired. Laboratories operate under manpower cap. There are no increases in permanent staff.

** Goals Status
- 1 - Goals Met
- 2 - Goals Substantially Met
- 3 - Goals Partially Met
- 4 - Goals Substantially Modified
- 5 - Goals Not Met
- 11 - Project Terminated

***Hypothesis Status
- 6 - Hypotheses Proved
- 7 - Hypotheses Remains Unchanged
- 8 - Hypotheses Modified
- 9 - Hypotheses Redefined
- 10 - Hypotheses Disproved
- 11 - Project Terminated

****These projects represent university fellowships and are not included in the totals.

Appendix D: DOE Critical Technologies

Pg #	Title	Project #	Science of Complex Systems	Modeling & Simulation of Complex Systems	High-Performance Computing	Nuclear Weapons Predictive Capability (Classified)	Safety Assessments & Engineering	Use Control & Security	Nonproliferation & Verification	Dynamic Testing in Severe Environments	High-Energy-Density Materials	Laser Technology	Pulsed Power and Accelerators	Microelectronics and Photonics	Nuclear Materials	Engineered Materials	Flexible Manufacturing	Environmentally Conscious Manufacturing	Intelligent Machines and Robotics	Waste Management	Other
41	Microfabrication with Femtosecond Laser Processing	38605							●			●		●			●				
44	Mesoscale Controlled Motion for a Microfluidic Drop Ejector	38606							●								●				
77	Physical and Electronic Changes Caused by Membrane Signaling as a Transduction Pathway in Affinity-Based Biosensors	38609		●					●			●		●							
116	Graduated Embodiment for Sophisticated-Agent Evolution and Optimization	38610	●	●	●																
119	Scalable Fault-Tolerant Algorithms for Linear-Scaling Coupled-Cluster Electronic Structure Methods	38613		●	●						●										
121	Micromagnetic Suspension	38614		●																	
123	Sensitivities for Large-Scale Simulation Codes	38615	●	●	●																
168	Engineered Superconductivity in Electron-Hole Bilayers	38616												●							
171	Silicon-Based RF MEMS Components	38617							●					●					●		
173	Nanoelectromechanical Oscillators (NEMOs) for RF Filtering	38619	●						●					●							
176	Continuous-Wave Intersubband Terahertz Sources	38620						●	●			●		●							
178	Microsystems for Chemical Signature and Reagent Delivery	38621							●					●							
180	Microfluidic Cellular-Sample Pretreatment	38622	●	●					●					●				●		●	
231	Automated Visual Direction of Mobile Manipulation	38623																	●		
233	Miniature Fourier-Transform Ion-Mobility Spectrometer for Real-Time Detection and Identification of Explosives and Chemical Agents	38624							●					●				●			●
235	EM Interactions with Systems to Enhance Security	38627	●					●					●								●
236	Use of Seismic and Acoustic Responses to Assess Bomb Damage to Underground Facilities	38629	●	●																	
238	Free-Space Electrooptic Sampling and Remote Mapping of Electromagnetic Fields from Emitting Structures Using Femtosecond Terahertz Transceivers	38655							●			●									
332	Natural-Gas Production Problems: Solutions, Methodologies, and Modeling	38662	●	●																●	●

Appendix D: DOE Critical Technologies

Pg #	Title	Project #	Science of Complex Systems	Modeling & Simulation of Complex Systems	High-Performance Computing	Nuclear Weapons Predictive Capability (Classified)	Safety Assessments & Engineering	Use Control & Security	Nonproliferation & Verification	Dynamic Testing in Severe Environments	High-Energy-Density Materials	Laser Technology	Pulsed Power and Accelerators	Microelectronics and Photonics	Nuclear Materials	Engineered Materials	Flexible Manufacturing	Environmentally Conscious Manufacturing	Intelligent Machines and Robotics	Waste Management	Other
335	Time-Domain Reflectometry for Remote, Real-Time Water-Quantity/-Quality Monitoring of Perennial and Ephemeral Streams	38665	●																		
338	Functionalized Nanoelectrode Arrays for *In Situ* Identification and Quantification of Regulated Chemicals in Water	38668							●					●				●		●	
341	Water Desalination	38673														●				●	
344	Revolutionary Systems for Catalytic Combustion and Diesel Catalytic Particulate Traps	38674														●	●	●	●		
348	Potential Application of Microsensor Technology in Radioactive-Waste Management—With Emphasis on Headspace Gas Detection	38677												●						●	
241	Identification of Chemical Plumes: Range-Resolved IR Lidar Enabled by New Photonic Technologies	38681							●			●		●							
434	A Robust, Coupled Approach for Atomistic-Continuum Simulation	38684	●	●																	
438	Microscale Rarefied-Gas Dynamics and Surface Interactions for EUVL and MEMS Applications	38685	●	●												●					
441	High-Fidelity Frictional Models for MEMS	38686		●																	
444	Soot Formation, Transport, and Radiation in Unsteady Diffusion Flames	38687	●	●			●														
493	The Basics of Aqueous Nanofluidics: "Interphase" Structure and Surface Forces	38688	●	●												●					
497	Design, Synthesis, and Characterization of Soft-Matter Nanolayer Superlattices	38689														●					
499	Photocontrol of Nanointeractions in Microsystems	38690						●				●		●							
501	Electrochemically Deposited Alloys with Tailored Nanostructures for LIGA Micromachines	38691	●													●	●				
503	Nanostructured Materials for Directed Transport of Excitation Energy	38692												●		●					
505	Modeling Local Chemistry in the Presence of Collective Phenomena	38693	●	●	●											●					
701	Nanoscale Energetic Materials by Inverse Micellar Synthesis	38717								●	●					●					
704	Modeling of Rock Penetration	38718		●		●				●											
572	Agile, Microsystems-Enabled Receiver	38722							●					●							
507	Solution-Based Nanoengineering of Materials	39017	●											●		●		●			

Appendix D: DOE Critical Technologies

Pg #	Title	Project #	Science of Complex Systems	Modeling & Simulation of Complex Systems	High-Performance Computing	Nuclear Weapons Predictive Capability (Classified)	Safety Assessments & Engineering	Use Control & Security	Nonproliferation & Verification	Dynamic Testing in Severe Environments	High-Energy-Density Materials	Laser Technology	Pulsed Power and Accelerators	Microelectronics and Photonics	Nuclear Materials	Engineered Materials	Flexible Manufacturing	Environmentally Conscious Manufacturing	Intelligent Machines and Robotics	Waste Management	Other
684	Simulations of Intense Petawatt Laser Pulses with Dense Z-Pinch Plasmas	39670		●							●		●								
473	Biomicrofuel Cell (BMFC)	41193							●					●		●					●
476	Augmented Cognition: Next-Generation Intelligent Systems	41194		●			●	●	●										●		
164	Microengine for Advanced Power Generation	41674							●								●		●		
707	Direct Simulation of Solid-Fluid Systems	41726	●	●	●																
710	Support–Active Site Interactions in Heterogeneous Catalysts	42461																			●
712	An Analysis of the Automotive Industry as a Source for Weapon Components and Manufacturing Processes	42483	●	●	●					●		●		●		●	●	●	●		
713	High-Speed Micro-EDM	46070															●				●
715	Microexternal-Combustion Engine: The P3 Engine Prototype	46686												●							
717	Lipid Membranes on Nanostructured Silicon	47795	●													●					
720	Resin Infusion Between Double Flexible Tooling	49769															●				
723	Studies on the Disbonding Initiation of Interfacial Cracks	49772				●				●				●		●	●	●	●		
243	Critical Technology Development for Hard-Target-Defeat High-G-Toleran Fuze and High Explosives	49915							●	●				●							
480	TALON	50065		●					●										●		
725	Compliant Membranes for MEMS Microphones	50396						●						●			●				
727	Multiscale Experimental/Numerical Study	50717		●																	
80	Cellular Observatory: Simultaneous Time- and Frequency-Resolved Microscopy	50772	●																		●
46	Atomic Layer Deposition of Highly Conformal Tribological Coatings	52523												●		●	●				
50	Assembly of Microsystems Using Exothermic Multilayer Thin Films	52524												●		●	●				
52	Intelligent Interaction Control as Applied to Metrology and Assembly of Microscale Components	52526	●	●															●		

Appendix D: DOE Critical Technologies

Pg #	Title	Project #	Science of Complex Systems	Modeling & Simulation of Complex Systems	High-Performance Computing	Nuclear Weapons Predictive Capability (Classified)	Safety Assessments & Engineering	Use Control & Security	Nonproliferation & Verification	Dynamic Testing in Severe Environments	High-Energy-Density Materials	Laser Technology	Pulsed Power and Accelerators	Microelectronics and Photonics	Nuclear Materials	Engineered Materials	Flexible Manufacturing	Environmentally Conscious Manufacturing	Intelligent Machines and Robotics	Waste Management	Other
55	Rapid-Prototyping High-Density Circuitry (RpHdc)	52527										●				●	●	●			
57	Elucidating the Mysteries of Wetting	52528	●	●	●									●		●	●	●		●	
60	Next-Generation Spindles for Micromilling	52530															●				
510	Assembly and Actuation of Nanomaterials Using Active Biomolecules	52531	●											●		●					●
82	Modeling Biomembranes	52532	●	●	●																
84	Reverse-Engineering Biological Networks: Applications in Immune Responses to Bioterrorism Threats	52533	●	●	●																●
88	High-Throughput Identification of Molecular Machines Involved in Membrane Signaling and Toxin Pathways	52536																			●
447	Coupled Solid-Fluid-Mechanical-Computational Modeling of Fracture and Fragmentation in Geomaterials, such as Hard and Deeply Buried Targets (HDBTs)	52537	●	●												●				●	
107	Sequestration of Pathogens on Nanoengineered Surfaces	52538	●	●												●					
111	A Combined Preconcentrator and Sensor for Live Waterborne Pathogens	52539							●							●					●
126	IP Storage: A Performance and Security Study	52540	●	●	●																
129	A Parallel Circuit Simulator for Cell Biology	52541	●	●	●																●
131	Developing a Computationally Efficient Dynamic Multilevel Hybrid Optimization Scheme Using Multifidelity Model Interactions	52542	●	●	●																
134	Robust Large-Scale Parallel Nonlinear Solvers for Simulations	52543		●	●																
137	Development of Computational Algorithms and Inversion Capabilities for Transport/Reaction Simulations of Chemical/Biological/Radiological Terrorist Attack Scenarios in Support of Homeland Security	52544		●	●																
140	Massively Parallel Linear Programming	52546			●																
183	Active Photonic-Crystal Devices for Integrated Photonics and Silicon Photonics	52548										●		●		●					
185	Co-Processing of Chalcogenide-Based Radiation-Hard Nonvolatile Memories by Sandia's MDL and BAE Systems	52549	●											●		●	●				
187	Functionalized Nanoparticles for Sensor Applications	52551												●		●					

Appendix D: DOE Critical Technologies

Pg #	Title	Project #	Science of Complex Systems	Modeling & Simulation of Complex Systems	High-Performance Computing	Nuclear Weapons Predictive Capability (Classified)	Safety Assessments & Engineering	Use Control & Security	Nonproliferation & Verification	Dynamic Testing in Severe Environments	High-Energy-Density Materials	Laser Technology	Pulsed Power and Accelerators	Microelectronics and Photonics	Nuclear Materials	Engineered Materials	Flexible Manufacturing	Environmentally Conscious Manufacturing	Intelligent Machines and Robotics	Waste Management	Other
190	Novel *In Situ* Mechanical Testers to Enable Integrated Metal Surface Micromachines	52552	●							●				●		●			●		
193	Compliant Thermomechanical MEMS Actuators	52553	●	●				●	●	●			●	●					●		
196	An Integrated, Stacked System-on-a-Chip	52554						●	●					●					●		
199	Micromass Spectrometer-on-a-Chip	52555							●					●							
201	Quantum Coherence in Semiconductor Nanostructures for Improved Lasers and Detectors	52556										●		●							
203	MOSFET–MEMS Integration	52557	●	●			●	●	●					●		●			●	●	
205	Microoptical Gyroscope Via Monolithic Active/Passive Optical Integration	52566						●				●		●					●		
207	Materials Physics and Device Development for Improved Efficiency of GaN HEMT High-Power Amplifiers	52570		●										●		●					
209	Leaky-Mode VCSELs for Photonic Logic Circuits	52571										●		●							
211	Advanced Polychromator Systems for Remote Chemical Sensing	52575	●					●	●					●				●		●	
245	Immunological Basis for High-Reliability Systems Control	52577	●					●		●									●		
247	Moving-Target Identification Using Ultrahigh-Range-Resolution Data	52580							●												●
249	Advanced Mobile Networking, Sensing, and Controls Using Graph Theory	52581	●	●															●		
252	Compact Terahertz Sources for Emerging-Threats Applications	52582										●	●	●							
255	Understanding Communication in Counterterrorism Crisis Management	52583		●																	
258	Hypervelocity Impact-Generated Flash	52584		●						●			●								
260	Improving Human/System Interactions in Systems-of-Systems	52585		●				●											●		
262	Distributed Detection and ID Algorithm Architecture for Unattended Ground Sensors	52586							●												
264	Secure Chaotic Communications	52587	●	●				●													
266	System-of-Systems Modeling and Analysis	52588		●																	

Appendix D: DOE Critical Technologies

Pg #	Title	Project #	Science of Complex Systems	Modeling & Simulation of Complex Systems	High-Performance Computing	Nuclear Weapons Predictive Capability (Classified)	Safety Assessments & Engineering	Use Control & Security	Nonproliferation & Verification	Dynamic Testing in Severe Environments	High-Energy-Density Materials	Laser Technology	Pulsed Power and Accelerators	Microelectronics and Photonics	Nuclear Materials	Engineered Materials	Flexible Manufacturing	Environmentally Conscious Manufacturing	Intelligent Machines and Robotics	Waste Management	Other
268	Eye-Safe Short-Range Standoff Aerosol-Cloud Finder	52589							●			●		●							
270	Microflame-Based Detector Suite for Universal Gas Sensing	52590					●		●					●		●				●	
351	Beyond Nanoparticles—Attack on a Chemical "Holy Grail"	52591																		●	●
354	Advanced Proton-Exchange Materials for Energy-Efficient Fuel Cells	52592	●													●				●	
357	Alanate-Hydride Fuel-Cell Demonstration Project	52593																			●
360	Real-Time Discriminatory Sensors for Water-Contamination Events	52595												●		●				●	
362	Advanced High-Efficiency Direct-Cycle Gas Power-Conversion Systems for Small Special-Purpose Nuclear-Power Reactors	52596		●			●								●						
365	Securing Mobile Code	52597						●	●												
368	Novel Catalysts for Hydrogen Fuel-Cell Applications	52598												●							
372	Linking Optimization and Simulation in Critical-Infrastructure Systems	52606		●	●																
514	Decomposition of Contaminants Using Photochemically Active Nanoparticles	52698														●					
516	Thermally Cleavable Surfactants	52699	●											●		●	●				
518	Transition-Metal Catalyzation of Complex-Hydride Absorption/Desorption Reactions	52700	●								●					●					
520	Quantification of Environments and Surfaces Within Micropackages	52701	●											●		●					
523	Assembly of Ordered Electrooptical and Bioactive Materials and Composites	52702	●											●		●					
525	Advanced Packaging/Joining Technology for Microsystems	52703	●	●								●		●							
528	Magnetostrictive Elastomers for Actuators and Sensors	52705	●	●												●					
576	Development of a High-Throughput Microfluidic Integrated Microarray for the Detection of Chimeric Bioweapons	52706	●						●					●		●					
578	Zero-Power Radio Receiver	52708							●					●						●	
581	Completely Passive Microwave Tag	52709							●					●						●	

Appendix D: DOE Critical Technologies

Pg #	Title	Project #	Science of Complex Systems	Modeling & Simulation of Complex Systems	High-Performance Computing	Nuclear Weapons Predictive Capability (Classified)	Safety Assessments & Engineering	Use Control & Security	Nonproliferation & Verification	Dynamic Testing in Severe Environments	High-Energy-Density Materials	Laser Technology	Pulsed Power and Accelerators	Microelectronics and Photonics	Nuclear Materials	Engineered Materials	Flexible Manufacturing	Environmentally Conscious Manufacturing	Intelligent Machines and Robotics	Waste Management	Other
584	Security Coatings for Multichip Modules	52710														●	●				
586	Detailed Modeling and Simulation of Contaminant Transport in Architectural Spaces	52711		●	●																
588	Content-Based Video and Image Indexing System	52712																			●
591	Bioaerosol Collection and Concentration for Microseparations-Based Detectors	52713							●												●
594	Detecting the Toolmarks of Genetic Engineering in Bioweapons Strains	52714							●												
596	Joint Authentication/Encryption	52716			●			●	●					●					●		
598	Ultrahigh-Temperature Ceramics for Hypersonic Vehicle Applications	52717														●					
601	Leveraging Robotic Planning for Physical-Security Analysis	52718		●				●	●										●		
604	Ultralightweight Telescope with MEMS Adaptive Optic for Distortion Correction	52720												●							
606	Modeling Signals from Earth-Penetrating Nuclear Weapons for Remote Kill Assessment	52721		●					●												
607	Novel Micropreconcentrators for CW, Explosives, and Water Surety	52723							●					●		●				●	
610	Ion-Mobility Spectrometer/Mass Spectrometer	52724							●		●			●							
612	Cryptographic Assurance of Execution Correctness and Confidentiality	52725			●			●	●										●		
615	Characterization, Performance, and Optimization of PVDF as a Piezoelectric Film for Advanced Space Mirror Concepts	52726							●							●					
730	Predictive Accelerated Aging of Microsystems: The Science of Dormancy	52727	●	●				●		●				●							
733	Surety and Accountability Enhancements for Storage Containers	52728														●					
735	Nuclear-Safety Weaklinks for Thermal and Mechanical Environments	52729					●	●								●					
738	Advanced Packaging Technology for Optical Firesets	52730												●		●					
740	Miniature Transmitter Filter for JTA Using LIGA Technology	52731												●							
743	Novel and Robust Environmental Sensing Devices (ESDs)	52732					●	●		●				●							

Appendix D: DOE Critical Technologies

Pg #	Title	Project #	Science of Complex Systems	Modeling & Simulation of Complex Systems	High-Performance Computing	Nuclear Weapons Predictive Capability (Classified)	Safety Assessments & Engineering	Use Control & Security	Nonproliferation & Verification	Dynamic Testing in Severe Environments	High-Energy-Density Materials	Laser Technology	Pulsed Power and Accelerators	Microelectronics and Photonics	Nuclear Materials	Engineered Materials	Flexible Manufacturing	Environmentally Conscious Manufacturing	Intelligent Machines and Robotics	Waste Management	Other
745	Advanced Neutron Monitors for JTA and Stockpile Monitoring	52733		●					●							●					
686	Development of an Efficient Large-Aperture High-Damage-Threshold Sol-Gel Diffraction Grating	52737										●	●								
689	Laser Triggering of Water Switches in Terawatt-Class Pulse-Power Accelerators	52738											●								
530	Experimental and Computational Study of Liquid-Solid Transition in Tin	52739				●									●						
747	Design and Control of the Magnetic Properties of Nanoparticles	52797	●	●			●		●					●		●	●				
749	Flow Control and Mixing in Microfluidic Devices	52977	●	●												●					
752	Atomic-Scale Scanning-Tunneling Microscopy Measurements of Nucleation and Growth of Ge/Si Alloy Structures	53464												●		●					
754	Micro-/Nanoscale Thermomechanical Manufacturing	53465	●	●												●	●				
450	Novel Diagnostics for Rarefied Flows in MEMS Applications	53585	●									●		●							
113	Geophysical Subsurface Imaging and Interface Identification	53586		●	●				●												
756	Evolution of Near-Surface Scalar Concentrations Through a Compact Cylinder Array Embedded in the Atmospheric Surface Layer	53587		●																	
63	Miniature High-Power RF Components Enabled by Mesoscale Manufacturing	53588															●				
691	Electrical Conductivity of Metal Alloys	53590		●							●		●								
375	Hydrogen Futures Dynamic Simulation Model	53591	●	●																	
757	Design of Biospecific Surfaces to Control Specific Cellular Responses	53681							●					●		●					
760	Nanomagnetic Films	54211							●					●		●					
762	A Multiscale Approach to Modeling Carbon Nanotube–Reinforced Composites	54213	●		●											●					
483	Near-Real-Time Characterization for Assured HDBT Defeat	55079		●	●																
486	Prompt Global Response	55086		●	●				●							●			●		
488	Winning the War: A Systems Approach to Defending Our Borders	55087	●	●								●		●							

Appendix D: DOE Critical Technologies

Pg #	Title	Project #	Science of Complex Systems	Modeling & Simulation of Complex Systems	High-Performance Computing	Nuclear Weapons Predictive Capability (Classified)	Safety Assessments & Engineering	Use Control & Security	Nonproliferation & Verification	Dynamic Testing in Severe Environments	High-Energy-Density Materials	Laser Technology	Pulsed Power and Accelerators	Microelectronics and Photonics	Nuclear Materials	Engineered Materials	Flexible Manufacturing	Environmentally Conscious Manufacturing	Intelligent Machines and Robotics	Waste Management	Other
765	Integrated Superhard and Metallic Coatings for MEMS	57300	●	●	●		●			●				●	●	●	●	●	●	●	●
769	Microscale Separations of Biological Compounds Using Novel Polymeric Separations Materials	57307	●													●					
772	Friction in Micromachine Interfaces	57308												●							
774	Lipid Microarray Biosensor for Biotoxin Detection	57309	●											●		●					
777	Advanced Manufacturing Techniques Using Rapid Prototyping	57310															●				
779	Robust Hermetic Packaging Techniques for MEMS Integrated Microsystems	57311												●							
532	Active Photonic Nanostructures	58907												●		●					
781	3-D Large-Eddy Simulation of Turbulent Flow Based on One-Dimensional Turbulence Modeling	59034	●	●																	
143	A Method of Evaluating Research Using New Innovation, Risk, and Impact Indicators	59916																			●
784	Photonic Encryption Using All-Optical Logic	61046						●				●		●							
786	Nanoporous-Carbon Adsorbers for Chemical Microsensors	62269							●												
273	Nonlethal Technologies for the War on Terrorism	62827						●					●	●							
377	Agent-Based Control of Distributed Infrastructure Resources	64811		●															●		●
789	Direct Single-Ion Machining of Nanopores	65559		●									●								
792	Investigation of the Effects of Intense Pulsed Particle Beams on the Durability of Metal-to-Plastic Interfaces	66170											●			●					
794	Advanced Techniques for Multiobjective Discrete Optimization	66450		●																	
796	Nonradioactive Safety and Performance Issues with Supercritical Water Reactor (SCWR) Safety Technologies	66809	●	●			●	●							●						
798	Radiation Performance Issues with Advanced Coolants for Next-Generation Reactor	66810	●	●			●								●						
66	Rapid Prototyping to the Nanometer Scale	67004												●		●	●				
67	Robust Manufacturing of Gel-Based Components for Nuclear Weapons	67005														●	●	●			

Appendix D: DOE Critical Technologies

Pg #	Title	Project #	Science of Complex Systems	Modeling & Simulation of Complex Systems	High-Performance Computing	Nuclear Weapons Predictive Capability (Classified)	Safety Assessments & Engineering	Use Control & Security	Nonproliferation & Verification	Dynamic Testing in Severe Environments	High-Energy-Density Materials	Laser Technology	Pulsed Power and Accelerators	Microelectronics and Photonics	Nuclear Materials	Engineered Materials	Flexible Manufacturing	Environmentally Conscious Manufacturing	Intelligent Machines and Robotics	Waste Management	Other
69	Meso-/Microoptical System Interface Coupling Solutions	67006										●		●		●					
71	Injection Molding of Net-Shape Active Ceramic Components	67007		●							●					●	●	●		●	
73	Macro-/Meso-/Microsystems Integration in LTCC	67008						●						●			●		●		
91	Studies of Signaling Domains in Model and Biological Membranes Through Advanced Imaging Techniques	67010	●																		
93	Imaging Self-Organization of Proteins in Membranes by Photocatalytic Nanotagging	67011	●	●												●				●	
96	Protein Microarrays for Biowarfare-Agent Detection and Characterization	67012												●							●
99	Interaction of Proteins with Lipid Films	67013	●	●												●					
103	New Technologies for Understanding Membrane-Protein Recognition and Signaling	67014	●																		●
145	Massively Parallel, Scalable Atmosphere Model	67015	●	●	●																●
147	High-Performance Processing Architecture	67016			●																
149	Substructured Multibody Molecular Dynamics	67017	●	●	●											●			●		
151	Enhancing Simulation Performance on Clusters with Configurable Auxiliary Devices	67018		●	●																
154	A Hybrid Level-Set/Particle Method for Modeling Surface Evolution During Feature-Scale Etching and Deposition Processes	67019		●										●							
157	Penetrator Reliability Investigation and Design Exploration (PRIDE)	67020	●	●			●														
160	Topology Optimization for Improving Sensor Performance	67021		●	●																
213	Characterization and Application of Dielectrics with Controlled Leakage	67022							●					●					●		
216	Nano-G Accelerometers Using Nanophotonic Motion-Detection System	67023												●							
218	Bragg Fiber Development	67024	●									●		●		●				●	
220	Microwave-to-Millimeter-Wave Electrodynamic Response and RF Applications of Semiconductor Quantum Nanostructures	67025												●							
222	Development of GaN 20–100 Watt Ku-Band Power Amplifiers for Micro-SAR	67026							●					●							

Appendix D: DOE Critical Technologies

Pg #	Title	Project #	Science of Complex Systems	Modeling & Simulation of Complex Systems	High-Performance Computing	Nuclear Weapons Predictive Capability (Classified)	Safety Assessments & Engineering	Use Control & Security	Nonproliferation & Verification	Dynamic Testing in Severe Environments	High-Energy-Density Materials	Laser Technology	Pulsed Power and Accelerators	Microelectronics and Photonics	Nuclear Materials	Engineered Materials	Flexible Manufacturing	Environmentally Conscious Manufacturing	Intelligent Machines and Robotics	Waste Management	Other
225	Evanescent-Wave Planar Photonic Biosensor	67027						●	●					●				●		●	
227	Passive Electronically Steerable Array (PESA) for Miniature Synthetic-Aperture Radar (Mini-SAR), Precision Guidance, and Intelligence/Surveillance/Reconnaissance (ISR)	67028												●							
275	Advancements in Sensing and Perception Using Structured Lighting Techniques and an Innovative Design Tool	67029		●								●							●		
278	Biophysics of BW-Warhead Defeat with a Kinetic Interceptor	67030		●																	●
281	Dispersal in Urban Canyons, Source Identification, and Collateral Damage/Mitigation Assessment	67031		●																	
283	Weaponization of Thermobaric Explosives	67032		●						●	●					●					
286	Development of an Enterprise-Scale Agent-Based Autonomic Logistics Simulation Model	67033	●	●	●																
289	Mobile-Node Authentication in a Wireless *Ad Hoc* Environment	67034																			●
292	Novel Processing, Affordable Motion Compensation, and Mode Multiplexing for Miniaturized Synthetic-Aperture Radar	67035		●					●					●							
295	Coilgun Technology Demonstration Test-Bed	67036											●			●					
298	Enhanced Perception for Remote 3-D Mapping of Unknown Indoor and Outdoor Environments	67037		●					●										●		
300	A Modular Micromagnetic Accelerometer in Support of the mTalon Vision	67038							●												
302	MICROFUZE Integration	67039						●			●			●							
304	Analysis of Technology Impacts on Operations in Complex Environments	67041	●	●	●		●	●											●		
306	CBW Cloud Knockdown and Neutralization	67042	●	●																	●
308	Assessment of Biokillers in EDS for Biological-Agent Destruction	67043							●												●
310	Adaptive-Force-Feedback Surface Control	67044												●					●		
312	High-Capacity Earth-Penetrator Instrumentation	67046								●				●							
314	Systems Analysis of Networked Sensors	67047	●	●															●		

Appendix D: DOE Critical Technologies

Pg #	Title	Project #	Science of Complex Systems	Modeling & Simulation of Complex Systems	High-Performance Computing	Nuclear Weapons Predictive Capability (Classified)	Safety Assessments & Engineering	Use Control & Security	Nonproliferation & Verification	Dynamic Testing in Severe Environments	High-Energy-Density Materials	Laser Technology	Pulsed Power and Accelerators	Microelectronics and Photonics	Nuclear Materials	Engineered Materials	Flexible Manufacturing	Environmentally Conscious Manufacturing	Intelligent Machines and Robotics	Waste Management	Other
317	Deployable Object Tracker for NMD Flights	67048							●			●		●					●		
319	Continuous-Flow Detector for Rapid Pathogen Identification	67049							●												●
380	Biological-Security Decontamination Technology—Reducing the Threat of Infectious-Agent Spread	67050	●					●													●
383	Consequence Management, Recovery, and Restoration after an Intentional Contamination Event	67051	●	●																	
386	Fully Integrated System-Dynamics Toolbox for Water Resources Planning	67052	●	●																	
390	Predicting System Performance of Proton-Exchange-Membrane Fuel Cells: Computational Modeling with Experimental Discovery and Validation	67053	●	●												●					
393	Optimal Allocation of Terrorist Countermeasures Using Risk-Based Systems Pathways Analysis	67054	●	●																	
396	Silicon Field-Emission Electric Propulsion Arrays (FEEP) Powered by Orbital Nuclear Reactors	67055												●							
398	Advanced Fuel-Cell Reactor for the Direct Cogeneration of Electricity During Selective Partial Oxidation of Hydrocarbons	67056	●													●	●				
401	New Hydrogen-Storage Material: Metal-N-H system	67057	●													●					
403	Intrusion Detection for Wireless Networks	67058						●													●
405	Membranes for H2 Generation from Nuclear Powered Thermochemical Cycles	67059					●									●					
408	Microfabricated BTU Monitoring Device for System-Wide Natural-Gas Monitoring	67060	●	●						●				●							
411	“Tunable” Ion Conductors for Low-Temperature Oxide-Based Fuel Cells	67061														●					
414	Nuclear Nanobatteries: On-Board Power for Independent MEMS Devices	67062												●	●	●					
417	Integrated Tunable Light Sources for Miniature Sensors	67063							●			●		●				●			
452	Ray Model of High-Frequency Cavity Scarring	67064	●	●	●																
455	New Smart Material to Address Issues of Structural Health Monitoring	67065	●	●						●				●		●			●		
458	Noncontact Surface Thermometry for Microsystems	67067	●	●										●							

Appendix D: DOE Critical Technologies

Pg #	Title	Project #	Science of Complex Systems	Modeling & Simulation of Complex Systems	High-Performance Computing	Nuclear Weapons Predictive Capability (Classified)	Safety Assessments & Engineering	Use Control & Security	Nonproliferation & Verification	Dynamic Testing in Severe Environments	High-Energy-Density Materials	Laser Technology	Pulsed Power and Accelerators	Microelectronics and Photonics	Nuclear Materials	Engineered Materials	Flexible Manufacturing	Environmentally Conscious Manufacturing	Intelligent Machines and Robotics	Waste Management	Other
461	High-Speed Interferometric Deformation Measurements	67068		●						●				●							
463	Fundamentals of Nanofluidics	67069	●	●																	
465	Simulating Self-Assembly and Growth of Biological Nanostructured Materials	67070	●	●																	
468	A Low-Power, Ultrafast-Current Transient Measuring Device	67071												●							
470	A Capillary Valve for Microfluidic Systems	67073		●					●												
534	Electrochemically Switchable Materials for (Bio)Microfluidics	67074														●					
537	Modeling of Friction-Induced Deformation and Microstructure	67075		●																	
540	Reversible Antibody Trapping for Selective Sensor Devices	67076	●													●					
542	Correlated and Comprehensive Analytical Techniques for Homeland Defense	67077			●																
545	Development of High-Energy-Density Dielectric Materials for Integrated Microsystems	67078	●								●										
549	Nanolithography-Directed Materials Growth and Self-Assembly	67079												●		●					
552	Development of a Novel Technique to Assess the Vulnerability of Micromechanical System Components to Environmentally Assisted Cracking	67080												●		●					
554	3-D Optical Sectioning with a New Hyperspectral Deconvolution Fluorescence Imaging System	67081	●	●	●									●		●	●				
558	The Science of Solutes: Transition Metals in LIGA Nickel	67082		●										●							
560	Novel Gel-Based Technology for Sensors and Weapons	67083	●											●		●					
562	Coupled Nanomechanical Oscillator Arrays for the Study of Internal Dissipation in Nanoscale Structures and Collective Behavior in Large Systems	67084	●											●							
565	Precisely Controlled Picoliter Vessels with Rapid Sample Preparation for Trace Biotoxin Detection	67085	●						●							●					
618	Adaptive Optics and Phase-Diversity Imaging for Responsive Space Applications	67086							●					●							
621	Infrastructural Development for Flexible Network of Devices	67087							●												

Appendix D: DOE Critical Technologies

Pg #	Title	Project #	Science of Complex Systems	Modeling & Simulation of Complex Systems	High-Performance Computing	Nuclear Weapons Predictive Capability (Classified)	Safety Assessments & Engineering	Use Control & Security	Nonproliferation & Verification	Dynamic Testing in Severe Environments	High-Energy-Density Materials	Laser Technology	Pulsed Power and Accelerators	Microelectronics and Photonics	Nuclear Materials	Engineered Materials	Flexible Manufacturing	Environmentally Conscious Manufacturing	Intelligent Machines and Robotics	Waste Management	Other
622	Monolithic Reconfigurable Radio-Frequency Microelectromechanical Systems (RF MEMS) Antennas	67088						●	●					●					●	●	
625	Next-Generation 3-D Inspection System for Facility Monitoring	67089	●		●		●	●	●										●		
627	Risk-Assessment Metatool	67090	●	●				●	●												
629	Featureless Spread-Spectrum Waveform Design and Processing	67091							●												
631	Tracking Slow-Moving Objects in a GPS–Denied Environment	67092		●				●	●					●							
632	Optical Communications	67093							●					●							
633	A Unique Vibration-Based Miniature Power Generator for National Security Applications	67094							●					●							
636	Image Georectification Using Digital Elevation Model Shadows	67095		●					●												●
639	Vulnerability Assessment of State-of-the-Art Microelectronics	67096						●	●					●							
640	Nonlinear Optical Detection of Biological and Chemical Aerosol Agents Using Femtosecond Lasers	67098							●			●		●							
643	Polymer Electronic Devices and Materials	67099						●	●					●			●	●			
647	Small Circuits for Cryptography	67101						●	●					●					●		
649	Analysis of Multichannel Internet Communication	67102							●												
650	Receiver for Ultralow-Power Wake-Up and Command	67104	●					●	●					●					●		
652	Extraordinary Optical Transmission Through Patterned Subwavelength Apertures	67105							●					●							
654	Reconstruction Algorithm Development and Assessment for a Computed Tomography–Based Spectral Imager	67107							●												
657	Power-Combining Techniques for Solid-State Power Amplifiers	67108		●					●					●							
659	Dispersive Diffractive Optical Elements for the Infrared	67109							●			●		●		●					
661	Atmospheric Propagation of Terahertz Radiation	67111							●		●	●		●							
663	High-Confidence Estimation of Relative Event Locations from Space-Based Sensors	67113							●										●		

Appendix D: DOE Critical Technologies

Pg #	Title	Project #	Science of Complex Systems	Modeling & Simulation of Complex Systems	High-Performance Computing	Nuclear Weapons Predictive Capability (Classified)	Safety Assessments & Engineering	Use Control & Security	Nonproliferation & Verification	Dynamic Testing in Severe Environments	High-Energy-Density Materials	Laser Technology	Pulsed Power and Accelerators	Microelectronics and Photonics	Nuclear Materials	Engineered Materials	Flexible Manufacturing	Environmentally Conscious Manufacturing	Intelligent Machines and Robotics	Waste Management	Other
665	Critical-Infrastructure System-of-Systems Assessment Methodology	67114	●	●																	
667	Dynamic Vulnerability Assessment	67115													●						●
669	Inflatable Antenna with Adaptive Actuators	67116							●												
671	Data-Driven Dynamic Models of Conflict	67117	●	●				●	●						●						
800	MEMS/Fuze Diagnostic Extraction in High-G Environments	67118								●				●							
694	Efficient Implicit Multigroup Radiation Calculations	67120		●	●								●								
696	Model for Channel Resistance in Water Breakdown	67121	●								●		●								
698	Embeddable Shock Physics Sensors	67122								●	●		●	●		●					
802	Smart Detectors of Enrichment of Bioaerosols	67716	●									●									●
805	Computational Studies of JP-8 Diffusion Flames with Detailed Chemistry and Particulate Formation	68063		●	●		●														
419	Design and Fabrication of Advanced Device Structures for Ultrahigh-Efficiency Solid-State Lighting	69143												●							
808	Molecular Simulation of Beta-Amyloid (A-beta) Peptide Interaction with Phospholipid Membranes	69145																			●
809	Nanoscale Testing of Deformation and Fracture in Engineering Materials	69146		●										●		●					
812	Nanocrystal-Polymer Composites for High-Luminous-Efficiency LEDs	69148												●							
817	Outstanding Challenges for AlGaInN MOCVD	69149												●							
820	Nanoporous Polymeric Materials for Chemically and Spatially Multiplexed Sensing of Bioagents	69150														●					
823	Evolutionary Complexity for Protection of Critical Assets	69151		●	●			●											●		●
825	Nanomechanical Stochastic Resonators	69152	●	●				●	●	●				●					●		
826	Augmented Musculature Device	69153																	●		
828	Biomolecular Decision-Making Processes for Self-Assembly	69154	●	●																	

Appendix D: DOE Critical Technologies

Pg #	Title	Project #	Science of Complex Systems	Modeling & Simulation of Complex Systems	High-Performance Computing	Nuclear Weapons Predictive Capability (Classified)	Safety Assessments & Engineering	Use Control & Security	Nonproliferation & Verification	Dynamic Testing in Severe Environments	High-Energy-Density Materials	Laser Technology	Pulsed Power and Accelerators	Microelectronics and Photonics	Nuclear Materials	Engineered Materials	Flexible Manufacturing	Environmentally Conscious Manufacturing	Intelligent Machines and Robotics	Waste Management	Other
830	Light-Powered Nanovehicle Propulsion	69155	●	●												●					
832	System-Dynamics Modeling to Assist Regional Water Planning: Modeling the Nonmarket Value of Water	69156	●	●																	
834	Interactive Water-Quality Modeling to Assist Regional Water Planning	69157	●	●																	
837	Microbe-Exuded Polymers and the Enhanced Corrosion of Carbonate Materials	69158	●	●																●	
840	Nerve-Cell Function and the Development of Cognitive Networks	69159	●													●					
843	Ultrahigh-Gain Fusion Concept	69160									●										
844	Nanofluidic Devices for Rapid Detection of Virus Particles	69161										●									
846	Solution Behavior of PEO: The Ultimate Biocompatible Polymer	69162	●	●	●																
848	New Self-Assembled Nanocrystal Micelles for Biolabels	69163														●					
851	Rapid Detection of Biothreat Agents Based on Cellular Machinery	69164							●												●
853	Patterning Quantum-Dot Arrays Using DNA Replication Principles	69165	●											●		●					
856	Adaptive Algorithms for Use in the Rejection of Periodic Disturbances of Unknown Frequency	69166	●	●	●																
858	Property-Based Testing for Cybersecurity Assurance	69168	●	●	●		●	●	●										●		
860	Self-Assembled Ordered Carbon-Nanotube Arrays and Membranes	69170							●					●							
863	Chemical Cross-Linking and Mass-Spectrometry Studies of the Structure and Dynamics of Membrane Proteins and Receptors	69189																			●
866	Toxin Studies Using an Integrated Biophysical and Structural Biology Approach	69190																			●
869	Top-Down Structural Studies	69191																			●
871	Molecular Dynamics of Membrane Proteins	69192	●	●																	●
874	Model-Building Codes for Membrane Proteins	69193			●																●
878	Poroelastic Wave-Propagation on the Earth Simulator	69198		●	●				●											●	

Appendix D: DOE Critical Technologies

Pg #	Title	Project #	Science of Complex Systems	Modeling & Simulation of Complex Systems	High-Performance Computing	Nuclear Weapons Predictive Capability (Classified)	Safety Assessments & Engineering	Use Control & Security	Nonproliferation & Verification	Dynamic Testing in Severe Environments	High-Energy-Density Materials	Laser Technology	Pulsed Power and Accelerators	Microelectronics and Photonics	Nuclear Materials	Engineered Materials	Flexible Manufacturing	Environmentally Conscious Manufacturing	Intelligent Machines and Robotics	Waste Management	Other
882	Development of Microreformers for Fuel Cells	69239														●					
568	Developing the Foundation for Polyoxoniobate Chemistry: Highly Tunable and Exploitable Materials	70799	●													●				●	
321	Simulating Human Behavior for National Security	71943	●	●															●		●
28	Agent-Based Modeling of Middle East Terrorist Recruitment	71944	●	●																	
30	Automatic Generation of Terrorist Operation Plan Hypotheses	71945	●																		
421	Develop a System-Dynamics Modeling Framework for Assessing Factors that Influence Water Resource Consumption	72599	●	●																	
423	Develop a Cooperative Water-Management Process, Creating a System-Dynamics Model of Water Resources in the Lower Rio Grande Basin	72600	●	●																●	
323	Compact Ultrabright Multikilovolt X-Ray Sources for Advanced Material Studies, 3-D Nanoimaging, and Attosecond X-Ray Technology	72715				●			●				●								●
425	Energy-Systems Analysis Framework and Modeling	72716		●																	
33	Radiation-/Geometry-Driven Jets: Proof-of-Principle Tests	73045			●	●					●		●								
884	Superhydrophobic Surface Coatings for Microfluidics and MEMS	73185	●											●		●					
673	Microoptical Radar (MOR) Facial-Recognition Project	73207	●					●				●		●			●		●		
886	Determining Explosive Ignition Criteria for Miniaturized Devices	74545									●					●					
888	Quantum Squeezed Light for Probing Mitochondrial Membranes and Study of Neuroprotectants	74546										●		●							
890	Characterization of a New Class of Surface-Micromachined Pumps	74547	●	●					●					●						●	
893	Risk of Biological Terrorism to Water-Distribution Systems	74548	●	●																	●
895	Explicit and Implicit Measures in Human Aversive Classical Conditioning	74759	●																●		
676	Automatic-Target-Recognition Algorithms for Uncooled Thermal Imagery	74760							●												
326	Magnetophoretic Bead Trapping in a High-Flowrate Biological Detection System	74795							●					●		●				●	
329	TPV Energy Scavenging for Hypervelocity Vehicles	75441												●		●					

Appendix D: DOE Critical Technologies

Pg #	Title	Project #	Science of Complex Systems	Modeling & Simulation of Complex Systems	High-Performance Computing	Nuclear Weapons Predictive Capability (Classified)	Safety Assessments & Engineering	Use Control & Security	Nonproliferation & Verification	Dynamic Testing in Severe Environments	High-Energy-Density Materials	Laser Technology	Pulsed Power and Accelerators	Microelectronics and Photonics	Nuclear Materials	Engineered Materials	Flexible Manufacturing	Environmentally Conscious Manufacturing	Intelligent Machines and Robotics	Waste Management	Other
898	Assessment of Advanced Pulsed-Power Fusion Concepts	75442		●					●		●		●								
427	A Mathematical Method for Quantifying the Effectiveness of Management Strategies	75443	●	●			●														
901	Developing Algorithms for Predicting Protein-Protein Interactions from Experimental Constraints	75513	●	●																	
904	Instrumentation Development for Real-Time Brain-Wave Monitoring	75514												●							
907	Miniaturized Electronic Steerable-Array Synthetic-Aperture Radar	76069							●					●							
910	Full-Earth-Monitoring Sensor MESAWorks	76070							●					●		●			●		
36	Systems Assessment of Water-Savings Impact of Controlled-Environment Agriculture Utilizing Wirelessly Networked SDACs	76305		●															●		
429	Inactivation of Avian Influenza (Bird Flu) with Sandia-Developed Decontamination Formulations	76306	●																	●	●
913	Deciphering the Genetic Regulatory Code Using an Inverse Error Control Coding Framework	78132	●	●															●		
38	Climate-Change Effects on International Stability	78307		●	●				●												
916	Generalized Continuum Models for Inelasticity in Solids: Formulation of Theories and Variational Methods for Computation	78783		●												●					
431	GeSi–Strained Nanostructure Self-Assembly for Nano- and Optoelectronics	79943												●		●					
678	Vulnerability Analysis for SCADA	80835	●				●														
918	Molten Salt-Based Growth of Bulk GaN and InN	80838										●	●	●							
679	Randomness Complexity and Cryptography	81209			●			●	●										●		
681	System Study: Adaptive Optics for Weapon, Reconnaissance, and Military Space Applications	81354							●					●							
			125	**136**	**46**	**5**	**19**	**43**	**99**	**20**	**17**	**32**	**19**	**138**	**8**	**100**	**31**	**16**	**49**	**29**	**45**

Appendix E: Major National Programs

Pg #	Title	Project #	Waste Management	Energy Efficiency	Renewable Energy	ES&H	Environmental Restoration	Fossil Energy	Radioactive-Waste Management	Economic Impact	Energy Research	Intelligence & National Security	Nuclear Energy	Science Education & Technical Information	Defense Programs	Department of Homeland Security (DHS)	Department of Defense (DoD)	Other Federal Agencies*	Other (Industry, Consortia…)**	Other Federal Agencies* Other (Industry, Consortia…)**
41	Microfabrication with Femtosecond Laser Processing	38605													●		●			
44	Mesoscale Controlled Motion for a Microfluidic Drop Ejector	38606													●	●				
77	Physical and Electronic Changes Caused by Membrane Signaling as a Transduction Pathway in Affinity-Based Biosensors	38609										●		●	●	●	●			
116	Graduated Embodiment for Sophisticated-Agent Evolution and Optimization	38610										●			●	●	●			
119	Scalable Fault-Tolerant Algorithms for Linear-Scaling Coupled-Cluster Electronic Structure Methods	38613			●		●	●			●			●	●	●				
121	Micromagnetic Suspension	38614									●				●					
123	Sensitivities for Large-Scale Simulation Codes	38615													●					
168	Engineered Superconductivity in Electron-Hole Bilayers	38616									●	●			●	●	●			
171	Silicon-Based RF MEMS Components	38617								●		●			●		●		●	**Industry
173	Nanoelectromechanical Oscillators (NEMOs) for RF Filtering	38619										●			●	●	●			
176	Continuous-Wave Intersubband Terahertz Sources	38620										●			●	●	●	●		*NASA
178	Microsystems for Chemical Signature and Reagent Delivery	38621										●				●	●		●	**Industry
180	Microfluidic Cellular-Sample Pretreatment	38622	●			●	●	●	●			●		●	●	●	●			
231	Automated Visual Direction of Mobile Manipulation	38623							●			●				●				
233	Miniature Fourier-Transform Ion-Mobility Spectrometer for Real-Time Detection and Identification of Explosives and Chemical Agents	38624					●					●			●	●	●			
235	EM Interactions with Systems to Enhance Security	38627														●	●			
236	Use of Seismic and Acoustic Responses to Assess Bomb Damage to Underground Facilities	38629													●		●			
238	Free-Space Electrooptic Sampling and Remote Mapping of Electromagnetic Fields from Emitting Structures Using Femtosecond Terahertz Transceivers	38655										●			●	●	●			

Appendix E: Major National Programs

Pg #	Title	Project #	Waste Management	Energy Efficiency	Renewable Energy	ES&H	Environmental Restoration	Fossil Energy	Radioactive-Waste Management	Economic Impact	Energy Research	Intelligence & National Security	Nuclear Energy	Science Education & Technical Information	Defense Programs	Department of Homeland Security (DHS)	Department of Defense (DoD)	Other Federal Agencies*	Other (Industry, Consortia…)**	Other Federal Agencies* Other (Industry, Consortia…)**
332	Natural-Gas Production Problems: Solutions, Methodologies, and Modeling	38662	●					●			●								●	**Industry
335	Time-Domain Reflectometry for Remote, Real-Time Water-Quantity/-Quality Monitoring of Perennial and Ephemeral Streams	38665					●							●				●		*USGS, B. of Rec., Army Corps of Engineers
338	Functionalized Nanoelectrode Arrays for *In Situ* Identification and Quantification of Regulated Chemicals in Water	38668	●			●	●					●				●	●			
341	Water Desalination	38673	●		●						●							●	●	*AWRF, B. of Rec., USGS, **Local Water Municipalities
344	Revolutionary Systems for Catalytic Combustion and Diesel Catalytic Particulate Traps	38674		●				●			●									
348	Potential Application of Microsensor Technology in Radioactive-Waste Management—With Emphasis on Headspace Gas Detection	38677	●						●											
241	Identification of Chemical Plumes: Range-Resolved IR Lidar Enabled by New Photonic Technologies	38681		●			●	●			●				●	●	●			
434	A Robust, Coupled Approach for Atomistic-Continuum Simulation	38684									●				●	●	●			
438	Microscale Rarefied-Gas Dynamics and Surface Interactions for EUVL and MEMS Applications	38685														●	●			
441	High-Fidelity Frictional Models for MEMS	38686													●					
444	Soot Formation, Transport, and Radiation in Unsteady Diffusion Flames	38687		●											●		●			
493	The Basics of Aqueous Nanofluidics: "Interphase" Structure and Surface Forces	38688									●				●					
497	Design, Synthesis, and Characterization of Soft-Matter Nanolayer Superlattices	38689													●					
499	Photocontrol of Nanointeractions in Microsystems	38690									●				●		●			
501	Electrochemically Deposited Alloys with Tailored Nanostructures for LIGA Micromachines	38691									●				●					
503	Nanostructured Materials for Directed Transport of Excitation Energy	38692		●																
505	Modeling Local Chemistry in the Presence of Collective Phenomena	38693					●				●				●					

Appendix E: Major National Programs

Pg #	Title	Project #	Waste Management	Energy Efficiency	Renewable Energy	ES&H	Environmental Restoration	Fossil Energy	Radioactive-Waste Management	Economic Impact	Energy Research	Intelligence & National Security	Nuclear Energy	Science Education & Technical Information	Defense Programs	Department of Homeland Security (DHS)	Department of Defense (DoD)	Other Federal Agencies*	Other (Industry, Consortia…)**	Other Federal Agencies* Other (Industry, Consortia…)**
701	Nanoscale Energetic Materials by Inverse Micellar Synthesis	38717													●		●			
704	Modeling of Rock Penetration	38718													●		●			
572	Agile, Microsystems-Enabled Receiver	38722										●			●	●	●		●	**LMSV
507	Solution-Based Nanoengineering of Materials	39017			●						●				●	●	●			
684	Simulations of Intense Petawatt Laser Pulses with Dense Z-Pinch Plasmas	39670													●					
473	Biomicrfofuel Cell (BMFC)	41193									●	●		●		●	●	●		*DARPA
476	Augmented Cognition: Next-Generation Intelligent Systems	41194										●	●		●	●	●			
164	Microengine for Advanced Power Generation	41674									●						●			
707	Direct Simulation of Solid-Fluid Systems	41726						●			●								●	**CRADA
710	Support–Active Site Interactions in Heterogeneous Catalysts	42461						●			●									
712	An Analysis of the Automotive Industry as a Source for Weapon Components and Manufacturing Processes	42483		●						●	●				●				●	**Industry
713	High-Speed Micro-EDM	46070													●	●				
715	Microexternal-Combustion Engine: The P3 Engine Prototype	46686									●	●				●	●			
717	Lipid Membranes on Nanostructured Silicon	47795														●		●		*DOE–BES
720	Resin Infusion Between Double Flexible Tooling	49769								●					●				●	**University Collaboration
723	Studies on the Disbonding Initiation of Interfacial Cracks	49772		●	●						●		●	●		●	●			
243	Critical Technology Development for Hard-Target-Defeat High-G-Tolerant Fuze and High Explosives	49915										●			●		●			
480	TALON	50065										●				●	●			
725	Compliant Membranes for MEMS Microphones	50396										●			●	●	●			
727	Multiscale Experimental/Numerical Study	50717													●					

Appendix E: Major National Programs

Pg #	Title	Project #	Waste Management	Energy Efficiency	Renewable Energy	ES&H	Environmental Restoration	Fossil Energy	Radioactive-Waste Management	Economic Impact	Energy Research	Intelligence & National Security	Nuclear Energy	Science Education & Technical Information	Defense Programs	Department of Homeland Security (DHS)	Department of Defense (DoD)	Other Federal Agencies*	Other (Industry, Consortia…)**	Other Federal Agencies* Other (Industry, Consortia…)**
80	Cellular Observatory: Simultaneous Time- and Frequency-Resolved Microscopy	50772									●								●	**Biotechnology
46	Atomic Layer Deposition of Highly Conformal Tribological Coatings	52523													●	●				
50	Assembly of Microsystems Using Exothermic Multilayer Thin Films	52524						●		●	●								●	**Industry, Consortia
52	Intelligent Interaction Control as Applied to Metrology and Assembly of Microscale Components	52526													●		●		●	**Industry
55	Rapid-Prototyping High-Density Circuitry (RpHdc)	52527													●		●		●	**Manufacturing Industry, University
57	Elucidating the Mysteries of Wetting	52528		●	●	●	●	●	●		●			●	●	●	●			
60	Next-Generation Spindles for Micromilling	52530										●			●		●			
510	Assembly and Actuation of Nanomaterials Using Active Biomolecules	52531													●	●	●	●		*NIH
82	Modeling Biomembranes	52532												●	●	●		●		*NIH
84	Reverse-Engineering Biological Networks: Applications in Immune Responses to Bioterrorism Threats	52533									●					●			●	**DOE GTL Program
88	High-Throughput Identification of Molecular Machines Involved in Membrane Signaling and Toxin Pathways	52536														●	●	●		*NIH
447	Coupled Solid-Fluid-Mechanical-Computational Modeling of Fracture and Fragmentation in Geomaterials, such as Hard and Deeply Buried Targets (HDBTs)	52537	●												●		●			
107	Sequestration of Pathogens on Nanoengineered Surfaces	52538														●				
111	A Combined Preconcentrator and Sensor for Live Waterborne Pathogens	52539														●	●	●	●	*CDC, **Industry
126	IP Storage: A Performance and Security Study	52540												●		●	●			
129	A Parallel Circuit Simulator for Cell Biology	52541	●				●												●	**Genomes-to-Life Initiative
131	Developing a Computationally Efficient Dynamic Multilevel Hybrid Optimization Scheme Using Multifidelity Model Interactions	52542													●		●			
134	Robust Large-Scale Parallel Nonlinear Solvers for Simulations	52543									●									

Appendix E: Major National Programs

Pg #	Title	Project #	Waste Management	Energy Efficiency	Renewable Energy	ES&H	Environmental Restoration	Fossil Energy	Radioactive-Waste Management	Economic Impact	Energy Research	Intelligence & National Security	Nuclear Energy	Science Education & Technical Information	Defense Programs	Department of Homeland Security (DHS)	Department of Defense (DoD)	Other Federal Agencies*	Other (Industry, Consortia…)**	Other Federal Agencies* Other (Industry, Consortia…)**
137	Development of Computational Algorithms and Inversion Cap- abilities for Transport/Reaction Simulations of Chemical/Biological/Radiological Terrorist Attack Scenarios in Support of Homeland Security	52544														●		●	●	*EPA, **Industry, Consortia
140	Massively Parallel Linear Programming	52546									●				●					
183	Active Photonic-Crystal Devices for Integrated Photonics and Silicon Photonics	52548		●							●						●			
185	Co-Processing of Chalcogenide-Based Radiation-Hard Nonvolatile Memories by Sandia's MDL and BAE Systems	52549										●		●	●	●	●			
187	Functionalized Nanoparticles for Sensor Applications	52551				●	●										●			
190	Novel *In Situ* Mechanical Testers to Enable Integrated Metal Surface Micromachines	52552												●	●					
193	Compliant Thermomechanical MEMS Actuators	52553		●	●				●		●	●	●		●	●	●			
196	An Integrated, Stacked System-on-a-Chip	52554										●			●	●	●			
199	Micromass Spectrometer-on-a-Chip	52555										●			●	●			●	**Industry
201	Quantum Coherence in Semiconductor Nanostructures for Improved Lasers and Detectors	52556										●		●	●	●	●			
203	MOSFET–MEMS Integration	52557	●			●						●	●		●	●	●			
205	Microoptical Gyroscope Via Monolithic Active/Passive Optical Integration	52566										●			●	●	●			
207	Materials Physics and Device Development for Improved Efficiency of GaN HEMT High-Power Amplifiers	52570										●			●	●	●			
209	Leaky-Mode VCSELs for Photonic Logic Circuits	52571															●			
211	Advanced Polychromator Systems for Remote Chemical Sensing	52575						●				●			●	●	●			
245	Immunological Basis for High-Reliability Systems Control	52577										●			●	●	●			
247	Moving-Target Identification Using Ultrahigh-Range-Resolution Data	52580															●			
249	Advanced Mobile Networking, Sensing, and Controls Using Graph Theory	52581										●			●		●			

Appendix E: Major National Programs

Pg #	Title	Project #	Waste Management	Energy Efficiency	Renewable Energy	ES&H	Environmental Restoration	Fossil Energy	Radioactive-Waste Management	Economic Impact	Energy Research	Intelligence & National Security	Nuclear Energy	Science Education & Technical Information	Defense Programs	Department of Homeland Security (DHS)	Department of Defense (DoD)	Other Federal Agencies*	Other (Industry, Consortia…)**	Other Federal Agencies* Other (Industry, Consortia…)**
252	Compact Terahertz Sources for Emerging-Threats Applications	52582										●		●	●	●	●			
255	Understanding Communication in Counterterrorism Crisis Management	52583													●	●	●			
258	Hypervelocity Impact-Generated Flash	52584													●		●			
260	Improving Human/System Interactions in Systems-of-Systems	52585										●			●	●	●			
262	Distributed Detection and ID Algorithm Architecture for Unattended Ground Sensors	52586														●	●			
264	Secure Chaotic Communications	52587													●		●			
266	System-of-Systems Modeling and Analysis	52588													●		●			
268	Eye-Safe Short-Range Standoff Aerosol-Cloud Finder	52589														●	●			
270	Microflame-Based Detector Suite for Universal Gas Sensing	52590	●	●		●	●	●		●		●			●	●	●			
351	Beyond Nanoparticles—Attack on a Chemical "Holy Grail"	52591						●		●	●									
354	Advanced Proton-Exchange Materials for Energy-Efficient Fuel Cells	52592	●	●							●									
357	Alanate-Hydride Fuel-Cell Demonstration Project	52593			●															
360	Real-Time Discriminatory Sensors for Water-Contamination Events	52595	●			●						●				●				
362	Advanced High-Efficiency Direct-Cycle Gas Power-Conversion Systems for Small Special-Purpose Nuclear-Power Reactors	52596		●							●		●							
365	Securing Mobile Code	52597										●				●	●		●	**Industry
368	Novel Catalysts for Hydrogen Fuel-Cell Applications	52598		●							●									
372	Linking Optimization and Simulation in Critical-Infrastructure Systems	52606													●	●	●			
514	Decomposition of Contaminants Using Photochemically Active Nanoparticles	52698									●				●	●				
516	Thermally Cleavable Surfactants	52699					●							●	●				●	**Industry

Appendix E: Major National Programs

Pg #	Title	Project #	Waste Management	Energy Efficiency	Renewable Energy	ES&H	Environmental Restoration	Fossil Energy	Radioactive-Waste Management	Economic Impact	Energy Research	Intelligence & National Security	Nuclear Energy	Science Education & Technical Information	Defense Programs	Department of Homeland Security (DHS)	Department of Defense (DoD)	Other Federal Agencies*	Other (Industry, Consortia…)**	Other Federal Agencies* Other (Industry, Consortia…)**
518	Transition-Metal Catalyzation of Complex-Hydride Absorption/Desorption Reactions	52700	●	●	●	●	●	●		●	●									
520	Quantification of Environments and Surfaces within Micropackages	52701													●		●			
523	Assembly of Ordered Electrooptical and Bioactive Materials and Composites	52702									●					●				
525	Advanced Packaging/Joining Technology for Microsystems	52703													●				●	**Microsystems
528	Magnetostrictive Elastomers for Actuators and Sensors	52705														●	●			
576	Development of a High-Throughput Microfluidic Integrated Microarray for the Detection of Chimeric Bioweapons	52706										●			●	●	●		●	**Industry
578	Zero-Power Radio Receiver	52708										●				●	●	●		*NASA
581	Completely Passive Microwave Tag	52709										●			●	●	●	●	●	*NASA, ** Industry—Motorola
584	Security Coatings for Multichip Modules	52710										●				●	●			
586	Detailed Modeling and Simulation of Contaminant Transport in Architectural Spaces	52711														●				
588	Content-Based Video and Image Indexing System	52712										●				●	●			
591	Bioaerosol Collection and Concentration for Microseparations-Based Detectors	52713										●			●		●			
594	Detecting the Toolmarks of Genetic Engineering In Bioweapons Strains	52714										●			●	●	●			
596	Joint Authentication/Encryption	52716										●		●	●	●	●			
598	Ultrahigh-Temperature Ceramics for Hypersonic Vehicle Applications	52717									●	●			●	●	●	●		*NASA
601	Leveraging Robotic Planning for Physical-Security Analysis	52718													●	●	●			
604	Ultralightweight Telescope with MEMS Adaptive Optic for Distortion Correction	52720										●			●	●	●			
606	Modeling Signals from Earth-Penetrating Nuclear Weapons for Remote Kill Assessment	52721										●								
607	Novel Micropreconcentrators for CW, Explosives, and Water Surety	52723	●			●	●			●		●			●	●	●			

Appendix E: Major National Programs

Pg #	Title	Project #	Waste Management	Energy Efficiency	Renewable Energy	ES&H	Environmental Restoration	Fossil Energy	Radioactive-Waste Management	Economic Impact	Energy Research	Intelligence & National Security	Nuclear Energy	Science Education & Technical Information	Defense Programs	Department of Homeland Security (DHS)	Department of Defense (DoD)	Other Federal Agencies*	Other (Industry, Consortia…)**	Other Federal Agencies* Other (Industry, Consortia…)**
610	Ion-Mobility Spectrometer/Mass Spectrometer	52724													●	●	●			
612	Cryptographic Assurance of Execution Correctness and Confidentiality	52725										●			●	●	●		●	**Secure Computing Infrastructure
615	Characterization, Performance, and Optimization of PVDF as a Piezoelectric Film for Advanced Space Mirror Concepts	52726												●						
730	Predictive Accelerated Aging of Microsystems: The Science of Dormancy	52727										●			●		●		●	**Industry
733	Surety and Accountability Enhancements for Storage Containers	52728													●					
735	Nuclear-Safety Weaklinks for Thermal and Mechanical Environments	52729													●		●			
738	Advanced Packaging Technology for Optical Firesets	52730										●			●	●	●			
740	Miniature Transmitter Filter for JTA Using LIGA Technology	52731													●		●			
743	Novel and Robust Environmental Sensing Devices (ESDs)	52732													●		●			
745	Advanced Neutron Monitors for JTA and Stockpile Monitoring	52733													●					
686	Development of an Efficient Large-Aperture High-Damage-Threshold Sol-Gel Diffraction Grating	52737									●									
689	Laser Triggering of Water Switches in Terawatt-Class Pulse-Power Accelerators	52738									●				●					
530	Experimental and Computational Study of Liquid-Solid Transition in Tin	52739													●					
747	Design and Control of the Magnetic Properties of Nanoparticles	52797		●										●	●	●	●			
749	Flow Control and Mixing in Microfluidic Devices	52977												●		●				
752	Atomic-Scale Scanning-Tunneling Microscopy Measurements of Nucleation and Growth of Ge/Si Alloy Structures	53464									●				●					
754	Micro-/Nanoscale Thermomechanical Manufacturing	53465										●		●		●				
450	Novel Diagnostics for Rarefied Flows in MEMS Applications	53585												●			●			
113	Geophysical Subsurface Imaging and Interface Identification	53586			●			●			●				●					

Appendix E: Major National Programs

Pg #	Title	Project #	Waste Management	Energy Efficiency	Renewable Energy	ES&H	Environmental Restoration	Fossil Energy	Radioactive-Waste Management	Economic Impact	Energy Research	Intelligence & National Security	Nuclear Energy	Science Education & Technical Information	Defense Programs	Department of Homeland Security (DHS)	Department of Defense (DoD)	Other Federal Agencies*	Other (Industry, Consortia…)**	Other Federal Agencies* Other (Industry, Consortia…)**
756	Evolution of Near-Surface Scalar Concentrations Through a Compact Cylinder Array Embedded in the Atmospheric Surface Layer	53587														●				
63	Miniature High-Power RF Components Enabled by Mesoscale Manufacturing	53588													●					
691	Electrical Conductivity of Metal Alloys	53590													●					
375	Hydrogen Futures Dynamic-Simulation Model	53591		●	●			●		●	●		●							
757	Design of Biospecific Surfaces to Control Specific Cellular Responses	53681					●					●		●	●	●	●			
760	Nanomagnetic Films	54211	●	●			●					●		●	●	●	●			
762	A Multiscale Approach to Modeling Carbon Nanotube–Reinforced Composites	54213		●											●					
483	Near-Real-Time Characterization for Assured HDBT Defeat	55079													●		●			
486	Prompt Global Response	55086										●			●	●	●			
488	Winning the War: A Systems Approach to Defending Our Borders	55087										●		●	●	●	●			
765	Integrated Superhard and Metallic Coatings for MEMS	57300	●	●	●	●				●	●	●	●	●	●	●	●		●	**Industry
769	Microscale Separations of Biological Compounds Using Novel Polymeric Separations Materials	57307									●					●				
772	Friction in Micromachine Interfaces	57308													●					
774	Lipid Microarray Biosensor for Biotoxin Detection	57309														●		●		*NIH
777	Advanced Manufacturing Techniques Using Rapid Prototyping	57310												●		●	●			
779	Robust Hermetic Packaging Techniques for MEMS Integrated Microsystems	57311										●			●					
532	Active Photonic Nanostructures	58907									●	●			●	●	●			
781	3-D Large-Eddy Simulation of Turbulent Flow Based on One-Dimensional Turbulence Modeling	59034		●				●			●					●			●	**Industry
143	A Method of Evaluating Research Using New Innovation, Risk, and Impact Indicators	59916												●						

Appendix E: Major National Programs

Pg #	Title	Project #	Waste Management	Energy Efficiency	Renewable Energy	ES&H	Environmental Restoration	Fossil Energy	Radioactive-Waste Management	Economic Impact	Energy Research	Intelligence & National Security	Nuclear Energy	Science Education & Technical Information	Defense Programs	Department of Homeland Security (DHS)	Department of Defense (DoD)	Other Federal Agencies*	Other (Industry, Consortia…)**	Other Federal Agencies* Other (Industry, Consortia…)**
784	Photonic Encryption Using All-Optical Logic	61046										●				●				
786	Nanoporous-Carbon Adsorbers for Chemical Microsensors	62269				●	●									●	●			
273	Nonlethal Technologies for the War on Terrorism	62827													●	●	●			
377	Agent-Based Control of Distributed Infrastructure Resources	64811		●	●			●		●						●	●		●	**Distributed Resource Utilization (elec. power, gas, water ...)
789	Direct Single-Ion Machining of Nanopores	65559									●					●				
792	Investigation of the Effects of Intense Pulsed Particle Beams on the Durability of Metal-to-Plastic Interfaces	66170									●		●				●			
794	Advanced Techniques for Multiobjective Discrete Optimization	66450														●	●			
796	Nonradioactive Safety and Performance Issues with Supercritical Water Reactor (SCWR) Safety Technologies	66809		●						●	●		●							
798	Radiation Performance Issues with Advanced Coolants for Next-Generation Reactor	66810		●					●		●		●							
66	Rapid Prototyping to the Nanometer Scale	67004																	●	**Industry
67	Robust Manufacturing of Gel-Based Components for Nuclear Weapons	67005		●											●	●	●			
69	Meso-/Microoptical System Interface Coupling Solutions	67006								●				●	●					
71	Injection Molding of Net-Shape Active Ceramic Components	67007	●												●		●		●	**Defense Programs
73	Macro-/Meso-/Microsystems Integration in LTCC	67008													●	●	●			
91	Studies of Signaling Domains in Model and Biological Membranes Through Advanced Imaging Techniques	67010												●		●				
93	Imaging Self-Organization of Proteins in Membranes by Photocatalytic Nanotagging	67011			●		●				●	●		●			●			
96	Protein Microarrays for Biowarfare-Agent Detection and Characterization	67012										●				●			●	**Industry, Medical Diagnostics, Basic Research
99	Interaction of Proteins with Lipid Films	67013														●				

Appendix E: Major National Programs

Pg #	Title	Project #	Waste Management	Energy Efficiency	Renewable Energy	ES&H	Environmental Restoration	Fossil Energy	Radioactive-Waste Management	Economic Impact	Energy Research	Intelligence & National Security	Nuclear Energy	Science Education & Technical Information	Defense Programs	Department of Homeland Security (DHS)	Department of Defense (DoD)	Other Federal Agencies*	Other (Industry, Consortia…)**	Other Federal Agencies* Other (Industry, Consortia…)**
103	New Technologies for Understanding Membrane-Protein Recognition and Signaling	67014			●		●				●					●		●	●	*NIH, **Biotechnology Industry
145	Massively Parallel, Scalable Atmosphere Model	67015								●		●				●	●	●		*NASA, NCAR
147	High-Performance Processing Architecture	67016													●					
149	Substructured Multibody Molecular Dynamics	67017								●		●		●	●	●	●			
151	Enhancing Simulation Performance on Clusters with Configurable Auxiliary Devices	67018		●	●		●	●			●		●		●	●	●			
154	A Hybrid Level-Set/Particle Method for Modeling Surface Evolution During Feature-Scale Etching and Deposition Processes	67019									●				●	●	●			
157	Penetrator Reliability Investigation and Design Exploration (PRIDE)	67020									●				●	●				
160	Topology Optimization for Improving Sensor Performance	67021		●												●				
213	Characterization and Application of Dielectrics with Controlled Leakage	67022								●		●			●	●	●		●	**Wireless and Radar Industry
216	Nano-G Accelerometers Using Nanophotonic Motion-Detection System	67023															●			
218	Bragg Fiber Development	67024								●		●				●	●			
220	Microwave-to-Millimeter-Wave Electrodynamic Response and RF Applications of Semiconductor Quantum Nanostructures	67025									●	●			●	●	●			
222	Development of GaN 20–100 Watt Ku-Band Power Amplifiers for Micro-SAR	67026										●			●	●				
225	Evanescent-Wave Planar Photonic Biosensor	67027	●			●	●					●				●	●			
227	Passive Electronically Steerable Array (PESA) for Miniature Synthetic-Aperture Radar (Mini-SAR), Precision Guidance, and Intelligence/Surveillance/ Reconnaissance (ISR)	67028										●			●		●			
275	Advancements in Sensing and Perception Using Structured Lighting Techniques and an Innovative Design Tool	67029										●			●	●	●			
278	Biophysics of BW-Warhead Defeat with a Kinetic Interceptor	67030										●			●	●	●	●	●	*Missile Defense Agency, **Industry

Appendix E: Major National Programs

Pg #	Title	Project #	Waste Management	Energy Efficiency	Renewable Energy	ES&H	Environmental Restoration	Fossil Energy	Radioactive-Waste Management	Economic Impact	Energy Research	Intelligence & National Security	Nuclear Energy	Science Education & Technical Information	Defense Programs	Department of Homeland Security (DHS)	Department of Defense (DoD)	Other Federal Agencies*	Other (Industry, Consortia…)**	Other Federal Agencies* Other (Industry, Consortia…)**
281	Dispersal in Urban Canyons, Source Identification, and Collateral Damage/Mitigation Assessment	67031														●				
283	Weaponization of Thermobaric Explosives	67032															●			
286	Development of an Enterprise-Scale Agent-Based Autonomic Logistics Simulation Model	67033													●		●			
289	Mobile-Node Authentication in a Wireless *Ad Hoc* Environment	67034														●	●			
292	Novel Processing, Affordable Motion Compensation, and Mode Multiplexing for Miniaturized Synthetic-Aperture Radar	67035										●			●	●	●	●		*DOE NA-22
295	Coilgun Technology Demonstration Test-Bed	67036									●					●	●			
298	Enhanced Perception for Remote 3-D Mapping of Unknown Indoor and Outdoor Environments	67037					●					●					●			
300	A Modular Micromagnetic Accelerometer in Support of the mTalon Vision	67038						●				●			●		●			
302	MICROFUZE Integration	67039													●		●			
304	Analysis of Technology Impacts on Operations in Complex Environments	67041										●			●	●	●			
306	CBW Cloud Knockdown and Neutralization	67042										●			●	●	●			
308	Assessment of Biokillers in EDS for Biological-Agent Destruction	67043														●	●			
310	Adaptive-Force-Feedback Surface Control	67044													●		●	●		*DARPA
312	High-Capacity Earth-Penetrator Instrumentation	67046													●		●			
314	Systems Analysis of Networked Sensors	67047										●		●	●	●	●			
317	Deployable Object Tracker for NMD Flights	67048								●		●			●	●	●	●	●	*NASA, **Commercial Applications
319	Continuous-Flow Detector for Rapid Pathogen Identification	67049										●				●	●			
380	Biological-Security Decontamination Technology—Reducing the Threat of Infectious-Agent Spread	67050														●	●	●		*USDA
383	Consequence Management, Recovery, and Restoration after an Intentional Contamination Event	67051					●		●			●		●		●				

Appendix E: Major National Programs

Pg #	Title	Project #	Waste Management	Energy Efficiency	Renewable Energy	ES&H	Environmental Restoration	Fossil Energy	Radioactive-Waste Management	Economic Impact	Energy Research	Intelligence & National Security	Nuclear Energy	Science Education & Technical Information	Defense Programs	Department of Homeland Security (DHS)	Department of Defense (DoD)	Other Federal Agencies*	Other (Industry, Consortia…)**	Other Federal Agencies* Other (Industry, Consortia…)**
386	Fully Integrated System-Dynamics Toolbox for Water Resources Planning	67052								●								●	●	*DOI, **Industry, local government
390	Predicting System Performance of Proton-Exchange-Membrane Fuel Cells: Computational Modeling with Experimental Discovery and Validation	67053			●						●						●			
393	Optimal Allocation of Terrorist Countermeasures Using Risk-Based Systems Pathways Analysis	67054			●					●	●	●	●		●	●	●	●	●	*FBI, CIA, State & Local Police, & Fire Agencies, **Utility
396	Silicon Field-Emission Electric Propulsion Arrays (FEEP) Powered by Orbital Nuclear Reactors	67055											●					●	●	*NASA, DoD, **Industry
398	Advanced Fuel-Cell Reactor for the Direct Cogeneration of Electricity During Selective Partial Oxidation of Hydrocarbons	67056		●	●						●									
401	New Hydrogen-Storage Material: Metal-N-H System	67057		●	●			●			●									
403	Intrusion Detection for Wireless Networks	67058										●				●				
405	Membranes for H2 Generation from Nuclear-Powered Thermochemical Cycles	67059		●				●			●		●						●	**INERI (International Nuclear Energy Research)
408	Microfabricated BTU Monitoring Device for System-Wide Natural-Gas Monitoring	67060									●							●	●	*DOT, **Oil and Gas Industry
411	"Tunable" Ion Conductors for Low-Temperature Oxide-Based Fuel Cells	67061		●	●			●			●									
414	Nuclear Nanobatteries: On-Board Power for Independent MEMS Devices	67062							●			●	●		●	●	●			
417	Integrated Tunable Light Sources for Miniature Sensors	67063		●				●			●					●	●			
452	Ray Model of High-Frequency Cavity Scarring	67064													●	●	●	●	●	**Airframe and Electronics
455	New Smart Material to Address Issues of Structural Health Monitoring	67065								●		●	●	●	●	●	●			
458	Noncontact Surface Thermometry for Microsystems	67067													●					
461	High-Speed Interferometric Deformation Measurements	67068												●	●					
463	Fundamentals of Nanofluidics	67069									●				●	●				

Appendix E: Major National Programs

Pg #	Title	Project #	Waste Management	Energy Efficiency	Renewable Energy	ES&H	Environmental Restoration	Fossil Energy	Radioactive-Waste Management	Economic Impact	Energy Research	Intelligence & National Security	Nuclear Energy	Science Education & Technical Information	Defense Programs	Department of Homeland Security (DHS)	Department of Defense (DoD)	Other Federal Agencies*	Other (Industry, Consortia…)**	Other Federal Agencies* Other (Industry, Consortia…)**
465	Simulating Self-Assembly and Growth of Biological Nanostructured Materials	67070									●				●	●	●			
468	A Low-Power, Ultrafast-Current Transient Measuring Device	67071													●					
470	A Capillary Valve for Microfluidic Systems	67073														●				
534	Electrochemically Switchable Materials for (Bio)Microfluidics	67074														●	●			
537	Modeling of Friction-Induced Deformation and Microstructure	67075								●					●		●			
540	Reversible Antibody Trapping for Selective Sensor Devices	67076									●					●				
542	Correlated and Comprehensive Analytical Techniques for Homeland Defense	67077										●			●	●				
545	Development of High-Energy-Density Dielectric Materials for Integrated Microsystems	67078									●	●		●	●	●	●			
549	Nanolithography-Directed Materials Growth and Self-Assembly	67079									●				●					
552	Development of a Novel Technique to Assess the Vulnerability of Micromechanical System Components to Environmentally Assisted Cracking	67080								●					●	●				
554	3-D Optical Sectioning with a New Hyperspectral Deconvolution Fluorescence Imaging System	67081		●								●			●	●				
558	The Science of Solutes: Transition Metals in LIGA Nickel	67082													●					
560	Novel Gel-Based Technology for Sensors and Weapons	67083					●							●		●	●		●	**Industry
562	Coupled Nanomechanical Oscillator Arrays for the Study of Internal Dissipation in Nanoscale Structures and Collective Behavior in Large Systems	67084										●			●	●	●			
565	Precisely Controlled Picoliter Vessels with Rapid Sample Preparation for Trace Biotoxin Detection	67085										●			●	●	●			
618	Adaptive Optics and Phase-Diversity Imaging for Responsive Space Applications	67086										●				●	●			
621	Infrastructural Development for Flexible Network of Devices	67087										●			●	●				
622	Monolithic Reconfigurable Radio-Frequency Microelectromechanical Systems (RF MEMS) Antennas	67088	●						●			●			●	●	●		●	**Industry
625	Next-Generation 3-D Inspection System for Facility Monitoring	67089				●						●			●	●	●	●	●	*FBI, CIA, ..., **Industry

Appendix E: Major National Programs

Pg #	Title	Project #	Waste Management	Energy Efficiency	Renewable Energy	ES&H	Environmental Restoration	Fossil Energy	Radioactive-Waste Management	Economic Impact	Energy Research	Intelligence & National Security	Nuclear Energy	Science Education & Technical Information	Defense Programs	Department of Homeland Security (DHS)	Department of Defense (DoD)	Other Federal Agencies*	Other (Industry, Consortia…)**	Other Federal Agencies* Other (Industry, Consortia…)**
627	Risk-Assessment Metatool	67090										●			●	●	●			
629	Featureless Spread-Spectrum Waveform Design and Processing	67091										●				●	●			
631	Tracking Slow-Moving Objects in a GPS–Denied Environment	67092										●			●	●				
632	Optical Communications	67093										●								
633	A Unique Vibration-Based Miniature Power Generator for National Security Applications	67094										●			●					
636	Image Georectification Using Digital Elevation Model Shadows	67095										●				●	●			
639	Vulnerability Assessment of State-of-the-Art Microelectronics	67096										●			●		●			
640	Nonlinear Optical Detection of Biological and Chemical Aerosol Agents Using Femtosecond Lasers	67098										●			●		●			
643	Polymer Electronic Devices and Materials	67099										●			●	●	●		●	**OLED industry, FPD and Flexible Display Industry
647	Small Circuits for Cryptography	67101										●		●	●	●	●			
649	Analysis of Multichannel Internet Communication	67102										●				●				
650	Receiver for Ultralow-Power Wake-Up and Command	67104										●			●		●			
652	Extraordinary Optical Transmission Through Patterned Subwavelength Apertures	67105										●								
654	Reconstruction Algorithm Development and Assessment for a Computed Tomography Based-spectral Imager	67107										●			●					
657	Power Combining Techniques for Solid-State Power Amplifiers	67108										●			●		●			
659	Dispersive Diffractive Optical Elements for the Infrared	67109										●		●	●	●	●			
661	Atmospheric Propagation of Terahertz Radiation	67111										●			●	●	●			
663	High-Confidence Estimation of Relative Event Locations from Space-Based Sensors	67113										●				●	●			
665	Critical-Infrastructure System-of-Systems Assessment Methodology	67114										●				●	●	●	●	*EPA, **Industry

Appendix E: Major National Programs

Pg #	Title	Project #	Waste Management	Energy Efficiency	Renewable Energy	ES&H	Environmental Restoration	Fossil Energy	Radioactive-Waste Management	Economic Impact	Energy Research	Intelligence & National Security	Nuclear Energy	Science Education & Technical Information	Defense Programs	Department of Homeland Security (DHS)	Department of Defense (DoD)	Other Federal Agencies*	Other (Industry, Consortia…)**	Other Federal Agencies* Other (Industry, Consortia…)**
667	Dynamic Vulnerability Assessment	67115															●		●	**DOE Sites
669	Inflatable Antenna with Adaptive Actuators	67116										●				●				
671	Data-Driven Dynamic Models of Conflict	67117		●				●		●	●	●	●			●	●			
800	MEMS/Fuze Diagnostic Extraction in High-G Environments	67118													●		●			
694	Efficient Implicit Multigroup Radiation Calculations	67120									●				●					
696	Model for Channel Resistance in Water Breakdown	67121									●				●		●		●	**Irradiation Systems
698	Embeddable Shock Physics Sensors	67122												●	●		●			
802	Smart Detectors of Enrichment of Bioaerosols	67716									●	●				●	●			
805	Computational Studies of JP-8 Diffusion Flames with Detailed Chemistry and Particulate Formation	68063		●				●			●				●		●			
419	Design and Fabrication of Advanced Device Structures for Ultrahigh-Efficiency Solid-State Lighting	69143		●						●	●		●	●	●	●	●			
808	Molecular Simulation of Beta-Amyloid (A-beta) Peptide Interaction with Phospholipid Membranes	69145																●		*NIH
809	Nanoscale Testing of Deformation and Fracture in Engineering Materials	69146															●			
812	Nanocrystal-Polymer Composites for High-Luminous-Efficiency LEDs	69148		●															●	**Industry
817	Outstanding Challenges for AlGaInN MOCVD	69149		●							●			●	●		●			
820	Nanoporous Polymeric Materials for Chemically and Spatially Multiplexed Sensing of Bioagents	69150													●	●			●	**Industry
823	Evolutionary Complexity for Protection of Critical Assets	69151										●								
825	Nanomechanical Stochastic Resonators	69152		●			●					●		●	●	●	●			
826	Augmented Musculature Device	69153										●		●	●	●	●			
828	Biomolecular Decision-Making Processes for Self-Assembly	69154										●			●		●			
830	Light-Powered Nanovehicle Propulsion	69155			●						●									

Appendix E: Major National Programs

Pg #	Title	Project #	Waste Management	Energy Efficiency	Renewable Energy	ES&H	Environmental Restoration	Fossil Energy	Radioactive-Waste Management	Economic Impact	Energy Research	Intelligence & National Security	Nuclear Energy	Science Education & Technical Information	Defense Programs	Department of Homeland Security (DHS)	Department of Defense (DoD)	Other Federal Agencies*	Other (Industry, Consortia…)**	Other Federal Agencies* Other (Industry, Consortia…)**
832	System-Dynamics Modeling to Assist Regional Water Planning: Modeling the Nonmarket Value of Water	69156										●		●				●		*U.S. Corps of Engineers, U.S. Bureau of Reclamation
834	Interactive Water-Quality Modeling to Assist Regional Water Planning	69157												●				●		*U.S. Corps of Engineers, U.S. Bureau of Reclamation
837	Microbe-Exuded Polymers and the Enhanced Corrosion of Carbonate Materials	69158	●				●				●			●						
840	Nerve-Cell Function and the Development of Cognitive Networks	69159														●		●		*NIH
843	Ultrahigh-Gain Fusion Concept	69160										●			●		●			
844	Nanofluidic Devices for Rapid Detection of Virus Particles	69161														●				
846	Solution Behavior of PEO: The Ultimate Biocompatible Polymer	69162														●				
848	New Self-Assembled Nanocrystal Micelles for Biolabels	69163				●										●				
851	Rapid Detection of Biothreat Agents Based on Cellular Machinery	69164										●			●	●				
853	Patterning Quantum-Dot Arrays Using DNA Replication Principles	69165										●			●	●				
856	Adaptive Algorithms for Use in the Rejection of Periodic Disturbances of Unknown Frequency	69166													●		●			
858	Property-Based Testing for Cybersecurity Assurance	69168										●		●	●	●	●			
860	Self-Assembled Ordered Carbon-Nanotube Arrays and Membranes	69170								●						●	●			
863	Chemical Cross-Linking and Mass-Spectrometry Studies of the Structure and Dynamics of Membrane Proteins and Receptors	69189														●		●	●	*NIH, **Industry–Biotechnology
866	Toxin Studies Using an Integrated Biophysical and Structural Biology Approach	69190														●			●	**Industry–Biotechnology
869	Top-Down Structural Studies	69191														●		●	●	**Industry–Biotechnology
871	Molecular Dynamics of Membrane Proteins	69192														●		●	●	**Industry–Biotechnology

Appendix E: Major National Programs

Pg #	Title	Project #	Waste Management	Energy Efficiency	Renewable Energy	ES&H	Environmental Restoration	Fossil Energy	Radioactive-Waste Management	Economic Impact	Energy Research	Intelligence & National Security	Nuclear Energy	Science Education & Technical Information	Defense Programs	Department of Homeland Security (DHS)	Department of Defense (DoD)	Other Federal Agencies*	Other (Industry, Consortia…)**	Other Federal Agencies* Other (Industry, Consortia…)**
874	Model-Building Codes for Membrane Proteins	69193														●		●		*NIH
878	Poroelastic-Wave Propagation on the Earth Simulator	69198	●				●	●			●				●					
882	Development of Microreformers for Fuel Cells	69239		●	●						●					●	●			
568	Developing the Foundation for Polyoxoniobate Chemistry: Highly Tunable and Exploitable Materials	70799		●					●					●		●				
321	Simulating Human Behavior for National Security	71943										●			●	●	●	●		*Law Enforcement
28	Agent-Based Modeling of Middle East Terrorist Recruitment	71944										●				●	●			
30	Automatic Generation of Terrorist Operation Plan Hypotheses	71945										●								
421	Develop a System-Dynamics Modeling Framework for Assessing Factors that Influence Water Resource Consumption	72599					●			●	●	●							●	**Water Sustainability
423	Develop a Cooperative Water-Management Process, Creating a System-Dynamics Model of Water Resources in the Lower Rio Grande Basin	72600	●				●	●		●									●	**Water Sustainability
323	Compact Ultrabright Multikilovolt X-Ray Sources for Advanced Material Studies, 3-D Nanoimaging, and Attosecond X-Ray Technology	72715													●	●				
425	Energy-Systems Analysis Framework and Modeling	72716		●	●			●		●	●					●	●			
33	Radiation-/Geometry-Driven Jets: Proof-of-Principle Tests	73045															●			
884	Superhydrophobic Surface Coatings for Microfluidics and MEMS	73185		●												●		●		*NIH, DARPA
673	Microoptical Radar (MOR) Facial-Recognition Project	73207										●			●	●	●			
886	Determining Explosive Ignition Criteria for Miniaturized Devices	74545													●		●			
888	Quantum Squeezed Light for Probing Mitochondrial Membranes and Study of Neuroprotectants	74546														●		●		*NIH
890	Characterization of a New Class of Surface-Micromachined Pumps	74547	●		●	●	●					●		●	●	●	●			
893	Risk of Biological Terrorism to Water-Distribution Systems	74548																●	●	*EPA, DHS, **Water Infrastructure

Appendix E: Major National Programs

Pg #	Title	Project #	Waste Management	Energy Efficiency	Renewable Energy	ES&H	Environmental Restoration	Fossil Energy	Radioactive-Waste Management	Economic Impact	Energy Research	Intelligence & National Security	Nuclear Energy	Science Education & Technical Information	Defense Programs	Department of Homeland Security (DHS)	Department of Defense (DoD)	Other Federal Agencies*	Other (Industry, Consortia…)**	Other Federal Agencies* Other (Industry, Consortia…)**
895	Explicit and Implicit Measures in Human Aversive Classical Conditioning	74759										●		●		●	●			
676	Automatic-Target-Recognition Algorithms for Uncooled Thermal Imagery	74760										●				●	●			
326	Magnetophoretic Bead Trapping in a High-Flowrate Biological Detection System	74795	●			●	●		●	●		●			●	●	●	●		*USDA, FEMA, DoJ
329	TPV Energy Scavenging for Hypervelocity Vehicles	75441		●								●			●					
898	Assessment of Advanced Pulsed-Power Fusion Concepts	75442									●		●		●					
427	A Mathematical Method for Quantifying the Effectiveness of Management Strategies	75443	●	●	●	●				●		●		●	●	●	●			
901	Developing Algorithms for Predicting Protein-Protein Interactions from Experimental Constraints	75513														●	●		●	**Pharmaceutics
904	Instrumentation Development for Real-Time Brain-Wave Monitoring	75514															●			
907	Miniaturized Electronic Steerable-Array Synthetic-Aperture Radar	76069										●			●	●	●			
910	Full-Earth-Monitoring Sensor MESAWorks	76070										●				●	●		●	**Electronics Industry
36	Systems Assessment of Water-Savings Impact of Controlled-Environment Agriculture Utilizing Wirelessly Networked SDACs	76305								●		●		●		●		●		*Agriculture
429	Inactivation of Avian Influenza (Bird Flu) with Sandia-Developed Decontamination Formulations	76306	●			●	●									●	●			
913	Deciphering the Genetic Regulatory Code Using an Inverse Error Control Coding Framework	78132					●							●	●	●			●	**Genomes-to-Life Program
38	Climate-Change Effects on International Stability	78307										●				●	●			
916	Generalized Continuum Models for Inelasticity in Solids: Formulation of Theories and Variational Methods for Computation	78783												●	●	●	●			
431	GeSi–Strained Nanostructure Self-Assembly for Nano- and Optoelectronics	79943									●				●					
678	Vulnerability Analysis for SCADA	80835										●				●	●		●	**SCADA Industry
918	Molten Salt-Based Growth of Bulk GaN and InN	80838		●	●						●	●			●	●	●			
679	Randomness Complexity and Cryptography	81209										●		●	●	●	●			

Appendix E: Major National Programs

Pg #	Title	Project #	Waste Management	Energy Efficiency	Renewable Energy	ES&H	Environmental Restoration	Fossil Energy	Radioactive-Waste Management	Economic Impact	Energy Research	Intelligence & National Security	Nuclear Energy	Science Education & Technical Information	Defense Programs	Department of Homeland Security (DHS)	Department of Defense (DoD)	Other Federal Agencies*	Other (Industry, Consortia…)**	Other Federal Agencies* Other (Industry, Consortia…)**
681	System Study: Adaptive Optics for Weapon, Reconnaissance and Military Space Applications	81354										●			●	●	●	●		*NASA
			25	**45**	**26**	**18**	**33**	**28**	**11**	**32**	**85**	**144**	**19**	**55**	**197**	**204**	**204**	**43**	**60**	

Appendix F: Dual-Benefit Areas and Single-Use Categories

Pg #	Title	Project #	Aeronautics	Applied Molecular Biology	Ceramics	Composites	Computer Simulation and Modeling	Data Storage and Peripherals	Electronics and Photonics	Energy	Flexible Computer-Integrated Manufacturing	High-Definition Imaging and Displays	High-Performance Computing and Networking	High-Performance Metals and Alloys	Intelligent Processing Equipment	Materials Synthesis and Processing	Medical Technology	Micro- and Nanofabrication	Micro- and Optoelectronics	Photonic Materials	Pollution Minimization, Remediation, and Waste Mgmt.	Sensors and Signal Processing	Software	Surface Transportation Technologies	Systems Management Technologies	Defense-Related (mostly or purely)	Dual-Use (defense and non-defense-related)	Non-Defense-Related (mostly or purely)
41	Microfabrication with Femtosecond Laser Processing	38605							●		●			●		●		●	●	●							●	
44	Mesoscale Controlled Motion for a Microfluidic Drop Ejector	38606							●						●	●		●									●	
77	Physical and Electronic Changes Caused by Membrane Signaling as a Transduction Pathway in Affinity-Based Biosensors	38609		●			●		●								●	●	●			●					●	
116	Graduated Embodiment for Sophisticated-Agent Evolution and Optimization	38610					●						●														●	
119	Scalable Fault-Tolerant Algorithms for Linear-Scaling Coupled-Cluster Electronic Structure Methods	38613					●						●										●				●	
121	Micromagnetic Suspension	38614					●																				●	
123	Sensitivities for Large-Scale Simulation Codes	38615	●				●						●										●				●	
168	Engineered Superconductivity in Electron-Hole Bilayers	38616							●	●								●	●			●					●	
171	Silicon-Based RF MEMS Components	38617							●								●	●	●			●					●	
173	Nanoelectromechanical Oscillators (NEMOs) for RF Filtering	38619							●									●				●					●	
176	Continuous-Wave Intersubband Terahertz Sources	38620							●										●			●					●	
178	Microsystems for Chemical Signature and Reagent Delivery	38621							●								●					●					●	
180	Microfluidic Cellular-Sample Pretreatment	38622		●			●		●							●	●	●	●		●	●					●	
231	Automated Visual Direction of Mobile Manipulation	38623																				●	●				●	
233	Miniature Fourier-Transform Ion-Mobility Spectrometer for Real-Time Detection and Identification of Explosives and Chemical Agents	38624							●										●		●	●				●		
235	EM Interactions with Systems to Enhance Security	38627							●																		●	

Appendix F: Dual-Benefit Areas and Single-Use Categories

Pg #	Title	Project #	Aeronautics	Applied Molecular Biology	Ceramics	Composites	Computer Simulation and Modeling	Data Storage and Peripherals	Electronics and Photonics	Energy	Flexible Computer-Integrated Manufacturing	High-Definition Imaging and Displays	High-Performance Computing and Networking	High-Performance Metals and Alloys	Intelligent Processing Equipment	Materials Synthesis and Processing	Medical Technology	Micro- and Nanofabrication	Micro- and Optoelectronics	Photonic Materials	Pollution Minimization, Remediation, and Waste Mgmt.	Sensors and Signal Processing	Software	Surface Transportation Technologies	Systems Management Technologies	Defense-Related (mostly or purely)	Dual-Use (defense and non-defense-related)	Non-Defense-Related (mostly or purely)
236	Use of Seismic and Acoustic Responses to Assess Bomb Damage to Underground Facilities	38629																				●	●			●		
238	Free-Space Electrooptic Sampling and Remote Mapping of Electro- magnetic Fields from Emitting Structures Using Femtosecond Terahertz Transceivers	38655							●										●	●		●					●	
332	Natural-Gas Production Problems: Solutions, Methodologies, and Modeling	38662					●			●																		●
335	Time-Domain Reflectometry for Remote, Real-Time Water-Quantity/-Quality Monitoring of Perennial and Ephemeral Streams	38665																				●						●
338	Functionalized Nanoelectrode Arrays for In-situ Identification and Quanitification of Regulated Chemicals in Water	38668							●								●	●			●	●						●
341	Water Desalination	38673								●						●					●						●	
344	Revolutionary Systems for Catalytic Combustion and Diesel Catalytic Particulate Traps	38674			●					●	●					●	●							●				●
348	Potential Application of Microsensor Technology in Radioactive-Waste Management—With Emphasis on Headspace Gas Detection	38677																			●	●						●
241	Identification of Chemical Plumes: Range-Resolved IR Lidar Enabled by New Photonic Technologies	38681							●	●								●	●	●	●	●					●	
434	A Robust, Coupled Approach for Atomistic-Continuum Simulation	38684					●																●				●	
438	Microscale Rarefied-Gas Dynamics and Surface Interactions for EUVL and MEMS Applications	38685					●											●									●	
441	High-Fidelity Frictional Models for MEMs	38686					●																				●	

Appendix F: Dual-Benefit Areas and Single-Use Categories

Pg #	Title	Project #	Aeronautics	Applied Molecular Biology	Ceramics	Composites	Computer Simulation and Modeling	Data Storage and Peripherals	Electronics and Photonics	Energy	Flexible Computer-Integrated Manufacturing	High-Definition Imaging and Displays	High-Performance Computing and Networking	High-Performance Metals and Alloys	Intelligent Processing Equipment	Materials Synthesis and Processing	Medical Technology	Micro- and Nanofabrication	Micro- and Optoelectronics	Photonic Materials	Pollution Minimization, Remediation, and Waste Mgmt.	Sensors and Signal Processing	Software	Surface Transportation Technologies	Systems Management Technologies	Defense-Related (mostly or purely)	Dual-Use (defense and non-defense-related)	Non-Defense-Related (mostly or purely)
444	Soot Formation, Transport, and Radiation in Unsteady Diffusion Flames	38687	●				●			●																●	
493	The Basics of Aqueous Nanofluidics: "Interphase" Structure and Surface Forces	38688		●			●									●	●	●	●			●				●	
497	Design, Synthesis, and Characterization of Soft-Matter Nanolayer Superlattices	38689							●									●	●	●						●	
499	Photocontrol of Nanointeractions in Microsystems	38690							●							●				●		●				●	
501	Electrochemically Deposited Alloys with Tailored Nanostructures for LIGA Micromachines	38691												●		●										●	
503	Nanostructured Materials for Directed Transport of Excitation Energy	38692							●									●		●							●
505	Modeling Local Chemistry in the Presence of Collective Phenomena	38693			●		●														●					●	
701	Nanoscale Energetic Materials by Inverse Micellar Synthesis	38717	●		●	●								●		●		●								●	
704	Modeling of Rock Penetration	38718					●																			●	
572	Agile, Microsystems-Enabled Receiver	38722							●									●	●			●					●	
507	Solution-Based Nanoengineering of Materials	39017			●		●									●		●	●	●		●						●
684	Simulations of Intense Petawatt Laser Pulses with Dense Z-Pinch Plasmas	39670					●			●																	●	
473	Biomicrofuel Cell (BMFC)	41193							●	●						●	●	●	●			●					●	
476	Augmented Cognition: Next-Generation Intelligent Systems	41194	●				●								●		●					●	●	●	●		●	
164	Microengine for Advanced Power Generation	41674								●								●									●	
707	Direct Simulation of Solid-Fluid Systems	41726					●			●			●										●					●
710	Support–Active Site Interactions in Heterogeneous Catalysts	42461								●																		●

Appendix F: Dual-Benefit Areas and Single-Use Categories

Pg #	Title	Project #	Aeronautics	Applied Molecular Biology	Ceramics	Composites	Computer Simulation and Modeling	Data Storage and Peripherals	Electronics and Photonics	Energy	Flexible Computer-Integrated Manufacturing	High-Definition Imaging and Displays	High-Performance Computing and Networking	High-Performance Metals and Alloys	Intelligent Processing Equipment	Materials Synthesis and Processing	Medical Technology	Micro- and Nanofabrication	Micro- and Optoelectronics	Photonic Materials	Pollution Minimization, Remediation, and Waste Mgmt.	Sensors and Signal Processing	Software	Surface Transportation Technologies	Systems Management Technologies	Defense-Related (mostly or purely)	Dual-Use (defense and non-defense-related)	Non-Defense-Related (mostly or purely)
712	An Analysis of the Automotive Industry a a Source for Weapon Components and Manufacturing Processes	42483				●	●		●	●	●		●	●	●							●		●	●		●	
713	High-Speed Micro-EDM	46070															●	●									●	
715	Microexternal-Combustion Engine: The P3 Engine Prototype	46686							●	●								●									●	
717	Lipid Membranes on Nanostructured Silicon	47795		●														●				●					●	
720	Resin Infusion Between Double Flexible Tooling	49769				●										●											●	
723	Studies on the Disbonding Initiation of Interfacial Cracks	49772	●			●			●	●	●							●	●	●	●	●		●			●	
243	Critical Technology Development for Hard-Target-Defeat High-G-Tolerant Fuze and High Explosives	49915							●													●				●		
480	TALON	50065													●							●			●		●	
725	Compliant Membranes for MEMS Microphones	50396																●				●					●	
727	Multiscale Experimental/Numerical Study	50717					●																				●	
80	Cellular Observatory: Simultaneous Time- and Frequency-Resolved Microscopy	50772		●						●																		●
46	Atomic Layer Deposition of Highly Conformal Tribological Coatings	52523							●							●		●									●	
50	Assembly of Microsystems Using Exothermic Multilayer Thin Films	52524							●	●				●		●		●	●								●	
52	Intelligent Interaction Control as Applied to Metrology and Assembly of Microscale Components	52526					●				●				●			●				●	●				●	
55	Rapid-Prototyping High-Density Circuitry (RpHdc)	52527							●		●				●	●											●	
57	Elucidating the Mysteries of Wetting	52528		●	●	●	●		●	●			●	●	●	●		●	●	●	●	●		●			●	

Appendix F: Dual-Benefit Areas and Single-Use Categories

Pg #	Title	Project #	Aeronautics	Applied Molecular Biology	Ceramics	Composites	Computer Simulation and Modeling	Data Storage and Peripherals	Electronics and Photonics	Energy	Flexible Computer-Integrated Manufacturing	High-Definition Imaging and Displays	High-Performance Computing and Networking	High-Performance Metals and Alloys	Intelligent Processing Equipment	Materials Synthesis and Processing	Medical Technology	Micro- and Nanofabrication	Micro- and Optoelectronics	Photonic Materials	Pollution Minimization, Remediation, and Waste Mgmt.	Sensors and Signal Processing	Software	Surface Transportation Technologies	Systems Management Technologies	Defense-Related (mostly or purely)	Dual-Use (defense and non-defense-related)	Non-Defense-Related (mostly or purely)
60	Next-Generation Spindles for Micromilling	52530									●				●			●									●	
510	Assembly and Actuation of Nanomaterials Using Active Biomolecules	52531		●		●			●									●		●							●	
82	Modeling Biomembranes	52532		●			●										●					●						●
84	Reverse-Engineering Biological Networks: Applications in Immune Responses to Bioterrorism Threats	52533		●			●						●				●											●
88	High-Throughput Identification of Molecular Machines Involved in Membrane Signaling and Toxin Pathways	52536		●																							●	
447	Coupled Solid-Fluid-Mechanical-Computational Modeling of Fracture and Fragmentation in Geomaterials, such as Hard and Deeply Buried Targets (HDBTs)	52537					●																				●	
107	Sequestration of Pathogens on Nanoengineered Surfaces	52538		●			●									●						●						●
111	A Combined Preconcentrator and Sensor for Live Waterborne Pathogens	52539		●													●	●			●	●					●	
126	IP Storage: A Performance and Security Study	52540					●	●					●														●	
129	A Parallel Circuit Simulator for Cell Biology	52541		●																								●
131	Developing a Computationally Efficient Dynamic Multilevel Hybrid Optimization Scheme Using Multifidelity Model Interactions	52542					●						●										●				●	
134	Robust Large-Scale Parallel Nonlinear Solvers for Simulations	52543					●																●				●	
137	Development of Computational Algorithms and Inversion Capabilities for Transport/Reaction Simulations of Chemical/Biological/Radiological Terrorist Attack Scenarios in Support of Homeland Security	52544					●																●					●

Appendix F: Dual-Benefit Areas and Single-Use Categories

Pg #	Title	Project #	Aeronautics	Applied Molecular Biology	Ceramics	Composites	Computer Simulation and Modeling	Data Storage and Peripherals	Electronics and Photonics	Energy	Flexible Computer-Integrated Manufacturing	High-Definition Imaging and Displays	High-Performance Computing and Networking	High-Performance Metals and Alloys	Intelligent Processing Equipment	Materials Synthesis and Processing	Medical Technology	Micro- and Nanofabrication	Micro- and Optoelectronics	Photonic Materials	Pollution Minimization, Remediation, and Waste Mgmt.	Sensors and Signal Processing	Software	Surface Transportation Technologies	Systems Management Technologies	Defense-Related (mostly or purely)	Dual-Use (defense and non-defense-related)	Non-Defense-Related (mostly or purely)
140	Massively Parallel Linear Programming	52546					●																			●	
183	Active Photonic-Crystal Devices for Integrated Photonics and Silicon Photonic	52548							●									●	●							●	
185	Co-Processing of Chalcogenide-Based Radiation-Hard Nonvolatile Memories by Sandia's MDL and BAE Systems	52549							●		●								●			●				●	
187	Functionalized Nanoparticles for Sensor Applications	52551																●	●			●				●	
190	Novel *In Situ* Mechanical Testers to Enable Integrated Metal Surface Micromachines	52552							●					●		●		●	●			●				●	
193	Compliant Thermomechanical MEMS Actuators	52553	●				●		●	●	●		●			●	●	●				●	●				●	
196	An Integrated, Stacked System-on-a-Chip	52554	●					●	●			●	●				●		●			●					●	
199	Micromass Spectrometer-on-a-Chip	52555							●									●				●					●	
201	Quantum Coherence in Semiconductor Nanostructures for Improved Lasers and Detectors	52556							●							●			●	●							●	
203	MOSFET–MEMS Integration	52557		●					●						●		●	●	●			●					●	
205	Microoptical Gyroscope Via Monolithic Active/Passive Optical Integration	52566	●						●										●			●					●	
207	Materials Physics and Device Development for Improved Efficiency of GaN HEMT High-Power Amplifiers	52570							●			●							●	●							●	
209	Leaky-Mode VCSELs for Photonic Logic Circuits	52571							●									●	●	●		●					●	
211	Advanced Polychromator Systems for Remote Chemical Sensing	52575							●									●	●	●	●	●			●		●	
245	Immunological Basis for High-Reliability Systems Control	52577						●							●		●					●	●		●		●	
247	Moving-Target Identification Using Ultrahigh-Range-Resolution Data	52580																				●				●		

Appendix F: Dual-Benefit Areas and Single-Use Categories

Pg #	Title	Project #	Aeronautics	Applied Molecular Biology	Ceramics	Composites	Computer Simulation and Modeling	Data Storage and Peripherals	Electronics and Photonics	Energy	Flexible Computer-Integrated Manufacturing	High-Definition Imaging and Displays	High-Performance Computing and Networking	High-Performance Metals and Alloys	Intelligent Processing Equipment	Materials Synthesis and Processing	Medical Technology	Micro- and Nanofabrication	Micro- and Optoelectronics	Photonic Materials	Pollution Minimization, Remediation, and Waste Mgmt.	Sensors and Signal Processing	Software	Surface Transportation Technologies	Systems Management Technologies	Defense-Related (mostly or purely)	Dual-Use (defense and non-defense-related)	Non-Defense-Related (mostly or purely)
249	Advanced Mobile Networking, Sensing, and Controls Using Graph Theory	52581													●							●					●	
252	Compact Terahertz Sources for Emerging-Threats Applications	52582							●									●	●	●		●					●	
255	Understanding Communication in Counterterrorism Crisis Management	52583					●																●				●	
258	Hypervelocity Impact-Generated Flash	52584					●															●				●		
260	Improving Human/System Interactions in Systems-of-Systems	52585	●				●						●		●												●	
262	Distributed Detection and ID Algorithm Architecture for Unattended Ground Sensors	52586											●									●				●		
264	Secure Chaotic Communications	52587							●													●					●	
266	System-of-Systems Modeling and Analysis	52588					●																●				●	
268	Eye-Safe Short-Range Standoff Aerosol-Cloud Finder	52589							●										●			●				●		
270	Microflame-Based Detector Suite for Universal Gas Sensing	52590			●				●						●		●	●			●	●					●	
351	Beyond Nanoparticles—Attack on a Chemical "Holy Grail"	52591								●											●							●
354	Advanced Proton-Exchange Materials for Energy-Efficient Fuel Cells	52592				●				●						●		●			●	●					●	
357	Alanate-Hydride Fuel-Cell Demonstration Project	52593								●																		●
360	Real-Time Discriminatory Sensors for Water-Contamination Events	52595																●			●	●					●	
362	Advanced High-Efficiency Direct-Cycle Gas Power-Conversion Systems for Small Special-Purpose Nuclear Power Reactors	52596	●				●			●													●				●	
365	Securing Mobile Code	52597																					●				●	
368	Novel Catalysts for Hydrogen Fuel-Cell Applications	52598								●																	●	

Appendix F: Dual-Benefit Areas and Single-Use Categories

Pg #	Title	Project #	Aeronautics	Applied Molecular Biology	Ceramics	Composites	Computer Simulation and Modeling	Data Storage and Peripherals	Electronics and Photonics	Energy	Flexible Computer-Integrated Manufacturing	High-Definition Imaging and Displays	High-Performance Computing and Networking	High-Performance Metals and Alloys	Intelligent Processing Equipment	Materials Synthesis and Processing	Medical Technology	Micro- and Nanofabrication	Micro- and Optoelectronics	Photonic Materials	Pollution Minimization, Remediation, and Waste Mgmt.	Sensors and Signal Processing	Software	Surface Transportation Technologies	Systems Management Technologies	Defense-Related (mostly or purely)	Dual-Use (defense and non-defense-related)	Non-Defense-Related (mostly or purely)
372	Linking Optimization and Simulation in Critical-Infrastructure Systems	52606					●						●														●	
514	Decomposition of Contaminants Using Photochemically Active Nanoparticles	52698			●											●											●	
516	Thermally Cleavable Surfactants	52699			●				●							●		●		●		●					●	
518	Transition-Metal Catalyzation of Complex Hydride Absorption/Desorption Reactions	52700								●						●					●			●				●
520	Quantification of Environments and Surfaces Within Micropackages	52701							●							●		●	●								●	
523	Assembly of Ordered Electrooptical and Bioactive Materials and Composites	52702				●										●		●										●
525	Advanced Packaging/Joining Technology for Microsystems	52703							●							●		●	●								●	
528	Magnetostrictive Elastomers for Actuators and Sensors	52705				●	●									●											●	
576	Development of a High-Throughput Microfluidic Integrated Microarray for the Detection of Chimeric Bioweapons	52706		●													●	●	●			●					●	
578	Zero-Power Radio Receiver	52708	●						●									●	●			●					●	
581	Completely Passive Microwave Tag	52709	●						●									●	●			●					●	
584	Security Coatings for Multichip Modules	52710	●		●				●						●	●										●		
586	Detailed Modeling and Simulation of Contaminant Transport in Architectural Spaces	52711					●														●	●					●	
588	Content-Based Video and Image Indexing System	52712																				●	●					●
591	Bioaerosol Collection and Concentration for Microseparations-Based Detectors	52713																				●				●		
594	Detecting the Toolmarks of Genetic Engineering in Bioweapons Strains	52714		●																							●	
596	Joint Authentication/Encryption	52716						●	●				●						●			●	●		●		●	

Appendix F: Dual-Benefit Areas and Single-Use Categories

Pg #	Title	Project #	Aeronautics	Applied Molecular Biology	Ceramics	Composites	Computer Simulation and Modeling	Data Storage and Peripherals	Electronics and Photonics	Energy	Flexible Computer-Integrated Manufacturing	High-Definition Imaging and Displays	High-Performance Computing and Networking	High-Performance Metals and Alloys	Intelligent Processing Equipment	Materials Synthesis and Processing	Medical Technology	Micro- and Nanofabrication	Micro- and Optoelectronics	Photonic Materials	Pollution Minimization, Remediation, and Waste Mgmt.	Sensors and Signal Processing	Software	Surface Transportation Technologies	Systems Management Technologies	Defense-Related (mostly or purely)	Dual-Use (defense and non-defense-related)	Non-Defense-Related (mostly or purely)
598	Ultrahigh-Temperature Ceramics for Hypersonic Vehicle Applications	52717	●		●											●										●	
601	Leveraging Robotic Planning for Physical-Security Analysis	52718					●																			●	
604	Ultralightweight Telescope with MEMS Adaptive Optic for Distortion Correction	52720							●									●	●	●						●	
606	Modeling Signals from Earth-Penetrating Nuclear Weapons for Remote Kill Assessment	52721					●															●				●	
607	Novel Micropreconcentrators for CW, Explosives, and Water Surety	52723		●		●			●						●		●	●			●	●				●	
610	Ion-Mobility Spectrometer/Mass Spectrometer	52724																●	●			●				●	
612	Cryptographic Assurance of Execution Correctness and Confidentiality	52725					●				●		●									●	●		●	●	
615	Characterization, Performance, and Optimization of PVDF as a Piezoelectric Film for Advanced Space Mirror Concepts	52726	●			●										●			●							●	
730	Predictive Accelerated Aging of Microsystems: The Science of Dormancy	52727					●		●							●		●								●	
733	Surety and Accountability Enhancements for Storage Containers	52728				●																			●		
735	Nuclear-Safety Weaklinks for Thermal and Mechanical Environments	52729			●											●										●	
738	Advanced Packaging Technology for Optical Firesets	52730							●										●						●		
740	Miniature Transmitter Filter for JTA Using LIGA Technology	52731																●								●	
743	Novel and Robust Environmental Sensing Devices (ESDs)	52732							●									●	●			●				●	
745	Advanced Neutron Monitors for JTA and Stockpile Monitoring	52733														●		●				●				●	
686	Development of an Efficient Large-Aperture High-Damage-Threshold Sol-Gel Diffraction Grating	52737							●										●								●

Appendix F: Dual-Benefit Areas and Single-Use Categories

Pg #	Title	Project #	Aeronautics	Applied Molecular Biology	Ceramics	Composites	Computer Simulation and Modeling	Data Storage and Peripherals	Electronics and Photonics	Energy	Flexible Computer-Integrated Manufacturing	High-Definition Imaging and Displays	High-Performance Computing and Networking	High-Performance Metals and Alloys	Intelligent Processing Equipment	Materials Synthesis and Processing	Medical Technology	Micro- and Nanofabrication	Micro- and Optoelectronics	Photonic Materials	Pollution Minimization, Remediation, and Waste Mgmt.	Sensors and Signal Processing	Software	Surface Transportation Technologies	Systems Management Technologies	Defense-Related (mostly or purely)	Dual-Use (defense and non-defense-related)	Non-Defense-Related (mostly or purely)
689	Laser Triggering of Water Switches in Terawatt-Class Pulse-Power Accelerators	52738								●																●	
530	Experimental and Computational Study of Liquid-Solid Transition in Tin	52739					●																			●		
747	Design and Control of the Magnetic Properties of Nanoparticles	52797			●	●			●		●			●	●	●	●	●	●	●								●
749	Flow Control and Mixing in Microfluidic Devices	52977					●									●	●	●				●						●
752	Atomic-Scale Scanning-Tunneling Microscopy Measurements of Nucleation and Growth of Ge/Si Alloy Structures	53464							●							●		●	●								●	
754	Micro-/Nanoscale Thermomechanical Manufacturing	53465					●	●								●		●	●			●						●
450	Novel Diagnostics for Rarefied Flows in MEMS Applications	53585	●																●								●	
113	Geophysical Subsurface Imaging and Interface Identification	53586					●			●													●				●	
756	Evolution of Near-Surface Scalar Concentrations Through a Compact Cylinder Array Embedded in the Atmospheric Surface Layer	53587					●														●						●	
63	Miniature High-Power RF Components Enabled by Mesoscale Manufacturing	53588														●											●	
691	Electrical Conductivity of Metal Alloys	53590					●							●													●	
375	Hydrogen Futures Dynamic Simulation Model	53591					●			●											●		●					●
757	Design of Biospecific Surfaces to Control Specific Cellular Responses	53681		●					●								●	●	●			●					●	
760	Nanomagnetic Films	54211					●	●	●							●		●				●						●
762	A Multiscale Approach to Modeling Carbon Nanotube–Reinforced Composites	54213	●			●	●							●													●	
483	Near-Real-Time Characterization for Assured HDBT Defeat	55079					●						●									●				●		

Appendix F: Dual-Benefit Areas and Single-Use Categories

Pg #	Title	Project #	Aeronautics	Applied Molecular Biology	Ceramics	Composites	Computer Simulation and Modeling	Data Storage and Peripherals	Electronics and Photonics	Energy	Flexible Computer-Integrated Manufacturing	High-Definition Imaging and Displays	High-Performance Computing and Networking	High-Performance Metals and Alloys	Intelligent Processing Equipment	Materials Synthesis and Processing	Medical Technology	Micro- and Nanofabrication	Micro- and Optoelectronics	Photonic Materials	Pollution Minimization, Remediation, and Waste Mgmt.	Sensors and Signal Processing	Software	Surface Transportation Technologies	Systems Management Technologies	Defense-Related (mostly or purely)	Dual-Use (defense and non-defense-related)	Non-Defense-Related (mostly or purely)
486	Prompt Global Response	55086	●		●	●								●												●	
488	Winning the War: A Systems Approach to Defending Our Borders	55087					●		●			●	●						●				●		●	●	
765	Integrated Superhard and Metallic Coatings for MEMS	57300	●	●	●	●	●		●		●	●	●	●	●	●	●	●	●	●	●	●				●	
769	Microscale Separations of Biological Compounds Using Novel Polymeric Separations Materials	57307		●												●		●								●	
772	Friction in Micromachine Interfaces	57308																●	●							●	
774	Lipid Microarray Biosensor for Biotoxin Detection	57309		●					●							●	●	●								●	
777	Advanced Manufacturing Techniques Using Rapid Prototyping	57310									●							●				●			●		
779	Robust Hermetic Packaging Techniques for MEMS Integrated Microsystems	57311							●									●								●	
532	Active Photonic Nanostructures	58907							●	●								●	●			●				●	
781	3-D Large-Eddy Simulation of Turbulent Flow Based on One-Dimensional Turbulence Modeling	59034	●				●			●																●	
143	A Method of Evaluating Research Using New Innovation, Risk, and Impact Indicators	59916					●																		●	●	
784	Photonic Encryption Using All-Optical Logic	61046							●				●													●	
786	Nanoporous-Carbon Adsorbers for Chemical Microsensors	62269																			●	●				●	
273	Nonlethal Technologies for the War on Terrorism	62827							●										●							●	
377	Agent-Based Control of Distributed Infrastructure Resources	64811					●			●					●								●		●	●	
789	Direct Single-Ion Machining of Nanopores	65559																●									●

Appendix F: Dual-Benefit Areas and Single-Use Categories

Pg #	Title	Project #	Aeronautics	Applied Molecular Biology	Ceramics	Composites	Computer Simulation and Modeling	Data Storage and Peripherals	Electronics and Photonics	Energy	Flexible Computer-Integrated Manufacturing	High-Definition Imaging and Displays	High-Performance Computing and Networking	High-Performance Metals and Alloys	Intelligent Processing Equipment	Materials Synthesis and Processing	Medical Technology	Micro- and Nanofabrication	Micro- and Optoelectronics	Photonic Materials	Pollution Minimization, Remediation, and Waste Mgmt.	Sensors and Signal Processing	Software	Surface Transportation Technologies	Systems Management Technologies	Defense-Related (mostly or purely)	Dual-Use (defense and non-defense-related)	Non-Defense-Related (mostly or purely)
792	Investigation of the Effects of Intense Pulsed Particle Beams on the Durability o Metal-to-Plastic Interfaces	66170												●		●											●	
794	Advanced Techniques for Multiobjective Discrete Optimization	66450																							●		●	
796	Nonradioactive Safety and Performance Issues with Supercritical Water Reactor (SCWR) Safety Technologies	66809								●											●							●
798	Radiation Performance Issues with Advanced Coolants for Next-Generation Reactor	66810								●											●							●
66	Rapid Prototyping to the Nanometer Scale	67004														●		●	●								●	
67	Robust Manufacturing of Gel-Based Components for Nuclear Weapons	67005				●			●							●			●			●					●	
69	Meso-/Microoptical System Interface Coupling Solutions	67006							●										●	●							●	
71	Injection Molding of Net-Shape Active Ceramic Components	67007			●		●									●					●	●					●	
73	Macro-/Meso-/Microsystems Integration in LTCC	67008			●				●								●	●	●	●		●					●	
91	Studies of Signaling Domains in Model and Biological Membranes Through Advanced Imaging Techniques	67010		●								●					●					●						●
93	Imaging Self-Organization of Proteins in Membranes by Photocatalytic Nanotagging	67011		●			●									●	●	●		●		●						●
96	Protein Microarrays for Biowarfare-Agent Detection and Characterization	67012					●										●	●				●					●	
99	Interaction of Proteins with Lipid Films	67013		●			●															●						●
103	New Technologies for Understanding Membrane-Protein Recognition and Signaling	67014		●			●																					●
145	Massively Parallel, Scalable Atmosphere Model	67015	●				●			●			●														●	

Appendix F: Dual-Benefit Areas and Single-Use Categories

Pg #	Title	Project #	Aeronautics	Applied Molecular Biology	Ceramics	Composites	Computer Simulation and Modeling	Data Storage and Peripherals	Electronics and Photonics	Energy	Flexible Computer-Integrated Manufacturing	High-Definition Imaging and Displays	High-Performance Computing and Networking	High-Performance Metals and Alloys	Intelligent Processing Equipment	Materials Synthesis and Processing	Medical Technology	Micro- and Nanofabrication	Micro- and Optoelectronics	Photonic Materials	Pollution Minimization, Remediation, and Waste Mgmt.	Sensors and Signal Processing	Software	Surface Transportation Technologies	Systems Management Technologies	Defense-Related (mostly or purely)	Dual-Use (defense and non-defense-related)	Non-Defense-Related (mostly or purely)
147	High-Performance Processing Architecture	67016											●														●	
149	Substructured Multibody Molecular Dynamics	67017		●			●						●			●	●	●				●	●	●			●	
151	Enhancing Simulation Performance on Clusters with Configurable Auxiliary Devices	67018					●						●										●				●	
154	A Hybrid Level-Set/Particle Method for Modeling Surface Evolution During Feature-Scale Etching and Deposition Processes	67019					●											●									●	
157	Penetrator Reliability Investigation and Design Exploration (PRIDE)	67020					●																●				●	
160	Topology Optimization for Improving Sensor Performance	67021	●				●											●									●	
213	Characterization and Application of Dielectrics with Controlled Leakage	67022							●									●				●					●	
216	Nano-G Accelerometers Using Nanophotonic Motion-Detection System	67023																	●							●		
218	Bragg Fiber Development	67024		●					●									●	●	●							●	
220	Microwave-to-Millimeter-Wave Electrodynamic Response and RF Applications of Semiconductor Quantum Nanostructures	67025							●	●								●	●			●					●	
222	Development of GaN 20–100 Watt Ku-Band Power Amplifiers for Micro-SAR	67026							●																	●		
225	Evanescent-Wave Planar Photonic Biosensor	67027		●					●								●	●	●		●	●					●	
227	Passive Electronically Steerable Array (PESA) for Miniature Synthetic-Aperture Radar (Mini-SAR), Precision Guidance, and Intelligence/Surveillance/ Reconnaissance (ISR)	67028							●									●				●				●		

Appendix F: Dual-Benefit Areas and Single-Use Categories

Pg #	Title	Project #	Aeronautics	Applied Molecular Biology	Ceramics	Composites	Computer Simulation and Modeling	Data Storage and Peripherals	Electronics and Photonics	Energy	Flexible Computer-Integrated Manufacturing	High-Definition Imaging and Displays	High-Performance Computing and Networking	High-Performance Metals and Alloys	Intelligent Processing Equipment	Materials Synthesis and Processing	Medical Technology	Micro- and Nanofabrication	Micro- and Optoelectronics	Photonic Materials	Pollution Minimization, Remediation, and Waste Mgmt.	Sensors and Signal Processing	Software	Surface Transportation Technologies	Systems Management Technologies	Defense-Related (mostly or purely)	Dual-Use (defense and non-defense-related)	Non-Defense-Related (mostly or purely)
275	Advancements in Sensing and Perception Using Structured Lighting Techniques and an Innovative Design Tool	67029					●															●				●		
278	Biophysics of BW-Warhead Defeat with a Kinetic Interceptor	67030		●			●										●									●		
281	Dispersal in Urban Canyons, Source Identification, and Collateral Damage/Mitigation Assessment	67031					●														●						●	
283	Weaponization of Thermobaric Explosives	67032					●																			●		
286	Development of an Enterprise-Scale Agen Based Autonomic Logistics Simulation Model	67033					●						●												●		●	
289	Mobile-Node Authentication in a Wireless *Ad Hoc* Environment	67034											●													●		
292	Novel Processing, Affordable Motion Compensation, and Mode Multiplexing fo Miniaturized Synthetic-Aperture Radar	67035							●			●										●	●				●	
295	Coilgun Technology Demonstration Test-Bed	67036				●				●																	●	
298	Enhanced Perception for Remote 3-D Mapping of Unknown Indoor and Outdoo Environments	67037																			●	●	●				●	
300	A Modular Micromagnetic Accelerometer in Support of the mTalon Vision	67038								●								●				●					●	
302	MICROFUZE Integration	67039														●		●	●			●				●		
304	Analysis of Technology Impacts on Operations in Complex Environments	67041					●						●									●	●				●	
306	CBW Cloud Knockdown and Neutralization	67042	●										●		●						●					●		
308	Assessment of Biokillers in EDS for Biological-Agent Destruction	67043																			●	●				●		
310	Adaptive-Force-Feedback Surface Contro	67044	●						●								●	●					●				●	

Appendix F: Dual-Benefit Areas and Single-Use Categories

Pg #	Title	Project #	Aeronautics	Applied Molecular Biology	Ceramics	Composites	Computer Simulation and Modeling	Data Storage and Peripherals	Electronics and Photonics	Energy	Flexible Computer-Integrated Manufacturing	High-Definition Imaging and Displays	High-Performance Computing and Networking	High-Performance Metals and Alloys	Intelligent Processing Equipment	Materials Synthesis and Processing	Medical Technology	Micro- and Nanofabrication	Micro- and Optoelectronics	Photonic Materials	Pollution Minimization, Remediation, and Waste Mgmt.	Sensors and Signal Processing	Software	Surface Transportation Technologies	Systems Management Technologies	Defense-Related (mostly or purely)	Dual-Use (defense and non-defense-related)	Non-Defense-Related (mostly or purely)
312	High-Capacity Earth-Penetrator Instrumentation	67046							●																	●		
314	Systems Analysis of Networked Sensors	67047							●													●			●	●		
317	Deployable Object Tracker for NMD Flights	67048	●						●			●							●			●				●		
319	Continuous-Flow Detector for Rapid Pathogen Identification	67049		●														●									●	
380	Biological-Security Decontamination Technology—Reducing the Threat of Infectious-Agent Spread	67050															●				●							●
383	Consequence Management, Recovery, and Restoration after an Intentional Contamination Event	67051					●														●				●			●
386	Fully Integrated System-Dynamics Toolbox for Water Resources Planning	67052					●																		●			●
390	Predicting System Performance of Proton-Exchange-Membrane Fuel Cells: Computational Modeling with Experimental Discovery and Validation	67053					●			●						●							●			●		
393	Optimal Allocation of Terrorist Countermeasures Using Risk-Based Systems Pathways Analysis	67054					●			●													●		●		●	
396	Silicon Field-Emission Electric Propulsion Arrays (FEEP) Powered by Orbital Nuclear Reactors	67055	●						●									●									●	
398	Advanced Fuel-Cell Reactor for the Direct Cogeneration of Electricity During Selective Partial Oxidation of Hydrocarbons	67056			●					●						●												●
401	New Hydrogen-Storage Material: Metal-N H system	67057								●						●					●			●				●
403	Intrusion Detection for Wireless Networks	67058								●			●									●					●	
405	Membranes for H2 Generation from Nuclear-Powered Thermochemical Cycles	67059			●	●				●				●		●		●										●

Appendix F: Dual-Benefit Areas and Single-Use Categories

Pg #	Title	Project #	Aeronautics	Applied Molecular Biology	Ceramics	Composites	Computer Simulation and Modeling	Data Storage and Peripherals	Electronics and Photonics	Energy	Flexible Computer-Integrated Manufacturing	High-Definition Imaging and Displays	High-Performance Computing and Networking	High-Performance Metals and Alloys	Intelligent Processing Equipment	Materials Synthesis and Processing	Medical Technology	Micro- and Nanofabrication	Micro- and Optoelectronics	Photonic Materials	Pollution Minimization, Remediation, and Waste Mgmt.	Sensors and Signal Processing	Software	Surface Transportation Technologies	Systems Management Technologies	Defense-Related (mostly or purely)	Dual-Use (defense and non-defense-related)	Non-Defense-Related (mostly or purely)
408	Microfabricated BTU Monitoring Device for System-Wide Natural-Gas Monitoring	67060								●					●			●				●					●	
411	"Tunable" Ion Conductors for Low-Temperature Oxide-Based Fuel Cells	67061			●	●				●						●		●										●
414	Nuclear Nanobatteries: On-Board Power for Independent MEMS Devices	67062							●							●	●	●	●			●					●	
417	Integrated Tunable Light Sources for Miniature Sensors	67063		●					●	●							●		●	●		●					●	
452	Ray Model of High-Frequency Cavity Scarring	67064					●		●													●					●	
455	New Smart Material to Address Issues of Structural Health Monitoring	67065				●	●									●		●				●					●	
458	Noncontact Surface Thermometry for Microsystems	67067							●									●	●			●					●	
461	High-Speed Interferometric Deformation Measurements	67068	●				●		●					●				●	●			●					●	
463	Fundamentals of Nanofluidics	67069					●											●									●	
465	Simulating Self-Assembly and Growth of Biological Nanostructured Materials	67070					●																				●	
468	A Low-Power, Ultrafast-Current Transien Measuring Device	67071							●										●	●							●	
470	A Capillary Valve for Microfluidic Systems	67073					●											●									●	
534	Electrochemically Switchable Materials for (Bio)Microfluidics	67074		●												●		●				●					●	
537	Modeling of Friction-Induced Deformation and Microstructure	67075												●		●		●									●	
540	Reversible Antibody Trapping for Selective Sensor Devices	67076														●	●					●					●	
542	Correlated and Comprehensive Analytical Techniques for Homeland Defense	67077														●		●				●	●				●	
545	Development of High-Energy-Density Dielectric Materials for Integrated Microsystems	67078	●		●	●			●	●					●			●	●							●		

Appendix F: Dual-Benefit Areas and Single-Use Categories

Pg #	Title	Project #	Aeronautics	Applied Molecular Biology	Ceramics	Composites	Computer Simulation and Modeling	Data Storage and Peripherals	Electronics and Photonics	Energy	Flexible Computer-Integrated Manufacturing	High-Definition Imaging and Displays	High-Performance Computing and Networking	High-Performance Metals and Alloys	Intelligent Processing Equipment	Materials Synthesis and Processing	Medical Technology	Micro- and Nanofabrication	Micro- and Optoelectronics	Photonic Materials	Pollution Minimization, Remediation, and Waste Mgmt.	Sensors and Signal Processing	Software	Surface Transportation Technologies	Systems Management Technologies	Defense-Related (mostly or purely)	Dual-Use (defense and non-defense-related)	Non-Defense-Related (mostly or purely)
549	Nanolithography-Directed Materials Growth and Self-Assembly	67079														●		●	●			●					●	
552	Development of a Novel Technique to Assess the Vulnerability of Micromechanical System Components to Environmentally Assisted Cracking	67080							●					●				●				●					●	
554	3-D Optical Sectioning with a New Hyperspectral Deconvolution Fluorescence Imaging System	67081		●								●			●	●	●	●	●	●		●	●				●	
558	The Science of Solutes: Transition Metals in LIGA Nickel	67082					●									●		●									●	
560	Novel Gel-Based Technology for Sensors and Weapons	67083		●					●			●				●	●	●	●	●	●	●		●			●	
562	Coupled Nanomechanical Oscillator Arrays for the Study of Internal Dissipation in Nanoscale Structures and Collective Behavior in Large Systems	67084							●									●				●					●	
565	Precisely Controlled Picoliter Vessels with Rapid Sample Preparation for Trace Biotoxin Detection	67085		●											●	●	●	●				●					●	
618	Adaptive Optics and Phase-Diversity Imaging for Responsive Space Applications	67086							●										●			●					●	
621	Infrastructural Development for Flexible Network of Devices	67087																					●		●		●	
622	Monolithic Reconfigurable Radio-Frequency Microelectromechanical System (RF MEMS) Antennas	67088							●									●			●	●					●	
625	Next-Generation 3-D Inspection System for Facility Monitoring	67089													●							●			●		●	
627	Risk-Assessment Metatool	67090					●																●			●		
629	Featureless Spread-Spectrum Waveform Design and Processing	67091																				●				●		
631	Tracking Slow-Moving Objects in a GPS–Denied Environment	67092							●						●			●	●			●		●		●		

Appendix F: Dual-Benefit Areas and Single-Use Categories

Pg #	Title	Project #	Aeronautics	Applied Molecular Biology	Ceramics	Composites	Computer Simulation and Modeling	Data Storage and Peripherals	Electronics and Photonics	Energy	Flexible Computer-Integrated Manufacturing	High-Definition Imaging and Displays	High-Performance Computing and Networking	High-Performance Metals and Alloys	Intelligent Processing Equipment	Materials Synthesis and Processing	Medical Technology	Micro- and Nanofabrication	Micro- and Optoelectronics	Photonic Materials	Pollution Minimization, Remediation, and Waste Mgmt.	Sensors and Signal Processing	Software	Surface Transportation Technologies	Systems Management Technologies	Defense-Related (mostly or purely)	Dual-Use (defense and non-defense-related)	Non-Defense-Related (mostly or purely)
632	Optical Communications	67093							●										●							●		
633	A Unique Vibration-Based Miniature Power Generator for National Security Applications	67094	●						●									●				●				●	
636	Image Georectification Using Digital Elevation Model Shadows	67095					●															●	●			●	
639	Vulnerability Assessment of State-of-the-Art Microelectronics	67096							●																	●		
640	Nonlinear Optical Detection of Biological and Chemical Aerosol Agents Using Femtosecond Lasers	67098							●													●				●		
643	Polymer Electronic Devices and Materials	67099	●						●		●	●				●		●	●	●	●	●					●	
647	Small Circuits for Cryptography	67101						●	●										●			●			●		●	
649	Analysis of Multichannel Internet Communication	67102																					●					●
650	Receiver for Ultralow-Power Wake-Up and Command	67104							●									●				●				●		
652	Extraordinary Optical Transmission Through Patterned Subwavelength Apertures	67105					●		●											●						●		
654	Reconstruction Algorithm Development and Assessment for a Computed Tomography-Based Spectral Imager	67107																				●				●		
657	Power Combining Techniques for Solid-State Power Amplifiers	67108					●		●																	●		
659	Dispersive Diffractive Optical Elements for the Infrared	67109							●										●	●		●				●		
661	Atmospheric Propagation of Terahertz Radiation	67111		●					●										●	●		●					●	
663	High-Confidence Estimation of Relative Event Locations from Space-Based Sensors	67113																				●	●			●		

Appendix F: Dual-Benefit Areas and Single-Use Categories

Pg #	Title	Project #	Aeronautics	Applied Molecular Biology	Ceramics	Composites	Computer Simulation and Modeling	Data Storage and Peripherals	Electronics and Photonics	Energy	Flexible Computer-Integrated Manufacturing	High-Definition Imaging and Displays	High-Performance Computing and Networking	High-Performance Metals and Alloys	Intelligent Processing Equipment	Materials Synthesis and Processing	Medical Technology	Micro- and Nanofabrication	Micro- and Optoelectronics	Photonic Materials	Pollution Minimization, Remediation, and Waste Mgmt.	Sensors and Signal Processing	Software	Surface Transportation Technologies	Systems Management Technologies	Defense-Related (mostly or purely)	Dual-Use (defense and non-defense-related)	Non-Defense-Related (mostly or purely)
665	Critical-Infrastructure System-of-Systems Assessment Methodology	67114					●			●															●		●	
667	Dynamic Vulnerability Assessment	67115					●																			●		
669	Inflatable Antenna with Adaptive Actuators	67116										●										●					●	
671	Data-Driven Dynamic Models of Conflict	67117					●																●		●		●	
800	MEMS/Fuze Diagnostic Extraction in High-G Environments	67118							●									●				●				●		
694	Efficient Implicit Multigroup Radiation Calculations	67120					●																				●	
696	Model for Channel Resistance in Water Breakdown	67121					●			●				●		●					●						●	
698	Embeddable Shock Physics Sensors	67122					●		●							●		●				●					●	
802	Smart Detectors of Enrichment of Bioaerosols	67716																				●					●	
805	Computational Studies of JP-8 Diffusion Flames with Detailed Chemistry and Particulate Formation	68063	●				●			●											●						●	
419	Design and Fabrication of Advanced Device Structures for Ultrahigh-Efficiency Solid-State Lighting	69143							●	●						●		●	●	●		●					●	
808	Molecular Simulation of Beta-Amyloid (A beta) Peptide Interaction with Phospholipid Membranes	69145															●											●
809	Nanoscale Testing of Deformation and Fracture in Engineering Materials	69146					●		●									●									●	
812	Nanocrystal-Polymer Composites for High Luminous-Efficiency LEDs	69148							●							●			●	●								●
817	Outstanding Challenges for AlGaInN MOCVD	69149							●	●					●	●		●	●			●					●	
820	Nanoporous Polymeric Materials for Chemically and Spatially Multiplexed Sensing of Bioagents	69150																●				●					●	

Appendix F: Dual-Benefit Areas and Single-Use Categories

Pg #	Title	Project #	Aeronautics	Applied Molecular Biology	Ceramics	Composites	Computer Simulation and Modeling	Data Storage and Peripherals	Electronics and Photonics	Energy	Flexible Computer-Integrated Manufacturing	High-Definition Imaging and Displays	High-Performance Computing and Networking	High-Performance Metals and Alloys	Intelligent Processing Equipment	Materials Synthesis and Processing	Medical Technology	Micro- and Nanofabrication	Micro- and Optoelectronics	Photonic Materials	Pollution Minimization, Remediation, and Waste Mgmt.	Sensors and Signal Processing	Software	Surface Transportation Technologies	Systems Management Technologies	Defense-Related (mostly or purely)	Dual-Use (defense and non-defense-related)	Non-Defense-Related (mostly or purely)
823	Evolutionary Complexity for Protection o Critical Assets	69151					●						●										●					●
825	Nanomechanical Stochastic Resonators	69152	●	●			●	●	●	●					●		●	●	●	●	●	●					●	
826	Augmented Musculature Device	69153	●														●										●	
828	Biomolecular Decision-Making Processes for Self-Assembly	69154		●			●											●									●	
830	Light-Powered Nanovehicle Propulsion	69155		●			●									●		●										●
832	System-Dynamics Modeling to Assist Regional Water Planning: Modeling the Nonmarket Value of Water	69156					●																		●			●
834	Interactive Water-Quality Modeling to Assist Regional Water Planning	69157					●																		●			●
837	Microbe-Exuded Polymers and the Enhanced Corrosion of Carbonate Materials	69158		●			●														●							●
840	Nerve-Cell Function and the Developmen of Cognitive Networks	69159		●														●				●						●
843	Ultrahigh-Gain Fusion Concept	69160								●																	●	
844	Nanofluidic Devices for Rapid Detection of Virus Particles	69161																				●					●	
846	Solution Behavior of PEO: The Ultimate Biocompatible Polymer	69162					●						●			●	●										●	
848	New Self-Assembled Nanocrystal Micelle for Biolabels	69163		●												●	●	●										●
851	Rapid Detection of Biothreat Agents Based on Cellular Machinery	69164		●																							●	
853	Patterning Quantum-Dot Arrays Using DNA Replication Principles	69165		●					●							●	●	●		●		●					●	
856	Adaptive Algorithms for Use in the Rejection of Periodic Disturbances of Unknown Frequency	69166					●						●														●	

Appendix F: Dual-Benefit Areas and Single-Use Categories

Pg #	Title	Project #	Aeronautics	Applied Molecular Biology	Ceramics	Composites	Computer Simulation and Modeling	Data Storage and Peripherals	Electronics and Photonics	Energy	Flexible Computer-Integrated Manufacturing	High-Definition Imaging and Displays	High-Performance Computing and Networking	High-Performance Metals and Alloys	Intelligent Processing Equipment	Materials Synthesis and Processing	Medical Technology	Micro- and Nanofabrication	Micro- and Optoelectronics	Photonic Materials	Pollution Minimization, Remediation, and Waste Mgmt.	Sensors and Signal Processing	Software	Surface Transportation Technologies	Systems Management Technologies	Defense-Related (mostly or purely)	Dual-Use (defense and non-defense-related)	Non-Defense-Related (mostly or purely)
858	Property-Based Testing for Cybersecurity Assurance	69168					●						●		●							●	●	●			●	
860	Self-Assembled Ordered Carbon-Nanotube Arrays and Membranes	69170							●			●				●	●	●	●	●		●					●	
863	Chemical Cross-Linking and Mass-Spectrometry Studies of the Structure and Dynamics of Membrane Proteins and Receptors	69189		●																								●
866	Toxin Studies Using an Integrated Biophysical and Structural Biology Approach	69190		●																							●	
869	Top-Down Structural Studies	69191		●																								●
871	Molecular Dynamics of Membrane Proteins	69192		●			●															●						●
874	Model-Building Codes for Membrane Proteins	69193					●						●															●
878	Poroelastic-Wave Propagation on the Earth Simulator	69198					●			●			●								●						●	
882	Development of Microreformers for Fuel Cells	69239			●					●								●									●	
568	Developing the Foundation for Polyoxoniobate Chemistry: Highly Tunable and Exploitable Materials	70799		●												●	●				●	●						●
321	Simulating Human Behavior for National Security	71943					●																				●	
28	Agent-Based Modeling of Middle East Terrorist Recruitment	71944					●																				●	
30	Automatic Generation of Terrorist Operation Plan Hypotheses	71945					●								●								●				●	
421	Develop a System-Dynamics Modeling Framework for Assessing Factors that Influence Water Resource Consumption	72599					●			●											●		●					●

Appendix F: Dual-Benefit Areas and Single-Use Categories

Pg #	Title	Project #	Aeronautics	Applied Molecular Biology	Ceramics	Composites	Computer Simulation and Modeling	Data Storage and Peripherals	Electronics and Photonics	Energy	Flexible Computer-Integrated Manufacturing	High-Definition Imaging and Displays	High-Performance Computing and Networking	High-Performance Metals and Alloys	Intelligent Processing Equipment	Materials Synthesis and Processing	Medical Technology	Micro- and Nanofabrication	Micro- and Optoelectronics	Photonic Materials	Pollution Minimization, Remediation, and Waste Mgmt.	Sensors and Signal Processing	Software	Surface Transportation Technologies	Systems Management Technologies	Defense-Related (mostly or purely)	Dual-Use (defense and non-defense-related)	Non-Defense-Related (mostly or purely)
423	Develop a Cooperative Water-Management Process, Creating a System-Dynamics Model of Water Resources in the Lower Rio Grande Basin	72600					●			●											●							●
323	Compact Ultrabright Multikilovolt X-Ray Sources for Advanced Material Studies, 3-D Nanoimaging, and Attosecond X-Ray Technology	72715																		●							●	
425	Energy-Systems Analysis Framework and Modeling	72716					●			●															●		●	
33	Radiation-/Geometry-Driven Jets: Proof-of-Principle Tests	73045					●						●													●		
884	Superhydrophobic Surface Coatings for Microfluidics and MEMS	73185								●						●		●	●			●					●	
673	Microoptical Radar (MOR) Facial-Recognition Project	73207	●						●		●				●				●	●		●	●	●			●	
886	Determining Explosive Ignition Criteria for Miniaturized Devices	74545																●								●		
888	Quantum Squeezed Light for Probing Mitochondrial Membranes and Study of Neuroprotectants	74546																				●					●	
890	Characterization of a New Class of Surface-Micromachined Pumps	74547		●					●							●	●	●			●							●
893	Risk of Biological Terrorism to Water-Distribution Systems	74548																			●							●
895	Explicit and Implicit Measures in Human Aversive Classical Conditioning	74759															●						●		●		●	
676	Automatic-Target-Recognition Algorithm for Uncooled Thermal Imagery	74760																				●					●	
326	Magnetophoretic Bead Trapping in a High Flowrate Biological Detection System	74795		●					●								●		●		●	●					●	
329	TPV Energy Scavenging for Hypervelocity Vehicles	75441	●							●								●	●	●							●	
898	Assessment of Advanced Pulsed-Power Fusion Concepts	75442					●			●																	●	

Appendix F: Dual-Benefit Areas and Single-Use Categories

Pg #	Title	Project #	Aeronautics	Applied Molecular Biology	Ceramics	Composites	Computer Simulation and Modeling	Data Storage and Peripherals	Electronics and Photonics	Energy	Flexible Computer-Integrated Manufacturing	High-Definition Imaging and Displays	High-Performance Computing and Networking	High-Performance Metals and Alloys	Intelligent Processing Equipment	Materials Synthesis and Processing	Medical Technology	Micro- and Nanofabrication	Micro- and Optoelectronics	Photonic Materials	Pollution Minimization, Remediation, and Waste Mgmt.	Sensors and Signal Processing	Software	Surface Transportation Technologies	Systems Management Technologies	Defense-Related (mostly or purely)	Dual-Use (defense and non-defense-related)	Non-Defense-Related (mostly or purely)
427	A Mathematical Method for Quantifying the Effectiveness of Management Strategies	75443					●			●					●						●				●		●	
901	Developing Algorithms for Predicting Protein-Protein Interactions from Experimental Constraints	75513		●			●																				●	
904	Instrumentation Development for Real-Time Brain-Wave Monitoring	75514																				●					●	
907	Miniaturized Electronic Steerable-Array Synthetic-Aperture Radar	76069					●		●										●			●					●	
910	Full-Earth-Monitoring Sensor MESAWorks	76070							●			●							●			●					●	
36	Systems Assessment of Water-Savings Impact of Controlled-Environment Agriculture Utilizing Wirelessly Networked SDACs	76305		●			●								●			●				●						●
429	Inactivation of Avian Influenza (Bird Flu) with Sandia-Developed Decontamination Formulations	76306		●													●				●						●	
913	Deciphering the Genetic Regulatory Code Using an Inverse Error Control Coding Framework	78132		●			●	●														●					●	
38	Climate-Change Effects on International Stability	78307					●						●														●	
916	Generalized Continuum Models for Inelasticity in Solids: Formulation of Theories and Variational Methods for Computation	78783	●			●	●		●					●			●										●	
431	GeSi–Strained Nanostructure Self-Assembly for Nano- and Optoelectronics	79943														●			●								●	
678	Vulnerability Analysis for SCADA	80835																							●		●	
918	Molten Salt-Based Growth of Bulk GaN and InN	80838			●				●	●						●	●		●	●		●					●	
679	Randomness Complexity and Cryptography	81209						●														●	●		●		●	

Appendix F: Dual-Benefit Areas and Single-Use Categories

Pg #	Title	Project #	Aeronautics	Applied Molecular Biology	Ceramics	Composites	Computer Simulation and Modeling	Data Storage and Peripherals	Electronics and Photonics	Energy	Flexible Computer-Integrated Manufacturing	High-Definition Imaging and Displays	High-Performance Computing and Networking	High-Performance Metals and Alloys	Intelligent Processing Equipment	Materials Synthesis and Processing	Medical Technology	Micro- and Nanofabrication	Micro- and Optoelectronics	Photonic Materials	Pollution Minimization, Remediation, and Waste Mgmt.	Sensors and Signal Processing	Software	Surface Transportation Technologies	Systems Management Technologies	Defense-Related (mostly or purely)	Dual-Use (defense and non-defense-related)	Non-Defense-Related (mostly or purely)
681	System Study: Adaptive Optics for Weapon, Reconnaissance, and Military Space Applications	81354							●													●				●		
			36	**55**	**22**	**23**	**127**	**10**	**124**	**63**	**15**	**13**	**37**	**19**	**32**	**82**	**54**	**131**	**91**	**40**	**49**	**157**	**48**	**12**	**29**	**45**	**246**	**60**

Author and Title Index

A B C D E F G H I J K L M N O P Q R S T U V W X Y Z

3-D
Eddy simulation, 781
Inspection, 625
Mapping, 298
Nanoimaging, 323
Optical sectioning, 554

A
Abbott, R. E.
Assessing Bomb Damage to Underground Facilities, 236
Characterization for Assured HDBT Defeat, 483
Tracking Slow-Moving Objects, 631
Abrams, B. L.
Nanocrystal-Polymer Composites for LEDs, 812
Nanoscale Energetic Materials, 701
Absorption, 518
Accelerator, 689
Accelerometer
Micromagnetic, 300
Nano-G, 216
Ackermann, M. R.
TALON, 480
Acoustic, 236
Actuation, 510
Actuator
Adaptive, 669
Magnetostrictive, 528
MEMS, 193
Adams, D. P.
Assembly of Microsystems Using Thin Films, 50
Rapid Prototyping to the Nanometer Scale, 66
Telescope with MEMS Adaptive Optic, 604
Adaptive
Actuator, 669
Algorithm, 856
Force-feedback, 310
See also: Optica
Adkins, D. R.
Micropreconcentrators for Surety, 607
Real-Time Sensors for Water-Contamination, 360
Adsorber, 786
Aerosol
Detection, 640
Finder, 268
See also: Bioaerosol
Affinity, 77
Agent
Infrastructure resources, 377
Logistics simulation, 286
Sophisticated, 116
Terrorist recruitment, 28
Agile, 572
Aging, 730
Agriculture, 36
Akau, R. L.
Full-Earth-Monitoring Sensor MESAWorks, 910
Alam, M. K.
Brain-Wave Monitoring, 904
Alam, T. M.
Polyoxoniobate Chemistry, 568
Alanate, 357
Aldridge, D. F.
Assessing Bomb Damage to Underground Facilities, 236
Characterization for Assured HDBT Defeat, 483
Poroelastic-Wave Propagation on the Earth Simulator, 878
Alford, C.
Microoptical Gyroscope, 205
AlGaInN, 817
Algorithm
Fault tolerant, 119
Ground sensors, 262
Periodic disturbances, 856
Protein interactions, 901
Spectral imager, 654
Target recognition, 676
Transport/reaction simulations, 137
Allen, C. L.
Dynamic Vulnerability Assessment, 667
Allen, J. J.
MOSFET–MEMS Integration, 203
Polychromator Systems for Remote Chemical Sensing, 211
Allen, S. E.
Miniaturized Electronic Steerable-Array SAR, 907
Silicon-Based RF MEMS Components, 171
Allerman, A. A.
Advanced Device Structures for Solid-State Lighting, 419
FGaN HEMT High-Power Amplifiers, 207
Outstanding Challenges for AlGaInN MOCVD, 817
Alloy
Conductivity, 691
Deposition, 501
Growth, 752
Altman, S. J.
Biological Terrorism to Water-Distribution Systems, 893
Amai, W. A.
Immunological Basis for Systems Control, 245
Infrastructural Development for Flexible Networks, 621
Ambrosini, A.
H2 Generation from Thermochemical Cycles, 405
Ames, A. L.
Intelligent Interaction Control for Metrology, 52
Ammerlahn, H. R.
A Systems Approach to Defending Our Borders, 488
Understanding Communication in Crisis Management, 255
Amplifier
Efficiency, 207
Micro-SAR, 222
Power combining, 657
Amyloid, 808
Anderson, D. J.
System-of-Systems Modeling and Analysis, 266
Anderson, G. R.
Polymer Electronic Devices and Materials, 643
Anderson, L. F.
Brain-Wave Monitoring, 904

Author and Title Index

A B C D E F G H I J K L M N O P Q R S T U V W X Y Z

Anderson, R. A.
Magnetostrictive Elastomers, 528
Anderson, R. J.
Automated Visual Direction of Mobile Manipulation, 231
Anderson, W. E.
Joint Authentication/Encryption, 596
Securing Mobile Code, 365
Small Circuits for Cryptography, 647
Antenna
Autodirective, 906
Inflatable, 669
RF MEMS, 622
Antibody, 540
Antolak, A. J.
Analytical Techniques for Homeland Defense, 542
Antoun, B. R.
Friction in Micromachine Interfaces, 772
High-Fidelity Frictional Models for MEMS, 441
Apblett, C. A.
Biomicrofuel Cell, 473
Microexternal-Combustion Engine, 715
Aperture
Diffraction grating, 686
Subwavelength, 652
See also: Synthetic Aperture Radar
Aqueous, 493
Architectural (contamination), 586
Architecture
Algorithm, 262
Processing, 147
Armendariz, M.
GaN 20–100 Watt Amplifiers for Micro-SAR, 222
Meso-/Microoptical System Interface Coupling, 69
Miniature Transmitter Filter for JTA, 740
Miniaturized Electronic Steerable-Array SAR, 907
Ultrafast-Current Transient Measuring Device, 468
Armijo, J. C.
Compact Terahertz Sources, 252
Armstrong, R. C.
Simulation with Configurable Auxiliary Devices, 151
Arnold, B. W.
Natural-Gas Production Problems, 332
Arnold, J. D.
Understanding Communication in Crisis Management, 255
Array
Antenna, 906
Carbon nanotube, 860
Compact cylinder, 756
Electric propulsion, 396
Nanoelectrode, 338
Nanomechanical oscillator, 562
Passively steerable, 227
Quantum dot, 853
Steerable, 907
See also: Microarray
Arviso, M.
High-Capacity Earth-Penetrator Instrumentation, 312
Ash, B. J.
Elucidating the Mysteries of Wetting, 57
Ashley, C. S.
High-Damage-Threshold Sol-Gel Diffraction Grating, 686
Assembly
Electrooptical, 523
Microscale components, 52
Microsystems, 50
Nanomaterials, 510
See also: Self-assembly
Assets (protection), 823
Assink, R. A.
PVDF as a Piezoelectric Film for Space Mirrors, 615
Assurance
Cryptographic, 612
Cybersecurity, 858
Atencio, M. O.
Rapid-Prototyping High-Density Circuitry, 55
Atherton, B. W.
Nonlinear Optical Detection of Aerosol Agents, 640
Atmospheric
Arrays, 756
Model, 145
Radiation, 661
Atomic
Deposition, 46
Microscopy, 752
Atomistic, 434
Attack, 137
Attosecond, 323
Atwood, C. J.
Controlled Motion for a Microfluidic Drop Ejector, 44
Miniature High-Power RF Components, 63
Aubry, S.
Atomistic-Continuum Simulation, 434
Augment
Cognition, 476
Musculature, 826
Austin, D. E.
Ion-Mobility Spectrometer/Mass Spectrometer, 610
Micromass Spectrometer-on-a-Chip, 199
Austin, F.
Agile, Microsystems-Enabled Receiver, 572
Authentication
Encryption, 596
Wireless, 289
Autodirective, 906
Automated, 231
Automatic
Operation plan, 30
Target recognition, 676
Automotive, 712
Autonomic
Antenna, 906
Logistics simulation, 286
Aversive, 895
Avian, 429

Author and Title Index

A B C D E F G H I J K L M N O P Q R S T U V W X Y Z

Axline, R. M.
Featureless Spread-Spectrum Waveform Design, 629
Ayson, M. J.
Dynamics of Membrane Proteins and Receptors, 863

B
Baca, A. G.
Agile, Microsystems-Enabled Receiver, 572
GaN 20–100 Watt Amplifiers for Micro-SAR, 222
GaN HEMT High-Power Amplifiers, 207
Miniaturized Electronic Steerable-Array SAR, 907
Nonlethal Technologies for the War on Terrorism, 273
Baca, P. M.
Biomicrofuel Cell, 473
Polymer Electronic Devices and Materials, 643
Bachand, G. D.
Assembly of Nanomaterials Using Biomolecules, 510
Light-Powered Nanovehicle Propulsion, 830
Optical Sectioning, 554
Patterning Quantum-Dot Arrays, 853
Reversible Antibody Trapping, 540
Transduction Pathways in Affinity-Based Biosensors, 77
Backer, A.
Augmented Cognition, 476
Bacon, L. D.
EM Interactions with Systems to Enhance Security, 235
Secure Chaotic Communications, 264
Bader, B. W.
Robust Large-Scale Parallel Nonlinear Solvers, 134
BAE Systems, 185
Baer, M. R.
Weaponization of Thermobaric Explosives, 283
Bailar, J. M.
Intelligent Interaction Control for Metrology, 52
Bailey, J. E.
Hypervelocity Impact-Generated Flash, 258
Baker, M. S.
Compliant Thermomechanical MEMS Actuators, 193
Silicon-Based RF MEMS Components, 171
Bambha, R. P.
Identification of Chemical Plumes, 241
Short-Range Standoff Aerosol-Cloud Finder, 268
Tunable Light Sources for Miniature Sensors, 417
Bammann, D. J.
Modeling of Friction-Induced Deformation, 537
Barbour, J. C.
Active Photonic Nanostructures, 532
Baron, R. V.
Gel-Based Components for Nuclear Weapons, 67
Barr, P. K.
Understanding Communication in Crisis Management, 255
Bartel, L. C.
Assessing Bomb Damage to Underground Facilities, 236
Characterization for Assured HDBT Defeat, 483
Poroelastic-Wave Propagation on the Earth Simulator, 878
Bartlett, R. A.
Sensitivities for Large-Scale Simulation Codes, 123
Simulations of Chemical/Biological Attacks, 137
Barton, D. L.
Polymer Electronic Devices and Materials, 643
Basin (Rio Grande), 423
Bastasz, R. J.
Nerve-Cell Function and Cognitive Networks, 840
Bateman, V. I.
A Modular Micromagnetic Accelerometer, 300
Bates, R. A.
Autodirective Antenna Array Technology, 906
Battaile, C. C.
Protection of Critical Assets, 823
Modeling of Friction-Induced Deformation, 537
Baynes, E. E., Jr.
Controlled-Environment Agriculture, 36
Bead (trapping), 326
Beam, 792
Beaver, C. L.
Joint Authentication/Encryption, 596
Securing Mobile Code, 365
Small Circuits for Cryptography, 647
Behrens, R., Jr.
Nanoscale Energetic Materials, 701
Nerve-Cell Function and Cognitive Networks, 840
Bell, N. S.
Active Photonic Nanostructures, 532
Photocontrol of Nanointeractions in Microsystems, 499
Benavides, G. L.
Adaptive-Force-Feedback Surface Control, 310
High-Speed Micro-EDM, 713
Bennett, R. S.
Radiation-Hard Nonvolatile Memories, 185
Berg, M. J.
Optimal Allocation of Terrorist Countermeasures, 393
Vulnerability Analysis for SCADA, 678
Berg, T. M.
Polymer Electronic Devices and Materials, 643
Bernard, M. L.
Augmented Cognition, 476
Human/System Interactions in Systems-of-Systems, 260
Simulating Human Behavior for National Security, 321
Understanding Communication in Crisis Management, 255
Berry, N. M.
Agent-Based Modeling Terrorist Recruitment, 28
Augmented Cognition, 476
Controlled-Environment Agriculture, 36
Bessette, G. C.
Characterization for Assured HDBT Defeat, 483
Bethke, D.
An Integrated, Stacked System-on-a-Chip, 196
Full-Earth-Monitoring Sensor MESAWorks, 910
Betty, R. G.
Biological-Security Decontamination Technology, 380
CBW Cloud Knockdown and Neutralization, 306
Biefeld, R. M.
Quantum Coherence in Semiconductor Nanostructures, 201
Bieker, J. M.
Biological-Security Decontamination Technology, 380
Inactivation of Avian Influenza, 429

Author and Title Index

A B C D E F G H I J K L M N O P Q R S T U V W X Y Z

Bielek, T. P.
  Novel Processing for Miniaturized SAR, 292
Bilayer, 168
Bilisoly, R. L.
  Reconstruction Algorithm Development, 654
Bioactive, 523
Bioaerosol detectors
  Microseparation, 591
  Smart, 802
Bioagent, 820
Biocompatible, 846
Biokiller, 308
Biolabel, 848
Biological
  Aerosol, 640
  Bead trapping, 326
  Biokillers, 308
  Cell, 129
  Decontamination, 380
  Self-assembly, 465
  Separation, 769
  Signalling domains, 91
  Structural, 866
  See also: Bioterrorism
  See also: Terrorism
Biomembrane, 82
(Bio)Microfluidic, 534
Biomicrofuel Cell (BMFC), 473
Biomolecular (self-assembly), 828
Biomolecule, 510
Biophysical, 866
Biophysics, 278
Biosensor
  Affinity-based, 77
  Lipid, 774
  Photonic, 225
Biospecific, 757
Bioterrorism, 84
Biothreat, 851
Biotoxin
  Biosensor, 774
  Sample preparation, 565
Biowarfare, 96
Bioweapon
  Chimeric, 576
  Genetic engineering, 594
Bird, 429
Bisson, S. E.
  Identification of Chemical Plumes, 241
  Tunable Light Sources for Miniature Sensors, 417
Bitsie, F.
  High-Fidelity Frictional Models for MEMS, 441
Blaich, J. D.
  Completely Passive Microwave Tag, 581
Blain, M. G.
  Functionalized Nanoparticles for Sensor Applications, 187
  Micromass Spectrometer-on-a-Chip, 199
Blevins, L. G.
  Soot Formation in Unsteady Diffusion Flames, 444
Bliss, D. E.
  Laser Triggering of Water Switches, 689
BMFC
  See Biomicrofuel Cell
Bochev, P. B.
  Geophysical Subsurface Imaging, 113
Bodette, D. E.
  Reconstruction Algorithm Development, 654
Bogart, G. R.
  Nano-G Accelerometers, 216
Bogart, K. H.
  Advanced Device Structures for Solid-State Lighting, 419
Boggs, P. T.
  Simulations of Chemical/Biological Attacks, 137
  Topology Optimization for Sensor Performance, 160
Boman, E. G.
  Massively Parallel Linear Programming, 140
Bomb (damage), 236
Bond, R. B.
  Prompt Global Response, 486
Bonhomme, F. R.
  Polyoxoniobate Chemistry, 568
Borders, 488
Borek, T. T., III.
  Analytical Techniques for Homeland Defense, 542
Borns, D. J.
  Energy-Systems Analysis Framework and Modeling, 425
  Hydrogen Futures Dynamic Simulation Model, 375
Boslough, M. B. E.
  Climate-Change Effects on International Stability, 38
  Massively Parallel Scalable Atmosphere Model, 145
  Sophisticated-Agent Evolution and Optimization, 116
Bouchard, A. M.
  Biomolecular Decision-Making for Self-Assembly, 828
  Risk-Assessment Metatool, 627
Bourdon, C. J.
  Diagnostics for Rarefied Flows in MEMS, 450
  Flow Control and Mixing in Microfluidic Devices, 749
Bowen, J. M.
  High-Capacity Earth-Penetrator Instrumentation, 312
Boyack, K. W.
  Evaluating Research Using Risk and Impact, 143
Boye, C. A.
  Telescope with MEMS Adaptive Optic, 604
Boyle, T. J.
  Active Photonic Nanostructures, 532
  Decomposition of Contaminants Using Nanoparticles, 514
  Self-Assembled Nanocrystal Micelles for Biolabels, 848
Bradshaw, R. W.
  Biokillers in EDS for Biological-Agent Destruction, 308
Bragg, 218
Brain-wave, 904
Brainard, J. R.
  A Model of Water in the Lower Rio Grande Basin, 423
  Real-Time Water-Quantity/-Quality Monitoring, 335

Author and Title Index

A B C D E F G H I J K L M N O P Q R S T U V W X Y Z

Braithwaite, M. J.
Controlled Motion for a Microfluidic Drop Ejector, 44
Branch, D. W.
Evanescent-Wave Planar Photonic Biosensor, 225
Branch, K. C.
Miniaturized Electronic Steerable-Array SAR, 907
Passive Electronically Steerable Array for Mini-SAR, 227
Brandt, D. J.
Miniature High-Power RF Components, 63
Bray, B. K.
Moving-Target Identification, 247
Bray, O. H.
Automatic Generation of Terrorist Operation Plan, 30
Breakdown, 696
Breckenridge, A.
Sophisticated-Agent Evolution and Optimization, 116
System-of-Systems Modeling and Analysis, 266
Brennan, J. S.
Genetic Engineering in Bioweapons Strains, 594
Toxin Studies Using an Integrated Approach, 866
Brewer, J. D.
Energy-Systems Analysis Framework and Modeling, 425
Brewer, L. N.
Analytical Techniques for Homeland Defense, 542
Briggs, R. D.
GaN 20–100 Watt Amplifiers for Micro-SAR, 222
GaN HEMT High-Power Amplifiers, 207
Brinker, C. J.
Assembly of Electrooptical and Bioactive Materials, 523
Self-Assembled Nanocrystal Micelles for Biolabels, 848
British thermal units (BTU), 408
Brocato, R. W.
Completely Passive Microwave Tag, 581
Miniaturized Electronic Steerable-Array SAR, 907
Receiver for Ultralow-Power Wake-Up, 650
Zero-Power Radio Receiver, 578
Brock, B. C.
Miniaturized Electronic Steerable-Array SAR, 907
Brockmann, J. E.
CBW Cloud Knockdown and Neutralization, 306
Modeling of Contaminant Transport, 586
Brooks, C. F.
Elucidating the Mysteries of Wetting, 57
Brotz, J. K.
A Modular Micromagnetic Accelerometer, 300
Brown, G. S.
Inactivation of Avian Influenza, 429
Brown, M. W.
Full-Earth-Monitoring Sensor MESAWorks, 910
Brown, W. M.
Deciphering the Genetic Regulatory Code, 913
Broyles, R. S.
High-Damage-Threshold Sol-Gel Diffraction Grating, 686
Brozik, S. M.
Biomicrofuel Cell, 473
Biospecific Surfaces to Control Cellular Responses, 757
Bragg Fiber Development, 218
Microfluidic Cellular-Sample Pretreatment, 180
Reversible Antibody Trapping, 540
Transduction Pathways in Affinity-Based Biosensors, 77
Brunner, T. A.
Efficient Implicit Multigroup Radiation Calculations, 694
Bryan, C. R.
Microsensors in Radioactive-Waste Management, 348
Bryson, P. R.
TALON, 480
BTU
See British thermal units
Buchheit, T. E.
Assembly of Microsystems Using Thin Films, 50
Mechanical Testers for Metal Surface Micromachines, 190
Buffleben, G. M.
Biokillers in EDS for Biological-Agent Destruction, 308
Building codes, 874
Bukaty, M. E.
Characterization for Assured HDBT Defeat, 483
Bunker, B. C.
Assembly of Nanomaterials Using Biomolecules, 510
Switchable Materials for (Bio)Microfluidics, 534
Reversible Antibody Trapping, 540
Solution-Based Nanoengineering of Materials, 507
The Basics of Aqueous Nanofluidics, 493
Buried targets, 447
Burns, A. R.
Imaging Self-Organization of Proteins, 93
Signaling Domains in Biological Membranes, 91
Toxin Studies Using an Integrated Approach, 866
Burns, B. L.
Miniaturized Electronic Steerable-Array SAR, 907
Burns, G. R.
Injection Molding of Net-Shape Ceramic Components, 71
Microfabrication with Femtosecond Laser Processing, 41
BW (Biological weapon)
See Biological
Byrne, R. H.
Advanced Mobile Networking Sensing, 249

C
Cable, G. D.
Modeling Signals from Earth-Penetrating Weapons, 606
Calderone, J. J.
MICROFUZE Integration, 302
Cameron, S. M.
Free-Space Electrooptic Sampling, 238
Campbell, D. V.
Miniaturized Electronic Steerable-Array SAR, 907

Author and Title Index

A B C D E F G H I J K L M N O P Q R S T U V W X Y Z

Campbell, J. E.
Multiobjective Discrete Optimization, 794
System-of-Systems Modeling and Analysis, 266
Campbell, P. L.
Critical-Infrastructure System-of-Systems Assessment, 665
Cryptographic Assurance of Execution Correctness, 612
Securing Mobile Code, 365
Campbell, R. B.
Advanced Pulsed-Power Fusion Concepts, 898
Simulations of Intense Petawatt Laser Pulses, 684
Cano, L. A.
Automatic Generation of Terrorist Operation Plan, 30
Canyon, 281
Capillary (valve), 470
Carbon
Adsorbers 786
Composite, 762
Corrosion, 837
Nanotube, 860
See also: Hydrocarbon
Carlson, J. J.
3-D Inspection System for Facility Monitoring, 625
Advancements in Sensing and Perception, 275
TALON, 480
Carr, D. W.
Coupled Nanomechanical Oscillator Arrays, 562
Nanoelectromechanical Oscillators for RF Filtering, 173
Nano-G Accelerometers, 216
Nanomechanical Stochastic Resonators, 825
Carroll, D. E.
Modeling Signals from Earth-Penetrating Weapons, 606
Carter, T.
Dispersive Diffractive Optical Elements for the IR, 659
Meso-/Microoptical System Interface Coupling, 69
Castaneda, J. N.
Microscale Rarefied-Gas Dynamics, 438
Castro, J. P.
Hybrid Optimization Schemes, 131
Catalyst
Heterogeneous, 710
Novel, 368
Catalytic
Combustion, 344
See also: Photocatalytic
Catalyzation, 518
Causey, R. A.
Nuclear Nanobatteries, 414
Cavity, 452
CBW
See Chemical/biological warfare
Ceccio, S. L.
Collateral Damage/Mitigation Assessment, 281
Cederberg, J. G.
Quantum Coherence in Semiconductor Nanostructures, 201
Celina, M. C.
PVDF as a Piezoelectric Film for Space Mirrors, 615
Cell
See Fuel cell
See also: Biomicrofuel cell
Cellular
Machinery, 851
Observatory, 80
Pretreatment, 180
Response, 757
Ceramic
Microsystems, 73
Molding, 71
Ultrahigh-temperature, 598
Cesarano, J., III.
Dielectric Materials for Integrated Microsystems, 545
Injection Molding of Net-Shape Ceramic Components, 71
Revolutionary Systems for Catalytic Combustion, 344
Chael, E. P.
Characterization for Assured HDBT Defeat, 483
Chalcogenide, 185
Chan, J. P.
Alanate-Hydride Fuel-Cell Demonstration Project, 357
Chanchani, R.
An Integrated, Stacked System-on-a-Chip, 196
Full-Earth-Monitoring Sensor MESAWorks, 910
Miniaturized Electronic Steerable-Array SAR, 907
Receiver for Ultralow-Power Wake-Up, 650
Chandler, D. W.
Cellular Observatory, 80
Chandross, M. E.
Protection of Critical Assets, 823
Modeling Local Chemistry, 505
Channel
Resistance, 696
See also: Multichannel
Chaotic (communication), 264
Chaplya, P. M.
Inflatable Antenna with Adaptive Actuators, 669
PVDF as a Piezoelectric Film for Space Mirrors, 615
Smart Material for Structural Health Monitoring, 455
Chavez, B. D.
Advanced Manufacturing Using Rapid Prototyping, 777
Rapid-Prototyping High-Density Circuitry, 55
Chavez, L. M.
Optimal Allocation of Terrorist Countermeasures, 393

Author and Title Index

A B C D E F G H I J K L M N O P Q R S T U V W X Y Z

Chemical
Aerosol, 639
Bioagent, 820
Biological warfare, 304
Cross-linking, 863
Micropreconcentrator, 607
Microsensor, 786
Nanoparticles, 351
Plume, 241
Remote sensing, 211
Signature, 178
Spectrometer, 233
Transport simulation, 137
Water, 338
See also: Electrochemical
See also: Photochemical
See also: Thermochemical
Chen, H. Y.
IP Storage: A Performance and Security Study, 126
Chen, J. H.
Microengine for Advanced Power Generation, 164
Chen, K. S.
Proton-Exchange-Membrane Fuel Cells, 390
Chenoweth Creel, B.
Agent-Based Autonomic Logistics Simulation Model, 286
Chhabildas, L. C.
Hypervelocity Impact-Generated Flash, 258
Chhabra, S.
Biomicrofuel Cell, 473
Molecular Machines Involved in Membrane Signaling, 88
Chiesa, M. L.
Penetrator Reliability Investigation, 157
Chimeric, 576
Chinn, D. A.
Nuclear Nanobatteries, 414
Polymer Electronic Devices and Materials, 643
Chip
System-on-a-chip, 196
See also: Multichip
Chirica, G. S.
Pathogens on Nanoengineered Surfaces, 107
Chow, W. W.
Active Photonic-Crystal Devices, 183
Quantum Coherence in Semiconductor Nanostructures, 201
Christensen, J. B.
Prompt Global Response, 486
Chu, D. D.
Full-Earth-Monitoring Sensor MESAWorks, 910
Meso-/Microoptical System Interface Coupling, 69
Miniaturized Electronic Steerable-Array SAR, 907
Circuit
Cryptography, 647
High-density, 55
Photonic logic, 209
Simulator, 129
Clark, B. F.
Adaptive Optics and Phase-Diversity Imaging, 618
Cleavable, 516
Clem, P. G.
Active Photonic Nanostructures, 532
Active Photonic-Crystal Devices, 183
Dielectric Materials for Integrated Microsystems, 545
Microflame-Based Detector for Gas Sensing, 270
Clemens, R. C.
Novel and Robust Environmental Sensing Devices, 743
Clement, J. J.
Vulnerability Assessment of Microelectronics, 639
Climate, 38
Cloud
Finder, 268
Knockdown, 306
Cluster
Coupled, 119
Simulation performance, 151
Coating
Metallic, 765
Security, 584
Superhydrophobic, 884
Tribological, 46
Cochrane, K. R.
Electrical Conductivity of Metal Alloys, 691
Code
Building, 874
Genetic, 913
Mobile, 365
Simulation, 123
Coffee, S.
Agile, Microsystems-Enabled Receiver, 572
Cogeneration, 398
Cognition, 476
Cognitive (network), 840
Coherence, 201
Coilgun, 295
Coker, E. N.
Catalysts for Hydrogen Fuel-Cell Applications, 368
Cole, E. I., Jr.
Vulnerability Assessment of Microelectronics, 639
Cole, P. J.
Gel-Based Components for Nuclear Weapons, 67
Novel Gel-Based Technology for Sensors, 560
Soft-Matter Nanolayer Superlattices, 497
Coleman, P. D.
Nonlethal Technologies for the War on Terrorism, 273
Collateral (damage), 281
Collective
Behavior, 562
Phenomena, 505
Collins, C. R.
Featureless Spread-Spectrum Waveform Design, 629
Collins, M. J.
Agent-Based Autonomic Logistics Simulation Model, 286
Collis, S. S.
Sensitivities for Large-Scale Simulation Codes, 123
Colmenero, C. C.
Full-Earth-Monitoring Sensor MESAWorks, 910

Author and Title Index

A B C D E F G H I J K L M N O P Q R S T U V W X Y Z

Combustion
Catalytic, 344
Microexternal engine, 715
Command, 650
Communication
Chaotic, 264
Crisis management, 255
Internet, 649
Optical, 632
Compliant
Actuators, 193
Membranes, 725
Composite
Assembly, 523
Carbon nanotube, 762
Nanocrystal-polymer, 812
Concentration
Bioaerosol, 591
Scalar, 756
Conditioning, 895
Conductivity
Metal alloys, 691
See also: Superconductivity
Conductor, 411
Confidentiality, 612
Configurable
Simulation, 151
See also: Reconfigurable
Conflict, 671
Conformal, 46
Conrad, G. N.
Automatic Generation of Terrorist Operation Plan, 30
Consumption (resources), 421
Container (storage), 733
Contamination
Decomposition, 514
Restoration, 383
Transport, 586
Water, 360
See also: Decontamination
Continuum
Atomistic simulation, 434
Inelastic solids, 916
Conversion (power), 362
Cook, B. K.
Direct Simulation of Solid-Fluid Systems, 707
Security Coatings for Multichip Modules, 584
Cook, M. A.
Agent-Based Control of Distributed Infrastructures, 377
Coolant, 798
Cooper, J. A.
The Effectiveness of Management Strategies, 427
Cooper, S. P.
Natural-Gas Production Problems, 332
Cooperative (water management), 423
Cornelius, C. J.
Biomicrofuel Cell, 473
Proton-Exchange Materials for Fuel Cells, 354
Proton-Exchange-Membrane Fuel Cells, 390
Corrosion, 837
Corwin, A. D.
High-Fidelity Frictional Models for MEMS, 441
Costin, L. S.
Characterization for Assured HDBT Defeat, 483
Modeling of Rock Penetration, 704
Countermeasure, 393
Counterterrorism, 255
Couple
Algorithm, 119
Atomistic simulation, 434
Oscillator array, 562
Microoptical interface, 69
Covan, J. M.
The Effectiveness of Management Strategies, 427
Cowan, W. D.
Adaptive Optics for Weapon and Space Applications, 681
MOSFET–MEMS Integration, 203
Telescope with MEMS Adaptive Optic, 604
Cowgill, D. F.
Nuclear Nanobatteries, 414
Cox, D. D.
Featureless Spread-Spectrum Waveform Design, 629
Cox, J. V.
Predictive Accelerated Aging of Microsystems, 730
Crack
Interfacial, 723
Micromechanical, 552
Craft, D. C.
Distributed Detection for Unattended Ground Sensors, 262
Craft, R. L.
Automatic Generation of Terrorist Operation Plan, 30
Optimal Allocation of Terrorist Countermeasures, 393
Crawford, M. H.
Advanced Device Structures for Solid-State Lighting, 419
Creighton, J. R.
Outstanding Challenges for AlGaInN MOCVD, 817
Criscenti, L. J.
Solution-Based Nanoengineering of Materials, 507
Crisis (management), 255
Critical
Assets, 823
See also: Infrastructure
See also: Supercritical
Crooker, P. J.
Biokillers in EDS for Biological-Agent Destruction, 308
Cross, K.
Outstanding Challenges for AlGaInN MOCVD, 817
Crowell, J. A.
Nuclear Nanobatteries, 414
Crown, K. K.
Patterning Quantum-Dot Arrays, 853

Author and Title Index

A B C D E F G H I J K L M N O P Q R S T U V W X Y Z

Crozier, P. S.
Molecular Dynamics of Membrane Proteins, 871
Substructured Multibody Molecular Dynamics, 149
Cruz, D.
Micromass Spectrometer-on-a-Chip, 199
Cryptography
Assurance, 612
Circuit, 647
Randomness, 679
Crystal
Photonic, 183
See also: Nanocrystal
Cummings, E. B.
A Capillary Valve for Microfluidic Systems, 470
Bioaerosol Microseparations-Based Detectors, 591
Continuous-Flow Detector for Pathogen Identification, 319
Preconcentrator and Sensor for Waterborne Pathogens, 111
Superhydrophobic Surface Coatings for Microfluidics, 884
Topology Optimization for Sensor Performance, 160
Cuneo, M. E.
Advanced Pulsed-Power Fusion Concepts, 898
Cuppoletti, C. M.
Advanced Neutron Monitors for JTA, 745
Current (measuring device), 468
Curro, J. G.
Pathogens on Nanoengineered Surfaces, 107
Solution Behavior of PEO, 846
Custer, R. P.
Intrusion Detection for Wireless Networks, 403
Vulnerability Analysis for SCADA, 678
CW (Chemical weapon)
See Chemical
Cybersecurity, 858
Cycle
Direct, 362
Thermochemical, 405
Cygan, R. T.
Microbe-Exuded Polymers, 837
Solution-Based Nanoengineering of Materials, 507
Cylinder (array), 756
Czaplewski, D. A.
Controlled Motion for a Microfluidic Drop Ejector, 44
Coupled Nanomechanical Oscillator Arrays, 562
Nanoelectromechanical Oscillators for RF Filtering, 173

D

Dagel, D. J.
Telescope with MEMS Adaptive Optic, 604
Daily, M. R.
Meso-/Microoptical System Interface Coupling, 69
Damage
Bomb, 236
Collateral, 281
Threshold, 686
Dargaville, T.
PVDF as a Piezoelectric Film for Space Mirrors, 615
Data
Model, 671
Moving-target, 247
Davalos, R. V.
Picoliter Vessels for Trace Biotoxin Detection, 565
Davidson, D. L.
Deployable Object Tracker for NMD Flights, 317
Davidson, G. S.
Evaluating Research Using Risk and Impact, 143
Optical Sectioning, 554
Reverse-Engineering Biological Networks, 84
Davidson, P. A., Jr.
Advancements in Sensing and Perception, 275
Davis, C. E.
Optimization in Critical-Infrastructure Systems, 372
Davis, D. W.
Rapid-Prototyping High-Density Circuitry, 55
Davis, J. Z.
Controlled-Environment Agriculture, 36
Davis, J.
Embeddable Shock Physics Sensors, 698
Study of Liquid-Solid Transition in Tin, 530
Day, D. M.
Geophysical Subsurface Imaging, 113
De Boer, M. P.
Assembly of Nanomaterials Using Biomolecules, 510
High-Fidelity Frictional Models for MEMS, 441
Superhard and Metallic Coatings for MEMS, 765
Mechanical Testers for Metal Surface Micromachines, 190
De Marquis, V. K.
Dielectric Materials for Integrated Microsystems, 545
Decomposition, 514
Decontamination
Avian influenza, 429
Infectious agent, 380
Deconvolution, 554
Dederman, D. A.
Characterization for Assured HDBT Defeat, 483
Dedrick, D. E.
Alanate-Hydride Fuel-Cell Demonstration Project, 357
Defeat
Biological weapon, 278
Hard target, 243
HDBT, 483
Defend
Borders, 488
Homeland, 542
Deformation
Friction, 537
Interferometric, 461
Testing, 809
Deland, S. M.
TALON, 480
Delivery (reagent), 178
Delnick, F. M.
Molten Salt-Based Growth of Bulk GaN and InN, 918

Author and Title Index

A B C D E F G H I J K L M N O P Q R S T U V W X Y Z

Demmie, P. N.
  Hybrid Optimization Schemes, 131
Dense (plasma), 684
Density
  Circuitry, 55
  High-energy, 545
Dentinger, P. M.
  Picoliter Vessels for Trace Biotoxin Detection, 565
Deoxyribonucleic acid (DNA), 853
Deployable, 317
Deposition
  LIGA micromachines, 501
  Modeling, 154
  Tribological coating, 46
Depoy, J. M.
  Critical-Infrastructure System-of-Systems Assessment, 665
Desalination, 341
Design
  Biospecific surfaces, 757
  Lighting, 419
  Magnetic properties, 747
  Penetrator, 157
  Sensing, 275
  Superlattices, 497
  Waveform, 629
Desjarlais, M. P.
  Electrical Conductivity of Metal Alloys, 691
Desonier, L. M.
  Real-Time Water-Quantity/-Quality Monitoring, 335
Desorption, 518
Destruction (biological-agent), 308
Detection
  Bioaerosol (microseparation), 591
  Bioaerosol (optical), 640
  Bioaerosol (smart), 802
  Biological (bead trapping), 326
  Biological (cellular machinery), 851
  Biological (chimeric), 576
  Biological (protein microarray), 96
  Biotoxin (lipid), 774
  Biotoxin (trace), 565
  Gas, 270
  Ground, 262
  Headspace gas, 348
  Intrusion (wireless), 403
  Ion-mobility spectrometer, 233
  Microflame, 270
  Nanophotonic (motion), 216
  Pathogen, 319
  Quantum coherence, 201
  Virus, 844
Diagnostic
  MEMS (extraction), 800
  MEMS (flows), 450
Diantonio, C. B.
  Injection Molding of Net-Shape Ceramic Components, 71
Dibble, D. C.
  Alloys for LIGA Micromachines, 501
Dickrell, D. J.
  Dielectrics with Controlled Leakage, 213
Dielectric
  Controlled leakage, 213
  High-energy-density, 545
Diesel, 344
Diffraction
  Infrared, 659
  Sol-gel, 686
Diffusion flames
  JP-8, 805
  Unsteady, 444
Digital, 636
Dirk, S. M.
  Functionalized Nanoparticles for Sensor Applications, 187
  Polymer Electronic Devices and Materials, 643
  Real-Time Sensors for Water-Contamination, 360
Disbonding, 723
Disch, E. A.
  Nonlinear Optical Detection of Aerosol Agents, 640
Discrete (optimization), 794
Dispersal
  Optics, 659
  Urban canyons, 281
Dissipation, 562
Distortion, 604
Distributed
  Detection, 262
  Infrastructure, 377
Distribution (water), 893
Diversity, 618
Dixon, D. A.
  Full-Earth-Monitoring Sensor MESAWorks, 910
Djordjevich, D. D.
  Understanding Communication in Crisis Management, 255
DNA
  See Deoxyribonucleic acid
Dodd, P. E.
  Full-Earth-Monitoring Sensor MESAWorks, 910
Doerry, A. W.
  Miniaturized Electronic Steerable-Array SAR, 907
  Novel Processing for Miniaturized SAR, 292
Dolan, P. L.
  Biomicrofuel Cell, 473
Domain
  Signaling, 91
  Time, 335
Domeier, L. A.
  Picoliter Vessels for Trace Biotoxin Detection, 565
  Thermally Cleavable Surfactants, 516
Dormancy, 730
Doser, A. B.
  Distributed Detection for Unattended Ground Sensors, 262
Doty, F. P.
  Nuclear Nanobatteries, 414
  Polymer Electronic Devices and Materials, 643
Doyle, B. L.
  Analytical Techniques for Homeland Defense, 542

Author and Title Index

A B C D E F G H I J K L M N O P Q R S T U V W X Y Z

Draelos, T. J.
Joint Authentication/Encryption, 596
Small Circuits for Cryptography, 647
Draper, B. L.
Radiation-Hard Nonvolatile Memories, 185
MOSFET–MEMS Integration, 203
Dreike, P. L.
Modeling Signals from Earth-Penetrating Weapons, 606
Drennen, T. E.
Hydrogen Futures Dynamic Simulation Model, 375
Drescher, S.
Event Locations from Space-Based Sensors, 663
Dubbert, D. F.
Miniaturized Electronic Steerable-Array SAR, 907
Novel Processing for Miniaturized SAR, 292
Dubicka, I.
Automatic Generation of Terrorist Operation Plan, 30
Dudley, P. A.
Miniaturized Electronic Steerable-Array SAR, 907
Duesterhaus, M. A.
Predictive Accelerated Aging of Microsystems, 730
Dugger, M. T.
Atomic Layer Deposition of Tribological Coatings, 46
Dielectrics with Controlled Leakage, 213
Predictive Accelerated Aging of Microsystems, 730
Dunkel, W. R.
Advanced Neutron Monitors for JTA, 745
Dunlap, S. K.
Full-Earth-Monitoring Sensor MESAWorks, 910
Microoptical Radar Facial-Recognition Project, 673
Dunn, R. G.
Semiconductor Quantum Nanostructures, 220
Superconductivity in Electron-Hole Bilayers, 168
Durability, 792
Durgin, N. A.
Property-Based Testing for Cybersecurity Assurance, 858
Dyck, C. W.
Agile, Microsystems-Enabled Receiver, 572
Dielectrics with Controlled Leakage, 213
Mechanical Testers for Metal Surface Micromachines, 190
Microelectromechanical Systems Antennas, 622
Miniature High-Power RF Components, 63
Miniaturized Electronic Steerable-Array SAR, 907
Nanoelectromechanical Oscillators for RF Filtering, 173
Passive Electronically Steerable Array for Mini-SAR, 227
Silicon-Based RF MEMS Components, 171

E
Earth
Penetrating (high-capacity), 312
Penetrating (nuclear), 606
Sensor, 907
Simulator, 878
Eddy, 781
EDM
See Electrical discharge machining
EDS
See Explosive destruction system
Einfeld, W.
Functionalized Nanoelectrode Arrays, 338
Real-Time Sensors for Water-Contamination, 360
Eisenbies, S. K.
Biomicrofuel Cell, 473
Ejector, 44
Elastomer, 528
Elbring, G. J.
Assessing Bomb Damage to Underground Facilities, 236
Characterization for Assured HDBT Defeat, 483
Eldridge, J. M.
Cryptographic Assurance of Execution Correctness, 612
Electrical
Conductivity, 691
Discharge machining, 713
Propulsion arrays, 396
See also: Dielectric
See also: Piezoelectric
Electricity, 398
Electrochemical
Alloys, 501
Switchable materials, 534
Electrodynamic, 220
Electromagnetic
Remote mapping, 238
Security, 235
Electron (hole), 168
Electronic
Membrane signaling, 77
Polymer, 643
Steerable array (miniature), 907
Steerable array (passive), 227
Structure methods, 119
See also: Microelectronic
See also: Optoelectronic
Electrooptic
Assembly, 523
Sampling, 238
Elevation 636
El-Kady, I. F.
Active Photonic-Crystal Devices, 183
Extraordinary Optical Transmission, 652
Ellis, A. R.
TPV Energy Scavenging for Hypervelocity Vehicles, 329
Ellis, C. R.
Bioaerosol Microseparations-Based Detectors, 591
Picoliter Vessels for Trace Biotoxin Detection, 565
Ellis, L. J.
TALON, 480
Ellison, J. A.
Microsystems for Chemical Signature, 178
EM
See Electromagnetic
Embed
Cylinder array, 754
Sensor, 698
Embodiment, 116

Author and Title Index

A B C D E F G H I J K L M N O P Q R S T U V W X Y Z

Emerson, J. A.
Meso-/Microoptical System Interface Coupling, 69
Prompt Global Response, 486
Emission, 396
Emit, 238
Encryption
Authentication, 596
Photonic, 784
Energetic (materials), 701
Energy
Excitation, 503
High-density, 545
Modeling, 425
Scavenging, 329
See also: Fuel cell
Engine
Microexternal, 715
See also: Microengine
Engler, B. P.
A Modular Micromagnetic Accelerometer, 300
Characterization for Assured HDBT Defeat, 483
Ennis, M. L.
A Model of Water in the Lower Rio Grande Basin, 423
Enos, D. G.
Vulnerability of Micromechanicals to Cracking, 552
Enrichment (bioaerosol), 802
Environment
Ad Hoc, 289
Complex, 304
Controlled, 36
Cracking, 552
GPS-denied, 631
High-gravity, 800
Mapping, 298
Quantification, 520
Sensing device, 743
Weaklinks, 735
Ephemeral (streams), 335
Eras, K.
Nuclear-Safety Weaklinks, 735
ESD
See Environmental sensing devices
Esherick, P.
Bragg Fiber Development, 218
Evanescent-Wave Planar Photonic Biosensor, 225
Transduction Pathways in Affinity-Based Biosensors, 77
Estimation, 663
Etching, 154
Etzkin, J. L.
Vulnerability Assessment of Microelectronics, 639
EUVL
See Extreme ultraviolet lithography
Evanescent, 225
Evans, G. H.
Modeling of Contaminant Transport, 586
Evans, L.
Water Desalination, 341
Evolution
Scalar concentration, 756
Sophisticated-agent, 116
Surface modeling, 154
Evolutionary (complexity), 823
Exchange (proton)
Materials, 354
Modeling, 390
Excitation, 503
Exothermic, 50
Explosive
Destruction system, 308
Detection, 233
Hard-target defeat, 243
Ignition criteria, 886
Micropreconcentrators, 607
Thermobaric, 283
Extraction, 800
Extreme ultraviolet lithography (EUVL), 438
Exuded, 837
Eye (safe), 268

F
Fabrication
Solid-state lighting, 419
See also: Microfabrication
Facial (recognition), 673
Fan, H.
Self-Assembled Nanocrystal Micelles for Biolabels, 848
Farkas, B. D.
Augmented Cognition, 476
Farnsworth, A. V., Jr.
Modeling Signals from Earth-Penetrating Weapons, 606
Radiation-/Geometry-Driven Jets, 33
Farrow, M.
Switchable Materials for (Bio)Microfluidics, 534
Faulon, J. M.
Model-Building Codes for Membrane Proteins, 874
Reverse-Engineering Biological Networks, 84
Fault, 119
Featureless, 629
Feddema, J. T.
Advanced Mobile Networking Sensing, 249
Tracking Slow-Moving Objects, 631
Feedback (adaptive force), 310
FEEP
See Field-emission electric propulsion
Feibelman, P. J.
The Basics of Aqueous Nanofluidics, 493
Feldner, L. M.
Microelectromechanical Systems Antennas, 622
Felix, J. A.
Full-Earth-Monitoring Sensor MESAWorks, 910
Femtosecond
Transceiver, 238
See also: Laser
Ferrizz, R. M.
Revolutionary Systems for Catalytic Combustion, 344

Author and Title Index

A B C D E F G H I J K L M N O P Q R S T U V W X Y Z

Fiber (Bragg), 218
Fidelity
  Frictional models, 441
  See also: Multifidelity
Fiechtner, G. J.
  Continuous-Flow Detector for Pathogen Identification, 319
Field-emission electric propulsion (FEEP), 396
Film
  Lipid, 99
  Multilayer thin, 50
  Nanomagnetic, 760
  Piezoelectric, 615
Filter
  Radio frequency, 173
  Transmitter, 740
Finch, N. S.
  Novel and Robust Environmental Sensing Devices, 743
Finnegan, P.
  Agile, Microsystems-Enabled Receiver, 572
Fireset, 740
Fischer, A. J.
  Advanced Device Structures for Solid-State Lighting, 419
Fischer, T. A.
  An Integrated, Stacked System-on-a-Chip, 196
  Full-Earth-Monitoring Sensor MESAWorks, 910
Flame
  Diffusion (JP-8), 805
  Diffusion (unsteady), 444
  See also: Microflame
Flash, 258
Fleming, D. D.
  Full-Earth-Monitoring Sensor MESAWorks, 910
Fleming, J. G.
  Active Photonic-Crystal Devices, 183
  Active Photonic Nanostructures, 532
  Bragg Fiber Development, 218
  Micromass Spectrometer-on-a-Chip, 199
  Silicon-Based RF MEMS Components, 171
  TPV Energy Scavenging for Hypervelocity Vehicles, 329
  Vibration-Based Miniature Power Generator, 633
Flemming, J. H.
  Biomicrofuel Cell, 473
Flexible
  Network, 621
  Tooling, 720
Flight (missile), 317
Flores, R. S.
  Radiation-Hard Nonvolatile Memories, 185
  Full-Earth-Monitoring Sensor MESAWorks, 910
  Miniaturized Electronic Steerable-Array SAR, 907
Floro, J. A.
  GeSi–Strained Nanostructure Self-Assembly, 431
  Nanostructured Materials for Directed Transport, 503
Flow
  Continuous, 319
  Control, 749
  High rate, 326
  Rarefied, 450
  Turbulent, 781
Flu (avian), 429
Fluid
  Direct simulation, 707
  Geomaterials, 447
  See also: Microfluidic
  See also: Nanofluidic
Fluorescence, 554
Fogler, R. J.
  Characterization for Assured HDBT Defeat, 483
  Moving-Target Identification, 247
Foiles, S. M.
  Mechanical Testers for Metal Surface Micromachines, 190
  Study of Liquid-Solid Transition in Tin, 530
  Transition Metals in LIGA Nickel, 558
Follstaedt, D. M.
  Direct Single-Ion Machining of Nanopores, 789
  GaN HEMT High-Power Amplifiers, 207
  Mechanical Testers for Metal Surface Micromachines, 190
Foltynowicz, R. J.
  Atmospheric Propagation of Terahertz Radiation, 661
  Continuous-Wave Intersubband Terahertz Sources, 176
  Ultrafast-Current Transient Measuring Device, 468
Force
  Feedback, 310
  Surface, 493
Ford, B. K.
  Optical Sectioning, 554
  Reconstruction Algorithm Development, 654
Forman, M. A.
  Miniature Transmitter Filter for JTA, 740
Formation
  Particulate, 805
  Soot, 444
  See also: Deformation
Forsythe, J. C.
  Augmented Cognition, 476
  Understanding Communication in Crisis Management, 255
Fossum, A. F.
  Modeling of Fracture in Geomaterials, 447
  Modeling of Rock Penetration, 704
Foulk, J. W., III.
  Modeling Carbon Nanotube–Reinforced Composites, 762
Fourier, 233
Fracture
  Geomaterials, 447
  Nanoscale testing, 809
Fragmentation, 447

Author and Title Index

A B C D E F G H I J K L M N O P Q R S T U V W X Y Z

Franco, R. J.
Characterization for Assured HDBT Defeat, 483
Frankel, D. J.
Signaling Domains in Biological Membranes, 91
Franklin, J. W.
Novel and Robust Environmental Sensing Devices, 743
Frederick, S. K.
Vibration-Based Miniature Power Generator, 633
Frequency
Cavity scarring, 452
Microscopy, 80
Radio frequency MEMS, 622
Rejection, 856
Frew, D. J.
Characterization for Assured HDBT Defeat, 483
Modeling of Rock Penetration, 704
Friction
Micromachine, 772
Model (deformation), 537
Model (MEMS), 441
Friedmann, T. A.
Coupled Nanomechanical Oscillator Arrays, 562
Dielectrics with Controlled Leakage, 213
Direct Single-Ion Machining of Nanopores, 789
Embeddable Shock Physics Sensors, 698
Nanoelectromechanical Oscillators for RF Filtering, 173
Frink, L. J. D.
Interaction of Proteins with Lipid Films, 99
Modeling Biomembranes, 82
Transduction Pathways in Affinity-Based Biosensors, 77
Frischknecht, A. L.
Modeling Biomembranes, 82
Solution Behavior of PEO, 846
Fruetel, J. A.
Pathogens on Nanoengineered Surfaces, 107
Fuel cell
Alanate-hydride, 357
Biomicro, 473
Catalysts, 368
Ion conductors, 411
Microreformers, 882
Proton exchange (materials), 354
Proton exchange (modeling), 390
Reactor, 398
Fujii, J. M.
Climate-Change Effects on International Stability, 38
Fujimoto, C. H.
Biomicrofuel Cell, 473
Proton-Exchange Materials for Fuel Cells, 354
Fuller, C. T.
Continuous-Wave Intersubband Terahertz Sources, 176
Fusion
Pulsed power, 898
Ultrahigh gain, 843
Fuze
Hard target, 243
MEMS diagnostic, 800
See also: Microfuze

G

Galambos, P. C.
Adaptive-Force-Feedback Surface Control, 310
Characterization of Surface-Micromachined Pumps, 890
Controlled Motion for a Microfluidic Drop Ejector, 44
Magnetophoretic Bead Trapping, 326
Microfluidic Cellular-Sample Pretreatment, 180
Gallegos, D. P.
Augmented Cognition, 476
TALON, 480
Gallis, M. A.
Diagnostics for Rarefied Flows in MEMS, 450
Microscale Rarefied-Gas Dynamics, 438
Gallium nitride
Amplifiers (HEMT), 207
Amplifiers (micro-SAR), 222
Growth, 918
Galloway, J. A.
Full-Earth-Monitoring Sensor MESAWorks, 910
Prompt Global Response, 486
GaN
See Gallium nitride
Ganter, J. H.
Augmented Cognition, 476
Ganti, A.
Power-Combining for Power Amplifiers, 657
Gantt, R. W.
Rapid Detection of Biothreat Agents, 851
Gao, H.
Microsensors in Radioactive-Waste Management, 348
Garasi, C. J.
Advanced Pulsed-Power Fusion Concepts, 898
Garcia, E. J.
Miniature Transmitter Filter for JTA, 740
Gardner, D. R.
Characterization for Assured HDBT Defeat, 483
Gardner, M. J.
Human/System Interactions in Systems-of-Systems, 260
Garikipati, K. K.
Continuum Models for Inelasticity in Solids, 916
Garino, T. J.
H2 Generation from Thermochemical Cycles, 405
"Tunable" Ion Conductors for Fuel Cells, 411
Garrison, J. C.
Content-Based Video and Image Indexing System, 588
Gartling, D. K.
Modeling of Contaminant Transport, 586
Gas
Headspace, 348
Natural (monitoring), 408
Natural (production), 332
Power conversion, 362
Rarefied, 438
Sensing, 270
Gaudioso, J. M.
Toxin Studies Using An Integrated Approach, 866
Geib, K. M.
Leaky-Mode VCSELs for Photonic Logic Circuits, 209

Author and Title Index

A B C D E F G H I J K L M N O P Q R S T U V W X Y Z

Gel
Diffraction grating, 686
Nuclear weapons, 67
Sensor, 560
Generator, 633
Genetic
Engineering, 594
Regulatory code, 913
Geomaterial, 447
Geometry, 33
Geophysical, 113
Georectification, 636
GeSi
See Germanium silicon
Germanium silicon (GeSi)
Growth, 752
Self-assembly, 431
Ghormley, R. C., II.
Receiver for Ultralow-Power Wake-Up, 650
Gilchrist, R. T.
Characterization for Assured HDBT Defeat, 483
Gilkey, J. C.
Deployable Object Tracker for NMD Flights, 317
Gill, D. D.
Next-Generation Spindles for Micromilling, 60
Giunta, A. A.
Hybrid Optimization Schemes, 131
Micromagnetic Suspension, 121
Givler, R. C.
Controlled Motion for a Microfluidic Drop Ejector, 44
Gladwell, T. S.
Automated Visual Direction of Mobile Manipulation, 231
Glass, S. J.
Ceramics for Hypersonic Vehicle Applications, 598
Nuclear-Safety Weaklinks, 735
Vulnerability of Micromechanicals to Cracking, 552
Global
Positioning satellite, 631
Response, 486
Goeke, R. S.
Atomic Layer Deposition of Tribological Coatings, 46
Goldsmith, C. L.
Agile, Microsystems-Enabled Receiver, 572
Goldsmith, S. Y.
Analysis of Multichannel Internet Communication, 649
Golling, D. F.
Biokillers in EDS for Biological-Agent Destruction, 308
Gonzales, M. A.
Hybrid Optimization Schemes, 131
Gonzales, M. E.
Characterization for Assured HDBT Defeat, 483
Goods, S. H.
Transition Metals in LIGA Nickel, 558
Vulnerability of Micromechanicals to Cracking, 552
Gorby, A. D.
Diagnostics for Rarefied Flows in MEMS, 450
Gourley, P. L.
Nanofluidic Devices for Detection of Viruses, 844
Light for Probing Mitochondrial Membranes, 888
GPS
See Global positioning satellite
Graph (theory), 249
Grasser, T. W.
Microscale Rarefied-Gas Dynamics, 438
Noncontact Surface Thermometry for Microsystems, 458
Grating, 686
Gray, G. A.
Hybrid Optimization Schemes, 131
Green, J. M.
Vulnerability Assessment of Microelectronics, 639
Grest, G. S.
Elucidating the Mysteries of Wetting, 57
Proton-Exchange Materials for Fuel Cells, 354
Griffith, M. L.
Microfabrication with Femtosecond Laser Processing, 41
Griffiths, S. K.
Fundamentals of Nanofluidics, 463
Grillet, A. M.
Elucidating the Mysteries of Wetting, 57
Injection Molding of Net-Shape Ceramic Components, 71
Grine, A. J.
Telescope with MEMS Adaptive Optic, 604
Gross, K. J.
Alanate-Hydride Fuel-Cell Demonstration Project, 357
Catalyzation of Complex-Hydride Reactions, 518
New Hydrogen-Storage Material: Metal-N-H System, 401
Grossetete, G. D.
Telescope with MEMS Adaptive Optic, 604
Grotbeck, C. L.
Dispersive Diffractive Optical Elements for the IR, 659
Reconstruction Algorithm Development, 654
Ground
Sensors, 262
See also: Underground
Growth
Biologically nanostructured, 465
Gallium nitride, 918
Germanium silicon, 752
Nanolithography, 549
Grubelich, M. C.
Assembly of Microsystems Using Thin Films, 50
Radiation-/Geometry-Driven Jets, 33
Guidance, 227
Guo, J.
Evanescent-Wave Planar Photonic Biosensor, 225
Microfabrication with Femtosecond Laser Processing, 41
Microoptical Gyroscope, 205
Gupta, V. P.
Controlled-Environment Agriculture, 36
Gurule, E. J.
Completely Passive Microwave Tag, 581
Zero-Power Radio Receiver, 578
Gyroscope, 205

Author and Title Index

A B C D E F G H I J K L M N O P Q R S T U V W X Y Z

H
H_2
See Hydrogen
Haaland, D. M.
Optical Sectioning, 554
Protein Microarrays for Biowarfare-Agent Detection, 96
Reverse-Engineering Biological Networks, 84
Habbit, R. D., Jr.
Microoptical Radar Facial-Recognition Project, 673
Hadi, M. Z.
Dynamics of Membrane Proteins and Receptors, 863
Hadley, G. R.
Bragg Fiber Development, 218
Extraordinary Optical Transmission, 652
Leaky-Mode VCSELs for Photonic Logic Circuits, 209
Hafenrichter, E. S.
Explosive Ignition Criteria for Miniaturized Devices, 886
Halbleib, L. L.
Injection Molding of Net-Shape Ceramic Components, 71
Hall, A. C.
Nuclear-Safety Weaklinks, 735
Security Coatings for Multichip Modules, 584
Hall, C. A.
Radiation-/Geometry-Driven Jets, 33
Hammerand, D. C.
Modeling Carbon Nanotube–Reinforced Composites, 762
Hampton, J. W.
TALON, 480
Hance, B. G.
Microsystems for Chemical Signature, 178
Hansche, B. D.
Interferometric Deformation Measurements, 461
Hanson, D. L.
Advanced Pulsed-Power Fusion Concepts, 898
Hard and Deeply Buried Targets
Characterization, 483
Fracture modeling, 447
Hardy, R. D.
Modeling of Rock Penetration, 704
Harmony, D. W.
Moving-Target Identification, 247
Haroldsen, B. L.
Microengine for Advanced Power Generation, 164
Harris, K. W.
EM Interactions with Systems to Enhance Security, 235
Harris, M. F.
Microfabrication with Femtosecond Laser Processing, 41
Harris, S. M.
MICROFUZE Integration, 302
Hart, B. E.
Human/System Interactions in Systems-of-Systems, 260
Hart, D. H.
Simulating Human Behavior for National Security, 321
Hart, W. E.
Agent-Based Autonomic Logistics Simulation Model, 286
Deciphering the Genetic Regulatory Code, 913
Micromagnetic Suspension, 121
Simulations of Chemical/Biological Attacks, 137
Hascall, A. G.
Heterogeneous Catalysts, 710
Haschke, G. B.
Automatic-Target-Recognition Algorithms, 676
Featureless Spread-Spectrum Waveform Design, 629
Haskins, W. E.
Dynamics of Membrane Proteins and Receptors, 863
Hassan, B.
Adaptive-Force-Feedback Surface Control, 310
Havenstrite, K.
Polymeric Materials for Sensing of Bioagents, 820
Hawley, M. F.
Understanding Communication in Crisis Management, 255
Hayden, C. C.
Cellular Observatory, 80
HDBT
See Hard and Deeply Buried Targets
Headley, T. J.
Compliant Thermomechanical MEMS Actuators, 193
Headspace, 348
Health (monitoring), 455
Heaphy, R.
Penetrator Reliability Investigation, 157
Hearne, S. J.
Assembly of Nanomaterials Using Biomolecules, 510
Mechanical Testers for Metal Surface Micromachines, 190
Heermann, P. D.
Augmented Cognition, 476
Heine, D. R.
Elucidating the Mysteries of Wetting, 57
Hekmaty, M. A.
Microengine for Advanced Power Generation, 164
Heller, E. J.
Completely Passive Microwave Tag, 581
Zero-Power Radio Receiver, 578
Helmick, P. H.
Conversion Systems for Nuclear-Power Reactors, 362
Hemmert, K. S.
High-Performance Processing Architecture, 147
HEMT (high electron mobility transistors)
See Transistors
Hendrickson, G. A.
Data-Driven Dynamic Models of Conflict, 671
Henry, W. D.
Risk-Assessment Metatool, 627
Hermetic, 779
Herr, A. E.
Polymeric Materials for Sensing of Bioagents, 820
Protein Microarrays for Biowarfare-Agent Detection, 96
Herrin, J. M.
Natural-Gas Production Problems, 332
Hertel, E. S., Jr.
Evolution of Near-Surface Scalar Concentrations, 756
Periodic Disturbances of Unknown Frequency, 856
Hetmaniuk, U.
Poroelastic-Wave Propagation on the Earth Simulator, 878
Hewson, J. C.
Computational Studies of JP-8 Diffusion Flames, 805

Author and Title Index

A B C D E F G H I J K L M N O P Q R S T U V W X Y Z

Hibbs, M.
Proton-Exchange Materials for Fuel Cells, 354
Hickman, R. J.
Embeddable Shock Physics Sensors, 698
Hickner, M. A.
Biomicrofuel Cell, 473
Proton-Exchange-Membrane Fuel Cells, 390
Hickox, C. E., Jr.
Modeling of Contaminant Transport, 586
Hietala, V. M.
Nonlethal Technologies for the War on Terrorism, 273
Optical Communications, 632
Highley, A. M.
Membrane-Protein Recognition and Signaling, 103
Top-Down Structural Studies, 869
Hill, T. A.
Radiation-Hard Nonvolatile Memories, 185
Hillaire, R. G.
A Systems Approach to Defending Our Borders, 488
Hindman, V. C.
TALON, 480
Hinkebein, T. E.
Water Desalination, 341
Hirschfeld, D. A.
Security Coatings for Multichip Modules, 584
Ho, C. K.
Macro-/Meso-/Microsystems Integration in LTCC, 73
Microsensors in Radioactive-Waste Management, 348
Holcomb, D. J.
Modeling of Rock Penetration, 704
Holdych, D. J.
Self-Assembly of Biological Nanostructured Materials, 465
Hole (electron), 168
Holland, J. F.
Natural-Gas Production Problems, 332
Hollenshead, J. T.
Characterization for Assured HDBT Defeat, 483
Holm, E. A.
Advanced Packaging Technology for Microsystems, 525
Holman, R. M.
Featureless Spread-Spectrum Waveform Design, 629
Holzrichter, M. W.
Novel Processing for Miniaturized SAR, 292
Homeland defense
Analytical, 542
Chem/bio attack, 137
Hong, J.
Dynamics of Membrane Proteins and Receptors, 863
Top-Down Structural Studies, 869
Hoover, E. R.
Characterization for Assured HDBT Defeat, 483
Hopkins, M. M.
Magnetophoretic Bead Trapping, 326
Hosking, F. M.
Assembly of Microsystems Using Thin Films, 50
Hostetler, S.
Characterization for Assured HDBT Defeat, 483
Hough, P. D.
Hybrid Optimization Schemes, 131
Penetrator Reliability Investigation, 157
Understanding Communication in Crisis Management, 255
Houston, J. E.
Reversible Antibody Trapping, 540
Superhydrophobic Surface Coatings for Microfluidics, 884
Howard, M. S.
Prompt Global Response, 486
Howell, S. W.
Functionalized Nanoparticles for Sensor Applications, 187
Howle, V. E.
Massively Parallel Linear Programming, 140
Hoyt, J. J.
Atomistic-Continuum Simulation, 434
Hsia, A. H.
MOSFET–MEMS Integration, 203
Hsu, J. W. P.
Nanolithography-Directed Materials Growth, 549
Huber, D. L.
Magnetostrictive Elastomers, 528
Pathogens on Nanoengineered Surfaces, 107
Reversible Antibody Trapping, 540
The Basics of Aqueous Nanofluidics, 493
Huber, R. J.
MOSFET–MEMS Integration, 203
Hudson, H. G.
Ray Model of High-Frequency Cavity Scarring, 452
Hughes, R. C.
Microsensors in Radioactive-Waste Management, 348
Transduction Pathways in Affinity-Based Biosensors, 77
Human
Aversive conditioning, 895
Simulating behavior, 321
System-of-systems, 260
Hunka, D. E.
Ion-Mobility Spectrometer/Mass Spectrometer, 610
Hunt, T. W.
Model-Building Codes for Membrane Proteins, 874
Hutchinson, S. A.
A Parallel Circuit Simulator for Cell Biology, 129
Hybrid
Level-set/particle, 154
Optimization scheme, 131
Hydride
Absorption/desorption, 518
Alanate, 357
Hydrocarbon, 398
Hydrogen
Catalysts, 368
Futures, 375
Membranes, 405
Storage, 401
Hypersonic, 598
Hyperspectral, 554
Hypervelocity
Impact, 258
Vehicles, 329

Author and Title Index

A B C D E F G H I J K L M N O P Q R S T U V W X Y Z

I

Identification
- Algorithm, 262
- Chemical plumes, 241
- Chemicals in water, 338
- Explosives, 233
- Gas source, 281
- Molecular machines, 88
- Moving target, 247
- Pathogen, 319
- Subsurface imaging, 113

Ignition, 886
Image
- Fluorescence, 554
- Geophysical, 113
- Georectification, 636
- Indexing, 588
- Phase-diversity, 618
- Proteins, 93
- Signaling domains, 91
- Spectral, 654
- Thermal, 676
- *See also*: Nanoimaging

Immune
- Bioterrorism, 84
- Systems control, 245

Impact
- Hypervelocity, 258
- Indicators, 143
- Technology, 304
- Water-savings, 36

In't Veld, P. J.
- Self-Assembly of Biological Nanostructured Materials, 465

Inactivation, 429
Independent (MEMS), 414
Indexing, 588
Indium nitride, 918
Industry (automotive), 712
Inelasticity, 916
Infectious, 380
Inflatable, 669
Influenza, 429
Infrared
- Chemical plumes, 241
- Optical elements, 659

Infrastructure
- Distributed, 377
- Flexible networks, 621
- Optimization/simulation, 372
- System-of-system, 665

Infusion, 720
Ingersoll, D.
- Biomicrofuel Cell, 473
- Development of Microreformers for Fuel Cells, 882
- Molten Salt-Based Growth of Bulk GaN and InN, 918
- Proton-Exchange Materials for Fuel Cells, 354
- Proton-Exchange-Membrane Fuel Cells, 390

Initiation, 723
Injection, 71
InN
- *See* Indium nitride

Insch, K. W.
- Cryptographic Assurance of Execution Correctness, 612

Inspection, 625
Instrumentation
- Brain-wave monitoring, 904
- Earth penetrator, 312

Integrated
- Biophysical/structural biology, 866
- Coatings, 765
- Macro-/Meso/Microsystem, 73
- Metal surface micromachines, 190
- Microarray, 576
- Microsystems, 779
- MOSFET-MEMS, 203
- Photonics, 183
- System-on-a-chip, 196

Intelligence (mini-SAR), 227
Intelligent
- Augmented cognition, 476
- Interaction control, 52

Interaction
- Electromagnetic, 235
- Human/system, 260
- Interaction control, 52
- Multifidelity model, 131
- Peptide-membrane, 808
- Protein-lipid, 99
- Protein-protein, 901
- Support-active site, 710
- Surface, 434
- *See also:* Nanointeraction

Interactive (modeling), 834
Interceptor, 278
Interface
- Coupling, 69
- Friction, 772
- Geophysical, 113
- Metal-to-plastic, 792

Interfacial (cracks), 723
Interferometric, 461
International (stability), 38
Internet
- Multichannel communication, 649
- Protocol (storage), 126

Interphase, 493
Intersubband, 176
Intrusion, 403
Inverse
- Error control, 913
- Micellar systhesis, 701

Inversion, 137

Author and Title Index

A B C D E F G H I J K L M N O P Q R S T U V W X Y Z

Ion
Conductors, 411
Machining, 789
Spectrometer (explosives), 233
Spectrometer (mass), 610
IP
See Internet protocol
IR
See Infrared
ISR
See Intelligence

J
Jacobsen, R. B.
Dynamics of Membrane Proteins and Receptors, 863
Jacobson, S. H.
Multiobjective Discrete Optimization, 794
James, C. D.
Magnetophoretic Bead Trapping, 326
Microfluidic Cellular-Sample Pretreatment, 180
James, S. C.
Management after an Intentional Contamination Event, 383
Jamison, G. M.
Photocontrol of Nanointeractions in Microsystems, 499
Thermally Cleavable Surfactants, 516
Janssen, C. L.
Simulation with Configurable Auxiliary Devices, 151
Jarek, R. L.
Catalysts for Hydrogen Fuel-Cell Applications, 368
Jenkins, M. W.
MOSFET–MEMS Integration, 203
Nanomagnetic Films, 760
Jennison, D. R.
Decomposition of Contaminants Using Nanoparticles, 514
Jensen, K. A.
Soot Formation in Unsteady Diffusion Flames, 444
Jensen, R. P.
Modeling of Fracture in Geomaterials, 447
Jets (radiation-driven), 33
Jiang, L.
Photocontrol of Nanointeractions in Microsystems, 499
Johnson, D. L.
Laser Triggering of Water Switches, 689
Johnson, M. M.
Understanding Communication in Crisis Management, 255
Johnston, A. M.
Deciphering the Genetic Regulatory Code, 913
Johnston, G. A.
Augmented Musculature Device, 826
Joint test assemblies (JTA)
Neutron monitors, 745
Transmitter filter, 740
Jokiel, B., Jr.
A Modular Micromagnetic Accelerometer, 300
Advanced Packaging Technology for Optical Firesets, 738
Controlled Motion for a Microfluidic Drop Ejector, 44
Full-Earth-Monitoring Sensor MESAWorks, 910
Miniaturized Electronic Steerable-Array SAR, 907
Predictive Accelerated Aging of Microsystems, 730
Vibration-Based Miniature Power Generator, 633
Jones, D. A.
Optimization in Critical-Infrastructure Systems, 372
Jones, G. D.
Optical Sectioning, 554
PVDF as a Piezoelectric Film for Space Mirrors, 615
Jones, H. D.
Optical Sectioning, 554
Jones, J. F.
Intelligent Interaction Control for Metrology, 52
Jones, R. E.
Atomistic-Continuum Simulation, 434
High-Fidelity Frictional Models for MEMS, 441
Modeling of Friction-Induced Deformation, 537
Jones, S. A.
Energy-Systems Analysis Framework and Modeling, 425
Hydrogen Futures Dynamic Simulation Model, 375
Jordan, S. E.
Dynamic Vulnerability Assessment, 667
Robotic Planning for Physical-Security Analysis, 601
Jorgensen, C. R.
Sophisticated-Agent Evolution and Optimization, 116
Jorgenson, R. E.
Model for Channel Resistance in Water Breakdown, 696
Ray Model of High-Frequency Cavity Scarring, 452
JP-8 (aviation fuel), 805
JTA
See Joint test assemblies
Jung, R. A.
Optimal Allocation of Terrorist Countermeasures, 393

K
Kaneshige, M. J.
Weaponization of Thermobaric Explosives, 283
Kanouff, M. P.
A Capillary Valve for Microfluidic Systems, 470
Alanate-Hydride Fuel-Cell Demonstration Project, 357
Bioaerosol Microseparations-Based Detectors, 591
Kao, G. K.
Multiobjective Discrete Optimization, 794
Karas, T. H.
Energy-Systems Analysis Framework and Modeling, 425
Karpetis, A. N.
Microengine for Advanced Power Generation, 164
Kast, B. A.
Automated Visual Direction of Mobile Manipulation, 231
Miniature High-Power RF Components, 63

Author and Title Index

A B C D E F G H I J K L M N O P Q R S T U V W X Y Z

Kay, R. R.
Full-Earth-Monitoring Sensor MESAWorks, 910
Kaye, R. J.
Coilgun Technology Demonstration Test-Bed, 295
Kearney, S. P.
Diagnostics for Rarefied Flows in MEMS, 450
Noncontact Surface Thermometry for Microsystems, 458
Soot Formation in Unsteady Diffusion Flames, 444
Keeler, B. N.
Coupled Nanomechanical Oscillator Arrays, 562
Nanoelectromechanical Oscillators for RF Filtering, 173
Nano-G Accelerometers, 216
Keenan, M. R.
Analytical Techniques for Homeland Defense, 542
Quantification of Environments within Micropackages, 520
Keese, D. L.
Adaptive-Force-Feedback Surface Control, 310
Keller, J. O.
Hydrogen Futures Dynamic Simulation Model, 375
Kellogg, R. A.
A Modular Micromagnetic Accelerometer, 300
Vibration-Based Miniature Power Generator, 633
Kelly, J. J.
Alloys for LIGA Micromachines, 501
Modeling of Friction-Induced Deformation, 537
Transition Metals in LIGA Nickel, 558
Vulnerability of Micromechanicals to Cracking, 552
Kelly, M. J.
Biomicrofuel Cell, 473
Catalysts for Hydrogen Fuel-Cell Applications, 368
Functionalized Nanoelectrode Arrays, 338
Kelton, J. M.
Rapid-Prototyping High-Density Circuitry, 55
Kemme, S. A.
Dispersive Diffractive Optical Elements for the IR, 659
Extraordinary Optical Transmission, 652
Meso-/Microoptical System Interface Coupling, 69
Kemp, R. A.
Beyond Nanoparticles, 351
Biomicrofuel Cell, 473
Decomposition of Contaminants Using Nanoparticles, 514
Heterogeneous Catalysts, 710
Kent, M. S.
Interaction of Proteins with Lipid Films, 99
Microbe-Exuded Polymers, 837
Quantification of Environments within Micropackages, 520
Pathogens on Nanoengineered Surfaces, 107
Kern, J. P.
Image Georectification, 636
Kholwadwala, D. K.
Adaptive-Force-Feedback Surface Control, 310
Augmented Musculature Device, 826
Kiffer, D. D.
Featureless Spread-Spectrum Waveform Design, 629
Kill
Assessment, 606
See also: Biokiller

Kilman, D.
Advanced Mobile Networking Sensing, 249
Intrusion Detection for Wireless Networks, 403
Systems Analysis of Networked Sensors, 314
Kim, J. K.
Microoptical Gyroscope, 205
Kim, T. J.
Novel Processing for Miniaturized SAR, 292
Kimmer, C. J.
Atomistic-Continuum Simulation, 434
Kinney, R. D.
Microoptical Gyroscope, 205
Kipp, M. E.
Assessing Bomb Damage to Underground Facilities, 236
Kirby, B. J.
High-Throughput Microfluidic Integrated Microarray, 576
Klebanoff, L. E.
Energy-Systems Analysis Framework and Modeling, 425
Klein, P. A.
Atomistic-Continuum Simulation, 434
Self-Assembly of Biological Nanostructured Materials, 465
Kliner, D. A.
Identification of Chemical Plumes, 241
Smart Detectors of Enrichment of Bioaerosols, 802
Klody, K. A.
Advanced Packaging Technology for Optical Firesets, 738
Predictive Accelerated Aging of Microsystems, 730
Knockdown, 306
Knorovsky, G. A.
Advanced Packaging Technology for Microsystems, 525
Knudson, M. D.
Embeddable Shock Physics Sensors, 698
Ko, T. H.
3-D Inspection System for Facility Monitoring, 625
Agent-Based Modeling Terrorist Recruitment, 28
Kobos, P. H.
Assessing Factors that Influence Water Consumption, 421
Data-Driven Dynamic Models of Conflict, 671
Hydrogen Futures Dynamic Simulation Model, 375
Koch, M. W.
Automatic-Target-Recognition Algorithms, 676
Deployable Object Tracker for NMD Flights, 317
Microoptical Radar Facial-Recognition Project, 673
Moving-Target Identification, 247
Kolda, T. G.
Robust Large-Scale Parallel Nonlinear Solvers, 134
Koleske, D. D.
Advanced Device Structures for Solid-State Lighting, 419
GaN HEMT High-Power Amplifiers, 207
Outstanding Challenges for AlGaInN MOCVD, 817
Kottenstette, R.
Micropreconcentrators for Surety, 607
Kotula, P. G.
Analytical Techniques for Homeland Defense, 542
Ceramics for Hypersonic Vehicle Applications, 598
Mechanical Testers for Metal Surface Micromachines, 190

Author and Title Index

A B C D E F G H I J K L M N O P Q R S T U V W X Y Z

Kotulski, J. D.
Ray Model of High-Frequency Cavity Scarring, 452
Kozlowski, D. M.
Intelligent Interaction Control for Metrology, 52
Kraus, G. M.
Agile, Microsystems-Enabled Receiver, 572
Passive Electronically Steerable Array for Mini-SAR, 227
Kravitz, S. H.
Biomicrofuel Cell, 473
MICROFUZE Integration, 302
Silicon Field-Emission Electric Propulsion Arrays, 396
Krumel, L. J.
Full-Earth-Monitoring Sensor MESAWorks, 910
Krumhansl, J. L.
Molten Salt-Based Growth of Bulk GaN and InN, 918
System-Dynamics Toolbox for Water Planning, 386
Water Desalination, 341
Kruppa, G. H.
Top-Down Structural Studies, 869
Ku-band, 222
Kulp, T. J.
Identification of Chemical Plumes, 241
Kuntz, D. W.
Ceramics for Hypersonic Vehicle Applications, 598
Prompt Global Response, 486
Kurtz, S. R.
GaN HEMT High-Power Amplifiers, 207
Quantum Coherence in Semiconductor Nanostructures, 201
Kuswa, G. W.
Energy-Systems Analysis Framework and Modeling, 425

L

Ladd, M. D.
TALON, 480
Laguna, G. A.
Remote 3-D Mapping of Unknown Environments, 298
Lamppa, K. P.
Full-Earth-Monitoring Sensor MESAWorks, 910
Landaker, W. J.
Full-Earth-Monitoring Sensor MESAWorks, 910
Lane, P.
Dynamics of Membrane Proteins and Receptors, 863
Genetic Engineering in Bioweapons Strains, 594
Toxin Studies Using an Integrated Approach, 866
Lane, T. W.
Genetic Engineering in Bioweapons Strains, 594
Rapid Detection of Biothreat Agents, 851
Lanes, C. E.
Extraordinary Optical Transmission, 652
Lanes, K. R.
Full-Earth-Monitoring Sensor MESAWorks, 910
Langley, C. C.
Top-Down Structural Studies, 869
Lanzone, A. J.
Mobile-Node Authentication, 289
Lapizco-Encinas, B. H.
Preconcentrator and Sensor for Waterborne Pathogens, 111
Larsen, L. E.
Biophysics of BW-Warhead Defeat, 278
Larson, K. W.
Augmented Cognition, 476
Laser
Femtosecond, 640
Microfabrication, 41
Petawatt, 684
Quantum coherence, 201
Triggering, 689
Lawrence, R. J.
Hypervelocity Impact-Generated Flash, 258
Radiation-/Geometry-Driven Jets, 33
Lawton, C. R.
Agent-Based Autonomic Logistics Simulation Model, 286
Layer
Atomic, 46
Surface (atmospheric), 756
See also: Bilayer
See also: Multilayer
See also: Nanolayer
Layne, D. A.
Biokillers in EDS for Biological-Agent Destruction, 308
Leak
Dielectrics, 213
Vertical-cavity surface-emitting laser, 209
Leatherwood, M. J.
Full-Earth-Monitoring Sensor MESAWorks, 910
Leavell, M. D.
Dynamics of Membrane Proteins and Receptors, 863
Membrane-Protein Recognition and Signaling, 103
LED
See Light emitting diode
Lee, E. J.
Intrusion Detection for Wireless Networks, 403
Vulnerability Analysis for SCADA, 678
Lee, E. S.
Picoliter Vessels for Trace Biotoxin Detection, 565
Lee, M.
Semiconductor Quantum Nanostructures, 220
Lehoucq, R. B.
Substructured Multibody Molecular Dynamics, 149
Lehr, J. M.
Model for Channel Resistance in Water Breakdown, 696
Leininger, M. L.
Algorithms for Electronic Structure Methods, 119
Simulation with Configurable Auxiliary Devices, 151
Lemp, T.
A Modular Micromagnetic Accelerometer, 300
Agile, Microsystems-Enabled Receiver, 572
Intelligent Interaction Control for Metrology, 52
Nonlethal Technologies for the War on Terrorism, 273
Novel and Robust Environmental Sensing Devices, 743
Vibration-Based Miniature Power Generator, 633
Lenard, R. X.
Silicon Field-Emission Electric Propulsion Arrays, 396

Author and Title Index

A B C D E F G H I J K L M N O P Q R S T U V W X Y Z

Lenhart, J. L.
Gel-Based Components for Nuclear Weapons, 67
Novel Gel-Based Technology for Sensors, 560
Lennox, R. C.
Intelligent Interaction Control for Metrology, 52
Leslie, S. J.
Receiver for Ultralow-Power Wake-Up, 650
Leung, K.
The Basics of Aqueous Nanofluidics, 493
Lewis, C. L.
Advanced Mobile Networking Sensing, 249
Remote 3-D Mapping of Unknown Environments, 298
Lewis, D. E.
Adaptive Optics for Weapon and Space Applications, 681
Lewis, P. R.
Microflame-Based Detector for Gas Sensing, 270
Micropreconcentrators for Surety, 607
Real-Time Sensors for Water-Contamination, 360
Liang, J. Z.
Infrastructural Development for Flexible Networks, 621
Libersky, J. A.
Assessing Bomb Damage to Underground Facilities, 236
Lidar, 241
LIGA (lithography, electroforming, and molding)
See Lithography
Light
Emitting diode, 812
Powered, 830
Quantum squeezed, 888
Solid-state, 419
Structured, 275
Tunable, 417
Light, Y. K.
Dynamics of Membrane Proteins and Receptors, 863
Genetic Engineering in Bioweapons Strains, 594
Lilly, M. P.
Superconductivity in Electron-Hole Bilayers, 168
Semiconductor Quantum Nanostructures, 220
Lin, S.
Active Photonic Nanostructures, 532
Photocontrol of Nanointeractions in Microsystems, 499
Linear
Programming, 140
Scaling, 119
See also: Nonlinear
Link, H. E.
Agent-Based Control of Distributed Infrastructures, 377
Securing Mobile Code, 365
Lipid
Film, 99
Membranes, 717
Microarray, 774
See also: Phospholipid
Liquid-solid, 530
Lithography
Micromachines, 501
Nickel, 558
Transmitter filter, 740
Ultraviolet, 438
See also: Nanolithography
Little, C. Q.
3-D Inspection System for Facility Monitoring, 625
Microoptical Radar Facial-Recognition Project, 673
Liu, J.
Solution-Based Nanoengineering of Materials, 507
Liu, S.
Microengine for Advanced Power Generation, 164
Live (pathogens), 111
Lloyd, J. A.
Optimization in Critical-Infrastructure Systems, 372
Location (estimation), 663
Locke, D. C.
Infrastructural Development for Flexible Networks, 621
Lockhart, R. R.
MEMS/Fuze Diagnostic in High-G Environments, 800
Loehman, R. E.
Advanced Fuel-Cell Reactor, 398
Ceramics for Hypersonic Vehicle Applications, 598
Prompt Global Response, 486
Logic
All-optical, 784
Photonic circuits, 209
Logistics, 286
Long, K. R.
Simulations of Chemical/Biological Attacks, 137
Topology Optimization for Sensor Performance, 160
Long, T. M.
Photocontrol of Nanointeractions in Microsystems, 499
Lopez, M. R.
Advanced Pulsed-Power Fusion Concepts, 898
Lorenz, J. C.
Natural-Gas Production Problems, 332
Lovelady, Z. L.
Infrastructural Development for Flexible Networks, 621
LTCC (Low-temperature co-fired ceramic)
See Ceramic
Lucero, D. A.
CBW Cloud Knockdown and Neutralization, 306
Lucero, F. L.
Polymer Electronic Devices and Materials, 643
Luck, D. L.
Controlled Motion for a Microfluidic Drop Ejector, 44
Luk, T. S.
Free-Space Electrooptic Sampling, 238
Microfabrication with Femtosecond Laser Processing, 41
Nonlinear Optical Detection of Aerosol Agents, 640
Luminous, 812
Lundstrom, J. M.
EM Interactions with Systems to Enhance Security, 235

Author and Title Index

A B C D E F G H I J K L M N O P Q R S T U V W X Y Z

Luo, W.
New Hydrogen-Storage Material: Metal-N-H System, 401
Luong, A. K.
Cellular Observatory, 80
Lutz, A. E.
Energy-Systems Analysis Framework and Modeling, 425
Hydrogen Futures Dynamic Simulation Model, 375
Lyo, S. K.
Quantum Coherence in Semiconductor Nanostructures, 201
Semiconductor Quantum Nanostructures, 220

M
Macha, J. M.
Prompt Global Response, 486
Machine
Molecular, 88
See also: Micromachine
Machinery (cellular), 851
Machining, 789
Maclin, R. F.
Analysis of Multichannel Internet Communication, 649
MacNab, S.
Biophysics of BW-Warhead Defeat, 278
Magnetic
Nanoparticles, 747
See also: Electomagnetic
See also: Micromagnetic
See also: Nanomagnetic
Magnetophoretic, 326
Magnetostrictive, 528
Maharrey, S. P.
Nanoscale Energetic Materials, 701
Maish, A. B.
Automated Visual Direction of Mobile Manipulation, 231
Majzoub, E. H.
Catalyzation of Complex-Hydride Reactions, 518
Malczynski, L. A.
Assessing Factors that Influence Water Consumption, 421
Data-Driven Dynamic Models of Conflict, 671
System-Dynamics Toolbox for Water Planning, 386
Malone, K. T.
Automatic-Target-Recognition Algorithms, 676
TALON, 480
Mangan, M. A.
Continuous-Wave Intersubband Terahertz Sources, 176
Manginell, M. M.
Biomicrofuel Cell, 473
Microfluidic Cellular-Sample Pretreatment, 180
Manginell, R. P.
Assembly of Nanomaterials Using Biomolecules, 510
BTU Monitoring Device for Natural-Gas Monitoring, 408
Microflame-Based Detector for Gas Sensing, 270
Micropreconcentrators for Surety, 607
Microsystems for Chemical Signature, 178
Real-Time Sensors for Water-Contamination, 360
Reversible Antibody Trapping, 540
Mani, S. S.
Bragg Fiber Development, 218
Controlled Motion for a Microfluidic Drop Ejector, 44
Microfluidic Cellular-Sample Pretreatment, 180
MOSFET–MEMS Integration, 203
Telescope with MEMS Adaptive Optic, 604
Mann, G. A.
Coilgun Technology Demonstration Test-Bed, 295
Manufacturing
Automotive industry, 712
Gel-based components, 67
Mesoscale, 63
Rapid prototyping, 777
Thermomechanical, 754
Mapping
Electromagnetic fields, 238
Unknown environments, 298
Mar, A.
Compact Terahertz Sources, 252
Multikilovolt X-Ray Sources for Material Studies, 323
Marin, E. B.
Modeling of Friction-Induced Deformation, 537
Marquis, E.
Transition Metals in LIGA Nickel, 558
Martin, J. E.
Magnetostrictive Elastomers, 528
Nanocrystal-Polymer Composites for LEDs, 812
Martin, J. W.
Inflatable Antenna with Adaptive Actuators, 669
PVDF as a Piezoelectric Film for Space Mirrors, 615
Martin, S. B.
Reverse-Engineering Biological Networks, 84
Martinez, M. J.
Modeling of Contaminant Transport, 586
Martinez, R. F.
Augmented Cognition, 476
Martinez, T. L.
High-Capacity Earth-Penetrator Instrumentation, 312
MEMS/Fuze Diagnostic in High-G Environments, 800
Martinez-Canales, M. L.
Penetrator Reliability Investigation, 157
Martino, A.
Reverse-Engineering Biological Networks, 84
Mascarenhas, N.
Advanced Neutron Monitors for JTA, 745
Massad, J. E.
Inflatable Antenna with Adaptive Actuators, 669
Mattsson, T. K.
Electrical Conductivity of Metal Alloys, 691
Matzke, C. M.
Assembly of Nanomaterials Using Biomolecules, 510
May, E. E.
A Parallel Circuit Simulator for Cell Biology, 129
Deciphering the Genetic Regulatory Code, 913
Reverse-Engineering Biological Networks, 84
Mayer, T. M.
Atomic Layer Deposition of Tribological Coatings, 46
Rapid Prototyping to the Nanometer Scale, 66

Author and Title Index

A B C D E F G H I J K L M N O P Q R S T U V W X Y Z

McBrayer, J. D.
Radiation-Hard Nonvolatile Memories, 185
McCarty, K. F.
Decomposition of Contaminants Using Nanoparticles, 514
McCormick, F. B.
Microoptical Gyroscope, 205
McDaniel, A. H.
Advanced Fuel-Cell Reactor, 398
McDaniel, B.
Systems Analysis of Networked Sensors, 314
McDonald, M. J.
A Systems Approach to Defending Our Borders, 488
Human/System Interactions in Systems-of-Systems, 260
Operations in Complex Environments, 304
McElhanon, J. R.
Soft-Matter Nanolayer Superlattices, 497
Thermally Cleavable Surfactants, 516
McEntire, R.
Hard-Target-Defeat High-G-Tolerant Fuze, 243
MICROFUZE Integration, 302
McFarland, R.
Radiation-Hard Nonvolatile Memories, 185
McGrath, L. K.
Biological Terrorism to Water-Distribution Systems, 893
McGraw, G. J.
Preconcentrator and Sensor for Waterborne Pathogens, 111
McKenna, S. A.
Simulations of Chemical/Biological Attacks, 137
McNamara, L. A.
Assessing Factors that Influence Water Consumption, 421
Climate-Change Effects on International Stability, 38
Data-Driven Dynamic Models of Conflict, 671
McWherter-Payne, M. A.
Prompt Global Response, 486
Mechanical
Solid-fluid, 447
Testers, 190
Weaklinks, 735
See also: Microelectromechanical
See also: Micromechanical
See also: Nanoelectromechanical
See also: Nanomechanical
See also: Thermomechanical
Medforth, C. J.
Imaging Self-Organization of Proteins, 93
Light-Powered Nanovehicle Propulsion, 830
Medlin, D. L.
Transition Metals in LIGA Nickel, 558
Mehlhorn, T. A.
Advanced Pulsed-Power Fusion Concepts, 898
Hypervelocity Impact-Generated Flash, 258
Radiation-/Geometry-Driven Jets, 33
Membrane
Compliant, 725
Fuel cells, 390
Hydrogen generation, 405
Lipid, 717
Mitochondrial, 888
Nanotube arrays, 860
Phospholipids, 808
Proteins (dynamics), 871
Proteins (model-building), 874
Proteins (nanotagging), 93
Proteins (recognition), 103
Proteins (structure and dynamics), 863
Signaling (domains), 91
Signaling (molecular machines), 88
Signaling (transduction pathways), 77
See also: Biomembrane
Memory (radiation-hard), 185
MEMS
See Microelectromechanical systems
Mendenhall, F. T.
TALON, 480
Mercier, J. A.
Image Georectification, 636
Merkle, P. B.
Measures in Human Aversive Classical Conditioning, 895
MESAWorks, 910
Metal
Coatings, 765
Electrical conductivity, 270
Hydrogen storage, 401
LIGA nickel, 558
Micromachines, 190
Organic chemical vapor deposition, 817
Organic semiconductor field-effect transistor, 203
Plastic interfaces, 792
Transition metal catalyzation, 518
Metatool, 627
Metrology, 52
Micelle
Biolabels, 848
Energetic materials, 701
Michael, J. R.
Advanced Packaging Technology for Microsystems, 525
Modeling of Friction-Induced Deformation, 537
Michalski, J. T.
Mobile-Node Authentication, 289
Microarray
Lipid, 774
Microfluidic, 576
Protein, 96
Microbe, 837

Author and Title Index

A B C D E F G H I J K L M N O P Q R S T U V W X Y Z

Microelectromechanical systems (MEMS)
- Actuators, 193
- Coating (metallic), 765
- Coating (superhydrophobic), 884
- Frictional models, 441
- Fuze diagnostic, 800
- Hermetic packaging, 779
- Metalorganic semiconductor transistor, 203
- Microphone, 725
- Nuclear nanobatteries, 414
- Radio frequency (antennas), 622
- Radio frequency (components), 171
- Rarefied gas (diagnostics), 450
- Rarefied gas (dynamics), 438
- Surface coatings, 884
- Ultralightweight telescope, 604

Microelectronic (vulnerability), 639
Microengine, 164
Microexternal (engine), 715
Microfabrication
- Laser, 41
- Natural-gas monitor, 408

Microflame, 270
Microfluidic
- Capillary valve, 470
- Coatings, 884
- Drop ejector, 44
- Flow control, 749
- Microarray, 576
- Sample pretreatment, 180
- Switchable materials, 534

MICROFUZE, 302
Micromachine
- Friction, 772
- LIGA, 501
- Metal surface, 190
- Pumps, 890

Micromagnetic
- Accelerometer, 300
- Suspension, 121

Micromass, 199
Micromechanical, 552
Micromilling, 60
Microoptical
- Gyroscope, 205
- Interface coupling, 69
- Radar, 673

Micropackage, 520
Microphone, 725
Micropreconcentrator, 607
Microreformer, 882
Microscopy
- Cellular observatory, 80
- Scanning-tunneling, 752

Microsensor
- Adsorbers, 786
- Waste management, 348

Microseparation, 591
Microstructure, 537
Microsystem
- Aging, 730
- Ceramic, 73
- Chemical signature, 178
- Dielectric materials, 545
- Packaging (hermetic), 779
- Packaging (joining), 525
- Photocontrol, 499
- Receiver, 572
- Thermometry, 458
- Thin films, 50

Microwave
- Quantum nanostructures, 220
- Tag, 581

Military, 681
Miller, D. P.
- Automatic Generation of Terrorist Operation Plan, 30
- Human/System Interactions in Systems-of-Systems, 260

Miller, J. E.
- Advanced Fuel-Cell Reactor, 398
- Beyond Nanoparticles, 351
- Catalysts for Hydrogen Fuel-Cell Applications, 368
- Revolutionary Systems for Catalytic Combustion, 344
- Water Desalination, 341

Miller, R. D.
- Joint Authentication/Encryption, 596
- Small Circuits for Cryptography, 647

Miniature
- Ignition criteria, 886
- Power generator, 633
- Radio frequency, 63
- Sensor, 417
- Synthetic aperture radar (miniature), 227
- Synthetic aperture radar (passive), 907
- Synthetic aperture radar (processing), 292
- Spectrometer, 233
- Transmitter filter, 740

Minton, M. A.
- Optimal Allocation of Terrorist Countermeasures, 393

Mirror, 615
Missert, N. A.
- GaN HEMT High-Power Amplifiers, 207

Mitchell, C. C.
- Outstanding Challenges for AlGaInN MOCVD, 817

Mitchell, J. A.
- Novel and Robust Environmental Sensing Devices, 743

Mitchell, R. T.
- Meso-/Microoptical System Interface Coupling, 69

Mitochondrial, 888
Mittas, A.
- MEMS/Fuze Diagnostic in High-G Environments, 800

Mobile
- Code, 365
- Manipulation, 231
- Network, 249
- Node authentication, 289

Author and Title Index

A B C D E F G H I J K L M N O P Q R S T U V W X Y Z

Mobility (ion)
See Spectrometer
MOCVD
See Metal-organic chemical vapor deposition
Mode
Leaky, 209
Multiplexing, 292
Model
Atmosphere, 145
Biomembranes, 82
Carbon nanotube composites, 762
Cavity scarring, 452
Channel resistance, 696
Conflict, 671
Contaminant transport, 586
Deformation, 537
Energy systems, 425
Fracture, 447
Friction, 441
Fuel cells, 390
Hydrogen futures, 375
Image georectification, 636
Kill assessment, 606
Local chemistry, 505
Logistics, 286
Natural-gas production, 332
Optimization scheme, 131
Proteins, 874
Rio Grande, 423
Rock penetration, 704
Solids, 916
Surface evolution, 154
System-of-systems, 266
Terrorist recruitment, 28
Turbulent flow, 781
Water (consumption), 421
Water (quality), 834
Water (value), 832
Modine, N. A.
Coupled Nanomechanical Oscillator Arrays, 562
Modeling Local Chemistry, 505
Quantum Coherence in Semiconductor Nanostructures, 201
Modular, 300
Modules, 584
Molding, 71
Molecular
Machines, 88
Membrane proteins, 871
Multibody dynamics, 149
Peptide, 808
See also: Biomolecular
Molina, L. L.
Secure Chaotic Communications, 264
Molten, 918
Mondy, L. A.
Injection Molding of Net-Shape Ceramic Components, 71
Monitor
Brain-wave, 904
Ephemeral streams, 335
Facility, 625
Full-earth, 910
Health, 455
Natural gas, 408
Neutron, 745
Montague, S.
Vulnerability Assessment of Microelectronics, 639
Montano, M. A.
Zero-Power Radio Receiver, 578
Moody, N. R.
Atomic Layer Deposition of Tribological Coatings, 46
Modeling of Friction-Induced Deformation, 537
Nanoscale Testing of Deformation and Fracture, 809
Moore, D. L.
Water Desalination, 341
Moore, J. T.
Beyond Nanoparticles, 351
Moore, R. H.
Injection Molding of Net-Shape Ceramic Components, 71
Moorman, M.
BTU Monitoring Device for Natural-Gas Monitoring, 408
Microflame-Based Detector for Gas Sensing, 270
Micropreconcentrators for Surety, 607
MOR
See Microoptical radar
Morales, A. M.
Soft-Matter Nanolayer Superlattices, 497
Microengine for Advanced Power Generation, 164
Miniature Transmitter Filter for JTA, 740
Morse, D. H.
Decomposition of Contaminants Using Nanoparticles, 514
MOSFET
See Metal organic semiconductor field-effect transistor
Motion
Compensation, 292
Controlled, 44
Detection, 216
Mou, S.
Continuous-Wave Intersubband Terahertz Sources, 176
Moving
Target identification, 247
Tracking, 631
Mowery, D. M.
PVDF as a Piezoelectric Film for Space Mirrors, 615
Mowry, C. D.
Real-Time Sensors for Water-Contamination, 360
Moy, T. D.
Agent-Based Modeling Terrorist Recruitment, 28
Moya, M. M.
Event Locations from Space-Based Sensors, 663
Moylan, S. P.
High-Speed Micro-EDM, 713

Author and Title Index

A B C D E F G H I J K L M N O P Q R S T U V W X Y Z

mTalon
Accelerometer, 300
See also: TALON
Muguira, M. R.
3-D Inspection System for Facility Monitoring, 625
Content-Based Video and Image Indexing System, 588
Tracking Slow-Moving Objects, 631
Mulder, S. A.
Infrastructural Development for Flexible Networks, 621
Muller, R. P.
Biomicrofuel Cell, 473
Multibody, 149
Multichannel, 649
Multichip, 584
Multifidelity, 131
Multigroup, 694
Multikilovolt, 323
Multilayer, 50
Multilevel, 131
Multiobjective, 794
Multiplex
Mode, 292
Sensing, 820
Multiscale
Experimental/numerical study, 727
Modeling carbon, 762
Muñoz, C.
Nuclear Nanobatteries, 414
Picoliter Vessels for Trace Biotoxin Detection, 565
Muron, D. J.
Functionalized Nanoelectrode Arrays, 338
Murphy, K. M.
Climate-Change Effects on International Stability, 38
Murphy, M. B.
Receiver for Ultralow-Power Wake-Up, 650
TALON, 480
Musculature, 826
Musson, L. C.
Modeling Surface Evolution During Etching, 154
Muyshondt, A.
Agile, Microsystems-Enabled Receiver, 572

N
Nanobattery, 414
Nanocrystal
Micelle, 848
Polymer, 812
Nanoelectrode, 338
Nanoelectromechanical (oscillators), 173
Nanoengineering
Solution-based, 507
Surfaces, 107
Nanofluidic
Aqueous, 493
Detection, 844
Fundamentals, 463
Nanoimaging, 323
Nanointeraction, 499
Nanolayer, 497
Nanolithography, 549
Nanomagnetic, 760
Nanomaterial, 510
Nanomechanical
Oscillator, 562
Resonators, 825
Nanometer, 66
Nanoparticle
Beyond, 351
Magnetic, 747
Photochemically active, 514
Sensors, 187
Nanophotonic, 216
Nanopore, 789
Nanoporous
Adsorbers, 786
Polymeric materials, 820
Nanoscale
Deformation, 809
Dissipation, 562
Energetic materials, 701
Thermomechanical manufacturing, 754
Nanostructure
Directed transport, 503
Photonic, 532
Self-assembly (growth), 465
Self-assembly (optoelectronics), 431
Semiconductor (lasers), 201
Semiconductor (radio frequency), 220
Silicon, 717
Tailored, 501
Nanotagging, 93
Nanotube
Modeling, 762
Self-assembled, 860
Nanovehicle, 830
Napier, M. P.
Full-Earth-Monitoring Sensor MESAWorks, 910
Naranjo, G. E.
Conversion Systems for Nuclear-Power Reactors, 362
Nasby, R. D.
Radiation-Hard Nonvolatile Memories, 185
Natek, N. H.
Assessing Bomb Damage to Underground Facilities, 236
National (missile defense), 317
Neiser, R. A., Jr.
Security Coatings for Multichip Modules, 584
Nellums, R. O.
Deployable Object Tracker for NMD Flights, 317
Interferometric Deformation Measurements, 461
Microoptical Radar Facial-Recognition Project, 673
Nelson, C. L.
Dynamic Vulnerability Assessment, 667
Nelson, T. R.
Nonlinear Optical Detection of Aerosol Agents, 640
NEMOs
See Nanoelectromechanical oscillators

Author and Title Index

A B C D E F G H I J K L M N O P Q R S T U V W X Y Z

Nenoff, T. M.
H2 Generation from Thermochemical Cycles, 405
"Tunable" Ion Conductors for Fuel Cells, 411
Water Desalination, 341
Nerve (cell), 840
Network
Biological, 84
Cognitive, 840
Flexible, 621
Mobile, 249
Sensors, 314
Wireless, 403
Neumann, W. D.
Securing Mobile Code, 365
Neuroprotectant, 888
Neutralization, 306
Neutron (monitors), 745
Newman, G. C.
A Model of Water in the Lower Rio Grande Basin, 423
Assessing Factors that Influence Water Consumption, 421
Nguyen, H. D.
Distributed Detection for Unattended Ground Sensors, 262
Self-Assembly of Biological Nanostructured Materials, 465
Nickel, 558
Nielsen, I. B.
Algorithms for Electronic Structure Methods, 119
Niese, A. D.
Deployable Object Tracker for NMD Flights, 317
Microoptical Radar Facial-Recognition Project, 673
Nilson, R. H.
Fundamentals of Nanofluidics, 463
NMD
See National missile defense
Noble, D. R.
Proton-Exchange-Membrane Fuel Cells, 390
Self-Assembly of Biological Nanostructured Materials, 465
Node, 289
Noncontact, 458
Nonlethal, 273
Nonlinear
Optical detection, 640
Solvers, 134
Nonmarket (value), 832
Nonradioactive, 796
Nonvolatile, 185
Nordquist, C. D.
Agile, Microsystems-Enabled Receiver, 572
Macro-/Meso-/Microsystems Integration in LTCC, 73
Microelectromechanical Systems Antennas, 622
Miniature High-Power RF Components, 63
Miniaturized Electronic Steerable-Array SAR, 907
Passive Electronically Steerable Array for Mini-SAR, 227
Silicon-Based RF MEMS Components, 171
Norman, A. K.
Direct Single-Ion Machining of Nanopores, 789
Norman, K.
Development of Microreformers for Fuel Cells, 882
Novak, J. L.
Biomicrofuel Cell, 473
Nano-G Accelerometers, 216
Tracking Slow-Moving Objects, 631
Novak, P.
Dynamics of Membrane Proteins and Receptors, 863
Membrane-Protein Recognition and Signaling, 103
Top-Down Structural Studies, 869
Nove, C. E.
Analysis of Multichannel Internet Communication, 649
Nozick, L. K.
Optimization in Critical-Infrastructure Systems, 372
Nuclear
Nanobatteries, 414
Reactors (orbital), 396
Reactors (special purpose), 362
Thermochemical cycles, 405
Weaklinks, 735
Weapons (gel-based components), 67
Weapons (kill assessment), 606
Nucleation, 752
Nyman, M. D.
Polyoxoniobate Chemistry, 568
Pathogens on Nanoengineered Surfaces, 107

O

O'Connor, J. W.
Surety and Accountability for Storage Containers, 733
O'Hern, T. J.
Collateral Damage/Mitigation Assessment, 281
O'Malley, P. D.
Hard-Target-Defeat High-G-Tolerant Fuze, 243
O'Rourke, W. T.
Distributed Detection for Unattended Ground Sensors, 262
Ober, C. C.
Sensitivities for Large-Scale Simulation Codes, 123
Observatory, 80
Ohlhausen, J. A.
Analytical Techniques for Homeland Defense, 542
Predictive Accelerated Aging of Microsystems, 730
Okandan, M.
Controlled Motion for a Microfluidic Drop Ejector, 44
Switchable Materials for (Bio)Microfluidics, 534
Microflame-Based Detector for Gas Sensing, 270
Microfluidic Cellular-Sample Pretreatment, 180
MOSFET–MEMS Integration, 203
Oliver, A. D.
Packaging for MEMS Integrated Microsystems, 779
Oliver, B. V.
Advanced Pulsed-Power Fusion Concepts, 898
Olsen, R. W.
Nuclear Nanobatteries, 414
Polymer Electronic Devices and Materials, 643
Olsson, R. H.
Nanomechanical Stochastic Resonators, 825
Olsson, W. A.
Natural-Gas Production Problems, 332

Author and Title Index

A B C D E F G H I J K L M N O P Q R S T U V W X Y Z

Omdahl, G.
Completely Passive Microwave Tag, 581
Zero-Power Radio Receiver, 578
Opalka, J. M.
Characterization for Assured HDBT Defeat, 483
Oppel, F. J., III.
Operations in Complex Environments, 304
TALON, 480
Optical
Adaptive optics (MEMS), 604
Adaptive optics (space), 618
Adaptive optics (weapon), 681
Communications, 632
Detection, 640
Firesets, 738
Infrared, 659
Logic, 784
Sectioning, 554
Transmission, 652
See also: Electrooptic
See also: Microoptical
Optoelectronics
Self-assembly, 431
See also: Electrooptic
Orbital (reactors), 396
Ordered
Electrooptical, 523
Nanotubes, 860
Organization (self), 93
Ortiz, P. G.
Novel Processing for Miniaturized SAR, 292
Osborn, T. D.
Full-Earth-Monitoring Sensor MESAWorks, 910
Tracking Slow-Moving Objects, 631
Osbourn, G. C.
Biomolecular Decision-Making for Self-Assembly, 828
Risk-Assessment Metatool, 627
Oscillator
Nanoelectromechanical (coupled), 562
Nanoelectromechanical (filtering), 173
Oswald, M. T.
Characterization for Assured HDBT Defeat, 483
Miniature Transmitter Filter for JTA, 740
Systems Analysis of Networked Sensors, 314
Outka, D. E.
Prompt Global Response, 486
Overberg, M. E.
GaN 20–100 Watt Amplifiers for Micro-SAR, 222
Oxidation, 398
Oxide, 411

P

P3 (engine), 715
Paananen, O. H.
Energy-Systems Analysis Framework and Modeling, 425
System-Dynamics Toolbox for Water Planning, 386
Pack, M. V.
Agile, Microsystems-Enabled Receiver, 572
Packaging
Firesets, 738
Hermetic, 779
Padilla, D. D.
Advancements in Sensing and Perception, 275
Pahl, R. J.
Explosive Ignition Criteria for Miniaturized Devices, 886
Weaponization of Thermobaric Explosives, 283
Palmer, J. A.
Adaptive Optics for Weapon and Space Applications, 681
Advanced Manufacturing Using Rapid Prototyping, 777
Microfabrication with Femtosecond Laser Processing, 41
Miniature High-Power RF Components, 63
Pan, W.
Coupled Nanomechanical Oscillator Arrays, 562
Pankretz, T. D.
Augmented Musculature Device, 826
Parallel
Circuit, 129
Programming, 140
Parekh, O. D.
Massively Parallel Linear Programming, 140
Parker, E. P.
Operations in Complex Environments, 304
Parks, R. C.
Critical-Infrastructure System-of-Systems Assessment, 665
Vulnerability Analysis for SCADA, 678
Parma, E. J., Jr.
Conversion Systems for Nuclear-Power Reactors, 362
Parson, T. B.
Compliant Thermomechanical MEMS Actuators, 193
Particle
Beams, 792
Level-set, 154
Virus, 844
See also: Nanoparticle
Particulate
Formation, 805
Traps, 344
Partridge, M. E.
High-Capacity Earth-Penetrator Instrumentation, 312
MEMS/Fuze Diagnostic in High-G Environments, 800
Passell, H. D.
A Model of Water in the Lower Rio Grande Basin, 423
Assessing Factors that Influence Water Consumption, 421
Modeling the Nonmarket Value of Water, 832
System-Dynamics Toolbox for Water Planning, 386
Passive
Electronically steerable array, 227
Microwave tag, 581
Optical integration, 205
Pate, R. C.
Controlled-Environment Agriculture, 36
Patel, K. D.
Macro-/Meso-/Microsystems Integration in LTCC, 73
Patel, R. K.
Full-Earth-Monitoring Sensor MESAWorks, 910
Radiation-Hard Nonvolatile Memories, 185

Author and Title Index

A B C D E F G H I J K L M N O P Q R S T U V W X Y Z

Pathogen
Identification, 319
Sequestration, 107
Pattengale, N. D.
Automatic Generation of Terrorist Operation Plan, 30
Pattern
Aperture, 652
Array, 853
Payne, J. A.
Receiver for Ultralow-Power Wake-Up, 650
Peake, G. M.
Leaky-Mode VCSELs for Photonic Logic Circuits, 209
Microoptical Gyroscope, 205
Peebles, D. E.
Quantification of Environments within Micropackages, 520
Peel, J.
Advanced Neutron Monitors for JTA, 745
Penetrate
Earth (high-capacity), 312
Earth (nuclear), 606
Reliability, 157
Rock, 704
PEO
See Polyethylene oxide
Peptide, 808
Perennial (streams), 335
PESA
See Passive electronically steerable array
Petawatt, 684
Peters, D. W.
Dispersive Diffractive Optical Elements for the IR, 659
Extraordinary Optical Transmission, 652
Peters, M. D.
Sophisticated-Agent Evolution and Optimization, 116
Peters, R. R.
Robotic Planning for Physical-Security Analysis, 601
Peters, T. H.
Robotic Planning for Physical-Security Analysis, 601
Peterson, D. W.
Advanced Packaging Technology for Optical Firesets, 738
An Integrated, Stacked System-on-a-Chip, 196
Meso-/Microoptical System Interface Coupling, 69
Peterson, G. D.
An Integrated, Stacked System-on-a-Chip, 196
Peterson, K. A.
Assembly of Microsystems Using Thin Films, 50
Macro-/Meso-/Microsystems Integration in LTCC, 73
Peterson, T. C.
Microoptical Gyroscope, 205
Pfeifer, K. B.
Fourier-Transform Ion-Mobility Spectrometer, 233
Functionalized Nanoelectrode Arrays, 338
MOSFET–MEMS Integration, 203
Polychromator Systems for Remote Chemical Sensing, 211
Pfeifle, T. W.
Characterization for Assured HDBT Defeat, 483
Phan, A.
Infrastructural Development for Flexible Networks, 621
Phan, A. H.
Fourier-Transform Ion-Mobility Spectrometer, 233
Phase
Diversity, 618
See also: Interphase
Phelan, J. M.
Critical-Infrastructure System-of-Systems Assessment, 665
Phelan, J. R.
Prompt Global Response, 486
Phenomena (collective), 505
Phillips, C. A.
Massively Parallel Linear Programming, 140
Optimization in Critical-Infrastructure Systems, 372
Simulations of Chemical/Biological Attacks, 137
Phillips, L. R.
Agent-Based Control of Distributed Infrastructures, 377
Phillips, M. C.
Quantum Coherence in Semiconductor Nanostructures, 201
Phillips, M. L.
Water Desalination, 341
Phinney, L. M.
Noncontact Surface Thermometry for Microsystems, 458
Phospholipid, 808
Photocatalytic, 93
Photochemical, 514
Photocontrol, 499
Photonic
Biosensor, 225
Crystal, 183
Encryption, 784
Lidar, 241
Logic, 209
Motion detection, 216
Nanostructure, 532
Physics
Materials, 207
Shock, 698
See also: Biophysics
Pickard, P. S.
Conversion Systems for Nuclear-Power Reactors, 362
H2 Generation from Thermochemical Cycles, 405
Hydrogen Futures Dynamic Simulation Model, 375
Picoliter, 565
Piech, M.
Photocontrol of Nanointeractions in Microsystems, 499
Pierson, L. G.
Cryptographic Assurance of Execution Correctness, 612
Securing Mobile Code, 365
Piezoelectric, 615
Pilcher, M. W.
Hard-Target-Defeat High-G-Tolerant Fuze, 243
Pitts, T. A.
Deployable Object Tracker for NMD Flights, 317
Microoptical Radar Facial-Recognition Project, 673
Nonlinear Optical Detection of Aerosol Agents, 640

Author and Title Index

A B C D E F G H I J K L M N O P Q R S T U V W X Y Z

Plan
Robotic, 601
Terrorist operation, 33
Water (integrated toolbox), 386
Water (regional), 832
Planar, 225
Plasma, 684
Plass, R. A.
Compliant Thermomechanical MEMS Actuators, 193
Predictive Accelerated Aging of Microsystems, 730
Quantification of Environments within Micropackages, 520
Plastic, 792
Pless, J. D.
Water Desalination, 341
Plimpton, S. J.
Modeling Biomembranes, 82
Substructured Multibody Molecular Dynamics, 149
Plume, 241
Plummer, K. W.
Receiver for Ultralow-Power Wake-Up, 650
Plut, T. A.
Agile, Microsystems-Enabled Receiver, 572
Passive Electronically Steerable Array for Mini-SAR, 227
Podgorski, J. R.
Tracking Slow-Moving Objects, 631
Pohl, P. I.
Microsensors in Radioactive-Waste Management, 348
Controlled-Environment Agriculture, 36
Polychromator, 211
Polyethylene oxide, 846
Polymer
Biocompatible, 846
Electronic devices, 643
Microbe-exuded, 837
Nanocrystal, 812
Separation materials, 769
Polyoxoniobate, 568
Polyvinylidene floride, 615
Poroelastic, 878
Power
Amplifier (GaN HEMT), 207
Amplifier (Ku-band), 222
Combining, 657
Conversion, 362
Light, 830
Low (measuring device), 468
Microengine, 164
Miniature, 633
Nuclear (nanobattery), 414
Nuclear (orbital), 396
Nuclear (thermochemical cycles), 405
Pulse (accelerator), 689
Pulse (fusion), 898
Receiver, 650
Zero, 578
Prasad, S. V.
Atomic Layer Deposition of Tribological Coatings, 46
Modeling of Friction-Induced Deformation, 537
Precise
Guidance, 227
Picoliter vessels, 565
Preconcentrator
Combined, 111
Novel, 607
Predict
Aging, 730
Fuel cells, 390
Protein interactions, 901
Preece, D. S.
Modeling of Fracture in Geomaterials, 447
Radiation-/Geometry-Driven Jets, 33
Prentice, W. J.
Intelligent Interaction Control for Metrology, 52
Pretreatment, 180
Prevost, G. E.
Controlled Motion for a Microfluidic Drop Ejector, 44
PRIDE (Penetrator Reliability Investigation)
See Penetrate
Programming, 140
Propagation
Poroelastic wave, 878
Radiation, 661
Propulsion
Electric, 396
Nanovehicle, 830
Protection (critical assets), 823
Protein
Interactions, 901
Membrane (chemical cross-linking), 863
Membrane (molecular dynamics), 871
Membrane (recognition), 103
Self-organization, 93
Proton (exchange)
Fuel cell (materials), 354
Fuel cell (modeling), 390
Prototype
Circuitry, 55
Engine, 715
Manufacturing, 777
Nanometer scale, 66
Provencio, P. P.
Durability of Metal-to-Plastic Interfaces, 792
GaN HEMT High-Power Amplifiers, 207
Pulse
Laser, 684
Particle beams, 792
Power, 898
Pump, 890
Pura, C. A.
A Systems Approach to Defending Our Borders, 488

Author and Title Index

A B C D E F G H I J K L M N O P Q R S T U V W X Y Z

PVDF
See Polyvinylidene floride

Q
Quantum
Coherence, 201
Dot arrays, 853
Nanostructures, 220
Squeezed light, 888

R
Raber, T. N.
Microengine for Advanced Power Generation, 164
Radar
Microoptical, 673
Synthetic aperture (miniaturized), 907
Synthetic aperture (passive), 227
Synthetic aperture (processing), 292
Rader, D. J.
Bioaerosol Microseparations-Based Detectors, 591
Microscale Rarefied-Gas Dynamics, 438
Superhydrophobic Surface Coatings for Microfluidics, 884
Radiation
Hard, 185
Jets, 33
Multigroup, 694
Performance, 798
Soot, 444
Terahertz, 661
Radio
Frequency (filtering), 173
Frequency (MEMS, antennas). 622
Frequency (MEMS, silicon). 171
Frequency (miniature), 63
Frequency (semiconductor quantum nanostructures), 220
Receiver, 578
Radioactive, 348
Rahimian, K.
Nuclear-Safety Weaklinks, 735
Polymer Electronic Devices and Materials, 643
Thermally Cleavable Surfactants, 516
Rahm, P. E.
A Capillary Valve for Microfluidic Systems, 470
Rambo, P. K.
High-Damage-Threshold Sol-Gel Diffraction Grating, 686
Randomness, 679
Range
Aerosol cloud, 268
Moving target, 247
Resolved, 241
Rapid
Biothreats, 851
Pathogen identification, 319
Prototyping (circuitry), 55
Prototyping (manufacturing), 777
Prototyping (nanometer), 66
Sample preparation, 565
Virus, 844
Rarefied
Flows, 450
Gas dynamics, 438
Rattan, N. S.
Infrastructural Development for Flexible Networks, 621
Rawlinson, K. S.
Full-Earth-Monitoring Sensor MESAWorks, 910
Microsystems for Chemical Signature, 178
Real-Time Sensors for Water-Contamination, 360
Reaction
Absorption/desorption, 518
Simulation, 137
Reactor
Fuel cell, 398
Nuclear (orbital), 396
Nuclear (special purpose), 362
Nuclear (supercritical water), 796
Reagent (delivery), 178
Real-time
Brain-wave monitoring, 904
Characterization (HDBT), 483
Chemical detection, 233
Water monitoring (contamination), 360
Water monitoring (streams), 335
Receiver
Microsystem, 572
Wake-up and command, 650
Receptor, 863
Reckase, E. N.
Event Locations from Space-Based Sensors, 663
Recognition
Facial, 673
Protein, 103
Target, 676
Reconfigurable, 622
Reconnaissance
Adaptive optics, 681
Passive electronically steerable array, 227
Reconstruction (algorithm), 654
Recovery, 383
Recruitment, 28
Reedy, E. D., Jr.
Coilgun Technology Demonstration Test-Bed, 295
Disbonding Initiation of Interfacial Cracks, 723
High-Fidelity Frictional Models for MEMS, 441
Reeves, P. C.
Augmented Cognition, 476
Reflectometry, 335
Regional
See Water planning
Regueiro, R. A.
Continuum Models for Inelasticity in Solids, 916
Modeling of Fracture in Geomaterials, 447
Regulated (chemicals), 338
Regulatory (genetic code), 913
Reichardt, T. A.
Short-Range Standoff Aerosol-Cloud Finder, 268

Author and Title Index

A B C D E F G H I J K L M N O P Q R S T U V W X Y Z

Reif, J. L.
Controlled Motion for a Microfluidic Drop Ejector, 44
Reineke, M. C.
TALON, 480
Reines, I. C.
Agile, Microsystems-Enabled Receiver, 572
Reinhart, W. D.
Biophysics of BW-Warhead Defeat, 278
Hypervelocity Impact-Generated Flash, 258
Rejection (disturbances), 856
Reliability
Penetrator, 157
Systems control, 245
Remote
Chemical sensing, 211
Kill assessment, 606
Mapping (electromagnetic fields), 238
Mapping (environments), 298
Water monitoring, 335
Renk, T. J.
Durability of Metal-to-Plastic Interfaces, 792
Renlund, A. M.
Explosive Ignition Criteria for Miniaturized Devices, 886
Weaponization of Thermobaric Explosives, 283
Renn, R. A.
Miniature Transmitter Filter for JTA, 740
Reno, J. L.
Continuous-Wave Intersubband Terahertz Sources, 176
Semiconductor Quantum Nanostructures, 220
Superconductivity in Electron-Hole Bilayers, 168
Replication, 853
Resin, 720
Resistance, 696
Resnick, P. J.
MOSFET–MEMS Integration, 203
Resolution, 247
Resolved
Lidar, 241
Microscopy, 80
Resonator, 825
Resource
Infrastructure, 377
Water (consumption), 421
Water (planning), 386
Restoration, 383
Reu, P. L.
Interferometric Deformation Measurements, 461
Reverse (engineering), 84
Reversible, 540
RF
See Radio(frequency)
Rice, S. F.
Advanced Fuel-Cell Reactor, 398
Richards, J. A.
Moving-Target Identification, 247
Rieger, D. J.
An Integrated, Stacked System-on-a-Chip, 196
Rigdon, J. B.
Robotic Planning for Physical-Security Analysis, 601
Simulating Human Behavior for National Security, 321
Rightley, M. J.
Full-Earth-Monitoring Sensor MESAWorks, 910
Miniaturized Electronic Steerable-Array SAR, 907
Rio Grande, 423
Risk
Assessment metatool, 627
Biological terrorism, 893
Evaluating research, 143
System pathways analysis, 393
Roberts, J. D.
Management after an Intentional Contamination Event, 383
Real-Time Water-Quantity/-Quality Monitoring, 335
Robertson, P. J.
Cryptographic Assurance of Execution Correctness, 612
Miniaturized Electronic Steerable-Array SAR, 907
Photonic Encryption Using All-Optical Logic, 784
Robino, C. V.
Advanced Packaging Technology for Microsystems, 525
Robinson, A.
BTU Monitoring Device for Natural-Gas Monitoring, 408
Microsystems for Chemical Signature, 178
Real-Time Sensors for Water-Contamination, 360
Robinson, A. C.
Advanced Pulsed-Power Fusion Concepts, 898
Robotic, 601
Rock (penetration), 704
Rodenbeck, C. T.
Microelectromechanical Systems Antennas, 622
Rodriguez, M. A.
Assembly of Microsystems Using Thin Films, 50
Dielectric Materials for Integrated Microsystems, 545
Polyoxoniobate Chemistry, 568
Roe, D. C.
Algorithms for Predicting Protein-Protein Interactions, 901
Protein Microarrays for Biowarfare-Agent Detection, 96
Roesler, A. W.
Assessing Bomb Damage to Underground Facilities, 236
Dielectric Materials for Integrated Microsystems, 545
MICROFUZE Integration, 302
Rogers, C. O.
Analysis of Multichannel Internet Communication, 649
Rohde, S. B.
Macro-/Meso-/Microsystems Integration in LTCC, 73
Rohrer, B. R.
Adaptive-Force-Feedback Surface Control, 310
Augmented Musculature Device, 826
Macro-/Meso-/Microsystems Integration in LTCC, 73
Rohwer, J. A.
Systems Analysis of Networked Sensors, 314
Rohwer, L. E.
Magnetophoretic Bead Trapping, 326
Nanocrystal-Polymer Composites for LEDs, 812
Romero, L.
Micromagnetic Suspension, 121

Author and Title Index

A B C D E F G H I J K L M N O P Q R S T U V W X Y Z

Ronnebro, E. E.
New Hydrogen-Storage Material: Metal-N-H System, 401
Rosenthal, S. E.
Electrical Conductivity of Metal Alloys, 691
Ross, J. R.
Biokillers in EDS for Biological-Agent Destruction, 308
Rossi, P.
Ultrafast-Current Transient Measuring Device, 468
RpHdc (Rapid-prototyping high-density circuitry)
See Rapid
Ruby, D. S.
Real-Time Water-Quantity/-Quality Monitoring, 335
Rucker, V. C.
Polymeric Materials for Sensing of Bioagents, 820
Protein Microarrays for Biowarfare-Agent Detection, 96
Rudd, J. V.
Free-Space Electrooptic Sampling, 238
Ruffner, J. A.
Resin Infusion Between Double Flexible Tooling, 720
Rush, B. M.
A Capillary Valve for Microfluidic Systems, 470
Russ, T. D.
Content-Based Video and Image Indexing System, 588
Microoptical Radar Facial-Recognition Project, 673
Russell, M. J.
Outstanding Challenges for AlGaInN MOCVD, 817
Rutledge, W. H.
Characterization for Assured HDBT Defeat, 483

S

Sa, T. J.
Understanding Communication in Crisis Management, 255
Saavedra, F. M.
Automated Visual Direction of Mobile Manipulation, 231
Saavedra, M. P.
Next-Generation Spindles for Micromilling, 60
Sackinger, P. A.
Elucidating the Mysteries of Wetting, 57
Safe (eye), 268
Salazar, J. S.
Moving-Target Identification, 247
Reconstruction Algorithm Development, 654
Salazar, R. A.
Brain-Wave Monitoring, 904
EM Interactions with Systems to Enhance Security, 235
Secure Chaotic Communications, 264
Sale, K. L.
Algorithms for Predicting Protein-Protein Interactions, 901
Membrane-Protein Recognition and Signaling, 103
Model-Building Codes for Membrane Proteins, 874
Salt, 918
Salters, B.
Microoptical Gyroscope, 205
Samara, G. A.
Dielectric Materials for Integrated Microsystems, 545
Samora, S.
Continuous-Wave Intersubband Terahertz Sources, 176
Dispersive Diffractive Optical Elements for the IR, 659
Meso-/Microoptical System Interface Coupling, 69
Sanchez, C.
Agile, Microsystems-Enabled Receiver, 572
Sandusky, J. V.
Deployable Object Tracker for NMD Flights, 317
Microoptical Radar Facial-Recognition Project, 673
Sapra, R.
Genetic Engineering in Bioweapons Strains, 594
Molecular Machines Involved in Membrane Signaling, 88
SAR
See Synthetic aperture radar
Sarkisov, G. S.
Laser Triggering of Water Switches, 689
Sasaki, D. Y.
Imaging Self-Organization of Proteins, 93
Interaction of Proteins with Lipid Films, 99
Lipid Membranes on Nanostructured Silicon, 717
Modeling Biomembranes, 82
Nanostructured Materials for Directed Transport, 503
Savignon, D. J.
Full-Earth-Monitoring Sensor MESAWorks, 910
Microoptical Radar Facial-Recognition Project, 673
Radiation-Hard Nonvolatile Memories, 185
SCADA
See Supervisory control and data-acquisition
Scalable
Algorithms, 119
Atmosphere model, 145
Scalar, 756
Scanning, 752
Scarring, 452
Scavenging, 329
Schare, J. M.
A Modular Micromagnetic Accelerometer, 300
Vibration-Based Miniature Power Generator, 633
Scharf, T. W.
Atomic Layer Deposition of Tribological Coatings, 46
Schefer, R. W.
Soot Formation in Unsteady Diffusion Flames, 444
Schelling, F. J., Jr.
Optimal Allocation of Terrorist Countermeasures, 393
Schendel, J. R.
Ultrahigh-Gain Fusion Concept, 843
Schiek, R. L.
A Parallel Circuit Simulator for Cell Biology, 129
Schmidt, C.
Biomicrofuel Cell, 473
Schmidt, R. C.
3-D Large-Eddy Simulation of Turbulent Flow, 781
Massively Parallel Scalable Atmosphere Model, 145
Schmidt, R. L.
Event Locations from Space-Based Sensors, 663

Author and Title Index

A B C D E F G H I J K L M N O P Q R S T U V W X Y Z

Schoeniger, J. S.
Dynamics of Membrane Proteins and Receptors, 863
Toxin Studies Using an Integrated Approach, 866
Schoenwald, D. A.
Agent-Based Autonomic Logistics Simulation Model, 286
Schroder, K. L.
Short-Range Standoff Aerosol-Cloud Finder, 268
Schroeppel, R. C.
Joint Authentication/Encryption, 596
Photonic Encryption Using All-Optical Logic, 784
Securing Mobile Code, 365
Small Circuits for Cryptography, 647
Schubert, W. K.
Compliant Membranes for MEMS Microphones, 725
Schwank, J. R.
Dielectrics with Controlled Leakage, 213
Full-Earth-Monitoring Sensor MESAWorks, 910
Schwarz, J.
High-Damage-Threshold Sol-Gel Diffraction Grating, 686
SCWR (Supercritical water reactor)
See Supercritical
SDAC
See Sense, decide, act, and communicate
Seager, C. H.
GaN HEMT High-Power Amplifiers, 207
Sears, M. P.
Interaction of Proteins with Lipid Films, 99
Sectioning (optical), 554
Security
Coating, 584
Communications, 264
Decontamination, 380
Electromagnetic interactions, 235
Generator, 633
Human behavior, 321
Internet protocol storage, 126
Mobile code, 365
Robotic planning, 601
Transport/reaction simulation, 137
See also: Cybersecurity
Seidel, D. B.
Nonlethal Technologies for the War on Terrorism, 273
Seismic, 236
Self-assembly
Biomolecular, 828
Micelles, 848
Nanolithography-directed, 549
Nanostructure, 431
Nanotube arrays, 860
Simulation, 465
Semiconductor (nanostructures)
Lasers, 201
Radio-frequency, 220
Sena, J. M.
Rapid-Prototyping High-Density Circuitry, 55
Sena, M. D.
Receiver for Ultralow-Power Wake-Up, 650
Sense, decide, act, and communicate, 36
Sensing
Bioagents, 820
Chemical, 211
Environmental, 743
Gas, 270
Graph theory, 249
Lighting, 275
See also: Sensor
Sensor
Ground, 262
Headspace gas, 348
Light sources, 417
Magnetostrictive elastomers, 528
Nanoparticles (functionalized), 187
Networked, 314
Photonic biosensor, 225
Topology, 160
Water contamination, 360
See also: Sensing
Separation
Polymeric, 769
See also: Microseparation
Sequestration, 107
Serkland, D. K.
Leaky-Mode VCSELs for Photonic Logic Circuits, 209
Meso-/Microoptical System Interface Coupling, 69
Serrano, J. R.
Noncontact Surface Thermometry for Microsystems, 458
Setchell, R. E.
Embeddable Shock Physics Sensors, 698
Shaddix, C. R.
Soot Formation in Unsteady Diffusion Flames, 444
Shadid, J. N.
Simulations of Chemical/Biological Attacks, 137
Shadow (model), 636
Shaner, E. A.
Semiconductor Quantum Nanostructures, 220
Shaneyfelt, M. R.
Dielectrics with Controlled Leakage, 213
Shaw, M. J.
Evanescent-Wave Planar Photonic Biosensor, 225
Microoptical Gyroscope, 205
Shediac, R.
Polymeric Materials for Sensing of Bioagents, 820
Shelnutt, J. A.
Imaging Self-Organization of Proteins, 93
Light-Powered Nanovehicle Propulsion, 830
Shepodd, T. J.
Biokillers in EDS for Biological-Agent Destruction, 308
Shields, E. A.
Event Locations from Space-Based Sensors, 663
Shirah, D. N.
System-of-Systems Modeling and Analysis, 266
Shirley, D. N.
Model-Building Codes for Membrane Proteins, 874
Shock (physics), 698

Author and Title Index

A B C D E F G H I J K L M N O P Q R S T U V W X Y Z

Shokair, I. R.
Short-Range Standoff Aerosol-Cloud Finder, 268
Showalter, S. K.
Microflame-Based Detector for Gas Sensing, 270
Micropreconcentrators for Surety, 607
Shul, R. J.
Advanced Device Structures for Solid-State Lighting, 419
Controlled Motion for a Microfluidic Drop Ejector, 44
GaN 20–100 Watt Amplifiers for Micro-SAR, 222
GaN HEMT High-Power Amplifiers, 207
MICROFUZE Integration, 302
Micropreconcentrators for Surety, 607
Vibration-Based Miniature Power Generator, 633
Shyr, L.
A Systems Approach to Defending Our Borders, 488
Optimal Allocation of Terrorist Countermeasures, 393
Sickafoose, S. M.
Analytical Techniques for Homeland Defense, 542
New Hydrogen-Storage Material: Metal-N-H System, 401
Siegal, M. P.
Micropreconcentrators for Surety, 607
Nanoporous-Carbon Adsorbers for Microsensors, 786
Self-Assembled Ordered Carbon-Nanotube Arrays, 860
Signals
Membrane (domains), 91
Membrane (molecular machines), 88
Membrane (protein recognition), 103
Membrane (transduction pathway), 77
Nuclear weapons, 606
Silicon
MEMS, 171
Nanostructured, 717
Photonics, 183
Propulsion arrays, 396
Simmons, B. A.
Assembly of Electrooptical and Bioactive Materials, 523
Biokillers in EDS for Biological-Agent Destruction, 308
Biomicrofuel Cell, 473
Continuous-Flow Detector for Pathogen Identification, 319
Decomposition of Contaminants Using Nanoparticles, 514
Design of the Magnetic Properties of Nanoparticles, 747
Picoliter Vessels for Trace Biotoxin Detection, 565
Polymeric Materials for Sensing of Bioagents, 820
Preconcentrator and Sensor for Waterborne Pathogens, 111
Thermally Cleavable Surfactants, 516
Simmons, J. A.
Semiconductor Quantum Nanostructures, 220
Superconductivity in Electron-Hole Bilayers, 168
Simonson, K. M.
Event Locations from Space-Based Sensors, 663
Simonson, R. J.
Functionalized Nanoparticles for Sensor Applications, 187
Microsystems for Chemical Signature, 178
Simulation
Atomistic-continuum, 434
Autonomic logistics, 286
Clusters, 151
Contaminant transport, 586
Earth, 878
Human behavior, 321
Hydrogen futures, 375
Large-eddy, 781
Large-scale, 123
Laser pulses, 684
Nonlinear solvers, 134
Optimization, 372
Parallel circuit, 129
Peptides, 808
Self-assembly, 465
Solid-fluid systems, 707
Transport/reaction, 131
Simultaneous, 80
Sinars, D. B.
Advanced Pulsed-Power Fusion Concepts, 898
Sinclair, M. B.
Active Photonic Nanostructures, 532
Nanostructured Materials for Directed Transport, 503
Optical Sectioning, 554
Polychromator Systems for Remote Chemical Sensing, 211
Rapid Prototyping to the Nanometer Scale, 66
Singh, A. K.
Continuous-Flow Detector for Pathogen Identification, 319
Imaging Self-Organization of Proteins, 93
Lipid Microarray Biosensor for Biotoxin Detection, 774
Microscale Separations of Biological Compounds, 769
Molecular Machines Involved in Membrane Signaling, 88
Protein Microarrays for Biowarfare-Agent Detection, 96
Superhydrophobic Surface Coatings for Microfluidics, 884
Skala, D. M.
Miniature Transmitter Filter for JTA, 740
Skousen, T. J.
Predictive Accelerated Aging of Microsystems, 730
Slade, A. L.
Toxin Studies Using an Integrated Approach, 866
Slater, L. S.
Automatic Generation of Terrorist Operation Plan, 30
Slepoy, A.
Model-Building Codes for Membrane Proteins, 874
Reverse-Engineering Biological Networks, 84
Slinkard, M. E.
Distributed Detection for Unattended Ground Sensors, 262
Sloan, G. R.
Agile, Microsystems-Enabled Receiver, 572
Miniaturized Electronic Steerable-Array SAR, 907
Novel Processing for Miniaturized SAR, 292
Slutz, S. A.
Advanced Pulsed-Power Fusion Concepts, 898
Ultrahigh-Gain Fusion Concept, 843

Author and Title Index

A B C D E F G H I J K L M N O P Q R S T U V W X Y Z

Small, D. E.
Augmented Cognition, 476
Smart
Detector, 802
Material, 455
Smart, K. J.
Systems Analysis of Networked Sensors, 314
Smith, A. V.
Continuous-Wave Intersubband Terahertz Sources, 176
Smith, B. J.
Optimal Allocation of Terrorist Countermeasures, 393
Smith, I. C.
High-Damage-Threshold Sol-Gel Diffraction Grating, 686
Smith, M. W.
Adaptive Optics and Phase-Diversity Imaging, 618
Adaptive Optics for Weapon and Space Applications, 681
Smith, R. B.
Agent-Based Control of Distributed Infrastructures, 377
Smith, T. M.
Sensitivities for Large-Scale Simulation Codes, 123
Smithpeter, C. L.
Hard-Target-Defeat High-G-Tolerant Fuze, 243
Smrcka, J. D.
Agent-Based Modeling Terrorist Recruitment, 28
Smythe, D. L.
Infrastructural Development for Flexible Networks, 621
Snell, M. K.
Robotic Planning for Physical-Security Analysis, 601
Soft (matter), 497
Sokolowski, S. S.
Micropreconcentrators for Surety, 607
Solids
Fluid (mechanical), 447
Fluid (simulation), 707
Inelastic, 916
Liquid, 530
Solid-state
Amplifiers, 657
Lighting, 419
Solutes, 558
Solvers, 134
Soot, 444
Sorensen, K. W.
Miniaturized Electronic Steerable-Array SAR, 907
Sounart, T. L.
Optical Sectioning, 554
Superhydrophobic Surface Coatings for Microfluidics, 884
Source
Automotive industry, 712
Identification, 281
Light, 417
Terahertz (compact), 252
Terahertz (intersubband), 176
X-ray, 323
Souza, C. A.
Biological Terrorism to Water-Distribution Systems, 893
Space
Adaptive optics (phase-diversity imaging), 618
Adaptive optics (system study), 681
Architectural, 586
Free, 238
Mirror, 615
Sensors, 663
Spahn, O. B.
Telescope with MEMS Adaptive Optic, 604
Spangler, S.
Alanate-Hydride Fuel-Cell Demonstration Project, 357
Catalyzation of Complex-Hydride Reactions, 518
New Hydrogen-Storage Material: Metal-N-H System, 401
Spatially, 820
Spectral
Imager, 654
See also: hyperspectral
Spectrometer
Ion-mobility (fourier-transform), 233
Ion-mobility (mass), 610
Membrane proteins, 863
On-a-chip, 199
Spectrum, 629
Speed (high)
Deformation measurements, 461
Micro-EDM, 713
Speed, A. E.
Augmented Cognition, 476
Spindles, 60
Spoerke, E. D.
Solution-Based Nanoengineering of Materials, 507
Spotz, W. F.
Massively Parallel Scalable Atmosphere Model, 145
Sprauer, D. C.
Miniaturized Electronic Steerable-Array SAR, 907
Sprigg, J. A.
Climate-Change Effects on International Stability, 38
Stability, 38
Stacked (system-on-a-chip), 196
Staiger, C. L.
Biomicrofuel Cell, 473
Stalker, K. T.
Characterization for Assured HDBT Defeat, 483
Receiver for Ultralow-Power Wake-Up, 650
TALON, 480
Stamber, K. L.
Energy-Systems Analysis Framework and Modeling, 425
Stamp, J. E.
Critical-Infrastructure System-of-Systems Assessment, 665
Systems Analysis of Networked Sensors, 314
Vulnerability Analysis for SCADA, 678
Standoff, 268
Stanley, J. B.
MOSFET–MEMS Integration, 203
Starkey, E.
Agent-Based Autonomic Logistics Simulation Model, 286

Author and Title Index

A B C D E F G H I J K L M N O P Q R S T U V W X Y Z

Starr, M. J.
High-Fidelity Frictional Models for MEMS, 441
Staton, A. W.
Microsystems for Chemical Signature, 178
Steen, W. A.
Advanced Fuel-Cell Reactor, 398
Catalysts for Hydrogen Fuel-Cell Applications, 368
Steerable (array)
Miniaturized, 907
Passive, 227
Steichen, R. J.
The Automotive Industry as a Source for Weapons, 712
Stephenson, L. L.
Superconductivity in Electron-Hole Bilayers, 168
Stevens, J. E.
Silicon-Based RF MEMS Components, 171
Stevens, M. J.
Modeling Biomembranes, 82
Molecular Dynamics of Membrane Proteins, 871
Self-Assembly of Biological Nanostructured Materials, 465
Substructured Multibody Molecular Dynamics, 149
Stewart, K. D.
Alanate-Hydride Fuel-Cell Demonstration Project, 357
New Hydrogen-Storage Material: Metal-N-H System, 401
Stickland, M. G.
Automatic Generation of Terrorist Operation Plan, 30
Stochastic, 825
Stockpile, 745
Stokebrand, D. D.
Prompt Global Response, 486
Storage
Containers, 733
Hydrogen, 401
Internet protocol, 126
Stotts, L. G.
TALON, 480
Strain
Bioweapons, 594
Nanostructures, 431
Strassner, B. H., II.
Microelectromechanical Systems Antennas, 622
Passive Electronically Steerable Array for Mini-SAR, 227
Power-Combining for Power Amplifiers, 657
Straumanis, A. R.
Biomicrofuel Cell, 473
Stream, 335
Structure
Alloy, 752
Biology, 866
Electronic, 119
Emitting, 238
Internal dissipation, 562
Interphase, 493
Lighting (solid state), 419
Lighting (techniques), 275
Membrane protein, 863
Monitoring, 455
Top-down, 869
See also: Infrastructure
See also: Microstructure
See also: Nanostructure
See also: Substructured
Stuecker, J. N.
Revolutionary Systems for Catalytic Combustion, 344
Subramania, G. S.
Active Photonic Nanostructures, 532
Active Photonic-Crystal Devices, 183
Substructured, 149
Subsurface, 113
Subwavelength, 652
Suite (detector), 270
Sukalski, M. W.
Simulation with Configurable Auxiliary Devices, 151
Sullivan, J. P.
Coupled Nanomechanical Oscillator Arrays, 562
Dielectrics with Controlled Leakage, 213
Nanoelectromechanical Oscillators for RF Filtering, 173
Ultrafast-Current Transient Measuring Device, 468
Sumali, H.
High-Fidelity Frictional Models for MEMS, 441
Inflatable Antenna with Adaptive Actuators, 669
Sun, A. C.
Flow Control and Mixing in Microfluidic Devices, 749
Micro-/Nanoscale Thermomechanical Manufacturing, 754
Sunnarborg, D. A.
Advanced Neutron Monitors for JTA, 745
Superconductivity, 168
Supercritical, 796
Superhard, 765
Superhydrophobic, 884
Superlattice, 497
Supervisory control and data-acquisition, 678

Author and Title Index

A B C D E F G H I J K L M N O P Q R S T U V W X Y Z

Surety
Micropreconcentrators, 607
Storage containers, 733
Surface
Biospecific, 757
Control, 310
Evolution, 154
Interactions, 438
Interphase, 493
Metal micromachines, 190
Micromachine pumps, 890
Nanoengineered, 107
Near, 756
Quantification, 520
Superhydrophobic, 884
Thermometry, 458
See also: Subsurface
Surfactant, 516
Surveillance, 227
Suspension, 121
Swartzentruber, B. S.
Nucleation and Growth of Ge/Si Alloy Structures, 752
Sweatt, W. C.
Rapid Prototyping to the Nanometer Scale, 66
Sweet, A. D.
Novel Processing for Miniaturized SAR, 292
Swiler, L. P.
Agent-Based Autonomic Logistics Simulation Model, 286
Penetrator Reliability Investigation, 157
Switchable, 534
Switches, 689
Symons, N. P.
Assessing Bomb Damage to Underground Facilities, 236
Characterization for Assured HDBT Defeat, 483
Poroelastic-Wave Propagation on the Earth Simulator, 878
Synthesis
Micellar, 701
Superlattices, 497
Synthetic Aperture Radar (SAR)
Mini-SAR (passive steerable), 227
Mini-SAR (processing), 292
Miniturized Steerable, 907

T

Tag
Microwave, 581
See also: Nanotag
Talin, A. A.
Transition Metals in LIGA Nickel, 558
Tallant, D. R.
Analytical Techniques for Homeland Defense, 542
Gel-Based Components for Nuclear Weapons, 67
Microfabrication with Femtosecond Laser Processing, 41
Quantification of Environments within Micropackages, 520
Catalyzation of Complex-Hydride Reactions, 518
TALON (Terrorist activity location, observation, and neutralization)
See Terrorist
Tam, R.
Understanding Communication in Crisis Management, 255
Tamez, C. J.
The Effectiveness of Management Strategies, 427
Tang, J. D.
Photonic Encryption Using All-Optical Logic, 784
Tanner, D. M.
Predictive Accelerated Aging of Microsystems, 730
Tanner, F. R.
Event Locations from Space-Based Sensors, 663
Taplin, R. B.
Microoptical Radar Facial-Recognition Project, 673
Tappan, A. S.
MICROFUZE Integration, 302
Nanoscale Energetic Materials, 701
Target
Defeat, 243
Identification, 247
Modeling, 447
Recognition, 676
Tarman, T. D.
Cryptographic Assurance of Execution Correctness, 612
Tarver, E. E., III.
Fourier-Transform Ion-Mobility Spectrometer, 233
Taylor, M. A.
Climate-Change Effects on International Stability, 38
Massively Parallel Scalable Atmosphere Model, 145
Telescope, 604
Temperature
Ceramics, 598
Fuel cell, 411
Terahertz (radiation)
Atmospheric propagation, 661
Compact sources, 252
Intersubband, 176
Transceivers, 238
Terawatt, 689
Terrorism/Terrorist
Attack simulation, 137
Biological, 893
Countermeasures, 393
Nonlethal, 273
Operation plan, 30
Recruitment, 28
TALON, 480
See also: Bioterrorism
See also: Counterterrorism
Thai, T. Q.
Infrastructural Development for Flexible Networks, 621
Thayer, G. E.
Switchable Materials for (Bio)Microfluidics, 534
Thermal
Cleavable surfactants, 516
Imagery, 676
Photovoltaic, 329
Weaklinks, 735

Author and Title Index

A B C D E F G H I J K L M N O P Q R S T U V W X Y Z

Thermobaric, 283
Thermochemical, 405
Thermomechanical
  Actuators, 193
  Manufacturing, 754
Thermometry, 458
Thin films, 50
Thoma, S. G.
  Nanocrystal-Polymer Composites for LEDs, 812
  Nanoscale Energetic Materials, 701
Thomas, E. D.
  Intrusion Detection for Wireless Networks, 403
Thomas, M. L.
  Microsensors in Radioactive-Waste Management, 348
Thomes, W. J., Jr.
  Photocontrol of Nanointeractions in Microsystems, 499
Thompson, A. P.
  Molecular Simulation of Beta-Amyloid Peptide, 808
Thompson, B. M.
  Agent-Based Autonomic Logistics Simulation Model, 286
Thompson, D. C.
  Simulation with Configurable Auxiliary Devices, 151
Thornberg, S. M.
  Catalysts for Hydrogen Fuel-Cell Applications, 368
  Quantification of Environments within Micropackages, 520
Thornhill, T. F., III.
  Hypervelocity Impact-Generated Flash, 258
Threat
  Bioterrorism, 84
  Infectious agent, 380
  Terahertz sources, 252
  See also: Biothreat
Throckmorton, D. J.
  Molecular Machines Involved in Membrane Signaling, 88
Thurston, B. D.
  High-Damage-Threshold Sol-Gel Diffraction Grating, 686
Tian, Z. R.
  Solution-Based Nanoengineering of Materials, 507
Tibbetts, D. R.
  Semiconductor Quantum Nanostructures, 220
Tidwell, V. C.
  A Model of Water in the Lower Rio Grande Basin, 423
  Assessing Factors that Influence Water Consumption, 421
  Interactive Water-Quality Modeling, 834
  Management after an Intentional Contamination Event, 383
  Modeling the Nonmarket Value of Water, 832
  Real-Time Water-Quantity/-Quality Monitoring, 335
  System-Dynamics Toolbox for Water Planning, 386
Tieszen, S. R.
  Computational Studies of JP-8 Diffusion Flames, 805
Tigges, C. P.
  Assembly of Microsystems Using Thin Films, 50
  GaN 20–100 Watt Amplifiers for Micro-SAR, 222
  GaN HEMT High-Power Amplifiers, 207
  Power-Combining for Power Amplifiers, 657
Time
  Resolved microscopy, 80
  See also: Real-time
Timlin, J. A.
  Analytical Techniques for Homeland Defense, 542
  Optical Sectioning, 554
  Reverse-Engineering Biological Networks, 84
Tin, 530
Tise, B. L.
  Miniaturized Electronic Steerable-Array SAR, 907
Tolerant
  Algorithms, 119
  High-G, 243
Tomography, 654
Tool
  Structured lighting, 275
  See also: Metatool
Toolbox, 386
Toole, T. J.
  Intrusion Detection for Wireless Networks, 403
Tooling, 720
Toolmarks, 594
Tooman, T. P.
  Short-Range Standoff Aerosol-Cloud Finder, 268
Topology, 160
Torczynski, J. R.
  Microscale Rarefied-Gas Dynamics, 438
Torgerson, M. D.
  Joint Authentication/Encryption, 596
  Mobile-Node Authentication, 289
  Randomness Complexity and Cryptography, 679
  Small Circuits for Cryptography, 647
Torres, T. M.
  Critical-Infrastructure System-of-Systems Assessment, 665
Toth, R. P.
  Biophysics of BW-Warhead Defeat, 278
Toxin
  Pathways, 88
  Studies, 866
  See also: Biotoxin
TPV (Thermal photovoltaic)
  See Thermal
Trace (detection), 565
Track
  Object (deployable), 317
  Object (slow-moving), 631
Transceiver, 238
Transduction, 77
Transform, 233
Transient, 468
Transistor (amplifier), 207
Transition
  Liquid-solid, 530
  Metal (catalyzation), 518
  Metals (nickel), 558

Author and Title Index

A B C D E F G H I J K L M N O P Q R S T U V W X Y Z

Transmission, 652
Transmitter, 740
Transport
  Contaminant, 586
  Excitation energy, 503
  Simulation, 137
  Soot, 444
Trapping
  Antibody, 540
  Bead, 326
Traps (particulate), 344
Tribological, 46
Triggering, 689
Trott, W. M.
  Microscale Rarefied-Gas Dynamics, 438
  Nanoscale Energetic Materials, 701
Trucano, T. G.
  Penetrator Reliability Investigation, 157
Tucker, M. D.
  Biological-Security Decontamination Technology, 380
  CBW Cloud Knockdown and Neutralization, 306
Tucker, R. D.
  Prompt Global Response, 486
Tucker, S.
  Human/System Interactions in Systems-of-Systems, 260
  Operations in Complex Environments, 304
Tuminaro, R. S.
  Geophysical Subsurface Imaging, 113
Tunable
  Ion conductors, 411
  Polyoxoniobate, 568
Tunneling (microscope), 752
Turbulence, 781
Turnley, J. G.
  Agent-Based Modeling Terrorist Recruitment, 28
  Assessing Factors that Influence Water Consumption, 421
Turnquist, M. A.
  Optimization in Critical-Infrastructure Systems, 372
Tuttle, B. A.
  Dielectric Materials for Integrated Microsystems, 545

U
Ulibarri, T. A.
  Polymer Electronic Devices and Materials, 643
Ulmer, C. D.
  Simulation with Configurable Auxiliary Devices, 151
Unattended (sensor), 262
Uncooled, 676
Underground (facilities), 236
Underwood, K. D.
  High-Performance Processing Architecture, 147
Unsteady (flame), 444
Urayama, J.
  Nonlinear Optical Detection of Aerosol Agents, 640
Urban, 281
Uribe, F.
  Macro-/Meso-/Microsystems Integration in LTCC, 73

V
Valdez, M. M.
  Energy-Systems Analysis Framework and Modeling, 425
Validation, 390
Valve, 470
Van Bloemen Waanders, B. G.
  Poroelastic-Wave Propagation on the Earth Simulator, 878
  Sensitivities for Large-Scale Simulation Codes, 123
  Simulations of Chemical/Biological Attacks, 137
  Topology Optimization for Sensor Performance, 160
Van Leeuwen, B. P.
  Advanced Mobile Networking Sensing, 249
  Mobile-Node Authentication, 289
  Operations in Complex Environments, 304
Van Swol, F. B.
  Assembly of Electrooptical and Bioactive Materials, 523
  Superhydrophobic Surface Coatings for Microfluidics, 884
Vanderveen, K. B.
  Energy-Systems Analysis Framework and Modeling, 425
Vanrandwyk, J.
  Intrusion Detection for Wireless Networks, 403
  IP Storage: A Performance and Security Study, 126
Varley, E. S.
  Ion-Mobility Spectrometer/Mass Spectrometer, 610
Varnado, G. B.
  Critical-Infrastructure System-of-Systems Assessment, 665
Vasile, M. J.
  Rapid Prototyping to the Nanometer Scale, 66
Vawter, G. A.
  Compact Terahertz Sources, 252
  Continuous-Wave Intersubband Terahertz Sources, 176
  Evanescent-Wave Planar Photonic Biosensor, 225
  Microoptical Gyroscope, 205
  Miniaturized Electronic Steerable-Array SAR, 907
VCSEL
  See Vertical-cavity surface-emitting laser
Vehicle
  Hypersonic, 598
  Hypervelocity, 329
  See also: Nanovehicle
Venturini, E. L.
  Dielectric Materials for Integrated Microsystems, 545
Vernon, M. E.
  Conversion Systems for Nuclear-Power Reactors, 362
Vertical-cavity surface-emitting laser, 209
Vesey, R. A.
  Advanced Pulsed-Power Fusion Concepts, 898
  Radiation-/Geometry-Driven Jets, 33
Vessel, 565
Vibration, 633
Video, 588
Virus, 844
Visual (direction), 231
Vogler, T. J.
  Biophysics of BW-Warhead Defeat, 278
  Embeddable Shock Physics Sensors, 698

Author and Title Index

A B C D E F G H I J K L M N O P Q R S T U V W X Y Z

Voigt, J. A.
Dielectric Materials for Integrated Microsystems, 545
Nanolithography-Directed Materials Growth, 549
Solution-Based Nanoengineering of Materials, 507
Water Desalination, 341
Volponi, J. V.
Biomicrofuel Cell, 473
Vulnerability
Dynamic assessment, 667
Microelectronics, 639
Micromechanical, 552
Supervisory control and data acquisition, 678

W
Wackerbarth, D. E.
Assembly of Microsystems Using Thin Films, 50
Wagner, G. J.
Atomistic-Continuum Simulation, 434
Wagner, J. S.
Augmented Cognition, 476
Wake-up, 650
Waldrip, K. E.
Development of Microreformers for Fuel Cells, 882
Molten Salt-Based Growth of Bulk GaN and InN, 918
Walker, C. A.
Macro-/Meso-/Microsystems Integration in LTCC, 73
Walker, C. L.
Image Georectification, 636
Wall, D.
Management after an Intentional Contamination Event, 383
Wally, K.
Bioaerosol Microseparations-Based Detectors, 591
Walraven, J. A.
Predictive Accelerated Aging of Microsystems, 730
Walther, E. A.
Immunological Basis for Systems Control, 245
Wang, G. T.
Outstanding Challenges for AlGaInN MOCVD, 817
Wang, Y.
Microsensors in Radioactive-Waste Management, 348
Wanke, M. C.
Continuous-Wave Intersubband Terahertz Sources, 176
Nonlethal Technologies for the War on Terrorism, 273
TPV Energy Scavenging for Hypervelocity Vehicles, 329
War
Borders, 488
Terrorism, 273
Warhead, 278
Warne, L. K.
Model for Channel Resistance in Water Breakdown, 696
Ray Model of High-Frequency Cavity Scarring, 452
Warrant, M. M.
Automatic Generation of Terrorist Operation Plan, 30
Warren, M. E.
An Integrated, Stacked System-on-a-Chip, 196
Waste (radioactive), 348
Water
Agriculture, 36
Biological terrorism, 893
Breakdown, 696
Contamination, 360
Desalination, 341
Management, 423
Reactor, 796
Regulated chemicals, 338
Pathogens, 111
Planning (quality), 834
Planning (toolbox), 386
Planning (value), 832
Streams, 335
Surety, 607
Switches, 689
Watson, J.
Agent-Based Autonomic Logistics Simulation Model, 286
Deciphering the Genetic Regulatory Code, 913
Wave
Brain, 904
Continuous, 176
Electrodynamic response, 220
Evanescent, 225
Poroelastic, 878
Spread-spectrum, 629
See also: Microwave
See also: Subwavelength
Waveform, 629
Waymire, R. L.
Simulating Human Behavior for National Security, 321
Weaklink, 735
Weapon
Adaptive optics, 681
Automotive industry, 712
Gel-based, 560
Nuclear (gel-based), 67
Nuclear (signals), 606
Thermobaric explosives, 283
See also: Bioweapon
Weaponization, 283
Webb, D. B.
An Integrated, Stacked System-on-a-Chip, 196
Full-Earth-Monitoring Sensor MESAWorks, 910
Webb, E. B., III.
Atomistic-Continuum Simulation, 434
Webster, J. R.
Dielectrics with Controlled Leakage, 213
Nanoelectromechanical Oscillators for RF Filtering, 173
Weichman, L. S.
Advanced Packaging Technology for Optical Firesets, 738
Weiland, L. A.
Agent-Based Control of Distributed Infrastructures, 377
Weir, N. A.
Intelligent Interaction Control for Metrology, 52
Weiss, C. J.
Geophysical Subsurface Imaging, 113

Author and Title Index

A B C D E F G H I J K L M N O P Q R S T U V W X Y Z

Welch, B. J.
High-Capacity Earth-Penetrator Instrumentation, 312
Welch, D. R.
Advanced Pulsed-Power Fusion Concepts, 898
Welle, E. J.
Hard-Target-Defeat High-G-Tolerant Fuze, 243
MICROFUZE Integration, 302
Wendt, J. R.
Active Photonic-Crystal Devices, 183
Advanced Device Structures for Solid-State Lighting, 419
Compact Terahertz Sources, 252
Completely Passive Microwave Tag, 581
Coupled Nanomechanical Oscillator Arrays, 562
Dispersive Diffractive Optical Elements for the IR, 659
GaN 20–100 Watt Amplifiers for Micro-SAR, 222
Microoptical Gyroscope, 205
Nanoelectromechanical Oscillators for RF Filtering, 173
Zero-Power Radio Receiver, 578
Wessendorf, K. O.
Microoptical Radar Facial-Recognition Project, 673
West, J. A.
High-Throughput Microfluidic Integrated Microarray, 576
Wetting, 57
Weyn, M. L.
EM Interactions with Systems to Enhance Security, 235
Wheeler, D. R.
Functionalized Nanoparticles for Sensor Applications, 187
Microflame-Based Detector for Gas Sensing, 270
Polymer Electronic Devices and Materials, 643
Real-Time Sensors for Water-Contamination, 360
Wheeler, J. W.
Adaptive-Force-Feedback Surface Control, 310
Whittet, L. J.
Risk-Assessment Metatool, 627
Wick, D. V.
Adaptive Optics and Phase-Diversity Imaging, 618
Wickstrom, R. D.
Event Locations from Space-Based Sensors, 663
Wiegandt, D. A.
TALON, 480
Wilcox, W. B.
Understanding Communication in Crisis Management, 255
Wilcoxon, J. P.
Nanocrystal-Polymer Composites for LEDs, 812
Nanoscale Energetic Materials, 701
Williams, P. J.
Penetrator Reliability Investigation, 157
Williams, R. L.
TALON, 480
Williams, T. C.
Soot Formation in Unsteady Diffusion Flames, 444
Wilson, C. W.
Advancements in Sensing and Perception, 275
Wilson, D. G.
Advanced Mobile Networking Sensing, 249
Intelligent Interaction Control for Metrology, 52
Wilson, M. P.
Image Georectification, 636
Reconstruction Algorithm Development, 654
Winters, W. S., Jr.
Modeling of Contaminant Transport, 586
Wireless
Ad Hoc environment, 289
Network (SDAC), 36
Network (wireless), 403
Witze, P. O.
Revolutionary Systems for Catalytic Combustion, 344
Witzke, E. L.
Cryptographic Assurance of Execution Correctness, 612
Woessner, S. M.
Nanocrystal-Polymer Composites for LEDs, 812
Nanoscale Energetic Materials, 701
Wolfenbarger, P. R.
Intelligent Interaction Control for Metrology, 52
Simulating Human Behavior for National Security, 321
Wong, C. C.
Full-Earth-Monitoring Sensor MESAWorks, 910
Wood, N. L.
Dynamics of Membrane Proteins and Receptors, 863
Woodard, J. B.
TALON, 480
Wooden, S. M.
Novel and Robust Environmental Sensing Devices, 743
Woodworth, J. R.
Laser Triggering of Water Switches, 689
Wouters, G. A.
Completely Passive Microwave Tag, 581
Power-Combining for Power Amplifiers, 657
Zero-Power Radio Receiver, 578
Wright, A. E.
GaN HEMT High-Power Amplifiers, 207
Understanding Communication in Crisis Management, 255
Wright, S. A.
Conversion Systems for Nuclear-Power Reactors, 362
Wyss, G. D.
Critical-Infrastructure System-of-Systems Assessment, 665

X
Xavier, P. G.
Augmented Cognition, 476
Robotic Planning for Physical-Security Analysis, 601
Simulating Human Behavior for National Security, 321

Y
Yang, P.
Injection Molding of Net-Shape Ceramic Components, 71
Microfabrication with Femtosecond Laser Processing, 41
Rapid-Prototyping High-Density Circuitry, 55
Yarrington, P.
Characterization for Assured HDBT Defeat, 483

Author and Title Index

A B C D E F G H I J K L M N O P Q R S T U V W X Y Z

Yelton, W. G.
Functionalized Nanoelectrode Arrays, 338
Nanoporous-Carbon Adsorbers for Microsensors, 786
Self-Assembled Ordered Carbon-Nanotube Arrays, 860
Yoder, J. R.
TALON, 480
Yoshimura, A. S.
Understanding Communication in Crisis Management, 255
Young, E. W.
Continuous-Wave Intersubband Terahertz Sources, 176
Young, M. F.
Conversion Systems for Nuclear-Power Reactors, 362
Young, M. L.
Optimal Allocation of Terrorist Countermeasures, 393
Young, R. W.
MOSFET–MEMS Integration, 203

Z
Z-pinch, 684
Zaha, J. S.
Advanced Neutron Monitors for JTA, 745
Zavadil, K. R.
Biomicrofuel Cell, 473
Quantification of Environments within Micropackages, 520
Switchable Materials for (Bio)Microfluidics, 534
Vulnerability of Micromechanicals to Cracking, 552
Zero (power), 578
Zhang, P.
Automatic Generation of Terrorist Operation Plan, 30
Zifer, T.
Decomposition of Contaminants Using Nanoparticles, 514
Thermally Cleavable Surfactants, 516
Zimmerly, C. A.
Polymer Electronic Devices and Materials, 643
Zimmerman, J. A.
Atomistic-Continuum Simulation, 434
Multiscale Experimental/Numerical Study, 727
Zubrzycki, W. J.
Deployable Object Tracker for NMD Flights, 317
Zuffranieri, J. V.
Energy-Systems Analysis Framework and Modeling, 425
Nonradioactive Safety with Water Reactors, 796
Radiation Issues with Advanced Coolants, 798
Zutavern, F. J.
Compact Terahertz Sources, 252
Free-Space Electrooptic Sampling, 238
Ultrafast-Current Transient Measuring Device, 468